

GREEN BUILDING, MATERIALS AND CIVIL ENGINEERING

PROCEEDINGS OF THE 4TH INTERNATIONAL CONFERENCE ON GREEN BUILDING,
MATERIALS AND CIVIL ENGINEERING (GBMCE 2014), HONG KONG, 21–22 AUGUST 2014

Green Building, Materials and Civil Engineering

Editors

Jimmy C.M. Kao

*Institute of Environmental Engineering, National Sun Yat-Sen University,
Kaohsiung, Taiwan, R.O.C.*

Wen-Pei Sung

National Chin-Yi University of Technology, Taiping City, Taiwan, R.O.C.

Ran Chen

Chongqing University, Chongqing, P.R. China



CRC Press

Taylor & Francis Group

Boca Raton London New York Leiden

CRC Press is an imprint of the
Taylor & Francis Group, an **informa** business

A BALKEMA BOOK

CRC Press/Balkema is an imprint of the Taylor & Francis Group, an informa business

© 2015 Taylor & Francis Group, London, UK

Typeset by V Publishing Solutions Pvt Ltd., Chennai, India

Printed and bound in Great Britain by CPI Group (UK) Ltd, Croydon, CR0 4YY

All rights reserved. No part of this publication or the information contained herein may be reproduced, stored in a retrieval system, or transmitted in any form or by any means, electronic, mechanical, by photocopying, recording or otherwise, without written prior permission from the publisher.

Although all care is taken to ensure integrity and the quality of this publication and the information herein, no responsibility is assumed by the publishers nor the author for any damage to the property or persons as a result of operation or use of this publication and/or the information contained herein.

Published by: CRC Press/Balkema

P.O. Box 11320, 2301 EH Leiden, The Netherlands

e-mail: Pub.NL@taylorandfrancis.com

www.crcpress.com – www.taylorandfrancis.com

ISBN: 978-1-138-02669-8 (Hbk)

ISBN: 978-1-315-75198-6 (eBook PDF)

Table of contents

Preface	xv
GBMCE 2014 committee	xvii
Analysis of reinforced concrete building structures using simple models <i>W. Kang, H. Chung & Y. Yungmin</i>	1
Green premium in green condo buildings? Evidence in Taiwan <i>F.-Y. Chen, I.-W. Peng, J.-H. Liang & Y.-Y. Liang</i>	7
To discuss the relationship between green building and regional housing price <i>T.-K. Hsieh, H.-Y. Tsai & Y.-R. Du</i>	13
Properties of asphalt mixtures with reclaimed material in Slovakia <i>S. Čápayová, A. Zuzulová & K. Bačová</i>	17
Solar technology of high-rise building integrated design in China <i>S. Y. Zhu & C.L. Ma</i>	21
A study of photovoltaic systems with a variable step size P&O MPPT algorithm <i>T.-C. Yu, C.-C. Liu, Y.-B. Lin, C.-H. Chen & Y.-C. Liou</i>	25
Experimental study on the axial behavior of perforated cold-formed steel wall frames <i>N.M. Mohsan, A. Sulaiman & M. Md. Tahir</i>	31
Integral analysis of laboratory and field electrical resistivity for soil density prediction <i>Z.A.M. Hazreek, A.T.S. Azhar, M. Aziman, S. Rosli, A. Fauziah & W.D. Chitral</i>	37
Structural behaviour of <i>Kekatong</i> glued laminated timber railway sleepers under 'sleepers static performance test' <i>M.B. Norshariza, A. Abu-Bakar, Z. Ahmad & P. Tahir</i>	45
Vibration control of stay cable with double Tuned Mass Damper <i>S. Luo, W. Liu & Z.S. Deng</i>	51
Biomass waste shells analysis and advanced gasification tests <i>L. Vecchione, M. Moneti, A. Di Carlo & E. Bocci</i>	55
Numerical simulation analysis on construction settlement of loess embankment <i>X.Q. Pang & Z.Q. Hu</i>	61
The effect of marketization of interest rate on the investing and financing of enterprise <i>X.-S. Zeng</i>	65
Application of viscous damper in reinforcement of frame structure <i>W. Han, M.J. Liao & X.Y. Jia</i>	69
Optimal dispatch of distributed generation system <i>D. Xu & P. Li</i>	73
Optimal allocation of distributed generation in smart grid <i>D. Xu & P. Li</i>	77

Regression, continuation, and innovation—contemplating upon the construction of livable communities <i>K. Yang</i>	83
On the study of spatial form and functional partition in the modern ceremony etiquette environment <i>Y. Li</i>	87
Analysis on the digital architectural construction of architectural surface <i>Y. Li</i>	91
Study the space environment accessories design and creation category <i>D. Wang</i>	95
The exchanged landscape: Reinterpretation of the site <i>D. Wang</i>	99
Analysis of Northeast Korean vernacular architectural landscape culture <i>Q. Yu & C.L. Wang</i>	103
Study on characteristics of the recycled cement mortar asphalt slurry <i>Z.L. Liu, Y.L. Du & J.J. Li</i>	107
Risk evaluation of hydroelectric asset-backed securitization using fuzzy triangular numbers <i>T. Ni, L. Tang & H. Wen</i>	111
The application of vortex squeeze expanding mechanism in geotechnical engineering <i>C.B. Li, S.F. Xue, R.G. Yu, Y.M. Zhang, M. Zhang, X.H. Liu & Z.J. Zhao</i>	117
Synthesis, characteristics conductivity of heteropoly compound $\text{Na}_6[\text{MnMn}(\text{OH}_2)\text{W}_{11}\text{O}_{39}] \cdot 16\text{H}_2\text{O}$ <i>M.-X. Zhu, L.-Q. Chen & X.-M. Lin</i>	121
Study on seismic behavior of pre-cast concrete joint with the capacity of self-centering <i>Y. Zou, C. Li & Q. Wang</i>	125
A parallel FEA computing kernel for ISSS <i>J. Duan, X.M. Chen, H. Qi & Y.G. Li</i>	131
The key points for ecological design during urbanization process <i>Z. Jia</i>	137
Optimal design of the flue size based on lagrangian algorithm <i>R.N. Zhang & Y.J. Yu</i>	141
Numerical simulation of indoor air quality and thermal comfort in typical office with stratum ventilation <i>J. Xu & Y.J. Yu</i>	145
Urban Heat Island and its influencing indicator of new central district in Guangzhou city <i>P. Wang & Q.L. Meng</i>	151
Study on surface performances of oxidation-sulfonated cellulose based superplasticizer <i>K. Rouzi, M. Mahemuti & M. Mamuti</i>	157
Study on numerical simulation of gas drainage drilling of rock drift of coal seam floor <i>W. Wu, Y.Y. Wang & J. Zhu</i>	163
Hydraulic fracturing anti-reflection technique and applications in soft and low permeability coal seam <i>X.X. Chen, W. Wang, W.G. Jin & Y. Xu</i>	169
Research of MATLAB modeling and vector control of brushless double-fed machine <i>Y. Deng, X. Jin & J. Chen</i>	173
Two dimensional numerical simulation of the flow transport in bend drains <i>C. Yang, C.-G. Li, W.-J. Zhao & L.-X. Zheng</i>	179

Recommendations on the reconstruction of the old market building in Xiamen—a case study of Xiamen's eighth market <i>J.H. He</i>	185
The application of payment guarantees to subcontracts <i>X.X. Ding & M. Y. Su</i>	189
Experimental study of double combination structural behavior of the negative bending region of Concrete-Partial-filled narrow-width steel box composite beams <i>H.L. Yang, Y. Zheng, X.K. Li, S. Li & S.X. Mo</i>	195
Optimize research in assessment system of green building indoor environment <i>X. Jiang & W. Cheng</i>	201
Seismic damage performance evaluation of special-shaped column frame <i>Y. Liu, X.M. Ren & H.B. Liu</i>	205
Design and construction of the high-support formwork for NingBo Cultural Plaza Grand Theatre <i>Y. Huang, Z.Q. Dong, J.M. Gu & L.J. Liang</i>	211
Analysis of the settlement of CFG pile composite foundation <i>L. Xie & B. Tang</i>	215
Test of surface free energy of asphalt by digital image processing <i>Q.X. Pan, X.D. Zha, W. Chen & B. Yang</i>	219
Experimental research on the flexural behavior of a new type of I shaped prestressed concrete sheet pile <i>H.D. Xu, K. Teng, X.J. Fu & K. Yuan</i>	225
Tests on the seismic behavior of cavity wall with phase change materials based on simulation masonry building <i>J.L. Shang, T.G. Zhang, S.Y. Lei & H. Zhang</i>	229
The calculation of composite beam's slippage formula and deflection formula considering the slippage of steel-concrete <i>X.J. Chen, Z. Tao & D.G. Zeng</i>	233
Experimental study on NO reduction by biomass reburning in Northern China <i>D. Yang, X.J. Zhang, Q.W. Chen, M. Zhang & S.J. Wei</i>	239
Experimental study on changes of CaCO ₃ concentration in FGD of falling films reactor <i>D. Yang, X. Lu, S.J. Wei & M. Zhang</i>	243
Development and research status of renewable energy utilization in Shandong province <i>D. Yang, Q.M. Wen & S.J. Wei</i>	247
A new prefabricated construction method based on building industrialization <i>J.N. Luo, H. Y. Zhu & H. Zhang</i>	251
An analysis of landslide thrust of each row of double-row and embedded anti-slide piles <i>J. Xu, Y.G. Pang, A.H. Li & X.H. Xue</i>	257
The research for the influence between the WVD and the amplitude of signals <i>Z.H. Yuan, M. Y. Xu & X.X. Qi</i>	263
Relationship between the stroke length of hydraulic cylinder and the attitude angle of shield during rectification <i>Y.P. Song & Y.X. Sun</i>	267
Exploration of extending the service life of the residential buildings in cold area <i>H.M. Liu & Z.H. Liu</i>	275
Finite element method analysis on slope stability under seismic dynamic <i>G.Y. Zhou & X. Zuo</i>	279
The stability research of hinge-chained concrete block slopes under water pressure <i>H. Su</i>	287

Research on ecological planning design of waterfront landscape belt in cold regions—with the riverside of Jilin city as a case study <i>H.M. Liu & Y. Su</i>	293
Study on the influence of the particle damping to sound field inside the closed cavity <i>L. Hu, Z. Tang, Q.L. Yang & X. Xu</i>	297
Microstructure and mechanical properties analysis of GH3030 alloy activity TIG welding <i>X.G. Zhu, W. Wang & C.L. Yang</i>	303
Study on the promotion of Liaoning rural roof insulation project <i>J. Liu, D.Q. Chen & R.Q. Liu</i>	307
Research on preparation of sulfate resistance foam concrete <i>J. Liu, Z.Y. Huang, R.Q. Liu & T.B. Hou</i>	313
Low cycle fatigue properties of anti-seismic steel HRB400E reinforcing steel bars <i>Y.R. Luo, T. Zeng, L. Fu, H.B. Lin & M.F. Huang</i>	319
GRNN model in the application of mixed-sand pumping concrete research <i>H. Li & X.W. Cheng</i>	323
The research on of drivers' shoulder fatigue when driving on the grassland highway <i>S.R.N. Bao, S.L. Zhu, C.H. Qi, M.X. Gao, H.T. Li & T. Zhao</i>	327
Effect of polypropylene fiber and silica fume on mechanical properties and durability improvement of high performance concrete <i>X.G. Zheng, J. Liu, S.M. Li, Z. Zeng, Z.C. Weng, D.J. Yang, D.H. Deng & R.S. Ding</i>	333
Reliability analysis of slope based on quantified Hoek-Brown strength criterion <i>H. Wu, X.C. Lin, J.G. Du & J.C. Xu</i>	343
Simulation of the superelasticity of Shape Memory Alloys by MATLAB programming <i>Y.H. Ling, Y.M. Huang, H.W. Ma, G.L. Guo & Y.Z. Wu</i>	347
Planning of slow traffic system from top-down perspective: Case study of Ersha Island <i>J.Y. Wu & Z.Y. Zeng</i>	353
Analyzing the key chain of railway accident causation based on community detection method <i>H.W. Xin, K.P. Li, H.F. Huang & X. Ma</i>	359
The investigation of financing models of Chinese highway <i>D. Fu, B. Tang & L. Xie</i>	363
A feasibility study on the subgrade compaction rapid detection using portable gravity punch <i>H.K. Zheng, C. Li, W.M. Wang, C.Y. Liang & J.J. Liu</i>	367
Experimental study on flexural behavior of High Titanium Heavy Slag Concrete beam <i>J.W. Long, X.Y. Guo & L. Song</i>	373
Applicability analysis on index values of water stability of asphalt mixture <i>Q.X. Pan, G.P. Qian, H.F. Liu & T. Huang</i>	377
The regular study of dry density for shear strength parameters of loess <i>K.F. Yuan & Z.J. Sun</i>	383
The regular study of water content for strength index of loess <i>K.F. Yuan</i>	387
Study on type selection of shield equipment in different geological conditions <i>F. Lin, S.G. Chen & H. Zhang</i>	391
The effect of the soil state on the soil physical properties <i>L. Ma</i>	395
Reduction of NO _x from biomass pyrolysis experiments <i>D. Yang, M. Zhang & X.J. Zhang</i>	399

Different approaches for energy saving in central air-conditioning system <i>L.H. Zhang, D. Yang, Y.X. Qu & L. Xu</i>	403
The analysis of hydraulic characteristics of central heating pipe network under typical conditions <i>L.H. Zhang, D. Yang, G.Y. Gao, Y.X. Qu & S.J. Jun</i>	407
Experimental study on recycled slag aggregate concrete-filled steel tube under axial compression <i>M.C. Chen, J.J. Liu & H. Huang</i>	413
Study of damage statistical elastic damage constitutive model for rock considering residual strength and threshold <i>Y.Q. Zhou, Q. Sheng, X.D. Fu, S.B. Chai & L.F. Li</i>	419
Experimental study on crack control of light gauge steel and foamed concrete wall <i>J.-J. Wang</i>	423
Study on the rutting resistance mechanism of Lucobit modifier <i>Y.M. Zhang, K. Wang & G.W. Hu</i>	429
Performance analysis and optimization of fuze TPV power supply <i>C.H. Yu, X.L. Qi & M. Gao</i>	435
The monitoring research on process of heat and moisture transfer in active layer of permafrost <i>M.L. Zhang, Z. Wen & K. Xue</i>	439
Triple objective evaluation model of green building based on whole life-cycle <i>Q.L. Han & X.L. Kong</i>	445
High-tech cabling system applied in green building <i>F. Fang & X.F. Yu</i>	451
Research and prospect on durability of reinforced concrete structures <i>Q.L. Li, X. Wang, Z.Z. Li, J.F. Li, X.M. Yang & Y.G. Han</i>	455
The research of selection of construction site of project based on grey correlation degree <i>Y.M. Lv, Y. Wei & L.Y. Zhang</i>	459
The research on developing eco-tourism in natural reserves in China <i>J.B. He & Z. Wang</i>	463
Numerical analysis of CFG pile arrangement by FLAC <i>L.H. Zhang, H.B. Liu & Q. Xu</i>	467
Measures to improve residential sound insulation property in severe cold region <i>Q.L. Zheng</i>	473
Equivalent solid-web beam method for steel truss based on the energy principle <i>Z.H. Zhang, X.P. Shu & M.L. He</i>	477
A realization method of massive log management system for crime forensics <i>H.-Y. Chen</i>	481
Research on the comprehensive evaluation of cuplock scaffolding <i>Y.R. Chen, L.J. Liu, W.G. Sun, L. Shen & P.Q. Yu</i>	485
Active control of structural vertical-vibration based on electromagnetic levitation technique <i>C. Xia, D.B. Fu & S.K. Liu</i>	495
Remedy chromium ions contaminated soil by electrolysis method <i>Z.Q. Zhang, Z. Gao, N. Liu, Y.W. He, Z. Wu, B.H. Lin, J.L. Chen & R.Y. Ma</i>	499
Statistical analysis of urban mass transit accidents and safety countermeasures study <i>Y.R. Fu & Y.D. Meng</i>	503
Study of minimum base shear on design seismic code <i>J. Setiawan & I. Imran</i>	507
Study of roadway layout in the σ_{HV} type in-situ stress field <i>P. Lv, X. Xi, L.-L. Shao & Z.-X. Zhang</i>	513

Study on the design of urban public facilities—take Hefei as an example <i>B. Zhang & B.N. Hu</i>	517
The application of conditional probability among Step-Stress Accelerated Life Testing <i>H.H. Guo, C.R. Li, K.S. Wang & Y.C. Pang</i>	521
Effect of band drain spacing on the improvement of hydraulic filled ultra-soft soil foundation <i>A.H. Liang, Z.J. Chen & J. Yu</i>	525
Analysis on the influence of the thickness of external insulation layer of building envelope on building energy consumption in Sunan Region <i>X.P. Feng & X. Liu</i>	529
An analysis of influence factors of income payment in developing countries <i>L. Zhang</i>	533
The authenticity of the images: “The real emotion”—reflection on the movies “Under the Hawthorn Tree” and “Avatar” <i>H.M. Lu</i>	537
Methods and measures of project cost implementation and control on all the stages of engineering project <i>J.X. Li</i>	539
A subgrade stability analysis method based on the strain monitoring information <i>Y.M. Xiang, W.X. Long, G.X. Ling & B. Du</i>	543
Research on differential settlement control standard of road subgrade in seasonal frozen area <i>Y.M. Xiang, W.X. Long, G.X. Ling & B. Du</i>	547
Analyzing the influential elements of FLAC strength reduction method of slope safety factor determined <i>J.L. Cai, Z.C. Ye, G. Li & L.H. Zhang</i>	553
Chaos behaviors of a class of constant-length substitutions and the hyperspace systems <i>W. Wang & X.G. Zhu</i>	557
Simulation tool application of energy consumption unit in sustainable residential building evaluation <i>Y. Su & Y. Fan</i>	561
Analysis of civil construction based on systems engineering theory <i>W.B. Xue & M.S. Yang</i>	565
The ventilation of traditional veranda style architecture in Haikou <i>Y. Wang, X. Chen & Y.P. Wang</i>	569
Evaluation of compressive strength of hardening concrete containing high calcium fly ash <i>W.J. Fan & X. Y. Wang</i>	573
Experiment validation of gravity feed liquid cooling evaporator simulation <i>Q.J. Liu, X.J. Ma, S. Y. Chen, F. Han & R.Q. Zhan</i>	577
Pricing and strategies of carbon emissions trading based on shadow price theory <i>S.Q. Li, X.Y. Wu, S.P. Hu & X. Sun</i>	581
Reliability distribution of traction system for rolling stock <i>S.J. Liu & Y. Lu</i>	585
Study on the problems and countermeasures of Urban Utility Tunnel construction <i>J.H. Wu & D.Z. Wu</i>	591
Application study of green building technology in universities and colleges in cold regions <i>J. Qiu & L.B. Xia</i>	595
Research on the influence of lean of bridge piers on continuous rigid frame bridge <i>W.Z. Ying</i>	599

The channel investigation of BIM technology localization <i>E.T. Qie, Y. Li, Y.Y. Jiao & C.T. Wang</i>	605
The architectural style characteristics of Enshi Tujia Diaojiaolou from Peng <i>Y. Hong</i>	611
The calculation methods of property of the parallel composite isolation system <i>H. Yan & F.M. Pi</i>	615
Gas-pressure sintered Si ₃ N ₄ fabricated by ceramics injection molding <i>X.F. Yang, J.H. Yang, X.W. Xu, M.M. Wang & Z.P. Xie</i>	619
Green SCC design algorithm and its performance <i>C.L. Hwang, Y. Risdianto, C.T. Chen, M.G. Tesfamariam, H.T. Phuoc, A.H. Limongan & B.L.A. Tuan</i>	623
Free and forced vibration of rectangular plates using the finite difference method <i>Y.S. Al Rjoub & O. Abdeljaber</i>	627
Tensile properties and water absorption of Recycle Polypropylene (rPP)/Oil Palm Empty Fruit Bunch (OPEFB) composites: The effect of Maleic Anhydride-g-Polypropylene (MAPP) addition <i>H. Nasution</i>	635
Evaluation of structural stability for beam made of submarine structural steels (SM 400, SM 490) at high temperature <i>I.-K. Kwon, O.-S. Kweon, H.-Y. Kim & S.-U. Chae</i>	639
Design and making of conformal cooling system for cycle time reduction in curvature and complex shape mold component <i>M. Hearunyakij & S. Chatakorn</i>	643
Study on the space layout of rural residents in Fusong county of Jilin Province <i>R.Q. Qie</i>	649
On the emotional orientation of surface architecture <i>H. Ma</i>	653
Effect of refrigerant charge and TXV opening on the performance of air-source heat pump water heater <i>Z.H. Wang</i>	657
Research on the urban plans of Xi'an (1950–1952) <i>Y. Xiao & Y.Y. Ren</i>	663
Integrating sustainability into design planning <i>R.J. Lu</i>	667
The research on the impact of external traffic organization of HOPSCA on urban space <i>Q.H. Hou & W.H. Wang</i>	671
An analysis on the social benefit of combining charities with road race events—with the 2011 Beijing Marathon as a case <i>Q.S. Zhu</i>	675
The social effects of traditional sports in the Yifan Festival of Molao people <i>Z.F. Huang & Y.L. Yang</i>	679
Contractor's claims management evaluation <i>L.M. Jia & S. Lu</i>	683
Matrix transfer method of the curved-wall type tunnel lining structure calculation <i>J. Yin, R.G. Deng, Z.B. Zhong, P. Wang & M. Hu</i>	689
The use of virtual water trade in water resources optimization in Minqin <i>J.M. Han, M. Liu & Y. Chen</i>	695

Study on model and design of old-age residence <i>L.L. Li & Y. Li</i>	703
Practice of new regionalism—taking “Design of Business Street at Zhuang Yuan Road along Xishui Bahe” for example <i>Y. Yang, M.X. Zhang & Q. Huang</i>	707
The experimental study on mechanical properties of elephant grass stem <i>X. Liang, B. Fang, D.P. Ye & H.J. Hu</i>	711
Architecture value and protection strategy of fortress settlement: A case study from Zhaibochang ancient residential <i>X.F. Bi, L. Wang & D.J. Xu</i>	715
Discussion of strata division of Bingmagou Formation in Yichuan of Yuxi region <i>J. Zhu, D.S. Zheng & S.H. Zhu</i>	719
Bon temples in Ding Qing of Qamdo <i>H.W. Qi, X.M. Zong & Y.P. Wang</i>	723
Study on innovation of Chinese elements in modern interior design <i>Y.F. Liu</i>	727
Adult picture book creation with mixed media—using a story of “Weirdness” as an example <i>R.L. Lin</i>	731
Adult picture book creation with mixed media—using a story of the case of the disappearing bodies as an example <i>R.L. Lin</i>	735
Adult picture book creation with mixed media—using a story of a crime of passion as an example <i>R.L. Lin</i>	739
Adult picture book creation with mixed media—using a story of “Forfeiting Lives” as an example <i>R.L. Lin</i>	743
Research on Chinese rural public security evaluation system based on fishbone diagram analysis—a case study of South Dagang district for the first partition <i>M. Sun & S.Y. Wang</i>	747
Predict of loss of fuel during the road reconstruction in Indonesia <i>D.K. Sudarsana, H. Sulistio, A. Wicaksono & L. Djakfar</i>	753
Optimizing transportation system planning design for campus in severe cold climates <i>Y. Zhang & Z.G. Chen</i>	757
Research advances and engineering application of energy pile system <i>C. Yang, Z.R. Zhu, G.L. Dai & W.M. Gong</i>	763
Investment efficiency analysis on installing coal ash system in power plants <i>F. Dai, J. Fan & Y.L. Xu</i>	769
Exploration on the ecology dominant development pattern along the Changshuang road <i>L.M. Bai</i>	773
Research on the green space system planning of Changchun and Eco-city construction <i>L.M. Bai</i>	777
The thinking of industrial heritage protection and reuse under the background of urban renewal <i>L.M. Bai</i>	781
Influence factors analysis of sulfate attack for cement concrete <i>Y.-C. Zhang & L.-L. Gao</i>	785
Experimental study on cementation strength of unsaturated granite residual soil <i>L.S. Tang, H.T. Sang, X.B. Deng, Z.G. Luo & H.K. Chen</i>	789

Application and experiment research on diaphragm wall foundation in bridge engineering <i>L. Wang, W.M. Gong, G.L. Dai & H. Guo</i>	795
The influence of Shrinkage-Reducing Agent on the early-age shrinkage under the different curing system and mechanical properties of concrete <i>Q.W. Fang, J.Y. Lai, X.Q. Qian & K. Dong</i>	801
Value for money and its application for infrastructure investment projects <i>J. Ceselsky, J. Kucera, B. Vojvodikova, M. Ferko & Z. Proske</i>	807
Finite element analysis of beam from rolled IPN 160 <i>O. Sucharda, J. Vasek & D. Mikolasek</i>	811
Numerical modeling of rotary stiffness of joint for rails <i>O. Sucharda, D. Mikolasek, J. Brozovský & L. Zidek</i>	817
Research on the influence of section size error on height of main beam on continuous rigid frame bridge <i>T.-L. Wan</i>	825
Classification and discussion of fastening system of ballastless track <i>J.C. Huang & C.H. Li</i>	829
The compared study of flexible central buckles cable girder anchorage system of steel truss girder suspension bridge <i>C.-D. Yang</i>	833
Study of greenway site selection based on cultural route: Research on grassland silk road (from Xanadu to Zhongdu) <i>P. Zhou, J.Y. Wu, X.F. Wu & Y.W. Huang</i>	841
Gaussian model investigation in modeling of air pollution diffusion using Geographic Information System (GIS) <i>F. Sabbagh, A. Afshari, M. Hassanzadeh, S. Kaveh & M. Amiri</i>	849
A comparative analysis to prioritize renewable energy alternatives using Fuzzy Analytic Hierarchy Process <i>V. Baratzadeh, S. Kaveh, Y. Edrisian, F. Sabbagh & A. Afshari</i>	855
Construction of a green golf club buildings on undermined area <i>R. Cajka, P. Labudek, K. Burkovic & M. Cajka</i>	861
Effect of the special environments on bond behavior of CFRP anchor <i>W.-R. Yang, X.-J. He, K. Zhang & P. Zhang</i>	869
Research on Tonga traditional houses adaptive to environment <i>S. Jin, H. Huang & Z. Yang</i>	873
Innovative design of integrated facility for the aged based on green building concept <i>Y. Chen & Y. Liu</i>	877
Simulation on visitor evacuation in large-space exhibition building <i>Y. Liu, Y. Chen & Q.C. Jiang</i>	883
Investigation on bond-slip behavior between Shape Memory Alloy and concrete by finite element method <i>D. Cui</i>	887
Study on architecture technology safety management <i>S. Wang</i>	891
Research on properties of GCL in MSW land <i>X.B. Xiong</i>	895
The analysis of the contrasted love in <i>Women in Love</i> <i>H. Y. Du, X.N. Peng & L. Zhang</i>	905

Design of a pallet pool in Inner Mongolia <i>J.W. Ren</i>	909
Design of a harbor station in Nansha Islands <i>J.W. Ren, J.W. Cao & X. Wei</i>	913
Re-discussion on the measurement of tourist environment capacity in large-scale scenic areas <i>K.Q. Wang & Q. Bai</i>	917
The design of dual purpose crib based on man-machine research <i>L.-L. Liu & J. Bian</i>	923
A design study on optoelectronic textiles in cases of LED lighting and solar powered handbags <i>J.-Y. Shih, S.-L. Lai & H.-T. Cheng</i>	927
Author index	935

Preface

On the successful basis of GBMCE 2011, 2012, 2013, the 2014 4th International Conference on Green Building, Materials and Civil Engineering (GBMCE) was held August 21–22, 2014 in Taiwan. The aim was to provide a platform for researchers, engineers and academics as well as industry professionals from all over the world to present their research results and development activities in green building, materials and civil engineering. The conference aims mainly at promoting the development of green building, materials and civil engineering, strengthening the international academic cooperation and communications, and exchanging research ideas. Submitted conference papers were reviewed by technical committees of the conference.

This book brings together 190 peer-reviewed papers on Green Building, Energy, Environment, Materials and Civil Engineering. This book provides the readers a broad overview of the latest advances in the field of Materials, Energy, Environment and Civil Engineering. We hope that this collection of papers will contribute in stimulating debate among scholars, researchers and academics and that you find them interesting and thought-provoking.

On behalf of the guest editors for this conference proceeding, we would like to thank the conference organization staff, and the members of the International Technological Committee for their hard work. We look forward to seeing all of you next year at GBMCE 2015.

Wen-Pei Sung
National Chin-Yi University of Technology
August, 2014

GBMCE 2014 committee

CONFERENCE CHAIRS

Prof. Wen-Pei Sung, *National Chin-Yi University of Technology, Taiwan*
Prof. Jimmy C.M. Kao, *National Sun Yat-Sen University, Taiwan*
Prof. Ming-Hsiang Shih, *National Chi Nan University, Taiwan*
Prof. Wen-Jie Luo, *National Chin-Yi University of Technology, Taiwan*

LOCAL ORGANIZING CHAIRS

Prof. Ron Chen, *Chung Hua University, Taiwan*
Prof. Wen-Sheng Ou, *National Chin-Yi University of Technology, Taiwan*
Prof. Yu-Kuang Zhao, *National Chin-Yi University of Technology, Taiwan*

INTERNATIONAL TECHNOLOGICAL COMMITTEE

Yoshinori Kitsutaka, *Tokyo Metropolitan University, Japan*
Nasrudin Bin Abd Rahim, *University of Malaya, Malaya*
Yan Wang, *The University of Nottingham, UK*
Zhi Jian Wang, *China Academy of Science, China*
Darius Bacinskas, *Vilnius Gediminas Technical University, Lithuania*
Qing-Lin Meng, *South China University of Technology, China*
Cheer Germ Go, *National Chung Hsing University, Taiwan*
Liu Yunan, *University of Michigan, USA*
Ye-Cai Guo, *Nanjing University of Information Science & Technology, China*
Wang Liying, *Institute of Water Conservancy and Hydroelectric Power, China*
Chenggui Zhao, *Yunnan University of Finance and Economics, China*
Rahim Jamian, *Universiti Kuala Lumpur Malaysian Spanish Institute, Malaysia*
Li-Xin Guo, *Northeastern University, China*
Gang Shi, *Inha University, South Korea*
Bhagavathi Tarigoppula, *Bradley University, USA*
Chen Wang, *University of Malaya, Malaya*
Wei Song, *Minzu University of China, Tsinghua University, China*
Shyr-Shen Yu, *National Chung Hsing University, Taiwan*
Shen-Chuan Tai, *National Cheng Kung University, China*
Jzau-Sheng Lin, *National Chin-Yi University of Technology, Taiwan*
Rong-Chang Jou, *National Chi Nan University, Taiwan*
Yean-Der Kuan, *National Chin-Yi University of Technology, Taiwan*
Fu-Jen Wang, *National Chin-Yi University of Technology, Taiwan*
Jeng-Min Huang, *National Chin-Yi University of Technology, Taiwan*
Jiunn-Min Chang, *National Chin-Yi University of Technology, Taiwan*
Chi-Wun Lu, *National Chin-Yi University of Technology, Taiwan*
Yu-Lieh Wu, *National Chin-Yi University of Technology, Taiwan*
Hua-Zhi Hus, *National Kaohsiung Marine University, China*
Shih-Heng Tung, *National University of Kaohsiung, China*
Chau-Cho Yu, *National University of Kaohsiung, China*

Kuo-Tsang Huang, *National Taiwan University, China*
Hsueh-Chun Lin, *China Medical University, China*
Yao-Chiang Kan, *Yuan Ze University, China*
Yao-Ming Hong, *Ming Dao University, China*
Rey-Chue Hwang, *I-Shou University, China*
Dyi-Cheng Chen, *National Changhua University of Education, China*
P.S. Pa, *National Taipei University of Education, China*
Shao-Wen Su, *National Chin-Yi University of Technology, Taiwan*
Yi-Ying Chang, *National Chin-Yi University of Technology, Taiwan*
Cheng-Yi Yu, *National Chin-Yi University of Technology, Taiwan*
Jun-Hong Lin, *Nanhua University, China*
Lei Wei, *National Chin-Yi University of Technology, Taiwan*
Kuang-Cheng Yu, *National Chin-Yi University of Technology, Taiwan*
Ting-Yu Chen, *National Chin-Yi University of Technology, Taiwan*
Chih-Neng Hsu, *National Chin-Yi University of Technology, Taiwan*

CO-SPONSORED BY

National Chin-Yi University of Technology
National Cheng Kung University
National Sun Yan-Sen University
National Chi Nan University
ChienKuo Technology University
Control Engineering and Information Science Research Association
International Frontiers of Science and Technology Research Association
Trans Tech Publications

Analysis of reinforced concrete building structures using simple models

W. Kang, H. Chung & Y. Yungmin

Dong-A University, Nakdong Daero, Saha-Gu, Busan, South Korea

ABSTRACT: This paper presents a finite element method to solve the axial, shear and moment coupled model for analysis of nonlinear structures. The Timoshenko fiber beam element was formulated according to force-based approach. The geometric nonlinearity or the P-Delta effect is considered in the formulation. The model is general and described for cyclic loading. The developed technique is useful to analyze structural components with any type of material. Comparisons with experimental results showed very good predictions with the numerical model. Both prepeak and post peak behavior was predicted well.

Keywords: finite element, beam model, P-Delta, nonlinear analysis

1 INTRODUCTION

The finite element analysis has become an important tool for understanding the behavior of structures. Fiber beam models are simplified versions of the finite element method used to reduce the computational cost. Fiber beam models use detailed geometry and material models to obtain an accurate representation of yielding and nonlinear behavior along the length of the member. Details of the section and geometry of the structural component and properties of the materials are essential components to build the fiber models; generally they are available and simple to obtain. Fiber models are also computationally efficient because of their minimal storage and processing requirements.

The analysis of Reinforced Concrete (RC) structures is highly nonlinear due to nonlinear nature of material and composite action of the concrete and steel materials. Various modeling approaches have been taken, differing such as constitutive modeling, formulation (displacement based, force based) and element preference (continuum model, lumped model, fiber model) (Vecchio & Collins 1986, Hsu & Zhu 2002, Balakrishnam & Murray 1988, Niwa et al. 1981, Barzerar & Schnobrich 1986, Stevens et al. 1987). In this research fiber model approach was used. The fiber model for Reinforced Concrete (RC) structures was developed by dividing each element into several sections along the member (Figure 1). The sections at each end of the element were further divided into several fibers which represent concrete and steel (Bazant & Bhat 1977). The strain in each fiber is calculated from the centroidal section strain and curvature with the help of the plane section remaining plane assumption. The stresses and modulus of fibers were calculated

from the fiber strain values. The constitutive relation of the section is derived by integration of the response of the fibers; the response of elements is also derived by integration of the response of sections along the length of the element. Mullapudi & Ayoub (2010a) formulated the displacement and force based two-dimensional (2-D) element based on the Timoshenko beam theory, with a fiber section accounting for axial and shear effects.

The nonlinear model is implemented in a computer program for the static analysis of Reinforced Concrete (RC) structures. This paper focuses on analytical modeling of highly nonlinear structural components with an efficient model which can be used to reduce the run time while maintaining accurate results.

The continuous material models such as micro-plane models, plasticity models with yield surface deals with several parameters and often needs thorough knowledge of the user and not efficient. Single or multi crack models (de Borst & Nauta 1985; Tots 1988) are useful but the crack pattern need to know in advance and continuous re-meshing is required. The lumped models are computationally efficient but they are unable to consider the gradual spread of nonlinearity along member length and uncertainties exist in assigning the required parameters of the model (Kanaan & Powell, 1973). In this research smeared crack approach with fiber formulation is used which is an efficient method while maintaining the required accuracy. For strain softening, the results with the fiber beam element are mesh dependent and as the size of the element reduces to zero, displacements localize into regions with zero volume (Bazant 1976). In this research, mesh sensitivity is conducted to simulate the experimental results.

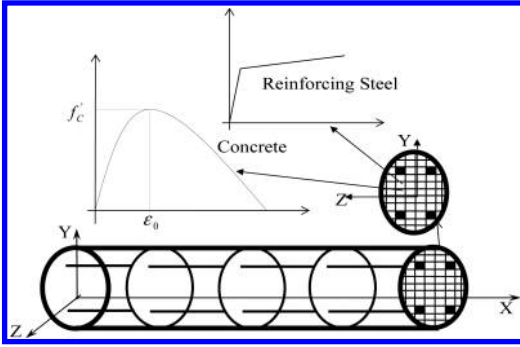


Figure 1. Fiber model beam representation (Mullapudi 2010).

Mullapudi (2010) developed an efficient theory for the analysis of RC structures subjected combined axial, bending, shear and torsional loads which is efficient in reducing computing cost while maintaining the accuracy. The coupling between axial, bending plays an important role in predicting the structural behavior under combined loadings (Mullapudi & Mullapudi et al. 2008a,b; Ayoub 2009a; Mullapudi & Ayoub 2010b). Therefore considered this aspect in the formulation. The crack shear transfer due to an aggregate interlock action depends on contact areas between crack faces. Crack shear stresses are formulated as function of crack normal and tangential displacements (Walraven & Reinhardt 1981; Bazant & Garbarova 1980). In this research, Reinforced Concrete is treated as a continuous material and the shear stresses along smeared cracks due to the projection of aggregate particles in a crack are considered as described in Mullapudi and Ayoub (2009b). The lateral movement of the structure to a deformed position generates second order overturning moments. The additional overturning moments on the structure are equal to the axial load “P” times the lateral displacement “Delta”. Therefore, the geometric nonlinearity or the P-Delta effect is also considered in the formulation. Several theories including modified compression field theory (MCFT) (Vecchio & Collins 1986, Mullapudi et al. 2008c) and soften membrane model (SMM) (Hsu & Zhu 2002, Mullapudi & Ayoub 2009a) were derived based on this principle which MCFT used an empirical equation to derive the shear stress and SMM used an equilibrium equation to derive the shear stress at crack. The RC is comparably ductile compared to the plain concrete and could strain more. Therefore, this phenomenon was taken into consideration with the implementation of modified poisson ratios suggested in Mullapudi and Ayoub (2013a). The required degree of freedom to analyze the nonlinear RC structure is high and

could take more computing time. The continuum element to analyze the RC structure was simplified with the use of Timoshenko beam element which also includes shear deformations in addition to the flexural deformations (Mullapudi et al. 2009c).

2 FIBER ELEMENT FORMULATION

The beam element was formulated with the incorporation of several fiber sections comprises of concrete and steel and the RC member was modeled with the interconnection of several beam elements. The beam element is proved to be efficient with force-based formulation and reduces the troubles caused from locking (Mullapudi & Ayoub 2012) and hence force-based formulation is used in this research.

In force-based formulation, an exact equilibrium between section and element forces is achieved. Section forces are determined based on interpolation between element loads. The compatibility between element and sectional forces are used using principle of virtual force relation.

The nodal forces and deformation of the element are

$$P = [N \ M_A \ M_B]^T \quad d = [u \ \theta_A \ \theta_B]^T. \quad (1)$$

where N is the axial force, M_A is the moment at end A , M_B is the moment at end B , u is the axial deformation, θ_A is the rotation at end A and θ_B is the rotation at end B .

The external and internal element deformations need to be in equilibrium and need to solve by an iterative procedure explained in Mullapudi and Ayoub (2009b).

3 CONSTITUTIVE LAWS

The stiffness matrix for an element depends on the material stiffness matrix and relates to the stress state and strain state. The compressive stress-strain curve of concrete in a structural element is softened because the perpendicular tensile stress will reduce the compressive strength and strain of concrete, with an appropriate softening coefficient. In this research the uniaxial compressive strength of concrete was reduced with softening coefficient as given in Mullapudi and Ayoub (2013b). The beam element is in lack of including the transverse reinforcement and it is solved with a special equilibrium condition which the net vertical stress along the stirrup is zero or is equal to the applied load at that location (Mullapudi and Ayoub 2013a). The geometric nonlinearity or the P-Delta effect was considered in the formulation. The post peak behavior of load-deformation curve of the RC

member also depends on the level of lateral confinement. For increasing confinement stresses, the response of concrete changes from brittle softening to ductile hardening (Kang et al. 1998, Smith et al. 1989). Under lateral tensile stresses, concrete cracks and eventually softens the strength of the concrete (Mullapudi 2010).

The concrete constitutive relations change according to the strain state in principal directions. If the uni-axial strain of concrete in principal direction one is in tension while the uni-axial strain in principal direction two is in compression, the compressive strength in principal direction two will soften due to the tension in the orthogonal direction. Hsu and Zhu (2002) derived a softening equation in the tension-compression region.

$$\xi = \left(\frac{5.8}{\sqrt{f'_c(\text{MPa})}} \leq 0.9 \right) \left(\frac{1}{\sqrt{1+400\varepsilon_1}} \right) \left(1 - \frac{|\beta|}{24^\circ} \right) \quad (2)$$

The softening coefficient is ξ , the uni-axial concrete compressive strength is f'_c , β is the deviation angle in degrees, ε_1 and ε_2 are lateral tensile strain in direction 1 and 2 respectively, γ_2 is the shear strain.

A simplified uniaxial concrete model modified from the Kent and Park model (Park & Priestley 1982) is used and implemented simple rules to account for softening of concrete and cyclic rules as described by Labib et al. (2013). The uniaxial behavior of steel is described by the nonlinear model of Menegotto and Pinto (Menegotto & Pinto 1973), as modified by Filippou et al. (1983) to include the isotropic strain hardening effects. The steel strain at cracked section increases rapidly to reach the strain hardening region of the stress-strain curve compared to the adjacent regions. Steel stresses are averaged along the steel bar traversing several cracks and the resulting smeared steel stress at first yield will be reduced compared to the local yield stress of a bare steel at the cracks. The smeared stress-strain relationships of steel embedded in concrete are included according to Belarbi & Hsu (1994).

4 NUMERICAL VERIFICATION

The confining effect on concrete in the member may be varied depending upon how a beam-column behaves under either a single curvature bending or under a double curvature bending. Takiguchi et al. (1992, 1997) conducted a series of experimental tests examining the RC beam-column members under several loading conditions, and the results showed that the characteristic of the compressive strength of concrete in the critical section of the members

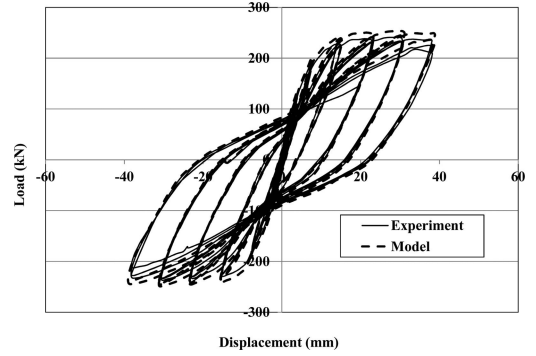


Figure 2. Comparison of experiment (2CLH18) and analytical model.

was inconstant due to the various loading and geometric conditions. In this paper, only double curvature column is tested with the developed model.

In this research, the geometric nonlinearity or the P-Delta effect is added to the original formulation given by Mullapudi and Ayoub (2013a). They previously able to simulated RC walls (Mullapudi et al. 2013c) accurately thus in this paper, RC columns are tested with the developed fiber model. The model consists of a single element with appropriate transverse reinforcement. The cross section was divided with 20 horizontal fibers. Five Gauss-Lobatto integration points are used for monitoring the inelastic behavior of the column. Numerical simulations are conducted under displacement control.

The model is used to simulate the results of one column 2CLH18 tested by Lynn (2001). The column was tested in double curvature under unidirectional lateral load. The length of the column is 2946 mm.

The specimen is a square column with a dimension of 457 mm. The concrete compressive strength is 33 MPa. The longitudinal reinforcement is 2.0% of the gross area of the specimen and the yield strength is 331 MPa. 13.5 mm diameter bars are used for transverse reinforcement with a spacing of 400 mm. The yield strength of the transverse reinforcement is 400 MPa. The axial load is 7% of the axial capacity of the column. The analytical results are compared with the measured load-displacement relation in Figure 2. The agreement between experimental and analytical results is accurate. The column failed in a flexure mode.

5 CONCLUSIONS

This paper presents a finite element method to solve the axial, shear and moment coupled model for analysis of nonlinear structures. The Timoshenko

fiber beam element was formulated according to force-based approach. The geometric nonlinearity or the P-Delta effect is considered in the original formulation given by Mullapudi (2010). The model is general and described for cyclic loading. The developed fiber beam column element was verified against experimental tests on RC columns. Comparisons with experimental result showed very good predictions with the numerical model.

REFERENCES

- Balakrishnam, S. & Murray, D.W. 1988. Concrete Constitutive Model for NLFE Analysis of Structures, *Journal of Structural Engineering, ASCE*, 114(7), 1449–1466.
- Barzerar-Jamshidi, F. & Schnobrich, W.C. (1986). Non-linear Finite Element Analysis of Reinforced Concrete under Short Term Monotonic Loading, Civil Engineering Studies *Report No. 530*, University of Illinois at Urbana-Champaign.
- Bazant, Z.P. 1976. Instability, ductility, and size effect in strain softening concrete, *J. Eng. Mech.*, 102(2), 331–344.
- Bazant, Z.P. & Bhat, P.D. 1977. Prediction of Hysteresis of Reinforced Concrete Members, *Journal of the Structural Division, ASCE*, 153–167.
- Bazant, Z.P. & Gambarova, P. 1980. Rough Cracks in Reinforced Concrete, *Journal of Structural Division, ASCE*, 106(4), 819–842.
- Belarbi, A. & Hsu, T.T.C. 1994. Constitutive Laws of Concrete in Tension and Reinforcing bars Stiffened by Concrete, *ACI Structural Journal*, 91, 465–474.
- de Borst, R. & Nauta, P. 1985. Non-orthogonal cracks in a smeared finite element model, *Engrg. Computations*, 2, 35–46.
- Filippou, F.C., Popov, E.P. & Bertero, V.V. 1983. Effects of Bond Deterioration on Hysteretic Behavior of Reinforced Concrete Joints. *Report SESM 77-1*, Division of Structural Engineering and Structural Mechanics, University of California, Berkeley.
- Hsu, T.T.C. and Zhu, R.R.H. 2002. Softened Membrane Model for Reinforced Concrete Elements in Shear, *ACI Structural Journal*, 99(4), 460–469.
- Kanaan, A.E. & Powell, G.H. 1973. DRAIN-2D, A general purpose computer program for dynamic analysis of inelastic plane structure. Rep. Nos. UCB/EERC/73/06 and 73/22, Univ. of California, Berkeley, Calif.
- Kang HD, Spacone E, Willam KJ. 1998. A study of compressive failure in over-reinforced concrete beams. In: FRAMCOS-3, Oct 12–16; Gifu, Japan, 2, 1195–1210.
- Labib, M., Mullapudi, R. & Ayoub, A. 2013. Analysis of RC Structures Subjected to Multi-Directional Shear Loads, *Journal of Advanced Concrete Technology*, 11, 22–34.
- Lynn, A.C. 2001. Seismic Evaluation of Existing Reinforced Concrete Building Columns, *Ph.D. Dissertation*, Department of Civil and Environmental Engineering, University of California, Berkeley.
- Menegotto, M., Pinto, P.E. 1973. Method of Analysis for Cyclically Loaded Reinforced Concrete Plane Frames Including Changes in Geometry and Non-Elastic Behavior of Elements Under Combined Normal Force and Bending, *Proceedings, IABSE Symposium on Resistance and Ultimate Deformability of Structures Acted on by Well-Defined Repeated Loads*, Lisbon, 15–22.
- Mullapudi, T.R.S., Ayoub, A. and Belarbi, A. 2008a. Fiber Section Formulation with Bi-Axial Strength Envelope for Analysis of Shear Dominant RC Structures, *Concrete bridge conference*, St Louis, Missouri, USA.
- Mullapudi, T.R.S., Ayoub, A. and Belarbi, A. 2008b. Effect of Coupled Shear-Bending Deformations on the Behavior of RC Highway Structures Subjected to Extreme Seismic Loading, *The Sixth National Seismic Conference on Bridges and Highways*, Charleston, South Carolina, USA.
- Mullapudi, T.R.S., Ayoub, A.S., Belarbi, A. 2008c. A Fiber Beam Element with Axial, Bending and Shear Interaction for Seismic Analysis of RC Structures, *14th World Conference on Earthquake Engineering*, Beijing, China.
- Mullapudi, T.R.S., Ayoub, A. 2009a. Non-Linear Finite Element Analysis of Concrete Structures with Softened Membrane Model, *ASCE Structures Congress*, Austin, Texas, USA.
- Mullapudi, R.T. & Ayoub, A.S. 2009b. Fiber Beam Element Formulation using the Softened Membrane Model, *American Concrete Institute, Special Publication*, 265, ACI, Farmington Hills, MI, 283–308.
- Mullapudi, R.T., Charkhchi, P. and Ayoub, A.S. 2009c. Evaluation of Behavior of Reinforced Concrete Shear Walls through Finite Element Analysis, *American Concrete Institute, Special Publication*, 265, ACI, Farmington Hills, MI, 73–100.
- Mullapudi, T.R.S. 2010. Seismic Analysis of Reinforced Concrete Structures Subjected to Combined Axial, Flexure, Shear and Torsional Loads, *Ph.D. thesis*, University of Houston, Houston, 328.
- Mullapudi, T.R. & Ayoub, A. 2010a. Modeling of the Seismic Behavior of Shear-Critical Reinforced Concrete Columns, *Engineering Structures*, 32(11), 3601–3615.
- Mullapudi, T.R.S. & Ayoub, A.S. 2010b. A 3D In-Elastic Beam Element Model for RC Members Subjected to Earthquake Loading, *14th European Conference on Earthquake Engineering*, Ohrid, Republic of Macedonia.
- Mullapudi, T.R.S. & Ayoub, A. 2012. Nonlinear Analysis of Reinforced Concrete Walls under Three-Dimensional Loading, *Magazine of Concrete Research*, ICE, 65(3), 172–184.
- Mullapudi, T. & Ayoub, A. 2013a. Analysis of Reinforced Concrete Columns Subjected to Combined Axial, Flexure, Shear and Torsional Loads, *Journal of Structural Engineering, ASCE*, 139(4), 561–573.
- Mullapudi, T.R.S. & Ayoub, A.S. 2013b. Constitutive Behavior of Reinforced Concrete Beam-Columns under Cyclic Loading, *Studies and Researches: Annual Review of Structural Concrete*, Politecnico di Milano, 32, 1–38.
- Mullapudi, T.R.S., Charkhchi, P. and Ayoub, A. 2013c. Behavior of Shear-Dominant Thin-Walled RC Structures, *Thin-Walled Structures*, 63, 134–146.

- Niwa, J., Maekawa, K. & Okamura, H. 1981. Nonlinear Finite Element Analysis of Deep Beams, *Int. Assoc. for Bridge and Struct. Engrg. Colloquium*, Final Report, Delft, Netherlands, 335–350.
- Park, R. & Priestley, M.J.N., Gill, W.D. 1982. Ductility of Square Confined Concrete Columns, *Journal of Structural Division, ASCE*, 108(4), 929–950.
- Smith SS, Willam KJ, Gerstle KH, Sture S. 1989. Concrete over the top, or: is there life after peak? *ACI Journal*; 86(5):491–7.
- Stevens, N.J. et al. 1987. Analytical Modeling of Reinforced Concrete Subjected to Monotonic and Reversed Loadings, *Publication No 87-1*, Dept. of Civ. Engineering, University of Toronto, Toronto, Ontario, Canada.
- Takiguchi K, Hotta H, Mizobuchi T and Morita S. 1992. Fundamental experiments on compressive properties of concrete around the critical section of R/C column. Architectural Institute of Japan. *J Struct Constr Eng*; 442:111–22.
- Takiguchi K, Imai K, Mizobuchi T. 1997. Compressive strength of concrete around critical section of R/C column under compressionbending-shear, *J Struct Constr Eng*; 496:83–90.
- Tots, J.G. 1988. Computational Modeling of Concrete Structures, *PhD Dissertation*, Delft, Netherlands.
- Vecchio, F.J. & Collins, M.P. 1986. The Modified Compression Field Theory for Reinforced Concrete Elements Subjected to Shear, *ACI Structural Journal*, 83(2), 219–231.
- Walraven, J.C. and Reinhardt, H.W. 1981. Theory and Experiments on the Mechanical Behaviour of Cracks in Plain and Reinforced Concrete Subjected to Shear Loading, *Concrete Mechanics—Part A, Heron*, 26(14), 65.

Green premium in green condo buildings? Evidence in Taiwan

Fong-Yao Chen & I-Wei Peng

National Chengchi University, Taipei, Taiwan

Jen-Hsu Liang

Chinese Culture University, Taipei, Taiwan

Yin-Yu Liang

University of San Diego, CA, USA

ABSTRACT: This study investigates price effects of green technology on residential property. It is argued that no green premiums are added for EEWH, a green certification in Taiwan. The hedonic regression analysis is used to estimate price premium of green label/green feature. Result shows that price premium exist with green features but premium for green label is not significant on residential property. Moreover, low maintenance costs features have a positive impact on prices; high maintenance costs features have a negative impact on prices. In other words, maintenance cost is the main concern. The result seems to be common sense but is not consistent with the energy saving effect of green building. Except increase incentives in urban renewal, consider how to improve efficiency in the use of green building is needed in the near future.

Keywords: green building; hedonic price theory; quantile regression

1 INTRODUCTION

LEED was established in 1995 in US. Up to April 2010, there were 5,384 certified office buildings, and 27,167 registered office buildings. In Taiwan, the EEWH (Ecology, Energy Saving, Waste Reduction, Health) system was established in 1999. Up to July 2013, there were only 84 residential green label certified buildings, and 179 candidate for certification. Obviously, the promotion of green building in Taiwan not as widely accepted. Developers could not see the value of green building, and consumers seem to underestimate its value to have reaction in housing price. Therefore, a negative cycle existed and a slowdown in the number of green building increased. Additionally green building related energy-saving certification has become an important factor in appraisal in foreign countries but the relationship between green building and housing price is not clear in Taiwan. Besides the floor area ratio rewards in urban renewal, Taiwanese appraiser did not experience addition to value for green building, not to mention its capitalization at market value.

In recent years, U.S. studies have found that green building is one of the factors that can be a rising factor in declination of real estate market. Literatures also showed that green building is a future trend, green label and building energy

conservation will become an important factor of real estate price. Furthermore, most studies point out that green building has a positive and significant influence on price. In other words, green building has benefit to health in individual level and is contributive to sustainable development in public level. Consumers “should” be cognitive, “should” be willing to spend more money to buy green building, and then green building price “should” be higher. Does it happen in Taiwan market or not is to be further discussed. This paper will also review literatures and construct empirical model of green building on residential sales price. Finally, we analyze the results and have a conclusion.

2 LITERATURE REVIEW

2.1 *The green impact on housing price*

There are many papers on this realm of the price impacts of green buildings, and most of them focus on commercial properties. Eichholtz et al. (2010a, 2010b) used hedonic regression to analyze the price premium, and found that certified buildings receive 16.8% premiums. The afterwards research on sustainability and dynamic analysis also found that certified building could raise sales price at 1.8%, 4.7% and 13.3%.

Dermissi (2009) showed that buildings certified with LEED could raise sales price at 18%; Eichholtz et al. (2013) indicated that both Energy Star and LEED have positive impacts on sales price, and the impact from two systems are subtle. Their empirical evidence indicated that the Energy Star labelled building could raise its sales price at 12.9%, while those labelled with LEED are at 11.1%.

Though Wiley et al. (2010), Fuerst and McAllister (2010) and Eichholtz et al. (2010b) found out those labelled with LEED gain the sales price premiums are \$130/sqm, 25% and 11%, while those labelled with Energy Star gain \$30/sqm, 18% and 13%. It's obvious to see that Energy Star performs better than LEED if we only consider the premium from sales price. As for those dual-labelled buildings, the positive impact on the rent or sales price is much more significant. Fuerst and McAllister (2010) indicates that those dual-labelled buildings' sales premium is 28–29%; Fuerst et al. (2012) then found that premium is 11%.

Besides focusing on Energy Star and LEED, there are researches from other green certificate systems. Chegut et al. (2012) found out that the premium of sales price is 38% with BREEAM labelled in UK. Fuerst et al. (2012) also pointed out that it could perform better and receive positive premium if the building obtains the EPC from EU.

On residential buildings, Aroul and Hanzs (2012) found out that Green buildings receive 2% premium. And when disaggregated into mandatory and voluntary green transactions, the respective premiums are 5% and 1%. Deng et al. (2012) examined the average green premium is 14–21% respectively.

Many studies support the idea that the green certificated buildings would make the house price higher. It comes with different levels of premium according to different level of green levels. Brounen and Kok (2011) indicated that, compared to buildings rated D, the premium estimated for A, B and C are 10%, 5.5% and 2.5% respectively. And for dwellings rated E, F and G, the estimated discounts are 0.5%, 2.5% and 5% respectively. Kok and Kahn (2012) found that the label of Energy Star puts positive impact on house price. However, impact from LEED is not significant. Miller et al. (2008) also shows that the green buildings hold no significant premium on sales price.

The main obstacles to promote green building are high cost in the initial stage. In addition, developers with no relative experience in green building know not much about green's risk, cost, benefit and value. It would perhaps assume negative impact on the sales price. Leopoldsberger (2011) showed that both maintenance cost and energy cost are significantly negatively correlated to rent. Fuerst and McAllister (2011) examined the effect of EPC rating on market value by 708 commercial properties

in UK, including 23 BREEAM certified. They found no significant effect of EPC rating on market value, and there was significantly negative impact at the 10% level for BREEAM certified building.

Yoshida and Sugiura (2012) pointed out green-labelled buildings exist a 5% discount. Besides the design for reducing heat island effect and longer building economic life that could lower renewal cost which reduce the discount; other green features like planting, green building materials, and the water circulation will make the sales price discounted due to extra maintenance cost and capital investment.

McAllister (2013) reviewed 29 literatures for green building. Most used hedonic regression to analyze the green impact on price, and commercial property is the main objects. Chen (2011) interviewed 120 Taiwanese appraisers and indicated that 87% of the appraisers agreed that green label would theoretically have positive impact on the sales price, 66% of the appraisers are conceived positive impact will be shown on the market, and most of them consider the impact to be around 10% of the price. There is a lack of empirical study in Taiwan on this subject due to lack of transparency for green related information.

2.2 *EEWH in Taiwan*

EEWH established in 1999, include nine categories: Biodiversity, Greenery, On-site Water Retention, Energy Saving, CO₂ Reduction, Construction Waste Reduction, Indoor Environment, Water Resource, and Sewage and Garbage Improvements.

Green label is rank as “Diamond”, “Gold”, “Silver”, “Bronze” and “Qualified”. However green label is non-mandatory registration, we could not get enough ranked samples to have an empirical study. Therefore we put it together and set a dummy variable to discuss whether green labelled or not. Moreover, we want to analyze more on price effect of green building in Taiwan. To deeper investigate green on sales price, we also analysis the price effect of green features. We refer to the categories to choose green features variables.

Our hypothesis is as following,

H₁: “Green label” is capitalized into housing prices.

H₂: “Green features” are capitalized into housing prices.

3 METHODOLOGY

3.1 *The model*

Hedonic regression model was adapted to analyze the effect of Green Building features as most literatures (Aroul and Hanzs, 2012; Chegut et al., 2012).

Besides normal building attributes, Green label is added as shown in Model (1) and Green features is added in Model (2). After trial and error, we find linear regression suits better for this study.

$$P_i = \alpha_0 + \sum_{j=1}^m \beta_j X_{ji} + \beta_G G_i + \varepsilon_i \dots \dots \quad (1)$$

$$P_i = \alpha_0 + \sum_{j=1}^m \beta_j X_{ji} + \sum_{g=1}^n \beta_g GF_{gi} + \varepsilon_i \dots \dots \quad (2)$$

In the equations, α_0 is the constant term, ε_i is assumed to be the residuals that comply with normal distribution, and the expected value of the error term is 0. The dependent variable is sales price. Independent variables X_{ji} are the j th physical characteristics of i th sample. The variables include transaction year, transaction floor, building size, age and shape. In the model, GF_{gi} indicates dummy variable where value equals 1 when g th feature implemented and 0 when it is not.

3.2 The data

This paper selected the Taipei University designated area for spatial extent. The region is relatively concentrated and the projects have higher likelihood for implementing green features. 359 transactions are recorded at the Interior Ministry from 2008 to 2012. The average sales price is 811.74 million, with standard deviation of 411.17 million and range between minimum of 2.2 million and maximum of 34 million.

Our information on Green label is cases approved by Taiwan Architecture and Building Center. 46 cases, or 12.74% of our data pool, are licensed Green label transactions.

As for the “green” impact on sales price, most literatures show positive effects, our expectation is positive. The impact of green feature depends on the maintenance and management of long-term benefits. We expect a negative impact in atrium garden, balcony garden, permeable paving, green roof, garbage room and refrigerated garbage storage device due to high maintenance frequency and cost. The feature with low maintenance frequency and cost, infiltration ponds, sun visors, energy saving lights, exposed pipework, light steel frame partitioning, recycled building materials, natural interior finishing materials and water-efficient appliance is expected to have a positive impact on the sales price.

4 EMPIRICAL RESULTS

4.1 Green label on sales price

How do they impact sales price? Firstly, we add a dummy variable for green label to regression. The results display in Table 1, which Adjust R^2 is 0.902.

Table 1. Green label result of OLS and quantile.

Variable	OLS	q10 (46 M)	q25 (57 M)	q50 (70 M)
Green label	33.63 (1.44)	28.80 (0.89)	46.54** (2.22)	47.42*** (2.66)
Adjust R^2	0.902	0.622	0.654	0.688

Note: ***indicates significance at the 1% level; **indicates significance at the 5% level.

The other building attribute variables beside green label are significant at the 1% level. However, the impact on sales price is not significant if it is green label. Age coefficient is negative while other factors are positive. The time variables, in 2010, 2011 and 2012, were significant and coefficient is positive. The result makes sense.

The total turnover of the study sample ranged between NT\$ 2.2 to 34 million, which is fairly wide. To understand whether there are differences in level of sales price, quantile regression is used. This study is limited to the number of samples; excluding 0.9 components analysis, build only 0.1, 0.25, 0.5 and 0.75 components. Empirical results are shown in Exhibit 4, each of the components of the coefficient of determination were 0.622, 0.654, 0.688 and 0.733. The higher sub bits indicate better fit of the model. Except for q10, most are at 10% level of significance. This result meets expectations, and higher price having greater impact. The green label certification will be able to play a bonus effect. The total price of NT\$ 5.7 million is a threshold of providing green building.

4.2 Green feature on sales price

In Table 2 we add dummy variables and green features in regression model, which Adjust R^2 is 0.919. Significant variable includes balcony garden, permeable paving, green roof, exposed pipework, light steel frame partitioning and natural interior finishing materials. In descending order for influences, significant negative variable are green roof, balcony garden and permeable paving, which are classified to high maintenance facility. Their coefficients are -180.112 , -75.321 and -36.93 .

On the other hand, in descending order the significant positive variable are light steel frame partitioning, natural interior finishing materials, exposed pipework. These are put into the construction period without regular maintenance of facility, which has a positive impact on house prices. Their coefficients are 113.196, 91.874 and 86.45. In other word, people prefer the green feature which has high initial investment costs and low maintenance cost in future economic life.

Table 2. Empirical result of green feature on sales price.

Variables	Coefficients
	t-value
Balcony garden	-75.321*** -2.668
Permeable paving	-36.930** -2.222
Infiltration ponds	18.276 -0.754
Green roof	-180.112** -2.392
Sun visors	18.242 -0.658
Energy saving lights	0.826 -0.039
Exposed pipework	86.450*** -4.342
Light steel frame	113.196*** -5.985
Recycle materials	16.01 -0.501
Natural materials	91.874*** -3.46
Water-efficient appliance	12.078 -0.579
Garbage room	-17.764 -0.910
Refrigerated garbage device	-1.856 -0.097
F value 157.11	

Note: ***indicates significance at the 1% level;
**indicates significance at the 5% level.

5 CONCLUSION

If green labelled buildings have effective energy-saving effect, the price would be higher. People do have this awareness. Since developers would follow the trend for where potential lies, the number of green building should increase. However, not many certified residential green building exist in the market since the promotion of green label in 1999. Empirical results also show that green labels have no significant impact on the sales price. Rationally, appraisers would not include green label as factor effecting valuation of price. This paper further used quantile regression analysis to show that housing in lower price range does not benefit from green building, but green residential in mid or high price range does experience the impact. And impact of green labels would scale with higher housing price.

People generally perceive green features to have positive effect on price. Our empirical research

shows that features would have both positive and negative impact on sales prices. Balcony garden, permeable pavement and roof gardens are facilities requiring frequent maintenance and therefore having negative impact on price. On contrary, features with longer economic life and lower maintenance requirement, such as exposed pipework, light steel frame partitioning and natural building materials, have positive impact on sales prices. In short, ease of management and low expense are key factors in promoting green building. Furthermore, features such as atrium garden and garbage handling area were perceived to have positive impact but was in fact statistically insignificant. The reason was that these features have already been incorporated into the design by developers. In order to promote green buildings, policy makers should view from end-user perspective. Not only should incentive program be provided for newer green building but should also be provided to product developers for better products with less maintenance requirement.

REFERENCES

- Aroul, R.R. & Hansz, J.A. 2012. The Value of "Green": Evidence from the First Mandatory Residential Green Building Program. *The Journal of Real Estate Research* 34(1):27-49.
- Brounen, D. & Kok, N. 2011. On the Economics of Energy Labels in the Housing Market. *Journal of Environmental Economics and Management* 62(2):166-179.
- Chegut, A., Eichholtz, P. & Kok, N. 2012. Supply, Demand and the Value of Green Buildings. *Rics Research*.
- Chegut, A., Eichholtz, P., Kok, N. & Quigley, J.M. 2011. The Value of Green Buildings: New Evidence from the United Kingdom. *ERES 2010 Proceedings*.
- Chen, I-Sheng 2011. *Green Value-A Valuation Point of View* National Taipei University.
- Deng, Y., Li, Z. & Quigley, J.M. 2012. Economic Returns to Energy-Efficient Investments in the Housing Market: Evidence from Singapore. *Regional Science and Urban Economics* 42(3):506-515.
- Dermissi, S., 2009. The Effect of LEED Rating on Office Property Assessed and Market Values. *Journal of Sustainable Real Estate* 1:23-47.
- Eichholtz, P., Kok, N. & Quigley, J.P. 2010a. Doing Well by Doing Good: Green Office Buildings. *American Economic Review* 100:2494-2511.
- Eichholtz, P., Kok, N. & Quigley, J.P. 2010b. Sustainability and the Dynamics of Green Building New Evidence on the Financial Performance of Green Office Buildings in the USA. *Rics Research*.
- Eichholtz, P., Kok, N. & Quigley, J.P. 2013. The Economics of Green Building. *Review of Economics and Statistics* 95(1):50-63.
- Fuerst, F. & McAllister, P. 2010. *What is the Effect of Eco-Labeling on Office Occupancy Rates in the USA?*. The Royal Institution of Chartered Surveyors, London.

- Fuerst, F. & McAllister, P. 2011. Green Noise or Green Value? Measuring the Effects of Environmental Certification on Office Values. *Real Estate Economics* 39(1):45–69.
- Fuerst, F., de Wetering, J van & Wyatt, P. 2012. Is Intrinsic Energy Efficiency Reflected in the Price of UK Office Leases? Working paper, October.
- Kok, N. & Kahn, M.E. 2012. The Value of Green Labels in the California Housing Market—An Economic Analysis of the Impact of Green Labeling on the Sales Price of a Home. Publication produced by UCLA.
- Leopoldsberger, G., Bienert, S., Brunauer, W., Bobsin, K. & Schutzenhofer, C. 2011. Energising Property Valuation: Putting a Value on Energy-Efficient Buildings. *The Appraisal Journal* 79(2):115–125.
- McAllister, P., 2013. Studies of Price Effects of Eco-Labels in Real Estate Markets: An ‘off the record’ record. Working paper, May.
- Miller, N., Spivey, J. & Florance, A. 2008. Does Green Pay Off? *Journal of Real Estate Portfolio Management* 14:385–400.
- Wiley, J.A., Benefield, J.D. & Johnson, K.H. 2010. Green Design and the Market for Commercial Office Space. *The Journal of Real Estate Finance and Economics* 41(2):228–243.
- Yoshida, J. and Sugiura, A. 2011. Which “Greenness” is Valued? Evidence from Green Condominiums in Tokyo. 46th Annual AREUEA Conference Paper.

To discuss the relationship between green building and regional housing price

Tsu-Kuang Hsieh & Han-Yu Tsai

Department of Natural Resources, Chinese Culture University, Taipei, Taiwan

Ying-Ru Du

Department of Urban Affairs and Environment Planning, Chinese Culture University, Taipei, Taiwan

ABSTRACT: This research was aimed to discuss on the relationship between the regional housing prices in Taipei and the certifications of green building labels by Taiwan Architecture & Building Center based on the actual selling prices registered in the competent authority by conducting the methodology of descriptive statistics and cross analysis for the empirical analysis on the connotation of green buildings' impacts on regional housing price; whereas it is hoped to enhance the public's comprehensions about green buildings, as well as to help the circles of industry, government and academy to realize the degrees of impacts of green building projects on regional housing prices; thus, the government may learn which effective policies to work on to promote green building development in Taiwan with a rather clarified impact on housing prices.

Keywords: green building; regional housing price

1 INTRODUCTION

There has been an on-going Green Building rating system for the building projects with construction costs over NTDS\$50,000,000.00 in Taiwan; however, most of the privates sectors in the industry would tend to get certified with Green Building Certificates and Labels for the honors and cognitions till year 2004, there had been 1,269 projects certified with Green Building Labels with a total of 3,153 application candidates. There might have been a certain degree of accumulated researches related to green building, sustainable building or healthy building in the perspectives of technology and system; however, only few has been studied on their impacts on the real estate market. Therefore, it is hoped that the research results on the connotation of green buildings' impacts on regional housing price will help to enhance the public's comprehensions about green buildings.

2 EMPIRICAL ANALYSIS

According to the data provided by Taiwan Architecture & Building Center, the inspection and rating organization established by Ministry of Interior Affairs, there have been up to 169 green building projects in the northern region during year 2000–2014. Based on the SPSS Analysis on

the data of the actual selling prices registered in Ministry of Interior Affairs, the research on the relationship between green building and regional housing price hence was studied.

Based on the amount of the green building projects, Neihu District and Da'an District as the top two districts with the green building projects had been selected as the subjects for the case studies.

There were up to 21 projects certified with Green Building Labels in Neihu District in year 2007. Therefore, the normal distribution curves of the average prices and the unit prices before and after year 2007 had been studied; whereas the results indicated of an unit price difference of NTD \$19140 between the unit price of NTD \$171317

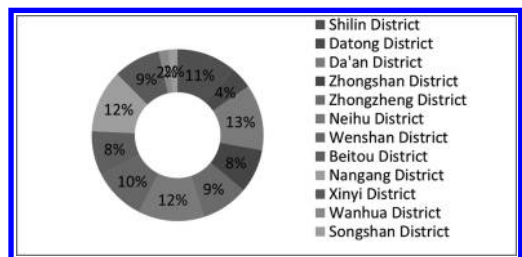


Figure 1. Green building cases in Taipei City.
Data source: sorted by this research.

Table 1. Average price in Neihu district.

	Neihu district before year 2007			Neihu district after year 2007		
	Total building transfer area (m ²)	Square meter per unit	Total price (NTD)	Total building transfer area (m ²)	Square meter per unit	Total price (NTD)
Effective	168	168	168	39	39	39
Average	86.17	171317.8	14475952	95.05	190457.1	19045641.3

Data source: Sorted by this research.

before 2007 and the unit price of NTD \$190457 after 2007. It indicated that green buildings actually helped to raise up the building unit prices and improve the living quality in the neighborhood, as well as to subsequently boost the regional housing prices.

A. Ranked first with the highest housing prices in the real estate market in Taiwan, Da’an District of Taipei City was allocated with 21 green building projects. According to the analysis, the unit price before the existence of any building certified with Green Building Label in this district before year 2003 was NTDS\$ 220,000.00; whereas the unit price was raised up with a growth of NTDS\$ 74,667 after year 2003. This should be deemed as the evidence of the trend that the housing prices rose under the indirect impact of the green building projects implemented in Da’an District and Neihu District.

According to the regression analysis on the impacts of the extraneous variables derived from the dimension of “green building performance”, such as energy resources conservation, living quality enhancement, environmental impact reduction and ecological and environmental preservation on the effects of economic efficiency and real estate market, the path analysis based on the output data shown in Figure 3 is described as follows: the path coefficient of energy resources conservation to real estate market was 0.28 (insignificant P-value) with a low predicted probability; however, the path coefficient of energy resources conservation to economic efficiency was 0.27 (P-value < 0.05) indicating a significant direct correlation. Meanwhile, the path coefficient of economic efficiency to real estate market was 0.47 (P-value < 0.05) indicating a significant direct correlations. Therefore, there was no significant direct correlation between energy resources conservation and real estate market but an intermediate correlation with economic efficiency by multiplying the two direct correlation coefficients as $(0.27 \times 0.47 = 0.13)$.

Moreover, the path coefficient of living quality enhancement to real estate market was 0.34 (P-value < 0.05) indicating a significant direct correlation;

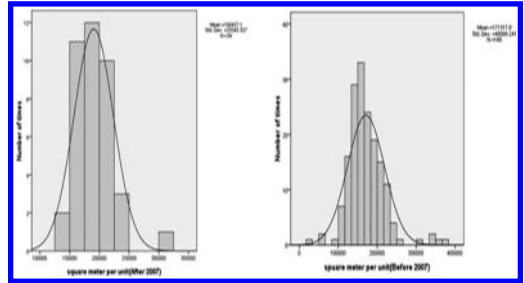


Figure 2. Unit price normal distribution in Neihu district.

Data source: Sorted by this research.

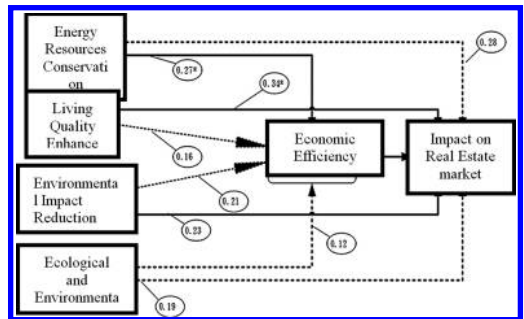


Figure 3. Path analysis of the impacts of green building on real estate market through economic efficiency.

Data source: Sorted by this research.

whereas the path coefficient of economic efficiency to real estate market was 0.47 (P-value < 0.05) indicating a significant direct correlation. However, the path coefficient of living quality enhancement to economic efficiency was 0.16 (insignificant P-value) indicating no direct correlation. Therefore, it is concluded that there was only direct correlation between living quality enhancement and real estate market, while no significant intermediate correlation with economic efficiency.

Furthermore, the path coefficients of environmental impact reduction to economic efficiency and

Table 2. Average price in Da'an district.

	Da'an district before year 2003			Da'an district after year 2003		
	Total building transfer area (m ²)	Square meter per unit	Total price (NTD)	Total building transfer area (m ²)	Square meter per unit	Total price (NTD)
Effective	219	219	219	32	32	32
Average	219	228856.24	27710602.13	57.2578	303523.24	16571562.501

Data source: Sorted by this research.

Table 3. The impact effects of green building performance on real estate market through economic efficiency.

Performance	Effect		
	Impacts of green building on real estate market (Direct effect)	Economic efficiency of green building (Indirect effect)	Sum of direct effect and indirect effect (Total effect)
Energy resources conservation	0.28	0.13 (0.27 × 0.47)	0.13
Living quality enhancement	0.34	–	0.34
Environmental impact reduction	0.23	–	–
Ecological and environmental preservation	0.19	–	–

Data source: Sorted by this research.

real estate market were 0.21 (insignificant P-value) and 0.23 (insignificant P-value) correspondingly with low predicted probabilities. Whereas, the path coefficient of economic efficiency to real estate market was 0.47 (P-value < 0.05) indicating a significant direct correlation, while there were no clarified direct impacts of environmental impact reduction on economic efficiency and real estate market.

Finally, the path coefficients of ecological and environmental preservation to economic efficiency and real estate market were 0.12 (insignificant P-value) and 0.19 (insignificant P-value) correspondingly with low predicted probabilities. Whereas, the path coefficient of economic efficiency to real estate market was 0.47 (P-value < 0.05) indicating a significant direct correlation. However, there were no clarified direct impacts of ecological and environmental preservation on economic efficiency and real estate market. The impact effects of green building performance on real estate market through economic efficiency are as follows in Table 3.

Finally, the analysis on questionnaire survey was conducted based on 100 valid copies and 5 invalid ones. Moreover, the reliability analysis was applied to verify the validity of the collected data; whereas reliability refers to the liability as the stability and consistency of the measuring instruments and the reliability coefficient between 0.7–0.9 indicates of

Table 4. Cronbach α of questionnaire dimension.

Questionnaire design			Cronbach α
Part I	Psychological dimension	Impacts of green building in real estate market	0.77
		Economic efficiency	0.75
		Environmental efficiency	0.73
		Social efficiency	0.81

Data source: Sorted by this research.

a good liability. According to Table 4 Cronbach α of questionnaire dimension, it indicated that the Cronbach α between the ranges of 0.7–0.9 implied a high consistency and liability. Furthermore, descriptive statistics were applied to discuss the impacts of green buildings on the regional housing prices in terms of the prices of the green building projects and the perceptions toward the housing prices in the region. According to Table 5, there were up to 80% of the respondents agreeing upon the statement that the prices of the green building projects would subsequently raise up the housing prices in the region. In other words, in the psychological dimension of the public, the prices

Table 5. Uprising house prices in the neighbourhood.

		Uprising house prices in the Neighborhood					Total
		1.00	2.00	3.00	4.00	5.00	
Uprising house prices in the individual project	1.00				100.0%		100.0%
	2.00		20.0%		40.0%	40.0%	100.0%
	3.00				100.0%		100.0%
	4.00	7.7%	3.8%	3.8%	50.0%	34.6%	100.0%
	5.00	6.7%	6.7%	20.0%	26.7%	40.0%	100.0%
Total		6.0%	6.0%	8.0%	46.0%	34.0%	100.0%

Data source: Sorted by this research.

of the green building projects might seem relatively high when it came to their house-purchase decisions; however, they would still consider it reasonable that the regional housing prices would rise along. The results had verified the hypothesis of this research in the beginning that the regional housing prices might rise up along with the implementations of the green building projects. It is hoped that based on the study, there will be further researches conducted on the impacts of green building performances on purchase decisions in terms of economic efficiency.

3 CONCLUSION

This research had successfully applied SPSS analysis software, questionnaire survey, green building certification data by Taiwan Architecture & Building Center, the samples of the actual selling price registrations for advanced statistical analysis to enhance the reliability and validity of the sample population of the real estate prices for more reliable research outcomes. The research results verified that the implementation of the green building projects in Neihu District and Da'an District had helped to raise up the regional housing prices in these two districts; Whereas it is hoped that more researches may be conducted for further analysis with alternative methodology in the future; finally, the variations and enlarged scopes of the correlations between green building and regional housing

prices may be subsequently derived as the future references in the circles of industry, government and academy.

REFERENCES

- [1] Chang Kuei-Feng (2008, June), *The Influence of the Residential Interest of Sustainable Building on House-purchase Choice*. Journal of housing studies, 17.
- [2] C.Y. Chen, E.C. Kao, (2005). *Development and analysis of green production and consumer system evaluation framework*. Journal of Humanities and Social Sciences, 1, 17.
- [3] Hong Jun Jia & Hui Wang. (2012). *Green Building and Sustainable Development*, Advanced Materials Research, 75, 55–58.
- [4] Pinchot, G. (1910), *The Fight For Conservation*, New York: Doubleday.
- [5] Tolba, M.K. (1987), *Sustainable development: Constraints and opportunities*. London: Butterworths.
- [6] Zhong K, Kang Y. Applicability of air-to-air heat recovery ventilators in China. *Applied Thermal Engineering* 2009;29:830.
- [7] GBCI (2011). Green Associate Candidate Handbook, <http://www.usgbc.org>.
- [8] Green Building Mark Q & A (2011). <http://twgbqanda.com/about.php?Type=45&menu=about> calss& pic dir list = 0.
- [9] Kazuo Iwamura (2010). CASBEE in Progress by JaGBC for Market Transformation.
- [10] J.N. Warfield. (1982). *Group planning and problem solving method in engineering interpretive structural modeling*, 5, 155–201.

Properties of asphalt mixtures with reclaimed material in Slovakia

S. Cápavová, A. Zuzulová & K. Bačová

Department of Transportation Engineering, Slovak University of Technology, Bratislava, Slovakia

ABSTRACT: The problem of environmental acceptability of technologies in road construction is since the 70s by introducing the technology of recycling and reuse of materials and since 90s of the 20th century by less energy intensive technologies dealt. All these mentioned technologies are still a hot topic due to price of the new input materials and energy consumption for production and processing of road building materials. It could use different types of new and reclaimed materials, various additives or those technologies which saving non-renewable natural resources and at the same ensuring the required properties of the road construction. This paper focuses on the application of reclaimed material to asphalt mixture and on the own results of research on Department of Transportation Engineering in Bratislava.

Keywords: asphalt mixture; reclaimed material; energy consumption; experimental verification

1 INTRODUCTION

In recent years there has been an increasing trend in the number of vehicles and the associated increase in traffic load on the existing road network, increase the use of private transport and prioritizing transportation of goods from rail to roads. In addition to traffic load other factors influencing the road, especially climatic factors (torrential rain, etc.). Need to use the highest quality materials and technologies that the road construction has required parameters and at the same time will be reduce the negative impact on the environment and ensure the required economic efficiency.

Tendency of modern society is to find the most acceptable way to reduce the possible negative impact of activities on the environment and humans. Total Energy Consumption (EC) in 2011 was in EU-27 1103.3 Mtoe (megaton of oil equivalent), (transport 33% and industry 26%), in Slovakia 10.8 Mtoe (transport 25% and industry 39.8%). Total CO₂ emissions in the EU-27 were 4173.8 million tonnes (transport 28.8%), in Slovakia 38.2 million tonnes (transport 17.6%). (European Commission 2013). The possibility of reducing the energy consumption and emissions can be achieved by applying of new technological processes, using modern machinery and right organization of transport.

Energy consumption of structure pavement is the energy required representing the total amount of energy input of each process (extraction, processing and transport of materials and other activities requiring the energy) about 3 MJ for 1 kg of produced asphalt mixture and about 1 MJ

for 1 kg produced cement concrete mixture. Data about total energy consumption of selected road material type are represented in Table 1 (CIPEC 2005).

From the perspective of sustainable development in road construction is necessary to use such as environmentally compatible, energy and economical acceptable materials and technologies. Use of recycled materials, technologies with production and processing at lower temperatures, new materials and additives and the use of appropriate techniques seems to be a suitable solution to reduce energy consumption. Except energy savings, which are related to economic savings, are technologies at lower temperatures classified as technologies taking into account the environmental aspects (greenhouse gases, vapors and aerosols reduction, acceptable environment for workers and the area near the building). Reduction of chemical

Table 1. Energy consumption of road material type (MJ/t).

Material	Total EC (MJ/t)
Hot mix asphalt	680
Warm mix asphalt	654
Cement concrete pavement	738
Continuously reinforced concrete pavement	1226
Recycled HMA with 10% RAP	642
Recycled HMA with 20% RAP	538
Recycled HMA with 30% RAP	510
Recycled HMA with 50% RAP	454

compounds (NAPA 2007): 10–30% CO, 20–40% CO₂, NO_x 60–70%, 20–40% of SO₂, volatile organic components of 50% and 30–50% of dust particles.

1.1 Technologies of asphalt mixtures

In case of asphalt technologies, Hot Mix Asphalt (HMA) is still the most widely used technology in most countries of the world. Alternative to classic hot mix technology could be Cold Mix Asphalt (CMA) with energy savings in 30% or hot in-place recycling with energy savings in about 15%. Combination of cold in-place recycling and CMA could be possible save around 80% of energy needed for production and processing of mixture (European Commission 2013). Technologies at lower temperatures (Warm Mix Asphalt—WMA, Half Warm Mix Asphalt—HWMA) are becoming popular in many countries. These modern technologies have many advantages, as mentioned energy and environment savings, and then depend on the particular low-temperature technology reduction of temperature in the range 10 to 50 °C, acceptable working environment for workers, better workability of the mixture and adding a higher amount of recycled material. The aim for the future is to increase the amount of reclaimed material in mixtures and the preference of real recycling, when the material reclaimed from the old road is reused to build new layer of road.

In EU the production of HMA and WMA from year 2009 decrease, in 2012 was it 276.4 million tonnes. In Slovakia was in 2012 the total production of HMA and WMA 1.9 million tonnes. Most of these mixtures (59%) were used to surface course, 30% to binder course and 11% to base course. In our country was the available amount of reclaimed asphalt 33.000 tonnes—90% was used in hot and warm recycling, 5% in cold recycling and 5% in unbound layers (EAPA 2013).

For comparison, we also describe the energy consumption of hydraulically bounded mixtures and the possibility of its reduction. The main energy part of cement concrete pavement is the energy needed for the production of cement. The solution is replacement of cement by other suitable material, for example blast furnace slag, natural cement, hydrated lime, fly ash and silica fumes. Another advantage of cement concrete pavement is unnecessary heating of aggregates. Energy consumption is also dependent on the distance the placement from the concrete mixing plant. Transport of cement concrete represents about 40% of the total energy needed for the construction of concrete road cover. Total energy consumption of production, transportation and construction of concrete-reinforced concrete cover is about 90 MJ/m³ (Zuzulová 2011).

2 USE OF RECLAIMED MATERIAL

2.1 Properties and recommended quantities

The uses of reclaimed asphalt for pavement construction layers in the each country regulate standards and regulations. In Slovakia, STN EN 13108-8 provides the maximum recommended amount of reclaimed asphalt in road construction asphalt layers (Table 2), content and defining of contaminants, categorization and information regarding the components of reclaimed material.

According to the valid standards is recommended max. 10% of reclaimed material in the surface course and 20% in the binder and base course. According to the standard, which was valid until 2006, it was possible to use 40% of reclaimed material to surface course, 50% to binder course and up to 70% to base course (depending on the type of mixture). Own national and foreign research shows that the mixtures containing varying amounts (and also more than 20%) of reclaimed material have better strength and deformation parameters.

In some countries, the legislation specifies the quantities of reclaimed asphalt that should be used in new road construction mixture. In Slovakia are no legislative measures or technical regulations that would govern the use of these materials. The issue of reclaimed material application in HMA deals the already mentioned standard and 3 technical regulations (Technical conditions 2011a,b,c).

The use of reclaimed material in WMA is not regulated by any standard. Design of WMA with reclaimed material is based on the standards requirements relating to HMA. Compared to conventional asphalt plants, is the requirement to lower temperature needed for the production and processing of the mixture.

Table 2. Applicability of reclaimed asphalt in asphalt mixtures according to STN EN 13 108-8.

Mixture	Maximum recommended amount of reclaimed asphalt	
	Surface course	Binder and base course
Asphalt Concrete AC	10%	20%
Béton Bitumineux Très Mince BBTM	10%	–
Porous Asphalt PA	10%	–
Stone Mastic Asphalt SMA	10%	20%
Mastic Asphalt MA	10%	–

3 EXPERIMENTAL VERIFICATION

The own research was focused on an experimental verification of the asphalt mixtures' characteristics determined for base courses with a certain portion of the reclaimed material (Reclaimed Asphalt Pavement—RAP).

3.1 Asphalt mixtures with RAP

Our department has recently focused on research into environmentally acceptable technologies of asphalt mixtures (Čápayová 2011; Gábor 2007). Except the application of recycled materials, we began to explore especially WMA technologies (Čápayová 2011; Čápayová 2014).

Experimental verification focused on selected laboratory tests with the relationship to previous research. There were verified properties of asphalt mixtures suitable to the base courses with different amounts of RAP—up to 20% according to STN EN 13108-8 and at the same at dosages up to 80% according to the withdrawn standards. The basic tests were Marshall test, indirect tensile strength and water sensitivity. Other important tests of strength and deformation characteristics of mixtures include resistance against permanent deformations, resistance to fatigue and determination of the stiffness modulus. Partial results of the research are presented in Figures 1–3. In Figure 1 is the Marshall stability, in Figure 2 Flow value. There were properties of three types of AC 22 mixture verified. Mixture 1 was with aggregate from Trstín and Lošonec and road asphalt 70/100, Mixture 2 with aggregate from Trstín and Sološnica and road asphalt 70/100. The first variant of Mixture 3 was with aggregate from Trstín and road asphalt 50/70

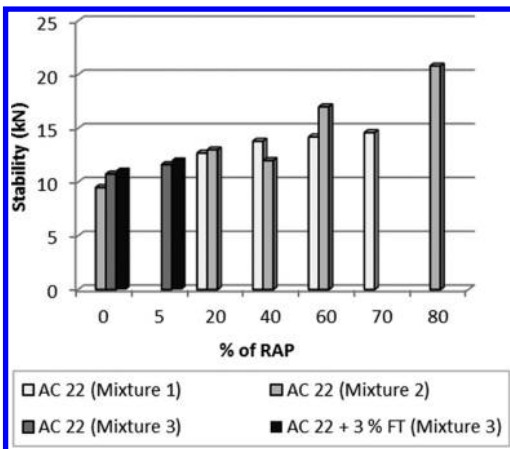


Figure 1. Marshall stability of asphalt mixture with RAP.

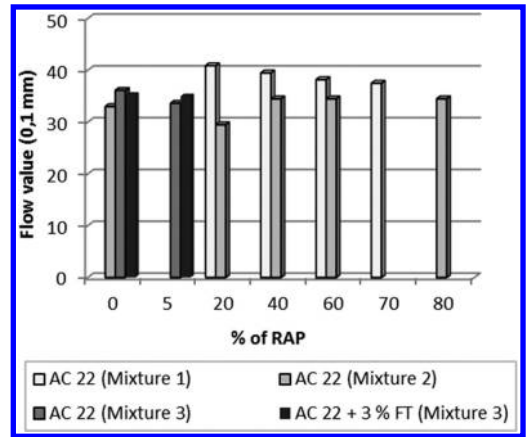


Figure 2. Marshall flow value of asphalt mixture with RAP.

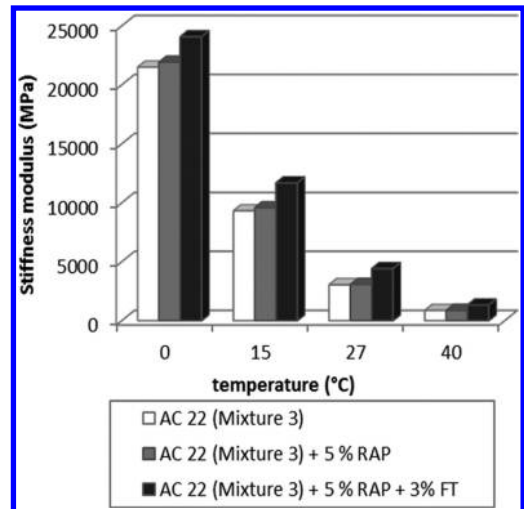


Figure 3. Stiffness modulus of asphalt mixture with RAP.

and the second variant was in addition with the low viscosity additive—3% of FT additive (Sasobit). At each change in the percentage of RAP is changed also grain size of mixture, which affects the values of the Marshall stability and flow value. In nearly all mixtures there was an increase of stability at higher doses of RAP. Only Mixture 2 has decrease of stability at 40% of RAP. Deformations expressed as a flow value are not entirely clear. Depending on the composition of mixtures flow values decreased with increasing amounts of RAP—Mixture 1 and 3. Mixture 2 has with more than 40% of RAP higher deformation than at 0% and 20% of RAP. Except Mixture 2 with 40% of

RAP there was an increase of Marshall stiffness the tested mixtures.

Properties of 2 variants of Mixture 3 were verified by other tests as determination of the stiffness modulus (Fig. 3), resistance against permanent deformations using the wheel tracking test and resistance to fatigue, that confirmed the positive impact of RAP.

The results of laboratory tests have demonstrated the possibility to design the mixture with higher amount of reclaimed material to meet the high requirements of standards.

4 CONCLUSION

Results of own and foreign researches confirm the appropriateness of the application of different types of reclaimed materials in road construction mixtures. Re-use of these materials in road construction may solve problems of waste management, save environment, natural resources and money. Mostly it assumes a positive impact of reclaimed materials on strength and deformation characteristics of asphalt mixtures but because of possible lower quality of some reclaimed materials, it is necessary to pay attention to laboratory tests, that was not reduced the quality of the resulting mixture.

Based on the experimental results, the following conclusions can be drawn:

- Results of laboratory tests of asphalt mixtures with RAP showed that mixtures can also be designed with a higher amount of reclaimed material as prescribed standard. But it is important to recognize the variety of the properties of reclaimed material—input components and their quantity, characteristics, age, exposure to climatic influences.
- In Mixture 1 with a fixed quantity of binder, increasing the amount of RAP caused reduction of some characteristics values, but in under the conditions of standards. At varying amounts of binder, increasing the amount of RAP caused an increase of stability and decrease of deformation and stiffness.
- For Mixture 2, 60% of RAP can be considered as the optimal amount.
- For Mixture 3, 5% of RAP was considered as the optimal and at the same time as a maximal amount, because higher amounts of RAP negative affect the content of gaps in mixture. The mixture with RAP has been shown a slight reduction in water sensitivity, the addition of FT-additive slightly increased the water sensitivity to 77%. However, in general can be concluded best parameters for mixtures with RAP

and FT additive—increase the value of indirect tensile strength of about 11%; stiffness modulus growth at 0 ° C and 12% at 40 ° C and 54% to 24 080 MPa. From the development of the fatigue lines it can be also stated that the longest degree of serviceability can be expected for AC 22 with the RAP and FT.

- The research results can be used to modification the current STN EN 13108-8 respectively to create a condition or standard for asphalt mixtures at low temperatures, which in Slovakia do not yet exist.

Paper was created with the support of the project VEGA 1/0351/13 “Traffic areas structures in integrated transport space”.

REFERENCES

- Čápayová, S. 2011 *Determination of qualitative parameters of construction layers of roads from repeatedly used materials*. Doctoral thesis. Faculty of Civil Engineering, Slovak University of Technology. Bratislava. (in Slovak).
- Čápayová, S. 2014 *WAM-DEF Deformation properties of low temperature asphalt mixtures*. Final report on project within the program to support young researchers. Slovak University of Technology. Bratislava. (in Slovak).
- CIPEC 2005. *Road rehabilitation energy reduction guide for Canadian road builders*: 16–17. Ottawa: CIPEC. http://www.nrcan.gc.ca/sites/www.nrcan.gc.ca/files/oe/pdf/industrial/technical-info/benchmarking/road-rehab/Roadhab_eng_web.pdf.
- EAPA (European Asphalt Pavement Association) 2013. *Asphalt in figures 2012*. <http://www.eapa.org>.
- European commission 2013. *EU Transport in figures 2013* (ec.europa.eu). Statistical pocketbook. Luxembourg: European Union.
- Gábor, P. 2007 *Characteristics of mixtures with recycled material in pavement base layers*. Doctoral thesis. Faculty of Civil Engineering, Slovak University of Technology. Bratislava. (in Slovak).
- NAPA (National Asphalt Pavement Association) 2007. *Warm-Mix Asphalt: Best Practices*. USA: NAPA.
- Technical conditions 2011a. *TP 07/2011 Cold in place reuse of flexible pavement layers*. Ministry of Transport, Construction and Regional Development of the Slovak Republic. Bratislava (in Slovak).
- Technical conditions 2011b. *TP 05/2011 Hot in place recycling for roads with traffic load of class I. to VI*. Ministry of Transport, Construction and Regional Development of the Slovak Republic. Bratislava (in Slovak).
- Technical conditions 2011c. *TP 04/2011 Hot recycling in asphalt plant*. Ministry of Transport, Construction and Regional Development of the Slovak Republic. Bratislava (in Slovak).
- Zuzulová, A. 2011. *The energy consumption of construction of cement pavement*. Proceeding of the Ivan Poliaček seminar: 48–54, 15–16 November 2011. Bratislava: Kongres studio. (in Slovak).

Solar technology of high-rise building integrated design in China

Shu Yan Zhu

Tianjin Architectural Physics Environment and Ecological Technology Key Laboratory,
School of Architecture in Tianjin University, China

Chen Long Ma

School of Architecture in South China University of Technology, China

ABSTRACT: Complete design building integrated with solar technology means that the solar energy system in the design process should be an integral part of the design: all contents of the solar system need to be considered as design elements, with various components of it coordinating with the architecture's style. The paper gives a research on how high-rise buildings integrate with Photovoltaic and Photo-thermal develop in China. By finding out the existing problems and shortcomings, the paper provides some references for the promoting of solar energy technology on urban high-rise buildings in the future.

Keywords: photovoltaic; photo-thermal; high-rise buildings; integration

1 BACKGROUND

With the rapid development of economy in cities, the high-rise building has become a typical representative of the city buildings in China. Because of its large size and complex functions, it plays a more and more important role in city construction process. Therefore, the research of high-rise buildings should not only be confined to their forms and structures, the technology-applications of them which are relevant to green buildings are extremely important. The solar energy technology, as a priority among priorities of green building technologies, should be actively promoted and applied in the high-rise building design.

At present, most of researches in solar energy are the application of solar photovoltaic and solar thermal technologies, of which the concern is the use of solar radiations and transforming them directly into electricity or thermal energies. Furthermore, the applications of solar cells and solar water heaters are two representatives of solar energy technology.

2 INTRODUCTION OF HIGH-RISE BUILDINGS

2.1 Definitions

Currently, the basic standards in China: Code of Design of Civil Buildings (GB50352-2005) and Code for Fire Protection Design of High-Rise Civil Buildings (GB 50045-95) stipulate that the high-rise buildings can be divided into two types:

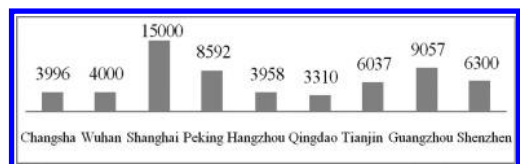
firstly, residential buildings with ten or more floors; secondly, public or comprehensive buildings with the height of more than 24 meters (monolayer public buildings which are higher than 24 meters are excluded). The civil buildings higher than 100 meters are defined as super high-rise buildings.

2.2 Quantity statistics

According to the statistics of collected informations from the Internet, the numbers of high-rise buildings in some main cities in China are shown as follows (the deadline of the statistics is the end of the year 2011).

These data are conservative, it is no doubt that after the recent two years, the numbers of high-rise buildings in the urban city are still increasing substantially, furthermore, with the developing trends of the economy and social, it will surely proceeding in the following years. Therefore, research on high-rise buildings is necessary and urgent; the design-method improvements of buildings integrated with the solar photovoltaic and solar thermal technologies are inevitable result of the sustainable developments in modern society.

Table 1. The statistics of high-rise buildings in main cities.



2.3 Expenditure

Based on the perspective of life cycle in architecture design, high-rise building is a high consumption building type, especially the expenditure of running and maintaining, both accounting for a large proportion in the total expenses.

While there are numerous high rise buildings of different functions, scales and constructions, they generally need to consume a large amount of energy, such as electric, gas, water, etc.

Taking an example of an ordinary high-rise office building with a central air conditioning system, it usually needs electricity of almost 80 to 100 VA/m², in order to meet the whole building demands of lighting, air conditioning, communication, equipment, emergency, firefighting, etc.

For there are so many people and a high level of security in the high-rise buildings, even if per capital amount keep steady, the total quantity of living water and fire water is always increasing rapidly and dramatically. At the same time, a large number of personnel activities need to be supported by providing all kinds of materials.

Therefore, the research in the high-rise buildings design integrated with solar energy is very significant and valuable for energy or resource savings.

2.4 Main functions

We have summarized the main functions of present high-rise buildings. Among them, office buildings demand less hot water, however, if there is a bath function in a commercial building, hot water demand will be higher. There are two mainly problems of solar technology application in high-rise buildings.

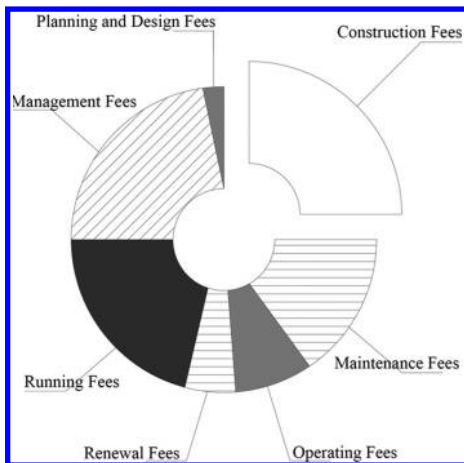


Figure 1. Ratio of cost in the high-rise buildings' life cycle.

First of all, solar thermal technologies are widely used in residential buildings, but there are still some disharmonious factors, such as, a lot of high-level, buildings in Kunming cannot be allowed to install solar devices. Because now high-rise buildings often install them on balcony wall to use solar energy, there will be existence of security risks. At the same time, the ones installed by individuals will make the community's environment messy. This is because the designer haven't considered the result of integration in the design in advance.

Secondly, in addition to residential buildings, other types of high-rise buildings can be classified to public buildings. This kind of building serve large numbers of users, so electric and hot water demand will increase accordingly. But the number of public buildings using solar photovoltaic and solar thermal technology is few, the projects designed from the perspective of integration are fewer.

3 CONCEPT OF INTERPRETATION

The word "integration" originates from the vocabulary of ecology, it also has the meaning of "emergent whole" or "integrated whole", just as some evolutionists say. In recent years, the concept of integration is often used in architecture design, especially in ecological building design.

The concept of solar integrated design technology and construction refers to construction should start from the design stage, we should not only consider aesthetics, but also the solar system should be considered as an indispensable factors of the building. One excellent integration design should have four key design points as the followings:

The first one is appearance. Solar energy collector component should be coordinate with buildings' facades. Whether it is placed on the roof or facades, its size, color, texture, and detail should all be considered during the architecture design process.

The second one is structure. Components should bear basic construction requirements to guarantee that the buildings' load-bearing, waterproof, impervious, insulation, lightning protection, drainage and other functions are not affected. At the same time, the components should consider the ability of antifreeze and wind resistance to enhance the practicability of function and structural durability.

The third one is pipeline layout. It should be considered during architecture design process to avoid some exposed pipelines' bad influence on architectural image. A perfect circulation line of solar system can reduce the energy loss of heat pipe, and avoid wasteful use of pipeline.

The last one is operating system. System design should be complete and reasonable to ensure its stability and safety; making it convenient to install

and repair to reduce unnecessary consumption; solving the problems of interconnection between the building the public power grid. The system should be achieved intelligently, automated as much as possible.

domestic applications of solar technology in high-rise building design.

Then we select nine typical scenarios of them for further study, their characteristics are summarized in [Table 2](#).








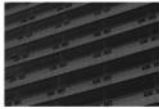





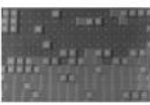




4 DOMESTIC PROJECTS STUDY

5 COMPARISON AND ANALYSIS

After reading the literature and collecting data on line, we have got great deal of information about

Through the study of the above projects, we can infer some regular patterns of solar technology

Table 2. Nine typical high-rise buildings of using solar technology.

PROJECT NAME	PHOTOS	DETAILS	PARTS & PATTERN OF INTEGRATION	UTILIZATION MODES	FUNCTION
SIEEB			Combined with visors (scaffolding)	Solar Photovoltaic	Office architecture
Shenzhen Jian-Ke mansion			The roof of the building, the south visors and the west curtain wall (scaffolding, curtain wall integration)	Solar Photovoltaic	Office architecture
Shenzhen Fang-Da mansion			Combined with flat roofs, and triangle walls (overhead placed)	Solar Photovoltaic	Office architecture
Wuhan torch tower			The photoelectric curtain wall and LED lighting system (curtain wall integration)	Solar Photovoltaic	Office architecture
Suntech photovoltaic research center			The photoelectric curtain wall (curtain wall integration)	Solar Photovoltaic	Office architecture
Baoding Power Valley Jin-Jiang International Hotel			Mainly use photoelectric curtain wall, equipped with photovoltaic components	Solar Photovoltaic	Hotel building
Beijing Hui-Huang - Jing-Ya hotel			The photoelectric curtain wall and LED lighting system (curtain wall integration)	Solar Photovoltaic	Hotel building
Dezhou solar energy international hotel			BIPV modules; solar heating system (add layer roof)	Solar Photovoltaic and Solar Thermal	Hotel building
Dezhou Wei-Lai-Cheng			Floating roof plate use of solar hot water system; Public space use photoelectric lighting (scaffolding)	Solar Photovoltaic and Solar Thermal	Residential building

used in high-rise building integrated design in contemporary China.

Firstly, among several different kinds of public high-rise buildings in the application of solar technology, the office buildings are the most. However, in recent years a large number of hotel buildings have begun to use it.

Secondly, at present model buildings and buildings invested by solar energy firms, such as the SIEEB in Tsinghua University is the typical project of ecological and low-energy consumption building; Fang-Da and Suntech were companies conducting the production and research of curtain wall and solar module; Dezhou solar energy international hotel and Wei-Lai-Cheng are both built by Huang-Ming Company which mainly focus on solar heat utilization.

Thirdly, solar thermal and solar photoelectric are disproportionate. Although the development of solar thermal industry in China is rapid and prosperous, it is mainly used in residential buildings, but high-rise public buildings mainly use the solar photoelectric technology. However, in the process of actual use, energy consumption for heating and air conditioning of public buildings is pretty large, hot water demand of medical buildings and hotel buildings is relatively large. Therefore, using mature and cheap solar-thermal technology has great economic and social significance.

Fourthly, the integration methods are still primary. Some scholars make statistics on the office building integration mode (Fig. 3). Most of the buildings still acquire solar energy by using scaffolding way, namely by using simple mechanical principle. The solar components are supported on the building through some metal structures. But according to the analysis of projects, in recent years, with the development of technology, the number of buildings using photoelectric curtain wall has started to increase, in addition, it can be combined with LED and other multimedia technology for lighting the hotel buildings at night.

Lastly, integration parts are not variety. Aforementioned solar energy utilizations are most for roofs, but due to the particularity of high-rise buildings, more and more research focus on the facades for using solar energy technology, especially the curtain wall structure of high-rise buildings. The examples given above have shown that in addition to solar photovoltaic panels, and hot collector component on the roof of buildings, now

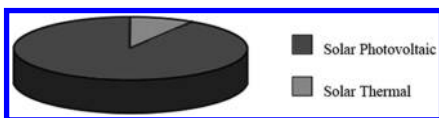


Figure 2. Ratio of photovoltaic and thermal in office building.

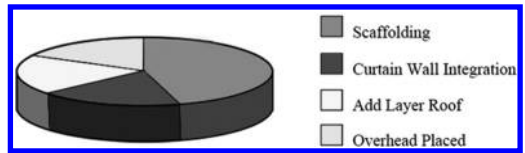


Figure 3. Ratio of four main integration ways in office building.

more and more buildings are designed with photovoltaic curtain wall elevations. The space of roof can be used is scarce, so using walls of high solar radiation can greatly increase the device area of solar energy utilization.

6 SUMMARY AND FORESIGHT

At present the application of solar photovoltaic and solar thermal technology in high-rise buildings still have not reached a satisfactory level. Real combination of solar energy technology and building design cannot be confined by just placing heat collectors or photoelectric devices on buildings' roof or walls. A building must be fully and reasonably applied with solar energy system to make the energy efficiency maximized. Therefore, if a building need both electricity and heat, how to achieve the building integrated with solar technology is a higher pursuit of rational use. High-rise building as a typical case of energy consumers, has much areas contacting with solar, so it is a really good research subject.

The research of solar energy integrated design is broad and profound, there are massive information need to be further explored. As architects, we should enhancing our theoretical knowledge, then resorting to constantly practice to find out more optimized photoelectric and heat integration system. Finally, the solar energy technology and building design process will be more closely. Besides, the most optimized integration design will meet the needs of social developments and public demands.

REFERENCES

- Qian Jianfeng, Zhang Jili, Analysis of a new photovoltaic thermal building integration system, Academic annual conference of the Chinese Association of Refrigeration, 2009, Conference proceedings: 907-912.
- Xu Shen, Li Baofeng, Modelling and detail design of photovoltaic architecture, Architectural journal, 2010.1: 60-63.
- Xue Menghua, Solar energy technology application of high-rise buildings, Construction science and technology, 2009.2:48-51.
- Yang Qian, Study on integrated design of active solar energy technologies and office building, Master's thesis of Chongqing University, May 2010.

A study of photovoltaic systems with a variable step size P&O MPPT algorithm

Ting-Chung Yu, Chih-Chieh Liu, Yih-Bin Lin, Chin-Hao Chen & Yan-Cheng Liou
Department of Electrical Engineering, Lunghwa University of Science and Technology, Taoyuan, Taiwan

ABSTRACT: A modified P&O MPPT algorithm of photovoltaic systems with a variable step size is proposed in this paper. It uses the slope of the tangent for the P-V curve as the judging condition in order to improve the MPPT performance of the photovoltaic systems. The Matlab/Simulink is used to perform the modeling and simulation tasks. The proposed system will be simulated with fixed and variable step size P&O MPPT algorithms, respectively, under different weather conditions in order to observe and analyze the improvements due to the variable step size algorithm on dynamic response and steady-state oscillation issues. From the simulation results, the proposed modified P&O MPPT algorithm with a variable step size spent less time than the fixed one to achieve the maximum power point tracking. It also shows similar oscillation magnitude to that of the traditional fixed step size algorithm when the operating point is near the MPP. The corresponding results validate that the proposed variable step size P&O MPPT algorithm can effectively improve the dynamic and steady state performances simultaneously.

Keywords: modified P&O MPPT algorithm; photovoltaic system; variable step size; dynamic response

1 INTRODUCTION

P&O algorithm is one of the most common used MPPT tracking techniques in the Photovoltaic (PV) systems due to its simple structure, less use of parameters and easy implementation. Traditional Perturbation and Observation (P&O) MPPT algorithm (Tavares et al. 2009) used a fixed step size to track the Maximum Power Point (MPP) during the perturbation period. The step size of perturbation is decided by the needs of tracking speed and steady state oscillations. When a larger perturbation step size is chosen, a faster tracking speed can be obtained. However, larger oscillations will be generated near the MPP and cause significant power losses. Conversely, to use a smaller perturbation step size can reduce the power oscillations and losses, but also the tracking speed. To solve this problem, a modified P&O MPPT algorithm is proposed to use a variable step size technique to perturb and track the MPP of the PV systems. When the operating point of PV modules is far away from the MPP, the system will automatically increase the perturbation step size to reinforce the tracking speed. When the operating point is close to the MPP, the system will also automatically reduce the perturbation step size to a certain extent in order to reduce power oscillations and losses.

In recent years, many scholars were devoted to the researches of the variable step size algorithm

(Al-Diab & Sourkounis 2010, Liu et al. 2008, Wang et al. 2013, Ahmed & Shoyama 2011). In the study (Al-Diab & Sourkounis 2010), the traditional fixed step size method was replaced by a gradually changing step size method. It could simultaneously improve the dynamic response and steady-state oscillation problems happened in the traditional P&O MPPT algorithm. In the research (Liu et al. 2008) proposed by F. Liu, S. Duan, F. Liu, B. Liu and Y. Kang, the variable step size method was applied to the Incremental Conductance (INC) MPPT algorithm, and it can also improve the dynamic responses and steady state oscillations of the MPPT algorithm. In the literature (Wang et al. 2013), P. Wang et al. proposed an improved variable-step INC MPPT algorithm. Compared with the traditional variable-step INC algorithm, this improved algorithm optimizes the selection of the step size so that the tracking of the MPP is more quickly and the steady-state performance is better.

2 VARIABLE STEP SIZE P&O MPPT ALGORITHM

The perturbation step size ΔV of the traditional P&O MPPT algorithm is fixed, and determined by the system designers' need. Using a larger step size would make the tracking speed boost,

but also lead to larger power oscillations near the MPP. On the contrary, the use of a smaller step size would result in smaller power oscillations and losses, however the tracking speed would be also reduced. Therefore, the use of fixed step size can not take both dynamic response and stability into account.

A modified P&O algorithm with a variable step size proposed in this paper is to use the slope of tangent of the typical P-V curve for the PV modules as the judgment basis in order to determine whether the perturbation grows or shrinks. It can be observed from the typical P-V curve that the slope of tangent at the operating point will appear a larger value when the point is away from the MPP. Conversely, when the operating point is close to the MPP, the slope of the tangent at the operating point gradually approaches zero.

In the literatures (Al-Diab & Sourkounis 2010, Liu et al. 2008), the perturbation step size were gradually adjusted and changed based on dP/dV or dP/dI . The disadvantage of this approach is that the step size will be gradually changed under any circumstance, even though the operating point is away from the MPP. This would make a certain impact on the tracking speed. In order to avoid the above effects, a multi-stage variable step size P&O MPPT algorithm is proposed in this paper to improve the performance of the traditional P&O MPPT algorithm. First, a basic step size ΔV_b is chose on the basis of the tolerance of the power oscillation near the MPP. Next, a scaling factor (N) related to the tracking speed is also determined. Finally, corresponding slop threshold values (S_{n-1} , S_{n-2} , ..., S_1) should also be selected according to the number of multi-stage (n). Mathematical relationships in multi-stage variable step size are summarized as follows,

$$\begin{aligned} \Delta V &= \Delta V_b \times N & \text{slop} > S_{n-1} \\ \Delta V &= \Delta V_b \times N(n-2/n-1) & S_{n-2} < \text{slop} < S_{n-1} \\ &\vdots & \vdots \\ \Delta V &= \Delta V_b & \text{slop} < S_1 \end{aligned} \quad (1)$$

Figure 1 is the flowchart of the proposed multi-stage variable step size P&O MPPT algorithm. The “slop” in Figure 1 represents the absolute value of the slope for the tangent on the operating point of the P-V curve. Its mathematical equation is expressed as follows,

$$\text{slop} = \left| \frac{P(n) - P(n-1)}{V(n) - V(n-1)} \right| \quad (2)$$

Next, a 3-stage variable step size algorithm is introduced to explain the variations of the perturbation step size in the tracking process. The

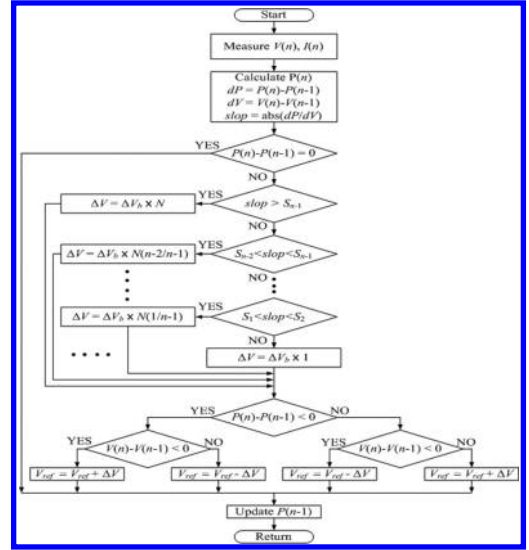


Figure 1. The flowchart of the proposed multi-stage variable step size P&O MPPT algorithm.

corresponding slop threshold values are set to be 1 and 5, respectively. When the system detects the absolute value of the slope is greater than 5 (away from MPP), the step size is automatically adjusted to the value of the basic step size multiplied by a scaling factor of N . The increased step size will accelerate the tracking speed, therefore, the tracking time is significantly reduced. When the operating point of PV modules approaches the MPP, the slope becomes smaller. When the system detects the absolute value of the slope is greater than 1 but less than 5, the step size is adjusted to the value of basic step size multiplied by $(N/2)$. At this time, the tracking speed will be slowed down to avoid excessive oscillations caused by bulky step size. Especially when the weather condition changes continuously, the absolute value of slope will not have much change. The use of larger step size will lead the tracking accuracy reduced. When the system detects the absolute value of the slope is less than 1, the operating point is very close to the MPP. The step size is reduced to the value of basic step size. It won't result in excessive steady state oscillations and power losses when the MPP is tracked. The mathematical relationship for the variation of the step size used in 3-stage variable step size algorithm is summarized as follows,

$$\begin{aligned} \Delta V &= \Delta V_b \times N & \text{slop} > 5 \\ \Delta V &= \Delta V_b \times (N/2) & 1 < \text{slop} < 5 \\ \Delta V &= \Delta V_b & \text{slop} < 1 \end{aligned} \quad (3)$$

3 ANALYSIS OF SIMULATION RESULTS

In order to validate the efficiency of proposed modified P&O algorithm, 3-stage variable step size P&O MPPT algorithm simulations under different weather conditions are carried out in this paper. The parameters of PV modules used in simulations are listed in Table 1. The block diagram of the simulation system is shown in Figure 2.

3.1 Single weather condition

The irradiance and temperature used in the simulation are 1000 W/m² and 40 °C respectively. The fixed step size and basic step size (ΔV_b) are all chose to be 0.01 V. The scaling factor (N) is set to be 30, and the slop threshold values are selected to be 5 and 1. Figure 3 is the comparison diagram for fixed and variable step size P&O algorithm

Table 1. Electrical specification of the PV module.

Item	Value
Rated maximum power (W)	200
Rated voltage (V)	40.0
Rated current (A)	5.00
Open circuit voltage (V)	49.6
Short circuit current (A)	5.5
Short circuit current temperature coefficient (mA/(C))	1.65
Open circuit voltage temperature coefficient (V/(C))	-0.129

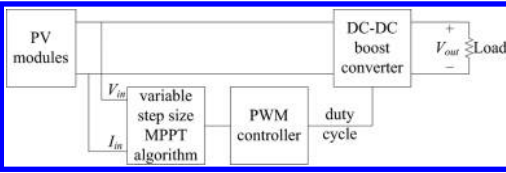


Figure 2. Block diagram of the PV simulation system.

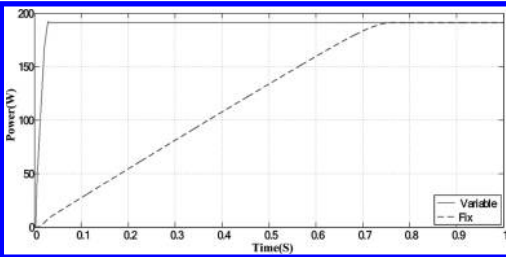


Figure 3. Comparison diagram for fixed and variable step size P&O algorithm simulations.

simulations. Figure 4 is an enlarged diagram of steady state power oscillations near the MPP.

According to Figure 3 and 4, the variable step size algorithm spends 0.03675s to reach the MPP, however, the fixed one needs 0.76335s to complete the task under the same power oscillation amplitude. The modified P&O algorithm still maintains the same steady-state oscillation amplitude while it increases its tracking speed. It won't get extra power losses when pursuing the tracking speed.

3.2 Changing weather conditions (I)

The irradiance and temperature in the simulation are set to be 1000 W/m² and 40 °C in the beginning, next directly dropped to 500 W/m² and 25 °C, and finally returned to 1000 W/m² and 40 °C. The fixed step size and basic step size (ΔV_b) are all chose to be 0.01 V. The scaling factor (N) is set to be 30, and the slop threshold values are selected to be 5 and 1. Figure 5 is the comparison diagram for fixed and variable step size P&O algorithm simulations. Table 2 is the statistics and comparison of the tracking time for fixed and variable step size P&O algorithms.

3.3 Changing weather conditions (II)

The irradiance and temperature in the simulation are set to be 400 W/m² and 25 °C in the beginning,

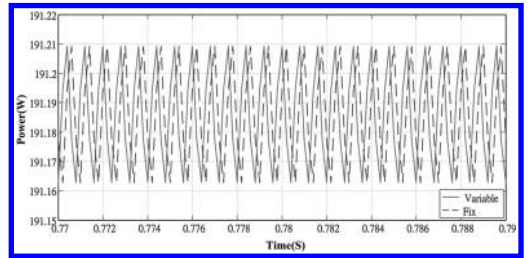


Figure 4. Enlarged diagram of power oscillations near the MPP.

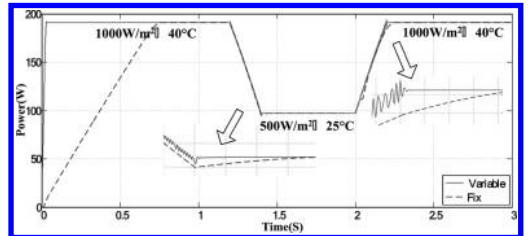


Figure 5. Comparison diagram for fixed and variable step size P&O algorithm simulations.

Table 2. Statistics and comparison of the tracking time for fixed and variable step size P&O algorithms.

Weather condition	Tracking time (s)		
	Fixed	Variable	Discrepancy
0~1000 W/m ² , 40°C	0.76335	0.03675	95.2%
1000 W/m ² , 40°C	0.246	0.212	13.8%
~500 W/m ² , 25°C			
500 W/m ² , 25°C	0.258	0.205	20.5%
~1000 W/m ² , 40°C			

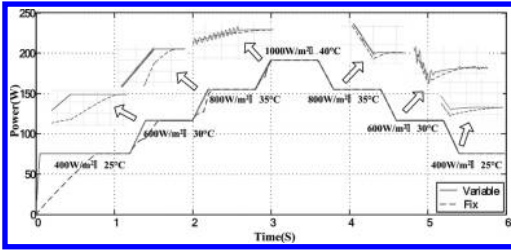


Figure 6. Comparison diagram for fixed and variable step size P&O algorithm simulations.

next gradually increased to 1000 W/m² and 40 °C, and then gradually returned to 400 W/m² and 25 °C. The fixed step size and basic step size (ΔV_b) are all chose to be 0.01 V. The scaling factor (N) is set to be 30, and the slop threshold values are selected to be 5 and 1. Figure 6 is the comparison diagram for fixed and variable step size P&O algorithm simulations. Table 3 is the statistics and comparison of the tracking time for fixed and variable step size P&O algorithms.

According to the results of Figure 5–6 and Table 2–3, it can be observed that the tracking times of the proposed variable step size P&O MPPT algorithm are shorter than those of the fixed step size algorithm in all simulations. The deficient extent of the tracking time is generally proportional to the changing magnitude of the weather condition. For example, in the simulations of Figure 5–6 the first variation of weather condition starts from zero, the terminal voltage of the PV module varies greatly. Therefore, the tracking time of the variable step size algorithm is less time-consuming than that of the fixed step size algorithm up to about 90%. In the next simulation, the variation of weather condition is about 500 W/m². Because of a smaller variation of terminal voltage of the PV module, the variable step size algorithm saves about 15–20% of the tracking time than the fixed step size algorithm. When the variation of weather condition is dropped to 200 W/m², the

Table 3. Statistics and comparison of the tracking time for fixed and variable step size P&O algorithms.

Weather condition	Tracking time (s)		
	Fixed	Variable	Discrepancy
0~400 W/m ² , 25°C	0.80635	0.08115	89.9%
400 W/m ² , 25°C	0.309	0.305	1.3%
~600 W/m ² , 30°C			
600 W/m ² , 30°C	0.516	0.505	2.1%
~800 W/m ² , 35°C			
800 W/m ² , 35°C	0.513	0.506	1.4%
~1000 W/m ² , 40°C			
1000 W/m ² , 40°C	0.519	0.505	2.7%
~800 W/m ² , 35°C			
800 W/m ² , 35°C	0.516	0.501	2.9%
~600 W/m ² , 30°C			
600 W/m ² , 30°C	0.52	0.51	1.9%
~400 W/m ² , 25°C			

variation of terminal voltage of the PV module is small. Therefore, the variable step size P&O algorithm saves only about 3–5% of the tracking time. On the whole, the proposed variable step size P&O MPPT algorithm can effectively improve the tracking speed (dynamic response) of the traditional fixed step size algorithm without losing the stability of simulation results.

4 CONCLUSION

A modified P&O MPPT algorithm of PV systems with a variable step size is proposed in this paper. It uses the slop of the tangent for the P-V curve as the judging condition in order to improve the MPPT performance of the PV system. When the operating point of PV module is far from the MPP, the step size will be automatically increased to enhance tracking speed. When the operating point approaches the MPP, the step size will be automatically reduced to a certain extent in order to reduce the steady-state oscillations and power losses. It can solve the dilemma of the traditional P&O MPPT algorithm between the dynamic response and stability.

According to the simulation results, it can be observed that the proposed variable step size P&O MPPT algorithm shows better performance on tracking speed than the traditional P&O MPPT algorithm regardless of weather conditions. In addition, the shortage of the tracking time is generally proportional to the changing extent of the weather condition. When a small amount of weather condition is changed, the proposed variable step size algorithm saves 3–5% of the tracking time. However, when a larger amount of weather

condition is changed, the proposed variable step size algorithm is possessed of the superiority of saving 15–20% of the tracking time. Overall, the proposed variable step size P&O MPPT algorithm shows better dynamic responses and steady state oscillations than the traditional P&O MPPT algorithm under any weather condition.

REFERENCES

- Ahmed, E.M. & Shoyama, M. 2011. Variable step size maximum power point tracker using a single variable for stand-alone battery storage PV systems. *Journal of Power Electronics* 11(2): 218–227.
- Al-Diab, A. & Sourkounis, C. 2010. Variable step size P&O MPPT algorithm for PV systems. *Proc. of the 12th International Conference on Optimization of Electrical and Electronic Equipment (OPTIM 2010)*, Brasov, Romania, 20–22 May 2010.
- Liu, F., Duan, S., Liu, F., Liu, B. & Kang, Y. 2008. Variable step size INC MPPT method for PV systems. *IEEE Transactions on Industrial Electronics* 55: 2622–2628.
- Tavares, C.A.P., Leite, K.T.F., Suemitsu, W.I. & Bellar, M.D. 2009. Performance evaluation of photovoltaic solar system with different MPPT methods. *Proc. of the 35th Annual Conference of the IEEE Industrial Electronics Society (IECON 2009)*, Porto, Portugal, 3–5 Nov. 2009.
- Wang, P., Zhou, Z., Cai, M. & Zhang, J. 2013. An improved multistage variable-step MPPT algorithm for photovoltaic system. *Proc. of the 2nd International Conference on Computer Science and Electronics Engineering (ICCSEE 2013)*, Hangzhou, China, 22–23 March 2013.

Experimental study on the axial behavior of perforated cold-formed steel wall frames

Nor Maslina Mohsan

Faculty of Civil Engineering, Universiti Teknologi MARA (UiTM) Pahang Jengka, Pahang, Malaysia

Arizu Sulaiman & Mahmood Md. Tahir

Faculty of Civil Engineering, Universiti Teknologi Malaysia (UTM) Skudai, Johor, Malaysia

ABSTRACT: This paper presents a full-scale experimental investigation on perforated cold-formed wall frames under axial compression load. The focus of this investigation is to study the axial buckling behavior as well as to obtain the axial load capacity of the wall frames. The wall frames specimens are divided into three different wall stud arrangements with two different cold-formed steel thicknesses which are 1.55 mm and 1.9 mm. During the testing, maximum failure load, horizontal displacement and strain distribution were recorded. The axial load capacity increases significantly as the cold-formed steel thickness increases and double bracing was used. The wall frame with Arrangement 2 shows higher axial load capacity among all specimens. Nearly all the wall frame specimens failed in Torsional Flexural Buckling (TFB) and Flexural Buckling (FB). Furthermore, the effect of holes can be seen where visible local buckling occurred at web and flanges near or in between holes.

Keywords: perforated cold-formed; wall frame; buckling behavior; axial load capacity

1 INTRODUCTION

The usage of cold-formed steel sections are getting popular in the construction of building especially as roof trusses, wall studs, floor joists and decking, and ceiling. This may be due to the sections are very efficient in terms of stiffness and strength (Dan Dubina, 2012). The cold-formed steel sections usually produced from cold rolled flat strips or coils by method of roll forming or press braking.

Load-bearing wall or non-load-bearing wall frames composed of cold-formed steel sections are widely used in construction since 1940s (Wang et al., 2005). Generally, cold-formed wall frames consists of several wall studs, top track and bottom track which can be braced by discrete bracing and may include sheathing materials to increase the buckling resistance.

Most of the previous researches focused on testing of cold-formed wall frames with sheathing either on one or both sides of the frames. Lee & Miller (2001), Tian et al. (2004), Telue & Mahendran (2004), Tian et al. (2007) and Vieira et al. (2011) performed experimental test on cold-formed steel wall frames with sheathing under axial loading. The axial load capacity, the behavior of wall frames, studs spacing, screw spacing and etc. were observed in the research. The results showed

that, the increase in axial load capacity of the cold-formed steel wall frames varies based on the sheathing types, thickness and material properties.

However, a small number of researches have been carried out on the unsheathed wall frames and with perforated studs. Miller & Pekoz (1993) conducted experimental test on 24 cold-formed wall frame assemblies without sheathing to investigate the structural behavior including the effect of bracing elements. The wall frames assemblies were found to fail by torsional-flexural which is the same as predicted by AISI 1986 Specification for wall frames without sheathing. The strap bracing and channel bracing used were effective in increasing the failure load up to 60%. As for the wall studs with perforations at the web, it is reported that the local and distortional buckling strength of the sections were reduced because of the availability of the perforations (Kesti & Davies, 1999).

This paper presents the results of the full-scale test on the axial load capacity and buckling behavior of the perforated cold-formed wall frames without sheathing. In addition, the influence of cold-formed steel thickness and the wall studs arrangement are discussed in detail. Although, the cold-formed wall frames are usually used in building with sheathing, in this case the wall frames will be used as the reinforcement in concrete wall panel.

2 EXPERIMENTAL STUDY

2.1 Specimens preparation

The cold-formed wall frames were fabricated from lipped channel sections and unlipped channel sections from Galvanised Hi-Tensile Steel Grade G450 (minimum yield strength of 365 MPa) and zing coating class Z275 (275 g/mm²). Two different series of lipped and unlipped channel sections were used as the wall frame stud and track having a nominal cross-section thickness of 1.55 mm and 1.90 mm. The studs are designated here as LC10016 (100 mm × 50 mm × 12 mm × 1.55 mm) and LC10020 (100 mm × 50 mm × 12 mm × 1.9 mm). Whilst for the wall frame tracks the channel without lips were used designated as TC10416 (104 mm × 60 mm × 1.55 mm) and TC10420 (104 mm × 60 mm × 1.9 mm).

The circular holes with diameter of 16 mm were drilled at the web and flanges of wall studs with spacing of 150 mm center to center as shown in Figure 1. The holes were drilled at the center of the web and flanges. The studs and tracks were arranged into three different arrangements as shown in Figure 2. Each ends of the wall studs were connected to the track by self-drilling screw with a

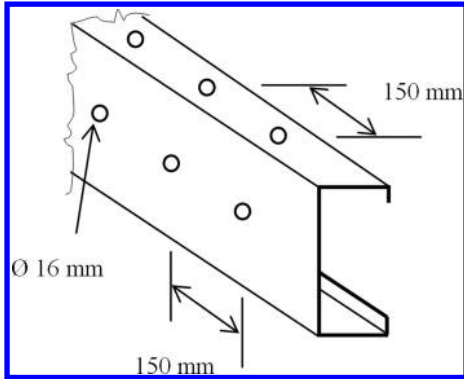


Figure 1. The position and spacing of holes.

diameter of 5.48 mm. The bracing was installed to the wall frame by using cold-formed steel bracket and fastened by using self-drilling screw at the side studs and bolt at the middle stud. The detail geometrical dimension of the assembled wall frames are shown in Table 1.

2.2 Test setup and instrumentation

The setup for the axial compression test of the wall frames is shown in Figure 3. A 50 ton hydraulic jack was used to supply the vertical load on top of the spreader beam. Spreader beam was used to ensure that the load applied to the wall frame is uniform. Linear Voltage Displacement Transducers (LVDT) were used to measure the horizontal displacements of the wall frame. Four LVDTs were positioned horizontally on the web and flange at quarter height from the top end of the wall frame. Another four LVDTs were placed horizontally at the mid-height of the middle and side stud. In addition to the horizontal displacement and loading, the strain in the wall frames were also measured by using strain gauges attached to the web of wall studs and track at various locations. However, the results for strain distributions are not reported in this paper. Readings from the LVDTs, strain

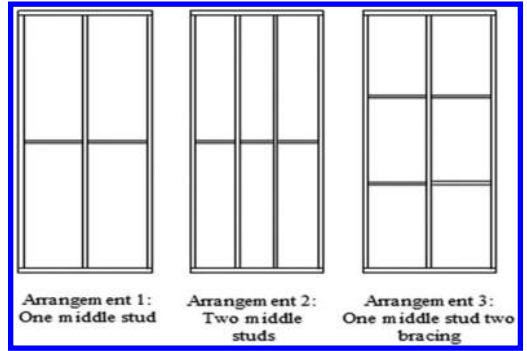


Figure 2. The geometrical arrangement of cold-formed wall frames.

Table 1. The geometrical dimension of cold-formed wall frames.

Specimen	Wall frame arrangement	Height, H (mm)	Width, B (mm)	Cold-formed thickness, t (mm)
1WFT1A1H1	1	2920	1120	1.55
1WFT1A2H1	2	2920	1120	1.55
1WFT1A3H1	3	2920	1120	1.55
1WFT2A1H1	1	2920	1120	1.90
1WFT2A2H1	2	2920	1120	1.90
1WFT2A3H1	3	2920	1120	1.90

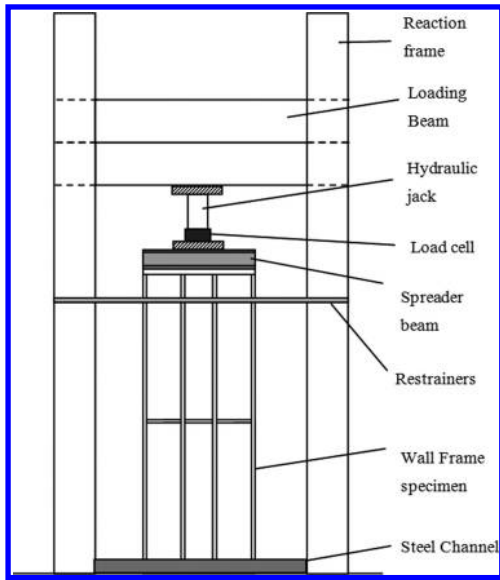


Figure 3. The schematic diagram setup for cold-formed wall frames test.

gauges and load cell were channeled to a data logger and recorded automatically in a computer.

3 RESULTS AND DISCUSSION

3.1 Axial load capacity

The axial load capacity is refer to the failure load or maximum load that can be attained during the loading process. The axial load capacity results for the cold-formed wall frames test are shown in Table 2. It can be seen from Table 2 that, the maximum axial load capacity for each thickness comes from specimen 1WFT1A2H1 and 1WFT2A2H1. This is because there are four number of wall studs used in Arrangement 2. The axial load capacity for specimens with Arrangement 2 was increased about 21% for specimen with 1.55 mm thickness and 40% for specimen with 1.90 mm thickness compared to specimens with Arrangement 1. However, the wall studs in Arrangement 1 is more effective in resisting the load since the axial load value per stud for Arrangement 2 was decreased by 9% for specimen with 1.55 mm thickness and increased by only 5% for specimen with 1.90 mm thickness. Furthermore, if compared with the results of Arrangement 1 and Arrangement 3, there were an increase of about 13% and 11% for each thickness. It shows that the bracing is effective in increasing the strength and stiffness of the wall frames and consistency with the statement made by Sputo & Beery (2008).

Table 2. The axial load capacity results.

Specimen	Wall frame arrangement	Failure load (kN)
1WFT1A1H1	1	140.7
1WFT1A2H1	2	170.7
1WFT1A3H1	3	159.8
1WFT2A1H1	1	191.9
1WFT2A2H1	2	270.5
1WFT2A3H1	3	215.0

Comparing with experimental programme reported by Mohsan et al. (2013), the results show that the stud in frames can carry more load than the corresponding individual stud with simple supports. As for the effect of the thickness, there is a significant increase with average of 43% of failure load with the increase of 22% of thickness.

3.2 Axial buckling behaviour

The axial buckling behavior results are summarized in Table 3 and discussed below.

3.2.1 Arrangement 1

Two cold-formed wall frames Arrangement 1 of two different thicknesses were tested. The measured horizontal displacements for both wall frames are presented in Figure 4. It can be seen that the horizontal displacements for specimen 1WFT1A1H1 and 1WFT2A1H1 are consistent. The highest value of 25.05 mm was recorded at the quarter height position of the middle stud. The middle and the side stud at quarter height position are not stiffened by bracing element. The typical buckling behavior for specimen with Arrangement 1 is as shown in Figure 5. Flexural buckling on the right side stud was observed in both wall frames as early as 75 kN of load for 1WFT1A1H1 and at 55 kN for 1WFT2A1H1. At the failure load, local buckling occurred at the web area of the left side stud coincide with the bracing connection.

3.2.2 Arrangement 2

There are four number of wall studs used and arranged in symmetrical order to form wall frames with Arrangement 2 (1WFT1A2H1 and 1WFT2A2H1). The horizontal displacements were measured at four locations on both wall frames as presented in Figure 6. It can be seen that the trend of horizontal displacement for both specimens is different where the horizontal displacement for specimen 1WFT2A2H1 increase approximately linear with the load. The typical buckling behavior for specimens with Arrangement 2 is as shown in Figure 7(a). Based on the observations during

Table 3. The axial buckling behavior results.

Specimen	Failure mode	
	Side stud	Middle stud
1WFT1A1H1	TFB at right stud LB at left stud	FB
1WFT1A2H1	TFB at left stud NB at right stud	FB at both middle studs
1WFT1A3H1	TFB at right stud FB at left stud	FB
1WFT2A1H1	TFB at right stud FB at left stud	FB
1WFT2A2H1	TFB at left stud NB at right stud	FB at both middle studs
1WFT2A3H1	TFB at right stud FB at left stud	FB

*TFB, torsional-flexural buckling. *LB, local buckling. *FB, Flexural buckling. *NB, no buckling. *Sd, Side stud. *Md, Middle stud. *Qh, Quarter height. *Mh, Mid-height.

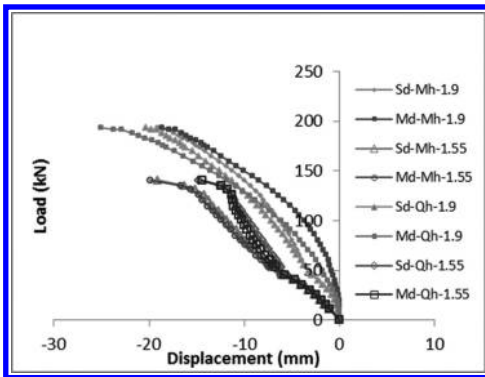


Figure 4. The load versus displacement graph for sample 1WFT1A1H1 and 1WFT2A1H1.

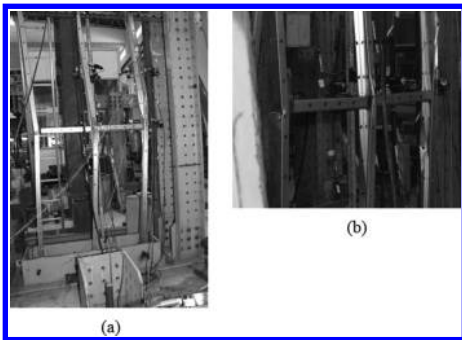


Figure 5. Typical buckling behavior of wall frame in Arrangement 1 (a) 1WFT1A1H1; (b) local buckling at web.

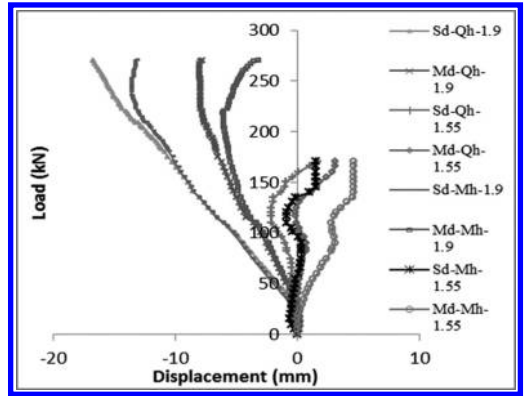


Figure 6. The load versus displacement graph for sample 1WFT1A2H1 and 1WFT2A2H1.

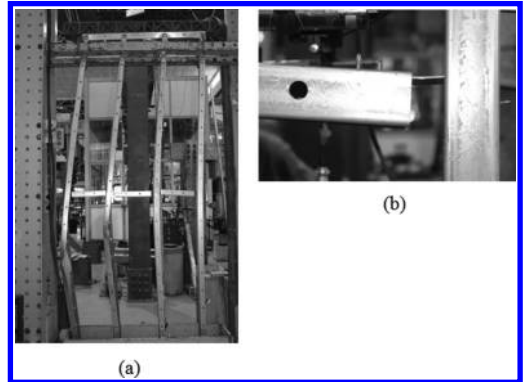


Figure 7. Typical buckling behavior of wall frame in Arrangement 2 (a) 1WFT2A2H1; (b) bracket in tension.

testing, both wall frames show a reaction of compressed symmetrically in the early stage of loading. When the load was further increased, the left wall stud starts to show some buckling toward the left side. However, the right studs showed minimal movement (no buckling) because of the existence of bracing that function effectively to restrain the movement. The effect of this movement can be seen at the bracket when is in the tension state as shown in Figure 7(b).

3.2.3 Arrangement 3

In Arrangement 3, two locations in the wall frames were installed with bracing. The measured horizontal displacements for both wall frames with Arrangement 3 are presented in Figure 8. Based on the results, the horizontal displacements measured are relatively small compared to other arrangements. This proves that the installation of double bracing can significantly control the

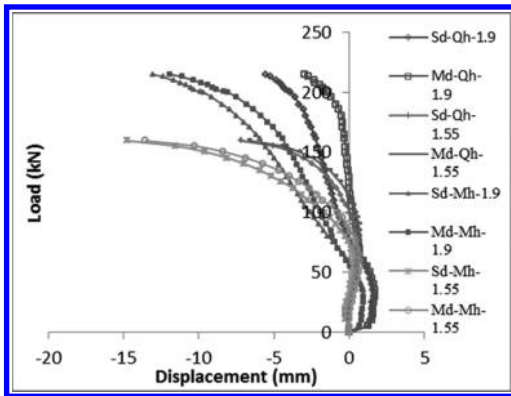


Figure 8. The load versus displacement graph for sample 1WFT1A3H1 and 1WFT2A3H1.

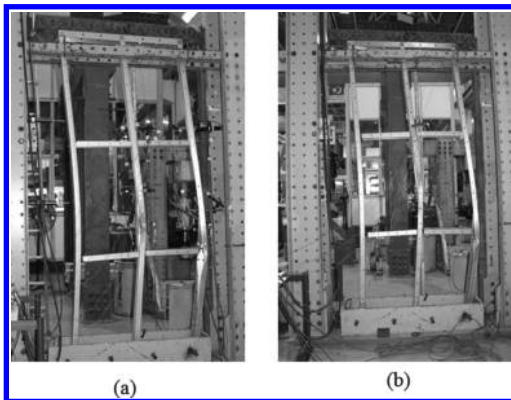


Figure 9. Buckling behavior of wall frame in Arrangement 3 (a) 1WFT1A3H1; (b) 1WFT2A3H1.

displacement of the wall frames. The horizontal displacement curve exhibits a similar trend for both wall frames, but specimen 1WFT2A3H1 are significantly smaller in magnitude. The buckling behavior for specimen with Arrangement 3 is as shown in Figure 9. From the observation, it can be seen that the changes due to loading were very gradual and the frame looks more stable. Both of the wall frames showed the same failure mode where the right stud experienced torsional flexural buckling and the overall frame buckled to the right since most of the studs minor axes lies at the right side.

4 CONCLUSION

The experimental results on perforated cold-formed wall frames are presented in this paper.

The axial load capacity and the axial buckling behavior of the wall frame are the main objectives in this study. The axial load capacity of the wall frames with Arrangement 2 is higher compared to other arrangements, since it has more wall studs. It is found that, the bracing is effective in increasing the strength and stiffness of the wall frames. As expected, the increase in the thickness of the cold-formed steel can significantly increase the axial load capacity of the wall frames. It was also found that almost all perforated cold-formed wall frame failed under flexural torsional buckling (TFB) and Flexural Buckling (FB), especially for the wall frames with Arrangement 1 which showed a very significant TFB. Permanent local buckling was also visible at the web area that coincided with the bracing connection and at the flanges in between the holes or near to the holes.

ACKNOWLEDGMENT

The authors gratefully acknowledge the Steel Technology Centre (STC) for providing materials used in this test. The authors also wish to thank all the technical support in the Structures Laboratory of Universiti Teknologi Malaysia for their assistance in carrying out the testing.

REFERENCES

- Kesti, J., & J. Davies, M. (1999). Local And Distortional Buckling of Perforated Steel Wall Studs. *Advances in Steel Structures, Volume 1*, 367–374.
- Lee, Y., & Miller, T.H. (2001). Axial Strength Determination For Gypsum-Sheathed, Cold-Formed Steel Wall Stud Composite Panels. *Journal Of Structural Engineering*, 127(6), 608–615.
- Miller, T.H., & Pekoz, T. (1993). Behavior of Cold-Formed Steel Wall Stud Assemblies. *Journal of Structural Engineering*, 119(2), 641–651.
- Mohsan, N.M., Sulaiman, A., & Tahir, M.M. (2013). Compressive Strength and Buckling Behaviour of Perforated Slender Lipped Channel Columns. In *Proceedings of 4th International Graduate Conference on Engineering, Science and Humanities IGCESH*, (pp. 440–445).
- Spoto, T., & Beery, K. (2008). Bracing Demand in Axially Loaded Cold-Formed Steel Stud Walls. *Journal Of Architectural Engineering*, (September), 85–89.
- Telue, Y., & Mahendran, M. (2004). Behaviour And Design of Cold-Formed Steel Wall Frames Lined With Plasterboard On Both Sides. *Engineering Structures*, 26(5), 567–579.
- The Dan Dubina, V.U., Raffaele Landolf. (2012). Design of Cold-Formed Steel Structures (1st ed.): *European Convention for Constructional Steelwork*.
- Tian, Y.S., Wang, J., & Lu, T.J. (2007). Axial load capacity of cold-formed steel wall stud with sheathing. *Thin-Walled Structures*, 45(5), 537–551.

- Tian, Y.S., Wang, J., Lu, T.J.Ã., & Barlow, C.Y. (2004). An experimental study on the axial behaviour of cold-formed steel wall studs and panels. *Thin-Walled Structures*, 42, 557–573.
- Vieira, L.C.M., Shifferaw, Y., & Schafer, B.W. (2011). Experiments on Sheathed Cold-Formed Steel Studs in Compression. *Journal of Constructional Steel Research*, 67(10), 1554–1566.
- Wang, J., Tian, Y.S., & Lu, T.J. (2005). The Role of Frame Members and Sheathing in Partition Wall Panels Subjected to Compression. *Thin-Walled Structures*, 43(6), 983–1002.

Integral analysis of laboratory and field electrical resistivity for soil density prediction

Z.A.M. Hazreek

Faculty of Civil and Environmental Engineering, Universiti Tun Hussein Onn Malaysia, Malaysia
School of Physics, Universiti Sains Malaysia, Malaysia

A.T.S. Azhar & M. Aziman

Faculty of Civil and Environmental Engineering, Universiti Tun Hussein Onn Malaysia, Malaysia

S. Rosli

School of Physics, Universiti Sains Malaysia, Malaysia

A. Fauziah

School of Civil Engineering, Universiti Sains Malaysia, Malaysia

W.D. Chitral

Research Center for Soft Soil, Universiti Tun Hussein Onn Malaysia, Malaysia

ABSTRACT: In the past, conventional technique to determine soil properties have faced serious problem in large scale project which related to the time and cost. Some alternative approach need to be used in order to solve or minimized those problem. Hence, this study was performed using integral analysis of laboratory and field electrical resistivity to determine basic properties of soil with particular reference to soil density. The electrical resistivity property of Clayey SILT was established using soil box test together with its density. Field electrical resistivity test was performed on site for Clayey SILT in order to determine its electrical resistivity and density properties. This study used pole-dipole array for field electrical resistivity test which supplied from ABEM SAS 4000 equipment. There was no similarity found of the resistivity value obtained from the laboratory with that of the field scale due to several reasons. Theoretically, the dissimilarity of resistivity array geometry factor, K used from laboratory and field test has strongly influenced the Electrical Resistivity Value (ERV) obtained from both different scales of experiment. The study aimed to establish a correction factor, c from lab and field scales based on ERV and soil density data was established at $1.94 \Omega m$. These c values were established to correct the field ERV based on laboratory data in order to reliably predict field soil density numerically using the equation derived through statistical analysis given by $\rho_{Bulk} = 1.9008\rho^{0.072}$. Hence, the mechanism of ERV from both scales has been investigated, presented and explained. Subsequently, this study will contribute to establish the electrical resistivity method as a supporting technique for geotechnical basic properties determination.

Keywords: electrical resistivity; soil density; array

1 INTRODUCTION

Soil Investigation (SI) commonly was associated with the aim of surface and subsurface geomaterials properties determination used for design and construction works. According to Clayton et al. (1995), the foremost classical geotechnical site investigation method for subsurface profile exploration is the application of boring (light percussion drilling, power augering and washboring), drilling (rotary drilling and coring), probing (Mackintosh probe, dynamic probing) and examination in-situ (trial pit-

ting, large bored shafts, tunnel and drifts). In recent years, rapid technology of electronics development has increased the popularization and utilization of geophysical method as an alternative tool in site investigation. Geophysical Method (GM) consists of several techniques such as electrical resistivity, seismic, magnetic, gravity, ground penetration radar, etc. The basis of the geophysical method is qualitative studying of earth using physical properties such as electrical resistance, velocity, magnetic susceptibility, density, etc. Since such potential of geophysics in engineering is yet to be realized and

fully developed, the application of these techniques are still not being fully utilized. Problems may arise during the applications when the GM is not being fully explored by the civil engineers due to their lack of exposure and expertise in this area. As reported by Clayton et al., (1995), some of the reasons are due to poor planning of geophysical survey by engineers who lack experience in the techniques, and over optimistic geophysicists leading to inappropriate application of the available techniques.

Conventional SI techniques always being the best approach due to its direct measurement in order to obtained the geomaterials properties. However, the problems in most traditional boring and drilling method encounter when the area of the investigation was large which will increase the number of borehole thus increasing money and time of the project. Moreover, this methods experience difficulties in steep and hilly terrain, swampy areas, coastal regions and complex geomaterial areas which need to be investigated (Khatri et al. 2011). Conventional SI work requires bulky and heavy machine (i.e. boring machine) to determine subsurface information thru geomaterial sampling which are prone to be less efficient in difficult site due to the difficulty of equipment mobilization, shifting, demobilization and operation. The information obtained was a single point data and the interpolation between a large boreholes spacing can lead to increase the degree of uncertainties of the subsurface profile investigated (Abidin et al. 2013, Hossain et al. 2012, Godio et al. 2006 & Mauritsch et al. 2000). According to Pozdnyakova & Pozdnyakova (2002), high number of soil sampling was required in order to achieve high accuracy of soil properties assessment and as reported by Siddiqui & Osman (2012), this objective was hard to achieve by borehole sampling which generally time-consuming and expensive. Traditional laboratory testing also can be very costly and took a longer time when dealing upon large number of soil. As a result, the solutions to these challenges will require multidisciplinary research across the social and physical sciences and engineering (Fragaszy et al. 2011). Geophysical methods such as ERM has increasingly become popular in geotechnical and structural engineering works due to its good efficiency in terms of cost (lower cost), time (less time) and provides large data coverage (2D image) which is therefore able to complement the existing borehole data (Abidin et al. 2013, Khatri et al. 2011, Liu & Evett 2008, Godio et al. 2006 & Cosenza et al. 2006). Hence, geophysical method offers the chance to overcome some of the problems inherent in more conventional ground investigation techniques Clayton et al. 1995.

In geotechnical engineering perspectives, sense of concern and appreciation is particularly viewed from the prospective contribution and significance

due to the geomaterial properties determination and its reliability. The application of alternative methods such as geophysical techniques can be increasingly meaningful provided it is able to contribute more than its well-known anomaly detection outcome since the main task and responsibility of engineers was to design and construct a structure safely. Studies which relate the geophysical data to geotechnical properties are rare and less known (Cosenza et al. 2006). Hence based on those issues, this study proposed to establish a study on geophysical techniques specifically using electrical resistivity method which is able to contribute the prediction of basic geotechnical properties thru the establishment of integral analysis between laboratory and field electrical resistivity value by introducing a correction factor, c which able to predict soil density statistically.

2 MATERIAL AND METHODS

This study consists of three stages: viz fieldwork, laboratory experimental and data processing and analysis using statistical analysis and utility software. Fieldwork was started by conducting a line of 2D electrical resistivity imaging using pole-dipole array. The testing configuration was given in Table 1. After completion of the field resistivity data acquisition, three specific point of location (A, B and C) as shown in Figure 1 was choose in line of the electrical

Table 1. Configuration used in 2D electrical resistivity test for both soil models.

No	Setting	Description
1	Array	Pole-dipole
2	Electrode specification	Small electrode (6 inch of length & 2 mm of diameter)
3	Electrode spacing	0.17 m (170 mm)
4	Total number of electrode	42 (in line electrode: 41 & remote: 1)
5	Total jumper cable	42

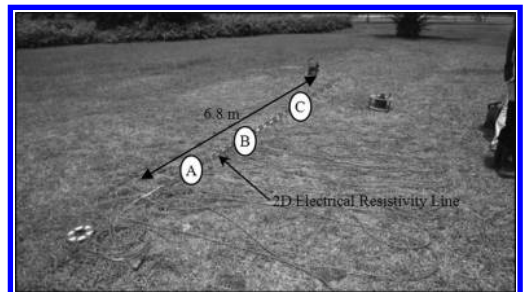


Figure 1. 2D resistivity data acquisition in progress and position of FDT.

resistivity survey for Field Density Test (FDT) using sand replacement method. Then, disturbed soil samples obtained from FDT was taken to the geotechnical laboratory for further laboratory study.

After completing the fieldwork task, laboratory experimental work was performed through classification and electrical resistivity soil box test. Soil classification test was performed using Particle Size Distribution (PSD) test specifically adopting the dry and wet sieve techniques. These tests were conducted as specified in BS1377 1990. Four number of PSD test was conducted based on soil samples at point A, B, C and a mixture of A, B and C soil. Then, laboratory electrical resistivity test was performed in a soil box test using specifically a Nilsson's soil resistance meter and Miller's soil box apparatus. A total of 1500 gram of oven dried soil samples was used for the soil box test. The process started by mixing an original mass of 1500 gram of oven dried soil with 2% of distilled water (30 ml) thoroughly. The soil box test was performed under dense condition assumption in order to match the site condition which was originally a dense soil. For dense condition, the soil needs to be compacted using a rammer with a fully flat wooden plate that was fully fitted and placed inside the soil box. The ramming process was completed step by step in three layers where each layer was compacted with a consistent energy from 27 impacts in order to determine the best uniform dense soil. After that, the soil electrical resistance was measured using the devices. The weight of the soil sample from the box was taken for immediate density determination after the soil electrical resistance was measured. The whole process of soil box test was continuously repeated 25 times.

Finally, data processing and analysis was performed in three stages as (1) the application of statistical analysis (Statistical Product and Service Solutions: SPSS and Microsoft Excel), (2) the analysis of field resistivity data using RES2DINV software of Loke et al. (2003) and (3) the interpolation of field and lab ERV and density in order to established a field ERV correction factor, c based on lab ERV.

3 RESULTS AND DISCUSSIONS

Three point of field ERV was extracted from the 2D Electrical Resistivity Tomography (ERT) based on the exact point of soil samples being taken for laboratory experiment. It was found that the highest field ERV was located at point A (46 Ωm) followed by point C (38 Ωm) and B (29 Ωm) respectively. The result of 2D resistivity section performed from the fieldwork and the location of data being extracted was given in Figure 2.

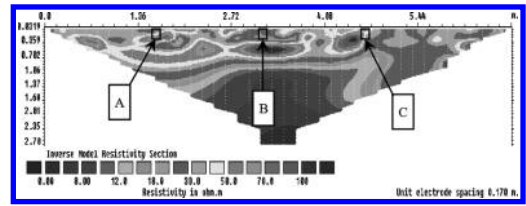


Figure 2. 2D ERT with location of ERV data extraction (based on location of FDT).

Sieve analysis showed that the soils were classed as Clayey SILT. It was found that the soil tested was dominated by fine grained soil. Majority of soil particle consisted of silt and clay followed by sand and gravel respectively. Particle size distribution curve and individual soil particle quantity obtained from the test was analyzed and are presented in Figure 3 and Table 2. Soil bulk density (ρ_{Bulk}) found at point A (1.69 Mg/m^3) was the highest followed by point C (1.55 Mg/m^3) and B (1.52 Mg/m^3) respectively.

The laboratory soil box resistivity experiment was performed using a mixed soil (soil A–C) due to the simplification and similarity of the soil type (Clayey SILT) which was deduced from the tests as presented in Figure 3 and Table 2. It was found that the lab ERV started to be recorded at 5600 Ωm (highest record) with ρ_{Bulk} of 1.16 Mg/m^3 while the lowest lab ERV was found to be at 14 Ωm for ρ_{Bulk} of 1.59 Mg/m^3 . All record for the lab ERV and its ρ_{Bulk} are given in Table 3. A series of ρ_{Bulk} versus ERV data was plotted using a statistical spreadsheet which demonstrated that the ERV gradually decreased with increasing value of ρ_{Bulk} in a curvilinear manner as shown in Figure 4. Lab ERV was recorded for 25 number of data due to the lowest consistent data recorded. According to statistical correlation, r analysis performed using SPSS, the r value was found to be 0.471 which indicated that the correlation level between ERV and ρ_{Bulk} was of medium strength level which further verified that the correlation between ERV and ρ_{Bulk} was acceptable. According to Yahaya et al. (2008), the strength of r can be defined to be medium when the r -value varied from 0.40 – 0.59. Then, the coefficient of determination, R^2 was determined to be 0.7882 which indicated that the data correlation was good being near to the value of 1.0. Hence, all statistical analysis showed that the lab ERV data has a good correlation to the soil density ρ_{Bulk} , as derived from the statistical equation given by $\rho_{\text{Bulk}} = 1.9008\rho^{-0.072}$. All statistical findings are presented in Table 4 and Figure 4.

This study has demonstrated that the ERV from lab and field are showing different values creating disillusionment for related parties. Basically,

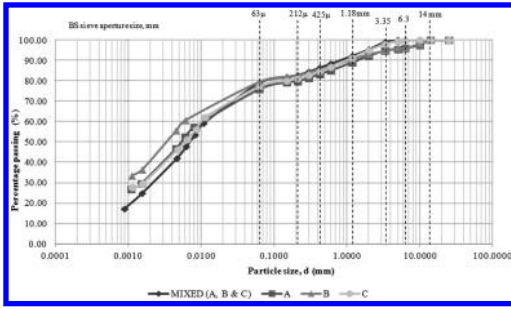


Figure 3. PSD curve for all soil samples.

Table 2. Quantification of soil particle of all soil tested.

Soil sample	Material	Quantity, %	Quantity, %
A	Gravel	7.85	24.19
	Sand	16.34	
	Silt	46.22	75.81
	Clay	29.59	
B	Gravel	6.85	20.51
	Sand	13.66	
	Silt	43.12	79.49
	Clay	36.37	
C	Gravel	5.12	22.86
	Sand	17.74	
	Silt	47.58	77.14
	Clay	29.56	
A-C	Gravel	4.59	21.10
	Sand	16.51	
	Silt	54.08	78.90
	Clay	24.82	

this factor occurred due to the different geometry factor, K used for the field and lab measurements. The value of apparent ERV (ρ_a) was greatly influenced by K factor applied in every measurement. Geometry factor, K describes the geometry of the electrode configuration used in data acquisition. Apparent resistivity (ρ_a) is ERV estimated based on half-pace geometry assumption which refers to the field ERV. According to Telford et al. (1990), apparent resistivity will be equal to the true resistivity provided the current and configuration was applied over the homogeneous isotropic ground. Lab ERV was determined using soil box apparatus with simple geometry factor as given in Equation 1. Field ERV was determined using Pole-dipole array with a geometry factor as given in final Eq. 2 which is derived from basic Equations. 3 and 4. Pole-dipole geometry factor, K used in this study was derived from Equation 4 based on basic four electrode system of measurement. The schematic diagram of Lab and field resistivity

Table 3. Laboratory data of ERV and ρ_{Bulk} .

Lab ERV, ρ (Ωm)	Bulk density, ρ_{Bulk} (Mg/m^3)
5600	1.16
2000	1.18
1100	1.20
800	1.16
380	1.19
250	1.19
160	1.17
100	1.21
80	1.28
58	1.29
40	1.36
31	1.44
21	1.64
19	1.68
18	1.63
19	1.63
16	1.65
16	1.58
17	1.54
15	1.61
14	1.69
15	1.57
15	1.54
14	1.59
14	1.59

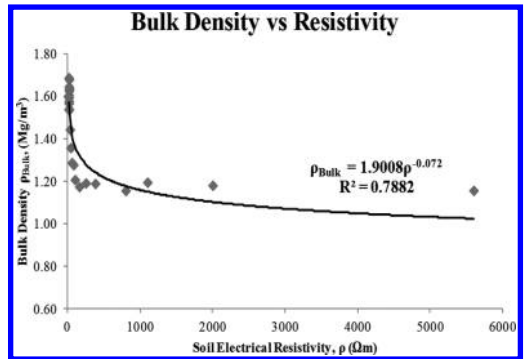


Figure 4. Laboratory ρ_{Bulk} versus ERV.

Table 4. Summary of statistical analysis.

Correlation (r)		Coefficient of determination (R^2)	Equation
Resistivity (ρ)	Bulk density, ρ_{Bulk} (Mg/m^3)	Bulk density, ρ_{Bulk} (Mg/m^3)	ρ_{Bulk}
1.0	-0.471	0.7882	$1.9008\rho^{-0.072}$

configuration was given in Figure 5 and Figure 6 while the schematic diagram for the four electrode system is given in Figure 7.

$$\rho = (A/L) * (R) \quad (1)$$

where R is a resistance term given by $R = \Delta V/I$, A/L is geometry factor, K of current and potential

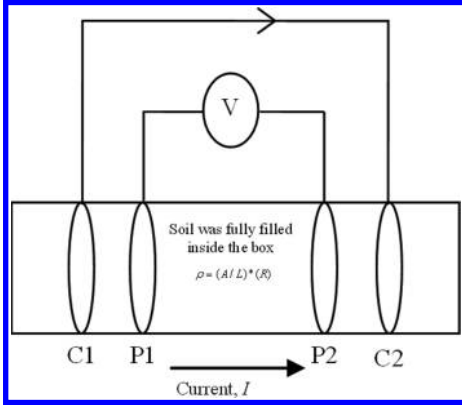


Figure 5. Soil box resistivity measurement involving its simple geometry factor, K.

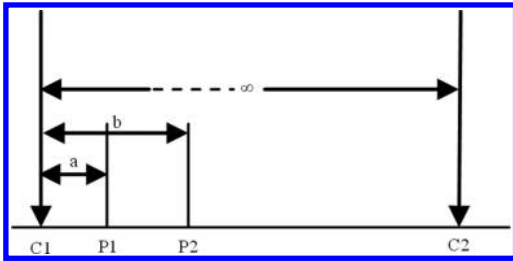


Figure 6. Pole-dipole electrode array used in field measurement.

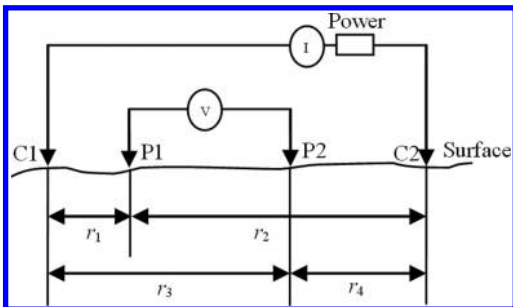


Figure 7. Four electrodes on the surface of homogeneous isotropic ground of resistivity.

in soil box apparatus, A is area of the conducting material and L is material length

$$\rho_a = ((2\pi ab)/(b-a)) * R \quad (2)$$

where R is a resistance term given by $R = \Delta V/I$

$$\rho_a = K * (R) \quad (3)$$

where R is a resistance term given by $R = \Delta V/I$, K is geometry factor based on pole-dipole electrode configuration

$$\rho_a = ((2\pi \Delta V/I)) * ((1/(1/r_1 - 1/r_2) - (1/r_3 - 1/r_4))) \quad (4)$$

where $K = ((1/(1/r_1 - 1/r_2) - (1/r_3 - 1/r_4)))$ and will be defined as a pole-dipole electrode geometry when one of the current electrodes is fixed at a greater distance away from the other three (substitute $r_1 = a, r_3 = b, r_2 = r_4 = \infty$ into equation of K).

Each array used in practice such as Wenner, Schlumberger, Pole-dipole, Dipole-dipole, etc has a different K value. Basically, any of the ρ_a was derived based on Eq. 4. As a result, the apparent resistivity (ERV) calculated from the electrical resistivity measurement is not the same due to the different K value. Hence, it was intrinsically clear that the ERV obtained from different scales using different types of arrays will produce a dissimilar ERV. The ERV was largely influenced by types of array used due to the different geometry factor (K) derived from each different types of array being applied (Abidin 2014 & 2013). Other factors which contribute to the dissimilar of ERV were the ge-materials physical and chemical influence. According to Griffith et al. (1991), resistivity value is highly influenced by water concentration and lithology variations. However this factor can be considered as a secondary factor since the main factor which causes the dissimilar ERV was strongly caused by a different type of array used. However, if the scale and type of array used was similar, then the ge-materials physical and chemical factor will possibly take a big role for influencing the ERV.

Both ERV lab and field scale was possibly being linked and correlated using moisture content interpolation in order to produce a correction factor, c which able to balanced the dissimilarity value of lab and field ERV. Soil bulk density measurement was considered similar for both scales of ERV measurement which able to be used as a guidance to correct the field ERV. As stated in previous section, the main aim of this study was to discover a new technique of electrical resistivity method which able to contribute for basic geotechnical properties determination as particular reference to soil density, ρ based on correlation of lab and field ERV. In order to achieve the aim of study,

Table 5. Correction factor, c of field ERV derive from the field and lab data.

Soil sample	A	B	C
Field ERV, ρ (Ωm)	46	29	38
Lab ERV, ρ (Ωm)	14	31–21	31–21
Field soil density, ρ_{Bulk} (Mg/m^3)	1.69	1.52	1.55
Lab soil density, ρ_{Bulk} (Mg/m^3)	1.69	1.44–1.64	1.44–1.64
Correction factor, c	3.29	1.07	1.49
Average correction factor, c	1.94		

the correction factor, c , has been established via corrected field ERV based on field and lab ρ_{Bulk} interpolation. This study found that the correction factor, c for field ERV of Clayey SILT was 3.29 Ωm (Point A), 1.07 Ωm (Point B) and 1.49 Ωm (Point C). Hence, the average c for Clayey SILT was found to be 1.94 Ωm . The summary of all c values and its related data analysis are given in Table 5. Finally, this study has established an alternative technique to determine the soil density using corrected field ERV based on lab ERV. The determination of soil density was being envisaged using the prediction equation produced by the statistical analysis as shown in Figure 4.

This study has demonstrated that the electrical resistivity method proves to have good prospects in determining basic geotechnical property correlations statistically. Prediction of soil density can easily be determined in the laboratory and field (using correction factor, c) which enables the engineers in less time, low cost and large number of data. In other words, the soil density value can be easily determined using laboratory or field (with use of an appropriate correction factor, c) resistivity method. This technique also can contribute to the enhancement of anomaly interpretation which is traditionally too much relative based on stand-alone qualitative approach. Methods are insufficient to stand alone in order to provide solutions to particular problems (Benson et al. 2003, Fraiha & Silva 1994). This technique was applicable to assist and improve the confidence level of conventional geophysical anomaly interpretation due to its ability to produce soil density value quantitatively. Geotechnical property quantification is an important factor for geophysical method used in engineering application (Kibria & Hossain, 2012). Hence, the reliability of traditional anomaly interpretation and conclusion can be increased using supported additional numerical data with particular reference to soil density value.

4 CONCLUSION

The ERV from field and laboratory scale was successfully performed on Clayey SILT soil. This study has discovered that the integration of ERV from lab and field scales can be a meaningful contribution since it was applicable to predict field and lab soil density parameter using numerical correlation with the application of field ERV correction factor (field scale). However, the ERV was largely influenced by geometry factor, K derived for each array used with different scale of measurement. This study has reduced few of the black boxes (uncertainties) through some of the basic resistivity theory presented.

ACKNOWLEDGEMENTS

This work was funded by Universiti Tun Hussein Onn Malaysia (ERGS from vote 40). First author wish to acknowledge gratefully to supervisors and research members for their tremendous guidance, work and cooperation.

REFERENCES

- Abidin, M.H.Z. Ahmad, F. Wijeyesekera, D.C. Saad, R. & Baharuddin, M.F.T. 2013. Soil Resistivity Measurements to Predict Moisture Content and Density in Loose and Dense Soil. *Applied Mechanics and Materials* 353–356: 911–917.
- Abidin, M.H.Z. Ahmad, F. Wijeyesekera, D.C. Saad, R. & Baharuddin, M.F.T. 2014. The Influence of Electrical Resistivity Array on its Soil Electrical Resistivity Value. *Applied Mechanics and Materials* 510: 185–192.
- Abidin, M.H.Z. Wijeyesekera, D.C. Saad, R. & Ahmad, F. 2013. Soil Resistivity Influence due to the Different Utilization of Electrical Resistivity Array. *Electronic Journal of Geotechnical Engineering* 18: 5643–5654.
- Benson, R.C. Yuhr, L. & Kaufmann, R.D. 2003. Some considerations for selection and successful application of surface geophysical methods, *The 3rd International Conference on Applied Geophysics*, 2003.
- British Standard 1377:1990. Methods of test for Soils for Civil Engineering Purposes.
- Clayton, C.R.I. Matthews, M.C. & Simons, N.E. 1995. *Site Investigation*. UK: Blackwell Science Ltd.
- Cosenza, P. Marmet, E. Rejiba, F. Jun Cui, Y. Tabbagh, A. & Charlery, Y. 2006. Correlations between geotechnical and electrical data: A case study at Garchy in France. *Journal of Applied Geophysics* 60: 165–178.
- Fragaszy, R. Santamarina, J. Amekudzi, A. Assimaki, D. Bachus, R. Burns, S. Cha, M. Cho, G. Cortes, D. Dai, S. Espinoza, D. Garrow, L. Huang, H. Jang, J. Jung, J. Kim, S. Kurtis, K. Lee, C. Pasten, C. Phadnis, H. Rix, G. Shin, H. Torres, M. & Tsouris, C. 2011. Sustainable development and energy geotechnology — Potential roles for geotechnical engineering. *KSCCE Journal of Civil Engineering* 15: 611–621.

- Fraiha, S.G.C. & Silva, J.B.C. 1994. Factor analysis of ambiguity in geophysics. *Geophysics*, 59: 1083–1091.
- Godio, A. Strobbia C. & Bacco, G. De. 2006. Geophysical Characterisation of a Rockslide in an Alpine Region. *Engineering Geology* 83: 273–286.
- Griffiths D.H. & King, R.F. 1981. *Applied Geophysics for Geologist and Engineers: The Element of Geophysical Prospecting*. Oxford: Pergamon Press.
- Hossain, J. Khan, M.S., Kibria, G. & Hossain, M.S. 2012. Determination of Moisture Content and Unit Weight of Clayey Soil Using Resistivity Imaging (RI). *Geo-Congress* 3398–3407.
- Khatri, R. Shrivastava, V.K. & Chandak, R. 2011. Correlation between vertical electric sounding and conventional methods of geotechnical site investigation. *International Journal of Advanced Engineering Sciences and Technologies* 4: 042–053.
- Kibria, G. & Hossain, M. 2012. Investigation of Geotechnical Parameters Affecting Electrical Resistivity of Compacted Clays. *Journal of Geotechnical and Geoenvironmental Engineering* 452: 1520–1529.
- Liu, C. & Evett, J.B. 2008. *Soils and Foundation*. Singapore: Pearson International.
- Loke, M.H. Acworth, I. & Dahlin, T. 2003. A comparison of smooth and blocky inversion methods 2-D electrical imaging surveys. *Exploration Geophysics* 34(3): 182–187.
- Mauritsch, H.J. Seiberl, W. Arndt, R. Römer, A. Schneiderbauer, K. & Sendlhofer G.P. 2000. Geophysical Investigations of Large Landslides in the Carnic Region of Southern Austria. *Engineering Geology* 56: 373–388.
- Pozdnyakova, A. & Pozdnyakova, L. 2002. Electrical fields and soil properties, *Proceedings of 17th World Congress of Soil Science*. 2002.
- Siddiqui, F.I. & Osman, S.B.A.B.S. 2012. Integrating Geo-Electrical and Geotechnical Data for Soil Characterization. *International Journal of Applied Physics and Mathematics* 2: 104–106.
- Telford, W.M. Geldart, L.P. & Sheriff, R.E. 1990. *Applied Geophysics*. Cambridge: Cambridge University Press.
- Yahaya, A.S. Ahmed, A. Gabda, D. & Na, C.S. 2008. *Problem and Solution in Statistics for Engineers and Scientist*. Selangor: Prentice Hall.

Structural behaviour of *Kekotong* glued laminated timber railway sleepers under ‘sleepers static performance test’

M.B. Norshariza & A. Abu-Bakar

Faculty of Civil Engineering, Universiti Teknologi MARA, Shah Alam, Selangor, Malaysia

Z. Ahmad

Institute of Infrastructure Engineering and Sustainability Management (IIESM), Universiti Teknologi MARA, Shah Alam, Selangor, Malaysia

P. Tahir

Institute of Tropical Forestry and Forest Product (INTROP), Universiti Putra Malaysia, Serdang, Selangor, Malaysia

ABSTRACT: Due to limited supply of large sections of solid timber for the production of railway sleepers, this study has initiated the use of glued laminated timber (glulam). This paper presents the structural behavior of the glulam timber sleepers made from selected Malaysian tropical timber namely *Kekotong*. In order to verify the performance of this glulam as railway sleepers, a series of test were conducted to determine the ultimate load test at rail seats and center of sleepers followed by performance tests under static bending in accordance with the American Railway Engineering and Maintenance-of-Way (AREMA) Manual and the results were then checked with the required mechanical properties set by the Malaysian Timber Industry Board (MTIB) for timber sleepers. The results showed that the *Kekotong* glulam sleepers complied with the requirement set by AREMA Manual for timber sleepers and the mechanical properties obtained exceeded the performance requirement values set by MTIB.

Keywords: glulam; heavy hardwood; performance test; timber sleeper; ultimate load

1 INTRODUCTION

Timber railway sleepers are one of the common sleepers used in railway track system. In a form of solid sawn rectangular cross-section, timber railway sleepers act as a beam located in between the rails and the ballast. The function of this component is to support the track loading and to distribute the oncoming load to the ballast (Mundrey, 2010). As the oldest material used in railway track, its capability in terms of workability, adaptability, good in absorbing damping and shock (Manalo, 2011) is better compared to Pre-Stressed Concrete (PSC) and steel sleepers.

There are more than 2.5 billion timber sleepers installed worldwide (Ets Rothlisberger SA, n.d.). As reported by Malaysian railway authority, *Keretapi Tanah Melayu Berhad* (KTMB), 26.4% from a total track length of 1724.50 km are installed with timber sleepers and the remaining are PSC sleepers (Norshariza, Ahmad, Bakar, & Tahir, 2013). Although the number of timber sleepers used in Malaysian railway track is getting less,

their demand in certain location is high such as at bridges, tunnels, stations, yard and industrial lines and at the soil area contributing extreme shocks and excessive force to the locomotives and sleepers (International Union of Railways (UIC), 2013; Mohamed, pers.comm).

The availability of good quality timber logs from higher Strength Groups (SG) such as SG1 and SG2 which are naturally durable with large diameter are limited and initiated the increasing in timber log price. The used of non-durable timber which is not properly treated resulting decreasing in its life span during services. With the above situations, the alternative to replace the solid timber sleepers is necessary and this has spurred the use of engineered timber products which is glued laminated timber or glulam.

This engineered timber product had been used as railway sleepers for many years on limited scale (Gong, Delahunty, Chui, & Li, 2013) but the timber used are from softwood and hardwood timber from European countries and Brazil. Studies have shown that the performance of glulam timber

railway sleepers is good compared to solid sawn timber sleepers (Carrasco, Passos, & Mantilla, 2012; Gallery, Gauntt, & Webb, 2000; Gong et al., 2013).

As Malaysia also facing shortage of large diameter logs for railway sleepers, therefore this study investigated the potential of glulam produced using Malaysian tropical hardwood timber species namely *Kekotong* (*Cynometra spp.*) in replacing solid timber sleepers. In earlier studies by authors (Norshariza et al., 2013) on the mechanical properties of glulam made from Malaysian tropical hardwood timbers showed that the strength properties of glulam is almost similar than that the strength properties of solid timber of the same species at the rail seats of sleepers.

As a new railway sleeper product, glulam timber railway sleeper which is manufactured by gluing together the individual pieces under controlled manufacturing conditions need to be verified under performance test as stipulated in the American Railway Engineering and Maintenance-of-Way Association (AREMA) Manual, 2012 (AREMA, 2012). Besides, the glulam timber railway sleepers are required to comply with criteria set by the Malaysian Timber Industry Board, MTIB (The Malaysian Timber Industry Board, n.d.) which stated that the timber must have Modulus of Elasticity (MOE) not less than 8132 N/mm². Therefore, this study is aimed to evaluate the structural behavior of *Kekotong* glulam timber railway sleepers under performance test as stipulated in (AREMA, 2012).

2 MATERIAL

Kekotong (*Cynometra spp.*) species was selected as prototype of glulam timber railway sleepers in this study. This timber species is one of species listed for railway sleepers in KTMB Technical Specifications (2005). This species was selected also based on the timber availability having SG2.

The glulam was manufactured at glulam factory in Johor Bahru. The timbers were visually graded in accordance with MS 1714: 2003 by MTIB grader and only timbers in HS grade were chosen.

The production of glulam was done in accordance with MS758:2001.

The timbers are naturally durable, untreated and suitable for outdoor environment conditions (MS 544: Part 2, 2001). Six (6) numbers of each *Kekotong* solid and glulam timber sleepers with sized 254 mm × 127 mm × 2000 mm length (KTMB, 2005) were prepared. The production of glulam timber sleepers were taken from normal and controlled manufacturing processes and Phenol-Resorcinol Formaldehyde (PRF) adhesive was used as recommended in MS758: 2001.

3 EXPERIMENTAL WORKS

3.1 *The ultimate strength at rail seat and center of sleepers (Phase 1)*

In Phase 1, the solid and glulam sleepers were tested in bending for determining the Modulus of Elasticity (MOE), Modulus of Rupture (MOR) and ultimate load at rail seats and center of the sleeper. However, the bending strength properties at rail seats has been reported in (Norshariza et al., 2013) and used in this study for performance test in Phase 2.

For bending test at the center, two (2) replicates each of solid timber and glulam timber sleeper were used. The three-point static bending test was setup in accordance with AREMA Manual (AREMA, 2012). The universal testing machine IPC 1000 kN capacity was used. The sleeper was loaded under a displacement control of 0.02 mm/sec (Norshariza et al., 2013). The load was applied until the tested sleepers totally failed. The first crack load at rail seat, P_1 ; first crack load at center, P_2 and; ultimate load, P_{max} were recorded and any structural cracks were inspected. Then, the MOE and the MOR for solid and glulam sleepers were computed. Table 1 shows the results of these tests.

3.2 *The performance test of Kekotong glulam timber railway sleepers (Phase 2)*

The performance test is a test required to evaluate whether the sleepers comply with requirements set by AREMA Manual. This manual was referred

Table 1. The average test results of ultimate strength of *Kekotong* solid and glulam timber sleepers.

Type of sleepers		P_{ult} (KN)	Δ_{max} (mm)	P_y (kN)	Δ_y (mm)	MOR (N/mm ²)	MOE (N/mm ²)	Density (kg/m ³)	Moisture content (%)
Kekotong solid	Rail seats	406.63	20.60	246.51 (P_1)	11.98	115.71	18533.72	1577.98	17.84
	Center	181.42	31.97	135.72 (P_2)	23.75	106.94	21459.65		
Kekotong glulam	Rail seats	431.04	15.92	389.65 (P_1)	13.00	111.87	30890.35	1629.40	9.69
	Center	146.86	27.31	111.61 (P_2)	15.97	80.44	21210.33		

because in the manual there is specification for engineered timber sleepers. In the absence of detailed procedures for conducting performance test for timber sleepers, the standard performance test for Pre-Stressed Concrete (PSC) sleepers was modified (Hamzah & Din, 2008). A series of flexural tests were conducted on the sleepers at the rail seats for negative and positive moments, as well as flexural test at the center of the sleepers for negative bending moment. These tests were conducted on the same sleepers.

The positive moment test setup was referred when the load was applied at the top of sleeper and the negative moment setup was referred when the load was applied at the bottom side from previous location. For the static bending test at the center of sleepers, only the test under negative moment was required since the shape and dimensions was similar at the top and bottom center (AREMA, 2012).

The load was applied at rail seat A, incrementally from zero to P_1 (see Table 1) under static bending at positive moment. The respective load was continuously applied to the test sample for three minutes. After that, the test sample was inspected for any structural crack. The test sample would comply with the requirement if there was no structural crack observed. Then, the test was repeated under the negative moment at the same rail seat (Seat A) with applied the load of P_1 .

The procedure was repeated for the static bending test at center for negative bending moment where the load was increasing from zero to P_2 (see Table 1). After the center bending test, the same procedures were repeated at rail seat B of the same sleepers.

3.3 Moisture content test and density of timber (Phase 3)

The test samples for moisture content and density were cut from the full cross-section with a thickness

of 25 mm after the ultimate strength test and the performance test. The moisture content and density were determine by oven-dry method (MS 837, 2006).

4 RESULTS AND DISCUSSIONS

4.1 The ultimate strength of the MOR and MOE of Kekatong solid and glulam timber sleepers

The strength performances were compared between the solid and glulam timber sleepers at the rail seats and at the center. These values were then verified with the performance requirement stipulated in the AREMA Manual and checked with the MTIB criteria. Table 1 and Figure 1 show the summary of the test results of ultimate strength at the rail seats and center of sleepers, and the graph of the load against the displacement respectively. From the results, the glulam timber sleepers at the rail seats has marginally higher load (6%) compared with solid timber sleepers. While at the center of sleepers the ultimate load of solid timber shows 23.5% higher than that of the glulam timber sleepers. Even though the difference of the ultimate load for solid timber sleepers shows a greater value at the centre, yet the ultimate load at the rail seats is much concerned since the wheel load is loaded at this location. Thus, glulam timber sleepers have the potential to replace solid timber sleepers. The displacement at maximum load, Δ_{max} (Table 1) and the area under the graph (Fig. 1) of solid timber sleepers at the rail seat and center of sleeper are slightly higher than the displacement and area under the graph of glulam timber sleepers. This indicates that the solid timber sleepers able to absorbed more energy and sustained a longer time before failure.

The design wheel load for normal train loading subjected to the rail seats is 120 kN (Mohamed, 2012). The displacement at 120 kN design load for

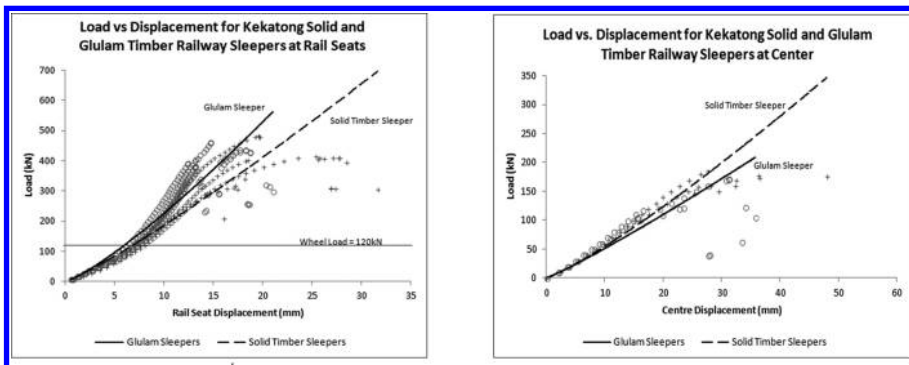


Figure 1. The flexural strength of timber sleepers at; (A) rail seats; (B) center.

both sleepers were compared with the average first crack load, P_y as highlighted in Figure 1(a). It was found that the displacement for solid timber sleepers (7.44 mm) is higher than the displacement for glulam timber sleepers (6.81 mm) at 120 kN design wheel load. The displacement at P_y for solid timber sleepers and glulam timber sleepers are reached about 61.02% and 90.9% higher than displacement at design load respectively. This means that glulam timber sleepers provide greater allowance before reached the P_y from the design load.

Table 1 gives an average value of the MOR and MOE. For bending at rail seat, the average MOR value for the glulam timber sleepers is close to the MOR of solid timber sleepers with percentage difference of 3.4%. However, the average MOR value for the solid timber sleepers at the center is almost 32.9% higher than the MOR of the glulam timber sleepers. The high differences in MOR for glulam timber sleepers be due to the longer span length and may contained numerous finger joints. However, both types of timber sleepers showed the MOR value exceeded the performance requirement of AREMA with MOR, 66.9 N/mm² (AREMA, 2012).

The average MOE value for glulam timber sleepers is higher than the MOE for solid timber sleepers at the rail seats, and almost similar at the center of the sleepers. The MOE value is more critical at the center of sleepers in the condition of unpacked ballast. According to AREMA and MTIB requirement, the MOE must be equal or higher than 11700 N/mm² and 8132 N/mm² respectively (AREMA, 2012; The Malaysian Timber Industry Board, n.d.). The MOE values found in this study for both solid and glulam timber sleepers were exceeded those requirements.

4.2 The crack pattern

This section discussed the crack behavior of sleeper at the rail seat and center of the sleeper. For solid and glulam timber sleepers at rail seats, the failure mode is in combination of bending and shearing. Solid timber sleeper generally showed simple tension failure type where the failure started at the soffit of the beam and then moved along the longitudinal grain. This types of failure normally occurred in dense timber (Bodig & Jayne, 1982).

As for glulam timber sleepers, the crack initiated at the finger joint in the tension zone. The cracks slowly propagated until it reached the weaker zone at upper lamella. Then, the cracks continued to the compression zone. However, the picture of crack pattern at the rail seat are shown in previous study (Norshariza et al., 2013). Figure 2 and Figure 3 show the crack pattern at the center of timber sleepers and the behavior of crack is similar as in the rail seat.

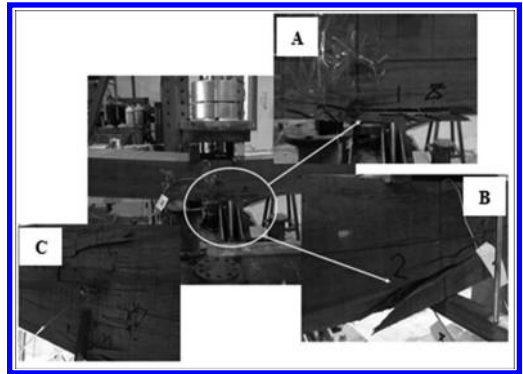


Figure 2. Solid *Kekatong* timber railway sleepers at the center showing; (A) failure at the tension zone; (B) cracks propagated toward the compression zone; (C) failure at bottom view of solid timber sleepers.

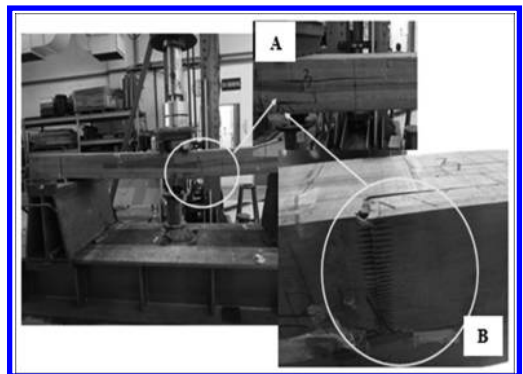


Figure 3. Glulam *Kekatong* timber railway sleepers at center showing; (A) failure started at finger joint at the lowest lamella and cracks propagated to the nearer finger joints and continually toward the compression zone; (B) failure at bottom view of glulam timber sleepers, failure at the finger joint.

4.3 The performance test of *Kekatong* solid and glulam timber sleepers

In this performance test, two (2) replicates each of solid and glulam timber sleepers were used. As followed the test procedures in AREMA (2012), both types of timber sleepers are complied with the performance requirement in AREMA (2012) with no structural cracked occurred during the static test.

5 CONCLUSIONS

From the study, the results show the glulam timber sleepers at the rail seats can sustained more load compared to the solid timber sleepers. However,

at the center of the timber sleepers, the ultimate load of solid timber sleepers is higher. Since at the rail seats are the loaded area for the wheel of train or locomotive, thus the glulam timber sleepers show good response. Both types of timber sleepers surpassed the design wheel load of 120 kN with higher percentage difference in displacement before reaching the first crack load. The average MOR and MOE values in this study exceeded the required value in the AREMA Manual and the MTIB criteria. In the static performance test, both types of timber sleepers show no cracks occurred and complied with the performance requirement. Further investigation on the performance test under flexural fatigue test will be conducted and the information from this study will be useful as references.

ACKNOWLEDGEMENT

The provision of glulam and solid timber railway sleepers by Woodsfield Timber Industry (M) Sdn. Bhd. and supported documents by *Keretapi Tanah Melayu Berhad* (KTMB) are gratefully acknowledged. The funding of this project is from Malaysian Timber Industry Board and Universiti Teknologi MARA. The authors wish to thank the laboratory technicians of Civil Engineering Faculty for their assistance.

REFERENCES

AREMA. 2012. *Chapter 30, Volume 1—Ties, The American Railway Engineering and Maintenance-of-Way Association (AREMA) Manual for Railway Engineering*. USA: Washington.

Bodig, J., & Jayne, B.A. 1982. *Mechanics of wood and wood composites*. New York, USA: Van Nostrand Reinhold Company Inc.

Carrasco, E.V.M., Passos, L.B., & Mantilla, J.N.R. 2012. Structural behavior evaluation of Brazilian glulam wood sleepers when submitted to static load. *Construction and Building Materials*, 26(1): 334–343.

Ets Rothlisberger SA. n.d. History and development of the wooden sleeper. Retrieved February 26, 2012, from www.corbat-holding.ch.

Gallery, D., Gauntt, J.C., & Webb, D.A. 2000. Progressively Engineered Hybrid Wood Crossties For The Next Century. In *The Roadmaster's Conference Proceedings of American Railway Engineering & Maintenance-of-Way Association*. AREMA.

Gong, M., Delahunty, S., Chui, Y.H., & Li, L. 2013. Use of low grade hardwoods for fabricating laminated railway ties. *Construction and Building Materials*, 41: 73–78.

Hamzah, S.H., & Din, K. 2008. Appraisal of used wooden railway sleeper. *Journal of Engineering Science and Technology*, 3(3): 224–233.

International Union of Railways (UIC). 2013. *Sustainable wooden railway sleepers*. France.

KTMB. 2005. *Technical Specifications*. Malaysia: Keretapi Tanah Melayu Berhad.

Manalo, A. 2011. *Behaviour of Fibre Composite Sandwich Structures: A case study on railway sleeper application*. PhD Thesis. University of Southern Queensland.

Mohamed, A.R. 2012. *Engineer of Permanent Way, KTMB in personal communication*.

MS 1714. 2003. *Specification for visual strength grading of tropical hardwood timber*. Malaysia: Department of Standards Malaysia.

MS 544: Part 2. 2001. *Code of practice for structural use of timber—Permissible stress design of solid timber*. Malaysia: Department of Standards Malaysia.

MS 758. 2001. *Glued laminated timber—Performance requirements and minimum production requirements (First revision)*. Malaysia: Department of Standards Malaysia.

MS 837. 2006. *Solid timber—Determination of moisture content (First revision)*. Malaysia: Department of Standards Malaysia.

Mundrey, J.S. 2010. *Railway Track Engineering* (4th ed.). New Delhi: Tata Mc Graw Hill Education Private Limited.

Norshariza, M.B., Ahmad, Z., Bakar, A.A., & Tahir, P. 2013. Ultimate Strength of *Kekatang* Glued Laminated Timber Railway Sleepers. In R. Hassan, M. Yusoff, Z. Ismail, N. Mohd Amin, & F. Mohd Arshad (Eds.), *The International Civil and Infrastructure Engineering Conference 2013*: pp. 97–105. Springer.

The Malaysian Timber Industry Board. n.d. *Malaysian Wooden Railway Sleepers*. Kuala Lumpur: MTIB.

Vibration control of stay cable with double Tuned Mass Damper

S. Luo, W. Liu & Z.S. Deng

Guangdong Communication Polytechnic, Guangzhou, P.R. China

ABSTRACT: This paper improved the double Tuned Mass Damper (TMD) system to reduce the frequency sensitive problem of single TMD system. In the mitigation model, as a rule of thumb, we placed two identical TMD on a stay cable at the three points of division. FEM investigation shows that double TMD system could control the cable vibration problem more efficiently than the single TMD system, and furthermore reduce the frequency sensitive problem.

Keywords: stay cable; vibration control; dynamic characteristics; Tuned Mass Damper (TMD)

1 INTRODUCTION

The vibration of the bridge deck and towers caused by wind, traffic loading or earthquakes produces indirect excitation of stay cables through the motion of their anchorages [1]. In certain circumstance, the induced cable vibrations attain large amplitudes [2]. Kovacs was the first to point out the possibility of parametric vibration under indirect excitation in the cables [3]. Compared with those conventional mechanical dampers, tuned mass dampers are relatively new countermeasures for stay cable vibrations. Tabatabai reported an experimental investigation on TMD performance [4]. Since the effectiveness of single TMD damper is sensitive to the frequency, this paper extends the existing research; a new mitigation strategy named the double TMD. Theoretical investigations for the damper performance on the cable vibration reduction are conducted, which provides the necessary theoretical basis for practical implementation.

2 NUMERICAL INVESTIGATION OF CABLE-TMD SYSTEM

The cable with TMD system was shown in Figure 1. The TMDs on a stay cable were located at the three points of division.

The dimensions and section properties of one cable in the Bill Emerson Memorial Cable-stayed Bridge was given in Table 1.

Numerical calculations are conducted here to investigate and understand the effect of different parameters on the system dynamics. A linear evaluation model is used in the former

benchmark study based on the Bill Emerson Memorial Cable-stayed Bridge [5]. The mass matrices M and stiffness matrices K used in the linear model are those of the structure determined through a static analysis corresponding to the deformed state of the bridge with dead loads [6]. The damping matrices C in the system are defined based on the assumption of modal damping. Then, the dynamic equilibrium equation of cable under load is:

$$M \cdot \ddot{X} + C \cdot \dot{X} + K \cdot X = L \cdot u(t) \quad (1)$$

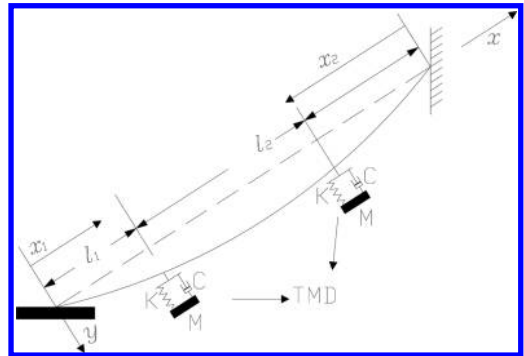


Figure 1. Investigation model for the mitigation system.

Table 1. Initial property of cable.

Area (m ²)	Length (m)	Tension (KN)	Modulus (GPa)	Density (kg/m ³)
0.00808	180.94	7482.38	200	7849.08

In which L is the loading vector, $u(t)$ is the time history of loading. Hence the standard form of system state space equations is:

$$\dot{Y} = \begin{Bmatrix} \dot{X} \\ \ddot{X} \end{Bmatrix} = A \begin{Bmatrix} X \\ \dot{X} \end{Bmatrix} + Bu(t) \quad (2)$$

In which, $Y = \begin{Bmatrix} X \\ \dot{X} \end{Bmatrix}$, $A = \begin{bmatrix} O_n & I_n \\ -M^{-1}K & -M^{-1}C \end{bmatrix}$, $B = \begin{bmatrix} O_n \\ M^{-1}L \end{bmatrix}$, and the output vector is:

$$\begin{Bmatrix} X \\ \dot{X} \\ \ddot{X} \end{Bmatrix} = C \begin{Bmatrix} X \\ \dot{X} \end{Bmatrix} + Du(t) \quad (3)$$

In which $C = \begin{bmatrix} I_n & O_n \\ O_n & I_n \\ -M^{-1}K & -M^{-1}C \end{bmatrix}$, $D = \begin{bmatrix} O_n \\ O_n \\ M^{-1}L \end{bmatrix}$.

In this analysis, as a rule of thumb, we placed two identical TMD on a stay cable at the three points of division. Parameters such as mass, stiffness, and damping of the TMD system were determined as:

Mass of TMD: $M_T = 1.5\% \times m \times L \approx 320 \text{ kg}$

Stiffness of TMD: $K_T = M_T(\omega_d)^2 \approx 2470 \text{ N} \cdot \text{m}^{-1}$.

Damping of TMD is $C_T = 1333 \text{ N} \cdot \text{s} \cdot \text{m}^{-1}$ which determined by dichotomy method in the program. The dynamic equilibrium equation of mitigation system at the located position of TMD (assume the FEM node point number is k) is:

$$\begin{aligned} m_k \ddot{X}_k - [c_k \dot{X}_k + C_T (\dot{X}_k - \dot{X}_T)] \\ - [-k_k X_{k-1} + (k_k + k_{k+1}) X_k \\ - k_{k+1} X_{k+1} + K_T (X_k - X_T)] = 0 \end{aligned} \quad (4)$$

where m_k , c_k , k_k is the mass, damping, and stiffness of cable at node k , and M_T , C_T , K_T is the mass, damping, and stiffness of TMD. Substitute [equation \(4\)](#) into state space [equation \(2\)](#). The acceleration time histories recorded during an earthquake that occurred at 12:37:32 (UTC) on Sunday, 1 May 2005, were taken and analyzed; only deck motion of the bridge was considered. The dynamic response at middle point of cable under the indirect excitation caused by the earthquake is shown in [Figure 2](#) and [Figure 3](#). [Figure 2](#) is about the time history response with single TMD, in which (a) is about displacement, (b) is about velocity, and (c) is about acceleration at middle point; and [Figure 3](#) is about the time history response with double TMD. From the comparison, we could make the

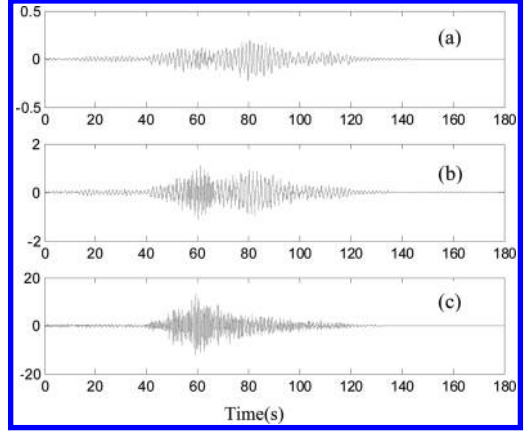


Figure 2. Time history response with single TMD.

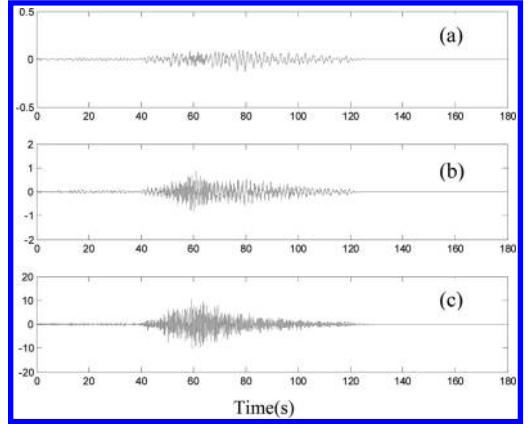


Figure 3. Time history response with double TMD.

following conclusions that double TMD system could control the cable vibration problem more efficiently than the single TMD system.

Since the effectiveness of the linear TMD damper is sensitive to the frequency; cable with double TMD is investigated in this study to broaden the tuning frequency. [Figure 4](#) is the bode diagram of different mitigation strategy. From the figure we could see that when the excitation frequency changes from 0.1–100 rad/s, the steady state response of cable with and without control at peak point is close, which means that the mitigation strategy of double TMD does not change the modal characteristics of cable. At the same time, we can see that single TMD could only control the odd order responsibility of cable, on the other hand, double TMD could damping not only the odd order responsibility of cable but also the even

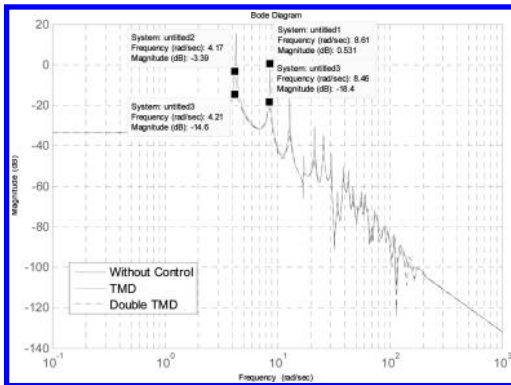


Figure 4. Bode diagram of different mitigation strategy.

order responsibility. Hence the new model matches well with the actual occurrence in bridge engineering. Furthermore, this study improved the double TMD system to reduce the frequency sensitive problem of single TMD system.

3 CONCLUSIONS

From this study, the double Tuned Mass Damper (TMD) system to control stay cable vibration is investigated. From the results of analysis, the dynamic characteristics of the mitigation system can be summarized as following: (1) Double TMD system could control the cable vibration problem

more efficiently than the single TMD system. (2) Double TMD could damping not only the odd order responsibility of cable but also the even order responsibility.

ACKNOWLEDGMENTS

This research is supported by the Guangdong Communication Polytechnic Doctoral Science Foundation (No. GG81080136). These supports are greatly appreciated.

REFERENCES

- [1] B.M. Pacheco, Y. Fujino. Keeping cables calm. *Civil Engineering*. 63(1993), pp. 56–58.
- [2] I. Kovacs. Zur frage der seil-schwingungen und der seildampfung. *Die Bautechnik*. 59 (1982), pp. 325–332(in German).
- [3] B. Pacheco, Y. Fujino, and A. Sulekh. Estimation Curve for Modal Damping in Stay Cables with Viscous Damper. *Journal of Structural Engineering*. 119(1993), pp. 1961–1979.
- [4] H. Tabatabai, A.B. Mehrabi. Tuned dampers and cable fillers for suppression of bridge stay cable vibrations. Final report to TRB IDEA program, Construction Technology Laboratories, Inc, Skokie, Illinois (1999).
- [5] S.J. Dyke, J.M. Caicedo, G. Turan, *et al.* Phase I benchmark control problem for seismic response of cable-stayed bridges. *Journal of Structural Engineering*. 129(2003). pp. 857–873.
- [6] J. Wilson, W. Gravelle. Modeling of a cable-stayed bridge for dynamic analysis. *Earthquake Engineering and Structural Dynamics*, 20(1991), pp. 707–721.

Biomass waste shells analysis and advanced gasification tests

L. Vecchione & Marta Moneti

Dafne, University of Tuscia, Viterbo, Italy

A. Di Carlo

DIMA, University Sapienza, Rome, Italy

E. Bocci

University Guglielmo Marconi, Rome, Italy

ABSTRACT: Cultivation of the hazel and almond is widespread in Italy, especially in those small and medium enterprises that work in the confectionery industry. The residual wastes of these productions are mostly shells, of ligno-cellulosic material, very suitable for combustion. The first aim of this work was to carry out the chemical characterization of such wastes (LHV, C, H, N, O, etc) for their energy exploitation. These analyses were performed in the laboratory CIRDER of Viterbo, in accordance with UNI standards. These wastes were then used in a fluidized bed bench scale gasifier to evaluate the composition of the raw gas (H_2 , CO, CO_2 , CH_4 , TAR) obtained during steam gasification tests. The TAR removal efficiencies of two different methods were finally investigated experimentally: catalytic cracking in a secondary reactor with Ni/ Al_2O_3 and scrubbing with vegetable sunflower oil.

Keywords: gasification; nichel; reforming; shell; TAR; bed fluidized

1 INTRODUCTION

Cultivation of the hazel and almond is widespread in Italy, especially in those small and medium enterprises that work in the confectionery industry. Particularly at the national level, the major producer regions are: Campania (40%), Lazio (33%), Piedmont (14%), Sicilia (10%) [1]. Almonds are instead produced in Sicily (72%), Apulia (25%), and Campania (2%) [1]. Due to the abundance in Italy (156.000 hectares [2]) of these wastes, this work will evaluate how different mixes could be exploited in small scale fluidized bed gasifier, rather than combustion in boilers and anaerobic digestion [3]. The biomass used is a mix composed of 50% of hazelnut shells and 50% of almond shells, each shell is taken from three different samples per each region. The Directive 2009/28/CE-implemented in Italy in 2010- set ambitious targets in order to ensure a clean and sustainable future. Its aim is to reduce greenhouses gases emissions by 20%, to produce 20% of energy from renewable sources and to decrease the consumption by 20% improving the energy efficiency. These goals must be reached by 2020. The above-mentioned regulation led the public administrations and private stakeholders to investigate new technologies which may face the growing energy demands by the use

of renewable sources alternative to fossil fuels. Thus, energy supply might change from being predominantly fossil fuelled to being fuelled by locally available sources. From alternative sources in Italy also advancing geothermal energy, for higher volcanic areas [4,5]. Energetically, biomass seems to be a valid alternative to the use of fossil fuels [6]. The term biomass refers to all organic materials, including biological wastes [7]. The biomass is that produced as a result of the process of chlorophyll photosynthesis with the help of solar radiation, water, and different nutrients. Biomass absorbs CO_2 , which is then released again in the atmosphere after its use as fuel. So at the end of its life cycle the CO_2 balance can be considered zero; the energetic use of biomass could thus reduce the greenhouse effect of the globe. In general biomass can be classified as [8]:

- The residues of agricultural production,
- The residues of forestry production,
- The dedicated cultures, both herbaceous and ligneous,
- The residues of agro-food processing,
- The residues of non-food processing industry.

According to the fifth agriculture census about 156.000 hectares are devoted to these crops with a consequent production of relevant amount of

biomass wastes. The disposal of these wastes is generally a problem for the industry. As indicated by the Legislative Decree 152/2006 residues from agricultural activities are classified as waste and therefore is within the scope of application of Part IV of the “Decreto Ambiente”. Article. 13 of Legislative Decree 205/2010 Italian (amendments to art. 185 of Legislative Decree 152/2006) states that “straw, pruning, mowing and other agricultural or forestry material” are not considered waste when used in agriculture, in forestry or for the production of energy. Thereby excluding the combustion of crop residues without energy production, this activity is configured as waste disposal of agricultural waste and must be submitted to the Italian Environmental Code. The energy use of these biomass residues could therefore involve both environmental and social benefits by promoting a new sector and the development of highly efficient energy conversion devices, with particular regard to emissions into the atmosphere [9]. The gasification process is a thermochemical process that allows the conversion of a solid fuel, biomass, in a gaseous fuel (syngas) usable in ICE and mTG [10]. Among the energy conversion processes of biomass, the used in this work is the fluidized bed gasification, with steam and catalytic cracking of the syngas. This type of gasification is preferable than others because the continuous mixing created within the reactor, brings to a uniform temperature in the bed, a production of syngas with a higher calorific value and because the use of olivine as hot sand, also a primary cracking of the TAR [11]. In the process of gasification biomass is thermally decomposed into syngas with the production of other compounds: char, ash and tar (Topic Atmospheric Residue, TAR) [12]. In this work two different types of residual agricultural biomass were considered, in particular almond and hazelnut shells. The biomass that will be introduced into gasifier is composed of 50% of hazelnut shells and 50% of almond shells. The samples, hazelnuts and almonds, were taken from three Italian regions. The samples were characterized and then used to perform gasification tests in order to verify the composition of the raw gas (in term of H_2 , CO , CO_2 , CH_4 and TAR) and to assess two techniques in series capable to ensure satisfactory TAR removal efficiencies for the use of the gas in cogeneration systems:

- Catalytic cracking/steam reforming in a secondary reactor at 800 °C
- Vegetable sunflower oil as scrubber for absorption tar.

The gasification process, designed to produce of mainly hydrogen and methane, appears to be quite complex and is implemented via use of two reactors. In the first, fluidizing, about 80 cm in

diameter, working at 850 °C with steam, there is the gasification of biomass, after, at the reactor outlet there is the removal of particulate through a particle filter and a cyclone ABB, then the cracking of the syngas product via the second small bed reactor packed catalyst [13]. In the output gas is filtered and sent in the second reactor, which works at 750 °C, where there is a packed bed consisting of 15% nickel supported by a matrix of alumina Al_2O_3 . In this second reactor occur cracking reactions of TAR and catalytic reforming of the syngas, primarily of methane [14]. The gas thus formed is passed through scrubbers vegetable oil and isopropanol cooled to condense the TAR dragged by the gas output and can be analyzed.

1.1 Biomass characterization

The biomass required for the performance of the tests was sampled, in accordance with the UNI EN 14778 and UNI EN 14780 [14,15].

In particular, tests were carried out to determine:

- The moisture content of the samples;
- The ash content;
- The total content of C, H, N, O.

The results of the tests performed on the samples are shown in [Table 1](#), where:

- Mar, moisture calculated on a dry basis as indicated by the UNI EN 14774-1 [16];
- LHV, lower calorific value calculated on a dry basis, as indicated by the UNI EN 14918 [17];
- C, H, N, O content percentage by mass of carbon hydrogen and nitrogen in the sample, determined in accordance with the UNI EN 15104 [18].

For each sample the ash content was also determined, as required by the UNI EN 14775 [19] ([Table 2](#)).

Analyzing the results it was verified that the energy characteristics of the samples are not much influenced by either the area or sampling



Figure 1. Gasifier on laboratory.

Table 1. Biomass analysis.

Shell	$M_{ar}^{0}/_{wt}$	LHV MJ/kg	$C^{0}/_{wt}$	$H^{0}/_{wt}$	$N^{0}/_{wt}$	$O^{0}/_{wt}$
Hazelnut Campania	9.16	20.37	48.66	6.4	1.33	33.44
Hazelnut Lazio	10.58	20.10	48.7	6.14	1.31	32.2
Hazelnut Piedmont	7.64	19.86	48.2	6.12	1.22	35.8
Almond Sicily	8.84	21.62	49.7	6.01	0.53	33.8
Almond Apulia	8.26	21.02	48.6	6.92	1.10	34.1
Almond Campania	7.92	20.92	48.5	6.63	0.95	34.7

Table 2. Ash content % wt.

Shell	Ash % wt. dry basis
Hazelnut Campania	1.71
Hazelnut Lazio	1.85
Hazelnut Piedmont	1.55
Almond Sicily	1.17
Almond Apulia	1.61
Almond Campania	0.92
Mean value	1.47

Table 3. The average values of the prepared sample for the gasification tests.

$C^{0}/_{vol}$	$H^{0}/_{vol}$	$N^{0}/_{vol}$	$O^{0}/_{vol}$	Ash $^{0}/_{wt}$	$M^{0}/_{wt}$	LHV (MJ/kg)
48.75	6.25	1.07	34.03	1.47	8.66	20.65

characteristics of cultivation. The average value of moisture is about 8.66% by mass, the LHV is 20.65 MJ/kg, the carbon content is equal to 48.75%, the hydrogen 6.25% and of nitrogen of 1.07% by weight, and the ash content is 1.47% by weight. The present samples were prepared for the experimental plant gasification. For a correct operation of the gasifier the biomass was triturated with knife mill to a particle size between 1–2 mm. The prepared sample for the test of gasification, has been realized taking 50% by weight of hazelnut shells and 50% of almonds. Table 3 shows the average values of the prepared sample for the gasification tests.

In particular, the low moisture, the small ash content, and the high carbon content of the sample obtained, makes the selected biomass feasible for the gasification process.

2 GASIFICATION PROCESS

The biomass analyzed has been used to feed the experimental gasification plant. Specifically 7 acquisitions every 3 min were performed, with a

constant biomass flow rate of 200 g/h. The gasification operating conditions were the same for each acquisition. The test results were the gas yields and composition, the TAR removal efficiency of the two methods and the composition of the TAR.

In Figure 2 gives a schematic diagram of the system under consideration.

On Figure 2 shows a schematic representation of the bench scale facility used during the work.

Its major components are: a solid fuel feeding system, a fluidized bed gasifier, a microreactor for catalyst tests, a bio-oil trap at ambient temperature, a gas cooling system, and metering and analyzing systems for the off-gases. The fluidized bed gasifier consists of an austenitic stainless steel cylindrical vessel of internal diameter 80 mm fitted with stainless steel porous distributor plate, designed to allow a good gas distribution at all temperatures. In particular a sintered stainless steel plate is used. The pressure drops through this plate are higher than 40% of those through the fluidized bed yet at ambient temperature, in order to guarantee a uniform gas distribution at every temperature. The entire reactor is located in a cylindrical electric furnace provided with temperature and heating rate control systems. Temperature within the reactor is measured by means of two thermocouples, one immersed in the bed and the other located under the distributor. The bed inventory is olivine sand. Olivine is a sand, natural source (MgO 48–50%, 39–42% SiO₂, Fe₂O₃ 8–10%), low cost (120 €/ton), which has been shown to have catalytic characteristics in relation to the reactions of reforming of tar. The olivine, unlike the calcined dolomite, it also used as catalyst [20], has the property of having a greater mechanical resistance to fracture similar to silica sand, so do not form dust, which can spoil the functioning of the gasifier [21]. The fluidized gas is a mix of steam and nitrogen: the flowrate of steam is set to obtain the desired steam to biomass ratio while nitrogen is added to guarantee a superficial velocity equal to two times of the minimum fluidization velocity. Water for the generation of steam is fed to an electrically heated boiler by means of a peristaltic pump at

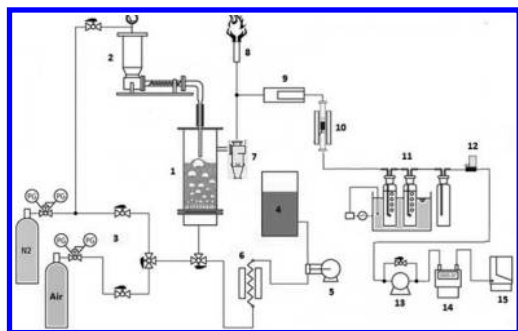


Figure 2. Scheme of the experimental system: (1) bubbling fluidized bed gasifier; (2) biomass feed system-hopper and screw feeder; (3) gasifying agents inlet system; (4) distilled H₂O storage; (5) water pump; (6) electric steam generator; (7) cyclone; (8) torch; (9) ceramic candle filter; (10) secondary reactor; (11) TAR condensation system; (12) mass flow controller (13) vacuum pump; (14) cumulative gas flow meter; (15) gas-chromatograph (TCD).

a constant flow rate. The biomass feeding system is designed to properly deliver the biomass inside the bubbling bed. During the start-up, the entire raw gas generated by biomass gasification feeds a torch to be completely burned. When gasification process reaches steady state conditions, a vacuum pump was switched on to feed the stainless steel microreactor (2 cm ID) for a catalysis test and the bio-oil trap with a slipstream of raw gas. A heated ceramic filter assures that no fine particles reach the microreactor. The microreactor (filled with catalyst) is located in a cylindrical electric furnace provided with a temperature and a heating rate control systems. The temperature of the catalyst bed is measured by a thermocouple inside the bed. For each run the permanent gas yield was measured by means of a volumetric gasmeter, after separation of the condensate (water and organic phases) in a cold bath of iso-propanol ($-10\text{ }^{\circ}\text{C}$). The flow rate of the slipstream was controlled by a needle valve downstream the microreactor. The TAR was measured after each test by means of Agilent GC-MS. Gas products were analysed by Varian micro-GC. Before any tests at different temperature catalyst were reduced in H₂ flow of 100 Nm³/min at the operative temperature of the tests.

The gasification process was performed at 850 °C. The biomass is fed from the top of the reactor directly in the bed, while the superheated steam at about 400 °C is fed from the bottom. The ratio between steam and biomass is approximately equal to 0.7, S/B = 0.7. The fluid bed, 20 cm in height consists of olivine particle with a Sauter mean diameter equal to 348 μm. Biomass has an granulometry between 1–2 mm.

The ceramic filter is heated to 300 °C to avoid TAR condensation. The fixed bed of Ni catalyst operates at 750 °C. The bed volume is about 15 ml and is made of nickel (15%) supported on an alumina matrix (Ni/Al₂O₃), the particle size of the bed ranges between 400 and 600 microns. In this reactor cracking and steam reforming of TAR and CH₄ occur, the outgoing gas is enriched in the hydrogen and depleted of methane and TAR [23]. The exit gas from the reactors can still contain traces of TAR which must be eliminated. To eliminate the TAR present, the gaseous stream is passed through first into a scrubber in vegetable oil (sunflower seeds), operating at ambient temperature, later in the traps to isopropyl alcohol (2-propanol) maintained at $-10\text{ }^{\circ}\text{C}$. From the analysis of TAR present in the traps in 2-propanol and in the vegetable oil is able to evaluate what has been the removal capacity of the TAR from gaseous stream [22].

3 DATA ANALYSIS

The average production of syngas, measured in output from the circuit for each test was 1.42 Nm³/kg of biomass fueled. The average composition of the gas after the catalyst bed, is given in Table 4.

Another important aspect to check is the concentration of TAR extracted from the syngas, and retained in vegetable oil sunflower and isopropyl alcohol. To implement these measures the GC-MS system Agilent Technologies 7890 was used. In order to evaluate the efficiency of the vegetable oil sunflower to remove TAR the concentration of these were evaluated without and with the vegetable oil. TAR concentration in the stream is shown in the next table (Table 5).

Table 4. Average composition of the gas output from the system.

Syngas composition	% Vol
H ₂	41.8
CO ₂	23.8
CH ₄	3.1
CO	31.3

Table 5. Composition TAR in the vegetable oil.

TAR	mg/Nm ³
Benzene	93
Toluene	40
Naphtalene	1964

Table 6. Capture efficiency of TAR of the vegetable oil.

Capture efficiency of TAR	%
Benzene	76
Toluene	76
Napthalene	96
Mean	83

Was estimated capture efficiency, the TAR present in the gaseous stream, from vegetable oil as illustrated in Table 6.

From the data shown is known as the vegetable oil is indicated for the capture of the TAR present in the gas [23], in particular, appears to be particularly responsive to the naphthalene.

4 CONCLUSION

Analyzing the data presented, it is possible to highlight that the presence of catalytic reforming reactor to Ni/Al₂O₃ downstream of the gasification reactor produces benefits both as regards the production of hydrogen, that for the reduction of TAR [24]. Also the systems capture TAR from the gas stream rich in hydrogen appear to be very effective, guaranteeing the production of a syngas cleaner for use in ICE, mGT and SOFC [25].

REFERENCES

[1] <http://www.enama.it/it/biomasse.php>.
 [2] <http://www.istat.it/it/archivio/111888>.
 [3] Carlini M, Castellucci S, Cocchi S. 2014. Mesophilic fermentation of SOMW in a micro pilot-scale anaerobic digester. *Advanced Materials Research*, vol. 827, p. 84–90, ISSN: 1022–6680, doi: 10.4028/www.scientific.net/AMR.827.84.
 [4] Carlini M, Castellucci S, Allegrini E, Tucci A. 2012. Down-hole heat exchangers: modelling of a low-enthalpy geothermal system for district heating. *Mathematical Problems in Engineering*, vol. 2012, 845192, ISSN: 1024–123X.
 [5] M.Carlini, S. Castellucci: “Modelling the vertical heat exchanger in thermal basin” ICCSA 2011, Parte IV, LNCS 6785, pp. 277–286, Springer Heidelberg Dordrecht London New York; ISSN 0302-9743, ISBN 978-3-642-21877-2, DOI 10.1007/978-3-642-21898-9.
 [6] Carlini M, Castellucci S, Cocchi S, Manzo A. 2013. Waste Wood Biomass Arising from Pruning of Urban Green in Viterbo Town: Energy Characterization and Potential Uses. In: ICCSA 2013. *Lecture Notes in Computer Science*, Berlin:Springer-Verlag, ISSN: 0302-9743, Ho Chi Minh City, Vietnam, 24-27 June 2013.
 [7] McKendry P., 2001. Energy Production from biomass (part 1): overview of biomass. *Bioresource technology* 83, 37–46.

[8] UNI EN 14588:2010, Solid biofuels, terminology definitions and descriptions.
 [9] Bocci E, Sisinni M, Moneti M, Vecchione L, Di Carlo A, Villarini. 2014. M. State of Art of Small Scale Biomass Gasification Power Systems: A Review of the Different Typologies. *Energy Procedia* 2014;45:247.
 [10] Monarca D., Colantoni A., Cecchini M., Longo L., Vecchione L., Carlini M., et al. 2012. Energy characterization and gasification of biomass derived by hazelnut cultivation: analysis of produced syngas by gas chromatography. *Mathematical Problems in Engineering* 2012;
 [11] Basu P. *Biomass Gasification and Pyrolysis: Practical Design and Theory*: Elsevier Science; 2010.
 [12] Vecchione L, Moneti M, Bocci E, Di Carlo A, Foscolo P. 2013. Steam Gasification of Pine Wood in a Fluidized Bed Reactor: Model Development and Validation at Different Operative Conditions. *21st European Biomass Conference and Exhibition* 2013:841.
 [13] UNI EN 14778:20011, Solid biofuels, sampling.
 [14] UNI EN 14780:2011, Solid biofuels, sample preparation.
 [15] UNI EN 14774-1:2009, Solid biofuels, moisture determination methods of drying in an oven.
 [16] UNI EN 14918:2010, Solid biofuels, determining the calorific value.
 [17] UNI EN 15104: 2011, Solid biofuels, determination of the total content of carbon, hydrogen and nitrogen.
 [18] UNI EN 14775:2010, Solid biofuels, determining the ash content.
 [19] P. Lv, J Chan, T. Wang, Y. Fu, Y. Chen, 2004. Hydrogen-rich gas production from biomass catalytic gasification, *Energy e fuel* 2004, 18, 228–233.
 [20] Sisinni M, Di Carlo A, Bocci E, Micangeli A, Naso V. 2013. Hydrogen-Rich Gas Production by Sorption Enhanced Steam Reforming of Woodgas Containing TAR over a Commercial Ni Catalyst and Calcined Dolomite as CO₂ Sorbent. *Energies* 2013;6:3167.
 [21] Rapagnà S, Jand N, Kiennemann A, Foscolo PU. 2000. Steam-gasification of biomass in a fluidised-bed of olivine particles. *Biomass and Bioenergy*. 2000;19:187–197.
 [22] Paethanom A., Nakahara S., Kobayashi M., Prawisudha P., Yoshikawa K. 2012. Performance of tar removal by absorption and adsorption for biomass gasification. *Fuel Processing Technology*. 2012;104:144–154.
 [23] Phuphuakrat T, Namioka T, Yoshikawa K. 2011. Absorptive removal of biomass tar using water and oily materials. *Bioresource Technology*. 2011;102: 543–549.
 [24] Kimura T, Miyazawa T, Nishikawa J, Kado S, Okumura K, Miyao T, et al. 2006. Development of Ni catalysts for tar removal by steam gasification of biomass. *Applied Catalysis B: Environmental*. 2006;68:160–170.
 [25] Di Carlo A, Borello D, Bocci E. 2013. Process simulation of a hybrid SOFC/mGT and enriched air/steam fluidized bed gasifier power plant. *International Journal of Hydrogen Energy* 2013;38:5857.

Numerical simulation analysis on construction settlement of loess embankment

Xu Qing Pang

*School of Civil Engineering and Architecture, Xi'an University of Technology, Xi'an, China
Railway Engineering Department, Shaanxi Railway Institute, Weinan, China*

Zai Qiang Hu

School of Civil Engineering and Architecture, Xi'an University of Technology, Xi'an, China

ABSTRACT: Loess embankment was dealt with by dynamic compaction with three different levels of 600 kJ, 1000 kJ, 1600 kJ in an experimental site. The settlement deformation of loess embankment was simulated by Marc finite element software after dynamic compaction of gradual loading and disposable loading. It drew a conclusion that the deformation gradual loading is bigger than disposable loading and the difference of two numbers reduced to a fixed number with increasing compaction levels, and the center of embankment settlement deformation took the form of a basin shaped settlement by a decreasing trend from the center to the two sides presenting. The result consists with the observation of settlement.

Keywords: loess; embankment; construction settlement; numerical simulation

1 INTRODUCTION

1.1 Marc finite element software

The stress-strain relationship of soil is very complex. The soil exhibits elasticity, viscosity, plasticity, and affected by stress history. Additional stress field is affected by the soil constitutive relationship, and has relation to superstructure and stiffness of foundation^[1]. The embankment and foundation should be look as a whole structure in the design and calculation. The finite element method reflects the influence factors of nonlinearity of soil, stress history on the settlement, so it is more reasonable than the usual stratified summation method. Marc supports the linear elastic model, nonlinear elastic model and elastic viscous plastic model as a nonlinear finite element analysis program^[2]. Therefore, it can simulate the mechanical behavior of soil^[3].

1.2 Engineering situation

The test area lies in the Malan loess region in Quaternary Pleistocene. MaLan loess thickness is 10–15 m. It presents some features which is porosity, loose structure, high compressibility and collapsible. We selected 100 m section in the testing site, divided it into four sections, each section of 25 m. We conducted dynamic compaction test with

three energy levels by 600 kJ, 1000 kJ, 1600 kJ, layout spacing is 3.5 m, and arranged the quincunx tamping point. We measure and record each settlement after dynamic compaction^[4].

2 THE ESTABLISHMENT OF FINITE ELEMENT MODEL

2.1 Parameter selection

The constitutive relation uses the linear elastic model for the upper part of the embankment. The calculation parameters set up for the finite element model of embankment mainly involves E , μ and γ . E is the elastic modulus of materials, μ is the Poisson's ratio, γ is the weight of soil. The subgrade can be divided into two layers. Upper loess layer is Q_3 loess, about ten meters. The lower layer is Q_2 loess, can be regarded as a relatively stable hard layer, deformation amount is very small. The upper Q_3 loess layer basic constitutive relation is the ideal elastic—plasticity model, E is the elastic modulus, μ is Poisson ratio, c is cohesion, ϕ is internal friction angle. The constitutive relation of the lower part of hard loess layer can be regarded as linear elastic model, calculation parameters reference to the embankment. The calculation parameters of subgrade bottom layer see for Table 1. The calculation parameters of embankment see for Table 2.

Table 1. Soil's parameters of subgrade subjacent.

Parameter	E (KPa)	μ
Value	15000	0.30

Table 2. Soil's parameter of embankment.

Parameter	E (KPa)	μ	γ (KN/m ³)
Value	20000	0.28	18~19

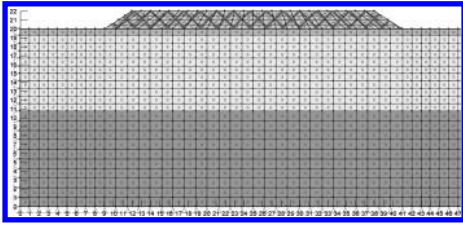


Figure 1. The finite element calculation model for settlement.

2.2 Loading method of embankment

We simulate the settlement with stepwise loading and disposable loading according to the different height of embankment. In stepwise loading, every layer filling as a loading, then calculate the deformation and stress in current construction of the soil everywhere. The deformation and stress caused by upper filling layer of soil superposed previous value until the whole structure completed, in this way, the simulation of the whole construction sequence realized^[5]. The disposable loading is loading the ultimate loading capacity of all on the subgrade one-time, then calculate the stress—strain relations of foundation and embankment. For example, finite element mesh for the embankment and subgrade area, calculation model of 2 m high embankment after dynamic compaction as shown in Figure 1.

3 NUMERICAL SIMULATION OF CONSTRUCTION SETTLEMENT

3.1 Coordinate deformation of subgrade and embankment

For comparison, the Marc finite element software was used to calculate the settlement of the subgrade^[6]. The embankment height is 10 m, the coordinate deformation of subgrade and embankment after the 600 KJ dynamic consolidation by step loading five times is shown in Figure 2. The coordinate deformation of subgrade and embankment after the 600 KJ dynamic consolidation by disposable

loading one time is shown in Figure 3. Settlement of subgrade surface by step loading five times is shown in Figure 4. Settlement of subgrade surface by disposable loading one time is shown in Figure 5. Settlement of subgrade vertical center point by step loading five times is shown in Figure 6. Settlement of subgrade vertical center point by disposable loading one time is shown in Figure 7.

The center point of settlement point disposable loading is located in embankment surface; step loading maximum settlement point is located in the first stage of the loading embankment center, both center settlements are more than the center point settlement of the ground surface^[7].

3.2 Settlement analysis

From Figure 1 to Figure 6 can be seen, most of the settlement of subgrade is caused by the foundation settlement, the settlement of subgrade decrease from the center to the two sides, the maximum settlement lies in the subgrade center line, present

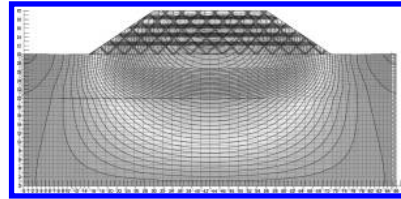


Figure 2. Coordinate deformation of subgrade and embankment (step loading five times).

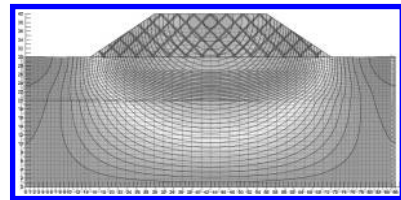


Figure 3. Coordinate deformation of subgrade and embankment (disposable loading one time).

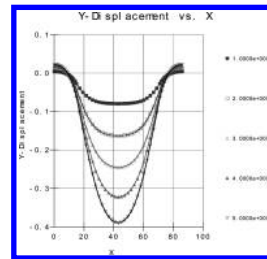


Figure 4. Settlement of subgrade surface (step loading five times).

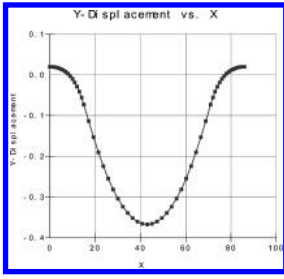


Figure 5. Settlement of subgrade surface (disposable loading one time).

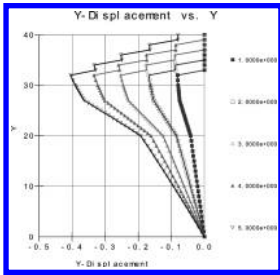


Figure 6. Settlement of subgrade vertical center point (step loading five times).

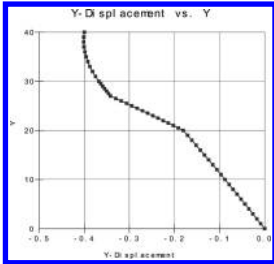


Figure 7. Settlement of subgrade vertical center point (disposable loading one time).

basin shaped settlement rule, and in accordance with the actual deformation of subgrade.

The central settlement amount and the maximum settlement are reduced with increasing compactation levels at the same height of embankment by two kinds of loading modes apparently. For the settlement deformation of subgrade center, the settlement of step loading is more than the disposable loading, and the difference between the two Loading modes decreases with the increase of impact compactation level. The maximum deformation settlement are or less the same under two loading modes. The settlement of embankment itself remained unchanged. The settlement value of embankment surface center reduced is equal to the decreasing value of the center of the subgrade surface. Loess subgrade settlement used Marc finite element simulation by dynamic compactation before and after see for [Table 3](#).

Table 3. The final settlement of loess foundation (cm).

Loading mode	Compact energy		
	Natural soils		Compact energy (2400 KJ)
Disposable loading	Subgrade center	The maximum settlement	Subgrade center
	42.87	46.58	29.39
	45.34	46.91	31.19
Step loading	Subgrade center	The maximum settlement	Subgrade center
	2.47	0.33	1.80
	2.47	0.33	1.80
Differential settlement			The maximum settlement
			32.51
			0
Compact energy (1600 KJ)			
		Subgrade center	33.23
		The maximum settlement	36.44
Compact energy (600 KJ)			
		Subgrade center	39.00
		The maximum settlement	40.14
		Subgrade center	2.23
		The maximum settlement	0.30

4 THE STRESS-STRAIN EXPERIMENT OF EMBANKMENT

4.1 Observation point and observation equipment layout

Sedimentation cup was embedded in the field test sections, and was numbered in accordance with the embedded sequence^[8]. For example, M1-1 stands for the embankment settlement cup of first layer center on the section M1^[9]. A experimental of M section sedimentation cup arrangement see for Table 4.

4.2 Rules of subgrade settlement

The embankment settlement observation results of the experimental section at the center, as shown in Figure 8 and Figure 9.

From roadbed settlement observation results can be seen, the embankment and subgrade settlement was increased as time went by, but the increase rate

Table 4. Sedimentation cup arrangement of M section.

Serial number	Width of subgrade (m)	Design altitude (m)	The ground elevation (m)	The height of embankment (m)
M1	28	421.48	409.64	11.84
M2	28	423.23	411.46	11.77
M3	28	419.73	408.66	11.07

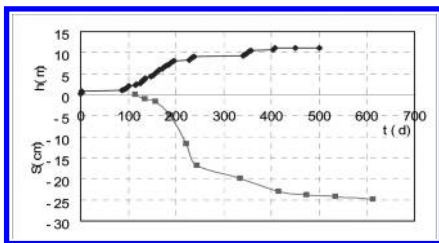


Figure 8. The embankment settlement observation results of Section M1-1 at the center.

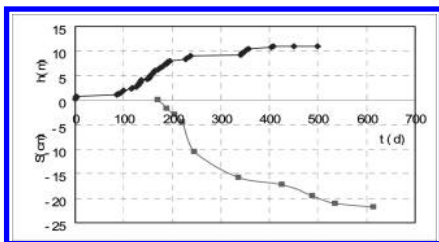


Figure 9. The embankment settlement observation results of Section M1-2 at the center.

is more and more small, and gradually stabilized as time went by. It is consistent with the finite element analysis results.

5 CONCLUSIONS

Adopting the simulation analysis of loess embankment settlement by using Marc software, the simulation result is consistent with the reality and the subgrade settlement deformation law can be obtained intuitively.

1. The subgrade surface settlement decreases from the center to both sides, the maximum soil pressure appeared in the embankment center.
2. The maximum settlement lies in the subgrade center line, present basin shaped settlement, the subsiding regularity is in accordance with the actual deformation of subgrade.
3. The settlement of step loading is more than the disposable loading for the settlement deformation of subgrade center, the difference between the two Loading modes decreases with the increase of impact compaction level. The maximum deformation settlement are or less the same under two loading modes.
4. Soil pressure increases with the filling height increasing during the embankment filling process, soil pressure tends to a stable value after the embankment construction.

REFERENCES

- [1] Li Guangxin. Advanced soil mechanics[M]. Beijing: Tsinghua University Press, 2006.
- [2] Zhang Qisen. Finite element analytical methods of highway[M]. Beijing: China Communications Press, 1987.
- [3] Chen Huohong, Yu Junquan, Xi Yuanshan. Marc 2003 foundation and application[M]. Beijing: Science Press, 2004.
- [4] JTG E40-2007. Test methods of soils for Highway Engineering[S]. Beijing: China Communications Press, 2007.
- [5] Yan Bin, Wang Hang, Ni Wankui. Settlement and deformation analyses before or after treatment on expressway loess foundation[J]. Journal of Engineering Geology, 2007, 15 (4):522-523.
- [6] Dai Jingliang. Expressway embankment research report on settlement law and prevention and curemethods in Shaan'xi province[R], 1997.
- [7] Dong Liang, Shi Cunlin, et al. On new computational method on settlement of ground[J]. Journal of engineering geology, 2005, 13(2): 227-230.
- [8] Li Mingling. Deformation monitoring and assessment technology for substructure of unballasted track on railway passenger dedicated line[J]. Engineering Science, 2009(1): 48-59.
- [9] Zhang Weibing. Study on settlement-deformation laws and calculation method of high Loess-filled embankment[D]. Xi'an: Changan University, 2007.

The effect of marketization of interest rate on the investing and financing of enterprise

Xiang-Shi Zeng

Jiujiang University, Jiangxi, China

ABSTRACT: The marketization of interest rates means the level of interest rates formulated by financial institutions for credit policy will depend on the supply and demand of the market. Just because of the not fully development of financial market in China, especially for the capital market, our enterprise still always finance on a bank-credit way. Therefore, the changes of interest rates will affect their investing and financing. In this paper, we will analysis the effect of interest rate fluctuation on the investing and financing of enterprise based on their behavior, so that we could make some recommendations and preventive measures on the risks presented by the marketization of interest rates.

Keywords: marketization of interest rates; strategies on investing; strategies on financing; preventive measures

1 INTRODUCTION

Marketization of Interest Rates is a kind of market mechanism based on capital price. Social capital resource always circulates among participants in financial market according to the law of market. The level of interest rates is determined by the supply and demand of market capital, which is quite different from liberalization of interest rates. In “12th Five-Year” plan, China has listed “gradually promoting market-oriented reform of interest rates” as an important part of financial marketization reform. China has made a great progress on reform of marketization of interest rates, based on the opening of interbank offered rate, also liberating the debt rate, coupons repo rate and spot trading rate of money market. It also uses the method of price bidding to issue financial bonds and treasury bonds and expand the floating range of lending rates to make interest rate management some certain market flexibility. After it gets marketization, interest rates has fluctuated more frequently, making enterprise directly face the effect brought. In 2007, Wang Dongjing and Zhang Xiangjian used analysis of covariance model, verifying the structural changes of corporate finance behavior equation after the abolition of interest rate caps happened. They believe that the reform of marketization of interest rates has got some success, leading financing constraints relieved and structure more reasonable. I do agree with the view of Zhang Wei that the standardization of enterprise and bank behavior is an important condition of marketization of interest rates. In modern enterprise

system, only this can improve the binding of the enterprise, helping enterprise consider more on the risk factors of investing and financing.

2 EFFECT OF MARKETIZATION OF INTEREST RATES ON INVESTING AND FINANCING OF ENTERPRISE

After the implement of marketization of interest rates, the effect will differ a lot to different countries and regions, but still having convention followed. This will offer the enterprise a direction that how to make a risk-averse determination of investing and financing. According to Shaqiri’s (1996) exploration, among 18 countries and regions which using marketization of interest rates, except interest rate in Poland decreased after the policy adopted, all others increased within varied degrees. During the implement of marketization of interest rates, interest rate in China kept increasing until in late 2008, for stimulating economy. The degree of interest rate fluctuation would cause great risk of enterprise financing. That’s why enterprise should make attention to management and control on interest rate risk to decrease the financing cost.

2.1 *Effect of marketization of interest rates on investing of enterprise*

In Keynesian macro model, volume of investment in a society is determined by the marginal efficiency of capital (r_c) and interest rate (r). Whether invest or not, is determined by the expected profits of

new investment, that is the comparison between the marginal efficiency of capital and the interest rate required by funds for purchasing these assets. If $r_e > r$, it invests. The higher expected return and lower investment cost, the stronger desire of invest.

Therefore, *ceteris paribus*, the lower interest rate, the higher volume of investment. So, interest rate and investment is inversely proportional.

1. Effect of Marketization of Interest Rates on Investment Scale of Enterprise

Under marketization of interest rates, the possible increasing of interest rates will lead the increasing of financing cost, but not the decreasing of investment scale. The two main facts are listed as below:

First, SMEs through the private lending market financing reversed transmission bank cut interest rates. Because of the long-time control of interest rates in China and interest rates and capital flows restriction of formal financial system, SMEs had to turn to the private lending market, leading the private interest rates increased. After the marketization of interest rates adopted, there is a kind of balance between the lower official interest rates and higher non-governmental lending interest rates. Some SMEs will enter the credit market, making the non-governmental interest rates decline.

Second, the interest rate volatility will affect corporate investment efficiency, the key is whether the enterprise real modern enterprise system is established. Non-standard business reputation poor enterprise will be reduced because of financing costs rise and loans, thus inhibiting the investment scale; And standardize the good reputation of enterprises will get more financial support, in order to gain more loans, thus promotes the increase of the size of its investment.

2. Effect of Marketization of Interest Rates on Investment Structure of Enterprise

The change of interest rate level and term will of course affect the investment structure of enterprise. If the level of interest rate becomes much higher, the enterprise will choose a project with a shorter term and higher profit to invest. The term structure of interest rate will also affect the investment term of enterprise. If the long-term interest rate is higher than the short-term interest rate, the enterprise will select short-term investment. Otherwise, it will choose long-term one.

2.2 Effect of marketization of interest rates on financing of enterprise

The main two channels of enterprise financing are internal one and external one. The external

financing includes direct financing and indirect financing. The direct financing is a kind of financial behavior directly formulated by the financial instruments from people who supply and demand funds. Direct financing instrument mainly includes stock, bond, commercial paper and borrowing certification. The indirect financing is a kind of financing formulated by intermediaries, in which the most common example is bank loan. Because of the great connection between the financing cost and interest rates of external financing, after the marketization of interest rates adopted, the frequently fluctuation of interest rates has become an important part of effect factor on external financing of enterprise.

1. Effect of Marketization of Interest Rates on Indirect Investment of Enterprise

During such a long time, financial market in China has been divided into two parts because of the restriction of interest rates and discrimination of SMEs, While private enterprises and SMEs only can get some little funds from banks, making them have to borrow from private lenders with higher interest rates. SMEs always face lack of funds. So in the process of marketization of interest rates, all these will get some improvements.

2. Effect of Marketization on Enterprise Financing in Stock Market

Changes of interest rates have great effect on the market value of stock. According to the discount theory of present value, we know that stock price is determined by the sum of dividends per share in the future and the sale price of stock in one day. The formula is listed as follow:

$$V = \sum_{i=1}^n \frac{D_i}{(1+R)^i} + \frac{M}{(1+R)^{n+1}}$$

In addition,

V —stock price;

D_i —the dividend in t year;

M —the sale price of stock;

R —discount rate.

From the formula, it can be inferred that stock price is proportional to the expected return D_i while it is inversely proportional to the discount rate R (including market interest rates and the risk free rate). When interest rates increase, stock price will decrease, vice versa. Enterprises can finance by stock when interest rates increase. According to the relationship (The following are shown in Table 1) between annual interest rate movements and domestic equity financing amount in China, when interest

Table 1. Unit: 0.1 billion Yuan.

2001	2002	2003	2004	2005	2006	2007	2008	2009
1182.13	779.75	819.56	835.71	338.13	2463.70	2722.99	3534.95	3894.52

Data Sources: 2001–2009 Financial Yearbook of China.

rate become higher, there are more opportunities of stock financing. When the interest rate decreased, SMEs with potential development would get amount of loans from banks with a lower interest rate than private market, which making them have more chances to enter into GEM market to finance.

3. Effect of Marketization on Bond Financing of Enterprises

After the marketization of interest rates adopted, interest rates of corporate bonds are determined by issuers and underwriters in accordance with credit status, solvency and credit rating results of enterprises. Those enterprises with good credit and high operating level can issue bonds at lower interest rates to reduce the cost of financing.

However, after the marketization of interest rates adopted, interest rates fluctuate more frequently, making investors face more risks. This will need investors have the ability of identify risks to take some certain risk prevention measures.

3 INVESTING AND FINANCING RISKS TO ENTERPRISES AFTER THE MARKETIZATION OF INTEREST RATES ADOPTED

3.1 *Investing risks to enterprises*

1. Interest Rate Risk

A significant feature of market-oriented interest rates is its complex and frequent fluctuation. In this circumstance, the increasing of interest rate will decrease the value of fixed rate bonds while the decreasing of interest rate will decrease the interest income of floating rate bonds. Even the investment of real economy will also make enterprises face risks. No matter with the floating or fixed rate, chooses of discount rate are full of risks. Different ways will make the possibility and combination of projects change. If you take the floating-rate financing when market interest rates increased sharply, projects under the original lower discount rate will become infeasible, which will lead the investment income greatly reduced.

2. Financial Risk

Non-anticipated changes in interest rates may adversely affect the value of the assets of enter-

prises. Higher interest rates will cause stock prices fall, while lower the value of mortgage assets, and may also reduce the size of the debt financing.

In addition, unreasonable duration of the investment and financing may also cause the company's cash flow risk, and even cause the financial crisis.

3. Trade Risk

The marketization of interest rates will cause the frequent flow of international hot money while large inflows of international hot money will make the spot exchange rate of RMB rise. To Chinese export enterprises, the RMB forward exchange earnings will be reduced.

3.2 *Financing risks to enterprises*

The uncertain changes of interest rates make the risks of financing rate greater to enterprises involved in the financial markets. Although the past loan contract with a fixed interest rate can be changed into a floating after the marketization of interest rates adopted, it will bring some negative effects to enterprises when the interest rate increase. If the interest rate stays unchanged, enterprises in general can smoothly finish their debt repayment. If the interest rate increases, cost of interests will also increase, making only some enterprises with high profits can repay debt in time. On the other hand, the increasing of interest rates will decrease cash flows of enterprises, decrease their capital liquidity and deteriorate its balance of payments. That will affect its development adversely.

Thus, with the deepening of the interest rate market, the interest rate risk should be paid more attention by enterprises.

4 PREVENTION ON INVESTING AND FINANCING RISK OF ENTERPRISES

4.1 *Internal control mechanisms of improving financing*

First of all, it should make feasibility studies on assets and liabilities of the business, forecasting and analyzing the size of the risk to provide a reference for the enterprise making the decision of whether intervene or exit the business. Second, funds should be invested rational into different

regions, industries and businesses to optimize the risk portfolio and distribute the loss of risk. Third, it should establish an internal linkage mechanism which can deal with the risks brought by the marketization of interest rates, not just in the risk control, but also management of all aspects like the target market positioning, business strategy adjustment, etc.

4.2 *Optimizing the structure of enterprise asset and liability*

Optimizing the structure of enterprise asset and liability that is in different strategies of interest rate fluctuation, management staff should make adjustment of the direction and size of the funding gap, to take advantage of changes of interest rates, generate the revenue and reduce financing costs.

4.3 *Establishing a modern enterprise system*

Modern Enterprise System making them play the main role to take investment responsibilities. It is a kind of modern enterprise system, which has clear property rights, responsibility, separation of enterprise from administration, and management

science, making enterprises enjoy the full investment autonomy. Enterprises should be responsible for their own investment behavior, bearing the investment risk. There is a great connection among investment activities, investment costs and possible future profits of enterprises. Maximizing the value of enterprises or profit is the primary choice of the investment strategy. The project that blind choice of investment, violate the decision-making process and cause serious economic lost, shall be prosecuted to the economic and legal responsibilities of key decision makers.

REFERENCES

- [1] N. Nie Yihui, Exploration on Marketization of Interest Rates and Determination of Investing and Financing of Enterprise, N. University News of Xi'an Petroleum University, 2008, (4).
- [2] J. Wang Dongjing, Zhang Xiangjian, Exploration on Marketization of Interest Rates, Financing of Enterprise and Credit Behavior of Financial Institutions, J. World Economy, 2007, (2).
- [3] J. Zhao Yanshen, Effect on Financing of SMEs by Liberation of Lending Rates in China, J. Financial Market, 2009, (10).

Application of viscous damper in reinforcement of frame structure

Wei Han & Ming Jun Liao

Automobile and Civil Engineering Institute, Beihua University, Jilin City, China

Xiao Yu Jia

Changchun Coal Design and Research Institute, Changchun, China

ABSTRACT: In seismic disaster reduction engineering, energy dissipation damping reinforcement technique are more and more brought to the attention of the construction industry because of its simple structure, low cost, short construction period, good damping effect and the advantages of wide scope of application. This paper discusses the characteristics and designing points of energy dissipation technology. There are many earthquakes occurred in the high intensity earthquake function. Improving its seismic performance is one of the difficulties in the current seismic design of buildings, the energy dissipation technology can effectively improve the seismic performance of the structure.

Keywords: viscous damper; energy dissipation bracing; seismic strengthening

1 INTRODUCTION

Energy dissipation bracing is an effective way to implement structural vibration control, which is widely used in various fields of civil engineering. Under the action of small earthquake and wind, it can increase the horizontal stiffness of the structure and reduce the lateral shift; in middle and strong earthquakes its stiffness becomes small, it can reduce the horizontal earthquake action of the structure, at the same time, it consumes a large amount of seismic energy, so that the seismic response of the structure is greatly attenuated. Energy dissipation brace is non load-bearing component, it does not constitute any influence and

threat to the bearing capacity and safety of the structure at the same time, it does not need manual input energy [1].

At present, the developing energy dissipation devices are displacement dependent damper (accumulator, friction dissipation metal) damper and velocity dependent (viscous dampers, viscoelastic dampers), and buckling restrained brace type energy dissipation damper and compound energy dissipation damper.

Energy dissipation technology increase the structural damping through some parts of the building structure (such as column, shear wall, node, link seam, floor space, adjacent buildings etc.) thereby reduces the reaction of structure under wind and earthquake [2]. Energy dissipation system is widely used in the energy dissipation bracing system (Fig. 1) [3]. This system is a kind of damping device and on the structure of oblique (cross). When the earthquakes take place, produces axial force and axial deformation, the damping device on the brace strut starts to work, such as friction variable damping (or other damping), consume a large number of seismic energy, reduce the deformation of structures.

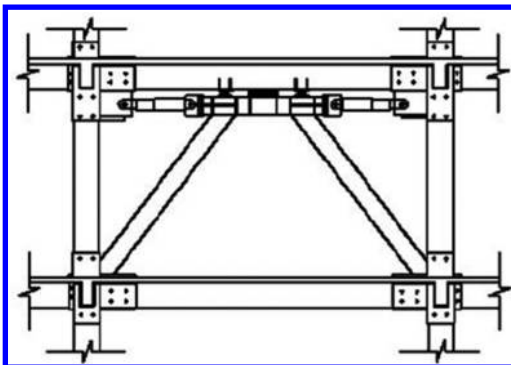


Figure 1. Double viscous dampers combination brace installation schematic diagram.

2 MECHANICAL PROPERTIES AND CALCULATION METHOD

Viscous damper, through the interaction between the components and its internal viscous medium, produce the viscous damping force and provide

additional damping for the main structure, thereby dissipate seismic energy inputting structure. Therefore, for the damper, the choice of viscous material is very important.

Currently Viscous materials on the market used in viscous dampers are methyl silicone oil, silicone rubber and the hydraulic oil, the methyl silicone and silicon rubber are more widely used [4]. The viscous damper damping can be divided into the cylinder type viscous fluid damper, cylinder type viscous dampers and viscous damping wall according to different principle of the viscous damper damping force Compared with the traditional seismic design, the effect of damper is better, seeing the comparative analysis in Table 1.

2.1 Mechanical models

Several common models describing the mechanics characteristics of viscous damper are as follows:

1. Restoring force model [5];
2. Kelvin model;
3. Maxwell model;
4. Maxwell model;
5. fractional derivative model.

We use accurate Maxwell calculation model for the viscous damping element in SAP2000 software, model expression is as follows: the damping coefficient, damping deformation speed; damping index, the scope of its application in 0.2~2.

2.2 Calculation methods

Common calculation methods are divided into modal decomposition response spectrum method and time history analysis, the essay mainly introduces the time history method. Time history analysis method integrates the dynamic equation by using finite element software, constitutive relation curves of structural member and the damper and the type of seismic wave. Time history analysis method calculates the

structural response at a certain moment through the integration. Time history analysis method will divide the whole process of earthquake ground motion into several small time periods, and that in the selected step Δt , the ground motion and structure of particle acceleration are linear change. The energy dissipation process damping structure analysis is divided into linear and nonlinear time history analysis. General speed linear damper uses linear time history analysis; while hysteretic damper only considers the restoring force nonlinear and use nonlinear time history analysis method.

While using the bottom shear method, the response spectrum method and the nonlinear static method, the effective damping ratio of the structure estimation added to energy consuming components is shown as follows:

$$\zeta_a = \sum_j \frac{W_{cj}}{4\pi W_s} \quad (1)$$

where ζ_a = the additional effective damping ratio of structure with energy dissipation; W_{cj} = cycle energy which the j performance parts consume in the structure of the expected inter story displacement; W_s = The total strain energy dissipating structure components in anticipation of displacement.

Viscous dampers consume energy under the action of horizontal earthquake, and make the preliminary estimation according to the following formula:

$$W_{cj} = \left(\frac{2\pi^2}{T_1} \right) \sum C_j \cos(\theta_j)^2 \Delta u_j^2 \quad (2)$$

where T_1 = represents fundamental vibration period of energy dissipation structure; C_j = j damper which is determined by the test of linear damping coefficient; θ_j = the angle of j energy dissipation of energy direction and the horizontal plane;

Table 1. Contrast of earthquake-reduction structure design and traditional seismic design.

Item	Traditional seismic design	Earthquake-reduction structure design
The characteristics of structural system	Each component can be connected reliably and consolidated on the base	Some parts of the structure with energy dissipation device, the remaining part with traditional structure
Shockproof means	Improve the structure of section size, reinforcement and ductility and prevent the weak structure from damaging	The ability to use dampers dissipation input
Seismic action	Related to the stiffness of the structure	The earthquake was significantly reduced
Seismic deformation	Mendable in moderate earthquakes and no collapsing with strong earthquake	Deformation is significantly reduced, strong earthquake can be fixed

Δu_i = relative horizontal displacement of damper both sides.

2.3 Seismic performance index

Chen Jianbin [6] viscous dampers are installed in the square steel tube concrete high-rise buildings, and analyzes the seismic performance of the structure with viscous dampers (angle of floor displacement, internal force, torsion effect factors such as layer); Weng Dagen and other persons [7] analyze the seismic performance of the viscous dampers supporting 8-storey steel frame shear wall buildings, it is obtained in different seismic wave structure in X, Y direction of bending moment, shear, axial force and displacement (displacement) size, and do not set the energy dissipation compared parameters of device situation. We draw the following conclusions: damper should be arranged in the building to enhance the energy dissipation effect, the energy dissipation bracing system can decrease the inter-story shear force and supporting the connecting shaft intersects the column, and viscous damper brace structure equivalent to provide additional stiffness is smaller, the actual engineering can be provided for each floor, which can also set layered energy dissipation brace. According to the needs.

At present, Improving the seismic performance of high-rise buildings mainly considers the following two aspects:

1. Improving the structural damping ratio

The elastic seismic response of structure. Is the function of damping and period. It decreases with the structural damping ratio increasing and the earthquake cycle extending. Structural damping is extremely effective for reducing the maximum resonance response. The structural damping changes with vibrational properties of all the materials, structures, and foundation soil. We should use the larger damping structure type and system in high-rise building design. Structure of damper can be installed on the structure to absorb the earthquake inputting energy so that it can reduce the structural deformation.

2. Setting energy dissipation device

Whether the building can resist earthquake or not mainly depends on the capability of structure of "energy absorption and dissipation", and it also depends on the ductility of the structure size, the former high-rise building design process mainly uses the strong column and weak beam, strong shear and weak flexure, strong node and weak component method to improve the ductility of structures. We generally uses energy dissipation device now, provide some additional stiffness or damping for the structure, energy dissipation device in the structure are mainly

used to dissipate earthquake energy and reduce the dynamic responses of structure, which is an effective, safe, economic and mature engineering seismic technology.

3 ENGINEERING EXAMPLES

A comprehensive office building in Wenchuan city Sichuan province was built in 2004, 6832 m², 6-storey, 24.6 meters high. The opening area is large, shape is complex, which apply the frame structure, in the zone with the seismic fortification intensity 8 (0.2 g), site is class II, basic wind pressure is 0.45 kN/m². After Wenchuan earthquake 2008, it was found that the frame structure was damaged along the longitudinal damage heavier (east-west), filled with fractures in external and internal wall of vertical column 2-5 floors, some bricks falling, cross wall damaged relatively light. A few Cracks appeared in beam end body structure, structure appears strong column and weak beam characteristics. It is concluded that the energy dissipation brace system should be installed in the original structure, a layer in the side span X direction and Y direction 6 buckling restrained braces should be installed on both sides, 32 viscous dampers should be installed between two to five layers, each viscous damping device energy dissipating support is supported by a viscous damping device and 2 butt welding of [20a] elimination support. Embedded parts are made up of 14 mm thick steel plate and 9φ20 connected by a node plate and embedded parts.

Structure design with PKPM software, the original structure and dissipating structure can support for the two model, force analysis and calculation. We get the figure of floor displacement, inter story displacement angle and floor shear related to the original structure under frequently occurred earthquakes and the structure setting up numerical dissipation viscous dampers, shown in Table 2. Through the data in Table 2, we get the following conclusions:

1. by setting energy dissipation brace, floor displacement significantly smaller. Because the building is not very high, and is not affected by the wind load, the top layer displacement, displacement is reduced by 55.6%;
2. the inter-layer displacement angle becomes smaller, the biggest changes is 40.9%;
3. because of some floors provided with viscous dampers, so the floor shear is larger, but the 6th layer which is not set viscous dampers, the floor shear is not large, so the shear ratio sometimes increases and sometimes reduces. The shear of the floor setting the energy dissipation brace maximizes in the rate of 45.3%.

Table 2. Under small earthquake, comparative analysis of structure before and after setting energy dissipating damper.

Floor	Floor displacement (mm)			Floor displacement angle (rad)			Floor shear (kn)			
	Before	After	Ratio	Before	After	Ratio	Before	After	Shear ratio	
X	6	14.4	6.4	55.6%	1/728	1/920	-20.9%	1249	1452	16.3%
	5	12.2	5.7	53.3%	1/623	1/840	-25.8%	1506	1545	2.6%
	4	10.9	5.4	50.5%	1/544	1/716	-24.0%	2167	1685	-22.2%
	3	8.9	4.9	44.9%	1/520	1/630	-17.5%	2654	1752	-34.0%
	2	6.6	4.2	36.4%	1/504	1/618	-18.4%	2775	1989	-28.3%
	1	4.9	3.0	38.8%	1/732	1/1080	-24.1%	3237	3014	-6.9%
Y	6	16.8	7.6	54.8%	1/858	1/820	4.6%	1361	1424	4.6%
	5	14.6	7.0	52.1%	1/632	1/915	-30.9%	1862	1608	-13.6%
	4	11.2	6.4	42.9%	1/549	1/853	-35.6%	2408	1316	-45.3%
	3	8.5	5.6	34.1%	1/527	1/892	-40.9%	2569	1524	-40.7%
	2	6.9	4.2	39.1%	1/526	1/838	-37.2%	2851	1856	-34.9%
	1	4.8	3.3	31.3%	1/462	1/650	-28.9%	3152	3285	4.2%

4 CONCLUSION

Advantages: ① from the earthquake reduction effect, when the earthquake comes, energy dissipation damping structure devices first enter the energy dissipation state and absorb a large amount of seismic energy. The earthquake-reduction structure response is reduced 40%~60% than the traditional one. ② From the economic point of view, the cost of the energy dissipation structure can be lowered 5% to 10% than that of traditional anti-seismic structure, while the cost of the existing building reinforcement can be reduced 10%~60%. ③ From the social point of view, compared with the traditional structure. The repair operation of energy dissipation damping structure is simpler after the earthquake. We only need to repair and replace the shock absorber, which has important significance for post earthquake life and recovery.

If the energy dissipation technology can be used more widely, we need to study the following issues:

The performance of the damper and the energy dissipation device still need to be strengthened, combine shock absorption technology with special new complex structure. We still need to further explore the formation of the new structure system.

The simplification of dissipation energy dissipation system model and development of software: the existing software SAP2000, ANSYS, ETABS and other software is only for numerical simulation analysis for the actual project, if we are able

to develop a special design of energy dissipation component software, which will be very good control of the disaster of earthquake.

REFERENCES

- [1] Wu Zehou, Zhou Fulin. Optimization of energy dissipation braces in frame structures[J]. J. of NW Inst. of Arch. Eng. (Natural science), 2002, 19(1):9-14. (in Chinese).
- [2] Lin Xinyang, Zhou Fulin. Theory and application of energy dissipation-seismic reduction technology [J]. world earthquake engineering, 2002, 18(3):48-51. (in Chinese).
- [3] Lv Xilin, Jiang Huanjun. Research progress of earthquake resistance and energy dissipation of complex tall buildings[J]. Journal of Building Structures, 2010, 31(6):52-61. (in Chinese).
- [4] Deng Xiaowu. Anti-seismic Performance Evaluation and Optimization for Frame Structure with Viscous Dampers[D]. Yangtze university graduate dissertation, 2012, 04. (in Chinese).
- [5] Wang Sheliang. The seismic structure design (Version 4) [M]. Wuhan university of science and technology press, 2011, 12. (in Chinese).
- [6] Chen Jianbin, Ding Jiemin. Aseismic Design of Tall Building of Concrete Filled Square Steel Tube with Energy Dissipation Braces[J]. Journal of TONGJI UNIVERSITY (natural science), 2006, 34(11): 1431-1435. (in Chinese).
- [7] Weng Dagen, Huang Wei, Lu Xilin. Analysis on Seismic Energy Dissipation Bracing Systems for Steel Frame Structures[J]. Journal of building structures, 2005, 35(3):42-47. (in Chinese).

Optimal dispatch of distributed generation system

D. Xu & P. Li

North China Electric Power University, Baoding, Hebei, China

ABSTRACT: Due to its flexible, clean and economic energy supply mode, and the high requirement of air pollution prevention in the energy field, distributed generation system which contains new energy, has become an important technology in the construction of smart grid. Indexes of energy and environment benefits are analyzed in this paper. Considering the energy and environmental benefits of distributed generation system, an optimal dispatch model is established. In order to better solve the model, crossover operator is introduced into particle swarm optimization algorithm to overcome its premature phenomenon. Simulation results show the correctness of the model and the effectiveness of the algorithm.

Keywords: distributed generation; energy and environmental benefits; optimal dispatch; improved particle swarm optimization

1 INTRODUCTION

Due to the increasingly concern about environment, Distributed Generation (DG) system which contains new energy and renewable energy, has become an important technology in the construction of smart grid. To give full play to the advantages of distributed generation systems in terms of energy and environmental benefits, domestic and foreign scholars have carried out lots of studies, including analysis of energy conservation efficiency, harmful gases emissions from energy supply systems, and renewable energy utilization (Giri, J. 2009, Benjamin, Kroposki et al. 2010).

In the meantime, the increasing use of DG has posed many challenges for the main grid (McDonald, J. D. 2009). DG system tries to supply economical, reliable and high quality electricity to customers. The primary aims of DG system are lower costs of operation while increasing network reliability (Mohab, M. et al. 2010). Therefore, the optimal dispatch of DG system becomes the research hot spot and difficulty (Matsuda, K. et al. 2007).

This paper studies energy and environmental benefits indexes of DG system, and establishes an optimal dispatch model of distributed generation system considering the energy and environmental benefits. The objective is to minimize the total operation cost of the DG system. An Improved Particle Swarm Optimization (IPSO) is proposed to solve the nonlinear optimization problem.

2 DISTRIBUTED GENERATION

2.1 Wind turbine

Wind power is safe and renewable energy. Besides, Wind Turbine (WT) has large growth space of installed capacity and its cost reduce fast (Dukpa, A. et al. 2010). The output power of wind turbines is determined by the characteristics of WT and the average wind speed at the height of the shafts. The output power equation is given by Equation 1:

$$P_{WT} = \begin{cases} 0 & V < V_{ci} \\ aV^3 + bV^2 + cV + d & V_{ci} < V < V_r \\ P_r & V_r < V < V_{co} \\ 0 & V > V_{co} \end{cases} \quad (1)$$

where P_r = rated power; V_{ci} = in wind speed; V_r = rated wind speed; V_{co} = out wind speed, and these parameters are usually given by manufactures of WT; a , b , and c = coefficients, and can be obtained by the fitting of the consumption characteristics curve of WT.

2.2 Photovoltaic cell

Based on solar photovoltaic effect, Photovoltaic cell (PV) converts solar radiation into electrical energy to supply load through cables, controllers, and storage devices. In order to facilitate the engineering application, the steady-state output power equation of PV is shown as Equation 2:

$$P_{PV} = P_{STC} G_{AC} [1 + k(T_c - T_r)] / G_{STC} \quad (2)$$

where G_{AC} = light intensity; $G_{STC} = 1000 \text{ W/m}^2$ = light intensity under the standard test condition, P_{PV} = output power of PV; P_{STC} = the maximum test power under the standard test condition ($G_{AC} = G_{STC} = 1000 \text{ W/m}^2$; ambient temperature = 77°F); k = temperature coefficient of power; T_c = working temperature of PV; T_r = reference temperature.

2.3 Micro turbine

Micro Turbine (MT) is a small heat engine developed in recent years. It has high starting speed, good flexibility, and high working efficiency. Due to these advantages, MT has gradually become a competitive form of distributed generation. Its fuel consumption cost equation is given by Equation 3:

$$F(P_{MT}) = c_n P_{MT} \Delta t / (\eta_{MT} L) \quad (3)$$

where $F()$ = fuel cost function; c_n = natural gas price; P_{MT} = output power of MT; η_{MT} = power generation efficiency of MT; Δt = the operating time; L = the low calorific value of natural gas.

2.4 Fuel cell

Fuel Cell (FC) is not affected by the Kano cycle limit, and does not burn, nor has a rotate generator. So compared to other forms of power generation technologies, its energy conversion efficiency is very high, up to 50%–70%. Moreover, FC is environmentally friendly with almost no emission of nitrogen oxides and sulfides, and little carbon dioxide emission. Without consideration of heat supply, its fuel consumption cost equation is given by Equation 4:

$$F(P_{FC}) = c_n P_{FC} \Delta t / (\eta_{FC} L) \quad (4)$$

where P_{FC} = output power of FC; η_{FC} = power generation efficiency of FC.

2.5 Diesel energy generator

The consumption characteristic of Diesel Energy Generator (DEG) is similar to the one of traditional fossil-fired generator, and it is given by Equation 5:

$$F(P_{DEG}) = a P_{DEG}^2 + b P_{DEG} + c \quad (5)$$

where P_{DEG} = output power of DEG; a , b , and c = coefficients of the fuel cost function and can be obtained by the fitting of the consumption characteristics curve of DEG.

3 OPTIMAL DISPATCH MODEL OF DISTRIBUTED GENERATION SYSTEM

3.1 Energy and environment benefits indexes

3.1.1 Pollutant emission index

With the power generation, DGs may have different pollutant emissions and the pollutant emission is calculated as Equation 6:

$$Q_e = \sum_{i=1}^n \sum_{j=1}^m (\lambda_{ij} P_i) \quad (6)$$

where Q_e = pollutant emission; λ_{ij} = emission coefficient of the j th type of pollutant from the i th distributed generation; P_i = output power of the i th distributed generation; n = the number of DGs; m = the number of the pollutant types.

3.1.2 Energy utilization reliability index

Energy utilization reliability is the ratio of energy reserves and energy utilization amount (Liu, J. et al. 2012). For nonrenewable energy sources, with exploitation their energy reserves decrease, but the energy utilization amount increases. For renewable energy sources, their energy reserves can be considered as large constant values which are far more than their utilization amount. Energy utilization reliability index can be expressed as Equation 7:

$$U = E_r / E \quad (7)$$

where U = energy utilization reliability index; E_r = energy reserves; E = energy utilization amount.

3.1.3 Static efficiency index

Static efficiency (Liu, J. et al. 2012) is the ratio of effective output work of DG and primary energy input, and its expression is as Equation 8:

$$\eta = W / H \quad (8)$$

where η = static efficiency; W = effective output work of DG; H = primary energy input.

3.2 Objective function

To achieve the optimal dispatch of DG system, the objective function is given in Equation 9:

$$\min \sum_{t=1}^{24} C^t = \sum_{i=1}^n \left(F_i(P_i^t) + \sum_{j=1}^m (c_j \lambda_{ij} P_i^t) \right) + c_{grid} P_{grid}^t \quad (9)$$

where C^t = total cost of DG system at time t ; c_j = the environmental conversion price of the j th type of

pollutant; P_{grid}^t = purchase power of DG system from main grid at time t ; c_{grid} = power price.

3.3 Constraints

Penalty function method is used in equality constraints. Meanwhile, off-limit values are set to their limit values in inequality constraints. Constraints of optimal dispatch of DG system are show as Equation 10:

$$\begin{cases} \sum_{i=1}^n P_i^t + P_{grid}^t = P_{load}^t \\ P_{i,min} \leq P_i^t \leq P_{i,max} \\ P_{grid,min} \leq P_{grid}^t \leq P_{grid,max} \end{cases} \quad (10)$$

where P_{load}^t = load power at time t ; $P_{i,min}$ = the minimum output power of the i th DG; $P_{i,max}$ = the maximum output power of the i th DG; $P_{grid,min}$ = the minimum purchase power between DG system and main grid; $P_{grid,max}$ = the maximum purchase power between DG system and main grid.

4 PSO ALGORITHM AND ITS IMPROVEMENT

4.1 PSO algorithm

PSO algorithm is a stochastic optimization algorithm based on swarm intelligence, proposed by James Kennedy and Russell Eberhart (Duong, S. et al. 2010). PSO algorithm simulates the foraging behavior of birds. In PSO a particle is regarded as one of the feasible solutions of the problem, and the optimum solution is searched in the solution space, according to the optimal position of the best individual position and the global optimal position evaluated by fitness function value. The update equation of the particle velocity and position is given in Equation 11:

$$\begin{cases} v_{i,j}^{k+1} = v_{i,j}^k + c_1 r_1 (p_{i,j}^k - x_{i,j}^k) + c_2 r_2 (p_{g,j}^k - x_{i,j}^k) \\ x_{i,j}^{k+1} = x_{i,j}^k + v_{i,j}^{k+1} \end{cases} \quad (11)$$

where k = iteration number; i = particle number; j = search space dimension number; v = particle velocity; x = particle position; p = best individual position of each particle; p_g = global optimal position of the whole particle population; c_1 and c_2 = learning factors, and are two positive constants; r_1 and r_2 = random numbers in the interval $[0, 1]$.

4.2 IPSO algorithm

PSO algorithm is easy to fall into local optimum. To overcome this disadvantage, this paper introduces

crossover operator from genetic algorithm into PSO algorithm (Kamalnia, S. et al. 2007). Specific processing is as follows: calculate the fitness value of all particles; half of the particles which have less fitness values are directly selected to go to the next generation, while genetic selection and crossover operation is applied to the other half particles, and only those whose fitness values are improved after genetic selection and crossover operation can be selected to go to the next generation (Deb, K. & Padhye, N. 2010, Allama, S.M. & Shatlab, M.M. 2010).

5 SIMULATION AND ANALYSIS

5.1 Simulation example

The DG system simulation example is based on the modification on the simulation example of Asari, M. et al. (2008). It contains PV with 10kW rated power, WT with 15 kW rated power, DEG, FC, and MT. The capacity of transmission lines is 50 kW. Pollutant emission coefficients and environmental conversion price is listed in Table 1. Power price is 0.7 yuan/kWh, and natural gas price is 2.48 yuan/m³. Figure 1 shows the output power prediction of PV and WT. Load prediction curve is shown in Figure 2.

Table 1. Pollutant emission coefficients and environmental conversion price.

Pollutant	Emission coefficient			Conversion price (yuan/kg)
	DGE	MT	FC	
NO _x	4.3314	0.6188	<0.023	36.04
SO ₂	0.4641	0.0009	0	12.79
CO ₂	232.04	184.08	635.04	0.142

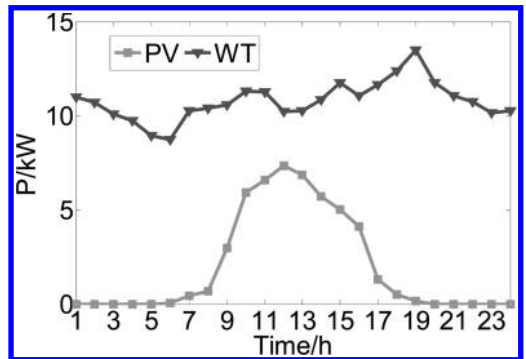


Figure 1. Output power prediction curve of PV and WT.

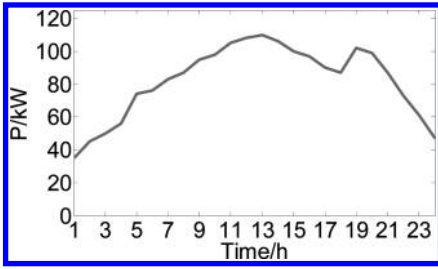


Figure 2. Load prediction curve.

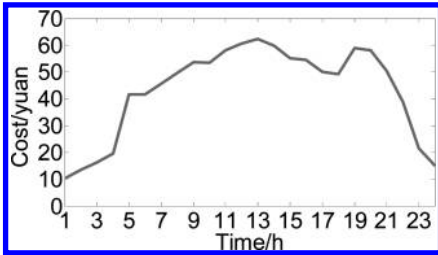


Figure 3. Total operation cost of the DG system within 24 hours of a day.

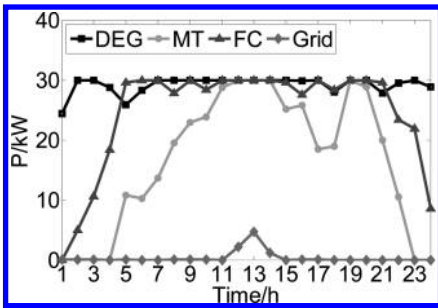


Figure 4. Output power of each DG.

5.2 Results analysis

IPSO is applied to solve the optimal dispatch of DG system, results are as follows. Figure 3 presents the total operation cost of the DG system within 24 hours of a day. Figure 4 presents the output power of each DG during the dispatch period.

The total operation cost curve in Figure 3 is similar to the load curve in Figure 2. This verifies the correctness of the algorithm. We can see from Figure 4, when the load is high at time 12–14, all DG output their maximum power, and purchase power from the main grid to meet the load demand. Because natural gas price is high, so even DEG has higher environmental conversion price, it still has lower power generation cost. Therefore, it

is the first DG to generate power followed by FC which is cleaner than MT, which is accord with the result shown in Figure 4.

6 CONCLUSION

To give full play to the advantages of DG system, this paper studied the indexes of energy and environmental benefits of DG system. On the basis of this, consider established an optimal dispatch mathematical model aiming for minimum total operation cost of DG system with consideration of the energy and environmental benefits. PSO algorithm is improved through the introduction of crossover operator from genetic algorithm. Simulation results show the validity of the model and the algorithm.

REFERENCES

- Allama, S.M. & Shatlab, M.M. 2010. Maximal optimal benefits of distributed generation using genetic algorithms. *Electric Power Systems Research* 80: 869–877.
- Asari, M. et al. 2008. Method for inferring operating state of distributed generator. *Electrical and Electronics Engineering; Proc. intern. conf., Japan, 18–20 March 2008*. Contern: IEE.
- Benjamin, Kroposki et al. 2010. Benefits of power electronic intel/aces for distributed energy systems. *IEEE Transactions on Energy Conversion* 25 (3): 567–574.
- Deb, K. & Padhye, N. 2010. Development of efficient particle swarm optimizers by using concepts from evolutionary algorithms. *Genetic and Evolutionary Computation; Proc. ann. conf., New York, 4–6 September 2010*. New York: ACM.
- Dukpa, A. et al. 2010. Optimal participation and risk mitigation of wind generators in an electricity market. *IET Renew. Power Gener.* 4 (2): 165–175.
- Duong, S. et al. 2010. Particle swarm optimization with genetic recombination: A hybrid evolutionary algorithm. *Artificial Life and Robotics* 15 (4): 444–449.
- Giri, J. 2009. Wanted: a more intelligent grid. *IEEE Power Energy Mag.* 7 (2): 34–40.
- Kamalinia, S. et al. 2007. A combination of MADM and genetic algorithm for optimal DG allocation in power systems. *Universities Power Engineering Conference; Proc. intern. conf., Brighton, 4–6 September 2007*. Piscataway: IEEE.
- Liu, J. et al. 2012. Impacts of distributed renewable energy generations on smart grid operation and dispatch. *Power and Energy Society General Meeting; Proc. intern. conf., San Diego, 22–26 July 2012*. Piscataway: IEEE.
- Matsuda, K. et al. 2007. Development of Method for Inferring Operating State of Distributed Generator. *Power & Energy Society; Proc. ann. conf., Japan, 12–14 September 2007*. Contern: IEE.
- Mcdonald, J.D. 2009. The next-generation grid. *IEEE Power Energy Mag.* 7 (2): 26–34.
- Mohab, M. et al. 2010. Optimum sitting and sizing of a large distributed generator in a mesh connected system. *Electric Power Systems Research* 80: 690–697.

Optimal allocation of distributed generation in smart grid

D. Xu & P. Li

North China Electric Power University, Baoding, Hebei, China

ABSTRACT: Smart grid has become the future development trend of electric power system, which is flexible, clean, secure, economic and environment friendly. The allocation of Distributed Generation (DG) in smart grid is researched in this paper. A multi-objective optimal allocation model is built with consideration of the network loss, investment cost, generation cost and the power supply reliability of DGs. Cuckoo Search (CS) algorithm is adopted to optimize the sitting and sizing of DGs. Simulation results of IEEE33 node system calculation example show that the proposed model is correct and the solving algorithm is effective.

Keywords: smart grid; distributed generation; optimal allocation; cuckoo search algorithm

1 INTRODUCTION

With the increasing concerns about environment, energy crisis, and higher requirements on power supply reliability, smart grid has become the future development direction of electric power system. As one of the key techniques of the construction of smart grid, Distributed Generation (DG) which contains renewable energy such as wind power, photovoltaic, fuel cell is a supplement of the centralized power supply, can effectively alleviate the environmental pollution and energy shortage, and improve power supply reliability and security of the main grid (Xu, S. 2009). However, the access of DG may have significant influence on the distribution network in the aspects of the power flow, voltage level, network loss, fault level and so on. The degree of detailed effects largely depends on the location and size of DG (Xu, S. 2009, Tsikalakis, A.G. & Hatziargyriou, N.D. 2008). So the allocation of DG in smart grid is a great challenge for the related research.

Scholars at home and abroad have carried out a lot of researches on the optimal allocation of DG, and have obtained some achievements of theory and practice. Based on sequential quadratic programming method, Wang, F. et al. (2012) puts forward a new method with second order distribution network power flow constraints. Calculation accuracy of this method is enhanced as a result of the good convergence of sequence quadratic programming method, and it is suitable for various complex distribution networks. An economical model aiming for the minimum annual operating cost of distribution network is established by Ye, D. et al. (2011). Weight factors of fixed installation cost are introduced into the proposed model to describe the cost variation of distribution network with

the connection of DGs. Hu, H. et al. (2006) builds a multi-objective programming model which takes the minimum distribution network loss, the minimum voltage deviation, the maximum static voltage stability margin as sub-objectives. Fuzzy set theory is utilized to transform the multi-objective optimization problem into a single objective problem. Li, G. & Lv, L. (2006) proposes a figure-based method which obtains the power distribution curve by the constant-power models. DGs are allocated according to the introduction on power flow and voltage. This method simplifies major objective functions and constraints of the optimal allocation problem and avoids the complicated solving process of traditional optimization algorithms.

A multi-objective optimal allocation model of DG is established in this paper. Sub-objectives are viewed in the aspect of economy, and transform the multiple objectives into a single objective aiming for maximizing annual economic benefits of the grid corporation. Cuckoo Search (CS) algorithm is adopted to solve the optimization problem.

2 OPTIMAL ALLOCATION MODEL OF DISTRIBUTED GENERATION

2.1 Objective function

The power generation of DGs can supply loads in the grid, and reduce the power purchase cost of the grid from the generation company. The total cost saved by the power generation of DGs is calculated in Equation 1:

$$F_1 = \sum_{i=1}^{N_{DG}} P_{DG_i} \times T_{max} \times C_d \quad (1)$$

where N_{DG} = the number of DGs; T_{max} = system maximum load utilization hours; P_{DG_i} = active power output of the i th DG; C_d = sale electricity price of the generation company.

When the grid has power failure or power quality problems, DGs can be disconnected to power grid through the main circuit breaker. In the isolated operation mode, DGs can still supply the loads, so as to reduce the loss caused by power failure. The reduced economic loss of power interruption is given in Equation 2:

$$F_2 = \sum_{i=1}^{N_{DG}} P_{DG_i} \times t_{max} \times C_l \quad (2)$$

where t_{max} = the duration of power interruption; C_l = unit economic loss of power interruption.

DGs are usually installed near load, so the network loss can be reduced greatly through reasonable allocation of DGs. This paper assumes that DG is directly installed on the same installation node of loads, and the network loss calculation equation can be simplified as Equation 3:

$$P_{loss} = \frac{rL}{3V^2} \left[(P_L - P_{DG})^2 + (Q_L - Q_{DG})^2 \right] \quad (3)$$

where P_{loss} = the network loss with the installation of DGs; r = unit impedance of line; L = the length of line; V = node voltage of the distribution network; P_L = active power of loads; Q_L = reactive power of loads; P_{DG} = active power output of DG; Q_{DG} = reactive power output of DG.

Given that the power factors of DGs are constants, the reduced network loss cost due to the installation of DGs can be expressed as Equation 4:

$$F_3 = (P_0 - P_{loss}) \times T_{max} \times C_e \quad (4)$$

where P_{loss} = the network loss without the installation of DGs; C_e = sale electricity price of the grid.

The total investment cost of DGs can be converted into the cost of each year as Equation 5:

$$F_4 = \sum_{i=1}^{N_{DG}} \frac{P_{DG_i} \times E_{DG_i}}{Y_{DG_i}} \quad (5)$$

where N_{DG} = the number of DGs; E_{DG_i} = the installation price of unit capacity of DGs; Y_{DG_i} = working life of DGs.

The generating cost of DGs can be expressed as Equation 6:

$$F_5 = \sum_{i=1}^{N_{DG}} (P_{DG_i} \times T_{max} \times C_{DG}) \quad (6)$$

where C_{DG} = the generation price of unit capacity of DGs.

Sub-objectives are viewed in the aspect of economy; the optimal allocation model of DG aims for maximizing annual economic benefits of the grid corporation is shown in Equation 7:

$$\max F = \max(F_1 + F_2 + F_3 - F_4 - F_5) \quad (7)$$

2.2 Constraint conditions

Constraint Conditions of the optimal allocation of DG are as follows.

2.2.1 Power flow equation constraint

$$\begin{cases} P_i = P_{i-1} - \frac{r_{i-1} (P_{i-1}^2 + Q_{i-1}^2)}{V_{i-1}^2} - P_{Li} + P_{DG_i} \\ Q_i = Q_{i-1} - \frac{x_{i-1} (P_{i-1}^2 + Q_{i-1}^2)}{V_{i-1}^2} - Q_{Li} + Q_{DG_i} \end{cases} \quad (8)$$

where P_i = injection active power at the i th node; Q_i = injection reactive power at the i th node; V_i = voltage amplitude at the i th node; P_i = active power load at the i th node; Q_i = reactive power load at the i th node; P_{DG_i} = injection active power of DGs at the i th node; Q_{DG_i} = injection reactive power of DGs at the i th node.

2.2.2 Node voltage constraint

$$K_{V_i} = \begin{cases} k_V (V_i - V_{imin})^2, & V_i < V_{imin} \\ k_V (V_{imax} - V_i)^2, & V_i > V_{imax} \\ 0, & V_i \leq V_i \leq V_{imin} \end{cases} \quad (9)$$

where V_{imax} = the upper limit of V_i ; V_{imin} = the lower limit of V_i ; K_{V_i} = the voltage penalty coefficient of the i th branch line; k_V = the node voltage penalty coefficient, and when the voltage meets the requirements it equals to zero, when the voltage deviates from operating limits it is assigned a very large value as penalty.

2.2.3 Total installation capacity of DGs constraint

$$K_{P_{\Sigma DG}} = \begin{cases} k_{P_{\Sigma DG}} (P_{\Sigma DG} - P_{Lmax})^2, & P_{\Sigma DG} > P_{Lmax} \\ 0, & P_{\Sigma DG} \leq P_{Lmax} \end{cases} \quad (10)$$

where $P_{\Sigma DG}$ = the total installation power of DGs; P_{Lmax} = the upper limit of the total installation

power of DGs; $k_{P_{s,DG}}$ = penalty coefficient of the DG installation power, and its principle of value assignment is as the one of k_v .

2.2.4 Node installation capacity of DGs constraint

$$0 \leq P_{DG_i} \leq P_{DG_{i \max}} \quad (11)$$

where P_{DG_i} = the installation power of DGs at the i th node; $P_{DG_{i \max}}$ = the upper limit of the installation power of DGs at the i th node.

3 OPTIMAL ALLOCATION OF DISTRIBUTED GENERATION BASED ON CUCKOO SEARCH ALGORITHM

3.1 Cuckoo search algorithm

In 2009, Xinshe Yang and Deb Suash put forward the cuckoo search algorithm based on the brood parasitism of some cuckoo species. Besides, the latter improved CS algorithm uses the Lévy flights instead of simple isotropic random walks to generate candidate nest (Yang, X.S. & Deb, S. 2009). Due to the simple setting of parameters, strong development capability in the optimization process, CS algorithm has been successfully applied to the practical problems in engineering optimization.

There are three idealized rules of the description of CS algorithm as follows (Yang, X.S. et al. 2012.):

1. Each cuckoo randomly chooses one host nest and lays one egg (representing one solution) in it at one time.
2. Among the randomly chosen host nests, the best host nest with the highest quality egg will remain to the next generation.
3. The number of the available host nest is constant, and a host bird can discover a foreign egg with a probability, i.e. $P_a = [0, 1]$. In this case, the host bird can either throw the egg away or abandon its nest and build a completely new nest elsewhere.

The host nest position is updated by Lévy flight as Equation 12 shows:

$$X_i^{k+1} = X_i^k + \alpha \otimes L(\lambda) \quad (12)$$

where X_i^k = the host nest position of the i th host nest in the k th generation; α = step size controlling factor which is related to the dimension of the optimization problem, and it is positive; \otimes = the entry wise multiplication; $L(\lambda)$ = the step size

drawn from a Lévy distribution, and its expression is given in Equation 13:

$$L(s, \lambda) = \frac{\lambda \Gamma(\lambda) \sin(\pi\lambda/2)}{\pi} \cdot \frac{1}{s^{1+\lambda}}, \quad (s \gg s_0) \quad (13)$$

where s_0 = the minimum step size; Γ = a Gamma function.

Flowchart of cuckoo search algorithm for solving the optimal allocation of DG is shown in Figure 1.

3.2 Coding program

In order to optimize the sitting and sizing of DG at the same time, this paper makes full use of the real coding characteristics of CS algorithm to avoid the tedious coding and decoding of binary coding.

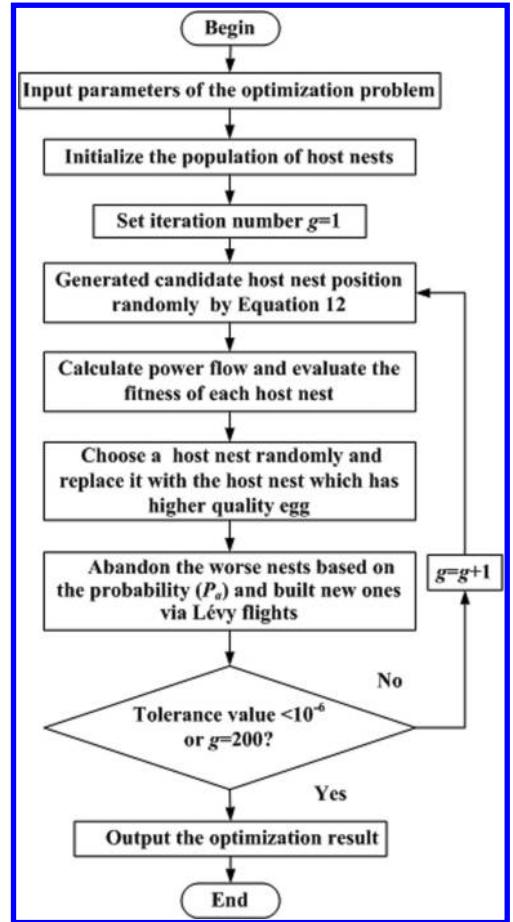


Figure 1. Flowchart of cuckoo search algorithm.

The rated power of DG is converted into a fixed number by Equation 14:

$$P_{DGi} = x_i P_s \quad (14)$$

where P_s = reference power; x_i = a real number between interval $[0, M]$, and $M = [P_{DGmax}/P_s]$.

Through the above process, the DG installation scheme of a radial distribution network which has N nodes available to install DGs can be presented by a set of variables as $X = \{x_1, x_2, \dots, x_N\}$. The value of x_i represents the condition of DG installation at the i th node. $x_i = 0$ means that there is no DG installed at the i th node. $x_i = C$ (C is a constant between interval $[0, M]$) means that there is DG installed at the i th node, and the installation power $P_{DGi} = CP_s$.

3.3 Fitness function

In this paper, the maximum annual comprehensive economic benefit is taken as the objective function, which belongs to the maximum optimization problem. With constraints the fitness function is given in Equation 15:

$$Fitness = \frac{1}{C_{max} + F} + \sum_{i=1}^{N_{DG}} K_{Vi} + K_{P_{\Sigma DG}} \quad (15)$$

where C_{max} = a large enough constant.

4 SIMULATION AND ANALYSIS

4.1 Simulation example

Figure 2 shows the IEEE33 node distribution system simulation example. The rated voltage of this distribution system is 12.66 kV. Total active power load is 3715 kW and total reactive power load is 2300 kvar. All DGs are viewed as PQ node and the power factor is 0.85. The maximum total DG installation power cannot exceed 25% of the total system loads, that is, the maximum DG installation power is 1114.5 kW. Besides, the maximum DG installation power at one node is 500 kW. The reference power

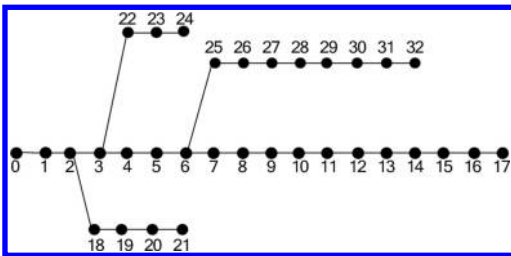


Figure 2. IEEE33 node distribution system.

Table 1. Installation location and capacity of DGs.

Location	11	16	17	29	31	Total
Capacity/kW	100	100	200	400	100	900

Table 2. Annual economic benefits of the grid corporation.

Function	F1	F2	F3	F4	F5	Total
Benefit/ 10 ⁴ yuan	262.92	9	44	-11.52	-299.59	4.81

is 10 kW. In addition, $C_e = 0.5$ yuan/kWh; $C_d = 0.3$ yuan/kWh; $C_{DG} = 0.38$ yuan/kW; $C_i = 1$ yuan/kWh; $E_{DGi} = 1280$ yuan/kW; $Y_{DGi} = 10$ years; $T_{max} = 8760$ hours; $t_{max} = 100$ hours; $k_v = k_{P_{\Sigma DG}} = 999$.

4.2 Results analysis

CS algorithm is applied to get optimal allocation of DG and the optimization results are presented in Table 1. Table 2 lists the annual economic benefits of the grid corporation.

It can be seen from Table 1 that the total install capacity of DG is 900 kW, which is 24.2% of the total loads of the system without exceeding the limit of 25%. In addition, $P_{loss} = 102.22$ kW but $P_0 = 202.68$ kW which is effectively reduced by 49.57%. This can be explained that because the five DG installation nodes are located approximately at the end of the network, so that the power flows between nodes reduces which consequently reduces the network loss. Table 2 shows that with the optimal allocation of DG, the annual economic benefit of the grid corporation amounts to 48100 yuan.

5 CONCLUSION

Aiming for the maximum annual economic benefit of the grid corporation, a multi-objective optimal allocation model of DG was established in this paper. Cuckoo search algorithm was adopted to solve the sitting and sizing of DGs. Results of simulation example showed that the reasonable allocation of DG was effective to reduce the network loss and increase the economic benefit.

REFERENCES

- Hu, H. et al. 2006. Computing the maximum penetration level of multiple distributed generators in distribution network taking into account voltage regulation constraints. *Proceedings of the CSEE* 26 (19): 13–19.

- Li, G. & Lv, L. 2006. A figure-based method of optimal placement of DG. *Relay* 29 (4): 91–96.
- Tsikalakis, A.G. & Hatziargyriou, N.D. 2008. Centralized control for optimizing micro grids operation. *IEEE Transactions on Energy Conversion* 23 (1): 1132–1144.
- Wang, C. & Nehrir, M.H. 2004. Analytical approaches for optimal placement of distributed generation sources in power systems. *IEEE Transactions on Power Systems* 19 (4): 2068–2076.
- Wang, F. et al. 2012. Optimal placement of distributed generations using sequential quadratic programming. *Computing Technology and Automation* 31 (3): 76–79.
- Xu, S. 2009. Consideration of technology for constructing Chinese smart grid. *Automation of Electric Power Systems*, 9 (33): 1–4.
- Yang, X.S. & Deb, S. 2009. Cuckoo search via Levy flights. *Proc. World Congress on Nature & Biologically Inspired Computing, Coimbatore, 9–11 December 2009*. Piscataway: IEEE.
- Yang, X.S. et al. 2012. Cuckoo search for business optimization applications. *Computing and Communication Systems, Durgapur, 21–22 November 2012*. Piscataway: IEEE.
- Ye, D. et al. 2011. Sitting and sizing of distributed generation planning based on adaptive mutation particle swarm optimization algorithm. *Power System Technology* 35 (6): 155–160.

Regression, continuation, and innovation—contemplating upon the construction of livable communities

K. Yang

Department of Architecture and Urban Planning, Jilin University of Architecture, Changchun City, Jilin Province, China

ABSTRACT: According to China's prospect of expansion and development, nationwide massive constructions are unavoidable. However, we still need to pay attention to the overall pattern of the constructing process of large-scale cities. Other than that, how to regulate the traffics by deploying compatible municipal administrative and public service facilities is equally important. Although citizens benefit from the fact that the majority of Chinese cities are bursting towards suburbanization, they are also experiencing unprecedented difficulties. Regarding this dilemma, on the one hand the researcher reflects on the lifestyles caused by modern cities' dwelling environment; on the other hand, the writer contemplates upon the construction of livable communities. Finally, the researcher attempts to propose novel modes of living, which will be compatible with China's direction of developing, and its cultural background.

Keywords: continuous creativity; urban vitality; livable community; "3D modality"

1 INTRODUCTION

Most of the Chinese cities are experiencing a phase of rapid development, which is catalyzed by the environmental advantages of the natural landscapes. Consequently, moving the production and living regions towards the edge, even the suburban area of cities is becoming mainstream. Moreover, private automobiles are turning into citizens' definitive way of trafficking, which is resulted from the newly expanded cities' lack of infrastructures and transport facilities. Under the scrutiny of urban expansion, massive constructions of residential areas, and the arrival of the age of automobile, traditional residential neighborhoods not only impede urban transportation, but it also causes public spaces to shrink, due to the privatization of living spaces.

As Modernism and residential neighborhoods are disappearing in developed countries such as the United States, China is also facing problems, which consist of the gradual separation of citizens and their outdoor environments, the alienation and disconnection among residents, living environment and city spaces' lack of vitality, etc. All these problems require us to examine our living styles in the modern cities from a new perspective; we also need to improve the social and urban problems caused by the reckless constructions of urban residential areas.

2 CONSTRUCTION OF RESIDENTIAL AREAS UNDER THE BACKGROUND OF MODERNISM

2.1 *Extensive constructions result in the "Suburbanization of residential areas" mode*

Firstly, the Modernist method of urban planning and its preference of "suburbanization of residential areas" result in the majority of the city's population to be living in the suburban area. Consequently, the disappearance of streets, along with the lack of urban public spaces, thoroughly decimate cities' environment for walking and pedestrianism.

Secondly, Modernist way of urban expansion, which is represented by zoning (the division of urban land according to their presupposed functions), residential neighborhoods, and boulevards designated to automobiles, impair the wholesomeness, which can only be found in traditional cities. Moreover, the fact that most of the citizens dwell in the suburban area yet work at downtown increases their commuting distances, causes traffic congestion, and ultimately leads to their lack of time for social activities.

Lastly, the Modernist mode of urban expansion causes urban space to become an unrestricted sprawl, which ultimately turns into a typical "rolling chapatti" mode of developing. (Chapatti is an

Indian dish, the pie gets bigger and thinner as the chef rolls it with a rolling stick.) Therefore, reckless expanding cities at the expense of their intrinsic values not only causes the cities to be disorganized, but is also a waste of resources.

2.2 *Residential neighborhoods under the age of automobile, and urban roads*

In her *The Death and Life of American Great Cities*, Jane Jacobs complains that the process of industrial revolution narrows down various functions of a city; the process also forced the streets to have a fixated role, as they are now used only as means of passages, which sucked the vitality out of originally lively cities. (Jacobs 1961) By further increasing the spacing of urban streets, large-scale “suburban residents” demolishes urban networks. The worsening of traffic congestion, along with endless urban expansion are indeed urban problems, yet they are also unavoidable end results caused by the residential neighborhoods, automobile-dependent mode of living.

When reviewing his design principles, Hertzberger also stated that, the purpose for centripetally converging spaces is to intensify the interactions among people who live together, to cultivate something consensual within regulated, limited spaces. Therefore, the spaces of urban roads ought to shift their reliance on the automobiles to a combination of pedestrianism, supported by motorized transportation. As a relaxing outer city space is created: on the one hand the city’s need for transportation is satisfied, while on the other hand, the negative effects of transportation exerted upon citizens are kept to the minimum. In order to achieve this ideal scenario, modifications ought to be made to the residential neighborhoods: instead of being discrete, urban trafficking spaces should be interspersed between housings to let the two effect and influence each other.

2.3 *The incompatibility between modern streets and pedestrianism*

Life is in itself complex and multifaceted, living at different locales further complicates the variations of lifestyles. The neighborhoods are in themselves independent, separated by urban road. However, among them there are scarcely any gratifying public spaces. On top of which, these public spaces lack a sense of communication; what is even worse is their deficiency of interaction with the city. As for China, urban problems caused by residential areas are gradually manifesting themselves started several years ago.

One of the disadvantages of modern cities is the lost of comfort and casualness of streets; streets’

complex outdoor functions are reduced to merely being passages for automobiles. The rejuvenation of streets is considered one of the key acts of the New Urbanism, which regards the pedestrian system as a complete network in and of itself. In order to encourage pedestrianism, pedestrian systems such as security pedestrian trails, shopping centers and auto-free streets are deployed to connect the plazas, hence forming a continuous network of public spaces, which will definitely improve the traffic status of that city.

3 REFLECTING ON THE REFORMATION OF FOREIGN DWELLING MODES

3.1 *The emergence of new urbanism*

The trend of large-scale urban constructions brings about numerous alterations to urban dwelling environment. As a result of which, people started meditating on the issue of residential suburbanization, and its end result is “New Urbanism”. People who are familiar with the American roots of New Urbanism, especially the ones who know about the history of how well post-Modernism was well received in the Chinese academic realm, will know that although the so called “New Urbanism” seems like a regression towards tradition, it is in fact a developing strategy which seeks new possibilities.

Accordingly, the practitioners of New Urbanism also came up with three primary planning principles: 1. Focus on regional planning; the wholesomeness of the region should be placed at top priority. 2. Place human at the center of the design, emphasize on the constructed site’s habitability, and its compatibility with human society. 3. Value history and nature, pay attention to how well does the plan fit its natural, cultural, historical background. New Urbanism also advocates for a “compact mode of development” that values frugality and moderation. The core competitive features of New Urbanism are its compactness, its pedestrian-friendly design, its composite functionalities, its accessibility, and its appreciation towards the ecosystem. Formed during the 1990s, New Urbanism is a set of tenets that concerns both community developing and the new movements in the realm of urban planning; its goal is to create a new generation of cities and housings by redefining the concept of city, as well as the meaning and form of communities. Hence, by applying concepts such as “traditional neighborhood development” and “transit oriented development,” New Urbanism successfully combined the sense of community, meaning of humanity, organically with today’s modern living environment.

3.2 *Community belief*

With the application of the theory of Habitability, lifestyles that support lively, livable communities are becoming accepted and understood by the general population, which is testified by the numerous community centers. To answer those who intend to know exactly what is the theory of habitability, its definition is briefly discussed in the book *New Community and New City—the Disappearing of Residential Neighborhoods and the Rise of New Communities*:

“Habitability of a community is a rather significant indicator of the quality of citizens’ lifestyles; it concerns the conditions of human communities’ level of comfort, security, economy, and welfare. Furthermore, it indicates how satisfied the dwellers/citizens feel about their community and their environment. To be more specific, habitability consists of the following aspects: 1. Security and health, which includes transportation safety, individual, and public wellbeing. 2. Environmental conditions, which concern hygiene, quietness, and the condition of air and water. 3. The quality of social communications, which concern the relationships between neighbors, their quality of communication (whether their communications are consensual; if they mutually respect each other, etc.), and their communal pride. 4. How well does the community support the dwellers’ need for entertainment, artistic pleasure, and unique cultural and historical consumptions.” (Yang 2006).

In the process of “community development,” solely accentuating the relationship between the dwellers and their physical and urban environment is not enough; what is more important is the interpersonal relationships among the residents. Community spirit is a conceptual idea, its origin is closely tied to the dwellers’ cultural awareness, which is also a cultural inclination. Planning processes that take the community spirit into account are qualified as community planning; otherwise they are merely plans for residential areas.

4 RATIONAL AND CREATIVE IDEAS THAT SUIT CHINESE MODES OF DWELLING

4.1 *The division of city blocks*

Through summarizing New Urbanism, it is clear that the construction of integrated hybrid communities is not only a Chinese trend, but also a global tendency. Firstly, by integrating the dwelling, entertaining, commercial, and serving facilities, the multi-functionality aspect of this type of

communities provide convenience for the dwellers, at the same time it also raises the city’s vitality and efficiency. Secondly, the lively community centers of this type of communities on the one hand generate convenient, comfortable public spaces, on the other hand, they provide the city with plenty of spatial areas for other activities. Lastly, the most competitive advantage of this concept of “city blocks” is its lively, high-quality auto-free zones, which in turn make the modern housing spaces that are constructed within this type of community more intimate and humane.

The pedestrian environments constructed in accordance with the “city block” theory are complete systems in and of themselves; the walking environments vary, as different public spaces tend to generate distinctive environments. As most of the Chinese cities are experiencing a phase of rapid development, urban public spaces are becoming key ingredients of citizens’ dwelling spaces, which ultimately qualify as an essential element of the structure of the cities. Moreover, the gradual integration of auto-free streets and housing spaces indirectly proves peoples’ intense aspiration for the organic merging between housing and urban spaces.

4.2 *Communal afforestation as opportunities for cities: The establishment of greenways in communities*

Situated in Chinese cities’ trend of rapid and intense development, communal greenways, being the basic framework and crucial component of urban greenways, will become important relaxing spaces in citizens’ daily lives. Since communal greenways are more intimate to dwellers’ daily lives, their latent advantages are not restricted as raising nearby residents’ living environments and qualities; they can also connect various types of city blocks, housings, neighborhoods, commercial streets, parks, and entertaining facilities, thus forming a self-sufficient urban living circle.

The concept of communal greenways is based on day-to-day lives, and is closely related to the residents’ customs of travelling, living, and their cultural backgrounds. Most of the Euro-American countries are experiencing a phase of counter-urbanization (or de-urbanization,) as the construction process of communal greenways in Western cities is based on the principles of low-carbon lifestyles and environment-friendly methods of travelling. However, as the researcher have mentioned before, the majority of Chinese cities are still in the phase of rapid development, as seen in Chinese cities’ dense population, lack of infrastructures, and deficiency of public spaces.

Therefore, aside than constructing communal greenways and advocating commuting methods that are environment-friendly, efforts should also be made to open up originally discrete communities; on top of that, we should also increase the density of China's network of communal greenways by enhancing the infrastructures, services, places for leisure activities, and greenbelts.

4.3 3D-modaility

4.3.1 "TND" mode of progressing—rethink the issue of neighboring units

Evolved from the traditional communities, TND (Traditional Neighborhood Development) is an entirely new mode of community planning. Presently, the semi-closed lifestyle is more favorable to the Chinese citizens, as it will be a gradual process for the extroverted way of living to be popularized in China, due to the conservative nature of Chinese traditional culture. Since the neighboring units are subordinated by several clusters, which together form the community, the idea is that while the community as a whole is opened to the city, the flow of automobiles is regulated at the entrances of each clusters. Similarly, the flow of pedestrians is regulated at the entrance of each neighboring units. Thus this complex system achieves the status of opened "roads" by deploying enclosed clusters. In order to infuse communities with vitality, shopping malls, auto-free streets, children's parks, clubs, bus stops and other indispensable organic facilities are disposed along the "roads." Moreover, the citizens can benefit from the commercial service facilities, as these facilities along with the construction of urban communal greenways have the potential to thoroughly improve the business arrangement along the city streets.

4.3.2 The application of TOD mode in large-scaled communities

Definition of TOD (Transportation Oriented Development): by appointing developing regions along the intersections of rail-based transportations and bus routes, more people get to utilize the public transit system. Hence, TOD in fact a unique perspective of urban planning which fully incorporates urban public transit systems such as subway, light rail, and buses, with land utilization. TOD tackles issues such as citizens' reliance on automobiles, and the stresses people put on infrastructures by advocating pedestrianism and the use of public transits. Lastly, TOD focuses on several aspects, including maintaining communities in certain sizes, restoring streets to its original role as multi-functioned spaces, thus truly turns a city into a pedestrian-friendly place.

4.3.3 POD (People/Pedestrian Oriented Development) mode of living and healthy methods of travelling

Although commuting methods such as rapid transit, railway based transit and public transit successfully shortens the citizens' sense of distance while commuting within the city, these transportation methods reduce the city's accessibility for pedestrians, as they omit the fact that a city should be a place where pedestrians are able to walk freely. Quite on the contrary, in reality it is quite difficult to incorporate non-motorized transportation into city planning. Therefore, urban transportation system should rethink the importance of pedestrianism and biking.

The researcher intends to argue that the optimal way of urban planning should seek to combine non-motorized transportation with motorized transportation. To be more specific, the establishment of non-motorized transpiration should not equate to adding dedicated lanes for pedestrians and bikers; efforts should be made to inform people of the convenience of getting to destinations on foot by manipulating land utilization and the design of communities.

5 CONCLUSION

The inquiry for theories that are able to deal with China's current communal lifestyles is of paramount significance. During the past several decades, social problems such as sustainable development, environmental conservation, and the emergence of residential communities, along with residential neighborhoods' inability to fulfill the potential of its dwellers' lives have exerted great impact on the interrelationship between people and their living environment. Since each city faces its unique problems, the researcher believes that there is no fixated way of defining optimal urban planning. However, the researcher does agree with the practitioners of New Urbanism that an optimal plan should be placing humans at its center. In order to solve the various urban problems through urban planning, we ought to seek to express our understanding of lifestyles and cultural trend in our designs.

REFERENCES

- Jacobs, Jane. 1961. *The Death and Life of Great American Cities*. New York: Random House.
- Wang, Hui. (3rd Edition.) 2002. *The Application and Theory of New Urbanism*, Foreign Urban Planning.
- Yang, DeZhao. 2006. *New Community and New City—the Disappearing of Residential Neighborhoods and the Rise of New Communities*. Beijing: China Electricity Power Press.

On the study of spatial form and functional partition in the modern ceremony etiquette environment

Ying Li

Art and Design Academy in Jilin Jianzhu University, Changchun, Jilin, China

ABSTRACT: Our country is a cultural ancient country with long history and has the civilized fine traditions. In political, economic and cultural exchanges with all other countries, we win the praise of “ceremonial country”. As the symbol of civilization, the traditional etiquette has long history. Etiquette is a self-disciplined and respect process which is expressed by the conventional procedures and ways in the people interaction and this process occurs in time and space. As a kind of etiquette culture, the ceremony etiquette penetrates into people’s life. This paper analyzes the spatial composition, classification, features in the ceremony etiquette environment, tries to find the effective means that can create decorative art of the ceremony etiquette space and so that lets people have a systematic understanding about the style, culture, color and texture of the ceremony etiquette space. The purpose of understanding the decorative design of the ceremony etiquette environment is to make our lives full, rich and full of new ideas.

Keywords: ceremony etiquette; environmental design; spatial characteristics

Ceremony etiquette is a part of the etiquette culture. As a culture, it penetrates into all aspects of people’s life. Big to the national holidays, important celebrations, religious rites, sports such as the opening and closing ceremonies of the Olympics and World Cup football match, etc. Small to the daily store opening ceremony, foundation stone laying ceremony, birthday, wedding, celebration, etc. Every day of human life will have a variety of large and small ceremony etiquette activities. Etiquette culture belongs to a part of superstructure and it is adapted to the economic base. With the sustained and rapid growth of the national economy, people’s living standard has been greatly improved and more and more people put forward higher requirements on the existing life. Under such situation, people need a kind of ceremony etiquette spatial environments with high quality. The aesthetic shift of the space emphasizes the participation and experience of people. The design of ceremony etiquette space pays more attention to artistic style, cultural features, the pursuit of aesthetic value and the creation of artistic conception. The decorative design of the ceremony etiquette environment is to make perfect design for the etiquette spatial environments and props, visual communication ways or means and light environment and then the environment condition is helpful to the audience to accept the etiquette information. This is a kind of creative art and design activity.

1 COMPOSITION OF CEREMONY ETIQUETTE SPATIAL FORM

Composition of the ceremony etiquette spatial structure refers to link the different characteristics local space mutually indoor and outdoor to constitute the overall space structure. It is closely connected with building structure and material. The visual image such as spatial shape, scale and proportion largely depend on structural organization form and material quality. The combination of technical and artistic form produces appealing interior spatial image and this reflects the nature of interior spatial art.

1. The open space

Open space belongs to export-oriented space. Its interface is transparent. It emphasizes the communication, flow, permeation and ambiguity of the spatial environments, stresses the borrowed scenery and opposite scenery and integrates with the natural scene or surroundings. It can enlarge visual field through borrowing outdoor landscape and gain the sense of infinite space. The flexibility of the open space is big. This is easy to change the spatial scene. This in the open space with psychological effect is often shown as a optimistic, lively and relaxed. On the landscape relation and spatial character, the open space has more receptivity, openness and commonality.

2. The enclosed space
Closed space is basically a stationary and sluggish. The interface is closed. It is surrounded by restricting maintenance entity. In the aspect of vision and audition, it has very strong isolation and seriousness. In the psychological effect, it has strong feeling of field, sense of security and privacy but it is easy to produce the depressing feeling.
3. The semi-open semi-enclosed space
The semi-open semi-enclosed space combines the flowing and resting interface enclosure. It can expand the space through borrowing the outdoor landscape but also has a relative feeling of field and privacy. It is between the indoor and outdoor and between the open and enclosed space, so it is difficult to determine its attribution. It breaks through the restriction of given space and gets more extensive contact with another space and then extends the implicative and intriguing artistic conception.

2 CLASSIFICATION OF CEREMONY ETIQUETTE FUNCTIONAL SPACE

Ceremony etiquette functional space refers to the most basic place where can realize the ceremony etiquette activities. It is mainly composed of public space, information space and auxiliary space.

1. The public space
Public space is also called shared space. It includes the channel, passageway and rest room in ceremony etiquette environment and is the area for the public use and activity. In principle, the design of public space should consider enough area and convenient for the audience to watch and exercise. At the same time, it should also provide the space for rest, stopping, talking and drinking water. In the public space, the channel is the most important part. It is directly related to that whether the audience can watch successfully and whether the ceremony etiquette information can be conveyed effectively.
2. The information space
Information space refers to the actual space of ceremony etiquette activity and is the main part of ceremony etiquette design. Whether can achieve a good visual effect, attract the attention of the guests, effectively convey information are the key of the design of information space. Information space is designed for the guests. The first thing is to consider the requirements of flow and vision, so the way and the setting of goal should be in the first place. Therefore, under the guarantee of the functional requirements of the channel and passageway, how to

provide guests with an exciting information place and an unforgettable visual perception or psychological experience should be paid more attention. This is the emphasis of the design of information space.

3. The auxiliary space
Auxiliary space refers to the space except the public space and information space. It mainly has reception space, staff space, storage space and maintenance space. Auxiliary space must be designed according to the actual situation and the area and the form of ceremony etiquette space. In general, public space should be expanded, information space should be ensured and auxiliary space should be reduced as much as possible.

3 THE BASIC FEATURES OF CEREMONY ETIQUETTE SPACE

The decorative design of ceremony etiquette spatial environments is the detailed design of architectural space and is to organize, adjust, improve and recreate the internal space provided by buildings. It further adjusts the spatial scale and proportion and solves the sequence, join, transition, contrast, and unified relationship of space.

In ceremony etiquette activities, space is in essence a kind of mutual relations produced between a kind of place, environment or an object and the people who feel it. In a certain spatial environments, it constitutes a series of intuitively visual pattern, provides a reasonable and effective communication between people and things or among people and people to ensure that the audience can accept enough information. In this sense, the ceremony etiquette space must satisfy the basic needs of people's flow or movement. That is to say, in the process of certain time, information will be obtained through the cognition and feelings for the ceremony etiquette space. The three-dimensional space aside from time is just a state of itself and then audience can't travel through the spatial kernel. To grasp the content of each local space and then to obtain the overall impression of artistic features of ceremony etiquette space. Therefore, as people's behavior activity process, time makes the entire ceremony etiquette space become real, "living" flowing space with "flesh and blood". In such flowing space, there are novel and chic prelude, tactful and moderate middle part, enthusiastic climax and wonderful ending. There are rhythmic rhythm, metrical rise and fall, gradually varied leisure, specific surprise, contrast ferment and harmonic order. Time becomes a kind of psychological experience of space and makes the audience feel a hyperspatial artistic charm in it.

In addition, the ceremony etiquette space reflects the strong functionality. Such using functionality is different from the pure art space create and also differs from the space of daily life and work and study. Any ceremony etiquette space is conducted with the functional partition or local organization for a certain purpose and constructs or shapes the visual form which can fully convey the ceremony etiquette information and is rich of artistic features by using all effective means. Therefore, in terms of ceremony etiquette spatial design, we not only need to study its basic features like flow, time and watching, at the same time, we should also analyze the audience activities, watching behavior carefully and pay sufficient attention to the related people and engineering. Then we can make the scale and proportion of each part in space corresponded with the behavior and perceptive mode of people in the space. Finally to create a humanized space which should be in accordance with the requirements of display.

AUTHOR BRIEF INTRODUCTION

Li Ying was graduated from Jilin College of the Arts in 2003 and now is the teacher of Art & Design Academy in Jilin Jianzhu University. Her research direction is interior design and its theory.

REFERENCES

- [1] Song Limin. Etiquette ceremony and environmental design. "Decoration". 2007 (3).
- [2] Tang Mingxing. The outline of decorative culture. Chongqing University Press. 2006 (10).
- [3] Wang Jiansong. Display design. China Architecture & Building Press. 2006 (5).
- [4] Lin Fuhou. Ma Weixing. Display art design. Beijing Institute of Technology Press. 2006 (7).

Analysis on the digital architectural construction of architectural surface

Ying Li

Art and Design Academy in Jilin Jianzhu University, Changchun, Jilin, China

ABSTRACT: With the development of time, digital technology more widely applied in the field of construction and the traditional architectural construction has been changed seriously. Through the analysis of the architectural surface digitization, the relationship between the architectural construction and the design process is investigated. The design process mainly includes the design method and design thinking, this lets us understand how the standard design changes. Facing a new environment, our thinking will be adjusted, integrated and transformed. Up to this day, it is urgently necessary to integrate organically the digital, traditional elements and processes in order to continue to develop the digital theory.

Keywords: architectural surface; digitization; new architectural construction

In this new age of building, connection is not the basic problem. The entire architectural surface has no thickness and can be accurately connected. There is no need to use the connection units, nails and screws and no need to be limited by the change of the materials. This is totally the game of space and surface.

The architectural theory we used in the past has not substantial effect in the virtual world. Due to the virtual space is in a state of weightlessness, so the weight and the load are not the basic factors to decide the component size, form and proportion. In the process, there is no concept of structural performance and reliability. In the virtual network world, object is just a kind of virtual embodiment which can arbitrarily scaling.

Architectural structure created by the virtual space will change the feature of a particular location. Such as the Sydney opera house, it greatly improves the look of the Angle of the country and the Sydney harbor and gives people the unforgettable impression. Virtual space can reestablish a specific physical environment and can illustrate to its content anytime and anywhere.

1 THE ADVANTAGES OF VIRTUAL TECHNOLOGY REALIZATION FOR ARCHITECTURAL DESIGN

1. Scrutiny on the early stage scheme of the construction

In modern times, people beset by materialization concepts may want to deny such construction state and there is a contradictory. But when

we find that the present technology can interchange the virtual space and physical space, this contradiction will be readily solved.

At present, there are many architectural design personnel can carry the expected virtual performance to the scheme by computer when protocol the design scheme firstly. Having a virtual visit to the building design scheme quickly and accurately through the 3D CAD system. Compare the virtual space data with the system database, the entity object and space 3D digital model can be accurately simulated. After the comparison, analyzing and assessing the design scheme carefully through the evaluation function of the internal system and making the feedback about whether the each index coefficient in the scheme is in line with the standard, whether the model is correct, whether the energy saving can reach to the maximum and so on.

After making modification suggestions and opinions for the scheme, the design personnel will modify the scheme according to the system feedback and will assess again using the CAAD system, and then established the final design plan after repeatedly assessment.

Therefore, virtual space plays a prediction role which lets architects and owners evaluate in advance. The ultimate aim is to simulate the building structure and material as much as possible and to realize the real experience.

2. Digital implementation constructed in the entity construction

Before, when the computer aided architectural technology did not be used, generally after the

architectural sketches were drawn, the designers made the plan for the building scheme according to the proportion, this could not express design intent intuitively and truly.

Through the use of the CAD technology to design graph and to build model. Designers use Auto CAD to draw construction drawings first, then use Sketch Up to amend the whole design sketches. This replaces the artificial hand painting and reduces the workload. Then designers use 3DMax software for building a simulation model preliminary according to the building on the design sketch and the size and proportion of construction. The digital work is convenient for us to review from various locations and can store the modification process of the plan at any time.

CAD breaks the deadlock which can not stereoscopic and omnibearing observe the design due to the space limitation before. The viewpoint of designers is no longer restricted and the design cost is saved. Also it is beneficial to the stereo change of the design scheme. The building designers are no longer affected by objective factors and their creative thinking is cultivated. This promotes the development of the architectural design industry.

2 DIGITAL CONSTRUCTION AND ANTI-CONSTRUCTION OF ARCHITECTURAL DESIGN

Construction is derived from the Greek and the word means a carpenter or builder. And then extended meaning is the production process, it refers to the artistic creation and covers the skills, methods, materials, even ideas. In 19th century, German scholar Botticher began to talk about the role of architectural construction in the field of building, he thought that buildings have “center and package” two parts and the external package must reflect the center nature. At the same time, he put forward the idea of “local and whole”. Another German scholar Semper thought that buildings have four types, they are foundation, fireplace, roof truss and rooftop and surrounding surface. In addition, he also stressed that “connection” is the most important factor for the construction, but also is the constitution to distinguish different materials.

In the 20th century, on the basis of above, researchers continue to innovative research. They put forward the relations between structure and construction, discussed the relationship between structure and construction technology and came up with that details are the principles of material and construction. They also pointed out that the meaning of the construction is the design of details,

opposed that the detailed control of technology for the architectural surface and argued that detail design is the application of a kind innovation and a kind judgment. They emphasized the connection of structure is the most basic elements.

In the modern research of architectural design and digital construction, people think that the traditional structure and digital construction basic elements and process are opposite and put forward the concept of “anti-construction” to expand the definition of traditional design and construction in the digital age. In the development age of science and technology, computer provides the possibility of a new production method and solution. With the development of science and technology, we can use all kinds of new materials and new production process to transform the information into a kind of material. Traditional architectural construction has been impacted by the digital technology. At present, we need a systematic new architectural construction which can integrate digital and classical elements in order to explore the digital theory of architectural surface preferably.

3 RETHINKING FOR THE ARCHITECTURAL DESIGN OF THE DIGITAL AGE

At the initial stage of the digital age in the 21st century, as a kind of information medium, architecture includes not only the structure, the construction and detail technical factors, it also carries a social life, aesthetic way and a lot of information and it plays the role of carrier of culture. Architectural form should express the natural rules and natural quality of form composition and should express the human’s cognition of elements and rules which form the nature. Composition of architectural form itself is a question of science and technology. The materials science and structure science are the scientific question of studying architectural form. But “the expression of architectural form” is not only a question of science and technology, “the characteristics of material” accords with some human emotion and the natural law revealed by the rationality in architectural structure system is the essence of architectural construction. And the expression of architectural construction is the essence of architectural art.

Architecture is one part of the art, but because of the limitation of technology in every age, we can’t image the free artistic creation. However, how to make the architectural works have better artistry in difficulties becomes an important task of the new age building designers.

4 CONCLUSION

Digital technology is not just a design tool, but also a kind of design media. Digital technology can make designers and social culture at that time in the design thinking process of individual and engine body produce unexpected ideas. The digital new architectural construction of architectural surface will inspire new unknown possibilities.

REFERENCES

- [1] Liu Yudong. The new architectural construction. China Architecture & Building Press, 2012.
- [2] Mao Honglin. Analysis on the combination of CAD and green architectural design [J]. *Kejichuanbo*, 2010, (12): 191,193.
- [3] Hu Xiaoqiang. Virtual reality technology. Beijing: Beijing University of Posts and Telecommunications Press, 2005.
- [4] Yan Junai. Intelligent architectural technology and design. Beijing: Tsinghua University Press, 2005.
- [5] Li Xinggang. Design of the national stadium. *Architectural Journal*, 2008.
- [6] Yu Chuanfei. Outside of the form—on the changes of the architectural connotation in the digital age. *New Architecture*, 2003.

Study the space environment accessories design and creation category

Di Wang

Art and Design Academy of Jilin Jianzhu University, Changchun, Jilin, China

ABSTRACT: The integrated use of analysis, induction, deduction and other methods are used, with social research as the practical basis, for this in-depth study of the creation of the accessories design and innovation in its environment, in an effort to seek the art of creating matching accessories their space environment, and to enhance how the design of cultural, their style, color, texture could empower interaction between human beings and nature, construction and the space environment. And on that basis, the depths of the emotional value of the accessories, could be fully tapped. And with the whole building's indoor and outdoor styles complementing each other's space environment, the individuality and spirituality of each piece of accessory could be utilized to the best.

Keywords: soft furnishings; mood; emotion; environmental

1 THE CONCEPT OF ACCESSORIES DESIGN

Accessories design is not about putting up craft-work, hanging up curtains, laying carpets alone... it is also a comprehensive art form to decorate the entire space, to reflect the content and charm of this space. Accessories design results in the refinement of one or a variety of materials, to produce an inspiring object, to strengthen the space of aesthetic effect, and enrich people's aesthetic needs of the space, to suggest or elevate the intended temperament and individuality of the space. To accessorize a space environment is to arrange the variety of objects in it. There is a wide range of accessories, in extremely diverse forms. Accessories design is an important component in space environment design. It is an emerging discipline, a young profession that serves to better create and deliver the style, taste, mood and atmosphere of the space.

However times may change, accessories always start from expressing certain ideas and culture, and play an irreplaceable role. They are the final complement to the creation of the image of a space environment, to the delivery of an atmosphere and adding a final touch to an environment. It is an integral part of a complete space environment, because the display of accessories must be in congruity an din coordination with other objects in that space and can not exist in isolation.

Accessories design is a big branch of space design. It drives space environment design towards perfection in space, environment, culture, aesthetics, behavior, ideology, etc. and keeps the residents of the building from monotonous life, and brings enrichment and variety to it. Individuals, families, and groups of people would then enjoy a harmonious, orderly, and lasting environment. As an important element in modern space design, accessories design is very important to the success of space design. Accessories to space environment are what flowers, grass, trees, rocks, creeks, zigzag alleys and cottages are to cottages—the element of life and spirit. How dull and boring would a space environment be without accessories? It would be incomplete like a body of only a skeleton without blood and flesh, thus the importance of the art of accessories in modern space design is plain to see.

2 DOMAINS OF ACCESSORIES DESIGN

The art of space accessories design is different from ordinary art of ornamentation that pursues Baroque grandeur or uncontrolled luxury, nor is it similar to the art of environment, which is much more scientific, technical and academic. It falls under popular sciences and it studies the internal and external functionality and artistic effects of buildings.

Space accessories design has two main tasks: one is to better serve the needs of use of that environment, or the functional needs; the second is to better express the atmosphere of the space and strengthen the style of design, or decorative needs.

The Education Department of Jilin Province “125” Social Science Research Project Contract Ji UNESCO combined words [2014] No667.

If space environment is the stage, space accessories play the part to express the essence of the space, to show the drama and metaphor in multi-dimensional space, and through appropriate combination the space environment is given certain meaning to establish various degrees of empathy with the audience.

2.1 *Functional accessories*

Functional accessories are those accessories with both practical value as well as ornamental value, such as furniture, lamps, textile and utensils. It is embodied in the specific, artistic and personalized means of decoration to reprocess and segment the horizontal and vertical indoor interface, to make the spatial layout more reasonable, layers more diversified, and the spatial flow more smooth. It also is a rearrangement or even re design of the space products and accessories, to maximize users' need being fulfilled.

Taking fabric accessories as an example, which have now permeated into every aspect of indoor space environment design, in modern indoor space design, the appropriate use of fabrics has become an important measurement of indoor accessories design. Fabrics often are soft and comfortable, making people feel warm and close. Natural fabrics such as cotton, wool, linen and silk are from nature, could easily create a natural space with a "feeling", and thus mediates with the "hard" feeling from furniture and walls with straight lines. And it brings curve to dull straight lines, softening the space. It is of practical use and is an ornament as well, and also enriches the color of the space. The softness of the fabrics not only brings a soft touch but also serves to absorb loud sound, and insulate sound and heat. Thus its application has been a long history and has been a must in indoor spaces. As fabrics could cover a large area, it plays a major role in the atmosphere, taste and feeling of the indoor space. What's more, fabrics are easy to change to fully express the individuality of the residents.

2.2 *Decorative accessories*

Decorative accessories are mainly to adopt modern ornamental methods such as sound, light and color to soften the space to create a certain vibration. And through various decorative skills, character and individuality are highlighted and the designers' insight is also showcased. The use of artistic accessories, placing statues, using different furniture and carpeting, suggests one's cultural values and is an extension of one's life style. Different cultural backgrounds and geographical differences will be distinct through the use of these

objects to directly touch people's hearts. But these decorations must be controlled and appropriate. Over decorating may not produce better results. Though modern spatial artistic accessories design need to rely on modern sciences and technologies, its ultimate goal is to cater to people and their lives. "All designs are all about people" is the permanent topic of the industry, which will lead people to use the latest and perfected modern technologies to improve life.

Accessories must match the overall style of the space design. So each member must do their best to follow the requirements of the intended artistic effects, to together create a highly useful space environment. Judging an object is pointless if it is taken out of context. Rather, the point is whether it is congruous with the overall space.

2.3 *Accessories chromatics*

Chromatic design and combination are the important link when we enter accessories design. People of different race, gender, age, culture, temperament and experiences have different tendencies and likings, which determines the chromatic style of accessories design.

2.4 *Furniture accessories*

An empty house, be it with fabulous walls, mean nothing practical to people. Only when furniture is installed can it meet the needs of people. Besides, furniture not only deliver practicality, but also aesthetic beauty of various styles. "furniture" has already been defined as a part of the human body. Designs "based on emotions" has become a necessity. "Furniture" is not only a mere function, rather, it has evolved into a house of peace for modern daily life. So it has become the basics of accessories design to make appropriate furniture arrangements.

Looking from the overall space environment, furniture, in addition to serving people' daily needs reflect the overall design styles of the space environment, the users' professional characteristics, aesthetics and cultural likings. It can be said that furniture the main part of accessories design. Furniture exists first of all because of its practical use. Then as times advance, apart from its practical use, furniture's artistic value becomes more and more valued. From the structure and categorization of furniture, we can give two main categories to furniture: practical, furniture for sitting, sleeping, storage, such as sofa, bed, wardrobe; the other, furniture for appreciation, shelves, windscreen, etc. in design space environment, after the space is determined, furniture becomes the main part of accessories design. Furniture arrangement could not

go without the requirements of the overall space design. Different spaces require different shapes and looks of furniture. Furniture is the most direct expression of space properties. Arrangement of furniture is the recreation of space organization. Good furniture design and arrangement reflect the purpose of use, and also the users' likings, status, and give character to the space. In using space, dividing space furniture has always been a good tool to improve the use of space, bring more layers and interest to the space. In creating artistic styles, as furniture takes up considerable space, thus it becomes important in creating space environment. Furniture, like architecture, often comes under the influence of cultures movements, so its styles are always in the change. So the design and arrangement of furniture need to be in congruity with the overall space design. Furniture also come to accentuate other accessories, in the forms of cupboards, shelves, etc.

3 CONCLUSION

The proposal of high class creative space environment is to cater to the current longing for a humane, interesting and ecological design, with strong

realistic value and responding to the zeitgeist. We long for a space with a theme, to reflect the deep and raw emotions for space. A design needs a theme. A society needs a special and humanistic building space. Starting from people, returning to nature, these two themes make the discussion on the creation of the indoor and outdoor space themes important in both theoretical and realistic terms. Studies on this topic will benefit: the creation of indoor atmosphere; overall unfolding of environmental artistic design; creating a venue for human environment emotional interaction. A theme is integral to writing. And so is it to design. It helps the whole design progress. Through "theme establishing" a design could have soul, meaning and culture and thus the unity of human, environment and space could be achieved.

REFERENCES

- [1] Huang Yan eds. *Furnishing Art and Design*. Anhui Fine Arts Publishing House.
- [2] Wang Qijun editor, Tian Yong, Hu Ke Dan, edited by Dan. *Furnishings and Accessories*, China Construction Industry Press.
- [3] Gao Xiangsheng. *Furnishings design* Jiangsu Science and Technology Press.

The exchanged landscape: Reinterpretation of the site

Di Wang

Art and Design Academy of Jilin Jianzhu University, Changchun, Jilin, China

ABSTRACT: The landscape has gradually replaced the building and became a kind of important organizational element. The intertexture of the horizontal surface and the infrastructure which across the earth has replaced the dense and compact spatial form and architectural texture in the traditional cities. In this new structure, landscape refers not only a park or a garden, it contains more connotation: from the highway, the polluted industrial field and even the exurban exploding population demand.

Keywords: landscape exchange; urbanism; field; spatial form

“Multidisciplinary is not self-comfort which is expressed through getting a sense of low-cost security. When the sturdiness of traditional disciplines breaks down, may be in the form of violence, such as under the impact of the popular culture—it (multidisciplinary) begins to work... this is in order to meet the birth of a brand new topic and a new vocabulary.....”.

—Roland. Barth

Because of the spanning of multiple disciplines, landscape becomes not only a lens which can get insight into the contemporary urban but also a medium which can help to rebuild contemporary urban. These views have been stated clearly in the “landscape urbanization” concept that put forward in recent years. Landscape urbanism shows a reorientation of discipline in the current. Among them, the landscape replaces the building and becomes the basic unit of contemporary urban development.

Exchange behavior—from ancient times to the trade route between Europe and Asia, to the rapid spread of the information on the Internet—has become the best interpretation for the public sphere since ancient times in the west. Optimization of exchange behavior itself always directly affected by the external force which used to bear the behavior, such as horse, railway and the Internet, etc—also a long-term relationship is built up among liquidity, exchange and clear interpretation for the field. This relationship continues to this day from the ancient Roman empire. The road map of Roman empire shows us the high density infrastructure which is formed by the trade within its territory. This is

an exchange network and mainly roots its control power of the vast and continuous land. In the middle ages, important trade routes will combine drawing knowledge with territorial control thought. This greatly improves the efficiency of the exchange behavior and symbolizes the beginning of organized business networks. However, this is realized through enhancing information and geographic knowledge and skills and by effectively promoting trade links between the previous fragmented zones.

These trading networks and their corresponding drivers determine the material space of different regions and characteristic of operation and management and then determine the form of urban and suburban landscape nowadays. In the past 25 years, process, ratio and the base of exchange have has great changes, at the same time the change for regional and site interpretation method has been caused.

In the past 2000 years, the constitute of a city public space in general contains business management, production and trade exchange activities, these have formed public space with natural forms which has strong identification: such as the Rome Forum, the middle ages square. The public parks in the early modern city are space types caused by business, even if there are some specious, but overall their produce is in order to counteract the effects of industrialization for the urban landscape and explore the potential of the city.

1 “CONFLICT” PLACE AND “CARRY” BEHAVIOR

The exchange network which is carrying on real-time massive deployment in the broad operation field promotes the circulation furthest and also

Ji UNESCO co word [2014] No. 667th.

enlarges the exchange with other networks, such as promoting the areas with interaction or conflict. High-speed infrastructure network, such as airports, highway interchange and some transport facilities, essentially belongs to conflict place. These conflicting areas do not tend to be randomly, on the contrary, they accumulate each other over time, they usually consistent with the preexisting condition of infrastructure, geographical features, natural resources and programs. In other words, it is formed through rearranging and polarizing the existing terrain but not through removing the old and building the new. Thus, exchange increases and gathers through multiple grid. This indicates that a larger transfer or internal exchange produces in time in a particular moment. At the time when the large exchange activities gathered, the possibility of design emerges. The opportunities of public space and other landscape projects also followed and occupy the area further, then produce a large number of activities and events which are not originally expected.

2 SUPERFICIAL GATHER

Exchange—adjusted network realizes the expansion by adding its own exchange resources. This excludes the land direct expansion of a block or a particular location, but their own distributed and organized expansion in different regions. In contrast, contemporary exchange network tends to be a cross-regional and staged interpretation in order to adapt to the diversified cross. This is indispensable for the success of the operation. Contemporary exchange network is usually not aimed at a particular location, but contains the coordination between the physical contact which is accomplished with the help of transportation infrastructure and the virtual connection which is realized through automatic transmission and communication system. As a result, regional development and structure will be more focused on efficiency and organization method. This is similar to the formation of high performance film—a kind of composite material. On the one hand, as the information receiver, infrastructure and superstructure. On the other hand, it is not limited to these, but falls in between traditional classification and the perception of spatial form. It is a kind of secondary landscape, it is the place where can provide support, service and areas for many exchanged and occupied possibilities that occur in the internal structure.

Therefore, once as the main content of public landscape, the meaning of architectural form is being empty. And the attention of investment and public has turned to their middle region. The region here does not mean the external environment or

the remaining space, it is a landscape full of tension and highly organization. So high efficient region can provide necessary logistical functions in exchange network and the traditional top security system either degenerates into a hierarchy of the system or integrates into the entire structure. This indicates a systematical rather than aesthetics method for the interpretation of the base. In this case, the sensitivity of design is more tend to performance and operating efficiency but not synthesis of traditional form. This points the way for the building innovation. This makes the design away from the demand of the pure aesthetics and integrate with the logic of operation strategy and the continuous and temporary spatial pattern. Furthermore, the effects from the long-term fluctuations and the various correction are avoided.

3 WEAKENED GEOGRAPHICAL FEATURES

In more traditional trade routes and trade organizations, by capturing the best time and place of exchange activities: personally exchange of goods, we can clearly interpret city landscape. Today the clear understanding of commercial area is realized through adapting the trading process or deploying the hand exchange. In the past, if time and place of an exchange are considered to be the best expression of the operation in the business and then they are the embodiment of commercial landscape from the form and symbolic meaning. Contemporary business exchange ecosystem pays more attention to the direct exchange behavior. Its success is determined by efficiency and the best scheme of exchange process. Thus, the adjustment and changes along the exchange path will be reduced to minimum, so they were thought to be the weakest time with many loopholes in the network. For a complex exchange system, the operation standards should be reducing the interruption and keeping the seamless implementation of exchange process—that is to say, the most flexible deployment process should have no necessary to correct to maintain the long-term effect of their trading trajectory or the flexibility should make continuous process won't be affected by modify. The frail moment in the network often has its own value, such as providing the sign that can help to identify the system and exploring the new space opportunity.

4 REGIONAL COMBINATION

The importance of combination and cooperation: either become a kind of economic union or form

the union between communication system and politics because of special interest. This short-term existed definition on its field depends on the interaction between many different levels information and leads to other operational definition for the field. In the site with collective exchange behavior, the separate individuals get together and look for self-expression in particular public practice, this reflects their social, political and cultural beliefs. These sites have been greatly promoted by increasing the precision of the communication technology. These technologies will help the combination between the public express and private purpose to form a tribal alliance type landscape. Thus, space region becomes more flexible and mobile, temporary correction can define the nature of area better relative to the specific environment.

5 CONCLUSION

Those familiar space types are formed after a long process. They are the optimized result of some event, until the new behavior begins to take over and leads to its restructuring, they are abandoned

from the original position. The complexity and strong liquidity of exchange process lead us to suspect the definition of the public area that we built up 15 years ago and always trust. As designers, when there is chance to participate in the design of new urban landscape and public project, we will be very glad to have this opportunity to consider how are these processes constantly challenging our traditional disciplines and professional response. Regardless of location and situation, landscape urbanism is not only discuss the design of new spatial form under the condition of integrating infrastructure, business and information system, but also explore its social, political and cultural influences in the process of reinterpreting the public space.

REFERENCES

- [1] "Landscape urbanism" (U.S.) Charles. Kurt Waldheim. Translated by Liu Hailong, Liu Dongyun, Sunlu. China Building Industry Press.
- [2] "The graphical introduction of landscape architecture form and texture" Catherine Dee. Dalian University of Technology Press.

Analysis of Northeast Korean vernacular architectural landscape culture

Qi Yu

School of Architecture and Planning, Jilin Jianzhu University, Changchun, China

Chun Liang Wang

Jilin Provincial Architecture Design Institute Co., Ltd., China

School of Architecture and Planning, Jilin Institute of Architecture and Civil Engineering, Changchun, China

ABSTRACT: Chinese Northeast Korean houses in Northeast residential buildings are very representative, has the unique local customs and practices and cultural legends, so far, there are still many well preserved reflects the Northeast regional architectural features of the vernacular architectural landscape, is the value of protection and research of certain. The overall layout characteristics, spatial combination characteristics, construction techniques in the formation and development of specific natural environment and social cultural background.

Keywords: Northeast; Korean vernacular; architectural landscape; folk culture

To live is to be able to make human a long stay in a certain place and build the human life, to live the residential culture is human in living life acquisition and inheriting way of life and all cultural phenomena related to live. Live in the northeast of Korean nationality is a hard-working and talented people, it not only has a colorful, form specific national costumes, and has the characteristic extremely the diet, sacrifice, funeral and so on national customs. Especially the Korean local-style dwelling houses building, more show distinct Korean ethnic culture and custom. Today, in the field of yanbian Korean autonomous prefecture, the country can still see many HeiWa white Korean traditional local-style dwelling houses of the wall. The dawn, under cover of smoke from the village, a yard, a small room, HeiWa and set each other off white walls, which work with the Korean men and women, a national graffiti accumulate flavour is dye-in-the-wood.

Northeast Korea nationality unique is in long-term residence form and residential culture from the northeast area the national culture of natural environment, cultural environment and under the influence of factors such as the formation and development. Residence is comprehensively reflect the natural environment, climate, environment, economic life and the influence of factors such as national culture building, and residential culture is generated on the basis of this. Therefore, residential culture is under the background of national social culture preserved, and constantly changing with The Times development. Among them, the customs associated with living best reflect the ethnic

characteristic of residential culture. As a result of the existence of the custom, of all ethnic groups of residential culture to inheritance and preserved for long, the appearance of the house of all ethnic groups and plays a significant role in the preservation of internal structure.

1 THE NORTHEAST NORTH KOREA LOCAL-STYLE DWELLING HOUSES BUILDING LANDSCAPE FEATURES

Korean is one of the main nationalities in northeast China, on the Korean peninsula or clustered, or for a long time and live together with other. North Koreans populated areas, fertile land, abundant resources, is one of the main forest region in China. Under the Changbai mountain, north Korean immigrants opens up the fertile territory. Under the abrupt show of Changbai mountain, yanbian Korean Chinese live. They have a large mountain development and paddy field, generation lived here, reproduction. The Korean folk house maintained the style of the dwellings before Tang dynasty, Japan in the form of local-style dwelling houses close to this. Korean mostly located in the flat ground of mountain villages, houses, having a unique style. North Korea ZuMin mostly to the top of the mountain park white wall construction, in addition to the urban residential has a simple wall, build walls and rural don't usually, and keep a certain distance between neighbors. Housing plane most of the rectangle and l-shaped, some

set verandah. Internal layout, the main room for the bedroom, straw bullpen and storing sundry “straw” on the side of the building, separated with kitchen and bedroom. How many bedroom, size, visual needs, separated by sliding door, more flexible and convenient. By a sliding door wall inside the bedroom closet, for storing clothing, bedding, make indoor appear capacious and refined. On the door of the family and visitors is kang, want to take off the shoes at the door, to keep the room clean.^[1]

Mostly distributed in yanbian area villages and towns along the mountain would strip. Village in the distance between the range, size and set, is based on how many natural expand acreage. Its terrain selection and han village, in the hill of Yang, close to the road traffic convenient place, or beside the river, the topography gao, there is no risk of flooding. Neighborhood, which is formed by space between road and trail is longer than the general things, have become between horizontal layout, there is also a part of the north and south direction long, vertical and horizontal cross become vertical layout. This shape along the mountains would transfer in length, regardless of the fixed direction; Otherwise arrangement according to the road, the road is very long, there is a certain direction, thus the trail was fellowship with trunk road into parallel or perpendicular direction. Road is the main traffic routes, residents and horses and chariots, no planning, construction house naturally formed after the road. Korean houses when decorate for whether the sun is not seriously, mainly along the road and construction. A house is given priority to with units, most of the courtyard and the walls, therefore, of the house decorate very casual. And because of the house a door access, both before and after the front yard open space and yard space are equal, gable place some connected on both ends of the houses, space zone are very few, is determinant. The Wells dry dwellings changbai mountain region, usually located in the leeward sunningdale flat area. Single-family less, generally is six or seven families live in a small village, arranged between families more loosely, not neat. This kind of settlement way is beneficial to reduce the influence of the winter cold wind.

2 TWO FACTORS AFFECTING THE FORMATION OF THE NORTHEAST NORTH KOREA LOCAL-STYLE DWELLING HOUSES BUILDING LANDSCAPE

2.1 *Natural factors*

Jilin city is an ancient city in central, northeast old name “shipyard” manchu “jilin ula”, is the meaning of living along the river. In jilin area is a

continental climate, cold winter, warm summer, be known according to investigation, the year is the highest temperature of 37 °C, the lowest to minus 42 °C, annual ice period of nearly five months. Annual rainfall of 1000 mm in eastern mountain area, the western desert alkali land precipitation is 635 mm. Most of jilin province for ethnic minority areas, the han, manchu, Korean and Mongolian. Folk residence, there are a lot of change in the form of railway east of the ground and mountains, is rich in timber and rainfall is large, so the houses with wood as the main body, with both ridge type double slope roof, the slope is very steep, tall. Railway, west of alkali soil, a series of wind for months, and the lack of wood, hence building construction short, do the tabular form, commonly known as “solonetz bungalow.

Since ancient times, Korean people like to choose lee sun, mountain, building environment is quiet and tastefully laid out place. Korean folk houses are beautiful appearance, house is in the shape of DaWuDing appearance is the middle flat, two head become warped, the middle flat, such as line, two head become warped flying crane. All of DaWuDing line and the curve and surface are slow, main contour line of the roof are apply for a thick white line. House flat short, the feeling of not high up the steep, especially long narrow Windows proportion, make flat short body and has the potential of high up, and the entire building is firmly located in the low level of stone on the stylobate. Sedate, plain curve and curved surface and the rafter child outside of the great white contour line, it is the difference between the Korean DaWuDing and han, Japan DaWuDing. North Korea’s residence is generally small, digging the so-called built, namely home ground on only a few feet shorter than the ground outside, outside with high barriers to keep out. Benefits is to prevent the northeast cold, heat preservation is wonderful, also be a feature. So the house from the outside is especially short. The chimney is mostly stand beside the house, not in the roof. The appearance of all ethnic groups in northeast China residential, mainly due to the impact of climate formation, which constitute the national housing shape elements—the slope of the roof, the thickness of the wall and other prominent reflect the influence of climate. In addition to that, of all ethnic groups of dwellings, deeply the influence of the local terrain, terrain and natural environment.

2.2 *Social and cultural factors*

The layout of all nationalities in the size of the houses and buildings, influenced by various national economic life level. Is due to the family’s economic strength is different, there differences in

the size of the house; Mode and economic life is different because people of all nationalities, and appear different spatial layout. The internal structure of the national housing is under the influence of national culture. The internal structure of the traditional dwellings, the various ethnic spirit culture is the inherent thought background and the influence of religious factors.

Population of ethnic Korean households is commonly 3–6, an average of around 5 people, housing construction area related to population, with a house for a family. Town house to have a simple wall, while the rural all no wall, no yard, nor a wing, for single detached house, this is one of the characteristics of Korean folk house. Their way of life is not in the yard for activity center, but the house as the center. Korean dance is beautiful and elegant, soft, or lyric natural and unrestrained, or enthusiasm is bold and unrestrained, full performance of the Korean soft, and not weak, elegant and not common national character.

Gallery for double sliding doors, Windows, and door window all Korean folk house, with a door as a window to the window as a door. Doors and Windows for mullion, horizontal Ling is less, the paste paper on the inside. In the northeast cold region, average house do with thick brick wall, adobe wall to prevent cold. While Korean folk house with thin wall and large fire resistance to keep out the cold, this is very distinctive. In the summer, shows its applicability., for single-family dwellings without wing mean single room, the vast majority have no yard and walls, the relationship of the goodwill, peace, and as a family. Traditional architecture in Windows and doors, door and window, is crisscrossed with fine wood lattice, and on paper. Variety of the shape of the window screen is very exquisite, beautiful case, length, fangyuan coordinate, the density interaction, neat, generous, bright-coloured, is rarely seen in northeast Asia.

3 NORTHEAST OF NORTH KOREA LOCAL-STYLE DWELLING HOUSES BUILDING LANDSCAPE RESIDENCE FORM AND TECHNICAL MEANS

The Korean housing structure, the main timber frame is bearing. The foundation earth mat stylobate within 30 centimeters high, surrounding rocks to build by laying bricks or stones. Stylobate foundations may be high up from the water, and was relieved, damp and indoor is relatively dry. Exterior wall is first set up the wood frame, two sides woven straw rope or wicker, wipe out the mud, and plaster finish, middle filling sand; Also have not fill sand, make the cavity wall. In the partition wall multi-purpose double slat wall plastering. Partition wall

is more light body structure, with plaster or clay-ing batten, surface paste paper again. Mostly made of sliding door door, door leaf double-sided pasting paper. This approach not only simple structure, light, the body wall of the area is too small. Summer when every room sliding door open, can each other ventilation, indoor air fresh, so it has both economic and suitable processing technique. But sound insulation, fire protection, this is the shortcoming of partition wall.^[2]

Door of push-pull type, the size of the door window is the same, is often the door regardless of, can make entrance, the vertical arrangement of the lattice, horizontal interval is far, to add the door window is long and narrow, the already low room give a person the sense with tall and beautiful. Roof made four slope, more common approach is to the rafters with straw shade or willow branches, the mud, then cover 30–50 cm thick straw, finally the rope into the grid, to encase the whole roof, or careless use step by step a lap joint, the roof covered, in case the wind will blow straw. In the town, residential use grey terracotta roofs. Tile roof slope curve slightly YanTou corners and tilted upward on both ends of the roof, eaves tiles and ridge and simple ornamental design, form a lively and lively style. It selects the appropriate local materials for building materials. Generally divided into two major categories of mineral and plant. Mineral, brick, stone, etc., including soil plant-based materials including wood pole stalk, etc. The Korean housing construction has certain regularity. Building foundation is very shallow, because the wall body weight is lighter, don't have to do under the permafrost, exterior wall foundation build by laying bricks or stones to 30 cm. The source of the gallery plate can be traced back to ancient buildings in China. In ancient times when built palaces, often take short pile stylobate, with small groups of short column as stylobate and foundation. Both to ventilation, and can be moistureproof. Gallery board it is evolved from it. Porch ground with planks, so called gallery board, Korean residential hall 40 cm higher than the platform base on the ground, the hall ground with planks, between the pillars on ZhuChuShi equipped with square bar, above the beam transverse spreads board.

4 CONCLUSION

Most of the houses in our country, the defense as a folk houses one of the important functions of consideration in the form of buildings, and Korean folk house is—a kind of highly consider residential form of defense. This reflects a—kind of old, goodwill interpersonal relationship harmony, as a rustic amorous feelings. In today's

society, there are very few such local-style dwelling houses building landscape, neighbourhood relations, see traditional residence in north Korea, we inspire? Full text, north Korea local-style dwelling houses building landscape forms, special construction technique, it can be seen around the people of all nationalities have to live, has played a great wisdom and creativity, other national local-style dwelling houses, such as manchu, Mongolian and

han Chinese local-style dwelling houses are worthy of our in-depth study.

REFERENCES

- [1] Jin Junfeng. Chinese Korean folk house. Ethnic publishing house, 2007-32.
- [2] Li-jun Zhou. China building industry press, 2009:212.

Study on characteristics of the recycled cement mortar asphalt slurry

Zhang Liang Liu, Yu Lin Du & Jun Jun Li

Shijiazhuang Institute of Railway Technology, Shijiazhuang, China

ABSTRACT: Based on a provincial highway cement concrete pavement reconstruction project in Handan area in Hebei province, the performance of the cement mortar renewable powder in cement concrete pavement were studied, using the three indicators of the asphalt, penetration, softening point and the ductility of the recycled mineral powder were researched through the contrast test of the limestone powder asphalt slurry, research showed that the renewable powder slurry of cement mortar has a good value.

Keywords: cement mortar; recycled powder

1 INTRODUCTION

A large amount of waste concrete was produced in the process of cement concrete pavement reconstruction, these are the main part of the construction garbage. Nowadays the most effective way to use the waste concrete is to make it to be the recycled aggregate, but large amount of the cement mortar powder was produced. The utilization of recycled cement mortar powder can not only solve the problems of shortages of raw materials in the highway construction, but also obtain remarkable economic and environmental benefits. The research and application of recycled powder at home and abroad is few and far between. This paper did some contrast research on characteristics between the recycled cement mortar asphalt slurry and the ordinary limestone ore powder asphalt mortar, providing a basis on the application of recycled cement mortar powder in asphalt mixture.

2 RAW MATERIAL

2.1 Asphalt

Korea SK heavy traffic AH-70 pavement petroleum asphalt was chosen in this paper. According to the test specification, the performance indexes

meet the requirement specification, the relevant technical indicators were shown in [Table 1](#).

2.2 Limestone ore powder

Ordinary limestone ore powder were compared with recycled cement mortar powder in this paper, limestone ore powder is produced by Hebei Handan Area. The particle size range of 0–0.3 mm. According to the test specification, the performance indexes meet the specification requirements, shown in [Table 2](#).

2.3 Recycled cement mortar powder

The recycled cement mortar powder studied in this paper was obtained by Handan local cement concrete pavement recycled fine aggregate (size 0–5 mm) through the ball mill processing. After examination, the indicators of recycled cement mortar powder also meet the specification requirements, shown in [Table 2](#).

3 TEST ON USING RECYCLE CEMENT MORTAR AS ASPHALT BINDER

3.1 The production of asphalt slurry

Number figures consecutively in the order in which reference is made to them in the text, making no dis-

Table 1. Asphalt performance indicators.

Items	Needle penetration (25°C, 100 g, 5 s)/0.1 mm	Ductility (5 cm min, 25°C)/cm	Softening point/°C	Flash point/°C
Test index	67	≥160	51	321
Code requirement	60–80	≥100	44–54	≥230

3.2 The penetration of the recycled powder asphalt slurry

Penetration is an important index representing the degree of hard and soft asphalt, which is a standard of classification of asphalt label. Introduce the penetration index into the characterization of asphalt mortar, used to characterize the consistency of the asphalt mortar.

Taking the *highway engineering asphalt and asphalt mixture test procedures (JTJ 052-2000)* as the basis. Select load 100 g, 5 s, the penetration experiment was carried out under the condition of test temperature 15°C, 25°C and 30°C. Regression analysis of test results is performed, the test data results as shown in [Table 3](#) and [Table 4](#).

From the test results we can learn that:

1. The common logarithm of the Penetration has a good linear relationship with temperature, three sample penetration increases with the rise of temperature. Under all temperature, penetration of asphalt mortar is lower than that of AH-70 matrix asphalt, which indicated that the samples become bodying and harden with the adding of filler. And the thickening and hardening effect of the recycled cement mortar powder is more significant than limestone ore powder. Therefore, the recycled cement mortar powder used as filler can make the asphalt mucilage harder, rigidity stronger.

Table 3. Regression analysis of penetration test results.

Sample types	Equation of linear regression	Correlation index
AH-70 asphalt	$\lg \text{Pen} = 0.8966 + 0.0383T$	0.999
Limestone ore powder asphalt mortar	$\lg \text{Pen} = 0.6984 + 0.0370T$	0.998
Cement mortar renewable powder asphalt binder	$\lg \text{Pen} = 0.6218 + 0.0378T$	0.999

Table 4. Calculation results of various index.

Items	PIlgPen	T800	T1.2	ΔT
AH-70 asphalt	0.29	52.4°C	-21.3°C	73.7°C
Limestone ore powder asphalt mortar	0.53	59.6°C	-16.7°C	76.3°C
Cement mortar renewable powder asphalt binder	0.38	60.4°C	-14.4°C	74.7°C

2. For penetration index, the addition of filler made the penetration index of sample rise, reduce the temperature sensitivity. And compared with limestone ore powder, the degree of penetration index rising caused by the addition of the recycled cement mortar powder is smaller. The penetration index of recycled cement mortar powder asphalt slurry is smaller than that of limestone ore powder, but the temperature sensitivity is higher.
3. As the equivalent softening point (T800), it increased with the addition of the filler, which help to improve the performance of asphalt mortar under high temperature. Compared with limestone ore powder, the rise range of equivalent softening point caused by the addition of recycled cement mortar powder is bigger, the equivalent softening point of recycled cement mortar asphalt slurry is higher than limestone ore powder, and the high temperature stability is better.
4. For the equivalent brittle point (T1.2), it rises with the adding of the filler, raising the temperature of low temperature embrittlement. Compared with limestone ore powder, the rise range of the equivalent brittle point caused by the adding the recycled cement mortar powder is bigger, the equivalent brittle point of recycled cement mortar powder asphalt slurry is higher than that of limestone ore powder, and low temperature embrittlement is higher, it's not good for the improvement of the anti-cracking ability at low temperature.
5. For plastic temperature range (ΔT), the addition of filler extended plastic temperature range of the sample. It helps asphalt mortar used in a wider range of temperatures. Compared with limestone ore powder, the expansion range of the plastic temperature caused by addition of the recycled cement mortar powder is much smaller. The range of the plastic temperature of the recycled cement mortar powder asphalt-binder is smaller than that of limestone ore powder.

3.3 The softening point of the recycled powder asphalt binder

Softening point of asphalt is the temperature of asphalt began to become soft. It represented the thermal stability of the asphalt. It means that higher the softening point of asphalt is, the higher temperature it needs to reach the same viscosity. This paper introduced the softening point into the asphalt binder characterization for representing the thermal stability of the asphalt mortar, and using the same test procedures as the asphalt sample. Test results such as [Table 5](#).

Table 5. Softening point test results.

Test type	AH-70 matrix asphalt	Limestone ore powder asphalt mortar	Cement mortar renewable rubber powder asphalt slurry
Softening point	51	58	61

Table 6. Mucilage asphalt ductility test results.

Items	5°C	15°C
Limestone ore powder asphalt mortar	2.12 cm	5.95 cm
Cement mortar renewable powder asphalt slurry	1.89 cm	5.64 cm

From the experimental results indicated that: the softening point of sample rise after adding filler, it shows that the filler is very outstanding in improving performance on high temperature stability of asphalt mixture, the asphalt mortar played an enhancement effect at high temperature, which made the asphalt mixture have enough strength to resist high temperature deformation at high temperature. Compared with limestone ore powder asphalt slurry, the softening point of recycled cement mortar powder of asphalt slurry rise more, the softening point of recycled cement mortar powder asphalt slurry is higher than that of limestone ore powder. Therefore, when the temperature rises, the recycled cement mortar powder asphalt slurry has a larger viscosity, higher strength to resist external forces to prevent the high temperature deformation, thus effectively preventing the rutting. This is because in the asphalt mortar, cement mortar powder enhancement effect is stronger, the addition of recycled cement mortar powder make asphalt slurry harder, high temperature performance is better.

3.4 Ductility of the renewable powder asphalt slurry

Asphalt ductility also calls the asphalt elongation, is an important performance index of flexibility, tensile and abrasive resistance. AH-70 matrix asphalt ductility is much bigger than ductility of asphalt mortar. Therefore, the ductility of the

matrix asphalt is not in the scope of discussion. This paper introduced the ductility into the characterization of the asphalt slurry, used to characterize the flexibility of the asphalt slurry. Shape the asphalt slurry into the asphalt sample. Determine ductility of asphalt mortar under two 5°C and 15 °C. The test results as shown in Table 6.

4 CONCLUSIONS

This article studied the performance of recycled cement mortar powder asphalt slurry from the penetration, ductility and softening point, and compared with limestone ore powder asphalt slurry, get the following conclusions:

1. Compared with limestone ore powder asphalt slurry, penetration, penetration index, equivalent softening point and equivalent brittle point of recycled cement mortar powder asphalt slurry was higher. This shows that temperature sensitivity of the recycled cement mortar powder asphalt slurry is high, temperature stability is good, low temperature crack resistance.
2. Under the condition of 5°C and 15°C temperature, the ductility of recycled cement mortar powder asphalt slurry is slightly lower than that of limestone ore powder. This indicated that the flexibility is not so good, easy to crack.
3. Softening point of the recycled cement mortar powder asphalt slurry is higher than that of limestone ore powder. When the temperature rises, it can resist external forces, prevent the high temperature deformation, prevent the occurrence of the rutting effectively.

REFERENCES

- [1] Technical specification for construction of highway cement concrete pavement [1] (JTG F30-2003) [S].
- [2] Aggregate for highway engineering test code (JTG E42-2005) [S].
- [3] Li Zhanyin. The properties of recycled aggregate concrete test research [D]. Xi'an University of Architecture and Technology, master thesis, 2003.
- [4] Li Ye, experimental study on the performance of recycled aggregates [D]. Master thesis of Chongqing University, 2009.
- [5] Jian Zhuang, Sun Zhenping, Li Jiabin, Gu Zhiqiang. Waste concrete crushing and regeneration technology research. Construction technology. 2005. 36 (2): 142-144.

Risk evaluation of hydroelectric asset-backed securitization using fuzzy triangular numbers

Ting Ni

Business School, Sichuan University, Chengdu, P.R. China

Lian Tang

School of Civil and Environment Engineering, Polytechnic University, Hong Kong, P.R. China

Hao Wen

Hydrochina Guiyang Engineering Corporation, Guiyang, P.R. China

ABSTRACT: In this paper, the risks of asset-backed securitization for hydropower stations are measured using analytic hierarchy process. Risk assessment indexes in levels are identified according to the general principles of risk identification and the nature of hydropower projects. In order to dealing with both qualitative and quantitative data, fuzzy triangular numbers are introduced. A case study on risk evaluation of hydropower project is used to illustrate the application potentiality of the proposed approach.

Keywords: hydroelectric asset securitization; risk evaluation; fuzzy triangular number

1 INTRODUCTION

The development of hydropower projects, particularly the cascade hydropower stations, needs huge amounts of money. Asset-Backed Securitization (ABS) with expanded borrowing capacity and lower financing cost than bank loans and enterprise bonds is helpful in improving traditional financing structure.

ABS is regarded as the most advanced financing technique innovation around the world. It got risen and grown in issuing scales, derived types and the application fields within less than forty years other than housing mortgage loan around the world. China has built asset securitization pilots since 2005 which mainly learned from American ABS including credit, non-performing loan, real estate, road & bridge.

Hydroelectric asset-backed securitization is being explored as a promising option in China. Researches in this field focus on (1) the necessity of asset securitization used in hydropower construction; (2) models for hydroelectric asset-backed securitization^[1]; (3) qualitative analysis of risks and risk response. Up to now, the income credential asset-backed securitization of Hydro Lancang is the first and only case in China^[2].

When considering risk management in asset securitization, quantitative analysis is required. Approaches vary, such as Back Propagation (BP), CreditRisk+, grey system theory, Analytic

Hierarchy Process (AHP). However, researches for quantitative analysis in risk evaluation under the consideration of characteristics of hydropower projects are less. Therefore, this paper tried to use well-known method, AHP combined with fuzzy triangular number into risk evaluation for hydroelectric asset-backed securitization.

2 RISK SYSTEM OF HYDROELECTRIC ABS

During the asset securitization, risks vary and have interaction effect and complexity relationship with each other. Risk identification according to stages is an available way.

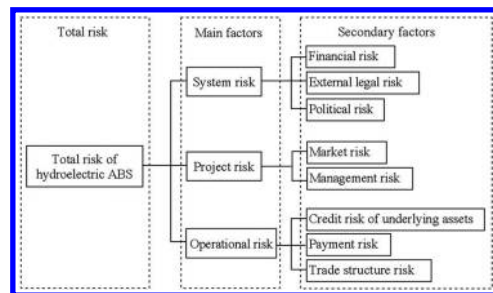


Figure 1. Hierarchy levels of the influencing factors.

Risk factors are identified according to the stages of hydroelectric asset securitization and the characteristics of hydro projects, as shown in Figure 1.

3 FUZZY TRIANGULAR NUMBERS IN AHP

Risk evaluation can be regarded as a decision problem, which is divided into three main steps in analytic hierarchy process^[3]: (1) problem structuring; (2) assessment of local priorities; (3) calculation of global priorities. In the first step, the risk evaluation problem is structured hierarchically at different levels, each level consisting of a finite number of decision elements. The relative importance of the risk elements (weights of criteria) is assessed indirectly from comparison judgments during the second step of the decision process. The last step of the AHP aggregates all local priorities from the decision table by a simple weighted sum. The global priorities thus obtained are used for final ranking of risks.

However, the judgment matrix made of 1–9 integers in AHP is unable to reflect the fuzziness of human judgment. A natural way to cope with such uncertain is to express the comparison ratios as fuzzy set or fuzzy numbers, which incorporate the vagueness of the human thinking. A fuzzy set uses the membership function, which assigns a membership value between 0 and 1 to each criterion or alternative. The Trapezoidal Fuzzy Numbers (TFN) are frequently employed to capture the vagueness of the parameters related to the risks. The fuzzy AHP, which was applied to the triangular membership function, was presented in the early 1980 by Van Laarhoven and Pedrycz^[4].

We define a fuzzy number M on R to be a triangular fuzzy number if its membership function $\mu_M(x): R \rightarrow [0,1]$ is equal to

$$\mu_M(x) = \begin{cases} \frac{x}{m-l} - \frac{l}{m-l}, & x \in [l, m] \\ \frac{x}{m-u} - \frac{u}{m-u}, & x \in [m, u] \\ 0, & \text{otherwise} \end{cases}$$

where $l \leq m \leq u$, l and u stand for the lower and upper value of the support of M respectively, and m for the modal value. The triangular fuzzy number can be denoted by (l, m, u) . The support of M is the set of elements $\{x \in R \mid l < x < u\}$. When $l = m = u$, it is a non-fuzzy number by convention.

Consider two TFN M_1 and M_2 , $M_1 = (l_1, m_1, u_1)$ and $M_2 = (l_2, m_2, u_2)$. Then, the operations laws are as follows.

$$(l_1, m_1, u_1) \oplus (l_2, m_2, u_2) = (l_1 + l_2, m_1 + m_2, u_1 + u_2) \quad (1)$$

$$(l_1, m_1, u_1) \otimes (l_2, m_2, u_2) = (l_1 \times l_2, m_1 \times m_2, u_1 \times u_2) \quad (2)$$

$$\lambda \otimes (l_1, m_1, u_1) = (\lambda l_1, \lambda m_1, \lambda u_1), \lambda > 0, \lambda \in R \quad (3)$$

$$(l_1, m_1, u_1)^{-1} \approx (1/l_1, 1/m_1, 1/u_1) \quad (4)$$

Let $A = (a_{ij})_{n \times m}$ be a fuzzy pairwise comparison judgments matrix and $M_{ij} = (l_{ij}, m_{ij}, u_{ij})$ denote a TFN. Then the steps are as follows:

Step 1: Pairwise comparison judgments of criteria are made by using the fuzzy scales in the same level of the hierarchy structure.

Step 2: The value of fuzzy synthetic extent with respect to the object is defined as:

$$S_k = \sum_{j=1}^m M_{kj} \otimes \left[\sum_{i=1}^n \sum_{j=1}^m M_{ij} \right]^{-1} \quad (5)$$

$$s.t. \sum_{j=1}^m M_{ij} = \left(\sum_{j=1}^m l_{ij}, \sum_{j=1}^m m_{ij}, \sum_{j=1}^m u_{ij} \right) \quad (6)$$

$$\sum_{i=1}^n \sum_{j=1}^m M_{ij} = \left(\sum_{i=1}^n \sum_{j=1}^m l_{ij}, \sum_{i=1}^n \sum_{j=1}^m m_{ij}, \sum_{i=1}^n \sum_{j=1}^m u_{ij} \right), \quad (7)$$

$$\left[\sum_{i=1}^n \sum_{j=1}^m M_{ij} \right]^{-1} = \left(1 / \sum_{i=1}^n \sum_{j=1}^m l_{ij}, 1 / \sum_{i=1}^n \sum_{j=1}^m m_{ij}, 1 / \sum_{i=1}^n \sum_{j=1}^m u_{ij} \right), \quad (8)$$

Step 3: The values of S_i are compared and the degree of possibility of $S_j = (l_j, m_j, u_j) \geq S_i = (l_i, m_i, u_i)$ is calculated. The corresponding value $V(S_j \geq S_i)$ can be expressed as follows.

$$V(S_j \geq S_i) = \begin{cases} 1, & m_j \geq m_i \\ 0, & l_i \geq u_j \\ \frac{l_i - u_j}{(m_j - u_j) - (m_i - l_i)}, & \text{otherwise} \end{cases} \quad (9)$$

Step 4: We calculate the minimum degree possibility d_j of $V(S_j \geq S_i)$, for $i, j = 1, 2, \dots, m$.

$$d_j = \min V(S_j \geq S_1, S_2, \dots, S_m) = \min \{V(S_j \geq S_1), V(S_j \geq S_2), \dots, V(S_j \geq S_m)\} \quad (10)$$

Step 5: We normalize d_i to derive the weight vector. The weight vector W' is defined as follows.

$$W' = \left(d_1 / \sum_{i=1}^m d_i, d_2 / \sum_{i=1}^m d_i, \dots, d_m / \sum_{i=1}^m d_i \right) \quad (11)$$

Step 6: Repeat this process for all levels of the hierarchy structure to obtain the weights of final level criteria.

4 NUMERICAL EXAMPLE

The solution process is based on the proposed fuzzy AHP method. The first step in applying the fuzzy

AHP is to construct a (three level) hierarchy of risk factors for hydroelectric ABS, as shown in Table 1.

30 experts in the hydropower field of the academic and management sectors responded to the questionnaire survey to give specific values (TFN scale in Table 2) to evaluate the risks of hydroelectric ABS.

In this example, we suppose that all pairwise comparison judgments are represented as fuzzy triangular numbers $\tilde{a}_{ij} = (l_{ij}, m_{ij}, u_{ij})$, such that $u_{ij} > m_{ij} > l_{ij}$. Table 3 shows the fuzzy evaluation results of criteria in the first level of the hierarchy with regard to the overall goal.

From Table 3 it is seen that Project risk is considered as the most important criterion, since all fuzzy numbers in the first row are greater than one.

Table 1. Risk assessment index of hydroelectric ABS.

Level 1	Level 2	Level 3
A	System risk	A ₁ Financial risk
		A ₂ External legal risk
		A ₃ Political risks
B	Project risk	B ₁ Market risk
		B ₂ Management risk
		C ₁ Credit risk of underlying assets
		C ₂ Prepayment risk
C	Operational risk	C ₃ Trade structure risk
		C ₁₁ Quality risk
		C ₁₂ Unable to take back generation income
		C ₁₃ The guarantor default
		C ₃₁ The mandatory default
		C ₃₂ Internal legal risk
		C ₃₃ Independent experts risk
		C ₃₄ Technical support risk
		C ₃₅ Interference risk
		C ₃₆ Downgraded securities

Table 2. Fuzzy scale.

Linguistic term	Fuzzy number	TFN
Equal importance	$\tilde{1}$	(1,1,1)
Intermediate values between $\tilde{1}$ and $\tilde{3}$	$\tilde{2}$	(1,2,3)
Moderate importance	$\tilde{3}$	(2,3,4)
Intermediate values between $\tilde{3}$ and $\tilde{5}$	$\tilde{4}$	(3,4,5)
Essential importance	$\tilde{5}$	(4,5,6)
Intermediate values between $\tilde{5}$ and $\tilde{7}$	$\tilde{6}$	(5,6,7)
Very vital importance	$\tilde{7}$	(6,7,8)
Intermediate values between $\tilde{7}$ and $\tilde{9}$	$\tilde{8}$	(7,8,9)
Extreme vital importance	$\tilde{9}$	(8,9,10)

Table 3. Fuzzy pairwise comparisons of the level criteria.

Primary risks	A	B	C
A	(1.000,1.000,1.000)	(0.273,0.375,0.600)	(0.375,0.600,1.000)
B	(1.677,2.677,3.677)	(1.000,1.000,1.000)	(1.333,2.333,3.333)
C	(1.000,1.677,2.677)	(0.300,0.429,0.750)	(1.000,1.000,1.000)

For example, Project risk is assessed as being about three times more important than System risk, and about two times more important than Operational risk.

Using Eq. 5–8, we obtained the TFN values of criteria in level 1 to be the following.

$$\begin{aligned}
 S_A(\text{System}) &= (1.648, 1.975, 2.600) \\
 &\otimes (1/15.017, 1/11.070, 1/7.948) \\
 &= (0.110, 0.178, 1.327) \\
 S_B(\text{Project}) &= (4.000, 6.000, 8.000) \\
 &\otimes (1/15.017, 1/11.070, 1/7.948) \\
 &= (0.266, 0.542, 1.007) \\
 S_C(\text{Operational}) &= (2.300, 3.095, 4.417) \\
 &\otimes (1/15.017, 1/11.070, 1/7.948) \\
 &= (0.153, 0.280, 0.556).
 \end{aligned}$$

We compared the values of S_j individually and identified the degree of possibilities of $S_j = (l_j, m_j, u_j) > S_i = (l_i, m_i, u_i)$ using Eq. 9. Table 4 shows the values of $V(S_j \geq S_i)$. Then, we determined the minimum degree of possibility d_j of $V(S_j \geq S_i)$ for $j, i = 1, 2, \dots, m$ using Eq. 10.

$$\begin{aligned}
 d_A &= \min\{V(S_A \geq S_B), V(S_A \geq S_C)\} = 0.1432 \\
 d_B &= \min\{V(S_B \geq S_A), V(S_B \geq S_C)\} = 1.0000 \\
 d_C &= \min\{V(S_C \geq S_A), V(S_C \geq S_B)\} = 0.5244.
 \end{aligned}$$

Using Eq. (11), we obtained the weight vector $W' = (0.0859, 0.5997, 0.3145)$, where W' is a non-fuzzy number. Therefore, the weights of 3 risks (system, project, operation) were found to be 0.0859, 0.5997, and 0.3145.

The weights of 8 risks for the second level of the hierarchy can be obtained by repeating the same process, as well as the weights of 20 risks in the third level.

After calculating the synthetic level value to order in single level and whole system, we get the rank of risks for hydroelectric asset-backed securitization in Table 5 and Table 6.

Table 4. Values of $V(S_j \geq S_i)$.

$V(S_A \geq S_i)$	$V(S_B \geq S_i)$	$V(S_C \geq S_i)$
$V(S_A \geq S_B)$ 0.1432	$V(S_B \geq S_A)$ 1.0000	$V(S_C \geq S_A)$ 1.0000
$V(S_A \geq S_C)$ 0.1012	$V(S_B \geq S_C)$ 1.0000	$V(S_C \geq S_B)$ 0.5244

Table 5. Risk rated ratio of level 1–2.

	L-1			W'
	A	B	C	
L-2	0.086	0.600	0.314	
A ₁	0.118			0.010
A ₂	0.573			0.049
A ₃	0.309			0.027
B ₁		0.165		0.099
B ₂		0.835		0.501
C ₁			0.008	0.002
C ₂			0.519	0.163
C ₃			0.473	0.149

The evaluation scores of 8 risks in level 2 of hydroelectric ABS risk systems (Financial risk, External legal risk, Political risk, Market risk, Management risk, Credit risk of underlying assets, Prepayment risk, Trade structure risk) were calculated as 0.010, 0.049, 0.027, 0.099, 0.501, 0.002, 0.163 and 0.149. Management risk received the highest evaluation score followed by Prepayment risk and Trade structure risk.

The overall evaluation scores of 22 risks (including 2 factors in level 2 and 20 in level 3) were calculated in Table 6. Facilities maintenance ranked the first. Prepayment risk still ranked the second. Stuff administration was the third. However, the scores of External legal risk, Output decline, Project competition risk and Downgraded securities were very close. It should be noted that the rank of the hydroelectric ABS risk system can be changed according to the different trade structure.

Table 6. Risk rated ratio of level 2–3.

	L-2								<i>W'</i>
	A ₁	A ₂	A ₃	B ₁	B ₂	C ₁	C ₂	C ₃	
L-3	0.010	0.049	0.027	0.099	0.501	0.002	0.163	0.149	
A ₁₁	0.561								0.006
A ₁₂	0.169								0.002
A ₁₃	0.271								0.003
A ₂		1.000							0.049
A ₃₁			0.250						0.007
A ₃₂			0.750						0.020
B ₁₁				0.166					0.016
B ₁₂				0.028					0.003
B ₁₃				0.455					0.045
B ₁₄				0.352					0.035
B ₂₁					0.165				0.082
B ₂₂					0.835				0.419
C ₁₁						0.042			0.000
C ₁₂						0.461			0.001
C ₁₃						0.497			0.001
C ₂							1.000		0.163
C ₃₁								0.146	0.022
C ₃₂								0.097	0.014
C ₃₃								0.251	0.037
C ₃₄								0.205	0.030
C ₃₅								0.063	0.009
C ₃₆								0.239	0.036

5 CONCLUSIONS

This paper attempts to evaluate risks of hydroelectric asset-backed securitization in China. The factors used in the evaluation systems are divided into System risk, Project risk and Operational risk, the selection of which considers the characteristics of hydroelectric assets from build-up hydropower stations.

According to the evaluation, risks from Facilities maintenance received the highest score (0.419). It also illustrated that Management risk from Project risk should be paid more attention. In hydroelectric ABS, the assets pool is made of hydroelectric stock assets which now have stable cash flows in the future. However, unpredictable factors still exist. They might affect the stable cash flows.

Prepayment risk (0.163) and Trade structure risk (0.149) followed the Management risk. Prepayment

has more occasionality than trade structure in the future. But we can well design the trade structure at the beginning of hydroelectric asset-backed securitization to control the total risk.

REFERENCES

- [1] Linping Zheng, Selection of financing patterns in the asset securitization of hydropower station, *Water Power*. 31 (2008) 8–11. (In Chinese).
- [2] Weimin Liao, Xiangjin Zhang, Financing initiatives and practice of the hydropower development in Lancang river basin, *Water Power*. 33 (2007) 4–6. (In Chinese).
- [3] T.L. Saaty, *Multicriteria Decision Making: the Analytic Hierarchy Process*, Cambridge, MA, 1982.
- [4] Van Laarhoven P.M.J., Pedrycz W. A fuzzy extension of Saaty's priority theory, *Fuzzy Sets Syst*. 134 (2003) 365–85.

The application of vortex squeeze expanding mechanism in geotechnical engineering

Chun Bao Li, Shi Feng Xue, Ran Gang Yu, Yan Mei Zhang, Ming Zhang & Xiao Hui Liu
College of Pipeline and Civil Engineering, China University of Petroleum, Qingdao, China

Zhi Jun Zhao
General Construction Company of Laixi, Qingdao, China

ABSTRACT: Proposed and verified the vortex squeeze expanding mechanism, and apply it to geotechnical engineering, introduced vortex extrusion equipments and construction process. It analyses the force relationship between vortex pressure blade, concrete and soil. Established there mechanics model. It discussed the mechanical conditions that the concrete medium squeezes into the soil medium. Put forward the construction scheme that the vortex squeeze expanding mechanism was adopted in compressive piles and uplift pile etc. The results show that Vortex squeeze expanding mechanism can be widely used in the field of geotechnical engineering, has strong applicability. Vortex squeeze expanding method will inject new vitality into the geotechnical engineering industry.

Keywords: vortex squeeze expanding mechanism; compressive pile; uplift pile; squeeze model

1 VORTEX SQUEEZE EXPANDING MECHANISM INSTRUCTIONS

It make the flowing concrete obtain kinetic and static by rotating the pressure vortex squeeze vane, the getting static energy flowing concrete will be squeezed into soil body that outside of the vortex tube by pressure vortex tube though vortex pressure chamber orifice, make the fluid concrete squeezed horizontally at a depth position of soil. This mechanism has been fully verificated in the laboratory (Fig. 1). Carried uplift pile by vortex squeeze expansion mechanism. It will form expanding body when stones being squeezed into the surrounding soil forming, can effectively compact soil pile. The slurry will condensate curing with gravel after it brought into the enlarged body, it formate the enlarged diameter portion in the solid. It will increases the contact surface and the soil compaction by setting enlarged diameter portion on different depths of the soil foundation. When tensioned and pressurized, the enlarged diameter portion will assign the axial load to different soil foundation, make full use of the bearing capacity of different level foundation soil. And will not bear load too much by the friction between pile and soil, or don't load too much transferred to the pile bottom^{[1][2]}.

2 THE MECHANICAL MODEL CONCRETE OUTWARD INTO OF SOIL FROM VORTEX PRESSURE CAVITY

In order to realize the vortex extrusion expansion concrete to the surrounding soil, need to analysis the stress relationship of vortex pressure blade, concrete and soil around. Establishing there mechanics model. Discussed the mechanical conditions that the concrete medium squeeze into the soil medium^[3].

Take "A" of Figure 2 as the research object, carry out mechanics analysis. Vortex pressure blade and it's around soil movement can be regarded as a parallel motion (Fig. 2), when instantaneous motion, The vortex pressure blade is equivalent to rigid (no deformation), keep the compressible soil with parallel motion, the coarse aggregate (stones) is idealized as a rigid sphere^[4]. To investigate the relative motion between the coarse aggregate and the compressible soil when the vortex pressure blade rigid in the force of F , the path and conditions that coarse aggregate squeeze into the compressible soil.

The coefficient of friction between the equivalent rigid body and rigid sphere is μ_1 , the normal force is N_1 , the friction force was f_1 , the coefficient of friction between compressed soil and rigid spheres was μ_2 , the normal force is N_2 , the friction force was f_2 , the stress relationship (Fig. 2).

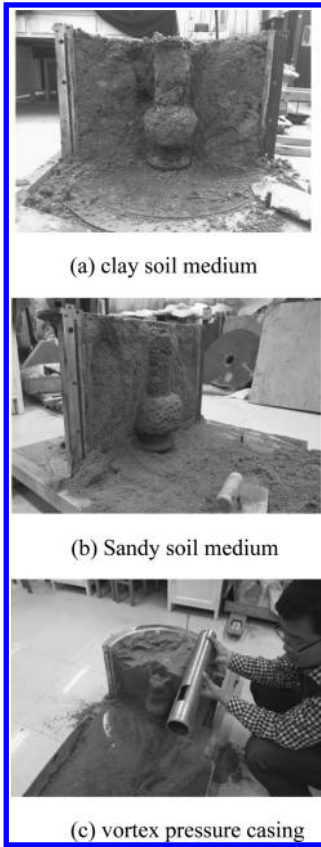


Figure 1. Experimental verification of vortex squeeze expanding mechanism.

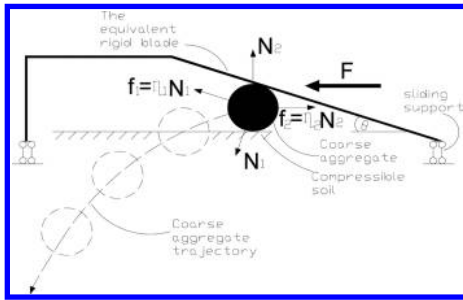


Figure 2. Mechanical model of coarse aggregate to squeeze into the soil.

From the balance we know:

$$\mu_1 N_1 \cos \theta + N_1 \sin \theta = \mu_2 N_2 \quad (1)$$

From the force relationship of the rigid spheres (Fig. 2) we know that in order to make rigid spheres

squeeze into the compressed into soil, it required to meet^[5]:

$$N_1 \cos \theta > \mu_1 N_1 \sin \theta + N_2 \quad (2)$$

Put (1) to (2), Derived as follows:

$$N_1 \cos \theta > \mu_1 N_1 \sin \theta + \frac{\mu_1 N_1 \cos \theta + N_1 \sin \theta}{\mu_2}$$

$$\mu_2 N_1 \cos \theta > \mu_1 \mu_2 N_1 \sin \theta + \mu_2 N_1 \cos \theta + N_1 \sin \theta$$

$$\mu_2 \cos \theta > \mu_1 \mu_2 \sin \theta + \mu_1 \cos \theta + \sin \theta$$

$$(\mu_2 - \mu_1) \cos \theta > (1 + \mu_1 \mu_2) \sin \theta$$

$$\tan \theta < \frac{(\mu_2 - \mu_1)}{(1 + \mu_1 \mu_2)} \quad (3)$$

It can be deduced, when θ , μ_1 , μ_2 meet the relationship $\tan \theta < (\mu_2 - \mu_1)/(1 + \mu_1 \mu_2)$, coarse aggregate (stones) can be squeezed into the soil which out of the vortex cavity. The coarse aggregate trajectory as shown in Figure 2.

3 VORTEX SQUEEZE EQUIPMENTS

Vortex squeeze equipments mainly include: vortex pressure casing, twist the gear, vortex pressure cavity. Precast concrete pile head, bodywork, upright column and diagonal brace (Fig. 3).

It's open at the bottom of Steel casing, set a gear matching with the twist equipment. Medial to ward the bottom of the steel casing is provided with a vortex cavity (Fig. 3-c), vortex pressure cavity is enclosed by the two vortex pressure vane and the two ends of the steel casing. Setting two export at the blade vortex, as the flowing concrete outward extrusion outlet horizontally, the width of each opening, that along the circumferential direction of the steel casing length is 1/4 perimeter of steel casing, opening height is equal to the height of vortex blade (Fig. 3-d). Vortex pressure blade is made of two identical semi-annular plate by anti-symmetric welded, the plane is in the shape of "S" (Fig. 3-b), the linear distance between the two ends of the vortex blade is the same as steel casing pressure diameter. The two "S" shaped vortex pressure blade are welded respectively with the vortex pressure cavity vertical side edge, grind weld smooth. Type of steel, the thickness of the steel plate that used for vortex pressure blade is same as the steel casing. Ensure the connection between vortex pressure blade and steel casing forming a smooth surface. In favor of squeezing the flowing concrete outward horizontal. The inner and outer bottom size of steel casing is matching with precast concrete pile head shape, size. Make concrete pile head that can embed steel

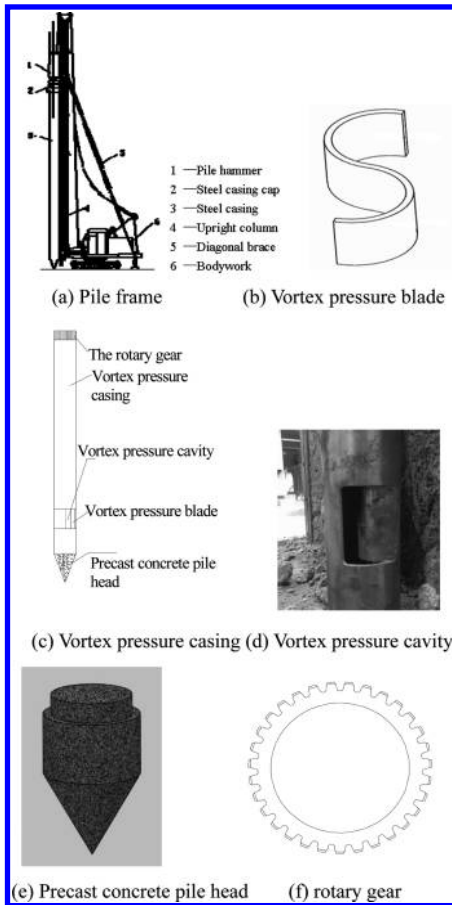


Figure 3. Vortex squeeze expanding equipments.

casing bottom. And have a certain gap to ensure the casing was divorced smoothly from precast concrete pile head when pulled out the casing (Fig. 3-c, 3-e). The inside of rotary is light cylinder, Lateral provided meshing teeth. The outer diameter of steel casing is equal to the inner diameter of the rotating gear. The top surface of the steel casing and the top face of rotation gear are flush. The rotary gear hoop welded on the outside top of the steel casing. The rotary gear is the force transmission device of the hammer and screwed (Fig. 3-c, 3-f).

4 THE APPLICATION PROGRAM OF VORTEX SQUEEZE EXPANDING MECHANISM IN GEOTECHNICAL ENGINEERING

The specific process for uplift expanding pile construction that using the foregoing equipment are as follows:

The specific process for uplift expanding pile construction that using the foregoing equipment are as follows:

The 1st step: Steel casing in place (Fig. 4-a), aim The precast concrete pile head alignment at the hammer pipe buried site.

The 2nd step: Hammer pipe buried (Fig. 4-b), use the hammer break the steel casing with precast concrete pile head together into the soil to a predetermined height.

The 3rd step: Pouring concrete(Fig. 4-c), poured the concrete into the steel casing from it's top.

The 4th step: Twist the casing (Fig. 4-d), connected the twist power device to the top of rotary gear steel casing. By rotating the rotary gear drives the steel casing to rotate together. The concrete in casing was squeezed to the surrounding soil along the horizontal direction through vortex pressure cavity under the vortex blade driven by pressure extrusion. Play expanding, compaction effect. Achieve the purpose of vortex pressure expanding. After knob to the predesigned expanding size, end twist.

The 5th step: Lifting the casing (Fig. 4-e), lifting the steel casing to the next soil layer that needing expanding portion, after completing the vortex pressure expanding.

The 6th step: Carry out upper soil layer vortex pressure expanding (Fig. 4-f), repeat the 3rd step to the 4th step, complete the upper soil layer vortex pressure expanding. The number of enlarged diameter is according to the quantity need of the project.

The 7th step: Pull off the steel casing (Fig. 4-g), after all which need to form expanding implementation completed, Pour the concrete into steel tube internal to the ground. Pull off the steel casing slowly. Take the steel in place.

The 8th step: Insert section steel (Fig. 4-h), insert the H section steel with anchor into concrete, Finish the work of stratified vortex extrusion expansion of reinforced uplift pile.

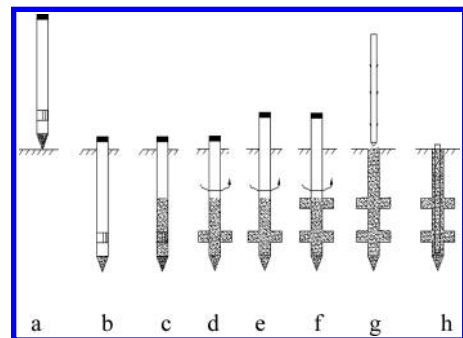


Figure 4. Process of stratified vortex-pressure expanded reinforced uplift pile.

5 CONCLUSION

First proposed the “vortex squeeze expanding mechanism”, and apply it to geotechnical engineering. Describe the design of vortex extrusion equipments and expanding pile construction process in detail. Vortex extrusion expansion equipment is simple and easy to manufacture. Comprehensive analysis showed that the application of vortex squeeze expanding mechanism in geotechnical engineering is feasible, has strong applicability. With the thorough research on the “vortex squeeze expanding mechanism”, it can also be applied to many other aspects in the field of geotechnical engineering. Such as the foundation treatment, shaft wall protection by drilling mud and bolting soil etc. And also applied to other technical fields, such as cement technology used in the oil industry and the mechanical field of fluid machinery.

REFERENCES

- [1] Shen Baohan. Teching Material for Pile Foundation Construction Technique (9). [J]. Construction technology. 2001, 30(1).51–53.
- [2] Sun Tailiang. Model tests on vertical bearing characteristics of variable-section pile. [D]. Shandong. Ocean University of China. 2011.
- [3] Y.Y.S., Barigou M., Seville J.P.K., Parker D.J. Fluid trajectories in a stirred vessel of non-Newtonian liquid using positron emission particle tracking [J]. Chemical Engineering Science, 2000, 55(24): 5969–5979.
- [4] Jiang Jihui. Motion analysis concrete mixing truck mixing process of mixing tube. [J]. Construction Machinery. 1991.2
- [5] Qin Yao. Mechanic analysis and lubrication performance research on V-seal ring. [D]. Shanghai. East China University of Science and Technology. 2013.

Synthesis, characteristics conductivity of heteropoly compound $\text{Na}_6[\text{MnMn}(\text{OH}_2)\text{W}_{11}\text{O}_{39}] \cdot 16\text{H}_2\text{O}$

Ming-Xia Zhu, Li-Qiang Chen & Xiu-Mei Lin

Department of Chemistry, Heihe University, Heihe, Heilongjiang, P.R. China

ABSTRACT: A new heteropoly compound $\text{Na}_6[\text{MnMn}(\text{OH}_2)\text{W}_{11}\text{O}_{39}] \cdot 16\text{H}_2\text{O}$ has been synthesized for the first time. The percentage composition of the product were determined by Inductively Coupled Plasma (ICP) and X-ray Photoelectron Spectroscopy (XPS). The product was characterized by Infrared Spectroscopy (IR) and X-ray Diffraction (XRD), which indicate it possesses the Keggin structure. The TG-DTA curve shows the sequence of water loss in the compound, the amount of the loss, as well as the thermostability. Conductivity of the compound was investigated by four-electrode method at room temperature and different measuring temperatures, the results reveal that its proton conductivity is $8.47 \times 10^{-7} \text{ S} \cdot \text{cm}^{-1}$ at 25°C and the activation energy for proton conduction is 27.96 kJ/mol .

Keywords: heteropoly compound; keggin structure; thermostability; conductivity

1 INTRODUCTION

Heteropoly compounds are a fascinating class of inorganic metal-oxygen cluster compounds^[1]. They are important because of their potential applications such as catalysis, biology, magnetism, photochemistry, medicine and good proton conductivity at room temperature^[2-5]. The heteropoly compounds belong to low temperature proton conductors generally^[6]. Nowadays, many heteropoly compounds have been reported for solid proton conductor, such as $\text{H}_7[\text{In}(\text{H}_7\text{O})\text{CoW}_{11}\text{O}_{39}]14\text{H}_2\text{O}$ ^[7]. Which show that this field continues to have a prominent place at the forefront of heteropoly compounds chemistry. We try to synthesize a heteropoly compound containing element manganese to investigate the conductivity with the change of heteroatoms. In the paper, we originally report the preparation of heteropoly acid $\text{Na}_6[\text{MnMn}(\text{OH}_2)\text{W}_{11}\text{O}_{39}] \cdot 16\text{H}_2\text{O}$ by acidification and the stepwise addition of solution containing the component elements. In addition, we report our result on its conductivity.

2 EXPERIMENTAL

2.1 Instruments and reagents

The Infrared Spectroscopy (IR) was recorded by KBr (S.P. grade) pellets on a 1730-FTIR (P.E. USA) spectrophotometer in the range of $400\text{--}4000 \text{ cm}^{-1}$. X-ray diffraction (XRD) patterns were measured using a D/MAX-3C diffractometer with a Cu target, Cu K_α radiation ($\lambda = 0.15405 \text{ nm}$). The elemental

analysis was performed by a PI ASMA-SPEC (1) ICPAES (Leeman Labs, USA) quantometer. The X-ray photoelectron spectroscopy (XPS) was executed on an ESCA LAB MARKII XPS spectroscopy. Thermal analysis was carried out on diamond TG-DTA P-E thermo-analysis system (USA), the rate of rising temperature was $10^\circ\text{C} \cdot \text{min}^{-1}$. The conductivity was obtained on a KEITHLEY2400 Digital Multimeter (USA). All the reagents used were of Analytical Reagent (AR) grade.

2.2 Preparation

$\text{Na}_2\text{WO}_4 \cdot 2\text{H}_2\text{O}$ (0.11 mol) was dissolved in 300 ml of water and the pH of the solution was adjusted to 6.5 with the acetic acid. After heating this solution to boiling, a solution of $\text{Mn}(\text{NO}_3)_2 \cdot 3\text{H}_2\text{O}$ (0.01 mol Mn^{2+}) dissolved in 100 ml of water was added dropwise while stirring, the stirring was continued for 45 min, and the temperature was kept 95°C . The stirring was continued for 1 h, and the temperature was kept at 75°C . The mixture was cooled at room temperature. A green oily liquid was obtained after adding the absolute alcohol into the above mixture. The red oily liquid was added the absolute alcohol for several times repeatedly, it turned into fine grained shapes finally and kept in a vacuum desiccator. The final yield was about 70%^[8].

2.3 Elemental analysis

Sodium, manganese, and tungsten were analyzed by Inductively Coupled Plasma (ICP) spectrometry. Water content was determined by

thermogravimetry. $\text{Na}_6[\text{MnMn}(\text{OH}_2)\text{W}_{11}\text{O}_{39}] \cdot 16\text{H}_2\text{O}$ is analysed for element(%): Na, 4.36; Mn, 3.33; W, 64.30; H_2O , 9.63. Found: Na, 4.30; Mn, 3.43; W, 63.20; H_2O , 9.57.

3 RESULTS AND DISCUSSION

3.1 IR

Figure 1 shows characteristic peaks of the sample in the range of $400\text{--}4000\text{ cm}^{-1}$. These peaks can be assigned to $\nu_{\text{as}}(\text{W} = \text{O}_d)$ 945 cm^{-1} , $\nu_{\text{as}}(\text{W} - \text{O}_b - \text{W})$ 889 cm^{-1} , $\nu_{\text{as}}(\text{W} - \text{O}_c - \text{W})$ 765 cm^{-1} , 617 cm^{-1} , $\nu_{\text{as}}(\text{O}_a - \text{Mn} - \text{O}_a)$ 412 cm^{-1} and $\nu_{\text{as}}(\text{Mn} - \text{O}_a)$ 573 cm^{-1} , respectively. These data indicate that the compound anions have the Keggin cage structure^[9–10]. We can see the sample has two obvious absorption peaks in 3448 cm^{-1} and 1637 cm^{-1} , they are treated as the stretching vibration of O–H bonds and the bending vibration of H–O–H bonds, respectively^[11,12], these results can illustrate that the sample has water molecules existing.

3.2 XRD

X-ray diffraction pattern of $\text{Na}_6[\text{MnMn}(\text{OH}_2)\text{W}_{11}\text{O}_{39}] \cdot 16\text{H}_2\text{O}$ powdered Sample obtained at room temperature is shown in Figure 2. The compound has distinct characteristic diffraction peaks at the 2θ angle of $6^\circ\text{--}10^\circ$, $17^\circ\text{--}22^\circ$, $26^\circ\text{--}33^\circ$. The positions and intensities of the main peaks are similar to those expected for the Keggin structure. Combined with IR. It can be considered

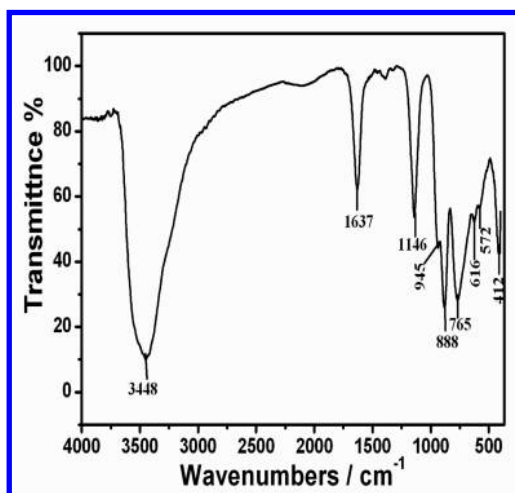


Figure 1. IR spectrum of $\text{Na}_6[\text{MnMn}(\text{OH}_2)\text{W}_{11}\text{O}_{39}] \cdot 16\text{H}_2\text{O}$.

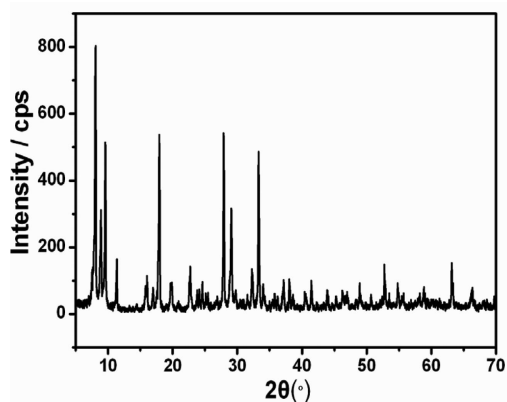


Figure 2. XRD pattern of $\text{Na}_6[\text{MnMn}(\text{OH}_2)\text{W}_{11}\text{O}_{39}] \cdot 16\text{H}_2\text{O}$.

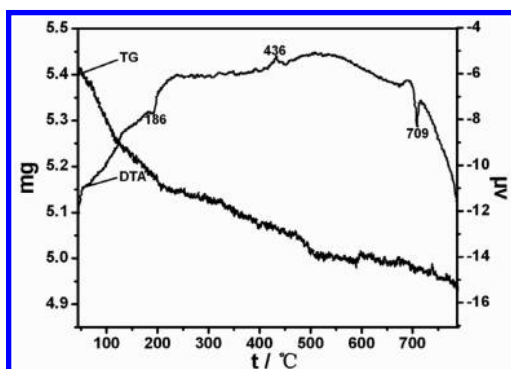


Figure 3. TG-DTA curve of $\text{Na}_6[\text{MnMn}(\text{OH}_2)\text{W}_{11}\text{O}_{39}] \cdot 16\text{H}_2\text{O}$.

that $\text{Na}_6[\text{MnMn}(\text{OH}_2)\text{W}_{11}\text{O}_{39}] \cdot 16\text{H}_2\text{O}$ possesses Keggin structure^[13–15].

3.3 Thermal stability

TG-DTA curves of $\text{Na}_6[\text{MnMn}(\text{OH}_2)\text{W}_{11}\text{O}_{39}] \cdot 16\text{H}_2\text{O}$ is shown in Figure 3. The TG curve can show the weight loss process of $\text{Na}_6[\text{MnMn}(\text{OH}_2)\text{W}_{11}\text{O}_{39}] \cdot 16\text{H}_2\text{O}$. The TG curve shows that the total percent of weight loss is 8.86%, which illustrates that there is three steps of weight loss. The first is the loss of 8 molecules of zeolite water from room temperature to 138°C , the second is the loss of 6 molecules of composition water from 140°C to 318°C , the third is the loss of 2 molecule of structural water from 318°C to 709°C . Furthermore, a strong exothermic peak appears at 436°C in the DTA curve, which is considered to be the decomposition temperature of the compound^[16–18]. A prominent endothermic

peak appears at 709°C in the DTA curve, which indicates the decomposition product melted.

3.4 XPS

XPS is one of common techniques on surface analysis, which can determine the elements of the materials and also can give the information of the elements' chemical states^[19]. To understand the elements consisting of the samples, XPS analysis are conducted on the the sample. The XPS total spectra of $\text{Na}_6[\text{MnMn}(\text{OH}_2)\text{W}_{11}\text{O}_{39}] \cdot 16\text{H}_2\text{O}$ is shown in Figure 4. It can be seen that, there are characteristic peaks of tungsten, manganese, Sodium, and Oxygen in the spectral graph. The calculation result of percentage composition of the product is consistent with ICP result.

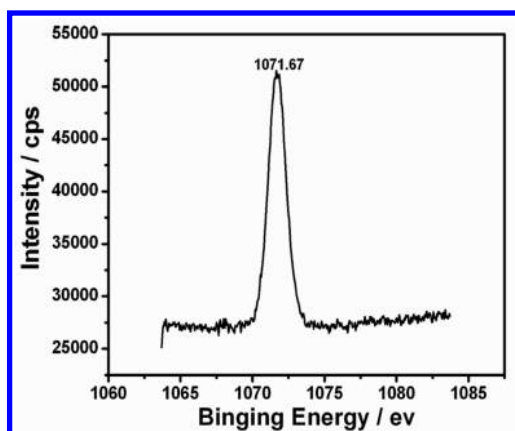


Figure 4a. XPS spectra of $\text{Na}_6[\text{MnMn}(\text{OH}_2)\text{W}_{11}\text{O}_{39}] \cdot 16\text{H}_2\text{O}$ for Na_{1s} .

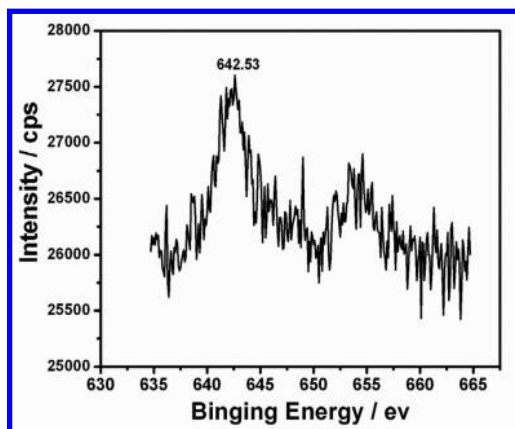


Figure 4b. XPS spectra of $\text{Na}_6[\text{MnMn}(\text{OH}_2)\text{W}_{11}\text{O}_{39}] \cdot 16\text{H}_2\text{O}$ for Mn_{2p} .

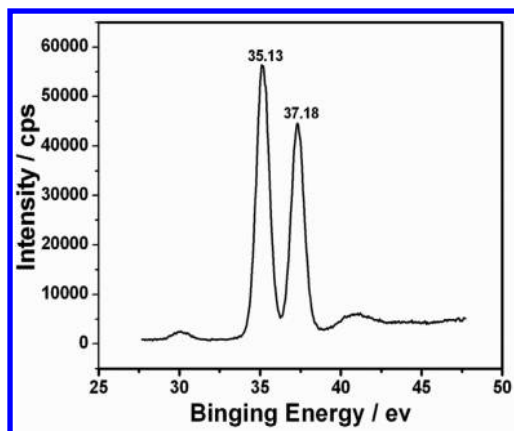


Figure 4c. XPS spectra of $\text{Na}_6[\text{MnMn}(\text{OH}_2)\text{W}_{11}\text{O}_{39}] \cdot 16\text{H}_2\text{O}$ for W_{4f} .

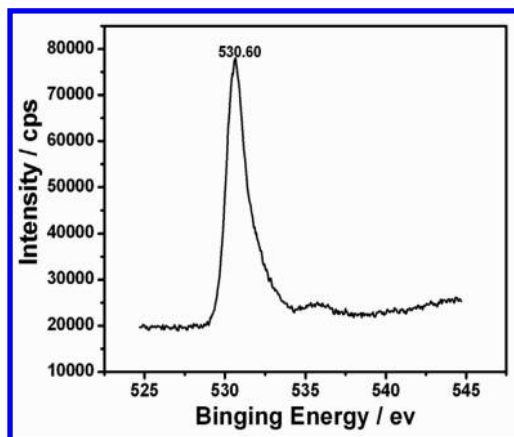


Figure 4d. XPS spectra of $\text{Na}_6[\text{MnMn}(\text{OH}_2)\text{W}_{11}\text{O}_{39}] \cdot 16\text{H}_2\text{O}$ for O_{1s} .

3.5 Conductivity

The conductivity of the compound is measured by four-probe method at room temperature and different measuring temperatures. The electric conductivities of the sample is $\sigma = 8.47 \times 10^{-7} \text{ S} \cdot \text{cm}^{-1}$ at room temperature. The compound of $\text{Na}_6[\text{MnMn}(\text{OH}_2)\text{W}_{11}\text{O}_{39}] \cdot 16\text{H}_2\text{O}$ is a new solid proton conductor. And the conductivity of the compound depends on the number of water molecules. The changes of the electrical conductivity with the increased temperatures meet the Arrhenius equation $\ln \sigma = -E_a/RT$ ^[20]. Figure 5 shows the Arrhenius plot. From the slope, we can calculate the activation energy of proton conduction. By using a curve-fitting algorithm, the activation energies (E_a) of the compound is 27.96 kJ/mol.

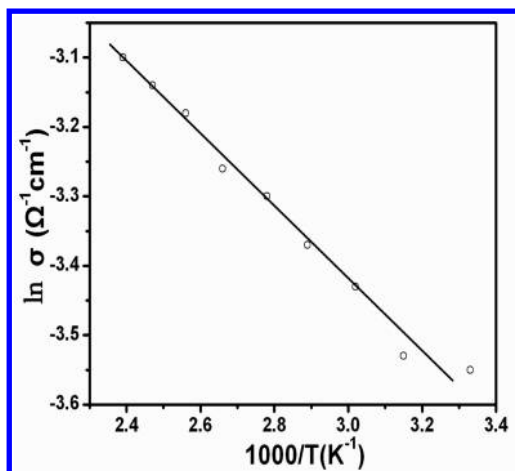


Figure 5. Arrhenius plot for $\text{Na}_6[\text{MnMn}(\text{OH}_2)\text{W}_{11}\text{O}_{39}] \cdot 16\text{H}_2\text{O}$.

4 CONCLUSION

In this paper, we report $\text{Na}_6[\text{MnMn}(\text{OH}_2)\text{W}_{11}\text{O}_{39}] \cdot 16\text{H}_2\text{O}$, a new solid proton Conductor was prepared and characterized for the first time. The IR and XRD indicate that its structure is Keggin structure. TG curve shows that there are three steps of weight loss. DTA curve shows that the thermal stability of the compound is higher than that of $\text{H}_6\text{CoW}_{12}\text{O}_{40}$ (320°C). We determined the conductivity of $\text{Na}_6[\text{MnMn}(\text{OH}_2)\text{W}_{11}\text{O}_{39}] \cdot 16\text{H}_2\text{O}$ by four-electrode method, its proton conductivity is $8.47 \times 10^{-7} \text{ S} \cdot \text{cm}^{-1}$ at room temperature (25°C).

ACKNOWLEDGEMENTS

This work was financially supported by the Science and Technology Foundation of Office of Education of Heilongjiang Province (No. 12521360).

REFERENCES

- [1] U. Kortz, M.G. Savelieff, F.Y.A. Ghali, L.M. Khalil, S.A. Maalouf, D.I. Sinno, *Angew. Chem. Int. Ed.* 41 (2002) 4070–4073.
- [2] R. Chakrabarty, P.S. Mukherjee, P.J. Stang, *Chem. Rev.* 111 (2011) 6810–6825.
- [3] Y.F. Zeng, X. Hu, F.C. Liu, X.H. Bu, *Chem. Soc. Rev.* 38 (2009) 469–480.
- [4] F. Xiao, J. Hao, J. Zhang, C. Lv, P. Yin, L. Wang, Y. Wei, *J. Am. Chem. Soc.* 132 (2010) 5956–5957.
- [5] Z.H. Li, X. Li, B.B. Zhou, Y.R. Guo, *J. Rare Earths* 20 (2002) 479–482.
- [6] G. Alberti, M. Casciola, *Solid State Ionics*. 145 (2001) 249–255.
- [7] Q.Y. Wu, X.G. Sang, F. Shao, W.Q. Pang, *Mater. Chem. Phys.* 92 (2005) 16–20.
- [8] L.Q. Chen, X.M. Lin, M.X. Zhu, L.M. Dai, *AMR*. 937 (2014) 224–228.
- [9] P.A. Jalil, N. Tabet, M. Faiz, N.M. Hamdan, Z. Hussain, *Appl. Catal. A: Gen.* 257 (2004) 1–6.
- [10] B.B. Zhou, Y.D. Wei, Z.H. Li, Y.R. Guo, *J. Chin. Rare Earth Soc.* 20 (2002) 83–87.
- [11] V.P. Tolstoy, L.B. Gulina, G.S. Korotchenkov, V.I. Brynsari, *Appl. Surf. Sci.* 221 (2004) 197–202.
- [12] Q.Y. Wu, G.Y. Meng, *Mater. Res. Bull.* 35 (2000) 85–91.
- [13] Z.H. Li, Y.D. Wei, B.B. Zhou, J. Meng, Y.R. Guo, Z. Lv, *J. Chin. Inorg. Chem.* 19 (2003) 1053–1058.
- [14] Y.P. Wang, B.B. Zhou, Y.L. Liu, *J. Alloys Compd.* 463 (2008) 333–337.
- [15] Q.Y. Wu, X.G. Sang, Y.C. He, X. Li, *Mater. Lett.* 57 (2003) 4028–4032.
- [16] Z.P. Wang, J.Y. Nu, L.Xu, *Acta Chim. Sin.* 53 (1995) 757–764.
- [17] A.V. Ivanov, T.V. Vasina, V.D. Nissenbaum, L.M. Kustov, M.N. Timofeeva, J.I. Houzvicka, *Appl. Catal. A: Gen.* 259 (2004) 65–72.
- [18] Q.Y. Wu, S.K. Wang, D.N. Li, X.F. Xie, *Inorg. Chem. Commun.* 5 (2002) 308–311.
- [19] Z.F. Li, J. Sun, L.P. You, Y.X. Wang, J.H. Lin, *J. Alloys Compd.* 379 (2004) 117–121.
- [20] A.S. Nowick, in: G.E. Murch, A.S. Nowick (Eds.), *Diffusion in Crystalline Solids*, Academic Press, New York, 1984, pp. 143–151.

Study on seismic behavior of pre-cast concrete joint with the capacity of self-centering

Yun Zou & Cheng Li

School of Environment Civil Engineering, Jiangnan University, Wuxi, Jiangsu, China

Qiang Wang

School of Civil Engineering, Shenyang Jianzhu University, Shenyang, China

ABSTRACT: This paper selected fabricated frame with post-tensioned reinforcement “dry type” stitching joint and post pouring “wet type” joint without post-tensioned reinforcement as research objects. Launched a monotonic loading and cyclical loading comparative computational analysis with the finite element software of ABAQUS. By comparing the bearing capacity, the self-centering capacity and the energy dissipating capacity of the two joints, the seismic behaviour of the “dry type” joint is studied. The results show that comparing to the post pouring “wet type” joint, the “dry type” stitching joint with post-tensioned reinforcement performs no worse in the energy dissipating capacity and ductility. Meanwhile, the “dry type” stitching joint performs better in rotation capacity, providing energy ductility in the earthquake, and reducing the extent of damage to beams and columns. Also, because of the rebound effect of post-tensioned reinforcement, the residual deformation of the structure is reduced, achieving the goal of restoration after the earthquake. The research results have certain guiding significance to the popularization and application of prefabricated frame.

Keywords: self-centering; precast concrete joint; finite element analysis; seismic behaviour

1 INTRODUCTION

Precast prefabricated construction is a construction structure of industrial production. It has advantage such as high quality, fast construction and so on. Seismic behaviour is the key point in the study of precast structure. The seismic principles of “three standards and two phase” in our country allow the structure to enter elastic-plastic stage in the medium or large earthquake. It makes large residual deformation and high repairing cost after the earthquake, though it protects the people's safety [1–3].

Fabricated frame with post-tensioned reinforcement joint uses “dry type” stitching method, providing the self-centering capacity by post-tensioned. Self-centering capacity is, after the load is unloaded, the structure or component has the characteristics that can reset to the initial state from a state of maximum deformation. A kind of precast concrete joint is studied, which has the capacity of self-centering. This new connection uses post-tensioned high-strength steel and dry joint method. The post-tensioned reinforcements tie the beam on the column to resist moment and provide self-centering force. In order to study the

seismic performance of such joints, the finite element software ABAQUS is used to analysis the capacity of self-centering and seismic behaviour.

2 FINITE ELEMENT ANALYSIS MODEL

2.1 Basic information of the model

The current domestic and international research shows that adding post-tensioned reinforcement in precast concrete beams can improve the ability to reset the joint, and reduce residual deformation after the earthquake [4]. Therefore, this paper designs a self-centering precast prestressed concrete frame with a joint JD-1, as shown in [Figure 1](#). And a common framework for the precast concrete pouring joint JD-2, as shown in [Figure 2](#). Dimensions and reinforcement of two joints are identical. In order to make the finite element model truly reflect the stress state of the joints in the actual project, the paper model is designed as a general framework for multilayer force across the bottom joint beams combination inflection points. In order to eliminate the interference of size effect, the model is the original ratio of full-scale model.

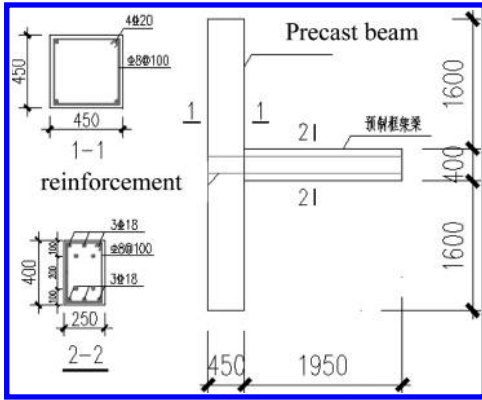


Figure 1. JD-1 size and reinforcement.

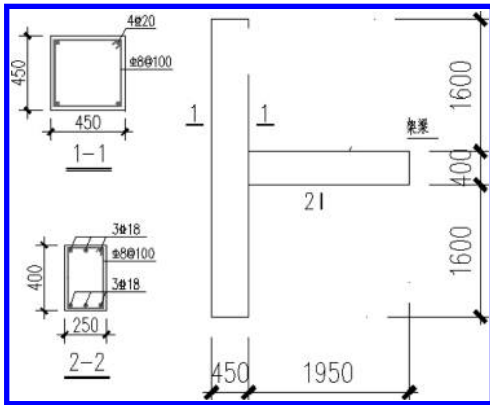


Figure 2. JD-2 size and reinforcement.

JD-1 splice connections use the dry method, when members of prefabricated corrugated pipe buried in the beams, the penetration of four pre-stressing steel is stranded. After using tensioned strand pore filling, joint area is also connected via a non-prestressed reinforcement after reservation pore filling method. Connection JD-2 after pouring the traditional method, some distance from the joint zone effluent pouring concrete at the site.

The distance between the joints column inflection point is 3.6 m. The distance between the beam inflection point is 2.4 m. The dimensions of column section are 450 mm × 450 mm. Sectional longitudinal reinforcement are 4Φ20 mm, and the column section Stirrup is Φ8@100. The dimensions of beam section are 250 mm × 400 mm. Sectional longitudinal reinforcement are 3Φ18+3Φ18, and the beam section stirrup is Φ8@100. Beam-column longitudinal reinforcement use HRB400 rebar, the stirrups use HPB335 reinforced, and the strength class of concrete is C45. Tendons select nominal

diameter of 15.2 mm, tensile strength is 2000 Mpa of 1–7 strand in applying 1000 Mpa pre-tensioning stage afterburner.

2.2 Concrete constitutive model

The concrete outside the stirrups is in uniaxial compressive stress state, using Saenz model to simulate the non-binding region uniaxial compressive stress-strain relationships. Concrete in the stirrups think multiaxial stress state, can be equivalent to uniaxial compressive stress state, the paper core area of concrete using Priestley improved Mander confined concrete model in order to consider constraints stirrups. Joints can be divided into unconstrained concrete area outside stirrups and constrained concrete area in stirrups. Stirrups outside the concrete are in uniaxial compressive stress state, and the stirrups think of concrete under biaxial stress state. In the joint both inside and outside the stirrups equivalent uniaxial compressive stress state. Concrete under uniaxial used compression stress situations—strain curves shown in Figure 3.

2.3 Steel constitutive model

Poisson's ratio of steel in elastic stage is 0.3. Constitutive relation uses ideal elastic-plastic model as shown in Figure 4. In this model, because the use of cooling method to prestress strand, so the prestressing strand uses similar parameters in addition to the definition of steel, but also gives a temperature coefficient of expansion (Expansion), the model of linear expansion of the strand coefficient value is 1e-5.

2.4 Boundary conditions and loading mode

Since the frame is statically indeterminate structure, its simulation boundary conditions is very important to the study of the performance of

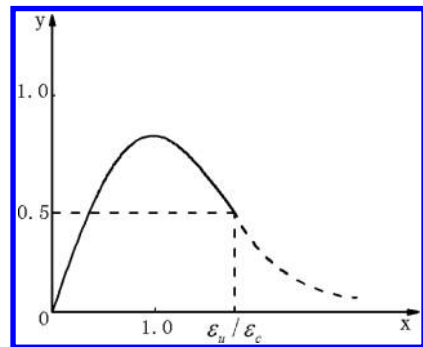


Figure 3. Concrete compression stress-strain relation.

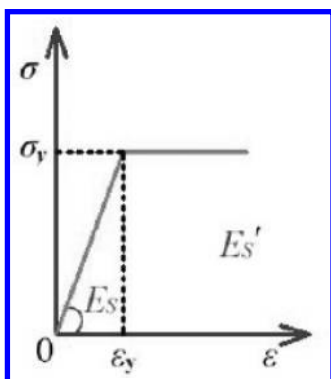
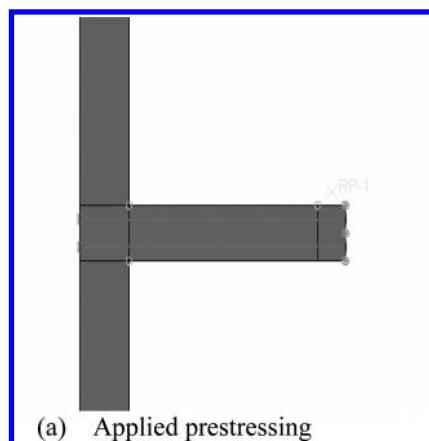


Figure 4. Steel constitutive relation.



(a) Applied prestressing

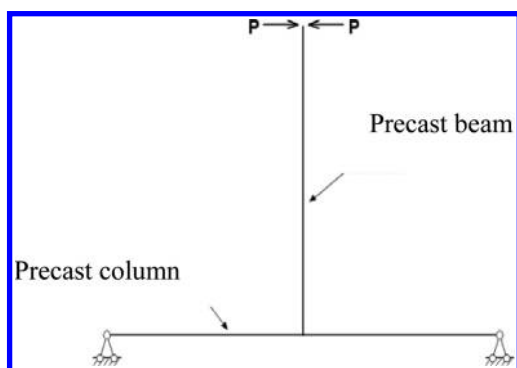


Figure 5. Loading diagram.

its beam-column joints. Reference here adopts Tsinghua University self-centering steel frame joint test program [5] [6], to facilitate loading adopts a “horizontal column vertical beam” mode. Set the hinge support both ends of column to simulation framework inflection point boundary conditions, and the support connected to the ground. Top of the beam is free end, applied the bidirectional horizontal load at the end of the beam to simulated earthquake load, shown in Figure 5.

In order to truly reflect the joint boundary conditions, three-line displacement X, Y, Z, is restrained on the dividing line of the middle of the bottom section of steel reinforced concrete columns of this model, and relax the bottom of the column rotational restraint. The line displacement of the X, Y directions at the cross-section of the concrete beam endpoint is restrained, so that it can not move around. In the column end where to load, Z direction displacement of load pads is controlled, which controls it can not move inside and outside. At the tops of columns where to add uniformly distributed load, Y direction displacement

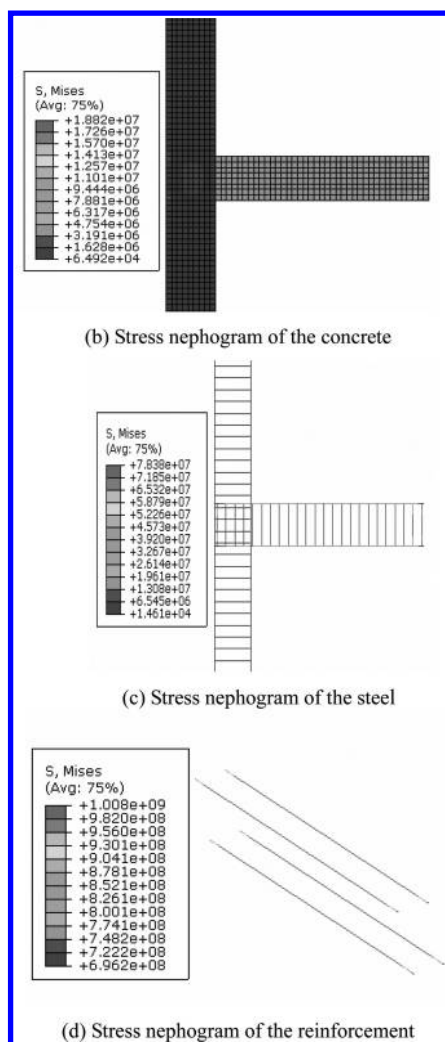


Figure 6. Applied prestressing process.

of load pads is controlled, which controls it can not move left and right.

In this paper of the two joints, the loading process of JD-1 has two stages, the first is to exert prestressed steel strand, then load on the beam end. JD-2 has not prestressed steel strand, load directly on the beam end. JD-1 after applying prestressed, the stress nephogram of concrete, steel bar and prestressed reinforcement are shown in Figure 6.

3 RESULTS AND ANALYSIS

3.1 Analysis of load-displacement curve

The load-displacement curve under monotonic load of JD-1 and JD-2 is shown in Figure 7. As can be seen from the figure, JD-1 due to the addition of the prestressing reinforcement and applying prestressing, its bearing capacity has a certain increase. In the course of the loading, JD-2 has a larger initial stiffness, but early enter into the elastic-plastic stage. Although JD-1 has a lower initial stiffness, but before load into 5 mm, it remained flexible working condition.

The load-displacement curve under monotonic load of JD-1 and JD-2 is shown in Figure 7. As can be seen from the figure, JD-1 due to the addition of the prestressing reinforcement and applying prestressing, its bearing capacity has a certain increase. In the course of the loading, JD-2 has a larger initial stiffness, but early enter into the elastic-plastic stage. Although JD-1 has a lower initial stiffness, but before load into 5 mm, it remained flexible working condition.

3.2 Analysis of hysteresis curve

The hysteresis curve of JD-1 and JD-2 is shown in Figure 8. As can be seen from the figure, the

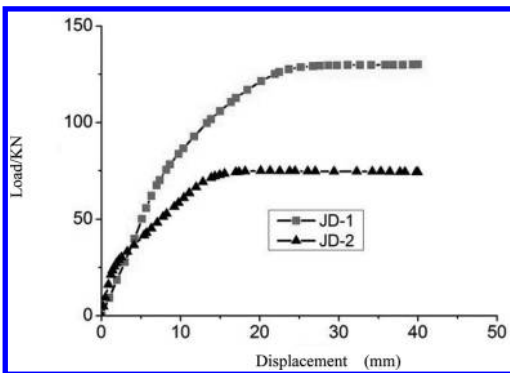


Figure 7. Load-displacement curve comparison reach the ultimate.

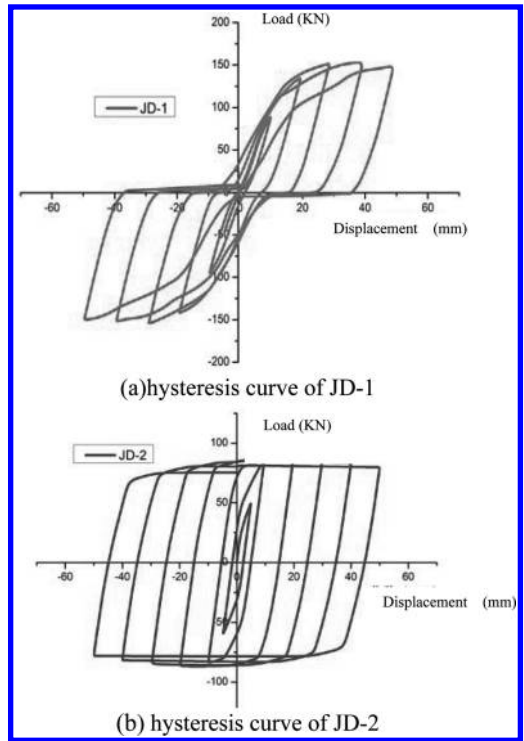


Figure 8. Analysis of hysteresis curve.

hysteresis curve of the post pouring JD-2 is in spindle type under cyclic loading. The graphics is full and stability, its absorption and dissipation are larger, which has better performance of the seismic behaviour. The curve of JD-1 although is not as full as JD-2, but each cycle unloaded, the displacement can be returned to the basic zero, indicating that JD-1 has a better ability to recenter. Meanwhile, JD-1 curve showing a clear “double banner” shape, showing good self-center feature. Because of the effect of stirrup in the joint area, when the load reaches a certain level, the beam is deviate form the column of JD-1, the steel of which reaches plastic quickly. In the effect of the cyclic load, the steel make an effect of energy dissipation.

3.3 Analysis of skeleton curve and the secant stiffness degradation

The skeleton curves of JD-1 and JD-2 are shown in Figure 9. The skeleton curve and load-displacement curve of self-centering joint and post pouring joint are similar to each other. When start loading, the member is substantially in elastic stage. When the load increases, post pouring joint JD-2 will be cracking, stiffness decreased significantly,

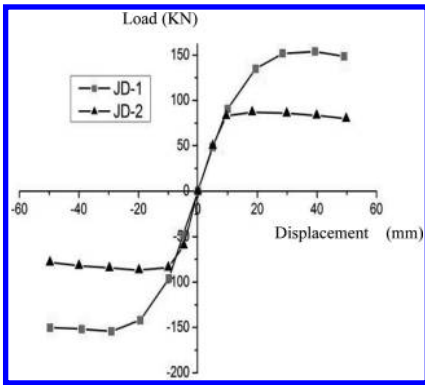


Figure 9. Skeleton curve comparison.

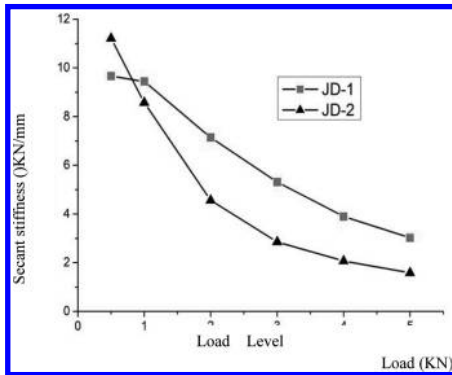


Figure 10. Stiffness degradation curve.

a significant reduction in the slope of the curve. JD-1 stiffness degradation is lower. When the load continues to increase, JD-2 first yield, the curve slope tends to horizontal.

JD-1 and JD-2 stiffness degradation curve are shown in Figure 10. Because the JD-2 post pouring precast joint, its initial stiffness is larger than the self-centering joint. However, with increasing load, the stiffness of JD-2 decreases quicker than JD-1, which tells that self-centering joint performs better in stiffness retention capacity.

3.4 Analysis of energy dissipation capacity

The hysteresis loop of JD-1 and JD-2 under cyclic loading are shown in Figure 11. As can be seen from that, self-centering joint JD-1 dissipated slightly lower than the post pouring joint JD-2. JD-1 dissipated 11.676 KJ, while JD-2 dissipated 13.806 KJ. Energy dissipation performance of two joint are similar.

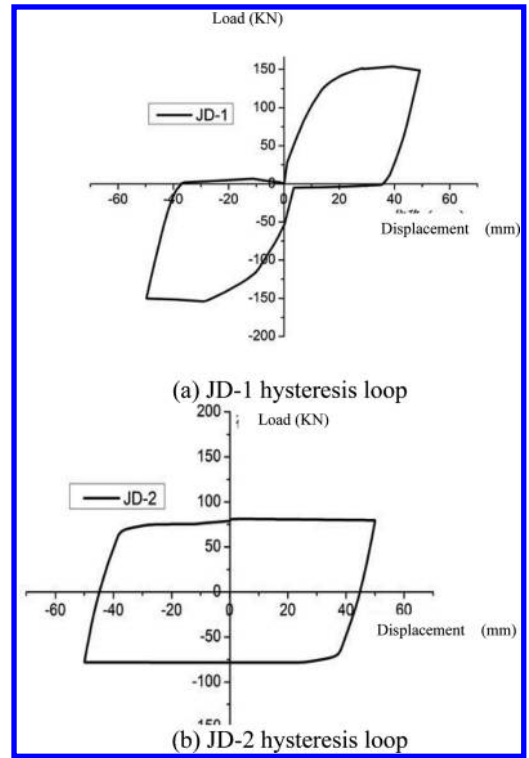


Figure 11. Joint hysteresis loop.

4 CONCLUSION

This paper designs a self-centering precast concrete frame joints JD-1 and a common post pouring precast concrete frame joint JD-2. Establish the finite element model of the two joints by ABAQUS. And apply monotonous and low cyclic load. The conclusions are as follows:

1. By the analysis of monotonic load, self-centering JD-1 performs better in bearing capacity than JD-2, but the initial stiffness of JD-1 is lower.
2. By the analysis of hysteresis curve, after the self-centering JD-1 unloaded, it can reset to initial position under the effect of prestressed reinforcement with a small residual deformation. Besides, JD-1 curve showing a clear “double banner” shape, showing good self-center feature.
3. By the analysis of skeleton curve and stiffness degradation, the stiffness of JD-2 decreases quicker than JD-1, which tells that self-centering joint performs better in stiffness retention capacity.
4. By the analysis of energy dissipation, self-centering joint JD-1 dissipated slightly lower than the

post pouring joint JD-2, but energy dissipation performance of two joint are similar.

ACKNOWLEDGEMENT

This work was financially supported by National Natural Science Foundation of China through Grant 51378240 and “Twelfth Five” science and technology support program (2012BAJ16B05).

REFERENCES

- [1] Lieping Ye, Xuchuan Lin, Xunliu Wang. Seismic Performance of Self-centering Prestressed Concrete Structures [C] “The development of green technology and building a conservation structure”—Fourteenth concrete and prestressed concrete Proceedings of the National Conference. 2007.
- [2] Palermo A, Pampanin S, Calvi G.M. Concept and development of hybrid solutions for seismic resistant bridge system [J]. *Journal of Earthquake Engineering*, 2005, 9(6):899–921.
- [3] Garlock M.M., Sause R, Ricles J.M. Behavior and design of post-tensioned steel frame system [J]. *Journal of Structural Engineering*, 2007, 133(3):239–299.
- [4] Priestley, M.J Nigel. Overview of PRESSS Research Program [J]. *PCI Journal*, 1991(4):50–57.
- [5] Zhenhua Pan. Study of Self-centering Steel Moment Frames [D]. Tsinghua University, 2010.
- [6] Zhenhua Pan, Peng Pan, Lieping Ye. Modeling and Parametric Study of Beam-to-Column Connection for Self-centering Steel moment Frames [J]. *Journal of Building Structures*, 2011, 32(3):35–42.

A parallel FEA computing kernel for ISSS

J. Duan, X.M. Chen, H. Qi & Y.G. Li

China State Construction Technical Center, Beijing, P.R. China

ABSTRACT: In this paper, a Finite Element (FE) analysis kernel is presented for ISSS, an Integrated Simulation System for Structures developed by the authors in Reference (Duan et al. 2014). This kernel is a parallel computing program coded by FORTRAN 2008 and based on the Intel Math Kernel Library (MKL). The famous PARDISO solver is called directly to solve the linear FE equations and to decompose the large sparse matrices in the modal analysis. The parallel concept of modern FORTRAN, elemental procedure, is applied extensively to parallelize the calculation of FE stiffness and stresses. Finally, some numerical examples of large-scale FE models would be presented. The validity and efficiency of the computing kernel would be demonstrated by comparing with ANSYS and SATWE.

1 INTRODUCTION

With the rapid development of high-rise buildings and long-span structures in the recent years, High Performance Simulation (HPS) is becoming more and more important, sometimes even crucial, for the structure design and building construction. The traditional design softwares, such as PKPM, ETABS, MIDAS, YJK, and so on, can't match the advanced requirements of HPS. On the other hand, the large scale general Finite Element Analysis (FEA) softwares, such as ABAQUS, ANSYS, ADINA, etc., although have the powerful computational abilities, but can't be applied directly to the architectural structure analysis and design, due to the fact that their preprocessors are inconvenient for building modeling and their postprocessors can't present computational results according to the building structure specifications, say, the civil codes and the customs of engineering.

Due to the above reasons, an Integrated Simulation System for Structures, or simply "ISSS" for short, has been developed for high performance computation of complex building structures by the authors of this paper in Reference (Duan et al. 2014). It is a coalition of abundant secondary software developments together with the traditional design softwares and the commercial FEA softwares. Since ISSS is designed for the building structure analysis, it is necessary to have an independent computing kernel due to the following reasons: above of all, ISSS should have a computing kernel of independent knowledge property rights; second, this computing kernel would facilitate the model-examination and trial-calculation of complex building structures; and furthermore, it would

serve as a supplement for the commercial FEA softwares and provide convenience for the special treatments in civil engineering, such as vibration isolation, comfort analysis, etc.

In this paper, a parallel FEA computing kernel would be presented for ISSS. It is developed by FORTRAN 2008 and based on the Intel Math Kernel Library (MKL). The famous PARDISO solver is called directly to solve the linear FE equations and to decompose the large sparse matrices in the eigenvalue solutions. The parallel concept of elemental procedure in modern FORTRAN is applied extensively to parallelize the calculation of FE stiffness and stresses. Some numerical examples of large-scale FE models would be presented and compared with ANSYS and SATWE to demonstrate the validity and efficiency of the computing kernel.

2 GENERAL DESCRIPTION OF ISSS

The interface of ISSS is shown in [Figure 1](#) (Duan et al. 2014). By this system, the building structure can be modeled within the popular design software, and then imported into the simulation system and transformed into FE models automatically, including FE meshing and boundary conditions setting. The general FE software can be called as a computing kernel to solve the above FE model. The calculated results of FEA would be transferred automatically to the post-processor, assessing the structural damage, estimating its security and comfort level, according to the theory of mechanics and building structure specifications. And finally, the post-processor would present the calculation reports with WORD and PDF files.

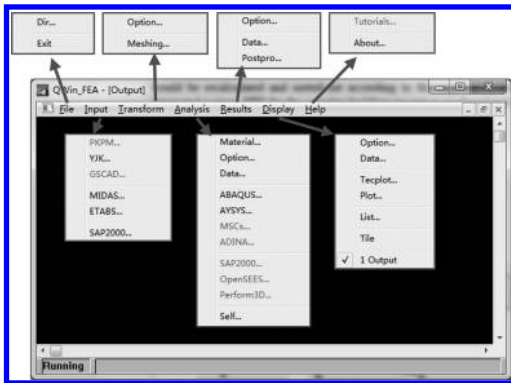


Figure 1. Interface of ISSS.

3 A PARALLEL FEA COMPUTING KERNEL

As an important part of ISSS, the FEA computing kernel is developed based on the Intel Math Kernel Library (MKL) and coded by FORTRAN 2008, a parallel computer language. To improve its capability and efficiency, the parallel concept of modern FORTRAN, elemental procedure, has been applied extensively in coding. Furthermore the famous PARDISO solver in MKL has been called to solve the large-sparse system of linear equations and to decompose the large sparse matrices in the modal analysis.

3.1 Parallel program using FORTRAN 2008

The ubiquity of computers with multiple processors and computers cooperating in some network has made parallel computing a mainstream subject, especially in the world of scientific and engineering calculation. Generally speaking, there are two kinds of parallel architectures, i.e. distributed memory and shared memory, shown in Figure 2. The former consists of many Personal Computers (PCs) and is integrated by the network. The latter is either a PC with a multi-core CPU or a mini-type server station with multi-CPU's and a shared memory. In regard to present stage, the parallel FEA computing kernel is designed and developed for the shared-memory architectures, especially for the low-cost PCs with multiple processing cores.

With respect to the FEA program, the most time-consuming tasks may be the linear equations solving and the FEs managements, such as the calculation of elemental stiffness and stresses. The former would be solved partly by calling PARDISO and the latter would be figured out by elemental procedure, a parallel syntax of FORTRAN 2003/2008 (WD 1539-1 2010 and Clerman & Speckor 2012).

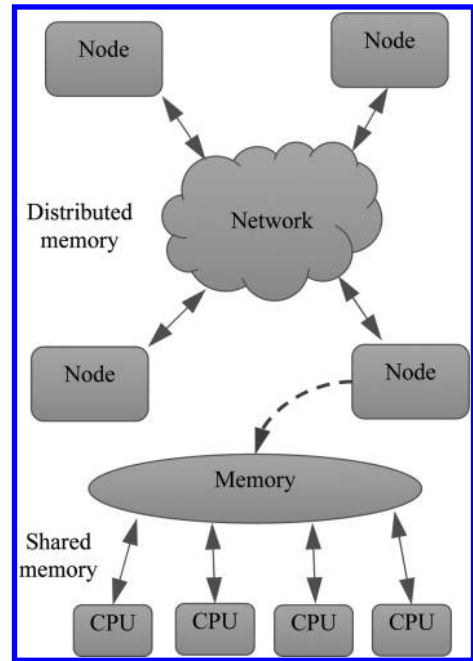


Figure 2. Illustration of parallel architectures.

Elemental procedures are written with all scalar dummy arguments, while called with array actual arguments. The compiler will automatically manage the distribution of threads and call the procedure for each array element. By means of elemental procedure, the computation of elemental stiffness and stress will be parallelized automatically, with no need for any other operation, shown in Figure 3. Furthermore, in addition to the calculation of finite elements, the concept of elemental procedure has been applied everywhere in the program to parallelize the data processing, as long as it is possible.

3.2 PARDISO solver

Solving linear systems of equations lies at the heart of many problems in computational science and engineering, particularly in FEA, because the FE system is often very large and the associated matrix, denoted by A , is extremely sparse. Among the currently-available software packages for the direct solution of sparse linear systems of equations, PARDISO (Parallel Sparse Direct Solver), coded by Schenk et al. (2000) and Schenk & Gartner (2006) with FORTRAN and c, may be the most popular one, partly because it has been integrated into the Math Kernel Library (MKL) of Intel Parallel Studio.

The PARDISO package is a high-performance, robust, memory-efficient and easy to use

```

module elem_duan
  type elem
    !.....
  contains
    procedure,pass :: stiff=>compute_stiffness
    procedure,pass :: stress=>compute_stress
    !.....
  end type
contains
  elemental subroutine compute_stiffness(self)
    class(elem),intent(inout) :: self
    !.....
  end subroutine compute_stiffness
  elemental subroutine compute_stress(self)
    class(elem),intent(inout) :: self
    !.....
  end subroutine compute_stress
end module elem_duan

```

```

subroutine test_duan
  use elem_duan,only:elem
  type(elem),allocatable :: elems
  !.....
  allocate(elems(n_e))
  call elems%stiff ()
  !.....
  call elems%stress ()
  !.....
end subroutine test_duan

```

Figure 3. An example of elemental procedure.

software for solving large sparse symmetric and non-symmetric linear systems of equations (Gould et al. 2007). Its most remarkable characteristic is parallel computing, not only for the shared-memory architectures but also for the distributed-memory architectures.

4 NUMERICAL VERIFICATION

Some numerical examples for large-scale FE models would be discussed in the follows to demonstrate the validity and efficiency of the present computing kernel.

4.1 Comparing with ANSYS

Figure 4 shows a wall-like block model subjected to gravity load and with bottom fixed. The static analysis results of this paper and ANSYS has been illustrated in Table 1, Figure 5 and Figure 6. Obviously, the results are in good agreement with each other.

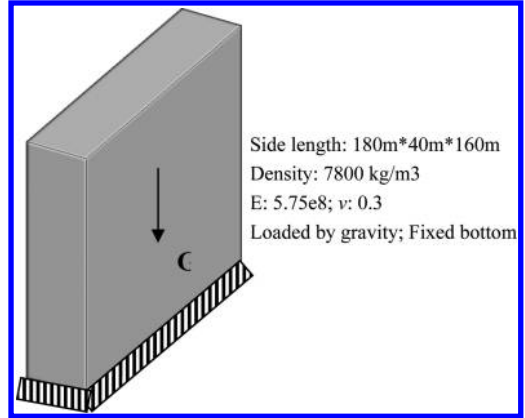


Figure 4. A wall-like block model.

Table 1. Results compared with ANSYS.

	ANSYS	This paper	Error
Mesh	90*20*80	90*20*80	–
Dofs (million)	0.45	0.45	–
Time (minute)	2.0	1.0	–
Max_Uz (mm)	1.67585	1.67549	0.02%
Max_Ux (mm)	0.32126	0.32122	0.01%
Max_Uy (mm)	0.13395	0.13381	0.1%

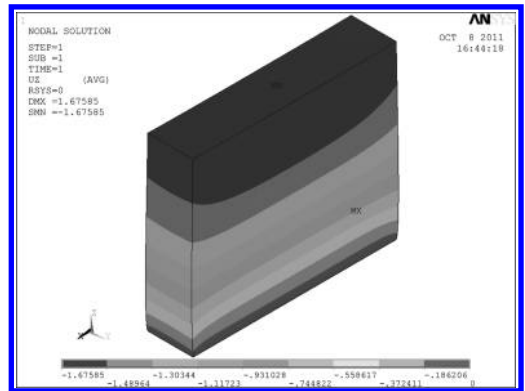


Figure 5. Displacement-contour plot of ANSYS.

To verify the validity and efficiency of the computing kernel furthermore, Table 2 presents the calculated results together with the consuming time according to different mesh size. It can be observed that the displacement results will increase gradually with the decrease of mesh size, and finally arrive at the convergence state. This phenomenon is in accordance with the FEA theory.

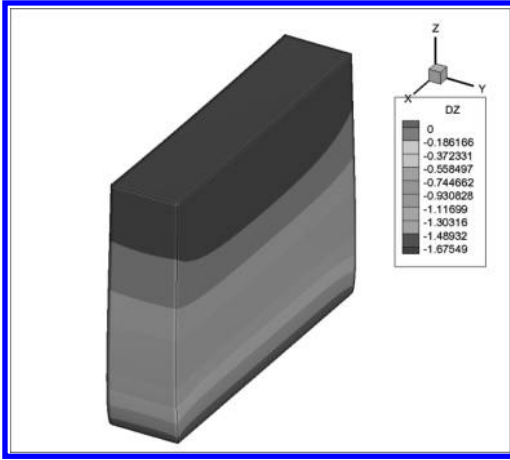


Figure 6. Displacement-contour plot of this paper.

Table 2. Results of the cube with different mesh size.

Mesh	Dof (Million)	Time (minutes)	Max_Uz (mm)
90*20*80	0.45	1.0	1.67549
108*24*96	0.75	3.2	1.67567
126*28*112	1.25	14	1.67579
144*32*128	1.85	28	1.67588
162*36*144	2.60	52	1.67595
180*40*160	3.60	100	1.67600

4.2 Comparing with SATWE

Figure 7 shows a multi-tower building. The natural frequency computed by SATWE software and the program in this paper has been shown in Table 3, Table 4 and Figure 8. Obviously, the results are very close, with the maximum error 7%~8% approximately, which may be resulted from the following reasons: (1) the FE DOFs scale of this model has exceeded the capacity of SATWE software, so the rigid slab hypothesis is introduced to decrease the DOFs scale of SATWE; (2) the SATWE software has introduced penalty function to simulate the restraints between the beams and walls, which is ignored in the program of this paper; (3) the lumped-mass models of the SATWE software and the present program are not identical, because the SATWE software has the mass of components, e.g. walls, beams, columns, braces etc., lumped at the top of itself.

For the multi-tower building shown in Figure 7, if the mesh size is set to 1.5 m, the DOFs scale will be 1.6 million; if the mesh size is set to a smaller one, the DOFs scale will get much larger; when

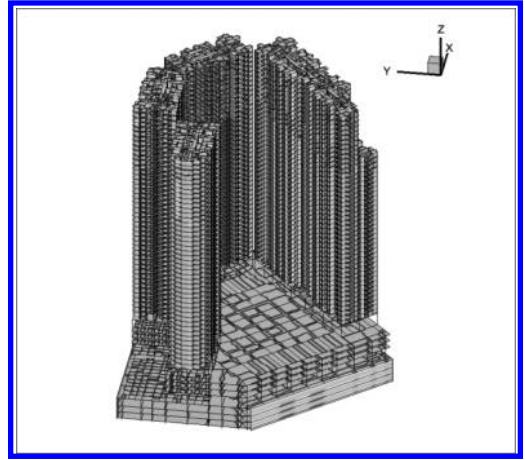


Figure 7. Multi-tower buildings.

Table 3. Computing scale and time compared with SATWE.

	SATWE	This paper
Mesh size (m)	1.5	1.5
Slab model	Rigid	Elastic
Dofs (million)	0.6	1.5
Dynamic dofs	690	500,000
Time (minute)	10	10

Table 4. Results compared with SATWE.

	SATWE	This paper	Error
Freq (Hz)	0.26	0.24	7.7%
1st, 30th	1.79	1.65	7.8%
Effective mass coefficient	0.60 (x)	0.61 (x)	1.7%
	0.62 (y)	0.63 (y)	1.6%

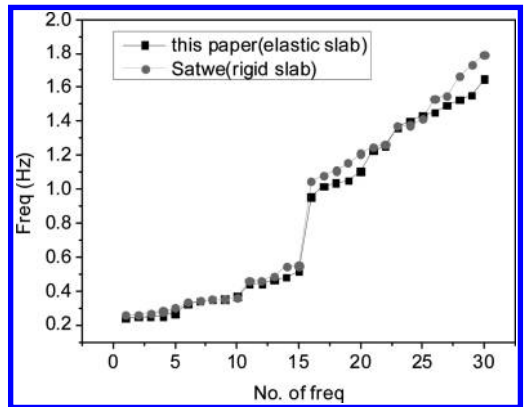


Figure 8. Natural frequencies.

the mesh size decreases to 0.5 m, the DOFs scale will increase to 11 million. The modal analysis results with the above different mesh size by the present program has been shown in the Table 5 and Figures 9–10. Observing the results, it can be easily concluded that the natural frequencies will decrease gradually with the decrease of mesh size, and finally arrive at a convergence state. This conclusion is exactly coincident with the FEA theory.

Table 5. Results for the building with different mesh size.

Mesh size (m)	Dofs (million)	Time (minute)	Freq (Hz) (1st, 30th)	
1.5	1.6	3.5	0.2364	1.6316
1.2	2	4.5	0.2321	1.5926
1.0	3.1	6.0	0.2256	1.5409
0.8	4.7	55	0.2200	1.4800
0.5	11	90	0.2156	1.4375

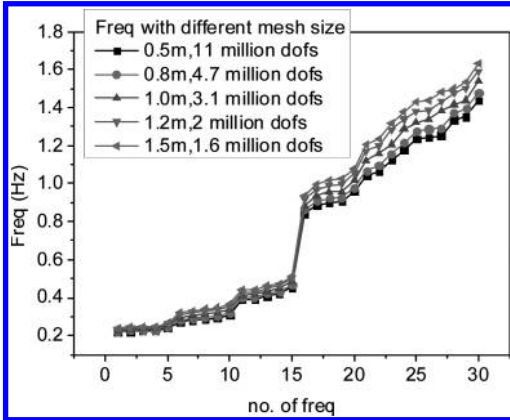


Figure 9. Frequencies with different mesh size.

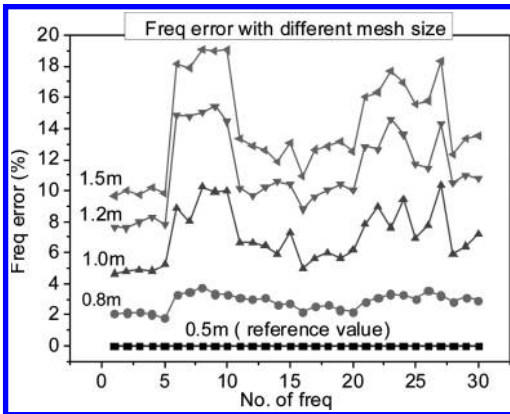


Figure 10. Frequency-errors with different mesh size.

5 CONCLUSION

A parallel FEA computing kernel is presented in this paper for the ISSS system. It is developed by FORTRAN 2008 and based on the Intel Math Kernel Library (MKL). The famous PARDISO solver is called directly to solve the linear FE equations and to decompose the large sparse matrices in the eigenvalue solutions. The parallel concept of elemental procedure in modern FORTRAN is applied extensively to parallelize the calculation of FE stiffness and stresses. Some numerical examples of large-scale FE models are presented and compared with ANSYS and SATWE, demonstrating the validity and efficiency of the computing kernel.

REFERENCES

- Clerman N.S. & Speckor W. 2012. *Modern Fortran Style and Usage*. New York, USA: Cambridge University Press.
- Duan J., Chen X.M., Qi H. & Li Y.G. 2014. An Integrated Simulation System for Building Structures. *Proceedings of the 4th International Conference on Civil Engineering, Architecture and Building Materials*, 24–25 May, 2014, Haikou, China. (Accepted).
- Gould N.I.M., Hu Y. & Scott J.A. 2007. A numerical evaluation of sparse direct solvers for the solution of large sparse, symmetric linear systems of equations. *ACM Transactions on Mathematical Software (TOMS)*, 33(2):10–45.
- Schenk O. & Gartner K. 2006. On fast factorization pivoting methods for symmetric indefinite systems. *Elec. Trans. Numer. Anal.*, 23:158–179.
- Schenk O., Gartner K. & Fichtner W. 2000. Efficient sparse LU factorization with left-right looking strategy on shared memory multiprocessors. *BIT*, 40(1):158–176.
- WD 1539-1. 2010. F2008 working document. J3/10-007r1.

The key points for ecological design during urbanization process

Z. Jia

Zhengzhou University, Zhengzhou, Henan, China

ABSTRACT: Urbanization is the major impetus of social economy and city development. However, this process also brings with environmental pollution, traffic congestion, ecological deterioration and other issues. At the same time, the urbanization policy has many problems, for instance, some people simply treat the urbanization process as more buildings and roads. In this paper, several design key points have been proposed to help promoting the development of the urbanization, such as land using, natural and cultural heritage preservation, low carbon architecture, transportation and building materials designing, and new green technology application.

Keywords: urbanization; ecology; nature; environment; transportation; building material; new technology

Urbanization is first written in the book “The Basic Theory of Urbanization” by A. Serda who is a Spanish engineer in 1867. The British economist Luis is the pioneer to propose the mode of urbanization development. Urbanization refers to a process that people as well as the secondary, tertiary industry move to town continually, and then the amount of the town and the scale of the town increase. For China, the urbanization process is an important stage that leading the country to modernization, it is promoting the development of social economy and regional coordination. In 2013 century economic working conference, the expert says it is important to integrate the concept of ecological civilization with the whole process of urbanization. The Chinese urbanization process is supposed to be more sustainable, intensive, and intelligence. This conference gives new connotation and points out the new direction for China’s urbanization. The urbanization planning requires using the concept of ecological civilization as the guide and regulates the process of urbanization under the principles of ecological design.

The urbanization process is a logical development. With the development of the economy, it is necessary to develop and gather together the industry fields. Accompanied by this process, rural labor force start to transfer to the city, various of resource start to reconfiguration and environmental resource has been fully use. These things help to promote the development of urbanization. Now days in many areas, people’s concept about urbanization lags behind the times. They treat urbanization equally as more construction. Many farm lands have been requisitioned and the city expands out of order. Urbanization is simply defined as

park development, building construction, road construction, new town development and random expanding. In contrast, the industry agglomeration is incomplete, the matching functions cannot keep up, the structure of city life is imbalance, environmental problem is very serious and lots of city became the same. While the people enjoy the convenience by the result of the economic development, they bear the consequence of energy emergency, resource shortage, climate change; ecological degradation and other environmental disaster emerge in endlessly. The essence of urbanization is the altering of production mode and life condition and it is also the process of civilization development. Therefore, taking in this sense, the statistics shows that the China’s urbanization rate has reached 52% while the real level is only about 37%. If we take the relationship between human, architecture and environment in consideration, plus the requirements of ecological city principles, we will face more problems and the number will become even lower. All in all, focusing on ecological city research is very important and necessary.

Ecological city planning is a comprehensive application of architecture, ecology, urban planning and other scientific subjects. It makes the whole city as an ecological system and various factors in this system contagiously circulating and transferring in order and finally reaches a state that is high efficiency, low consumption, no waste, no pollution and ecological balance. During the state of urban planning, respecting the nature and living with a harmony relationship with the nature should be taken into consideration. This is the core requirements of ecological design. The era requires the application of ecological design for the

urbanization and the design is also focus on the key points of the ecological urban planning. This article will discuss some basic principles of ecological urban planning.

1 FROM THE SPACE PLANNING AND STRATEGY, THE CITY DEVELOPMENT SHOULD MAKE FULL USE OF THE ADVANTAGE OF LARGE URBAN AGGLOMERATION TO PROMOTE THE URBANIZATION

China is a country with large area and population. Urban and rural development is very different. The way towards urbanization should be diverse. Therefore, the process of urbanization should not imitate what Japan and South Korea did which they only relying on the big city, neither Germany's way of development because its urbanization relies on the small towns. Instead, the way for China's own development should be more in a way of coordination of all the city scale. The small town is better for offering the public service for the residence. In recent years, there are lots of breakthroughs for the expanding goal of the big city. Although this result shows that there is a giant attraction and grow effect for the development, the negative impact is become increasing apparent. For example, the development of the city infrastructure lags behind, city operation cost is high, life quality deteriorates and the developing resource was taken out to the bigger city. Therefore, the urbanization process is imbalance, the gathering effect does not work and it is very hard to continue the process of the urbanization. The core concept for improving the urbanization is the coordination development of the metropolitan area. The structure of the metropolitan should be like a pyramid. The small towns locate at the bottom of the pyramid as the foundation of the urbanization.

2 AS FOR THE DESIGN METHOD, REGIONAL PLANNING SHOULD INSIST THE INTENSIVE DEVELOPING CONCEPT

The core idea of the sustainable development is "Development that meets the needs of the present without compromising the ability of future generations to meet their own needs. Therefore, it requires the planner designing the city according to the principles of the eco theory. The town's different area should achieve the goal of micro, composite and intensive effect in terms of ecological resource, production mode and operating methods. In the design, the key aspect would be combine the

land, water, bio-resource, architecture style, public service, infrastructure and transportation as a whole. As for the land uses, the huge land should be divided into several functional partitions so that the "short path" will promote mixed using of the land and avoid the single-function city or district. Each partition should include commercial, residential, cultural, recreational and other functional space. As for the transportation routine, it is suggested to use two layer structures to separate the pedestrians and vehicles. All of these measures will prompt the citizens to obtain a simple and sustainable living style as well as help implement the Eco-life for the city.

3 THE ECO-DESIGN SHOULD BLEND INTO THE EXISTING CITY CONTEXTURE

First, it is important to keep a harmony relationship between the city and the nature environment. Regionalism is the main characteristic of the ecological urbanization. The original landform is the result of the natural selection and it has its own texture. The new urban design should be combined with the original terrain characteristic, respect the ecological elements as much as possible and altering the natural environment as few as we can to retain the harmony relationship between the nature and the city. Hengqin district is the new designed area located in the city of Zhuhai. It is an island which surrounded by the ocean. The structure of the water system and farm land in the island is based on the construction of the artificial island. The contexture of the land and water system has already become the main morphological characteristics. Hengqing new district is designed by AMA architecture from France. This design is focus on keeping the original land feature. It preserves the existing drainage, the channel, the Hengqing Mountain which bulges out of the sea, the mud flat and the fields. Therefore, the whole design automatically constitutes the original ecology and landscape system and strengthens the people's memory of the nature.

Second, it is important to keep the style consistent between the old and the new districts. The old and the new town should be linked through the way of ecological design and then form the new urban landscape. Each town has its own history context development process. The urban space and landscape are the ground context of the city in different era. If we only broaden the road for the heavy traffic or demolish the buildings for renovate the historic area, the history trait of the town will slowly disappear and the culture function of the city will not be complete. The new town should

not only keep the coordinated relation between the old town in terms of the culture, history, color, scale and street texture, but also need to keep the diversity of the develop methods which include the space and the function.

Therefore, the city needs wide road as well as the narrow historic road. The old house should blend with the new city contexture. The new town should connect the old town by the ecological corridor and blend with each other naturally. The city of Wuhan changes the previous way of urbanization process which is the “random expanding” to the new way which forms to a very open city space structure. The structure uses the main city as the core and then builds up six new city agglomerations along the main transportation route. The space between the main city and the new city agglomeration has the ecological zone while there are six green zones among the six new city agglomerations as well. This design becomes the role model of the ecological design.

4 NATURAL GREEN SPACE PRESERVATION FOR REUSE AND TRANSPORTATION DESIGN ARE THE KEY ASPECTS OF THE LOW CARBON DESIGN

The green space is the foundation of the city life’s vitality and it is the natural driving force of the sustainable development. Giving great importance for the “wild land” in the city and trying to preserve it; Establishing the contacting band between different water zones; Considering setting up the reservation zone for the wild life and restrict people’s access to the zone; Plus the landscape are all having the responsibility to ease the environmental problem, guarantee the urban ecological security, and maintaining the natural ecology and bio-diversity. In this way, the human and the nature could reach the harmony relationship.

Urban traffic network design aims at separating different functional areas effectively and re-organizing them into towns. The common traffic organization forms have grid network, ring network, center divergence network, etc. These organization forms should be based on the actual situation and convenient the people as much as they can. It is very important to reduce the distance for car using and the dependency level on the motor vehicle. It is also very important to pay attention to the seamless design of the public transportation among different towns. All these measures will help guide people to a low carbon travel and achieve the best circulation and access in between the towns with the minimum fossil energy consumption. In Louvain-la-Neuve, Belgium, the town is adopting the elastic asymmetric method for urban planning. There are

400 hectares out of 900 lands are reserved for the city green space and this number has been written in the laws so it becomes the rigid requirements for the planning. The design of the pavement in the city is very distinctive. The railway station square is rising up and support by concrete columns. The train is passing by under the square and the motor vehicle could either go through the loop line or under the square. The sidewalk stretches along the square in all directions and connects other squares in different scale and finally reaches to every corner of the city. By doing this, the city becomes a whole and Louvain-la-Neuve becomes a walk-able city.

5 FOR THE ASPECTS OF BUILDING MATERIALS, IT IS BETTER TO CHOOSE THE LOCAL MATERIALS, SELECT THE APPROPRIATE TECHNOLOGY AND FOCUS ON RECYCLING THE MATERIALS

There are different geographical environment and climate conditions in different regions. Local inhabitants have different methods to pick up the building materials and solve the housing problem. Adopting the local resource and traditional construction techniques to solve the local urbanization problem is the fundamental strategy of ecological design. It also helps maintain the historical continuity. At the same time, it is supposed to consider from the view of the economy. The designer should solve the materials recycling problem and set up the “resource-product-renewable resource” mode. This method not only reflects the local customs, living habits and aesthetic taste, but also shows the development of the urbanization structure. The 2012 Pritzker price winner Wang Shu’s work emphasizes the ecological aspect of the architecture. In the museum of Ningbo and Xiangshan campus of China Academic and Fine Art school, he uses large amount of recycled bricks, tiles and bamboo. Plus he uses the local construction skills to build up the architecture. Therefore, the design of the building facade has the sense of history and the original materials have been reused in a good way. Furthermore, the ecological design emphasizes the land resource saving strategy, which refers to choose the suitable new technology for the town construction and use other materials for making bricks instead of the soil. To the point of low carbon design, the construction process should focus on applying the prefabricated technology which mainly refer to the precast the building components and assemble them on the site. By doing this, the pollution could be reduced during the construction process. This is the inevitable requirement of industrialized and ecological urban construction.

6 THE BUILDINGS IN THE TOWN ARE BETTER TO BE ENERGY EFFICIENCY IN ORDER TO MAKE FULL USE OF THE NATURAL RESOURCES

The eco city is mainly presented by the specific design strategies of different buildings. In the process of designing, passive and active design methods are applied to learn how to make full use of the solar power, wind power, rain water and so on. Through the architecture project, it is better to combine different environment to design the building's floor plans, shape, elevation and section. This strategy will not only fulfill the functional needs but also fulfill the ecological needs which makes fully use of the natural resource to create the complex interior and exterior space. It will help collecting the natural resource and apply different green technology on the building. At the same time, it is important to include the green space into the design. Green roof and the vertical green system need to be considered for the architecture. The ground of town is suggested to use 100% water permeable material which makes the urban green space play a role of wetland with a functional of water supply and drainage. By doing this, the whole town becomes an ecosystem. From the historic point of view, architects from all over the world in different periods have explored the ecosystem of the building. The modernism architects Frank Lloyd Wright considers the architecture as a living organism. From Le Corbusier's 5 points of new architecture, setting green roofs and the free designing of the ground plan aim to have a close relationship in between the architecture and environment. Osaka Gas Company builds the "21st century lab building" which is a typical ecological architecture. The building's exterior wall is adopted the new tech insulation layer to improve the heat preservation. The building also uses the special equipment to collect the heat energy and transform it into electricity. Architect Charles Correa from India has always emphasized his view of ecological design which

is "form follows climate". He invented the tube housing refers to the building has an open courtyard located in the middle of a narrow architecture. This kind of layout will help reduce the solar radiation because the entrance is designed at the section of the building and a gap has been cut on the roof to form an air ventilation system to cool the building. Ken Yeang from Malaysia is focus on the green high rise design through bioclimatology. He designs varieties of concave space on the building skin and has green space in it so that the users could still meet with nature even when they stay inside the high rise. Energy saving design is the premise and foundation of the ecology design and it is one of the main focuses of the ecological city.

In conclusion, in order to reach the goal of ecological city, first, the lands need to be mix effectively to have the composite effect. Second, it is important to preserving the nature environment and obtains the continuity of the landscape and architecture style. Third, it is important to focus on the design of traffic network and low-carbon traveling. Finally, the designer needs to focus on using the local materials and applying the appropriate technology on the design, especially the technique used for recycling the natural resource. With these design points, the ecological urbanization construction will have a good start.

REFERENCES

- Chen, Bozhong. & Hao, Shouyi. 2005. The Discussion of China's Rapid Urbanization Process. *Humanistic Geography*: 44-47.
- Dai, Zhizhong. *Architecture Concept Analysis-The idea of Bionic*. China Plan Press: 1-100.
- Gao, Jiehua. 1999. *Architecture and Culture*. Tianjin Science and Technology Press.
- He, Jiajia. 2012. Ecological Design Analysis. *Architecture and Environment*.
- Liu, Bo. & Ying, Tan. 2009. Creating Green City. *Journal of Architectural Study*.
- "National New Urbanization Planning 2014-2020".

Optimal design of the flue size based on lagrangian algorithm

Ruo Nan Zhang & Yue Jin Yu

College of Energy and Power Engineering, Nanjing Normal University, Nanjing, Jiangsu, China

ABSTRACT: Based on the numerical simulation results of the velocity field about gas pollutants under different flue sizes, variation characteristics of the outlet average velocity with the changes of flue size should be discovered. Fit the 3D surface between the outlet average velocity and the width of two flue walls, surface equation of the outlet average velocity are further determined. The convergence of the equation should be verified by the determination coefficient. Regard the flue section area as a definite condition, applying the lagrangian algorithm for solving the different width of flue size, which maximize and minimize the outlet average velocity respectively. When outlet of the flue is equipped with a dust-collecting equipment, the flue size should be recommended to minimize the velocity. While export is equipped without the equipment, recommends for maximize the velocity.

Keywords: flue size; outlet average velocity; section area; conditional extremum; numerical simulation

1 INTRODUCTION

Cooking fume generates from burned edible oil and fuel combustion, which includes a mass of small oil droplets and gas pollutants (Saha S, Guha A & Roy S, 2012; Lee S C, Li W M & Yin Chan L, 2001; Lai A C K & Ho Y W, 2008). Inhalable particles account for 93% of total cooking fume. As the particle size decreases, the number of particles increases gradually (Gao J et al. 2013; Liao C M, Chen S C & Chen J W, 2006; Zhang Q, Gangupomu R H & Ramirez D, 2010). The kitchen environment should be purified when the diluted cooking fume exhausted by range hood. Only large particle particles (including solid and liquid) are trapped, the rest of fume such as inhalable particles are released into the atmosphere directly (Schrock D W, Olson B A & Urness R J, 2006; Katragadda H R, Fullana A & Sidhu S, 2010).

The gas pollutants extracted low to the ground, where is man's living area (Lai A C K & Ho Y W, 2008; Lai A C K & Chen F Z, 2007). It will produce concentration gradient and velocity gradient, and the gas pollutants pollute our living surroundings immediately under the turbulence effect. In order to control gas pollutants emission and reduce the pollution, we need to control them in concentration and velocity terms.

Improving the range hood efficiency of absorption of gas pollutant or setting a dust-collecting equipment on outlet of the flue could effectively decentralize the concentration of gas pollutants emissions. where as, the velocity will be merely controlled when the gas pollutants are exhausted

by range hood. Relevant standards only lay claim to the area of cross section but not including the width of each flue wall (GB5009-2011). Whether the outlet average velocity could change with the variation of flue size?

Would this change cause further impact on the diffusion rate of the gas pollutants? Would it put forward any new requirements for outlet average velocity if a dust-collecting equipment is set on the outlet?

In this paper, the numerical simulation is operated when the width of flue walls vary within a certain range. Based on the results, characteristics of outlet average velocity change as width of flue walls vary are found. Subsequently, 3D surfaces of the changes of outlet average velocity is fitted. By using determination coefficient, surface equation is determined, and goodness of fit is worked out. Assume the flue section area is fixed, the optimal width of flue walls could be analyzed when outlet of the flue is equipped with or without a dust-collecting equipment.

2 NUMERICAL SIMULATION

For 30-storey high-rise residential buildings, the flue section area is recommended as 0.2~0.25 m². In practical projects, high-rise residential buildings are generally less than 30 storeys in china. Therefore, the maximum flue section area of the 30 storeys is regarded as the upper limit, and the flue width up to 0.5 m under this condition. The flue width of the residential building in our country is

generally greater than 0.3 m according to a survey. Consequently, this paper hypothesize 0.3 m as flue width lower limit, 0.5 m as flue width upper limit, 0.02 m as step size. Choosing a layer of flue as the research object, we simulate the outlet average velocity of gas pollutants in flue.

The physical structure of the flue is shown in Figure 1. Flue height is 3 m, the distant between the hood entrance and the ground is 1.6 m, and the pipeline radius of the range hood is 0.15 m. Define each flue wall as a , b as shown in Figure 1.

We assume the gas pollutants can not be compressed. According to the calculation formulas of viscosity and density at constant pressure, as shown in Eq. (1), Eq. (2). We can get the gas pollutants viscosity is $24.49 \times 10^{-6} \text{ Pa}\cdot\text{s}$ and the density is 0.751 kg/m^3 . While the air viscosity is $25.82 \times 10^{-6} \text{ Pa}\cdot\text{s}$, the density is 0.746 kg/m^3 . So we can considered that the physical properties of gas pollutants are similar to the air. During the simulation, the gas pollutants can be regarded as air.

$$\mu_m = \frac{\sum y_i \mu_i M_i^{1/2}}{\sum y_i M_i^{1/2}} \quad (1)$$

$$\rho_m = \sum \rho_i y_i \quad (2)$$

where μ_m = gas mixture viscosity; ρ_m = gas mixture density; y_i = mass fraction of gas; M_i = relative molecular mass of gas; μ_i = gas viscosity; ρ_i = gas density.

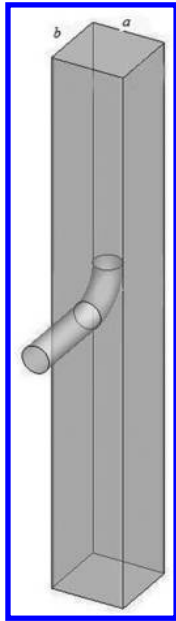


Figure 1. The physical structure of flue.

In the process of cooking fume exhausted by range hood, the cooking fume would diluted by the amount of air. So the extracted gas temperature as low as 40°C , while maximum temperature in the cooking as high as 300°C (Wu M T, Lee L H & Ho C K, 2004; Yang J, Jia J et al. 2005). Currently, the flue is made of fiber glass mesh reinforced cement concrete pipes, with the absolute roughness of about 1.0~2.0 mm. In the flue, the gas pollutants flow fully developed, with a typical turbulence characteristic. So the standard $k-\varepsilon$ equation model is adopted in this paper.

3 NUMERICAL RELATIONS OF OUTLET AVERAGE VELOCITY AND FLUE SIZE

3.1 Effect of flue size change on outlet average velocity

As shown in Figure 2, 3D surface are fitted on the results of the numerical experiments. With the increasing of flue size, the outlet average velocity goes down firstly, then rises, and drops again at the last, several maximums and minimums appeared in this processing.

Assumed that hypothesize b is fixed with a ranges from 0.3 m to 0.5 m. It turns out that we have two maximums and two minimums of the outlet average velocity. With the increasing of a , the period of the alternation of peak and valley gradually increases. When a is 0.32 m or 0.42 m respectively, the average velocity reaches the maximum. And when a is 0.36 m or 0.5 m respectively, the average velocity is the minimum. The average rate of change of average velocity arrives to 18.8%.

While a is fixed and the range of b changes from 0.3 m to 0.5 m, the average velocity reach up to maximum when b is 0.32 m or 0.42 m, respectively. The average velocity is as low as the minimum when

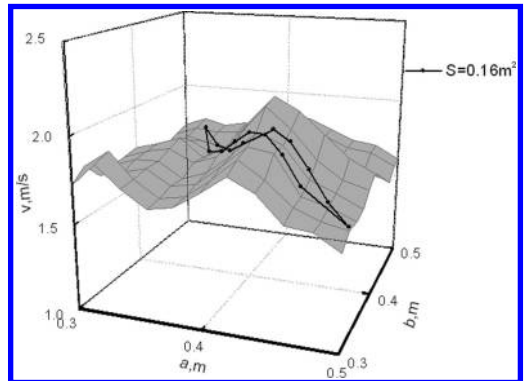


Figure 2. Relationship between outlet average velocity and flue size.

b is 0.34 m or 0.46 m, respectively. The average rate of change of average velocity arrived 13.6%. Obviously, the change of a has more influence on the outlet average velocity than b .

When a and b change simultaneously, the outlet average velocity trend also is wavy type. As is shown in Figure 2, the flue section area is 0.16 m², the variety rate of outlet average velocity is large. The velocity attained the peak when a is 0.34 m and b is 0.46 m, while velocity arrived the valley when a is 0.42 m and b is 0.38 m. The rate of change of average velocity arrives to 19.3%. It can be found in the results in the investigation that when a and b change simultaneously within the certain conditions, the rate of change of the outlet average velocity arrived the maximum.

3.2 Numerical equation about outlet average velocity and flue size

According to the surface, the surface equation between outlet average velocity and a , b is determined, as in Eq. (3). Parameters in the equation are shown in Table 1.

$$V = w_1 + w_2 \exp\left[-\frac{(\ln a - \ln w_3)^2}{2w_4}\right] + w_5 \exp\left[-\frac{1}{2}\left(\frac{b - w_6}{w_7}\right)^2\right] \quad (3)$$

where V = outlet average velocity; a = wall a width; b = wall b width; w_1 ~ w_7 = parameters.

Determination coefficient is the parameter which can reflect the goodness of fit of the numerical equations, as in Eq. (4). Determination coefficient of Eq. (3) is 0.91, which reflects 91% of the variation on outlet average velocity depends on the change of a , b . Therefore the equation can be considered as appropriate. The equation can effectively forecast the outlet average velocity, when the width of flue wall ranges from 0.09 m² to 0.25 m².

Table 1. Parameters in the equation.

	Value
w_1	1.67
w_2	0.23
w_3	0.42
w_4	0.05
w_5	0.14
w_6	0.39
w_7	-0.02

$$R^2 = 1 - \frac{\sum_n (V_i - \hat{V}_i)}{\sum_n \left(V_i - \frac{1}{n} \sum_n V_i \right)} \quad (4)$$

where R^2 = determination coefficient; V_i = numerical simulation value of outlet average value; \hat{V}_i = function value of outlet average value; n = the number of numerical simulation point.

4 DETERMINATION OF THE OPTIMAL FLUE SIZE

It is sure that the cooking fume exhaust efficiency is a key factor in determining the flue size. Only the flue section area is limited, but the choice of wall width have the higher flexibility. In order to reduce the concentration of gas pollutants, dust-collecting equipment should be installed at the outlet of the flue. In the meantime, the outlet average velocity should be reduced to ensure the equipment works fully. If the equipment is not installed, the outlet average velocity should be improved to accelerate the diffusion rate. Consequently, the different optional flue size should be determined in different conditions, which would further control the outlet average velocity.

Hypothesize the flue section area is Z m². The extreme points of Eq. (3) would be calculated by Lagrange conditional extremum method. In other words, the maximum and minimum of Eq. (5) would be calculated. So the partial derivative equations between L and a , b , λ would be computed, as in Eq. (6). The maximum L_{\max} (a_{\max} , b_{\max} , λ_{\max}) and the minimum L_{\min} (a_{\min} , b_{\min} , λ_{\min}) can be got.

$$L = w_1 + w_2 \exp\left[-\frac{(\ln a - \ln w_3)^2}{2w_4}\right] + w_5 \exp\left[-\frac{1}{2}\left(\frac{b - w_6}{w_7}\right)^2\right] + \lambda(ab - Z) \quad (5)$$

$$\begin{cases} \frac{\partial L}{\partial a} = \lambda b - \frac{w_2(\ln a - \ln w_3)}{aw_4} \exp\left[-\frac{(\ln a - \ln w_3)^2}{2w_4}\right] = 0 \\ \frac{\partial L}{\partial b} = \lambda a - \frac{w_5(b - w_6)}{w_7} \exp\left[-\frac{1}{2}\left(\frac{b - w_6}{w_7}\right)^2\right] = 0 \\ \frac{\partial L}{\partial \lambda} = ab - Z = 0 \end{cases} \quad (6)$$

As shown in Figure 1, V may arrives peak or valley when a , b takes the boundary value, respectively. Therefore more conditions need to be considered, namely, $a_1 = 0.3$ m, $b_1 = Z/0.3$ m; $a_2 = 0.5$ m,

$b_2 = Z/0.5$ m; $a_3 = Z/0.3$ m, $b_3 = 0.3$ m; $a_4 = Z/0.5$ m, $b_4 = 0.5$ m, the corresponding results are L_1, L_2, L_3, L_4 . By Comparative analysis $L_1, L_2, L_3, L_4, L_{min}$ and L_{max} , we can get the peak value V_{max} and the valley value V_{min} , as in Eq. (5), Eq. (6).

$$V_{max} = \max(L_1, L_2, L_3, L_4, L_{max}) \quad (7)$$

$$V_{min} = \min(L_1, L_2, L_3, L_4, L_{min}) \quad (8)$$

When a is a_m with and b is b_m , the outlet average velocity arrives the peak value; a is a_n and b is b_n , the outlet average velocity arrives the valley value.

Take $Z = 0.16$ as a example, the V arrives peak when $a = 0.42$ m and $b = 0.38$ m; the V arrives valley when $a = 0.5$ m and $b = 0.32$ m.

5 CONCLUSIONS

Changing of the width of flue wall which is connected with branch flue shows greater influence on outlet average velocity than that of the flue wall which is not connected with branch flue.

The equation between the outlet average velocity and the flue size can effectively forecast the outlet average velocity, when the flue area ranges from 0.09 m² to 0.25 m².

In order to ensure the equipment work fully, the outlet average velocity should be adjusted to a lower level when a fume removal equipment is installed at the outlet of the flue. To accelerate the diffusion rate, the outlet average velocity should be increased when a fume removal equipment is not installed.

REFERENCES

Gao J, Cao C, Zhang X, et al. 2013. Volume-based size distribution of accumulation and coarse particles (PM_{0.1-10}) from cooking fume during oil heating. *Building and Environment* 59: 575–580.

GB5009-2011. Design code for residential buildings.
 Katragadda H R, Fullana A, Sidhu S, et al. 2010. Emissions of volatile aldehydes from heated cooking oils. *Food Chemistry* 120(1): 59–65.
 Lai A C K, Chen F Z. 2007. Modeling of cooking-emitted particle dispersion and deposition in a residential flat: a real room application. *Building and environment* 42(9): 3253–3260.
 Lai A C K, Ho Y W. 2008. Spatial concentration variation of cooking-emitted particles in a residential kitchen. *Building and Environment* 43(5): 871–876.
 Lai A C K, Ho Y W. 2008. Spatial concentration variation of cooking-emitted particles in a residential kitchen. *Building and Environment* 43(5): 871–876.
 Lee S C, Li W M, Yin Chan L. 2001. Indoor air quality at restaurants with different styles of cooking in metropolitan Hong Kong. *Science of the Total Environment* 279(1): 181–193.
 Liao C M, Chen S C, Chen J W, et al. 2006. Contributions of Chinese-style cooking and incense burning to personal exposure and residential PM concentrations in Taiwan region. *Science of the total environment* 358(1): 72–84.
 Saha S, Guha A, Roy S. 2012. Experimental and computational investigation of indoor air quality inside several community kitchens in a large campus. *Building and Environment* 52: 177–190.
 Schrock D W, Olson B A, Urness R J, et al. 2006. A New Standard Method of Test for Determining the Grease Particulate Removal Efficiency of Filter Systems for Kitchen Ventilation. *ASHRAE transactions* 112(1).
 Wu M T, Lee L H, Ho C K, et al. 2004. Environmental exposure to cooking oil fumes and cervical intraepithelial neoplasm. *Environmental research* 94(1): 25–32.
 Yang J, Jia J, Wang Y, et al. 2005. Treatment of cooking oil fume by low temperature catalysis. *Applied Catalysis B: Environmental* 58(1): 123–131.
 Zhang Q, Gangupomu R H, Ramirez D, et al. 2010. Measurement of ultrafine particles and other air pollutants emitted by cooking activities. *International Journal of Environmental Research and Public Health* 7(4): 1744–1759.

Numerical simulation of indoor air quality and thermal comfort in typical office with stratum ventilation

Jian Xu & Yue Jin Yu

School of Energy and Mechanical Engineering, Nanjing Normal University, Jiangsu, China

ABSTRACT: In this paper, the Navier-Stokes equations and the RNG $k-\epsilon$ turbulence model are used to predict three-dimensional CO₂ pollutant concentration distribution in the ventilation office. It also has computed PPV and PPD to evaluate human thermal comfort at the same time. The result shows that, with the stratum ventilation, occupants can have better IAQ when it used upper part air return in the breathing zone while the thermal comfort have no significant difference.

Keywords: stratum ventilation; air distribution; IAQ; thermal comfort; numerical simulation

1 INTRODUCTION

The energy consumption of HVAC system accounts for more than 50% of building energy consumption, therefore it has a big potential for energy saving in it. In order to control the energy consumption of the building HVAC system, new standards have been adopted in mainland China and other parts of the world. In general, the ideal temperature for the summer air-conditioning is 25.5°C, the National Development and Reform Commission advocated 26°C as the summer air-conditioning temperature. It can be seen that increasing air-conditioning temperature can save energy, but as the air-conditioning temperature rises, there will be an impact on the indoor thermal environment and airflow. It will affect the thermal comfort, increase the energy consumption of HVAC system, and even cause serious harm to human health such as sick building syndrome.

As an effective way to solve the contradiction between energy saving and thermal comfort, stratum ventilation, this new type of ventilation has a strong potential for energy savings and application prospects. In order to study the airflow parameters of this ventilation. Professor Wang Fenghao who from Xi'an Jiaotong University and Lin Z from the City University of Hong Kong made a model experiment on its airflow distribution (Lin Z 2008; Liu Xiaodong et al. 2009; Wang Fenghao et al. 2009). Lin pointed out that the stratum ventilation can provide better thermal comfort and save more energy than conventional ways in high temperature air conditioning office. However studies about this ventilation are still relatively few, airflow parameters under different conditions need to be studied

and optimized in the future. Using the RNG $k-\epsilon$ turbulence model and CFD numerical simulation, the author studied the IAQ and thermal comfort in working area of stratum ventilation under different air return methods. The results can be used for future study and engineering reference.

2 CONCEPT AND DEVELOPMENT OF STRATUM VENTILATION

As shown in [Figure 1](#), the concept of stratum ventilation comes through four stages (Lin Z 2005): confluence jet, opposed jet, transition ventilation and stratum ventilation.

Firstly, confluence jet is the ventilation which flows down attached to the vertical wall. The fresh cold air goes into the room from the top inlet, and then flows along the wall to the ground. It gradually replaces the stale air out of the room by forming an "air pool" which is similar to displacement ventilation. After that the opposed jet is the ventilation which use the nozzle setting correspond to the position, then in the vertical direction the air formed a horizontal air layer in the middle of the room after the jet collided. In this air layer, the mean age of the air is quite low, but there also have some serious entrainment phenomenon which is not very ideal. Transition ventilation is to forming the horizontal air layer by bending the air-flow with setting diversion board at an appropriate position. However, the results show that it is still has serious entrainment phenomenon. Stratum ventilation is characterized by forming fresh air layer and sending directly to the breathing zone. The air is supplied by the inlet located on the side

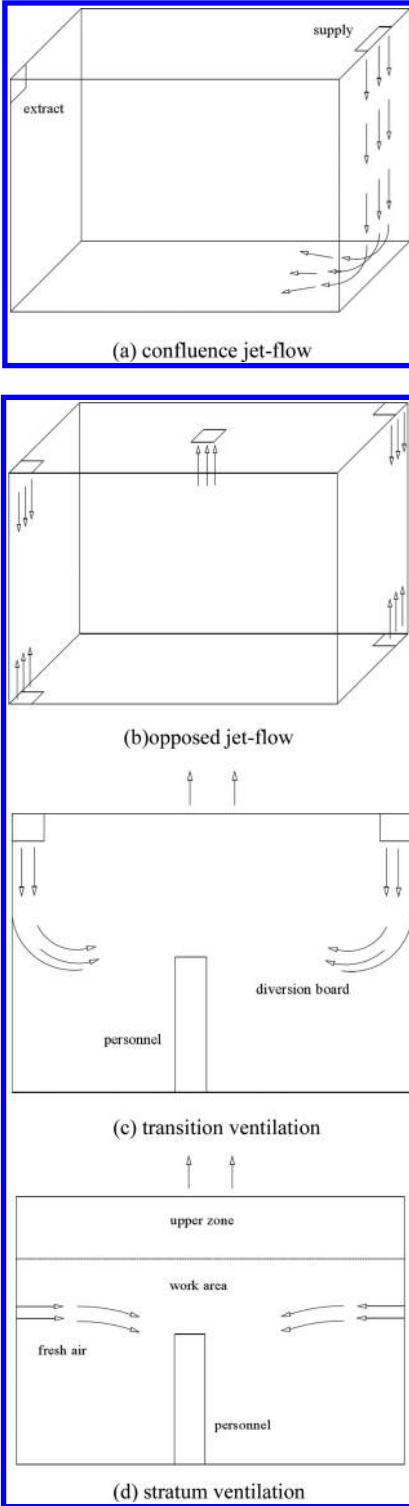


Figure 1. Development of stratum ventilation.

wall just above the height of the work area. The specific height is designed by whether occupant is standing or sitting in the room. Because the fresh air is delivered directly to the breathing zone, the fresh air which needs to be supplied can get significantly reduced. Meanwhile, the supply air temperature can be higher than mixing ventilation at the same level of thermal comfort. Reducing the fresh air and increasing the temperature of supply air created a space for energy saving.

3 NUMERICAL SIMULATION OF STRATUM VENTILATION

3.1 Mathematical model

The air flow in the room was low speed flow. In that case the air was in the incompressible range. Assuming that air flow was unsteady incompressible viscous three-dimensional flow. The control equation of the eddy viscosity turbulence model used the average continuity equation and Reynolds-averaged Navier-Stokes equation (Cho Y et al. 2005; Cho Y et al. 2008):

Continuity equation

$$\frac{\partial \bar{u}_i}{\partial x_i} = 0 \quad (1)$$

Reynolds-averaged equation

$$\frac{\partial}{\partial x_j} (\bar{u}_i \bar{u}_j + \tau_{ij}) = \bar{f}_i - \frac{1}{\rho} \frac{\partial p}{\partial x_i} + \frac{\partial^2}{\partial x_j^2} \left[\mu_t \left(\frac{\partial \bar{u}_i}{\partial x_j} + \frac{\partial \bar{u}_j}{\partial x_i} \right) \right] \quad (2)$$

where u_i is the velocity component, μ_t is the eddy viscosity coefficient, τ_{ij} is the viscous stress, ρ is density, p is pressure, f_i is mass force. Here used air-flow ventilation to dilute the indoor air pollutants, meanwhile, it used components transport equation:

$$\frac{\partial (\rho Y_i)}{\partial t} + \nabla \cdot (\rho \bar{U} Y_i) = -\nabla \cdot \bar{J}_i + R_i + S_i \quad (3)$$

where Y_i is the quality component concentration of \bar{J}_i each component, kg/m^3 ; R_i is the net production rate of chemical reactions; here the R_i is 0 because no chemical reactions were involved in this study. S_i is the discrete phase and additional production rate which caused by user-defined source term, kg/s ; is the diffusion flux, $\text{kg}/(\text{m}^2 \cdot \text{s})$.

$$\bar{J}_i = - \left[\rho D_{i,m} + \frac{\mu_t}{Sc_t} \right] \nabla Y_i \quad (4)$$

where $D_{i,m}$ is the mass diffusion coefficient of component i in the mixture, Sc_i is turbulent Schmidt number, which is 0.7; μ_t is the eddy viscosity coefficient, $N \cdot s/m^2$; D_i is the mass diffusion coefficient.

SIMPLE algorithm was used in Pressure and velocity coupling system, the model initialization R_e was 1.75×10^4 , the air flow was turbulent. Space discrete method adopt the Second Order in pressure and momentum, all residuals were set below 1×10^{-3} , and the residual of kinetic energy term which below 1×10^{-6} .

3.2 Physical model

The model built as a typical office which is shown in Figure 2, the coordinate origin set in the center of the ground, the size of the room is $4 \text{ m} \times 3 \text{ m} \times 2.7 \text{ m}$, it is decorated with simulated occupant (sitting), computers, lamps, bookcases, etc. The grill type air inlet's size is $0.2 \text{ m} \times 0.2 \text{ m}$ which setting in the middle area of side wall. The outlet is $0.5 \text{ m} \times 0.5 \text{ m}$ and four different kinds air return methods have been considered which are same sidewall upper return (A), opposite sidewall upper return (B), opposite sidewall lower return (C), roof return (D).

3.3 Boundary conditions

The inlet used the given boundary conditions, the air flow velocity $V_{in} = 1.28 \text{ m/s}$ and the CO_2 concentration of the air flow was 300 ppm. The ventilation volume was set by 6 times the number of

ventilators. The occupant as a source of pollutants released CO_2 at the rate of 7.9 mg/s . The heat dissipating capacity of the computer is 100 W , lamp is 34 W and occupant is 100 W . The body surface temperature set at 36°C , the indoor air-conditioning temperature took 26°C as NDRC recommended, the other walls were set as adiabatic wall.

4 RESULT

4.1 Distribution of pollutant concentration

As shown in Figure 2 the study used the observation flow lines which near the simulated human body to analyze data. The position and height of the flow line were taken to represent the upper and lower halves of the body respectively. It divided into two flow lines in the vertical direction which the lower section is from 0.1 m (ankle) to 0.6 m (waist) and the upper section is from 0.6 m to 1.3 m (head). Figure 3 shows the distribution of pollutant concentration on observation flow lines.

It can be seen from the results that the CO_2 concentration distribution of the four different conditions fluctuated slightly in the lower half of the observation flow line. The CO_2 concentration of condition A and D were relatively low. While the CO_2 concentration fluctuated heavily in the upper half of observation flow line. It started at the position of the head which was around 1.1 m , the CO_2 concentration had a clear upward trend with the height getting increased. It indicated that the contaminant near the breathing zone was brought to the upper area of the room with the air flow and influence of the body thermal plume. The CO_2 concentration of condition A, C and D were relatively low In the breathing zone where the height is around 1.0 m to 1.1 m , and the difference of them were all below $2 \times 10^{-5} \text{ g/L}$. However, the condition B had a maximum CO_2 concentration which was

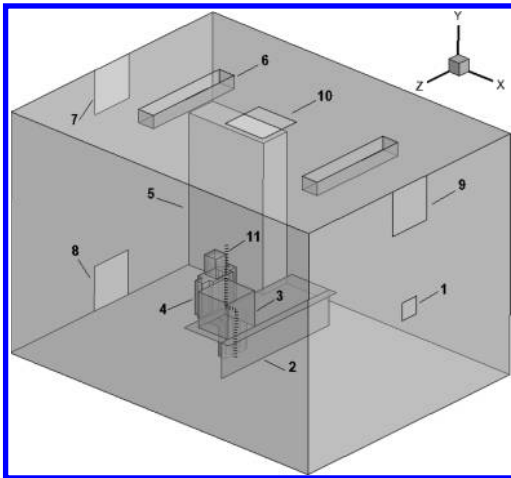


Figure 2. Layout of the modeling room. 1. inlet 2. table 3. computer 4. occupant 5. bookcase 6. lamp 7. outlet A 8. outlet B 9. outlet C 10. outlet D 11. observation flow line.

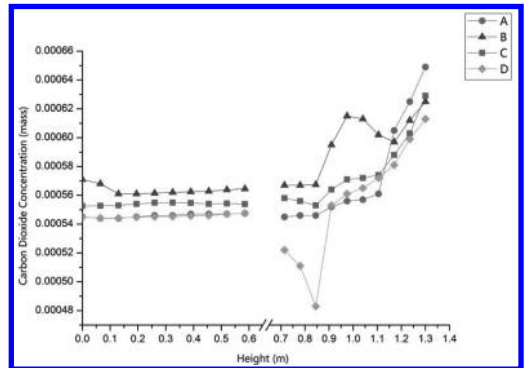


Figure 3. Distribution of pollutant concentration.

nearly 6.2×10^{-4} g/L. It can be seen that the upper air return is significantly better than the lower air return in terms of the contaminant removal. Besides, the opposite sidewall return has a better performance comparing with the same sidewall back.

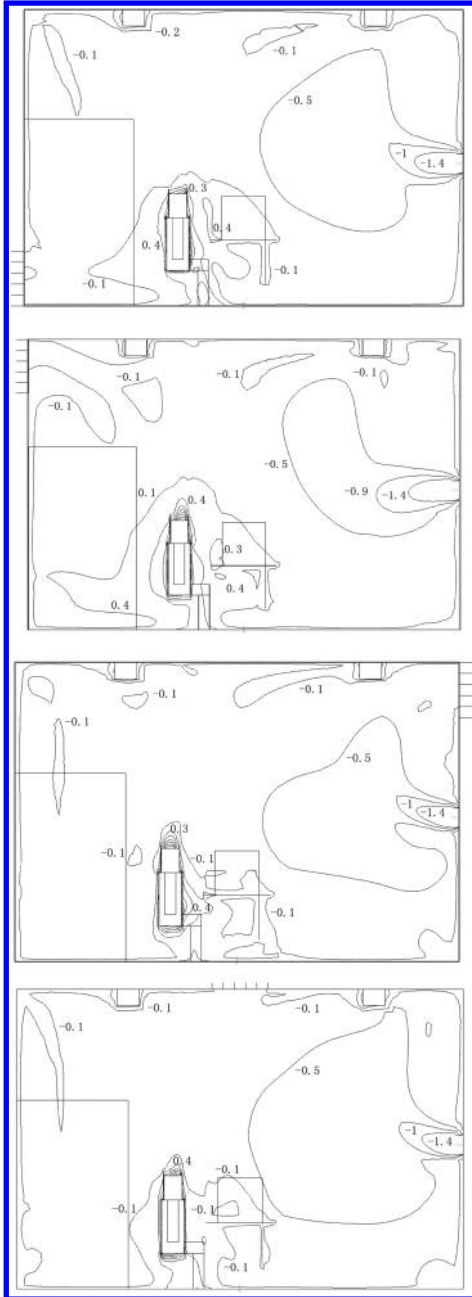


Figure 4. PMV in four kinds of working conditions.

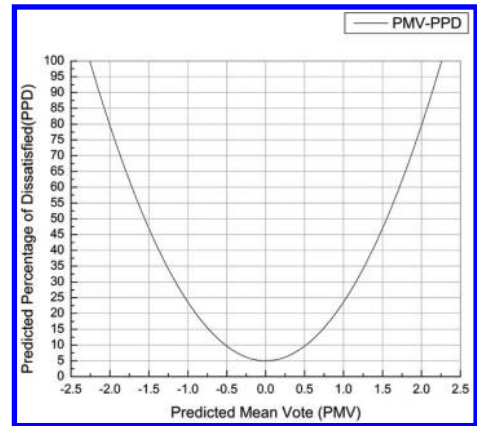


Figure 5. PMV-PPD.

4.2 PMV and PPD

Figure 4 shows the PMV in four kinds of conditions ($Z = 0$ section). To calculate the PMV, here takes the computational condition which the occupant is sitting and relaxed wearing trousers and shirt. It is shown that the difference of the PMV between these working conditions are small. The PMV values are mostly between -0.1 to $+0.4$ in the working area. The overall thermal comfort is at the neutral state which is good for occupant. Figure 5 shows the relationship between PMV and PPD (Rongyi Zhao et al. 2009), it can be seen that the $PPD = 5\%$ when the $PMV = 0$, which means that even if the indoor thermal comfort is optimal, there still has 5% of the people who are not satisfied due to physiological differences between individuals. ISO 7730 recommended $PPD < 10\%$ (Fanger et al. 2005), so the PMV is between -0.5 to $+0.5$, it means that 10% of the people are allowed felt dissatisfied. It can be known from Figure 5 that the PPD of the four conditions are between 5% to 10% near the working area, so the four different conditions can meet the thermal comfort requirements, and the different conditions had a little effect on thermal comfort.

5 CONCLUSION

The four different air return methods of stratum ventilation have a big impact on the CO_2 concentration distribution of the working area. To be more specific, the upper part air return generally has a lower pollutant concentration than the lower part air return, and in the breathing zone (1.0 m–1.1 m), the difference is particularly obvious. Roof air return and opposite side air return are better than lower air return and same

side air return. In order to make better indoor air environment, the project should adopt the roof air return or opposite side air return. In terms of the thermal comfort, the four air return methods have a little effect on it. The PMV where near the working area are in the comfort range, in accordance with ISO 7730.

REFERENCES

- Cho Y, Awbi HB, etc. 2005. Comparison between wall-confluent jets and displacement ventilation in aspect of the spreading ratio on the floor [J]. *Indoor Air 2005: Proceedings of the 10th International Conference on Indoor Air Quality and Climate, Vols 1–5*, 2005: 3249–3254.
- Cho Y, Awbi HB, Karimipannah T. 2008. Theoretical and experimental investigation of wall confluent jets ventilation and comparison with wall displacement ventilation [J]. *Building and Environment*, 2008, 43(6): 1091–1100.
- Fanger et al. 2005. ISO 7730. Moderate thermal environments-Determination of the PMV and PPD indices and specification of the conditions for thermal comfort [S].
- Lin Z. 2005. Stratum ventilation-a conceptual introduction[C]// *Proceedings of the 10th International Conference on Indoor Air Quality and Climate*, 2005, Beijing, China. Sep 2005: 3260–3264.
- Lin Z. 2008. Ventilation system for higher room temperature setting [J]. *Journal of Chemical Industry and Engineering*, 2008, 59(S2): 235–241.
- Liu Xiaodong, Yan Caiqiu, Li Yuanbin, Wang Fenghao. 2009. Experimental study of the air distribution characteristics in room of stratum ventilation [J]. *Refrigeration & Air-conditioning*, 2009, 9(2): 57–60.
- Rongyi Zhao et al. 2009. Air conditioning [M]. China Architecture & Building Press.
- Wang Fenghao, Liu Xiaodong, Li Yuanbin, Lin Zhang. 2009. Experiment and Numerical Simulation on Ventilation System of Office Building [J]. *Journal of Refrigeration*, 2009, 30(5): 45–50.

Urban Heat Island and its influencing indicator of new central district in Guangzhou city

P. Wang & Q.L. Meng

Building Environment and Energy Laboratory, State Key Laboratory of Subtropical Building Science, South China University of Technology, Guangzhou, P.R. China

ABSTRACT: Urban new central district is the area characterized with high density and has unique underlying surface, its outdoor spacial quality is of importance. Therefore, studying its heat island problem and thus finding methods to optimize its thermal environment, has important research value. In this paper, Zhujiang New Town, the representative of new central district in Guangzhou city, was taken as the research object. Meteorological data from Haixinsha weather station were collected to analyze the heat island intensity. A field experiment in a typical block was conducted to investigate the thermal environment from the neighborhood level. Then cases were set and simulated by the numerical simulation software ENVI-met, and respective contribution of different planning indicators to control heat island intensity was evaluated. It was proved that Greenery Ratio is the most outstanding indicator in lowering daytime heat island intensity.

Keywords: new central district; Urban Heat Island; Heat Island Intensity; Greenery Ratio

1 INTRODUCTION

Urban Heat Island (UHI) is a phenomenon that the temperature within the city is higher than in the suburb. Since it was first documented by British scholar Howard L in 1818, UHI has been an important issue over more than one hundred years. A lot of investigations were done and confirmed that UHI is a consequence of urbanization (Oke 1982, Shashua-Bar et al. 2004, Botlyán et al. 2005, Rizwan et al. 2008, Hart et al. 2009). Higher temperature results in decreasing outdoor air quality, worsening human thermal co (Chen et al. 2009, Lin et al. 2010, Zhao et al. 2011, Ng et al. 2012).

Guangzhou is the centre of the Pearl River Delta, one of the most prosperous economic zones in China. It is located in the hot and humid climate zone, and thus has a long and hot summer. It is proved that the air temperature in Guangzhou is rising in recent years (Wu 1986, Weng et al. 2004). Some researches took meteorological data of several weather stations in the city to compute the Urban Heat Island Intensity (UHII), which showed the spatial variation of UHI in the whole of Guangzhou (Jiang et al. 2007), even the hourly UHII values (Li et al. 2007). The other researches focused on some specific district, and the field experiment was done when there existed no weather station in targeted area, which showed the frequency and intensity of UHI in different functional areas (Ye et al. 2008). It can be found that the influence of urban center landscape on UHI was significant.

Urban center is developed with detached close-set high-rise buildings, and its aspect ratio as well as impervious area is large. New central district, which is the new urban center by centralized planning due to requirements of population, land or functional structure development, is more characterized with high density. Such underlying surface influences local microclimate environment prominently. On the other hand, its outdoor spacial quality is of importance. Therefore, studying its UHI problem and thus finding methods to optimize its thermal environment, has important research value.

In this paper, Zhujiang New Town, the representative of new central district in Guangzhou city, was taken as the research object. Meteorological data from weather station as well as the field experiment were used to analyze its UHI condition. By employing the numerical simulation software ENVI-met, respective contribution of different planning indicators to control heat island intensity was also evaluated.

2 SUMMERTIME UHI CONDITION OF ZHUJIANG NEW TOWN

2.1 *UHI analysis by meteorological data from weather station*

Haixinsha is the weather station lies in the south of Zhujiang New Town, it could describe the background climate environment of this new central district. At the same time, Luogang weather

station, that is the national basic weather stations located in suburb, represents the urban climate of suburban areas (Fig. 1).

The hourly meteorological data of July, 2013 from above two stations were compared (Fig. 2). The average UHII in the whole month was 1.7°C. The maximum of average UHII of each hour, 2.5°C, occurred at 7:00, while the minimum of average UHII, 0.8°C, occurred at 13:00. Besides, It can be seen that daytime UHII, when the air temperatures is high, is much lower than that of nighttime or early morning. If we defined 8:00–18:00 as daytime period according to Design Standard for Thermal Environment of Urban Residential Areas (JGJ 286-2013) and Evaluation Standard for Green Office Building (GB/T 50908-2013), the average daytime UHII is 1.2°C, and the average nighttime UHII is 4.4°C.

2.2 UHI analysis by the field experiment

In order to empirically investigate the local microclimate environment from the neighborhood level, a field experiment was conducted in a typical block, Block I2, of Zhujiang New Town in July 11–13,

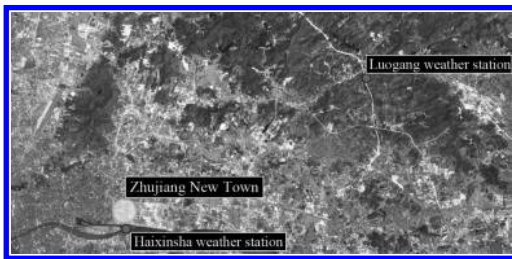


Figure 1. Locations of Zhujiang New Town and two weather stations.

2013 (Fig. 3). Each measuring point with its experiment device and underlying surface condition were shown in Figure 4. The experiment lasted for 47 hours, from July 11 21:00 to July 13 20:00.

The result shows that air temperature variation trends of all the measuring points were consistent. They fell to the lowest at around 6:00, then climbed up until reached to peak at 16:00, 4 hours later than the moment when the solar radiation was the most intense. The drizzle at around 13:30 on July 12 caused the temperature to drop and soon rebound.

Nighttime UHII of every measuring point was higher than daytime UHII obviously. The maximum UHII, 6.0°C of measuring point 1, just occurred at early morning on July 13. During the period from 10:00 to 18:00 there were at least one measuring point whose UHII was negative value.

Temperature difference of each measuring point was within 1°C at night, while during the day it turned to be bigger. Measuring point 1, which was set on light color pavement without shade had highest temperature among all the points during the experiment time. Measuring point 6, which was located on the granite plaza without building shadow, also had high temperature. On the contrary, the temperatures of measuring points between high-rise buildings were generally lower because of getting enough building shadow, e.g. measuring point 3. Measuring point 5, which was located both to the north of a tall building and under the dense shade from a tree, had lowest temperature among all the points during the daytime (Fig. 5). It is supposed that high-rise building shadow and greening shade play an important cooling role.

The average temperature of all measuring points was close to the value of Haixinsha weather station at night, and was lower at daytime (Fig. 6).

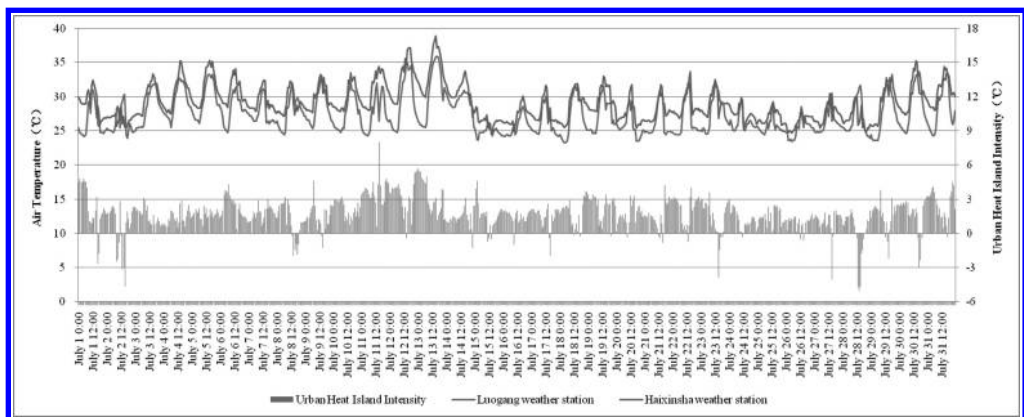


Figure 2. Hourly air temperature and UHII in July 2013.



Figure 3. Location of the typical block in Zhujiang New Town.

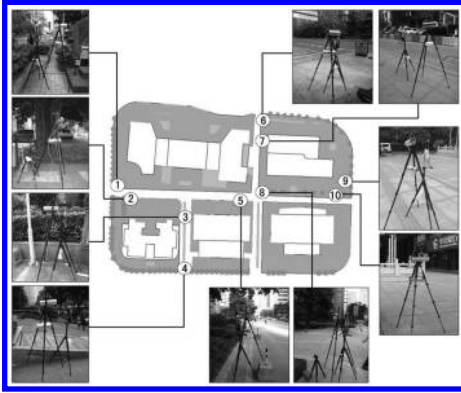


Figure 4. Location of ten measuring points.

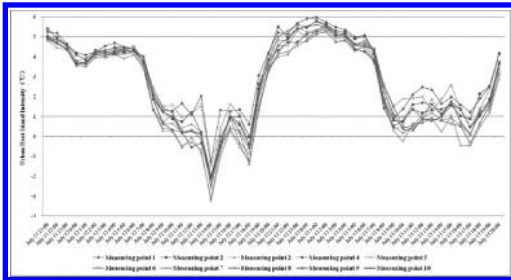


Figure 5. Hourly UHII of ten measure points.

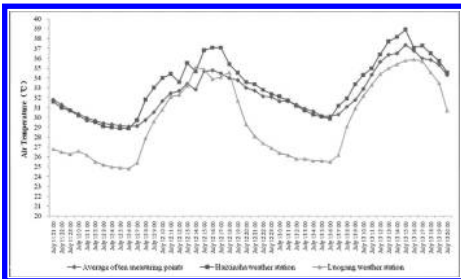


Figure 6. Average air temperature of ten measure points and comparison with weather stations.

The reason may be that there are no buildings or trees to provide shelter from solar radiation within a certain distance around the observation instrument in Haixinsha weather station.

3 SIMULATION AND RESULTS

The UHI condition of Zhujiang New Town was analyzed in the previous chapter. Next the verification of the numerical simulation software ENVI-met was done based on the measured meteorological data from above-mentioned field experiment. Then simulating cases were established and simulated, to discuss the main planning indicators affecting UHII.

3.1 A brief introduction of ENVI-met

ENVI-met is a three-dimensional microclimate model designed to simulate with a typical resolution of 0.5 to 10 m in space and 10 sec in time. It is a tool for studying the surface-plant-air interactions in the urban environment at the microclimate scale. Some recent studies have adopted ENVI-met to simulate urban microclimate (Ali-Toudert et al. 2007, Ng et al. 2012), demonstrating that it could describe urban micro-environment relatively accurately.

The results of simulation (Fig. 7) and measured temperature were strongly correlated ($R^2 = 0.917$, $P < 0.001$), and this numerical simulation software was proved to be available in predicting thermal environment of high density blocks (Fig. 8).

3.2 Setting of cases to be simulated

By reviewing the related literature at home and abroad, Floor Area Ratio (FAR), Building Density (BD) and Greenery Ratio (GR) are found

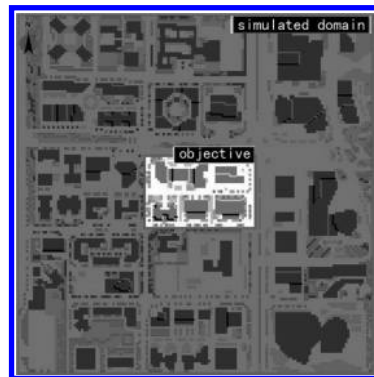


Figure 7. Simulation and target domain in ENVI-met.

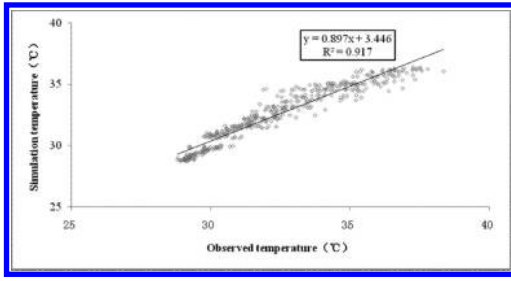


Figure 8. Correlation between observed temperature and simulated temperature.

Table 1. Cases established for simulation.

Case name*	Floor area ratio	Building density	Greenery ratio
8-35-15	8	35%	15%
4-35-15	4	35%	15%
6-35-15	6	35%	15%
10-35-15	10	35%	15%
8-25-15	8	25%	15%
8-45-15	8	45%	15%
8-55-15	8	55%	15%
8-35-0	8	35%	0%
8-35-30	8	35%	30%

*Naming rule for cases is Floor area ratio—Building density (%)—Greenery ratio (%).

to be important planning indicators. According to the field survey we have done before in Zhujiang New Town, their respective changing range were determined. The I2 block was chosen as the prototype case (case 8-35-15) and the other simulating cases were set up (Table 1). Meteorological data of typical summer day of Guangzhou is used as the boundary condition when we simulated with ENVI-met.

3.3 Results and discussions

Average daytime UHII during 8:00–18:00 is taken as the evaluation index of each case.

Simulation results are presented in Figures 9–11. The larger BD, FAR and GR are, the better outdoor thermal environment is. We may figure out that more building shade and greening can effectively mitigate the heat island problem.

When BD rises from 25% to 35%, the UHII reduction is minimal, and when BD rises from 35% to 55%, the UHII reduction reaches to 0.1°C. As for FAR, average daytime UHII reduces nearly 0.1°C when FAR rises from 4 to 6, while the UHII reduction less than 0.01°C when FAR rises from

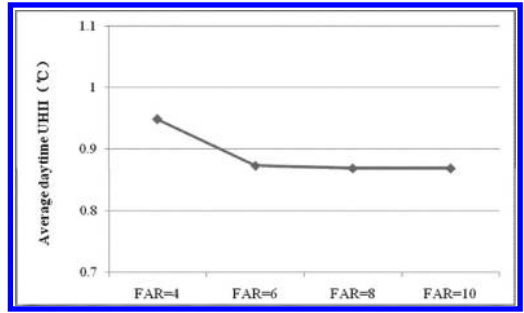


Figure 9. Average daytime UHII with changing of Floor Area Ratio (FAR).

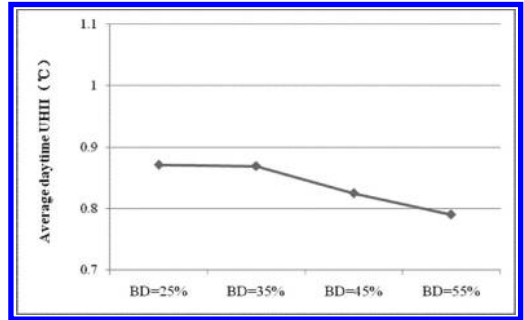


Figure 10. Average daytime UHII with changing of Building Density (BD).

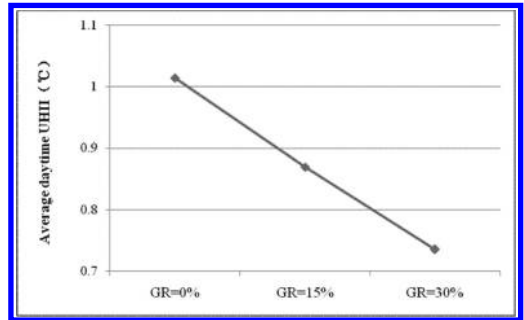


Figure 11. Average daytime UHII with changing of Greenery Ratio (GR).

6 to 10. GR is the most significant impact variable. when GR rises from 0 to 30%, the total UHII reduction is nearly 0.3°C. That is to say, when GR increases by 10%, average daytime UHII decreases by close to 0.1°C.

GR is the most outstanding indicator in mitigating UHI. According to the field survey we have done before, GR value is generally between 10% and 20% actually within the block, there

exists great potential for GR in improving thermal environment. In view of the high density block in new central district, creating more green space, especially more lush trees, within the block may be the most suitable method at present.

4 CONCLUSIONS

Urban new central district is the area characterized with high density and has unique underlying surface. Studying its UHI problem and thus finding methods to optimize its thermal environment, has important research value.

This paper took Zhujiang New Town as the research object. Meteorological data from weather station were collected to compared and analyze, it showed that the average daytime UHII is 1.2°C, and the average nighttime UHII is 4.4°C.

What's more, a field experiment in a typical block, I2, was conducted to empirically investigate the local microclimate environment from the neighborhood level. It was proved that thermal environment of different areas within the block were non-uniform, and high-rise building shadow as well as greening shade played an important cooling role.

I2 block was also chosen as the prototype case, and the other cases were established and simulated by ENVI-met. Respective contribution of different planning indicators to control heat island intensity was evaluated. On the premise of urban high density development, GR is the most outstanding indicator in improving thermal environment. When GR increases by 10%, average daytime UHII decreases by 0.1°C. Considering GR value in actual blocks in new central district, there exists great potential for GR to mitigate UHI problem.

Since the ratio of trees was set nearly 50% (according to the ratio of I2 block) of the greenery areas, and greening forms were unitary, in the future work, we will consider different kinds of greening forms and different ratios of trees, to further investigate their influences on thermal environment, and provide more scientific reference for urban planners and governments.

ACKNOWLEDGEMENTS

The author wishes to give special thanks to the students in Building Environment and Energy Laboratory who took part in the field experiment. The project was supported by National Key

Technology R&D Program of China (Project No. 2012BAC21B03).

REFERENCES

- Ali-Toudert, F. et al. 2007. Effects of asymmetry, galleries, overhanging facades and vegetation on thermal comfort in urban street canyons. *Solar Energy* 81(6): 742–754.
- Bottyán, Z. et al. 2005. The relationship between built-up areas and the spatial development of the mean maximum urban heat island in Debrecen, Hungary. *International Journal of Climatology* 25(3): 405–418.
- Chen, H. et al. 2009. Study on mitigation measures for outdoor thermal environment on present urban blocks in Tokyo using coupled simulation. *Building and Environment* 44(11): 2290–2299.
- Hart, M.A. et al. 2009. Quantifying the influence of land-use and surface characteristics on spatial variability in the urban heat island. *Theoretical and Applied Climatology* 95(3–4): 397–406.
- Jiang, X.D. et al. 2007. Characteristics of multi-scale temporal-spatial distribution of urban heat island in Guangzhou. *Chinese Journal of Applied Ecology* 18(1): 133–139 (in Chinese).
- Li, C.M. et al. 2007. Characteristics of Urban Heat-island Intensity of Guangzhou in 2005. *Guangdong Meteorology* (4): 30–33 (in Chinese).
- Lin, T.P. et al. 2010. Shading effect on long-term outdoor thermal comfort. *Building and Environment* 45(1): 213–221.
- Ng, E. et al. 2012. A study on the cooling effects of greening in a high-density city: An experience from Hong Kong. *Building and Environment* 47: 256–271.
- Oke, T.R. 1982. The energetic basis of the urban heat island. *Quarterly Journal of the Royal Meteorological Society* 108(455): 1–24.
- Rizwan, A.M. et al. 2008. A review on the generation, determination and mitigation of Urban Heat Island. *Journal of Environmental Sciences* 20(1): 120–128.
- Shashua-Bar, L. et al. 2004. Thermal effects of building geometry and spacing on the urban canopy layer microclimate in a hot-humid climate in summer. *International Journal of Climatology* 24(13): 1729–1742.
- Weng, Q.H. et al. 2004. Managing the adverse thermal effects of urban development in a densely populated Chinese city. *Journal of Environmental Management* 70(2): 145–156.
- Wu, Y.B. 1986. Heat Island character and its influence on air pollution over Guangzhou. *Journal of Tropical Meteorology* 2(3): 212–250 (in Chinese).
- Ye, Y.H. et al. 2008. Influence of landscapes on the frequency and intensity of urban heat island. *Ecology and Environment* 17(5): 1868–1874 (in Chinese).
- Zhao, C. et al. 2011. Urban planning indicators, morphology and climate indicators: A case study for a north-south transect of Beijing, China. *Building and Environment* 46(5): 1174–1183.

Study on surface performances of oxidation-sulfonated cellulose based superplasticizer

Kuerbanjiang Rouzi, Mailikezati Mahemuti & Maliya Mamuti

Institute of Chemistry and Chemical Industry, Xinjiang University, Urumqi, Xinjiang, China

ABSTRACT: Surface and dispersing performances, zeta potentials and effects on the fluidity of cement paste using two water reducing agents traditional naphthalene sulfonated formaldehyde (FDN) and Oxidation-Sulfonated Cellulose (OSC) based superplasticizer were investigated. According to the result of performance test, OSC mechanism is discussed. The results show that OSC is a type of air entraining superplasticizer and it can reduce the surface tension of water. It's adsorption amount on the surface of cement are smaller than FDN, but OSC has better dispersing capability and higher zeta potential than FDN, and the compressive strength of concrete treated with OSC is higher than that treated with FDN. Excellent dispersing performance of OSC is the result of co-action of electrostatic repulsion and steric hindrance.

Keywords: oxidation-sulfonated cellulose; superplasticizer; surface performance; dispersion; mechanism

Water reducing agent is an important chemical admixture that can be added to cementitious pastes to improve the workability and strength of concrete (Zhang, Shang, Yin, Aishah, Salmiah, & Ooi, 2001). The application of water reducing agent into the building energy consumption, improve the durability of the concrete engineering, it is of great economic and social benefits (Sylvie, Solenne, David, & Isabelle, 2012).

Cellulose is the most widely used type of completely biodegradable natural polysaccharide polymer (Ragauskas, Williams, Davison, Britovsek, Cairney, Eckert, Frederick, Hallett, Leak, Liotta, Mielenz, Murphy, Templer, & Tschaplinski, 2006). It has the raw material sources, the advantages of low cost, easily biodegradable (Liu, Guo, Ha, & Liao, 2008). For a long time, people use various methods to cellulose modification, in order to broaden its application domain (Xiong, Ye, He, & Wu, 2000; Simone, & Birgit, 2003; Wang, Hang, Zhang, & Ma, 2008). In the field of construction, the cellulose derivatives as water reducing agent research has also received attention (Halidan, Kurbanjian, Wang, & Chen, 2011; Caroline, Nathalie, & Pascal, 2014; Yoshioka, Sakai, Daimon, & Kitahara, 1997).

The effect mechanism of concrete water reducing agent is the lack of a thorough system research. Correct understanding of the interaction of water reducing agent and cement on the performance of the application of water reducing agent to make reasonable explanations and improve the

existing water reducing agent performance and developing new water reducing agent has important guiding significance, but the researches on the mechanism of the dispersion is a very complicated work, although now many research tried to use the space steric hindrance and electrostatic repulsion theory of principle to explain the interaction of water reducing agent and cement, but for many of the results are often inconsistent, and even contradictory (Yoshioka, Tazawa, & Kawai, 2002; Fernández, Duran, Navarro-Blasco, Lanas, Sirera, & Alvarez, 2013; Didamony, Heikal, Khalil, & Al-Masry, 2012). In this paper, through the selection of FDN and OSC two types of water reducing agent, the comparison and analysis on its performance, revealing the sulfonated cellulose water reducing mechanism of water reducing agent.

1 EXPERIMENTAL

1.1 *Materials*

A commercially manufactured ordinary portland cement 42.5R based on Chinese National Standard GB/T 8077-2000 was used (came from Urumqi Cement Plant in China). Cotton pulp (DP:576) supplied by AO yang technology limited liability company, Manas, Xinjiang, China; FDN used in this study was commercial products. All other reagents were commercially available and were used without further purification.

1.2 Synthesis of OSC

A certain amount of cotton pulp (after appropriate pieces) into a three-neck flask with stirring heat up was hydrolyzed by diluted hydrochloric acid a certain time. After cooling to room temperature, the micro crystalline cellulose (MCC, a certain degree of polymerization) was collected by filtration and washing to neutral, dried under 50°C. Then a slurry of oven-dried crystalline cellulose and distilled (DI) water (200.00 mL) was treated with sodium periodate and stirred for three days at room temperature in absence of light. The product was filtered, repeatedly washed with DI water to remove the spent oxidant, and then air dried. The oxidation cellulose was dispersed in deionized water and reacted with sodium bisulfite (6.00 g). After stirring for 72 h at rt, the resulting product was dialyzed using cellulose acetate membrane followed by freeze drying.

2 EXPERIMENTAL METHODS

2.1 Surface tension measurement

Accurate confecting different concentration of sample solution, using 70545 type surface tensiometer tensile membrane method is used to measure the surface tension.

2.2 Adsorption amount measurement

FDN adsorption amount measurement: according to the literature (Lei, & Plank, 2014): The concentrations of FDN were measured by UV adsorption spectrophotometer (UV240, JAPAN), it was calculated from the difference in the equilibrium concentrations of the polymers in the liquid phase before and after adsorption.

OSC adsorption amount measurement: OSC belongs to polysaccharide derivatives, it showed very weak adsorption within UV-visible region, so choose method of Chemical Oxygen Demand (COD) testing. Test method/principle was used according to the literature (Sun, & Guan, 2009).

2.3 Adsorption layer thickness measurement

Sulfonated cellulose on the cement particle adsorption layer thickness by Thermo ESCALAB type 250 multi-function X-ray photoelectron spectrometer (Thermo Electron Corporation, U.K measurement), method of measurement see references (Zheng Da feng, Qiu Xue qing, & Lou Hongming, 2008).

2.4 FTIR measurement

The IR spectra of cellulose and OSC were recorded with a FT-IR spectrometer (EQUINOX 55, Germany).

2.5 Fluidity of cement of paste

A certain amount of water-reducing agent was added to water in advance. And then cement paste was prepared with a water/cement weight ratio of 0.35:1. The fluidity of cement paste was evaluated by pullout spread of a sample from a flow cone specified according to GB8077-2000.

The maximum diameter of the spread sample and the maximum width perpendicular to that diameter were measured and the average of these two values was defined as the flow value.

2.6 ζ -Potential measurement

A certain amount of cement was added to the solution with certain concentration of water-reducing agent. The ratio of solute to solvent by weight was 0.0025:1. After mixing for 5 min in the blender, the ζ -potential of particles in the clarified liquor was analyzed using a Zeta Potential Analyzer ZETA PLUS (Brookhaven Instruments Corporation, New York, U.S.A) and the average of ten measurements was regarded as the ζ -potential of the cement particles.

3 RESULTS AND DISCUSSION

3.1 Surface tension analysis of the OSC

As shown in Figure 1, oxidation-Sulfonated cellulose aqueous solution surface tension and decreased with the increase of solution concentration, when the concentration of the solution quality of 4 g/L, the oxidation-sulfonated cellulose solution surface tension decreased to 52.98 mN/m, continue to increase concentration, remain unchanged, the surface tension of the solution that OSC is a kind

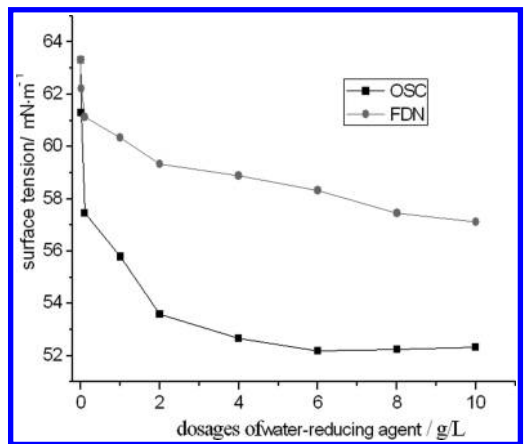


Figure 1. The relationship between the surface tension and the concentration of FDN and OSC.

of surface active agent, can reduce that of the liquid surface tension.

3.2 FTIR analysis of the OSC

As shown in Figure 2, IR spectrum of OSC (b) had two new and strong characteristic absorption peaks in comparison with IR spectrum of cellulose (a). The peaks located at 818 cm^{-1} , 1338 cm^{-1} and 615 cm^{-1} were stretching vibration of C-O-S and S=O, respectively, which indicated that sulfuric acid groups were introduced into the cellulose molecule.

3.3 Effect of water-reducing agents on the fluidity of cement paste

The fluidity and fluidity loss of cement paste are important application performance parameters for water-reducing agent. To evaluate the applied capability of OSC, the relationship between the fluidity of cement paste and dosage/storing time of OSC were studied and compared with that of FDN.

As shown in Figure 3, the addition of water reducing agent can significantly improve the fluidity of cement paste. The fluidity of cement paste with OSC and FDN increased from 65 to 294 and 252 mm, respectively, when their dose was increased from 0% to 2.5%, which indicated that the dispersion capacity of OSC was stronger than that of FDN at the same dose.

In addition, with the increase of FDN dose, the fluidity of cement paste also increased until it reached about 1.4%. While for OSC, when the dosage exceeded 0.8%, the fluidity was maximum. So compared with FDN, OSC could produce more dispersing ability for cement particles. Figure 4 examines the storing time dependency of the fluidity of cement paste in the same dosage (0.8%). During the process of hydration, the fluidity of cement paste

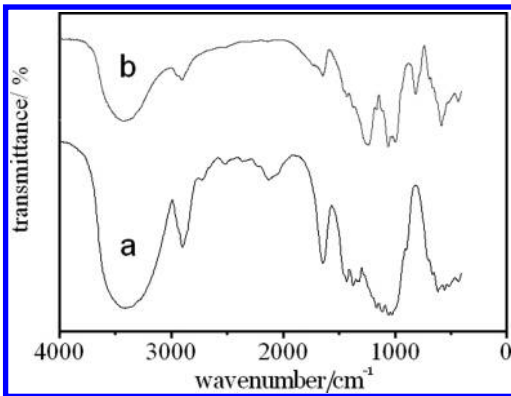


Figure 2. IR spectra of cellulose (a) and OSC (b).

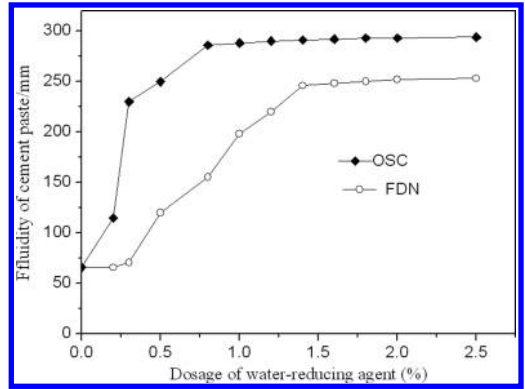


Figure 3. Effect of water-reducing agents addition on the fluidity of cement paste.

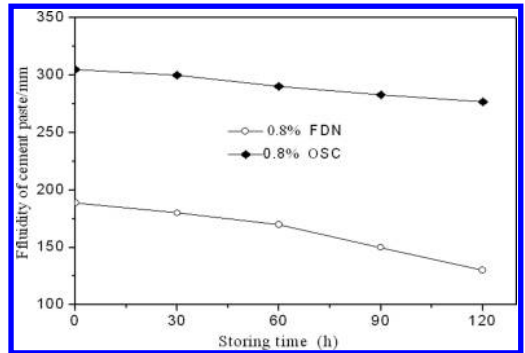


Figure 4. The storing time dependency of the fluidity of cement paste.

with FDN reduced from 189 to 130 mm, loss was 31.2%. Whereas the fluidity of cement paste with OSC reduced from 305 to 277 mm, loss was just 9.2% in the same storing time.

The results show the the dispersion stability of OSC was superior to that of FDN. Because of the dispersion mechanism of water reducing agent and its adsorption characteristics are closely related. In order to explain the reason for why the dispersion capacity and stability of OSC are better than that of FDN, the investigation of adsorption characteristics of OSC should be carried out since they are closely correlated to dispersing mechanism.

3.4 Adsorption characteristics of water-reducing agents on cement surface

Water reducing agent in cement particles on the surface of the adsorption characteristic parameters including zeta potential of water—OSC—cement system, adsorption amount and adsorption layer

thickness. They are discussed in detail in the following text.

3.4.1 Effect of water-reducing agent on ζ -potential of cement particles surface

Figure 5 shows that the zeta potential for cement particle without addition admixture was +9.8 mV, and while it rapidly decreased to about -38 mV - 45 mV with OSC and FDN, respectively. The absolute value increases, this is because the anion adsorption of FDN and OSC changed the charge distribution of the electrical double layer of the cement surface.

3.4.2 Adsorption amount of water-reducing agent on cement surface

Water reducing agent concentration and its adsorption on cement particles as shown in Figure 6, figure curve shape was like Langmuir adsorption. Water reducing agent on the surface of the cement particles, generally conform to the Langmuir

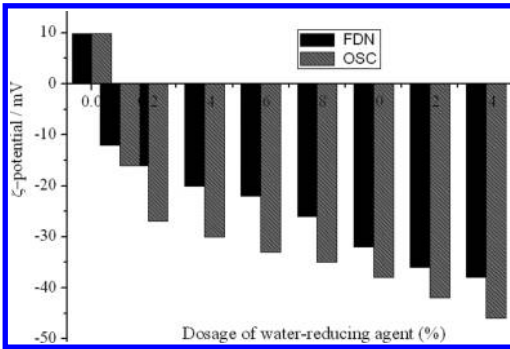


Figure 5. ζ -Potential of water-reducing agents with different concentration.

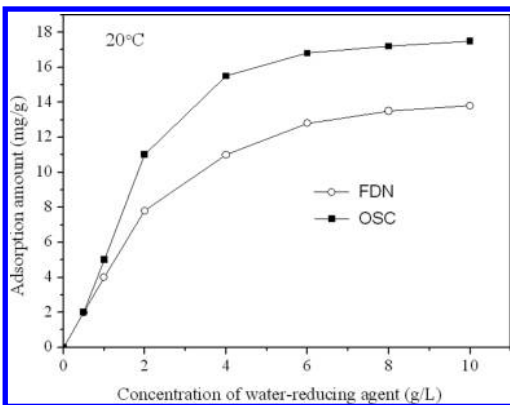


Figure 6. Relationship between concentration and adsorbed amount of water-reducing agent.

adsorption isothermal adsorption equation (Zhao, Ying, & Zang, 2011):

$$\Gamma = \Gamma_{\infty} \frac{kc}{1+kc} \quad (1)$$

The type is to:

$$\frac{c}{\Gamma} = \frac{c}{\Gamma_{\infty}} + \frac{1}{\Gamma_{\infty} k} \quad (2)$$

where c and Γ are equilibrium concentration (g/L) and equilibrium adsorption capacity (mg/g), respectively; Γ_{∞} and k are the Langmuir constants representing maximum adsorption capacity (mg/g) and adsorption constant, respectively.

According to the Langmuir equation (3) the use of drawing a straight line, the intercept and slope of two kinds of water reducing agent FDM and OSC limit adsorption capacity were 13.8 mg/g and 16.5 mg/g. Since the linear correlation of two straight line close to 1 (see Fig. 8), so the knowable FDM and OSC in the cement particles on the surface of a belongs to the Langmuir adsorption monolayer adsorption.

3.4.3 The adsorption layer thickness of the water reducing agent

As shown in Figure 7, the thickness of the adsorption layer OSC and FDM were 5.09 and 0.62 nm, respectively. It can be calculated that the adsorption layer thickness ratio was 8:1, which indicated that the molecular adsorption state of FDM and OSC on cement articles was quite different. OSC mixed with cement particle interactions lead to system happen very big change, on the one hand, the electrostatic repulsion between particles increase, on the other hand, due to the adsorption

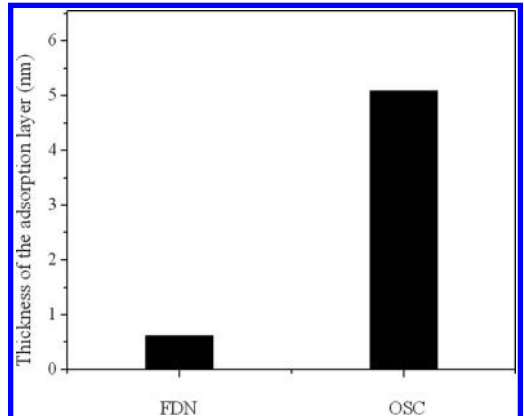


Figure 7. The thickness of adsorption layer of water-reducing agent.

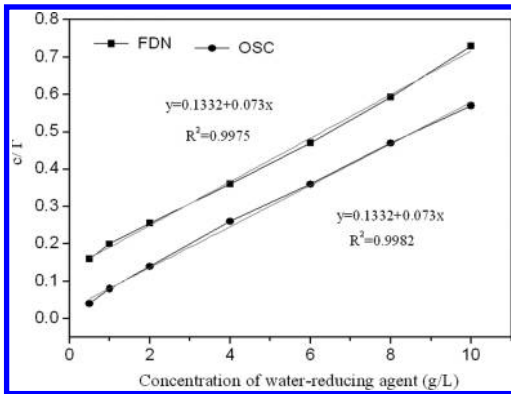


Figure 8. Langmuir adsorption isotherm for the adsorption of OSC and FDN on cement particles.

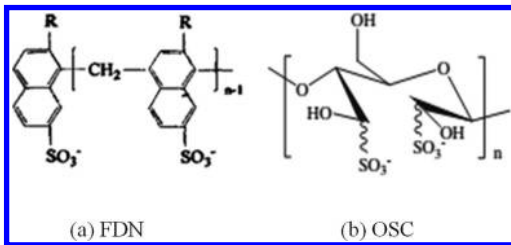


Figure 9. The molecular structure of FDN and OSC.

on the surface of cement particles of OSC adsorption layer formation (5.09 nm), has a strong space steric effect, and the space steric forces play a leading role in a certain scope, it shows that OSC mainly depends on the space steric effect to achieve between cement particles dispersed, and electrostatic repulsion is indispensable to the dispersed water reducing effect. That is the space steric effect is dominant, the result of the synergy with the effects of the electrostatic repulsion.

3.5 The dispersing mechanism of OSC

The molecular structures of FDN and OSC are shown in Figure 9, respectively. It can be seen that the dispersing mechanism that the dispersing mechanism of water-reducing agent is closely related to not only the adsorption characteristics but also the configuration of the molecule.

The molecular structure of FDN is linear with short branched, to stick lying on the surface of cement particles (Dong, Ben, Shu, Lu, & Jin, 2007). The adsorption layer thickness of this kind of adsorption state was too thin (0.62 nm) to contribute to steric stabilization. Therefore, the dispersing ability of FDN mainly comes from

the electrostatic repulsive force produced by the adsorption double-electrical layer. In the cement particles on the surface of FDN are easily covered by the hydration product, resulting in a paste fluidity a rapid loss in a certain time.

4 CONCLUSION

1. The adsorption of OSC and FDN on cement particles both conform to Langmuir single layer adsorption, but the dispersion mechanism of OSC is quite different from that of FDN. Although maximal adsorption OSC higher than that of FDN, but the cement paste with OSC can reach maximal fluidity (294 nm) at lower adsorption amount. And the fluidity of cement past may achieve maximal fluidity (252 mm) with FDN may achieve most only at maximal adsorption.
2. Sulfonated cellulose in the molecular structure of water reducing agent—OSO₃Na groups and—OH groups, and uneven distribution, adsorption on the surface of cement particles, forming different morphology, molecular chain on the cement particles can form annular structure or caudate. It can be concluded that the OSC to cement water reducing dispersion effect mainly depends on the space steric effect, electrostatic repulsion play a supporting role. Thus, the dispersing stability generated by steric hindrance is much better than that by electrostatic repulsive force.

ACKNOWLEDGEMENT

We are grateful to the Xinjiang Uygur Autonomous region of China Nature Science Foundation (No. 2012211A017) for financial support of this research.

REFERENCES

- Caroline Autier, Nathalie Azéma, & Pascal Boustingorry. (2014). Using settling behaviour to study mesostructural organization of cement pastes and superplasticizer efficiency. *Colloids and Surfaces A: Physicochemical and Engineering Aspects*, 450(20):36–4.
- Didamony H. El, Heika Mohamedl, Khalil Kh. A., & S. Al-Masry. (2012). Effect of delaying addition time of SMF superplasticizer on the physico-mechanical properties and durability of cement pastes. *Construction and Building Materials*, 35(10):261–269.
- Dong Fang Zhang, Ben Zhi Ju, Shu Fen Zhang, Lu He, & Jin Zong Yang. (2007). The study on the dispersing mechanism of starch sulfonate as a water-reducing agent for cement. *Carbohydrate Polymers*, (70):363–368.

- Fernández J.M., Duran A., Navarro-Blasco I., Lanas J., Siraera R., & Alvarez J.I. (2013). Influence of nanosilica and a polycarboxylate ether superplasticizer on the performance of lime mortars. *Cement and Concrete Research*, 43(1):12–24.
- Halidan Mamat, Kurbanjian Rouzi, Wang Xin, & Chen Song lin. (2011). Development and application of sulfobutylated cellulose ether (SBC) based water-reducing agent. *Concrete (China)*, 256(2):75–82.
- Kurbanjian Rouzi, Halidan Mamat, Alimujiang, & Hajinsa. (2011). Synthesis and dispersing mechanism of cellulose sulfonate as a water-reducing agent for cement. *Concrete (China)*, 7(261):69–74.
- Liu Sa, Guo Jianwei, Ha Chengyong, & Liao Bing. (2008). Synthesis of novel adamantane carboxylic acid esters of cellulose using co-reagent. *Journal of Chemical Industry and Engineering (China)*, 59(12):3178–3183.
- Lei L., & Plank J. (2014). A study on the impact of different clay minerals on the dispersing force of conventional and modified vinyl etherbased polycarboxylate superplasticizers. *Cement and Concrete Research*, 60:1–10.
- Ragauskas A.J., Williams C.K., Davison B.H., Britovsek G., Cairney J., Eckert C.A., Frederick W.J. Jr., Hallett J.P., Leak D.J., Liotta C.L., Mielenz J.R., Murphy R., Templer R., & Tschaplinski T. (2006). The path forward for biofuels and biomaterials. *Science*, 311(5760):484–489.
- Simone Knaus, & Birgit Bauer-Heim. (2003). Synthesis and Properties of Anionic Cellulose Ethers: Influence of Functional Groups and Molecular Weight on Flowability of Concrete. *Carbohydrate Polymers*, 53:383–394.
- Sun Dongyue, & Guan Xianguan. (2009). Elimination of Interference on COD Measurement by $K_2Cr_2O_7$ Method. *Environmental Science and Management, (China)*, 34(6):124–126.
- Sylvie Pourchet, Solenne Liautaud, David Rinaldi, & Isabelle Pochard. (2012). Effect of the repartition of the PEG side chains on the adsorption and dispersion behaviors of PCP in presence of sulfate. *Cement and Concrete Research*, 42(2):431–439.
- Wang Li jiu, Huang Feng yuan, Zhang Hong, & Ma Xi chen. (2008). Preparations and applications of cellulose -based concrete high-range water-reducing agent. *Journal of Dalian University of Technology (China)*, 48(5):679–684.
- Xiong J, Ye J, He X, & Wu Z. (2000). The improved heterogeneous reaction of the oxidation of cellulose by periodic. *Polym. Mater. Sci. Eng.*, 16(3):172–175.
- Yoshioka K, Sakai E., Daimon M., & Kitahara A. (1997). Role of steric hindrance in the performance of superplasticizers for concrete. *J. Am. Ceram. Soc.*, 80(10): 2667–2671.
- Yoshioka K., Tazawa E., Kawai K., et al. (2002). Adsorption characteristics of superplasticizers on cement component minerals. *Cement and Concrete Research*, 32(10):1507–1513.
- Zhang, T., Shang, S., Yin, F., Aishah, A., Salmiah, A., & Ooi, T.L. (2001). Adsorption behavior of surfactants on surface of Portland cement. *Cement and Concrete Research*, 31(7):1009–1015.
- Zheng Da feng, Qiu Xue qing, & Lou Hongming. (2008). Measurement of adsorption layer thickness of water reducing by using XPS. *Journal of Chemical Industry and Engineering (China)*, 59(12):57–259.
- Zhao Fenghua, Ying Guangjun, & Zang Fengzhong. (2011). Study On Adsorption Behavior of Water Reducer in Cement-based Materials. *Building Materials world (China)*, 32(2):9–12.

Study on numerical simulation of gas drainage drilling of rock drift of coal seam floor

Wei Wu

Modern Educational Technology Center, Henan Polytechnic University, Jiaozuo, China

Yuan Yuan Wang

Institute of Higher Education, Henan Polytechnic University, Jiaozuo, China

Jie Zhu

Modern Educational Technology Center, Henan Polytechnic University, Jiaozuo, China

ABSTRACT: At present the gas drainage effect is not good in many high gas coal mines and gas outburst coal mines, gas drainage rate can not reach the standard, one important reason is that drill hole sealing effect is not good. However, if selection of starting sealing depth of drill hole is not reasonable, then drill hole sealing effect is bad. So this article researches that numerical simulation on rock drift of coal seam floor and drilling of rock drift of coal seam floor by using COMSOL Multiphysics software. It obtains the reasonable starting sealing depth of drill hole of rock drift of coal seam floor and works out the problem that gas drainage efficiency can not reach the standard.

Keywords: gas drainage; drill hole sealing; numerical simulation; drill hole starting sealing depth

1 INTRODUCTION

Coal resource is one of the main energy in our country, along with the increase of mining depth, the gas accident probability is increased. In the 1950s, gas drainage was as an important measures of prevention and management of coal mine gas in our country. After decades of development, the gas drainage technology has made significant progress^[1]. However, at present our country still has a lot of high gas coal mines and gas outburst coal mines and their gas drainage effect is bad, the gas drainage rate is very difficult to reach the standard, in addition to the permeability of coal seams is relatively poor and the gas drainage method is not appropriate, the drill hole sealing effect of gas drainage is bad is also one of the important reasons^[2]. If the selection of starting sealing depth of gas drainage is not reasonable, it will directly affect the hole sealing effect. Selection of starting sealing depth is not reasonable, mainly because of stress and strain characteristics of rock drift surrounding and stress and strain characteristics of rock drift borehole surrounding is not thorough analyzed. Based on drilling of rock drift of coal seam floor, this article researched stress and strain characteristics of rock drift surrounding and stress and strain characteristics of rock drift borehole

surrounding and finally determined reasonable gas drainage drilling starting sealing depth. To improve the effect of drill hole sealing, so as to improve the gas drainage rate, solve the problem of coal mine gas drainage rate is substandard.

2 THEORETICAL RESEARCH OF STRESS AND STRAIN CHARACTERISTICS OF ROCK DRIFT SURROUNDING

At the beginning, the coal and rock is in thermodynamic equilibrium state, once rock drift was excavated, this state of equilibrium will be destroyed, into a new kind of non equilibrium state^[3]. If the rock drift is a circle, its external force [equation \(1\)](#):

$$\sigma_{\infty} = \gamma H \quad (1)$$

In the [equation \(1\)](#):

σ_{∞} —Infinity static level pressure;

γ —Specific gravity of rock;

H —Buried depth of rock drift.

R , φ plane, r , z plane, φ , z plane maximum shear stress [equation \(2\)](#) as below:

$$T = \frac{\sigma_{\varphi} - \sigma_r}{2} \quad T_1 = \frac{\sigma_z - \sigma_r}{2} \quad T_2 = \frac{\sigma_{\varphi} - \sigma_z}{2}, \quad (2)$$

3 THEORETICAL RESEARCH OF STRESS AND STRAIN CHARACTERISTICS OF DRILLING SURROUNDING OF ROCK DRIFT

Assume that produce the plastic yield shear stress is $T = T_0$, the yield limit under uniaxial compression is σ_0 .

The main shear stress increases with the increase of buried depth of rock, when $T = T_0$, drift wall began to yield, then the following equation (3):

$$\Gamma = \frac{\sigma_\varphi - \sigma_r}{2} = \sigma_\infty = T_0 = \frac{\sigma_0}{2} \quad (3)$$

when $\sigma_\infty = T_0 = \sigma_0/2$, r, φ plane produce slip line.

When T reach the yield limit, material yield is part of the plastic.

If the buried depth continue to increase, and the other a maximum shear stress plane also reach the yield condition:

$$\Gamma_1 = \frac{\sigma_z - \sigma_r}{2} = \frac{\sigma_\infty}{2} = T_0 = \frac{\sigma_0}{2} \quad (4)$$

According to theory of plasticity, attain the state of plastic of rock must meet two main shear stress sliding surface. Then it happens in column r , φ plane sliding phenomenon, and generates the slip line.

In addition, it can occur in column r , z plane slip phenomenon, also produces slip plane if early rock balance is broken, and can damage rock, once external disturbance, then gas outburst and rock burst will occur easily.

Gravity equation and yield stress equation (5):

$$\sigma_\infty = 2T_0 = \sigma_0 \quad (5)$$

Control the rock drift strain parameters is equation (6):

$$\Gamma = \varepsilon_r - \varepsilon_\varphi \quad (6)$$

Take the ideal elastic-plastic model of rock, when $T = T_0$, into the plastic state, but once $\Gamma \geq \Gamma_0$ (Γ_0 is limit value), rock will be destroyed, brittle rock Γ_0 is elastic limit Γ_e .

The plastic deformation zone of rock drift surrounding stress equation (7):

$$\sigma_r = 2T_0 \ln \frac{r}{a}, \quad \sigma_\varphi = 2T_0 \left(\ln \frac{r}{a} + 1 \right) \quad (7)$$

In the equation (7):

r —The current point coordinates;

a —The radius of rock drift.

The radius of plastic zone equation (8):

$$\left(\frac{c}{a} \right)^2 = e^{\frac{\sigma_\infty - T_0}{T_0}} \quad (8)$$

When $\sigma_\infty = 2T_0 = \sigma_0$, $c = 1.65a$.

Assume that drilling surrounding rock is in all directions for homogeneous elastic medium, no viscous behavior or creep. The original rock stress state is hydrostatic pressure, Round hole in the rock drift surrounding characteristics is the same^[4].

Studies show that when the buried depth $H \geq 20R_0$, R_0 is drilling radius, does not consider influence area of its own gravity, influence area of the borehole surrounding is 3 to 5 times, and the error of the original problem is not more than 11%. So borehole stress problems can be regarded as homogeneous state, thus formed the space structure and loading in the axisymmetric case, reduced to a plane strain problem of drilling^[5].

From Figure 1 we can get the following equation (9):

$$(\sigma_r + d\sigma_r)(r + dr)d\theta - \sigma_r r d\theta - 2\sigma_r dr \sin \frac{d\theta}{2} = 0 \quad (9)$$

In the equation (9):

σ_r —tangential stress;

σ_r —radial stress;

r —The radius of the micro unit;

θ —coordinate angle.

Because $d\theta/2$ is very small, so $\sin d\theta/2 = d\theta/2$.

Then get equation (10):

$$\sigma_r - \sigma_t + r \frac{d\theta}{dr} = 0 \quad (10)$$

When radial strain $\mu \rightarrow \mu + d\mu$, then radial strain ξ_r equation (11):

$$\xi_r = \frac{(\mu + d\mu)d\theta - r d\theta}{rd\theta} = \frac{d\mu}{dr} \quad (11)$$

When tangential strain $rd\theta \rightarrow (r + \mu)d\theta$, then get tangential strain ξ_t equation (12):

$$\xi_t = \frac{(r + \mu)d\theta - rd\theta}{rd\theta} = \frac{\mu}{r} \quad (12)$$

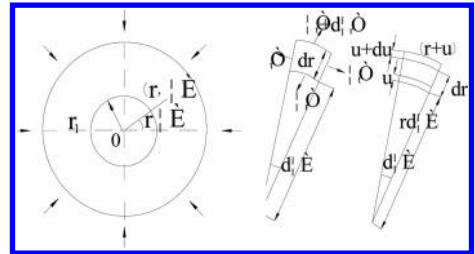


Figure 1. Drilling surrounding unit stress distribution.

After calculation:

$$\frac{d\xi_i}{dr} = \frac{1}{r} \frac{d\mu}{dr} - \frac{\mu}{r^2} = \frac{1}{r} \left(\frac{d\mu}{dr} - \frac{\mu}{r} \right) = \frac{1}{r} (\xi_r + \xi_i)$$

According to generalized Hooke law, then get the equation (13), (14):

$$\xi_i = \frac{1}{E} [\sigma_i - \mu(\sigma_r + \sigma_s)] \quad (13)$$

$$\xi_r = \frac{1}{E} [\sigma_r - \mu(\sigma_i + \sigma_s)] \quad (14)$$

In equation (13), (14):

σ_s —round hole axial stress.

Because:

$$\frac{d\xi_i}{dr} = \frac{1}{E} \left(\frac{d\sigma_i}{dr} - \mu \frac{d\sigma_r}{dr} \right)$$

Finally get equation (15):

$$\frac{d\sigma_i}{dr} - \mu \frac{d\sigma_r}{dr} = \frac{1+\mu}{r} (\sigma_r - \sigma_i) \quad (15)$$

According to equation (10) and equation (15), assume that σ_i is caused by gravity, $\sigma_i = \gamma H$, the drilling radius is r , then can get the drilling radial stress σ_r and tangential stress σ_t equation (16) and equation (17):

$$\sigma_r = \gamma H \left(1 - \frac{r_1^2}{r^2} \right) \quad (16)$$

$$\sigma_t = \gamma H \left(1 + \frac{r_1^2}{r^2} \right) \quad (17)$$

In the equation (16) and equation (17): r_1 is the drilling radius.

According to the above derivation, the maximum stress of borehole surrounding is tangential stress, when $\sigma_t = 2\gamma H$ exceeds borehole surrounding elastic limit, will enter a state of the plastic around the borehole.

4 NUMERICAL SIMULATION OF STRESS AND STRAIN CHARACTERISTICS OF ROCK DRIFT DRILLING SURROUNDING AND STARTING SEALING DEPTH RESEARCH

After studying the stress and strain theory of rock drift and drilling surrounding, using comsol Multiphysics software to simulate the stress and strain of drilling of rock drift surrounding.

According to the results of simulation, finally confirm reasonable drilling starting sealing depth.

Using rock drift of coal seam floor of 2145 working face of Hebi the sixth coal mine as an example to simulate, according to the calculation results, ultimately determine reasonable drilling starting sealing depth.

Buried depth of rock drift of coal seam floor of 2145 working face of Hebi the sixth coal mine is 500 m, length of 980 m, is located in the sandstone rock formations, distance between the drill fields layout from 15 m to 20 m^[6].

Using Mohr-Coulomb criterion to simulate stress and strain of the buried depth of 500 m, radius of 2.2 m circular rock drift. Because the buried depth is in the area from 500 m to 700 m, crustal stress is about from 15 MPa to 25 MPa, so choose to impose from 15 MPa to 25 MPa crustal stress on the top, left and right boundaries, the lower boundary is fixed boundary. Due to the rock drift is in sandstone formation, so select the physical and mechanical properties of sandstone as the rock drift surrounding physical parameters (as shown in Table 1).

Calculation results is as shown in Figure 2 and Figure 3, Figure 2 is numerical simulation of stress of rock drift surrounding of coal seam floor of 2145 working face of Hebi the sixth coal mine, Figure 3 is numerical simulation of strain of rock drift surrounding of coal seam floor of 2145 working face of Hebi the sixth coal mine, it describes the distribution characteristics of elastic-plastic region of rock drift surrounding.

From Figure 2 we can see clearly rock drift surrounding of coal seam floor of 2145 working face, especially use rock drift center position as reference coordinate, area of 7 m radius appeared the phenomenon of stress concentration.

From Figure 3 we can see clearly we can see clearly rock drift surrounding of coal seam floor of 2145 working face, especially use rock drift center position as reference coordinate, area of 4.5 m radius appeared the phenomenon of elastoplastic state. Thus in this area rock deformation amount is large, rock permeability is good, if choose this section of the area for drill hole sealing, even if miner finished drill hole sealing, the sealing effect is not good, because of the action of gas drainage negative pressure, there may be cause this area air leakage. So when choosing drill hole starting sealing position should avoid this section area, namely drill hole starting sealing depth should be greater than 4.5 m.

After numerical simulation of stress and strain of rock drift surrounding of coal seam floor of 2145 working face of Hebi the sixth coal mine, then start to simulate stress and strain of drilling of rock drift surrounding of coal seam floor of 2145 working face of Hebi the sixth coal mine,

Table 1. Numerical simulation parameters selection.

Rock type	Elasticity modulus (MPa)	Cohesion (MPa)	Internal friction angle (°)	Poisson's ratio	Density (g/cm ³)
Sandstone	2×10^4	19	39	0.2	2.5

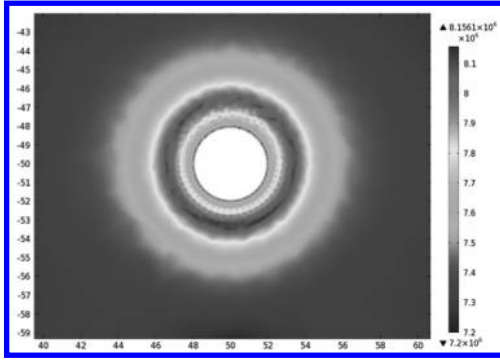


Figure 2. Numerical simulation of stress of rock drift surrounding of coal seam floor of 2145 working face of Hebi the sixth coal mine.

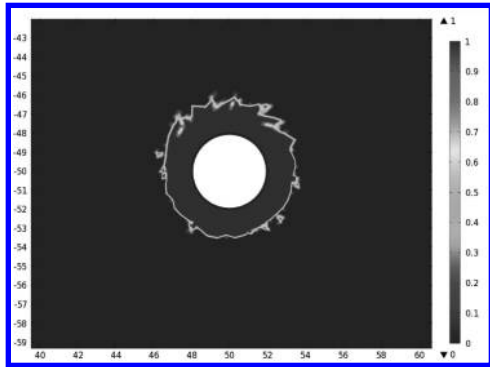


Figure 3. Numerical simulation of strain of rock drift surrounding of coal seam floor of 2145 working face of Hebi the sixth coal mine.

and then to coal floor rock wear layer surrounding the borehole stress strain numerical simulation, the length of the drilling is about 30 m in rock drift of coal seam floor of 2145 working face of Hebi the sixth coal mine, drill hole diameter is 110 mm, so select 30 m drill hole length and 110 mm drill hole diameter as numerical simulation parameter.

Calculation results is as shown in Figure 4 and Figure 5, Figure 4 is numerical simulation of stress of drilling of rock drift surrounding of coal seam floor of 2145 working face of Hebi the sixth coal mine, Figure 5 is numerical simulation of strain

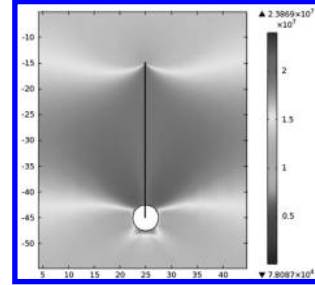


Figure 4. Numerical simulation of stress of drilling of rock drift surrounding of coal seam floor of 2145 working face of Hebi the sixth coal mine.

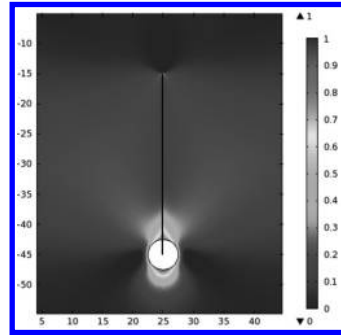


Figure 5. Numerical simulation of strain of drilling of rock drift surrounding of coal seam floor of 2145 working face of Hebi the sixth coal mine.

of drilling of rock drift surrounding of coal seam floor of 2145 working face of Hebi the sixth coal mine, it describes the distribution characteristics of elastic-plastic region of drilling of rock drift surrounding.

From Figure 5 we can clearly see that drilling orifice strain is larger and other points, after simulation calculation, for drill hole orifice as a starting point to 6 m above the rock drift, this area strain is relatively large. Due to this section of the area of rock deformation is big, choose the drilling starting seal depth should also avoid the this area, namely the drilling starting seal depth should be greater than 6 m.

Through the numerical simulation analysis and comparing, the final selection is 6 m as the

drilling starting seal depth of rock drift drilling of coal seam floor of 2145 working face of Hebi the sixth coal mine, because 6 m is longer than 4.5 m. According to coal mine site drilling hole sealing depth 8 m, gas drainage effect is good, the numerical simulation select start sealing depth of 6 m is reasonable and reliable, in line with the actual situation. If choose to start from 6 m deep drill hole sealing, does not affect the hole sealing effect, moreover can save drill hole sealing material, thus saving the cost of single drill hole sealing.

5 CONCLUSIONS

Through studying the stress and strain theory of rock drift and drilling surrounding, and then using comsol Multiphysics software to simulate the stress and strain of drilling of rock drift surrounding combining with field case. According to the results of simulation, finally confirm reasonable drilling starting sealing depth. Finally has chosen the reasonable and reliable the drilling starting seal depth of rock drift drilling of coal seam floor after numerical simulation, reduce unnecessary drill hole sealing material cost and improve the effect of drill hole sealing quality, laid a theoretical foundation to improve the gas drainage rate. This method simulated the numerical results are accurate and can be used as choosing the drilling starting seal

depth of rock drift drilling of coal seam floor. It will have the very good application prospect.

ACKNOWLEDGEMENT

The corresponding author of this article is Yuanyuan Wang.

REFERENCES

- [1] Wang Zhaofeng, Liu Jun. 2005. The existing problems and the countermeasures in the coal mine gas drainage in our country. *Coal mine safety*. 36(3):29–32.
- [2] Huang Xinye, Jiang Chenglin. 2011. The coal seam gas drainage drilling hole sealing with pressure technology research. *Coal Science and Technology*. 39(10): 45–48.
- [3] Qi Zhicheng, Qian Qihu. 2009. The fundamental problem of the rock deformation and damage under the power. Beijing. science press. 330–332.
- [4] Qian Minggao, et al. 2003. The key strata theory under rock formation control. Xu Zhou. China mining university press. 11–17.
- [5] Hao Zhiyong. 2010. Material composite technology and its application in the borehole sealing study. Beijing. China mining university press. 11–13.
- [6] Zhang Minjie, Hua Junjie, Hua Jingtao. 2011. Single coal seam floor gas drainage drilling in a gas stripe region outburst prevention technology. *Coal mine safety*. 42(6):30–32.

Hydraulic fracturing anti-reflection technique and applications in soft and low permeability coal seam

Xue Xi Chen

North China Institute of Science and Technology, East Yanjiao, Beijing, China
Key Laboratory of Coal Mine Disaster Prevention and Control, Langfang, Hebei, China

Wei Wang, Wen Guang Jin & Yong Xu

North China Institute of Science and Technology, East Yanjiao, Beijing, China

ABSTRACT: For the problem of low coal seam permeability and difficult gas extraction at Wangxing Zhuang Coal Mine 2₁ coal seam, proposed hydraulic fracturing anti-reflection technique, studied the processes and parameters of fracturing equipment, fracturing borehole layout, fracturing power and so on, the hydraulic fracturing technique experiment and effect inspection was carried out at 11091 haul road of Wangxing Zhuang 2₁ coal seam. The results showed that: after the implementation of hydraulic fracturing, the average extraction of coal seam gas concentration had increased about 5-fold, the amount of gas extraction had increased about 6-fold. The effect of increasing seam permeability and improving gas drainage efficiency was ideally.

Keywords: hydraulic fracturing; coal seam permeability; gas drainage concentration; the amount of gas drainage

1 INTRODUCTION

In recent years, most mines of our country have entered a phase of deep mining, the stress increasing that comes along makes the seam and rock permeability get worse, gas pressure and gas content has greatly increased^[1]. According to statistics, more than 95% of the high gas and outburst mines coal seam in our country have a low coal seam permeability, gas extraction is difficult, drainage is not ideal^[2]. To improve the coal seam permeability, domestic and foreign scholars have proposed a variety of methods, such as hydraulic cutting, hydraulic punching, hydraulic fracturing, loosening blasting, protective layer of pressure relief. Due to the simple process and broad applicability, the hydraulic fracturing has been more and more applied^[3-6].

Gas permeability coefficient of Wangxing Zhuang Coal Mine 2₁ is 0.051 m²/MPa²·d, coal seams are difficult to draw, currently coal extraction, the pressure relief zone shallow borehole extraction and other extraction methods have taken. But the existence of pre-pumping time constraints, large projects and low gas pre-pumping rate have a greater impact on production safety. In order to solve difficult problem of gas drainage bring on by low permeability coal seam, proposed to carry out hydraulic fracturing antireflection

technique experiment at 2₁ coal seam, through the implementation of hydraulic fracturing, increase coal seam permeability, expand borehole radius of influence, improve gas extraction rate, shorten the coal seam gas extraction time, and ultimately achieve the purpose of safe and efficient coal mining.

2 HYDRAULIC FRACTURING ANTIREFLECTION MECHANISM

Coal and rock mass is a kind of porous media consist of many cracks and pores, these cracks and pores in the original state is mostly mutually connected. When making water injection borehole, crack will produce in coal and rock around borehole. These fissure circles are interlaced with coal native fissures. Hydraulic Fracturing use the initially fissures of water injection borehole, putting high-pressure water into the coal rock, to overcome coal rock fracture surface minimum principal stress and the tensile strength of coal and rock, making these fractures occurred after effects of high pressure water expansion and extension, thereby forming an internal split seam, forming a number of interwoven multi-fractured connected network. The formation of the network had created conditions for the flow of the gas in the coal seam,

accelerated the speed of the gas from the adsorption state to free, greatly improved the permeability of the coal seam, then created good conditions for the effect of coal seam gas extraction.

3 HYDRAULIC FRACTURING FIELD TEST

3.1 Test location description

Fracturing place was seated in Wangxing Zhuang Coal Mine 2₁ coal seam south wing mining area 11091 working face haul road. 2₁ coal seam thickness 0 ~ 24.76 m, the average thickness is 7.07 m, Buried stability, outpitted in the form of powder and flake-like, intensity is low, belonging to lean coal and meager-lean coal. 2₁ coal seam false roof is mudstone, thickness 0.13 ~ 0.65 m, the average thickness is 0.38 m. Immediate roof is silty mudstone, mudstone and siltstone, the average thickness is 4.43 m, Big of sandstone in most areas is immediate roof, the average thickness of sandstone is 9.95 m. Immediate bottom is silty mudstone, mudstone and siltstone, the average thickness is 5.27 m, Lithology is a little weak, bedding development, belonging to moderate stability. The failure pattern of coal at Wangxing Zhuang Coal Mine 2₁ coal seam is V; ruggedness coefficient is 0.21; initial speed of methane diffusion is 19.16.

3.2 Hydraulic fracturing process and parameters

3.2.1 Fracturing equipment

Hydraulic fracturing system of field test this time consisted of fracturing pump, pressure gauge, water tanks, high pressure pipe and special sealing borehole device. Fracturing pump was YLB1000/40-P with the maximum displacement of 1.3 m³/min, fracturing pump rated at 40 MPa, and equipped with pressure gauges, water meter and pressure relief valve. Tank used a dedicated underground fracturing tanks, more than just parallel. High pressure connecting pipe chosen high quality seamless steel tube and the pressure hose, seamless steel tube could be weighed on 40 MPa, pressure hose could be weighed on 38 MPa, pressure sealing and pressure hose connected with quick connector. The outer diameter of the sealing device was 65 mm, inner diameter was 45 mm, pressurized expansion factor was 2 to 3, the compressive strength was not less than 40 Mpa.

3.2.2 Borehole layout

When the fracturing experiment began 11091 working face had formed the ventilation circuit but not put into production. So hydraulic fracturing borehole and gas drainage borehole were arranged in the haul road, borehole length for an average of

100 meters, 8 meters borehole spacing, the specific arrangement was shown in Figure 1. Using special sealing device sealing, sealing length was 20 meters, external sealing device was connected to the high pressure line. After construction of hydraulic fracturing borehole and gas drainage borehole were completed, fracture hydraulic fracturing borehole. After the on-site implementation of hydraulic fracturing was completed, draining the hydraulic fracturing borehole until gas occurred, associated with the investigation borehole near the drainage pipe together carrying gas extraction. For analyzing before and after hydraulic fracturing of gas drainage borehole results, choose two normal drainage boreholes in the same roadway but different locations for data comparison.

3.2.3 Fracturing pressure

Injecting water makes coal produce fissures, is the result of the original rock stress and the interaction of high-pressure water in borehole, somewhere in vivo coal tangential tensile stress should be greater than the tensile strength of coal^[7]. That is:

$$|\sigma_{\theta}| > |R_t| \quad (1)$$

In the formula: σ_{θ} is tangential tensile stress, the unit is MPa; R_t is tensile strength of coal, the unit is MPa. The easiest crack location of coal is water injection borehole edge, so the tangential tensile stress when cracks is^[8]:

$$\sigma_{\theta} = (1 + \lambda) p_0 + 2(1 - \lambda) p_0 \cos 2\theta - p_0 \quad (2)$$

In the formula: λ is lateral stress coefficient;

$$\lambda = \frac{1500}{H} + n(n = 0.3 \sim 0.5);$$

H is vertical depth underground, the unit is m; p_0 is vertical stress, $p_0 = \gamma H$, γ is the average bulk density of coal strata overlying, the unit is KN/m³;

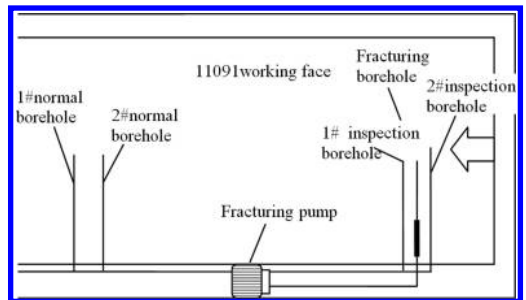


Figure 1. The arrangement diagram of hydraulic fracturing and gas drainage borehole.

θ is the angle between radial direction where crack initiation point is located in and the horizontal direction, the unit is $^{\circ}$.

Hydraulic fracturing along the seams around the water injection borehole only forced by vertical stress and horizontal stress two directions, so only considering $\theta=0^{\circ}$ and $\theta=90^{\circ}$ two cases, respectively taking $\theta=0^{\circ}$ and $\theta=90^{\circ}$ into formula (2), could be obtained minimum water injection pressure of crack initiation from the edge of water injection borehole is:

$$p = \min \{ (3 - \lambda) p_0 + R_r, (3\lambda - 1) p_0 + R_r \} \quad (3)$$

Geological exploration report of Wangxing Zhuang Coal Mine could calculate the lateral stress coefficient $\lambda = 2.07$, $p_0 = 20.825$ MPa, coal tensile strength is 1.5 MPa. According to fracture initiation pressure formula could calculate initiation pressure of this time is 20.87 Mpa, combining with the actual situation of Wangxing Zhuang Coal Mine, assessing the highest fracturing pressure as 30 Mpa, assessing the initial pressure as 4 Mpa.

3.3 Field test situation

At the beginning of fracturing, pressure in hydraulic fracturing borehole fluctuated slightly, but only slightly, at the same time fracturing water flow increased significantly with time, at the moment borehole space and the original crack around coal body were filled with fracturing fluid. As the fracturing is conducted, the original space in borehole is filled with fracturing fluid, then raised the fracturing pressure, fracturing water flow would increase slowly. After a while, the coal began to appear noise sounds like “pipa”, this explained the coal began to produce new fissures. At this point the fracturing pressure began to fluctuate, new cracks began to develop and run-through, the water flow increased rapidly, the fracturing

effect was obvious. At about 50 minutes we could hear the voice sounds like “pipa”, notice to stop the pump, pressure of hydraulic fracturing borehole decreased rapidly, pressure was close to about 0 MPa at 55 min, fracturing end. Specific changes of fracturing pressure and gas concentration in the roadway with time was shown in Figure 2.

Stop fracturing and drain away the water from fracturing borehole, then detect orifice concentration of 1# inspection borehole with portable gas detector, immediately rang out a warning sound. With the palm near the orifice, could feel methane gas ejected outwards. Within 20 min after water injection, gas concentration in the roadway where fracturing borehole was located in from 0.091% before fracturing increased to 0.154%, the highest concentration had risen 0.063%, indicated that the fracturing effect is remarkable.

4 HYDRAULIC FRACTURING ANTIREFLECTION EFFECT ANALYSIS

After finished fracturing, as the water slowly drained out of the drainage borehole, gas concentration of each drainage boreholes could increase in some extent, both of drainage concentration and scalar had shown significant volatility. After the “Fluctuation” drainage concentration and gas drainage scalar began to decline, and finally stabilized.

Gas drainage concentration and gas drainage scalar of 1, 2 inspection borehole and 1,2 normal borehole changed with time were shown in Figure 3, Figure 4. As can be seen from the figure, normal borehole gas drainage concentration and gas drainage scalar were at a low level and changes are not obvious, the maximum drainage concentration was 15.8%, with an average of 12.01%, the average gas drainage scalar was 0.084 m³/min. But both of inspection borehole gas drainage concentration and drainage scalar were at a high level,

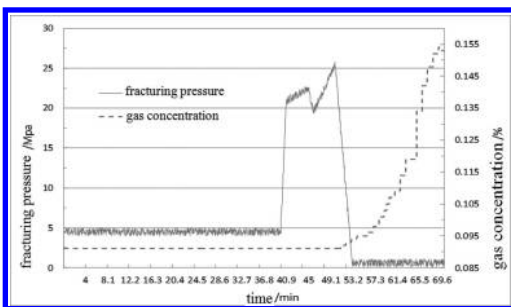


Figure 2. The graph about the relationship of fracturing pressure and gas concentration.

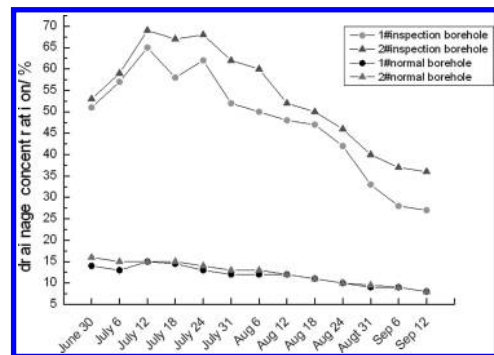


Figure 3. Comparison of gas drainage concentration.

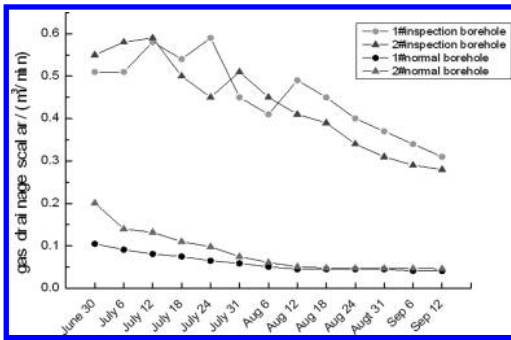


Figure 4. Comparison of gas drainage scalar.

the maximum drainage concentration was 59.5%, with an average of more than 39%; the average of drainage scalar was above 0.3 m³/min. Compared to normal borehole, the amount of fracturing borehole gas drainage improved 4.1 times.

5 CONCLUSION

1. Hydraulic fracturing enlarged and extended coal fissures by high-pressure water, intertwined to form a multi-fractured connected network, thereby greatly increased the permeability of coal seam.
2. After hydraulic fracturing, inspection borehole gas drainage concentration and gas drainage scalar were always at a high level, presented fluctuated state; but normal borehole gas drainage concentration and gas drainage scalar were always at a low level, no significant changes.
3. The average gas drainage concentration of hydraulic fracturing inspection borehole had reached 39.29%, the average gas drainage scalar was 0.34 m³/min; higher than normal borehole respectively 3.3 times and 4.1 times, hydraulic fracturing antireflection effect was significant.

ACKNOWLEDGEMENTS

The corresponding author of this paper is Wang Wei. This paper is supported by Program for New

Century Excellent Talents in University (NCET-11-0837), the Fundamental Research Funds for the Central Universities (3142014012; 3142014310; 3142013110; 3142013126) and Safty Technology and engineering (coal safety) key disciplines (HKSJZD201401).

REFERENCES

- [1] Jinpeng Yan, Zegong Liu, Xiulei Jiang and so on. Numerical simulation on hydraulic fracturing procedure of coal seam with high gas and low air permeability [J]. China Safety Science and Technology Production, 2013, 9(8):27–32.
- [2] Jingui Li, Cheng Zhai, Boquan Lin and so on. Application of Hydraulic Fracturing and Permeability Improvement Technology to Low Permeability Seam [J]. Coal project. 2012(1):31–36.
- [3] Changjiang Qin, Yunsheng Zhao, Changsong Li. Field Test on the Technology of Hydraulic Fracturing of Coal between Holes. Safety and environmental engineering. 2013, 20(5):126–129.
- [4] Yaofeng Wang, Yanzeng Li. Technology and application of directional hydraulic penetration permeability improvement by guided groove [J]. Journal of China Coal Society. 2012, 37(8):1326–1331.
- [5] Binwei Xia, Ke Hu, Yiyu Lu. Mechanism of crack-oriented of hydraulic fracture and its technique in mine [J]. Journal of Chongqing University. 2013, 36(9):8–13.
- [6] Zhijun Wang, Ruilin Zhang, Sen Zhang and so on. Numerical analysis of fracture guide & control of directional hydraulic fracturing in coal body containing gas [J]. Journal of henan university of technology. 2013, 32(4):373–379.
- [7] Guohua Zhang, Guangping wei, Fengcai Hou. Theory of stark split affusion stress and stark split location about trough coal delaminations' bore of hydraulic fracture [J]. Journal of China Coal Society. 2007, 32(1):52–55.
- [8] Daoxiong Tan, Hongqing Niu, Minbo Zhang and so on. Application and Research on Seam Hydraulic Fracture Permeability Improvement Technology [J]. Coal science and technology. 2013, 41(5):79–85.

Research of MATLAB modeling and vector control of brushless double-fed machine

Yi Deng & Xin Jin

Hankou University, Wuhan, China

Jing Chen

Wuhan University of Technology, Wuhan, China

ABSTRACT: This paper is concerned with the problem of MATLAB modeling and vector control of brushless double-fed machine. Firstly, the structure of BDFM is analyzed and a mathematic model of BDFM based on the rotor $d-q$ model is set up in order to carry out the accurate simulation model via MATLAB. Secondly, a new vector control strategy for BDFM is proposed, which is verified by simulation. The results show that the proposed method can achieve a wide range control speed of BDFM with good static and dynamic characteristics.

Keywords: BDFM; vector control; mathematic model; simulation

1 INTRODUCTION

In recently, variable frequency speed adjusting technology has been widely applied in many fields. The installed capacity of the traditional squirrel cage and wound rotor asynchronous motor has been greatly restricted because of respective disadvantages and limitations with the need of energy and cost saving^[1,2].

For Brushless Double-Fed Machine (BDFM), double-fed refers to connect the power winding and control winding of BDFM with AC current grid or other circuit respectively, which made them can send electric power.

BDFM develops from the cascade brushless doubly fed machine with the characteristics of simple and durable structure, and no brushes and slip rings, whose operation are reliable, speed and power factor are adjustable and it can get a single-fed or double-fed operation with the small capacity frequency converter and low cost. It has a broad application prospect in the variable frequency speed drive and gearshift invariable frequency systems^[3].

In this paper, proposed closed loop vector control method based on the BDFM mathematic model is presented to MATLAB simulation. And the result shows that the proposed method can realize the stepless speed regulation and has good static and dynamic characteristics.

2 STRUCTURE THEORY OF BDFM

Brushless Double-Fed Machine has the same theory with two cascaded induction machine. Based on the cascaded induction machine, the theory of brushless double-fed machine is presented in Figure 1.

P_p , P_c are the pole-pairs number of power windings and control windings;

If the stator's output power of the first machine is P_N , the slip of the two machines are s_p , s_c when running in a speed. The mechanical power of the first machine can be obtained as follows:

$$P_{wp} = (1 - s_p)P_N \quad (1)$$

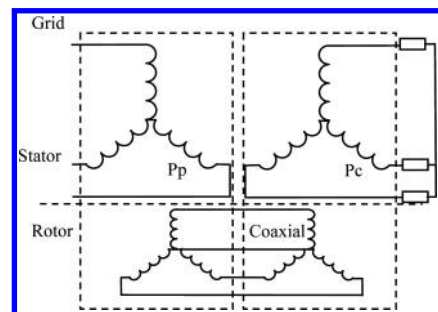


Figure 1. Winding model of cascade double-fed machine.

$s_p P_N$ is the power that the first machine transmit to the second machine by rotor when ignore the motor loss. For the power of the second machine comes from its rotor, according to the principle of transform, the rotor of the second machine is the primary side while the stator is the secondary side. The mechanical power of the second motor shaft are expressed as

$$P_{wc} = (1 - s_c) s_p P_N \quad (2)$$

and the output power of the whole cascade shaft is:

$$P_w = P_{wp} + P_{wc} = 1 - s_c s_p P_N \quad (3)$$

where $s_c s_p P_N$ is the electric power consumed on the resistance of the second machine.

If the resistance of the secondary side of the second machine is changed, the power $s_p s_c P_N$ are also changed. Under the assumption of the P_N , the $s_c s_p$ will change, namely the equivalent slip s changes ($s = s_c s_p$), and the current frequency of the second machine' secondary side will change accordingly. Therefore, if we can change the current frequency of the second machine' secondary side, the speed of machine can be changed.

Brushless double-fed machine use the Variable-frequency Drive replace the external resistance in the model machine, and through the changing of the current frequency of the secondary side, the external resistance in the model machine, and through the changing of the current frequency of the secondary side, the equivalent slip can be changed.

Based on this evidence it will make a improved and practical cascade brushless double-fed variable speed machine (as show in Fig. 2). Using the Variable-frequency Drive replaces the external resistance of the machine, on the one hand, it can realize the voltage frequency regulation in order to change the speed, on the other hand, it can transmit energy to improve the efficiency of the system.

For the cause of comprehension, let the first machine as power machine, and the second machine as control machine.

Through the analysis and calculation of cascade system which run in different speed and phase

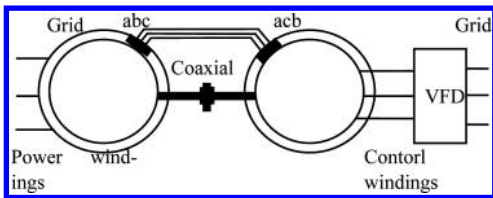


Figure 2. Structure diagram of cascade double-fed machine.

sequences, it can be found out that the electromagnetic torque of two machines in the same direction when the rotors of two machines connect in negative phase sequence. Thus it is the exactly efficient and practical that the rotor of brushless double-fed variable speed machine connecting in a negative phase sequence.

Suppose that the current frequency is f_r , the stator current frequency of the first machine is f_p and the stator current frequency of the second machine is f_c , the speed of the power machine can be presented as:

$$n + n_{rp} = n + \frac{60 \times f_r}{p_p} = \frac{60 \times f_p}{p_p} \quad (4)$$

meanwhile the speed of control machine is

$$n - n_{rc} = n - \frac{60 \times f_r}{p_c} = \frac{60 \times f_c}{p_c} \quad (5)$$

The rotors of two machine, usually connected in negative sequence, which are mechanical coaxial named as ... The power machine has the same current frequency f_r with control machine, thus the actual speed of rotor is

$$n = \frac{60 \times (f_p + f_c)}{p_p + p_c} \quad (6)$$

Although the cascade BDFM will reduce the capacity of frequency converter without the running and maintain inconvenience caused by the mechanical brush, the cascade BDFM still needs two machines, which increase the cost and volume. Based on these results, there is a practical BDFM improved by researchers (as show in Fig. 3).

Denote $n_{s0} = 60 \times f_p / p_p + p_c$, the equation can be rewritten as

$$n = n_{s0} + \frac{60 \times f_c}{p_p + p_c} \quad (7)$$

n_{s0} is the equivalent synchronous speed of the brushless double-fed machine when $f_c = 0$, it

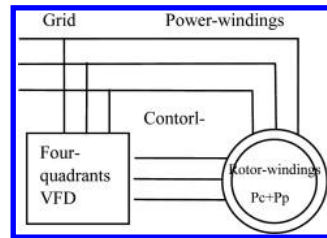


Figure 3. Schematic diagram of BDFM operation.

corresponds with magnetic pole number $P_p + P_c$ and f_p . Therefore the brushless double-fed machine can be looked as ordinary single winding machine with brush whose magnetic pole number is $P_p + P_c$, the frequency is f_p and the speed is n .

3 THE MATHEMATICAL MODEL OF BDFM

The mathematical model of brushless double-fed machine usually drive from cascade machine model, including in network model, circuit model, rotor speed model and double synchronous speed model and so on.

Generally speaking, the speed in d - q coordinate frame is arbitrary. However, the power winding of brushless double-fed machine is unequal to the pole number of control winding or current frequency, and the angular frequency ω_p and ω_c of equivalent sinusoidal currents induced in the rotor windings are also unequal. It's difficult to reconcile two windings into a d - q coordinate frame through uniform coordinate transformation matrix.

In this paper, we analyze and simulate BDFM by rotor speed model.

Rotor speed model which converts the voltage, current and magnetic flux of three phase static coordinate system into the d - q coordinate frame synchronized with rotor speed through coordinate transformation, has realized the simplification about the state variable of rotor current. The rotating d - q coordinate system relative to the rotor is still at the rotor speed coordinate. Therefore, there are no alternating quantities in voltage, current and magnetic linkage equation, which simplify the mathematic model. The operating characteristics of BDFM can be exactly simulated by this model.

When we use the cascade double-fed machine model to analyze the BDFM, we can respectively establish the voltage current model of power machine and control machine^[4]. And the mathematic model based on rotor speed coordinate of BDFM can be carried out by using the characteristic that the rotor is reverse phase closed connection. The BDFM can be presented as follows^[5]:

where P_p, P_c are the pole-pairs number of power windings and control windings; $U_{qp}, U_{dp}, I_{qp}, I_{dq}$ are the d - q voltage and current of power windings; $U_{qc}, U_{dc}, I_{qc}, I_{dc}$ are the d - q voltage and current of control windings; $U_{qr}, U_{dr}, I_{qr}, I_{dr}$ are the d - q voltage and current of rotor windings; R_p, R_c, R_r are the resistances of the power windings, control windings and rotor windings; L_{sp}, L_{sc}, L_r are the inductor of the power windings, control windings and rotor windings; M_p, M_c are mutual inductance of the power windings, control windings and rotor windings; W_r is mechanical angular velocity of rotor; P is differential operator.

3.1 The torque equation of BDFM

According to the torque equation of asynchronous motor

$$T_e = n_p L_m (i_{qs} i_{dr} - i_{ds} i_{qr}) \quad (9)$$

where n_p is pole-pairs number, L_m is equivalent inductance, thus the torque equation of the cascade double-fed power and control machines can be represented by

$$\begin{cases} T_{ep} = P_p M_p (i_{qp} i_{drp} - i_{ds} i_{qrp}) \\ T_{ec} = P_c M_c (i_{qc} i_{drc} - i_{ds} i_{qrc}) \end{cases} \quad (10)$$

where T_{ep}, T_{ec} are electromagnetic torque of power machine and control machine; i_{drp}, i_{qrp} are rotor d - q current of power machine; i_{drc}, i_{qrc} are rotor d - q current of control machine.

The power and control machine rotor d - q currents can be given by three phase winding current, and they are reverse phase connected, we can figure out that

$$\begin{cases} i_{drp} = i_{drc} \\ i_{qrp} = -i_{qrc} \end{cases} \quad (11)$$

We can set $i_{drp} = i_{dr}, i_{qrp} = i_{qr}$, the torque equation of BDFM can be designed as

$$\begin{bmatrix} U_{qp} \\ U_{dp} \\ U_{qc} \\ U_{dc} \\ U_{qr} \\ U_{dr} \end{bmatrix} = \begin{bmatrix} R_p + PL_{sp} & P_p W_r L_{sp} & 0 & 0 & 0 & PM_p & P_p W_r M_p \\ -P_p W_r L_{sp} & R_p + PL_{sp} & 0 & 0 & 0 & -P_p W_r M_p & PM_p \\ 0 & 0 & R_c + PL_{sp} & P_c W_r L_{sc} & -PM_c & P_c W_r M_c & \\ 0 & 0 & -P_c W_r L_{sc} & R_c + PL_{sc} & P_c W_r M_c & PM_c & \\ PM_p & 0 & -PM_c & 0 & R_r + PL_r & 0 & \\ 0 & PM_p & 0 & PM_c & 0 & R_r + PL_r & \end{bmatrix} \begin{bmatrix} I_{qp} \\ I_{dq} \\ I_{qc} \\ I_{dc} \\ I_{qr} \\ I_{dr} \end{bmatrix} \quad (8)$$

$$T_e = T_{ep} + T_{ec} = P_p M_p (i_{qp} i_{dr} - i_{dp} i_{qr}) + P_c M_c (i_{qp} i_{dr} + i_{dp} i_{qr}) \quad (12)$$

according to kinetic equation

$$T_e = T_L + J \frac{dW_r}{dt} \quad (13)$$

where T_L is load torque, J is moment of inertia, we can set up the matlab simulation model.

3.2 The vector control strategy of BDFM

Since BDFM is a nonlinear, multivariable, strong coupling complex systems, the traditional VF control, vector control and DTC control in theory and practical applications are difficult to achieve effective control of BDFM. Therefore, it is necessary to propose new ideas and control methods of BDFM based on structure and electromagnetic properties.

Since the power windings is given by the grid and beyond control, if the speed-power of field windings considered as f_p . According to the Motor theory, only rotating magnetic fields in same frequency can produce a constant torque and realize electro-mechanical energy conversion; we can consider the control DC value given as the DC equivalent value of control winding converted to synchronous coordinate f_p , its rotational speed is same to power winding magnetic field speed. Through theoretical analysis, equivalent three-phase windings " f_c " in slip frequency f_p - f_c coordinates is same to actual control of three-phase windings f_c ^[6].

According to Eq. (6), there is

$$f_r = \frac{f_p + f_c}{P_p + P_c} \quad (14)$$

and at the double-fed mode the slip frequency can be written as

$$\begin{aligned} f_d &= f_p - f_c \\ &= f_p - (f_r(P_p + P_c) - f_p) \\ &= 2f_p - f_r(P_p + P_c) \end{aligned} \quad (15)$$

Based on the results, the real three phase current of control winding can be driven from 2r/2s and 2s/3s conversion of the equivalent DC and the slip frequency coordinate system equivalent conversion of the equivalent windings.

Taking XiangTanYSNT450-16 brushless double-fed machine for example, the voltages in power windings and control windings are respectively 6000 V and 660 V. The power flow in the 6000 V grid and the frequency converter provides

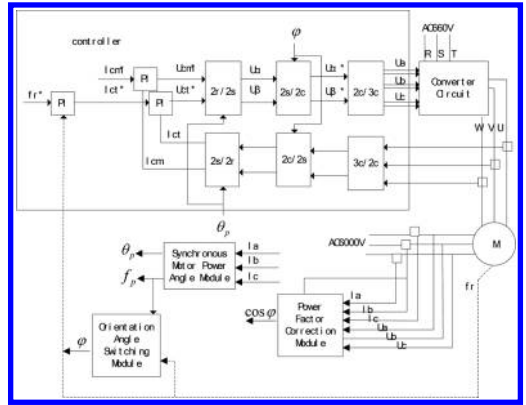


Figure 4. Schematic diagram of the vector control of BDFM.

the source of control windings. The schematic diagram of the vector control is shown in Figure 4.

The f_r (given mechanical speed) and I_{cm}^* (given excitation) are determined by frequency converter. And the difference of the f_r^* and f_r (speed feedback) enter the PI control and the output is I_{ct}^* (given torque). After the conversion of coordinates as shown in Figure 4, the equivalent three-phase current flow in brushless double-fed machine, the stepless speed regulation can be realized in theory.

4 SIMULATION

4.1 The simulation model of BDFM

The BDFM simulation model can be set up based on the current equation, voltage equation torque equation and kinetic equation, as shown in Figure 5.

In the model, U_{pabc} is the input three-phase current of power windings, U_{cabc} is the input three-phase current of control windings. Currently the U_{pabc} is power frequency voltage. The U_{pabc} is high voltage power supply input which is uncontrollable source, who works as electromotor providing active power for brushless double-fed machine, or works as electric generator returning the power to grid. The power factor and speed can be controlled effectively by controlling U_{cabc} .

In Figure 5, $P_{3s/2r}$ is the module that converts three-phase stator into two-phase rotor in usual vector control of the power windings. It has the same expression with control windings of $C_{3s/2r}$. $BDFM_{Te}$ is the module of torque equation and kinetic equation. We can establish the Matlab simulation model according to the control method above.

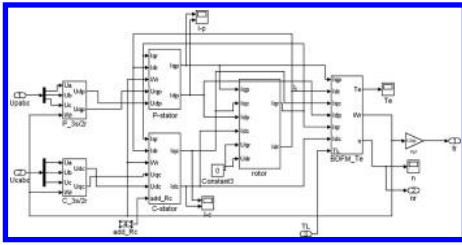


Figure 5. Simulation model of BDFM.

4.2 Simulation result

Choosing the ode23tb as the simulation arithmetic, and the maximum step is 0.0001s. The machine parameters are as follows:

Power Windings: $P_p = 3$; $L_{sp} = 71.52e-3$; $R_p = 0.51$; $M_p = 69.45e-3$
Control Windings: $P_c = 1$; $L_{sc} = 65.48e-3$; $R_c = 0.46$; $M_c = 60.5e-3$;
Rotor Windings: $R_r = 1.653$; $L_r = 145.5e-3$;
 Rotational Inertia: $J = 0.3kg \cdot m^2$;

The power windings fg was put in at 0.3 s. At first, connect the control windings, next put in it at 0.5 s, finally put in the load at 1.2 s when the speed is stable. The three-phase current waves is shown in Figure 7, we can see that power windings current is larger than normal load work or unload when put in the power windings. The control windings current waves are shown in Figure 8. When connecting the control windings before 0.3 s, the current will be larger. In practical application, we can add resistances in control windings in order to prevent from frequency converter alarming which caused by large current, or conduct soft boot of BDFM by changing the start control method. We also can see from given speed and actual speed wave in Figure 9, after putting in the control windings the BDFM go into double-fed pattern rapidly from asynchronously pattern, and the waves reflect the characteristic actual system accurately. The active power and reactive power waves are shown in Figure 10. There is little influence on reactive power but big effect to active power caused by putting load when the machine running steadily, which proves the simulation system is correct.

As we can see from the simulation result, the rotational speed begins to slow down during the 1.2 s loading time. When we check the control winding current, we can see that the control winding frequency gets higher as the rotational speed slows down, this is mainly because the frequency slip orientation angle we use is calculated by the speed feedback f_s , so when loading the motor speed slows down because the speed reduction caused by the load will adversely affect the slip

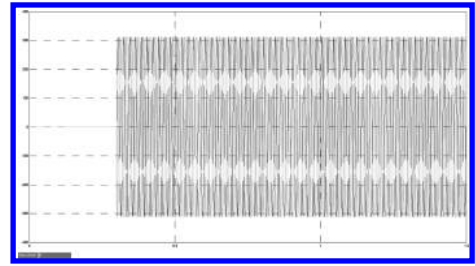


Figure 6. Voltage waveform of power winding.

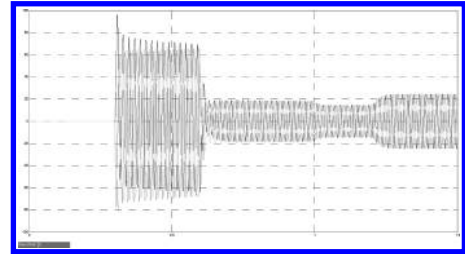


Figure 7. Current waveform of power winding.

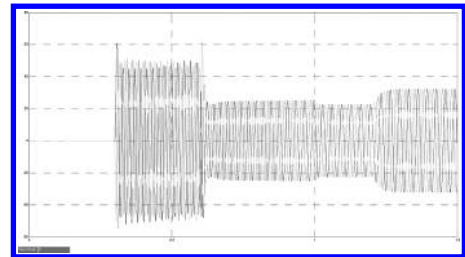


Figure 8. Voltage waveform of control winding.

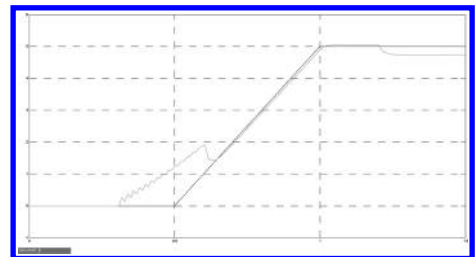


Figure 9. Waveform of speed.

frequency modulation, thereby affecting the slip angular orientation, thus resulting in a decrease rotational speed.

In a real system, this situation will get the motor load capacity weak. In order to improve BDFM with a load capacity and a higher hard features,

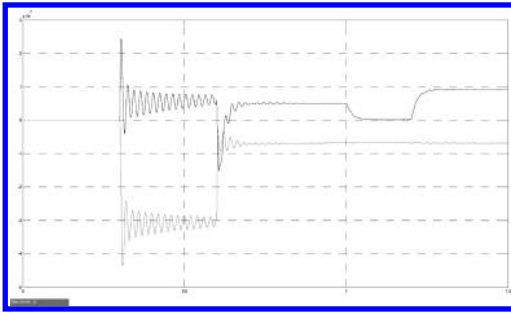


Figure 10. Waveforms of reactive and active power.

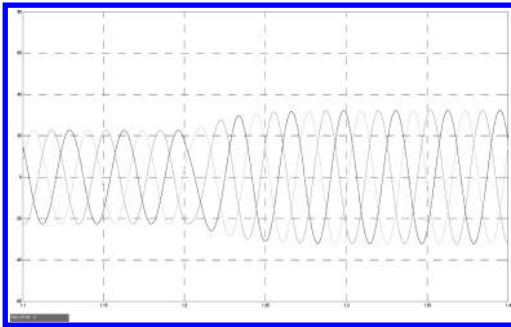


Figure 11. The changes of Three-phase current waveform of control winding when take loads test.

we can use BDFM in the doubly-fed mode, the control winding current frequency directly affect the basic characteristics of speed, we use f_r^* (mechanical speed is given) to calculate slip frequency angle, then the speed fluctuations now will not affect

the modulation of output f_c , thereby enabling the motor speed quickly stabilized, and can greatly improve the load capacity of the motor.

5 CONCLUSION

The simulation results show that the method of vector control this paper proposed can achieve a smooth and stepless BDFM speed change. The simulation results show that this method has a wide speed range, with good static and dynamic characteristics.

REFERENCES

- [1] Wentao Zhang, Shu Chen, Jianzhong Xu, Na Li. Complication and Reliability Evaluation of Brushless Doubly Fed Machine Frequency Conversion Speed Control System in Pump Stations, *China Rural Water and Hydropower*, 2012(7):102–105.
- [2] Yuan Chen, Zhong Li. The Brushless Doubly-fed Machine Control and Application Prospect, *TheWorld of Inverters*, 2012(3):69–73.
- [3] Bao-long Gao. Overview on New Control Strategies of Brushless Doubly-Fed Machine, *Small and Special Electrical Machines*, 2012(12):59–63.
- [4] Boshi Chen. Automatic control system of electric traction, China Machine Press, 2003.
- [5] Hanghang Liu, Li Han. Overview on Control Strategies of Brushless Doubly-Fed Machines, *Small and Special Electrical Machines*, 2010(6):69–73.
- [6] Zheng Wang. Study on the Mathematic Model and Vector Control of Doubly Fed Brushless Machine Based on Slip-Frequency Rotating Reference Frame, Shenyang University of Technology, 2006.

Two dimensional numerical simulation of the flow transport in bend drains

Cheng Yang & Chun-Guang Li

College of Civil Engineering, Beifang University of Nationalities, Yinchuan, China

Wen-Juan Zhao & Lan-Xiang Zheng

College of Civil and Hydraulic Engineering, Ningxia University, Yinchuan, China

ABSTRACT: The effects of the radius of curvature and the angle of drains bend to the water movement of drains are studied using a two-dimensional mathematical model of turbulent water movement. The model considering the impact of the transverse circulation in curved channel, and an adaptive algorithm of Manning's roughness was constructed. The governing equations of the model are discretized with Finite Volume Method (FVM) on unstructured grids. The water movement of a variety of different drains is simulated. The results show that: the numerical value meets the basic laws of Bend Flow movement; at the same hydraulic parameters, with the increase in the radius of curvature, the difference of the velocity and water level between the left bank and right bank of the top section gradually reduced; When the curvature radius is 6 times that of the width of water surface, and the angle of drains bend greater than 90°, the angle increases have little effect on the velocity and water level in the canal bend; also verified in the channel design, the provisions of the radius of curvature and bending angle is reasonable.

Keywords: bend drains; the radius of curvature; numerical simulation; unstructured grids

1 INTRODUCTION

Most drains in the project include corners, such as hydropower aqueducts, water canals and irrigation canals and so on. The general requirements of design curve section drains are the radius of curvature of the curve is 5-6 times the width of the drains, and drains bend angles greater than 90°. Currently, the use of numerical simulation study on the curve type drains, primarily research into the water and sediment transport rule, but few studies the effects of the radius of curvature and the angle of drains bend to the water movement of drains.

Two-dimensional turbulence mathematical model has been widely used to study the movement of laboratory flume, drains and the natural water bodies. Based on the research of the project group, two-dimensional mathematical model of turbulent water movement is established, and an adaptive algorithm of Manning's roughness was constructed. The water movement of a variety of different drains is simulated.

2 MATHEMATICAL MODEL AND DISCRETE

2.1 Mathematical model

The two-dimensional RNG flow mathematic model [2] include: continuity equation, momentum equation, k -equation, and ϵ -equation. The general form of this equations [2-4]:

$$\begin{aligned} \frac{\partial}{\partial t}(h\phi) + \frac{\partial}{\partial x}(hu\phi) + \frac{\partial}{\partial y}(hv\phi) \\ = \frac{\partial}{\partial x}\left(h\Gamma_{\phi}\frac{\partial\phi}{\partial x}\right) + \frac{\partial}{\partial y}\left(h\Gamma_{\phi}\frac{\partial\phi}{\partial y}\right) + S_{\phi}(x,y) \end{aligned} \quad (1)$$

where ϕ is common variables, Γ_{ϕ} is the diffusion coefficient and $S_{\phi}(x,y)$ is the source term, its meaning and calculation formula of the coefficient of reference literature [2]. The transverse circulation in curved channel has a great impact on flow transport in drains.

This article adopts the method of literature [3], that is, without any increase in a large amount of

calculation, we improve the source term of the momentum equation to reflect the effect of the transverse circulation.

The flow condition and comprehensive resistance characteristics of river morphology was reflected Manning coefficient, which value affected by velocity, water level, slope, shape cross-section of other factors. And the value will affect the results of the numerical simulation in the great degree of accuracy. In this paper, with reference to the literature [2], established the Manning coefficient calculation method of adaptive adjustment.

2.2 Discrete mathematical model

Using unstructured grid, finite volume method and Gauss's theorem integral formula (1) on the control unit. Then formula (1) can be converted into the form below:

$$\int_A \frac{\partial(h\Phi)}{\partial t} dA + \int_A h\Phi U \cdot n dA = \int_A \Gamma grad\Phi \cdot \bar{n} dA + \int_A S_\Phi dA \quad (2)$$

where A is the area of control unit, U is the velocity vector grid unit, \bar{n} is the normal vector grid interface.

To discrete formula (2), using first-order discrete transient format, the source term using linearization, the specific process can be found in literature [5].

Inlet boundary: setting velocity, the computation formulas of k and ε are as follows:

$$k = \frac{3}{2} (IU_{in})^2, \varepsilon = \frac{0.09^{0.75} k^{1.5}}{0.1R}$$

Outlet boundary: setting export levels;

Banks of the river boundary: According to the no-slip handle.

3 STUDY ON FLOW FIELD OF DIFFERENT RADIUS OF CURVATURE OF THE DRAINS

According to the radius of curvature, we set several different drains. The water movement of a variety of these drains is simulated.

3.1 Working conditions

Design drains corners, radius of curvature preferable 5 to 6 times of the width of the channel [7]. We combine this standard set several conditions, and all conditions are detailed in Table 1. Other parameters are: channel depth: $h = 2.5$ m, the

Table 1. Different radius of curvature of the channel.

Working conditions	Channel width (m)	Radius of curvature (m)	Import flow (m ³ /s)	Export level (m)
1-1	2	6	9.3	1.95
1-2		8		
1-3		10		
1-4		12		

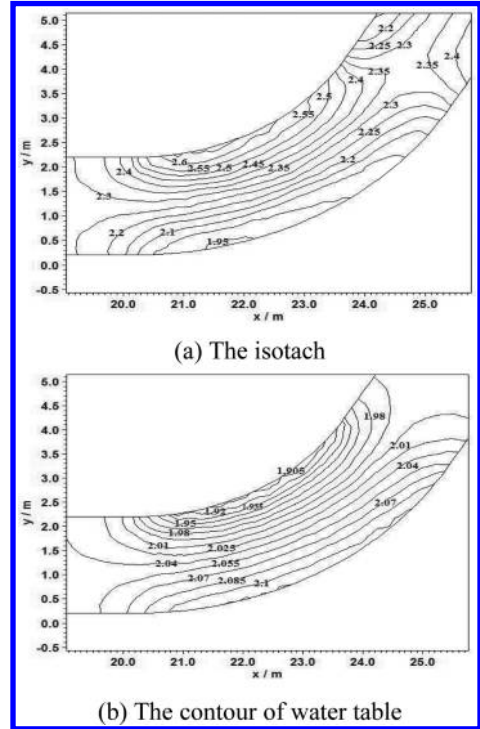


Figure 1. Condition 1-1.

angle of drains bend is 120° , roughness: $n = 0.03$, slope: $J_b = 0.7 \text{ ‰}$, the initial water level is 1.97 m. In order to make the water flow into the channel bend can fully development, set the length of the straight section of the curve is 10 times the channel width [8].

3.2 The simulation results and analysis

The simulation results of condition 1 shown in Figure 1–Figure 4.

From Figure 1 to Figure 4 we can see that: ① The simulation results accord with the basic laws of flow transport, that is the velocity on the left is greater than the right, the water level of the

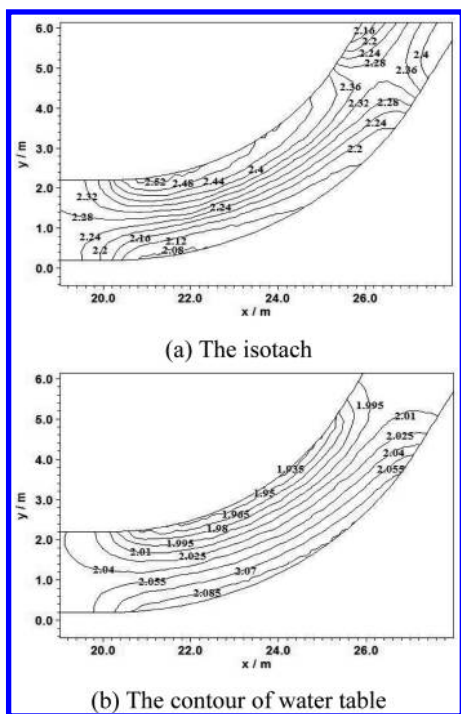


Figure 2. Condition 1-2.

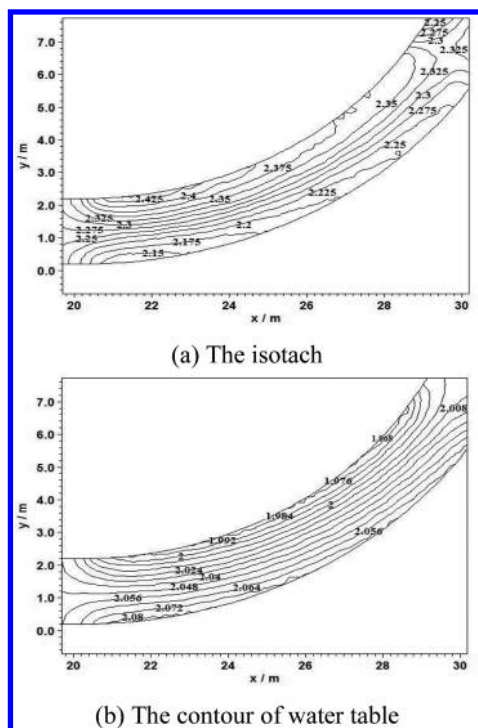


Figure 4. Condition 1-4.

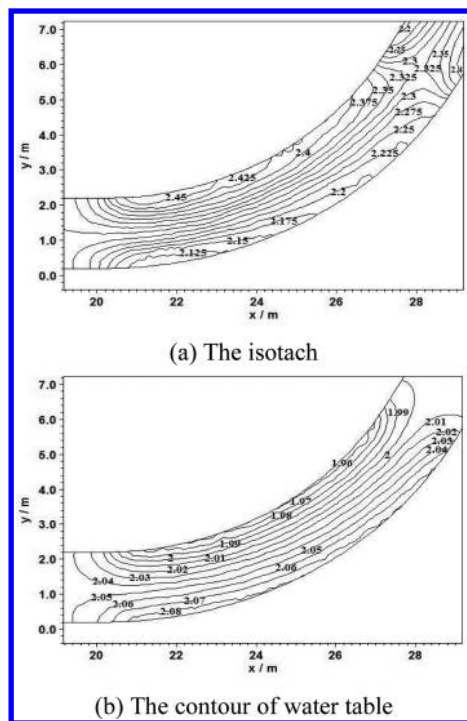


Figure 3. Condition 1-3.

left bank is lower than the right bank; ② Along with the increase of the radius of curvature, the velocity and water level of both sides of the bend are falling. In particular, when the radius of curvature is greater than or equal to 5 times of the width of the channel, this decline was obvious; ③ In all conditions, the maximum velocity of the left bank, the minimum velocity of the right bank and the highest water level of the right bank always in the same section; ④ With the increase of the radius of curvature, in the bend, the water level of right bank is gradually decreased, and the range of the high water level is significantly reduced, thereby greatly reducing the chance of channel bend flow out of the ditch; ⑤ Simulation results further validate the design of canal, the radius of curvature should be greater than 5 times of the width of the channel.

The top section of the curve is the focus of the study. We take the top section of the curve of four channels in condition 1 for example, to compare the simulated values of depth-averaged velocity and water level. The results are shown in Figure 5.

The Figure 5 shows that: ① The water level on the left bank of the section is lower than the right bank, and the depth-averaged velocity on the left bank is greater than the right bank; ② By figure (a) shows that with the increase of radius

of curvature, the depth-averaged velocity of the top section of curve is shown as: on the left bank gradually decreases, and the right bank increases gradually, and on the left bank is still greater than the right bank; ③ Comparison on the difference between the depth-averaged velocity of both sides, the biggest is condition 1-1, and the minimum is condition 1-4; ④ The figure (b) shows that with the increase of radius of curvature, the change of the water level of the top section of curve is on the left bank gradually increased, decreased on the right bank. And the transverse gradient of the water surface slope decreases; ⑤ The simulation result shows that the radius of curvature is more than five times the width of the canal is reasonable.

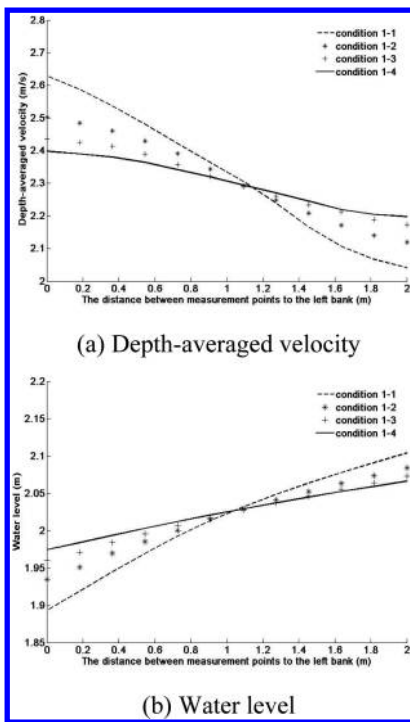


Figure 5. Compare the simulated values of depth-averaged velocity and water level of the condition 1.

4 STUDY ON FLOW FIELD OF DIFFERENT ANGLE OF DRAINS BEND

In combination with the research above, and consider the effects of the angle of drains bend to the flow transport in drains. The condition 2 includes four different channels. Among them, the condition 2-3 and the condition 1-4 are the same. some parameters are shown in Table 2, other parameters are the same as in Section 3.

The simulation results of condition 2 shown in Figure 6–Figure 8.

By Figure 4, Figure 6, Figure 7 and Figure 8, ① In the condition 2, the situation of the bend is: the greater the flow velocity, the lower the water level; ② The results of flow field show that: when the radius of curvature is constant, and the angle of drains bend is greater than 90° , the angle of drains bend will impact on the flow transport and water level in drains, and the effect is very small; ③ When the radius of curvature meet the design requirements, as long as the angle of drains bend is greater than 90° , the flow rate will not be too fast or ultra-high-level phenomena in the bend of the canal, which can meet the engineering requirements; ④ Simulation results show that in the design of channel, the requirements for the design of the river bend is reasonable.

We take the top section of the curve of four channels in condition 2 for example, to compare the simulated values of depth-averaged velocity and water level. The results are shown in Figure 9.

The Figure 5 shows that: ① With the increase of the angle of drains bend, the change law of water level at the top section of the curve is: the water level on the left bank gradually reduce, increased on the right bank; ② Comparison on the difference between the depth-averaged velocity of both sides, the biggest is condition 2-3, and the minimum is condition 2-1; ③ When the radius of curvature is constant, and the angle of drains bend is greater than 90° , the angle of drains bend will impact on the flow transport and water level in drains, and the effect is very small; ④ The simulation result shows that when the radius of curvature is 6 times of the width of the channel, the angle of drains bend is greater than 90° can satisfy engineering demand.

Table 2. Different the angle of drains bend of the channel.

Working conditions	Channel width (m)	Drainage bend angle	Import flow (m ³ /s)	Import flow (m ³ /s)	Export level (m)
2-1	2	12	100°	9.3	1.95
2-2			110°		
2-3			120°		
2-4			130°		

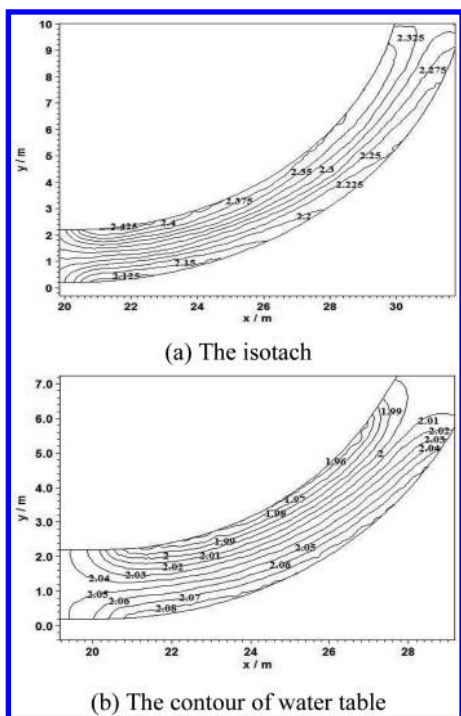


Figure 6. Condition 2-1.

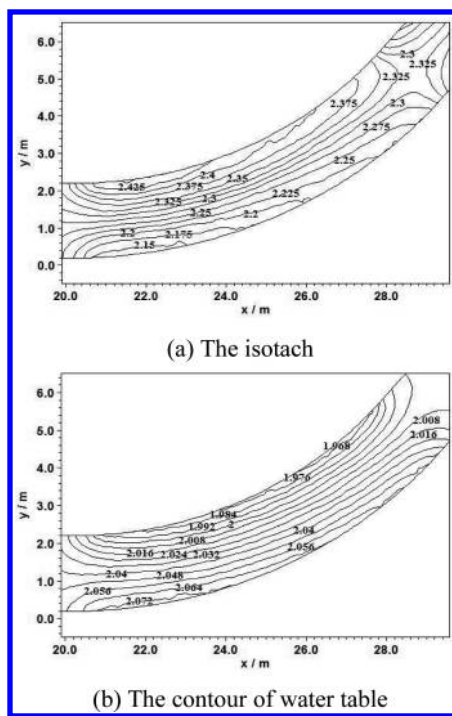


Figure 8. Condition 2-4.

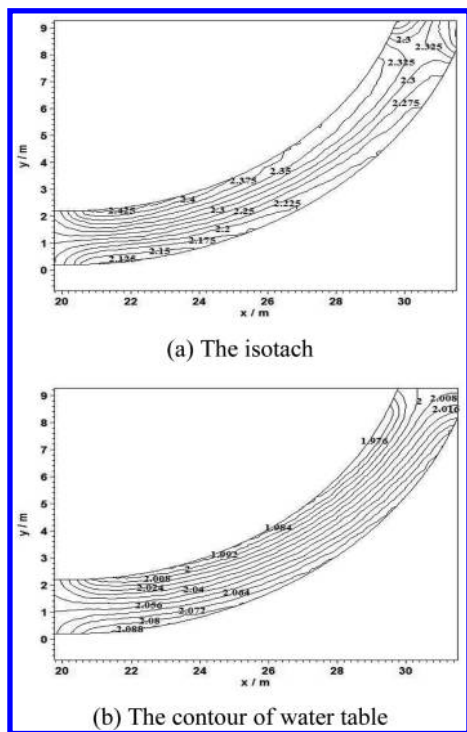


Figure 7. Condition 2-2.

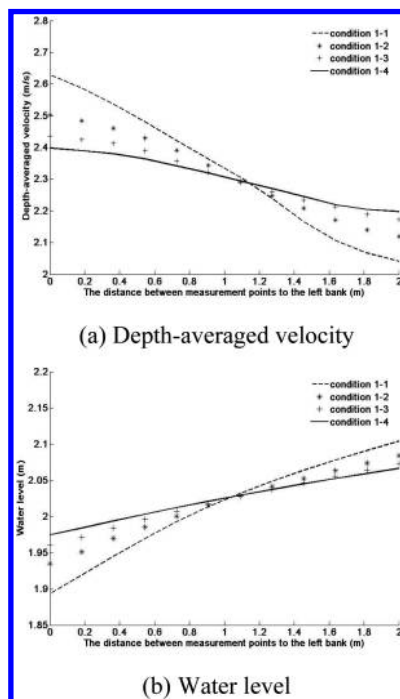


Figure 9. Compare the simulated values of depth-averaged velocity and water level of the condition 2.

5 CONCLUSION

In this paper, the flow transport in a variety of different drains was studied, using a two-dimensional turbulent flow model, unstructured grid and finite volume method. The results show that: the velocity in the left bank of the drains bend is greater than the right, the water level of the left bank is lower than the right, which conform to the basic rules of flow movement; when the angle of the drains bend is greater than 90° , with the increase of the curvature radius, the difference of the depth-averaged velocity between the left and right banks is gradually reduced, and the water surface transverse slope is also gradually reduced; the radius of curvature should be more than five times the width of the channel, and has little effect on the speed and level of increase in the radius of curvature; when the radius of curvature is 6 times the width of the channel and the angle of the channel bend is greater than 90° , with the increase of angle, the change of speed and water level is very small; In the design of canal, the radius of curvature should be 5-6 times the channel width and the drains bend should be greater than 90° is reasonable.

Research of this paper is to further verify the reliability of the mathematical model and numerical methods, and provide reliable mathematical model and numerical methods, for the study of practical engineering problems, such as: the design of the canals, drains the scheme design of water supply, etc. Also for the further study of water quality, water temperature and ice research laid the foundation.

ACKNOWLEDGEMENT

Grant sponsor: the National Natural Science Foundation of China (grant number: 91230111, 41301533).

Grant sponsor: the Scientific Research Grant of Beifang University of Nationalities, China (grant number: 2014XYZ06).

Author: Yang Cheng, Email: yangchenglll@163.com, Tel: 0951-2068011.

REFERENCES

- [1] Liu Yuling, Liu Zhe. Numerical Simulation to Flows in Curved Channels[J]. Chinese Journal of Applied Mechanics, 2007, 24(2):310-312.
- [2] Yang Cheng. Numerical Simulation of the Flow and Sediment Transport of the typical Reservoir in Ningxia[D]. PhD thesis of Ningxia University, 2013.
- [3] Jing Hefang. Numerical Study on the Yellow River Flow and Bed Deformation of the Continuous Bends from Daliushu to Shapotou[D]. PhD thesis of Ningxia University, 2011.
- [4] Li Chun-guang, Jing He-fang, Lv Sui-ju, etc. Two dimensional numerical simulation of the sediment transport in Daliushu-Shapotou reach of the Yellow River[J]. Hydro-Science and Engineering, 2011, 4:102-107.
- [5] Lai X.J., Wang D.G., Chen Y. Pressure correction method on unstructured Grids [J]. Hydrodynamics, 2004, 16(3):316-324.
- [6] Yang Cheng, Li Chungang, Jing Hefang, etc. Two dimensional numerical simulation of the flow in Shuidonggou Reservoir[J]. Advances in Science and Technology of Water Resources, 2013, 33(6):56-60.
- [7] The national standard of the People's Republic of China—irrigation and drainage. GB50288-99. The Ministry of Water Resources of the People's Republic of China.1999-8-1.
- [8] Tao Wen-quan. Numerical heat transfer (second edition) [M]. Xi'an: Xi'an Jiaotong University Press, 2001.

Recommendations on the reconstruction of the old market building in Xiamen—a case study of Xiamen’s eighth market

Jun Hua He

Department of Architecture, Xiamen University Tankahkeei College, Xiamen, China

ABSTRACT: With the alterations of Zhongshan Road and the surrounding neighborhood blocks in Xiamen. The development of this ancient blocks has been affected more or less. This is full of contradictions how to protect external architectural form of the store, how to make better use of interior space under the impact of the urbanization and the market economy. Messy and spontaneous formation of Market Street is resulting in congestion of the traffic line. From the analysis of the architectural features of the Xiamen eighth market, to expound the importance of markets of architectural culture, and to put forward the recommendations of the remediation market space from the perspective of architecture symbols. And the recommendations of the rectification market block of space from the architecture Semiology.

Keywords: architectural style; symbol; renovation for space

1 INTRODUCTION

1.1 *The formation process of the market of the Xiamen eighth market*

The very keen atmosphere of old market block is in the Xiamen eighth market. This is Zheng Cheng-gong’s military camp is at in 300 years ago. There used to be water transport of goods distributing center in Xiamen.

There are many piers, including Dian bao pier, Hong benbu pier, Datie pier, Desheng pier, and so on. Desheng pier also known as Admiral pier. Tongan fishermen, Nanan fishermen had berthing in the Datie pier. Hong Benbu pier is located in Hong Xu Minister Yamen ruins. Coastal territory turmoil time, Hong Xu is Zheng Chenggong’s military officer. [1] Take advantage of the tide comes, the fishermen to sell fresh seafood to the local population.

Local hawkers also sell vegetables. In the 1920 of the 20th century, Xiamen built the first road—Kaiyuan Road. The above said fish aquatic product rural fair on in this road neighbor. The 20th century 30’s, the eighth market is located between Yingping Road and Guying Road. Yingping Road connected to Kaiping Road and Kaihe Road. Area the Guying Road was fish aquaculture market. This developed for afterwards the grocer has laid the foundation. It is occupying a land area of about 400 to 500 square meters. The internal space was already accommodating more than 20 stalls, sells the vegetables, the fruit,

the aquatic product, the meats in indoor business space. In the 1930 of the 20th century the local population increases, eighth market extended into Kaiping Road, increased to more than 60 more stalls. In the 1980s, the eighth market expansion Yingping Road agricultural trade market. With an area of 1720 square meters, temporary corrugated belong to the open steel frame structure. The plane assumes the cruciform. The intersection has the octagon turret. [2]

1.2 *The current situation of the market of the Xiamen eighth market*

But 200 meters east along Kaiyuan Road to the eighth market, looking at the ancient facade, the old Xiamen feeling immediately feel. The Epitaxial length was equal to one kilometer from the transit hub. Contain Kaiping Road, Yingping Road, Kaihe Road, Guying Road and other main roads linear swing.

And more interesting is that there are many residents here, where you can see a very authentic old Xiamen life. Xiamen eighth market near the pier, convenient traffic, here is the freshest and cheapest seafood distribution center in Xiamen; half the size of the restaurant is open everyday seafood procurement in eighth market.

Eighth market is known for its seafood and snacks around for nearly a century, approximately 750 existing fixed pitch. Eighth market has the most cherished Guzao styles. Eighth market was undergoing a transformation, from May 2012.

2 THE ARCHITECTURAL FEATURES OF THE XIAMEN EIGHTH MARKET

2.1 *Featured architectural style*

Copy the template file Speaking of the architectural features of the eighth market, but it is very rich. From two part talk, these are the layout about traditional store, and building facade above the second floor and the second floor.

2.1.1 *The layout about traditional store*

But to talk about the layout of the store are the traditional Chinese mode, the front counter, back in the operating room or the treasury. Underlying facade door are wooden, suffused with a dark color. The arcade space has become a business space, lost its purpose as a transportation space.

The first floor space uses for to exhibit the goods or to act as the storehouse. The upstairs, it is taken shop owner's residence, or rent to those who need it. The underlying traffic space was admitted to the indoor space. Counter position can also be moved to the road, and excavated trenches in the ground to fix the counter. In order to protect the cleanliness of the counter, the store installed outrigger steel frame under the skin along the ground floor beams, covered with corrugated sheets.

2.1.2 *Rich facade styles of the second floor and the second floor above*

People can see the architectural modeling considerations and the craftsmanship of the builders. Although in some arcade grow the roots of trees, some put up the chimney, and some were built, lost their original appearance. However, part of the arcaded facade forms well-preserved. If the canopy is not removed, and I'm also not found the eighth market arcade has such a rich facade forms.

Fine lintel decoration, the superb craftsmen used cement to complete these patterns carved on the wall. Red brick and white seam of arcade corner walls were in stark contrast with freshly trimmed window frames and pilasters. It is indeed

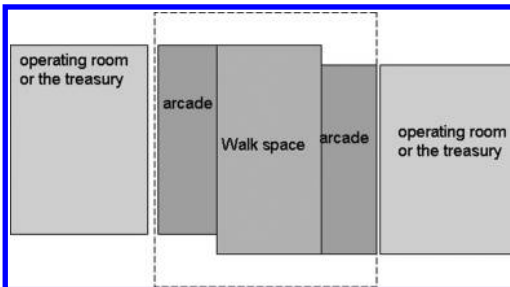


Figure 1. The layout about traditional store.

Professional maintenance. Reinforcement of cornice was painted brilliant white, contrasted with old walls. Fine streamline line foot and treasured vase decoration in balcony, exquisite workmanship lets me be startled. The cement carving flower proportion is moderate. Exterior wall using Rouge-brick masonry, and is by far the best preserved. Brick moldings on Parapet are very rhythmic, coherent and natural. Rouge-brick masonry is unique brick art of the Minnan region.

2.2 *Interesting ceiling space*

As a large market for seafood, the canopy is the necessary facilities.

First, Xiamen's plenty of rain; the umbrella is the goods which the pedestrian must bring along with. The canopy likely is the market umbrella. The stall keepers have supported the canopy. In order to cause the seafood to be bright, they have placed the seafood under the awning. And they worried the rain water has diluted in the trough sea water, affects the seafood quality.

The eighth market canopy is set up between opposite arcade. The following pictures reveal a message. That is the importance of the canopy. For the purpose of transformation, cross-shaped canopy demolished. But the shopkeepers have supported many large umbrella and shade nets. Contradictory, if the recoveries of the canopy, then you see less than arcaded facade beautifully.

Moreover this roof function is not merely rain-proof, but also provides the interior lighting, has been hanging very many light bulbs on the steel frame. While shops for the convenience of customers to choose the goods, partial lighting is also set on the counter. Customer can clearly look for the goods in the space. The market is in place from morning to night. Markets are doing business from morning to night. The night market is equally bustling with the daytime.

2.3 *Symbolic regional patterns*

It is surrounded by a lot of houses in the market, along with the eighth market development, and today has become old and high-density residential areas. There are Bagua Cheng Lane, Jiutiao Lane, Shiyi Jian Lane, Hezai Gan Lane, Datie Street, Daoping Road near the market.

Kaiping Road is divided into three sections, respectively, the sale of cooked food, vegetables and groceries. The Longquan Temple is Buddhist architecture. Inside the temple is worshipped Bodhisattva. The devout Buddhists in Xiamen were greater than the number of Christians.

The Cathedral, Zhushu Chapel in the Kaiyuan Road. The infield section of the eighth market is



Figure 2. Old and high-density residential areas.

precisely a cross, and this is a coincidence this? Or the familiarity of local church, thus affecting the city's self-organizing form. Yingping Road that length is approximately 190 meters. The east side aims at Lujiang Road, west side aims Sibe Road. Guying Road that length is probably 140 meters, its southern section perpendicular to Kaiyuan Road. Yingping Road and Guying Road, which the two roads constitute symbolic Latin cross. This is precisely a core part of the eighth market. It is a symbol, from the geometric figure. This symbol has been deeply printed on the satellite map. Cross is easy to spot on a map, will not confuse other streets.

3 THE RECOMMENDATIONS OF THE RECTIFICATION OF THE XIAMEN EIGHTH MARKET

3.1 Two different opinions

About this transformation, I have heard two different opinions.

The first viewpoint is as follows. The eighth market carries on the promotion transformation, scheduled for completion at the end of September. The main projects of reconstruction of the old market included underground drainage system and the road surface, as well as the original stalls. We want to change the status quo of the "dirty and messy".

Then it is a different view. The transformation of the old city turns a city full of warmth and memories into history debris, and then a piece of thoroughly crushed, and allows them to disappear permanently. Stele in Hong Benbu street, water

distributing point in Danshui Lane, water well in Guying Road, and so on, whether these traces of history with the pace of reconstruction and gradually disappear.

3.2 Referencing examples

We look at how to transform the old market in Istanbul and Barcelona.

GAD designed a concrete deck triangular-shaped shell that covers all the space that invites visitors to enter through large openings at street level. The new design injects a contemporary and pragmatic solution, while preserving the history of the fish market. Both the internal market as its outer covering is used occasionally for art events. [3] This Besiktas Fishmarket design methods can be used within the range observed in the close-range perspective.

The proposal for the rehabilitation of the old Santa Caterina Market, located in the Ciutat Vella district of Barcelona, involves action on the urban tissue adjacent to the existing structure to streamline its location. At the same time, the intervention aims to mixed and confused with the original structure. Cover becomes more important in the facade of the building, with the disadvantage that is only visible from the air and, for now, there is the possibility that there is a viewpoint which would cover. [4] This rehabilitation of the old Santa Caterina Market design methods can be used within the range observed in the Medium shot perspective and Long-range observation.

Both of these designs are to deal with market relations with the surrounding historic district.

3.3 Thinking on protection and reconstruction

Market transformation should not be done overnight, to be sustainable and to protect the original traces of the traditional culture and architectural features.

3.3.1 Market environment or the living environment

This Besiktas Fishmarket is Protection of the living environment of the original, and surrounded by a certain distance.

Lies in this compared with the contradictory place, the eighth market gathers the human spirit is not merely comes from the customer, but also comes from the inhabitant.

This mix kind of Commercial-residential environment is Xiamen's characteristic, I also may see in Xiamen's other places. This is perhaps the portrayal of the usual life of the ancient heritage of coastal fishermen. Even in the high-speed development, people still like the market, like the life.

The rehabilitation of the old Santa Caterina Market wants to make history in the building, with a great roof structures. The city and the market can not be split, and then we have to accept them.

3.3.2 *Sustainable transformation*

The traditional market cannot turn the supermarket. Each supermarket goods are similar; we will find not many types of fresh food and seafood. Why is this? Many traditional shops, low prices, and profit margins are low. This one, they can not afford the cost hydropower and rent as supermarkets. Several old market is in Xiamen is after reconstruction, land prices rising, they can hardly compete with newly opened super markets, withered in abundance.

There may be a need to consider the existing fire safety issues of the location. The transformation of the wire and cable also must be considered. With respect to energy, solar energy technology can be used in the multi-storey house in the roof has a lot of room to use.

In terms of protection of architectural features, we should take the attitude responsible to history. This is a great project, need experts to participate in the drawing of the construction drawings, specialized craftsmen to participate in the construction, and expertise in quality control for acceptance.

The functional partition problem, you can refer to the design of the two markets. To consider now is to build a kind of roof, is to adopt the old shape or new consideration. How to do both shelter for the market space and do not affect the arcaded facades overall sense. This as if is a difficult problem, but I thought we the designer may solve this problem.

3.3.3 *For the next generation*

With the pace of real estate development, many places in Xiamen Island have been developed. More and more supermarkets substituted traditional Market position. Everything is new, can not find the mark in the past.

What kind of environment we want to leave to future generations? We think clean is really be? I have witnessed a reconstruction on the Zhonghua road, Centuries-old arcade building become construction trash in an instant. Now here is the very big shop. They Sets up the surface to defer to beforehand appearance reconstruction along the street, but the line foot is such roughness and the stiffness. The sham forever is unable with the original work to compare.

I saw in the eighth market such a special building. Lujiang Kindergarten is located on the Kaiping Road. After business hours, parents with children through the eighth market, teaches children recognition recognition of marine fish, communicate with the store. Then forward a hundred years there may be a lot of kids play through the arcade, leaning against the wooden door side, listens to my grandfather talk about the history of Xiamen. After 100 years, Xiamen eighth market will survive? Beautiful arcade facade will survive? Flood Street in this part will be in? Old folk customs of local people still exist? What type is Xiamen in descendant's eye? This is not alarmist; the key is how we want to leave a Xiamen to future generations.

REFERENCES

- [1] Xiamen Local Records Compilation Committee office. 1999. "Republic of Xiamen Chi". Chronicles Press.
- [2] Wang Dongcheng, Su Qi. 2011. "Xiamen retain only the eighth market Minnan old-fashioned style, business was still prosperity most cherished". http://news.xmnn.cn/xmxw/201112/t20111222_2115349.htm.
- [3] WikiArquitectura—Buildings of the World. 2010. "Besiktas Fishmarket", http://en.wikiarquitectura.com/index.php/Besiktas_Fishmarket.
- [4] WikiArquitectura—Buildings of the World. 2010. "Santa Catarina Market", http://en.wikiarquitectura.com/index.php/Santa_Catarina_Market.

The application of payment guarantees to subcontracts

Xiao Xin Ding & Meng Yuan Su

Department of Construction Management, Jilin Jianzhu University, Changchun, China

ABSTRACT: The guarantee system in construction projects is, as an international practice, an important means of credit for getting and awarding contracts. At present, many problems, such as poor quality, default in funds, etc., arising from Chinese construction industry, are closely linked to poor performance on getting and awarding contracts. Analyzing the guarantee system in the industry under Chinese conditions, this paper puts forward a concept that a payment guarantee system should be executed in the model texts of subcontracts, thus offering sensible suggestions for perfecting professional subcontracts for construction projects (model text) and labor subcontracts for construction projects (model text).

Keywords: payment guarantee; professional subcontract; labor subcontract

1 INTRODUCTION

The model texts for subcontracts widely used in China at the present time, i.e. *Professional Subcontracts for Construction Projects (Model Text)* and *Labor Subcontracts for Construction Projects (Model Text)*, are issued by the Housing and Construction Ministry and the General Administrative Bureau for Industry and Commerce in August 2003, both of which lay down detailed stipulations for and standardize subcontracting that frequently occurs in construction projects in China. Ten years' use of the texts has found that there are many unreasonable, nonstandard and imperfect problems in them, which grow more serious with the sudden boom in the industry. Moreover, construction workers demanding for wages and claiming for rights from time to time recently have considerably stunted and damaged the growth of the industry, and have seriously affected the stability of society. This paper aims to perfect the model texts of the subcontracts so that disputes arising from imperfections of the texts among parties concerned can be reduced and the interests of the downstream labor force in the industry chain can be defended. Only in this way can the construction market in China achieve a healthy growth.

Project Resources: The Project of Planning Fund for Humanities and Social Sciences Research of Ministry of Education. Project Number: 12YJAZH010; The Key Research Base and Open Project of Humanities and Social Science in Colleges and Universities in Jilin Province, Number: (2012) 551; Jilin Scientific Development and Plan Project, Number: 20130420086FG.

2 PAYMENT GUARANTEES IN SUBCONTRACTS

Payment guarantees refers to the guarantees for payment of goods issued by the buyer or proprietor to the seller or contractor, which ensures that the buyer or the contractor shall fulfill its obligation of payment according to the commercial contract. The payment guarantees in subcontracts are classified into those by the contractor and those by the subcontractor, of which that by the contractor refers to guarantees of the contractor for its subcontractors, suppliers and workers (including peasant workers, same below), ensuring that the contractor shall pay its subcontractors, suppliers and workers for all costs and wages under the terms of the contract, while those guarantees by the subcontractor refers to guarantees of the subcontractor for the contractor, ensuring that the subcontractor shall pay suppliers and workers for all their costs and wages under the terms of the construction contract. The two types of guarantees play an important role in standardizing subcontracting in the construction market in China.

3 THE SITUATION OF PAYMENT GUARANTEES AT HOME AND ABROAD

3.1 *The employment of payment guarantees in foreign countries*

1. The United States has the most complete system of construction guarantees in the world. The US, which owns the biggest guarantee market in the world, has a 100-year history of

construction guarantees. Unlike other countries, the US has 50 states that have adopted mainly the system of guarantees by companies and expressly forbidden banks from guaranteeing by law, while other countries provide guarantees through letters of guarantee issued by banks. The complete operation of guarantee credit in the US has been established, in which the government has improved strict entrance requirements on guarantees by company. The company is required to have not only superior strength in funds but also a high credit rating. Once it has guaranteed for a construction project, the guarantor company shall intervene in the whole process of construction, and meanwhile the sponsor and the builder will regulate the survey, design and building of the project in order for it to be carried out well rather than only compensate. It should also offer sensible suggestions for the sponsor and the builder so as to avoid blame shifting between the two parties^[1].

2. The Trust Fund Mode in Great Britain

Great Britain adopts trust fund in construction guarantees, a mode which means that the sponsor shall transfer a certain amount of money equivalent to the original fund to the trustee within a certain period of time after the date when the contract takes effect, or offer a letter of guaranty of immediate payment equivalent to the original value issued by banks or other financial institutions and hereby a trust fund guarantee is created. The original value of the trust fund shall be 1.5 times as much as the cost of the contract on the date when it takes effect, and then the value shall be divided by the number of months of the contract period. The sponsor is under an obligation to keep the trust fund at the original value. The beneficiaries of the trust fund shall be the contractor and subcontractors or suppliers subordinate to the contractor. If the sponsor goes into liquidation and becomes insolvent, the beneficiaries may make a claim to the trustee, who may pay the beneficiaries on its own a sum of money not more than the amount deserved. This procedure can effectively prevent harmful deeds of the sponsor, such as intentional insolvency^[2].

3.2 Application of payment guarantee in China

The current subcontracts in China contain stipulations on guarantees as follows: “31.1 If subcontracts require the contractor to provide payment guarantees for subcontractors, the two parties shall negotiate on the way of guarantees and the amount guaranteed, which shall be set in the special terms of the contract. 31.2 If subcontracts

require subcontractors to provide guarantees of performance for the contractor, the two parties shall negotiate on the way of guarantees and the amount of guarantees, which shall be set in the special terms of the contract. 31.3 The performance bond provided by subcontractors shall not exceed the amount guaranteed which is provided by the contractor for subcontractors in the general contract.” The current subcontracts do not contain detailed provisions for guarantees, which makes the payment guarantee merely a formality during its operation.

In order to execute the guarantee system for the construction industry as soon as possible, China has experimented with the system in some of its economically developed cities, among which are Beijing, Shanghai, Shenzhen and Xiamen, who have done a admirable job by solving problems that they keep on looking for and analyzing, and have gained more and more experience by doing so in the guarantee system^[3].

1. Keeping a record of the professional guarantor companies and standardizing the qualifications of them.

By keeping a record of the guarantor companies and strictly examining their qualifications, the job has become standardized.

2. Managing the letter of guarantee for the construction project, and enhancing the sense of risk.

The government stipulates mandatorily that before the application for the construction license, formalities for keeping safe the letter of guarantee shall be completed in the municipal trading center of construction after the signing of the contract between the sponsor and the builder. It also stipulates that the original may be taken back on condition that a certificate issued by the competent department is presented after the project completed and accepted. This policy plays an important role in the regulation of construction guarantees.

3. Dynamically managing the funds of the guarantor company to ensure its capability for compensation.

By creating a statistical analysis of construction guarantees, the capability of the guarantor can be monitored in real time so that the guarantor can compensate for any dispute within the amount guaranteed.

4. Standardizing the format and the contents of the contract of construction guarantees to uphold its legal validity.

The Board of Arbitration in Xiamen is commissioned to formulate the *Model Text of the Contract of Construction Guarantees in Xiamen City*, which should be made a universal practice.

The model text stipulate expressly the scope of mandatory guarantees, requirements for the qualifications of the guarantor, time limits of guarantees and so on, which can safeguard effectively the interests of the parties concerned.

5. Introducing professional agencies of credit rating for financial institutions to create a credit rating system for guarantor companies of construction.

By the introduction of credit rating agencies for financial institutions, the guarantor companies of construction of whom a record has been kept can be rated, and their credentials can be determined accordingly, and thus they can be regulated through market competition.

6. Publicizing the necessity of the guarantee system for construction for good performance of the system.

Through wide publicity and hard training, the builder and the workers can recognize the real role of the guarantee system and learn how to safeguard their interests by legal means^[4].

4 THE TERMS OF PAYMENT GUARANTEES IN THE SUBCONTRACT TO BE IMPROVED

4.1 *Mandatory payment guarantees both for the contractor and the subcontractor*

Payment guarantees of the contractor refers to the guarantees offered by the guarantor to the contractor for its subcontractors, guaranteeing that the contractor will pay its subcontractors for all costs according to the terms of the construction contract. The period of validity of the payment guarantees of the contractor shall be provided in the contract. The deadline for the period of validity of the contract shall not be more than 30 to 150 days later than the deadline for payment provided in the relevant construction subcontract (the general contract). If the contractor fail to pay all costs in time according to the terms of the contract, the guarantor will take the responsibility of guarantees according to the letter of guarantee or the promise of guaranteeing the contract. When the contractor subcontract by law a project whose cost is 500 thousand yuan or above or whose service cost is above 100 thousand yuan, he shall offer to its subcontractor the payment guarantees, and at the same time the subcontractor shall offer to the contractor its guarantees for fulfilling the contract. The payment guarantees shall be equal in amount to the fulfillment guarantees, amounting generally to 5% of contract cost^[5].

Payment guarantees of the subcontractor refer to guarantees offered by the guarantor to the subcontractor for the contractor, guaranteeing that

the subcontractor will pay the suppliers, workers for all costs and wages according to the terms of the construction contract. The payment guarantees of the subcontractor may adopt such professional guarantors as letters of guarantee by banks. If the subcontractor fails to pay all costs and wages to the suppliers and workers according to the terms of the contract, the guarantor shall take the responsibility of guarantees according to the letter of guarantee or the promise of guaranteeing the contract.

4.2 *Establishment of the detailed procedure for payment guarantees*

1. The Amount of Payment Guarantees

Considering the flow of funds of the contractor and the subcontractor, the amount of their payment guarantees should be determined by the scale of the project. For the project that lasts for one year, the amount guaranteed may be 5% of the contract cost; for the project to be carried over to the next year, the amount guaranteed may be 5% of the contract cost to be finished within the year. For the benefit of the suppliers and the workers, the contractor and the subcontractor should guarantee the fixed amount that must not be cut down with the progress of the project and the payment of wages^[6].

2. Validity Period of Payment Guarantee

In order to settle the “triangular debts” completely in the settlement of a project, the deadline for the validity period of the payment guarantees of the contractor and the subcontractor shall expire on the date of settlement when subcontractors have completed all projects according to the terms of the subcontract. After the completion of the project, the court or any institutions of arbitration will not hear the any disputes of defaults in payment if there is any.

3. Submission of Payment Guarantees

If payment guarantees of the contractor and the subcontractor are established, both parties shall submit the guarantees upon signing the construction contract. All letters of payment guarantees shall be kept by the administrator of the special account of the money guaranteed who must be recognized by the administrative department of the project in order that the guarantees can be best regulated and executed, and can be used immediately to compensate and in settling disputes once claims occur. If subcontractors win a bid or undertake a project as a union, each party or the leader of the union shall submit the payment guarantees and the guarantees shall be binding on all the members of the union.

4. Deferment of Payment Guarantees

Payment Guarantees of the contractor and the subcontractor shall be effective throughout the whole process of the project. As there are inevitably changes during the execution of a project, or breaches of the contract by proprietors, the time limit for the project will inevitably be affected. Payment guarantees of the contractor and the subcontractor must be deferred with the delay of the project. If the deferment is not caused by the subcontractor, he should defer payment guarantees with the cost to be born by the proprietor or the contractor and the settlement should be carried out at the time of the re-submission of payment guarantees. If the deferment is caused by the subcontractor, he should defer payment guarantees with the cost to be born by himself, and the re-submission of payment guarantee shall not be 28 days later than the original submission^[7].

5. Supplementation of Payment Guarantees

In order to prevent the decrease in payment guarantees of the contractor and the subcontractor due to claims, the two parties shall supplement the amount of the guarantees within 28 days upon receipt of claims by the guarantor of the L/G or the administrator of the special account of guarantee so that the guarantees may be sufficient to compensate within the period of its validity.

6. Return of Payment Guarantees

The contractor and the subcontractor shall issue an release within 14 days after the completion and settlement, and with the issued release and the report of supervision and acceptance of completion of the project and the report of verification of settlement of the project completion, the two parties shall request the termination of payment guarantees from the administrator of the special account of the guarantee. The administrator of the special account shall return the letter of guarantee or guarantees automatically (including interest)^[8].

7. Workflow of Payment Guarantee

When the contractor and the subcontractor fails to pay costs according to the service contract or purchase contract, the obligee may make a claim to the guarantor according to the contractor of the project and the guarantee contract of the project, and meanwhile it may issue a notice in writing to the proprietor and the contractor. After the competent department has checked, the guarantor must compensate for it. In the actual projects under supervision, the qualifications of the claimer and the reasons for claiming shall be recognized in writing by the general supervising engineer of the project.

4.3 *Specific prescriptions to be laid down for the guarantors to be selected*

According to regulations, the guarantor of a project shall be a financial institution founded by law within Chinese territory that has been licensed by a administrative institutions of banking to conduct its guarantee business and whose business site shall be in the same district as the project site, including branches of various commercial banks, sub-branches (not including sub offices and savings banks), a special guarantor whose business scope shall be mainly guaranteeing activities, and who shall be registered and kept a record at the local competent administrative department where the project takes place. In the meantime, the government should make every effort to strengthen the relevant regulations, creating credentials for guarantors and requiring them to undertake business within their scope of capability. The government should establish strict control over the criteria for starting a guarantor and create a standard and stable guarantee market.

4.4 *Devising the governmental plan and strategy of regulation*

The project that satisfies the amount of guarantee but has not been guaranteed according to the procedure shall be banned from a license of construction. The original of the letter of guarantee shall be submitted to the local competent department for safekeeping and its amount of guarantee must be kept at a sufficient level. If the amount of guarantee is not sufficient due to compensation or other causes and the amount is not supplemented on time, the project shall be ordered to stop for scheduled rectification.

5 CONCLUSION

There are many problems in the lawfulness, mechanism feasibility and reasonableness of mandatory execution of payment guarantees by the government at present, which makes the system stagnating in operation. One of its sources lies in that we have not found an appropriate, lawful, reasonable and reliable mechanism of operation. We should improve safeguards for the operation of construction regulations, impose responsibility of license of construction and payment guarantees, and determine the autonomy of the proprietor through regulations and the autonomy exerted by the big proprietor standardly. And what's more, we should determine the approaches to mandatory and optional guarantees, together with their items, and reach a consensus on the amount of general guarantees,

together with their reasonable division. To match with all that, we should provide the mechanism of differentiation of guarantees so as to form a mechanism of operation that will conform with both the international practices and Chinese conditions. We should also nurture professional guarantors and heighten the sense of interest safeguarding of the workers. Finally, a suggestion goes to the competent departments or associations that they should issue a joint order to specify the operational structure and to solve the intractable problems of mechanism of project investment and operation that the local government can do little about, a suggestion that can smooth the way for the achievement of system feasibility and regional unity.

REFERENCES

- [1] Shibing Feng. On Establishment and Perfection of the Building Engineering Guarantee System in China. *Market Weekly*, March 2008.
- [2] Xinjie Liu. Consideration on Implementing Engineering Guarantee System in China-Fujian Building Materials, Vol. 3 (2012).
- [3] Yisheng Liu, Xiaolong Wang, Zhonglin Chen. Engineering Guarantee System Abroad and Its Inspiration [J]. *Journal of Engineering Management*, 2010. 24(1):15.
- [4] Genshan Zhao. Discussion on the Feasibility of Implementing the Engineering Guarantee System in China [J]. *Management Science*, 2009 (127).
- [5] Dejuan Kong. Research on Supervisal Mode of Construction Guarantee Market [D]. Hangzhou: Zhejiang University, 2008.
- [6] Yisheng Liu, Xiaolong Wang, Zhonglin Chen. Enlightenments of Construction Bond Systems in Overseas-Construction Management Modernization. Vol. 24, pp. 13–17, 2010.
- [7] Chunyang Wang. Investigation and Research on the Engineering Guarantee System in China [D]. Beijing: Tsinghua University, 2005.
- [8] Rui Zhang, Xiaomei Deng. Comparative Study on Builder's Lien and Priority of Compensation of Construction Project [J]. *Construction Economy*, 2005 (8).

Experimental study of double combination structural behavior of the negative bending region of Concrete-Partial-filled narrow-width steel box composite beams

Hai Lin Yang

College of Civil Engineering, Guilin University of Science and Technology, Guilin, China

Yan Zheng

GuangXi Key Laboratory of Geomechanics and Geotechnical Engineering, Guilin, China
College of Civil Engineering, Guilin University of Science and Technology, Guilin, China

Xing Ke Li & Sheng Li

College of Civil Engineering, Guilin University of Science and Technology, Guilin, China

Shi Xu Mo

GuangXi Key Laboratory of Geomechanics and Geotechnical Engineering, Guilin, China
College of Civil Engineering, Guilin University of Science and Technology, Guilin, China

ABSTRACT: In order to study the double combination structure behavior of Concrete-Partial-filled narrow-width steel box composite beam in negative moment regions, three beams have been tested. Test results show that the behaviors of the continuous beams are improved obviously after filling concrete in partial steel box and the beams possess high loading capacity and rigidity and good ductility. Combined with experimental comparison pure shear connection design of composite beams and the influence of relative sliding on deflection, the different reinforcement amount of the crack in the negative moment region of development were analyzed.

Keywords: Concrete-Partial-filled steel box continuous beam; negative moment; double combination

1 INTRODUCTION

Concrete-Partial-filled narrow-width steel box composite beam is a new type of steel composite beams based on the rectangle steel tube concrete structures and steel box-concrete composite beams. Its positive bending section is the same as the common steel box-concrete composite beams and in the negative moment region compression area of the steel box girder is filled with concrete^[1]. So it can improve the structure behavior of the continuous composite beams in the negative moment regions and make its stress characteristics similar to concrete-filled rectangular steel tube eccentric compression member. Compared with the traditional steel box-concrete composite beams not only have large stiffness, light weight, high bearing capacity but also the local stability and global torsion performance are

good characteristic^[2,3]. Three-dimensional pressure state of concrete is better to play its compression resistance capability. Through experimental research, this paper expounds the experimental phenomena, component characteristics of local damage, the cracking mechanism and development regularity of cracks in the negative moment region and composite beams section stress distribution.

2 TEST SURVEY

In order to study the Concrete-Partial-filled narrow-width steel box continuous composite beams mechanical properties in the negative moment region, making three beams with static load conditions under negative moments (PSCB1-1, PSCB1-2, PSCB1-3). The parameters of the test beam is shown in [Table 1](#). Test device and the loading device are shown in [Figure 1](#). Composite beams section parameter is shown in [Figure 2](#). The strength of the steel box filled concrete is C40. The strength of steel

Fund project: The national natural science fund project (51168011, 51108109).

Table 1. Parameters of test specimens.

Number	Ratio	Stud spacing	Degree	Reinforced	Spacing
PSCB1-1	1%	2 × Φ13 400	1.00	11Φ12	85
PSCB1-2	2%	2 × Φ13 250	0.75	22Φ12	85
PSCB1-3	3%	2 × Φ13 140	1.00	32Φ12	60

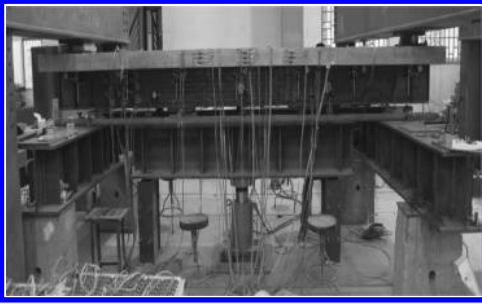


Figure 1. Test device and loading equipment.

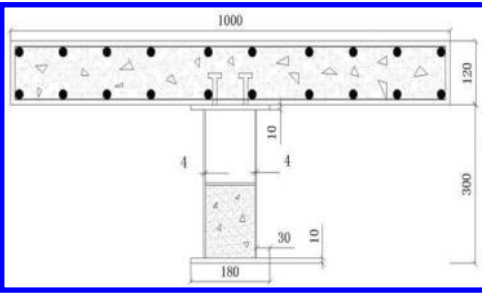


Figure 2. Section of the composite beam.

Table 2. Mechanical properties of steel.

Name	Type	Yield strength (MPa)	Tensile strength (MPa)	Elongation (%)
Reinforced	Φ12	446	564	30.4
Reinforced	Φ6	342	489	32.2
Steel plate	Q235	295	373	31.5

plate is Q235. Longitudinal reinforcement strength is HRB335, stirrup strength is HPB300. Steel of the related mechanical parameters are shown in Table 2.

3 EXPERIMENT PROCESS

Test process can be divided into three stages: the first stage from starting loading to the composite

beams crack—the elastic state of composite beams. The second stage of crack development process, with the increase of load, development of cracks basically stable, width and depth of cracks changed little, composite beams shows the characteristics of obvious elastic-plastic stage of work. The third stage of bending failure, composite beams shows the characteristics of obvious plasticity.

In the initial stages of load application, steel box girder and concrete flange plate showed a good combination. With the gradual increase of load, when the specimen is loaded to $(0.23\sim 0.35)M_u$, a crisp void noise ringing out, the natural bond between the steel box girder and concrete flange plate damaged (M_u = ultimate bearing capacity). The profile and surface junction of concrete flange plate in the middle of span appeared micro cracks that can be detected by naked eyes. With the increase of load, in the internal of steel box girder ringing noise. When the load applied to $(0.64\sim 0.8)M_u$, the buckling of steel box girder web plates appeared to drum, surface cracks on the concrete flange plate developed into the main cracks. Meanwhile, new cracks appeared constantly and surface cracks on the concrete flange plate encrypted gradually along with cracks gradually growing width and depth and extending to the plate of the below surface. Outer convex buckling of steel box girder web plates was more apparent, most of the longitudinal reinforcement reached the yield strength, and composite beams achieved the ultimate bending capacity.

4 THE TEST RESULT ANALYSIS

4.1 Load—deflection curves

To avoid fast loading, concrete flange plate crack development process cannot be reflected, the loading per level 10 kN. Through the collation of test data, the load deflection curve of specimens cross section could be drawn. The curve reflects the basic properties, such as stiffness, bearing capacity and ductility of the specimen. The whole load deflection curve of different reinforcement ratio specimen is shown in Figure 3.

From Figure 3 we can see that there is a linear relationship about mid span's deflection curve before the load applied to $0.35M_u$. The load-

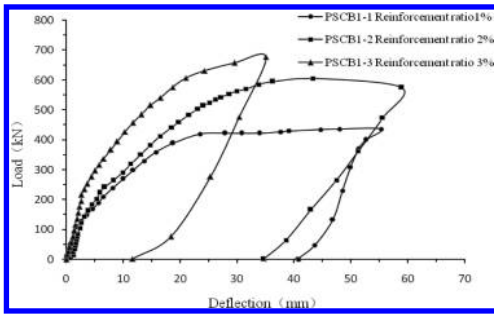


Figure 3. Different ratio of reinforcement load-deflection curves.

deflection curve of different reinforcement ratio rising stage's slope difference is bigger. After the first turning point, load-deflection curve characterized by nonlinear, composite beams bending stiffness decrease is noticeable. Local buckling of steel box girder web plates occurred in succession, composite beams came into the failure stage and the sectional flexural stiffness drastically reduced.

4.2 Buckling failure

Specimen is loaded to $0.4\sim 0.55M_u$, composite beams in the cross region and load bearing place around the web and filled concrete disengaging, and is accompanied by the ringing noises. Load to $0.65\sim 0.8M_u$ near the loading point of steel box girder began to appear to the outside, the basis of local produce web buckling outer convex half wave, and the load of $3\%\sim 5\%$. When the load applied to $0.95M_u$, bearing accessory flexor wave began to web on both sides of the expansion and deformation, mid span deflection increases with load increasing rapidly, the composite beams in large deformation stages, but composite beams still showed good ductility. All load deflection curves of the rising and falling period are basic parallel, specimen capacity no significant decline. Specimen PSCB1-1 buckling mode and buckling position are shown in Figures 5 to 6.

4.3 The strain distribution of reinforced and steel box

Figure 7 is the longitudinal reinforcement's curve of stress-strain relationship in the middle of span. From the picture we can see that from starting loading to the first turning, the three specimens' longitudinal reinforcement and concrete had uniform stress and deformed coordinately. After the first turning, three curves appear steps, accompanying longitudinal reinforcement strain increase sharply. This



Figure 4. PSCB1-1 the biggest deformation.



Figure 5. PSCB1-1 local buckling.



Figure 6. PSCB1-1 local buckling.

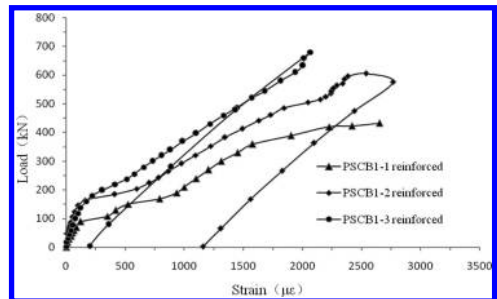


Figure 7. Curves of load and strain.

phenomenon shows that the concrete flange plate begins to crack and quits work, most of the tensile stress transfers to the longitudinal reinforcement. The peak strain of the whole curve corresponds to the ultimate bearing capacity of the specimen. When PSCB1-1 reached the bearing capacity, steel box yielded sooner than longitudinal reinforcement, specimen occurred bending failure. The curve is similar with the load deflection curves.

Specimen PSCB1-1 bottom transverse strain distribution is shown in Figure 8. Due to the influence of shear lag effect, it cannot make full use of the steel strength, reducing the bearing capacity of composite beams. Before the load applied to $0.68M_u$, bottom transverse strain distribution is even. Along with the load increasing, shear lag phenomenon of the steel box plate in the bottom is very obvious.

Specimen PSCB1-1 cross section steel box girder on the surface strain along the depth of beam is shown in Figure 9. In the early stage of the loading, specimen cross section along the height strain values are linear relationship, basically accord with the flat section assumption. When the load closed to the elastic limit state, the strain value closest to the steel box bottom plate occurred tension mutation. It showed that steel box girder web section that bearing the maximum

bending moment began slightly convex outward buckling.

4.4 The development of concrete flange plate crack

The test results show that when the load is applied to $0.12M_u$, pure bending section of PSCB1-1 in the central of concrete flange plate began to appear a few micro cracks on the surface. With the increase of load, cracks extended toward either side of the flange plate and the width of cracks also increased gradually. The maximum of crack width are also located in the middle part of the flange plate, apparently caused by the shear lag effect of the negative bending section. Demarcate each through crack in a certain order in the process of test, and these cracks are main cracks that developed rapidly and the width is relatively big. Load tests showed that the series of load effected little on the main cracks width, but had a large impact on the flange plate cracks' distribution.

The strain distribution of concrete flange plate is shown in Figure 10. The first turning point of these curves are precursors for the cracking of concrete flange.

With the increase of load, specimen occurred bending failure. The distribution of concrete flange plate's cracks is shown in Figure 11.

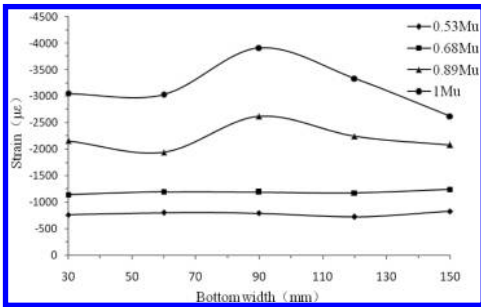


Figure 8. PSCB1-1 steel slab strain distribution.

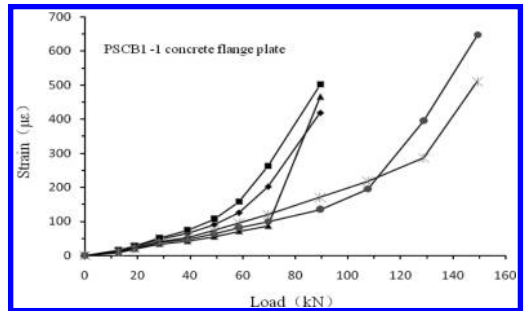


Figure 10. Curves of load and strain.

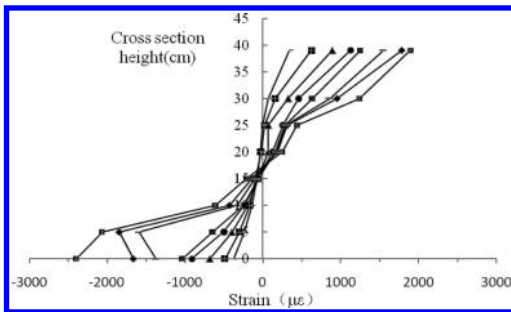


Figure 9. Strain distribution of mid-span section.



Figure 11. Concrete flange plate crack distribution.

5 CONCLUSION

Concrete-Partial-filled narrow-width steel box composite beams in bending failure test showed a good structural ductility and plastic characteristics such as high strength reserve. Compared with the literature^[4], because the steel box compression area filled concrete in the negative moment region, the deformation of the steel box girder's web plate and bottom plate only is convex outward, delays the local buckling of composite beams, and improves the local stability of steel box. The structure deformation is limited, so the flexural bearing capacity of composite beams is improved. At the same time, the increase of reinforcement ratio can effectively control the crack width of concrete flange plate.

REFERENCES

- Mo Shixu, 2008. Test research and bearing capacity calculation of concrete-partially-filled steel box beam [J]. *Industrial Construction* (z1): 499–503 (in Chinese).
- Nie Jianguo, 1997. Research on the cracking of negative bending regions of composite steel concrete beams[J]. *Journal of Tsinghua University*, 37(6): 95–99 (in Chinese).
- Shu Xiaojuan, 2011. Preliminary design and application of steel-box concrete composite beam[J]. *China Civil Engineering Journal*. (in Chinese).
- Tan E.L., 2012. Behaviour and design of composite beams subjected to negative bending and compression[J]. *Journal of Constructional Steel Research*, 79: 34–47.

Optimize research in assessment system of green building indoor environment

Xue Jiang & Weng Cheng

Harbin Institute of Technology, Harbin, China

ABSTRACT: Along with the progress of the society, healthy indoor environment has become the common expectation. It is one of the most important composition contents of green building assessment in the evaluation of the indoor environment. At present, the green building assessment system of many countries is in gradual improvement. The evaluation indexes of indoor environment are contrasted in green building assessment system from China, America, England and Japan. The similarities and differences between the index weight, index content and scoring mechanism are analyzed. Sound, light, heat and air quality, the four specific index scores, are compared and analyzed in the evaluation system. On this basis, the optimization direction of index system of indoor environment is proposed, which can provide reference information for sustainable building system.

Keywords: green building; indoor environment; evaluation index optimization

1 INTRODUCTION

The 2/3 time is spent in the interior in a person's lifetime. Indoor environment is very important for people, therefore, evaluation of indoor environment is an important part of green building assessment system. The evaluation index of indoor environment in this paper is discussed based on the contents of the evaluation indexes based on green building, including Chinese "green building evaluation criteria" (hereinafter referred to as GBT) GB/T50378-2014. The mature international evaluation system are compared in this study, including the UK's BREEAM, Japan's CASBEE and American LEED. The overall framework of GBT and LEED are similar. BREEAM introduces objective selection and implementation ways in detail. Japanese CASBEE is a more comprehensive evaluation index. These typical indoor environment evaluation systems of green buildings can make contribution to the indoor environment index evaluation system of China.

2 COMPARATIVE ANALYSIS OF INDOOR ENVIRONMENT EVALUATION

2.1 Index comparison

Evaluation of indoor environmental standards in GBT is divided into two parts, control items and grading items. The main contents of the control items are evaluation of noise, illumination,

humidity and air quality; Grading items are sound environment, light environment, thermal environment and air quality.

Through the comparative analysis of the four evaluation system, the common contents are natural ventilation performance, room temperature control, partition coefficient of natural lighting, noise and sound insulation performance (except LEED). People need a healthy and comfortable indoor environment, which lead to more application project of green technology. Modern people spend more time in air conditioning room and artificial light. It is harmful to the human body hugely, therefore, the desire for natural ventilation are increasingly in recent years. It is hoped that indoor environment rely on more natural ventilation in summer and winter and more to natural light to reach the desired illumination. It is the pursuit of the green natural environment performance.

2.2 Evaluation and scoring method comparison

The scoring method of LEED, BREEAM and GBT is similar. The main difference is the setting of scores and the proportion of quantitative indexes, which will lead to the operational difficulty. Although CASBEE provided many evaluation levels, the operation is more difficult than other three. According to the existing mechanisms, the more qualitative indicators are, the harder for technical personnel to control. Therefore, quantitative indexes proportion should be increased in

Table 1. Corresponding relationship between the GBT and other typical indoor environment evaluation systems.

GBT	LEED	BREEAM ECOHOMES	BREEAM OFFICE	CASBEE
Acoustic environment	Non	Sound insulation	Acoustic properties	Sound environment
Light environment	System controllability	Lighting and vision lighting	Lighting, vision, glare control, high frequency light, indoor and outdoor lighting light level, regional control	Light environment
Hot and humid environment	System controllability, thermal comfort	Non	Thermal partition	Thermal environment
Air quality	Air quality, environmental control of smoking, outdoor air monitoring, improve ventilation, the construction of IAQ management plan, low emission materials, indoor chemicals and pollution source control	Non	Potential of indoor air quality, volatile organic compounds in natural ventilation	Air quality of the environment
Other	Non	Non	Microbial pollution	Non

the revision of the index, or converting qualitative indexes into quantitative through scientific conversion method.

2.3 The weight comparison

2.3.1 Weight distribution

The four kinds of index system of indoor environment index can be classified into indoor air quality, humid environment, light environment and sound environment. GBT is set up with a total evaluation score of 100 points. The highest score is the air quality index evaluation. The score in LEED is 15, the air quality index is significantly higher than the other three types of indicators. The residential part of BREEAM is 7 points and the construction part is 13 points, so the total score is 20 points. As can be seen, the system is more emphasis on public construction indoor environment and more attention is paid to the light environment. The total score of CASBEE is 110 points, the weights on air quality and light is larger but the four indicators are almost basic balance.

It can be seen from the weight of index, the indoor air quality, which is affected by many factors, is the focus of attention of these typical index system in the assessment of green building; the second is the light environment; finally is the hot and humid environment and sound environment. Among them, the focus of the indoor air quality is indoor ventilation and pollutant control. The light environment evaluation focuses on indoor daylight coefficient and vision. The hot and humid environment is focus on the air velocity and temperature control. Noise insulation control is the most important part of acoustic environment.

2.3.2 Air quality

In each evaluation system, air quality takes the largest weight. It reflects the degree to meet environmental requirements for people. The evaluation factors are mainly the air velocity and the clean degree of air. If the air velocity is not enough, people will feel uncomfortable; if rapid velocity will affect the temperature and cleanliness. According to the different environment, the amount of fresh air is adjusted appropriate to control air cleanliness and velocity makes air quality to achieve the optimum condition.

It is one of the important ways to improve the indoor environment that take effective control of indoor air pollutants. There are tens of thousands of kinds of effects of pollutants of indoor air quality, including influence of indoor decoration materials for air quality should be within the scope of evaluation. Green building evaluation should not only make the pollutant concentration in the air at a harmful concentration index the accepted, but

Table 2. Weights of air quality indexes.

FIRST CLASS	SECOND CLASS	THIRD CLASS	GBT	LEED	BREEAM	CASBEE
Air quality	Minimum air quality	–	–	–	1 (0.05)	–
	Pollution countermeasures	Chemical pollutants	5 (0.05)	3 (0.2)	–	1-5 (0.05)
		Pollution of mineral	–	–	1	1-5 (0.05)
		Mites and molds	–	–	–	1-5 (0.05)
		Legionella	–	–	–	1-5 (0.05)
		Low emission materials	–	4 (0.27)	1 (0.05)	–
	Fresh air system	Fresh air volume	–	1 (0.07)	–	1-5 (0.05)
		Natural ventilation performance	10 (0.1)	1 (0.07)	1 (0.05)	1-5 (0.05)
		new tuyere location	–	–	–	1-5 (0.05)
		Air supply design	5 (0.05)	–	–	1-5 (0.05)
	Operation management	CO ₂ monitoring	3 (0.03)	–	–	1-5 (0.05)
		Control of smoking	7 (0.07)	–	–	1-5 (0.05)

also make the quality of indoor air to be satisfied with most people are in the room.

2.3.3 Heat and humid environment

Heat and humidity significantly affect the working efficiency and living comfort. It should be paid attention to in the evaluation system. In addition to guarantee human overall heat balance, utilization of natural energy should also be included in the evaluation of green buildings. Large glass surface is often used in buildings. It may cause the greenhouse effect in summer and cold glass surface radiation effects in winter. Evaluation of thermal radiation should also be included. Therefore, in addition to air conditioning design conditions, local climate and the internal load variation on indoor environment should also be analyzed.

It has not been considered such as temperature control, thermal comfort control and air velocity on the humidity in GBT. But overall, the temperature control, humidity control have been a certain consideration. There are many control indexes of LEED on thermal comfort; they are divided into different stages. BREEAM in the control of hot and humid environment have two score items, but the two projects are described in detail; they also stressed the importance of thermal comfort and the partition of the important. Heat and humid environment indexes in CASBEE distributed uniformly and it involves more projects than the other three. However, it is lack of the evaluation of adjustable measures and thermal comfort of whole environment.

2.3.4 Light environment

Light is another basic conditions for normal daily activities. Light environment is an important index to evaluate the quality of the indoor environment.

Evaluation indicators of natural lighting are paid the highest attention. It makes people more familiar and comfort visually. But in the actual living and working, buildings that can achieve natural lighting during the day are less. Light environment evaluation of the indoor environment should be classified reasonable. Less evaluation projects are included in the GBT, but the content is rich. If it is divided into more sub-indexes, it will become clearer. It is the lack of evaluation of lighting equipment and lighting control. There is only one index for light environmental assessment in LEED. It includes the evaluation of the coefficient of lighting and vision. It is divided into two parts, space lighting 75% and 90%. The purpose of the evaluation is through the introduction of natural light and view of regional architecture to build a relationship between indoor and outdoor of the buildings. There is only one item in the lighting part of BREEAM; it describes lighting and vision requirements in detail. The score of the different functional areas have detailed grading rules. The distribution of indexes in CASBEE is uniform but lack of evaluation field. Each of the indexes compared to other systems is not detailed enough.

2.3.5 Acoustic environment

From the different evaluation index systems, the GBT evaluation has more indexes. At present, compared with other typical evaluation systems, it is still lack of evaluation of the opening part of the sound insulation performance. There is no evaluation of acoustic environment in LEED; there is only one item in BREEAM. It is divided into 4 degree evaluation. It can be obtained the corresponding value according to different circumstances and the highest score is 4 points. Acoustic environment is also less than other assessment in

CASBEE, without considering the influence of layout design. But the noise insulation is considered in details. People want to have a relatively quiet environment and healthy and comfortable sound environment is good for human health. The control and construction of noise should be strengthened from two aspects. The green sound environment evaluation is not to damage hearing and reduce the noise source, which need to be considered in the design (such as the equipment generating noise separately arranged in away from using the room location). But the index to control of the sound environment is not perfect.

3 INDEX OPTIMIZATION

Through the analysis of indexes, the content of evaluation and weight distribution, the main results are as follows,

1. The indoor evaluation indexes should be made closer to the quantitative indicators to enhance maneuverability.
2. It is not only objective numerical indicators concern, but also the application of energy saving technology and green technology should be paid attention to in the indoor environment design and evaluation.
3. The evaluation should be four aspects include air quality, hot and humid environment, light environment and sound environment. Air quality is the focus of the indoor environment evaluation, including the choice of building materials.
4. In the gradually improving evaluation of system, acoustic environment should be strengthened.

REFERENCES

Ministry of housing and urban rural development, *Green building evaluation criteria GB/T50378-2006* [s], 2007.

Ministry of housing and urban rural development, *Green building evaluation criteria GB/T50378-2014* [s], 2014.

Bre G, *BREEAM ECOHOMES* [s] 2006.

Bre G, *BREEAM OFFICE* [s] 2008.

USGBC. *LEED2009 for New Construction and Major-Renovations Rating System* [s], 2008.

Japanese Association for sustainable construction, [s] Performance evaluation system of CASBEE integrated building environment, 2005.

He Yun. Green building indoor environment design (J), *The Chinese residential*, 2012, (10): 17–18.

S. Abbaszadeh, L. Zagreus, D. Lehrer1 and C. Huizenga. Occupant Satisfaction with Indoor Environmental Quality inGreen Buildings, *Proceedings of Healthy Buildings 2006, Lisbon* (Vol., III): 365–370.

Yang Xincheng Liu Meng. The typical green building assessment system of indoor environment index comparative analysis of, *Construction and environmental engineering* [J], 2013, (35): 174–176.

Seismic damage performance evaluation of special-shaped column frame

Yang Liu, Xing Min Ren & Hong Bing Liu

School of Mechanics and Civil and Architecture, Northwestern Polytechnical University, Xi'an, Shaanxi Province, P.R. China

ABSTRACT: Base on the elastic-plastic analysis method and two-parameter seismic damage model, the concrete special-shaped column frame structure was analyzed. With the Pushover method, the displacement response of structure and the development and distribution of component plastic hinges was obtained. Calculate the seismic damage indexes with Park-Ang model and achieve the analysis results of Pushover, then evaluate the seismic performance of specially shaped column frame. Use the above methods to study three typical special-shaped column frame structures of different height, which provides some theoretical reference for its engineering practice.

Keywords: special-shaped columns; seismic performance evaluation; Park-Ang model; Pushover method

1 FOREWORD

As a new structure, the special-shaped column structure has no much time in service and its project experience has not been accumulated enough. So far, scholars from various countries have researched on the relative performance of special-shaped column component much. But the theoretical research of seismic behavior of special-shaped column structure as a whole has been relatively little (Yan 2007, Shen 2010).

Calculate and analyze the seismic response of the regular special-shaped column structure with Pushover method, which can reflect the overall deformation of the structure well and show the plastic deformation mechanism of structural members clearly. In 1985, a seismic damage model which is linear combination of seismic elasto-plastic deformation and cumulative hysteretic energy was proposed by Park and Ang (Park & Ang 1985). This model considers the coupling effect of maximum deformation and cumulative hysteretic energy, and can evaluate damage of special-shaped column structure subjected to earthquake successfully.

On the base of Pushover analysis (Zhang 2002), this paper made reference to the basic idea of the reinforced concrete structure damage assessment, adopted the Park-Ang seismic damage model to analyze three special-shaped column frame models of different height and assess their seismic performance.

2 SEISMIC DAMAGE ASSESSMENT MODEL

2.1 Park-Ang damage model

Define the seismic damage index of special-shaped column structure as follow:

$$D_i = \frac{X_{im}}{X_{icu}} + \beta \frac{E_{ih}}{V_{iy} X_{icu}} \quad (1)$$

where X_{im} = the maximum inter-storey displacement of floor i under the earthquake; E_{ih} = the cumulative energy consumption of floor i ; V_{iy} = the yield shear force of floor i ; X_{icu} = the destruction limit displacement of floor i ; and β = the energy dissipation factor. The result is more stable when $\beta = 0.15$ (Cosenza et al. 1990).

The relationship between floor elasto-plastic deformation energy consumption and maximum displacement response of structure (Ye & Otani 1999):

$$E_{ih} = \frac{1}{2} V_{iy} X_{iy} + (1 + 4\rho) V_{iy} (X_{im} - X_{iy}) \quad (2)$$

where X_{iy} = inter-storey yield displacement; V_{iy} = inter-storey yield shear.

Maximum inter-storey displacement, inter-storey limit displacement, yield displacement and yield shear can be calculated by the Pushover method.

2.2 Park-Ang inter-storey damage index

This paper referred to the relevant literature (GBJ50011-2010 2010, Hu 2006) and divides the damage of building structures under earthquake action into the following five levels: Basically intact, Slight damage, Moderate damage, Severe damage and Collapse. Correspondingly, this paper gives the boundary damage index as shown in Table 1.

3 LAYOUT OF TEXT

3.1 Special-shaped column structure model

This paper selected three typical special-shaped column frame models of different height as examples, established their finite element analysis models. The models have 2 spans along the horizontal, 6 spans along the vertical. Each span is 4.5 m. The plane layouts of the models are the same, the height of all storeys is 2.9 m. There is no rectangular columns in all models.

Model 1 has 3 storeys, Model 2 has 6 storeys, Model 3 has 9 storeys, as shown in Figure 1. The columns in the corner of the structure model are L-shaped, in the circumference are T-shaped, in the middle are cross-shaped. Section dimensions and reinforcements of columns are shown in Figure 2. The rectangular beam section is 200×400 mm. The thickness of the floor is 200 mm. The concrete strength grade of structure is C30, longitudinal force steel bars of beams and columns are HRB335 as the floor reinforcement.

3.2 Seismic response analysis of special-shaped column structure model

Loading horizontal force along the two-span direction (the weak direction) of structure models with SAP2000. The global displacement and inter-storey displacement of structure models under the different intensity earthquake effect were obtained by this Pushover calculation. And the plastic deformation of structure is clearly reflected.

As shown in the plastic hinge distribution Figure 3, end of columns of Model 1 forms undeveloped plastic hinges first under the 7-degree

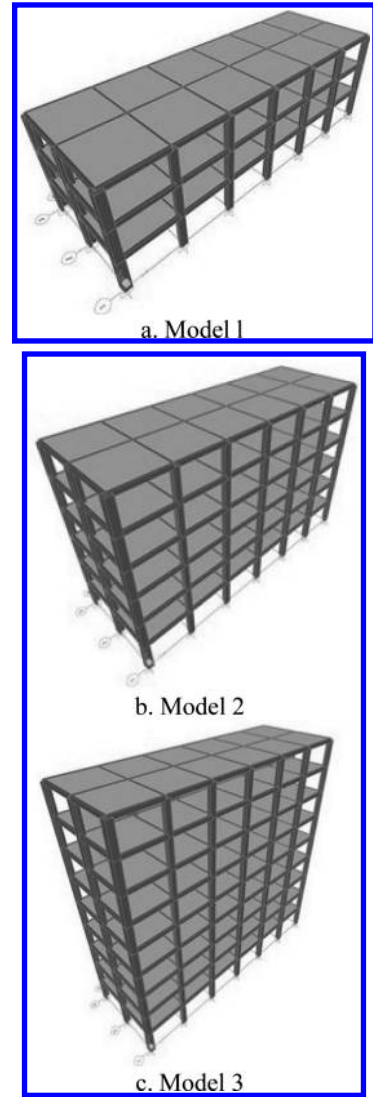


Figure 1. Structure models.

earthquake. It manifests that there are small cracks in the end of columns, or concrete cover of beam-column joints partly peels. Under the 8-degree earthquake, all the beams and columns of the structure form undeveloped plastic hinges. Under the effect of 9-degree earthquake, the beams on second floor of model 1 form developing plastic hinges. It manifests that there are cracks in beam-column joints, concrete cover of beam-column joints partly peels, the structure is slightly damaged.

As shown in the plastic hinge distribution Figure 4, almost all the frame beams of Model 2 form underdeveloped plastic hinges under the

Table 1. Inter-storey damage index of frame structure.

Earthquake damage grade	Damage index
Basically intact	0–0.2
Slight damage	0.2–0.4
Moderate damage	0.4–0.65
Severe damage	0.65–0.9
Collapse	>0.9

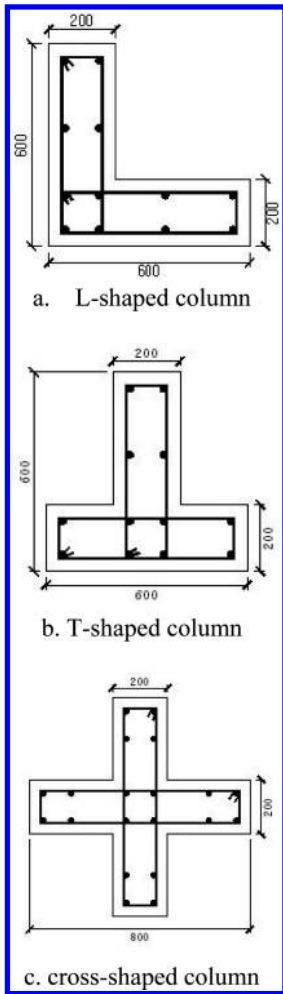


Figure 2. Sectional view of special-shaped columns.

7-degree earthquake, the columns of bottom floors also form underdeveloped plastic hinges. Under the 8-degree earthquake, the beams of bottom floors form developing plastic hinges which manifests that there are cracks in beam-column joints and concrete cover of beam-column joints partly peels. Under the 9-degree earthquake, the beams of lower portion of model form more developing plastic hinges which shows the joints are seriously cracked.

As shown in the plastic hinge distribution Figure 5, under the 7-degree earthquake, all the beams of the structure form underdeveloped plastic hinges except beams in the top floor, the columns in the bottom three floors also form underdeveloped plastic hinges. Under the 8-degree earthquake, beam plastic hinges in lower part of the

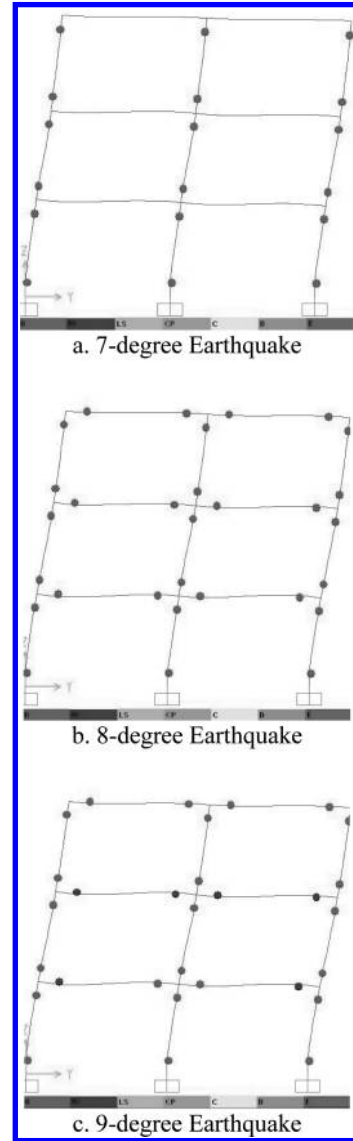


Figure 3. Plastic hinge distribution of model 1 under multi-intensity earthquakes.

structure continue to develop. Beams of second, third and fourth floor start to run out of capacity. Under the 9-degree earthquake, all the beams of the model start to lose capacity, the structure is severely damaged.

3.3 Calculation of structure inter-storey seismic damage index

According to the formula (1) and (2), calculate the inter-storey hysteretic energy of the models under

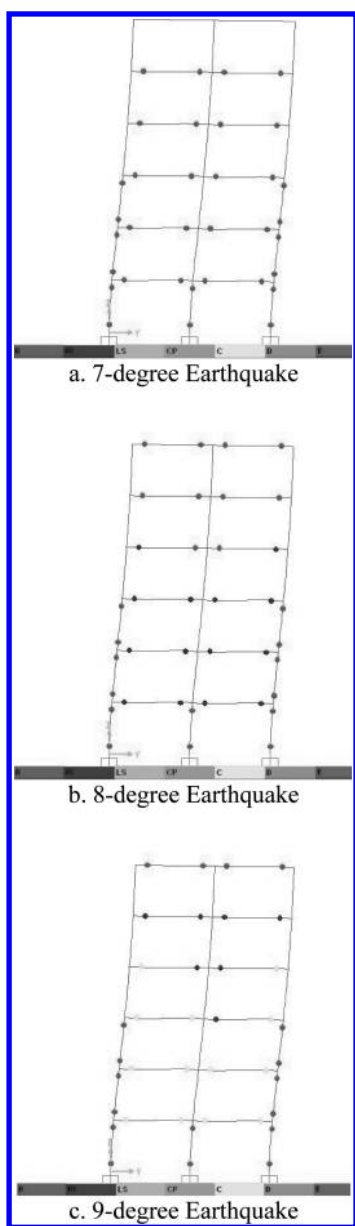


Figure 4. Plastic hinge distribution of model 2 under multi-intensity earthquakes.

multi-intensity earthquakes, and then inter-storey seismic damage indexes can be gotten. The results are shown in Table 2-4.

Draw the inter-storey damage assessment Figures 6-8 of the models under 7-degree, 8-degree and 9-degree earthquake.

Compare the inter-storey damage degrees calculated with Park-Ang model to plastic deformation

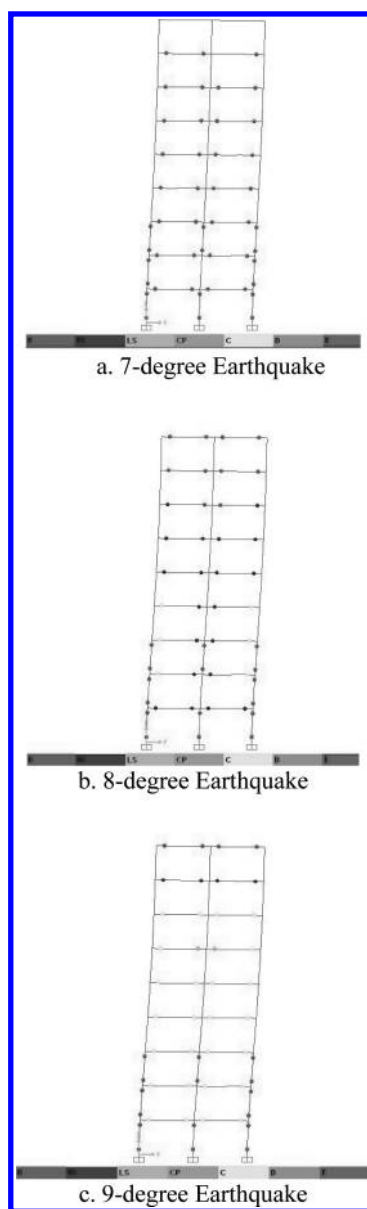


Figure 5. Plastic hinge distribution of model 3 under multi-intensity earthquakes.

Table 2. Inter-storey damage indexes of model 1.

Storey	7-degree (0.1 g)	8-degree (0.2 g)	9-degree (0.4 g)
1	0	0.0091	0.1991
2	0	0.0817	0.3639
3	0	0.0166	0.2232

Table 3. Inter-storey damage indexes of model 2.

Storey	7-degree (0.1 g)	8-degree (0.2 g)	9-degree (0.4 g)
1	0.0054	0.1860	0.5081
2	0.1153	0.4262	0.9866
3	0.1190	0.4318	1.0034
4	0.0780	0.3517	0.8451
5	0.0184	0.2307	0.6068
6	0	0.0948	0.3405

Table 4. Inter-storey damage indexes of model 3.

Storey	7-degree (0.1 g)	8-degree (0.2 g)	9-degree (0.4 g)
1	0	0.3163	0.8786
2	0.1208	0.6757	1.7034
3	0.1432	0.7595	1.8729
4	0.1320	0.7334	1.8207
5	0.1097	0.6645	1.6606
6	0.0780	0.5677	1.4558
7	0.0333	0.4318	1.1579
8	0	0.3052	0.8693
9	0	0.1711	0.5696

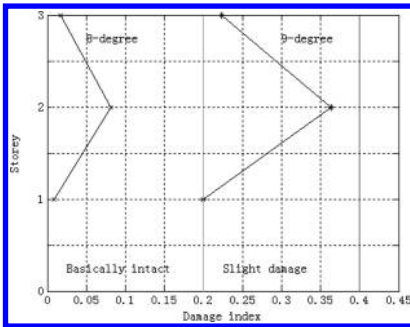


Figure 6. Inter-storey damage indexes of model 1.

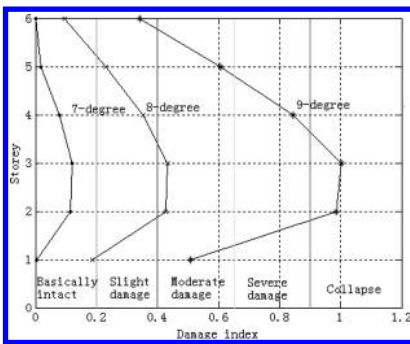


Figure 7. Inter-storey damage indexes of model 2.

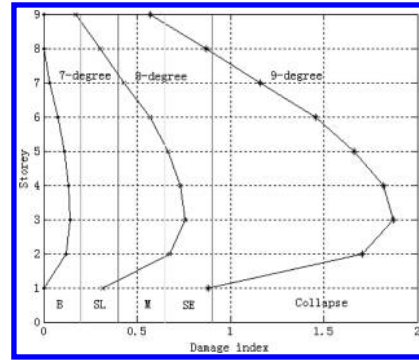


Figure 8. Inter-storey damage indexes of model 3.

Table 5. Seismic performance comparison of model 1.

	Park-Ang model	Pushover
7-degree (0.1 g)	Basic intact	Basic intact
8-degree (0.2 g)	Basic intact	Basic intact
9-degree (0.4 g)	Slight damage	Slight damage

Table 6. Seismic performance comparison of model 2.

	Park-Ang model	Pushover
7-degree (0.1 g)	Basic intact	Basic intact
8-degree (0.2 g)	Moderate damage	Moderate damage
9-degree (0.4 g)	Collapse	Severe damage

Table 7. Seismic performance comparison of model 3.

	Park-Ang model	Pushover
7-degree (0.1 g)	Basic intact	Basic intact
8-degree (0.2 g)	Severe damage	Moderate damage
9-degree (0.4 g)	Collapse	Severe damage

obtained with Pushover method, we can get the results as shown in Tables 5-7.

4 CONCLUSION

Based on the Pushover analysis and Park-Ang seismic damage model, this paper evaluated the seismic damage performance of three frame finite element models with special-shaped columns, and draws the following conclusions:

1. The seismic performance levels of special-shaped column structures evaluated by Park-Ang model

are safer than the results analyzed by Pushover method. It's because Park-Ang model taking into account the effect of hysteretic energy to the structure.

2. The weak storeys of regular concrete equiaxial special-shaped column frame show up in the lower part of the structure. With the increase of the floors, the position of weak storeys also raise. Under the same earthquake, the higher the floor, the more serious damage it affords. And the damage mode belongs to beam plastic hinge mechanism.

This paper made a preliminary discussion on seismic performance of special-shaped column frame structure, obtained some results which can provide some reference for practical application of special-shaped column structure.

REFERENCES

Cosenza, E. et al. 1990. An evaluation of the use of damage functional in earthquake-resistant design. *Proc. 9th Eur. Conf Earthquake Engineering*: 303–312. Moscow.

GBJ50011-2010 2010. *Code for Seismic Design of Buildings*. Beijing: China Architecture and Building Press. (In Chinese).

Hu, Y. 2006. *Earthquake Engineering* (Second Edition). Beijing: Seismological Press. (In Chinese).

Park, Y. & Ang, A. H. 1985. Mechanistic Seismic Damage Modes for Reinforced Concrete. *Journal of Structural Engineering. ASCE*. 111(4):722~739.

Shen, P. 2010. *Design and Construction of Special-Shaped Column Structure*. Beijing: China Mechanical Industry. (In Chinese).

Yan, S. 2007. *Understanding and Application of Technical Specification for Concrete Structures with Specially Shaped Columns*. Beijing: China Architecture and Building Press. (In Chinese).

Ye L.P. & Otani S. 1999. Maximum seismic displacement of inelastic system based on energy concept. *Earthquake Engineering & Structural Dynamics*. 28: 1483–1499.

Zhang, X. 2002. *Nonlinear Analysis of Reinforced Concrete Aseismatic Structure*. Beijing: Science Press. (In Chinese).

Design and construction of the high-support formwork for NingBo Cultural Plaza Grand Theatre

Yuan Huang, Zhong Qi Dong & Jun Ming Gu
Hebei College of Industry and Technology, Shijiazhuang, China

Lu Jun Liang
Zhejiang Provincial Erjian Construction Group Co., Ltd., Ningbo, China

ABSTRACT: The project of NingBo Cultural Plaza Grand Theatre adopts the fastener type high modulus construction technology. This engineering safety conditions high, difficult construction. Combining NingBo Cultural Plaza Grand Theatre, the paper discussed the high-support formwork calculation, including construction safety, construction technology etc.

Keywords: high-support formwork calculation; construction technology; templates support system

1 SUMMARY OF PROJECT

The project is located in the middle of Central Corridor the Eastern District of Ningbo City. The east side is HeQing Road, north side is NingChuan Road, west side is the third tender of cultural square, and the south side beyond the HouTang River. The total construction area is 70458 m² where the basement one and local three takes 24073 m². The ground floor is divided into 1# cinema and 2# cinema separately with 46385 m² which the 1# cinema has a construction area of 22952 m² with five floors and 2# has 23433 m² with 4 floors and local 5 floors. This project's building structure is frame structure, the security level is secondary and the foundation design level is A. When doing this project, it will multi-use the tall formwork, which girder frame body is 6.35 m with maximum height and no floor connected. There is one overweight beam with the cross section of 800*3350 ~ 4160 mm, the span of the beam is 19.8 meters, and the surface of beam is 35.28 ~ 35.60 m. The pole base is 150 mm thick reinforced concrete slab, and the height of board is 0.8 m. This 800*3350 ~ 4160 mm fastener type steel tube scaffold include in the tall special project template.

2 HIGH MODULUS SYSTEM CHOICE

The template support system utilize $\Phi 48 \times 3.5$ mm fastener type Q235A full house scaffolding, and at the top of the worksite is adjustable on the loan and at bottom use steel base which through adjusting

the drag to adjust the height of template support. Column side beam bottom and bottom template use 18 mm plywood and the support material use 50 mm*80 mm wood square.

2.1 Design of the formwork system

The beam size is 800 mm*4160 mm, the side of template is using the nine plywood, keelson is using the wood square of 50 mm*70 mm, and the outer keel is using double steel pipe with 48 mm*3.5 mm which connected by the screw of diameter of 12 mm. The horizontal spacing of the screw is 500 mm and vertical screw spacing is not more than 450 mm, all of the first line of the screw from the bottom is 200 mm, keelson wood square of the distance is 250 mm uniformly. By analyzing the most unfavorable side form as the sides form for the high beam side which side is 800 mm*4160 mm, then it can be used to calculate its bearing capacity. The beamform support system construction is shown in Figure 1.

2.2 Basic parameters of beam side

Calculation of section width 800 mm, height 4160 mm, both sides of the floor thickness 0 mm. Stencil Palette use general use plywood. Inner keel spacing is 250 mm. Inner keel use the plank which size is 50*70 mm. Outer keel use steel pipe which size is 48 mm *3.2 mm. The bolts arrange 10. The section ranges 200 mm + 400 mm + 400 mm + 400 mm + 400 mm + 400 mm + 450 mm + 450 mm. Section span direction spaces

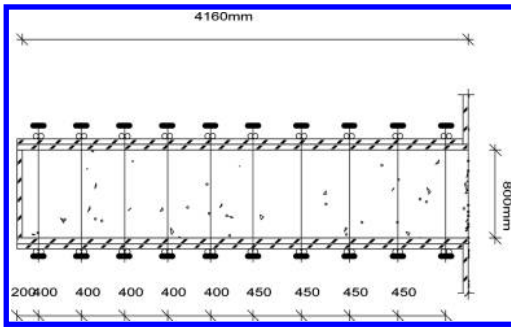


Figure 1. The practice of beamform support system construction.

500 mm, diameter is 12 mm, panel depth is 15 mm, shear strength is 1.4 N/mm², bending strength is 15.0 N/mm², modulus of elasticity is 6000.0 N/mm². The shear strength of wood is 3 N/mm², bending strength is 13.0 N/mm², modulus of elasticity is 9000.0 N/mm².

2.3 Standard calculation of template loading beam side

The strength calculation need consider the lateral pressure of new pouring concrete and the load design value when dumping the concrete. The deflection calculation only considers the load standard value of lateral stress of new pouring concrete. The formula to calculate of the lateral stress of new pouring concrete is the minimum value:

$$F = 0.22\gamma_c t \beta_1 \beta_2 \sqrt{V} \quad F = \gamma_c H \quad F = \gamma_c H \beta_2$$

Among them, γ_c is the gravity and density of concrete that is 24.000 kN/m³. t is the initial setting time of new concrete. When it equals 0, then pick up $200/(T+15)$ and 5.000 h. T is the concrete's temperature when into the mold which is 298 K. V is the pouring speed of concrete that pick 1.200 m/h. H is the total height between the position to calculate the lateral pressure and the top side of the new concrete that is 4.160 m. β_1 is the correction coefficient of additive which is 1.000 and β_2 is the correction coefficient of concrete slump which is 1.150. By the calculation of formula, the side pressure standard value of new pouring concrete is $F_1 = 33.250$ kN/m². The important coefficient of structure is 0.9, and then in the real calculation it usually use the side pressure standard value of the new pouring concrete $F = 0.9 \times 33.260 = 29.934$ kN/m². With the important coefficient of structure, the load standard value when pouring concrete is $F_2 = 0.9 \times 4.000 = 3.600$ kN/m².

2.4 The calculation of the panel of beam side template

The panel is flexural structure which need check its bending strength and stiffness. The template panel need follow simply supported beam to calculate, and the width of panel is 0.25. The calculated value of load $q = 1.2 \times 29.934 \times 0.250 + 1.40 \times 3.600 \times 0.250 = 10.240$ kN/m as is the Figure 2.

In this example, the cross section moment of inertia I and sectional resistance moment are separately $W = 25.00 \times 1.50 \times 1.50 / 6 = 9.38$ cm³ and $I = 25.00 \times 1.50 \times 1.50 \times 1.50 / 12 = 7.03$ cm⁴.

The calculation of deformation need use static load standard value by the specific requirements. As Figure 5 and 6:

After the calculation, the bearing forces from left to right are separately:

$N_1 = 1.024$ Kn; $N_2 = 2.816$ Kn; $N_3 = 2.816$ kN; $N_4 = 1.024$ Kn. The maximum bending moment $M = 0.064$ kN·m (as Fig. 3) and the maximum dysmorphosis $V = 0.469$ mm.

1. Calculation procedure for bending strength.

The panel bending strength calculated values: $F = M/W = 0.064 \times 106/9375 = 6.827$ N/mm²; Calculated bending strength panel $[f]$, equal 15.00 N/mm². If Flexural strength checking calculation $f < [f]$, correct.

2. Shear calculation [dispensable]. Shear strength calculation section $T = 3Q/2bh = 3 \times 1536 / (2 \times 250 \times 15) = 0.614$ N/mm²; strength design value of shear $[T] = 1.40$ N/mm². If shear strength checking calculation T , correct.

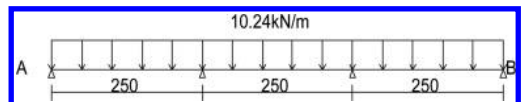


Figure 2. The calculated value of load.

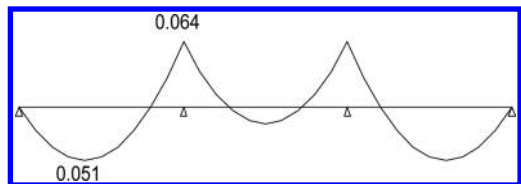


Figure 3. The bending moment diagram.

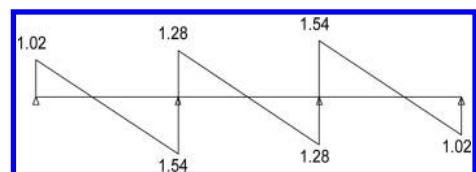


Figure 4. The shear diagram.

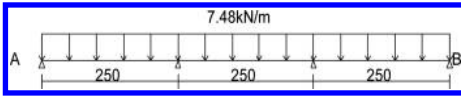


Figure 5. The deformation calculation diagram.

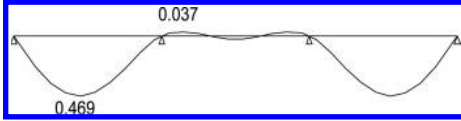


Figure 6. The deformation pattern.

3. Deflection calculation. The maximum deflection of the panel $v = 0.469$ mm. If the maximum deflection of the panel less than $[v] = l/250 = 250/250 = 1.0$ mm, correct.

2.5 Calculation of the beam side keelson

The keels load transfer directly template, calculated in accordance with uniform load continuous beam usually.

Calculation of uniformly distributed load keelson strength $q = 1.2 \times 0.25 \times 29.93 + 1.4 \times 0.25 \times 3.60 = 10.240$ kN/m. Deflection calculation of beam side keelson $q = 0.25 \times 29.93 = 7.484$ kN/m. As shown in Figures 7, 8, 9 and 10.

Deformation is calculated by static load standard value according to the requirement of standard, force diagram and calculation shown in Figure 11.

The maximum bending moment after calculation $M = 0.204$ kN · m (Fig. 12); the maximum support after calculation $F = 4.761$ kN; the maximum Deformation after calculation $V = 0.109$ mm, moment of inertia I and sectional resistance moment w are: $W = 5.00 \times 7.00 \times 7.00/6 = 40.83$ cm³, $I = 5.00 \times 7.00 \times 7.00 \times 7.00/12 = 142.92$ cm⁴.

The internal keel bending strength is calculation. Calculation of bending strength: $F = 3 \times 2422 / (2 \times 50 \times 70) = 1.038$ N/mm². If the numerical less than 13, is correct. Shear calculation of the beam side keelson (dispensable). Shear strength must meet: $T = 3Q/2bh < [T]$; the calculation value $T = 3 \times 2422$; the design value $[T] = 1.30$ N/mm²; the result is correct. The beam side keelson is deflection calculation. The maximum deformation value $v = 0.109$. If the maximum deformation value of the beam side keelson less than $[v] = l/250$, correct.

2.6 Calculation of outer keel

The outer keel load transfer inner keel, according to the calculation of continuous beams under concentrated load (Fig. 12). Calculation of the outer keel load follows the concentrated load. Point load P value the horizontal support pipe transfer force.

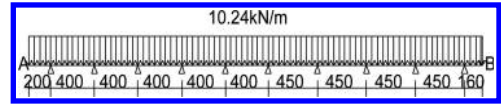


Figure 7. The calculation diagram keelson.

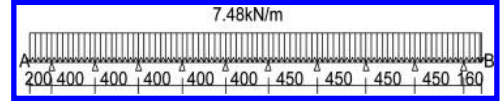


Figure 8. The calculation of deformation to the keel.

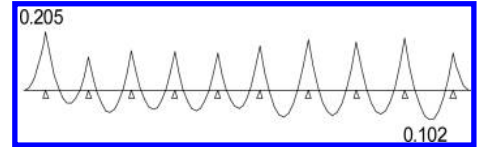


Figure 9. The keelson bending moment diagram.

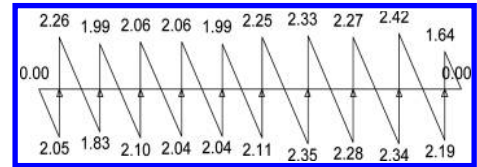


Figure 10. The keelson shear diagram.

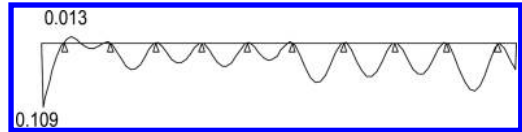


Figure 11. The deformation of the keelson.

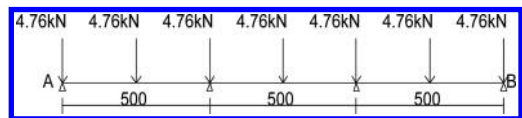


Figure 12. Calculation diagram of supporting pipe.

The calculation of deformation need use static load standard value by the specific requirements.

After the serial calculation, the maximum bending moment $M_{max} = 0.416$ kN · m (Fig. 13). The biggest deformation $V_{max} = 0.108$ mm and the largest bearing force $Q_{max} = 10.237$ kN. The intensity of the bending calculation: $f = M/W = 0.416 \times 106/9458000.0 = 43.98$ N/mm².

The intensity of the bending calculation to support the steel tube is less than 205.0 N/mm² that can satisfy the requirements. The maximum deflection to support the steel tube is less than $[v] = 500/150 = 250/250 = 3.33$ mm that can satisfy the requirements.

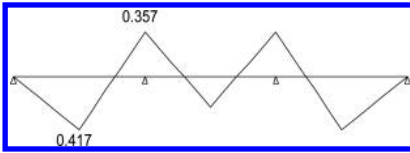


Figure 13. The supporting steel tube bending moment diagram.

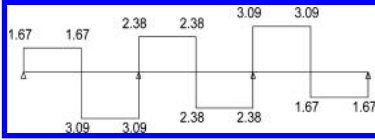


Figure 14. The supporting steel tube shear diagram.

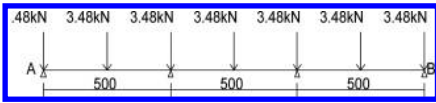


Figure 15. Calculation of deformation of the support tube.

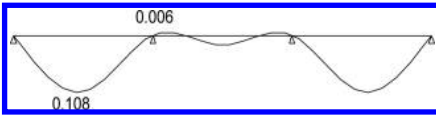


Figure 16. Deformation of the supporting steel tube.

4 SAFETY TECHNICAL MEASURES OF HIGH SUPPORT FORMWORK

1. Workers of high template support should have the appropriate operating licenses for employment. Construction workers and technical directors should provide a safety technology declaration to all the construction teams before construction. Workers should set up high template support strictly in accordance with program requirements.
2. Detect steel tubes and fasteners before entering the site; furthermore, provide an examining report to supervisors for inspection to ensure the quality of steel tubes and fasteners to meet the requirements. Prohibit the use of significant deformation, cracks and severe corrosion of steel fasteners.
3. When build or remove the templates, unrelated persons are not allowed to access the templates, moreover, warning signs should be hung in place and specialized workers need to be arranged there for safety.
4. Links of nodes must be tightened, tightening torque of fasteners should between $40 \text{ N} \cdot \text{M}$ to $60 \text{ N} \cdot \text{M}$, representative node samplings should be selected when taking a spot check.
5. When high template building or removing, steel banding, concrete pouring; In order to avoid focus stacking of materials, equipments and

tools, the load capacity of template columns shall not exceed the designed load value at any circumstances. All materials, equipments and tools need to put to the appropriate locations when construction is completed.

6. Project department should organize construction workers, quality inspectors and safety officers and project directors to give a Comprehensive inspection and acceptance corporate with Supervision Department before pouring concrete. Once reached the requirements, project could carry on.
7. In the process of concrete pouring, slump of concrete should be strictly controlled; concrete pouring plan should be elaborately designed, which will influence the loading balance of those templates.
8. In the process of pouring concrete, specialized workers are needed to keep close watch in the site, once subsidence, looseness or deformation happened; stop pouring immediately and reinforcement measures need to be taken.
9. Concrete strength of those template need to meet the requirements of "Concrete Construction Quality Acceptance" GB50204-2002, and demolition approval procedures must be applied before removal, strictly compliance with the principles of removing from the top to the bottom, non-load-bearing templates shall be removed firstly, template fling is forbidden.

5 CONCLUSION

The template support system of fasteners and steel tube erection, construction requirements could meet by calculation and checking, on the basis of the erection plan and structural measures, the structural layer construction task could be completed successfully without any security incidents or accidents of structural quality.

ACKNOWLEDGEMENTS

This work was financially supported by the Hebei college of industry and technology (BZ1001) and study on unsaturated $12\text{CaO} \cdot 7\text{Al}_2\text{O}_3$ crystal structure, the Hebei college of industry and technology (ZZ-1301). Correspondding author is Associate Professor Dong Zhongqi.

REFERENCES

- [1] Safety Specifications of Steel Tubular Scaffold of Construction, JGJ162-2008.
- [2] Technical Regulations of Steel Tubular Scaffold Template of Construction, BD33/1035-2006.
- [3] Specification of Concrete Structures Design, GB50010-2010.

Analysis of the settlement of CFG pile composite foundation

Liang Xie & Bin Tang

Wuhan University of Science and Technology, Wuhan, Hubei, China

ABSTRACT: As a technology of foundation treatment, the application of CFG pile composite foundation is very broad in recent years. This paper describes the CFG pile composite foundation settlement characteristics and mechanism of action, summarizes and analyzes the influence factors of its settlement. Cushion, pile length, influence of pile on the deformation of soil between piles, and area displacement ratio have relatively large impact on settlement, the analysis of the settlement of CFG pile composite foundation in this paper has a certain reference value for practical design of composite foundation.

Keywords: CFG pile; composite foundation; settlement

1 INTRODUCTION

With the rapid development of the domestic economy as well as the need for opening to the outside world, mass transport facilities and a variety of building continuously constructed, accompanied by a variety of complex engineering geological conditions, including the unfavorable geological conditions which is one of the major causes of accident. In order to meet the needs of construction, we must carry on foundation treatment of the natural ground. CFG pile (Cement Fly-ash Gravel pile) composite foundation was developed in 1985 by the foundations research institute of China Academy of building research, which is currently extended and applied to nearly 20 provinces and regions of the country^[1]. Because of its low cost, short construction period, great reinforcing effect, outstanding economic benefits, it has received more and more attention by the engineering in recent years.

2 ACTION MECHANISM OF CFG PILE COMPOSITE FOUNDATION

As shown in Figure 1, CFG pile composite foundation is made up by cushion, CFG piles and soil between piles, belongs to the rigid pile composite foundation. The mechanisms of reinforcement mainly are: cushion effect, piles effect and compaction effect.

Under the load of upper structure and foundation, settlement occurred in both piles and soil between piles, the CFG piles as high bond strength piles, their modulus are bigger than the modulus of the soil, so the settlement of piles is smaller, then the load gradually concentrated on top of the piles^[2]. As a result, a layer of cushion is laid between foundation

and piles, soil, which transmits the pressure from the basis (or horizontal force) to the piles and the soil, and adjusts the relative displacement between piles and soil in order to make them work together.

3 THE SETTLEMENT CHARACTERISTICS OF CFG PILE COMPOSITE FOUNDATION

3.1 The transfer characteristics of the load

The differences between pile composite foundation and pile foundation, mainly is the conditions modification of pile stress, and the foundation load will be assigned to the piles and soil through the cushion. Under the load, the pile body pricks to the cushion, and the cushion materials also constantly fill to the soil between piles, then the soil will undertake quite large part of the load all along, fully reflects the characteristic of composite foundation which the base and the reinforcement bodies work together^[3].

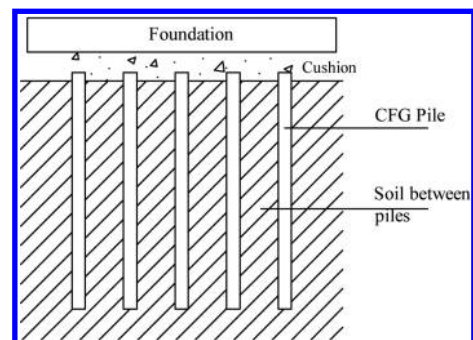


Figure 1. CFG pile composite foundation.

In CFG pile composite foundation, as the modulus of the piles and the soil between piles are different, under the corresponding load, the settlement of the bottom of basis, the head of pile and the soil are all different. When the pile settlement is bigger compared with the soil, which means that the pile has the upward relative displacement, at this time, the soil around the pile can have upward friction to the pile body surface, which called positive friction. But when the soil settlement surpasses the pile settlement, the soil will have the downward friction to the pile body surface, called negative friction. The pile body dividing line place is a neutral point, as shown in Figure 2, in depth Z_0 place is the neutral point. The boundary point of positive and negative friction of the pile is a neutral point, as shown in Figure 2, in depth Z_0 place is the neutral point. When the depth $Z < Z_0$, the soil settlement is bigger than the pile settlement, the soil will have negative friction to the pile body surface, that means the pile axial stress increases along with the depth in the Z_0 scope; On the contrary, when the depth $Z > Z_0$, the soil will have positive friction to the pile, the pile axial stress decreases along with the depth, so the maximum axial stress is in the neutral point.

3.2 Settlement mechanism

Compared to the piles, due to the addition of cushion of pile composite foundation, makes the settlement more complex, as shown in Figure 3 which is the settlement diagrams of CFG pile composite foundation. Figure 3a for before they are loaded, that is the deformation when $P = 0$. After loading, $P > 0$, the settlement quantity of the surface of the soil between piles is S_s , the settlement

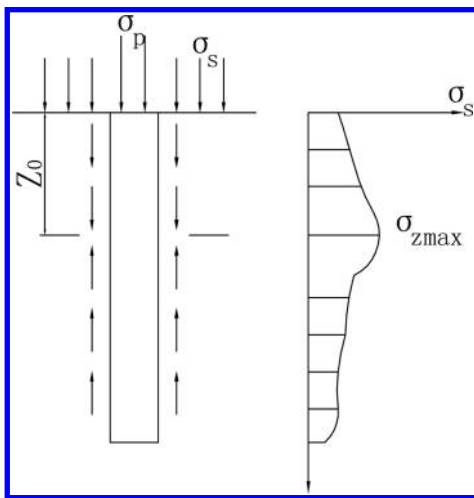


Figure 2. Variation of CFG pile axial force with depth.

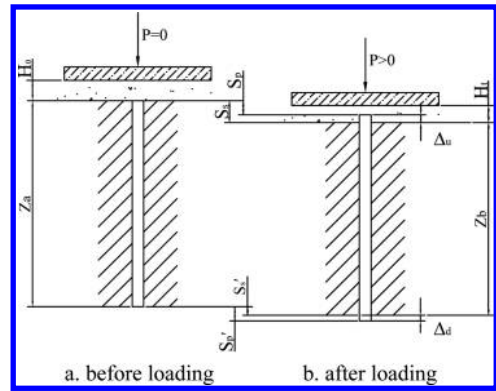


Figure 3. The settlement of CFG pile composite foundation.

quantity of the head of pile is S_p , the soil of the end of pile occurs settlement S_p' , and the settlement quantity of the end of pile is S_p' . Due to a high modulus of CFG pile, under normal load, the axial deformation of the pile is negligible, that means $S_p = S_p'$. As shown in Figure 3b.

The upward pricking quantity of the head of pile is $\Delta_u = S_s - S_p$;

The downward pricking quantity of the end of pile is $\Delta_d = S_p' - S_s'$;

So, the soil deformation quantity in the pile length range is $S_1 = \Delta_u + \Delta_d$;

Deformation of the subjacent bed of the composite foundation is S_2 ;

Deformation of the cushion is $S_3 = H_0 - H_1$, H_0 , H_1 is the thickness of cushion before and after loading;

So, total settlement of the bottom of basis is $S = S_1 + S_2 + S_3$, which is composed of three parts:

- ① the soil deformation in the pile length range;
- ② the deformation of the subjacent bed;
- ③ the deformation of cushion^[4].

4 INFLUENCE FACTORS OF SETTLEMENT OF CFG PILE COMPOSITE FOUNDATION

4.1 Influence of cushion on settlement

The cushion mainly has three aspect functions: ① to ensure soil-pile interaction; ② to adjust the sharing ratio of load or horizontal force between piles and soil; ③ to prevent excessive stress at the bottom of the basis. Influence of cushion on settlement mainly shows on the modulus and thickness of cushion.

In the case of certain thickness and the same load, the variation of the modulus of cushion which influence on settlement is relatively significant, and mainly shown through the influence of the side

friction of pile and pile-soil stress^[5]. This will affect the soil deformation in the pile length range S_1 and the deformation of the subjacent bed of the composite foundation S_2 , which will have an impact on the total settlement. When cushion modulus decreases, the ratio of pile-soil stress decreases, the effect of pile-soil increases, at the same time the length of the friction area also increases, thereby increases the total amount of settlement. Therefore, in order to make cushion play its role in spreading concentrated stress, the cushion modulus must be above a certain value.

When the thickness of cushion is different, the influence on settlement mainly shown by the assignment of load of the pile. When cushion thickness is too small, the stress will significantly concentrates on the head of CFG pile, which needs to thicker design size of the base, and increase the length and number of CFG piles; However, when the thickness of cushion is too large, the soil between piles shares too much load, then the load shared by piles decreases, the settlement of foundation increases, but the bearing capacity of composite foundation has not been significantly improved. Therefore, in the application of CFG pile composite foundation, the thickness of cushion should be paid attention to adjust, so as to alleviate the inhomogeneity of foundation, and make the composite foundation deformation in coordination, generally is 10~30 cm thick.

4.2 Influence of pile length on the settlement

CFG pile length, that is, the reinforcing layer thickness of CFG pile composite foundation, which plays an important role on the settlement of composite foundation. Along with the pile length changes, under the same conditions of loading, the sharing ratio of load between piles and soil varies as well^[6]. When the pile length decreases, the sharing-load of the soil between piles increases relatively. But when the load on the soil increases, its deformation will also increase, which means the soil deformation in the pile length range S_1 increases as well, thereby the total settlement S will increase. On the contrary, when the pile length increases, the sharing-load of the soil between piles decreases relatively, its deformation also decreases, which means S_1 will decrease and the total settlement S will decrease.

The variation of the pile length, which will have a certain impact on Δ_u and Δ_d , when other conditions are certain, the longer the pile, the smaller the Δ_u and Δ_d , and the soil deformation quantity in the pile length range S_1 will decrease; conversely, the pile length decreases, Δ_u , Δ_d and S_1 will increase.

In general, when other conditions are certain, along with the pile length increases, the total settlement will reduce. When the pile is short, the settlement is very large, this time increasing the pile length to reduce the settlement will be

remarkable; when the pile is long enough, as the pile length increases, while the settlement can be further reduced, but the effect is not great; when the pile length increases to a certain degree, the pile side friction and the load of the head of pile are approximate into linear relationship, it has little to do with the pile length itself, settlement tends to be stable, the increase of the pile length can nearly no longer cause the further settlement. In the process of the engineering applications, in accordance with the principle which to control the settlement of composite foundation in the allowable deformation value, design the pile length reasonably, so as to avoid the use of the piles which are too long or too short, in order to achieve the goal that economical use, avoiding construction difficult.

4.3 Influence of pile on the deformation of soil between piles

The CFG pile comes from gravel pile, just puts cement, fly ash and other adhesive materials into the gravel pile, then the pile becomes a whole, its side friction is much bigger than the ordinary steel pile and the precast concrete pile. In the CFG pile composite foundation, the existence of the pile has restrained the deformation of the soil between piles, reduces the deformation of the soil.

Before the destruction of the pile, the load of the head of pile transmits to the soil between piles and the subjacent bed through bearing force from the end of pile and the pile side friction, as a result of the establishment of the cushion, under the load, the stress concentrates on the top of the pile, the pile body pricks upward into the cushion, the relative displacement will occur between the pile and the soil, then the negative friction appears in the certain depth scope of the pile body, resulting in a plane of equal settlement of the pile and the soil. When the depth $Z < Z_0$, namely in the negative friction area, at this time, the soil has the downward migration compared with the pile, then the soil will have the negative friction on the pile, the settlement of the soil limited, thereby the total settlement S affected.

When the upper load P is small, the pile friction plays a major role, the bearing force from the end of pile play less relatively, the overall effect is to make the deformation of the soil decrease; contrarily, when the upper load P is large, the pile friction plays a secondary role, the deformation of the soil increases^[7]. In addition, because a portion of the pile load is passed directly to the underlying layer of the pile, the compression deformation of the subjacent bed will be greater than the natural foundation deformation at the same depth. In conclusion, the influence of pile on the soil between piles has a great impact on the settlement of the CFG pile foundation.

4.4 Influence of the area displacement ratio

In the pile composite foundation, one pile and the soil which the pile undertakes assumed as a compound unit. In the compound unit, the ratio of the sectional area of pile to the area of the compound soil unit, called area displacement ratio, namely the area displacement ratio is $m = A_p/A$, A_p is the sectional area of the pile; A is the area of the compound soil unit. It can also be defined as $m = d^2/d_e^2$, d is the average diameter of pile, d_e is the diameter of the equivalent circle which is the foundation area shared by one pile.

Area displacement ratio can be changed by changing the size of the cushion cap and the diameter of pile, reduces the size of the cushion cap or increases the pile diameter, the pile and the soil between piles both will decrease, but there is a certain degree of difference of the influence on the settlement between the two, the impact on settlement of reducing the size of the cushion cap will be much greater than the impact of increasing diameter. Reduce the size of the cushion cap, which is equivalent to reduce the total load, so the decrease of the settlement is greater. Therefore, when changing the area displacement ratio, reducing the size of the cushion cap (such as increasing the number of piles under the cap, which is equivalent to decrease the radius of cushion cap of the single pile), is more effective to control the settlement deformation than increasing the pile diameter.

Area replacement ratio is an important parameter of the design of composite foundation, when the pile length is certain, while the area displacement ratio changes, the change of additional stress of the composite foundation along with the depth is consistent, the additional stress decreases sharply in the reinforcement area; At the border of the reinforcement layer and the subjacent bed, the diffusion degree of the additional stress increases, but the rate of increase is small; In the subjacent bed, the additional stress decreases along with the increase of the area displacement ratio, and the rate of decrease is small^[8]. However, it is important to note that, when the replacement ratio keeps in a certain range, along with the increase of the replacement ratio, the settlement of the reinforcement area and the total settlement are great; but when the ratio is beyond a certain value, the decrease of the settlement will not be obvious. In the design process, there is an optimal replacement ratio, which can make the pile composite foundation play with a maximum of efficiency to restrict settlement.

5 CONCLUSION AND PROSPECTS

This paper starts from the action mechanism of CFG pile composite foundation, explains the settlement characteristics of CFG pile composite foundation,

and makes the further analysis of the main influence factors of settlement. The pile composite foundation has the working properties of both natural foundation and pile foundation at the same time, but it also has the clear distinction with the two. Pile composite foundation under vertical loads, the piles and soil undertake the loads together, but the settlement of the bottom of basis, piles and soil between piles are all different, this shows that the complexity of the pile composite foundation settlement.

We need to be aware of the fact that the seepage consolidation caused by groundwater also affects the final settlement of the composite foundation, but at present the research of the composite foundation settlement is rarely associated with the groundwater impact, and the most corresponding settlement calculation formulas also ignore the problem, which requires the further research. What's more, in composite foundation design, the optimized design through dual control of the bearing capacity and settlement, that is a very complex calculation model, there is no sound theoretical knowledge yet, and its stability and versatility require esoteric mathematical knowledge to calculate, large finite element software to simulate, it also need to be test in the practical engineering.

ACKNOWLEDGEMENTS

This work was financially supported by Natural science fund of China (41372299).

REFERENCES

- [1] Gao Junzhao, et al. 2007. Analysis of bearing capacity of the composite foundation of CFG, *Hydrogeology & Engineering Geology* 04:31–35.
- [2] Zeng Qiao. 2013. Design calculation and engineering application of CFG pile composite foundation, Chongqing: Chongqing Jiaotong University.
- [3] Gao Junzhao & Gao Pu. 2007. Current research and prospect of the composite foundation of CFG, *Journal of Xuchang University*, 2007, 26(5): 118–119.
- [4] Zhu Ruijun, et al. 2007. Settlement of CFG pile composite foundation in silt soil region, *Journal of University of Science and Technology* 29(4): 363.
- [5] Wang Zhongshi, et al. 2007. Influence of cushion on the settlement of CFG pile composite foundation, *Geotechnical engineering world* 11(5): 31–32.
- [6] Pan Xing. 2005. Discussion on the settlement calculation of CFG pile composite foundation, *Rock and Soil Mechanics* 26: 248–249.
- [7] Jia Xuejun & Jiang Xiaodong. 2006. Calculation of Settlement and Deformation Monitoring of CFG Piles Composite Foundation, *Construction Technology* 35(6): 54.
- [8] Liu Zhifeng, et al. 2001. The effect of area replacement ratio and pile length on the stress and deformation of composite foundation, *Industrial Construction* 31(11): 18–19.

Test of surface free energy of asphalt by digital image processing

Qin Xue Pan & Xu Dong Zha

Changsha University of Science and Technology, Changsha, China

Wu Chen

Planning and Design Institute of Hubei Province, Wuhan, China

Bo Yang

Changsha University of Science and Technology, Changsha, China

ABSTRACT: In order to reasonably evaluate the adhesion of asphalt, test method of asphalt surface free energy with digital image processing technology is proposed on the basis of the test principles on surface free energy. Then the contact angles between 6 kinds of asphalt and three different liquid were comparatively tested as the method. The results show that the tested data are small in variability. There are very good linear correlations between the contact angles and the surface free energy. This shows that testing contact angles by using the method of digital image processing have a good repeatability, and the test data are reliable and effective. Therefore, it is a fast and feasible method that is used to test the contact angles among asphalt of droplet and then get surface free energy.

Keywords: asphalt; surface free energy; digital image processing; contact angle; ellipse fitting

1 INTRODUCTION

At present, a lot of research on surface free energy of asphalt and aggregate have been made at home and abroad, such as Elphinstone, Cheng, Bhasin^[1-3] etc, which show that using the surface free energy theory can well predict the properties of the mixture on anti-water damage and fatigue. Therefore, it is of great significance to develop a rapid, accurate and reasonable test methods to asphalt surface free energy for studying on performance of asphalt and asphalt mixture especially in providing the rational basis for anti-water damage ability of asphalt surface. Method for determination of the contact angles are more, however, which have their limitations. Such as the contact angles tested by capillary rise method^[4] is between toluene-asphalt solution and mineral aggregate, which deviate from real situation. There is a big error in the results on the height of liquid and time measured by people; What tested by Wilhelmy hanging slice method^[5-12] is a dynamic contact angle, and its equipment cost is high. Therefore, this article will use the image processing method for determining the contact angles between asphalt and the droplet, which is a recommended method for its accurate determination, reliable data and low cost.

2 SURFACE FREE ENERGY OF ASPHALT TESTING BASIC PRINCIPLE

Surface free energy is defined as the work consumed in separating solid or liquid in the vacuum to create a new interface. Surface tension is a vector, equal value to surface free energy, whose direction is tangent with the liquid surface, and line perpendicular to the separatrix between any two parts in liquid surface. Because of asphalt being a visco-elastic-plastic body at room temperature, only picture at room temperature in experiments, don't consider the viscoplasticity of asphalt, and can be regarded approximately as solid. According to the theory of Fowkes, it below can be gotten by expanding Young Equation as follows:

$$1 + \cos \theta = 2\sqrt{\gamma_s^d} \frac{\sqrt{\gamma_l^d}}{\gamma_l} + 2\sqrt{\gamma_s^p} \frac{\sqrt{\gamma_l^p}}{\gamma_l} \quad (1)$$

In Formula (1): θ is contact angle ($^\circ$); γ_s is solid surface free energy (mJ/m^2); γ_l is liquid surface free energy (mJ/m^2); γ_s^d is dispersion component of solid surface free energy (mJ/m^2); γ_s^p is polar component of solid surface free energy (acid-alkali force) (mJ/m^2); γ_l^d is dispersion component of liquid surface free energy (mJ/m^2); γ_l^p is polar component of liquid surface free energy (mJ/m^2).

According to Formula (1), solid surface free energy and its components can be calculated by the contact angles and the corresponding surface tension of liquid. Then using Young Equation

$$\gamma_l \cos \theta = \gamma_s - \gamma_{sl} \quad (2)$$

to verify the validity of the data: for a given solid, there is linear relationship between $\gamma_l \cos \theta$ and γ_l of different liquid, otherwise, it means that the test data exist errors or variability and need to be tested anew. It can be known from the above that calculating asphalt surface free energy needs the contact angle between asphalt and droplet and surface tension of the corresponding liquid. As a result, the contact angles between asphalt and droplet should be measured at first.

3 SURFACE FREE ENERGY OF ASPHALT TESTING BASIC PRINCIPLE

According to the principle of digital image processing and the measurement requirements of asphalt—droplet contact angles, this paper put forward the analysis process on contact angles by digital image processing including image acquisition and cutting, image format conversion, image enhancement, image segmentation and binarization, boundary ellipse fitting, contact angles calculation. Analysis process is shown in Figure 1.

3.1 Image acquisition and cutting

In the preparation of asphalt sample, choose a slide glass standard 76.2 mm long and 25.4 mm wide as a base plate. First the base plate was placed on the heater, temperature was maintained at around 60°C, then heated asphalt to 160°C, holding the base plate with clip in the asphalt to infiltrate, and then removed unnecessary asphalt, make it a smooth surface. when asphalt sample

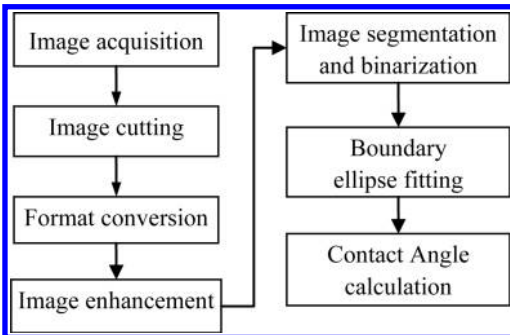


Figure 1. Contact angles analysis process by digital image processing.

prepared cool to room temperature, placing it in the dryer for 6 hours for next test. When shooting by digital camera, adjusted the camera height through tripod, and it must be the orthographic projection. Dropping the droplets, to ensure start filming after it has dropped 2 s lest droplet shape has been affected by time. Figure 2 is the asphalt—droplets image.

3.2 Image enhancement and smoothing processing

The image cut will be converted to a grayscale image (as shown in Fig. 3a), then took the gray balance at it, to transform it into uniform distribution forms, so as to enhanced the overall image contrast and highlighted the details of the original image. And then adopted smoothing processing in the method of median filter on the image to suppress, weaken or eliminate details, mutants, edges in it and noise interference (as shown in Fig. 3b).

3.3 Image cutting

Edge is a sideline made up with pixel point of grayscale or color changing greatly in the image. Usually the boundary of different parts of the object or object in the image were determined by edge detection. In the article, we would make edge detection at binary image according to Canny edge operator theory, whose result is shown in Figure 4.

3.4 Image boundary fitting

According to the actual shape of the droplets and extract the boundary of the graphics, it is proposed to two assumptions while fitting boundary:

1. The shape of the droplet is a part of elliptical spherical, droplet is vertically symmetrical in the



Figure 2. Asphalt—droplets image.

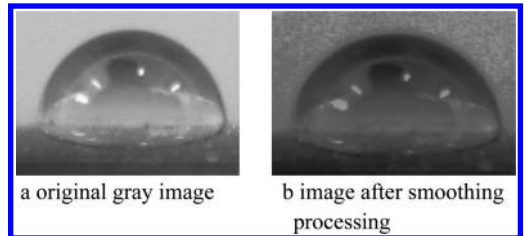


Figure 3. Comparison diagram of droplet processed before and after.



Figure 4. Droplet boundary detected in Canny method.

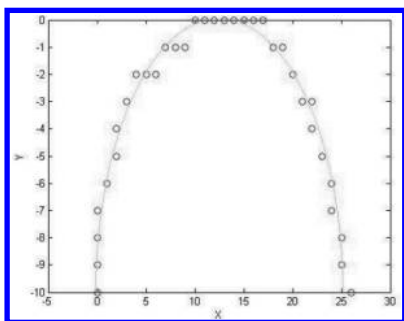


Figure 5. Example for ellipse boundary fitting.

middle, which indicate that the droplet are the same from any angle to observe.

2. The shape of the drop is only related to its grav-ity and interfacial tension.

Ellipse fitting is to define the fitting in an area but not on the whole number axis, however, the ordinary least squares method can't meet the requirements, therefore improved least-square method is adopted to fit the ellipse. Letbe the general formula of elliptical is:

$$F(x, y) = ax^2 + bxy + cy^2 + dx + ey + f \quad (3)$$

$$A = [a \ b \ c \ d \ e \ f]^T \quad (4)$$

The coefficient of elliptic parameter equation can be obtained by programming based on the improved algorithm, and then draw the ellipse fitting curve. Figure 5 is the example for elliptic curve fitting, small circles representing pixels on the asphalt—droplet boundary, coefficient of elliptic parameter equation $A = [0.53255 \ -0.0029613 \ 0.84639 \ -13.312 \ -16.86 \ 82.394]^T$.

The contact angles would be solved on the basis of the example on elliptic curve image in Figure 5 and coefficients of elliptic parameter equation. Firstly, solve out the intersection points of elliptic curve with datum plane, to letbe it as (x_1, y_1) , (x_2, y_2) . Then take $F(x, y)$ for x derivation according to the Formula (5):

$$F'_x = -\frac{2ax_0 + by_0 + d}{bx_0 + 2cy_0 + e} \quad (5)$$

In Formula (5): (x_0, y_0) is the coordinates of points, other letters meanings are the same as above.

Slope of two intersection points: $K1 = 196.6120$, $K2 = 210.77$, are obtained by programming according to the example in Figure 5 and the Formula (5). Then, according to their slopes, the angles gotten by the back calculation: $\theta_1 = 89.71^\circ$, $\theta_2 = 89.97^\circ$, which are asphalt—droplet contact angles of the image in above example.

4 TEST RESULTS ANALYSIS

This paper selected five kinds of A-70 road asphalt (Taizhou-Zhonghai, Zhejiang-Donghai, South Korea-SK, South Korea-Caltex, Liaohe-Maoming) and a SK modified asphalt (SBS I-D type) for testing, the liquid tested were distilled water, glycerin and formamide. First, chose 10 clear photos of asphalt—droplet in each kind of asphalt with 3 kinds of liquid selected, then, whose contact angles would be tested in the method above. Table 1 is the three test liquid surface free energy and component values. Table 2 is the value for contact angles and coefficient of variation of the asphalt—droplets. From Table 2, all of variation coefficient of contact angles in test ranged from 0.95% to 1.71%, which shows that it has a good repeatability to use the method of digital image processing to test contact angles.

Table 3 lists the regression formula and related relations between each kind of asphalt's $\gamma \cos \theta$ and their γ , which were shown in Figure 6.

From Table 3 and Figure 6, it can be obtained that the correlation coefficient (R^2) of asphalt selected in test ranged from 0.9833 to 1, which showed that there were good linear relationship between $\gamma \cos \theta$ and γ . Finally, surface free energy and their components of asphalt were calculated out by Formula (1) with the measured contact angles and surface tension of the liquid, which can be seen in Table 4.

Table 1. Surface free energy and component of three test liquid (22 °C).

Liquid	Surface free energy (mJ/m ²)		
	γ	γ^d	γ^p
Distilled water	72.3	18.7	53.6
Glycerin	65.2	28.3	36.9
Formamide	59.0	39.4	19.6

Table 2. Testing results on contact angles and coefficient of variation of the asphalt—droplets.

Asphalt kinds	Distilled water		Glycerin		Formamide	
	Angle (°)	Variation coefficient (%)	Angle (°)	Variation coefficient (%)	Angle (°)	Variation coefficient (%)
Zhonghai	107.2	1.25	95.2	1.54	82.8	1.35
Donghai	108.9	1.71	96.3	1.51	83.6	1.26
SK	103.3	1.46	96.7	1.14	85.2	1.20
Caltex	97.9	1.17	89.2	1.25	81.5	1.48
Maoming	96.8	1.02	87.4	1.24	78.7	1.17
SBS I-D	105.1	0.95	97.1	1.10	88.3	1.18

Table 3. Correlation on $\gamma\cos\theta$ & γ of each asphalt.

Asphalt kinds	Regression formula	Correlation coefficient (R^2)
Zhonghai	$\gamma\cos\theta = -2.1622 \gamma + 135.04$	1.0000
Donghai	$\gamma\cos\theta = -2.2545 \gamma + 139.72$	0.9999
SK	$\gamma\cos\theta = -1.6143 \gamma + 99.364$	0.9833
Caltex	$\gamma\cos\theta = -1.4042 \gamma + 91.956$	0.9974
Maoming	$\gamma\cos\theta = -1.5139 \gamma + 101.20$	0.9980
SBS I-D	$\gamma\cos\theta = -1.5381 \gamma + 92.427$	0.9998

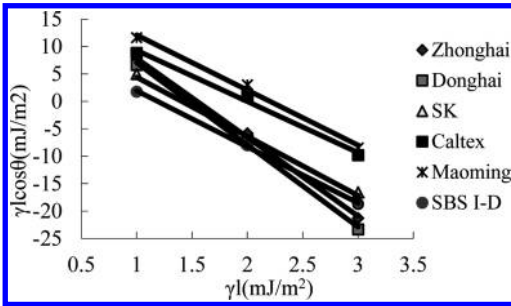


Figure 6. Correlation on surface free energy of asphalt.

Table 4. Surface free energy and their components for asphalt.

Asphalt kinds	Surface free energy (mJ/m ²)		
	γ	γ^d	γ^p
Zhonghai	24.08	23.71	0.37
Donghai	24.56	24.37	0.19
SK	18.09	16.18	1.91
Caltex	20.25	16.85	3.40
Maoming	22.31	19.16	3.15
SBS I-D	16.68	14.78	1.90

5 CONCLUSIONS

In this paper, according to the testing principle of surface free energy, digital image processing technology was used in the research on testing surface free energy of asphalt, which can be mainly obtained the following conclusions:

1. According to the measurement requirements to the contact angles of asphalt—droplet and the basic principle of digital image processing, the testing analysis process on contact angles of asphalt—droplet by digital image processing was put forward. Boundary fitting at asphalt—droplet image was made by improved ellipse fitting algorithm, whose results showed that the algorithm can make very precise fitting at elliptic curve of the droplet, the calculation results being stable, and meeting the requirements of real-time speed, this showed that the algorithm is a reliable, effective and easy-to-use method.
2. The results, using the method of digital image processing to determine the different liquid and the contact angles of asphalt, showed that all variation coefficients of contact angles in test ranged from 0.95% to 1.71%, which showed that testing contact angles by the method of digital image processing has a good repeatability. And the Young Equation is used to test the effectiveness of the data for the asphalt chosen in the test. The variation range on linear correlation coefficient of $\gamma\cos\theta$ & γ was between 0.9833 ~ 1, so as to verify the reliability of the data and the correctness of this test method.

ACKNOWLEDGEMENTS

The authors appreciate the support of Projects of National Natural Science Foundation of China (51078045); Technology Project of Communications Department in Hebei Province

(Y-2010025-9); Projects of Graduate Student Research Innovation Fund in Hunan Province (CX2013B364, CX2013B365).

REFERENCES

- [1] Elphinstone G.M. Adhesion and cohesion in asphalt-aggregate systems [D]. College Station, USA: Texas A&M University, 1997.
- [2] Cheng D. Surface free energy of asphalt-aggregate system and performance analysis of asphalt concrete based on surface free energy [D]. College Station, USA: Texas A&M University, 2002.
- [3] Bhasin A., Masad E., Little D., et al. Limits on adhesive bond energy for improved resistance of hot-mix asphalt to moisture damage [J]. Transportation Research Record, 2006, 1970: 3–13.
- [4] Xiao Qing-yi, Xue Hang, Xu Jin-zhi, etc. Moisture damage model of asphalt mixture based on surface and interface theory [J]. Journal of Wuhan University of Technology, 2007, 29(5): 71–73.
- [5] Zhu She-yao, Zhao Zhen-guo. Fundamental of interface chemistry [M]. Beijing: Chemical Industry Press, 1996.
- [6] Wei Jian-ming, Zhang Yu-zhen, Zhan Yan, et al. Effect of anti-stripping agents on surface free energy of asphalt binders [J]. Journal of China University of Petroleum: Natural Science Edition, 2011, 35(2): 162–165.
- [7] He Xing-hua, Zhou Yuan-yuan. Image Processing of Matlab 7.X [M]. Beijing: Posts and Telecom Press, 2006.
- [8] Pauli A.T., Grimes W., Huang S.C., et al. Surface energy studies of asphalts by AFM [J]. Preprints—American Chemical Society. Division of Fuel Chemistry 2003, 48(1): 14–18.
- [9] Miknis F.P., Pauli A.T., Beemer A., et al. Use of NMR imaging to measure interfacial properties of asphalts [J]. Fuel, 2005, 84(9): 1041–1051.
- [10] Hefer A.W., Bhasin A., Little D.N. Bitumen surface energy characterization using a contact angle approach [J]. Journal of Materials in Civil Engineering, 2006, 18(6): 759–767.
- [11] Jonathan E. Howson, Amit Bhasin, Eyad Masad, et al. Influence of material factors on surface free energy and performance related parameters [A]. Advanced Characterisation of Pavement and Soil Engineering Materials [C]. 2007, Taylor & Francis Group, London, 2007.
- [12] Hefer A.W., Bhasin A., Little D.N. Bitumen surface energy characterization using a contact angle approach [J]. Journal of Materials in Civil Engineering, 2006, 18(6): 759–767.

Experimental research on the flexural behavior of a new type of I shaped prestressed concrete sheet pile

Han Dong Xu, Kun Teng & Xin Jun Fu

Changzhou Architectural Research Institute Co., Ltd., Changzhou, China

Kang Yuan

State Key Laboratory of Mining Disaster Prevention and Control, Shandong University of Science and Technology, Qingdao, China

ABSTRACT: Prestressed concrete sheet pile has been playing more and more important role in pit maintenance by virtue of its special advantages with the increasing of cutting depth of foundation trench in recent years. A new type of I shaped prestressed concrete sheet pile is introduced in this paper, and its flexural behavior and deformation characteristic as well as failure process are analyzed. After the four-point bending test, the cracking bending moment and ultimate bending moment are obtained and these values are consistent with the theoretical calculating value. The research result shows that it has superior flexural bearing capacity and it can satisfy for the requirement of the code. Besides, due to the simpleness in construction craft and low cost, it has a better value for engineering reference and practical significance.

Keywords: prestressed concrete sheet pile; flexural behavior; failure process

1 INTRODUCTION

With the continuous development of economic society, a large number of urban space will be developed and utilized. Consequently, numerous deep foundation pit engineering will come into being. Under the influence of modern ideas such as environmental protection and efficient, traditional supporting pattern has couldn't meet the requirement of economy and environmental protection in engineering construction. Therefore, it should require to research and develop new construction technology and new building materials.

After many years of engineering practices, the prestressed concrete sheet pile shows a lot of advantages such as good quality, high construction speed, low construction costs and environmental protection as well as industrial use production and so on which has been widely used in deep foundation pit supporting and has achieved good effect of engineering. Therefore, it is one of the effective way to develop the prestressed concrete sheet pile in solving the problems in deep foundation pit supporting.

In recent years, Changzhou Architectural Research Institute Co. Ltd developed a new construction method which is called HCMW on the reference of SMW construction method and

prefabricated underground continuous wall. In the HCMW method, the main construction point is the usage of the I shaped prestressed concrete sheet pile whose cross section is shown in Figure 1.

In order to research the pile's mechanical property so as to checkout whether or not it can satisfy the requirement of engineering application, four-point bending test is usually conducted to measure its cracking bending moment and ultimate bending moment^[1-3]. In this paper, the four-point bending tests are conducted using a new type I shaped prestressed concrete sheet pile so as to obtain its flexural behavior index.

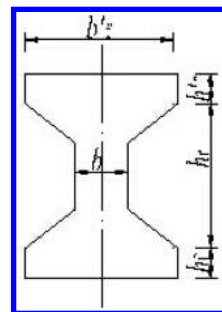


Figure 1. Section of the concrete sheet pile.

2 FOUR-POINT BENDING TEST

The experimental program was conducted on 4 prestressed concrete sheet pile with total length of 9.6 m or 10 m with the dimension of cross section 700 mm × 400 mm and 1000 mm × 400 mm respectively. All the sheet pile specimens are made of C60 concrete, and the bending test is shown in the Figure 2. During the test, the load was applied by multi-stage and the change of the deflection of the sheet piles as well as the change of a load was monitored using displacement-monitoring instrument, as is shown in Figure 3. Besides, the cracking bending moment and the ultimate bending moment are calculated based on the crack load and the ultimate load of the test specimen. In addition, during load increasing, tension damage to the

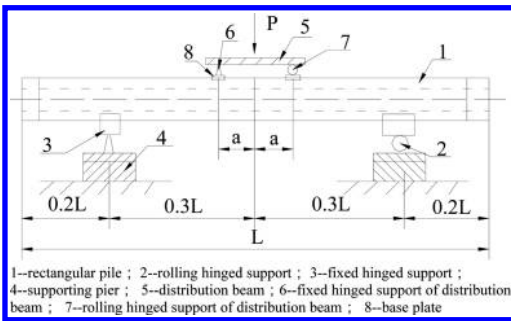


Figure 2. Schematic diagram of four-point bending test.

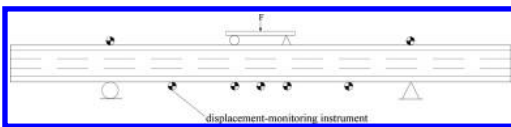


Figure 3. The arrangement of displacement-monitoring instrument during testing.



Figure 4. The device graph of bending test.

bottoms of the sheet piles and crushing damage to the tops of the sheet piles can be caused easily after the sheet piles are bent, cracks of a structure or a component can occur and can also expand, so the positions, distribution, lengths and widths of the cracks are important indicators for reflecting the structural performance, and particularly, for a prestressed concrete structure, it is extremely important to study the crack resistance and deformation performance. Therefore, the expansion condition of the fissures is also monitored during the test. The real experiment conditions can be seen in Figure 4.

3 RESULTS AND DISCUSSION

3.1 Analysis of deflection-load

Figure 5 and Figure 6 are the deflection-load curve obtained during the loading process of sheet pile samples with sectional dimension 700 mm × 400 mm and 1000 mm × 400 mm respectively. The deflection-load curve can be divided into two stages from these two figures, one is elastic stage and the other is elastic-plastic stage. In the elastic stage, the applied load and the deflection of sheet pile is linear relationship. The higher growth rate of load and the lower growth rate of deflection reflect the bigger flexural stiffness of sheet pile. With the increasing of the external load, a turning point of load-deflection curve is appeared. The growth rate of deflection is begin to increase while the load is begin to decrease. This is because the cracks are begin

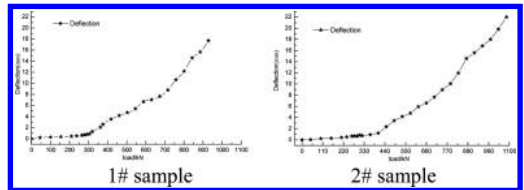


Figure 5. Deflection-load curve of 700 mm × 400 mm sample.

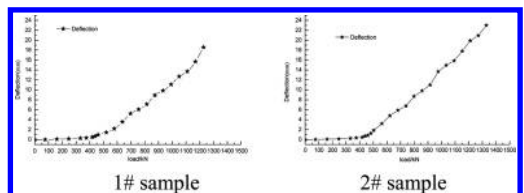


Figure 6. Deflection-load curve of 1000 mm × 400 mm sample.

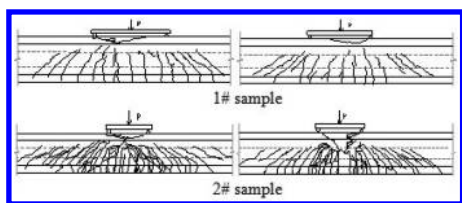


Figure 7. Crack pattern of 700 mm × 400 mm sample after test.

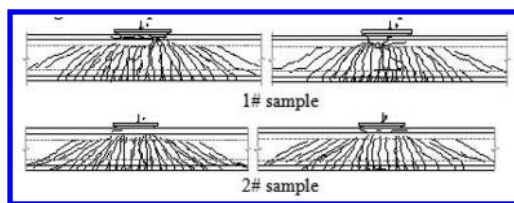


Figure 8. Crack pattern of 1000 mm × 400 mm sample after test.

Table 1. Experiment results of specimens.

Dimension (mm)	Number	Cracking load (kN)	Cracking bending moment (kN·m)	Ultimate load (kN)	Ultimate bending moment (kN·m)
700 × 400	1#	319.5	391.2	914.8	1099.6
	2#	319.5	391.2	957.3	1150.2
1000 × 400	1#	460.5	588.5	1227.5	1547.2
	2#	503.3	642	1270.3	1600.7

to appear in the sheet pile which results in the decrease of the whole flexural stiffness of sheet pile and the deflection-load curve has been into the elastic-plastic stage. During the stage of elastic-plastic, the initiation of cracks and extension as well as coalescence is evolving all the time, the whole flexural stiffness of sheet pile is becoming smaller and smaller.

3.2 Analysis of crack propagation

During the loading process, the applied load will transmit to the sheet pile sample through the distributive girder which will result in the bend of sheet pile sample. At the same time, the bottom of sheet pile will be in the tension state while the top of sheet pile in the compression state. Because the concrete's tension strength is far lower than its compressive strength. The crack will initiate in the bottom of the sheet pile at the constant moment zone perpendicular to the center line of the sheet pile. With time going on, more and more cracks will emerge with split sound in the constant moment zone and these cracks are distributed symmetrically. As the applied load increase to the ultimate load, the width of cracks in the constant moment zone will widen gradually and diagonal cracks will appear and extend in the bending-shear section but with low spreading velocity. However, the compression zone of sheet pile has never destroyed. Only when the applied load exceeds the ultimate load, the compression zone of concrete will crush. Finally, the whole crack pattern in the concrete sheet pile when the experiment finished is shown in Figures 5 and 6.

3.3 Analysis of flexural capacity

Table 1 gives the details of the crack bending moment and ultimate bending moment of four groups of sheet pile samples obtained during the process of loading. According to these values, it is concluded that the crack bending moment and ultimate bending moment with sectional dimension of 1000 × 400 is larger than that of 700 × 400. And this shows that the sectional dimension of sheet pile has a great influence on the flexural bearing capacity. When the width of section is constant, the crack bending moment and ultimate bending moment will be larger with the increasing of height of section. Therefore, we can change the section dimension of sheet pile so as to obtain the required flexural bearing capacity.

4 CONCLUSIONS

The four-point bending tests of four groups of concrete sheet pile are conducted in this paper and the conclusions are obtained as follows:

1. It is observed that the measured bending moment of these two pieces of sheet pile are large enough to guarantee the reliability of design so as to meet the application condition in engineering. The cracking bending moment and ultimate bending moment of a sheet pile with the height of 1000 mm are far higher than those of a sheet pile with the height of 700 mm.
2. During a four-point bending test, the deflection-load curve of a sheet pile has the elastic characteristic at the initial loading stage, the overall flexural stiffness is quite high, while the

- deflection-load curve of the sheet pile will be in the elastic-plastic stage after cracks occur, and the overall flexural stiffness will become smaller.
3. During the test, a crack firstly appears in a tension zone in the constant moment zone and then gradually expands and extends towards the two sides, finally a lot of oblique crack appears on a bending-shear section, and concrete in the compression zone can also be crushed.

REFERENCES

- [1] H. Manalip, M. Pinglot, M. Lorrain. 1994. Behavior of the Compressed Zone of Reinforced and Prestressed High Strength Concrete Beams, *ACI Journal*, 149, 209–226.
- [2] Zhang Peng, Yan Ping. 2012. Experimenta studies on the flexural bearing capacity of prestressed concrete I-shaped pile. *Low Temperature Architecture Technology*. 4: 77–79.
- [3] Y. Zandi, Y. Akgün, A. Durmuş. 2012. Investigating the Use of High Performance Concrete in Partially Prestressed Beams and Optimization of Partially Prestressed Ratio, *Indian Journal of Science and Technology*, 2991–2996.
- [4] Shady H. Salem, Khalid M. Hilal, Tarek K. Hassan, et al. 2013. Experimental behavior of partially prestressed high strength concrete beams. *Open Journal of Civil Engineering*, 3: 26–32.
- [5] Lu Lei, Huang Guang-long, Zhou Wen-yuan. 2014. Deformation analysis of rectangular prestressed high strength concrete supporting pile [J]. *Journal of Nanjing University of Technology (Natural Science Edition)*, 36(1): 60–65.

Tests on the seismic behavior of cavity wall with phase change materials based on simulation masonry building

J.L. Shang, T.G. Zhang, S.Y. Lei & H. Zhang

Department of Materials and Mineral Resource, Xi'an University of Architecture and Technology, Xi'an, China

ABSTRACT: To study the seismic behavior of cavity wall filled with phase change material, tests of the sandwich housing model made by 1/4 reduced scale was carried out, which mainly focused on the influence of different vibration location (EL-wave and Taft wave) and acceleration on seismic performance of cavity wall composite masonry building. The frequency and damping ratio of the model, peak acceleration, power amplification coefficient, strain of tie have also been studied. It is shown that deformation capacity of model are high due to the tie in wall can play a keyword role. The phase change material filled between two leave walls has not much influence on the seismic performance of the cavity wall.

Keywords: cavity wall masonry building; phase change material; shaking table test; stress and strain of tie

1 INTRODUCTION

Sandwich composite wall is composed of two leaves wall, which can be put phase change material and tie. As there are phase change materials in wall, the wall has a good stored energy. But China is in the Eurasian and the Pacific seismic belt, seismic performance of sandwich composite wall structure have to study [1]. In this paper, the test of simulated seismic for sandwich masonry structure is innovative.

2 SIMULATED SEISMIC SHAKING TABLE TEST SCHEME

2.1 Test model design

1. Porous brick size

Because of the reduced scale, the model brick in the actual test was cut saws molding and the performance of test model brick is shown in Table 1.

2. Building model size

Due to the limited zone, the shaking table size is determined primarily by the geometric shrinkage ratio of 1:4 [2]. Counterweight calculation is considered and shown in Figure 1.

3. Reinforcement of building model (design values)

According to the requirement of the masonry structure, side pillar, middle column, stirrup and reinforcement of ring beam are considered according to the scale requirement and the standard provisions design [3–5].

2.2 Tie design

Z type tie has been used in between internal and external leaves wall, as shown in Figure 2.

2.3 Phase change material

Phase change material can be put between internal and external leaves wall, as shown in Figure 2.

3 SIMULATED SEISMIC SHAKING TABLE TEST

3.1 Test control system

The single parameter feedback control list of shaking table systems is used in the vibrating table simulation control part.

Table 1. Performance of test model brick.

Layer of cavity wall	Size (mm)	Porosity (%)	Compressive strength (MPa)	Bibulous rate (%)
EL-1 (EL-2)	112 × 22 × 40	32.65 (27.6)	22.88	8.2
IL	112 × 46 × 40	27.71	45.57	7.9

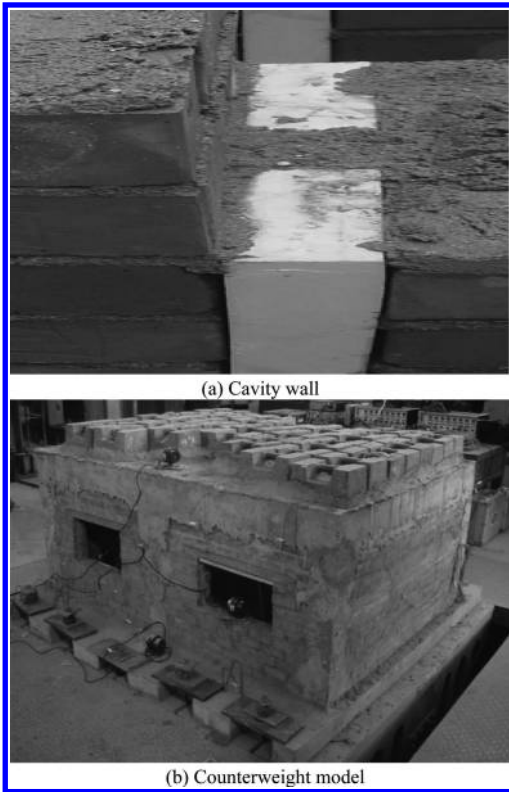


Figure 1. Building model size.



Figure 2. Tie and PCM between two leaves wall.

3.2 Sensor arrangement

The sensor includes the accelerometer and displacement meter. An accelerometer is fixed in vibration table (A1), mat layer (A2), wall (A3), ring beam (A4) respectively bottom-up. The displacement meter is placed in the door (E1-E3) and the

Table 2. Seismic wave peak and seismic intensity.

Order	Acceleration peak (gal)	Seismic intensity (deg.)	Seismic description
1	36	6	S
2	110	6	S
3	220	8	S
4	300	7	M
5	620	7	M
6	700	8.5	M
7	800	9	M
8	1020	8	L
9	1240	9	L
10	1360	10	-

Note: S—small, M—moderate, L—large.

window. (E6-E8). Moreover, strain film is stuck on the tie of the wall and forced steel bar in constructional column.

3.3 Loading process

In the experiment, EL-central wave and Taft wave are input in each working condition. The actual cycle of EL-central wave is 30 s but the cycle should be $T_1 = 30 \times 0.35 = 10.5$ s considering the similar ratio ST 0.35. According to the actual situation of instrument, the input cycle should be $T = 10.5 \times 4096/1500 = 28.69$ s, frequency $f = 1/T = 34.9$ MHz. The actual cycle of Taft wave is 54 s but the cycle should be $T_1 = 54 \times 0.35 = 18.9$ s considering, the similar ratio ST 0.35. According to the actual situation of instrument, the input cycle should be $T = 18.9 \times 4096/2720 = 28.46$ s, frequency $f = 1/T = 35.1$ MHz.

The waves are input several times for the observation of the building models' working conditions at various stages. In the experiment, different seismic intensities are controlled by the corresponding maximum acceleration of input seismic waves, as shown in Table 2.

4 TEST RESULTS AND ANALYSIS

4.1 Dynamic characteristic analysis

Frequency and damping ratio of the model are shown in Table 3.

Dynamic feature is the inherent characteristics of the structure itself, including the natural frequency, mode shape, damping ratio and other parameters [6]. In this test, the parameters of single-layer sandwich wall masonry structure housing have been inspected, the change of two parameters along hammer detection as shown in Table 3.

Table 3. Frequency and damping ratio of the model.

Number	Frequency (Hz)	Damping ratio (%)
1	15.3074	1.3982
2	14.9082	1.6219
3	14.6917	1.2948
4	14.5044	1.7857
5	14.0981	1.5904
6	14.5064	2.0493
7	14.1045	2.1529
8	13.8985	2.7755
9	13.2745	2.7874
10	13.4991	3.1582

Table 3 shows that structural vibration frequency is gradually declines. According to the relationship between frequency and stiffness, we can see that the second hammer frequency value (14.9082 Hz) decreases by 2.61% than the first hammer frequency value (15.3074 Hz), with the increase of peak acceleration, structure stiffness decreases slowly, when the cracks are not obvious. After the third hammering, the frequency (14.6917 Hz) drops by 4.02% and cracks begin to increase. After the eighth hammering, the frequency has fallen by 9.20% and cracks appear in large numbers. The original cracks have widened and prolonged. At the end of the test, the frequency declines by 11.81%.The test shows that earthquake damage is a cumulative damage process.

It can be seen from the figure that the damping ratio is also gradually increases (from 1.3982 gradually to 3.1582). The result shows that the overall stiffness of the structure is not decreasing, the tie of two leaves wall can play an important role and slow the stiffness degradation and prevent the accumulation of damage.

4.2 Acceleration response analysis

Peak acceleration under various operating conditions is shown in Table 4.

According to the above table, the peak acceleration of model increases with the increase of measured height. It is indicated that seismic wave has been responding to upper structure in the whole process of vibration and that mark between wall piece and components and reinforcement are perfect. No obvious destructive cracks appear in the whole model with loading increase.

4.3 Power amplification coefficient analysis

Power amplification coefficient is the ratio between acceleration maximum and the maximum input acceleration. Power amplification coefficient can

Table 4. Peak of EL-Centro wave under various stages.

Order	Measuring point			
	A1	A2	A3	A4
1	38.644	36.525	39.766	50.360
3	121.119	106.554	89.775	118.21
6	223.91	224.58	237.693	247.879
8	315.463	322.683	326.565	368.804
11	620.639	582.882	610.954	748.163
14	683.317	725.358	710.068	862.453
16	835.299	841.572	933.000	967.998
17	1011.48	992.198	1008.61	990.011
20	1319.95	1173.61	1516.84	1572.92
22	1407.18	1151.88	1370.73	1691.13

reflect change and destruction dynamic response of the model [7–8].

Power amplification coefficient under various operating conditions is shown in Table 5.

Because EL-Centro wave and Taft wave spectrum are different, the responses of the model are different when the two waves approximate the input table at the acceleration rate. With each wave, the model response acceleration and power amplification coefficient also have big differences. Power amplification coefficient change is amplitude with the stronger impact of EL-Centro on the structural dynamic effects (EL-Centro wave: 0.741~1.262, Taft wave: 0.930~1.272).

For example, with the impact of seismic wave, the measuring point of the EL-Centro wave's power amplification coefficient is varies. The model of the input seismic wave amplification is not obviously affected by the load that causes model number to increase and makes model stiffness down [9].

4.4 Strain response of tie

Doors and windows are the weak parts of the structure, so the tie stress changes of this part is analyzed. Change of the strain peak is shown in Figure 3 and Figure 4.

From the Figures 3–4, rachel reinforcement strain change at the place of doors and windows is varies with peak acceleration under the same wave pattern: the maximum tie strain appears in E1, E6 when EL-Centro wave increases to 1924.967 $\mu\epsilon$, 1374.4 $\mu\epsilon$. That steel strain significantly increases in the EL-Centro waves, which shows that the model structure is more sensitive to this waveform. The stress of the tie can be calculated according to the tie elastic modulus.

In the test, the maximum strain of the measurement is 2272.19 $\mu\epsilon$. Reinforced for hard-drawn wire, the elastic modulus E is 2×10^6 MPa, so the stress

Table 5. Power amplifier coefficient under various stages.

Order	Measuring point		
	A2	A3	A4
1	0.945	1.029	1.303
3	0.880	0.741	0.976
6	1.003	1.062	1.107
8	1.023	1.035	1.169
11	0.939	0.984	1.205
14	1.062	1.039	1.262
16	1.008	1.117	1.159
17	0.981	0.997	0.979
20	0.889	1.149	1.192
22	0.819	0.974	1.202

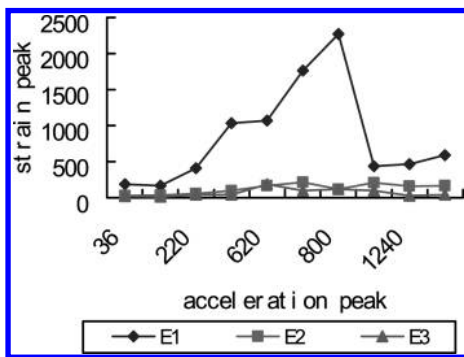


Figure 3. EL-Centro wave, strain peak curve of tie near doors.

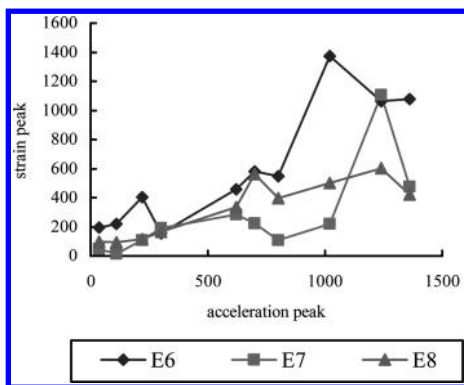


Figure 4. EL-Centro wave, strain peak curve of tie near window.

of hard-drawn wire σ is $\xi \times E = 2272.19 \times 10 \times 2 \times 106 = 554.5$ MPa, close to the yield strength of tie 555 MPa. With the increase of the input earthquake force, the wall and the tie coordinate are well and the security of the tie is guaranteed.

5 CONCLUSION

1. With the increase of input seismic wave, peak acceleration and structure stiffness slowly decrease while the damping ratio gradually increases. The whole structural stiffness decreases with the cracking appearing but if the wall tie and structural column are added, then it can play a constraint role in slowing its stiffness degradation and preventing damage accumulation.
2. The model of the input of seismic wave amplification is not obviously affected despite the increasing loading number causing model cracks and making model stiffness down.
3. With the increase of input earthquake forces, wall and tie coordinate well. With the peak acceleration increasing, sensor strain peak is also growing. The stress of tie inside the wall does not exceed yield stress.

ACKNOWLEDGEMENTS

This work is financially supported by National Natural Science Fund (51172176) and the National Eleventh Five-Year Plan Project (2006BAJ02B01), and Shaanxi Provincial Science and Technology Innovation Project (2013KTCL03-17).

REFERENCES

- [1] Li, H.N. & Zhang, J.W. 2004. Seismic behavior of insulated hollow-brick cavity walls using quasi-static experimentation. *Experimental Mechanics* 44(4): 396–406.
- [2] Tokui, N. 2004. Simplified shaking table test methodology using extremely small scaled models. *13WCEE*: 156–158.
- [3] Hendry, A.W. 2001. Masonry walls: materials and construction. *Construction and Building Materials* 15(8): 323–330.
- [4] Moustafa, K. F. 2004. Shaking table testing and analysis of two column bents. *13WCEE*: 201–204.
- [5] Sinha, B.P. & Hendry, H.W. An Investigation into the Behavior of a Five-story Cavity wall Structure. *University of Edinburgh*.
- [6] Lu, X.L. & Li, P.Z. 2004. Shaking table model testing on dynamic soil structure interaction system. *13WCEE*: 134–145.
- [7] Sun, J.J. 2004. Earthquake simulate or tests of one sixth scale nine-story RC model. *13WCEE*: 75–78.
- [8] Zhou, Y. & Lu, X.L. 2006. Shaking table test model design in different structures. *Structural Engineers* 22(4): 37–39.
- [9] Wang, Y.H. & Cheng, W. 2008. Elementary introduction to shanking table test of seismic simulation. *Industrial Construction* 38(7): 34–36.

The calculation of composite beam's slippage formula and deflection formula considering the slippage of steel-concrete

Xu Jiao Chen & Zhong Tao

Kunming University of Science and Technology, Kunming, China

De Guang Zeng

Metallurgical Planning and Design Institute of Henan, Zhengzhou, China

ABSTRACT: The main content is to calculate the slippage formula and deflection formula of composite beam considering the slippage of steel-concrete under different loads. Establish the differential equation of the slippage of steel-concrete interface of composite beam, and calculate the slippage of steel-concrete interface formula under different loads according the boundary conditions. Then we conducted the elasticity calculation of the flexible composite beams by using the program that made by myself, and we get a result that while maintaining the shear connectors without changing, the greater the shear stiffness of the shear connector is, then the smaller of composite beam's deflection and section slippage is.

Keywords: composite beam; slippage of steel-concrete; share connectors

1 INTRODUCTION

Steel-concrete composite beam is a kind of flexural member composed by concrete slab and steel beam via shear connectors. Because composite beams have good behaviors, so they are widely used in architecture fields.

In the early 1920s, Canada Dominion Bridge Company Machay and other people were simply supported composite beam research, they take T-shaped composite beam as the research object for the study, after testing, the final results showed that: If the steel beams with concrete to maintain sufficient adhesion, the steel beams of composite beams and concrete will have full interaction.

In the early 20th century, E.S. Andress proposed the transformed section theory, because the beams consist of two materials that is concrete and steel beams, so the composed section need to be translate into cross-section of the same material, only be translated the composed section can be calculated by using the material mechanics theory.

But this theory does not take the relative slip of the composite beam into account, so there is still have a certain gap between the calculation results and the actual situation. To the 1950s, N.M. Newmark proposed a calculate theoretical which considered the relative slip of composite beam cross-section, but in the calculation process which requires to solve differential equations, and the results are very complex, so this theory does not

apply to the actual project. However, it also has a very important theory significance.

This article is mainly to calculate the section shear force and derivation formula of composite beams when considering different combinations of beam. Establish the differential equation of the slippage of steel-concrete interface of composite beam, and calculate the slippage of steel-concrete interface formula under different loads according the boundary conditions.

2 INTERFACE SLIP CALCULATION OF COMPOSITE BEAM D

2.1 *Differential equations of slip*

In the actual project, the shear connectors of composite beam are flexible connectors, then there will have slip inevitably in the junction between the concrete slab and the steel beams. So to calculate the value of interfacial slip, it is more in line with the actual composite beam stress state. It needs to do some assumptions, before calculating slip differential.

1. Steel beams and concrete slabs were in line with the plane section assumption.
2. Steel beams and concrete slabs bonded with each other.
3. Shear connectors is always in the state of flexible working.

4. Shear connectors uniformly distributed along the beam length. And assuming the shear-slip relationship of single shear connectors is $Q = ks$.

where k is the slip stiffness of shear connectors, s is the interface slip of composite beam. Assuming the spacing of shear connectors is a , then the slip stiffness per unit length of the beam is

$$k_L = \frac{k}{a}$$

The shear-slip relationship of the beam per unit length is $V = k_L s$.

Taking an element in the composite beam, as it is showed in the Figure 1, according to the unit body force equilibrium conditions we can get

$$\begin{cases} dM_c - V_c dx - \frac{1}{2} v h_c dx = 0 \\ dM_s - V_s dx - \frac{1}{2} v h_s dx = 0 \end{cases} \quad (1)$$

We can get the result (2) by dealing with the upper equation:

$$\frac{dM_c}{dx} + \frac{dM_s}{dx} - V = hv \quad (2)$$

Based on the assumption (2), the curvature of the steel beam and concrete slab is the same, and then we can get:

$$\Phi = \frac{M_c}{E_c I_c} = \frac{M_s}{E_s I_s} = -\frac{d^2 y}{dx^2} \quad (3)$$

The strain of the concrete slab's interface surface and steel beam's upper surface of the composite beam is

$$\begin{cases} \varepsilon_{AB} = \frac{1}{2} h_c \Phi - \frac{N_c}{E_c A_c} \\ \varepsilon_{CD} = \frac{N_s}{E_s A_s} - \frac{1}{2} h_s \Phi \end{cases} \quad (4)$$

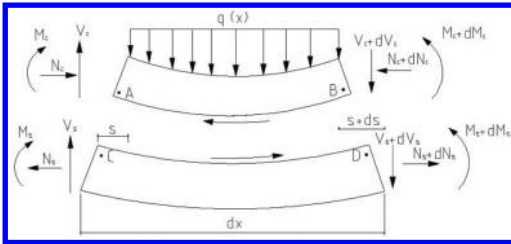


Figure 1. Force diagram of the element.

$$\text{And } \frac{ds}{dx} = \varepsilon_{AB} - \varepsilon_{CD} \quad (5)$$

Taking (4) into (5), we can get:

$$\frac{ds}{dx} = h\Phi - \frac{N}{EA} \quad (6)$$

Form (3) we can get:

$$\frac{dM_c}{dx} + \frac{dM_s}{dx} = \frac{d\Phi}{dx} (EI) \quad (7)$$

By differentiating (6), we can get:

$$\frac{d^2 s}{dx^2} = h \frac{d\Phi}{dx} - \frac{N}{EA} \quad (8)$$

Taking (2) and (7) into (8), we can get:

$$\frac{d^2 s}{dx^2} = h \frac{1}{EI} (hv + V) - \frac{N}{EA} \quad (9)$$

Based on the assumption (4), we can know that $v = k_L s = ks/a$, taking them into (9), we can get:

$$\frac{d^2 s}{dx^2} - \frac{k}{a} \left(\frac{1}{EA} + \frac{1}{EI} h^2 \right) s = \frac{h}{EI} V \quad (10)$$

Assuming

$$\alpha^2 = \frac{k}{a} \left(\frac{1}{EA} + \frac{1}{EI} h^2 \right) \quad \beta = \frac{h}{EI}$$

Then we can get

$$\frac{d^2 s}{dx^2} - \alpha^2 s = \beta V \quad (11)$$

Formula (11) is the interface slip differential equations of the composite beam.

2.2 Deformation calculation of composite beam when considering the slippage

We can know that form (6) equation:

$$\frac{ds}{dx} = h\Phi - \frac{N}{EA} \quad (12)$$

The moment that the section of the composite beam bended is

$$M = M_c + M_s + N \cdot h \quad (13)$$

We can know that form (3) equation:

$$M_c = E_c I_c \Phi \quad M_s = E_s I_s \Phi$$

Taking them into (13), we can get:

$$M = EI\Phi + N \cdot h$$

where $EI = E_s I_s + E_c I_c$.

We can get that form (14) equation:

$$\Phi = \frac{1}{EI}(M - Nh)$$

Taking (15) into (12), we can get:

$$\frac{ds}{dx} \frac{1}{h} EI = -h \left(\frac{1}{EA} \frac{1}{h^2} EI + 1 \right) N + M$$

$$\text{Assuming } \frac{1}{\alpha} = \frac{1}{EA} \frac{1}{h^2} EI$$

We can rewrite the (16) as the flowing:

$$\frac{ds}{dx} \frac{EI}{h} = -h \left(\frac{1 + \alpha}{\alpha} \right) N + M$$

Based on the assumption (4), we can know that $v = k_L s = ks/a$, and $vdX = dN$, we can get:

$$\frac{ds}{dx} = -\frac{a}{k} \frac{d^2 N}{dx^2}$$

Taking (18) into (17), we can get:

$$\frac{d^2 N}{dX^2} - \frac{k}{a} \frac{h^2}{EI} \frac{1 + \alpha}{\alpha} N - \frac{k}{a} \frac{h}{EI} \frac{q}{2} (lx - x^2) = 0$$

$$\text{Assuming } \omega^2 = \frac{k}{a} \frac{h^2}{EI} \frac{1 + \alpha}{\alpha} \quad \beta_1 = \frac{q}{2h} \frac{\alpha}{1 + \alpha}$$

We can rewrite the (19) as the flowing:

$$\frac{d^2 N}{dx^2} - \omega^2 N + \omega^2 \beta_1 (lx - x^2) = 0$$

By solving equation (20) we can get the general solution (21)

$$N_1 = c_1 e^{\omega x} + c_2 e^{-\omega x} - \beta_1 x^2 + \beta_1 lx - \frac{2\beta_1}{\omega^2}$$

Consider the boundary conditions when $X = 0$, $N = 0$; When $x = l/2$, $N' = 0$, then the undetermined coefficient of (21) equation is:

$$c_1 = \frac{\beta_1 e^{-\frac{l}{2}}}{\omega^2 \cosh \frac{l}{2} \omega} \quad c_2 = \frac{\beta_1 e^{\frac{l}{2}}}{\omega^2 \cosh \frac{l}{2} \omega}$$

Taking c_1 and c_2 into (21), we can get:

$$N = \frac{2\beta_1}{\omega^2} \left[\frac{\cosh \left(\frac{l}{2} - x \right)}{\cosh \frac{l}{2} \omega} - 1 \right] - \beta_1 x(x-l)$$

Taking (22) into (15), we can get

$$y(x) = -\frac{1}{EI} \left[-\frac{2h}{\omega^4} \frac{\beta_1 \cosh \omega \left(\frac{l}{2} - x \right)}{\cosh \frac{l}{2} \omega} + \frac{ql}{12} x^3 - \frac{qx^4}{24} + \frac{h\beta_1 x^2}{\omega^2} + \frac{h\beta_1}{12} x^4 - \frac{h\beta_1 l}{6} x^3 + c_3 x + c_4 \right]$$

Consider the boundary conditions when $x = 0$ $N = 0$ when $x = l/2$ 时, $dy/dx = 0$ then the undetermined coefficient of (23) equation is:

$$c_3 = \frac{l^3}{24} (2h\beta_1 - q) - \frac{h\beta_1}{\omega^2} \quad c_4 = \frac{2h\beta_1}{\omega^4}$$

Taking C_3 and C_4 into (23), we can get:

$$y(x) = -\frac{1}{EI} \left[-\frac{2h}{\omega^4} \frac{\beta_1 \cosh \omega \left(\frac{l}{2} - x \right)}{\cosh \frac{l}{2} \omega} + \frac{2h\beta_1 - q}{24} \times (x^4 - 2x^3 l + l^3 x) + \frac{h\beta_1}{\omega^2} \left(x^2 - xl + \frac{2}{\omega^2} \right) \right]$$

Formula (24) is the composite beams' deflection formula under uniform loads.

3 THE ELASTICITY CALCULATION OF THE FLEXIBLE COMPOSITE BEAMS

There is a steel-mixed composite beam, the cross section is shown in Figure 2, the length of beam is $l = 10$ M, and uniformly distributed load that acts upon the beam is $q = 50$ KN/m. The elastic modulus of concrete is $E_c = 3 \times 10^{10}$ N/m², the elastic modulus of the steel beam is $E_s = 2.1 \times 10^7$ N/m². Spacing of shear connectors are $a = 0.2$ m, the two stiffness are: (1) $k = 2 \times 10^7$ N/m; (2) $k = 2 \times 10^{13}$ N/m; According to the length of composite beam, we divided it into 10 units when calculating.

According to the beam length and spacing of the shear connectors, calculating the number of shear connectors and shear stiffness of all shear connectors, and then divided all shear stiffness into each unit according to the number of beam elements.

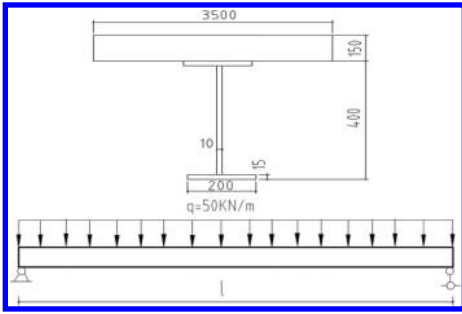


Figure 2. The section of composite beams.

Table 1. Deflection of flexible composite beam ($k = 2 \times 10^7$ N/m).

Node	1	2	3	4	5	6
f_1	0	1.531	2.890	3.947	4.616	4.844
f_2	0.000	1.536	2.898	3.959	4.629	4.858
f_1/f_2	-	0.996	0.997	0.997	0.997	0.997

Table 2. Deflection of flexible composite beam ($k = 2 \times 10^{13}$ N/m).

Node	1	2	3	4	5	6
f_1	0	8.714	1.649	2.266	2.665	2.798
f_2	0.000	8.727	1.658	2.277	2.671	2.807
f_1/f_2	-	0.998	0.994	0.995	0.9978	0.996

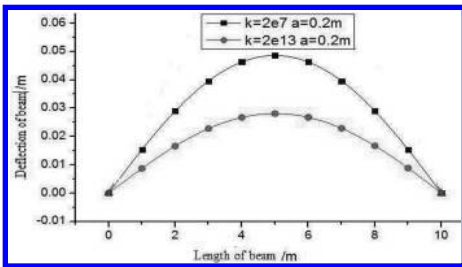


Figure 3. Deflection distribution of different shear stiffness composite beam.

Deflection calculation results of composite beam are as follows: f_1 is analytical solution, f_2 is program solution.

The figure of deflection distribution along the length of beam as follow:

According to Table 1 and Table 2, we can get a result that the program solutions have a very high

Table 3. The composite beam's slippage.

Node	1	2	3	4	5	6
$k = 2 \times 10^7$	-2.766	-2.588	-2.138	-1.512	-7.803	3.207
$k = 2 \times 10^{13}$	-6.105	-4.428	-3.447	-2.428	-1.064	2.845

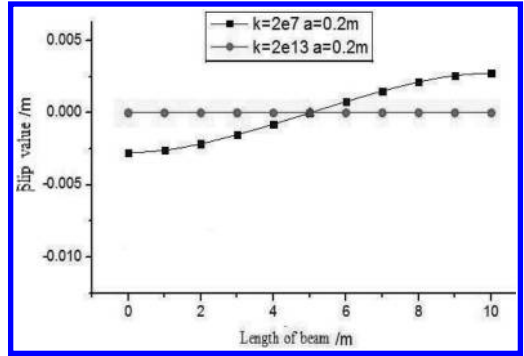


Figure 4. The section slippage of flexible composite beam's different shear stiffness.

accuracy and it is credible, because the small difference between the calculated analysis solutions and program solutions, then calculating the interface slip value of the composite beam by using the program:

We can see from Figure 3 and Figure 4 that while maintaining the shear connectors without changing, the greater the shear stiffness of the shear connector is, then the smaller of composite beam's deflection and section slippage is.

That is because the greater shear stiffness is, the combined effect of the combination of concrete flange beams and steel beams will be better. Above the three different stiffness of shear connectors, we can know that the maximum rigidity lead very small interfacial slip value, if the stiffness of the shear connector tends to infinity, then the composite beam will become a normal beam; Conversely, if shear stiffness approaches Infinitely small, that means there is no shear stiffness, then it becomes a simple composite beam.

4 CONCLUSIONS

Firstly, the main content is to calculate the slippage formula and deflection formula of composite beam considering the slippage of steel-concrete under different loads.

Secondly, calculate the deformation of composite beam and redistribution of internal forces of reinforced concrete beam with the calculation program. And calculate the relevant formula.

In the analysis of composite beam in plastic stage, calculate and analysis the section stress considering the different locations of neutral axis.

Establish the differential equation of the slippage of steel-concrete interface of composite beam, and calculate the slippage of steel-concrete interface formula under different loads according the boundary conditions.

Then we conducted the elasticity calculation of the flexible composite beams by using the program that made by myself. The result had shown that the difference between the calculated analysis solutions and program solutions is very small, so it has reference significance. And we also get a result that while maintaining the shear connectors without changing, the greater the shear stiffness of the shear connector is, then the smaller of composite beam's deflection and section slippage is.

REFERENCES

- Johnson R.P. Composite structural of steel and concrete, vol 1: Beams, columns, frames and applications in building. 2nd Ed. Oxford: Blackwell Scientific, 1994.
- Johnson R.P., I.M. May. Partial-Interaction Design of Composite Steel and Concrete Structure. *The Structure Engineering*, 1975, 53 (8):305–311
- New mark, C.P. Siess, L.M. Viest. Test and Analysis of Composite Beams with Incomplete Interaction (J), *Experimental Stress Analysis*, 1951, (9):31–45.
- Ollgaard J.G, Stutter R.G Fisher J.W, Shear Strength of Stud Connectors in Light weight and Normal Weight Concrete. *AISCC. Engrg*, 1971, 8 (4):55–64.
- Rotter M., P. Ansourian. Cross-Section Behavior and Ductility of Composite Beams. *Proceedings of the Institution of Civil Engineerings*. 1979, 2(67):453–474.
- Yam L.C.P, Chapman J.C. Inelastic Behavior of Continuous Composite Beams of Steel and Concrete, *Proc. Instn Civ. Engrs, Part 2*, 1972, 53(12):487–501.
- Yam L.C.P, *Ultimate-load Behavior of Composite T-Beams Having Inelastic Shear Connection (D)*. London University of London. 1996.

Experimental study on NO reduction by biomass reburning in Northern China

Dong Yang

Key Laboratory of Renewable Energy Utilization Technologies in Buildings of the National Education Ministry, Jinan, China

Xiao Jie Zhang, Qing Wen Chen, Meng Zhang & Shi Jun Wei

Department of Thermal Engineering, Shandong Jianzhu University, Jinan, China

ABSTRACT: Nitric Oxide (NO) removal characteristics were studied on the biomass reburning experiment platform by reburning various kinds of biomass, such as corn stalk, cotton stalk, apple wood and poplar, during which the influence of following factors on the NO removal was analyzed, like the sort and grain size of the reburning fuel, reaction temperature in the reburning zone. The experiment result indicates that for the selected four kinds of biomass, the greatest denitration effect is XX. The smaller the biomass particle size, the higher the denitration efficiency. Again at about 1100 °C, the biomass reburning NO removal efficiency has the maximum. In a temperature below 1100 °C, denitration efficiency will showed a trend of increase accompanied by a rise in temperature. The reburning denitrification efficiency is unchanged the reburning denitrification efficiency is unchanged.

Keywords: biomass; particle size; reburning zone temperature; NO removal

1 INTRODUCTION

Reburning technology is one of the most promising and cost-effective Nitrogen Oxides (NO) reduction strategies for combustion systems which use reducing product by the pyrolysis of fuel in reburning zone. Therefore, the properties of the reburning fuel play a vital role in NO removal. It generally thought that the ideal reburning fuel, which requires it have low N element content and generate small amounts of NO The product of combustion contains a large reducing groups of CHI which can react with NO to reduce the pollution emissions under the condition of high temperature.

China is an agricultural country and has plenty of biomass resources. Biomass energy can use to combust in boiler replace coal as a result of small quantity nitrogen and sulfur. Meanwhile the pollution gas of NO and SO₂ exhaust more less with coal after combustion. Biomass combustion products have alkali metal salt which can improve the efficiency of the denitration. Biomass energy is a kind of renewable clean energy, CO₂ absorption for plant photosynthesis from the burning of recycling, no carbon dioxide emissions.

2 EXPERIMENT

2.1 *Experimental material*

This paper discusses the proximate and ultimate analysis of the test material what are four kinds of biomass in northern China. The results as shown in [Table 1](#).

2.2 *The experimental apparatus and methods*

According to the requirement of the biomass reburning denitration experiments, the experimental design of fixed bed reactor system is shown in [Figure 1](#).

Simulated flue gas was used in the experiment which include O₂, N₂, CO₂, and NO be controlled by a flow meter to adjust flow rate according to certain proportion. N₂ gas for balance, the experiment adopted for high purity gas, O₂, N₂, CO₂ gas purity are 99.999%, NO gas adopts distribution (1% NO + 99% N₂). The flow valve of mixed flue gas was controlled in 8 L/min.

Simulated flue gas mixed in the mixing tank is warmed up through the air preheater which is a steel tube for a length of 600 mm, inner diameter of 80 mm. The air preheater can control temperature

Table 1. Proximate and ultimate analysis of biomass.

Biomass	Proximate analysis			
	Mad/%	Aad/%	Vad/%	FCad/%
Corn stalk	9.23	2.89	68.83	17.85
Cotton stalk	9.21	3.29	71.19	16.31
Apple wood	5.87	2.15	75.34	16.64
Poplar	5.81	2.20	76.40	15.59

Biomass	Ultimate analysis				
	C/%	H/%	O/%	N/%	S/%
Corn stalk	45.95	6.00	46.58	1.21	0.26
Cotton stalk	48.30	5.65	45.60	1.08	0.17
Apple wood	51.02	5.94	42.35	0.64	0.05
Poplar	51.43	6.22	41.68	0.61	0.06

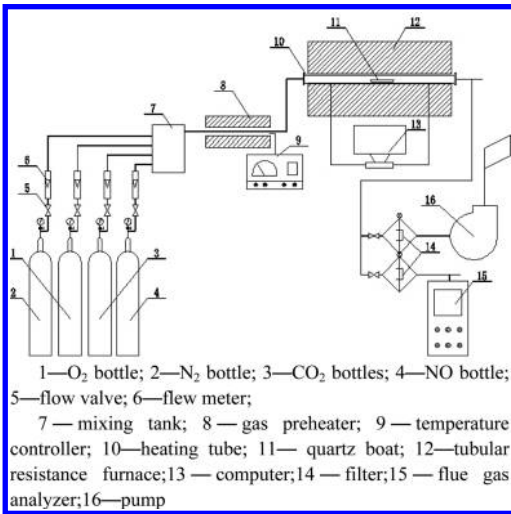


Figure 1. Biomass reburning laboratory furniture.

from 200 ~ 1000 °C. Preheat the simulated flue gas is mainly in order to make it close to the actual situation, reduce the error.

Tube furnace system is mainly composed of furnace, quartz tube, the temperature control system in which simulating flue gas react with biomass fuels in the quartz tube. Flue gas analyzer was York OPTIMA7 handheld flue gas analyzer which made in Germany. The instrument with data acquisition and processing software can be connected to a computer and also alone. Its technical indicators as follows: O₂: 0~21%; CO (high): 0~2000 ppm; CO (very high): 0~10000 ppm; NO: 0~5000 ppm; CO₂: 0~20%.

The denitration efficiency of biomass reburning is computed from Eq. 1.

$$\eta_{NO} = (1 - C_{NO,out}/C_{NO,in}) \times 100\% \quad (1)$$

η_{NO} —NO denitration efficiency, %;
 $C_{NO,out}$ —Export concentration of NO in reburning zone, $\mu\text{L/L}$,
 $C_{NO,in}$ —Inlet concentration of NO in reburning zone, $\mu\text{L/L}$.

3 RESULT AND ANALYSIS

3.1 The influence of different reburning biomass on the denitration efficiency

Corn stalk and cotton stalk are a representative of the herbs, apple wood and poplar are representative of woody plants. Under the experimental condition of the reburning zone temperature 1000 °C, fuel ratio 20%, the same atmosphere, the result as shown in Figure 2. Herbaceous and woody plants all have high denitration efficiency. The byproduct of denitration effect is lower than that of cotton in Herbaceous plants. Meanwhile, the denitration effect of apple wood is weak than that in woody plants. But the experiment result was not particularly evident.

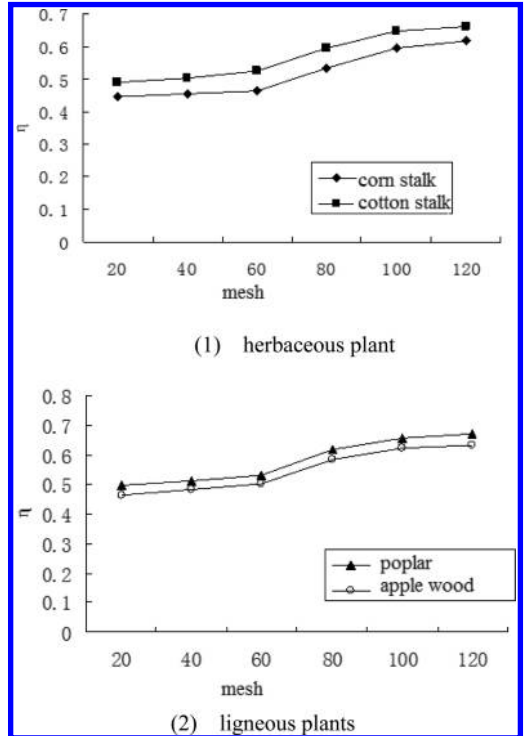


Figure 2. The influence of different reburning biomass on the denitration efficiency.

Generally recognized, the stand or fall of denitration effect is closely related to reburning fuel volatile. In the reburning zone, when the reducing atmosphere of excess air coefficient is less than 1, CHI for removal of NOX play a major role, and biomass in reducing atmosphere generated under high temperature cracking, coke, etc., so that, when burned, biomass in the volatile content, the greater the denitration effect is better. From the previous industrial analysis results, the cotton volatile content is higher than that of corn stalk, cypress volatile content is higher than the apple wood, and this difference corresponded to their denitration effect happens to conform. Woody plant volatile share is greater than the herbs, yet they denitration effect were similar, this is mainly because of herbs of pyrolysis and combustion temperature are lower than that of woody plants, pyrolysis, combustion is relatively difficult, volatile woody plants in the same temperature conditions, the precipitation is incomplete, it caused the herbs and woody plants denitration effect were similar results.

3.2 The influence of fuel particle size on the denitration efficiency

Four kinds of biomass with 20 mesh, 40 mesh, 60 mesh, 80 mesh, 100 mesh and 80 mesh 6 kinds of sieve sieve to separate different size of sample, respectively, under the condition of the working condition of the same biomass reburning the NO reduction experiment, the result is shown in Figure 3. By the figure is not hard to see, the smaller the particle size of fuel denitration effect is better. The main reason is: biomass fuel particle size is smaller, it always will be, the greater the surface fuel and gas contact area. Under the same conditions the heating temperature, the faster the heating rate, the faster the thermal decomposition and precipitation of the more volatile, so with the NO reduction reaction is the sooner the fully. Although fuel particle size, the smaller

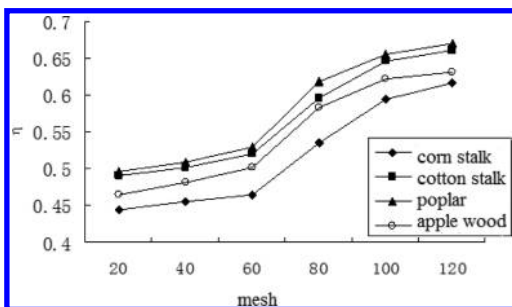


Figure 3. The influence of fuel particle size on the denitration efficiency.

the denitration efficiency is higher, but can be seen from the chart, with further fuel particle size decreases, and denitration efficiency increase degree is becoming more and more low, this is mainly because the volatile rapid exhalation will be formed on the surface of particles is very abundant pore structure, increase the specific surface area of biomass tar, thus promoted the phase-out of bio-char and NO reduction reaction, and inhibit the reduction of NO. Preparation of smaller particle size of biomass can increase the power consumption of grinding, it increases the difficulty and higher cost, at the same time because of biomass granule has a particularly strong adhesion, to cause feeding difficulties. Therefore, in the use of biomass fuel reburning denitration, to comprehensively consider denitration effect and economical, practical, selecting the best particle size range.

3.3 Reburning zone temperature affect denitration efficiency

Screening particle size range of four kinds of biomass in 0.150 ~ 0.180 mm, initial concentration of NO in the reburning zone is 600 PPM, and fuel ratio is 20% under the condition of reburning denitration experiment, the experimental results are shown in Figure 4. It is not hard to see from the table, the reburning zone temperature is decided to burn denitration efficiency and working condition of the content of volatile one of the key. In the reburning zone temperature smaller area, woody plants is far lower than the denitration effect of woody plants, with the increase of temperature, biological texture and denitration effect increased, woody plants to increase speed is greater than the herbs to increase speed, after up to 900 °C for 4 kinds of biological effect of texture. And the temperature rise to about 1100 °C, herb denitration efficiency highest, denitration efficiency is 69.2% cotton, 66.8% corn denitration efficiency peak. After 1100 °C, herb denitration effect decreased, while

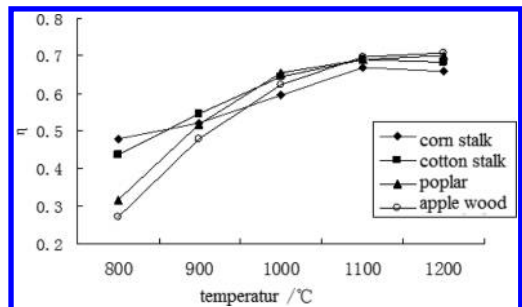


Figure 4. Reburning zone temperature affect denitration efficiency.

the denitration effect of the woody plants continues to increase, but not stronger amplitude, 1200 °C cypress denitration efficiency of 70.1%, while apple wood denitration efficiency reached 70.7%. In the high temperature phase, compared with herbs of the woody plants denitration effect is better.

4 CONCLUSION

With corn stalk, cotton in this chapter are two kinds of herbs and apple wood, have two kinds of woody plants, for example, the effects of the variety of biomass in the process of biomass to fuel, fuel particle size, reburning zone temperature, working condition of several parameters on the denitration efficiency, obtained the following conclusion:

1. The four kinds of biomass as reburning fuel to be able to achieve better denitration efficiency, effectively reduce NO emissions. The effect of different biomass burning again also has a certain difference, in general, woody plants reburning denitration efficiency is higher than the denitration efficiency of herbs.
2. Biomass particle size has a certain influence on the denitration efficiency, the smaller the particle size, the higher the denitration efficiency.
3. At low temperature, as the temperature increases, the denitration efficiency of biomass burning again followed rise in temperature to 1100 °C, the denitration efficiency of herbaceous plants reached a maximum, continue to raise the temperature, herbaceous plants declined, the denitration efficiency of woody plants of reburning denitration efficiency while continue to increase, but the increasing amplitude is small.

ACKNOWLEDGEMENTS

This paper was financially supported by the Doctor Foundation of Shandong Jianzhu University (No.XNBS1223) and the independent innovation project of academics in Jinan (No.201401223). The authors would also like to acknowledge the extended help from the Department of Thermal Engineering.

REFERENCES

- [1] Chen Qingwen. The mechanism research on biomass reburning denitration [D]. Shandong Jianzhu University. 2014.
- [2] Yang Dong, Chen Qingwen. The TG-DTG Analysis and Kinetics of Typical Biomass in Northern China[J]. Journal of Combustion Science and Technology. 2014, 20(3).
- [3] J. Ballester, R. Ichaso, A. Pina, et al. Experimental evaluation and detailed characterization of biomass reburning. Biomass and Bioenergy. 2008, 32(10): 959–970.
- [4] C. Casaca, M. Costa. NOx control through reburning using biomass in a laboratory furnace[J]. Effect of particle size. Proceedings of the Combustion Institute. 2009, 32(2):2641–2648.
- [5] P. Dagaut, F. Lecomte, S. Chevailler, et al. Experimental and detailed kinetic modeling of nitric oxide reduction by a natural gas blend in simulated reburning conditions. Combustion Science and Technology. 1998, 139(1): 329–363.
- [6] C.L. Yeh*, C.W. Liang. NOx reduction in a Carbon Monoxide boiler by reburning[C]. 7th Asian-Pacific Conference on Aerospace Technology and Science, 7th APCATS 2013:378–387.

Experimental study on changes of CaCO_3 concentration in FGD of falling films reactor

Dong Yang

Key Laboratory of Renewable Energy Utilization Technologies in Buildings, Ministry of Education, Jinan, China

Xiao Lu

Shandong Key Laboratory of Building Energy-saving Technique, Jinan, China

Shi Jun Wei & Meng Zhang

Key Laboratory of Renewable Energy Utilization Technologies in Buildings, Ministry of Education, Jinan, China
Shandong Key Laboratory of Building Energy-Saving Technique, Jinan, China

ABSTRACT: In view of the existing problem of traditional FGD, we combined two techniques to establish the double circulating falling film wet flue gas desulfurization test system, studied the effects of parameters on the performance of gas—liquid two—phase operation of wet flue gas desulfurization tower desulfurization in low pH, and found the absorption efficiency of SO_2 and changes of CaCO_3 concentration under the environment of Wet flue gas desulfurization. The study found: the SO_2 absorption efficiency increases with increasing pH of slurry and liquid-gas ratio, decreases with the increasing concentration of SO_2 entrance, slurry concentration and Superficial gas velocity; the concentration of CaCO_3 increases with increasing pH of slurry and concentration of SO_2 entrance.

Keywords: falling films; CaCO_3 concentration; FGD

1 INTRODUCTION

Since 21 Century, the environment problem is one of the most serious challenges in the world. China's coal-fired power, large consumption of coal has caused a large amount of SO_2 discharged. Pollution caused by acid rain is becoming more and more serious in our country [1]. In order to reduce the thermal power plant emissions of SO_2 and the pollution of the atmosphere further, to meet the relevant national standards for the discharge of requirements, especially to meet particular emission limit value index of key areas, according to the characteristic of the wet flue gas desulfurization process, there is the urgent need for further research, more greatly improve the desulfurization efficiency, achieved discharge standards [2].

Dominant in the wet flue gas desulfurization technology of the current is the spray type limestone gypsum flue gas desulfurization. Spray absorption tower has many advantages, but there are some problems. Experts and scholars from home and abroad, for the spray absorption tower and scaling problems solved based on the model, proposed the falling film wet flue gas desulfurization process [3–4]. At the same time, some foreign companies firstly proposed the double circulation

of wet flue gas desulphurization technology, using low pH, mainly used for cooling the hot flue gas and the calcium sulfite oxidation to gypsum, promote the dissolution of CaCO_3 ; high pH mainly used for the absorption of SO_2 . So we combine the two new techniques to establish the double circulating falling film wet flue gas desulfurization test system, but by the test conditions are only tested tower, studied the effects of various operating parameters on the desulfurization process [5–7].

2 EXPERIMENTAL STUDY

2.1 Research contents

On the falling film desulfurization test system of double-pH, under 45 ° C, gas—liquid two-phase operating parameters on single tower falling film desulfurization process, of which, including the pH of liquid phase parameters (3.5, 4, 4.5, 5, 5.5), slurry concentration (130, 145, 160 g/L) and liquid-gas ratio (15, 20, 25 L/Nm³); vapor parameters including the velocity of flue gas (3.2, 3.7, 4, 4.5 m/s) and absorption tower entrance SO_2 concentration (2000, 3000, 4000, 5000, 6000, 8000 mg/Nm³). In the process of test on the system performance parameters were measured, the

wet flue gas desulfurization environment SO_2 absorption variation characteristics and CaCO_3 concentration.

2.2 The experimental system

Through small the falling film reactor simulation of double-pH wet removal system, we studied process of SO_2 absorption characteristics and the concentration of CaCO_3 in wet FGD. The system as shown in Figure 1.

In the falling film reactor, absorption desulfurization slurry goes along the wall under the action of gravity, at the same time, thus removing the SO_2 . Falling film tube diameter is 29 mm, effective removal of height 2 m, oxidation zone for circulating slurry tank, 4 sets of gas and slurry sampling points in the height direction of falling film reactor, sampling measurement on the desulfurization process. The wall of the tank is provided with a plurality of different heights of the overflow port, experiment with different overflow port to control the liquid residence time in the pool. Slurry added groove in the corresponding CaCO_3 slurry added in the measurement of circulating pool of slurry pH. The experimental system is divided into four parts: smoke simulation system, the slurry circulating system, oxidation system and limestone slurry and sewage system [8].

2.3 The experimental method

The concentration of CaCO_3 will affect the efficiency of desulfurization in slurry, which affects the consumption of desulfurization agent and system economical operation. Therefore, in the process of test, always online monitoring of CaCO_3 concentration is important. In order to avoid slurry dissolved on measurement deviation, sample liquid filtration take a certain amount of, then the filtered solid content by titration. CaCO_3 content

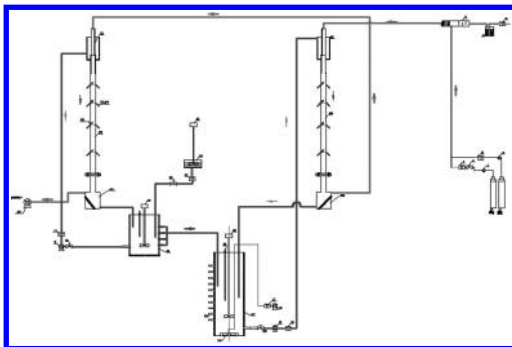


Figure 1. Falling film reactor desulfurization test system diagram.

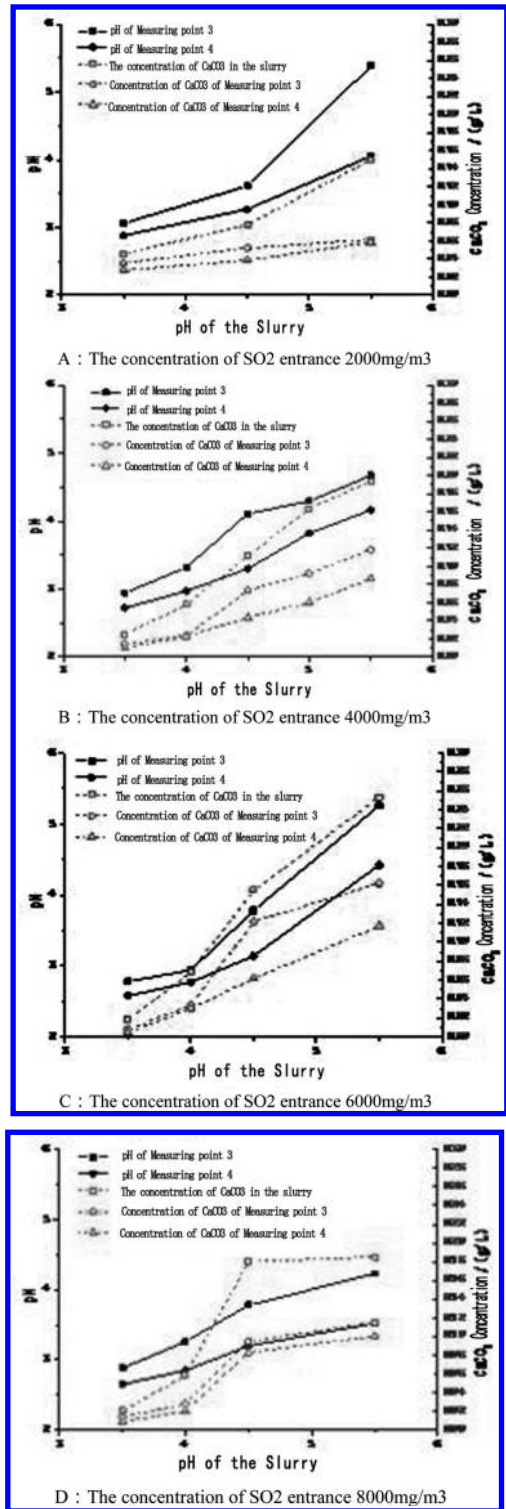
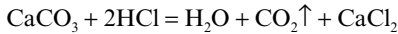


Figure 2. The pH and CaCO_3 concentration.

was determined by acid titration method, CaCO_3 was determined by HCl standard solution and the dilute solution, reaction products were CaCl_2 and H_2CO_3 , titration reaction is:



To the end point of titration when the pH value is about 3.9, can choose 0.1% methyl orange as the indicator, the end solution changed from yellow to orange. HCl solution for titration of CaCO_3 , because the reaction to produce H_2CO_3 , titration process pH change is not obvious, the color of the solution changed not sensitive enough. Therefore, close to the end point of titration, the solution is heated to boiling the solution CO_2 out, and accelerate the decomposition of H_2CO_3 , cooling to room temperature and then continue the titration [9–10].

2.4 Experimental results and discussions

1. By 2–2 analysis, pH of slurry decreased along the process of absorption of SO_2 , and high pH value in the pulp tank along the slurry pH value greater changes. At the same time, a slurry tank pH value is high, is relatively along the pH is higher, the corresponding points of CaCO_3 concentration is higher. As in a slurry tank pH = 4.5, measuring point 2 of the pH value is 4.1, and the measuring point 4 of the pH value is 3.1; and the slurry tank pH = 3.5, measuring point 2 of the pH value is 2.9, measured 4 pH value is 2.75, the higher pH value of slurry tank, is relatively along the the pH value is high.
2. As also can be seen in 2–2, as slurry tank raises the pH, the concentration of CaCO_3 in circular groove increases. Such as the entrance to 6000 mg/m^3 SO_2 , slurry pH from 3.5 to 4.5, the contents of limestone slurry tank from 0.06 g/L to 0.085 g/L, relatively slow growth; but the slurry pH from 4.5 to 5.5, the contents of limestone slurry tank from 0.085 g/L to 0.150 g/L, the limestone content increases sharply. This is due to the dissolution of limestone is between Ca^{2+} and CO_3^{2-} through a solid surface of solid phase and liquid phase liquid solid film subject to the main liquid phase diffusion process.
3. From Figure 2, as SO_2 entrance concentration raised, CaCO_3 concentration in the slurry increases. As pH = 5.5 entrance SO_2 concentration 2000 mg/m^3 , CaCO_3 concentration of circular groove 0.17 g/L; entrance SO_2 concentration 4000 mg/m^3 , CaCO_3 concentration of circular groove 0.195 g/L; entrance SO_2 concentration 6000 mg/m^3 , CaCO_3 concentration of circulating tank 0.255 g/L. This is because, SO_2 entrance concentration increased, the need to increase the concentration of limestone slurry tank to keep the system stable chemical.

3 CONCLUSION

Double-pH test system of limestone gypsum wet flue gas desulfurization based on, on a single pH value of desulfurization performance falling film reactor, and get the change law of CaCO_3 concentration in wet desulfurization absorption slurry SO_2 and:

1. The SO_2 absorption is effected by SO_2 entrance concentration, pH of slurry, liquid gas ratio, gas velocity and slurry concentration;
 - ① The entrance concentration is lower to higher absorption efficiency, and low concentrations decreased faster absorption efficiency;
 - ② The pH of slurry SO_2 the higher absorption efficiency is high, the test cycle slurry tank slurry pH is 5.5, SO_2 the best absorption effect, with the ratio of liquid to gas to increase desulfurization efficiency increases;
 - ③ The empty tower gas velocity increasing section, desulfurization efficiency will reduce;
 - ④ The slurry concentration is higher, the lower the SO_2 absorption efficiency;
2. Factors affecting the CaCO_3 concentration of slurry are the SO_2 entrance concentration and pH of slurry tank;
 - ① The entrance concentration SO_2 , CaCO_3 concentration in the slurry;
 - ② The higher pH value of slurry tank, along the higher concentration of CaCO_3 ;
3. Desulfurization system operation at low pH, will increase the solubility of CaCO_3 ; but when the pH value is less than 4.5, the absorption efficiency of SO_2 will greatly reduce the risk at the same time, increase equipment corrosion. Therefore, the desulfurization system should be run in 4.5 ~ 5.5.

ACKNOWLEDGEMENT

This paper was financially supported by the Doctor Foundation of Shandong Jianzhu University (No. XNBS1223) and the independent innovation project of academics in Jinan (No. 201401223). The authors would also like to acknowledge the extended help from the Department of Thermal Engineering.

REFERENCES

- [1] Dongmei Cao. Harm and control technology of SO_2 pollution in China [J]. Chinese Journal of Environmental Science, 2013, 02:73–74.
- [2] Zhongxing Shao, Hongjian Li. Present situation and control pollution of coal-fired SO_2 Counter measures in China [J]. Shanxi chemical industry, 2011, 01:46–48+57.

- [3] Qian Du. Study on process of SO₂ removal by orderly falling films with cocurrent gas-liquid contacting [D]. Harbin Institute of Technology, 2004.
- [4] Xuejing Zhang. Falling film desulfurization gas-liquid mass transfer theory and experimental research [D]. Beijing Institute of Civil Engineering and Architecture, 2012.
- [5] Wenju Jiang. Flue gas desulfurization and denitration Handbook [M]. Beijing: Chemical Industry Press, 2012.
- [6] Zhibing Fan. Hazards of sulfur in coal for power plant equipment and Countermeasures [J]. Hebei Electric Power Technol, 1994, 03:45–48.
- [7] Jianjun Liu, Zhihua Zhao, Xuean Yan. To investigate the uprating scheme system of wet desulphurization device SO₂ absorption [J]. Electric power technology and environmental protection, 2011, 06:33–35.
- [8] Jinglong Liu. Experimental study on double-pH wet flue gas desulfurization [D]. Shandong University, 2012.
- [9] Wang Huo. The oxidation and crystallization mechanism of Limestone—gypsum wet desulphurization absorption process [D]. Zhejiang University, 2009.
- [10] Qian Du, Chunyuan Ma, Yong Dong. Influence of gas velocity of empty tower section of limestone/gypsum wet flue gas desulfurization process [J]. Power Engineering, 2007, 02:267–272.

Development and research status of renewable energy utilization in Shandong province

Dong Yang

Key Laboratory of Renewable Energy Utilization Technologies in Buildings of the National Education Ministry, Jinan, China

Qing Mei Wen

Shandong Provincial Key Laboratory of Building Energy Saving Technology, Jinan, China

Shi Jun Wei

School of Thermal Energy Engineering, Shandong Jianzhu University, Jinan, China

ABSTRACT: Introduce the renewable energy development and application status in Shandong Province, in view of the problems encountered in the process of the use of renewable energy, puts forward some reasonable suggestions and measures.

Keywords: renewable energy; development situation; measures

1 INTRODUCTION

At present, the green wave on the theme of energy revolution and low carbon economy is sweeping the world, energy strategy has a decisive role in the international competition. Widely used in solar, wind and biomass for renewable energy [1–4], not only has the advantages of energy saving, emission reduction and low carbon environmental protection role, but also can create new industries, to create a new round of economic growth, promote national economic development and social stability. Actively promote renewable energy application in buildings, is the most economical choice to solve the problem of building energy use, has very important significance to meet the growing demand for energy construction, improving people's quality of life, improve building energy efficiency and promote the energy-saving of construction.

2 ENERGY SITUATION

Shandong province is an important energy base in China. Coal, oil and other fossil energy resources are more abundant, widely distribution of new energy and renewable energy resources, has favorable conditions of development. Wind energy resources of about 88000000 kilowatts, among them the land-based wind energy resources develop about 20000000 kilowatts, mainly distributed in

Yantai, Weihai, Qingdao, Dongying, Binzhou and other coastal city. Biomass with the using conditions such as crop straw, livestock manure, waste water and living garbages can reach more than 20000000 tons of standard coal per year. Nearly 1/3 area in 2200 hours of annual sunshine, solar total radiation value is equivalent to 731 tons of standard coal. In the 17 cities have geothermal resources, the total heat equivalent to 312 tons of standard coal. The coastline length is more than 3000 kilometers, near shore waters are rich in marine energy resources, can develop and make full use of tidal and wave energy.

3 THE HUGE POTENTIAL OF APPLICATION

Shandong is a big province of energy resource consumption, relative lack of conventional energy resources, the mineral resources per capita amount is about 49% of the national average level. The province is currently in the stage of accelerate development of industrialization and urbanization, higher energy consumption intensity, and expanding consumption scale make the contradiction between energy supply and demand have become increasingly prominent. Construction field is the large consumption of energy, according to estimates, in 2007 the province building energy consumption was 43800000 tons of standard coal,

about 23.6% of total energy consumption. With the development of urbanization and the improvement of people's living standards, building energy consumption will increase rapidly, according to estimates, by 2012, the construction of the total energy demand of 49500000 tons of standard coal, accounting for about 25% of the total energy consumption of the whole society, building energy-saving situation grim. Shandong province existing residential construction area is about 112000000 square meters, expected in the next five years the average annual increase about 50000000 square meters, and the province's cities and towns in solar water heater installation area is about 6000000 square meters, shallow geothermal energy building area is 3000000 square meters, architectural applications of renewable energy has great potential, the task is very formidable. We must further enhance the sense of urgency and responsibility, take effective measures to accelerate the pace of building applications of renewable energy, rapidly improve the use proportion of renewable energy in buildings, make contributions to the province's energy-saving emission reduction work [5].

4 APPLICATION STATUS

The construction industry is a big energy consumption, will have a significant impact on the environment. At present, the city building is transform traditional to high efficient green type development mode, the green building is the inevitable trend of architectural development. For the development of renewable energy technologies also tend to diversification, technology increasingly diverse, as shown in Figure 1.

Solar energy and heat pump is the renewable energy technology applied more widely. For the

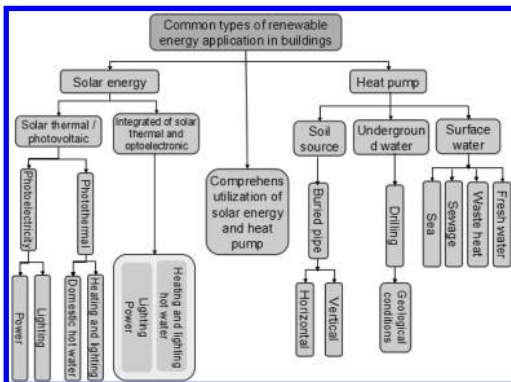


Figure 1. Types of technology in renewable energy application.

application of solar energy, the form from the simple preparation for domestic hot water, as well as the solar cooker, has been developed to the complexity form such as solar heating, lighting, photovoltaic power generation and combined with ground source heat pump. Ground source heat pump are not limited to the application of shallow geothermal energy, soil source, underground water, industrial waste heat and city waste water as a possible cold and heat sources has also been into the demonstration projects of the renewable energy construction application.

The development and utilization of solar energy in Shandong mainly concentrated in the photovoltaic and thermal. The solar water heater production has been basically formed a complete industrial system merge into raw material processing, technology development, product production and marketing services together, also gives impetus to the development of glass, metal, heat insulating materials and vacuum equipment and other related industries, has become a rapidly emerging industry. Geothermal development in Shandong is mainly used in medical, health, bathing, heating etc. Currently the geothermal field has initially proved reserves and has been developed and used are in Dongying, the northern city of Ji'nan, Liaocheng, and several other areas. Notable is, the application of ground source heat pump has gradually emerged in Shandong in recent years. The ground source heat pump system has broad energy saving value in the indoor temperature regulation of office, hotel, residential and other buildings.

5 PROBLEMS IN THE USE OF RENEWABLE ENERGY PROCESS

With the continuous expansion of the scale of the industry, many problems and obstacles that the development of renewable energy facing shows gradually.

5.1 Weak independent innovation capability, low technology level

Although our country has increased in the key technology R & D and innovation ability of new energy utilization, but on the whole, regardless of level of scientific research or input in our country, compared with foreign developed countries still have obvious difference. Its weakness in basic research, innovation, basic research work carried out less, late start, low level. The lack of powerful technology support platform, the lack of a clear system of technology roadmap and long-term development of ideas, not continuous, rolling investment plan, funding for research and development support is

obviously insufficient, leading to the core technology of most of the domestic enterprises are from abroad, technology of heteronomy buried a crisis for the development of the whole industry.

5.2 *Administrative management is loose, the standard system is not perfect*

Over the long term, renewable energy management function of our scattered in a number of departments, the cross department functions, separate management, funds dispersed, the lack of coordination, conflict, and can not form a cohesive force, to a certain extent, weakened the national macro-control capacity, there is "have mechanism no management" problem. In addition, along with the development of the industry and expand the domestic market, lack of technical standard, and lack of personnel issues have become increasingly prominent, the need for new energy industry development direction related departments to coordinate research, introduced the system of strong support policy, torsion of funds in the development of disordered state.

In such an environment, Shandong province by using the technology of new energy to face the same problem. The majority of renewable energy commercialization degree is low and the cost is too high, the market development is not mature and capacity is relatively small. Wind, ocean, geothermal energy development in the initial stage. Biomass still accounted for a considerable proportion in rural energy consumption in Shandong province, most of the direct combustion of firewood. Biomass gasification, liquefaction technology in its early stages, biogas utilization has not yet reached the level of business application. To realize industrialization, must eliminate the disorder of technology, capital, market and mechanism. To reduce the cost and promote the implementation of incentive policies.

6 DEVELOPMENT STRATEGY

6.1 *Speeding up the research and innovation, improve the technical standards*

Actively supports the development, integration and applicate demonstration of the application of renewable energy buildings [6], organize the introduction, digestion, absorption of foreign advanced technology, encourages the research and development of renewable energy application products that with high technology content, good economic performance and remarkable energy-saving effect to enhance the capability of independent innovation. Research on the standardized production pattern of renewable energy production equipment

combined with construction, improve the level of technology and application.

6.2 *Insist that the government guidance, increase capital investment*

Put the application of renewable energy buildings into all levels of the national economic and social development planning, formulate preferential policy, increase financial support, the relevant departments and social forces to actively participate in, establish diversified channels of investment and financing mechanism [7–10]. Do well the technical research and development, and gradually establish and improve the technical support system of renewable and new energy development, to promote it as an important area of research work. Major scientific research and technology development projects should be listed in priority in technology plan, policy to guide, investment to tilt, renewable energy industry development will be included in all levels of government develop and scientific research plan, and into the fiscal budget.

6.3 *Increase publicity and training, strengthen the organization and leadership*

Give full play to the guiding role of public opinion and supervision, vigorously promote the status of renewable energy resource and significance of the use in buildings. Actively promote and expand the influence of successful experience in the demonstration project operation mode, technology, operation and management. Strengthen the propaganda and guidance, make the construction sector and the vast majority of people recognize the importance of renewable energy, as well as the advantages of renewable energy application in buildings, actively participate in the building applications of renewable energy, to form a market driven mechanism of building applications of renewable energy.

6.4 *Improve policy support, establish perfect mechanism*

According to the national policy, the province should be timely introduce matching administrative regulations, administrative rules and the corresponding technical specification of development plan, sound regulations and standards, strengthen supervision and management. Assigned a part of renewable energy middle or long-term development goals to each area, refine the problems such as the total system of renewable energy targets, renewable energy power generation approval, price and full acquisition system, renewable energy special funds and tax, credit and others, make them easy to operate.

ACKNOWLEDGEMENTS

This work was supported by Shandong Province in 2014 of urban and rural housing construction science and technology project (KY013) and Ji'nan university institute innovation project (201401223) supported.

REFERENCES

- [1] Yang Ji-chun. Some Thoughts on Application of New Energy in Energy-Saving Buildings[J]. Applied Energy Technology, 2008, 03: 32–34.
- [2] He Wen-jing, Li Pei, Liu Ya-mei. The application planning of renewable energy building in Jinan[J]. Journal of Shandong Jianzhu University, 2011, 03: 251–255.
- [3] Liu Zhen, Zhang Xi-liang, Gao Hu et al. Study on Design and Evaluation of the Development Scenarios of Renewable Energy[J]. Chinese population, resources and environment, 2011, 21 (7): 28–32.
- [4] Xiao Guoxing. The legal path of renewable energy development[J]. Academic Journal of Zhongzhou, 2012, (5): 79–85.
- [5] Yang Xiaomei, Xu Mingxian, Sun long higher. Renewable energy industry in Shandong province development and utilization in Shandong Industrial[J]. Technology, 2014, 01:72–72.
- [6] Han Bao-hua, Qiao Liang, Liu Bin-yong. Application Situation of Renewable Energy in Construction and Development Approach of Shandong Province[J]. Building Energy Efficiency, 2008, 06:56–58.
- [7] Li Jun-feng, Shi Jing-li, Wang Zhong-ying. New progress of renewable energy policy in Europe and its reference for China[J]. Renewable Energy Resources, 2007, 25 (3): 1–3.
- [8] Xie Xu-xuan, Wang Zhong-ying, Gao Hu. Advanced national renewable energy development subsidy policy and Its Enlightenment to China[J]. Renewable Energy, 2013, 35 (8): 15–19.
- [9] Li Hong, Dong Liang, Duan Hongxia et al. On Comprehensive Evaluation and Optimization of Renewable Energy Development in China[J]. Resources Science, 2011, 33 (3): 431–440.
- [10] Li Xiao-long. Source, use and management of China's renewable energy development fund[J]. Consumer Guide, 2013, (6): 39–40.

A new prefabricated construction method based on building industrialization

J.N. Luo

School of Architecture, Southeast University, Nanjing, China

H.Y. Zhu & H. Zhang

Department of Building Science and Technology, Southeast University, Nanjing, China

ABSTRACT: Cities in China now are facing eager demand of residences. To achieve environmental sustainability, industrialized housing based on prefabricated construction system is an effective way. But the single construction technology had posed adverse effect on the building industrialization. The article analyses the problems of current prefabricated construction method-Prefabricated Concrete system (PC) and proposes a new prefabricated construction method called “Frame formwork” based on building industrialization, trying to solve the problems through a demonstration project practice-Nanjing Jiangning Galley of Modern Art. Then the article comes to the conclusion that “Frame formwork” is a way to solve the problems and is worth further researching.

1 INTRODUCTION

Today’s cities are responsible for the vast majority of the world energy consumption and ever-increasing greenhouse gas emissions, making them instrumental in driving the global urban metabolism. Greater concentrations of people will soon be living in cities than in rural areas. As cities across the globe increasingly adjust to accommodate the rapidly expanding population, cities in China now are facing eager demand of residences. To achieve environmental sustainability, industrialized housing based on prefabricated construction technology is obviously an effective way to achieve the goal. In addition, because of population problem and economic and environment situations of China, it is widely believed that high-rise residential on reinforced concrete system is the most needful housing type in China. So it is imperative that we begin to find a feasible building construction technology and how it can achieve global environmental sustainability.

Nowadays, prefabricated reinforced concrete construction system (PC) had played the absolutely leading role in the industrialized housing over the past decades in China and many houses were under construction based on PC system. Some of them had come into use for several years, but PC system had not truly spread across China. It is also well known that it has its drawbacks such as hard to transport, poor in physical properties

and so on, which were hard to solve systematically. The single construction technology also had posed adverse effect on the building industrialization. So it is also crucial to find a more reasonable and effective prefabricated construction method to accomplish the building industrialization in China.

2 CURRENT PREFABRICATED CONSTRUCTION TECHNOLOGY

2.1 *Situation analysis*

The construction activities of Prefabricated Concrete System (PC) based on the building industrialization now already become the main direction to accomplish the building industrialization in China. But PC construction technology cannot fully replace and update the traditional patterns of architectural design and construction. Introducing the most advanced precast concrete production CNC equipment, competing patent applications, preparing the technical regulations for PC become fashionable phenomenon in China now. These reflect the overwhelming dependence on the single prefabricated construction technology and the neglect of the true purpose of the building industrialization. In addition, many projects were pursuing the simple form of “industrialization” such as the simple prefabrication but lack the systematical analysis of the whole building system.

2.2 Problem description

In China, it is widely believed that high-rise residential on reinforced concrete system is the most needful housing type now and reinforced concrete structure is the main structural type for most buildings. From the perspective of building industrialization, the accomplishment of building industrialization depends heavily on the structure. According to the current reinforced concrete construction technology of structure, there are two kinds of construction methods in general: Precast Concrete, Cast-in-Place Concrete. In brief, there are three critical problems that hard to solve systematically in the construction of reinforced concrete:

1. Fixed position of steel bar
2. Fixed form of concrete
3. Fixed position of structural components.

2.3 Precast concrete construction technology

For the precast concrete construction method, the main purpose is to divide the whole structure to the precast concrete elements that can be prefabricated in the factory, delivered on the road, assembled on the construction site. This construction method is to pursue the high rate of prefabrication and decrease the construction site working as much as possible. The enterprises such as Vanke and Dadi are using this technology now, but they have not truly popularized this technology successful. In general, the reasons are as follows:

1. Structural System: The single technology pathway (PC system)
2. Manufacture: Underdeveloped mechanical technologies
3. Delivery: Huge precast components and high transport costs in China
4. Building Construction: Unsatisfactory joining technology between precast elements
5. Building Performance: Unsatisfactory joining technology between prefabricated building components and poor in physical properties.

2.4 Cast-in-place concrete construction technology

For the Cast-in-Place Concrete construction method, this is the most widely used construction technology now. Cast-in-place concrete is transported in an unhardened state and placed in forms. Ready mixed concrete is proportioned and mixed off the project site. Because of the low cost, the low technology and the well structural integrity, it is the best choice for the high-rise residential. But it has the low level of industrialization and poses adverse effect on the environment. So developing

an improved prefabricated construction technology based on cast-in-place concrete could be a new way.

2.5 Methodology of industrialization in architectural design and formation

The perspective of research about building industrialization mostly concentrated in the construction techniques, construction equipment, professional design standards, production equipment and so on. The research of architectural design is usually from the perspective of “modular”, “standardized”, lacking the order in architectural design and formation. Methodology in Architectural Design and Formation tries to establish a set of rules and regulations of design and construction principles based on a new prefabricated construction system towards building industrialization and balance the desirable integration of architecture and structural design.

3 A NEW PREFABRICATED CONSTRUCTION METHOD

3.1 “Frame formwork” construction system

Our team has been working on a new construction method called “Frame Formwork” for several years. To solve three critical problems mentioned above in the construction of reinforced concrete, we fabricate steel frame with formwork without pouring the concrete in the factory which are too much lighter than PC components and delivered them to the construction site and assemble them. Actually, it is formwork with frame (steel skeleton) on it to replace the heavy prefabricated concrete structural components and it is steel structure before pouring the concrete on the construction site. In other words, it is a type of improved cast-in-place concrete structural construction system. “Frame

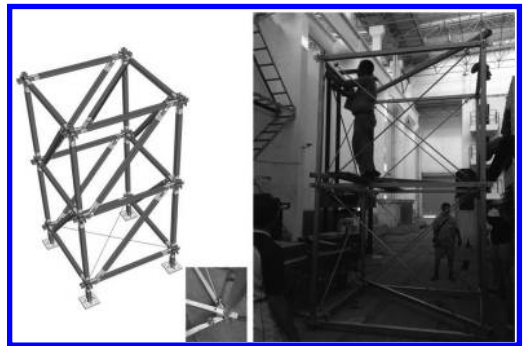


Figure 1. “Composite Grid Scaffold”.

Formwork” can be seen as some prefabricated service elements for the structural components so as to maintain the advantages of the cast-in-place concrete system and meanwhile the advantages of precast concrete construction technology.

3.2 “Composite Grid Scaffold”

Scaffold plays very crucial role in building process. “Composite Grid Scaffold” is actually one kind of improved scaffold whose standard components are the same as that of “Frame Formwork”. So the function of this new scaffold can take more responsibilities: formwork supports, skeleton of formwork, construction platform and even the location of different prefabricated building components. Because of its standardization, it is easier to manufacture in the factory, delivery on the road and assemble on the construction site.

4 DEMONSTRATION PROJECT- NANJING JIANGNING GALLERY OF MODERN ART

4.1 Introduction

The building will be built in the Jiangning District of Nanjing. The function and the space of the building is very simple. Its building area is only about 700 m² and the height is 8 m. It is just for the exhibition of the modern art works that are from local artists. The main purpose of the building is to accumulate some technical details and experience.

4.2 Construction idea

The whole building can be divided into four parts according to the building process: structure, building envelope, interior decoration, service system. The main purpose was to pursue the maximal independence of the four parts so as to enhance

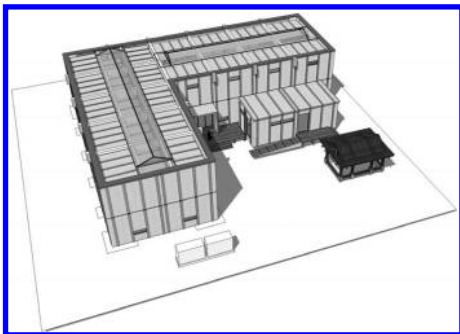


Figure 2. Nanjing Jiangning gallery of modern art.

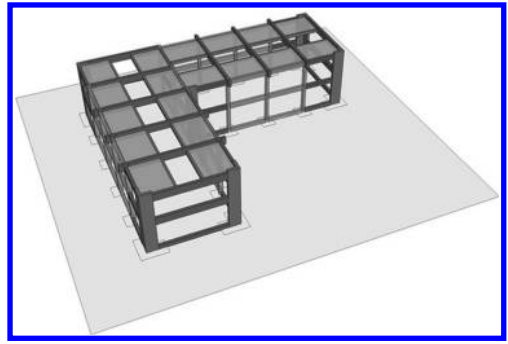


Figure 3. Independent structure.

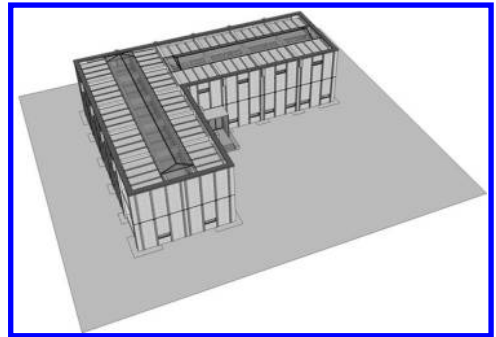


Figure 4. Independent building envelope.

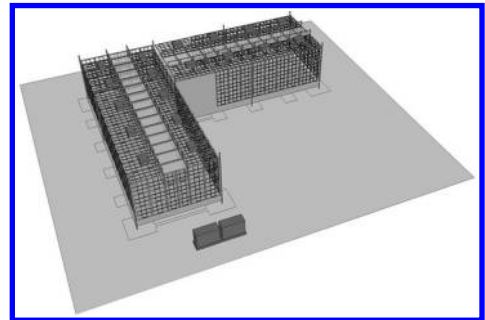


Figure 5. Independent service system.

the prefabrication rate in the factory. In the design phase, we followed this principal and converted the traditional construction drawings to the four parts of drawings which only had the information that different kinds of workers (in construction site or in factory) needed.

In addition, there are more benefits to divide the whole building into four parts. Because of their independence, they can provide essential tolerance and diversity. For structure, it can provide

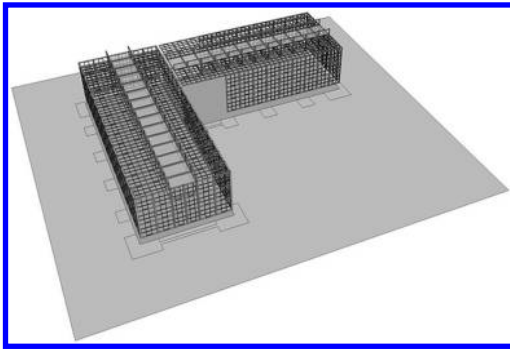


Figure 6. Independent interior decoration.

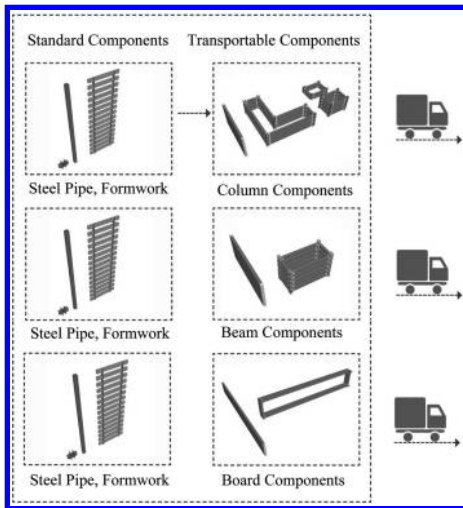


Figure 7. Prefabricated components in factory and delivered.

more possibilities for the diversity of the building envelope. For building envelope, it can realize not only the high prefabrication rate in the factory, but also the tremendous convenience for the maintenance. For example, the architects just need to replace some parts of the components of the building envelope to satisfy the building performance requirement in different place or the different aesthetic needs of clients. For interior decoration, it can provide more space possibilities. With the process of the project, we would renew the information at any time to guarantee the consistence with construction site.

4.3 Building process

The project used “Frame Formwork” construction method. Compared to the current prefabricated

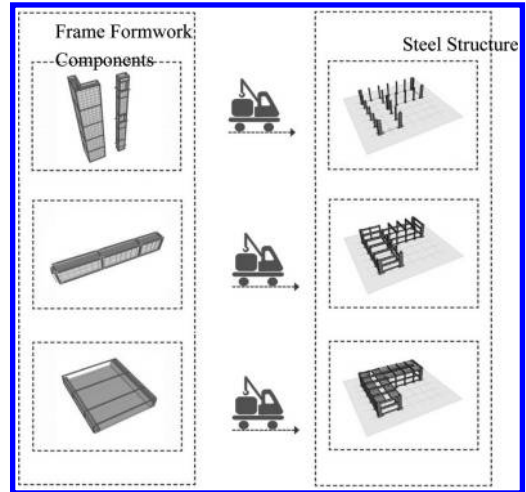


Figure 8. Preassembled in on-site factory and hoisted in position.

construction technology, the new construction tried to find another prefabricate construction way to solve the five problems that mentioned above.

Following the four parts of the building, the construction of the building could be more effective and reasonable than the PC system. Building process contains four steps: producing standard components, fabricating transportable components in the factory, preassembling big components in the on-site factory and installing them to the building. Taking structure for example, the building process can be shown as follows.

5 PRODUCTIZATION CONSTRUCTION MODE

5.1 Productization of building

Productization construction mode could be summarized to manufacture and sale building sub-assembly based on architectural industrialization mode, to assemble building products based on building industrialization mode, to maintenance building components based on product pattern. Compared to the current construction mode towards building industrialization, productization construction mode has more characteristic of industrial product.

5.2 BIM based on the new construction mode

In the future, based on building information modeling software such us Revit Architecture, the object of this software is to manage all lifetime of

building and will try hard to satisfy the needs of six aspects on “Frame Formwork” prefabricated construction system from design to using. It will be the necessary tool to realize the productization construction mode.

6 CONCLUSION AND PROSPECT

To sum up, both precast concrete construction method and cast-in-place concrete construction method have their advantages and disadvantages. How to keep balance among prefabrication rate, transportation and construction is core issue. “Frame Formwork” prefabricated construction method based on productization construction mode towards building industrialization provides a kind of thought to try to avoid drawbacks and maintain the advantages of the two construction methods. It is worth further researching.

This work was supported by National Key Technology R&D Program under Grant No.2012BAJ16B03.

REFERENCES

- Carlos H. Caldas, Lucio Soibelman, Les Gasser. 2005. Methodology for the Integration of Project Documents in Model-Based Information Systems. *Journal of Computing in Civil Engineering*. 19(1):25–33.
- Gao, Y. 2010. The developing trend and measures of building industrialization. *Industrial & Science Tribun.* 9(5):117.
- Ji, Y.B. 2011. *The development research of Building Industrialization*. Beijing: China Architecture & Building Press.
- Zhu, H.Y, P. 2013. *Assemble and Disassemble method of “Frame Formwork”*. China: 201310037930.X, 2013.05.
- Zhu, H.Y, P. 2013. *Assemble and Disassemble method of “Composite Grid Scaffold”*. China: 201310037858.0, 2013.05.
- Zhu, H.Y, P. 2013. *Assemble and Disassemble method of “Split Node”*. China: 201310037922.5, 2013.05.
- Zhu, H.Y, P. 2013. *The installation method of “Stair Frame Formwork”*. China: 201210370715.7, 2013.01.

An analysis of landslide thrust of each row of double-row and embedded anti-slide piles

Jun Xu, Ying Gang Pang & An Hong Li

China Railway Eryuan Engineering Group Co., Ltd., Chengdu, Sichuan, P.R. China

Xin Hua Xue

State Key Laboratory of Hydraulics and Mountain River Engineering, College of Water Resource and Hydropower, Sichuan University, Chengdu, Sichuan, P.R. China

ABSTRACT: Now in the treatment of large-scale landslide, double-row or multi-row and embedded anti-slide piles has been widely used. Yet the traditional limit equilibrium method can't calculate the landslide thrust of each row of piles. Then it is difficult to ensure the safe, reliable, economical and reasonable design of anti-slide piles in large-scale landslides. Based on full-scale geomechanical model test and strength reduction method of finite element, the landslide thrust of each row of piles in landslide with curve slip surface and linear slip surface is studied. Also the rule of landslide thrust of each row of piles varying with the row distance and buried depth is further analyzed. And after that, the design rule of double-row and embedded anti-slide pile is presented which is helpful for improving the multi-row anti-slide piles' design in large-scale landslide.

Keywords: large-scale landslide; thrust of piles; double-row and embedded anti-slide pile

1 INTRODUCTION

In the recent years, the double row pile or multi-row and embedded anti-slide pile for landslide treatment also gradually obtained the application (CREEC 1981; Xiong et al. 2002; CREEC 2010). As the double-row pile or multi-row pile has larger resistance and their thrust against landslide is better than general anti-slide pile, so they have been widely used in the large and super large landslide treatment. However, the calculation theory on multi-row pile combination system is not enough mature: such as how to know the interaction between pile and pile-soil, the influence factors of soil body and the stiffness characteristics of pile shaft, the influence of boundary stress characteristics of single pile in the multi-row pile system on shaft stress characteristics of single pile, and how to distribute the external load in different pile-rows, etc. For the multi-row anti-slide pile, how to know the landslide thrust is borne by each row pile, how to determine the reasonable pile row distance, how to know the thrust is borne by embedded pile, the thrust distribution form, and how to determine the pile buried depth, etc., these cannot be effectively solved according to the current conventional limit equilibrium design calculation method.

The recently developing finite element strength reduction method can give full consideration to the pile-soil common function. Through the strength reduction the internal force of structure (Zhen et al. 2004, 2005, 2009; Xu et al. 2010; Yang et al. 2010) can be calculated. As compared with the traditional limit equilibrium method, the finite element strength reduction method is used not only for accurately calculating the safety coefficient and the critical slip surface, and can be for reproducing the development process of rock mass deformation, especially in the retaining structure design, the advantages are more obvious. The calculation of Wulong county large landslide and large geological mechanical model test results and centrifugal model test results also proved the applicability of finite element strength reduction method (Zhao et al. 2009; Xu et al. 2009, 2010).

Taking the double row pile as an example, this paper has researched the two kinds of typical landslide with linear and curve slip surface. The finite element numerical calculation program is used for analyzing the landslide thrust borne by each row of piles with different pile row distance and pile length, and for summing up the rule of landslide thrust borne by double-row and embedded anti-slide pile: (1) the landslide thrust received by front and rear pile and their distribution change

rule when analyzing different pile row distance; (2) the thrust size received by front and rear pile and their distribution change rule when analyzing the different buried depth of rear pile to provide a theory basis for the design optimization of anti-slide pile.

2 THRUST SHARING RULE WHEN DOUBLE-ROW ANTI-SLIDE PILE'S ROW DISTANCE CHANGES

2.1 The landslide with curve slip surface

For this kind of landslide, the main sliding section is the curve slip line, the front anti-sliding section is longer, resistance slide feature is apparent. Calculation model is shown in Figure 1, the calculation model is about 170 m long and 105 m high. The pile section is 3.0 m wide and 2.0 m long.

The material parameters for calculation are shown in Table 1, and the Drucker-Prager (DP) soil model is adopted.

Calculation is carried out using ANSYS finite element program according to the plane strain model, and the front-row pile is fixed. When the pile distance changes, the calculated landslide thrust borne by each row pile is shown in Figure 2. The reduction coefficient is 1.27.

According to the calculation, it can be found out that (1) when the curve slip surface landslide

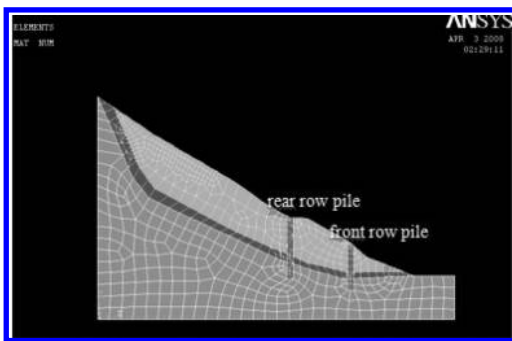


Figure 1. Calculation model of landslide with curve slip surface.

is reinforced using double-row pile, the total thrust borne by double-row pile is more than that of only a single pile, namely when the reduction coefficient is same, the sum of landslide thrust borne by double-row pile is more than 14%~41% of only a single pile; (2) with the increase of the row distance, the thrust borne by front row pile increases gradually, the thrust borne by the rear row pile increases firstly, then decreases; (3) the front pile is located in the front landslide sliding section, the rear row pile is located in middle-front landslide sliding section or in the middle slide down section, most of the landslide thrust is borne by the rear row pile, namely the landslide thrust of 30%~40% for the front row pile, and the landslide thrust of 60%~70% for the rear row pile.

As shown in Figure 2, when the front row pile position is fixed, and the distance between the rear and front row piles is increased gradually, the thrust ratio of the front row pile increases, the thrust ratio of the rear row pile decreases. But two row of piles is spaced within the range of 10~70 m, the landslide thrust proportion for each row pile is basically unchanged or slightly changed. Only when the rear row pile is arranged in the landslide rear edge, the thrust proportion for each row pile is changed sharply.

2.2 The landslide with linear slip surface

This landslide slides along the bedding or the structure surface, and the main sliding section is linear. Its front sliding section is small and the sliding resistance characteristic isn't obvious. The calculation model is about 220 m long and 130 m high, and the calculation model is shown in Figure 3. The material parameters for calculation are as same as the landslide with curve slip surface.

Calculation is carried out using ANSYS finite element program according to the plane strain model. The front row pile position is fixed and the rear row pile position can be changed. When the pile distance change is calculated the landslide thrust borne by each row pile is shown in Figure 4. The reduction coefficient is 1.25.

Table 1. The material parameters for ANSYS simulation.

Material type	Density (kN/m ³)	Cohesion (kPa)	Friction (°)	Young's modulus (kPa)	Poisson's ratio
Sliding body	20	20	30	—	—
Sliding surface	20	5	23.4	—	—
Bedrock	27	1800	37	—	—
Pile	25			3.45e7	0.2

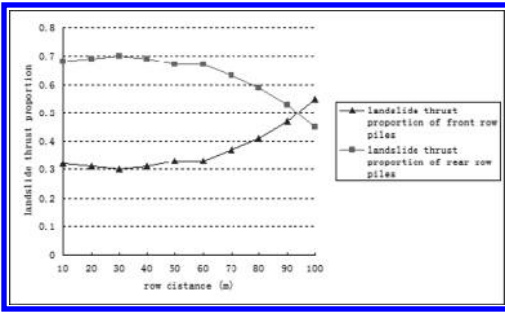


Figure 2. The landslide thrust proportion to row distance in the landslide with curve slip surface.

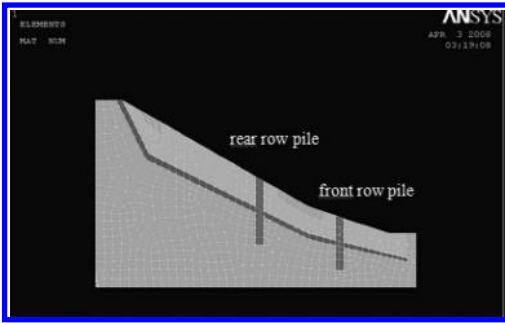


Figure 3. Calculation model of landslide with linear slip surface.

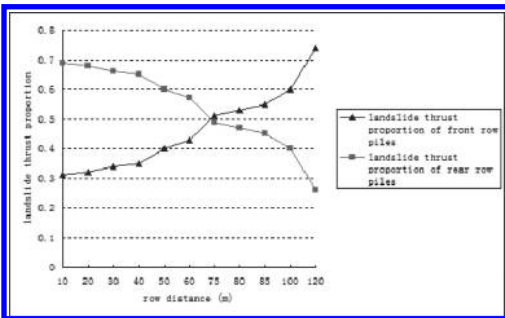


Figure 4. The landslide thrust proportion to row distance in the landslide with linear slip surface.

According to the calculation and Figure 4, it can be found out that (1) when the linear type landslide is reinforced using double-row pile, the total thrust borne by double-row pile is more than that of only a single pile, namely when the reduction coefficient is same, the sum of landslide thrust borne by double-row pile is more than 1.03–1.29 times only a single pile; (2) with the increase of the row distance, the thrust borne by front row pile increases

gradually, the thrust borne by the rear row pile increases firstly, then decreases; (3) the landslide thrust ratio of the rear row pile gradually decreases and that of the front row pile increases, and such change rule is shown in Figure 4.

3 THRUST SHARING RULES WITH DOUBLE-ROW PILE'S BURIED DEPTH CHANGES

3.1 The landslide with curve slip surface

The dimensions of curve slip surface landslide model is shown in Figure 1. The thickness of the sliding zone is 1 m. The length of the rear row pile is 45 m and that of the front row pile is 25 m. The distance between the front and rear row piles is 40 m. Calculations were carried out according to no buried depth reduction in considering the front row pile length and according to the 1/4, 1/3 and 1/2 of buried depth reduction, the thrust size and distribution change of front and rear row piles.

1. Influence of pile top buried depth change on the landslide thrust borne by double-row piles
The thrust calculation results for different pile length are shown in Figure 5.

The calculation results show that with the rear row pile top buried depth increases, the landslide thrust of the rear row pile decreases, and decrease amplitude is about 20%, at this time the landslide thrust of the front row pile increases somewhat, increase rate is only 3%, the sum of the thrust for double-row pile decreases. The conclusion shows that when the rear row pile buried depth increases, the landslide thrust decrease amplitude of this pile is obvious, but the thrust borne by the front row pile is almost unchanged.

2. Distribution mode of thrust in different buried depth

Figure 6 shows the distribution mode of thrust acting on the pile when the rear row pile

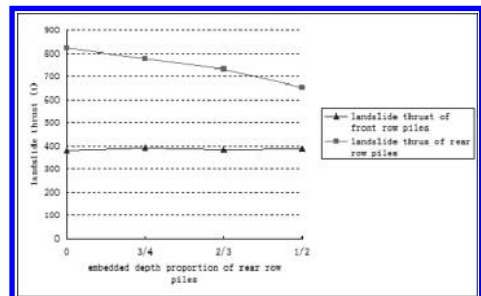


Figure 5. The landslide thrust of double-row piles with different buried depth of rear row piles in landslide with curve slip surface.

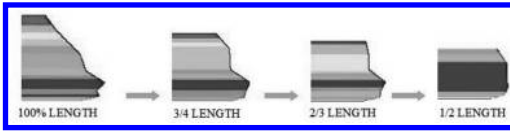


Figure 6. Distribution mode of landslide thrust along the pile with different pile length.

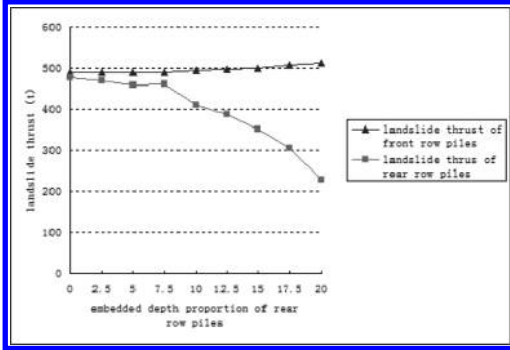


Figure 7. The landslide thrust of double-row piles with different buried depth of rear row piles in landslide with linear slip surface.

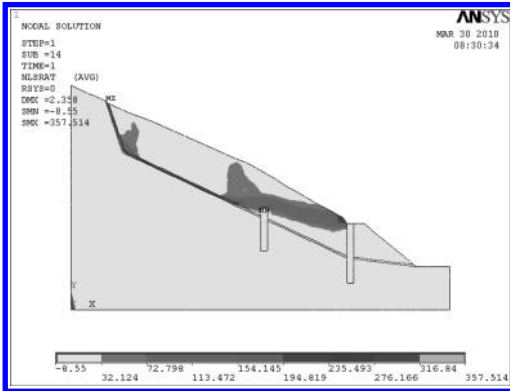


Figure 8. The slip surface of landslide with linear slip surface with 20 m buried depth of rear row piles.

has different buried depth, and different color means different range of the stress value. It can be seen from Figure 6 that when the pile is embedded, with the increase of pile top buried depth, effective landslide thrust gradually changes from a triangular distribution to rectangular distribution.

3.2 The landslide with linear slip surface

Linear slip surface landslide's typical section is shown in Figure 3. Landslide is 220 m long and

130 m high, the front row pile is 34.6 m long and rear row pile is 45 m long. Fix the front row pile position and buried depth, and constantly adjust the buried depth of the rear row pile. The influence of the rear row pile buried depth change on the thrust borne by double-row pile is shown in Figure 7.

It can be seen from Figure 7 that with the increase of the rear row pile buried depth, the landslide thrust of the front row pile increases somewhat and that of the rear row pile gradually reduced. When the buried depth of the rear row pile is up to 20 m (about 1/2 of the pile length), the potential sliding surface appears on the upper part of slope and goes through the rear row pile top, as shown in Figure 8.

4 CONCLUSIONS

Based on the finite element strength reduction method, this paper has discussed the thrust share change rule of front and rear pile with pile spacing change for the double-row piles in curve slip and linear slip surface landslide, and thrust change rule of double-row piles when the rear row pile changes with pile top buried depth, which are shown as follows:

1. When the landslide is reinforced using double-row pile and the reduction factor is same, the total thrust borne by double-row pile is more than that of only a single pile and the sum of landslide thrust borne by double-row pile is more than 10%~40% of only a single pile. If possible, using composite pile such as a chair type pile may be more economical.
2. With the increase of pile spacing, the thrust share ratio of the rear row pile reduces and that of the front row piles increases.
For the linear landslide, the landslide thrust share proportion of the rear row pile reduces, and that of the front row pile increases gradually.
Therefore, adjusting multi-row pile spacing can make the double row pile's landslide thrust more even reasonable.
3. With the increases of rear row pile buried depth, the landslide thrust of the rear row pile is decreased gradually, that if the front row pile almost unchanges or slightly increases. The sum of thrust for double-row pile decreases gradually. So to change the buried depth of the rear row pile in double-row pile can optimize two row of piles' stress.
4. When the pile is embedded, with the increase of pile top buried depth, effective landslide thrust gradually changes from a triangular distribution to rectangular distribution.

This is useful for optimization design of large-scale landslide using the double-row or multi-row

and embedded anti-slide pile for reinforcement (Yang et al. 2010).

REFERENCES

- China Railway Eryuan Engineering Group Co., Ltd. (1981) "Design and Calculation of Anti-slide Pile." *China Railway Press*, Beijing (in Chinese).
- China Railway Eryuan Engineering Group Co., Ltd. (2010) "Research on multi-row and embedded anti-slide piles applied in controlling large-scale landslide." (in Chinese).
- Xiong, Z.W., Ma, H., Zhu, H.D. (2002). "Forceing Distribution of Buried Double Row Anti-slide Piles." *Subgrade Engineering*, (3): 5–11 (in Chinese).
- Xu, J., Li, A.H., Ma, J.L. (2009). "Numerical Analysis of Optimal Design for Wulong Landslide." *Journal of Southwest Jiaotong University*, Vol. 44(S1): 69–73 (in Chinese).
- Xu, J., Li, A.H., Zhao, X.Y. (2010). "Study on Thrust-Sharing Ratio of Large-sized Landslide Pile Row through Centrifugal Model Test." *Subgrade Engineering*, (3): 57–59 (in Chinese).
- Xu, J.B., Zhen, Y.R., Zhao, S.Y., Feng, X.T., Ye, H.L. (2010). "Comparison and analysis of landslide thrust by use of finite element and limit analysis methods." *Chinese Journal of Geotechnical Engineering*, Vol. 32(9): 1380–1385 (in Chinese).
- Yang, B., Zhen, Y.R., Zhao, S.Y., Li, A.H. (2010). "Two-row anti-slide piles in three kinds of typical landslide computations and stress rule analysis." *Rock and Soil Mechanics*, Vol. 31(S1): 237–244 (in Chinese).
- Yang, B., Zhen, Y.R., Tang, X.S., Li, A.H. (2010). "Application of Artificial Intelligence in the Design of Full-length Anti-slide Pile." *Chinese Journal of Underground Space and Engineering*, Vol. 6(2): 358–363 (in Chinese).
- Zhen, Y.R., Zhao, S.Y. (2005). "Limit state finite element method for geotechnical engineering analysis and its applications." *China civil engineering journal*, Vol. 38(1): 91–99 (in Chinese).
- Zhen, Y.R., Zhao, S.Y. (2004). "Calculation of inner force of support structure for landslide/slope by using strength reduction FEM." *Chinese Journal of Rock Mechanics and Engineering*, Vol. 23(20): 3552–3558 (in Chinese).
- Zhen, Y.R. (2009). "New design method of anti-slide pile: strength reduction method of finite element." (in Chinese).
- Zhao, S.Y., Zhen, Y.R., Li, A.H., Qiu, W.P., Tang, X.S., Xu, J. (2009). "Application of multi-row embedded anti-slide piles to landslide of Wulong county government." *Rock and Soil Mechanics*, Vol. 30(S1): 160–164 (in Chinese).

The research for the influence between the WVD and the amplitude of signals

Z.H. Yuan, M.Y. Xu & X.X. Qi

College of Information and Engineering, Shenyang University, Shenyang, China

ABSTRACT: The regulation of variation of the frequency of signals with time is important. WVD that has many great qualities is one of the most imperative method and as a method of analysis in time-frequency domain. However, the relationship between the WVD and the amplitude of signals is always ignored. In this paper, the WVD of signals that has different amplitude is compared and a conclusion about the relationship between WVD and amplitude is achieved.

Keywords: WVD; time-frequency analysis; the amplitude of signals

1 INTRODUCTION

Nowadays, the analysis of signal is that the signal is mapped in time-domain, frequency-domain and time-frequency domain. The time-frequency analysis plays an important role in signal processing. Generally, cross-terms always be concerned and the influence between the result of analysis and parameters of signal is always ignored. In the paper, commonly, the signal amplitude in time-frequency analysis of WVD has a certain influence.

2 THE FOUNDATION OF SIGNAL ANALYSIS THEORY

2.1 Time-domain analysis

Time-domain analysis is the most directly method to analyze in processing of signals. It means that the signal will be filtrated, magnified and disposed by correlation analysis, etc [1]. It can improve SNR through the method of time-domain analysis and get many parameters for providing effective information to fault analysis and diagnosis. Time domain analysis is including parameter value analysis and time domain waveform analysis [2]. The former is used for getting fault information by statistical method, such as mean value, variance and kurtosis.

2.2 Frequency-domain analysis

Frequency-domain analysis is the most common method in project. It means the signal is put in frequency-domain and to analyze its frequency qualities. Commonly, both low-frequency and high-frequency is included in signals, and every

faults has its special frequency [3]. Therefore, separating the special frequency from the rest of frequency and then analyzing it in order to make sure where is wrong and what kind of fault. Frequency-domain is including Fourier transform, power spectrum analysis and Cepstral analysis [4].

2.3 Time-frequency-domain analysis

Stationary signal and time-invariant signal, generally, is analyzed in time-domain and frequency-domain. But for non-stationary signal and time-varying signals, they always is mapped in time-frequency domain to analyze [5]. Good time-frequency analysis method can detect the non-stationary signal frequency's change with time, and

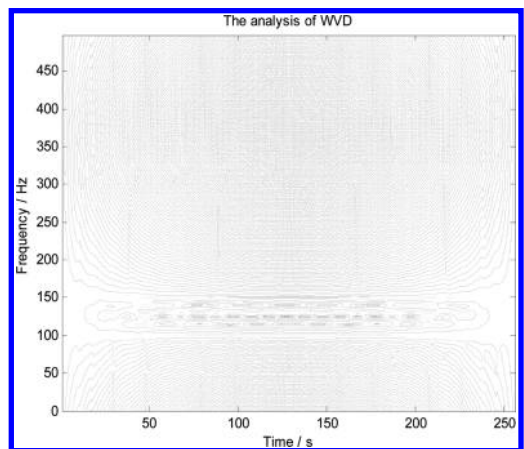


Figure 1. The WVD of signals.

get the two dimensional time-frequency distribution of the energy of signals. Simultaneously, the ingredient of signals will be exactly displayed [6]. Time-frequency analysis is including many methods, such as WVD, PWVD, Cohen time-frequency distribution and so on.

WVD has some great qualities in the process of stationary signals and non-stationary signals. Relatively, WVD has a higher resolution than STFT [7]. To simple signals, WVD can precisely describe the process of changing of signals in time-frequency domain. Figure 1 is showed to describe the situation of signals.

3 THE INFLUENCE BETWEEN AMPLITUDE OF SIGNALS AND WVD

There are still some problems, even though getting a precise process in time-frequency domain by WVD. When the WVD time-frequency analysis was carried out on the signal, the result will be different because the amplitude of signals is different. For example, the signal that has a large amplitude is not easy submerged by cross-terms, at the same time, a small amplitude signal is easier submerged by cross-terms.

In this paper, an analog signal include two signal components is introduced to explain the influence of WVD with amplitude. Firstly, an analog signal is built

$$y = A \cdot \sin(2\pi \cdot 20 \cdot t) + B \cdot \sin(2\pi \cdot 80 \cdot t)$$

A and B respectively is amplitude of two signal component. The frequency of the first signal component is 20 Hz, and the frequency of the second component is 80 Hz. The sampling frequency (F_s) is 1000 Hz, sampling interval is $1/F_s$, the length of signal is 1000. Matlab is used for simulating signals, in the end, contour lines is used for drawing the spectrum of signals.

1. If $A = B = 0.5$, there are same amplitudes between two signals.

There are two active line in 20 Hz and 80 Hz in Figure 2, which is standing for frequency of real signals. The rest is cross-term.

2. If $A < B$, and when $A = 0.5$, $B = 0.3$,

There is an active line in 20 Hz in Figure 3, and the line in 80 Hz is shorter.

When $A = 0.5$, $B = 0.1$,

There is still an active line in 20 Hz in Figure 4, and the line in 80 Hz is submerged completely by cross-term.

3. If $A < B$, and when $A = 0.5$, $B = 0.7$,

And the same time, when $A = 0.5$, $B = 1$,

From (2) and (3), when B is less than A, the frequency of the signal has amplitude B

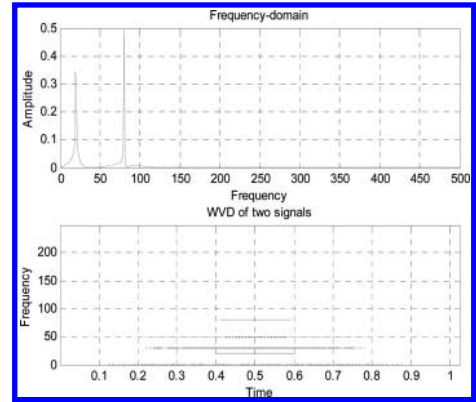


Figure 2. When $A = B$, the WVD of two signals.

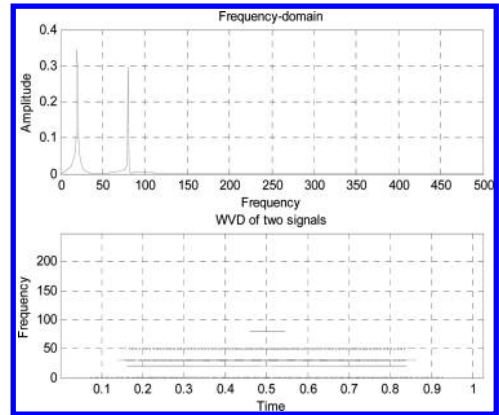


Figure 3. When $A = 0.5$ and $B = 0.3$, the WVD of two signals.

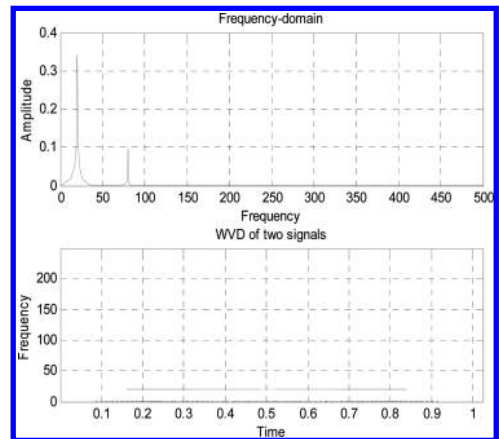


Figure 4. When $A = 0.5$ and $B = 0.1$, the WVD of two signals.

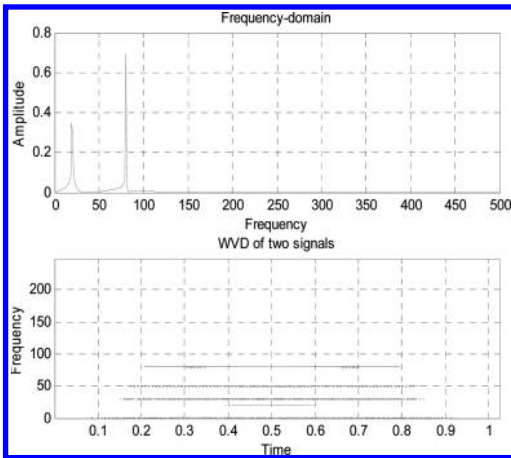


Figure 5. When $A = 0.5$ and $B = 0.7$, the WVD of two signals.

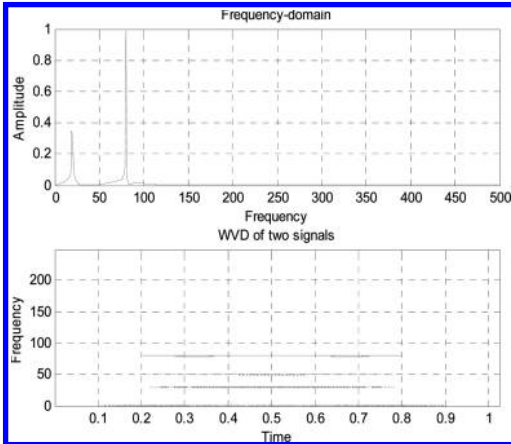


Figure 6. When $A = 0.5$ and $B = 1$, the WVD of two signals.

in spectrogram is phasing down or disappear. When B is greater than A , the frequency of the signal has amplitude A is submerged gradually. Due to the nature of the WVD, this phenomenon also exists in many analog signals and the signal in practical engineering.

4 SUMMARY

In the analysis of time-frequency, the result of WVD of signal is influenced by cross-terms, at the same time, the result is influenced by amplitude of all kinds of signals, either. In sum, a relatively large amplitude of frequency component has a higher resolution, and it is not easy to be swallowed up by the cross-terms. On the contrary, a relatively small amplitude of frequency component is easy to be submerged by cross-terms and is not easy to find out.

ACKNOWLEDGEMENT

It is a project supported by Science and Technology Foundation of Shenyang (Grant No. F12-169-9-00, F13-298-1-00) and Technology Project of Shenyang (Grant No. F13-055-2-00). The corresponding author is Zhonghu Yuan.

REFERENCES

- [1] Bin Wu, Minjie Wang, Jing Kang. Rolling bearing fault vibration signal characteristics and diagnostic methods[J]. Journal of dalian university of technology, 2013, 53(1):76–81.
- [2] Xiaodong Ye. Study on the method of rolling bearing fault vibration signal analysis[J]. Coal Mine Machinery, 2012, 33(12):257–259.
- [3] Zhengjia He, Yanyang Zi, Xining Zhang. Modern signal processing technology and application[M]. Xi'an: Xi'an Jiaotong University Press, 2007.
- [4] Jinfu Wang, Fucai Li. Mechanical fault diagnosis method of signal processing: Time-frequency analysis[J]. Noise and Vibration Control, 2013, 1(2):173–179.
- [5] Xiaoping LI, Guangming Shi. Optimizing kernels of quad-ratic time-frequency representation [J]. Chinese Journal of Radio Science, 2013, 18(2):208–211.
- [6] Tonghong Jin, Zhengbo Mo, Deliang Zheng. The time-frequency analysis technology and application research[J]. Mechanical Science and Technology, 2009, 28(1):75–78.
- [7] Xiaofen Meng, Wenchao Du, Dayong Zhang. The method of cognition of cross-term in WVD. Journal of Dalian University of Technology. Vol. 21(2012), p. 187–191.

Relationship between the stroke length of hydraulic cylinder and the attitude angle of shield during rectification

Yun Pu Song & Yi Xing Sun

School of Mechanical Engineering, Tongji University, Shanghai, China

ABSTRACT: This article analyze the relationship between the stroke length of hydraulic cylinder and the attitude angle of the shield via simulating the differential process of the shield hydraulic cylinder based on finite element method. The simulation result shows that the effects of the soil parameters and the buried depth are relatively low compared to that of the action spot of the hydraulic cylinder. On the basis of this result, we can get the conclusion that we should apply the exact position of the hydraulic cylinders when we consider establishing the theoretical model of shield operation system. We can also obtain the corrected coefficient of the attitude angle via analyzing the difference between the simulation result and the mathematical result.

Keywords: finite analysis method; action spot of cylinder; shield rectification; soil parameters

1 INTRODUCTION

Nowadays, the existing control strategies of shield rectification are mostly based on the operators' judgments after the analysis of the measured data [1]. With the continuous development of computer technology, more and more researchers start to focus on the work of auto-rectification of shield machine. In the procedure of this, analyzing the earth pressure around the shield and establishing an accurate theoretical model of shield during excavation is an important process [2, 3]. We think that analyzing the relationship between the stroke length of cylinder and the attitude angle of shield through studying the theoretical model is helpful to establish the model. Unfortunately, it is extraordinary difficult to establish an accurate mathematical model in traditional ways because of the heavy load, dynamic load and offset load characteristics presented by the shield machine during excavation [1, 2, 3]. In order to solve this problem, finite elements methods are involved by many researchers to simulate the driving process of shield, which is helpful in establishing the theoretical model [1, 4, 5].

Sun Wei considered the relationship between the rectification moment and angle of shield via finite element method and explored the influence of different parameters to obtain the expression formula which indicates the role of earth elastic modulus playing in the corrected coefficient [1], which assumes the effect of driving system as a rectification moment instead of studying the relationship between the movement of driving system and the shield attitude angle. To solve this issue, we will

try to analyze the real relationship between the stroke length of hydraulic cylinder and the attitude angle of shield based on simplified driving system through finite element method. In this article, we will implement a comparative analysis of the simulation result and theoretical result to explore the influence of different parameters and obtain the corrected coefficient.

2 THEORETICAL MODEL

Firstly we need to simplify the driving system reasonably to build a theoretical model of hydraulic cylinders' movement. The present researches related to the driving system of shield are mostly based on four-region system which simplifies the driving system by dividing the cylinders into four sections, namely top region, bottom region, left region and right region [6], as showed in Figure 1. During the excavation of shield, it will drive straightly when all the cylinders in four regions work together; it will

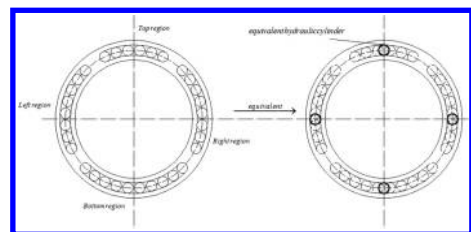


Figure 1. Hydraulic cylinder regions.

turn left or right when the cylinders in the top and bottom regions work normally while the cylinders in the left and right region thrust in differential action; it will move towards up or down direction when the cylinders in the left and right regions work normally while the cylinders in top and bottom region thrust in differential way [7].

In this article, we assume the driving system as a parallel mechanism which is driven by four equivalent hydraulic cylinders according to Deng Yingcong's article [6]. The differential action of the cylinders in the left and right region will affect the yawing deviation angle $\Delta\alpha$; the differential action of the cylinders in the top and bottom region will affect the pitching deviation angle $\Delta\beta$. As for the rolling deviation angle $\Delta\gamma$, we will not discuss it in this article because that the rolling deviation angle $\Delta\gamma$ will be small enough due to the friction between shield and the soil. As for the yawing deviation angle $\Delta\alpha$ and the pitching deviation angle $\Delta\beta$ of shield during rectification, the former shows the attitude deviation of shield in the horizontal plane and the other indicates that in the vertical plane. And both of the analysis procedures are similar except we will consider the effect of the gravity in the vertical plane, so we will just study the pitching deviation angle $\Delta\beta$ in this article.

As showed in the Figure 2, the stroke length of the equivalent cylinder in the top region is Δl_1 and that in the bottom region is Δl_3 .

As Figure 3 shows, $\Delta\beta$ is the pitching deviation angle and θ is the angle between the initial line and

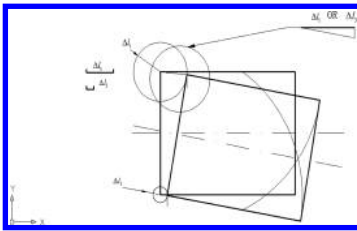


Figure 2. The attitude of shield in non-deformable rigid state.

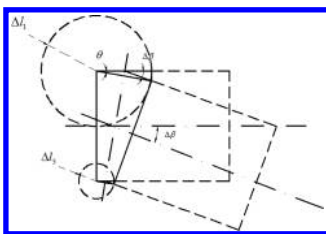


Figure 3. The pitching deviation angle $\Delta\beta$.

the line connecting the new and old position of the same vertex. (Note: we have amplified the angles for clear demonstration).

There is an isosceles triangle between the new and old position of the shield tail plane as showed in the Figure 3. The lengths of the equal sides are the diameter of the shield because of the non-deformable characteristic of the rigid. After geometry processing, we can get:

$$\frac{1}{2} \left(\frac{\Delta l_1}{\cos \theta} - \frac{\Delta l_3}{\cos \theta} \right) = D \cdot \sin \theta$$

While D is the diameter of the shield.

Obviously, we can get the relationship between θ and $\Delta\beta$ according to the geometry knowledge: $\Delta\beta = 2\theta$. Then:

$$\Delta\beta = \arcsin \frac{\Delta l_1 - \Delta l_3}{D}$$

Particularly we wish to point out that the shield may move towards down or up direction, but the analysis processes are similar. In this article, we will consider the situation of moving towards down direction.

3 ANALYSIS WITH FE METHOD

3.1 Basis of finite element method

Finite element method will be used to explore the effect of soil density, buried depth of shield, soil elastic modulus and the action spot of cylinders acting on the relationship between the stroke length of hydraulic cylinder and the attitude angle of shield during rectification. We need to prepare some parameters for the FE analysis, including the soil parameters, the structure parameters of shield machine and the frictional coefficient between the soil and the shield. According to a real tunneling construction condition, we can get the structure parameters of the shield, as shown in Table 1.

In order to analyze the effect of soil density, buried depth, soil elastic modulus and the action spot of cylinder, there should be 18 groups of

Table 1. Structure parameters of shield.

Item	Value	Unite
Diameter	6.25	m
Length	7.57	m
Elastic modulus	210000	MPa
Poisson ratio	0.3	-
Density	15.6	KN/m ³

parameters for different simulation environments as showed in Table 2. To simplify the procedure, this simulation is based on the assumption that the shield tunnels in a single soil layer in this article.

There will be a slide distance between shield and the soil in the simulation, so we need to consider the dynamic friction coefficient between shield and the soil, named μ_{ms} . And μ_{ms} usually equal to the tangent value of the friction angle ϑ between the soil and the shield [8].

$$\mu_{ms} = \tan \vartheta$$

Because the friction angle ϑ is affected by the properties of the soil, the roughness of the shell of shield machine and the operation factors (For example, the grouting process), it is difficult to measure the angle. It can be limited between the maximum and minimum angle. The maximum angle is soil internal friction angle φ and the minimum angle is $\varphi/2$ or $\varphi/3$. Zhu Hehua takes the middle value as the friction angle between the soil and shield, namely $2\varphi/3$ and get an excellent result [8], so we will also take the $2\varphi/3$ as the friction angle:

$$\vartheta = \frac{2\varphi}{3}$$

As showed in Table 2, the internal friction angle is 26.5° , so the friction coefficient in the simulation is:

$$\mu_{ms} = \tan 26.5^\circ = 0.3184$$

In this article, Ansys Workbench will be applied as the FEA software. And we would like to use the classical Drucker-Prager (D-P) model as the soil analysis element.

3.2 The establishment of the finite element model

In this FE model, we use element solid 95 to simulate the soil and element solid 186 to simulate the shield. In order to simplify the simulation process and accelerate the analysis procedure, a comparative small model will be established: width 40 m; length 20 m; height 40 m. After the pre-process, we can get the meshing of the FE model, showed in Figure 4.

3.3 Analysis of the simulation result

Because the topic of this article should focus on the relationship between the stroke length of the equivalent cylinders and the attitude angle of the shield, we will use the value that the settlements of the Cutter Face (CF) minus the settlements of the Shield Tail (ST) as the shield's descend value (It should be ascend value if the shield moves towards up direction). From Figure 5 to Figure 8, they are examples based on the parameters of the No. 1 group.

Following conclusions can be obtained from these displacement contours:

1. There is almost no change in the y direction of the shield;
2. The deformation amounts of the CF in x direction are corresponding to the displacements of

Table 2. Simulation environment parameters.

No.	Fixed radius of cylinders/m	Soil elastic modulus/MPa	Poisson ratio	Soil density/ $\text{kN} \cdot \text{m}^{-3}$	Cohesion/kPa	Internal friction angle/ $^\circ$	Buried depth of shield/m
1	2.8	53.5	0.25	19.5	18.6	26.5	15.375
2	2.8	53.5	0.25	21.5	18.6	26.5	15.375
3	2.8	53.5	0.25	23	18.6	26.5	15.375
4	2.8	53.5	0.25	18	18.6	26.5	15.375
5	2.8	53.5	0.25	16.5	18.6	26.5	15.375
6	2.8	53.5	0.25	19.5	18.6	26.5	11.375
7	2.8	53.5	0.25	19.5	18.6	26.5	13.375
8	2.8	53.5	0.25	19.5	18.6	26.5	17.375
9	2.8	53.5	0.25	19.5	18.6	26.5	20.375
10	2.8	15.5	0.25	19.5	18.6	26.5	15.375
11	2.8	25.5	0.25	19.5	18.6	26.5	15.375
12	2.8	35.5	0.25	19.5	18.6	26.5	15.375
13	2.8	45.5	0.25	19.5	18.6	26.5	15.375
14	2.8	60.5	0.25	19.5	18.6	26.5	15.375
15	2.6	53.3	0.25	19.5	18.6	26.5	15.375
16	2.7	53.3	0.25	19.5	18.6	26.5	15.375
17	2.9	53.3	0.25	19.5	18.6	26.5	15.375
18	3.0	53.3	0.25	19.5	18.6	26.5	15.375

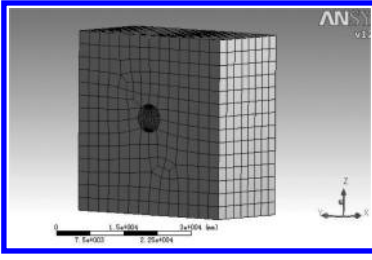


Figure 4. Meshing of the FE model.

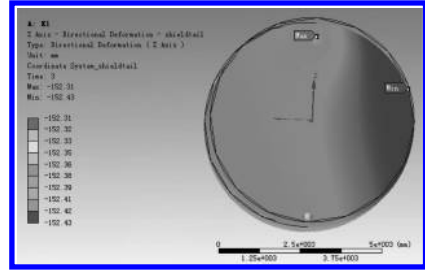


Figure 7. No. 1 deformation of the ST in z axis.

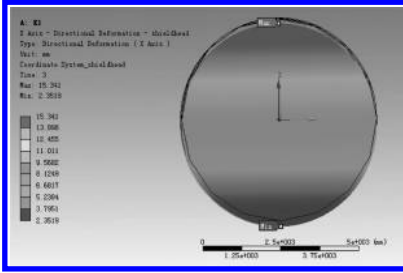


Figure 5. No. 1 deformation of the CF in y axis.

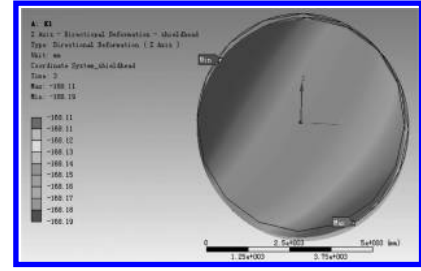


Figure 8. No. 1 deformation of the CF in z axis.

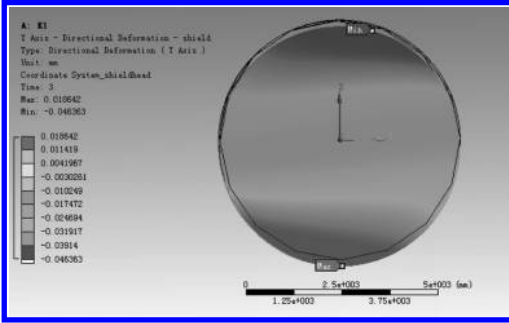


Figure 6. No. 1 deformation of the CF in x axis.

the equivalent cylinders acting on the shield tail (Equivalent cylinder for the top region: 15 mm. Equivalent cylinder for the bottom region: 3 mm).

3. The deviation value of the maximum deformation amount and the minimum deformation amount in the CF plane and the ST plane are respectively 0.08 mm and 0.12 mm, which means that there is no big deformation happened to either the CF plane or the ST plane. So we can use the average value of the maximum and the minimum displacement as the displacement of the plane's center correspondingly.

We can get the following function after study the Figure 9:

$$\Delta z = \left(\frac{\Delta l_1 + \Delta l_3}{2 \cos \theta} \times \cos \theta + L \right) \sin \Delta \beta$$

While L —the length of the shield;
 Δl_1 , Δl_3 are the stroke lengths of the equivalent cylinders in the top and bottom region respectively.

So we can get the pitching deviation angle $\Delta \beta$ if we can get the displacements of the CF plane center from the simulation:

$$\Delta \beta = \arcsin \left(\frac{\Delta z}{L + \frac{\Delta l_1 + \Delta l_2}{2}} \right)$$

Additionally, we introduce the corrected coefficient $K1$ to consider the difference between the pitching deviation angle in real condition and that in the theoretical condition.

$$K1 = \frac{\Delta \beta_{\text{Simulation}}}{\Delta \beta_{\text{Theoretical}}}$$

3.3.1 The influence of the soil density

According to the simulation results of groups from No. 1 to No. 5, we can get the influence effect of soil density acting on the relationship, which is

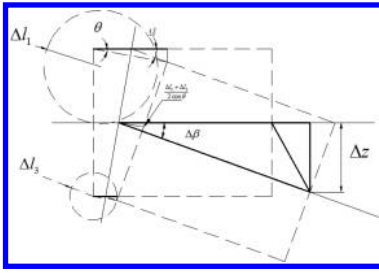


Figure 9. Relationship between the attitude angle and the displacement of the CF plane center.

demonstrated on Figure 10. The x axis indicates the shield excavation time and the y axis indicates the pitching deviation angle $\Delta\beta$ (Applied to the similar pictures).

As showed in Figure 10, the gradient of the fitting lines only decrease by 0.11% while the soil density almost increase by 40%. So we can say that the effect of the soil density acting on the relationship between the stroke length of the equivalent cylinder and the attitude angle of the shield is relatively small.

We can get the effect of the soil density acting on the K1 after compared the simulation results to the theoretical results, as showed in Figure 11.

We can see that the corrected coefficient K1 just fluctuate in 0.97 to 0.98 although the soil densities change a lot, which also indicates that the influence of the soil density acting on the K1 is relatively small.

3.3.2 The influence of the buried depth

According to the simulation results of groups from No. 1 and group No. 6 to No. 9, we can get the influence effect of the shield buried depth acting on the relationship, which is demonstrated in Figure 12.

Obviously, the gradient of the fitting lines just change by 0.25% while the buried depth increase by 80%. So we can also tell that the effect of the shield buried depth acting on the relationship between the stroke length of the equivalent cylinder and the attitude angle of the shield can be ignored in the theoretical model.

At the same time, we can also get the effect of the shield buried depth acting on the K1, as showed in Figure 13.

As it indicates in Figure 13, K1 stay in the range of 0.95 to 0.96 all the time, which also means the influence of the buried depth is small.

3.3.3 The influence of the soil elastic modulus

According to the simulation results of groups from No. 1 and group No. 11 to No. 14, we can get the effect of the soil elastic modulus acting on the relationship, which is demonstrated in Figure 14.

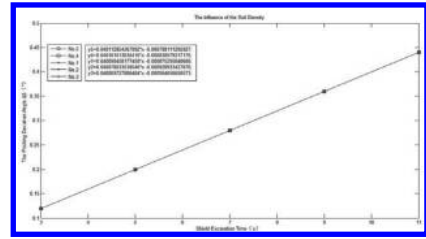


Figure 10. The influence of the soil density.

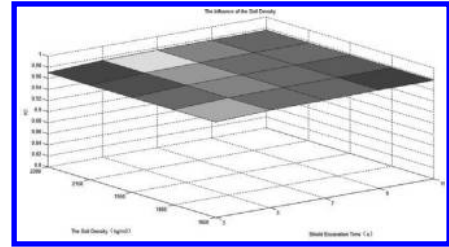


Figure 11. The influence of the soil density.

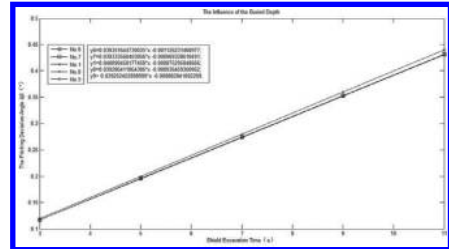


Figure 12. The influence of the shield buried depth.

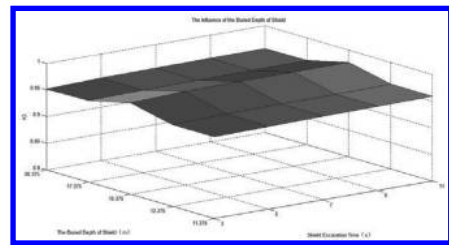


Figure 13. The influence of buried depth.

The gradients of the fitting lines just change by 0.85% while the soil elastic modulus increase by 190.32%. So it is obvious that the effect of the soil elastic modulus acting on the relationship between the stroke length of the equivalent cylinder and the attitude angle of the shield can also be ignored in the theoretical model.

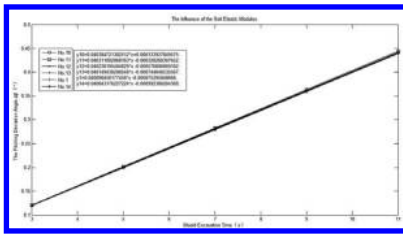


Figure 14. The influence of the soil elastic modulus.

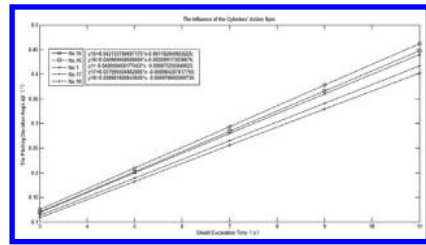


Figure 16. The influence of the cylinders' action spot.

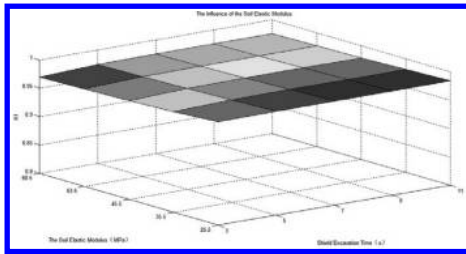


Figure 15. The influence of the soil elastic modulus.

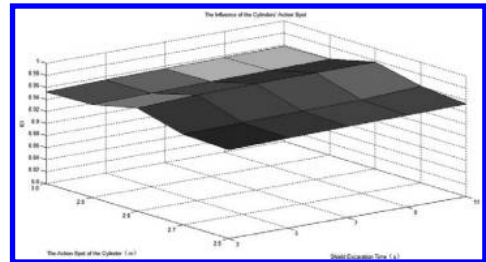


Figure 17. The influence of the cylinders' acting spot.

Figure 15 shows the influence of the soil elastic modulus acting on the K1.

As demonstrated in Figure 15, K1 always fluctuates in 0.96 to 0.98 no matter what change the soil elastic modulus has made. So we can also get the same conclusion that the soil elastic modulus barely affects the corrected coefficient K1.

3.3.4 The influence of the cylinders' action spot

According to the simulation results of groups from No. 1 and group No. 15 to No. 18, we can get the effect of the cylinders' action spot acting on the relationship, which is demonstrated on Figure 16.

According to the simulation result, the gradients of the fitting lines decrease by 12.94% while the fixed radius of equivalent cylinders increase by 15.38%. There is no doubt that the action spot of cylinders we used in the theoretical model will affect the accuracy of the model. But sometimes we would like to use approximate radius as the action spot to simply the establishment of the model. From the Figure 16, we can get the conclusion that it is very important to takes the exact position of hydraulic cylinder into account in order to enhance the accuracy of the theoretical model of hydraulic cylinders' movement.

In order to analyze the influence of the cylinders' action spot acting on K1, we take different action spots into the theoretical model and compare the results to the simulation results, as showed in Figure 17.

As showed in Figure 17, K1 still stays around 0.95 to 0.97 while the action spot changes a lot, which means that the corrected coefficient K1 will be steady if we applied the exact value of the fixed radius into the theoretical model. When we use the exact value of the cylinders' fixed radius instead of approximate radius, it may eliminate large fluctuations of the corrected coefficient K1 so that we can apply the K1 as a constant in the establishment of the model. In this way, we will enhance the accuracy of the theoretical model.

4 CONCLUSION

This article analyze the relationship between stroke length of equivalent hydraulic cylinders and the attitude angle of shield during rectification and explores the influences of soil density, buried depth, soil elastic modulus and the action spot of hydraulic cylinders acting on the relationship. This article also obtains the corrected coefficient K1 with the comparative analysis of simulation and theoretical results.

1. The influences of soil density, buried depth and soil elastic modulus affecting on the relationship between stroke length of equivalent hydraulic cylinders and the attitude angle of shield during rectification are relatively small and can be ignored in the process of establishing theoretical model.

2. The exact action spot of hydraulic cylinders should be applied in the theoretical model of the driving system because it affects the relationship greatly.
3. On the basis of applying the exact action position of the cylinders, the corrected coefficient of the simulation condition and the theoretical condition, namely K_1 , stays around 0.95 to 0.98 steadily. It should be applied in the process of establishing the theoretical model of the driving system so that the model can demonstrate the rectification procedure of shield accurately.

ACKNOWLEDGEMENT

This work is supported by National Natural Science Foundation of China (51105276). The authors would like to express the appreciation to the financial support of NSFC.

REFERENCES

- [1] Sun Wei, Yue Ming. Relationship between rectification moment and angle of shield based on numerical simulation [J]. *Journal of Central South University*. 2012(19):517–521.
- [2] Mitsutaka Sugimoto, Aphichat Sramoon. Theoretical Model of Shield Behavior During Excavation. I: Theory [J]. *Journal of Geotechnical and Geoenvironmental Engineering*. 2002(128):138–155.
- [3] Mitsutaka Sugimoto, Aphichat Sramoon. Theoretical Model of Shield Behavior During Excavation. II: Application [J]. *Journal of Geotechnical and Geoenvironmental Engineering*. 2002(128):156–165.
- [4] Mitsutaka Sugimoto, Aphichat Sramoon. Simulation of Shield Tunneling Behavior along a Curved Alignment in a Multilayered Ground [J]. *Journal of Geotechnical and Geoenvironmental Engineering*. 2007(133):684–694.
- [5] Thomas Kasper, Gntüher Meschke. A 3D Finite Element Simulation Model for TBM Tunnelling in Soft Ground [J]. *International Journal for Numerical and Analytical Methods in Geomechanics*. 2004(28):1441–1460.
- [6] Deng Yingcong, Guo Weizhong. Analysis the Function of Divided Region of Shield's Driving System Based on the Equivalent Model [J]. *Journal of Mechanical Engineering*. 2010, 46(13):122–127 (In Chinese).
- [7] Tang Jingshi, Gao Guoan. Analysis on the Shield Machine (3) [J]. *Road Machinery & Construction Mechanization*. 1990, 7(2):32–36 (In Chinese).
- [8] Zhu Hehua, Xu Qianwei. Analysis the Driving Force of Earth Pressure Balance Shield Based on the experimental model [J]. *Rock and Soil Mechanics*. 2007, 28(8):1587–1594 (In Chinese).
- [9] Xiao Shiyun, Lin Mou. Constitutive Model Based on Drucker-Prage Material Consistent Rate [J]. *Engineering Mechanics*. 2003, 20(4):147–151 (In Chinese).

Exploration of extending the service life of the residential buildings in cold area

Hong Ming Liu & Zhao He Liu

Jilin Jianzhu University, Changchun, China

ABSTRACT: Construction industry as a high energy consuming industries play a decisive role for sustainable development, especially for residential construction, is closely linked with people's life, but the life is too short to become restricting execution of the strategy of sustainable development. This paper summarizes the reasons affecting the residential building life in severe cold area of China, and puts forward the method to extend the service life of the residential building.

Keywords: cold area; residential building; sustainable development; service life

In the middle of the eighteenth Century, spinning machine and steam engines have been invented and applied opened the first industrial revolution the curtain. Manual labor to the power machine production, greatly improved productivity, science and technology progress, the city changes a process to accelerate, much closer links between the world, changed the face of the world, human life more and more rich. The results of the industrial revolution has brought joy and hope, but at the same time, the negative effects of environmental pollution, ecological destruction, waste of resources also slowly formed in the history of industrialization process, and continue to expand.

After entering twentieth Century, the international community generally recognize that environmental pollution, ecological destruction, resource scarcity will bring serious threat to human survival. Thus, the concept of "sustainable development" in 1972 at the United Nations Conference on the human environment emerge as the times require held in Stockholm. Sustainable development includes all aspects of human life, is related to the natural, social, environmental, economic, technological, political and other areas, according to the architecture, green building is the embodiment of an important proposal of its environmental friendly.

According to the statistics of some authority, every year the construction industry consumes nearly 50% human natural resources use, 40% of the total energy, as well as produce large amounts of construction waste. Can be said that the construction industry for sustainable development play a decisive role. And the construction industry in China is more extensive, our resources are

also paid a heavy price. However, although the construction industry consumes such a large share of resources, but Chinese building relatively short life, especially for the construction of residential buildings total proportion of such phenomenon is particularly serious, even appeared only built years house was torn down the phenomenon. Life is too short building has become chronic in implementation of the strategy of sustainable development. According to statistics, China and Korean residential average useful life of less than 30 years, with only about half of the design life. By contrast, American residential life is much longer American: about 80 years, Switzerland, Norway, about 70–90 years, the British first—up to 132 years in western developed countries, "Centennial" meet the eye everywhere(1).

In recent years, the discussion on the problems of the service life of the housing has not stopped. Some residential not to use fixed number of year is dismantled or the collapse of the reports in the newspapers. On the face of it, this may simply be due to the quality of construction, but if you go into the reason, in fact the quality is just one of the many reasons why, or is the cause of the surface. The author thinks, caused by the following reasons of residential building in cold regions life not long.

1 POLICY

(1) China now still lack a clear legal provisions stipulated if buildings due to quality problems and did not reach the design life of disciplinary measures, the construction is completed or inspection

process of some quality problems in the construction is not scientific. Lack of long-term supervision mechanism for subsequent use of quality problems in the process of building. This has caused some construction units and individuals to cut corners in the construction, reduce the quality standard construction.

(2) the development plan as a whole city changed frequently, inconstant in policy, a leader of a city planning, the lack of overall planning and adjustment direction, resulting in a large number of buildings were demolished.

Support life extension construction of the problem depends on the government. The author believes that countries need to introduce some punitive policies and regulations, to further regulate the construction of the service life of the problem, and strengthen the supervision mechanism, for the normal use of the building because of its quality and the reasons for failure to reach the required service life of building units and forcibly removed did not reach the people responsible use fixed number of year residential impose a certain discipline. Only in this way can effectively contain some or due to the pursuit of local economic interests or due to the pursuit of personal interests at the expense of the environment and ecological practice. In addition to formulate the overall planning of the city, scientific planning is the foundation to improve the residential life, only to maintain the stability of exploration planning, to provide a guarantee for the residential long-life. So through detailed investigation, analysis, demonstration, ensure rigorous planning, comprehensive, scientific. And planning once determined, must be strictly enforced, not random adjustment, implementation of the planning process into the orbit of the legal system, and strengthen accountability. Necessary adjustments, to strictly enforce the statutory procedures, be open and transparent, avoid the chief will.

2 THE PATTERN OF HOUSING

With the development of economy Chinese, people's living standard has improved significantly, the living standards also has a higher standard. Residential from the initial shelter sites become now meet the recreational, social comprehensive place, can say, the development of residential is accompanied by the residential cognitive deepening and development, but whether the brick wall structure or frame structure can not avoid is, once the room because the old pattern can not meet the use requirements of daily or is the room because the nature of the use of change, need to

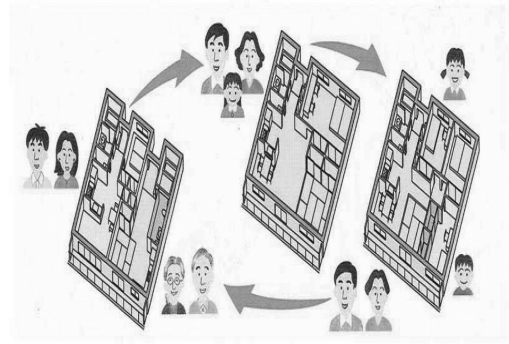


Figure 1. Yan Yinjun. Dry construction technology of Japanese and Chinese built residential [Z]. Pu design firm, 2009, 12-5.

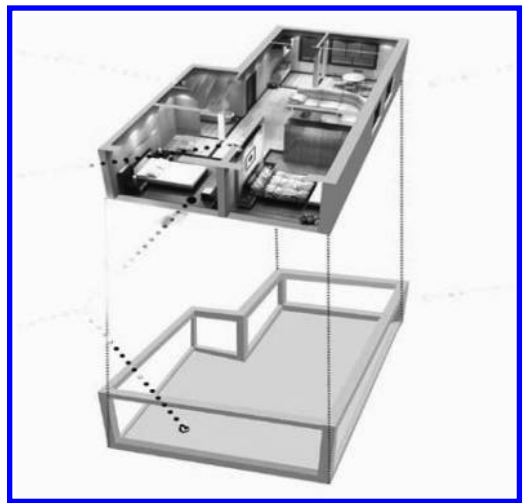


Figure 2. Liu Yingchao. Ji'nan will pilot China supporting housing houses such as building blocks [N]. China broadcast network, 2011:8-14.

change the room pattern, the original building is difficult to easily with the new demand change easily, which now houses the elimination rate is high.

Most of the time not because of quality problems of building but because housing patterns can not meet the growing needs of people living, entertainment, office etc. Cold regions often uses both residential brick structure and framework structure can not meet the similar to Smith proposed "circulation space", "the overall space" concept. I think, first of all need to improve the technical standard system of construction, carry out structural system in China, to establish the coordination system of product modular construction and department as soon as possible, unified modular system, coordination of different buildings and

each part of the component size, formulate technical specifications and standards of practice, unified construction and node structure, and carry out the standard of research and interchangeability of parts commonality, separate the building structure and equipment pipeline, without changing the main body structure under the premise, the design pipeline replacement, building maintenance and renovation to update spatial layout adjustment. Not only ensure the safety and reliability of the whole image, style of residential building on the consistency of the public interest; while also providing a full performance of self creative platform for users. But if the replaceable module standard construction is not perfect, will cause the design and residential Bup in production at random, resulting in similar product specifications clutter, seriously affect the installation quality and efficiency. So the design of standardization is not only a technical problem, but also involves the scientific management, need to carry out systematic research more (2).

3 THE DAILY MAINTENANCE

Aging people to use in everyday life, the material itself and the weather for the construction of the weathering, corrosion will affect the quality of the construction of their. The building as a necessity of a human life need to regularly check and maintenance. But whether developers or property owners are often ignored or is concerned about this. Not clearly divided and maintenance cost expenditure, also often make the idea ran aground, eventually building maintenance and repair is not timely, serious damage, affect the service life. To solve this problem by checking the macro-control of relevant government authorities and details. First of all, should establish corresponding construction archives, including the registration date of construction, architectural level, fire rating, construction materials and other projects, and regularly check the maintenance of the existing housing, found problems in a timely manner to timely repair.

Secondly, to clear the responsibility scope, avoid mutual shirk responsibility phenomenon. Routine maintenance and repair is the main content of scheme selection, repair plan refers to the building in the use of life cycle period to develop repair several applicable solutions corresponding, scheme should fully consider the repair costs, repair effect and sustainable development issues. So, can gradually with the restoration and reconstruction of the new building to replace, can prolong the service life, reduce the resource occupation and destruction of the environment.

4 THE CONSTRUCTION PROJECT

Selection and structure in architectural details, should suit one's measures to local conditions. For example, in the cold area, every year nearly 70 degrees Celsius temperature requirements in facing to meet the physical characteristics of normal at the same time also has good freezing and thawing. But we see more of is the most decorative materials at lea stone to two years, up to four or five years or even the whole piece of cracks, peeling off phenomenon, can not be expected to play a decorative effect, but the impact of normal use, and even lead to the structure itself is directly affected by the rain and snow weather invasion, which leads to the decrease of the construction itself the service life of the.

Therefore, in the architectural surface tiles, decorative paint and detailing the choice also should choose more suitable for cold region climate characteristic of materials, regardless of color, material or paste process should suit one's measures to local conditions to choose. Especially for the residential, comfort and applicability is the focus of the design, its durability and full consideration.

5 THE CONSTRUCTION OF THE GUIDING IDEOLOGY

Some parts of the city construction in order to image feature and the outstanding achievements of individuals, for instant success in the guiding ideology, speed, light weight, large demolition Dajian, achievement projects and developers of commercial interests, do not consider their own economic capacity and the objective need of macro regulation, long-term development is not a city, focus only on the pursuit of personal administration achievements, leading to its seek high, demand and the so-called "modernization", the construction of Development Zone, the central business district, a large theme park, resulting in a large number of old buildings in the normal design using the demolition period, resulting in land and resources waste, as well as the expansion of the bubble economy and the city.

For policymakers especially as in the face of the construction of this humanistic color things, its economic benefits should not be used as the only evaluation index. Especially for residential construction, its role in society should be far more than its economic effect. Rating standards only reform and the officials, area, not only the economic growth rate, the annual increase of the construction area as a basis for a year, but a combination of sustainable development, ecological

protection, green building and other aspects of the contribution and comprehensive evaluation, which can effectively curb the broken window theory (the broken window theory that is to break a window to promote a series of transactions occur, thus to bring business opportunities, create wealth can occur [3]).

In addition, the demolition to establish perfect laws and regulations system to control building will be one of the essential social policy, should be based on the assessment mechanism construction of the type, structure, building materials, the scale, the city environment and other specific factors with corresponding, to definite limit its demolition period, so as to manage the whole city building renewal development.

Residential building is one of the longer service life of economic products, guarantee or whole

life cycle extension of residential buildings can greatly reduce the waste of resources, promote the green environmental protection. In the global climate warming, the background of rising resource environment crisis awareness, China development practice of green building initiatives, are an important contribution to the consumers and society.

REFERENCES

- [1] Li Dexi . The long-life residential design research [D]. Tsinghua University, 2007:12-01.
- [2] Liu Zhifeng hundred years to build housing has an important strategic significance [J]. China real estate information, 2010:7-15.
- [3] Hu Ke. City building short-lived phenomenon in China [D]. Huazhong University of Science and Technology, 2010:1-01.

Finite element method analysis on slope stability under seismic dynamic

Gui Yun Zhou & Xi Zuo

Jinling Institute of Technology, Nanjing City, Jiangsu Province, China

ABSTRACT: The basic principle and calculation method for analysis on slope stability under seismic dynamic are discussed in this study. The seismic wave is input through artificial truncated boundaries, and the stress and deformation of the slope induced by seism loading are determined by time-integration method. The effect of foundation radiation damping is simulated by adopting visco-elastic artificial boundaries condition on artificial truncated boundaries. Safety factor of slope stability is solved by finite elements strength reduction method. The displacement saltation of feature points when the connection of plastic zone occurs is considered as an instability criterion of the slope. A quantitative evaluation method of slope dynamic stability is put forward through combining the dynamic finite element method with the visco-elastic artificial boundaries condition. Finally, for Shilipu hydropower station as an engineering application, the slope dynamic stability of the reservoir slope is analyzed, and the time history of the slope dynamic displacement and the safety coefficient of dynamic stability are obtained. The calculation results agree very well with geological survey and are close to the actual situation, indicating that the method can be used to evaluate dynamic stability of the practical engineering.

Keywords: slope stability; seismic dynamic; visco-elastic artificial boundaries; strength reduction; dynamic finite element method; safety factor; shilipu hydropower station

1 INTRODUCTION

Analysis on slope stability under the role of seismic dynamic is one of main research objectives of geotechnical dynamics referring to many disciplines such as earthquake engineering, soil dynamics, earthquake resistance of structure, geological engineering and etc. Currently, there are many developed methods for analysis on static slope stability, yet dynamic stability research is an ongoing activity (e.g. Hong Haichun and Xu Weiya, 2005; Liu Liping et al., 2001). The methods for analysis on dynamic stability include: pseudo-static method, Newmark sliding block method, numerical simulation method, survey comprehensive assessment, theory research and test and other methods. Numerical simulation method mainly include: Finite Element Method (FEM), discrete element method, Lagrange Method etc. Terzaghi (1950) is the first man using pseudo-static method in dynamic analysis on slope stability. When traditional pseudo-static method used in analysis, seismic loading was embodied mainly by means of inertia force, only horizontal motion was considered and the least stability safety coefficient could not be easy to be determined. Although pseudo-static method will simplify calculation resulting in a coarse calculation result, it was used in the earlier analysis on seismic slope stability widely

owing to its simple and practical use (e.g. WU XY et al., 1991). Finite Element Method (FEM) has been used in dynamic analysis early since 1970s, many scholars have made enormous beneficial researches in such field (e.g. Ito H et al., 1995; He Yunlong and Lu Shuyuan, 1998; Tang Hongxiang and Shao Longtan, 2004; Bo Jingshan et al., 2001). As it is applicable to complex media and terrain conditions, not only potential failure surface can be determined, but stress, strain and permanent deformation of under the role of seismic loading can be simulated accurately, Dynamic Finite Element Method (DFEM) has been used more and more widely in practical engineering. The main aspects of the current research on DFEM are as follows: dynamic loading consideration (how dynamic to play its role in slope), location and shape of failure surface (the position where slope instability lied), instability criteria of slope (whether the slope will be instable), instability results of slope (the calculation of permanent displacement or deformation).

In view of the existing problems above, it was recommended that slope stability was analyzed by DFEM, during the analysis process, the effect of foundation radiation damping is simulated by adopting visco-elastic artificial boundaries conditions on artificial truncated boundaries through which Seismic wave is input and slope stress and deformation under the role of seism loading is

determined by time-integration method. Due to the quite short process of earthquake happening, therefore, shear strength parameter change during the period of earthquake happening in the analysis of slope stability should not be considered, earthquake resistance Safety Coefficient for Slope Stability is intended to provide a safety reservation for deduction of material shear strength parameters resulted from precipitation, corrosion and weathering in a long period. The specific steps of DFEM analysis on slope stability are as follows: 1) firstly, to analyze static on the deduction process of material parameters by finite element strength reduction method; 2) to analyze combining static with dynamic on the deduction process of material parameters by finite element strength reduction method; 3) to analyze the calculation results of static and dynamic, and build the relationship between deduction coefficient of shear strength parameter and slope control point displacement or plasticity area, increasing suddenly displacement of control point or plasticity area covering right the whole sliding area as a judgment criterion for slope instability, at the moment, deduction coefficient of shear strength parameter is namely Safety Coefficient of earthquake resistance for Slope Stability.

2 BASIC PRINCIPLE FOR STATIC AND DYNAMIC ANALYSIS BY NFEM

2.1 Safety coefficient of slope stability

Nonlinear finite element strength reduction method (e.g. Zhou Guiyun and Li Tongchun, 2006) represents that adding c , φ , the indicators of material strength, to the equation (1) and (2) and meanwhile divided by F , a deduction coefficient, a group of new strength indicators c' , φ' can be obtained, and then the new indicators as new material parameters are put into finite element formula to participate in calculation, through F , deduction coefficient, increasing constantly and repeated analysis, until the slope have reached the critical damage, at the moment, the deduction coefficient shall be the minimum of safety coefficient of slope stability, the connecting part of plastic zone is the slipping surface.

$$c' = c / F \quad (1)$$

$$\tan \varphi' = \tan \varphi / F \quad (2)$$

2.2 Finite element equations

In analysis of slope stability, the finite element movement balance equation is as follows (e.g. Qian Jiahuan and Yin Zongze, 1996):

$$M\ddot{u} + C\dot{u} + Ku = F \quad (3)$$

In the equation, \ddot{u} , \dot{u} , u represent respectively acceleration, velocity and displacement vector, M , C , K respectively quality matrix, damping matrix and stiffness matrix, Rayleigh damping ratio assumptions are adopted here, i.e., $C = \alpha M + \beta K$, α , β are Rayleigh Proportional damping coefficients, F is an external loading column vector.

Generalized Newmark method used to discrete time domain, i.e., the following integral format will be used:

$$\dot{u}_{n+1} = \dot{u}_n + \Delta t \ddot{u}_n + \beta_1 \Delta t^2 \Delta \ddot{u}_n \quad (4)$$

$$u_{n+1} = u_n + \Delta t \dot{u}_n + 0.5 \Delta t^2 \ddot{u}_n + \beta_2 \Delta t^2 \Delta \ddot{u}_n \quad (5)$$

The finite element balance equation of loading increment at No. $n+1$ steps obtained from Equation (3) is:

$$M\ddot{u}_{n+1} + C\dot{u}_{n+1} + Ku_{n+1} = F_{n+1} \quad (6)$$

Put equation (4) and equation (5) into equation (6), the equation about $\Delta \ddot{u}_n$ can be obtained:

$$\bar{K} \Delta \ddot{u}_n = \Delta \bar{F}_n \quad (7)$$

where \bar{K} represents equivalent stiffness matrix, $\bar{K} = (1.0 + \alpha\beta_1\Delta t)M + (\beta_1\beta_1\Delta t + \beta_2\Delta t^2)K$; $\Delta \bar{F}_n$ is equivalent loading increment, $\Delta \bar{F}_n = F_{n+1} - (\dot{u}_n + \alpha\dot{u}_n^p)M - (u_n^p + \beta\dot{u}_n^p)K$, $u_n^p = u_n + \Delta t\dot{u}_n + 0.5\Delta t^2\ddot{u}_n$, $\dot{u}_n^p = \dot{u}_n + \Delta t\ddot{u}_n$. As setting of parameter β_1 , β_2 values will affect the accuracy and stability of algorithm, in general, if $\beta_1 = 1/2$ and $\beta_2 = 1/8 \sim 1/4$ are set, stable solutions will be obtained. To solve linear equation group (7), the value of $\Delta \ddot{u}_n$ can be obtained, by gradual iteration to achieve displacement of nodes, the state of unit stress can be obtained by using constitutive relationship so as to analyze the stability of the slope.

3 DYNAMIC ARTIFICIAL BOUNDARIES CONDITIONS

Under the role of seismic loading, fluctuation energy will be transferred from structure to foundation, when a finite element discrete model is used to simulate the infinite foundation, wave reflection will occur on the artificial truncated boundaries, which will lead to wave oscillation and at last result in distortion simulation. To solve the problem, the most effective way is to introduce dynamic artificial boundary conditions, such as viscous boundary, paraxial approximation boundary, transmission boundary, visco-elastic boundary and etc. (e.g. Clayton R and Engquist B., 1997; Clayton R and Engquist B., 1980; Shen Jumin, 2000; He Xiangli

and Li Tongchun, 2005). Where visco-elastic boundary makes calculation not only have a higher accuracy but also simple, practical and available to realize in programming. Visco-elastic boundary was used in dynamic analysis on slope stability in this paper.

3.1 Visco-elastic artificial boundary

In practical problems, scattering wave produced from partial irregular region or structure and foundation may have ordinarily geometric proliferation, therefore, for scattering wave, the assumption of cylindrical wave (2D) or spherical wave (3D) is more reasonable. Cylindrical wave equation for Out-of-plane in Polar coordinates is the following:

$$\frac{\partial^2 w}{\partial t^2} = c_s^2 \left(\frac{\partial^2 w}{\partial r^2} + \frac{1}{r} \frac{\partial w}{\partial r} \right) \quad (8)$$

where w is out-of-plane displacement of medium, c_s is shear wave velocity, $c_s = \sqrt{G/\rho}$, G is shear modulus, ρ is mass density.

For the Cylindrical wave scattering from coordinate origin, the following equation can be used to seek solution

$$w(r,t) = \frac{1}{\sqrt{r}} f \left(t - \frac{r}{c_s} \right) \quad (9)$$

Through using equation (9) and shear stress formula, $\tau(\gamma,t) = G \partial \omega / \partial \gamma$, shear stress of any point in the medium can be achieved, the equation is as follows:

$$\tau(r,t) = -G \left[\frac{1}{2r\sqrt{r}} f \left(t - \frac{r}{c_s} \right) + \frac{1}{c_s\sqrt{r}} f' \left(t - \frac{r}{c_s} \right) \right] \quad (10)$$

where f' represents the derivative of f with respect to the variables in the brackets. The velocity of any point can be expressed as follows:

$$\frac{\partial w(r,t)}{\partial t} = \frac{1}{\sqrt{r}} f' \left(t - \frac{r}{c_s} \right) \quad (11)$$

Put equation (9) and (11) into equation (10), then any radius γ_b can be obtained, which was divided by arrow outside diameter, $\bar{\gamma}_b$, then stress on the micro-element surface of exterior normal was obtained, the relationship between stress and velocity and displacement on the surface above is:

$$\tau(r_b,t) = -\frac{G}{2r_b} w(r_b,t) - \rho c_s \frac{\partial w(r_b,t)}{\partial t} \quad (12)$$

We can see that if medium was truncated at radius γ_b , meanwhile, the corresponding distribution physical components, viscous damper C_b , and linear spring K_b were imposed on the truncated boundaries, then:

$$C_b = \rho c_s, \quad K_b = \frac{G}{2r_b} \quad (13)$$

Consequently, $\gamma = \gamma_b$ are fully same as those of equation (12). If the distance γ_b from wave source to the artificial boundaries can be accurate determined, the coefficients of physical components imposed on the artificial boundaries can be determined by equation (13), so that reflection of scattering wave on the artificial boundaries can disappear fully, i.e., the spread of wave from definite to infinite domain can be simulated accurately.

3.2 Input method of earthquake fluctuation

Suppose that $\omega_0(x,y,t)$ is known input field, i.e., free wave field, the angle of wave incidence may be arbitrary, the displacement resulted from incidence wave at any point B on artificial boundary is $\omega_0(x_B, y_B, t)$, the condition makes fluctuation input accurately is to impose equivalent load on artificial boundary and make the displacement and stress on artificial boundary same as the origin wave, namely:

$$\omega(x_B, y_B, t) = \omega_0(x_B, y_B, t) \quad (14)$$

$$\tau(x_B, y_B, t) = \tau_0(x_B, y_B, t) \quad (15)$$

where τ_0 is the stress produced by the displacement ω_0 in the original continuous medium.

To achieve fluctuation input, the stress should be imposed at the node B is $F_B(t)$. Use the concept of detachment body in the normal dynamic analysis, to make artificial boundary detach with additional physical components (spring and damping), the stress at the node B on artificial boundary is as follow:

$$\tau(x_B, y_B, t) = F_B(t) - f_B(t) \quad (16)$$

The movement equation consists of spring and damper is as follow:

$$f_B(t) = C_b \dot{\omega}(x_B, y_B, t) + K_b \omega(x_B, y_B, t) \quad (17)$$

Substitute equation (15) and equation (17) into equation (16), the following equation can be obtained:

$$F_B(t) = \tau_0(x_B, y_B, t) + C_b \dot{\omega}_0(x_B, y_B, t) + K_b \omega_0(x_B, y_B, t) \quad (18)$$

In equation (18), ω_0 is known, $\dot{\omega}_0$ and τ_0 can be solved according to ω_0 , therefore, the total loading $F_b(t)$ imposed on artificial boundaries can be obtained, and then fluctuation input on visco-elastic artificial boundary can be achieved.

4 ENGINEERING APPLICATION

Shilipu hydropower station lies in the upper reaches of Minjiang River in Sichuan Province, which is situated in Alpine valley belt in the northeastern of the Plateau, the dam type is gravelly soil core wall rock-fill dam with the normal water level 1681.0 m, groundwater 1622.0 m, crest elevation 1685.7 m, the biggest dam height 133 m and total storage capacity about 470 million m^3 . The project site is located in seismic peak acceleration of 0.15 g, equivalent to the basic seismic intensity Surface lithology are mainly epimetamorphic, sandstone, siltstone and crystalline limestone, quartz schist, tuffaceous phyllite, tuffaceous rocks and volcanic conglomerate, etc. By the influence of terrain, lithology, geological structure, multiple landslides are found in the rock of the upper reaches and both laterals, In order to study whether seismic loading effect will have an influence on the security of the dam and power plant after reservoir filling, the dynamic stability of the reservoir slope needs to be analyzed. In the paper, the landslide near the water lawns landslides, which may significantly affect the project, is chosen to be made a finite element analysis in a representative profile. Geological survey shows that the overall water level landslides are in stability, and small landslides and local instability may occur on seismic loading effect. The upper part of the slope is covered with gravel layers of which the soil density is $2.01 \times 10^3 kg/m^3$, the cohesive force is 15 kPa, the friction angle is 25°, the Poisson's ratio is 0.30, the elastic modulus is 30 MPa; while the lower part is bedrock of which the density is $2.05 \times 10^3 kg/m^3$, elastic modulus is 2.5 GPa. During dynamic calculations, the elastic modulus is increased by 30%, that is, static elastic modulus multiplied by the coefficient of 1.3.

Landslide typical profile mesh partition figure, shown in Figure 1, adopts a free-partitioned quadrilateral element, and only horizontal motion is considered in calculation. The seismic waves are inputted from the bottom of the foundation. Taking into account the amplification the foundation acted on elastic waves during the process that seismic waves are transferred from the foundation to the slope, reduce the input waves by half. Computing time step is 0.01s, altogether is 30s. Time-histories of acceleration, velocity and displacement of input wave were shown in Figure 2.

The slope dynamic response results and its stable safety are analyzed through the calculation of time

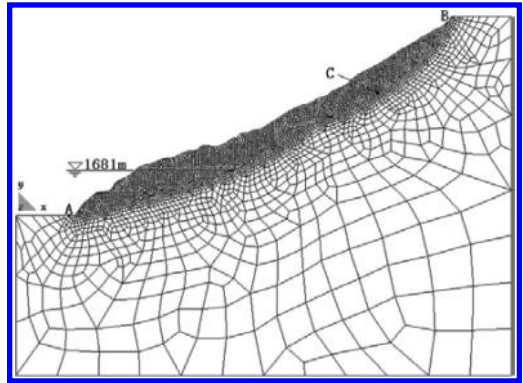


Figure 1. Numerical calculation model of slope.

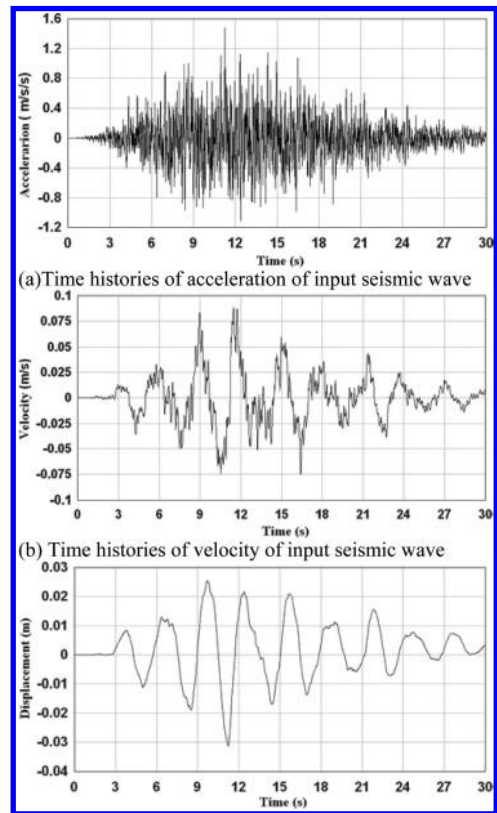


Figure 2. Time histories of acceleration, velocity and displacement of input wave.

histories of slope dynamic displacement under the role of seismic loading. Several major parts are analyzed by taking three characteristic points, A, B, C, from the base, crest and body of the slope (see Fig. 1). The time histories of displacement of the

points, A, B, C, in X direction with different reduction coefficients of materials strength are as shown in Figure 3, Figure 4 and Figure 5 respectively.

From the time histories of displacement in Figure 3, Figure 4 and Figure 5, we can see the

displacement of Point A, Point B varies slightly under different reduction coefficients of materials strength, while the displacement of Point C varies greatly as the reduction coefficients are between 1.042~1.136, knowing that the slope instability

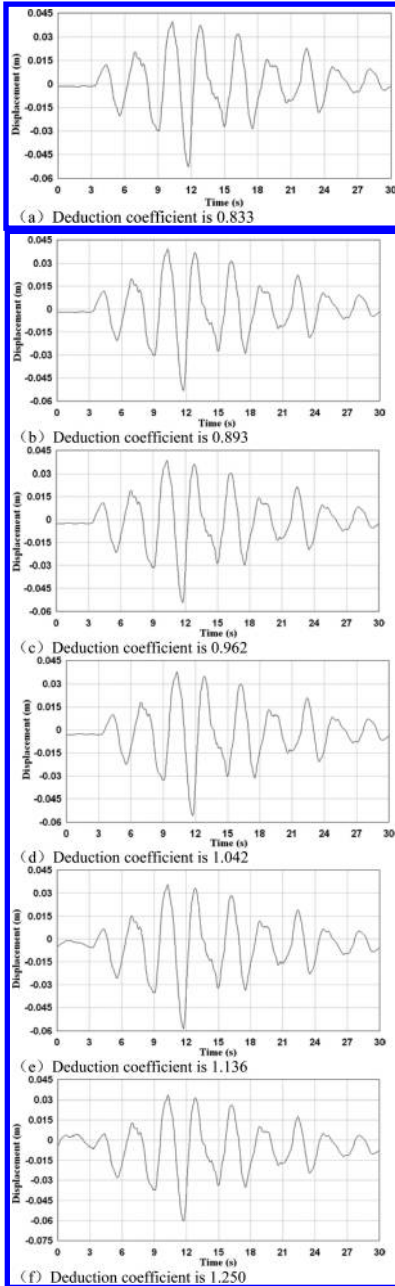


Figure 3. Time histories of displacement at Point A under different reduction coefficients of slip resistance.

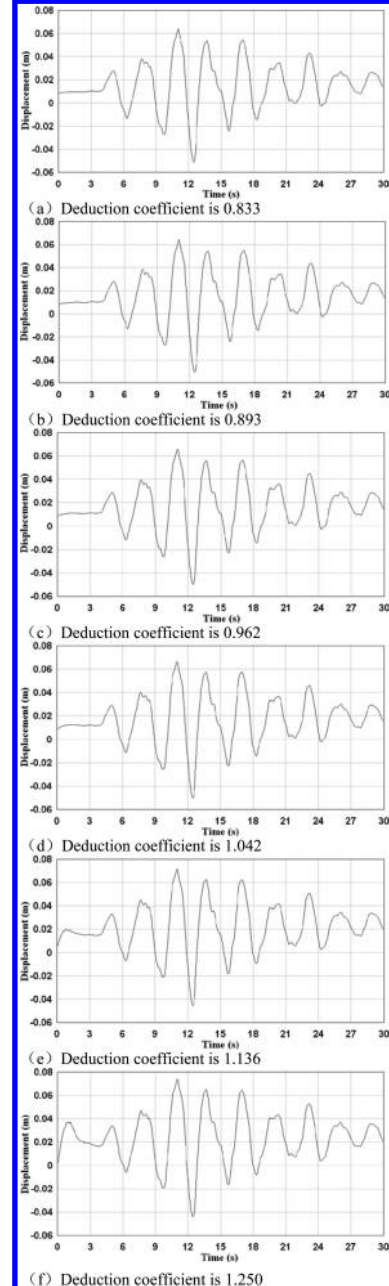


Figure 4. Time histories of displacement at Point B under different reduction coefficients of slip resistance.

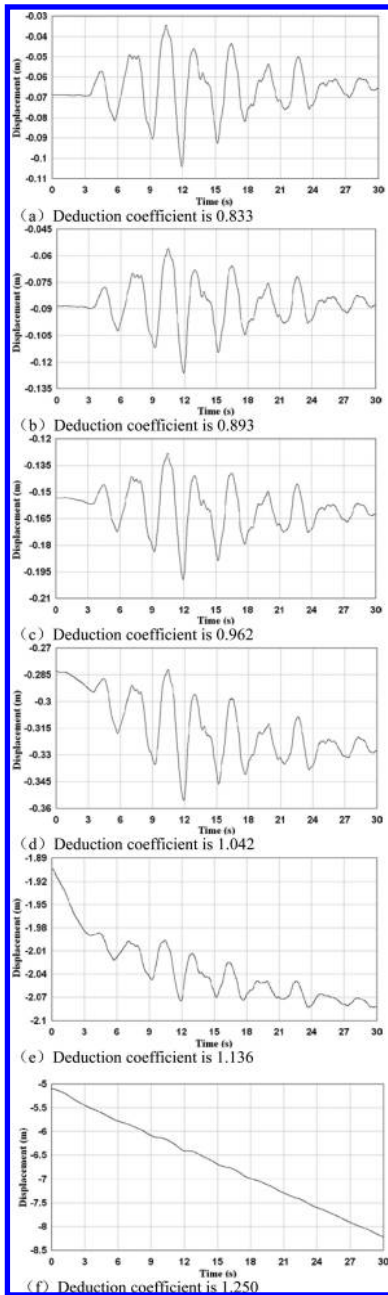


Figure 5. Time histories of displacement at Point C under different reduction coefficients of slip resistance.

damage will occur when the reduction coefficient is a certain value among 1.042~1.136. Figure 6 is the distribution of plastic zone inside the slope when the strength reduction coefficient is 1.136, from which we can see that the middle and upper

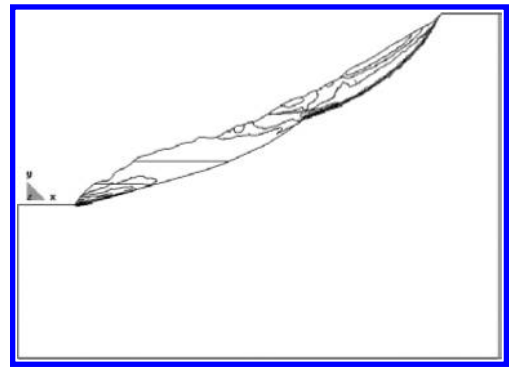


Figure 6. Plastic region distribution in slope body when the shear strength reduction coefficients is 1.136.

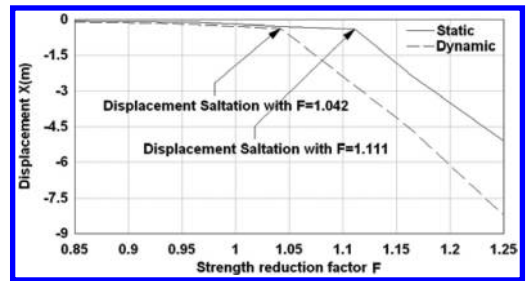


Figure 7. Control point (Point C) displacement—curve for the shear strength reduction coefficients.

parts of the plastic zone are linked up and local slope instability occurs. So, we can take Point C as displacement control point and establish material-shearing parameters (that is, the shear strength reduction coefficients) and displacement curves for slope control points, as shown in Figure 7.

Figure 7 indicates that abrupt change of X displacement will occur at Point C when strength reduction coefficient is 1.111 under static condition, while such change will occur when strength reduction coefficient is 1.042 under dynamic condition. From the definition of stability safety coefficients of strength reduction, static stability safety coefficient is 1.111 and dynamic stability safety coefficient is 1.042, and if the side-slope instability occurs, the upper partial instability will happen. The instability scope is shown in the plastic zone distribution, see Figure 6. By traditional rigid limit equilibrium method, we calculated the stability safety coefficient of the slope was 0.96 under the role of seism loading and from this we considered the overall slope instability occurred. By the calculation results, the analysis results of dynamic finite element agreed very well with those of geological survey and are close to the actual situation. But the

calculation results by traditional rigid limit equilibrium method are conservative slightly, and cannot get an exact failure location of slope instability. All these show that DFEM in the paper is feasible and effective.

5 CONCLUSION

Based on several main aspects of the current analysis on slope dynamic stability such as dynamic loading, location and shape of failure surface, slope instability criteria and results, the DFEM for analysis on slope dynamic stability is put forward. Seism wave is input through artificial truncated boundaries as dynamic loading, visco-elastic artificial boundaries conditions is used to simulate the effect of foundation radiation damping, the slope stress and deformation under the role of seism loading can be determined by time-integration method. Non-linear finite elements strength reduction method is used to calculate the safety factor and the displacement saltation of control points when the connection of plastic zone occurs is considered as an instability criterion of the slope. The results of the engineering application above agree well with those of geological survey and actual engineering situation, hence the DFEM for analysis on slope dynamic stability put forward in the study is reasonable and effective.

This article was supported by Colleges and Universities Natural Science Research Project of Jiangsu Province (Grant No. 14KJB560007), Natural Science Foundation of Jiangsu Province (Grant No. BK20140108), and Natural Science Foundation of Jiangsu Province (Grant No. BK20141090).

REFERENCES

[1] Bo Jingshan, Xu Guogong, Jing Liping. Seismic Response and Dynamic Stability Analysis of Soil Slopes, *Earthquake Engineering and Engineering Vibration*, Vol. 21, No.1, 2001, pp.116–120.

[2] Clayton R., Engquist B., Absorbing boundary conditions for acoustic and elastic wave equations, *Bull. Seism. Soc. Amer.*, No.76, 1977, pp.1529–1540.

[3] Clayton R., Engquist B., Absorbing boundary conditions for wave-equation migration, *Geophysics*, No.45, 1980, pp.895–904.

[4] He Xiangli, Li Tongchun, Dynamic Artificial Boundaries Condition for Infinite Domain, *Chinese Journal of Advance in Science and Technology of Water Resources*, Vol.25, No.3, 2005, pp.64–67.

[5] He Yunlong, Lu Shuyuan, A Method for Calculating the Seismic Action in Rock Slope, *Chinese Journal of Geotechnical Engineering*, Vol.20, No.2, 1998, pp.66–68.

[6] Hong Haichun, Xu Weiya, Review on the Stability of Slope under Seismic Loading, *Chinese Journal of Rock Mechanics and Engineering*, Vol.24, No.suppl.1, 2005, pp.4827–4836.

[7] Ito H., Sato K., Sawada Y., Consideration on the Seismic Method and the Design Seismic Coefficient of Large cut slope under the strong earthquake, In: *International Congress on Rock Mechanics*, Japan, 1995, pp.413–416.

[8] Liu Liping, Lei Zunyu, Zhou Fuchun, The evaluation of seismic slope stability analysis methods, *Chinese Journal of Chongqing Jiaotong University*, Vol.22, No.3, 2001, pp.83–88.

[9] Qian Jiahuan, Yin Zongze, *Principle of Geotechnique and Calculations*, China Water Power Press, 1996.

[10] Shen Jumin, *Aseismic Engineering*, China Architecture and Building Press, 2000.

[11] Tang Hongxiang, Shao Longtan, Finite Element Analysis on Slope Stability of Earth-rock Dam Under Earthquake, *Chinese Journal of Rock Mechanics and Engineering*, Vol.23, No.8, 2004, pp.1318–1324.

[12] Terzaghi K, *Mechanisms of landslides, Engineering Geology (Berdey) Volume*, Geological Society of America, 1950.

[13] Wu XY, Law KT. Selvadurai, APS. Examination of the Pseudostatic Limit Equilibrium Method of Dynamic Stability Analysis of Slopes, *Canadian Geotechnical Conference pt 1 Sep 29-Oct 2 1991*.

[14] Zhou Guiyun, Li Tongchun, Rocky Slope Stability Analysis Taking into Account Saturated-unsaturated Seepage Flow, *Chinese Journal of Water Resources and Power*, Vol.24, No.5, 2006, pp.79–82.

The stability research of hinge-chained concrete block slopes under water pressure

Hui Su

Jinling Institute of Technology, Nanjing City, Jiangsu Province, China

ABSTRACT: This paper studied the stability of the hinge-chained concrete block slopes under water pressure. And it introduced two solutions of basic slope stability safety factors. Then the finite element method is used to analyze and compare the selected appropriate finite element models in four different working conditions, thus some conclusions were received.

Keywords: hinge-chained concrete block; slope stability safety factor; finite element method; calculation model

1 INTRODUCTION

Slope protection is not only a significant unit in keeping river embankments safety but also an important aspect of dyke reinforcement project. Traditional slope protection patterns include block stone, cast-in-place concrete, pouring mold bag concrete pavement, asphalt concrete and so on. Different slope protection forms together play a very important role in withstanding killer waves, protecting slope from being washed out by rains, preventing frost heave and dryness of dyke clayey soil, avoiding clay be blown about by wind. However, according to the long-term practice, it is found that traditional slope protection exist some drawbacks in engineering application. For instance, to artificially and canalized natural river by using impervious artificial hard material will impede ecological function and affect the structure integrity of biological system. With economic and social development and improving people awareness, river ecology, landscape and water function have gradually been taken seriously. For modern slope protection project, riverbank should not only own the basic protective function but also the ecological functions harmonize with the surrounding environment. Therefore, in order to adapt to the need of new situation, the slope protection technology of river regulation should gradually develop from originally pure physical measures to ecological slope protection technology.

2 BASIC PRINCIPLES OF THE STRENGTH REDUCTION METHOD OF FINITE ELEMENT

Strength reduction was adopted abroad in the 1980s, but due to the mechanical concept is not

very clear, and affected by calculation procedures and calculation accuracy, thus it was not popular in China. With the advancement of computers and the advent of various types of general-purpose software, strength reduction has been widely used to calculate the slope stability safety factor. Strength reduction and iterative solution are the same in the definition of the slope stability safety factor.

The slope stability safety factor can be defined as the reduction extent of the shear strength when the slope just reached critical damage state. The safety factor is the ratio of the actual shear strength of soil and shear strength after reduction when it is in critical damage state.

$$K = \frac{c}{c_e} = \frac{tg\phi}{tg\phi_e} \quad (1)$$

where K is safety factor; c , ϕ is the actual shear strength parameters of the soil; c_e , ϕ_e is shear strength parameters of soil when the limits of state is reached.

The basic principle of strength reduction is using the formula (1) and (2) to adjust the strength indicators of soil, and then the slope is analyzed using finite element method. By increasing the reduction factor and repeating the analysis of the slope, a reduction factor in critical state is obtained, which is the slope stability safety factor.

3 CALCULATION MODEL AND CALCULATION PARAMETERS

The finite element strength reduction is used to calculate and analyze the stability of the hinged

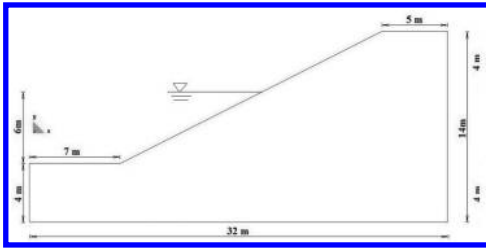


Figure 1. Reservoir slope model size.

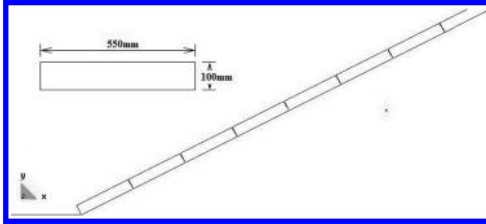


Figure 2. Pavement and size of concrete block revetment.

ecological slope protection. The model and the size of the reservoir slope is shown in Figure 1, and the reservoir water level is 6 m. The laying and dimensions of concrete block slope protection is illustrated in Figure 2. Material parameters for the calculation is as follows: For slope body, $\rho = 1700 \text{ kg/m}^3$, $c = 5 \times 10^3 \text{ Pa}$, $\phi = 20$, $E = 30 \times 10^9 \text{ Pa}$, $\nu = 0.3$; for concrete block, $\rho = 2400 \text{ kg/m}^3$, $E = 30 \times 10^9 \text{ Pa}$, $\nu = 0.17$.

4 THE CALCULATION WORKING CONDITIONS AND CALCULATION METHOD

The working conditions below were considered in the calculation:

Working condition one: Without revetment and without water. Working condition two: With revetment and without water. Working condition three: Without revetment and with water. Working condition four: With revetment and water.

The first working condition is to consider the reservoir without impoundment before the revetment pavement, the second working condition is to consider the reservoir without impoundment after the revetment pavement, the third working condition is to consider the reservoir with impoundment before the revetment pavement, and the fourth working condition is to consider the reservoir with impoundment after the revetment pavement. Those working conditions were compared after calculation. The influence of concrete block revetment on reservoir slope stability was analyzed by the safety factor of slope stability.

5 THE CALCULATION RESULTS

5.1 Without revetment and without water

In this situation, the reservoir is without impoundment and revetment. The computational grid meshing of slope is shown in Figure 3. According to the analysis of calculation results, some results are acquired. During the strength reduction process, if the reduction factor is taken as 0.76, the plastic zone inside the slope starts to distribute throughout the cross section. The distribution of plastic zone is shown in Figure 4 at this time. The distribution of the X direction displacement is shown in Figure 5. The distribution of the X direction stress is shown in Figure 6. The relation between the strength reduction factor and X direction displacement is shown in Figure 7. As can be seen from Figure 7, the slope of X displacement curve takes mutation as the strength reduction

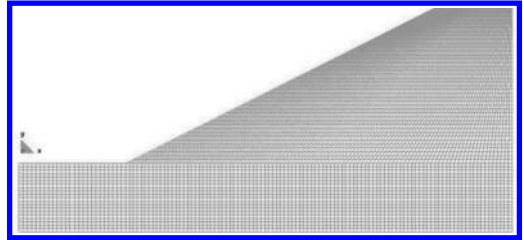


Figure 3. Meshing.

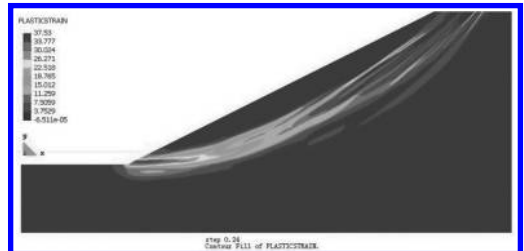


Figure 4. The distribution of plastic zone.

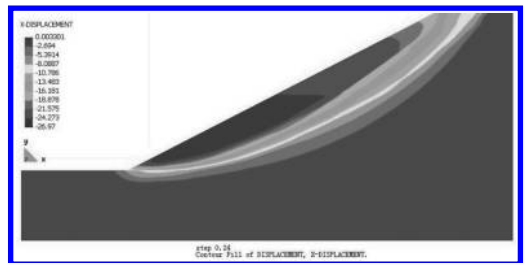


Figure 5. The distribution of X displacement.

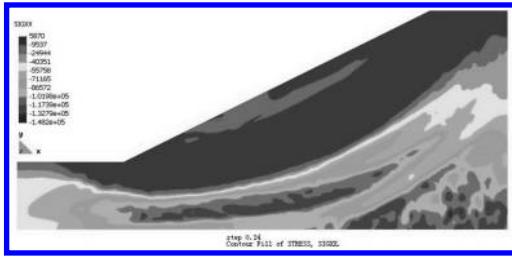


Figure 6. The distribution of X stress.

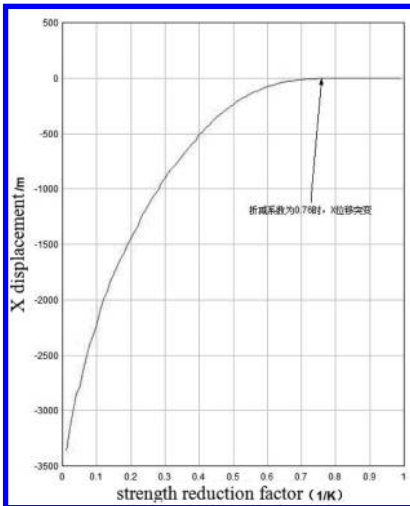


Figure 7. The relation between the strength reduction factor and X displacement.

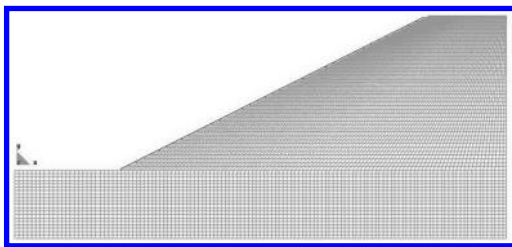


Figure 8. Meshing.

factor arriving 0.76, so the safety factor of slope stability was $1/0.76 = 1.316$.

5.2 With revetment and without water

In this situation, the reservoir is without impoundment and with revetment. The computational grid meshing of slope was shown in Figure 8. According to the analysis of calculation results, some results are acquired. During the strength reduction process,

if the reduction factor is taken as 0.71, the plastic zone inside the slope started to distribute throughout the cross section. The distribution of plastic zone is shown in Figure 9 at this time. The distribution of the X direction displacement is shown in Figure 10. The distribution of the X direction stress is as shown in Figure 11. The relation between the strength reduction factor and X direction displacement is shown in Figure 12. As can be seen from Figure 12, the slope of X displacement curve takes mutation as the strength reduction factor arriving 0.71, so the safety factor of slope stability was $1/0.71 = 1.408$.

5.3 Without revetment and with water

In this situation, the reservoir is with impoundment and without revetment. The computational grid meshing of slope is shown in Figure 13. According

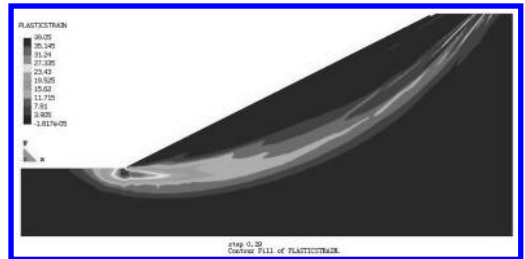


Figure 9. The distribution of plastic zone.

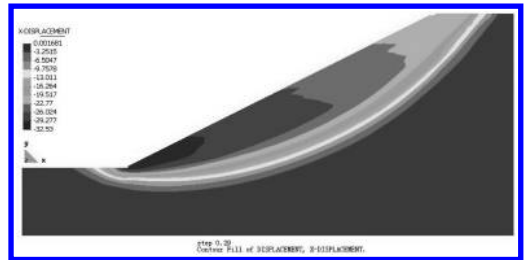


Figure 10. The distribution of X displacement.

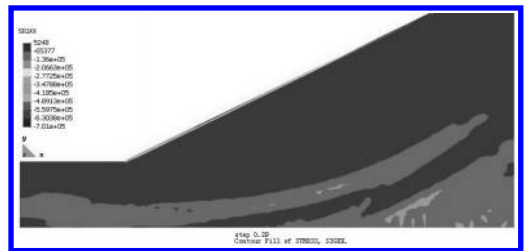


Figure 11. The distribution of X stress.

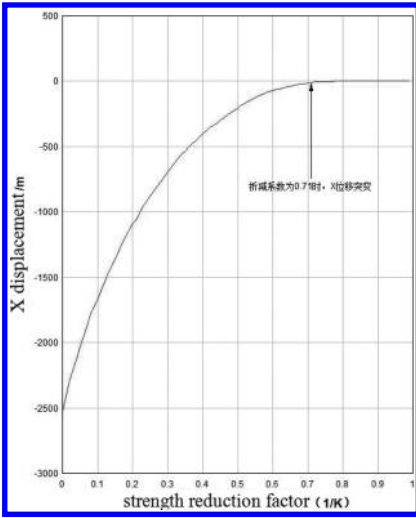


Figure 12. The relation between the strength reduction factor and X direction displacement.

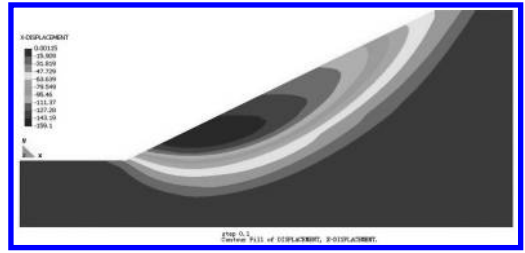


Figure 15. The distribution of X displacement.

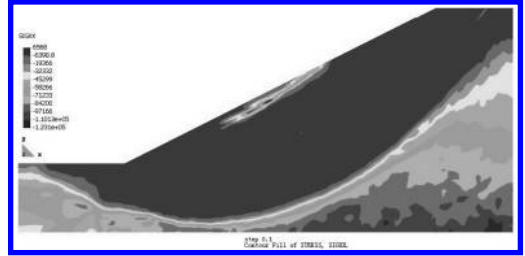


Figure 16. The distribution of X stress.

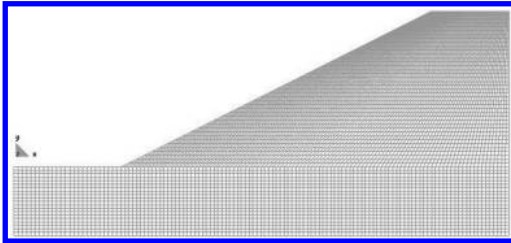


Figure 13. Meshing.

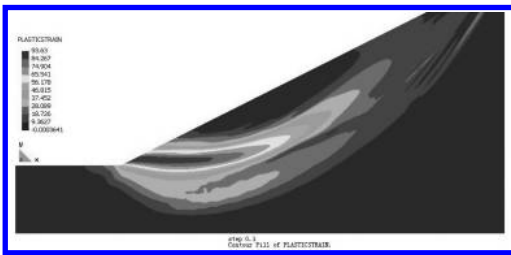


Figure 14. The distribution of plastic zone.

the analysis of calculation results, some results are acquired. During the strength reduction process, if the reduction factor is taken as 0.9, the plastic zone inside the slope starts to distribute throughout the cross section. The distribution of plastic zone is shown in Figure 14 at this time. The distribution of the X direction displacement is shown in Figure 15. The distribution of the X direction stress is as shown in Figure 16. The relation

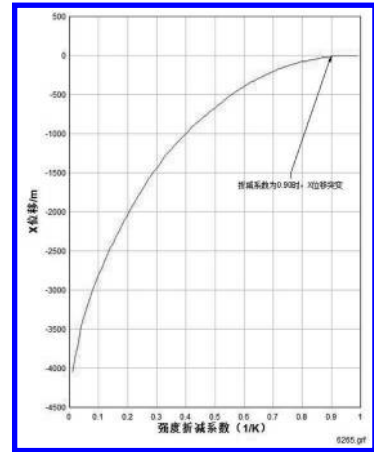


Figure 17. The relation between the strength reduction factor and X direction displacement.

between the strength reduction factor and X direction displacement is shown in Figure 17. As can be seen from Figure 17, the slope of X displacement curve takes mutation as the strength reduction factor arriving 0.9, so the safety factor of slope stability is $1/0.9 = 1.111$.

5.4 With revetment and with water

In this situation, the reservoir is with impoundment and with revetment. The computational grid

meshing of slope is shown in Figure 18. According to the analysis of calculation results, some results are acquired. During the strength reduction process, if the reduction factor is taken as 0.82, the plastic zone inside the slope starts to distribute throughout the cross section. The distribution of plastic zone is shown in Figure 19 at this time. The distribution of the X direction displacement is shown in Figure 20. The distribution of the X direction stress is shown in Figure 21. The relation between the strength reduction factor and X direction displacement is shown in Figure 22. As can be seen from Figure 22, the slope of X displacement curve takes mutation as the strength reduction factor arriving 0.82, so the safety factor of slope stability is $1/0.82 = 1.220$.

5.5 The calculation results analysis under the working conditions

For the four kinds of working conditions, the safety factor of slope stability are shown in Table 1.

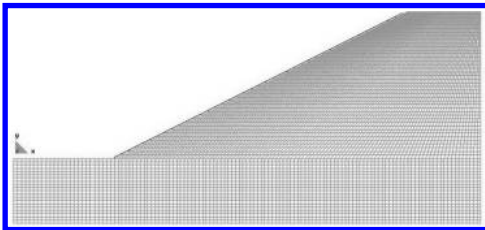


Figure 18. Meshing.



Figure 19. The distribution of plastic zone.

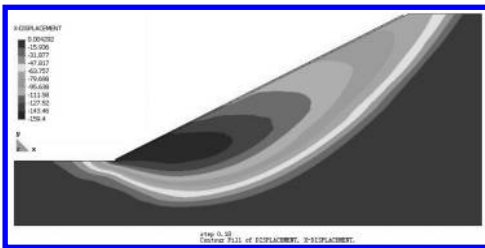


Figure 20. The distribution of X displacement.

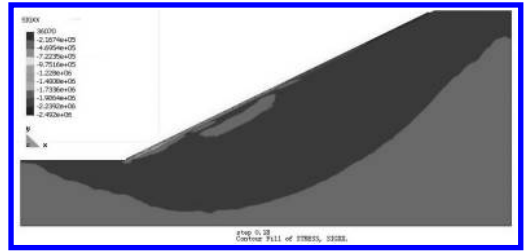


Figure 21. The distribution of X stress.

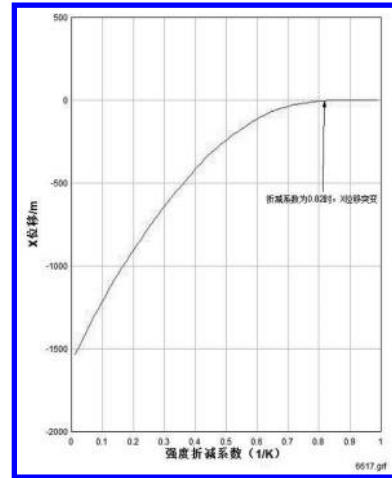


Figure 22. The relation between the strength reduction factor and X direction displacement.

As can be seen from Table 1, with the same calculation model and calculation parameters, the safety factor of slope stability under different working conditions are different. For the reservoir without revetment and water, the safety factor is 1.316. Whereas the safety factor of slope stability of reservoir with revetment but without water is 1.408, taking a significant increasing compared to the first working condition. For the reservoir without revetment but with water, the safety factor of slope stability is 1.111, taking a significant decreasing compared to the first working condition. The safety factor of slope stability decreases mainly owing to the fact that unit weight of underwater slope is buoyant unit weight after the reservoir impoundment. However, the safety factor of slope stability of reservoir with revetment and water is 1.220, taking a significant decreasing relative to reservoir without revetment and water (the third working condition). It is apparent that concrete block revetment can make a contribution to improving the safety factor of slope stability, so it can be used in actual revetment engineering.

Table 1. The safety factor of slope stability of working conditions.

Working condition	Without revetment and without water	With revetment and without water	Without revetment and with water	With revetment and with water
Safety factor	1.316	1.408	1.111	1.220

6 CONCLUSION

In this paper, it studied the stability of the hinge-chained concrete block slopes under water pressure. And it introduced two solutions of basic slope stability safety factors. Then the finite element method is used to analyze and compare the selected appropriate finite element models in four different working conditions.

This article was supported by Natural Science Foundation of Jiangsu Province (Grant No. BK20141090).

REFERENCES

- [1] Li Zhi-jiang, Duan Fei, Li Wei-lin. Research on and Practice of Hinged Mattress Applied in Beach Protection Engineering on the Middle & Lower Reaches of the Yangtze River [J]. *Port & Waterway Engineering*, 2006, (4): 80–81.
- [2] Simons D.B, Senturk F.Y. *Sediment Transport Technology*. [M] Water Resources Publications. 1976.
- [3] Klein Breteler M, Bezuijen A. Simplified design method for block revetments [A]. *Proceedings ICE Conference on Coastal Structures and Breakwaters* [C]. London: Thomas Telford, 1991. 423–436.

Research on ecological planning design of waterfront landscape belt in cold regions—with the riverside of Jilin city as a case study

Hong Ming Liu & Yu Su

Jilin University of Architecture, Changchun, China

ABSTRACT: Under the background of globalization, the strategic status of characteristic winter cities in urban competition has been greatly increased. From the perspective of ecology, the paper is to discuss about the deficiency in waterfront view for winter cities, and make multiple researches on plant species, artificial facilities and regional culture in waterfront area and expounds about how to create a good ecological environment in the hope of developing a plan suitable for the orderly development of the water-front landscape in cold regions. Besides, this paper applies its research findings into the waterfront landscape planning and design for riverside of Jilin province.

Keywords: cold regions; riverside landscape belt; planning and design

The waterfront ecological landscape in the cold regions is the representative for riverside cities in the cold regions. It is also the concentrated reflection of the city's characteristics, which can endow the cities in the cold regions with typical city landscape characteristics, which is harmonious with nature. The ecological planning design of the waterfront landscape is an important way for the cities in the cold regions to create natural environment and artificial environment, to promote their landscape development and guide the city construction to achieve the goal of creating city ecological landscape characteristics. The waterfront ecological landscape design is a restoration and treatment of the cold regions, in terms of the water quality improvement of lakes, rivers, oceans and marshy, water and soil maintenance, habitat of flora and fauna, and making the environment greener and more beautiful. Through conducts planning and design of the coastal space, facilities and environment, it aims to create a beautiful and vivid waterfront landscape environment with its own characteristics. The waterfront landscape belt of the cities in the cold regions is an important part of the public opening space of the cities in the cold regions. By artistically combining the natural and artificial landscape, it enhances the intimacy between humans and nature. Based on the idea of protecting ecological environment and sustainable development, this paper puts forward as series of approaches and methods to restore the waterfront ecology, including phytoremediation, reconstruction of systematic food chain and waterfront landscape, implementation of ecological

bank protection and increase of species to recreate communities.

1 BACKGROUND OF THE RESEARCH TOPIC

The ecological design of the waterfront landscape belt in the cold regions started at a very late date. Due to lack of proper models to refer to, the landscape belt design, being dull and formalized, is faced with many problems and difficulties, and opportunities as well. With the speeding up of urbanization, waterfront ecological landscape design has a great room for development and more attention has been paid to it. Designers should make full use the climate and unique regional cultural characteristics in the cold regions to explore proper design principles and strategies and achieve the goal of protecting environment in the real sense, putting people in the first place and sublimating the value of the waterfront landscape in the cold regions.

2 ECOLOGICAL LANDSCAPE DESIGN PRINCIPLES FOR WATERFRONT LANDSCAPE BELT IN THE COLD REGIONS

2.1 *The principle of ecology*

The water space is a very complex system, so it requires the design to show the multiple functions of the space environment. Apart from the requirements of flood control, water conservancy and

beautifying the city, the design should also provide conditions for the reproduction of the flora and fauna so as to protect biological diversity. Through enhancing the treatment efforts, the design should focus on the planting of local trees and combining fallen leaves and needle-point evergreen plants for plant furnishing, thus making better use of the waterfront environment, promoting the natural circulation, constructing the urban ecological passage and creating an ecological environment full of vigor. In this way, the waterfront landscape design can reach the realm of “originating from nature but being superior to nature, and returning to nature.”⁽¹⁾ Only by employing scientific methods and design methods to analyze, evaluate and improve the design can ecological development and sustainable development be achieved in the real sense.

2.2 *The principle of putting people first*

The waterfront landscape belt design in the cold regions should conform to the living habits and behavior styles of the local residents. The design should fully demonstrate the care of “putting people first,” such as laying anti-slipping tiles on the square and footpaths and consider the convenience for people to go outside and the accessibility of the place that people wants to go to. Moreover, the positive factors like ice and snow can be made use of to mobilize people’s interest for the outdoor activities in winter and make people better experience the nature, such as the winter sunshine. The design shouldn’t be just for the sake of beauty, but should stick to the principle of “putting people first” in the material and spiritual level in the real sense.

2.3 *The principle of regionalism*

Each city has its own history, which can give full expression to the development and changes of a city. Usually, this is where the charm of a city lies. The waterfront landscape design in the cold regions should fully employ the climate characteristics and regard them as the theme to create the city’s image, achieving the combination of natural landscape treatment and cultural landscape protection and utilization, restoration and improvement of the vigor of the landscape and shaping of the new image of the city. The designer should fully dig the historical and cultural deposit of a city and fully analyze the status quo so as to make full use of the historical and cultural characteristics of a city and adopt landscape design expression method to vigorously promote them. This is of vital significance to the continuity of the city’s history and culture.

2.4 *The principle of safety*

With the increasing expansion of city scale, floods are posing a greater threat to the expanded city. Especially to material and technical conditions of the riverside cities in the mountainous region, that cannot be avoided completely. Therefore, landscape design should consider the influence of floods, and the special climate characteristics and movement rules and characteristics of water body in the cold regions. Designers should regard safety as an important principle in riverside landscape design. Only when the safety is ensured can people get closer to the nature to experience it better.

3 ANALYSIS AND STATUS QUO OF THE CLIMATE AND ENVIRONMENT IN THE RIVERSIDE WEST ROAD IN JILIN CITY

The Jilin City is characterized with temperate continental monsoon climate, whose four seasons are distinctive. In spring, it is arid and lacks precipitation. In summer, it is hot, humid and rainy. In autumn, it is cool and sunny. In winter, it is cold and snowy. Thanks to the special climate environment, Jilin City is a great summer resort; in winter it is paradise of ice and snow. The Songhua River is abundant with species, being beautiful, wide and long, which is like a green ribbon flowing through the whole city of Jilin. The landscape belt along the Songhua River is an important landscape for Jilin City. The landscape belt planning and design of Riverside in Jilin City has shown many shortcomings, mainly the dull planning and design content, formalized design and planning form, and impoverishment of the landscape, failure of fully employing the local climate characteristics, simple overlaying of riverside green belt, riverside square, various activity arenas, parks and landscape pieces, lack of unique waterfront landscape belt design in the cold regions, failure to meet the diversity and complexity of the social activities and low development and utilization rate of the natural resources. This paper will conduct planning and reform of the waterfront landscape belt in the Riverside in Jilin City.

4 METHODS AND STRATEGIES FOR THE WATERFRONT LANDSCAPE DESIGN IN THE COLD REGIONS

4.1 *The influence of sunshine and shadows*

Properly plan the sunshine area and shadow area after considering the sun exposure period; fully utilize the beneficial influence of the near water body and design according to different seasons,

especially winter and summer; protect the current vegetation and conduct plant furnishing in the place if necessary. Plant furnishing can control the microclimate, mitigate the strong wind, and the leaves can protect the soil to prevent against the drying of wind and sunshine. In winter, it can absorb or transform the heat of the sun so as to protect the soil from being frozen.

4.2 *Water body recovery*

In order to protect Songhua River from being polluted, it should firstly be forbidden that the city sewage, failing to be up to stands and or without being treated, is directly discharged into the water body; secondly, the wetland along the shore can be created to restore the ecological environment of the water body. The wetland soil contains some special hydrological and physical properties, which make it into a natural reservoir, being able to cut down flood peaks and homogenize flood through the method of intercepting runoff and accumulate rainstorms, and can eliminate the organic, inorganic and toxic substances from the water body. Some substances entering the wetland water body can absorb the chemical substances and deposit. In this way, the water quality is purified.

4.3 *Design of the green land and pavement*

The waterfront space is increasingly become a leisure and relaxing ground for people. The waterfront green land landscape can give people a comfortable and pleasant feeling of being far away from the noisy metropolitan life, so it has become more and more popular. At the same time, the greening rate has exceeded 50% of the other cities. In summer, it can effectively reduce dust and temperature, enrich the riverside plants and achieve the virtuous cycle through landscape and ecology.⁽²⁾ In winter, ice lanterns and sculptures and snow sculptures can be established. All these snow and ice landscape ornaments can change on an annual basis, thus enriching the city appearance and the color in the winter and making up for the shortages of the dull winter plants. The combined application of plants and pavements can guide people's transportation sight. However, it should be remembered that anti-slipping measures should be adopted for the pavements in the cold regions.

4.4 *Plant furnishing*

Plant large areas of tall trees along the waterfront landscape area to keep the cold and chill; plant some special tree species in some locations as decorations or landmarks. The plants will show different

shapes and changes of color due to the climate change of the four seasons, such as the yellow leaves in summer and the beautiful icicles hanging on the branches in winter. Moreover, large quantities of evergreens, such as pines and cypresses, can be adopted. At the same time, make the area along the Songhua River into the natural food resources and habitats for birds and other animals, and a main living environment for the biosphere.

4.5 *Service facilities*

set up public phones, road instructions, road signs, waterers, benches, trash cans, decorative lighting, toilets, recreational and sports facilities, passages, pavilions and attics to meet people's different demands; try one's best to adopt the blight colors, combine with the theme of snow and ice in the cold regions to design and widely apply ice and snow to make up for the inadequate greening area in winter.⁽³⁾

5 CONCLUSIONS

To sum up, the potential value of the waterfront public space in the cold regions to the city's general landscape and development of the surrounding area has been extensively recognized. Urban waterfront green landscape ecological planning is an important part of urban landscape planning. Based on the specific region of Songhua river waterfront area in the Jilin City, this paper focuses on analyzing and designing the natural elements, artificial elements and cultural elements, and puts forward relevant strategies to create an artistic, humanistic, ecological and safe waterfront landscape environment with the characteristics of the cold regions. This paper applies the landscape planning idea to the planning of waterfront space so as to enable the urban waterfront landscape to create a livable metropolitan environment. This paper hopes to serve as a modest spur to induce more valuable contributions in the construction of waterfront ecological landscape in the cold regions and the creation of urban environment with characteristics.

REFERENCES

- [1] Liu Binyi. Modern landscape planning and design [M] Nanjing: Southeast University press, 1999.
- [2] Zhu Junzhen garden art [M] Beijing: Chinese Forestry Press, 1998.
- [3] Wang Kaihong Zhang Shi Cong. The design of cold area city waterfront landscape and research of [J] art research 2008, 2.

Study on the influence of the particle damping to sound field inside the closed cavity

Li Hu, Zhe Tang & Qi Liang Yang

School of Automobile and Traffic Engineering, Wuhan University of Science and Technology, Wuhan, China

Xian Xu

Technology Center of Dongfeng Commercial Vehicle Co., Ltd., Wuhan, China

ABSTRACT: The simulating calculation and modal experiment verification of a model car have been carried on which was made from thin steel plates. Then, sound pressure of the field points inside the model car which was pasted with particle dampers were got by using the vibration-acoustic coupling calculation and acoustic experiment. The comparison of the simulation and experimental results verified the acoustic simulation model of the model car with particle dampers was right. Finally, the influence to sound field inside the model car with particle dampers at different position were studied by simulating calculation.

Keywords: particle damping; vibration-acoustic coupling; the sound pressure of field points; sound field distribution

1 INTRODUCTION

The car bodies are mainly consisted of thin-wall parts. They vibrate obviously and radiate noise to the surroundings when they are motivated by outside actuators. Most of sound energy inside the car is produced by vibration of thin-walled car body. So, damping materials are often used to suppress the vibration of the thin wall parts. Then the noise inside the car was under control. The viscoelastic damping materials were used in domestic auto industry commonly such as asphalt composite material. But the disadvantages of asphalt material are that its damping characteristics change with the temperature, stability is poor and it will release harmful gas at high temperature (Zhou et al. 2003).

NOPD is to fill tiny particles into the accessory cavity of vibration structure according to fill rates. Structural vibration result in inelastic collision and friction among particles and the cavity walls, consuming energy, generating damping effect. Then the purpose of suppressing structural vibration is reached. Its influence on the structure stiffness is very small almost without additional quality. And it can significantly improve the system damping. Not only NOPD is suitable to be used in high temperature, corrosion and other relatively harsh environment, but also its vibration reduction performance may not reduce along with

time (Panossian 1989, 1991). Therefore, it has good prospects for vibration reduction instead of asphalt materials. Li Hu and Qibai Huang of Huazhong university of science and technology established the mathematical model of particle damping based on the discrete element method. They also established the powder mechanics model of particle damping to study the effects of the cross-section shape and size of particle damper cavity to particle damping characteristics in order to reveal the nonlinear characteristics of particle damping. Then, Li Hu designed the quadratic regression orthogonal experiment of particle damper to obtain the relationships between the particle damping vibration characteristics and the main parameters (Hu, et al. 2008, 2009).

In this paper, particle dampers were pasted on the model car which was made from thin steel plate. Sound pressure of the field points inside the model car were obtained by vibration-acoustic coupling simulation and acoustic experiment separately. The acoustic simulation model of the model car with particle dampers is validated through the contrast of the simulation results and experimental data. On the basis, the difference of sound pressure inside the model car were studied which was pasted by particle dampers at different positions. The research will provide a good reference for the application research of the thin-walled car body with the particle damping.

2 THE MODAL SIMULATION CALCULATION AND EXPERIMENT OF THE MODEL CAR

2.1 The modal simulation calculation of the model car

The geometric model of the model car was imported into the Virtual Lab, meshed and simulated by setting correct parameters. The meshing grid sizes of the model car are set to be 10 mm. And the steel material properties are filled into the software. Then, free modes of the model car were calculated without any constrains.

2.2 The modal experiment of the model car

The model car was welded by some steel plates with 1 mm thickness. Its geometric sizes were as follows: length was 1015 mm, width was 414 mm, the maximum height was 293 mm. The model car structure was shown in [Figure 1](#).

The modes of the model car were tested by the signal collection and analysis system named LMS Test Lab. Geometric line diagram model of the model car was shown in [Figure 2](#), including a total of 172 nodes. Several acceleration sensors are fixed at the surfaces of the model car to gather the acceleration signal respectively. Four corners of the model



Figure 1. The model car structure.

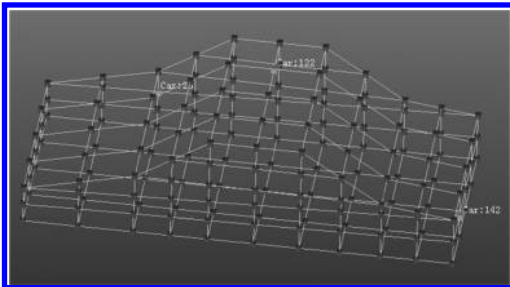


Figure 2. Geometric line diagram of the model car.

Table 1. The contrast of top 10 order modes between test and simulation.

Order	Test results	Simulation results	Deviation (%)
	Frequency (Hz)	Frequency (Hz)	
1	22.17	24.90	12.32
2	32.13	32.71	1.82
3	44.58	44.20	0.85
4	54.07	54.29	0.41
5	58.22	60.25	3.50
6	60.94	61.44	0.82
7	64.46	66.05	2.47
8	69.41	73.76	6.27
9	77.18	78.03	1.09
10	80.47	82.22	2.18

car were hung with rubber band during the test process in order to keep it at free state. The model car was hit with the force hammer. The response signals were measured by the acceleration sensors, enlarged via the built-in amplifier and passed into the signal acquisition instrument to be stored in the computer. Then, the output of the force hammer and input of acceleration sensors were processed by the modal analysis function of the software to obtain the modal parameters of the model car. The test and analysis results were shown in [Table 1](#).

2.3 The contrast of the test and simulation modes

In order to verify the correctness of the finite element model of the model car, the simulation and test of the first 10 order modes were compared. It can be seen from [Table 1](#), the simulation errors of the modes and test modes were controlled within 15%. Although difference of the first order modal frequency between the simulation and test is 12.3%, other difference was controlled within 5%. It proved the finite element model of the model car was relatively accurate. The acoustic simulation calculation of the model car may be carried out on the basis of this model.

3 THE SIMULATION AND TEST OF THE SOUND PRESSURE AT THE FIELD POINTS INSIDE THE MODEL CAR WITH PARTICLE DAMPERS

3.1 The basic principles of acoustic coupling simulation

In the acoustic fluid-structure coupling interaction problems, if energy dissipation on the fluid

boundary caused by damping was taken into consideration, the discretization of the wave equation can be acquired as following.

$$m_e^a \ddot{P}_e + c_e^a \dot{P}_e + k_e^a P_e + \rho_0 R^T \ddot{u}_e = 0 \quad (1)$$

In the formula, m_e^a is the fluid mass matrix. c_e^a is the fluid damping matrix. k_e^a is the fluid stiffness matrix. $\rho_0 R^T$ is the coupling mass matrix of interface to describe fluid-solid interaction. P_e is the node stress vector. u_e is the node displacement vector.

The fluid pressure load on the fluid-solid interfaces were put into the structural dynamics equation, structural discretization equation can be obtained as follows.

$$m_e^s u_e + c_e^s u_e + k_e^s u_e - R_e P_e = F_e^s \quad (2)$$

In the formula, m_e^s is the structural unit mass matrix. c_e^s is the structural unit damping matrix. k_e^s is the structural unit stiffness matrix. $R_e P_e = F_e^a$ is fluid pressure load vector on the fluid-solid interfaces, which is the direct coupling term related on fluid pressure on the fluid-solid interfaces. F_e^s is the structural load.

The finite element discrete equation of full fluid-structure interface can be obtained from formula (1) and formula (2) and unified as the following.

$$\begin{pmatrix} m_e^s & 0 \\ m_e^{as} & m_e^a \end{pmatrix} \begin{pmatrix} \ddot{u}_e \\ \ddot{p}_e \end{pmatrix} + \begin{pmatrix} c_e^s & 0 \\ 0 & c_e^a \end{pmatrix} \begin{pmatrix} \dot{u}_e \\ \dot{p}_e \end{pmatrix} + \begin{pmatrix} k_e^s & k_e^{sa} \\ 0 & k_e^a \end{pmatrix} \begin{pmatrix} u_e \\ p_e \end{pmatrix} = \begin{pmatrix} F_e^s \\ 0 \end{pmatrix} \quad (3)$$

This is the coupling equation of sound and structure, $m_e^{as} = \rho_0 R_e^T$ and $K_e^{sa} = -R_e$ are coupling terms. It shows the structural vibration under the action of load will produce sound waves, and the radiation sound wave can also cause the vibration of the structure.

3.2 Simulations of the sound pressure at the field points inside the modal car

First of all, the acoustic finite element simulation model of model car with particle dampers was established. All free degrees of four angles on the top of the finite element model are constrained. Three field points were set up respectively at the position of the engine compartment, driver's and rear passenger's ear area. Force signals were collected in the subsequent validation experiments (180 Hz and 240 Hz steady signal were selected to simulate the model car in this paper) and regarded as exciting signal. Then, the damping loss factor of particle dampers were imported in, which

measured by the steady-state flow method (Cheng et al. 2013). The finite element simulation model is shown in Figure 3. Overall sound pressure level of three field points are calculated as well as experimental verification and analysis.

3.3 The measurement of sound pressure at the field points inside the model car

According to the process of acoustic simulation of the model car, 4 corners of the model car were fixed on the bracket by bolts, and 3 particle dampers whose size are $120 \times 20 \times 10$ (mm) and was filled with 0.7mm steel ball were pasted at the bottom of the model car. Microphones were placed at field points. Sine excitations were applied at the bottom of the model car. And sound pressure signals were recorded. The measurement for sound pressure at the interior field points was shown in Figure 4 test figure.

3.4 Comparison and error analysis between the experiment and the simulation of the sound pressure at the field points

The experiment and simulation date of the sound pressure were compared at the field points inside model car. It can be seen from Table 2 that, the



Figure 3. The simulation model of the model car with particle dampers.

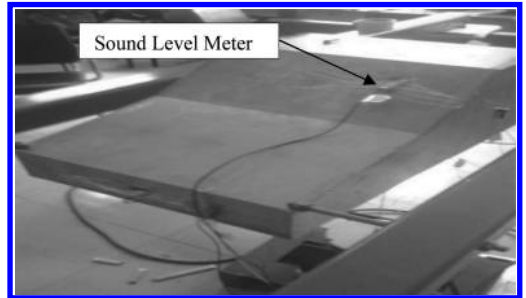


Figure 4. Measurement of the sound pressure at the interior field points.

Table 2. Comparison between the experimental and simulation date of the sound pressure at the field points inside the model car.

Excitation frequency (Hz)	Field points	Simulation results (dB)	Test results (dB)	Deviation (%)
180 Hz	Field point 1	90.51	98.96	8.5
	Field point 2	93.13	93.92	0.8
	Field point 3	88.36	93.37	5.4
240 Hz	Field point 1	110.05	109.06	0.9
	Field point 2	97.07	92.85	4.5
	Field point 3	103.34	100.44	2.9

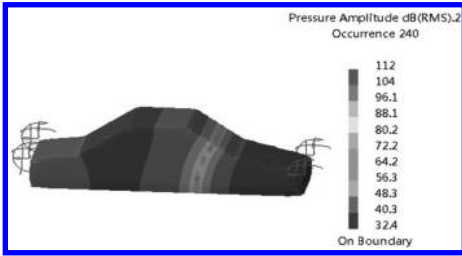


Figure 5. The sound field of the model car without a particle damper at 240 Hz.

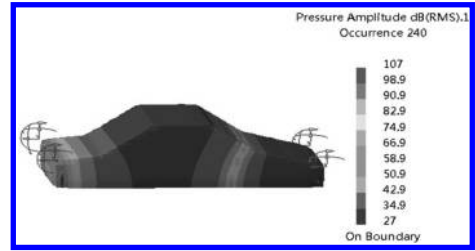


Figure 8. The sound field of model car with particle dampers above the engine ceiling at 240 Hz.

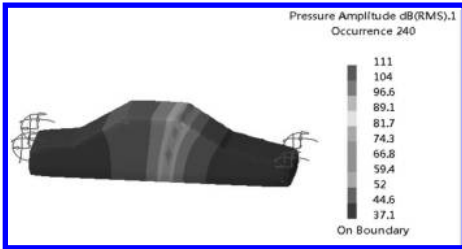


Figure 6. The sound field of the model car with particle dampers at flank at 240 Hz.

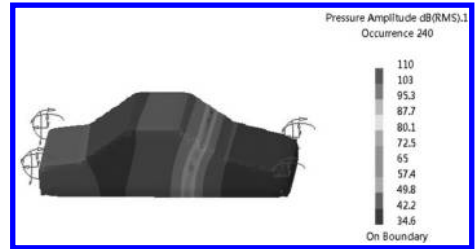


Figure 9. The sound field of model car with particle dampers under the floor at 240 Hz.

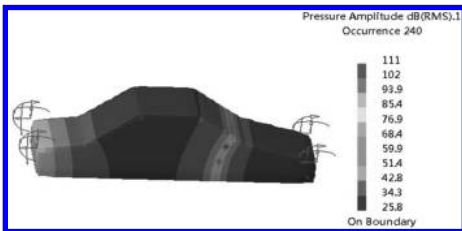


Figure 7. The sound field of the model car with particle dampers above the hood at 240 Hz.

error of the experiment and simulation result of the sound pressure at the field points are within 10% in 180 Hz and 240 Hz. It shows that the acoustic simulation model is relatively accurate. The major reasons of error are perhaps as followings.

- (1) The experiment of the ambient noise results in the error.
- (2) The vibration of the actuator makes a noise and results in caused by the error.

4 THE CHANGES OF INTERIOR ACOUSTIC FIELDS WITH THE DIFFERENT POSITIONS PARTICLE DAMPERS ARE PASTED ON

The difference of the interior acoustic fields was compared of the model car which wasn't pasted particle dampers, the model car which was pasted particle dampers at flank, or above the engine nacelle, or above the ceiling, or under the model car. In the simulation process, the force of 240 Hz which was collected in the experiment was applied.

Conclusion can be drawn from the above comparison of the results of different simulation calculations. (1) After the particle dampers were pasted at the model car, the interior sound field was changed. (2) Pasting particle damper at the different positions of the model car, changes of the interior sound field are different. The maximum sound pressure was reduced. (3) When particle dampers were pasted above the ceiling, the noise reduction effect was the best one.

5 CONCLUSION

1. The correct finite element model of the model car was built through comparing the modal simulation with the test data.
2. The correct acoustic finite element model of the model car with particle dampers was built through the comparison of the acoustic simulation and the test data at field points inside the model car.
3. By comparing the sound field distribution inside the model car with or without particle dampers, it can be drawn that the interior sound field is changed and particle dampers play a certain noise reduction role. The noise reduction effect was best when particle dampers are pasted above the ceiling.

ACKNOWLEDGEMENTS

This work was financially supported by Nation Natural Science Foundation of China (No: 51105283), Institute of vibration noise and fault diagnosis, School of Mechanical Science & Engineering of Huazhong University of Science and Technology (HUST).

REFERENCES

- Cheng Xiang-ke, Yang Qi-liang, Hu Li, Yuan Shuang Tang Zhe. Study on the Method of Particle Damping Loss Factor Experiment [C]. *Advances in Civil and Structural Engineering*, 2013.
- Feng Zhou, Shigui Zhou, Haishen Yang. *Damping Materials and Automobile Vibration Noise Reduction* [J]. *Automobile Technology*, 2003.
- Hu Li, Huang Qi-bai, Liu Zhan-xin. Study on Characteristics of Particle Dampers [J], *Journal of Vibration and Shock*, 2009.
- Hu Li, Huang Qi-bai, Ma Wei-ci. Experimental Research on the Damping Performance of Particle Dampers [J], *Noise and Vibration Control*, 2008(5).
- Panossian, H.V., *Non-Obstructive Impact Damping Applications for Cryogenic Environments*. *Proceedings of Damping*, 1989, pp. KBC 1–9.
- Panossian, H.V., *Non-Obstructive Particle Damping: A New Passive Damping Technique Shock and Vibration*, Vol. 1, No. 6, 1991: 4–10.

Microstructure and mechanical properties analysis of GH3030 alloy activity TIG welding

Xiao Gang Zhu

Changchun Institute of Engineering and Technology, Changchun, Jilin, China

Wei Wang

Jilin Agricultural University, Jilin, China

Chun Li Yang

Harbin Institute of Technology, Harbin, Heilongjiang, China

ABSTRACT: According to the metallurgical characteristics of GH3030, several single-component compounds were selected, such as TiO_2 , MoO_3 , AlF_3 , etc. The influence of these compounds on the welding penetration, welding voltage and weld forming are measured. The experiments indicated that different single-component compounds differ in the power of increasing the penetration. The penetration of AlF_3 flux is the most distinct. MgF₂ weld strength is the highest, with several other compound strength are accounted for more than 90% of the parent material.

Keywords: super alloy; A-TIG welding; orthogonal experiment; aging treatment; mechanical properties

1 INTRODUCTION

Nickel base superalloy with high temperature, high strength, high durability and good comprehensive properties such as resistance, welding performance. At present, in the actual production of nickel based superalloy welding is the most widely used manual electric arc welding and argon tungsten arc welding. The conventional TIG welding with the welding arc stability, weld can ensure internal quality, appearance, suitable for welding in the advantages of difficult places, under the protection of inert gas. But the conventional TIG welding single pass welding depth, is only suitable for welding thin plate^[1]. If the increase in input current, the weld width will be very wide, and the increase of penetration depth is not obvious. By using helium as a protective gas penetration is very limited, and will greatly increase the cost of production. A-TIG compared with the conventional TIG welding, in the same welding condition, can greatly improve the penetration depth (as shown in Fig. 1-1), at the same time reduce welding time 50%, improve the welding efficiency 2-6 times, reduce the cost of welding.

2 TEST MATERIAL AND METHODS

2.1 Test material

Nickel based alloy used in most aerospace engine field is GH4263, and the experiment for this material are studied. GH3030 alloy composition as shown in Table 1.

2.2 Test method

In welding test before, on the surface plate removing oxide, oil processing, first with a wire brush to remove the oxide film on the surface of polished specimens, with metallic luster; and then wipe with anhydrous ethanol or acetone, remove oil

Table 1. Chemical composition of GH3030.

Element	Content (%)	Element	Content (%)
C	0.04-0.08	Cr	19.00-21.00
Mn	≤0.60	Co	19.00-21.00
Si	≤0.40	Mo	5.6-6.10
P	≤0.015	Ti	1.90-2.40
S	≤0.007	Ni	Margin

and dry. In order to facilitate the welding effect comparison, as shown the welding plate is divided into two regions, in which, a region with flux A-TIG welding, the other part of the common TIG welding. Powdered active agent in ethanol mixing into suspension, the suspension with a flat brush evenly coated on the surface of the specimen, the ethanol evaporate completely, can carry out welding^[2].

The specimen is also used in argon (flow in order to prevent welding oxidation, welding process on weld take three argon protection. In addition to argon gas protection welding torch (flow 10 L/min), and in the opposite direction of 150 mm welding with long drag cover butt welding Joint positive protection (flow 15 L/min). Welding parameters.

3 THE RESULTS OF EXPERIMENT

3.1 Active agent to the effect of welding penetration

By contrast the following rules, activating agent, the weld penetration increased significantly, the weld width narrowing, corresponding to the depth to width ratio increases; for the different compounds penetration increases are also different; single element compounds on penetration has increased in varying degree. As you can see in Figure 1, the penetration of 1.5 mm welding of uncoated and coated with surfactant, AlF₃ penetration depth can reach 4 mm, an increase of 160%, in the following several kinds of compounds, AlF₃ on the penetration increased significantly. Other compounds penetration as shown in Table 2-2. TiO₂ welding penetration increases smaller,

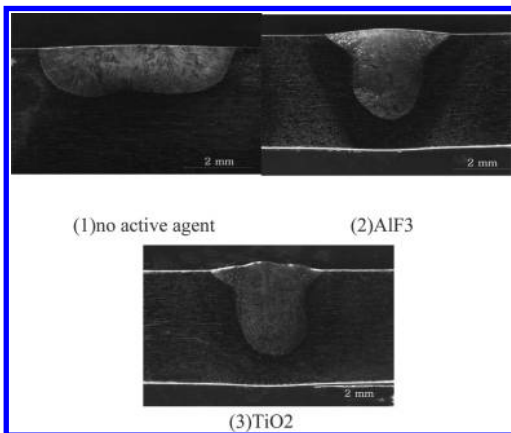


Figure 1. Active agent to the effect of welding penetration.

3.2 Effect of surfactant on the welding voltage

Welding voltage is an important index of the welding process, it has great influence on the line heat input welding, welding arc shrink and judge the most clear and convincing way is the change of arc voltage^[4]. The same arc in the same welding current, arc length and protective atmosphere, if the arc voltage increase, is somehow make arc generated contractive. However in the arc contraction, the arc force is more concentrated, the weld pool surface will produce depression greater, the arc length is increased, in this case with arc voltage value of the measured to judge arc contraction with uncertainty, which has not been a major cause of arc voltage evaluation of the arc contraction. The crux of the problem lies in considering voltage changes brought about by the arc length change, change the arc voltage is proved the most effective way for the arc contraction^[3].

Figure 2 measurement results of arc voltage (not considering the introduction of active agent, because the arc force is more concentrated, the weld pool surface increase). The measurement results show that, in the 3 kinds of active agent selected, in addition to the AlF₃ on the arc voltage of no effect, other active agent makes the arc voltage increased in different degrees. Among them, TiO₂ coating agent after the arc voltage increase the greatest degree of arc voltage, welding parameters corresponding to the increase of 11.5V, the arc voltage is increased by 40% (arc voltage without flux is 8.8v). The arc voltage is increased for two reasons: one is the number of electrons arc increases, another is the arc contraction conductive area and decrease. Although the metal atom active agent after the decomposition of ionization is easier than the Ar atom, but ionic binding energy of metal oxide is very big, so,

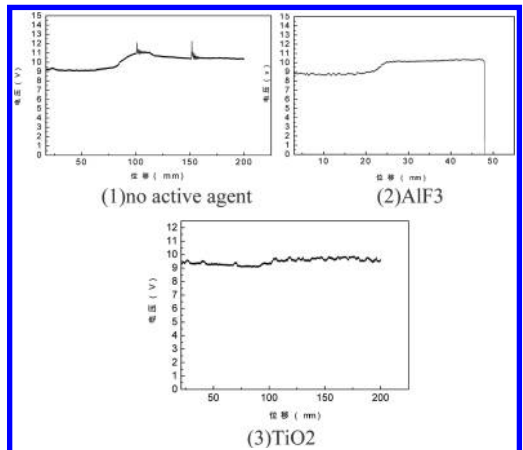


Figure 2. Effect of surfactant on the welding voltage.

metal ions ionization out rarely, electronic increased in number and not the main reason, and the conductive area of Jian Xiaocai by the arc contraction caused is the main reason.

3.3 Analysis of weld line microstructure

The alloy welding, heat affected zone is not obvious in Figure 4-2 (b) are shown. The main reason is that the thermal conductivity of nickel base superalloys difference from the parent material, weld to great temperature gradient, temperature drops quickly. In addition, the alloy temperature at 730 °C, 750 °C grain won't grow up, that is, nickel base superalloy grain growth of low temperature high. Based on the above two reasons, nickel base superalloy in welding, heat affected zone is very small.

The weld zone is in as cast microstructures of typical, see 4-2 (d), the middle of weld is equiaxed crystal, however, the active agent formulation different, different welding processes, welding seam center equiaxial crystal width is not the same, even some active agent without intermediate equiaxial crystal. Both sides of thee Equiaxed grains are columnar crystal zone. Because of the poor thermal conductivity of nickel base superalloy, the cooling rate of the weld is slow, is also the weld cooling undercooling is small, easy to coarse grain. The second phase particle distribution in the columnar dendrite. In addition, some impurity elements are easily gathered in the inter dendritic. Dendrite and welded seam region of equiaxed grains compared to large lot. Therefore, the weld strength is lower than the base metal strength, the tensile fracture at the weld, shall be.

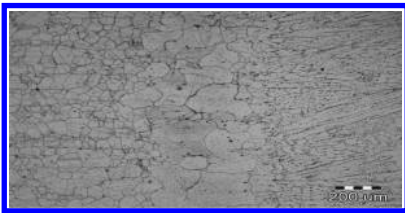


Figure 3. Base meta + heat affected zone.

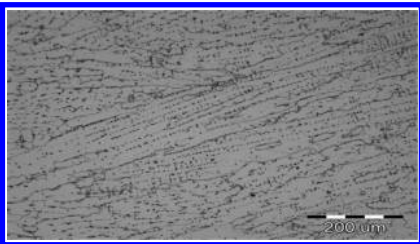


Figure 4. Weld zone.

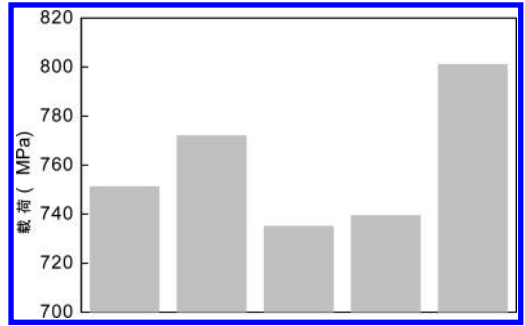


Figure 5. Analysis of weld performance.

3.4 Analysis of weld performance

The coating agent, performance and parent material and weld declined slightly, the highest MgF2 welding tensile strength, can reach 770 MPa, accounting for 96.1% of the base metal strength. Surfacing and the tensile strength of AlF3 was 740 MPa, accounting for 92.5% of the base metal strength. But the welding tensile strength of TiO2, MoO3 were 725 MPa and 730 MPa, accounting for 90.6% of the base metal strength, 91.2%.

4 CONCLUSION

1. Coating on AlF3 welding of GH3030 alloy deep increases remarkably; surface coating of AlF3 weld forming the best; the most significant increase of welding voltage MoO3.
2. The weld zone grain than the base metal and heat affected zone large root.
3. With MgF2 weld strength is the highest, with several other compound strength are accounted for more than 90% of the parent material.

REFERENCES

- [1] H. Carpenter. Alloy 903 Helps Space Shuttle Fly [J]. Metals Progress, Aug, 2009, 32(2):25-29.
- [2] S. Leconte, P. Paillard, J. Saindrenan. Effect of fluxes containing oxides on tungsten inert gas welding process [J]. Science and Technology of Welding and Joining, 2008, 45(1):12-15.
- [3] P.C.J. Andersonand, R. Wiktorowicz. Improving Productivity with A Welding & Metal Fabrication [J]. Science and Technology of Welding and Joining. 2011, 6(3):108-109.
- [4] D.C. Johnson, E.F. Pfender. The Effects of Low ionization potential Contaminants on Thermal Plasmas [J]. Plasma Chemistry and Plasma Processing. 1983, 3(2):258-273.

Study on the promotion of Liaoning rural roof insulation project

Jun Liu, Ding Qiang Chen & Run Qing Liu

Shenyang Ligong University, Shenyang, Liaoning Province, China

ABSTRACT: The roof insulation project has a significant meaning in building energy conservation. According to the survey of roofing heat preservation performance of the rural construction in Liaoning province, this paper put forward the concrete measures for Liaoning rural roof insulation project, based on the analysis of its rural problems on the roof insulation project promotion.

Keywords: rural construction; roofing project; thermal insulation material

As the main part of building protection, the roof plays a crucial role in building energy conservation. Relevant data shows that roof energy consumption accounts for about 8%~10% of total energy consumption of the building in our city area, while the figure in rural area is about 40%^[1]. Two main reasons account for the large rural roof energy consumption. First, it is not conducive to building energy-saving, because the rural buildings are low layer building whose shape coefficient are large^[2]; second, due to the limit of construction technology, rural residential design often ignores the energy-saving factor, rarely adapt new thermal insulation materials and often choose natural materials from local area. The roof insulation project not only can relieve the condition of cold winter hot summer which reduces the residents' bitter, but also reduce the waste of heat energy and electric energy for the heavy use of heating and air conditioning. If the insulation layer is on the top of waterproof layer, that is the inverted roof. It can avoid the waterproof layer being exposed in a constantly changing environment for a long-term, and then improve the performance of the waterproof layer^[3]. Thus see, the rural roof insulation design has an important significance to reduce building energy consumption, improve the indoor temperature and enhance the roof safety performance. In this paper, field research method is employed to study the rural building roof thermal insulation performance in Liaoning District. Based on the analysis of the existing problems on the promotion of the rural roof insulation project, the concrete measures are put forward to construct the promotion system.

1 THE STATUS OF THE RURAL ROOF INSULATION PROJECT OF LIAONING PROVINCE

According to the climatic subdivision standard of building energy efficiency design in our national rural areas, this research involved a total of 15 villages and towns and 87 farm rooms in Liaoning province, that are distributed in Shenyang City belong to the severe cold region and Chaoyang City, Jinzhou, Dalian City, Yingkou City, Dandong City belong to the cold region. It mostly reflects the basic situation of the rural roof insulation project in Liaoning area. The survey shows that the energy conservation wasn't taken into consideration in the process of the construction. Therefore, the new thermal insulation material is rarely used in the roof project.

Among the 87 farmhouse in this survey, there are 10 were built in nineties, 28 were built from 1990 to 2000, 36 were built from 2000 to 2010, 13 were built after 2010. **Table 1** lists the housing roof forms and main thermal insulation materials at different age.

The houses built in Nineties look shabby, and the heating facilities only have heated brick bed and the stove. The indoor temperature in winter is relatively low, but it is relative cool in summer. The most of flat-topped houses built during the period of 1990 to 2000 are precast concrete floor structure, and most of the houses did not consider insulation problems in construction. Therefore, the indoor temperature is low in winter and high in summer. Compared with the houses built from 2000 to 2010, it paid more attention to firmness and beauty of the material to build houses in nineties; however

Table 1. The rural building roof forms and thermal insulation materials in Liaoning areas.

Construction time	Roof forms	Proportion (%)	Thermal insulation materials
Nineties ago	Sloping roof	90	Straw, Clay and rice straw
	Flat roof	10	Straw, Clay and rice straw
From 1990 to 2000	Flat roof	85	Stove ash, spall (53% of the roof without insulation layer)
	Sloping roof	15	Straw, Clay and rice straw
From 2000 to 2010	Flat roof	85	Slag, benzene board
	Sloping roof	15	Straw, Clay and rice straw
Since 2010	Flat roof	60	Benzene board
	Sloping roof	40	Slag, straw, Clay and rice straw

Table 2. Indoor temperature in different districts.

District	Construction time	Indoor temperature in winter (°C)	Indoor temperature in winter (°C)	Outdoor temperature description
Shen yang	Nineties ago	12.7	27.6	Outdoor temperature
	1990–2010 (with no insulating layer)	8.2	30.5	in winter is -18.9°C
	1990–2010 (with the insulating layer)	10.2	29.8	Indoor temperature in summer is 32°C
	After 2010	12.6	28.2	
Dalian	Nineties ago	14.4	25.3	Outdoor temperature
	1990–2010 (with no insulating layer)	12.6	27.6	in winter is -10.6°C
	1990–2010 (with no insulating layer)	13.2	26.8	Indoor temperature in summer is 26.2°C
	After 2010	14.6	26.1	
Chao yang	Nineties ago	13.7	26.3	Outdoor temperature
	1990–2010 (with no insulating layer)	12.5	27.4	in winter is -15.6°C
	1990–2010 (with the insulating layer)	12.9	26.8	Indoor temperature in summer is 28.2°C
	After 2010	14.6	26.4	
Jin zhou	Nineties ago	13.9	28.3	Outdoor temperature
	1990–2010 (with no insulating layer)	12.7	29.6	in winter is -14.5°C
	1990–2010 (with the insulating layer)	12.9	29.1	Indoor temperature in summer is 32.1°C
	After 2010	13.6	28.4	
Ying kou	Nineties ago	14.1	25.3	Outdoor temperature
	1990–2010 (with no insulating layer)	13.1	26.8	in winter is -13.8°C;
	1990–2010 (with the insulating layer)	13.4	26.4	Indoor temperature in summer is 28.4°C
	After 2010	14.2	25.8	
Dan dong	Nineties ago	13.9	25.9	Outdoor temperature
	1990–2010 (with no insulating layer)	12.1	26.8	in winter is -13.9°C
	1990–2010 (with the insulating layer)	12.7	26.4	Indoor temperature in summer is 28.1°C
	After 2010	13.8	25.6	

the thermal insulation materials in the roof almost didn't changed. With the improvement of rural living standards, the houses built after 2000 were equipped with indoor heating, and some families also installed air conditioning. It is basically realized the warm in winter and cool in summer. Driven by the country vigorously promote green policies, the houses built after 2010 began to consider the energy conservation and environmental protection problems. More and more houses began to simply use the insulation layer, almost of which are benzene board and slag, and the insulating property is

ordinary. Table 2 lists the indoor temperature of the houses built in different areas and time. In nineties, the sloping roof houses built with the thermal insulation materials of straw or Clay and straw or rice straw was selected. From 1990 to 2010, the flat roof houses with no insulating layer and were selected, and the material of the insulating layer is the furnace ash. After 2010, the selected houses were with flat roof, and material of the insulating layer is slag and benzene board. The measurement of the housing temperature was chosen in the same area and at the same time. The winter temperature

was measured from 8:00 to 10:00, and in the summer it was from 13:00 to 15:00. All of which were measured by the digital thermometer. All heating facilities were closed 2 hours in advance for the measurement of the housing temperature in winter, while in summer; it was 1 hour in advance to close all cooling facilities. Before measuring the room temperature, it needs to close all doors and windows until the room temperature was constant. It was the time to end the test when the numerical value of temperature measuring instrument was stable. The house was tested for three times, and the final value was the average.

Table 2 shows that the rural roof insulation system in Liaoning is not improved in the past 30 years. There was no difference in the thermal insulation performance of the houses built in Nineties and after 2010. The main roof thermal insulation materials such as the original ecology of straw, rice straw and clay in Nineties are adopted, that have good thermal inertia. The roof structure is the wood frame, the houses combine the structure, environmental protection and heat preservation together and achieve the purposes of improving the indoor thermal comfort by lowering the roof heat transfer coefficient. However, in order to improve the insulation performance of the roof structure, the thickness of the grass-mud was large, generally above 100 mm, which increased the roof load. What's more, the aesthetics, durability and waterproof are bad. The building with the reinforced concrete prefabricated plate roof was employed in the houses built in nineties. Even though the housing safety and aesthetics had been improved, poor insulation was also obtained. The insulating layer had been used in the built houses after 2010, such as laying the slag or asbestos board, but the real effect is ordinary. In order to improve the indoor temperature in winter, the coal is heavy used for heating. Compared with other heat sources, the efficiency of the coal is low, only accounting for 30%–40%, which is not conducive to Chinese building energy conservation.

2 THE EXISTING PROBLEMS ON THE PROMOTION OF THE RURAL ROOF INSULATION PROJECT IN LIAONING

The insulation technology has been widely used in the buildings built in the city of Liaoning province, that the good results are achieved. However, there are many obstacles on the promotion of the rural roof insulation project, which mainly showed in the following areas.

1. Construction level restricts the application of new thermal insulation materials.
At present, rural housing construction is carried out by local farmers. Those people, who

combine into a temporary construction team, usually do not have professional knowledge and construction technology, completely follow the master study. They aren't familiar with the new type of thermal insulation material and can't apply it, whatever they do is all according to the traditional service. In accordance with the relevant national norms, construction of the insulating layer has strict requirements, and need specialized equipment. But these for the majority of rural construction teams in our province do not have. The research on rural construction team shows 97.3% of construction workers didn't have the work license. Almost all of the construction team doesn't have the professional construction equipment for the insulating materials. All of what restrict the application of the insulating material in the construction of rural roof are that the construction team don't grasp the key points of the construction of the hydrophobic waterproof pearl stone products, the new expansion pearl stone insulation board, the extruded polystyrene board and the foamed concrete construction.

2. Residents have an insufficient understanding of the importance of the insulation project.

With the improvement of rural living standards, the residents' need of the residential appearance increase continuously, but the issues of the roofing material are rarely considered. In the survey, only 32.6% of residents thought it is necessary to arrange the insulating layer, while 40.6% of residents considered that there was no need to set the insulating layer. The residents who believed the insulating layer should be arranged were all in the severe cold area of Shenyang, others did not think it was a necessity was in the cold area of Dalian, Dandong. With the improvement of the rural living standards and infrastructure, many new houses now are equipped with heating and air-conditioning, the phenomenon of the room like an "icehouse" in winter has been nearly non-existent. While in summer, the majority of the rural residents would go outside to enjoy the cool, they do not know the hot room. It has a little effect on the promotion of the roof insulation project simply from the aspect of improving the residential comfort. However, the notion of the building energy conservation is too broad and abstract, so it is a hard job to enhance the awareness of the residents about the insulating project.

3. It is not suitable for the using of some new thermal insulation material in the rural area because of its unstable property.

At present, the new thermal insulation material is adopted in the Chinese urban construction, mainly is the expanded pearl stone and

its products, the expanded vermiculite and its products, the mineral wool and its products, and the foamed concrete and extruded polystyrene^[4]. These thermal insulation materials are hard to find in the rural construction in Liaoning province, besides the price factors, the performance of the material that is not fit with the characteristics of rural buildings also limits the using. For example, the heat insulation sandwich board which is made of a variety of pearls tone that's abundant in our country has many features such as heat preservation, heat insulation, sound absorption, non-toxic, non-flammable, odorless, and so on. It is very suitable for acting as the roofing materials. But the expanded pearl stone and its products tend to have a lot of water. The insulation performance would reduce and the absorption strength would decline after absorbing water. The construction condition in the rural is not as good as in the cities, which can make the pearl stone products absorb a lot of water, then as the loss of heat preservation, the insulation thermal conductivity would increase. What's more, water cannot be drained in the process of construction. However, the waterproof layer would split up caused by the changes in temperature, which result in the phenomenon of water seepage and leakage. While the exhaust steam layer is needed by the hydrophobic waterproof pearl stone products and the new expanded pearl stone insulation board, which bring higher request for the construction level, thus the new insulation products with low price, good heat preservation. And the extruded polystyrene boards which are the most common used as the roofing heat preservation and heat insulation material in urban areas now, it is just the opposite in the countryside. In addition to the price factor, another important factor hindering its promotion is the fireproofing performance. The indoor naked light is often used for the cooking and heating in the rural areas, so the fire prevention performance of roofing materials is the main factor. Since the extruded polystyrene foam plastics belong to the thermoplastic plastic, it has the poor heat resistance. Compared with inorganic materials, the fire prevention performance will be improved by adding the flame retardant, but there is still a considerable gap. In addition, as the service life of the material is about 20 years and the "white pollution" caused by the waste materials can't be degraded, which isn't conducive to the protection of environmental. Therefore this affects the long-time application and development. So the extruded polystyrene boards used commonly in the city are not the ideal thermal insulation material in the countryside^[5].

3 THE CONSTRUCTION OF THE POLICY SYSTEM ON THE PROMOTION OF THE RURAL ROOF INSULATION PROJECT IN LIAONING PROVINCE

The roof insulation project is of great significance for the rural building energy conservation since it can reduce building energy consumption caused by adjusting indoor temperature so as to improve the ecological environment and the quality of the residents' life. At present, the government of Liaoning province has not formulated any relevant policies to incentive the promotion of the rural roof insulation project, thus, it is necessary to build multi-level policy system aimed at the sustainable development of rural house to promote the using of new roofing thermal insulation material in rural house.

The policy system of the rural insulation project in Liaoning province should include the following three aspects, the first is to establish the public awareness, the second is to guide the construction, and the third is to provide the technical support.

1. Raising the public cognitive of the insulation project

The government should formulate the relevant policies to raise the cognitive of the application of the insulation project among the rural residents, construction team, the material production enterprises, and the relevant research institutions. This kind of policy is aimed at rural residents, the following are specific measures:

1. The demonstration project building can be built in the rural areas, so that the rural residents can know the advantages of the insulation project;
2. Some seminars can be held by the experts in the agricultural leisure time to propagate the advantages of insulation project by face-to-face;
3. Printing the promotional materials, and providing some interpretation and technical support.

2. Guiding more participation in the promotion of the insulation project

The government should make relevant policies to support the parties to be involved in the promotion of rural insulation project. The measures include:

1. Taking the way of offering subsidies to encourage the rural residents to use the new roofing thermal insulation material, and the monetary compensation is paid in accordance with the using of the area of the thermal insulation material.
2. Encouraging the thermal insulation material production enterprises to promote the new roofing thermal insulation material to the

rural area by reducing the taxes. The amount of the tax reduction is in accord with the amount of the materials used by rural residents. What's more, the fixed and intangible assets that enterprises have purchased for producing the roofing thermal insulation material for the rural area should give an appropriate tax relief.

3. Adopting the way of science and technology fund to encourage the scientific research institutes and enterprises to increase the intensity of the research and development in the new rural roofing thermal insulation material as soon as possible, which can conform to the climate characteristics and the living conditions of rural areas in our country.

3. Providing technical support services

The complete specification should be drafted by relevant experts organized by government to support the construction units to use the new type of roof insulation materials. The drafted specification of the new rural roof insulation material in our country should depend on the virtual circumstances, such as the situation of the rural economic development, the climatic features, the local materials and other factors. The issues meet in the process of compiling should be paid attention to, which are as follows:

1. The professional terms of the new roofing material specification should be explicated so as to make the staff without professional knowledge can also understand the basic meaning.
2. The drawings and texts should be employed in the design and construction of the new roof material specification, which can make the builders do simple design and construction from the drawings.
3. The acceptance check of the new roofing materials can follow the principal of the pursuit of the most important, ignoring minor. The features of the rural construction should be fully considered, maximizing the match with the conditions of rural construction, rather than in accordance with the standards of urban housing, and using the high cost of equipment, machines and tools. At the same time, rural construction experience and habit should be considered. The working

conditions can be relaxed appropriately on the premise of security.

4 CONCLUSIONS

The promotion of the roof insulation project in the rural houses has great significance in the building energy conservation. At present the most of rural houses in our country pay no attention to the heat preservation and insulation. The different thermal insulation materials are used in different historical period, but the effects of heat preservation are not remarkable. With the continuous development of new rural construction in our country, it is necessary to promote and use the roofing materials actively, which are economic, applicable, energy-saving and environmental protection. Therefore the government need to do a good job of propaganda and support, and should also encourage the relevant enterprises and scientific research units to actively develop the new insulation material that match with the rural economy and ecological environment in Liaoning.

ACKNOWLEDGEMENTS

The authors gratefully appreciate the financial support from The 12th Five-Year Plan by Ministry of Science and Technology support of major projects (2012BAJ20B03).

REFERENCES

- [1] Miao, H.D. 2009. *Study on the thermal insulation system of the rural residential energy conservation roof*. Master's thesis of Dalian University of Technology.
- [2] Liu, F.L., & Pan, Y.Q., & Du, Y.H. 2010. Analysis of the thermal insulation property of the rural residential roof in Henan province. *Energy Conservation Technology*, (2):158–164.
- [3] Wang, B.M., & Miao, H.M., & Li, J. 2010. Study on the application of the roof thermal insulation materials in Chinese rural residents. *Technology and application of building materials*. (1):7–10.
- [4] Wei, B.P., & Li, X.H. 2008. Discussion on energy saving roof. *Information technology (Science Edition)*, (6):274–274.(1):7–10.
- [5] Zhang, D.X. 2006. *Building thermal insulation materials*. Beijing: Chemical Industrial Press.

Research on preparation of sulfate resistance foam concrete

Jun Liu

Shenyang Ligong University, Shenyang, China

Zi Yan Huang

College of Materials Science and Engineering, Shenyang Jianzhu University, Shenyang, Liaoning, China

Run Qing Liu

Shenyang Ligong University, Shenyang, China

Tian Bo Hou

College of Materials Science and Engineering, Shenyang Jianzhu University, Shenyang, Liaoning, China

ABSTRACT: In order to study preparation method of sulfate-resistance foam concrete, the sulfate-resistance ability of foam concrete foamed using hydrogen peroxide was tested, the impact of water-cement ratio and rubber powder dosage on sulfate resistance of foam concrete was analyzed. Moreover it is found that by changing agitation and curing methods, the sulfate-resistance of foam concrete was optimal. The results showed that when water-cement ratio is 0.54 and powder dosage is 0.11%, by adding hydrogen peroxide before mixing rubber powder with mould and humidification, sulfate resistance of foam concrete is optimal and the corrosion factor is 103.48%.

Keywords: foam concrete; sulfate-resistance ability; hydrogen peroxide

1 INTRODUCTION

Currently, there is no complete standards for trial or production for foam concrete in China, thus large-scale promotion of the foam concrete is constrained^[1]. Sulfate-resistance is an important part for durability of foam concrete, which is also seen as the most complex and harmful environmental water erosion. Studies on foam concrete is still confined to the macroscopic mechanical properties, literature on the durability of foam concrete didn't publish frequently^[2] and research on sulfate-resistance of foam concrete is little. Few studies have involved foam concrete microstructure and related study on composition, properties and microstructure of foam concrete is not systematic. Abroad, Jones and McCarthy spent 12 months studying sulfate erosion. The excellent chemical resistance of foamed concrete was revealed. It is found that the lower the density, the faster the rate of carbonation^[4,5].

As there is a large number of pores in foam concrete, it has sulfate resistance and freeze-thaw resistance^[6]. Mainly reasons that impact sulfate resistance of concrete are internal and external. The internal ones mainly refer to the material of the foam concrete, such as water-cement ratio^[7].

The external ones are environmental factors such as concentration of sulfate solution and the pH value.

Research on sulfate resistance of foam concrete is still in its infancy. In this experiment the foam concrete was prepared using hydrogen peroxide. By analyzing the impact of water-cement ratio, powder content and the order of mixing on sulfate resistance of foam concrete we got the optimal preparation method of sulfate resistance foam concrete.

2 TEST MATERIALS AND METHODS

2.1 Materials

Cement: Test Cement is the ordinary portland cement, numbered PO 42.5 made by Shenyang Jidong Cement production, its chemical composition is shown in [Table 1](#).

Table 1. Cement chemical composition (%).

SiO ₂	Al ₂ O ₃	Fe ₂ O ₃	CaO	MgO	SO ₃	R ₂ O	LOI
21.72	5.81	4.33	62.41	1.73	2.56	0.50	1.47

Table 2. Fly ash chemical composition (%).

SiO ₂	Al ₂ O ₃	CaO	MgO	Fe ₂ O ₃	K ₂ O	Na ₂ O	LOI
59.95	26.78	4.35	2.30	1.53	1.25	2.75	1.29

Fly ash: Test fly ash is made by Shenyang Shenhai company, is rated “I” grade. Its chemical composition is shown in Table 2.

Vesicant: Hydrogen peroxide is concentration of 30% hydrogen peroxide AR. It is made by Shenyang Xinhua Reagent Factory. It meets the “GBT” 6684-2002 “Chemicals 30% hydrogen peroxide”.

Foam stabilizer: Na₂SO₄ is analytical grade anhydrous sodium by Tianjin Chemical Regent Limited.

2.2 Preparation and maintenance

The production and conservation of specimens is in accordance with “ordinary concrete mechanical test method standards” GB/T 50081 provisions. Conservation of specimens should cover film.

2.3 Test methods

Accordance with the “foam concrete standard” JG_T266-2011 and “ordinary concrete long-term performance and durability test method standards” GB-T50082-2009, test foam concrete’s dry and wet cycle, density, sulfate resistance.

3 RESULTS AND DISCUSSION

3.1 The influence of water-cement ratio on the sulfate resistance of foam concrete

In order to study the influence of water binder ratio on sulfate resistance of foam concrete, Testing foam concrete’s water-cement ratio are 0.54, 0.62, 0.70, 0.78 respectively. Measure its Dry density and true density, do wet and dry cycle sulfate attack test, calculate compressive strength corrosion coefficient. For comparison with freezing, wet and dry strength loss rate, calculate the rate of sulfate attack quality change.

Figure 1 shows, Foam concrete’s mass loss in sulfate is less than in freeze-thaw cycles and wet and dry cycles. Its variation is same with the variation of mass loss in wet-dry cycle. When the water-cement ratio is 0.54, the minimum mass loss is -10.5%. Water-cement ratio is 0.78, the maximum mass loss is 3%, mostly are negative loss.

Figure 2 shows, Foam concrete compressive strength corrosion coefficient decreases with the increase of water-cement ratio. Combine with

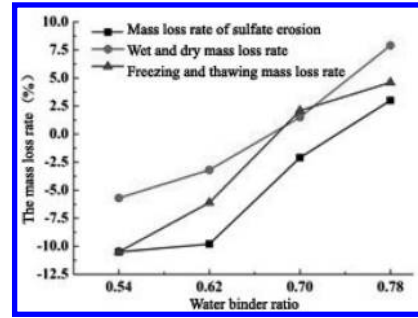


Figure 1. Relationship between water-cement ratio and mass loss rate.

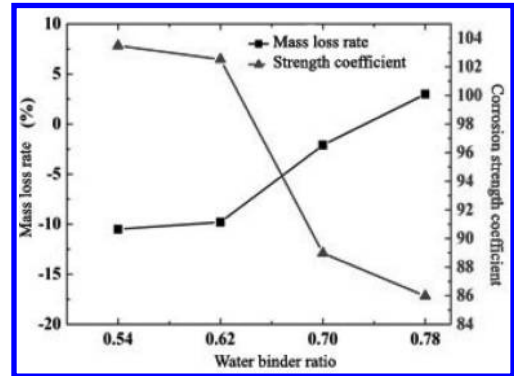


Figure 2. Relationship between water-cement ratio and corrosion resistance.

the change of mass loss rate. Increasing of foam concrete’s water-cement ratio leads weakening of sulphate resistance. When the water-cement ratio is 0.54, the maximum compressive strength corrosion factor is 103.48%. When the water-cement ratio is 0.87, the minimum compressive strength corrosion factor is 85.89%. Prove that smaller water-cement ratio can improve foam concrete sulfate resistance. The increasing water causes that structure is not dense. Lead sulfate easier access test block, make sulfate resistance of test block is poor, they filling the cement matrix and the pores of foam concrete.

Figure 3 shows, Mass loss rate of foam concrete decrease as dry density increased. When the dry density is 305 kg/m³, mass increase after foam concrete sulfate attacking by 10.5%. After drying the foam concrete infiltrating of sulfate solution precipitates sulfate crystals. The smaller dry density is, the bigger foam concrete sulfate crystals precipitated space is. Mass loss is also smaller, even negative growth.

Figure 4 shows that, when subjected to sulfate attack, compressive strength corrosion coefficient

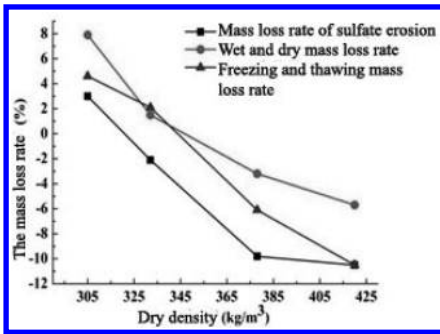


Figure 3. Relationship between dry density and mass loss rate.

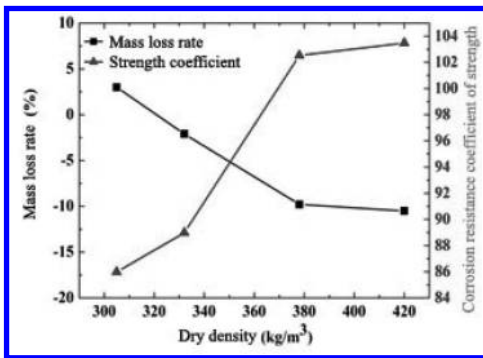


Figure 4. Relationship between water-cement ratio and corrosion resistance.

of foam concrete with dry density increases. When the dry density is 420 kg/m^3 , the maximum corrosion resistance coefficient is 103.48. After the foam concrete subject to sulfate attack, showed a higher compressive strength than the original. This shows that the foam concrete cement matrix of sulfate crystals precipitated for enhancement effect of the cement matrix is greater than the density of the cement matrix destruction effects. The greater dry density, the easier the internal test block formed of independent closed pores. Even in the case of a certain number of open holes, independent and the closed hole with a stronger ability to prevent sulfate attack.

3.2 Powder dosage effect on the anti-sulfate erosive of foam concrete

The foam concrete respectively mix sum quality of the cement and fly ash, and the rates were 0.11%, 0.17%, 0.23%, 0.29% of the powder. Measure 4 groups of specimens' dry density and true density, test its 15 sulfate attack, calculated compressive

strength corrosion coefficient and compared to the freezing and thawing, wet and dry strength loss rate similarly calculate the rate of change of mass of sulfate attack.

According to Figure 5, the erosion loss of quality of foam concrete sulfate content powder trends opposite with the quality of freeze-thaw. Its increasing trend is similar with foam concrete quality loss rate of wetting-drying cycles powder content greater than 0.23% increase in the extent. This shows that the sulfate resistance of foam concrete in terms of quality content along with the increase of the powder, but the degree of increase is very slow. When the powder content is 0.11%, the mass loss rate minimum is -3%.

According to Figure 6, the high-performance sulphate resistance of foam concrete compressive strength corrosion coefficient resistant changes tremendous in between powder dosage of 0.11%, and 0.17%. When the powder content is 0.11%, the maximum compressive corrosion coefficient is 102.3%, when powder content is 0.17%, the compressive corrosion coefficient is reduced to 90.72%.

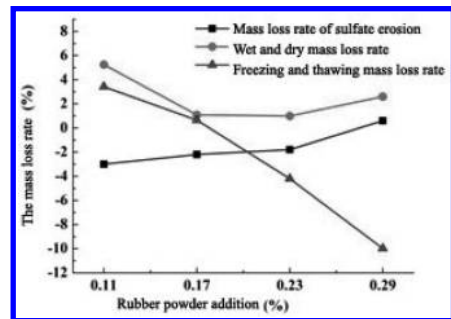


Figure 5. Relationship of foam concrete powder content and the rate of mass loss.

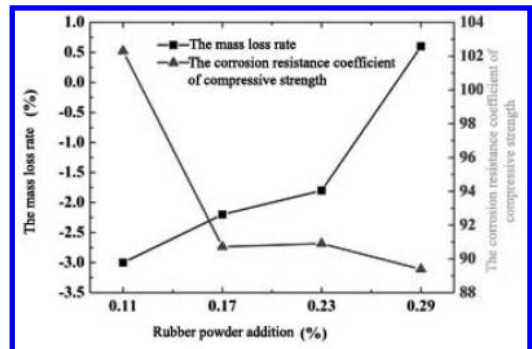


Figure 6. Relationship of foam concrete powder dosage and sulphate resistance.

close to the minimum value of 89.39%. This shows that when the powder content is over 0.11, sulfate resistance of foam concrete suffers tremendous damage.

According to Figure 7 shows that quality loss of foam concrete sulfate attack dry density increases with rise. Its increasing trend and the cycle of wet and dry foam concrete mass loss rate is similar with that in dry density greater than 462 kg/m³ trend increases. This shows that the more dense foam concrete cement matrix, sulphate crystals precipitated can be reduced space, adding foam concrete is less than the damage received during crystal precipitation, thereby increasing the mass loss rate.

Combined with variation of compressive strength corrosion coefficient in Figure 8 shows that, when dry density foam concrete is less than 462 kg/m³, the compressive corrosion factor greatly improved. This represents a density of 462 kg/m³ explained by the powder content control to ensure that foam concrete sulfate resistance a limit.

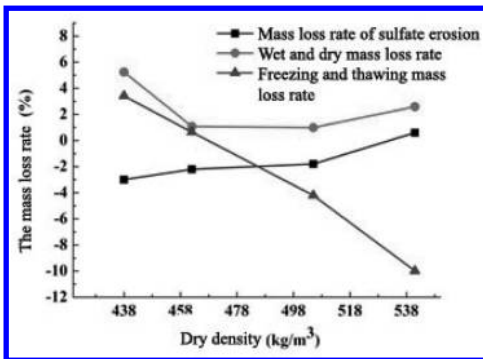


Figure 7. Foam concrete dry density and quality loss rate.

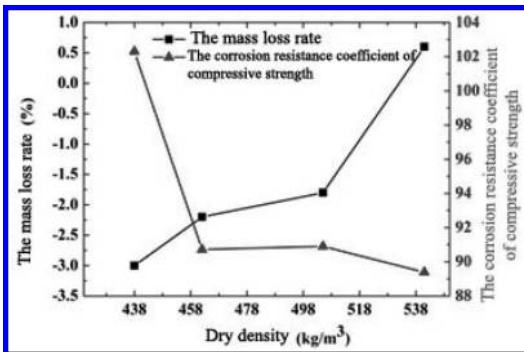


Figure 8. Relationship of dry density of foam concrete and sulfate resistance.

3.3 The impact of foam concrete mixing sequence sulfate resistance

Use four kinds of mixing sequence corresponding to variable production of foam concrete. Four groups were set to test the mixing order: ① premixed powder premixed hydrogen peroxide, ② premixed powder and then mixed with hydrogen peroxide, ③ premixed powder and then mixed with hydrogen peroxide, ④ then mixed powder and then mixed with hydrogen peroxide.

Measure 4 group specimens' dry density and true density, and its 15 sulfate weathering test. Calculate the compressive strength corrosion coefficient, compared to freezing and thawing, wet and dry strength loss rate similarly calculate the rate of change of mass of sulfate attack.

According to Figure 9 shows that the mass loss of foam concrete sulfate attack, with the mixing order change except hydrogen peroxide mixed powder after mixing, and the rest are with the freeze-thaw cycles of wet and dry cycle sequence with mixing trends are very different. When premixed hydrogen peroxide and premixed powder, foam concrete erosion mass loss rate of the minimum is -2.5%, and the rest are due to be mixed with hydrogen peroxide or re-mixed powder and successive increases.

According to Figure 10 shows that the mixing of hydrogen peroxide mixed order makes foam concrete compressive strength corrosion factor reduction, pre-mixed powder mixed with the powder was respectively 92%, and 87%. Combined to mass loss determine, premixed hydrogen peroxide and premixed powder mixing order method is most favorable to formulated the high performance sulphate resistance foam concrete.

According to Figure 11 shows that when the density is controlled by the mixing order, sulphate resistant foam concrete mass loss variation with density and mass loss of wet and dry cycle variation of density with similar. Binding assay test sulfate attack soaking wet and dry cycle drying step is

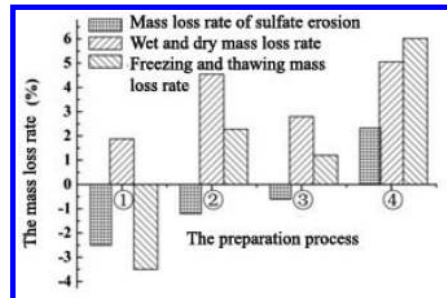


Figure 9. Foam concrete mixing order and mass loss rate.

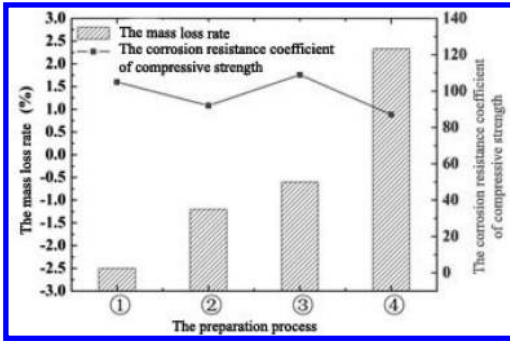


Figure 10. Relationship of foam concrete mixing sequence and sulphate resistance.

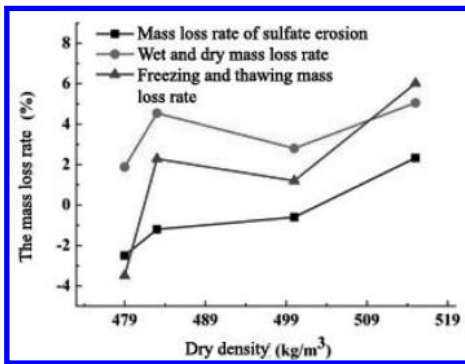


Figure 11. Relationship of foam concrete dry density and mass loss rate.

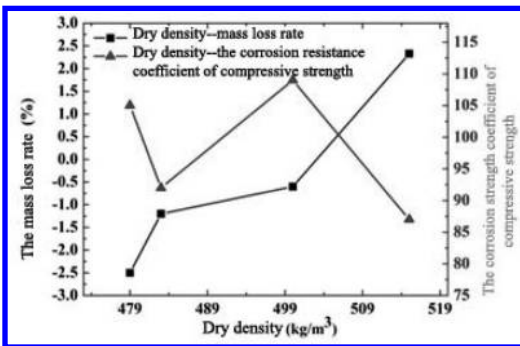


Figure 12. Relationship of foam concrete dry density and sulphate resistance.

similar, indicating that similar testing methods will produce similar test results. Overall, the minimum is mass loss rate of sulfate attack. Wherein when dry density is 479 kg/m³, the mass loss rate minimum of -2.5%.

According to Figure 12 shows that, when dry density is 483 kg/m³ to 500 kg/m³ in the change, compressive strength corrosion coefficient changes is the same with the density and mass loss rate. The rest is the opposite. This shows that in addition to in this section are accompanied by loss of quality with loss of strength. Also shows it is possible that the mass loss rate is increased and increase strength. This is due to the cement matrix reasonable quality loss is just a new form of better mechanical properties of the structure. However, because of this process has a great chance, so do not rely on this method to study the sulphate resistance foam concrete preparation methods.

4 CONCLUSION

Based on the preparation of sulfate-resistance foam concrete, this paper conducted wet-dry cycle, sulfate resistance testing as well as freeze-thaw test. The impact of the water-cement ratio, powder dosage, mixing order corrosive on sulfate-resistance of foam concrete we got the following conclusions:

1. In the preparation of sulfate resistance foam concrete, water-cement ratio should not be more than 0.78, powder dosage should not be in excess of 0.29%, and otherwise it will affect the sulfate resistance.
2. When the water-cement ratio is 0.54, powder content is 0.11%, the foam concrete resistant sulfate corrosion reaches optimal performance and corrosion factor is 103.48%.
3. In the preparation of sulfate-resistance foam concrete, the method by adding hydrogen peroxide before mixing rubber powder with mould and humidification should be employed, which can help to improve the sulfate attack resistant performance of foam concrete.

ACKNOWLEDGEMENTS

This work was financially supported by International cooperation project (KJDR-2013-01 L).

REFERENCES

- [1] Liu Xiaoyan, Wangxin Rui, Liu Lei, Jiang Lin-sheng Research progress and application of foam concrete [J]. Concrete, 2012, 06:34-36.
- [2] Tianxue Chun, Zhao Hui, Chen Jie, Shao Ying Ying. Summary of the relationship between materials research and performance of foam concrete [J]. Building Block and Block Building, 2010, 06:49-52.

- [3] Jones M.R., McCarthy A. Preliminary views on the potential of foamed concrete as a structural material [J]. Magazine of Concrete Research 2005; 57:21–31.
- [4] Jones M.R., McCarthy A. Utilizing unprocessed low-lime coal ash in foamed concrete [J]. Fuel 2005; 84:1398–1409.
- [5] Wang Zhaoqiang, Tanke Feng, Xu Xiuxia. Research status of foam concrete [J]. Concrete, 2013, 12:34–36.
- [6] Zheng research and FAQs foam concrete analysis and countermeasures [J]. Shanxi Architecture, 2008, 34 (32):166–167.
- [7] Xu Fenlian, late Zhao Qun, Jiang Shan Lei, Su Hua research and application of foam concrete in China [J]. Commodity concrete, 2011, 11:24–26, 44.

Low cycle fatigue properties of anti-seismic steel HRB400E reinforcing steel bars

Yun Rong Luo, Tao Zeng, Lei Fu, Hai Bo Lin & Mao Fei Huang

College of Mechanical Engineering, Sichuan University of Science and Engineering, Zigong, China
Key Lab in Sichuan Colleges on Industry Process Equipments and Control Engineering, Zigong, China

ABSTRACT: Low Cycle Fatigue (LCF) experiments on anti-seismic steel HRB400E reinforcing steel bars under constant total strain control were carried out on a MTS 809 servo-hydraulic material testing machine. Cycle stress-strain response character was analyzed carefully. The strain-life data from the axial tests were used to derive suitable *Coffin-Manson* parameters for the test material. And the half-life plastic strain energy was determined and found as an important characteristic in prediction of low-cycle fatigue life. The fracture surfaces of the fatigue samples were characterized by scanning electron microscope and the fracture mechanisms were discussed.

Keywords: low cycle fatigue; steel bar; fatigue life

1 INTRODUCTION

Since the 2004 Sumatra earthquake, the occurrence of earthquake becomes very frequent all over the world [1, 2]. In china, 33% earthquakes are inherited on 7% land of the world, so it has most strong earthquakes in the world. Each strong earthquake may destroy a large number of buildings, which results in huge disasters and damage to property and inevitably causes some damage to the surviving buildings. As one of the most important materials to ensure the structural safety of buildings under seismic loads, the performance of the rebar will determine the anti-seismic performance of buildings [3]. At present, the HRB400E III grade steel has been promoted heavily in the construction of the earthquake zone in China. Construction steel experiences high strain low cycle fatigue process under seismic loading [4]. Zhan Suyu et al. [5] have reported the low-cycle fatigue properties of HRB400E III grade steel with diameters of 25 mm and 20 mm on Instron-Model 1342 fatigue test machine.

The main objective of this paper is to investigate the low cycle fatigue behaviors, such as cyclic

stress response, stress-strain curve, strain-life relationship and damage mechanisms of HRB400E III grade steel with diameters of 22 mm on a MTS 809 servo-hydraulic material testing machine under completely reversed strain control. These investigations would provide reference for engineering application and subsequent welded joint and oxidation corrosion LCF tests of HRB400E reinforcing steel bars.

2 MATERIAL AND TESTING ARRANGEMENTS

The experiments were conducted on the hot-rolled HRB400E reinforcing steel bars (using 22.0 mm hot-rolled bars). The chemical compositions and mechanical properties (performed in accordance with [6]) of the rebar are given in [Table 1](#) and [Table 2](#), respectively. The cylindrical fatigue specimens with gauge length of 20 mm and diameter of 7.25 mm were used ([Fig. 1](#)). The dimension of the specimen was set to avoid the buckling under the highest compressive force anticipated in the test. The specimens were machined by a NC machine.

Foundation Item: Item Sponsored by Project of Sichuan Provincial Department of Education (13ZA0129), Key Lab in Sichuan Colleges on Industry Process Equipments and Control Engineering (GK201205), Fund of Sichuan University of Science and Engineering (2010XJKYL006) and Fund of Key Laboratory of corrosion and protection of Sichuan Province Materials (2012CL10, 2013CL07).

Table 1. Chemical composition of test material (mass percent, %).

C	Si	Mn	P	S
0.22	0.34	1.44	0.021	0.029

Table 2. Mechanical properties of test material.

	σ_y /MPa	σ_b /MPa	δ_{10} (%)	A_{gt} (%)
Measured value	422	653	22.2	14.3
National standard	≥ 400	≥ 540	—	≥ 9

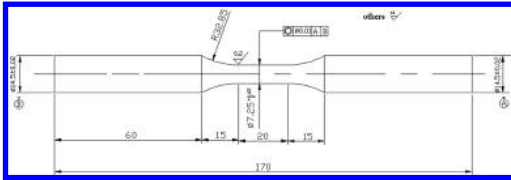


Figure 1. Geometry of test specimen.

The specimen surfaces were carefully ground and polished using abrasive paste (Model W3.5) along the axial to remove scratches.

The low cycle fatigue tests were conducted on a servo-valve controlled electro-hydraulic testing machine (MTS 809) in ambient air at room temperature. The tests were carried out under uniaxial tension-compression loading with total strain control at strain ratio of -1 and frequency of 1 Hz. The total strain was measured by a dynamic extensometer attached to the specimen having span length 10.0 mm. Triangular waveform was used for all the fatigue tests. The cyclic loading started from the tensile side. The displacement, load and strain signals were measured for each cycle.

A 10% drop of the peak load was defined as specimen failure. The data was considered ineffective unless the site of the fracture or the initiation of cracks was within the gauge length of the dynamic extensometer. The number of cycles to failure was recorded as the fatigue life. The response at half of the fatigue life was used to obtain cyclic stress-strain curves in this study.

3 EXPERIMENTAL RESULTS

The variation of fatigue life with strain amplitude is shown in Figure 2. It can be seen that the LCF life decreases gradually with increasing strain amplitude. The fatigue life distribution is concentrated and the life fluctuation range of effective data is small, indicating that the test process is under good control.

3.1 Strain amplitude—dependent cyclic stress response

During cyclic process, the cyclic stress of metal material is relative to its deformation resistance,

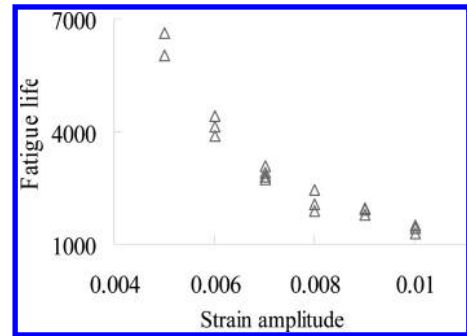


Figure 2. Results of tests.

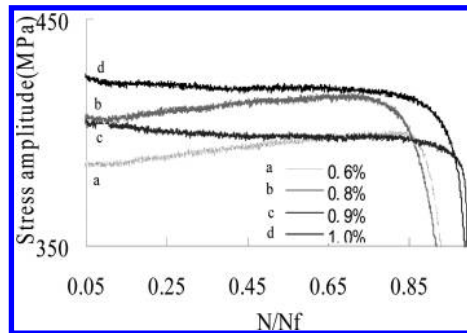


Figure 3. Cyclic stress response.

and metal material may occur cyclic hardening, cyclic softening or cyclic stability. The cyclic stress response of the test material at different strain amplitudes is shown in Figure 3. The test material exhibited slight cyclic hardening for the strain amplitudes lower than 0.8%. However, for the strain amplitudes higher than 0.8%, the test material exhibited cyclic stability or slight cyclic softening. The cyclic hardening of the test material could prevent the material from prematurely damage or failure due to the material softening under high cyclic loading. The cyclic softening of this material at higher strain amplitudes may be due to the annihilation of dislocations with a net decrease in dislocation density and rearrangement of dislocations into the configuration of cells and subgrains [7].

3.2 Stress-strain curve

Figure 4 shows the hysteresis loops in the first cycle, the half-life cycle and the failure cycle at the strain amplitude of 0.6%. The plastic strain energy dissipated during the fatigue process could be represented by the area surrounded by the hysteresis loop [8]. The larger the area is, the more energy it could absorb. As can be seen from Figure 4, the hysteresis loop

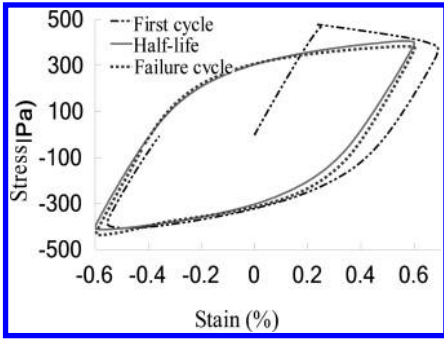


Figure 4. Hysteresis loops.

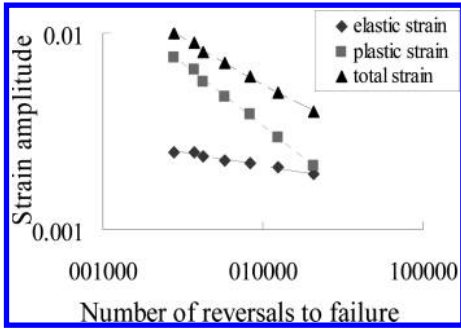


Figure 5. Prediction of N_f based on Manson-Coffin law.

in the first cycle is not closed; the hysteresis loop at half-life is smooth, closed and symmetric, indicating a good control of load during the test process; the compression part of the hysteresis loop in the failure cycle has a significant turning point. The large area surrounded by the hysteresis loop in Figure 4 indicates that the test material has a good ability to absorb the earthquake energy.

3.3 Strain-life relationship

The total strain amplitude (ϵ_a or $\Delta\epsilon_f/2$) can be expressed as [9]:

$$\Delta\epsilon_f/2 = \sigma'_f/E(2N_f)^b + \epsilon'_f(2N_f)^c \quad (1)$$

where σ'_f is the fatigue strength coefficient; b is the fatigue strength exponent; E is the elastic modulus; ϵ'_f is the fatigue ductility coefficient and c is the fatigue ductility exponent.

From the test results in Figure 5, the four material parameters in Eq.(1) have been derived and the $\Delta\epsilon_f/2 - 2N_f$ relationship can be expressed as:

$$\Delta\epsilon_f/2 = 0.00739(2N_f)^{-0.136} + 1.199(2N_f)^{-0.638} \quad (2)$$

3.4 Prediction of fatigue life from energy

The stress and plastic strain or dissipated hysteresis energy are considered as the main cause of fatigue failure [9]. Hence, an energy-based approach using plastic strains energy (ΔW^p) may be proposed to

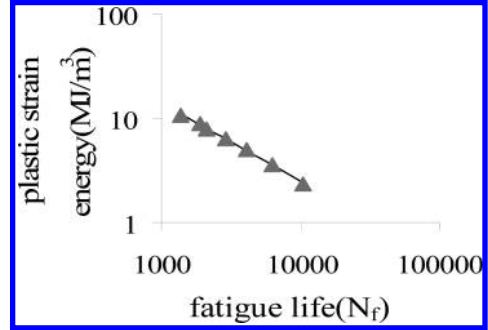


Figure 6. Prediction of N_f based on half-life plastic strain energy.

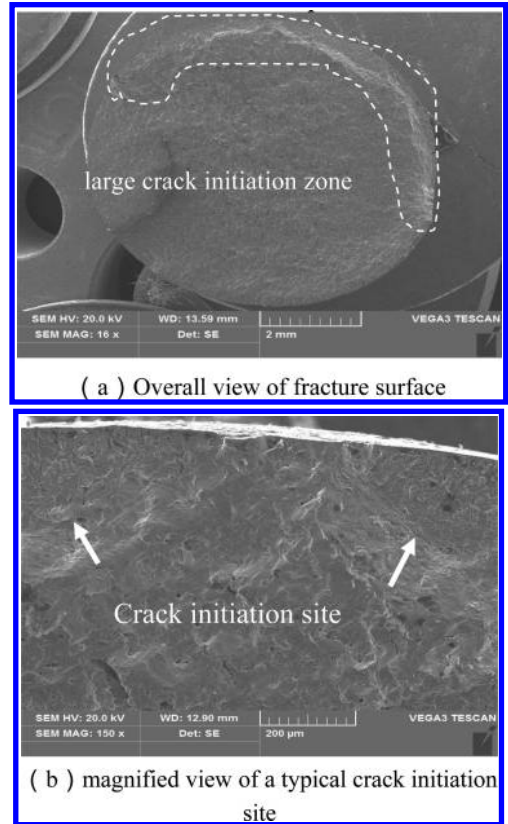


Figure 7. Representative SEM micrographs of fracture surface fatigued at strain amplitude of 0.8%.

predict the fatigue life of materials. And it was calculated at the half-life (0.5 N_f) hysteresis loop using the following power relationship [8]:

$$\Delta W_{ave}^P = A(N_f)^\alpha \quad (3)$$

where A is the plastic strain energy coefficient and α is the plastic strain energy exponent.

The constants in Eq. (3) were obtained from least square regression analysis of the experimental data in Figure 6 and found as 2558.7 and -0.754 , respectively. It can be seen that the fitted curve is very close to the experimental data, suggesting that the fatigue life could be well predicted by $\Delta W_{ave}^P - N_f$ relationship.

3.5 Damage mechanisms

Figure 7(a),(b) show representative micrographs of the fracture surfaces of the specimen cycled to failure at strain amplitude of 0.8%. Figure 7(a) shows general appearance of fracture surface. It is seen that a large crack initiation zone (including more than one crack initiation sites) exists on the fracture surface. Figure 7(b) shows magnified view of a typical crack initiation site and characteristic features of fracture surface at high magnification. It can be seen that fatigue crack initiated from the specimen surface.

4 CONCLUSIONS

1. The cyclic stress response is strain amplitude-dependant, showing a transition point at strain amplitude of 0.8%.

2. The strain-life data may be seen to be well predicted by the *Coffin-Manson* relationship. And the energy dissipation in average of cycles is an important parameter in prediction of low-cycle fatigue life.

3. Multiple fatigue crack initiation sites initiated from the specimen surface.

REFERENCES

- [1] J.Y. Wu: J. SCU. Sci. & Eng. (Nat. Sci. Edi.) Vol. 24(2011), P. 125. (In Chinese).
- [2] Y.L. Zhao: J. SCU. Sci. & Eng. (Nat. Sci. Edi.) Vol. 24(2011), P. 129. (In Chinese).
- [3] Y.L. Zhao: J. SCU. Sci. & Eng. (Nat. Sci. Edi.) Vol.24 (2011), P. 249. (In Chinese).
- [4] S.H. Gong, G.M. Sheng.: Earthquake Resistant Eng. Iss.3 (2004), P. 41. (In Chinese).
- [5] S.Y. Zhan, G.M. Sheng, X.D. Liu, M.S. Yu: Mat. Heat Treatment Vol. 39 (2010), P. 22. (In Chinese).
- [6] GB/T228-2002 Metallic Materials-Tensile Testing at Ambient Temperature. China Standards Institution: 2002. (In Chinese).
- [7] M.D. Callaghan, S.R. Humphries, M. Law, et al. J. Mater. Sci. Eng., A, Vol. 527 (2010), P.5619.
- [8] Y.R. Luo, C.X. Huang, Y. Guo, Q.Y. Wang. J. Iron and Steel Res. Int. Vol. 19 (2012), P. 47.
- [9] Y.R. Luo, Q.Y. Wang, Y.J. Liu, C.X. Huang. J. SCU. (Eng. Sci. Edi.), Vol. 44(2012), P. 169. (In Chinese).

GRNN model in the application of mixed-sand pumping concrete research

Hong Li & Xing Wang Cheng

Chang'an University, Xi'an Municipality, Shaanxi Province, China

ABSTRACT: According to GRNN (General Regression Neural Network) theory, combined with genetic algorithm, the paper established an artificial neural network model of mixed-sand pumping concrete, amount of test materials as input, compressive strength and slump as output. The results show that: the network model can accurately predict the compressive strength and slump, and can guide the design of mixed-sand pumping concrete mixture ratio by multi-objective optimization.

Keywords: GRNN; prediction model; mixed-sand pumping concrete; multi-target optimization

1 INTRODUCTION

The proper use of mixed-sand, which is blended from machine-made sand and natural sand, in pumping concrete will not only help to relieve the situation of severe shortage of excellent natural sand. The strength and working performance of pumping concrete are the core contents of quality control. While in mixed-sand, factors such as stone powder, grading, particle shape and so on, have complex and ignorable influence on the intensity and working property of concrete^[1,2], which leads to the high-complex and non-linear relationship between materials of different mix proportions and concrete.

Artificial neural network has excellent nonlinear adaptive information processing ability, without any transcendental function, it can realize self-learning, self-organization and approximating any nonlinear mapping from the test data information, and it's the ideal way to solve the problem of nonlinear mixed-sand pumping concrete^[3,4]. Compared with the traditional BP neural network, GRNN has advantages such as the strong ability of nonlinear mapping, fast convergence, and good fault tolerance. And when the data are from small samples, its predictive effect is still excellent.

In this paper, according to certain amount of testing data on compressive strength and slump of pumped concrete made from blended sand, GRNN model which can predict and evaluate its strength and working performance was established, and combined with genetic algorithm to perform the multi-objective optimization on the compressive strength and slump of the pumped concrete of blended sand under multiple factors.

2 GRNN FORECAST MODEL AND MULTI-TARGET OPTIMIZATION

GRNN is a branch of the radial basis function neural network, whose theoretical basis originates from nonlinear regression analysis, and the regression analysis of the non-independent variable Y in relation to the independent variable X is actually to calculate y that has the biggest probability value. The network structure of GRNN is simple. Besides the input layer and output layer, there are only two definite hidden layers, namely, the mode layer and the summation layer, and the number of the unit nodes in the hidden layers is also uniquely definite according to the sample. The activation function of the nodes in GRNN's hidden layer adopts Gaussian function which has a property of local activation for the input information, making it have a strong attraction for the input that is close to the local neuron property. There is only one artificially set parameter smoothing factor SPREAD, and the connection weights between the network layers are uniquely definite due to the training sample. Network training is one-way training with no need for iteration, and the results have global convergence. Thus, it can rapidly predict the model with relative large computing advantage.

The multi-objective optimization is the problem which frequently encounter in scientific research and engineering practice. In multi-objective optimization control system, objectives restrict each other through decision variables, and the optimization of one objective must be at the cost of other objectives, so it's difficult to evaluate pros and cons of multi-objective problem objectively. The

result of multi-objective optimization is normally not an absolute optimal solution, but a set of equilibrium solutions (namely Pareto optimal solution set), thus, the genetic algorithm leading to global optimization is introduced to calculate.

The design of the mixing proportion of the pumping concrete of mixed-sand should meet the requirements of strength and working performance at the same time, which is a typical multi-objective optimization problem. Combined with genetic algorithm, GRNN prediction model was used to calculate target function, and the optimal Pareto solution was obtained finally. The algorithm procedure is shown in Figure 1.

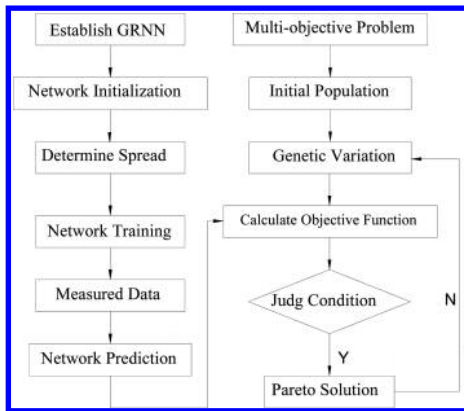


Figure 1. The algorithm procedure.

3 GRNN PREDICTION MODEL OF THE MIXED-SAND PUMPING CONCRETE

3.1 Modeling method

As for the pumping concrete of mixed-sand, the ratio of the weight of per unit volume of crushed sand and the total weight of the mixed-sand is defined as the replacement rate. Set the replacement rate, the water binder ratio, the sand ratio and water reducer respectively as the independent variable x_1, x_2, x_3, x_4 , set the compressive strength of the mixed-sand concrete as variable Y_1 , and the slump as Y_2 . The paper created the GRNN model which adopts the typical network structure including 4 layers, as shown in Figure 2. The value of the smoothness factor SPREAD in GRNN has relatively significant influence on the precision of the final approximation of network and the best SPREAD is found by use K-fold cross-validation.

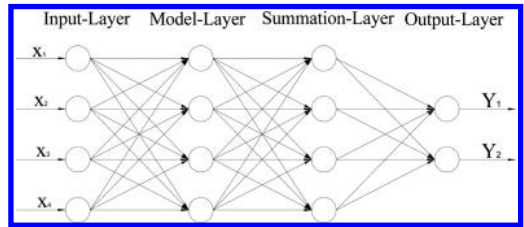


Figure 2. The structure of GRNN.

Table 1. Network training set.

Number	x_1	x_2	x_3	x_4	Y_1 [mp]		Y_2 [cm]	
					Test	Forecast	Test	Forecast
1	0	0.53	0.4	1.5	31.5	31.88	143	137.2
2	1	0.53	0.4	1.5	33.2	33.32	95	97.6
3	0.15	0.5	0.38	1.2	35.1	35.18	108	102.5
4	0.15	0.56	0.42	1.8	29.1	29.20	156	155.2
5	0.33	0.5	0.4	1.8	34.8	34.70	153	151.9
6	0.33	0.53	0.42	1.2	34.2	34.01	145	140.6
7	0.33	0.56	0.38	1.5	30.2	30.81	55	57.3
8	0.5	0.5	0.42	1.5	36.5	35.94	168	164.4
9	0.5	0.56	0.4	1.2	31.5	31.42	72	73.2
10	0.67	0.5	0.38	1.2	37.2	36.98	78	85.1
11	0.67	0.53	0.4	1.5	33.5	33.34	118	107.8
12	0.75	0.56	0.38	1.5	31.8	31.50	44	53.5
13	0.75	0.53	0.42	1.2	34	33.90	128	118.8
14	0.9	0.53	0.38	1.8	32.7	32.79	81	84.3
15	0.9	0.56	0.4	1.2	31.1	31.40	68	70.2
16	0.9	0.5	0.42	1.5	35.7	35.69	150	153.2

Table 2. Network test set.

Number	x_1	x_2	x_3	x_4	Y_1 [mp]		Y_2 [cm]	
					Test	Forecast	Test	Forecast
17	0.15	0.53	0.4	1.5	32.1	32.21	136	132.7
18	0.5	0.53	0.38	1.8	32.6	32.60	93	97.6
19	0.67	0.56	0.42	1.8	29.8	29.78	148	148.1

3.2 The construction of sample

The experimental material: the cement adopts P.O 42.5; coarse aggregate is the 4.75–26.5 mm continuous grading screen, whose apparent density is 2550 kg/m³; two kinds of fine aggregates are selected. One is natural river sand, whose fineness is 2.20 and apparent density is 2610 kg/m³, while the other is machine-made sand, whose fineness is 2.73 and apparent density is 2790 kg/m³. Polycarboxylate efficient pumping aid whose main component is carboxylic graft polymer is selected as the admixture and its recommended mixing amount is 0.5%–2.0% of the amount of cementing material. According to concrete strength of C25 and orthogonal thought, different level combinations of replacement rate (x_1), water-binder ratio (x_2), sand percentage (x_3), and water reducer (x_4) were set.

3.3 Sample training and result prediction

The value of the smoothness factor SPREAD in GRNN has relatively significant influence on the precision of the final approximation of network. Using four-fold cross-validation to find the best SPREAD: divide the learning samples of table one into four sub samples, take the single sub sample for validation data, with the other three samples used for practice about four times. Each sub sample is verified once to forecast the mean square error and take it as Network training goal. In the range of [0.01,1], the best SPREAD obtained is 0.75. After network training is finished, the Table 2 is used as test sample to verify the generalization ability of the network.

It can be seen from Tables 1 and 2 that when sample data are relatively few and unstable data exist, the relative error of GRNN prediction is always kept at a relatively low level, which means that through neural network, the purpose of predicting test result could be achieved.

4 MULTI-OBJECTIVE OPTIMIZATION OF THE MIXED-SAND PUMPING CONCRETE

In practical project, there are different restrictions on slump for the pumping concrete according

to different pumping height, and the strength requirements should be met at the same time. Use established GRNN prediction model to search optimization to the quality target of strength and slump, which can cut unnecessary tests and greatly enhance work efficiency.

4.1 The mathematical model of multi-objective optimization

The establishment of mathematical model is firstly to determine the object to optimize: the large value of compressive strength of network prediction is got in the reasonable range; the best slump is required to be set according to different pumping heights, and the network projection slump is required to be close to or even reach the best slump. Set Set substitution rate as x_1 , water-binder ratio as x_2 , sand ratio as x_3 , admixture as x_4 , network projection compressive strength as GRNN₁, and network projection slump as GRNN₂. The best slump is set as K according to different requirements of pumping heights. Its mathematical description is as below:

Objective function:

$$f_1(x_1, x_2, x_3, x_4) = \max[\text{GRNN}_1(x_1, x_2, x_3, x_4)]$$

$$f_2(x_1, x_2, x_3, x_4) = \min[|K - \text{GRNN}_2|(x_1, x_2, x_3, x_4)] \quad (1)$$

Constraint condition:

$$0 \leq x_1 \leq 1$$

$$0.5 \leq x_2 \leq 0.56$$

$$0.38 \leq x_3 \leq 0.42$$

$$1.2 \leq x_4 \leq 1.8 \quad (2)$$

4.2 Multi-objective optimization solution

As the most widely used and successful multi-objective optimization algorithm, NSGA-II owns good convergence and robustness performances, and Pareto solutions are distributed evenly in the targeted space^[5]. The multi-objective optimization

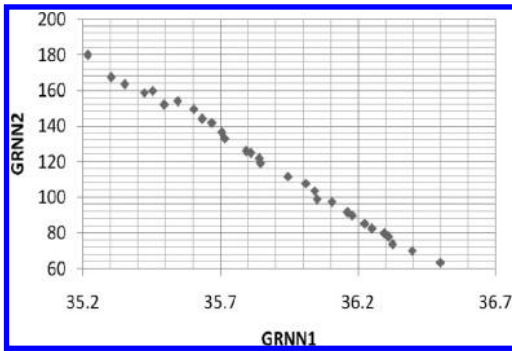


Figure 3. The first front-end Pareto solution.

Table 3. C25 concrete recommended mixture ratio.

	x_1	x_2	x_3	x_4	GRNN ₁	GRNN ₂
K = 140	0.57	0.50	0.40	1.36	35.63	144.2
	0.55	0.50	0.40	1.33	35.67	141.5
	0.60	0.50	0.41	1.42	35.70	136.9

adopted by the function “gamultiobj” provided in the genetic toolbox of the software MATLAB is modified from NSGA-II. The GRNN prediction model is embedded into the objective function of the function “gamultiobj”. Considering the extrapolation capacity limitations of sample data and neural network, choose the best slump $K_1 = 140$, to get the front-end individual scatter gram of Pareto solutions by computing the function “gamultiobj”. The specific parameter settings are as follows: the optimal front-end individual coefficient is 0.3, the population size is 100, the largest evolution algebra is 100, the introductory evolution algebra is 100, and the deviation of the fitness function value is $1e-100$.

It can be seen from the Figure 3, with the increase in the compressive strength, the slump decreases, which correctly reflects the contradiction between the two target quality properties.

According to the Pareto’s optimal solution, C25 mixed-sand pumping concrete recommended mixture ratio can be gotten, as shown in Table 3.

5 SUMMARY

Aiming at the compressive strength and slump of mixed-sand pumping concrete, the GRNN prediction model has been established. It is concluded that the predicted values with the test of the theoretical results fit well with the numerical. Based on established GRNN, the paper conduct multi-target optimization model by combining genetic algorithm and get the recommended mix proportion of delivered concrete of C25 mixed-sand pump under the condition that the optimum slump is for $K = 140$. Research shows that GRNN has excellent generalization ability at the condition of small specimen amount, and has broad application prospects in the prediction and evaluation of concrete performance, mix proportion optimum design of concrete and so on.

REFERENCES

- [1] Wang JiLiang. Machine-made Sand in the Application of High Performance Concrete Research [D], Wuhan: Wuhan University of Technology, 2008. (in Chinese).
- [2] Ai Long, Peng Hao, et al. Influence Law and Action Effect of Manufactured Sand Gradation on Concrete Performance[J]. Concrete, 2013 (1): 73–76. (in Chinese).
- [3] Wu Wei, Wang Jian, et al. Convergence Analysis of Onlin Gradient Method for BP Neural Networks[J]. Neural Networks, 2011 (24): 91–98.
- [4] Li Hong, Peng Tao. Prediction of Concrete Compressive strength Based on BP, RBF neural network Theories[J]. Journal of Wuhan University of Technology, 2009, 31 (8): 33–36. (in Chinese).
- [5] Xiao Xiaowei, Xiao Di, et al. A Research Summary on Multi-objective Optimization Application Research of Computers[J], 2011, 28 (3): 805–808. (in Chinese).

The research on of drivers' shoulder fatigue when driving on the grassland highway

Sa Ri Na Bao, Shou Lin Zhu, Chun Hua Qi, Ming Xing Gao, Hang Tian Li & Ting Zhao
College of Energy and Traffic Engineering, Inner Mongolia Agriculture University, Hohhot Inner Mongolia, China

ABSTRACT: Compared with other kinds of roads, the grassland highway has the features of low gradient, simple linear structure, less traffic flow and monotonous surrounding scenery. Driving in such monotonous surroundings, drivers tend to feel tired physically and mentally, because of the continued same operation. This dissertation will report four selected drivers' real driving experiments on the typical grassland road, using MPI50 multi channel physiologic recorder to collect information. Besides, analyze the regulation of the surface electromyography of the deltoid muscle of drivers' shoulders with its Mean Power Frequency (MPF) and Median Frequency (MF). According to the research, both MPF and MF have clear and similar tendency of decline, which proves that drivers' shoulders have already felt tired. This conclusion can be a theoretical support for the deep research of drivers' exhaustion condition.

Keywords: grassland highway; shoulder fatigue; Mean Power Frequency (MPF); Median Frequency (MF); Surface Electromyography (SEMG)

1 INTRODUCTION

Because of its special geographic and geomorphic conditions, the grassland highway has become the typical highway of Inner Mongolia. It has the features of low gradient, simple linear structure, less traffic flow and monotonous surrounding scenery^[1-2]. Driving in such monotonous surroundings for a long time will cause negative effect on driving. Drivers are easy to feel tired physically and mentally, which will affect the safety of driving. It is quite necessary to do research on the relationship between the muscle fatigue and the time of driving so as to reduce the traffic accidents caused by drivers' muscle fatigue.

Nowadays, most researches on the fatigue conditions of driving on the grassland highway based on the Surface Electromyography (SEMG) from home and abroad are completed on driving simulator, however they neglect the influences of highway, surroundings both inside and outside cars and other factors. This dissertation is based on the research on the typical grassland highway in Xilinhot city, Inner Mongolia, including lots of driving tests, based on analysis of electromechanical power spectrum, studying the change of the Mean Power Frequency (MPF) and Median Frequency (MF) of electromechanical power spectrum along with time during the driving process, from which we can learn the condition of drivers' muscle fatigue on their shoulders. This research has great importance

of limiting the driving time, relieving drivers' fatigue and enhancing the driving safety.

2 DATA AND METHODOLOGY

2.1 Experimental highway

This driving test was carried in typical grassland summer. The experimental section is the provincial road S101, a typical grassland highway located in Xilinhot city from Saihan town to Mandula town, Inner Mongolia, which is designed as a secondary road whose designed vehicle speed is 80 km/h^[3]. Compared with other roads, this section has the features of low gradient, simple linear structure, less traffic flow and monotonous surrounding scenery. As it is, this section of highway is relatively representative.

2.2 Experimental subject

Among the selected experimental subjects, there are four healthy teachers aging from 40 to 53, two of whom are males. Their average age is 46.3 years old (SD = 5.8), and they have averagely been driving for eight years (SD = 2.9). All the drivers are in good condition, have no illness or injuries on shoulders, and they are not quite familiar with the condition of the roads. The basic information about the four drivers are shown in [Table 1](#).

Table 1. Basic information on drivers.

Driver	Gender	Age	Driving years	License	Familiar with the road
01	F	53	7	C1	AVERAGE
02	M	51	13	C1	AVERAGE
03	F	40	6	C1	AVERAGE
04	M	41	6	C1	AVERAGE

2.3 Experimental instruments and assistant facilities

One MP150 multichannel physiologic recorder produced by American BIOPAC company, one laptop, some disposable electrode plates, alcohol, cotton swabs, and several storage batteries.

2.4 Procedure and requirements of experiment

1. Drivers should get enough sleep before the test. Drinking alcohol and driving fatigue are not allowed.
2. Before the test, stick electrode plates to the drivers, adjust and plug in the MP150 multichannel physiologic recorder and the computer.
3. In case of the disturbance of other electronic signals, all people inside the car shall turn off their cell phones.
4. Before the test, use MP150 multichannel physiologic recorder to collect the data of drivers' static electromyography as original reference data for later research.
5. This experiment shall not set speed limitation under safe conditions. After covering 145 kilometers, the car will return back to the beginning.

3 THE SELECTION OF TESTED TARGET

The surface electromyography signal refers to bio-electronic signal sent from the surface of skeletal muscle during the neuromuscular system reaction, which is recorded by electrode plates. It is one-dimensional time-series signal whose change is influenced by related activity pattern and quantity of motor unit, and metabolism. At the same time, the test will do no damage to the drivers. It is easy to operate, and it can keep testing and it is quite convenient to locate the tested area^[4-6]. There are many ways to analyze electromyography, mainly including time domain analysis method, frequency domain analysis method and time and frequency domain analysis method.

Time domain analysis method is a very practical way, whose index is Integrated Electromyography (IEMG) and Root Mean Square (RMS).

However, whether using time domain analysis methods to assess the condition of muscle fatigue is useful or not is still quite disputed^[7].

Frequency domain analysis method is using the change of fast Fourier Transform (FFT) to turn the time-domain signal into frequency domain signal^[8-10]. In addition, MPF and MF, as the most common characteristic parameter, can effectively reflect the features of electromyography signal.

Time and frequency domain analysis method is a common way to deal with signal, which can reflect the distribution of signal energy in time and frequency domain, and efficiently describe the feature of the non-stationary signal^[8,11]. However, the relevant research about whether electromyography signal is stationary signal or not is not consistent. Therefore, more research is needed.

Combined with the characteristics of the three methods above, this dissertation will apply Frequency domain analysis methods based on FFT to dealing with and analyzing electromyography signal. Use MPF and MF to study the muscle fatigue on drivers' shoulders.

4 ACQUISITION AND ANALYSIS OF SIGNAL

The study will use MP150 multichannel physiologic recorder to collect data of electromyography signal of shoulders to get EMG signal waveform. We will use Acknowledge software to collect data whose its sampling frequency is 1000 Hz, and use SPSS software to carry on statistical analysis. At last, we will export the trend chart of MF and MPF.

4.1 Analysis of the change of MF/MPF on drivers' shoulders

Acknowledge software will collect signal with 5-minute time interval. The picture of trend of the change of MPF and MF of the deltoid muscle of drivers' shoulders long with time driving on grassland highway is shown in [Figures 1-4](#):

1. During the experiment, because there is no speed limitation, every driver drove in a different speed. Compared with males, females drove more slowly and longer. According to the four pictures, two females' driving time is averagely 185 minutes, while the other two males' driving time is averagely 160 minutes.
2. Choose four different frequency domains: 180-260 Hz, 80-220 Hz, 120-300 Hz, 140-260 Hz to show the regulation of change more clearly.
3. According to [Figures 1-4](#), the regulation of the change of MPF and MF of the deltoid muscle of drivers' shoulders along with time has almost

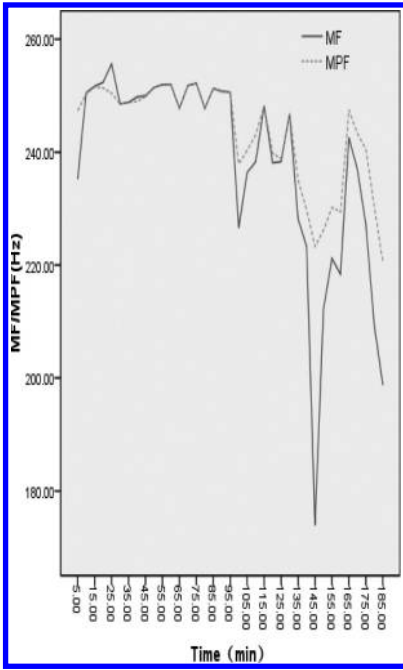


Figure 1. The regulation of the change of MPF and MF of drivers' shoulders along with time.

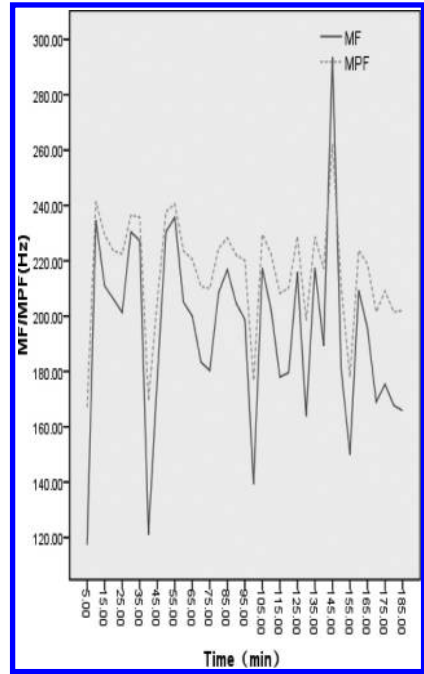


Figure 3. The regulation of the change of MPF and MF of drivers' shoulders along with time.

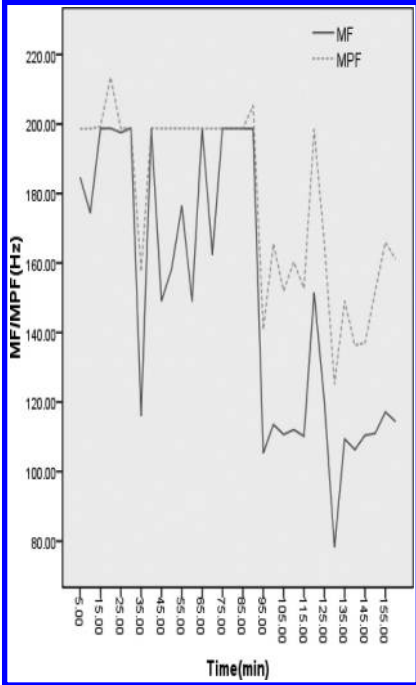


Figure 2. The regulation of the change of MPF and MF of drivers' shoulders along with time.

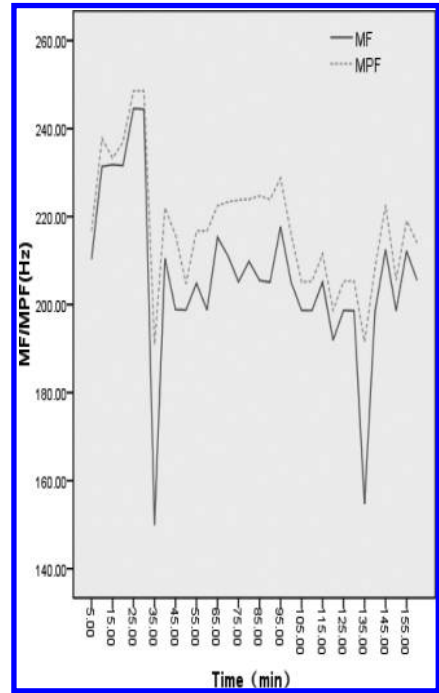


Figure 4. The regulation of the change of MPF and MF of drivers' shoulders along with time.

a consistent apparent declining tendency, and after 35 minutes, there is an obvious ascending node. According to Figure 1, at the beginning, the change of the MF and MPF is relevantly steady, which proves that the drivers' shoulders haven't felt tired yet. As time goes by, it shows an apparent declining tendency, which proves the drivers' muscle shows accumulated fatigue.

4. According to Figure 2, the wave is gradual and the expand time between the two waves is relevantly longer. As time goes by, it has an apparent declining tendency, which proves the drivers' muscle shows accumulated fatigue. As No. 2 driver is an experienced driver of 13 years, he can adjust himself effectively during the driving process to make himself comfortable, but as time goes by, his muscle also shows accumulated fatigue.
5. According to Figures 3 and 4, the wave of MF and MPF rise and fall frequently and compared with No. 3 driver, the wave of MF and MPF of No. 4 driver changes more. Because No. 3 driver and No. 4 driver both have been driving for 6 years, and they are less experienced than

other drivers. Therefore, they are easy to feel nervous. It also may because the female is more likely feel nervous than the male, which leads to the greater change of the wave of MF and MPF.

4.2 The change of MF/MPF on drivers' shoulders and goodness of fit

In order to see the regulation of the change of MPF and MF along with time more directly, we counterpoised the four drivers MF and MPF, and used SPSS to test goodness of fit of the regression equation. The goodness of fit of the regression equation is to test the intensiveness of data points around regression line in tested samples so that we can judge how representative the regression equation is to the sample data. Refer to Figures 5 and 6, Tables 2 and 3 as follow:

1. According to Figures 5–6, the regulation of the change of MPF and MF of the drivers' shoulders along with time has almost a consistent apparent declining tendency, which proves the drivers have already felt tired on their shoulder.

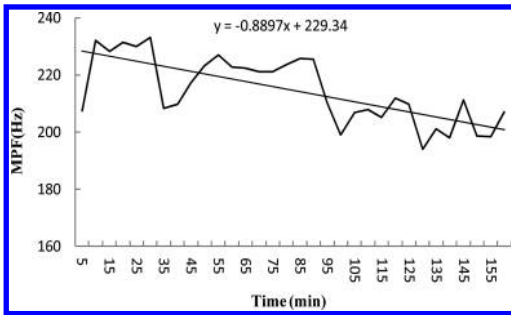


Figure 5. The trend of the change of average MPF of drivers' shoulders along with time.

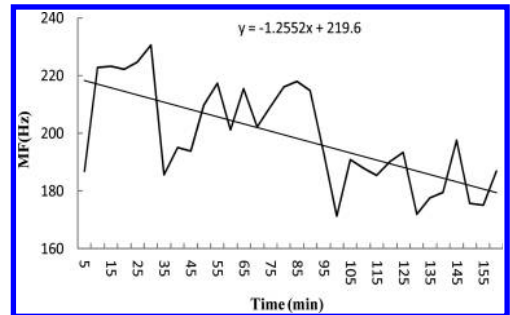


Figure 6. The trend of the change of average MF of drivers' shoulders along with time.

Table 2. The goodness of fit of the regression equation testing (MPF).

Model	R	R ²	Adjusted R ²	Std. error of the estimate	Change statistics		
					R ² change	F change	Sig. F change
1	0.716 ^a	0.513	0.497	8.26262	0.513	31.631	0.000

Table 3. The goodness of fit of the regression equation testing (MF).

Model	R	R ²	Adjusted R ²	Std. error of the estimate	Change statistics		
					R ² change	F change	Sig. F change
2	0.669 ^a	0.447	0.429	13.30933	0.447	24.265	0.000

The regulation of the change of MPF and MF of the drivers' shoulders along with time is similar.

2. According to Tables 2 and 3, R^2 is respectively 0.513 and 0.447. R is respectively 0.716 and 0.669. This proves it is advisable to adopt one element linear to fit the regulation of the change of MPF and MF of the drivers' shoulders along with time.

5 CONCLUSIONS

This dissertation is based on the data of real driving tests of four drivers on the typical grassland highway in Xilinhot city, Inner Mongolia, which analyzes the regulation of the surface EMG of the deltoid muscle of drivers' shoulders, and concludes the regulation of the change of MPF and MF along with time as follows:

1. The regulation of the change of MPF and MF of the deltoid muscle of drivers' shoulders along with time has almost consistent apparent declining tendency, which proves that driving on a grassland highway for a long time will easily cause muscle fatigue on shoulders.
2. Driving time has obvious linear effect on MPF and MF.
3. Analyzed data shows that compared with males, females are more easily to get nervous. However, because the samples are fewer than required, we can not draw the conclusion. And we will put more samples in later driving tests to compare analyze the difference performance of males and females.
4. After driving for 35 minutes, the MPF and MF of drivers' shoulders will decline evidently.

ACKNOWLEDGEMENT

This dissertation is approved by Project supported by National Natural Science Foundation (51168036). Great gratitude to all the drivers who participated in this experiment.

REFERENCES

- Dongqing Xu. 2011. Study on the Effect of the Continuous Driving Time on the Driving Fatigue under Environment of Prairie Highway. *Inner Mongolia Agricultural University*, master's degree thesis. (in Chinese).
- Kun Jiao, Zengyong Li, Ming Chen, et al. 2004. SEMG Analysis of Lumbar Fatigue during Simulated Driving. *Chinese Journal of Ergonomics* 10(3):10-14. (in Chinese).
- Le Kang, Jianguo Zhang, Herong Liu. 2012. Surface Electromyography of Lower Limbs during Activities of Daily Living for Normal Adults. *Chinese Journal of Rehabilitation Theory and Practice* 18(9):816-819. (in Chinese).
- Qiang Tian, Liping Huang, Shiqing Yu, et al. 2008. The effect of 8 hour driving on sEMG signal changes of lumbar muscles and the tibialis anterior muscles in middle-aged male taxi drivers. *Chinese Journal of Rehabilitation Medicine* 23(1):19-22. (in Chinese).
- Shangle Feng. 2012. Research on the Effect of Grassland highway Curve Combination on Drivers ECG Characteristics. *Inner Mongolia Agricultural University*, master's degree thesis. (in Chinese).
- Shoulin Zhu, Chunhua Qi, Mingxing Gao, et al. 2013. Research on the Effect of Grassland Highway Curves on Drivers HRV. *Advanced Materials Research* 779-780:584-591. (in Chinese).
- Taoran Liu. 2009. Research on The Surface Electromyographic Characteristics of Human. *Tianjin University of Science and Technology*, master's degree thesis. (in Chinese).
- Wei Peng, Duming Wang, Shuang Yin, et al. 2013. Exploring the Characters of Physiological Signals for Fatigued Drivers. *Chinese Journal of Ergonomics* 19(1):24-28. (in Chinese).
- Wei Zhou. 2009. SEMG Signal Processing Base on Histogram and Spectrum. *Hangzhou University of Electronic Science and Technology*, master's degree thesis. (in Chinese).
- Yongchao Zhao. 2009. The Study on Work Fatigue of Tractor Drivers Based on SEMG. *Northeast Agriculture University*, master's degree thesis. (in Chinese).
- Yongge Mu. 2004. Study and Application of Surface electromyography Signal Based on Time-Frequency and Time-Seale Analysis. *Chongqing University*, master's degree thesis. (in Chinese).

Effect of polypropylene fiber and silica fume on mechanical properties and durability improvement of high performance concrete

Xin Guo Zheng, Jing Liu, Shu Ming Li, Zhi Zeng, Zhi Cai Weng & De Jun Yang
Railway Engineering Research Institute of China Academy of Railway Science, Beijing, China

De Hua Deng
Civil Engineering and Architecture College, Central South University, Changsha, China

Ren Sheng Ding
Hangzhou-Changsha Railway Passenger Dedicated Line Zhejiang Co., Ltd., Hangzhou, China

ABSTRACT: Polypropylene fibers and silica fume were used to get high impermeability and cracking resistance concrete. Results showed the fibers improved the concrete performance of anti-cracking resistance and decreased plastic shrinkage at early age significantly; moreover, the fibers reduced the adverse influence of both early plastic cracking on chloride permeability and improper consolidation or materials sedimentation on concrete homogeneity. However, just incorporating fibers (without silica fume) had no obvious improvement on strength and impermeability of concrete. The usage of polypropylene fibers and silica fume together in concrete increased the compressive strength and caused a significant reduction in chloride permeability in both rapid chloride penetration test and wetting and drying cycles in 1.9% NaCl solution; the drop of relative dynamic modulus and mass loss of concrete after 300 freezing-thawing cycles in simulative seawater were only 8.7% and 1.84%, respectively; its corrosion potential of internal steel bar bearing acceleration of corrosion was higher than others without addition of polypropylene fibers or silica fume in the corresponding periods showing more excellent steel bar protection performance of the concrete. So the addition of silica fume significantly enhanced the comprehensive effectiveness of the polypropylene fibers on properties of concrete. Consequently, the improvement of fibers and silica fume on concrete properties may be attributed to both the anti-cracking effect from polypropylene fibers and densification reinforcement action to the interfacial transition zones of both fiber—matrix and aggregate—cement paste from silica fume.

Keywords: polypropylene fiber; silica fume; high performance concrete; compressive strength; chloride permeability; cracking resistance; frost resistance; corrosion potential

1 INTRODUCTION

In China, a lot of major infrastructures are being built and will be built in the marine and coastal environment, such as coastal railway, sea-crossing bridges and tunnels, ports and harbors, oil drilling platforms, parking apron, etc. These buildings are generally built by concrete which is one of the most widely-used construction materials because of its low cost, high compressive strength, high durability and versatility. Since these major infrastructures play an important role in the national economy, high durability of concrete is required necessarily, and the service life requirement is generally more than 100 years. But the survey of buildings durability in the marine environment at home and abroad indicated many concrete structures

appeared premature destruction and deterioration in just 20 to 30 years after being built, far from reaching the designed service life and had to be rehabilitated costly. The main reason for premature deterioration is steel bar corrosion in concrete caused by chloride ion permeability and freezing-thawing damage of concrete [1–4]. As we know, concrete is intrinsically porous and may deteriorate or depredate as a result of harsh environmental exposure such as marine environment. The deterioration effect on concrete structure has led to the realization that durability of concrete should be improved by adding into extra suitable constituent materials in normal concrete. An effective way to minimize durability problem is to make the composite less permeable and the paste denser or to inhibit crack propagation and provide enough

cover thickness for concrete structures especially in the marine environment [5–7].

Over the last nearly 30 years, High Performance Concrete (HPC) has been widely used in marine construction engineering. Its preparation is characterized by low water-cement ratio, sufficient mineral admixtures and superplasticizers. Durability is the most important property except for meeting the strength requirement. It's denser and possesses excellent cementitious pore structures and high impermeability [8–12]. The addition of silica fume into HPC can further improve the cementitious pore structures and densify the interfacial transition zone between cement pastes and aggregate [13]. In addition, silica fume can also fill the capillary pores of the composites and reduce water permeability, penetration of chloride ion as well as corrosion rate of reinforcements [14]. However, the addition of silica fume may cause HPC cracking more early and seriously due to higher plastic shrinkage of concrete [15–16]; while the addition of polypropylene fibers can improve the toughness and cracking resistance of concrete effectively [17]. Fiber is one of the commercially available additives and has been added in concrete since 1960 to enhance tensile strength, abrasion resistance and energy absorbing capacity [18–21]. The concrete with fiber have much higher ductility than those without fiber, and demonstrate a significant increase in energy absorption [22–23]. Therefore, to combine the advantages of silica fume and fibers to HPC, the simultaneous addition of silica fume and polypropylene fibers on properties improvement of HPC was studied by experiments including compressive strength, rapid chloride penetration, chloride penetration depth in wetting and drying cycles, flat restrained cracking resistance test, chloride permeability test after cracking, shrinkage test, freezing-thawing cycles and accelerated corrosion potential test of steel bar in concrete. The aim of the study is to research and develop a kind of concrete with excellent impermeability, frost resistance and cracking resistance properties, and then to provide more durable materials for exploitation and utilization of marine resources sufficiently.

2 EXPERIMENTAL MATERIALS

2.1 Materials

1. Cement: 42.5 ordinary Portland cement (C) confirming to GB 175 was used; its compressive strength of 28d was 46.3 MPa.
2. Fine aggregate: Locally available natural sand with a specific gravity of 2.69 and fineness modulus of 2.7 was used.

Table 1. Chemical composition of cement, fly ash and silica fume/%.

	P.O 42.5	FA	SF
SiO ₂	24.3	52.8	85.36
Al ₂ O ₃	4.9	25.7	0.06
Fe ₂ O ₃	3.8	9.7	7.04
CaO	55.2	3.7	0.56
MgO	4.3	1.2	1.10
SO ₃	2.2	0.2	–

Table 2. Mixture proportions of concrete and slump.

Mix no.	C0	C1	C2
C (kg/m ³)	360	360	360
FA (kg/m ³)	120	120	96
SF (kg/m ³)	0	0	24
Fiber (kg/m ³)	0	0.9	0.9
Superplasticizer [#]	0.4%	0.6%	0.6%
Slump (cm)	21.5	21.0	19.5

[#]represents dosage of superplasticizer is the percentage of binder in weight.

3. Coarse aggregate: Locally available crushed stone with a maximal nominal size of 19 mm and crushed index of 7.8 was used.
4. Mineral admixtures: Level I Fly Ash production (FA) with specific surface area of 5400 cm²/g was used; Silica fume with specific surface area of 35000 m²/kg was used.
5. Superplasticizer: Polycarboxylate superplasticizer confirming to GB 8076 with 30% water reducing rate was used.
6. Fiber: Polypropylene monofilament fiber with density of 0.91 g/cm³, length of 19 mm, diameter of 18–48 μm was used.

The chemical compositions of cement, fly ash and silica fume are given in Table 1.

2.2 Concrete mix proportions

Mixture proportions of HPC were given in Table 2. The water/binder ratio and sand rate for every mix was 0.32 and 40%, respectively. The concrete slump was 20 cm ± 2 cm by adjusting superplasticizer dosage. The mixing procedure adopted was as follows: First, the cement, mineral admixtures and fibers were dry mixed till a uniform color was obtained without any clusters of binders and fibers to make fibers distributed uniformly. Weighed quantities of coarse aggregates and sand were then mixed in dry state, thoroughly until a homogene-

ous mix was obtained. Water was then added in three stages as 45% of total water to the dry mix of concrete in first stage; 45% of water and superplasticizer to the wet mix; Remaining 10% of water was sprinkled on the above mix and thoroughly mixed. Total mixing time of C1 and C2 with fibers is 2 minutes longer than ordinary HPC of C0 without fibers.

3 EXPERIMENTAL METHODS

3.1 Compressive strength test

In accordance with “Standard for test method of mechanical properties on ordinary concrete” (GB/T50081-2002), the cubic specimen size is 150 mm × 150 mm × 150 mm.

3.2 Chloride permeability test

3.2.1 Rapid chloride penetration test

To simulate actual field placement of concrete better, PVC pipes were used to make cylinder specimens with the dimension of 16 cm (diameter) × 100 cm (height). After consolidated, specimens were cured in the standard condition. Three groups of Φ100 mm × 50 mm cylinders were cut and cored in the upper, middle and lower of the specimens, respectively. Every group had three specimens. Specific coring positions: in the upper coring downwards 50 mm from the top; in the middle coring the center of specimen; in the lower coring upwards 50 mm from the bottom. The Nordtest NT build 492 method was used to test chloride diffusion coefficient of specimens coring from different height positions. The concrete age was 28 days when testing.

3.2.2 Chloride penetration depth in wetting and drying cycles

The ocean tidal cycle is half a day or a day, so 24 hours per wetting and drying cycle of was designed. Placed test devices in the open environment. 100 mm × 100 mm × 100 mm cubic specimens were exposed to the sunlight directly during the day and immersed in 5% NaCl solution at night. Immersed time in a cycle should be no less than 16 hours, the solution surface should be above the specimens more than 50 mm, and space between specimens should be more than 50 mm. Drying time should be the maximum temperature interval in a day, and no less than 4 hours. Split the specimens and sprayed 0.1M AgNO₃ solution on the splitting surface after 3 months and 6 months. The distance between white color boundary and the surface was the chloride penetration depth.

3.3 Cracking resistance test

3.3.1 Qualitative evaluation of concrete cracking resistance

The flat restrained cracking resistance test method was used. The flat platform size was 600 mm × 600 mm × 63 mm with the short restraining steel bars inlaid around shown in Figure 1. Placed and consolidated fresh concrete in the platform. A plastic film covered on the surface till concrete initial setting. Fans were used to blow specimens directly. The development of cracking on the surface including initial cracking time, crack length, width, area and appearance was observed as the qualitative evaluation of concrete cracking resistance.

3.3.2 Chloride penetration after cracking

When the development of concrete cracking on the surface of the platform was stable, cored three Φ100 mm × 50 mm cylinders at most representative cracking positions from every platform, respectively. The method explained in Section 3.2.1 was used to test chloride diffusion coefficient of cracking concrete. They were compared to evaluate crack resistance of every kind of concrete with different mix proportion quantitatively. The influence of cracking on chloride permeability was also evaluated.

3.4 Frost resistance test

To simulate concrete freezing and thawing in sea water, the 10 cm × 10 cm × 40 cm prismatic specimens were immersed in 1.9% NaCl solution during freezing and thawing cycles. The central temperature was controlled (-17 ± 2) – (8 ± 2) °C, one cycle took about 2–4 hours. Specimens were immersed

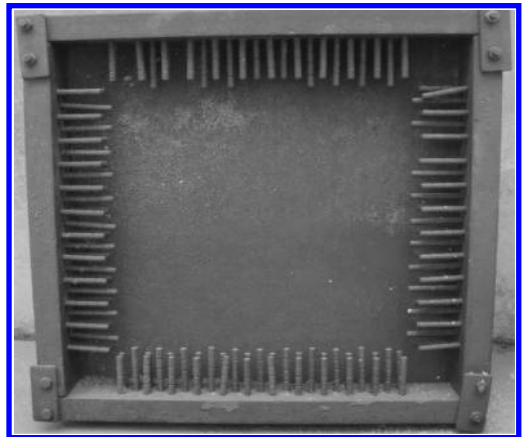


Figure 1. Flat restrained cracking resistance test instrument.

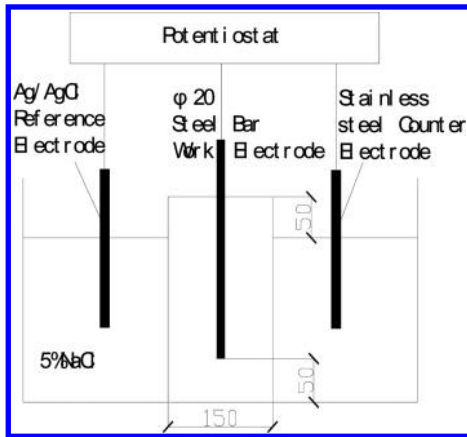


Figure 2. A sketch of corrosion potential measurement.

in 1.9% NaCl for 4 days, and then the cycles were started at the concrete age of 28 days. The relative dynamic elastic modulus and mass loss of concrete were used to evaluate concrete frost resistance.

3.5 Corrosion potential of steel bar

One end of $\Phi 20 \text{ mm} \times 250 \text{ mm}$ steel bar was located in the central concrete cylinder with the dimension of $\Phi 150 \text{ mm} \times 250 \text{ mm}$. Specimens were cured in the standard condition for 28 days before test. A sketch of corrosion potential measurement equipment was shown in Figure 2. The steel bar was sealed with epoxy coating except the area where corrosion was monitored. Both ends of concrete cylinder were also sealed with impermeable coating to insure the ingress of chloride only from surrounding perimeter. To accelerate the corrosion of reinforced, 30 V direct voltage was imposed. The potential difference between steel bar and the reference electrode was measured every 24 hours in the absence of applied voltage, which is called the corrosion potential (E_{corr}). Based on ASTM C876-91 steel corrosion potential evaluation criteria, when corrosion potential is less than -426 mV , it means the corrosion of steel is very severely. The time for the corrosion potential reaching -426 mV and declining rate were used to evaluate the concrete protective performance of steel bar.

4 RESULTS AND DISCUSSION

4.1 Compressive strength

As shown in Figure 3, the compressive strength of C1 was slightly lower than that of C0 all the time; the compressive strength of C2 was significantly

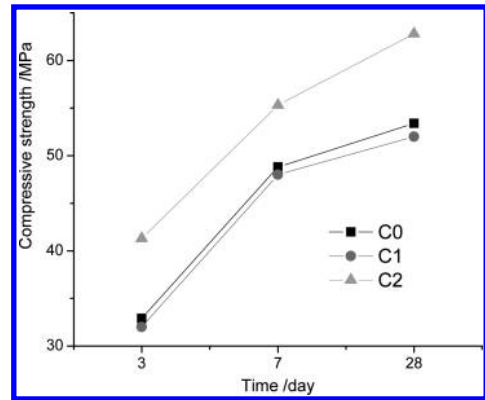


Figure 3. Compressive strength of different mix concrete.

higher than that of C0 and C1, especially higher nearly 10 MPa at the age of 28 days. These may be due to on one hand polypropylene fibers are soft and thin, and the surface is hydrophobic. A great deal of weak interfacial transition zone is formed between fibers and matrix when cement hardened; the water/cement ratio there is higher resulting in more porous and internal weak interfaces. It has adverse effects on mechanical strength of concrete; on the other hand superfine silica fume can effectively fill the pore gaps between gel and fibers to make the matrix and interfacial transition zone denser. The hydration of silica fume improves and enhances weak interfaces, not only eliminates adverse effects of fibers on strength also increases compressive strength [24].

4.2 Chloride permeability test

As shown in Figure 4, the chloride diffusion coefficient of C2 was significantly lower than that of C0 and C1 in the upper, middle and lower position. On one hand it's due to the filling effect of silica fume, on the other hand silica fume and $\text{Ca}(\text{OH})_2$ occur the secondary hydration to generate C-S-H gel, then the pore structures of hydrated cement paste have been changed by reducing the diameter greater than $0.5 \mu\text{m}$ harmful pores and increasing the diameter less than $0.02 \mu\text{m}$ harmlessly pores. Pores are refined [25]. The reaction of silica fume makes capillary porous more tortuous to extend or block the permeable channel; while the amount and size of $\text{Ca}(\text{OH})_2$ crystals are reduced and its directional enrichment is also alleviated, which reduces concrete porosity efficiently.

With coring positions changing from upper to lower (U-M-L), the chloride diffusion coefficient showed a downward trend, of which C0 was the most obvious, its chloride diffusion coefficient in the upper was higher than the middle and lower

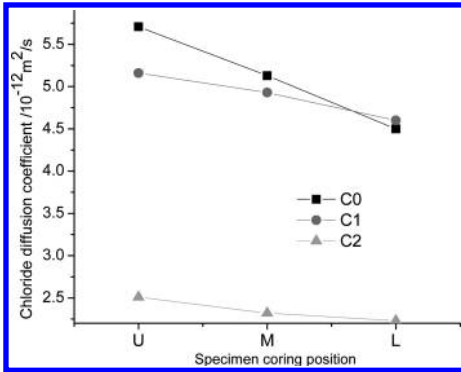


Figure 4. Chloride diffusion coefficient at different position. U, M, L—represents the Upper, Middle, Lower position of the specimen explained in the test procedure 3.2.1, respectively.

parts by 12% and 23%, respectively. However, the chloride diffusion coefficient fluctuations of C1 and C2 were much gentler. For C2, the difference between upper and lower was only 8%. It showed that when the concrete-pouring at a higher altitude, consolidation especially over vibration makes water or paste easy to float up and bleed, which causes the upper water-binder ratio is higher than the lower in the same concrete placement layer; While the specific gravity of aggregate is greater, the sedimentation of aggregates can cause many tiny settlement cracks before hardened. So the lower concrete impermeability is higher than the upper's. When adding some fibers, the overall uniformity and consistency of fresh concrete were enhanced, and the trend to bleeding and segregating was reduced just like the matrix formed into 3D grids by fibers. Equal dispersion in the matrix of fibers alleviated coarse aggregates subsiding and water floating, which hindered the amount and scale of settlement cracks. Moreover, silica fume can further reduce bleeding because of its very small particles and huge specific surface area. Thus for the discrete of chloride permeability at different placement heights, C2 was the smallest followed by C1 and C0. So the addition of fiber and silica fume can insure the uniformity and stability of hardened concrete best. Despite the slump was reduced, it could be reached to the same slump level by increasing 0.2% superplasticizer dosage shown in Table 2.

As shown in Figure 5, the chloride penetration depth of C2 in wetting and drying cycles was less than 6 mm after six months. The chloride penetration depth of C1 is a bit smaller than that of C0, but the difference was only within 2 mm. It showed just adding fibers couldn't increase concrete impermeability significantly. The effects of fibers on the

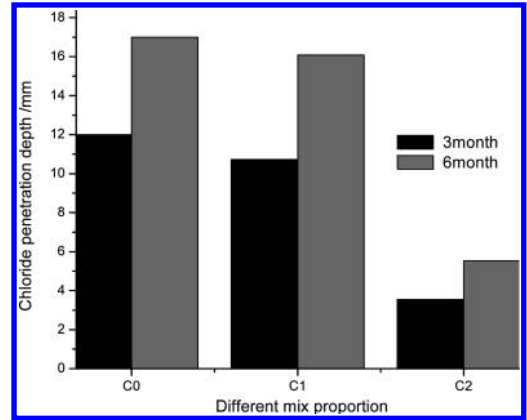


Figure 5. Chloride penetration depth in dry and wet cycles.

properties of concrete stem from the counteracting action between fibers reinforced cracking resistance advantageously and fibers increasing weak interfacial transition zone adversely. If these actions are equivalent, the effect of fiber on concrete permeability is not obvious. Maybe the indoor laboratory conditions, which means the standard sample size and curing without restrained, aren't conducive for fibers to exert cracking resistance role. So the improvement of fiber on concrete impermeability wasn't evident.

4.3 Cracking resistance test

4.3.1 Flat restrained cracking resistance test

As listed in Table 3, the cracking area of C1 was only 12.2% of that of C0. This indicated fibers could sharply increase concrete early cracking resistance. During the experiment, surface water evaporated rapidly in the blow of fans and caused shrinkage tensile stress. Nevertheless, at the beginning, the hardening concrete didn't have sufficient strength to resist the stress; so cracking occurred on the surface. The addition of fibers make per cubic concrete evenly dispersed more than 10 million fibers, which enhances the concrete ability to resist the tensile stress, thereby inhibits the formation and development of cracking. But the addition of fibers and silica fume at the same time made C2 crack first and appear a relatively larger amount of minute cracks. It may result from the specific surface area of silica fume is huge enough to make fresh concrete more viscous and easily prone to plastic shrinkage because of the lack of moisture on the surface. In addition, the development of early strength is rapid and stress relaxation ability is small [16], cracking is more easily to occur. However, under the constraint of fibers, the width of cracks wasn't greater than 0.5 mm.

Table 3. Cracking properties on concrete surface.

No.	Initial rack min:sec	Cracking width A/(mm)	Cracking length B/(mm)	A×B/mm ²
C0	4:00	1.0	150.5	150.5
		0.5	230.6	115.3
		0.3	403.9	101.0
C1	4:50	1.0	0.0	0.0
		0.5	0.0	0.0
		0.3	178.4	44.6
C2	3:15	1.0	0.0	0.0
		0.5	0.0	0.0
		0.3	304.2	76.1
No.	Gross area/mm ²	Relaive percentage/(%)	Crack description	
C0	366.8	100.0	The amount was great, wider and longer than C1 and C2	
C1	44.6	12.2	The amount of cracks was the least, just very minute cracks	
C2	76.1	20.7	The amount of minute cracks was larger than C1, no wider than 0.5 mm and distributing in a clutter	

4.3.2 Chloride penetration after cracking

As can be observed in Figure 6 clearly, all chloride diffusion coefficients of concrete after cracking were much higher than that of corresponding concrete cured in the standard condition. Therein, C0 is the most obvious, which was raised by 50.1%. The variation of C1 was the smallest. This demonstrated the effect of fiber inhibiting cracking at early age made impermeability of hardened concrete not decline much. And the curly fibers staggered to make chloride permeability channels more tortuous, thereby lowered chloride penetration depth. Though the chloride diffusion coefficient of C2 was still the lowest, the change of C2 was relatively larger with almost close to 50%. It may be due to the silica fume concrete requirement for early curing condition was stricter. During the cracking test, the specimens weren't provided wet curing but to accelerate the surface wind speed and moisture evaporation, so the cement hydration was badly influenced, especially serious for C2. This also reflects laterally the early curing condition is very important for hardened concrete impermeability. The curing should be taken more seriously on construction site.

4.4 Frost resistance test

For the drop rate of relative dynamic modulus in Figure 7, C0 was higher than C1 before the first 150 freezing thawing cycles. After then, C1 was higher than C0. This showed the internal damage of C0 was more serious than C1 at early cycles; thereafter, the internal damage of C1 was more serious

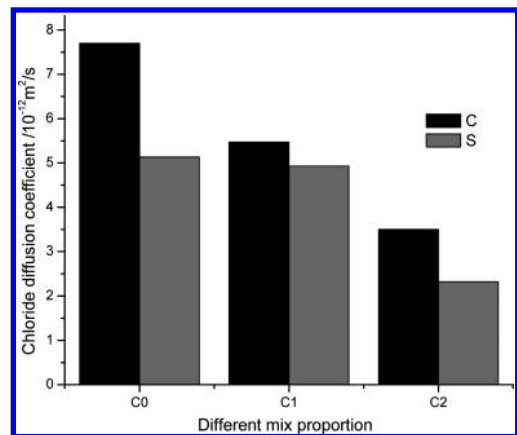


Figure 6. Influence of cracking on chloride diffusion coefficient. C represents chloride diffusion coefficient after cracking test S represents chloride diffusion coefficient under Standard curing condition

than C0. The ices in micro pores grew directionally and melt, and icing pressure acted on the pore walls repeatedly along with the freezing and thawing cycles [26–27]. Because of the three-dimensional binding and cross-linking of fibers, the early damage of C1 is less serious. With continuous freezing and thawing action, ice pressure fatigued the weak interfacial transition zone between fibers and matrix. The fiber gradually lost bonding strength to the matrix and the action of re-distributing pressure. Water penetrated more easily into the

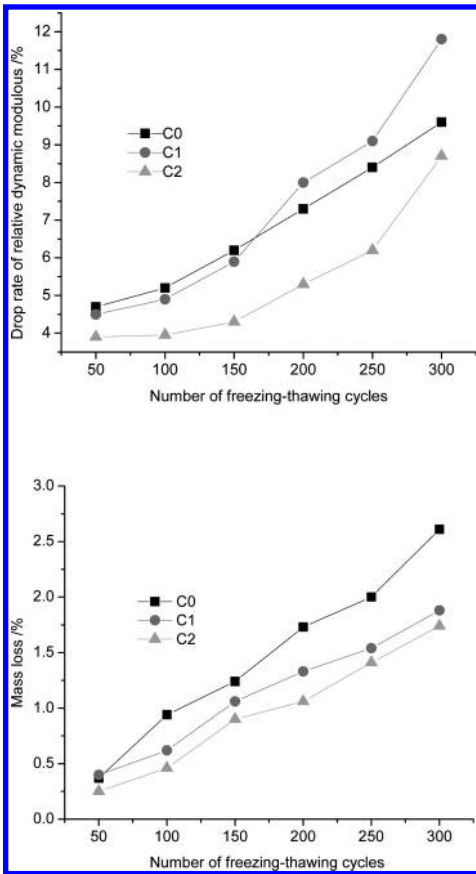


Figure 7. Relative dynamic modulus and mass loss of concrete during freezing-thawing cycles in simulative sea water.

matrix because of more interfacial fatigued cracks. The more the internal frozen water, the greater the pressures which will bring more serious damages to concrete [28]. In 300 cycles, the drop rate of relative dynamic modulus of C1 was significantly higher than C0 proved this point. However, for mass loss in Figure 7, C1 was always less than C0. This indicated fibers can reduce the surface spalling and be conducive to maintaining the appearance of concrete integrity during freezing and thawing cycles. For both the drop rate of relative dynamic elastic modulus and mass loss, C2 was always lower than the C0 and C1. This may be due to densely filling and high activity effect of silica fume.

4.5 Corrosion potential of steel bar

The sequence for steel corrosion potential reaching -426 mV indicating serious corrosion of steel bar in concrete was C1, C0 and C2 shown in Figure 8.

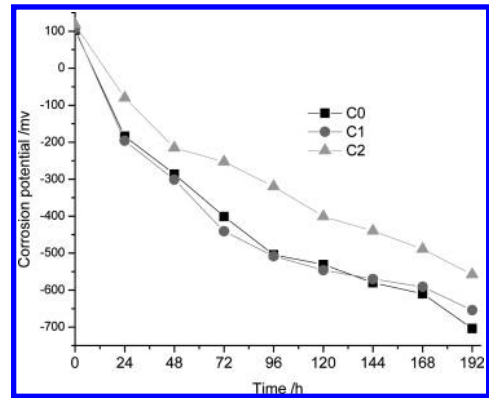


Figure 8. Corrosion potential alteration of steel bar in concrete.

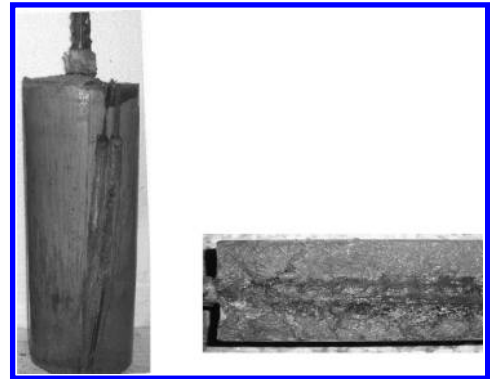


Figure 9. Cover cracking of C0 and corrosion situation of steel bar in C0.

And the corrosion potential of C2 was higher than that of C0 and C1 in the same period; the cylinders of C0 and C1 could be seen emerging cracks in the 96 hours after electrification, while cylinders of C2 had no cracks at that time. This indicated C2 had more excellent steel bar protecting performance. Chloride ions can penetrate through the concrete cover and migrate to steel surface rapidly in the electric field. When the concentration reaches a critical value, chloride can cause the passive films of steel bar begin to corrode into Fe^{2+} . With the sustaining enrichment of chloride, Fe^{2+} and Cl^- generate water-soluble $FeCl_2$, and then diffuse outward and form into $Fe(OH)_2$ with OH^- in the pore solution; latterly it may transfer into other rust when meeting oxygen. The volume of rusted productions expands 2–7 times which generates great tensile pressure and causes cover cracking (Fig. 9). Chloride ions released and newly penetrated can migrate to the anode

again and bring out more Fe²⁺. The corrosion of steel becomes more and more serious causing steel corrosion potential of the steel bar getting smaller and smaller. Cl⁻ are not consumed and only to catalyze the corrosion [29–31]. Based on the electrochemical mechanism, the above results indicated the HPC with fibers and silica fume not only possessed a relatively higher external electrical impedance to reduce the volume of external Cl⁻ penetrating into the matrix, so the time of reaching chloride critical value in concrete had been significantly delayed; but also had greater internal electrical resistance to inhibit internal Cl⁻ depolarization and catalyst to the corrosion of steel bar, so the process of the rust generation and cracks inducing by expansive stress of rusted had been postponed. These may be the reasons why the cylinders of C2 hadn't cracked yet when corrosion potential reached -558 mv.

5 CONCLUSION

The effects of polypropylene fiber and silica fume on properties improvement of HPC were studied by series of experiments. These results can be summarized as follows:

1. The single addition of fibers without silica fume makes compressive slightly lower than concrete without addition of fiber, and has little effect on improvement of strength, impermeability, frost resistance, though the mass loss is less in the freezing and thawing cycles. The effects of fibers on the properties of concrete result from the counteracting actions between fibers enhance concrete cracking resistance advantageously and fibers increase weak interfacial transition zones adversely.
2. The incorporation of both polypropylene fibers and silica fume increased compressive strength obviously, and caused a significant reduction in chloride permeability both in rapid chloride permeability test and wetting and drying cycles in 1.9% NaCl solution. Relative dynamic modulus and mass loss of concrete after 300 freezing-thawing cycles in simulative sea water were 8.7%, 1.84% respectively; its corrosion potential of steel bar was higher than others in corresponding period, showing excellent steel bar protection performance. Therefore, the significant improvement on concrete properties may result from both the anti-cracking effect of polypropylene fibers and densification reinforcement action to the interfacial transition zone of fiber—matrix and aggregate—cement paste by silica fume.
3. The addition of fibers inhibits the plastic cracking and early shrinkage significantly, reduces

the adverse influence of early plastic cracking on chloride permeability and improper placement and consolidation and materials sedimentation on the homogeneity of concrete.

4. The curing condition at early age is also confirmed extraordinarily important for crack resistant and permeability of hydrated cement paste.

ACKNOWLEDGEMENT

This research was supported, in part, by China Railway Corporation Science and Technology Research and Development Program under Grant No.2013G008-D, National Basic Research Program of China (973 Program) under Grant No.2010CB736102 and China Academy of Railway Science Foundation under Grant No.2010YJ75. The authors are grateful to Prof. XieYongjiang and Li Huajian for their useful comments and suggestions. The authors are also grateful to Prof. Xin Xuezhong, the chief engineer of Hangzhou-Changsha Railway Passenger Dedicated Line Zhejiang Co., Ltd for his useful comments and suggestions. The authors are also grateful to Mr. Qiu Jiagen, the minister of Safety and Quality Department of Beijing-Fuzhou Railway Passenger Dedicated Line Anhui Co., Ltd. for his support with test program design.

REFERENCES

- [1] Luc Schueremans, Dionys Van Gemert, Sabine Giessler. Chloride penetration in RC-structures in marine environment—Long term assessment of a preventive hydrophobic treatment. *Construction and Building Materials*, 2007, 21: 1238–1249.
- [2] L. Bertolini, B. Elsener, P. Pedeferra, R. Polder. *Corrosion of Steel in Concrete—Prevention, Diagnosis, Repair*, Wiley VCH, 2004.
- [3] Yu Pusong, Li Yuansong, Guo Fanzhao. Factors affecting corrosion and approaches for improving durability of ocean reinforced concrete structures. *Ocean Engineering*, 2004, 31: 779–789.
- [4] Economics of Corrosion (1994). NACE International Publication 3C194. Report prepared by the NACE International Task Group T-3C-1 on Industrial Economic Calculational Techniques, Unit on Economics of Corrosion, September 1994.
- [5] Oh B.H., Cha S.W., Jang B.S., et al. Development of High-performance Concrete Having High Resistance to Chloride Penetration [J]. *Nucl. Eng. Des.* (Switzerland), 2002, 212(1–3): 221–231.
- [6] Sahmaran M., Li V.C. Influence of Microcracking on Water Absorption and Sorptivity of ECC [J]. *Mater. Struct.*, 2009, 42(5): 593–603.
- [7] Antoni H.T., Saeki N. Performance of FRC Against Chloride Penetration under Loading [J]. *Proceedings of the JCI*, 2004, 26(1): 921–926.

- [8] Li Z., Ma B., Peng J., Qi M. The microstructure and sulfate resistance mechanism of high-performance concrete containing CNI. *Cement Concrete Composites* 2000, 22: 369–77.
- [9] Tahir Gonen, Salih Yazicioglu. The influence of mineral admixtures on the short and long-term performance of concrete. *Building and Environment*, 42(2007): 3080–3085.
- [10] Khan M.I., Lynsdale C.J. Strength, permeability, and carbonation of high-performance concrete. *Cement and Concrete Research*. 2002, 32: 123–131.
- [11] Use of Fly Ash in Concrete. ACI Manual of Concrete Practice 2001. Reported by ACI Committee 232, ACI 232.2R-96.
- [12] Al-Amoudi O.S.B., Maslehuddin M., Bader M.A. Characteristics of silica fume and its impact on concrete in the Arabian Gulf. The Sixth International Conference on Deterioration and Repair of Reinforced Concrete, 2000: 80–165.
- [13] Wang Dongmin, Zuo Yanfeng. Chloride Ions Diffusion Properties in High Performance Concrete with Different Materials. *Journal of the Chinese Ceramic Society*, 2004, Vol. 32: 1345–1361.
- [14] Mejia R., Delvasto S., Gutierrez C., et al. Chloride Diffusion Measured by A Modified Permeability Test in Normal and Blended Cements [J]. *Adv. Cem. Res.*, 2003, 15(3): 113–118.
- [15] Gao Xiaojian, B.A. Hengjing. Effect of mineral admixture on early age cracking. *Journal of Architecture and Civil Engineering*, 2006, Vol.23: 19–20.
- [16] Wang Yingfei, Huang Yanfei. Experimental Study on Cracking Sensitivity of Hardened Cement-based Paste at Early Age. *Materials Journal of the Chinese Ceramic Society*, 2006, 05: 44–46.
- [17] A. Garcia Santos, J. Ma. Rincón, M. Romero, R. Talero. Characterization of a polypropylene fibered cement composite using ESEM, FESEM and mechanical testing. *Construction and Building Materials*, 2005, 19: 396–403.
- [18] Li H., Zhang M.H., Ou J.P. Abrasion Resistance of Concrete Containing Nano-particles for Pavement[J]. *Wear*, 2006, 260(11–12): 1 262–1 266.
- [19] Song P.S., Wu J.C., Hwang S., et al. Assessment of Statistical Variations in Impact Resistance of High-strength Concrete and High-strength Steel Fiber-reinforced Concrete[J]. *Cem. Concr. Res.*, 2005, 35(2): 393–399.
- [20] Lin W.T., Huang R., Lee C.L., et al. Effect of Steel Fiber on the Mechanical Properties of Cement-based Composites Containing Silica Fume [J]. *J. Mar. Sci. Tech.*, 2008, 16(3): 214–221.
- [21] Swaddiwudhipong S., Seow P.E.C. Modeling of Steel Fiber Reinforced Concrete under Multi-axial Loads[J]. *Cem. Concr. Res.*, 2006, 36(7): 1354–1361.
- [22] Kesner K., Billington S.L. Investigation of Infill Panels Made from Engineered Cementitious Composites for Seismic Strengthening and Retrofit [J]. *J. Struct. Eng.*, 2005, 131(11): 1712–1720.
- [23] Cheng A., Huang R., Wu J.K., et al. Influence of GGBS on Durability and Corrosion Behavior of Reinforced Concrete[J]. *Mater. Chem. Phys.*, 2005, 93(2–3): 404–411.
- [24] Houssam A. Toutanji. Properties of polypropylene fiber reinforced silica fume expansive-cement concrete. *Construction and Building Materials*, 1999: 171–177.
- [25] Ma Kunlin, Xie Youjun, Long Guangcheng. Study on Preparation of High Performance Concrete with Imperability to Chloride Ions. *Industrial Construction*, 2006, 11: 90–93.
- [26] Taejun Cho. Prediction of cyclic freeze–thaw damage in concrete structures based on response surface method. *Construction and Building Materials*, 2007: 254–262.
- [27] Bryant Mather. *Concrete Durability*. Cement Concrete Composites, 2004, 26: 3–4.
- [28] Xie Youjun, M.A. Kunlin. Research on the Frost-resistant Capability of Concrete in Different Solutions. *Journal of Railway Science and Engineering*, 2006, 8: 29–34.
- [29] Gustafsson M.E.R., Franzén L.G. Dry Deposition and Concentration of Marine Aerosols in a Coastal Area, *Atmos Environ*, 1996, 30(6): 977–989.
- [30] Mustafa M.A., Yusof K.M. Atmospheric Chloride Penetration into Concrete in semi-tropical marine environment. *Cement Concrete Research*, 1994, 24(4): 661–70.
- [31] Mangat P.S., Khatib J.M., Molloy B.T. Chloride Diffusion and Reinforcement Corrosion in Blended Cement Paste and Concrete. *Cement Concrete Composites*, 1994, 16: 73–81.

Reliability analysis of slope based on quantified Hoek-Brown strength criterion

Hao Wu & Xing Chao Lin

China Institute of Water Resources and Hydropower Research, Beijing, China

Jian Gang Du & Jia Cheng Xu

China International Engineering Consulting Corporation, Beijing, China

ABSTRACT: Based on a database of water conservancy and hydropower slope established by IWHR, quantitative scoring RMR system as a bridge, GSI achieve quantified targets. According to Hoek-Brown strength criterion, Monte Carlo method simulation, statistical get rock shear strength parameters mean and standard deviation. Rock shear strength characteristics of the obtained values for slope reliability analysis is a useful supplement to slope safety factor method, a combination that can project a comprehensive evaluation of the slope.

Keywords: quantified GSI; RMR; Hoek-Brown criterion; rock shear strength; reliability analysis

1 INTRODUCTION

Currently slope stability analysis is the most commonly used deterministic model, a single safety factor as the evaluation index. But parameters have great variability and uncertainty in slope stability analysis, which led to safety factor more than 1 of the slope is still possible landslides. A variety of factors affect slope stability variability can be considered in slope reliability analysis. Slope reliability analysis can serve as a useful complement to the safety factor method, a combination that can make a comprehensive evaluation of the slope.

Key to slope reliability analysis is to determine the parameters of the rock material, slope engineering design mostly used the recommended value, that is a certain empirical and can not give the coefficient of variation of the material. Hoek-Brown strength criterion first proposed in 1980 provides a new way to determine the parameters of rock material, in slope engineering that has been widely used. In 2002 GSI established based on Hoek-Brown strength criterion was amended, confining stress on slope engineering methods for determining the upper limit and the introduction of amendments to the disturbance parameters to better apply in slope engineering. But GSI is a completely qualitative evaluation, GSI variability can not be estimated, to obtain the variability of rock material becomes difficult. Many experts and scholars made a lot of research on the GSI quantify and obtain corresponding results.

China Institute of Water Resources and Hydropower Research, etc established a slope database for

water conservancy and hydropower, that contains a total of 152 slopes and test data. On this basis, the quantitative assessment criteria of RMR system as a bridge to achieve quantified GSI indicators, according to Hoek-Brown strength criterion, draw rock shear strength parameters. The mean and standard deviation of the shear strength obtained by this method can be used for reliability analysis of slope. This paper describes the theoretical and computational steps of the method, reliability analysis carried out on left bank slope of Manwan hydropower engineering, the analysis results is consistent with the actual situation of the project.

2 THEORY & METHODS

2.1 *Quantitative RMR system*

When the GSI system was put forward by Hoek, The original RMR system was not completely abandoned and the transformation relations of the RMR system with GSI system of edition 1989 were also given, such as [Equation \(1\)](#). The RMR system is a scoring system with consideration of rock uniaxial compressive strength of σ_c , structural plane spacing SP, rock mass quality indicator RQD. So based on the database of IWHR, included a large number of experimental data, RMR index of rock is accurately scored, eigenvalues of rock RMR index is derived.

Through a large number of experimental data, the accurate statistical mean and standard deviation of each parameter in the RMR system can be accessed. Using the RMR system as a bridge,

the mean and standard deviation of the GSI system are also obtained. According to the above and based on the Hoek-Brown criterion, the eigenvalue of the rock shear strength can be get as follows.

$$GSI = RMR_{1989} - 5 \quad (1)$$

The RMR rating scale given by Hoek-Brown criterion published in 1989 provided guidelines for how to score rock mass on the basis of eigenvalues of each parameter (Such as rock uniaxial compressive strength and rock mass quality indicator RQD, etc). But it brings certain difficulty to score because of all the indexes in the table are given in the form of discrete data. Therefore, in order to get the accurate scoring and statistical eigenvalue according to the test results, it's needed to apply cubic spline interpolation to the discrete data in classification tables, namely, to establish the continuous function relationship between eigenvalues and score. Based on the theory of the two ranks quadrature, the statistical characteristics of each classification index can be get.

The function relations between score of rock mass quality and rock uniaxial compressive strength of σ_c , structural plane spacing SP, rock mass quality indicator RQD are shown as Equation (2)–(4).

$$f(\sigma_c) = \begin{cases} 0(x < 1) \\ -6.31E - 06x^3 + 5.11E - 04x^2 + 7.59E - 02x + 0.768(1 \leq x < 37.5) \\ -1.11E - 07x^3 - 1.86E - 04x^2 + 0.102x + 0.441(37.5 \leq x \leq 250) \\ 15(x > 250) \end{cases} \quad (2)$$

$$f(RQD) = \begin{cases} -4.30E - 06y^3 + 4.84E - 04y^2 + 0.185y + 0.626(0 \leq y < 62.5) \\ 2.96E - 05y^3 - 5.07E - 03y^2 + 0.582y - 7.651(62.5 \leq y < 82.5) \\ 2.96E - 05y^3 - 6.32E - 03y^2 + 0.643y - 10.714(82.5 \leq y \leq 100) \end{cases} \quad (3)$$

$$f(SP) = \begin{cases} 1.06E - 04z^3 - 1.20E - 02z^2 + 0.469z + 3.697(0 \leq z < 40) \\ -2.22E - 06z^3 + 9.2E - 04z^2 - 4.82E - 02z + 10.598(40 \leq z < 130) \\ -2.22E - 06z^3 + 9.2E - 04z^2 - 4.84E - 02z + 10.607(130 \leq z \leq 200) \\ 20(z > 200) \end{cases} \quad (4)$$

The relationship between rock mass quality indicator and each parameter in the RMR system is linear shown as Equation (5). The mean value u_{RMR} and standard deviation σ_{RMR} are shown as

Equation (6)–(7), based on the theory of the two ranks quadrature.

$$RMR = f(\sigma_c) + f(SP) + f(RQD) + C \quad (5)$$

$$u_{RMR} = f(u_{\sigma_c}) + f(u_{SP}) + f(u_{RQD}) + C \quad (6)$$

$$\sigma_{RMR} = \zeta \sqrt{(f'(u_{\sigma_c})\sigma_{\sigma_c})^2 + (f'(u_{SP})\sigma_{SP})^2 + (f'(u_{RQD})\sigma_{RQD})^2} \quad (7)$$

Above, f' is a derivative of function, u is the average corresponding indexes, σ is the standard deviation of corresponding indicators. ζ is a constant, it is mainly used for considering the impact on the classification index standard deviation in the RMR system caused by uncertain factors such as groundwater, joint conditions.

2.2 GSI quantification

By Equation (1), GSI and RMR is a linear relationship. So u_{GSI} —the mean value and σ_{GSI} —the standard deviation of the GSI system, shown as Equation (8)–(9).

$$u_{GSI} = u_{RMR} - 5 \quad (8)$$

$$\sigma_{GSI} = \sigma_{RMR} \quad (9)$$

2.3 Rock shear strength index

GSI indicators have been quantified by RMR system, gives the eigenvalues of GSI indicators—mean and standard deviation. Monte Carlo method simulate a set of GSI values. Based on Hoek-Brown strength criterion, a set of rock shear strength can be obtained, statistics gives the eigenvalues.

3 ENGINEERING APPLICATION

3.1 Background of engineering

Manwan is built on the Lancang River in Yunnan Province's first large-scale cascade hydropower stations. Type of gravity is dam, the largest dam height is 132 m, crest length is 418 m, the total installed capacity of 1.5 million kilowatts. Due to the structure of the left bank of downslope side development, during excavation, cut off a large range longitudinal structural plane, which happened several times landslide. Maximum landslide total is about 106,000 m³, thickness is about 10 m, width is 70–80 m, height is 112 m. Therefore, the slope reliability of Manwan hydropower left bank was studied.

3.2 Determine the material parameters

In the investigation stages Manwan hydropower station for the study and classification of rock mass,

conducted shear deformation and other groups inside and outside surface of the test as well as structural survey, geological exploration drilling RQD statistical work, and has done 71 group uniaxial compressive strength test, and 13 adit 249 sampling group (total 1145 rock samples), taken within 11 drill core samples were 373 point load strength test.

Based on the above information on a large number of tests on the uniaxial compressive strength σ_c , structure spacing SP and rock mass quality indicators RQD were collated and statistics, most of the indicators normally distributed, each index eigenvalues statistical results shown in Table 1.

According to Table 1 Test statistics, By the Equation (2) to (7) RMR rating eigenvalues is derived. By the Equation (8) and (9) GSI score eigenvalues is Derived Scores shown in Table 2.

The use of Monte Carlo method simulation, based on Hoek-Brown strength criterion for shear strength parameters were statistically different from the weathered zone, as shown in Table 3.

Table 1. Statistical test results.

Weathered zone	Strongly			Weakly			Slightly		
σ_c (Mpa)									
Mean	25.00			40.90			49.10		
Standard deviation	6.00			8.18			9.82		
RQD (%)									
Mean	30.20			35.70			41.50		
Standard deviation	7.25			1.66			1.77		
SP (cm)									
Mean	10.60			8.10			13.40		
Standard deviation	2.26			0.91			2.89		

Table 2. Rock mass classification scores.

Weathered zone	Strongly			Weakly			Slightly		
σ_c									
Mean	2.89			4.3			4.99		
Standard deviation	0.537			0.631			0.723		
RQD									
Mean	6.52			7.64			8.81		
Standard deviation	1.464			0.336			0.339		
SP									
Mean	7.42			6.72			8.08		
Standard deviation	0.588			0.271			0.232		
Jointed conditions	4			9			9		
Groundwater	15			15			15		
Total (RMR)									
Mean	35.83			42.66			45.88		
Standard deviation	5			2.294			2.495		
GSI									
Mean	30.83			37.66			40.88		
Standard deviation	5			2.294			2.495		

* $\zeta = 3$, in the engineering.

3.3 Slope reliability analysis

It conducted a slope stability analysis for Manwan hydropower station left bank landslide area that has occurred, typical sections as shown in Figure 1.

We use Sarma method to calculate the slope safety factor, shear strength parameters as shown in Table 3. Rosenblueth method is a method of calculating the reliability based only on the mean and standard deviation of random variables, calculated model shown in Figure 2, safety factor and reliability index as shown in Table 4.

Know from Table 4, the safety factor of typical cross-sections is slightly larger than 1, slope is in a critical state that may be landslide occurred. Reliable indicator of typical cross-sections is a lot worse than reliable indicator 3.7 of grade II structure set by normative standards (GB50199-94, China), landslide has great possibilities. The results is consistent with the actual situation of the project.

Table 3. Shear strength parameters of rock.

Weathered zone	c (Mpa)		Φ (°)	
	Mean	Standard deviation	Mean	Standard deviation
Strongly weathered	0.073	0.015	31.55	3.66
Weakly weathered	0.114	0.010	39.95	1.53
Slightly weathered	0.138	0.004	43.41	0.56

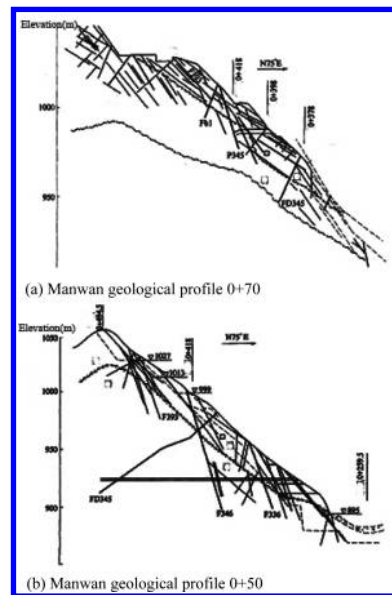


Figure 1. Manwan landslide typical geological profile.

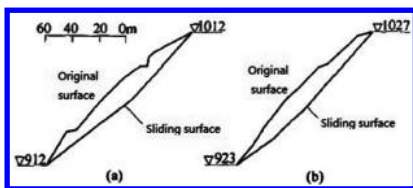


Figure 2. Model.

Table 4. typical cross-sections safety evaluation.

Typical cross-sections	(a)	(b)
Safety factor	1.14	1.04
Reliable indicator	2.11	1.50

4 CONCLUSION

(1) In the slope stability analysis, the safety factor method does not consider the variability and uncertainty of the parameters. Slope reliability analysis considers a variety of factors affect slope stability variability, can serve as a useful complement to the safety factor method, the rock material parameter is a key in slope reliability analysis. GSI established based on Hoek-Brown strength criterion to determine the shear strength parameters of rock slope engineering methods in a wide range of applications.

(2) GSI system is a qualitative scoring system, GSI score difficult during use. China Institute of Water Resources and Hydropower Research has established a slope database of water conservancy and hydropower, based on the quantitative score of RMR system as a bridge to achieve quantified targets for GSI. According to Hoek-Brown strength criterion, Monte Carlo method simulation, the results mean and standard statistical difference in shear strength parameters of rock can be get.

(3) The GSI quantitative methods described herein in Manwan application, to evaluate its left bank slope reliability evaluation result is consistent with the engineering practice. This GSI quantify get rock strength parameters is feasible in the reliability analysis of slope engineering.

ACKNOWLEDGEMENTS

The paper is the final product with founding from the National Basic Research Program of China (973 Program: 2013CB036405). And the authors would like to thank IWHR, that provides engineering data.

REFERENCES

- Chen Zuyu. 2003. *Soil Slope Stability Analysis-Theory Methods and Programs*. Beijing: China WaterPower Press.
- Chen Zuyu et al. 2005. *Rock Slope Stability Analysis-Theory Methods and Programs*. Beijing: China WaterPower Press.
- Hoek, E. & Brown, E.T. 1980. Empirical strength criterion for rock masses. *Journal of Geotechnical and Geoenvironmental Engineering* 106(9): 1013–1035.
- Hoek, E. et al. Hoek-Brown failure criterion-2002 edition. In Hammah, R. (eds), *Proceedings of the North American Rock Mechanics Society NARMS-TAC 2002*. Toronto: University of Toronto Press.
- Hoek, E. et al. 1995. *Support of underground excavations in hard rock*. Rotterdam: A.A. Balkema.
- Hoek, E. & Brown, E.T. 1988. The Hoek-Brown criterion-a 1988 update. In Curran, J.C. (ed.), *Proceedings of the 15th Canada Rock Mechanics Symposium, 1988*. Toronto: University of Toronto.
- Hu Shengming & Hu Xiuwen. 2011. Estimation of rock mass parameters based on quantitative GSI system and Hoek-Brown criterion. *Rock and Soil Mechanics* 32(3): 861–866.
- Lin Daming et al. 2013. Research on parameters of Hoek-Brown criterion and application based on core classification. *Chinese Journal of Rock Mechanics and Engineering* 32(1): 143–149.
- Lu Wenqiang & Gong Jue. 2003. Application of Rosenblueth Moment Estimation Method into Probabilistic Analysis of Slope Stability. *Chinese Journal of Rock Mechanics and Engineering* 22(2): 232–235.
- Sonmez, H. & Ulusay, R. 1999. Modifications to the geological strength index(GSI) and their applicability to stability of slopes. *International Journal of Rock Mechanics and Mining Sciences* 36(6): 743–760.
- Sun Jinshan & Lu Wenbo. 2008. Modification of Hoek-Brown criterion and its application. *Engineering Journal of Wuhan University* 41(1): 63–66.
- Su Yonghua et al. 2009. Quantification of elements for geological strength index in Hoek-Brown criterion. *Chinese Journal of Rock Mechanics and Engineering* 28(4): 679–686.
- Song Yanhui & Ju Guanghong. 2012. Determination of rock mass shear strength based on in-situ tests and codes and comparison with estimation by Hoek-Brown criterion. *Chinese Journal of Rock Mechanics and Engineering* 31(5): 1000–1006.
- Wu Zhenjun et al. 2010. A new optimization approach for slope reliability analysis. *Rock and Soil Mechanics* 31(3): 713–718.
- Wu Debin & Xu Weiya. 2005. Hoek-Brown criterion-based study on mechanical parameters of excavated slope rock masses. *Journal of Hohai University: Natural Sciences* 33(1): 89–93.
- Xia Kaizong et al. 2013. Estimation of rock mass mechanical parameters based on ultrasonic velocity of rock mass and Hoek-Brown criterion and its application to engineering. *Chinese Journal of Rock Mechanics and Engineering* 32(7): 1458–1466.
- Yao Zeliang et al. 2005. Simple and Quadratic of the Two Ranks Quadrature of the Structure Reliability. *Journal of Northwest Hydroelectric Power* 21(3): 20–23.

Simulation of the superelasticity of Shape Memory Alloys by MATLAB programming

Yu Hong Ling, Ye Ming Huang, Hong Wei Ma & Gan Liang Guo
 South China University of Technology, Guangzhou, China

Yun Ze Wu
 HuaYi Designing Consultant Ltd., Shenzhen, China

ABSTRACT: The Brinson constitutive model can accurately describe the super elastic effect of Shape Memory Alloys (SMAs) by dividing the internal variable, martensite fraction, into stress induced part and temperature induced part. To simulate mechanical behavior of superelastic SMAs under strain load cycle, the MATLAB programming method is introduced. The programming results based on the Brinson model are compared with both the test results and numerical simulation results based on the Auricchio model at ANSYS environment. They agree well and this indicates that the proposed programming method offers an alternative numerical simulation tools for SMA materials.

Keywords: Shape Memory Alloy; constitutive model; numerical simulation

1 INTRODUCTION

Shape Memory Alloys (SMAs) are a class of metal with excellent characteristics including the shape memory effect, super elastic effect, high damping, and good corrosion resistance, therefore, SMAs find many applications in structural vibration control fields.

Many experimental studies on SMAs have been conducted, and many types of constitutive models of SMAs were presented based on experimental results.

The constitutive models are classified as: based on thermodynamic and free energy type (Falk 1980, Falk 1983), based on mathematical constitutive model type (Abeyartane & Knowles 1991, Abeyartane & Knowles 1993), based on thermodynamics and thermal dynamics type (Brinson 1993, Auricchio and Taylor 1997), based on mesomechanics model type (Patoor, Eberhardt et al. 1993, Patoor and Eberhardt 1996).

The Brinson constitutive model can accurately describe the super elastic effect of Shape Memory Alloys (SMAs) by dividing the internal variable, martensite fraction, into stress induced part and temperature induced part. The formulas for the Brinson model are complex, and they are difficult to be applied for theoretical analysis since these formulas just have numerical solution without analytical solution. To figure out the stress values for a given strain load cycle, the programming method at MATLAB environment is introduced based on

the Brinson model in this paper. The difficulty in the constitutive model is how to solve the implicit cosine-type transcendental equation.

2 SIMULATION OF SUPERELASTICITY BY MATLAB PROGRAMMING

2.1 The Brinson model

The Brinson Constitutive model (Brinson 1993) based on the concept of free energy driving force can avoid the problem of measuring parameters. It defined the parameters to apply for engineering calculation. Because the form of model is simple, it is widely been applied. For the constant temperature $T \equiv T_0$, simplified equations are as follows:

$$\sigma_i - \sigma_0 = D(\xi_i)(\varepsilon_i - \varepsilon_0) + \Omega(\xi_i)(\xi_i - \xi_0) \quad (1)$$

$$D(\xi_i) = D_A + \xi_i(D_M - D_A) \quad (2)$$

$$\Omega(\xi_i) = -\varepsilon_L D(\xi_i) \quad (3)$$

$$\xi_i = \frac{1}{2} \cos \left\{ \frac{\pi}{\sigma_s^{cr} - \sigma_f^{cr}} \left[\sigma_i - \sigma_f^{cr} - c_M(T - M_s) \right] \right\} + \frac{1}{2} \quad (4)$$

$$\xi_i = \frac{\xi_0}{2} \left[\cos \left(\pi \frac{c_A T - c_A A_s - \sigma_i}{c_A A_f - c_A A_s} \right) + 1 \right] \quad (5)$$

where D_A and D_M is the elastic modulus of fully austenitic and martensitic respectively; A_s and A_f is

the starting and finishing temperature of austenite respectively; M_s and M_f is the starting and finishing temperature of martensitic respectively; C_m and C_a is the slope of martensite and reverse martensite phase transformation respectively; ε_L is the largest recoverable strain of materials respectively; σ_s^{cr} and σ_f^{cr} is the starting and finishing stress limit of martensitic respectively; T is the temperature; σ_i is the stress and σ_0 is the starting stress; ξ_i is the intermediate variable.

The drive installed on the energy dissipation device in the internal structure can reduce adverse effect from earthquake or wind to structure. Therefore, in the simulation, strain is determined as independent variable and stress is determined as dependent variable.

The implicit cosine-type transcendental Equation 6 and 7 about unknown quantity σ_i can be fixed through variable substitution:

$$\sigma_i - \left\{ D_A + \frac{\xi_0}{2} \left[\cos \left(\pi \frac{c_A T - c_A A_s - \sigma_i}{c_A A_f - c_A A_s} \right) + 1 \right] \cdot (D_M - D_A) \right\} \cdot \left\{ \varepsilon_i - \varepsilon_L \cdot \frac{\xi_0}{2} \cdot \left[\cos \left(\pi \frac{c_A T - c_A A_s - \sigma_i}{c_A A_f - c_A A_s} \right) + 1 \right] \right\} = 0 \quad (6)$$

$$\sigma_i - \left\{ D_A + \left[\frac{1 - \xi_0}{2} \cos \left\{ \frac{\pi \cdot [\sigma_i - \sigma_f^{cr} - c_M (T - M_s)]}{\sigma_s^{cr} - \sigma_f^{cr}} \right\} + \frac{1 + \xi_0}{2} \right] \cdot (D_M - D_A) \right\} \cdot \left\{ \varepsilon_i - \varepsilon_L \cdot \left[\frac{1 - \xi_0}{2} \cos \left\{ \frac{\pi \cdot [\sigma_i - \sigma_f^{cr} - c_M (T - M_s)]}{\sigma_s^{cr} - \sigma_f^{cr}} \right\} + \frac{1 + \xi_0}{2} \right] \right\} = 0 \quad (7)$$

For every giving strain value, Stress value can be solved by transcendental Equation 6 or 7. The martensite value, the modulus of elasticity and the transformation modulus can be solved through equations. As a result, all unknown quantities in equations can be found.

2.2 Programming in MATLAB environment

The Brinson Constitutive model was simulated accurately by MATLAB. Flow chart of MATLAB is shown in Figure 1. The main difficulty in program is to solve transcendental Equation 6 and 7. Usually, the zero function in MATLAB is to solve equations about nonlinear including transcendental

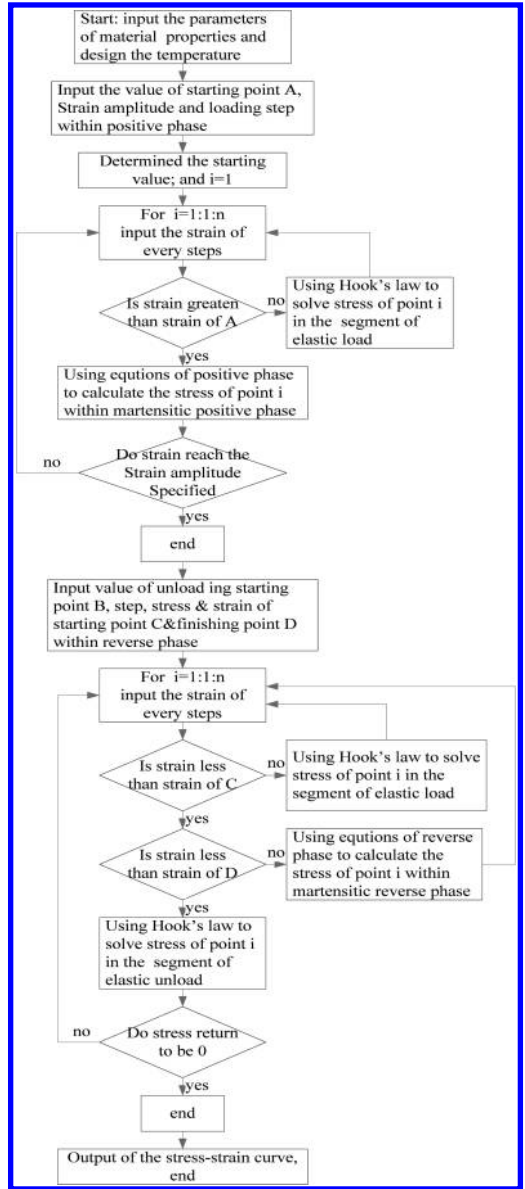


Figure 1. Flow chart of MATLAB.

equations. Action of the function is to find zero of function for unknown quantity.

Taking reverse transformation transcendental Equation 6 for example, the equation curve in the stress range $[0, 800]$ was drawn, and it corresponded different unloaded starting point. As shown in Figure 2, it is easy to know basic characteristic of the transcendental equation.

The curve shows that the greater strain amplitude, the more obvious the peak point of the curve.

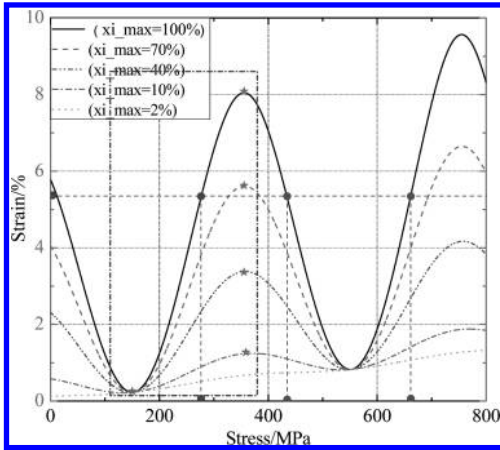


Figure 2. Transcendental equation curves of reverse phase.

Assuming the first derivative of the transcendental Equation 6 as zero, the stagnation point of the curve can be found. In reality, the curve of the transcendental equation will lose the peak point when the strain amplitude is less than 1%. But the curve is the wave shape curve, and it should have inflection point through mathematical proof.

Therefore, when the second derivative is zero, the inflection point of transcendental Equation 6 can be found. As shown in Figure 3, the stress range segment endpoint may be the average stress gotten by two inflection point beside peak point. The diamond marked points are peak points; the circle marked points are inflection points; the star marked points are the average stress points in the Figure 3. So the stress-strain relationship curve about reverse transformation can be gotten, and Brinson Constitutive model relationship curve also can be gotten.

2.3 Simulation results

After a series of procedural improvement and repeated calculation, Brinson Constitutive model relationship curve about different Strain amplitude can be gotten by MATLAB, as shown in Figure 4.

When the program calculates, it needs 12 material parameters. It contains the elastic modulus of fully austenitic and martensitic D_A and D_M , the starting and finishing temperature of austenite A_s and A_f , the starting and finishing temperature of martensitic M_s and M_f , the slope of martensite and reverse martensite phase transformation C_m and C_a , the largest recoverable strain of materials ϵ_L , the starting and finishing stress limit of martensitic σ_s^{cr} and σ_f^{cr} , the temperature T .

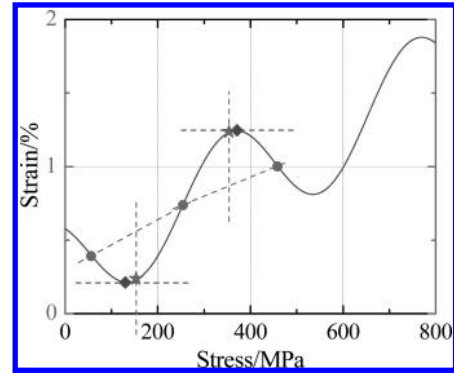


Figure 3. Solution for peak point of transcendental equation.

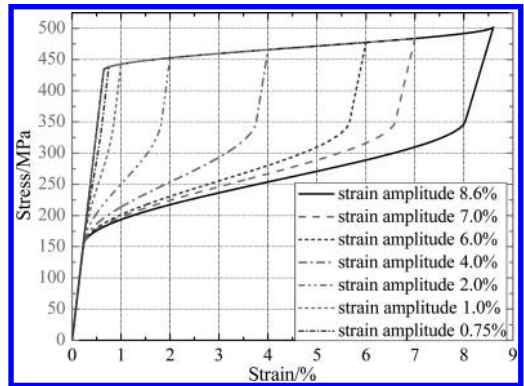


Figure 4. Brinson constitutive model curves in strain amplitude.

3 SIMULATION OF SUPERELASTICITY IN ANSYS ENVIRONMENT

3.1 The Auricchio model

In ANSYS, the deformation of finite element model and constitutive model of material are needed to calculate by ANSYS. The constitutive model of material is needed to input by clients. The simulation to SMA by ANSYS was based on Auricchio model (Auricchio & Taylor 1997, Auricchio & Taylor 1997), and it considers transformation from austenitic to martensitic (A→S), martensitic to austenitic (S→A) and martensitic to martensitic (S→S). It described properties of super elastic and single, two-way shape memory. The model calculated by ANSYS defined three transformation areas. Those are the elastic area, positive phase area and reverse phase area shown in Figure 5.

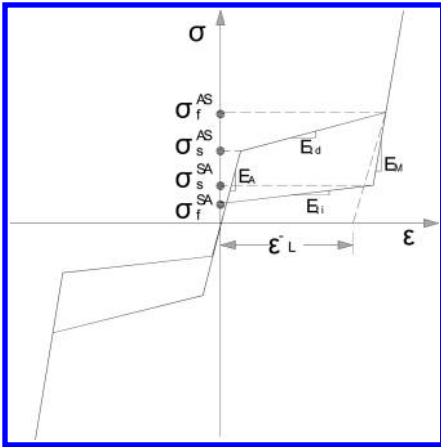


Figure 5. SMA constitutive model in ANSYS.

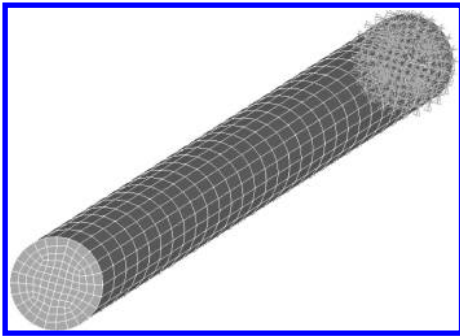


Figure 6. Grid division of model in ANSYS.

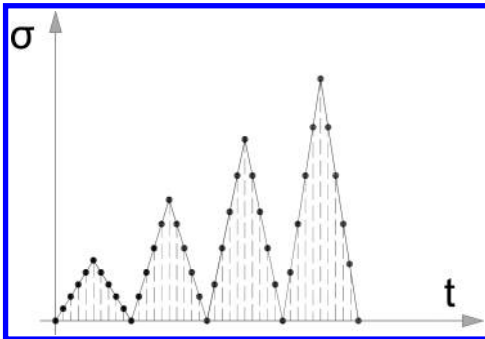


Figure 7. Loading procedure.

Every subcycles load or unload all simplify as elastic loop. The line between σ_s^{AS} and σ_f^{AS} is reverse phase area. Every operational rules used by subcycles are simplified from constitutive model equations of SMA.

For the mixed deformation, ANSYS calculates every deformation and contributes all to the total deformation.

The properties of material are defined by 7 parameters specified as follows: C_1 is the starting stress of positive phase σ_s^{AS} ; C_2 is the finishing stress of positive phase σ_f^{AS} ; C_3 is the starting stress of reverse phase; C_4 is the finishing stress of reverse phase σ_f^{SA} ; C_5 is the maximum recoverable strain $\bar{\epsilon}_L$; C_6 is the phase rate of material α ; C_7 is the elastic modulus of martensitic E . All of these mentioned above are called phase parameters of SMA.

Models in ANSYS contain unit types of PLANE182, PLANE183, SOLID185, SOLID186, SOLID187 and SOLID190. SOLID186 was used to simulate.

3.2 The simulation in ANSYS environment

Simulation by ANSYS for SMA is used to fulfill simple stretching cycle, and it simulates SMA super elastic characterization in ANSYS. The diameter of SMA section is 1 mm; the length of SMA section is 100 mm. After establishing model, unit SOLID185 can be used to divide unit for material shown as Figure 6. The one end of column model is fixed and another free end is put load to simulate the stretching cycle of material shown as Figure 7.

4 ASSESSMENT ON THE PROGRAMMING RESULTS

The phase parameters are determined as shown in Table 1 based on document (Ling, Y.H. et al. 2010, Peng, H.H. 2010). E_x is the elastic modulus of austenitic. The parameters of Brinson model compiled by MATLAB are shown in Table 2. The simulations of different strain amplitude are shown as Figures 8–10.

Generally, the parameters of simulation and experiment contain lap energy, equivalent secant stiffness and equivalent damping ratio. A stress-strain curve of simple and typical load-unload cycle is shown as Figure 11. The ultimate tensile strength is σ_u , and the residual strain is ϵ_{res} . The maximum phase transition strain loaded is ϵ_f , and

Table 1. The parameters of material phase in ANSYS.

E_x /GPa	C_1 /MPa	C_2 /MPa	C_3 /MPa
48	498	608	343
C_4 /MPa	C_5	C_6 ($m \cdot s^{-1}$)	C_7 /GPa
220	0.067	0	18

Table 2. The parameters of Brinson constitutive model.

Parameters	Value	Parameters	Value
Elastic modulus (MPa)	$D_a = 48000$ $D_m = 18000$	Maximum residual strain	$\epsilon_L = 0.067$
Phase-transition temperature ($^{\circ}\text{C}$)	$M_f = -40.8$ $M_s = -26.8$ $A_s = 5.3$	Critical stress (MPa)	$\sigma_s^{cr} = 80$ $\sigma_f^{cr} = 270$
Conversion factor (MPa/ $^{\circ}\text{C}$)	$A_f = 12$ $C_m = 7.6$ $C_a = 17.2$	Material design temperature ($^{\circ}\text{C}$)	$T = 25$

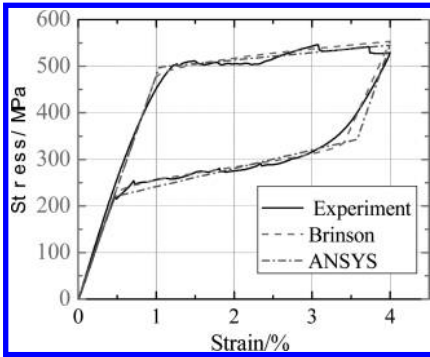


Figure 8. Stress-strain curve with 4% strain amplitude.

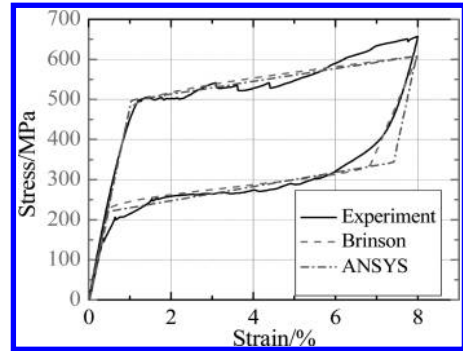


Figure 10. Stress-strain curves with 8% strain amplitude.

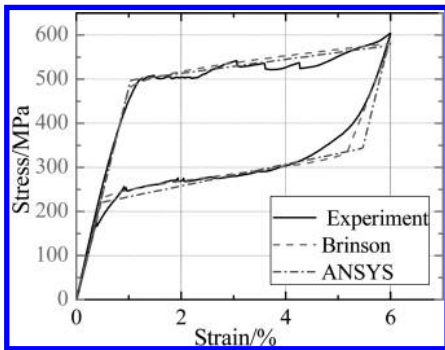


Figure 9. Stress-strain curves with 6% strain amplitude.

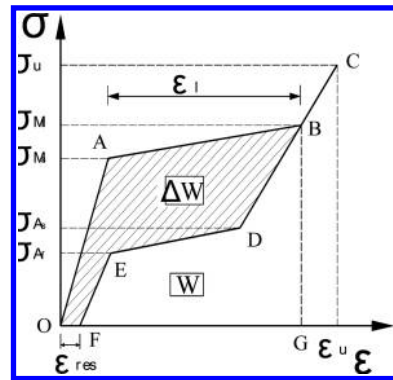


Figure 11. Stress-strain curves of super elastic SMA material.

it is also called the length of the yield platform. The ultimate tensile strain is ϵ_u . ΔW is the total energy loss in a load-unload cycle of super elastic SMA, and its area is enclosed by OABDEF. And W is the total strain energy in a load-unload cycle of super elastic SMA, and its area is enclosed by OABGO. Therefore, the equivalent damping ratio is $\xi_{eq} = \Delta W / (2\pi K \delta^2)$; the equivalent secant stiffness is $K = (F_{max} - F_{min}) / (\delta_{max} - \delta_{min})$.

The displacement amplitude is δ ; the maximum and minimum load are F_{max} and F_{min} ; the maximum and minimum stretching displacement are δ_{max} and δ_{min} .

From Figures 8 to 11, the solutions of simulation are similar with experiment, and it is mentioned above. Two simulation methods can perfectly reflect the super elastic properties of SMA. In order to verify effectiveness, Table 3 shows differ-

Table 3. The contrast between experiment and simulation.

Strain (%)	Results of	Equivalent stiffness (N/mm)	Lap energy dissipation (N/mm)	Equivalent damping ratio
4	Experiment	103.8	521.0	0.0499
	The Brinson model	108.6	527.9	0.048
	ANSYS	107.0	539.6	0.0501
5	Experiment	87.5	688.6	0.050
	The Brinson model	89.1	728.1	0.052
	ANSYS	88.9	734.0	0.053
6	Experiment	79.1	880.1	0.049
	The Brinson model	76.1	938.1	0.054
	ANSYS	76.0	953.5	0.055
7	Experiment	70.9	1110.3	0.051
	The Brinson model	66.7	1150.6	0.056
	ANSYS	66.4	1196.7	0.059
8	Experiment	64.4	1411.1	0.054
	The Brinson model	59.8	1370.4	0.057
	ANSYS	59.9	1428.7	0.059

ence between experiment and simulation. Accuracy of both can demand engineering. The simulation accuracy of little strain amplitude is better than the large. With the increase of strain amplitude, the fluctuation of stress platform of material positive phase will be obvious. And the end of curve is convex. However, the fluctuation of stress platform of material reverse phase is unobvious. The accuracy of Brinson simulation is better than ANSYS simulation. As a result, the program compiled by MATLAB can describe for super elastic properties of SMA.

5 CONCLUSION

This paper introduces accurate and simulation programming methods based on the Brinson constitutive model in MATLAB environment. The finite models of SMAs were set up in ANSYS environment. The numerical results of superelastic SMAs based on the Auricchio model at ANSYS are figured out. The programming results based on the Brinson model are compared with both the test results and numerical simulation results based on the Auricchio model at ANSYS environment. They agree well. This shows that the MATLAB programming based on the Brinson constitutive model can more accurately describe the superelastic and shape memory properties of SMA.

REFERENCES

- Abeyartane, R. & Knowles, J. 1991. Kinetic relations and propagation of phase boundaries in solids. *Arch Rational Mechanics* 114(2): 119–154.
- Abeyartane, R. & Knowles, J. 1993. A continuum model of a thermoelastic solid capable of undergoing phase transitions. *Journal of Mechanics and Physical Solids* 41(3): 541–571.
- Auricchio, F. & Taylor, R.L. 1997. Shape memory alloys: modeling and numerical simulations of the finite strain superelastic behavior. *Computer Methods in Applied Mechanics and Engineering* 143(1–2): 175–194.
- Brinson, L.C. 1993. One-Dimensional Constitutive Behavior of Shape Memory Alloys: Thermomechanical Derivation with Non-Constant Material Functions and Redefined Martensite Internal Variable. *Journal of Intelligent Material Systems and Structures* 4(2): 229–242.
- Falk, F. 1980. Model free energy, mechanics, and thermodynamics of shape memory alloys. *Acta Metallurgical* 28(12): 1773–1780.
- Falk, F. 1983. One-dimensional model of shape memory alloys. *Arch Mechanics* 35(1): 63–84.
- Patoor, E. & Eberhardt, A. 1996. Micromechanical modeling of superelasticity in shape memory alloys. *J Phys IV* 1(6): 277–292.
- Patoor, E., Eberhardt, A. & Berveiller, M. 1993. Micro-mechanical modeling of superelasticity in shape memory alloys. *Arch Mech* 296: 38–54.
- Ling, Y.H., Peng, H.H. & Zhang, S. 2010. Effect of Several Evaluation Metric on Inbalance Data Learning. *Journal of South China University of Technology* 38(4): 131–135.
- Ling, Y.H., Peng, H.H. & Zhang, S. 2011. A Novel SMA Damper and Its Vibration Reduction Performance. *Journal of South China University of Technology* 39(6): 119–124.

Planning of slow traffic system from top-down perspective: Case study of Ersha Island

Juan Yu Wu

*State Key Lab of Subtropical Building Science, Guangzhou Key Lab of Landscape Architecture,
School of Architecture, South China University of Technology, Guangzhou, Guangdong Province, China*

Zi Yang Zeng

School of Architecture, South China University of Technology, Guangzhou, Guangdong Province, China

ABSTRACT: The motorization of urban transportation makes the urban human space which consists of slow traffic gradually transforms into segmented car space which is departed by the road network. However, with the growing attention from all over the world, the slow traffic system is becoming emphasized these years. Development of slow traffic system in China has also achieved some results. In order to seek, analyze and research the problems of the slow traffic system, the thesis focuses on studying the theoretical information of slow traffic system, as well as surveying the slow traffic system of Ersha Island in Guangzhou. And this paper tries to explore suitable planning strategies for the slow traffic system combining greenway in the central part of Guangzhou from the macroscopic angle to the microcosmic angle.

Keywords: slow traffic system; greenway; Ersha Island; problems; planning strategies; macroscopic angle to microcosmic angle

1 INTRODUCTION

Urban slow traffic system acts an important part in urban transportation system. In a broad sense, it is a transportation mode which takes human as main body of transportation mobility and its travel speed is no more than 15 km per hour. In a narrow sense, it is a transportation mode for pedestrian and bicycle.

Slow traffic is a basic trip mode for travel. Under the promoting of the globally sustainable development ideas, the slow low carbon traffic is being emphasized, while the motorized transportation is being reviewed. Specifically, considerable countries start promoting the comprehensive transportation strategy which aims to encourage the slow traffic and control the motor vehicle. In recent years in China, lots of metropolises have started structuring slow traffic system and some are representative. Therefore, by surveying the slow traffic in Ersha Island in Guangzhou, the thesis aims to exploring the planning methods and strategies to optimize the slow traffic system to a more systematic and orderly one.

2 PLANNING CONCEPT OF SLOW TRAFFIC SYSTEM

The slow traffic system in modern city emphasizes the coexistence between the motor vehicle and

non-motor vehicle. It is predictable that the future goal is to structure a diversified and harmonious transportation system including slow traffic system. One of the most important factors in planning slow traffic system is to regard slow travelers as the main body, and to protect their right-of-way. Consequently, the main core idea of slow traffic planning is humanization and detailed designs.

Some foreign countries such as Holland, Denmark, America etc. have high level of importance on slow traffic. Moreover, they have developed relatively mature slow traffic system whether the overall planning or the details designing. The planning of slow transportation in Amsterdam, Copenhagen, Portland, and Chicago are successful cases. From the macro scope, the government establishes policies and regulations to help and support the slow traffic development. From the micro scope, the planners focus on the implementation of the slow lanes, such as the classification of bikeways and the design of crossing facilities. Holland can be a representative example to illustrate such process. Since the oil crisis in the 70's of last century, Holland has invested a large amount of money to support bikeway facilities and the slow traffic construction. Such strategies not only help structure and improve the environmental energy saving slow transportation system, but also make slow traffic a better trip mode for local residents.

Gradually, because of great bicycle traffic network and high proportion of trips done by bike, Holland becomes one of the countries which has the most perfect slow traffic system. Such success can't be achieved without the appropriate policies from government and systemic planning from the planner. Such as the overall slow system planning of Delft in 1987, the planners put forward the bikeway hierarchy plan and classified the bikeways into city level, district level, and community level, and they successfully enhanced the quality of the local slow traffic system. But in China, since the reform and opening-up policy in 1970s, considerable problems of city traffic and pollution have erupted because of the blind pursuit to rapid urbanization and motorized transportation. However, in 21st century, citizens have eventually realized the importance of slow traffic. Studies on theories and methods of slow traffic gradually develop at a preliminary stage.

Based on these, by studying the theoretical information of slow traffic system, and surveying the slow traffic system of Ersha Island in Guangzhou, the thesis focuses on seeking, analyzing and researching the problems of the slow traffic system in the site. By these researches, from the macroscopic angle to the microcosmic angle, the thesis continues exploring suitable planning strategies for the slow traffic system combining greenway in the central part of Guangzhou.

3 RESEARCH ON SLOW TRAFFIC SYSTEM IN ERSHA ISLAND, GUANGZHOU

3.1 Study background

The Ersha Island containing huge green spaces locates in the city center of Guangzhou. And it represents the spatial structure which is known as "open green spaces with slow system", and the direction in which the plan of slow traffic in the city center of Guangzhou will follow. However, this mode still has much room to improve. And we explore to put forward a practical planning to improve the existing slow traffic system.

3.2 Study object

The object of the research is the western of Guangzhou Development Park in Ersha Island. The south of the site is Yanyu Road, the north connects Datong road, the west borders the cross of Datong Road and Yanyu Road, and the east closes to Xiaowu Street.

3.3 Study method

The specific methods used for the study are as follows: information consultation, site investigation,

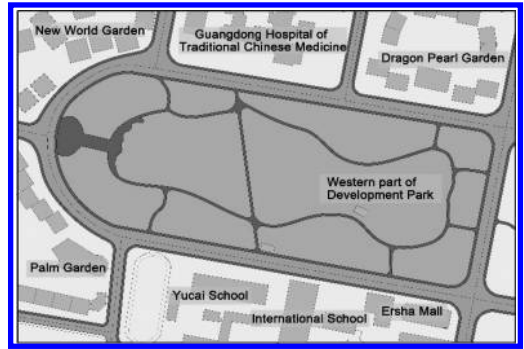


Figure 1. Site plan of Ersha western Development Park.

satellite map analysis, and space tracking note. The research process and analysis are from three perspectives. Firstly, from the macro perspective, we consult the information about the overall plan in the region of which Ersha Island is a part, to study the broader strategies of slow traffic system. Secondly, from the medium perspective, we analyze the satellite map of the site and its surrounding areas, to study the integrity and rationality of slow traffic roads. Finally, by narrowing the study perspective to the site itself, we analyze the details of the slow traffic roads. Through the different methods presented above, the status of the slow traffic system in the site can be analyzed deeply.

3.4 Analysis of the slow traffic system in Ersha Island

As a green space in the city center, there are large amount of citizens here every week. The majority of the users are walkers and cyclists who will certainly use the slow lanes. Through the research on different scales, we find out different kinds of problems about the lanes system.

3.4.1 Macro scale

On the regional level, the site demands a complete slow traffic system. The Development Park, which locates in the core position of the Island, crosses the east-west axis of the Ersha Island and connects the traffic of the east-west part and the north-south part. Majority of the citizens coming to the site are for passing through or commuting. Besides, there are different kinds of public buildings, such as hospital in the north, and two schools, two museums and a concert hall in the south. Therefore, such composite land has great demands for suitable slow traffic system.

3.4.2 Medium scale

By analyzing the site, we found that there are bus stations which need slow lanes to be connected

are located in the both sides of the park. This will create large amount of people who intend to get on or off the bus, and they need safe and convenient slow lanes to get to their destination. However, the roadways bordering the park are the one-way three lanes which is long and wide enough for the motor vehicles to reach the speed of more than 40 km/h. There is no doubt that there are conflicts between the fast traffic and the slow traffic. In order to ensure the walkers and cyclists the right-of-way, planning strategies have to be made to improve slow lanes.

3.4.3 Microcosmic scale

From the microcosmic scale, we found that there aren't enough convenient connections between the slow traffic lanes and the crossing facilities. For instance, the facility helping the walker or the cyclist to cross the road is only the zebra crossing. Actually, compared with Holland, this will bring inconvenience for the slow traffic system.

4 PLANNING ASSUMPTION OF THE SLOW TRAFFIC SYSTEM IN ERSHA ISLAND

The above problems about the slow traffic system in Ersha Development Park are so representative that basically such problems can be found in all the big cities in China. Therefore, exploring ways to solve the problems is meaningful for the improvement of the slow traffic system in China. By summing up the successful slow traffic practices in the foreign cities like Portland, Chicago, and Amsterdam etc., conclusion can be made that overall planning strategies and details construction are contributing factors of their successes. If the planer can draw the merits from these practices and use them in the domestic slow traffic planning, to some extent, the slow traffic can be improved not only in Ersha Island but in Guangzhou. Based on this, with the exploration on strategies about the slow traffic development, we next put forward some planning ideas in both the policy aspect and the construction aspect.

4.1 Suggestions for the policy

4.1.1 Planning strategies

As Holland, America etc., the governments will establish detailed framework for slow traffic system planning. The framework can be shaped in three stages: public opinion collection, route selection of slow traffic network, and detailed subsection planning. The process strives to provide a rational and clear guidance for the slow traffic planning.

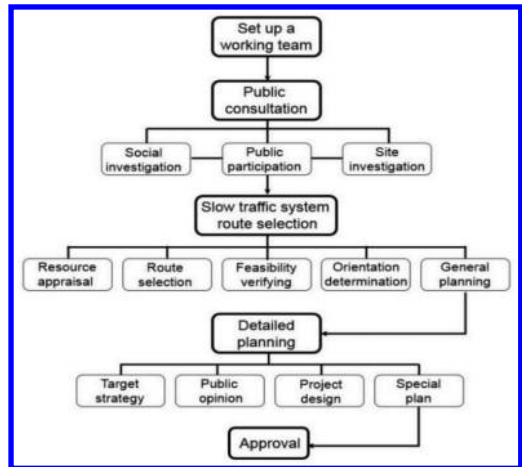


Figure 2. Suggested planning framework.

4.1.2 Transportation strategies

The above context shows that the autos are also a contributing factor influencing the slow traffic system in China. The existing traffic strategies in China concerns more in the motor traffic, while corresponding to guide policies of slow traffic are insufficient. Therefore, the complete guidance of traffic strategies can help improving the slow system. In order to encourage the slow traffic, the planners should properly limit the autos in some area. For instance, in the vehicle traffic aspect, the speed limited regulation can be formulated in the areas like Ersha Island. In addition, the planners can also use specific strategies such as traffic calming, and pedestrian-oriented development etc.

4.2 Suggestions for the construction

4.2.1 Transformation of roads plane

First of all, it is reasonable that the roadways surrounding the park operate one way direction, and it can avoid several intersection conflict points. However, the disadvantage is that the speed of motor vehicle is easy to reach high due to the less traffic conflicts. Therefore, based on these problems, we provide some suggestions of transformation.

Datong Road and Yanyu Road, as the urban subsidiary roads, are the boundary of Development Park and they traverse the Ersha Island. The west side of the roads is Yangjiang east Road, the east connects Guangzhou Avenue. Both of these roads are one-way three lanes. We choose a part of them for the exploration of slow traffic optimizing. There are several problems of the roads: the 1.5 m-width of bicycle lane is narrow, the relationship between roadside parking and bike lanes is improper, and

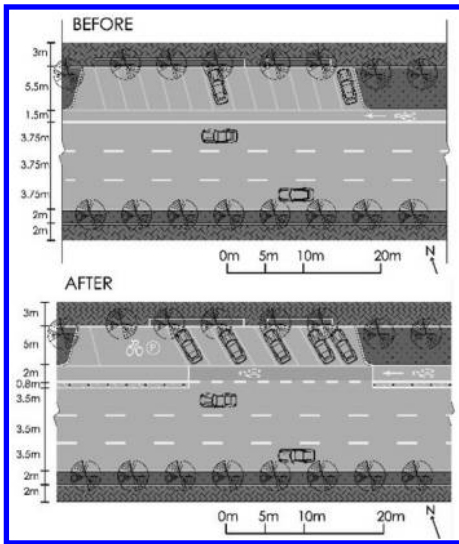


Figure 3. Diagram of transformation of Datong Road.

the safety of cyclists may reduce due to the fast motor vehicles.

Transformation: According to the practices in Portland and Chicago, under the parallel operating of motor vehicles and non-motor vehicles, the isolation belt can be structured to make the slow lane prevent cars from entering the bikeway so that cycle tracks will be safe. Without changing the width of the road, a low barrier can be used as the isolation belt. In addition, pavement in bright color can be used for warning in the area where there are conflicts between parking lots and bike lanes.

Xiaowu Street, is a north-south branch way of the Ersha Island, which segment the green space. Similar to last two roads, there are so wide roadway, while the bikeway is narrow. Moreover, because of lacking the consideration of on-street parking lane, the parked cars has occupied and cut the slow lanes.

Transformation: According to the traffic calming strategy and the practices of the bikeways in Portland, in the branch way level, the position of non-motor vehicles weighs more than autos'. Therefore, one roadway is reduced and an on-street vehicle parking lane is set up. In addition, to enhance the safety and the convenience of the slow lanes, we suggest to widen the bikeway and add the car-deceleration facilities like pedestrian crossing facilities and special pavement.

4.2.2 Transformation of roads section

According to the survey, we refine to the design of road sections, to improve the relations

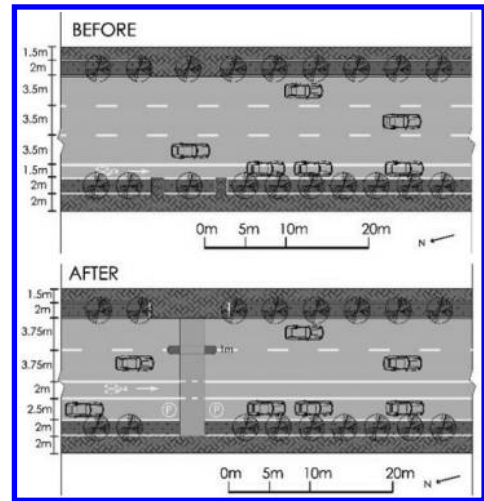


Figure 4. Diagram of transformation of Xiaowu Street.



Figure 5. Section of transformation of Datong Road.

among motor vehicles, non-motor vehicles, pedestrians and road facilities. The sections can be divided into three types: the subsidiary road with barrier, the branch way which motor and non-motor vehicles can share, and the greenway in the park.

The section of subsidiary roads: On the section of Datong Road, between the roadway and the bikeway, the low pillar can be the visual and sensory barrier with which makes the riders feel more comfortable. In addition, there can be parking lots, green belt of bus stops between the bikeway and the sidewalk, just the same as the original.

The section of branch roads: The road mode of roadways with on-street parallel parking in Chicago roadways system can be applied on the Xiaowu Street with high parking demands. Besides, in order to make the walkers and cyclists cross the road more conveniently, facilities of pedestrians twice crossing street should be added in to reduce the speed of autos.

The section of greenways in the park: The practice in San Diego in California is instructive that



Figure 6. Section of transformation of Xiaowu Street.



Figure 7. Section of transformation of greenway.



Figure 8. Transformation of the intersection between Datong Road and Xiaowu Street.

the greenway is wide enough to accommodate the walker and the cyclist standing in parallel. Besides, there should be at least a 3 m vertical safe sight distance, in order to guarantee the safety of the greenway and create a comfortable space effect.

4.2.3 Transformation of intersection

The intersection is the node where there are the most intense conflicts between the slow traffic and the motor traffic. We take the intersection between the Datong Road and the Xiaowu Street as an example, to explore a proper mode which can reduce the conflict for the intersection transformation. Some measures can be applied: One, add a bike box which is formed by pulling the stop line for vehicles back from the intersection and adding a stop line for bicyclists behind the crosswalk for cyclists; two, use the pedestrian

priority zone instead of the existing zebra crossing as the crossing facilities and cover the zone with eye-catching pavement. Such transformation methods can also be used not only on the intersection in this case but on those of one way roadways in other urban road system.

4.2.4 Facilities

Interesting facilities such as leisure chairs, public bicycle rental point, and parking facilities for non-autos will increase the attraction to slow system. Bicycle parking area with leisure and recreational facilities can be set at some distance from each other. And the parking area can distribute near bus stops for the convenient interchange between slow traffic and public transport. Furthermore, following types of spaces can be used for bicycle parking: grey spaces under stereo intersection, green spaces on the street, and the on-street vehicle parking lane etc.

5 CONCLUSION

The urban slow traffic system is so complex that it involves much more than urban transportation system. It includes aspects of urban society, urban geography and urban management. The planning of slow traffic from Guangzhou to China is in its infancy and has a long way to go. However, although there are different levels of problems, the slow traffic system will develop with the optimization from strategies to the details just as the top-down perspective. In the future, the slow traffic will become a sustainable trip mode and make urban transportation more humanized and systematic. According to the analysis of the strategies and ideas of the overall slow traffic planning on macro level, the analysis of the city area on the medium level, and the analysis of specific site on micro level, the thesis merely conducts orientation studies on the planning strategies and the detailed construction, in order to cast a brick to attract jade. Finally, we hope that the study can play a proper reference role for the future planning and construction of urban slow traffic system in China.

ACKNOWLEDGEMENT

This research is supported by National Natural Science Foundation of China (No. 51208204), 2013 Central University Research Grant of South China University of Technology (No: x2jzD213058w), 2012 State Key Lab of Subtropical Building Science Project (No. 2012KB27), 2011 Guangdong Province Ordinary University

Humanities and Social Science Research Project
(No. 11 WYXM006).

REFERENCES

- Amiton David. 2010. *Portland bikeway design best practices*. Portland: Denver Igarta.
- Feng Jianxi, Dijkstra M. & Prillwitz J. 2009. Historical evolution and planning of the Dutch bicycle traffic design. *International Urban Planning* 28: 29–35.
- Pan An. 2006. Path of urban transportation. *Practice of Guangzhou traffic planning*.
- Public Works. 2008. *Bicycle Master Plan California Roseville*. Roseville: Fehr & Peers in association with Alta Planning & Design.
- Xia Tian. 2010. Analysis of design strategy of the urban slow traffic system. *Traffic information and safety* 28: 81–82.
- Yu Wei, Qian Kefeng, Gao Jiang & Qian Jianhua. 2009. Guidelines of slow traffic system planning and design in Hangzhou City. *Urban transportation*.

Analyzing the key chain of railway accident causation based on community detection method

Hui Wen Xin

State Key Laboratory of Rail Traffic Control and Safety, Beijing, P.R. China

Ke Ping Li

State Key Laboratory of Rail Traffic Control and Safety, Beijing, P.R. China
Beijing Laboratory of Urban Rail Transit, Beijing, P.R. China

Hang Fei Huang & Xin Ma

State Key Laboratory of Rail Traffic Control and Safety, Beijing, P.R. China

ABSTRACT: The demand of enhancing the prevention of railway accidents is ever increasing so that the study of railway accident causation becomes important. A number of methods have been proposed to analyze the causation of railway accidents, however, few try to discover implicit relationships between accident factors. This paper innovatively apply the theory of complex network as a tool to analyze the railway accident causation. Based on 2009–2013 rail equipment accident records from FRA, a community detection method called FastNewman is mainly utilized. Several key chains are found by the combination of other measurement from complex network theory. The ultimate relationships extracted can be used for controlling authority to develop rules and regulations.

Keywords: complex network; community structure; railway accident; node strength

1 INTRODUCTION

As a result of technical progress and nowadays' ever increasing demand of efficiency, railway has become an increasingly significant means of transportation. Today's railway meets people's needs of convenience with high speed and frequency, making it a vital necessity to insure railway safety.

For years, researchers have devoted much efforts in understanding how and why accidents occur. An accident was seen by Heinrich (1980) as a consequence of a set of factors which occur in a logic order. Reason (1990) proposed the most influential Swiss cheese model, which views an accident as the consequence of failures at four stages.

Specifically, in railway accident studies, researchers focus on to aspects of analysis of railway accident: one to find the critical factor, or, more generally, to find a set of factors tending to appear together and to play an important role in accidents' happening and the other to find cause chains of accidents, i.e. how an accident forms step by step. In the former aspect, Mirabadi & Sharifian (2010) apply association rules of data mining in Iranian railway accident data and reveals unknown relationships and patterns among them. Wang et al. (2012) adopt grey system theory to analyze railway

accident causes, identifying the primary and secondary factors in different types of incidents. Ma et al. (2013) construct a model based on complex network theory and illustrate it with China's "7.23" railway accident. In the latter way, Kim & Yoon (2013) presents a computer-aided system called CAS-HEAR to find multiple levels of error causes and their casual relations and then evaluate this model with 80 railway accident reports in UK. Wang et al. (2013) establish the accidents influence elements evolution network based on emergency of complex network and system entropy, analyzing the correlation and interaction mechanism of different elements.

2 CONCEPT AND METHOD

2.1 *Community structure of complex network*

Community structure is one of the most important features found in many different real network, including the Internet, biochemical network, social network and so on. When a network has an obvious community structure, it means that this network is composed of several clusters or groups. Each cluster is considered as a "community". The nodes are

found to link to each other tightly by high-density within-group edges and relatively to have sparse links to those in other groups.

2.2 Community detection

The detection of community structure plays an important role in understanding the topological structure and overall function of a network. Two classical theories, Graph Partition from Graph Theory and Hierarchical Clustering from sociology, are applied in many kinds of community detection algorithms.

Kernighan-Lin algorithm, known as KL algorithm, and Spectral Bisection are two classical community detection methods that utilize Graph Partition theory. However, there are defects in both of these algorithms which make them relatively unpractical. For the former, the size of each community must be known before using it (Wang et al. 2006). For the latter, the algorithm can only divide the whole network equally once a time, which means that it must be used repeatedly if the network is supposed to be divided into several communities.

Hierarchical Clustering has two strategies, agglomerative method and divisive method, according to adding or deleting edges from a network. The basic idea of agglomerative method is to calculate the similarities between each node and then to add edges to an empty network, taking similarity as an order. This process can stop at any point. On the contrary, divisive method tries to find node pair which has the lowest similarity and then delete the edge between them. Also, this process can stop at any point. The FastNewman algorithm used in this essay is a kind of agglomerative method.

2.3 FastNewman algorithm

The FastNewman (FN) algorithm proposed by Newman (2004) is relatively a faster one between community detection algorithms based on the theory of modularity. The main process of FN can be described in three steps.

Step 1 Initialize the network to be divided as n communities. It means that each node represents an independent community. The initial value of e_{ij} accords with $e_{ij} = 1/2m$, if there is an edge between node i and node j , in which m is the number of total edges in the network. Otherwise e_{ij} equals to zero. a_i is calculated as $a_i = k_i/2m$ by noting that k_i is the degree of node i .

Step 2 Combine community i and community j successively and calculate the change in Q upon joining two communities.

$$\Delta Q = e_{ij} + e_{ji} - 2a_i a_j = 2(e_{ij} - a_i a_j) \quad (1)$$

According to greedy algorithm, every time the combination should be along the direction in which the maximum or minimum change of Q can be reach. Note that there must be edges between the two communities.

Step 3 Check if all nodes are in one community, if not, go back to step 2. Otherwise the process is completed.

3 COMPLEX NETWORK OF RAILWAY ACCIDENT CAUSATION

Railway accidents can be caused by a wide variety of factors. Generally, more factors than one would cause a railway accident. The rate by which two or more factors tend to occur simultaneous is not irregular or just random if we consider a large number of railway accidents. It implied internal relations between these concurrent factors. These potential connections mentioned above play a significant role in accident prevention.

To construct and analyze the complex network of railway accident causations, we choose to use 1514 records out of 12,200 records from the latest five year's rail equipment accident records of USA's Federal Railroad Administration (FRA). Each of these records includes a primary cause and a contributing cause, which makes it easy to build the causation network.

To make the analysis of the network reasonable, we build the railway accident causations network by following the rules below.

Rule 1 Define each related accident cause as a node in the complex network. There are 254 causes involving in these five-year records. It means that the complex network consist of 254 nodes. FRA classifies all the railway accident causations into five different categories.

Rule 2 The network is constructed on the basis of adjacent matrix. Elements of the matrix stand for the inner connections between these causes. If two causes used to be in the same accident, the element is greater than zero, otherwise zero. Whether there is an edge between two nodes depends on the element related to them. If the element is greater than zero, there is an edge and vice versa.

Rule 3 We define this network as a weighted and undirected graph. The weight of each edge, which is the corresponding element in adjacent matrix, represents the times these two factor appeared in the same accident in the past five years, regardless the order (primary cause or contributing cause).

The railway accident causation network built following principles above is shown in [Figure 1](#).

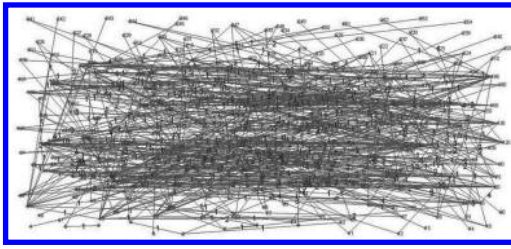


Figure 1. The complex network of railway accident causation.

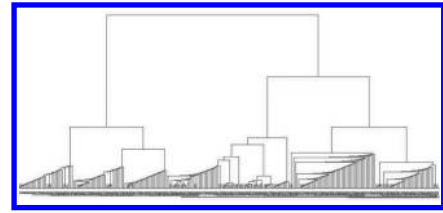


Figure 2. Dendrogram of communities found by FN algorithm in the complex network of railway.

4 ANALYSIS ON RAILWAY ACCIDENT CAUSATION NETWORK BASED ON COMMUNITY DETECTION

4.1 Result of FastNewman algorithm

We utilize the FN algorithm to detect community structure in the complex network of railway accident causation. The dendrogram generated by the algorithm is shown in Figure 2.

The result of the application shows a high peak modularity of $Q = 0.6075$, corresponding to a split into 14 communities. In order to demonstrate clearly in the rest parts of this essay, a list of members in each community is presented in Table 1.

4.2 Key Chain from the Complex network

Table 1 reveals that half of the communities have small sizes which contain less than ten members. In order not to lose the generality, these communities are out of our consideration. It means that we only focus on Community 8 to 14 in our research.

However, in the communities that have larger size than others, not all of their members are equally important. For example, some nodes just have one edge to connect them to other nodes. Obviously, these nodes mentioned are not very important in the network or the community. To identify the most important factors in each community, i.e. members of the key chain, a special measure (Opsahl & Panzarasa 2010) is used as follow.

$$C_D^{w\alpha} = k_i \times \left(\frac{s_i}{k_i} \right)^\alpha = k_i^{(1-\alpha)} \times s_i^\alpha \quad (2)$$

This formula combines the concept of degree (k_i) with node strength (s_i) (Barrat et al. 2004) and add a tuning parameter α . This parameter represents a preference to the number of edges or to the weights. If α is between 0 and 1, the number of

Table 1. The result of community detection in the complex network of railway accident causation by using FN algorithm.

Community number	Member
1	151,245
2	16,206
3	57,58,101,109,148,222
4	14,205
5	38,216
6	39,217
7	153,246
8	127,128,129,130,131,132,203,239,240,241
9	12,46,79,81,82,83,84,85,87,88,89,90,91,92,93,94,95,96,113,218,219,226,228,229,230,231
10	7,8,13,44,45,47,48,50,53,59,66,68,69,71,72,73,80,97,98,99,114,119,137,152,220,227,232,233,237,243
11	43,49,51,52,54,60,61,62,63,64,65,67,74,76,78,103,105,106,107,108,110,111,115,141,142,149,221,223,224,225,234,235,236
12	2,3,5,15,18,19,20,22,23,25,26,100,102,104,118,121,123,124,135,154,155,156,157,158,159,160,161,162,163,164,165,166,167,168,169,172,173,174,176,178,179,180,182,185,187,188,196,199,200,208,247,249
13	1,4,6,9,10,11,28,30,34,37,40,41,42,55,56,75,77,116,117,120,122,125,126,133,134,136,138,140,143,144,145,146,147,170,175,186,202,204,209,210,211,212,213,215,238,242
14	17,21,24,27,29,31,32,33,35,36,70,86,112,150,171,177,181,183,184,189,190,191,192,193,194,195,197,198,201,207,214,244,248,250,251,252,253,254

edges is preferable, while if it is over 1, the weights are favorable. In this research, both the number of edges and the weights have significant influences in the importance of a node. So we set $\alpha = 1$, which means the two parts are equally important and

Table 2. Key chain from communities.

Community number	Key chain
8	127,128,129,131
9	81,94,82,95
10	72,47,45,73,68,98,48,66
11	106,64,64,103,60,61,108,62
12	163,154,158,157,161,164,172,155,18,135, 166,20,169,124,162,247,165
13	117,120,134
14	195,197,31

that makes the measure to have the same form as the node strength.

$$s_i = \sum_j^N w_{ij} \quad (3)$$

Here w_{ij} is the weight of the edge that connects node i to node j .

We consider every community as an independent network and calculate each node's node strength. Finally, we rank the entire members in each community according to the node strength.

Some key factors in each community are more important and the inner connections in these members are closer. So we extract these nodes and show them in Table 2.

The key chains shown in Table 3 are causation which tend to appear simultaneously in railway accidents. The result illustrates that there are repetitive patterns in railway accidents to be discovered. An intervention to one member of them can lead to a series of influences on others. Therefore, rules and regulations should be formulate and modify according to these patterns.

5 CONCLUSIONS

This paper was motivated by the need of discovering implicit relationships between key factors. Although many models of accident causation have been developed to analyze key factors, relatively few of them focused on mining the real existing relationships between them. In this paper, we apply rules of complex network to find these real relationships, considering the capability of revealing features of real networks.

We constructed a complex network based on the latest five year's data from FRA and utilized FN algorithm as a method to detect community structure in the network. Considering both the number and weights of edges as influential elements

to the importance of nodes in each community, a rank according to node strength was established to distinguish key chains from others. Eventually, seven key chains were extracted according to which the supervision should focus on to prevent accidents.

It should be noticed that the relationships we found in this paper were not shown as casual relationships and that the real complex formation mechanism of the relations is still unknown. Also, like other social networks, the railway accident causation network is dynamic, therefore, a dynamic community detection method could be more precise to be used in it. And these two aspects should be our future topics.

ACKNOWLEDGEMENTS

Project supported by the National Natural Science Foundation of China (Grant No. 71271022), and the Research Foundation of State Key Laboratory of Rail Traffic Control and Safety, China (Grant No. RCS2012ZQ001).

REFERENCES

- Barrat, A. et al. 2004. The Architecture of Complex Weighted Networks. *Proceedings of the National Academy of Sciences* 101(11): 3747–3752.
- Heinrich, H.W. et al. 1980. *Industrial Accident Prevention*. New York: McGraw-Hill.
- Kim, D.S. & Yoon, W.C. 2013. An accident causation model for the railway industry: Application of the model to 80 rail accident investigation reports from the UK. *Safety Science* 60: 57–68.
- Ma, X. et al. 2013. Analyzing the causation of a railway accident based on a complex network. *China Physics B* 23: 028904.
- Mirabadi, A. & Sharifan, S. 2010. Application of association rules in Iranian Railways (RAI) accident data analysis. *Safety Science* 48: 1427–1435.
- Newman, M.E.J. 2004. Fast Algorithm for Detecting Community Structure in Networks. *Physical Review E* 69: 066133.
- Opsahl, T. & Panzarasa, P. 2010. Node Centrality in Weighted Networks: Generalizing Degree and Short Paths. *Social Networks* 32: 245–251.
- Reason, J. 1990. *Human Error*. New York: Cambridge University Press.
- USA Department of Transportation Federal Railroad Administration. <<http://www.fra.dot.gov/Page/P0001>>.
- Wang, X.F. et al. 2006. *Theory and Application of Complex Network*. Beijing: Tsinghua University Press.
- Wang, Y.L. et al. 2013. Safety Assessment Method Application for Urban Rail Transit Operation Based on Entropy and Emergence. *Journal of the China Railway Society*. 35(4): 1–9.
- Wang, Z. et al. 2012. Analysis of Railway Accident Causes and Risk. *China Safety Science Journal*. 22(6): 79–85.

The investigation of financing models of Chinese highway

Dong Fu, Bin Tang & Liang Xie

Wuhan University of Science and Technology, Wuhan, Hubei, China

ABSTRACT: Highway is the important national infrastructure. The lack of construction funds is an important factor restricting the development of Chinese highway. This article has deeply discussed the present status and problems of the financing of Chinese highway, suggests that perfect the highway management system, improve the highway financing environment, optimize the highway financing structure, so that we can attract more capitals to enter the market of Chinese highway by diversified, multi-channel and innovative financing, promoting the faster and better development of Chinese highway.

Keywords: financing; models; highway

1 INTRODUCTION

The highway is an important symbol of the modern transportation. Highway will lead and promote the development of the regional economy along the routes, shows its huge economic and social benefits. The financing models and structure based on national financial allocations and bank loans can no longer meet the needs of funds for Chinese highway construction[1]. Therefore, studying the present status of the financing of Chinese highway, analyzing the existing problems in financing activities and exploring the new financing channels actively have great significance for the lack of funds for Chinese highway construction.

2 THE STATUS AND MAIN MODELS OF THE FINANCING OF CHINESE HIGHWAY

Under the planned economic system, highway construction mainly relies on the national investment, the main body of financing and the channels of funding sources are single. Because of the large investment and difficult financing in highway construction, in 1984, the 54th Executive meeting of the State Council had developed several measures to accelerate highway construction in China, identified the policy called “loans to build roads, collect fees owing on the loan”. Under the guidance of state policies, the enthusiasm of the local communities to invest in highway goes up significantly, highway financing developed from the pure government investment, gradually to the diversified direction of a combination of government fund raising and market financing. We have

developed the investment and financing system as “state investment, local financing, social fund raising, and utilization of foreign capitals”[2].

At present, the main financing models of Chinese highway are the government investment, bank loans and securities financing, management transfer, BOT model and so on. Government investment, including financial allocations and financial loans, which is the traditional way for the financing of the highway construction in China, and is also one of the important sources of the funds for Chinese highway construction. Bank loan is the most important model of the financing of highway construction in China now, and it's the largest proportion of the capital source. Bank loan funds mainly come from domestic banks, foreign banks and multilateral financial institution, such as the World Bank, the Asian Development Bank and so on. Securities financing is a direct financing method which means all kinds of stocks, bonds and other securities are issued in the domestic and foreign financial market for financing. Stock financing and bond financing have become the important ways to attract social funds and to mobilize private capitals to enter the field of highway. The highway in China are basically toll roads, you can recover the investment of the project ahead of schedule, make an inventory of the existing stock of assets to raise funds for other construction projects through the transfer of operating right of the built toll roads. BOT (Build-Operate-Transfer) is point to the franchise agreements between project sponsors and government, and then the sponsors organize and found project companies which are responsible for financing, design, construction, and operation and maintenance tasks. The project companies have the ownership of projects and will collect fees, so they

can pay off debts with the obtained income, make up for the projects management costs and obtain the anticipated return on investment in the provision of franchising. And then the projects handed over to the government freely after the end of the concession[3].

3 ANALYSIS ON THE PROBLEMS EXISTED IN FINANCING OF CHINESE HIGHWAY

There are many problems existed in financing activities of Chinese highway, mainly displays in the following respects.

3.1 *The irrational financing structure, the high proportion of bank loans*

Highway financing structure is irrational, which mainly displays in the state finance insufficient investment, the lack of own funds, the high proportion of bank loans. The high quota bank loans overwhelm the highway construction department, resulting in the high asset-liability ratio, the toll revenues of many built highways are insufficient to pay the interest of bank loans, and it's unable for them to repay the principal and interest when a large number of credit funds become due.

3.2 *The imperfect financing environment*

The financing environment, which affects highway financing activities, is a collection of various factors, including financial environment, economic environment and legal environment. China has not yet established a highly efficient financial market system, the policy environment and financing system are also incomplete, relevant regulations and laws are not perfect, highway financing shows many characteristics of plan economy, the abilities in the construction and management are not strong enough to adapt to the rules of economy and to avoid market risks, it is excessively dependent on systems, policies and regulations, once it meets national policies adjustment, especially the adjustment in finance and currency, the highway financing will be influenced deeply sometimes.

3.3 *The insufficient investment of central finance and the high pressure of the local government finance*

The highway defined as public goods, which decides that the government should put in more funds, government financial fund is an important source of funds to support and guarantee the rapid development of highway, and is also

the basic standpoint of raising highway funds. However, in the current investment and financing system of highway construction, the loans from banks have occupied the major share, the investment from central finance is few. On the other hand, in order to promote the growth of local economy, or to pursue the achievements in their official career, the enthusiasm of local government for highway construction is very high, but the massive investment of local government on highway aggravates the financial and public burden.

3.4 *Imperfect development of the capital market*

Highway financing has a great prospect in the securities market; the extraneous source financing model based on issuing stocks and bonds can raise large amounts of private capital. However, the development of China's capital market is still imperfect, due to the system, mechanism and historical reasons; the highway financing has been marginalized in the stock market. With the decline in self-financing capacity and the continuous improvement of the state requirements for listed companies, the cost and difficulty in raising the funds of highway construction in the stock market increase largely.

3.5 *Insufficient capital investment in enterprise*

With the development of economy, the strength of the large state-owned enterprises and private enterprises for investment gradually increased, compared with the foreign investors, they are familiar with national conditions, closely associated with government, and there is no exchange rate risk of domestic funds, the cost of capital is lower than outside. Therefore, this part of the funds should also be positively strived for highway industry of construction funds. In addition, some of the non-bank financial institutions, such as trust and investment companies, securities companies, insurance companies, financial companies of the enterprise groups, which have already accumulated massive funds in recent years. If we can fully mobilize their interest on the highway investment, it will become another major funding source for the highway construction.

4 THE WAYS OF IMPROVING THE PRESENT SITUATION OF CHINESE HIGHWAY FINANCING

Facing the fund gap of highway construction in China, as well as the problems on the management and financing system of the highway, we

must perfect the relevant laws and regulations, improve the financing environment, and consummate the market mechanism and financing structure, we should not only make good use of the existing and mature financing models, but also constantly expand the space of financing, actively explore new financing ideas, and bravely innovate the financing methods to attract more capitals smoothly enter the market of domestic highway construction, we can implement specifically from the following aspects.

4.1 *Perfect the management system of highway*

On the basis of the coordinated planning, the traffic management departments of state should gradually establish easily centralized, unified, efficient highway management regulations which conforms to the Chinese national conditions in order to standardize the highway management in different places, only in this way can the managers and users of the highway work by the rules, avoid the risks and improve the efficiency of resource use, there are laws for people to follow and we must handle cases in conformity with the laws. Moreover, in order to avoid redundant and overlapping management between authority and enterprises, we have to clear about the main body of the highway management.

4.2 *Optimize the financing structure of highway*

Financing structure usually refers to a composition ratio of borrowed funds and own funds. Lack of own funds, excessively borrowed funds, the high proportion of bank loans, the small share of market financing, and the inadequate investment of private capital are the main performance of the irrational financing structure now. Therefore, in order to optimize the financing structure, we can only increase the capital investment, the main methods include: 1) Increase the investment of state funds. With the increase of the central fiscal revenue, the state should increase its investment in highway funds, local governments should also support the construction of highway by the establishment of special funds and self-raised funds of local finance; 2) Attract more foreign investment by the way of joint investment and cooperation; 3) Issue stocks to raise its own funds.

4.3 *Improve the financing environment of highway*

Highway is public product and national infrastructure; the government should assume the major role and play the leading role in highway financing and construction activities. First, the

state should set up an efficient financial market system, establish and improve the highway regulations, standardize the construction and management activities of the highway in different places, and actively guide the financing of highway enterprises. Second, the highway construction should be given the more relaxed fiscal policies and market access conditions by the state to relax the restrictions for listing and issuing bonds of the highway enterprises, increase the investment of non-repayment capital, lower the loans ratio, and improve the credit rating of banks and transportation enterprises, ensure the supply of funds for highway construction.

4.4 *Diversified, multi-channel and innovative financing*

1) We should continue to make good use of the traditional models of financing, such as making efforts for the state investment, making full use of bank loans and so on. 2) Expand the market space of financing, such as increasing the bond financing, more preferred stock financing, fund financing and so on. 3) Actively promote the project financing, such as the BOT model, ABS model, PPP model and so on. 4) Establish a special fund for highway construction, such as the establishment of "Special Fund for the Highway Construction" and so on. 5) Encourage the well-funded enterprises to invest highway. 6) Try to absorb folk private capitals. 7) Bold attempt and promotion of new financing methods, such as the cooperative operation of collective land, bundled financing, the sale and leaseback of fixed assets, natural resources mining right financing, property transactions, the issue of highway infrastructure lottery, finance leasing and so on.

5 CONCLUSIONS

Highway is the important infrastructure for the development of national economy and society, the scale of highway construction is huge in China, the construction and development of highway will be severely constrained if there are no adequate funds. There are many problems in the financing structure, financing environment and management system of highway at present, we have to optimize the financing structure, improve the financing environment, and perfect the management system, reasonably apply and explore the various financing channels. Based on the application of traditional financing model, we should seek various ways to make full use of the capital from financial markets and idle funds from society to invest in the construction of the highway project.

ACKNOWLEDGEMENTS

This work was financially supported by Natural science fund of China (41372299).

REFERENCES

- [1] Zixi Pan, The limitations and improvements of the financing models of highway construction, *J. Science and Technology Innovation Herald*, 2008, 19(7):37. (in Chinese).
- [2] Chaohui Xiang, The investigation on the highway investment and financing model of China's loans to build roads, collect fees owing on the loan, *J. China Economist*, 2009, (3):52–53. (in Chinese).
- [3] Miaofang Zheng, Zhongmin Fang, The analysis of the financing models of highway construction funds, *J. Modern economic information*, 2009, (20):102–103. (in Chinese).

A feasibility study on the subgrade compaction rapid detection using portable gravity punch

Hua Kai Zheng, Ce Li, Wen Ming Wang & Chun Yu Liang
College of Transportation, Jilin University, Changchun, Jilin, China

Jing Jian Liu
School of Civil Engineering and Architecture, East China Jiaotong University, Nanchang, China

ABSTRACT: Firstly design the portable gravity punch according to the principle of mechanics and the concept of the compaction degree, then detect the compaction degree of the soil specimen using this punch in the laboratory, establish the quantitative relationship between the test data and the compaction degree of the specimen. The result shows that the portable gravity punch can detect the compaction degree of subgrade rapidly. Finally put forward the specific ideas for the application of the portable gravity punch in the construction process.

Keywords: portable gravity punch; compaction degree; field detection of subgrade and pavement

1 INTRODUCTION

Highway subgrade is the foundation of the road, it will not only bear the self-weight of the soil and the pavement structure, at the same time it will also suffer the traffic load transferred from the road pavement. So it is the main bearing structure of the road. A strong subgrade is not only important to the pavement strength and stability, but also can create favorable conditions for prolonging its service life. To the fill and natural subgrade, it is necessary to compact if the strength is insufficient, and how to detect the density to control the compaction quality is very important to ensure the project quality and the economic benefit.

Subgrade evaluation indexes mainly include the intensity, degree of compaction, modulus of resilience, CBR and deflection value. And degree of compaction is widely applied in the practical construction because it is easy to measure comparing to other indexes. At present, compaction degree is stipulated to determine the construction quality of highway subgrade in China's highway construction standards. Measuring roadbed compaction degree can use sand filling method, irrigation method, cutting ring method and nucleon density instrument. Although the above methods are accurate, they are too complex and adopted in the after construction period. Portable Gravity punch has the advantages of low damage, rapid, real-time detection of the degree of compaction in the compacting process, and it can improve the efficiency of construction.

2 CONCEPT OF THE COMPACTION DEGREE AND PROFESSION EVALUATION METHODS

The degree of compaction is the ratio of the dry density of soil or other construction materials after compaction to its maximum dry density obtained by the standard compaction test in the laboratory. It is used to represent the density in the construction site after compaction. The higher compaction degree means the greater density and the better overall quality of the material.

At present, the traditional compaction degree detection methods commonly used in the engineering are cutting ring method, sand filling method, nuclear density apparatus, core drilling method and non-nuclear density gauge method. And now a new method called intelligent compaction quality detection method (ICCC method) is used at home. *Specifications for design of Highway Subgrade (JTG D30-2004)* specifies using ring method, sand filling method and the nuclear density apparatus to detect the degree of compaction in-situ. Though the principles are not the same, the purposes are all to measure the degree of compaction of soil or other materials accurately. To ensure the accuracy of the test results, the above methods have strict requirements on the operation and precise control process, and are used to identify the final compaction effect in the engineering.

3 DESIGN PRINCIPLE OF GRAVITY PUNCH

3.1 Instrument work principle

In order to obtain the advantages of simple operation, rapid detection of the compaction effect, gravity punch device is designed by the energy principle. That means a standard energy applied on the compacted soil (or other materials). Measuring the compaction effect, then establish the mapping relationship between the measured data with the degree of compaction gained by the standard test method, so as to use the gravity punch for compaction degree detection.

The detection principle of the designed gravity punch is that a member (mass is M) is fixed on a frame which height is H , and the member can resist shock and wear. So it reserved certain gravitational potential energy which can indicate by $W = MgH$.

Then the member is dropped through a control device, and during this process the gravity potential energy of the member transfer to kinetic energy as certain impact energy Q exert on the roadbed.

Finally, measure the penetration depth (s) and the damage diameter (d) of roadbed, the mass of the broken soil (m) as the test result, and we can use the three quantities s , d , m to characterize the roadbed compaction degree.

3.2 Detection principle of the compaction degree

Prepare several soil specimens which have the same moisture content (the optimum water content) but different compaction levels in the laboratory, then measure and calculate the degree of compaction γ with the standard test method. At the same time test each of the specimens using the gravity punch, and record s_i , d_i and m_i values. Establish the following mapping relationship through statistical analysis to the test data.

$$s, d, m \rightarrow \gamma$$

So we can achieve an equivalent representation between the degree of compaction with a standard test method and the gravity punch measurements.

4 INSTRUCTION OF THE PORTABLE GRAVITY PUNCH

4.1 Structure composition

Following are the main components and their functions of the gravity punch:

- ① Support frame: Support instruments to ensure the instrument stability
- ② Hooke: Hold the hammer and probe

- ③ Sleeve: Constraint hammer falling trajectory
- ④ Impact probe: Transfer hammer energy, impact the soil directly
- ⑤ Pressure lever: Recovery the position of hammer and probe

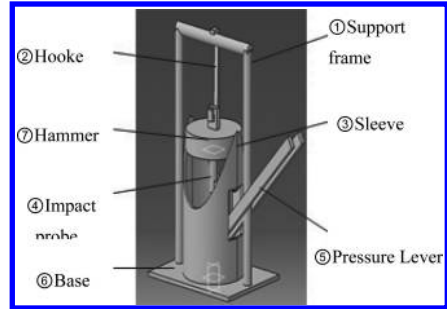


Figure 1. Dimensional model diagram of the gravity punch.



Figure 2. Real map of the gravity punch.

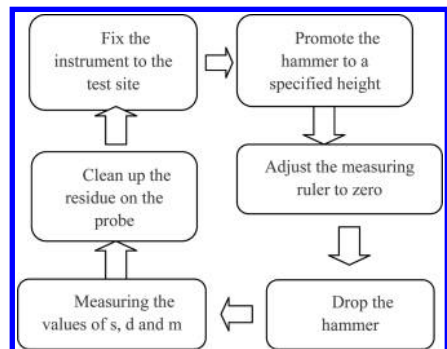


Figure 3. Test operation flow chart.

- ⑥ Base Support and steady the instrument
- ⑦ Hamme: Provide gravitational potential energy, increase the impact energy.

Simple model diagram: See Figure 1.

Real map: See Figure 2.

4.2 Operational approach

Following is the Operation flow chart See Figure 3.

5 TEST STUDY OF THE INSTRUMENT PERFORMANCE

5.1 Laboratory test method

In order to verify instrument performance, we first carry simulation tests in the laboratory. Specific test procedure is as follows:

1. Preparation of test soil. Choose silty clay as the test soil, and dry in the oven after fully crush, then add water evenly to the optimum moisture content 15%. Cover by film for 24 hours.
2. Using heavy compaction meter to prepare soil specimen which divided into three layers based on standard methods. Simulate different degree of compaction by controlling the number of compaction. Make three specimens by compacting 27 times each layer, marked 1₁, 1₂, 1₃; make three specimens by compacting 22 times each layer, marked 2₁, 2₂, 2₃, make three specimens by compacting 17 times each layer, marked 3₁, 3₂, 3₃, make three specimens by compacting 12 times each layer, marked 4₁, 4₂, 4₃.
3. Calculate the wet density of Specimen. Let's assume the mass and the volume of the clean sleeve is M and V, then measure the mass of each group specimens (including sleeve) m₁₁, m₁₂, m₁₃, m₂₁, m₂₂, m₂₃, m₃₁, m₃₂, m₃₃, m₄₁, m₄₂, m₄₃. Calculate the average wet density of each group soil specimens according to the following formula, and the test results are summarized in Table 1.

$$\bar{\rho}_{i\text{wet}} = \frac{\bar{m}_i - M}{V}, \quad \bar{m}_i = \frac{1}{4}(m_{i1} + m_{i2} + m_{i3} + m_{i4}),$$

i = 1, 2, 3, 4

4. Detecting the degree of compaction of soil specimens using gravity punch. Detect each of group specimens with different degree of compaction, and measure the penetration depths (We just analyze the penetration depth 's' of the parameter), then record the test results and summarize in Table 1.
5. Calculate the compaction degree of soil specimens. Calculate the average dry density

Table 1. Experimental data and calculated results

Specimens	1 ₁	1 ₂	1 ₃
Mass [m(g)]	2106	2104	2110
Volume [V(mm ³)]	99700	99700	99700
Wet density (10 ³ kg/m ³)	21.12	21.1	21.16
Average	21.13		
Moisture content (%)	15.1		
Dry density (10 ³ kg/m ³)	18.36		
Compaction degree	100		
Q ₁ Penetration [s(mm)]	16.2	17.2	16.4
	17.1		
Q ₂ Penetration [s(mm)]	25	25.8	25.7
	25.5		
Specimens	2 ₁	2 ₂	2 ₃
Quality [m(g)]	2067	2076	2071
Volume [V(mm ³)]	99700	99700	99700
Wet density (10 ³ kg/m ³)	20.73	20.82	20.77
Average	20.78		
Moisture content (%)	15.1		
Dry density (10 ³ kg/m ³)	18.05		
Compaction degree	98.3		
Q ₁ Penetration [s(mm)]	18.1	17.9	18
	18		
Q ₂ Penetration [s(mm)]	27.1	26.3	27.6
	27.3		
Specimens	3 ₁	3 ₂	3 ₃
Quality [m(g)]	1986	2026	1993
Volume [V(mm ³)]	99700	99700	99700
Wet density (10 ³ kg/m ³)	19.92	20.32	19.99
Average	20.08		
Moisture content (%)	15		
Dry density (10 ³ kg/m ³)	17.46		
Compaction degree	95.1		
Q ₁ Penetration [s(mm)]	20.4	20.1	19.8
	20.1		
Q ₂ Penetration [s(mm)]	29.4	28.7	29.5
	29.2		
Specimens	4 ₁	4 ₂	4 ₃
Quality [m(g)]	1958	1951	1960
Volume [V(mm ³)]	99700	99700	99700
Wet density (10 ³ kg/m ³)	19.64	19.57	19.66
Average	19.62		
Moisture content (%)	14.9		
Dry density (10 ³ kg/m ³)	17.08		
Compaction degree	93		
Q ₁ Penetration [s(mm)]	23.5	22.4	23.2
	23.4		
Q ₂ Penetration [s(mm)]	32.1	32.6	31.3
	32.3		

* Impact energy: Q₁ = 1253 J, Q₂ = 1825 J.

of each group specimen according to following formula:

$$\bar{\rho}_{iDry} = \frac{\bar{\rho}_{iwet}}{1 + 0.01\bar{\omega}_i}, \quad i = 1, 2, 3, 4, \bar{\omega}_i = 15$$

Finally, calculate the degree of compaction of the specimen:

$$\gamma_i = \frac{\bar{\rho}_{iDry}}{\rho_{iDry}} \times 100\%, \quad i = 1, 2, 3, 4$$

5.2 Data analysis and establishment of transfer relationship

From the data in the table, we can obtain the relationship curve between the degree of compaction and penetration of the specimens as shown in Figure 4.

From the distribution of the data points in the coordinate axes, we can know the degree of compaction and penetration is approximately linear relationship in the 90–100 range. Using the method of least squares linear fit, the fitting relationship formula is:

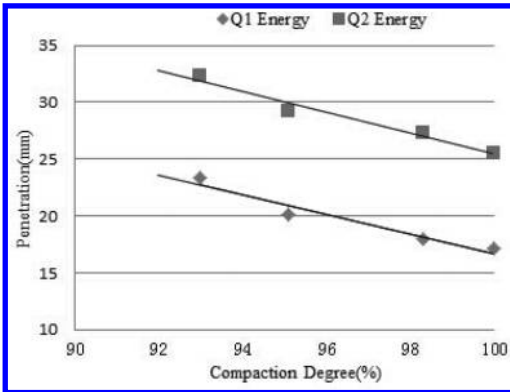


Figure 4. Correlation of compaction degree and penetration.

$$Q_1 : \gamma_1 = 119.2 - 1.16s$$

$$Q_2 : \gamma_2 = 126.8 - 1.08s$$

Thus, a function relationship of penetration using portable gravity punch with the degree of compaction is established when the soil compaction degree is relatively large (more than 90).

5.3 Test of corresponding relationship between penetration and the degree of compaction

Make specimens by compacting 24 times and 15 times respectively on the basis of the test method in 5.1 (two specimens in each group), then use the portable gravity punch device to detect. Compare the compaction degree calculated by the function relationship with what measured based on the standard method, and the results are shown in Table 2.

The results show that the error rates are all less than 0.5% and within the acceptable range. So we can say the fitting relationship meets the operating requirements of the actual engineering.

6 ASSUMPTION IN THE PRACTICAL APPLICATION OF ENGINEERING

Laboratory test results show the feasibility of using a portable gravity punch to test compaction degree on fine-grained soil. For the detection of the compaction degree to the actual project subgrade soil still need the relevant test to improve and perfect. The following proposed application are envisaged.

We should select several typical subgrade soils under construction conditions, and use portable gravity punch to test different degree of compaction of the soil, then use ring method to test compaction degree by standard testing. Adopt the experimental data analysis method similar to 5.2 to establish the correlativity between penetration and degree of compaction, and then revise the parameters of the formula. Finally sum up the correction factor of relationship to the typical subgrade soil. Thus, in the construction, the relationship between penetration depth and the degree of compaction

Table 2. Degrees of compaction obtained by penetration and by standard test method.

Hitting times	Impact energy	Penetration (mm)	Calculation of compaction degree	Compaction degree measured by standard method	
24 times	Q ₁	17.5	98.89	99.0	0.1
	Q ₂	26.1	98.73		0.3
15 times	Q ₁	21.5	94.26	94.1	0.2
	Q ₂	30.5	93.86		0.3

can be obtained through choosing the correction coefficient according to the used foundation fill. Substitute the test data to the formula; we can calculate the corresponding degree of compaction.

In addition, the instrument can also have the following improvement:

1. Add a distance-measuring sensor so that the instrument can measure penetration automatically and accurately;
2. Embedded microcontroller to storage the relationship of penetration and the degree of compaction and depth—correction factor of soil in the memory module, and then write a program

to achieve the function of selecting the correction coefficient, attaining the sensor testing data automatically and calculating the degree of compaction.

REFERENCES

- [1] Deng, Xuejun. 2013, *Road Subgrade and Pavement Engineering*, Beijing: China Communications Press.
- [2] Gao, Dazhao. 1979, *Soil Properties and Soil Mechanics*, Beijing: China Communications Press.
- [3] Sun, Jiasi. 2012, *Road Survey and Design*, Beijing: China Communications Press.

Experimental study on flexural behavior of High Titanium Heavy Slag Concrete beam

Jian Wen Long, Xiao Yu Guo & Lei Song

School of Civil Engineering and Architecture, East China JiaoTong University, Nanchang, P.R. China
National Tower and Steel Structure Quality Supervision Inspection Center, Fuzhou, P.R. China
Jiangxi Province Steel and Grid Structure Quality Testing Center, Fuzhou, P.R. China

ABSTRACT: To ensure the mechanical properties of high titanium heavy slag concrete beams. This test made three High Titanium Heavy Slag Reinforced Concrete (HTHSRC) beams and three Ordinary Reinforced Concrete (ORC) beams. The type of concrete aggregate and ratio of reinforcement were regarded as parameter variable of the experiment. Through the observation and comparison study of the cracking load, ultimate bearing capacity, deflection change, it found that increasing the steel reinforcement ratio can significantly improve the ultimate bearing capacity of high titanium heavy slag concrete beams as well as the ordinary concrete beams. The kind of high titanium heavy slag aggregate had no significant effect on the ultimate flexural bearing capacity. The calculation results of the bearing capacity of all specimens, calculated by the method in *code for design of concrete structures (GB50010-2010)*, were proved safe and reasonable.

Keywords: high titanium heavy slag; reinforced concrete; flexural capacity; cracking moment; ultimate bearing capacity

1 INTRODUCTION

HTHSRC is a kind of reinforced concrete which is utilized by high titanium heavy slag sand and gravel, a kind of waste blast furnace slag from Panzhihua iron and steel group, in replace of ordinary aggregate. Rational use of HTHSRC can effectively solve the problem of large accumulation of waste of blast furnace slag in Panzhihua area, also can relieve the problem of high cost of sand and gravel in this region, in accordance with national requirements of sustainable development.

In the past few decades, The material properties of high titanium heavy slag has been fully studied. At present, The preparation of high performance concrete with high titanium heavy slag sand and gravel had demonstrated available. In addition, There have been a number of engineering structure tentatively adopt high titanium heavy slag concrete in Panzhihua.

So this paper intends to study the mechanical properties of HTHSRC beam, discuss the feasibility on high titanium heavy slag as coarse and fine aggregate concrete used in practical engineering.

2 TEST PLAN

2.1 Test materials and specimens design

Experiment the designed variables starting from the material of the aggregate. The concrete of one

series of specimens use High Titanium Heavy Slag (HTHSC), the another group of specimens used ordinary gravel and sand (OC). This two kinds of concrete mixture ratio design are shown in [Table 1](#).

[Figure 1](#) shows that the size of specimens is 100 mm × 160 mm × 1200 mm. The concrete protective layer thickness is 20 mm. N_1 is erect steel wire which used 8 well. The reinforcement ratio (ρ) of all specimens are in the proper range, the reinforcement ratio listed (ρ) in [Table 2](#). [Table 2](#) is the material list of specimens, The specimens numbered SL2-1~SL2-3 made of high titanium heavy slag aggregate, the beams numbered OL1-1~OL1-3 are ordinary aggregate concrete.

2.2 Test method

[Figure 1, 2](#) show that test install a fixed hinge support at the one end of the beam, and set rolling bearings at the other end. The thin steel sheet is installed between the specimen and pad to avoid concrete damage due to local compression.

As is shown in [Figure 1](#), the experiment bonded strain gauge at pure bending section of the test beams to measure the concrete strain changes along the height of specimens. In order to measure deflection of specimens, the paper arranged dial indicators on the lower part of the mid-span and the upper part of the supports. Then get the actual maximum deflection, determinate the cracking

Table 1. Concrete mixture ratio design (kg).

Concrete	Cement	Coal fly	Ordinary sand	Slag sand	Ordinary gravel	Slag gravel	Water	Water reducing agent
OC	430	60	780	–	1040	–	160	4.9
HTHSC	430	60	–	780	–	1040	160	4.9

Table 2. Material list of specimens.

Specimens	Concrete	N_1	Steel	f_y (MPa)	N_2	ρ
OL1-1	OC	$3 \times \phi 6.5$	HPB300	303.5	$\phi 4@100$	0.71%
OL1-2		$2 \times \phi 10$	HRB335	306.6	$\phi 4@100$	1.12%
OL1-3		$2 \times \phi 16$	HRB335	525.3	$\phi 6.5@100$	2.87%
SL2-1	HTHSC	$3 \times \phi 6.5$	HPB300	303.5	$\phi 4@100$	0.71%
SL2-2		$2 \times \phi 10$	HRB335	306.6	$\phi 4@100$	1.12%
SL2-3		$2 \times \phi 16$	HRB335	525.3	$\phi 6.5@100$	2.87%

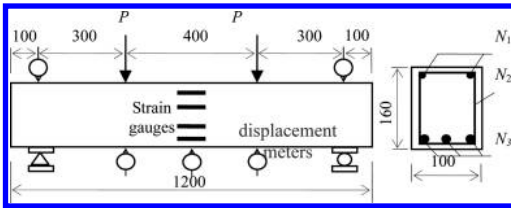


Figure 1. Size of specimen (mm).



Figure 2. Loading device.

moment (M_{cr}) and ultimate moment (M_{uc}) of beams.

3 TEST RESULTS AND ANALYSIS

3.1 Crack resistance analysis

The article observes the development of crack in the course of experiment and layout the propagation

of all the specimens in Figure 3. Analysis shows that the first cracks of the HTHSRC specimens appeared near the mid span, which is similar to the ordinary reinforced concrete beams, and the width of all crack are between 0.02 mm and 0.03 mm. With the increase of load, new cracks appear and become wider. Some of cracks through the neutral axis and extend upwards along the height direction of beams. When the load is close to the limit load, the diagonal crack developed at the shear-bending section. Finally, the fracture spacing are kept between 80 mm to 100 mm. The crack, crack spacing and maximum crack width of HTHSRC specimens are similar to Ordinary Reinforced Concrete (ORC) specimens.

Based on the cracking moment (M_{cr}) in Table 3, the cracking moment comparison chart of all specimens in different case of reinforcement was showed at Figure 4. It is proved that the cracking moment of HTHSRC beams are higher than the cracking moment of ordinary beams in the same conditions. The reason is that the physical and chemical properties of high titanium heavy slag aggregate can significantly improve the pore characteristics of concrete, improve interface structure of cement slurry and aggregate, enhance the bond performance of concrete interface. At the same time, with increasing of reinforcement ratio, the crack resistance performance improved, and crack resistance of HTHSRC beams are improved much more significant in the lower ratio of reinforcement. The growth of crack resistance performance of the two types of concrete beams is close to each other.

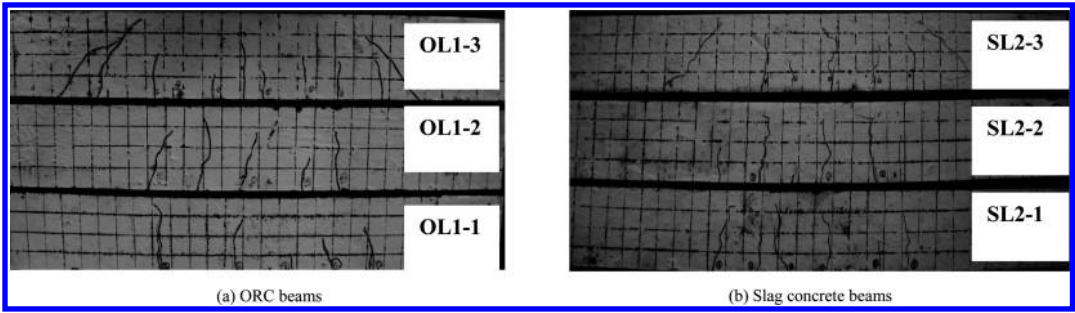


Figure 3. Cracks figure.

Table 3. Cracking moment and ultimate bending moment.

Specimens	Concrete	f_c (MPa)	M_{cr} (kN·m)	M_{uc} (kN·m)	M_{uc} (kN·m)
OL1-1	OC	55.3	1.88	6.09	4.01
OL1-2			2.05	6.34	6.36
OL1-3			2.69	23.23	23.81
SL2-1	HTHSRC	53.5	2.02	6.38	4.01
SL2-2			2.27	7.03	6.35
SL2-3			2.77	23.24	23.62

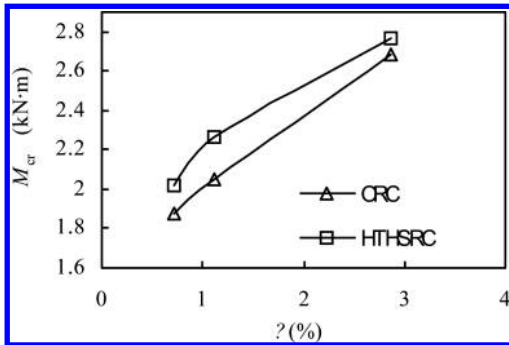


Figure 4. Comparison of cracking bending moment under different reinforcement ratio.

3.2 Analysis of bearing capacity

Figure 5 shows the strain distribution, along the height direction of concrete section, of typical specimens in the mid-span. It is proved that the strain distribution characteristics in the section of HTHSRC specimens and ORC specimens are similar to each, and both of them are basically consistent with the assumption of plane cross section.

Figure 6 lists the bending moment (M) – deflection (u_m) curves of the two types of concrete

specimens under three kinds of reinforcement. It shows that all specimens can still bear the load while reach limit bearing capacity. The failure mode of HTHSRC specimens has obvious ductility characteristics as well as ORC specimens. In the same condition of reinforcement, there is a slight increase of ultimate bearing capacity of HTHSRC specimens compared with ORC specimens, but it is not obvious. The reason is that the tensile strength of the both concrete are at a low level, the pulling force that bending beam can bear is mainly limited by the bottom rebar, and the tensile stress of concrete beneath the neutral axis can be ignored. So the ultimate moment of beams that can withstand is mainly determined by the reinforcement situation.

Table 3 lists the calculated ultimate bending moment (M_{uc}) and the measured bending moment (M_{uc}) through experiment of all specimens. The M_{uc} are calculated by actual strength of materials according to the formula in the present code for design of concrete structures. As can be seen from Table 3, all ratio of calculation and measure (M_{uc}/M_{uc}) of specimens are greater than one. Furthermore, the M_{uc}/M_{uc} of HTHSRC specimens are larger than the ORC specimens. Therefore, using the present code for design of concrete structures to calculate the flexural bearing capacity of HTHSRC specimens is safe and available.

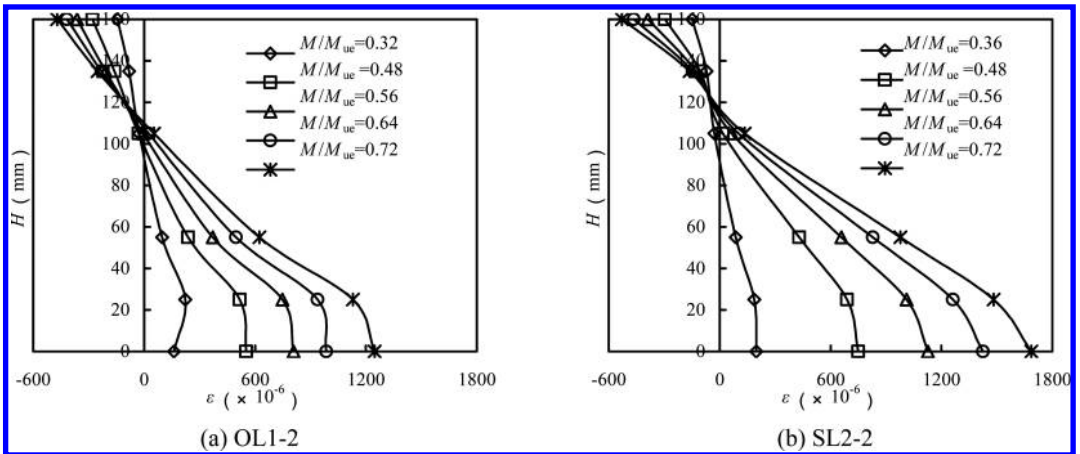


Figure 5. Strain distribution of typical specimens along the section height.

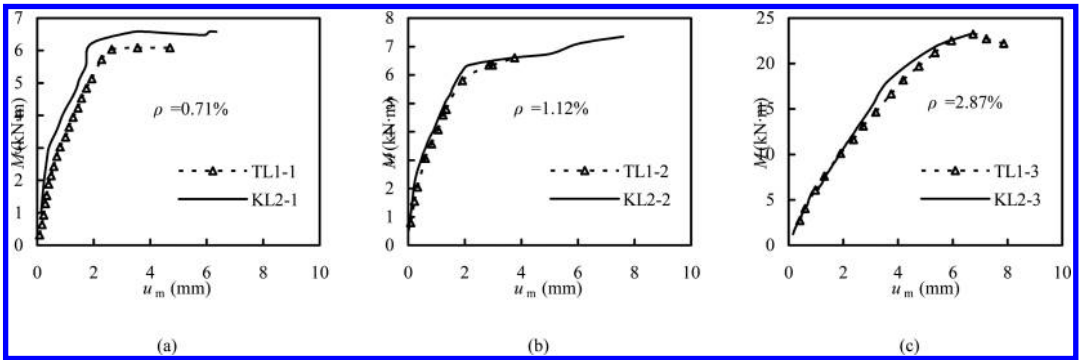


Figure 6. Test beams' $M-u_m$ graph.

4 CONCLUSION

- The Crack propagation forms of high HTHSRC beams are similar to OCR beams. However, the HTHSRC specimens have better crack resistance than OCR.
- The failure mode and ultimate flexural bearing capacity of HTHSRC specimens are similar to OCR specimens. The HTHSRC has no significant effect on the ultimate flexural bearing capacity. It is reasonable using *code for design of concrete structures* to calculate the the normal section bearing capacity of HTHSRC beams.

REFERENCES

Jin Kun-sun, Wei Chen, Shuang Hua-huang, et al. 2010. Mechanics performance of complex high Titanium heavy SLAG reinforcement concrete beam [J]. *Advanced Materials Research*, 168(2011): 2013–2020.

Siddique R, Kaur D. 2011. Properties of concrete containing ground granulated blast furnace slag (GGBFS) at elevated temperatures[J]. *Journal of Advanced Research*, 3(1): 45–51.

The National Standards of People's Republic of China. 2010. GB 50010-2010. Code for design of concrete structures [S].

Wang G, Wang Yu-hong, Gao Zhi-li. 2010. Use of steel slag as a granular material: volume expansion prediction and usability criteria [J]. *Journal of Hazardous Materials*, 184(1–3): 555–560.

Wang Qing-li, Kang Qing-liang, Cao Ping-zhou. 1999. Flexural strength for engative bending and vertical shear strength of composite steel slag-concrete beams [Z]: 5.

Zhou Le, Liu Hong-tao. 2011. Calculation method of flexural bearing capacity of Carbon fiber reinforced concrete beam [C] //Frontiers of Green Building, Materials and Civil E. Shangri-La, China, Shangri-La, China: 5080–5083.

Applicability analysis on index values of water stability of asphalt mixture

Qin Xue Pan, Guo Ping Qian, Hong Fu Liu & Tuo Huang
Changsha University of Science and Technology, Changsha, China

ABSTRACT: In view of the singleness of index values determined by the current standard on water stability of asphalt mixture, immersing Marshall test and freeze-thaw splitting test were carried out with 10 kinds of continuous dense gradation asphalt mixture. The test results show that the water stability of the low grade asphalt mixture is better than that of high grade asphalt, modified asphalt is better than the same label ordinary asphalt, and the difference is large between AC class and ATB class mixture, whose laws differ with different test methods. The standard requirements can not control the standard stability values of 30[#] asphalt and ATB class mixture. The water stability of asphalt mixture has great relationship with asphalt's kinds and gradation, types of mineral aggregate gradation and test methods. Therefore, in the actual mixture design, we should respectively define different control standards of testing indexes according to different kinds of asphalt mixture and test methods.

Keywords: road engineering; asphalt mixture; water stability; immersion marshall; freeze-thaw splitting

1 INTRODUCTION

The water damage of asphalt pavement is one of the mainly early diseases of high-grade asphalt pavement in our country, which reduced the driving performance of road severely, shorten the service life of the asphalt road, causing huge economic losses and adverse social impact. Besides unreasonable drainage design, poor water stability of asphalt mixture is also the important reasons for the water damage of asphalt pavement. And research on water stability of asphalt mixture was generally commenced from the following two aspects: one is the evaluation on adhesion between asphalt and mineral aggregate; The second is to evaluate the water stability of asphalt mixture. The latter test methods used the most widely were immersing Marshall test and freeze-thaw splitting strength test^[1-9]. There are only two control standards (the ordinary asphalt or modified asphalt) for the test indexes in current 《Technical Specifications for Construction of Highway Asphalt Pavements》(JTG F40-2004). But the kinds of asphalt mixture are many. If we take a single value as a standard for all mixture, it will lead that the excellent water stability mixtures are very easy to meet the specification requirements and the worse's are difficult to achieve. Meanwhile, there are big differences between the test results also because of different test methods and test conditions. Which above-mentioned will limit the applicability for the required values of the specification and make it cannot provide a good guide for engineering practice.

Based on this, this article relying on Yudeng highway construction project, 10 continuous

dense gradation asphalt mixture, used in highway construction commonly now, were selected to take the immersion Marshall test and freeze-thaw splitting test as the specifications. Then the law that the water stability of asphalt mixture was affected by mixture types and materials can be concluded according to comparative analysis for the test results, which can provide the reference for determining more proper and detailed test indexes to the water stability of asphalt mixture.

2 TECHNICAL PERFORMANCE OF RAW MATERIAL AND MIXTURE RATIO DESIGN

2.1 *Technical performance of raw material*

Aggregate and four kinds of asphalt (30[#], 70[#], 50[#] asphalt and SBS modified asphalt (I-D)) selected in this study were tested about main technical performance indexes based on 《Test Method of Aggregate for Highway Engineering》(JTG E20-2005) and 《Standard Test Methods of Bitumen and Bituminous Mixtures for Highway Engineering》(JTG E20-2011). The test results show that the technical performances of the selected raw materials are all qualified for the specification requirements.

2.2 *Mixture gradation and optimum oil-stone ratio*

Gradation of four kinds of mixture (AC-20, AC-25, ATB-30, ATB-40) selected in the article was design by Bailey method, the design results as

Table 1. Gradation composition on four kinds of mixture.

Graduation type	Item	Mass passage rate in different mesh size (mm)/%														
		54	37.5	31.5	26.5	19	16	13.2	9.5	4.75	2.36	1.18	0.6	0.3	0.15	0.075
AC-20	SR	-	-	-	100	90-100	78-92	62-80	50-72	26-56	16-44	12-33	8-24	5-17	4-13	3-7
	DG	-	-	-	100	97.6	87	70.4	56.7	36.5	25.2	19.1	12.7	9.1	8.1	6.3
AC-25	SR	-	-	100	90-100	75-90	65-83	57-76	45-65	24-52	16-42	12-33	8-24	5-17	4-13	3-7
	DG	-	-	100	99.2	84	73	61.6	49.4	34	24.8	16	10.2	7.8	6.3	5.2
ATB30	SR	-	100	90-100	70-90	53-72	44-66	39-60	31-51	20-40	15-32	10-25	8-18	5-14	3-10	2-6
	DG	100	100	99.3	85.2	62.4	57.7	50.4	40.8	33.3	23	17.8	10.9	7.4	5.5	4.2
ATB40	SR	100	90-100	75-92	66-85	49-71	43-63	37-57	30-50	20-40	15-32	10-25	8-18	5-14	3-10	2-6
	DG	100	97.8	85.3	79.4	64.9	56.9	48.9	39.1	31.9	22.4	17.4	10.8	7.4	5.6	4.4

Notes: SR is standard requirements; DG is designed gradation.

shown in Table 1. From which we can see that the gradation designed can satisfy the requirements of current standards. is used to determine the oil-stone ratio of four kinds of a mixture with 30# asphalt were determined according to Marshall test, which are 4.6%, 4.0%, 3.4%, 4.0% in order. with first-class match types of different types of asphalt mixture are used to 30# oil-stone ratio of asphalt design. The same gradation mixtures with the different kinds asphalt used the same ratio as 30# asphalt.

3 ANALYSIS ON TEST RESULTS OF WATER STABILITY

According to T0709-2011 and T0729-2011 in 《Standard Test Methods of Bitumen and Bituminous Mixtures for Highway Engineering》 (JTG E20-2011), 10 kinds of asphalt mixture designed above were tested in the immersion Marshall stability test and freeze-thaw splitting test, whose results were shown in Table 2. From which we can see that all the mixture's test results basically meet the specification requirements.

3.1 Immersion Marshall test

According to Table 2, stability test results of all kinds of asphalt mixture were plotted by classification in Figure 1 to Figure 3.

From Figure 1 and Figure 2, we can see that the stability to the asphalt mixture of AC class are is sensitive to asphalt types but ATB class's is not, 30# asphalt mixture's is 3-4 times than 50# and 70# asphalt mixture's. AC-20 (70#)'s is bigger than AC-20# (50) because of using the SBS modified in it, which show that the SBS modified asphalt can improve the stability of the mixture. Meanwhile, it can be found that the standard requirements can only control the standard stability values of the 50# and 70# asphalt mixture, 30# and ATB class asphalt mixtures's standard stability were respectively 3 times and 2 times to the values specification required.

From Figure 3, it can be found that there are small differences between the AC and ATB class mixture of residual stability ratio. 30# and 50# asphalt mixture residual stability are bigger, and 70# asphalt mixture's are smaller, even some are slightly lower than the standard requirements. This shows that the water stability of 30# and 50# asphalt mixture are better than 70# mixture's.

3.2 Freeze-thaw splitting test

According to Table 2, freeze-thaw splitting test results of all kinds of asphalt mixture were plotted by classification in Figure 4 to Figure 6.

Table 2. Results of water stability tests of asphalt mixture.

Mixture types	Stability				Splitting strength				
	Standard conditions (KN)	SR (KN)	Immersion 48 h (KN)	RSR (%)	SR (%)	Freeze-thaw before (MPa)	Freeze-thaw after (MPa)	TSR (%)	SR (%)
AC-20C (30#)	39.5	AC#8	35.0	89	Common asphalt #80	1.46	1.40	96.1	Common asphalt #75
AC-25C (30#)	31.2		26.5	85		1.48	1.31	88.3	
AC-20C (50#)	8.0		7.4	92		1.06	0.88	83.0	
AC-25C (50#)	8.9		8.3	93		1.13	0.93	82.3	
AC-20C (70#SBS)	11.1		8.9	80		0.95	0.89	94.0	
AC-25C (70#)	7.4	ATB#15	5.7	78	Modified asphalt #85	0.82	0.75	91.3	Modified asphalt #80
ATB30 (30#)	28.6		26.8	93		1.86	1.53	82.0	
ATB40 (30#)	27.5		24.8	90		2.17	1.63	75.1	
ATB30 (70#)	31.2		24.4	78		1.14	0.87	75.6	
ATB40 (70#)	29.3		27.9	95		1.18	0.89	75.2	

Notes: SR is standard requirements; RSR is residual stability ratio; TSR is residual splitting strength ratio.

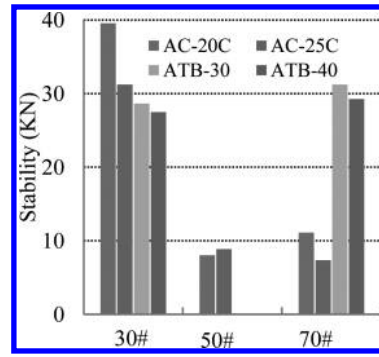


Figure 1. Standard stability.

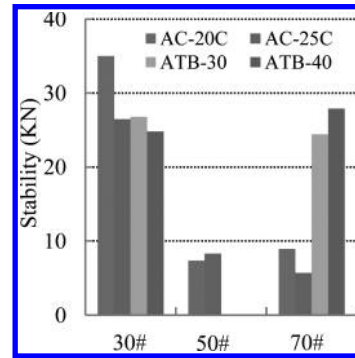


Figure 2. Stability after immersed 48 h.

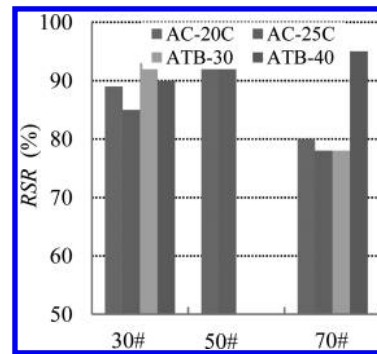


Figure 3. Residual stability ratio.

From Figure 4 and Figure 5, it can be found that the mixtures' splitting strength before freeze-thaw and after are sensitive to the grade label of the asphalt, its value decreases with the label increasing. The splitting strength of ATB class are higher than that of AC class, and along with the increase of asphalt grade, the gap of splitting strength between the two kinds of mixture become smaller.

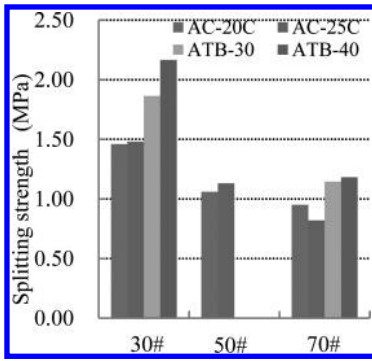


Figure 4. Splitting strength before freeze-thaw.

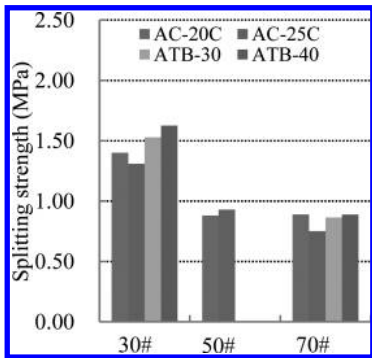


Figure 5. Splitting strength after freeze-thaw.

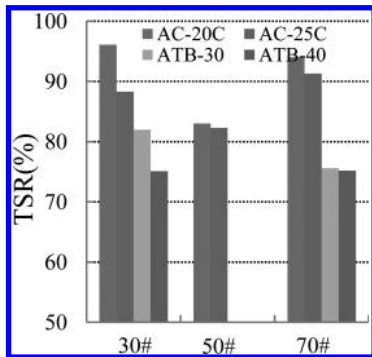


Figure 6. Splitting strength ratio-TSR.

From Figure 6, we can see that *TSR* of 10 kinds of mixture can satisfy the requirements of the specification, and have a regular pattern: the *TSR* of 30# and 70# asphalt mixture are bigger than that of 50# asphalt mixture smaller. *TSR* of ATB class mixture being not sensitive to asphalt label; AC class mixture's are significantly higher than that of ATB class's, and also over

specification requirements more. This shows that the water stability of AC class mixture is excellent, and it only has guiding significance for the design to mixture when raising the standards for the control values.

By comparative analysis between Figure 3 and Figure 6, it can be found that, differences on Marshall immersion test results with the same grade label asphalt are small, especially 30# and 50# asphalt mixture's residual stability ratio are at about 90%, higher than the standard value (80%). This shows that the experimental method's evaluation for the water stability of asphalt mixture is relatively cursory; However, gaps of freeze-thaw splitting test results among 10 kinds of mixture are obvious, and have a regular pattern, which shows that the experiment method to evaluate effect is excellent. Therefore, it is proper that using this method to the water stability test in the actual design for mixture.

4 CONCLUSIONS

According to the analysis on test results of water stability for 10 kinds of continuous dense gradation asphalt mixture, this article can obtain the conclusions below:

1. The stability of the ATB class mixture is not sensitive to asphalt grade label and gradation type, and standard stability of the mixtures of 30# asphalt and ATB class are the respectively 3 times and 2 times to specification requires, which show that the requirements of the specification have not control the standard stability values of the two kinds of mixture.
2. *TSR* of ATB class mixture are not sensitive to asphalt label; AC class mixture's are significantly higher than that of ATB class's, and also over specification requirements more. This shows that their water stability is excellent.
3. Summarizing two kinds of test results, the law about 10 kinds of water stability of asphalt mixture selected in the article is: low grade asphalt mixture is better than high grade class asphalt, and modified asphalt is better than the same grade label ordinary asphalt; evaluation result of freeze-thaw splitting test on the water stability of asphalt mixture is better than that of Marshall immersion test.

To sum up, test method, asphalt and mineral aggregate type affect the water stability of asphalt mixture greatly. It can not evaluate the water stability accurately by existing specification requirements values. Therefore, in actual mixture design, we should define the test indexes respectively

depending on the type of asphalt grade, mineral aggregate gradation and test method.

ACKNOWLEDGEMENTS

The authors appreciate the support of Projects of National Natural Science Foundation of China (51038002); Projects of Graduate Student Research Innovation Fund in Hunan Province (CX2013B364, CX2013B365); The project was supported by Open Fund of the Key Laboratory of Highway Engineering (kfj120101, kfj120204, kfj130103); The scientific research project of education department in hunan province (13C1028).

REFERENCES

- [1] Cui Xin-zhuang, Jin Qing, Zhang Na, et al. Experiment on Permeability Model and water Stability of Damaged Asphalt Mixture [J]. China Journal of Highway and Transport, 2014, 27(3):1–10.
- [2] Liu Tang-zhi, Zhu Hong-zhou, LI Jia-kun, et al. Research on Water Stability of Warm-recycled Asphalt Mixture [J]. Journal of Wuhan University of Technology, 2013, 35(3):54–58.
- [3] Jiang Wang-heng, Zhang Xiao-ning, Li Zhi. Mechanical Mechanism of Moisture-induced Damage of Asphalt Mixture Based on Simulation Test of Dynamic Water Pressure [J]. China Journal of Highway and Transport, 2011, 24(4):21–25.
- [4] Deng Zong-cai, Wei Zhon-gxing, Zhang Zhi-qing. Experiment of Road Performance of Asphalt Mixtures Mixed with Different Kinds of Recycled Coarse Aggregate [J]. Journal of Highway and Transportation Research and Development, 2013, 30(2):9–13.
- [5] He Liang, Wang Zhen, Ma Yu, et al. Effect of Foaming Agent on Asphalt Foaming and Water Stability of Mixture [J]. Journal of Building Material, 2010, 13(2):198–202.
- [6] Yang Rui-hua, Xu Zhi-hong, Li Yu-zhi. Research on Evaluation Method for Moisture Susceptibility of Asphalt Mixture [J]. Journal of Tongji University (Natural Science), 2007, 35(11):1486–1491.
- [7] Yu Hai-chen, Sun Li-jun, Zhang Li-jie, et al. Analysis of Water Stability of Sulphur Extended Asphalt Mixture [J]. Journal of Building Material, 2009, 12(6):679–683.
- [8] Transportation Industry Standard of the People's Republic of China. Standard Test Methods of Bitumen and Bituminous Mixtures for Highway Engineering (JTG E20-2011) [S]. Beijing: China Communications Press, 2011.
- [9] Transportation Industry Standard of the People's Republic of China. Technical Specifications for Construction of Highway Asphalt Pavements (JTG F40-2004) [S]. Beijing: China Communications Press, 2004.

The regular study of dry density for shear strength parameters of loess

Kang Feng Yuan & Zhi Jie Sun

Key Laboratory of Highway Construction and Maintenance Technology in Loess Region, Ministry of Transport, P.R. China

Shanxi Key Laboratory of Highway Construction and Maintenance Technology in Loess Region, Shanxi Transportation Research Institute, Shanxi, Taiyuan, China

ABSTRACT: At present, the research is not enough for the correlation of dry density and shear strength parameters in domestic. The paper aims how the change of dry density influence the shear strength parameters of reshaped loess by consolidation drained triaxial shear test for the loess. The results showed that: with the increasing of dry density, the strength of reshaped loess will tend to strengthen. With the increasing of dry density, the changing of shear strength parameter c and ϕ all become larger with the increasing of dry density.

Keywords: consolidation drained; reshaped loess; dry density; strength parameter c ; strength parameter ϕ

1 INTRODUCTION

The strength is an important mechanical properties for loess, involving many engineering problems which associated with the loess stability, such as foundation bearing capacity, slope stability. Many scholars have completed a lot of research work for the strength of the loess. Wang Shuo et al^[1] think that the cohesion of unsaturated remolded loess will increase with the increment of dry density due to the influence of reciprocity of particles and tension action of inter-granular water. Internal friction angle of unsaturated remolded loess get a little increasing with the increment of dry density, approximately showing linear variation. Wang Hui et al^[2] think that the intact loess microstructure is destroyed after disturbance and remodeling, and dry density changes have a significant impact on penetration coefficient, which tend to decrease while the dry density increases. The studies showed that: the stress-strain is influenced by boundary conditions such as stress path. The different conditions have distinct effect. However, there is rare research for the affect of dry density to strength characteristic of loess^{[3]-[10]}.

With the help of consolidated drained triaxial test to research the characteristics of reshaped loess for different dry density. Analysis the correlation of dry density and shear strength parameter. The study have some theoretical significance for the research of loess characteristics.

2 THE LOESS OF TEST

The loess of test is taken from certain slope at the Jinnan district, which is silty clay, soil evenly. The loess samples have been whittled to length 30 cm cube in the field. The natural moisture content of loess samples was 9.9%, the natural dry density was 1.39 g/cm³.

3 TEST INSTRUMENTS AND TEST METHOD

3.1 Test instruments

The test instrument is the conventional triaxial shear apparatus. The pressure will pass to the specimen with the help of the fixed beam.

3.2 Test method

The natural moisture content of loess was 9.9%. Prepare reshaped triaxial specimen which dry density were separate 1.39 g/cm³, 1.43 g/cm³, 1.47 g/cm³, 1.51 g/cm³ and the amount is four for each dry density specimen. The confining pressure were separate 50 kPa, 100 kPa, 200 kPa, 400 kPa for shear test which is consolidation drained. For consolidated drained shear test, specimen installed before applying confining pressure, open the drain valve to consolidation, start motor to cut after the end of consolidation. The final shutdown standard is to see the loess samples which have obvious

cracks or dislocation or axial deformation reaches 12 mm.

4 TEST RESULTS AND ANALYSIS

4.1 The law of stress-strain characters changing with dry density for reshaped loess

The law of stress-strain characters changing with dry density under different confining pressure is indicated in Figures 1 to 4.

Figures 1–4 show that the shear strength of loess become larger with the increasing of dry density.

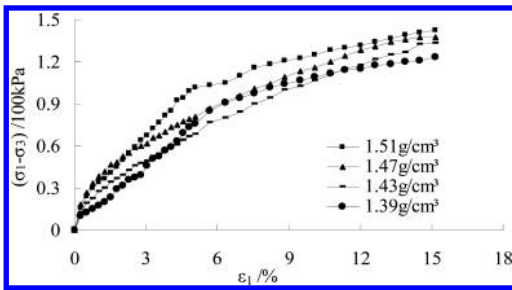


Figure 1. The stress-strain curves for $p = 50$ kPa.

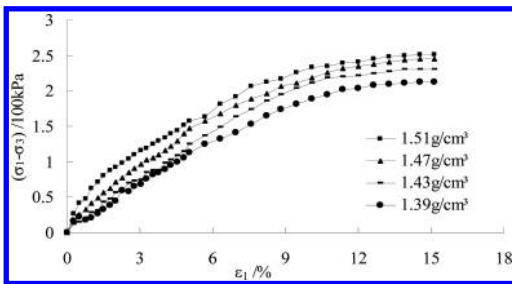


Figure 2. The stress-strain curves for $p = 100$ kPa.

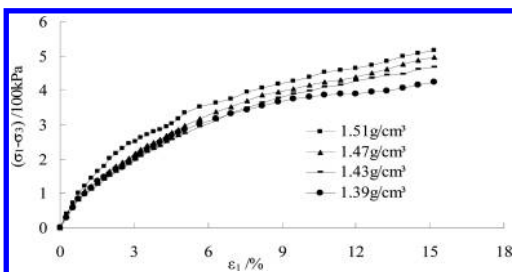


Figure 3. The stress-strain curves for $p = 200$ kPa.

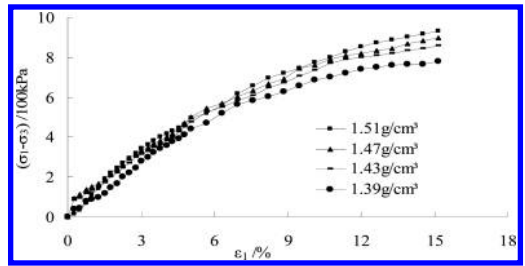


Figure 4. The stress-strain curves for $p = 400$ kPa.

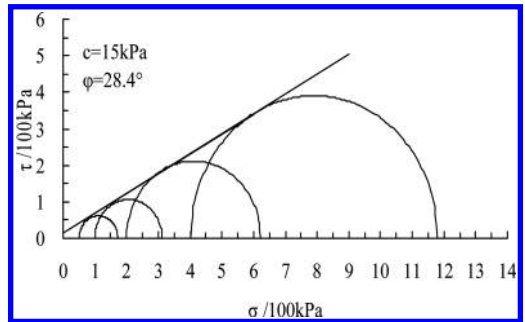


Figure 5. The strength lines for $\rho_d = 1.39$ g/cm³.

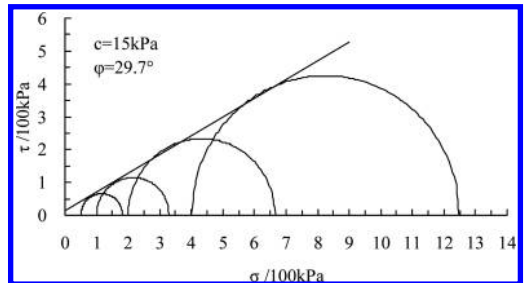


Figure 6. The strength lines for $\rho_d = 1.43$ g/cm³.

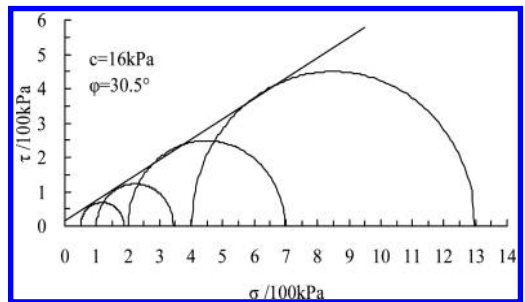


Figure 7. The strength lines for $\rho_d = 1.47$ g/cm³.

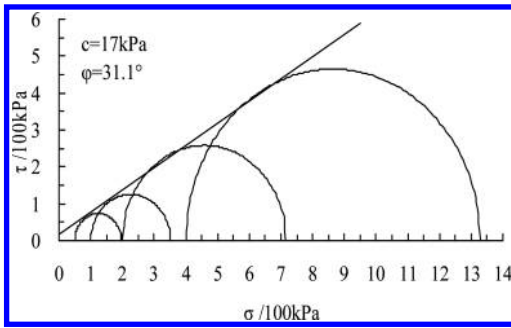


Figure 8. The strength lines for $\rho_d = 1.51 \text{ g/cm}^3$.

With the increasing of confining pressure, the dry density have weak impact for the strength.

4.2 The law of shear strength parameters changing with dry density for reshaped loess

The shear strength lines under different dry density is indicated in Figures 5 to 8.

Figures 5–8 show that the change of shear strength parameter c and ϕ all become larger with the increasing of dry density.

5 CONCLUSIONS

In this paper, triaxial test apparatus is applied to study reshaped loess shear strength parameters under dry density. The main conclusions are as follows:

1. With the increasing of confining pressure, the stress-strain curve of reshaped loess will tend to overlap which indicates the strength gap become small.
2. With the increasing of dry density, the changing of shear strength parameter c and ϕ all become larger with the increasing of dry density.

ACKNOWLEDGEMENTS

The paper is Sponsored by the Research Project of Shanxi Provincial Communication Department [2012-1-3].

REFERENCES

- [1] Wang Shuo, Liu Zhan-hui. Test Study on Influence Factor of Shear Strength of Unsaturated Remolded Loess [J]. Journal of Shijiazhuang Tiedao University (Natural Science), 2010, 23(3):86–89.
- [2] Wang Hui, Yue Zu-ren, Ye Chao-liang. Experimental Investigation of Permeability Characteristics of Intact and Reshaped Loess [J]. Journal of Shijiazhuang Tiedao University (Natural Science), 2009, 22(2):20–22.
- [3] S.K. Vanapalli, D.G. Fredlund D.E. Pufahl and A.W. Clifton, Model for the Prediction of Shear Strength with respect to Soil Suction, Can. Geotech. J. Vol.33, 1996.
- [4] Song Fei. The study on the stability and deformation mechanism of huazicun loess landslide [J]. Shanxi Science & Technology of Communications, 2012, 216(3):13–15. (in Chinese).
- [5] Li Xu-hua. The Rational Slope Type Research on Loess High Slope [J]. Shanxi Science & Technology of Communications, 2012, 214(1):29–30. (in Chinese).
- [6] Fredlund D.G, Morgenstern N.R. Stress state variables for unsaturated soils [J]. Journal of the Engineering Division, ASCE, 1997, 103(GT5):477–466.
- [7] Bian Jia-min, Wang Bao-tian. The research of shear strength and water for unsaturated soil [J]. Yellow River, 2010, 32(11):124–125. (in Chinese).
- [8] Xiong Chuan-xiang, Gong Xiao-nan. An updated elastoplastic damage model for structural soft-clays [J]. Rock and Soil Mechanics, 2006, 27(3):395–397. (in Chinese).
- [9] Sheng Wei-gao, Li Guo-wei, Yuan Jun-ping. Stability analysis of high slopes based on the influence of water content change on soil strength [J]. Advances in Science and Technology of Water Resources, 2009, 29(1):12–15. (in Chinese).
- [10] Wang Yong-zhong, Liu Xiong-jun, Ai Chuan-jing, et al. Experimental investigation on shear strength parameters c and ϕ for a temporarily frozen soil in South China [J]. Engineering Journal of Wuhan University, 2010, 43(2):198–202. (in Chinese).

The regular study of water content for strength index of loess

Kang Feng Yuan

Key Laboratory of Highway Construction and Maintenance Technology in Loess Region, Ministry of Transport, P.R. China

Shanxi Key Laboratory of Highway Construction and Maintenance Technology in Loess Region, Shanxi Transportation Research Institute, Shanxi, Taiyuan, China

ABSTRACT: At present, the research is not enough for the correlation of water content and strength index in domestic. The paper aims how the change of water content influence the strength index of intact loess by consolidation drained triaxial shear test for the Jinnan loess. The results showed that: when the confining pressure is same, with the increasing of water content, the strength of intact loess will tend to weaken. The strength index c increased obvious with the increasing water content. The change of strength index ϕ is not obvious with the increasing water content.

Keywords: consolidation drained; intact loess; water content; strength index c ; strength index ϕ

1 INTRODUCTION

The stress-strain relationship is the basis which described deformation and strength characteristics under load, and also the evaluation prerequisite of loess deformation and strength characteristics. Zhu Zhi-duo et al^[1] think that the latter part strength and deformation characteristics of silt change small and with the increase of stabilizer amount, the curve of uniaxial stress-strain changes significantly. Leng Yi et al^[2] think that under drained condition sand specimens with stress history of different type do not change their shear strength for a given mean principal stress. On the other hand, the stress-strain characteristics behaved different with respect to the stress history. The studies showed that: the stress-strain is influenced by boundary conditions such as stress path confining pressure. The different conditions have distinct effects for the stress-strain characteristics of loess. However, for the strength characteristics of intact loess, there is rare research on the water content^{[3]-[10]}.

With the help of consolidated drained triaxial tests to research the characteristics of intact loess for different water content and confining pressure. Analysis the reason that loess stress-strain curve tends to coincide for intact loess, coming up with some conclusions. The study have some theoretical significance for the research of loess stress-strain characteristics. And it will provide reference for the future research of loess strength.

2 THE LOESS OF TEST

The loess of tests is taken from certain slope at the Jinnan district, in a depth of 5 m below the surface, which is silty clay, soil evenly. The soil samples have been whittled to length 25 cm~30 cm cube in the field. The natural moisture content of loess samples was 8.7%, through the burette method to configure the required moisture content for the sample.

3 TEST INSTRUMENTS AND TEST METHOD

3.1 Test instruments

The test instrument is the conventional triaxial shear apparatus which come from a Nanjing experimental instrument factory. The pressure will pass to the specimen with the help of the counterproductive of fixed beam.

3.2 Test method

Prepare intact triaxial specimen which water content were separate 10%, 14%, 18%, 22% and the amount is also four. The confining pressure were separate 50 kPa, 100 kPa, 200 kPa, 400 kPa for consolidated drained shear test. The specimen installed before exert confining pressure, open the drain valve to consolidation, and start motor to cut after the end of consolidation. The final shutdown standard is the axial deformation which reach 12 mm.

4 TEST RESULTS AND ANALYSIS

4.1 The law of stress-strain characters changing with water content for intact loess

The law of stress-strain characters changing with water content under different confining pressure is indicated in Figures 1 to 4.

Figures 1–4 show that the shear strength of loess decreases larger with the increasing of water content. With the increasing of confining pressure, the water content have a weak impact for the strength.

4.2 The law of shear strength index changing with water content for intact loess

The shear strength lines for intact loess under different water content is indicated in Figures 5 to 8.

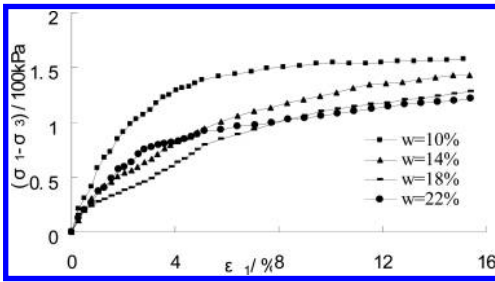


Figure 1. The stress-strain curves for $p = 50$ kPa.

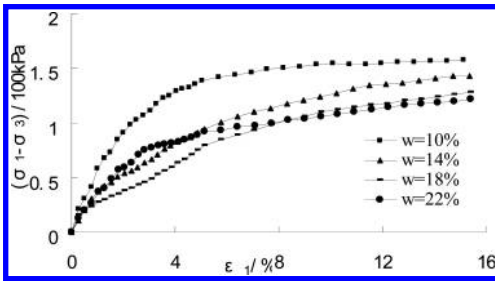


Figure 2. The stress-strain curves for $p = 100$ kPa.

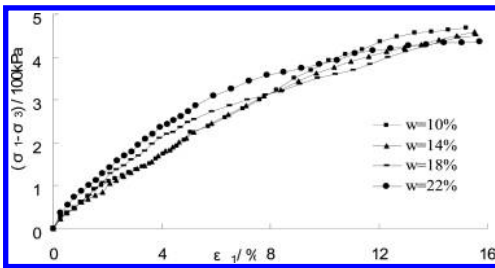


Figure 3. The stress-strain curves for $p = 200$ kPa.

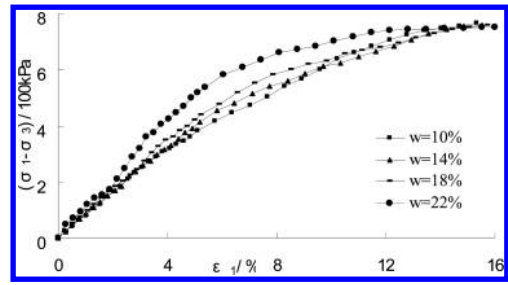


Figure 4. The stress-strain curves for $p = 400$ kPa.

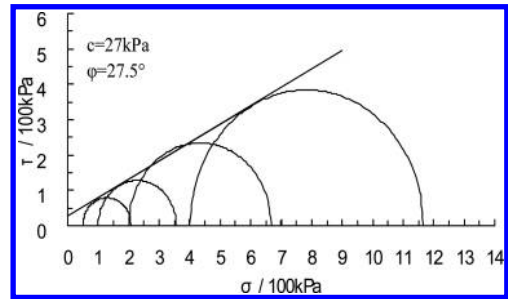


Figure 5. The shear strength lines for $w = 10\%$.

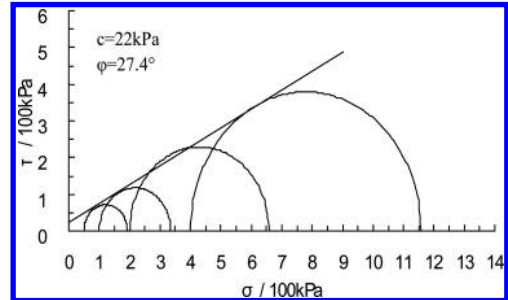


Figure 6. The shear strength lines for $w = 14\%$.

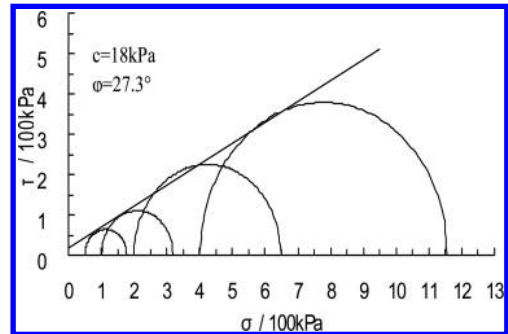


Figure 7. The shear strength lines for $w = 18\%$.

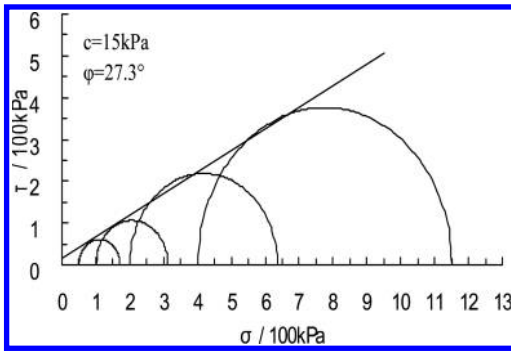


Figure 8. The shear strength lines for $w = 22\%$.

Figures 5–8 show that the change of shear strength index c is obvious with the increasing water content. The change of shear strength index ϕ is not obvious with the increasing water content.

5 CONCLUSIONS

In this paper, conventional triaxial test apparatus is applied to study loess stress-strain characteristics under water content. The main conclusions are as follows:

1. When the confining pressure is same, with the increasing of water content, the strength of intact loess will tend to weaken.
2. With the increasing of water content, the change of shear strength index c is obvious. The change of shear strength index ϕ is not obvious.

ACKNOWLEDGEMENTS

The paper is Sponsored by the Research Project of Shanxi Provincial Communication Department [2012-1-3].

REFERENCES

- [1] Zhu Zhi-duo, Hao Jian-xin, Zhou Li-hong. Experimental study of stress-strain characteristics of stabilized silt [J]. *Rock and Soil Mechanics*, 2008, 29(8):2199–2202. (in Chinese).
- [2] Leng, Yi, Luan Mao-tian, Xu Cheng-shun, et al. Experimental study of effect of stress history on mechanical properties of saturated sand under complex stress conditions [J]. *Rock and Soil Mechanics*, 2009, 30(5):1257–1263. (in Chinese).
- [3] S.K. Vanapalli, D.G. Fredlund D.E. Pufahl and A.W. Clifton. Model for the Prediction of Shear Strength with respect to Soil Suction, *Can Geotech. J.* Vol. 33, 1996.
- [4] Song Fei. The study on the stability and deformation mechanism of huazicun loess landslide [J]. *Shanxi Science & Technology of Communications*, 2012, 216(3):13–15. (in Chinese).
- [5] Li Xu-hua. The Rational Slope Type Research on Loess High Slope [J]. *Shanxi Science & Technology of Communications*, 2012, 214(1):29–30. (in Chinese).
- [6] Fredlund D.G, Morgenstern N.R. Stress state variables for unsaturated soils [J]. *Journal of the Engineering Division, ASCE*, 1997, 103(GT5):477–466.
- [7] Wang Li-zhong, Zhao Zhi-yuan, Li Ling-ling. Non-linear elastic model considering soil structural damage [J]. *Journal of Hydraulic Engineering*, 2004, (1):83:89. (in Chinese).
- [8] Xiong Chuan-xiang, Gong Xiao-nan. An updated elastoplastic damage model for structural soft-clays [J]. *Rock and Soil Mechanics*, 2006, 27(3):395:397. (in Chinese).
- [9] Shen Zhu-jiang, Liu En-long, Chen Tie-lin. Generalized Stress-Strain Relationship of Binary Medium Model for Geological Materials [J]. *Chinese Journal of Geotechnical Engineering*, 2005, 27(5): 489–494. (in Chinese).
- [10] Qi Ji-lin, Xie Ding-yi, Shi Yu-cheng. Status Quo and Method of Quantitative Study on Soil Structure [J]. *North-western Seismological Journal*, 2001, 23(1): 99–103. (in Chinese).

Study on type selection of shield equipment in different geological conditions

Fang Lin, Shou Gen Chen & Heng Zhang

Key Laboratory of Transportation Tunnel Engineering, Southwest Jiaotong University, Chengdu, China

ABSTRACT: This study summarized classification of shield machines in different geological conditions. This summary covered all the more frequently used types. And this study also sorted the types selection of cutter head. It offers references for associated projects.

Keywords: shield construction, shield selection, cutter head

1 INTRODUCTION

Underground space has become more and more important in modern city construction. And shield method is the best choice. Shield machine as the main machine in shield construction can not only hold formation pressure, but also push on active seal-tube structures [1]. After development of shield machine according to different geological conditions, it equips with excavation, jacking, diversion, support, slagging, lining and transportation machines in the front, middle, end and subsequent sections of shield machine and on earth, which makes up a complete system [2].

Shield method construction consists of stability of excavation face, shield tunneling and lining. Shield selection is a job to select shield machine on different tunnel dimensions, length, thickness of earth covering and geologic situation. Different shield methods adapt to different conditions [3–5]. If wrong methods are chosen, construction schedule will be delayed, and collapse, stratum settlement, water burst, may happen in excavation face. Shield selection should consider the type of the whole machine, coordination of every unit and how to cooperate with auxiliary methods. A reasonable shield selection contributes to successful, safe and economical construction [6,7].

2 TYPE OF SHIELD MACHINE AND SCOPE OF APPLICATION

Shield machines are sorted into three types: open shield machine, semi-open shield machine and sealed shield machine, according to partition structures between excavation face and workroom said in *new technic of shield tunnel in Japan* [8,9].

Specific categories: a. open shield machine: hand-operated type, semi-mechanical type and mechanical type; b. semi-open shield machine: extruder type; c. sealed shield machine: slurry type, earth pressure balanced type and soil pressured type (soil pressured type and slurry type).

Scope of application: a. earth pressured shield machine can be suitable for most kinds of geological conditions, ranges from soft sand soil stratum to sandy gravel stratum. Excavated soil layers are separated into soil particles and muddy water when they are transported to the ground as slurry status. The separation equipment set on the ground occupy such a large area that the recent use has been limited; b. earth pressure balanced shield machine is suitable for plastic liquid clay with less sediment concentration which can be excavated by cutters; c. soil pressured shield machine is equipped with added materials like bentonite, CMC, clay, super absorbent resin, vesicant and so on, which can be selected by different soil properties. This kind of machine is suitable for a wide range of geological conditions such as alluvial clay, pluvial clay, sandy soil, gravel, grit and alternation of beds among these stratum. At the back of cutter of soil pressured shield machine is equipped with agitating vane which can stir the whole soil space compulsively. Excavated soils are mixed with bentonite, CMC, clay or foam materials to transfer into plastic liquid clays with impermeability. Such clays are full of soil space and screw conveyer, can balance earth pressure and water pressure in excavation face. This machine with spoke cutter can be applied to a wide range of soil [7]; c. slurry shield machine transform excavated soils into slurries by adding materials. This is more suitable for huge gravel bed and is less used in practical project. [Figure 1](#) shows some typical types of shield machines.

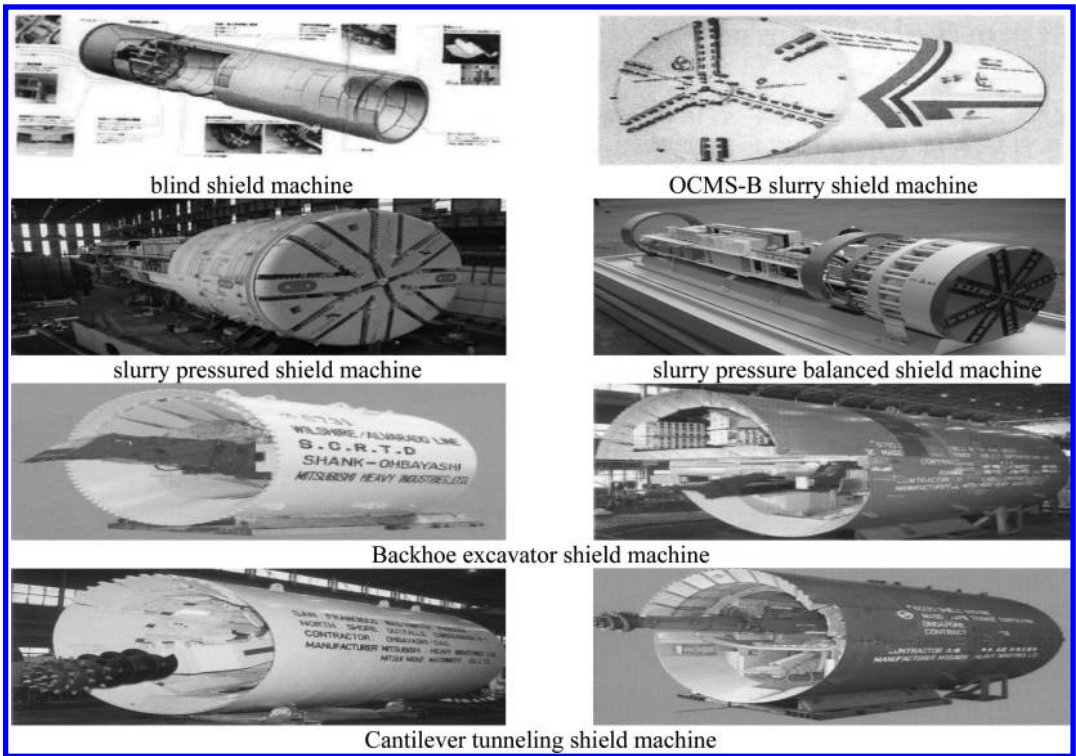


Figure 1. Type of shield tunnelling.

3 BODY SELECTION OF SHIELD MACHINE

3.1 Factors in shield's selection

Figure 2 shows the relationship of factors in shield's selection.

3.2 Shield selection in soft stratum

Shield method in soft stratum should keep shield-tunneling face and surrounding soils of shield periphery steady. And reduce soil disturbance to avoid surface deformation. This is the key to select shield machine in soft stratum [10–12]. A. Normal earth pressure balance shield machine is suitable for soft clay (low intensity, high compressibility, low permeability and high sensitivity). B. Slurry pressured shield machine is suitable for soft clay and sandy soil even gravel bed, but it needs mud separation equipment, which occupy large area and high cost. C. Grid extruding shield is suitable for not self-stabilization, liquidity soft cohesive soil, especially cross the river, lake, underground engineering on the bottom of the sea or swamp area which are less strict with the surface deformation along the shield tunneling route.

3.3 Shield selection in collapsibility loess soil

It is quite complicated to use shield method to construct tunnel in collapsibility loess soil. It's better to avoid such soil layer and use open type shield including artificial excavation of shield, half machinery excavation and excavation of shield when meet this soil layer.

3.4 Shield selection in lateritic layer

Earth pressure balance shield is the best choice for tunnel of the lateritic layer. It is better to choose mud type earth pressure balanced shield when shield drive comes across high strength of red clay. Earth pressure balance shield compound is more suitable for red clay with unweathered and weakly weathered rocks. When driving in the general red soil, enclosed earth pressure balance shield should be used, when shield drive comes across lithosphere, open mechanical excavation of shield should be used.

3.5 Shield selection in expansive clay layer

Soil massing expansive clay layer can maintain stability under the natural state, include: artificial excavation of shield, half machinery shield

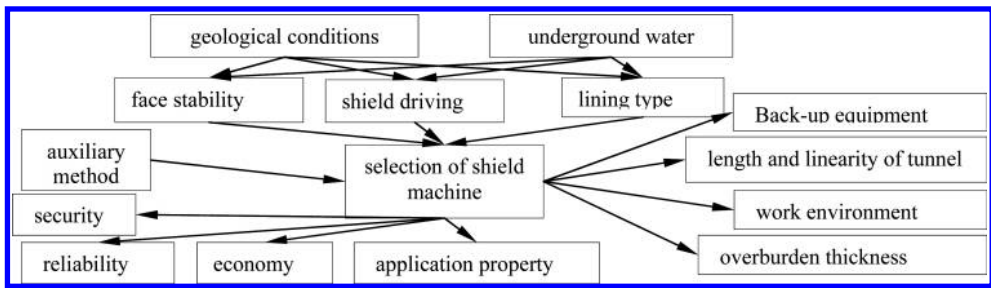


Figure 2. The relationship of factors in shield's selection.

excavation and excavation of shield. But water injection or grouting process are prohibited. Strength reduces obviously when soaking, so we should choose earth pressure balance or mud pressure type of shield. When shield drive come cross soil both with expansive clay under natural state and soil is soaked by water, composite shield should be closed.

3.6 Shield selection in sandy cobble stratum

Stabilizing measure of excavated soil must be considered when shield tunneling in gravel bed, sealed shield machine is the best. A. slurry pressured shield machine is the best choice of gravel bed. B. earth pressure balance shield machine can satisfy construction requirements by adopting different soil improvement measures along with different geological conditions. C. open shield machines including hand-operated type, semi-mechanical type and mechanical type are used in pebble bed. Slurry pressurized composite shield machine should be chosen when it comes cross alternation of gravel bed and gravel bed. For cobbles, stone breaker must be set in the shield cabinet.

3.7 Shield selection in weathered rock

Long tunnels may run across complicated stratum soft and strong/medium/weak weathered rock interacted. In this case, composite shield machine should be chosen: slurry pressured shield machine, earth pressure balance shield machine and open composite shield machine. The following shield machines have been widely used so far in domestic. A. earth pressure balance shield machine: mainly used in densely built-up and populated areas like subway engineering. B. slurry pressured shield machine: mainly used in extremely challenging geologies or in crossing-sea/river engineering like river-crossing tunnels engineering in the Huangpu River of Shanghai. C. Composite shield machine: mainly used in weathered changeable stratums like subway engineering of guangzhou 2nd metro line between Haizhu square and Shiergong. D. grid compressive shield machine: mainly used in soft soil and in open space with

surface deformation without strict requirement like inflowing and draining shield tunnels in Shanghai and riverside and seaside areas of Zhejiang.

3.8 Shield selection of large diameter shield machine selection problem

Selection of large diameter slurry balance shield construction machine should consider the following problems: construction parameters match, construction of underwater shallow overburden soil, close structures across the ground floor or building pile foundation, underground pipeline, anti-floating of advance in the tunnel construction, out of the hole or holes construction, special strata in the construction, close of shield tunnel construction and debugging of mud system running and construction management.

4 SELECTION OF SHIELD MACHINE CUTTERS

4.1 Shield cutter head type

Cutter is key technologies of Shield design. Opening rate and the cloth knife must be adjustment of different strata of the tunnel in time. A. panel cutter disk: applied to solid rock, opening rate is only about 30%. Working surface keeps stable by the knife dish pressure formation, soil pressure, mud pressure only part of the stability of working face. B. spoke type cutter: usually, the shield machine through the soft stratum, torque is bigger! Thrust is smaller! Earth pressure! Mud pressure balance working face, the knife dish of tool wear is also small, it should be promoted. C. without the knife dish of shield in place of no water or less water. D. applicable range: quicksand! Rich water and unstable strata like the metro of south and unstable strata in the application. Defect: Price difference, not easy to localization.

4.2 Selection of shield machine cutters

Different knife dish types suit for different formation. Features of different types of cutter heads are shown in Table 1.

Table 1. Features of different types of cutter heads.

Forms of cutters	Panel	Spoke type
The excavation surface soil pressure control	Generally there are three pressure: P1: between excavation face and panel; P2: between import and export of the panel; P3: between panel and capsule wall (soil pressure gauge pressure) Among: P2 may not easily confirm which affected by the panel opening, $P3 = P1 - P2$ the excavation face pressure is not easy to control. At the same time control pressure lower than actual excavation face.	There is only one stress P. Chamber pressure and soil pressure gauge pressure in the excavation face is equal. Pressure is easy to control and balance.
Sand, soil adaptation (grain size <15 cm)	Because the soil excavation surface affected by panel opening, enter inside the capsule is not smooth, it is easy to bond and susceptible to plugging.	Only a few spokes, at the same time with mixing blades after the spokes. Sand flows smoothly and not easy to block.
Sandy gravel adaptation (grain size >15 cm)	Strong adaptability, if necessary, add hob.	Can't add hob, forms and small number of the cutting tools.
Cutter torque	Cutter head torque resistance is big, need to increase equipment capability, high cost.	Cutter head torque small resistance and low cost.
Security of segment change in tunnel	Due to the panel, replace the cutting head in the tunnel safe and reliable.	Replacing cutting head poor safety inside the tunnel, the high cost of reinforced soil.

5 CONCLUSION

Shield machines as large special mechanical equipment in shield construction are different of the general construction machinery. Shield selection relates the design of the shield machine itself, parts of configuration and adaptability for formation condition of shield machine. Because of the high cost for shield machine, our national conditions and the financial capacity of the enterprises should also be considered in shield selection. The production of shield machine in our country has better to walk our own feature way from equipment introduction technologies absorption independently developed to adapt to our national conditions and formation conditions. Reasonable shield machine selection is of great concern to not only the technology of shield tunnel construction but also the costs and benefits of shield tunnel construction. So shield selection must be attract much attention.

REFERENCES

- [1] Song Kezhi, Zhu Jiande, Wang Mengshu, Liu Baosong. Selection of tunneling shield for waterless sandy cobble stratum [J]. Railway Standard Design, 2004(11): 51–53. (in Chinese).
- [2] Yuan Minzheng, Ju Shijian, Zhu weibin. Study and discussion of adaptability of shield machine in Guangzhou Metro Lines No. 1 and No. 2[M]. Modern Tunneling Technology, Vol. 41, No. 3, 2004, 31–34. (in Chinese).
- [3] Rowe, Kack. A method of estimating surface settlement above tunnels constructed in soft ground[J]. Canadian Geotechnical Journal. 1983, 20(8): 11–22.
- [4] Haukur Ject. The significance of mixed face conditions for TBM performance [J]. World Tunneling Annual Technical Review, 2002.
- [5] Nomoto, T., Imaura, S, Hagivara, T. et al. Shield tunnel construction in centrifuge[J]. Journal of Geotechnical and Geoenvironmental Engineering, 1999, ASCE 125(4):289–300.
- [6] Williams T.M. Using a Risk Register to integrate Risk Management in Project Definition[J]. International Journal of Project Definition[J]. International Journal of Project Management, 1994, 12: 17–22.
- [7] Clough G.W. EPB shield tunneling in mixed face conditions[J]. Journal of Geotechnical Engineering, 1993, 119: 1640–1656.
- [8] Lee K.M, Rowe, R.K. An analysis of three-dimensional ground movements: The thunder bay tunnel[J]. Canadian Geotechnical Journal, 1991, 28: 25–41.
- [9] J.H.M. Tah, V. Carr. Towards a framework for project risk knowledge management in the construction supply chain[J]. Advance in Engineering Software, 2001, 32: 835–836.
- [10] Weibin, Ju Shijian. Shield construction technology in plex strata[M]. Beijing: China Science and Technology Press, May, 2006, pp57–58. (in Chinese).
- [11] Jiang Zhaosheng, Huang Weiran, Zhu weibin. Reconstruction of shield excavation machine for composite strata[M]. Guangdong Building materials, 2006(3), pp138–139. (in Chinese).
- [12] Liu Gaofeng, Song Tiantian. Analysis and Study on Wearing of Cutting Tools of Shield Machines used in Chengdu Metro Construction[J]. Tunnel construction, 2007(6): 89–93. (in Chinese).

The effect of the soil state on the soil physical properties

Lin Ma

Key Laboratory of Highway Construction and Maintenance Technology in Loess Region,
Shanxi Transportation Research Institute, Ministry of Transport, Taiyuan, China

ABSTRACT: The soil state is one of the most important factor that affecting the engineering mechanical properties of soil. The paper discusses the mechanical properties of the soil from the perspective of testing, analyzes internal differences of the stress value under soil each state. Studies shows that the destruction stress of intact soil is the maximum, remolded soil is the second, and saturated soil is the minimum; The stress difference between intact and remolded soil is less than the difference between remolded and saturated soil as well as intact and saturated soil. This difference is about 2 to 3 times.

Keywords: intact soil; remolded soil; saturated soil; stress difference

1 INTRODUCTION

The general nature of the natural soil undisturbed soil^[1], due to the formation of such soil consolidation in Sedimentary action has a high strength. Just as high loess slope, it can remain upright and stable without supporting role. When the construction of the subway in the city, the more common kind of soil is saturated soil^[2]. The pores in soil particles are filled with water molecules due to prolonged immersion in water. Cementing substance between the particles are basically dissolved so that saturated soil has a very low intensity saturated soil and poor engineering properties. When the construction of the subway, it often encounters tunnel face collapse, substantial gushing and other projects diseases. The third is remolded soil, common encounters in fill subgrade^[3,4]. Such soil is a product of natural undisturbed soil. It formed due to the spatial structure of intact soil is severely damaged. Remolded soil forms secondary structures due to compaction in subgrade engineering. It makes that remolded soil has a certain shear strength and engineering performance is relatively intact.

In summary the paper analyzes the mechanical properties of three kinds of soil from the test and studies the internal mechanism of their differences.

2 TEST METHOD

The test performed strictly according to the “road soil test procedures”. Intact samples are

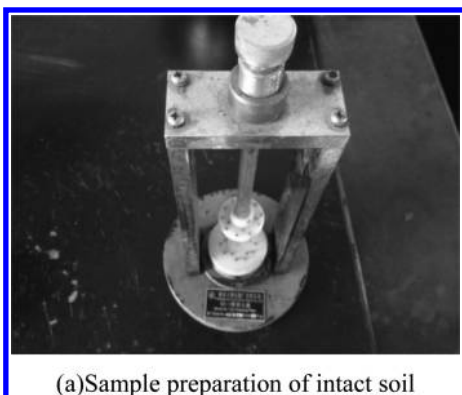
cut by a rotary specimen maker. Remolded samples are made by stratified compaction specimen maker. Saturated samples are made by vacuum pumping and saturation with intact samples prepared. Sample preparation equipment is shown in [Figure 1](#). The tests were carried out that the triaxial compression test of intact soil, remolded soil and saturated soil when moisture content is 15% and confining pressure are 50 kPa, 100 kPa, 200 kPa and 300 kPa. The test method used the consolidation non drainage method. The aim analyzes mechanics differences of intact soil, remolded soil and saturated soil under the same confining pressure and moisture conditions.

3 THE ANALYSIS OF TEST RESULT

Firstly the basic physical properties indicators of the soil are tested. The results shows in [Table 1](#).

Not difficult to see from [Figure 2](#) that the majority soil samples particle size are between 0.01 to 0.1. The soil effective diameter is 0.022 mm. Controlled diameter is 0.66 mm. Its uniformity coefficient C_u is 3 that less than 5. The curvature coefficient C_c is 0.75 that less than 1. It can determine the soil gradation bad.

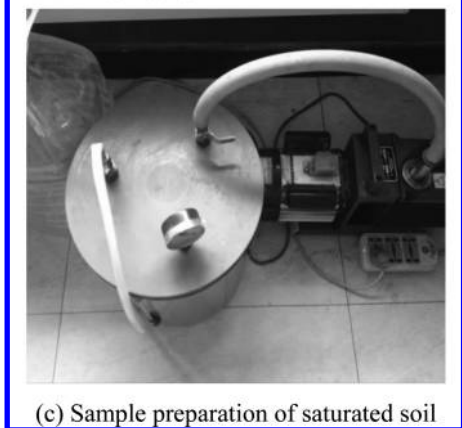
As can be seen from [Figure 3](#), the stress values of intact soil is maximum. Remolded soil followed, and saturated soil is minimum. The reason is that intact soil maintain overhead structure which formed by the effect of natural history deposition.



(a) Sample preparation of intact soil



(b) Sample preparation of remolded soil



(c) Sample preparation of saturated soil

Figure 1. Three kinds of sample preparation.

This structure can effectively resist the effects of external load, and it shows larger stress value; Spatial structure of remolded soil is destroyed, only to resist external loads through interactions of soil particles, so the stress values exhibited relatively low; The structure of saturated soil is fully damaged. The bonding material between the particles are dissolved. Large particles are dispersed into small particles, Cohesion between soil particles completely lost, resulting in soil resistance to external loads greatly reduced. So it is the minimum stress value.

Figure 4 illustrates that stress difference of intact and remolded soil increases with the confining pressure increasing. The internal structure of intact soil has large pores which are filled with water and air compared with remolded soil. Since remolded soil is a product of natural undisturbed soil, the internal structure is almost non-porous. As water and air can't be compressed, the resistance of intact soil is larger under the same volume and confining pressure. Meanwhile, with the confining pressure increases, the incompressible effect of intact soil is more significant. But remolded soil is less affected. So it shows as the curve shape in Figure 4. At the same time the stress difference between intact and remolded soil is less than the difference between remolded and saturated soil as well as intact and saturated soil. This difference is about 2 to 3 times.

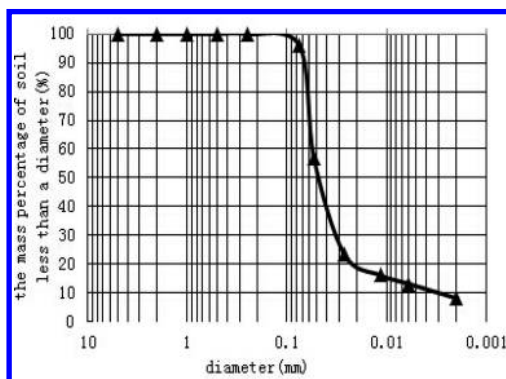


Figure 2. Graph of soil sample pieces.

Table 1. List of soil samples physical indicators.

Name of soil samples	Natural moisture content/%	Dry density/ g · cm ⁻³	Porosity ratio	Proportion	Liquid limit/%	Plastic limit/%
Soil samples	15.03	1.52	0.784	2.71	24.5	17.87

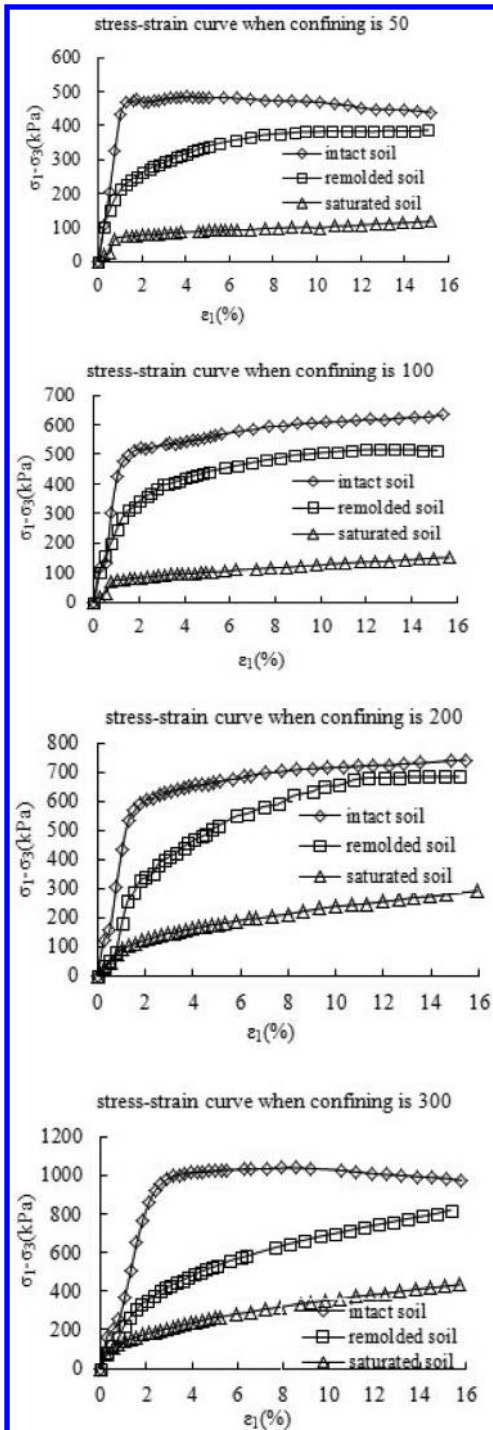


Figure 3. Different confining pressures three state soil stress-strain curve.

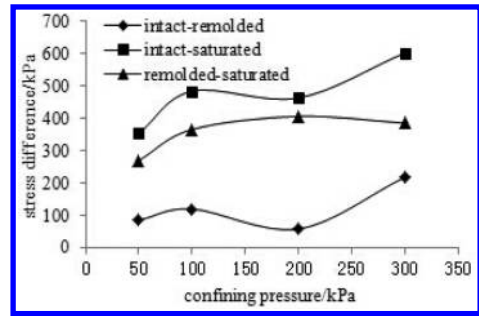


Figure 4. Three states stress the difference between the soil and the confining pressure curve.

4 CONCLUSION

The soil state is one of the most important factor that affecting the engineering mechanical properties of soil. It is one of the core content that studies the engineering state of soil by the majority of scientific workers. The paper discusses the mechanical properties of the soil from the perspective of testing, analyzes the internal differences of soil stress value under each state, reveals the formation mechanism of each state's soil. It can provide some guidance for engineering design.

ACKNOWLEDGMENTS

The paper is Sponsored by the Research Project of Shanxi Provincial Communication Department [2013-1-12].

REFERENCES

- [1] Liu Zudian. Loess Mechanics and Engineering[M]. Shaanxi science and Technology Press, 1997.
- [2] Zhao Xiangmin. The subgrade CBR values test analysis [J]. Shanxi traffic science and technology, 2012, 6(3): 17-19.
- [3] Wu Minzhe, Zhang Ke, Hu Weibing. Cumulative plastic strain of saturated loess due to metro traffic loading [J]. J. Xi an Univ.of Arch. & Tech.(Natural Science Edition) 2011, 43(2):316-322.
- [4] Zhang Peiyun. Role of control of water content in the roadbed compaction [J]. Journal of Liaoning Technical University (Natural Science), Vol. 30 Suppl:114-116.

Reduction of NO_x from biomass pyrolysis experiments

Dong Yang, Meng Zhang & Xiao Jie Zhang

Key Laboratory of Renewable Energy Utilization Technologies in Buildings of the National Education Ministry, Jinan, China

School of Thermal Energy Engineering, Shandong Jianzhu University, Jinan, China

ABSTRACT: Biomass combustion again reducing NO_x technology is a low cost low NO_x emission technology. Through the selection of cypress wood, apple wood, corn straw and cotton pole four analyzed the characteristics of biomass, biomass N element content is very low and almost does not contain S elements, and biomass is a kind of clean energy. At the same time, the biomass high volatile content, ash content is low, easy to catch fire, burning volatile analysis out of focus, and precipitation speed faster, so the biomass is a kind of ideal reburning fuel. The experimental results show that the biomass of reburning can effectively reduce NO_x emissions. The smaller the fuel particle size, the higher the rate of NO reduction. Reburning zone temperature is higher, the higher the NO reduction rate. The optimum excess air coefficient is between 0.6 to 0.8, and the NO reduction rate is above 50%.

Keywords: biomass; pyrolysis; NO_x; reburning denitration

1 INTRODUCTION

Biomass is a renewable energy, and is also one of the important energy to the survival of humans. In the world energy consumption, biomass accounted for 13% ~ 14%^[1], second only to coal, oil and natural gas, one of the world's fourth of the total energy consumption. Biomass energy accounted for 33% of primary energy in our country, and is second to the coal energy^[2]. Biomass is a kind of low nitrogen and low sulfur of renewable energy, using biomass as reburning fuel to replace part of fossil fuels, reducing the fuel nitrogen output and the formation of SO₂, and a net reduction of CO₂ release^[3]. Biomass resource is abundant in our country, the distribution range is wide, such as biomass combustion and reburning denitration technology can be combined, develop efficient large-scale biomass reasonable use, to open up new areas of energy utilization, improve the benefit of environmental protection has important significance.

Biomass reburning denitration reactions including gas phase homogeneous reaction are in contrast with the biomass coke heterogeneous reaction, thomogeneous reaction living pyrolysis and partial oxidation of CH₄ and HCCO radicals react with NO to generate HCN, HCN produced by the following reaction the conversion of NO to N₂^[4]:



At the same time, through the type (1) ~ (4) and biomass pyrolysis of H₂, CO by type (5) ~ (6) response, will be NO reduction removal^[5]:



Biomass reduction NO coke surface for a vision of the reaction^[6]:



By the homogeneous reaction mechanism is: under the reducing atmosphere, the biomass of volatile hydrocarbons (CH₄), H₂ and CO by type (1) ~ (6) and NO reduction reaction occurs, the CH₄ group on the NO reduction plays a leading role^[7]. On the analysis of the efficiency of biomass burning out of stock again, must consider biomass vision reaction on the surface of the coke.

2 THE EXPERIMENT TO PREPARE

2.1 The experimental device

Instrument of the experiments mainly include the tubular resistance furnace atmosphere, the heating

tube, air pretreatment equipment, air flow measurement device, flow control valve, temperature control instrument, mixed gas, flue gas analyzer, computer software system, etc. Experimental system diagram as shown in Figure 1.

This experiment flue gas source using simulated flue gas, gas ratio when simulating flue gas field configuration through the flowmeter. After the furnace exhaust concentration by flue gas analyzer measurement. The experimental system diagram as shown in Figure 2.

2.2 Test the raw material

This experiment used four kinds of biomass are from shandong jinan area, respectively for cypress wood, corn stalk, cotton pole, apple wood. First four kinds of biomass samples using the crusher for crushing, then put the raw material sample sieve sieve with 80 mesh points, make its granularity is smaller than 0.2 mm, then select a kind of typical biomass, the screen is divided into 80 mesh, 120 mesh and 120 mesh in three different particle

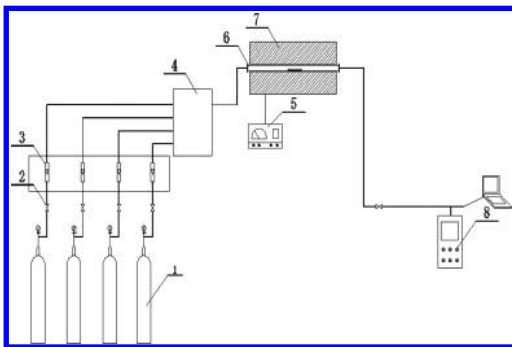


Figure 1. The experimental system diagram. 1—air tank 2—flow control valve 3—flow meter 4—mixed gas 5—temperature control instrument 6—tubular resistance furnace atmosphere 7—flue gas analyzer.

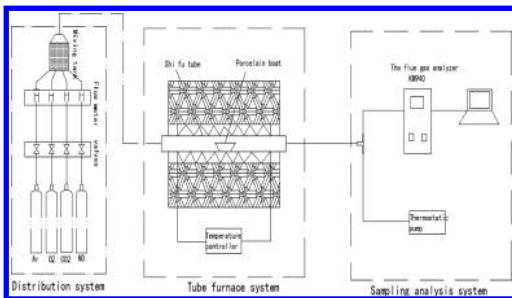


Figure 2. Biomass combustion NO_x reduction system graph again.

Table 1. Four kinds of raw materials of industrial analysis and elemental analysis.

Experimental sample	Industrial analysis/%ad				
	M_{ad}	A_{ad}	V_{ad}	V_{ad}	
Cypress wood	2.71	0.92	84.04	12.33	
Apple wood	3.31	3.31	79.99	15.57	
Cotton pole	5.1	3.1	74.6	17.2	
Corn stalk	17.2	5.93	71.45	17.75	
	Elemental analysis/%ad				
	C	H	O	N	S
Cypress wood	47.28	6.29	41.40	1.40	0.01
Apple wood	44.45	8.85	43.48	2.6	0.3
Cotton pole	41.2	5.1	28.75	1.39	0.12
Corn stalk	41.6	5.6	43.7	0.8	0.2

size. After the screening, the biomass in the electric heating oven drying into the glasswares standby after 4 ~ 6 hours. Four kinds of raw materials of industrial analysis and elemental analysis are shown in Table 1.

Can be seen by elemental analysis, lower biomass C content and higher content of H, four kinds of biomass C content is under 50%. The lower C content determines the biomass, the lower calorific value. Four kinds of biomass S content are below 2%, corn stalk almost do not contain S, so biomass combustion produces less sulfur oxides and nitrogen oxides. Through the analysis of biomass high volatile content, ash content is low, easy to burn, after combustion produces fewer pollutants, and is a kind of clean energy, suitable for as reburning fuel used for reburning denitration.

3 THE EXPERIMENTAL SYSTEM

The experiment system is mainly including the distribution system, tube furnace system and flue gas sampling analysis system, the introduction of each system are as follows:

3.1 Distribution system

Experiments using CO_2 , NO , O_2 and N_2 gas mixture by certain proportion to simulate flue gas, gas components, 99.9% purity of CO_2 and O_2 purity is 99.9%, and N_2 purity is 99.999%, NO purity of 1% (1% NO + 1% N_2). Simulated flue gas total flow of 1.68 L/min, the concentration of each component of the gas is respectively: CO_2 concentration is 15%, NO concentration respectively 500, 1000, 1500 ppm, and O_2 concentration is 3%.

3.2 Tube furnace system

Experimental heat tube furnace used for wuxi Belize engineering company produces the KTF-12 type tubular electric furnace. Electric furnace temperature control system with artificial intelligence technology, with the PID, fuzzy control, self-tuning capabilities and to prepare various temperature program, and other functions, the temperature control system shows that accuracy of 1 °C, ±5 °C temperature field stability, and heating rate of 1 ~ 20 °C can be set freely. Furnace adopts double furnace shell structure, double layer between the furnace shell is equipped with fan, cool can quickly rise, making the low surface temperature of the boiler shell. Furnace tube with high purity quartz tube, both ends with 304 high vacuum stainless steel flange sealing, two side sealing selects high heat-resistance quartz refractory fire bolt, used to heat sealing, to prevent the high temperature flue gas of instruments and equipment damage. Chamber of a stove or furnace material is made of high quality imported polycrystalline alumina fiber vacuum adsorption, energy saving 50%, heating element using silicon molybdenum rods. Heating tube in tube furnace gas section, connected with pressure monitoring devices, and connected to the flue gas analyzer.

3.3 The flue gas sampling analysis system

Experiment process, flue gas after filtering, enter OPTIMA7 handheld flue gas analyzer component measurement, O₂, NO, CO and SO₂ in flue gas concentration measurement by flue gas analyzer. O₂ concentration in the flue gas analyzer measurement range is: 0 ~ 21%, the accuracy of plus or minus 0.2%, NO: 0 ~ 5000 PPM, NO_x: 0 ~ 5000 PPM, flue gas temperature: 0 ~ 1200 °C.

Biomass reduction NO experiment, experiment measuring 0.500 g biomass in each group. Each group before the experiment, the first will be equipped with biomass porcelain boat into the quartz tube cold end, and to the quartz tube ventilation with high purity N₂ for a period of time, to eliminate the residual gas of the tube. Stay tube furnace temperature after reaching the set value, the simulated flue gas into the tube furnace, open the flue gas analyzer, to measure gas composition concentration of outlet of the quartz tube. After waiting for the gas composition concentration stability, quickly push the porcelain boat into the tube furnace central heating zone, system continue to record the gas composition concentration of outlet of the quartz tube.

Under different working conditions, the biomass burning the NO reduction rate is defined as:

$$\text{NO (reduction rate)} = (1 - [\text{NO}]_r / [\text{NO}]) * 100\%$$

Type, [NO] as the basic operating mode (before into biomass) measured under NO density; [NO]_r for reburning conditions (into) after the biomass under NO level was measured.

4 THE EXPERIMENTAL RESULTS AND ANALYSIS

4.1 The influence of biomass species of reduction NO

Reburning conditions, selection of reburning fuel directly affect denitration effect, different reburn fuel due to its characteristics vary, denitration effect is also different. Such as reburning zone temperature is 1000 °C, the initial concentration of NO is 1000 PPM remains the same, taking 0.500 g size for 120 to four kinds of biomass, under the condition of four kinds of biomass in the same oxygen concentration differences between the NO reduction rate is obtained. Experimental conditions, the use of cotton stalk, cypress, apple wood and corn stalk four kinds of biomass have been good denitration effect, using four kinds of biomass as reburning fuel can significantly reduce the NO emission concentration. Under the same experimental conditions, four kinds of biomass, cypress and apple wood reduction effect is NO best, cotton rod with corn stalk is close to NO effect, efficiency of maize straw sold out of the worst. Cypress, apple wood, cotton and corn straw reburning denitration rate were 83.1%, 80.3%, 69.6% and 83.1% respectively, and this is closely related to different biomass fuel properties.

4.2 Impact on the reduction of NO reburning zone temperature

From the chemical reaction kinetics, the reaction temperature for chemical reactions have important influence, therefore, in the process of biomass burning again, suitable reburning zone temperature is critical for the higher rate of NO reduction. The study shows that with the increase of pyrolysis temperature (673 k to 1173 k) in the biomass pyrolysis gas CO, H₂ concentration increased, CH group concentration decreased after rising first, and the ability of CO and H₂ removal NO compared with CH is very small, therefore, to volatile combustion temperature is too high to biomass homogeneous reaction efficiency of removing NO adverse. Moreover, reburn temperature can improve the phase-out of biomass char surface reaction intensity, but reburn temperature is too high will reduce the biomass char surface area and make the biomass char produces glass structure, blockage of biomass char pore, hindered the coke and NO contact, which would reduce the biomass

char surface heterogeneous reduction removal of NO strength. Therefore, biomass burning again is the best reburn temperature range, under this experimental condition, the biomass best reburn temperature range is 1073 ~ 1173 k.

By the experimental data can be seen that, in the case of oxygen ($O_2 = 3\%$), four kinds of biomass for the NO reduction rate increased with reburning zone temperature. The characteristics of biomass at different temperatures show is growing in different temperature reduction efficiency of NO matter the main reason for the differences. Based on different temperature or material will be the study of the release of the pyrolysis gas product, it can be seen that when the pyrolysis temperature from 800 °C to 1100 °C, the biomass pyrolysis of CH_4 concentration increasing, and CH_4 as biomass burning again restore NO quotiety of the main components in the process, its concentration increases for the NO reduction plays an important role in promoting. In addition, the Arrhenius equation shows that increasing reburning zone temperature, which improve the NO reduction reaction temperature, can strengthen the NO positive reaction rate of reduction reaction, thus promotes the NO reduction reaction.

4.3 Biomass particle size effect on reduction of NO

Biomass fuel combustion including volatile thermo-lysis, the homogeneous and residual phase-out of fixed carbon combustion. Small particle size, specific surface area is big, in the same condition, the volatile pyrolytic exhalation faster, able to quickly reach the ignition temperature began to burn, and residual carbon through heat conduction, convection and radiation heat faster, also the temperature in a short period of time to achieve the requirement of the fire, and immediately began to burn. Again at the same temperature, the faster the smaller the particle size of biomass heating rate, volatile the faster release rate and the higher the production rate of the volatile, homogeneous reaction known removal by NO more; Generated at the same time, the smaller the particle size, specific surface area increased, the biomass of coke on the surface of heterogeneous reaction intensity is enhanced, but coke decreased biomass, biomass of coke denitration biomass denitration the contribution rate of decline.

5 CONCLUSIONS

Due to the introduction of biomass gas in flue gas of biomass gas will NO dilution effect of flue gas, so when considering reburning reduction effect can't with the initial concentration of NO in flue gas and the exhaust measured concentration

of NO direct comparison. In experimental data processing when the concentration conversion method was adopted, which assumes that join the biomass gas has NO reduction effect but only NO dilution in flue gas, at the same time given to meet the requirements of automobile exhaust gas analyzer to measure flow rate and join the N_2 to exhaust measuring results, the influence of so I can get a reduced initial concentrations of $NO [NO]_0$.

Different kinds of biomass contains different volatile and coke content, volatile high biomass, rekindle high denitration efficiency; Biomass char surface heterogeneous reaction of NO removal is also very important.

Biomass, the smaller the particle size, the higher the volatile yield of biomass pyrolysis, the bigger the specific surface area of the biomass char, and heterogeneous reaction coke surface are enhanced, biomass combustion removal again NO efficiency increases, but the biomass burning biomass particle size selection must reference biomass grinding costs.

Biomass burning again is the best reburn condition parameters: the best reburn temperature is 1073 ~ 173 k, reburning zone excess air coefficient, fuel ratio and reburning zone residence time of 0.6 20% and 0.81 s, respectively.

ACKNOWLEDGEMENTS

This work was financially supported by the Doctor Foundation of Shandong Jianzhu University (XNBS1223) and the independent innovation project of academics in Jinan (No. 201401223).

REFERENCES

- [1] Hao Zhong, Jian Xie, Zongtao Yang, et al. The research status and development of biomass pyrolysis gasification technology [J]. Journal of yunnan normal university, 2001, 21(1): 41–45.
- [2] Qingshi Zhu, Lifeng Yan, Qingyang Guo. Biomass clean energy[M]. Beijing: Chemical Industry Press, 2002.
- [3] Stanley Harding N, Bradley Adams R. Biomass as a reburning fuel: a specialized cofiring application [J]. Biomass and Bioenergy, 2000, 19(6): 429–445.
- [4] Shen Boxiong Yao Qmag, Xuchang Xu. Kinetic model for natural gas reburning [J]. Fuel Processing Technology, 2004, 85: 1301–1315.
- [5] Pin Lu, ShengRong Xu, XiuMing Zhu. Study on NO heterogeneous reduction with coal in an entrained flow reactor [J]. Fuel, 2009, 88: 110–115.
- [6] Dong Li, Shiqin Gao, Wenli Song, et al. Experimental study of NO reduction over biomass char [J]. Fuel Processing Technology, 2007, 88: 707–715.
- [7] Wu Zhou, Kunzan Qiu, Zhihua Wang, et al. Coal and pulverized coal fineness of furnace combustion process denitration and burning characteristics [J]. Journal of chemical fuel, 2004, 2(2): 146–150.

Different approaches for energy saving in central air-conditioning system

Lin Hua Zhang, Dong Yang, Yun Xia Qu & Lin Xu

Key Laboratory of Renewable Energy Utilization Technology in Building of National Education Ministry, Jinan, China

Shandong Provincial Key Laboratory of Building Energy-Saving Technology, Jinan, China

School of Thermal Energy Engineering, Shandong Jianzhu University, Jinan, China

ABSTRACT: Energy consumption of central air conditioning system draws more attention to the public. Currently, electricity contributes to more challenges such as globe warming as the basic energy in the central air conditioning system. The severe situation of accelerating global warming and high consumption drive people to find some approaches to solve the problems. Therefore, it is essential to settle the problem. In this essay, three different methods are given to deal with energy consumption such as make use of heat pipe air-handing coil to save energy, based on the fuzzy logic for energy saving and decomposition-coordination method.

Keywords: central air conditioning system; energy saving; heat pipe air-handing coil; fuzzy logic; decomposition-coordination method

1 INTRODUCTION

The air-conditioning system plays a vital important role in refrigeration to adjust the air temperature and humidity in summer. However, the world energy demand will increase by 35 percent from 2010 to 2035. Increased energy demand leads to more greenhouse gas emission and accelerating globe warming. Therefore, the demand of air-conditioning system is increasing incredibly due to the effect of climate change and globe warming [1].

Cooling loads, especially the air-conditioning units, makes a great contribution to the energy consumption in tropical areas, especially in China. The central air conditioning system, which is one of the air-conditioning systems, is a typical AC system widely-used in commercial, administrative and institutional building [2]. At present, the central air conditioning units consume nearly 20% of electricity consumption in China [3]. Furthermore, 19 provinces in China have suffered the blackout because of the Excessive electricity consumption. In future China, Lu and Ma [4] stated that the commercial and residential areas will contribute to the large energy consumption. Hence, it is of vital importance to reduce the consumption of central air conditioning units for future life. In this essay, three kinds of methods are given to achieve the energy saving in central air conditioning system.

2 DIFFERENT METHODS FOR ENERGY SAVING

2.1 Heat pipe air-handing coil

In order to save energy in central air conditioning system, heat pipe air-handing coil is able to be used in the central air conditioning system. To reduce the energy consumption in the building, dew-point of the air supply is always used in the air-conditioning system. Compared with other heat recovery equipments, heat pipe is capable of not only giving people a better living environment but also saving energy, because it needs no energy or mechanical parts which can reduce energy consumption [5]. In Wan et al study, the loop heat pipe is preceded by a short circuit portion and a heat pipe in the cooling coil (Fig. 1). Heat pipe comprises a closed container which contains a two phase working fluid, such as refrigerant. When the hot air flow in the evaporator, the refrigerant absorbs heat from the liquid, and at the same time, the boiling liquid refrigerant becomes a refrigerant vapor then travels to the cooling section of the high-speed pipe (condensing unit). The pre-cooled air flows through the cooling coil. After further cooled and dehumidified, the moist air passes through the condensing section of heat pipe with lower temperature and humidity ratio, where the free air is reheated by using warm air from the evaporator into the heat recovery in the air condition. Meanwhile, the refrigerant vapor

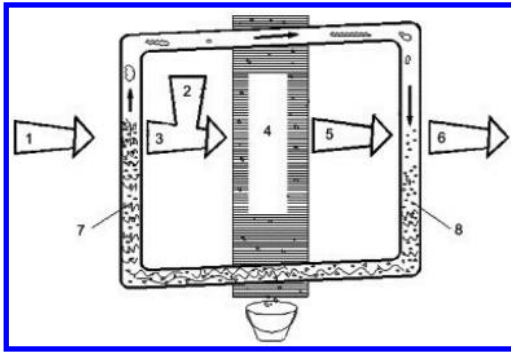


Figure 1. Arrangement of heat-pipe air-handling coil. (1) Outdoor air; (2) return air; (3) pre-cooled air; (4) cooling coil; (5) cooled and dehumidified air; (6) reheated air; (7) evaporating section of heat-pipe; (8) condensing section of heat-pipe.

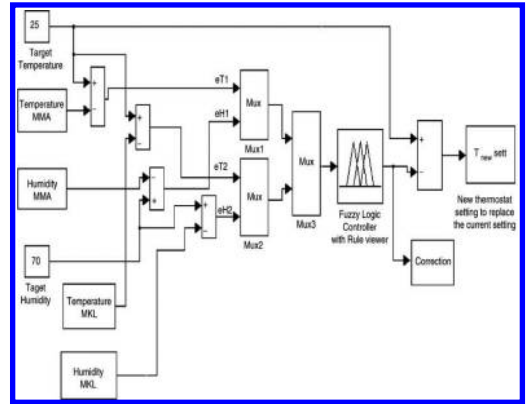


Figure 2. Simulink model of the developed fuzzy scheme.

is condensed into liquid refrigerant by giving up heat and returns to the evaporating section by gravity or by capillary action. By means of the heat pipe action, less sensible cooling is required so that the cooling coil is able to offer more latent capacity and superior dehumidification ability, and lower relative humidity supply air is obtained, which can improve the indoor air quality and thermal comfort. In addition, the peak cooling load is reduced by using heat pipe to pre-cool outside air, which contributes to the reduction of the equipment size such as chiller, chilled water pump.

According to Wan [5], a heat-pipe air-handling coil is able to be employed to store heat from outside air to reheat the apparatus dew point state air and as a result to save reheat energy.

2.2 Energy saving method based on fuzzy logic

Other scientists, such as Ahmed [2] pointed out the energy saving approach based on the Fuzzy logic in central air conditioning system. They proposed to control the temperature and humidity in one room which is served by a central air conditioner unit as well as reduce the electricity consumption.

Figure 2 shows the computer model that has been developed using the MATLAB-SIMULINK [6] for the proposed scheme. Input to this model cannot be applied immediately before the corrected instantaneous temperature setting AHU indoor temperature and humidity, and the temperature and relative humidity of the laboratory. The output is a correction in a thermostat (AHU located within a room) is set above 25 °C. The model is also considered using MATLAB fuzzy toolbox [7] as an input, respectively blur differences from objectives, namely 25 °C and 70%, and the output of the fuzzy decision-making. Figure 3(ac) are

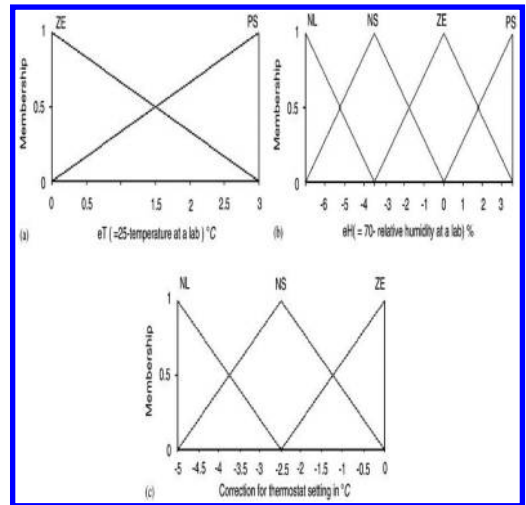


Figure 3. Fuzzy memberships of inputs and output variables respectively (a) differences of the labs' temperature from 25 °C, (b) differences of the labs' humidity from 70%, (c) correction in thermostat setting above 25 °C.

shown for input and output of the triangular fuzzy membership functions. The laboratory differences ZE 'zero and the "PS" (positive small)' temperature from 25 ° C is composed of two properties, it is clear. "Laboratory differences NL (negative large)," NS (negative small), "ZE 'from a relative humidity of 70% using a four qualifiers that blur", "(zero), and the" PS "(positive small). The output (corrected) has used three attributes were "NL", "NS", and "ZE 'which is limited. Thermostat sets (25 °C correction) after the change, and it turned out to be a positive number equal to or exceeding 25 °C. However, the thermostat is set up to study

the system can be changed to 30 °C maximum alignment marks. Therefore, any amendments that may need constant temperature exceeds 30 °C this is truncated to comply with the limits.

And then, Ahmed [2] came to the conclusion that it is evident that the proposed scheme has produced comfortable cooling and humidity level inside the labs for reduced energy intake of the AHU even when the outside weather was very warm and humid.

3 DECOMPOSITION-COORDINATION METHOD

Apart from the techniques above, some other methods are able to deal with the energy consumption in central air conditioning system.

Yao and Chen [5] advised to use decomposition-coordination method for global optimization. They first studied the components of the energy model, such as coolers and air heat exchanger surface. Then, the global optimization model to function is handed out normally by the target, and a series of constraint equations. The main task of the optimization model includes two aspects:

1. Determine the number of devices you want to run (such as chillers, cooling towers and cooling/chilled water pumps) to meet the cooling load requirements, while consuming the least energy;
2. The decision aimed at minimum energy consumption optimum operating conditions of the equipment. The former task can be viewed as the control variable for the device to perform a specific combination of integer programming problems operation, which is usually a non-linear programming problem Sun [6], central air conditioning system is a large scale complex system, which consists of numerous coupling components. To make the problem more clearly, in terms of the type of a local device list the optimization model, based on this, the entire system is a global integration.

It may have some difficulties to solve large-scale, and the use of traditional methods (such as direct search simplex method, gradient method) highly nonlinear optimization problem. Even a significant increase in computing power is not sufficient to offset the ever-increasing, such as the complexity of the central air-conditioning systems, energy systems. Therefore, it is necessary to solve the equation using a more efficient and reliable method [9]. in which a larger number of decision variables to be determined. Mathematical programming decomposition techniques have been extensively studied and has been shown to

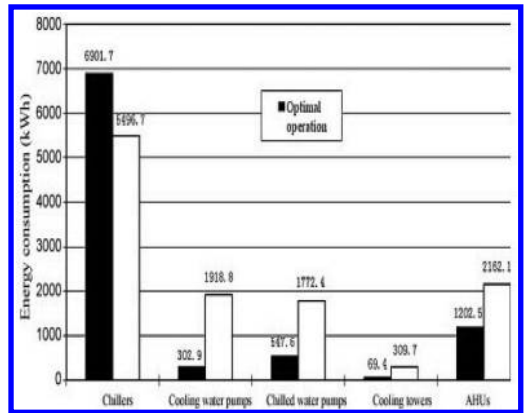


Figure 4. Energy consumption of different type of equipments in the system under optimal and actual operation.

be high-dimensional optimization problem solving on a global scale [10] [11] is an effective way to break down the main idea of the method is to split large system into many weakly coupled subsystems; partition variables or constraints set isolated sub-problems easier, and decentralization of decision-making of local decision-making between the global optimum [12]. With decomposition matrix elements one by one now, you can reduce the dimensionality of the original problem, and allows us to solve the problem the child has a smaller size than the overall problem in parallel, thereby reducing storage requirements and computational effort. Consequently, global optimization model based on the overall control of local energy saving device models developed central air conditioning system. Decomposition-coordination and effective way to solve the optimization problem with high dimension, introduced to solve the global model may involve large-scale air-conditioning system; a large number of decision variables are optimized.

Figure 4 shows the data that based on the method. The results in Figure 4 shows that the global optimization scheme will save the system about 2635 kWh of electrical energy on the focused day. Therefore, It is obvious that the method is useful for energy saving.

4 CONCLUSION

The energy consumption in central air conditioning system is always paid more attention by the society. In China, because of the severe environment and lack of natural resource, the energy saving becomes more important to the development of society. In this essay, those three methods are able to help local government to deal with the electricity

consumption. Furthermore, new approaches and technologies for saving energy will be studied in the future and new attempt will be conducted by the researchers to give the public a better life.

ACKNOWLEDGEMENTS

This paper was financially supported by the Doctor Foundation of Shandong Jianzhu University (No. XNBS1223) and the independent innovation project of academics in Jinan (No. 201401223).

REFERENCES

- [1] Daut, I., Adzrie, M., Irwanto, M., Ibrahim, P., and Fitra, M. Solar Powered Air Conditioning System. *Energy Procedia*, 2013, 6, 444–453.
- [2] Ahmed, S.S, Majid, M.S, Novia, H & Rahman, H.A. Fuzzy logic based energy saving technique for a central air conditioning system. *Energy*. 32 (7), 1222–1234.
- [3] Lu, W. Potential energy savings and environmental impacts of energy efficiency standards for vapor compression central air conditioning units in China. *Energy Policy*, 35(3), 1709–1717.
- [4] Lu, W., & Ma, Y. Image of energy consumption of well off society in China. *Energy Conversion and Management*, 45(9), 1357–1367.
- [5] Wan, J.W, Zhang, J.L. & Zhang, WM. The effect of heat-pipe air-handling coil on energy consumption in central air-conditioning system. *Energy and Buildings*, 39(9), 1035–1040.
- [6] Sun, J & Reddy, A. Optimal control of building HVAC and R systems using Complete Simulation-Based Sequential Quadratic Programming (CSB-SQP). *Building and Environment*. 40(5), 657–559.
- [7] MathWorks, Inc, & Wang, W.C. Fuzzy Logic Toolbox: for Use with MATLAB: User's Guide. MathWorks, Incorporated.
- [8] A Sun, J & Reddy, A. Optimal control of building HVAC and R systems using Complete Simulation-Based Sequential Quadratic Programming (CSB-SQP). *Building and Environment*. 40(5), 657–559.
- [9] Thi, H.A.L, Pham, D.T & Thoai, N.V. Combination between global and local methods for solving an optimization problem over the efficient set. *European Journal of Operational Research*, 26(6), 863–873.
- [10] Wang, Y.J & Ying, L. Global optimization for special reverse convex programming. *Computers and Mathematics with Applications*. 55(6), 1154–1163.
- [11] Artuto, M.C & Lorenz, T.B. A stable elemental decomposition for dynamic process optimization. *European Journal of Operational Research*. 142(2). 258–270.
- [12] Abdelouahed, H. Two-level primal-dual proximal decomposition technique to solve large scale optimization problems. *Applied Mathematics and Computation*. 160(3), 921–938.
- [13] Shahnawaz Ahmed, S., Shah Majid, M., Novia, H., & Abd Rahman, H. Fuzzy logic based energy saving technique for a central air conditioning system. *Energy*, 32(7), 1222–1234.
- [14] The Student Edition of SIMULINK: Dynamic System Simulation for MATLAB; Modeling, Simulation, Analysis. The Student Edition of SIMULINK for Windows 95/NT [M]. Prentice Hall, 1997.

The analysis of hydraulic characteristics of central heating pipe network under typical conditions

Lin Hua Zhang, Dong Yang, Guang Yang Gao, Yun Xia Qu & Shou Jun Jun

Key Laboratory of Renewable Energy Utilization Technology in Building of National Education Ministry, Jinan, China

Shandong Provincial Key Laboratory of Building Energy-Saving Technology, Jinan, China

School of Thermal Energy Engineering, Shandong Jianzhu University, Jinan, China

ABSTRACT: In this paper, we shall first briefly introduce the central heating pipe network hydraulic basic model and computation model. Through the simulation of primary pipe network, the two kinds of typical operation modes (the pump set the lift and at the end of constant pressure difference) at the beginning of the heating pipe network under adjustment, user valve adjustment of the hydraulic characteristics are analyzed.

Keywords: centralized heating; set head; the constant terminal differential pressure; hydraulic model

1 INTRODUCTION

The late 1970s and early 1980s, on the basis of China's research on water heating system working conditions, to study the thermal expansion conditions, and on the relationship between hydraulic conditions and thermal conditions, giving the lay of the conclusions: hydraulic systems are the important cause of system imbalance Enthusiasm [1]. Currently, Central heating system exist prevailing hydraulic imbalance generally, the actual operation of the heating system in each unit of heat users of heating medium flow heating area does not match with the design flow, which results in nearly cold thermal heat far imbalances [2]. To achieve a stable thermal condition of the heating system reasonably, it must be a stable hydraulic conditions and reasonable flow distribution. Typically, initial adjustment is before the central heating system is running (or running), so that each user to achieve the desired flow conditions (or design conditions). But the initial adjustment can only adjust the central heating system deployed by the heat load evenly, thereby enabling each user's average temperature to reach consensus. To ensure the central heating system throughout the heating period are running well, on-demand heating, also need running adjustment, at any time based on the outdoor temperature changes, and user self-regulate, regulate water temperature and flow pipe network [3]. Therefore, researching the hydraulic characteristics of urban centralized heating hot water pipe network in different operation mode,

can provide guidance for the actual operation of the pipe network, which has a very important practical significance.

2 MODELING HYDRAULIC CONDITIONS OF CENTRAL HEATING PIPE NETWORK

2.1 The basic model hydraulic conditions of central heating pipe network I

Central heating pipe network is a fluid network, which is similar to electrical network, complying with Kirchhoff's current and voltage laws, and the slip flow, pressure drop and pipeline resistance coefficient characteristics analogous to electric current branch network, voltage and resistance. For any network, you can get the basic model of central heating pipe network hydraulic conditions [4]

$$Aq_g = q_j \quad (1)$$

$$B_p p = 0 \quad (2)$$

$$p = S|q_g|q_g + \rho gh - \rho gH \quad (3)$$

A : tubes gateway linking matrix of $n \times m$ matrix of order, it is the sole representative of the topology of the network, its rank is n

q_g : pipe flow vector

$q_{g1}, q_{g2}, \dots, q_{gm}$: the 1, 2...pipe sections flow, m^3/h ;

q_j : net flow vector node ($q_{j1}, q_{j2}, \dots, q_{jn}$, m^3/h)

$q_{j1}, q_{j2}, \dots, q_{jm}$: the traffic nodes, m^3/h ;
 B_j : the basic loop matrix pipe network for $(m-n) \times m$ matrix;
 p : pipe pressure drop vector;
 p_1, p_2, \dots, p_m : the pressure drop tube segment, Pa;
 S : pipe resistance characteristics coefficient matrix (m-order diagonal matrix);
 $|q_g|$: q_g absolute value of (m-order diagonal matrix), $|q_g| = \text{diag}\{|q_{g1}|, |q_{g2}|, \dots, |q_{gm}|\}$, m^3/h ;
 ρ : fluid density, m/s^2 ;
 g : acceleration due to gravity, m/s^2 ;
 h : Vector pipe segment elevation difference of two nodes, $h = (h_1, h_2, \dots, h_m)$, m;
 H : Pump head vector pipe section, $H = (H_1, H_2, \dots, H_m)$, m.

2.2 The hydraulic conditions' calculation model of central heating pipe network

The calculating hydraulic conditions model (linear equations) [4] can be established after more than transformation the basic model of nonlinear hydraulic conditions:

$$M^k \Delta q_g^{k+1,k} = -\Delta q_z^k \quad (4)$$

M : Maxwell (Max Well) matrix, based on Bf-based $(mn) \times (mn)$ order symmetric positive definite matrix. M matrix corresponding to a certain tree, different tree, the corresponding matrix M is different, $Pa/(m^3 \cdot h^{-1})$

$k, k+1$: iterations

Δp_g : With sticks flow section (+1) th iteration of the first iteration of the difference vector, m^3/h

Δp_z : The basic circuit pipe pressure drop, Pa.

2.3 Level pipe network hydraulic modeling simulations

Simulation of A pipe network (see Fig. 1) is a single heat source branched pipe network, including 10 thermal stations, thermal stations using plate heat exchanger (hereinafter referred to as thermal stations each user). The model contain the main features of the city's district heating network, but

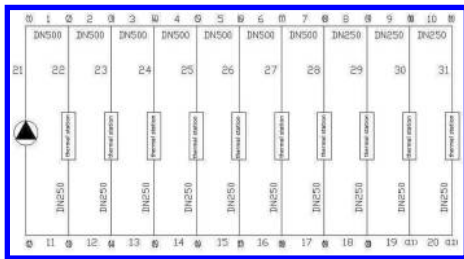


Figure 1. Simulation of a heating pipe network hydraulic model.

in some of the details were properly streamlined to facilitate pipe network modeling and dynamic characteristics of network analysis. Simulation of A pipe network design heat load is 67670 kW, average allocated to 10 thermal stations that each thermal station design heat load is 6 767 kW. The design supply and return water temperature of level network are 120, 60°C, namely the design flow rate of each thermal station is 100 m^3/h , the total flow of 1000 m^3/h .

The simulation takes users branch network to the connected branches, the length of each branch pipe section (Fig. 1 horizontal pipe) is 750 m, with sticks of supply and return pipe in two parts, both 50 m. The most unfavorable heat users (the most remote heat users) design pressure drop of 938.99 kPa, select the node 12 (ie, return the pump inlet) as a point of constant pressure, constant pressure point pressure pipeline network considering prevent vaporization, intrusion and other factors, taking 0.15 MPa [3].

3 THE RESULTS OF PUMP HEAD AND THE END OF THE SET PRESSURE HYDRAULIC CONDITIONS

To facilitate the discussion, defined here as the pump fixed head condition SBD conditions, the end of a given pressure conditions for the MDD conditions. The results were the first two of these conditions run after regulation and regulation were analyzed and compared.

3.1 SBD conditions

By calculating the most adverse thermal pressure drop of the entire pipe network users, the pump head is 938.99 kPa. Now the entire pipe network' run regulation can be made true by using Matlab software programming operation. SBD conditions for backwater pressure before and after the initial adjustment shown in Figure 2. The beginning of each branch of the flow regulator shown in Table 1.

Since before the initial adjustment, the proximal pressure is much greater than the user-owned by remote users, each user flow distribution is very uneven, appear consistent hydraulic imbalance. If operate as this conditions, the pump will lead to greatly increased power consumption, energy waste is enormous. Therefore, here, all the simulated networks have carried out the first adjustment pipe network hydraulic conditions to meet the design conditions.

3.2 MDD conditions

The constant pressure difference of the pipe network is 556.96 kPa, using differential pressure

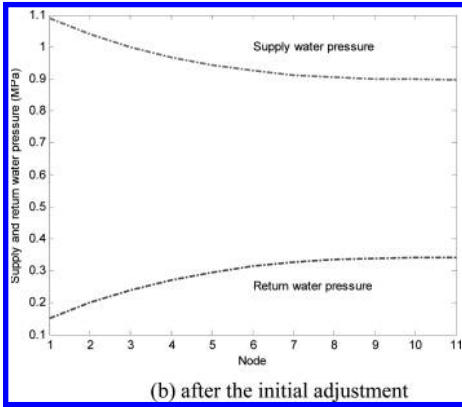
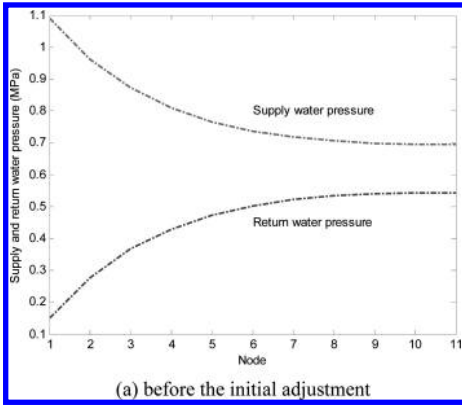


Figure 2. Supply and return water pressure before and after the initial adjustment under SBD.

Table 1. Each branch flow of SBD conditions before the initial adjustment.

User	Flow/(m ³ ·h ⁻¹)
1	253.5
2	217.9
3	188.9
4	165.8
5	148.2
6	135.4
7	126.9
8	122.1
9	119.9
10	119.3
Total	1598.0

way to the end, the pressure of near-user-owned is about 3550 kPa, which is seven times of the end user. Figure 3 gives the supply and return water pressure conditions before and after the initial adjustment under MDD.

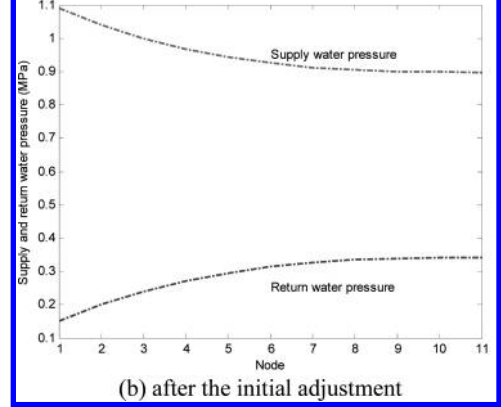
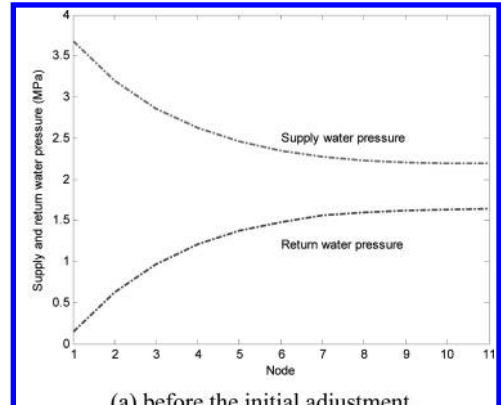


Figure 3. Supply and return water pressure before and after the initial adjustment under MDD.

Table 2. Each branch flow of MDD conditions before the initial adjustment.

User	Flow/(m ³ ·h ⁻¹)
1	496.8
2	426.2
3	368.8
4	323.2
5	288.3
6	263.0
7	246.3
8	236.6
9	232.3
10	231.2
Total	3113.0

Before the initial adjustment, the flow of each branch under MDD is shown in Table 2. Before the initial adjustment under the MDD condition, the total flow is 3113 m³/h, far beyond the design flow (1000 m³/h), hydraulic imbalance of the near-end

Table 3. The opening of the percentages control valve, after initial adjustment, in user road network under MDD.

User	Valve opening/%
1	70.18
2	71.61
3	72.85
4	73.88
5	74.70
6	75.28
7	75.67
8	75.89
9	75.99
10	76.02

user of 4.97, leading severe hydraulic imbalance. Long time of running down, not only cause some pressure on the pipe but also to the pump, causing operation to overload and great waste of energy.

The supply and return water pressure after the initial adjustment is shown in Figure 3(b), the backwater pressure curve is relatively flat, indicating a steady decline in funding for each user with pressure, operating conditions have been greatly improved. At the same time, each user' traffic has reached the design flow. Now, the opening of the percentages control valve in user road network is shown in Table 3.

4 THE HYDRAULIC CONDITIONS ANALYSIS AND COMPARISON OF THE PIPE NETWORK IN TWO WAYS

Based on initial adjustment of the pipe network adjustment, the article analyzed the valve pipe network hydraulic characteristics of the user to adjust under the two conditions.

4.1 Pressure analysis

Using the valve adjustment on the road of the 5 for example, analyze and compare the hydraulic conditions when the valve opening is 0.5, 0.9 and 0.747 (design conditions of the valve opening). Valve opening SBD conditions of shown as MSBD, and valve opening MDD conditions shown as MMDD. In the different backwater, the pressure charts under two operation modes are shown in Figure 4.

In the same valve opening, the users' supply water pressure reducing one by one, while backwater pressure increased in turn. As can be seen from Figure 4(a) and Figure 4(d), for the same network, either the pump or the end of a given set lift pressure, when early for hydraulic adjustment

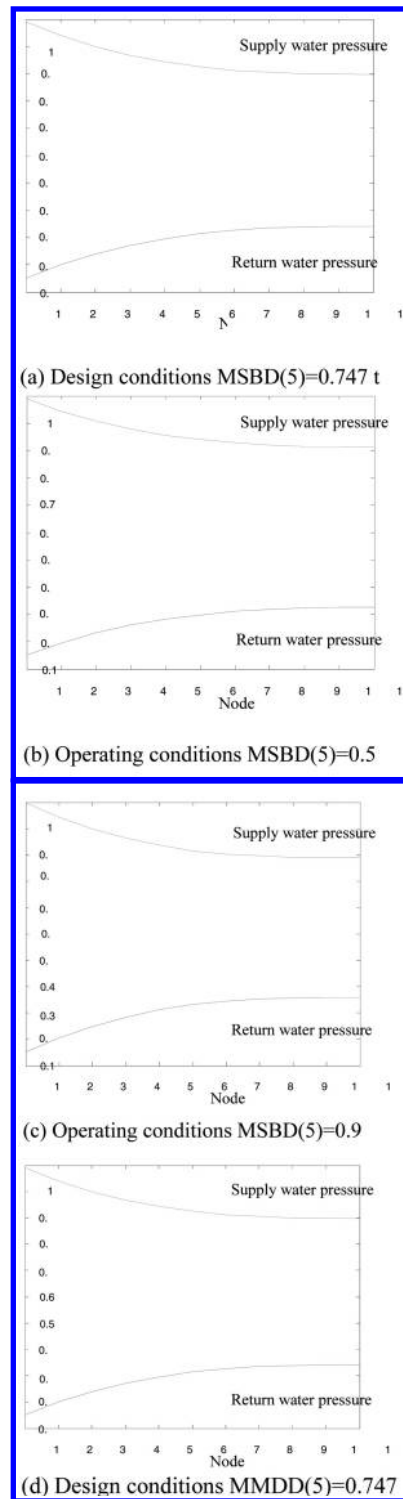


Figure 4. Supply and return water pressure under the two conditions in different valve opening.

and achieve the ideal conditions, the pipe network hydraulic engineering exactly the same conditions, and further illustrates the importance of early heating pipe network hydraulic adjustment. As can be seen from Figure 4(b), adjust the conditions of the water pressure is higher than when the design conditions, backwater pressure decreased, therefore each user's owned by the pressure increases. As can be seen from Figure 4(c), the water pressure in design conditions are lower than it in regulate working conditions, backwater pressure increases, thus reducing the funding for each user with the pressure.

Users water pressure regulating valve after the magnitude of the increase is equal to the magnitude of backwater pressure increases, so after the user's owned by pressure constant. The comparison of supply and return water pressure and owned by pressure of branch to Num. 5 user in different valve opening degree is shown in Figure 5.

From Figure 5 can be drawn from the laws of the pressure characteristics of the two conditions:

1. For SBD conditions, when the valve opening is changed on one of the road, the remaining water pressure increases with each user of the valve opening is reduced, the pressure increases with backwater valve opening and elevated, so the owned pressure decreases with the increase of the valve opening pressure.
2. For MDD conditions, with the increase of the valve opening, each user's supply and return water pressure increases; regardless of how regulating valve opening changes, adjust the valve after the user-owned branches unaffected by pressure, does not change; users before the regulator valve branch (including the adjustment of the user) with the valve opening increases, capital increases with pressure.

4.2 Traffic analysis

User traffic in the different valve opening under two conditions is shown in Table 4.

As can be seen from Table 4, the SBD condition, adjust the valve opening degree of the road user 5, when the branch where the user appears in the user's line before adjusting the offset, and the farther away from the pump, the greater the degree of hydraulic imbalance; appear after the user geometric disorder. Design conditions to the valve opening as a reference, when the valve opening becomes hours before, after adjusting users and traffic are greater than the design flow (100 m³/h), but after the user traffic are equal; when the valve opening becomes large, and traffic regulation before and after the user is less than the design flow rate, but the user traffic behind are equal.

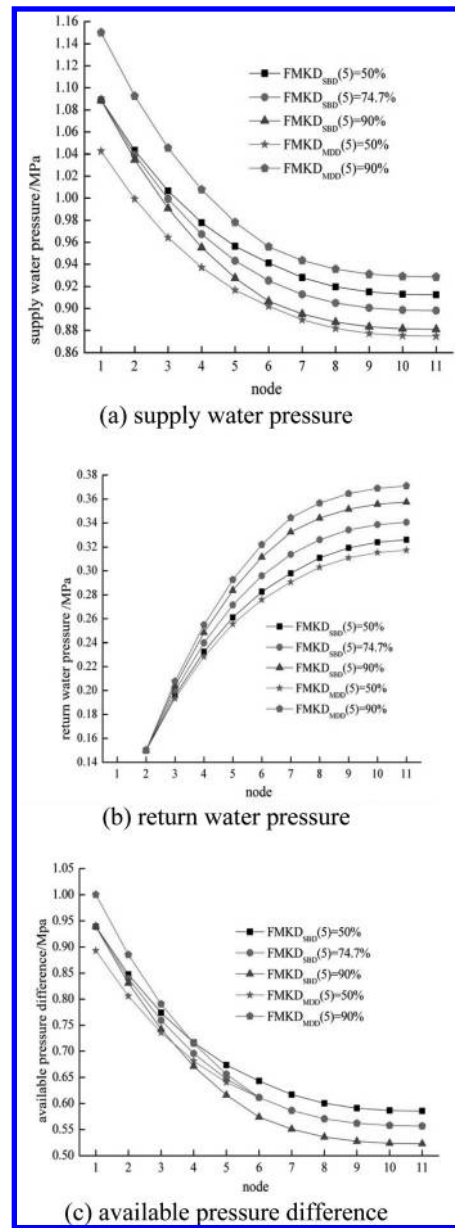


Figure 5. The comparison of supply and return water pressure and owned by pressure of branch to Num.5 user in different valve opening degree.

As for MDD conditions, regulating valve opening where the branch road users 5 users appear before adjusting user agreement disorders, and farther away from the pump, the smaller the hydraulic imbalance. The user traffic behind has no change in the design flow. Design conditions to the valve opening as a reference, when the valve opening

Table 4. User traffic in the different valve opening under two conditions (m³/h).

User	MSB D(5) = 50%	MSB D(5) = 90%	MMD D(5) = 50%	MMD D(5) = 90%	Design conditions
1	100.5	99.5	97.9	102.7	100.0
2	101.0	98.9	98.4	102.0	100.0
3	101.5	98.2	99.0	101.4	100.0
4	102.0	97.6	99.5	100.7	100.0
5	42.8	165.2	41.0	170.5	100.0
6	102.6	96.9	100.0	100.0	100.0
7	102.6	96.9	100.0	100.0	100.0
8	102.6	96.9	100.0	100.0	100.0
9	102.6	96.9	100.0	100.0	100.0
10	102.6	96.9	100.0	100.0	100.0
Total	960.8	1044	935.8	1 077	1000.0

becomes smaller, adjust the user before the user traffic is less than the design flow; when the valve opening becomes larger, adjust the user before the user traffic is greater than the design flow.

Therefore, the flow variation can be drawn under two operation modes:

Impact of changes in the valve opening: For SBD conditions, the valve before the user to adjust the slip, the closer the regulating valve branch, the greater the deviation from the design value of the flow, ie the greater the impact; while for MDD conditions, the before adjusting the valve branch users, the closer the slip regulator valve, the flow deviates from the design value is smaller, that is, the smaller the impact.

For the same branch (non-slip regulation), with the increase of the valve opening degree, the SBD conditions, flow gradually decreases; MDD condition when the slip regulator valve to gradually increase until the user traffic. When slip is a slip regulation, regardless of conditions, traffic will increase the valve opening as increases.

5 CONCLUSIONS

1. SBD conditions, changes in the user adjust the valve opening, have impact on other users' traffic and pressure, and the valve before users slip regulation, from the user to adjust the closer, the greater the impact.
2. MDD conditions, the user adjusted had no effect on the behind users' traffic and resource use pressure, keep the hydraulic characteristics of the design condition, the closer with the previous user adjusted, the smaller the impact.

3. SBD conditions, the regulated users have greater impact on its neighboring users, users in order to meet their requirements will turn up the heat with the valve, increasing the flow rate, which is bound to bring the pump power consumption increases.

The conclusions have great guiding significance on the promotion of district heating system operating adjustment and optimization control technology development and the improvement of urban central heating system operation and management level; which provide reliable theoretical basis systems to reduce energy consumption and improve energy efficiency.

ACKNOWLEDGEMENTS

This paper was financially supported by t the independent innovation project of academics in Jinan (No. 201401223).

REFERENCES

- [1] Shi Zhaoyu. Reconsider hydraulic balance of heating system [J]. District heating, 2010(1):4.
- [2] Bao Dunyan, Wang Xiaodong. Heat balance of Heating system and the hydraulic control [J]. The gas and heat, 2005, 25(10):25.
- [3] Zhou Shoujun. Based on network dynamic model of the urban centralized heat supplying system parameter prediction and operation optimization research (PhD thesis) [D]. Jinan: Shandong university, 2012:56-57.
- [4] Shi Zhaoyu. Fluid network analysis and synthesis [M]. Beijing: Tsinghua university press, 1993:5-14.

Experimental study on recycled slag aggregate concrete-filled steel tube under axial compression

Meng Cheng Chen, Jing Jian Liu & Hong Huang

School of Civil Engineering and Architecture, East China Jiaotong University, Nanchang, China

ABSTRACT: In order to study the influence of the types of recycled aggregate to recycled aggregate concrete-filled steel tube column, 11 short columns were tested under axial compression load. The major changes in parameters of specimens were the types of cross sections (including circle and square), the types of aggregates (including natural aggregate, 50% natural aggregate and 50% high titanium slag recycled aggregate, 50% natural aggregate and 50% normal recycled aggregate) and the sizes of steel tubes. The results show that the recycled aggregate concrete-filled steel tube short column's loading process, failure pattern, load-longitudinal strain curve are similar to normal concrete-filled steel tube short column. The changes of the type of recycled coarse aggregate have little effect on the properties mentioned above. Specimens with circular section show failure mode of shear type. Partial bucklings occur on four sides of square specimens after the test, and the degrees of bucklings are substantially the same. Compared circle specimens and square specimens with the same external size, it can be seen that the bearing capacity of square specimens is significantly higher than that of circular specimens, for the reason that the square specimens have a larger cross sections; and the strain correspond to peak load of square specimens is far less than that of circular specimens, and there is a rapid decline of the load when it meet the peak. The ductility of square specimens is significantly weaker than circular ones. The bearing capacity of recycled aggregate concrete-filled steel tube column is lower than normal concrete-filled steel tube column. The bearing capacity of recycled slag aggregate concrete-filled steel tube column is generally no less than recycled normal aggregate concrete-filled steel tube column. If the formula of normal concrete-filled steel tube column is used to calculate the bearing capacity of recycled aggregate concrete-filled steel tube column, the calculated value of circular specimens is conservative, while the calculation value of square specimens should be reduced.

Keywords: recycled aggregate concrete-filled steel tube; short column; axial compression; aggregate; bearing capacity

1 INTRODUCTION

There are 6 billion tons of garbage produced by Chinese city every year, in which there are about 2.4 billion tons of construction garbage. Waste concrete account 30%~40% [1] of the construction garbage. Waste concrete's negative impact on the environment is enormous. The issues of how to deal with waste concrete fragments are becoming more and more challenging. Besides, the production of concrete requires a lot of sand and gravel aggregate, but with the continuous exploitation of nature sand and gravel, natural resources also trend to be exhausted. The ensurance of the supply of high quality aggregate will be more and more difficult. To solve these issues, the production and construction of concrete must be applied with latest and high level of technology and management to save resources and energy, to reduce environmental

burden and to maintain ecological balance for sustainable development, rather than consuming a large amount of resources and energy.

At present, related researchs to using waste concrete as recycled aggregate to produce recycled concrete were done by domestic and foreign scholars, and they are used in road, building foundations cushion and reinforced concrete structural engineering. However, the strength and elastic modulus of recycled concrete is lower and durability is power compared to normal concrete. The common strength class of recycled concrete range from C20 to C50. As a result, recycled concrete may not applied directly in engineering structure. The best combination of proportioning of recycled concrete is studied by Zhou Jinghai et al [3]. They analysis the impact of replacement ratio of recycled aggregate to recycled concrete according to orthogonal experiments. The results show

that the best replacement ratio of recycled coarse aggregate is 50%.

If recycled concrete is poured into steel tube, due to the restriction effect from steel tube to concrete, the strength is improved. Meanwhile, the recycled concrete obstruct the inward buckling of steel tube. This method not only take the advantage of two kinds of material, but also avoid the disadvantage of them. Experimental study on recycled aggregate concrete-filled steel tube under axial compression is done by references [1–9]. The study results show that the mechanical properties of recycled aggregate concrete-filled steel tube is similar to corresponding normal concrete-filled steel tube under axial compression. Besides, the experimental results of Zhou Jinghai et al [3], Han L H and Yang Y F [4] show that the bearing capacity of recycled aggregate concrete-filled steel tube column is lower than normal concrete-filled steel tube column. The experimental results of Wang Yuyin et al [1] show that the replacement ratio of recycled coarse aggregate's influence to concrete-filled steel tube short column's bearing capacity is relatively small. The experimental study of Qiu Cichang et al [8] analysis the failure deformation features of thin wall recycled aggregate concrete-filled steel tube in different types of cross sections. The results show that the failure deformation features of thin wall recycled aggregate concrete-filled steel tube is similar to normal thin wall concrete-filled steel tube. The influence of the types of recycled aggregate to recycled aggregate concrete-filled steel tube column need to be studied.

To study the influence of the types of recycled aggregate to recycled aggregate concrete-filled steel

tube column, 11 short columns were designed and their mechanical properties under axial load were studied by the experiments. The major changes in parameters of specimens were the types of cross sections, the types of aggregates and the sizes of steel tubes.

2 EXPERIMENT DESCRIPTION

2.1 Design and production of test pieces

11 short columns were designed. The parameters of specimens are shown in Table 1. the major changes in parameters of specimens were the types of cross sections (including circle and square), the types of aggregates (including natural aggregate, 50% natural aggregate and 50% high titanium slag recycled aggregate, 50% natural aggregate and 50% normal recycled aggregate) and the sizes of steel tubes. The lengths of specimens were 3 times of the sizes of steel tubes. Four steel plates used to make tube wall were cut into predetermined size and then welded into steel tube when making square steel tube. Two square steel plates of thickness of 16 mm were made for each specimens. The strength of steel was tested by standard tensile experiment.

Normal concrete all used natural aggregate. Recycled normal concrete used 50% natural aggregate and 50% normal recycled aggregate, recycled slag concrete use 50% natural aggregate and 50% slag recycled aggregate. Normal recycled aggregate was from normal reinforced concrete specimens whose original strength class were c40. Recycled slag aggregate was from slag reinforced concrete specimens made by high titanium weight slag

Table 1. Parameters of specimens.

Number	Section	D or B /mm	t /mm	D/t or B/t	f_y /MPa	f_{cu} /MPa	f_{ck} /MPa	ξ	N_{uc} /kN	N_{uc} /kN	N_{uc}/N_{uc}
C-NC-114	Circle	114	2.65	43.0	336.6	41.5	27.7	1.212	750	673	1.12
C-NC-140	Circle	140	2.59	54.1	362.5	41.5	27.7	1.023	1030	932	1.10
S-NC-114	Square	114	2.97	38.4	391.2	41.5	27.7	1.592	950	914	1.04
C-RC-114	Circle	114	2.65	43.0	336.6	43.1	28.9	1.165	750	685	1.09
C-RC-140	Circle	140	2.59	54.1	362.5	43.1	28.9	0.984	1030	952	1.08
S-RC-114	Square	114	2.97	38.4	391.2	43.1	28.9	1.532	860	931	0.92
S-RC-140	Square	140	2.97	47.1	391.2	43.1	28.9	1.228	1250	1258	0.99
C-RS-114	Circle	114	2.65	43.0	336.6	42.8	28.6	1.175	790	683	1.16
C-RS-140	Circle	140	2.59	54.1	362.5	42.8	28.6	0.992	990	948	1.04
S-RS-114	Square	114	2.97	38.4	391.2	42.8	28.6	1.544	860	927	0.93
S-RS-140	Square	140	2.97	47.1	391.2	42.8	28.6	1.238	1325	1252	1.06

Notes: 1. Naming method of specimens: first number C represents that section type is circle, S represents that section type is square; middle number NC represent normal concrete, RC represent recycled aggregate concrete, RS represent recycled slag concrete; Arabic numbers represent the sizes of steel tubes. 2. D represent circular steel tube's outer diameter; B represent square steel tube's outer side length; t represent steel tube's thickness; f_y represent steel tube's yield strength; f_{cu} represent concrete's cubic compressive strength; f_{ck} represent concrete's axial compressive strength; ξ represent specimen's confining factor; $\xi = A_s f_y / (A_c f_{ck})$; N_{uc} represent the tested ultimate load of specimen by the experiment; N_{uc} represent theoretical value of ultimate load.

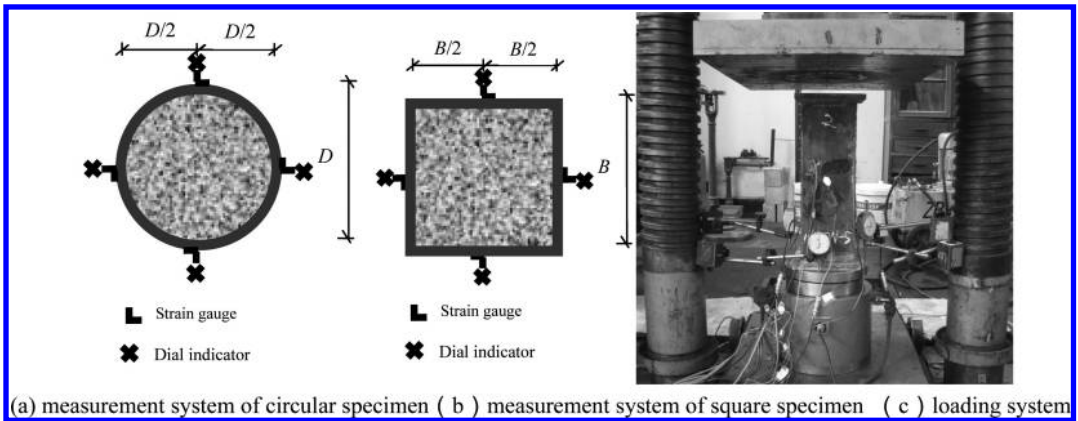


Figure 1. Loading and measurement system.

whose original strength class were C40. The waste concrete was crushed artificially and then screened. Then recycled coarse aggregate meet the standard of GB/T 25177-2010 Recycled coarse aggregate for concrete was available. The particle size of recycled coarse aggregate range from 4.75 mm to 31.5 mm. Normal concrete of strength class of C40 was poured according to JGJ 55-2011 Specification for mix proportion design of ordinary concrete. Recycled concrete of strength class of C40 was poured according to JGJ/T 240-2011 Technical specification for application of recycled aggregate. Cement was HAILUO brand 42.5R normal portland cement. Normal coarse aggregate was natural gravel. Fine aggregate was natural sand. Water was city water. Concrete was poured artificially. Steel tube stand and was poured into concrete from the top hierarchically and poker vibrator is used when pouring. The conservation methods of specimen were the nature conservation. Surface laitance of concrete was chiseled away two weeks later. Then the surface of concrete and steel tube were wiped by high-strength epoxy mortar. They were polished smooth after their hardening. Then upper cover plates were welded to ensure the steel tube and core concrete can bear the load together at the beginning of the load.

2.2 Loading and measurement system

The experiments were conducted in 500t Hydraulic pressure test machine, Structural Engineering Laboratory, East China Jiaotong University. Step load system was applied in the experiment. Each stage of load was 1/10 of expected ultimate load in elastic range. Each stage of load was 1/15 of expected ultimate load after the yield of steel tube. Holding time of each load stage is 2 to 3 minutes. Load slowly and continuously when approaching failure.

Strain and displacement were collected automatically by computer data acquisition system.

Loading and measurement system are shown in Figure 1. 4 series of longitudinal strain gauges and transverse strain gauges were pasted symmetrically in middle section of steel tube. 4 WBD-30B dial indicator resistance strain displacement transducers (electromechanical dial indicator) whose accuracy was 0.001 mm and range was 30 mm were arranged at four corners of specimens. 5000 kn load transducer was arranged under the specimens to monitor the axial force loaded on the specimens.

3 EXPERIMENTAL RESULTS AND ANALYSIS

3.1 Failure modes

Failure modes of specimens are shown in Figure 2. It can be seen that recycled aggregate concrete-filled steel tube short column's failure pattern is similar to normal concrete-filled steel tube short column. The changes of the type of recycled coarse aggregate have little effect on the properties mentioned above. Specimens with circular section show failure mode of shear type and there are several places of buckling on the surface of outer steel tube. Partial bucklings occur on four sides of square specimens after the experiment, and the degrees of bucklings are substantially the same. Weld cracking occur at some part of serious buckling.

3.2 Relationship of load and deformation

Experimental results of N (axial load)- ϵ (notional longitudinal strain) curves of all specimens are shown in Figure 3. N - ϵ relationship of concrete-filled steel tube and recycled aggregate concrete-filled



Figure 2. Failure modes of specimens.

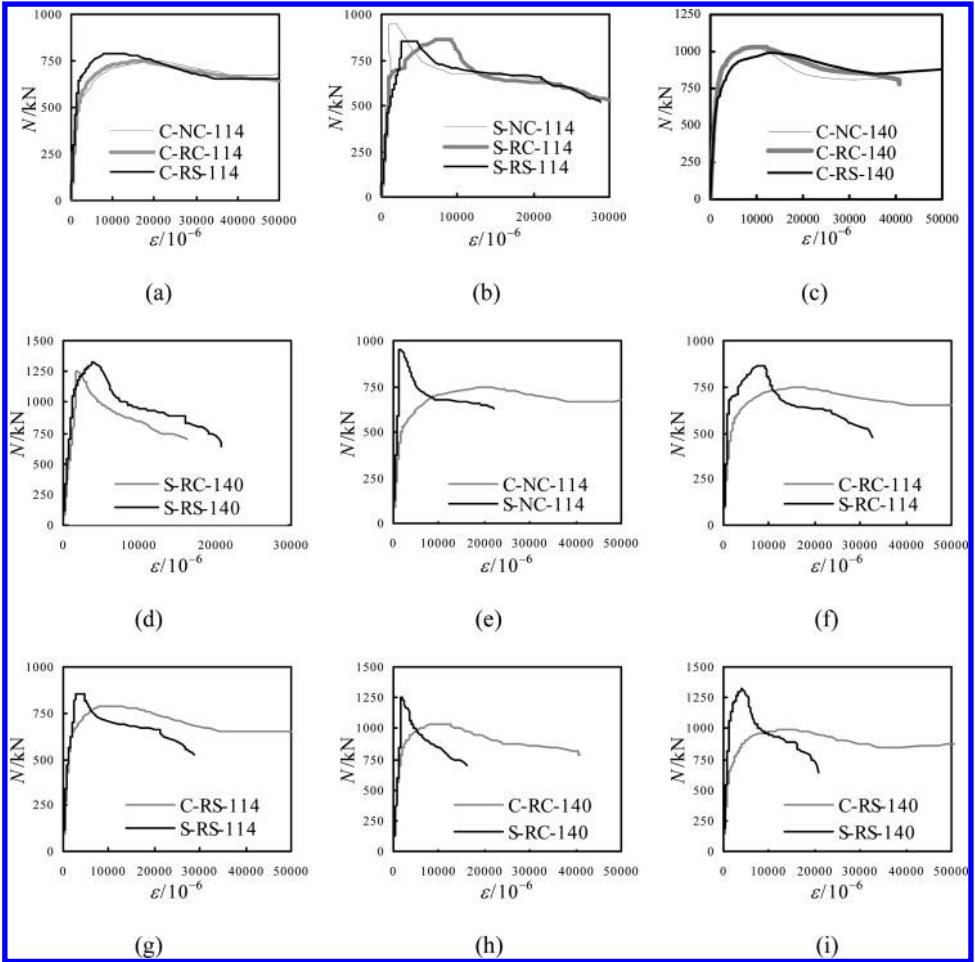


Figure 3. N - ϵ curves of specimens.

steel tube of different recycled coarse aggregate are compared in Figure 3(a)-(d). It can be seen that recycled aggregate concrete-filled steel tube short column's load-notional longitudinal strain relationship is similar to normal concrete-filled steel tube short column. The changes of the type

of recycled coarse aggregate have little effect on the properties mentioned above. N - ϵ relationship of different section type are compared in Figure 3(e)-(i). Compared circle specimens and square specimens with the same external size, it can be seen that the bearing capacity of square

specimens is significantly higher than that of circular specimens, for the reason that the square specimens have a larger cross sections; but the strain correspond to peak load of square specimens is far less than that of circular specimens, and there is a rapid decline of the load when it meet the peak. The ductility of square specimens is significantly weaker than circular ones.

4 CALCULATION OF BEARING CAPACITY

To verify the applicability of the formula of bearing capacity of normal concrete-filled steel tube to recycled aggregate concrete-filled steel tube, each specimen's ultimate load is calculated by the formula of bearing capacity of normal concrete-filled steel tube put forward by reference [4]. The formula is:

$$N_{uc} = A_{sc} f_{scy}$$

N_{uc} represent theoretical value of ultimate load of concrete-filled steel tube under axial load; A_{sc} represent cross section area of concrete-filled steel tube ($A_{sc} = A_s + A_c$); f_{scy} represent strength index of concrete-filled steel tube under axial load, to circular concrete-filled steel tube $f_{scy} = (1.14 + 1.02\xi) f_{ck}$, to square concrete-filled steel tube $f_{scy} = (1.18 + 0.85\xi) f_{ck}$.

N_{uc} of all specimens are shown in Figure 1, after comparing N_{uc} and N_{ue} , it is shown that:

The formula of bearing capacity mentioned above has a good applicability to normal concrete-filled steel tube.

N_{uc}/N_{uc} of recycled aggregate concrete-filled steel tube is lower than that of normal concrete-filled steel tube. It is shown that the bearing capacity of recycled aggregate concrete-filled steel tube column is lower than normal concrete-filled steel tube column.

N_{uc}/N_{uc} of recycled slag aggregate concrete-filled steel tube is generally higher than that of recycled aggregate concrete-filled steel tube. The bearing capacity of recycled slag aggregate concrete-filled steel tube column is generally no less than recycled normal aggregate concrete-filled steel tube column.

If the formula of normal concrete-filled steel tube column is used to calculate the bearing capacity of recycled aggregate concrete-filled steel tube column, the calculated value of circular specimens is conservative, while the calculation value of square specimens should be reduced.

5 CONCLUSION

Recycled aggregate concrete-filled steel tube short column's loading process, failure pattern,

load-longitudinal strain curve are similar to normal concrete-filled steel tube short column. The changes of the type of recycled coarse aggregate have little effect on the properties mentioned above.

1. Specimens with circular section show failure mode of shear type and there are several places of serious buckling on the surface of outer steel tube. Partial bucklings occur on four sides of square specimens after the experiment, and the degrees of bucklings are substantially the same. Compared circle specimens and square specimens with the same external size, it can be seen that the bearing capacity of square specimens is significantly higher than that of circular specimens, for the reason that the square specimens have a larger cross sections; hut the strain correspond to peak load of square specimens is far less than that of circular specimens, and there is a rapid decline of the load when it meet the peak. The ductility of square specimens is significantly weaker than circular ones.
2. The bearing capacity of recycled aggregate concrete-filled steel tube column is lower than normal concrete-filled steel tube column. The bearing capacity of recycled slag aggregate concrete-filled steel tube column is generally no less than recycled normal aggregate concrete-filled steel tube column. If the formula of normal concrete-filled steel tube column is used to calculate the bearing capacity of recycled aggregate concrete-filled steel tube column, the calculated value of circular specimens is conservative, while the calculation value of square specimens should be reduced.

ACKNOWLEDGEMENTS

The research reported in the paper is part of the Project 51378206, 51008122 and 50968006 supported by the National Natural Science Foundation of China (NSFC), Jiangxi Provincial Department of Education Technology Plan Landing Project (Jiangxi Finance and Education (2011) 243), Jiangxi Young Scientists of Cultivation Project (20133BCB23015) as well as Jiangxi Focus Fund (20114 ACB01000, 20122BAB206006). The financial support is highly appreciated.

REFERENCES

- [1] Wang Yuyin, Chen Jie, Zong Bin, et al. Mechanical behavior of axially loaded recycled aggregate concrete filled steel tubular stubs and reinforced recycled aggregate concrete stubs [J]. *Journal of Building Structures*, 2011(12):170–177. (in Chinese).

- [2] Xiao Jianzhuang. *Recycled concrete* [M]. Beijing: China Architecture & Building Press, 2008: 5–7. (in Chinese).
- [3] Zhou Jinghai, Su Ming, Meng Xianhong, et al. Recycled Self Compacting Concrete-Filled Steel Tube Stub Columns Tests [J]. *Journal of Shenyang Jianzhu University* (Natural Science), 2011(2):266–271. (in Chinese).
- [4] Han L.H, Yang Y.F. *Modern Concrete filled steel tube structures technology* [M]. Second Edition. Beijing: China Architecture & Building Press, 2007. (in Chinese).
- [5] Konno K, Sato Y, Kakuta Y, et al. Property of recycled concrete column encased by steel tube subjected to axial compression [J]. *Transactions of the Japan Concrete Institute*, 1997, 19(2):231–238.
- [6] Yang Y.F, Han L.H. Compressive and flexural behaviour of recycled aggregate concrete filled steel tubes (RACFST) under short-term loadings [J]. *Steel and Composite Structures*, 2006, 6(3):257–284.
- [7] Qiu Changlong. Study on recycled concrete and analysis of mechanical properties of steel tube recycled concrete short column [D]. Chengdu: Southwest Jiaotong University, 2009:62. (in Chinese).
- [8] Chen Z.P, Liu F, Zheng H.H, Xue J.Y. Research on the bearing capacity of recycled aggregate concrete-filled circle steel tube column under axial compression loading [C]/2010 International Conference on Mechanic Automation and Control Engineering. Wuhan: Wuhan Institute of Technology, 2010:1198–1201.
- [9] Qiu Cichang, Wang Qingyuan, Shi Xiaoshuang, et al. Experimental investigation on the behavior of recycle concrete-filled thin-walled steel tube under axial compression [J]. *Journal of Experimental Mechanics*, 2011, 26(1):8–15. (in Chinese).
- [10] GB/T 25177-2010 *Recycle coarse aggregate for concrete* [S]. (in Chinese).
- [11] JGJ 55-2011 *Specification for mix proportion design of ordinary concrete* [S]. (in Chinese).
- [12] JGJ/T 240-2011 *Technical specification for application of recycled aggregate* [S]. (in Chinese).

Study of damage statistical elastic damage constitutive model for rock considering residual strength and threshold

Yong Qiang Zhou, Qian Sheng, Xiao Dong Fu, Shao Bo Chai & Long Fei Li

State Key Laboratory of Geomechanics and Geotechnical Engineering, Institute of Rock and Soil Mechanics, Chinese Academy of Science, Wuhan, China

ABSTRACT: Based on the statistical theory and damage theory, the article, considering the residual strength and damage threshold of the rock, establishes a damage statistical model for rock under tri-axial compression condition. On the basis of the damage model, using the extreme characteristics of rock stress-strain at low confining pressure, a unified solution of the model parameters is derived. By comparison with the experimental data, it is discovered that: It shows the breakdown of rock and its extension is closely related to the stress state; through the introduction of the correction factor of damage variable, the residual strength of rock is solved. As well, a new method is proposed for solving the correction factor, which makes the theoretical curve, derived from the damage model, not only can be a good close to the experimental data, but also overcome the various issues of the previous solving methods of correction factor; That the stress yield point as the damage threshold point, it can avoid the situation that value of damage factor is not from 0 to 1 in the low load.

Keywords: Weibull distribution; correction factor; threshold; residual strength

Rock under outer loads will produce many random distributive micro cracks which make rock have part of the strength lost as well as stiffness deteriorated at the macro level. The statistical theory will be the most important method on the analysis of the micro-cracks distribution.

The theoretical methods for studying the influence of the micro-cracks distribution are essentially based on different types of statistical distribution. Many studies assume that micro-unit strength obey Weibull distribution (1). Jiang et al. (2) used lognormal distribution. Cao et al. (3) expanded study on statistical constitutive model and determination of parameters of rock by using normal distribution. By comparing and analyzing, Zhang (4) suggested that Weibull distribution is more applicable than normal distribution or like Weibull distribution in elastic damage probability models and Weibull distribution will be the preferred one. Based on Weibull distribution, Cao (5) proposed a new representation based on Drucker-Prager criterion, which provides a new way to determine the micro-unit strength.

According to the definition of damage, damage will occur not as soon as rock under deformation or bearing but when the deformation or the internal stress exceeds a certain level, namely, the material exists of the so-called damage threshold. Li (7) deemed that damage threshold related to yield strain. Besides, threshold variable relates to

stress state. Therefore, it is reasonable to choose damage threshold the stress related to the stress amount described in more reasonable. Due to friction and confining pressure, rock in the latter part of full of stress-strain curves still has some residual strength, which is expressed as pure friction. Although some scholars consider the impact of residual strength, and the introduction of the initial number of injuries or damage variable correction factor, however, it can only describe the correlation between residual strength and peak intensity, but not quantitatively reflect the residual strength, but also its determination method is not given. So far there are a few, even few, rock models considering the residual strength and damage threshold.

1 ROCK SOFTENING MODEL WITHOUT THE DAMAGE THRESHOLD

1.1 Damage variable

According to Lemaitre [6] strain equivalence hypothesis, the stress-strain relationship of damaged materiel can be replaced by that in lossless state with replacing the nominal stress σ_i to effective stress σ_i' , i.e.,

$$\sigma_i = (1 - D) \sigma_i' \quad (1)$$

where D is the damage variable. According to continuum mechanics, D means the infinitesimal number of damaged rock to that of all. Assuming rock particles obey the Weibull distribution, the damage variable can be expressed as

$$D = \frac{n}{N} = \frac{\int_0^F NP(F) dF}{N}$$

$$= \frac{\int_0^F N \frac{m}{F_0} \left(\frac{F}{F_0}\right)^{m-1} \exp\left[-\left(\frac{F}{F_0}\right)^m\right] dF}{N}$$

$$= 1 - \exp\left[-\left(\frac{F}{F_0}\right)^m\right] \quad (2)$$

where m and F_0 are distribution parameters, respectively, m , means rock brittleness, and if F is axial strain, F_0 means ultimate strain, else if F is the stress function, then F_0 means the macro rock strength.

1.2 Rock damage model without the damage threshold

Elastic constitutive model of lossless rock under triaxial confining pressure is:

$$\sigma_i = E\varepsilon_i + \mu(\sigma_j + \sigma_k) \quad (3)$$

where i, j, k , are 1, 2, 3, respectively. E and μ are general parameters of rocks, i.e., elastic modulus and Poisson's ratio, respectively. Based on the above equation, damaged rock can be assumed to obey Hook's law, i.e.,

$$\sigma'_i = E\varepsilon'_i + \mu'(\sigma'_j + \sigma'_k) \quad (4)$$

Assuming the damaged part and lossless part of the rock keep deformation compatibility, the strain in the rock is constant. According to the definition, Poisson's ratio is also constant.

By substituting Eqs. 1 and 4 into Eq. 3, the damage model with threshold under triaxial confining pressures is obtained:

$$\sigma_i = E\varepsilon_i(1-D) + \mu(\sigma_j + \sigma_k)$$

$$= E\varepsilon_i \left[\exp\left[-\left(\frac{F}{F_0}\right)^m\right] \right] + \mu(\sigma_j + \sigma_k) \quad (5)$$

From Eq. 5, damage variable, D , can be derived as

$$D = \frac{E\varepsilon_i + \mu(\sigma_j + \sigma_k) - \sigma_i}{E\varepsilon_i} \quad (6)$$

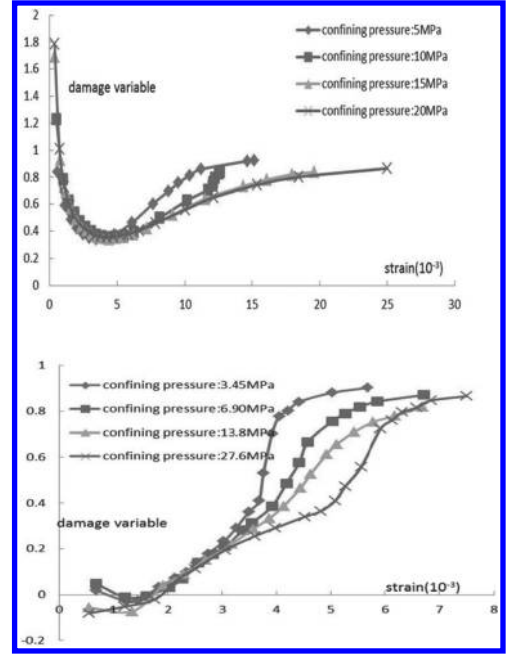


Figure 1. The changing process of damage variable as strain.

With Eq. 6 and the axial stress and strain relationship under different confining pressures (8–9), damage variables in different axial strains are obtained, as Figure 1 shows.

From Figure 1, the value of damage variable is not in the interval $[0, 1]$. That is inconsistent with the reasonable value interval. With increasing load, the value of damage variable is increasing, and finally converges to 1, which means rock is instability; with the confining pressure increases, the damage variable correspondingly increased. These phenomena illustrate the damage on the rock has a threshold, and is associated with stress, which just verifies the above conclusions. So when you create the model of rock damage, threshold should be considered.

2 ROCK DAMAGE MODEL WITH THE THRESHOLD AND RESIDUAL STRENGTH

Damage occurs when rocks bear the load especially the confining pressure, its strength will not immediately become 0 but some residual strength caused by friction.

For that, many studies take the damage variable correcting parameters or initial damage value

$$\sigma_i = (1 - \delta D) \sigma_i' \quad (7)$$

where δ is the damage variable correcting parameters or initial damage value. There is two ways to determine its value, one is fitting rock stress-strain curve by changing δ value, the other is definition that δ is the ratio of residual strength to the peak intensity or its 1/2 power. The first way is too tedious and more difficult and has a terrible shortage. When δ is less than 1, With increasing strain, the stress after the peak stress is reduced, but when the strain reaches a certain value, with increasing strain, but stress has increased, and the smaller, the greater the stress increasing, which does not accord with actual situation seriously. The second class method solves the problems of the first class method, but in a certain confining pressure, along with the δ increase, residual strength and the peak intensity reduce, and the residual strength decreases far greater than the amplitude of the peak intensity, which is contrary to the definition. Therefore, the front two methods are not very desirable, this paper proposes an alternative approach to consider residual strength: use the same introduction damage variable correction parameters, like the formula (7), but when solving the model parameters, it needs to meet the following condition:

$$\sigma_1 \Big|_{\sigma_1 = \sigma_u, \varepsilon_1 = \varepsilon_u} = \sigma_u \quad (8)$$

$$\frac{d\sigma_1}{d\varepsilon_1} \Big|_{\sigma_1 = \sigma_c, \varepsilon_1 = \varepsilon_c} = 0 \quad (9)$$

$$\sigma_1 \Big|_{\sigma_1 = \sigma_u, \varepsilon_1 = \varepsilon_u} = \sigma_u \quad (10)$$

By Eqs. 5, 9, 8 and 10, the expression of model parameters m , F_0 and δ under different criterions or axial strains is obtained as

$$m = - \frac{\frac{\sigma_c - \mu(\sigma_2 + \sigma_3)}{\varepsilon_c} F \Big|_{\sigma_1 = \sigma_c, \varepsilon_1 = \varepsilon_c}}{\left[\sigma_c - \mu(\sigma_2 + \sigma_3) - E\varepsilon_c(1 - \delta) \right] \frac{dF}{d\varepsilon_1} \Big|_{\sigma_1 = \sigma_c, \varepsilon_1 = \varepsilon_c} \ln \left[\frac{\sigma_c - \mu(\sigma_2 + \sigma_3)}{\delta E \varepsilon_c} - \frac{1}{\delta} + 1 \right]} \quad (11)$$

$$F_0 = \frac{F \Big|_{\sigma_1 = \sigma_c, \varepsilon_1 = \varepsilon_c}}{\left(-\ln \left[\frac{\sigma_c - \mu(\sigma_2 + \sigma_3)}{\delta E \varepsilon_c} - \frac{1}{\delta} + 1 \right] \right)^{1/m}} \quad (12)$$

$$\begin{aligned} & F \Big|_{\sigma_1 = \sigma_c, \varepsilon_1 = \varepsilon_c} \ln \frac{F \Big|_{\sigma_1 = \sigma_c, \varepsilon_1 = \varepsilon_c}}{F \Big|_{\sigma_1 = \sigma_u, \varepsilon_1 = \varepsilon_u}} \\ & + \ln \frac{\ln \left[\frac{\sigma_c - \mu(\sigma_2 + \sigma_3)}{\delta E \varepsilon_c} - \frac{1}{\delta} + 1 \right]}{\ln \left[\frac{\sigma_u - \mu(\sigma_2 + \sigma_3)}{\delta E \varepsilon_u} - \frac{1}{\delta} + 1 \right]} \\ & \left[\sigma_c - \mu(\sigma_2 + \sigma_3) - E\varepsilon_c(1 - \delta) \right] \frac{dF}{d\varepsilon_1} \Big|_{\sigma_1 = \sigma_c, \varepsilon_1 = \varepsilon_c} \\ & \frac{\ln \left[\frac{\sigma_c - \mu(\sigma_2 + \sigma_3)}{\delta E \varepsilon_c} - \frac{1}{\delta} + 1 \right]}{\frac{\sigma_c - \mu(\sigma_2 + \sigma_3)}{\varepsilon_c} F \Big|_{\sigma_1 = \sigma_c, \varepsilon_1 = \varepsilon_c}} = 0 \end{aligned} \quad (13)$$

where Eq. 13 is an implicit equation, which is solved by iteration. The value of δ , not limit between 0 and 1, can be any one.

On this basis, considering the damage threshold, which is:

$$\sigma_i = \begin{cases} E\varepsilon_i + \mu(\sigma_j + \sigma_k) \\ E\varepsilon_i \left(1 - \delta + \delta \exp \left[- \left(\frac{F}{F_0} \right)^m \right] \right) + \mu(\sigma_j + \sigma_k), \\ \sigma_u \end{cases} \quad (14)$$

$$F < F_s$$

$$F \geq F_s \text{ 且 } \sigma_i > \sigma_u$$

$$\sigma_i = \sigma_u$$

Eq.14 is rock damage statistical model with the threshold and residual strength.

3 COMPARISON AND VERIFICATION

In this section, the damage statistical model is investigated and compared. The rock mass parameters as follows: the Young modulus E is 90 GPa, the Poisson's ratio μ is 0.25, the internal friction angle φ is 31.30 and the cohesive force is 45.1648 MPa. Figure 2 shows the model parameters m , F_0 regardless of the residual strength effect obtained under different criterions. From Eqs. 11–13, the parameters of the damage model under different confining pressure can be obtained and shown in Figure 3. It can be seen from Figure 3 that the damage model considering residual strength under different confining pressure is more close to the experimental

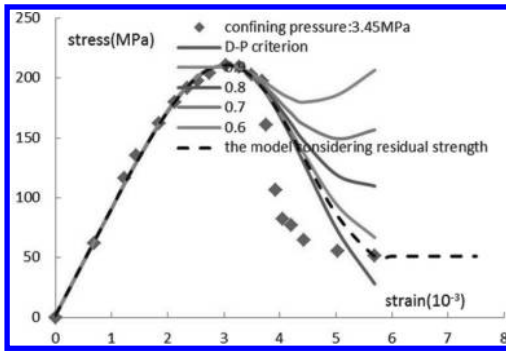


Figure 2. The fitting of experimental data and theory data derived from damage model based on the Drucker-Prager criterion under different confining pressure (regard of the residual strength).

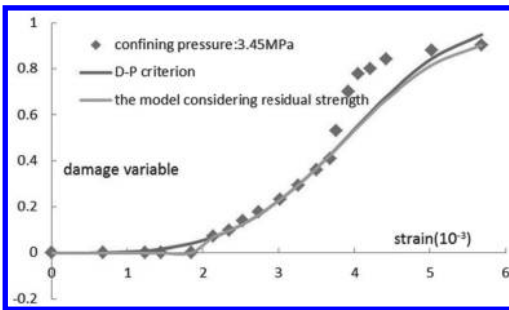


Figure 3. The changing process of damage variable as strain.

curve than the damage model based on conventional D-P criterion which is not considering residual strength.

4 CONCLUSION

1. Rock has a threshold of damage, which is associated with stress state.
2. Through the use of extreme value theory, the unity solving style of three parameters m , F_0 , δ is derived, which is good way to solve the problems of previous damage due to the introduction of variable correction parameters.
3. Damage model presented in this paper, is a good solution to the problem of residual strength and damage threshold of rock, but the model

is based on linear elastic theory, and does not reflect the plastic deformation of the rock.

ACKNOWLEDGMENT

We acknowledge the financial supports of National Natural Science Foundation of China (91215301).
Corresponding Author: Zhou Yong-qiang
852538607@qq.com 13554656059.

REFERENCES

- [1] Liu Qi-jian, Yang Lin-de, Cao Wen-gui. Statistical Damage Constitutive Model for Rock and Back Analysis of its Parameters [J]. Chinese Journal of Rock Mechanics and Engineering, 2005, 24(4): 616–621. (in Chinese).
- [2] Jiang Wei, Deng Jian, Si Qingchao. Study on the constitutive model and its modifying for rock damage based on Mohr criterion [J]. Journal of Hebei University of Engineering (Natural Science Edition), 2010, 27(2): 30–33. (in Chinese).
- [3] Cao Wen-gui, Mo Rui, Li Xiang. Study on statistical constitutive model and determination of parameters of rock based on normal distribution [J]. Chinese Journal of Geotechnical Engineering, 2007, 29(5): 671–675. (in Chinese).
- [4] Zhang Ming, Li Zhong-kui, Su Xia. Probabilistic Volume Element Modeling in Elastic Damage Analysis of Quasi-Brittle Materials [J]. Chinese Journal of Rock Mechanics and Engineering, 2005, 24(23): 4282–4288. (in Chinese).
- [5] Cao Wengui, Zhao Minghua, Liu Chengxue. Study on the model and its modifying method for rock softening and damage based on Weibull random distribution [J]. Chinese Journal of Rock Mechanics and Engineering, 2004, 23(19): 3226–3231. (in Chinese).
- [6] Lemaitre J. Application of damage concepts to predict creep-fatigue failure [J]. Journal of Engineering Materials and Technology (ASME), 1979, 101(1): 202–209.
- [7] Li Shu-chun, Xu Jiang, Li Ke-gang, et al. Study on Damages Constitutive Model of Rocks Based on Weibull Distributing [J]. Journal of Hunan University of Science & Technology (Natural Science Edition), 2007, 22(4): 65–68. (in Chinese).
- [8] Kang Yaming, Liu Changwu, Jia Yan, et al. Research on Statistical Damage Constitutive Model and Critical Damage for Rock Subjected to Triaxial Stress Condition [J]. Journal Of Si Chuan University (Engineering Science Edition), 2009, 41(4): 42–47. (in Chinese).
- [9] J.C. Jaeger, N.G.W. Cook. Fundamentals of rock mechanics [M]. Third Edition chapman and Hall, London, 1979.

Experimental study on crack control of light gauge steel and foamed concrete wall

Jian-Jun Wang

China Academy of Building Research, Beijing, China

ABSTRACT: Although light gauge steel and foamed concrete composite wall has the advantages of light weight, heat insulation, sound insulation and fire resistance, wall shrinkage and cracking are often found. In order to improve its crack resistance, tests of the foamed concrete shrinkage, wall elements with added structure detailing measures and curing measures of wall were conducted. The results indicated that: on the premise that construction is not affected, the reduction of water cement ratio and the increase of fiber and lightweight aggregate are effective measures to reduce foamed concrete shrinkage; by fixing wire meshes on both sides of light gauge steel wall, using coated curing and prolonging the curing time the wall cracks can be effectively controlled.

Keywords: light gauge steel and foamed concrete wall; wall cracks; shrinkage; experimental study

1 INTRODUCTION

Light gauge steel and foamed concrete wall is a new composite wall using the thin-walled light gauge steel as the wall framework and cast-in-situ foamed concrete as the filler, which has such advantages as high load-bearing capacity, thermal insulation, sound insulation, fireproofing, etc.^[1,2] The filling of foamed concrete not only increases the bearing capacity of the light gauge steel wall, but also plays a role in enclosure; foamed concrete, with light and porous characteristics, improves heat insulation and sound insulation performance of wall. Cast-in-situ process gets the light gauge steel framework fully covered by foamed concrete, which not only enhances the integrity and strong sense of the walls, but also protects light gauge steel from fire. Therefore, light gauge steel and foamed concrete composite wall possesses significant comprehensive advantages and meets the current development trend of the wall material reform and building energy efficiency in China.

Compared with ordinary concrete, foamed concrete is subject to more serious shrinkage and cracking due to containing no coarse aggregate; the thin-walled light gauge steel has a smooth surface; as a result, the bonding stress of light gauge steel and foamed concrete is much weaker than ribbed bar. These reasons are why light gauge steel and foamed concrete wall is more likely to show shrinkage and cracking, which can affect wall

safety and durability and will further affect the normal service life of whole project. Therefore, it is of significant importance to carry out research on the crack control of light gauge steel and foamed concrete wall, improve its crack resistance and quicken the promotion of this new wall technology.

References [3] to [7] have studied the influence factors of foamed concrete shrinkage and cracking, such as admixture, foam parameters, etc. This paper studies the shrinkage performance of foamed concrete from the point of materials, carries out experimental study on the crack control effect of light gauge steel and foamed concrete wall after taking design details requirements and construction curing measures from the point of engineering application, and puts forward targeted measures on wall crack control.

2 TEST OVERVIEW

2.1 Raw material

Cement: P.O.42.5R; Sand: washed-out sand with a maximum particle size of 4 mm and a silt content of no more than 5%; Foaming agent: composite forming agent; Fiber: polypropylene staple fiber, 6 mm–10 mm long; Lightweight aggregate: clays haydite with aggregate size of 5 mm–15 mm and bulk density of 800 kg/m³; Light gauge steel: rectangular thin-walled steel tubes, two specifications of 40 × 40 × 1 mm and 40 × 60 × 1 mm; Wire mesh:

three specifications: $\Phi 1.2@25 \times 25$, $\Phi 2.8@50 \times 50$, and $\Phi 2.0@100 \times 100$; high-ribbed formwork: ribbed mesh and corner mesh.

2.2 Design and preparation of specimens

1. Design of specimens

6 units (26 specimens in total) are designed in terms of foamed concrete mix proportion, details requirements and construction curing measures for light gauge steel and light concrete wall. See Table 1, 2, and 3 for the design parameters of these specimens.

2. Preparation of specimens

Preparation of foamed concrete shrinkage specimen: prepare a $40 \times 40 \times 160$ mm mold, punch a $\Phi 6.5$ hole respectively in the center of both sides of the mold, fix the feeder head to the two holes with (8 ± 1) mm longer than the specimen; pour foamed concrete mixed by the mix

proportion into the mold, and then measure the initial length, and the length after natural drying at the 7th, 14th, 28th, and 56th day according to the curing and test environment requirements in JGJ70-2009 *Standard for Test Method of Performance on Building Mortar*.

Preparation of light gauge steel and foamed concrete wall specimen: process and produce a light gauge steel wall framework (Fig. 1) and prepare according to the steel mesh structure measures (Figs. 2 and 3) and the construction measures in Table 3.

3. Test method

The foamed concrete shrinkage test is conducted according to JGJ70-2009 *Standard for Test Method of Performance on Building Mortar*; test method of light gauge steel and foamed concrete wall crack: observe the occurrence time and quantity of cracks, maximum crack width, and total length of specimen crack.

Table 1. Details for mix proportion of foamed concrete.

Group	Specimen no.	Cement (kg)	Sand (kg)	Foam (L)	Water (kg)	Fiber (kg)	Haydite (kg)	Description
Group 1: different W/C ratio	1-1	320	400	630	96	–	–	W/C ratio: 0.30
	1-2	320	400	630	112	–	–	W/C ratio: 0.35
	1-3	320	400	630	128	–	–	W/C ratio: 0.40
	1-4	320	400	630	144	–	–	W/C ratio: 0.45
	1-5	320	400	630	160	–	–	W/C ratio: 0.50
Group 2: different fiber contents	2-1	320	400	630	120	–	–	None
	2-2	320	400	630	120	0.96	–	Fiber content: 0.3%
	2-3	320	400	630	120	1.92	–	Fiber content: 0.6%
	2-4	320	400	630	120	3.2	–	Fiber content: 1.0%
Group 3: different haydite contents	3-1	400	750	460	180	–	–	Haydite: 0%
	3-2	400	750	460	180	–	250	Haydite: 20%
	3-3	400	750	460	180	–	350	Haydite: 30%
Group 4: different dry densities	4-1	310	210	715	110	–	–	600 kg/m ³
	4-2	320	400	630	120	–	–	800 kg/m ³
	4-3	350	560	560	120	–	–	1000 kg/m ³
	4-4	360	750	460	140	–	–	1200 kg/m ³

Table 2. Design parameters for design structure measures for light gauge steel and foamed concrete wall.

Group	Specimen no.	Wall steel mesh specification	External-corner steel tube construction	Light gauge steel wall framework	Foamed concrete mix proportion
Group 5: different detailing requirements	5-1	–	N/A	Figure 1	The same as specimen 2-2
	5-2	$\Phi 1.2@25 \times 25$	N/A	Figure 1	The same as specimen 2-2
	5-3	$\Phi 2.8@50 \times 50$	Corner mesh	Figure 1	The same as specimen 2-2
	5-4	$\Phi 2.0@100 \times 100$	Corner mesh	Figure 1	The same as specimen 2-2
	5-5	High-ribbed formwork	N/A	Figure 1	The same as specimen 2-2

Table 3. Design parameters for construction curing measures for light gauge steel and foamed concrete wall.

Group	Specimen no.	Curing method	Curing time	Light gauge steel wall framework	Foamed concrete mix proportion
Group 6: different construction measures	6-1	Curing by watering and covering with straw	7d	Figure 1	The same as specimen 2-2
	6-2	Curing by watering and covering with straw	10d	Figure 1	The same as specimen 2-2
	6-3	Curing by watering and covering with a film	7d	Figure 1	The same as specimen 2-2
	6-4	Curing by watering and covering with a film	10d	Figure 1	The same as specimen 2-2
	6-5	Curing by watering and covering with a film	14d	Figure 1	The same as specimen 2-2

Notes: 1. Specimens in Group 5 are cured by watering for 7d; 2. Specimens in Group 6 are provided with the construction measures of $\Phi 2.8@50 \times 50$ steel mesh and corner mesh.

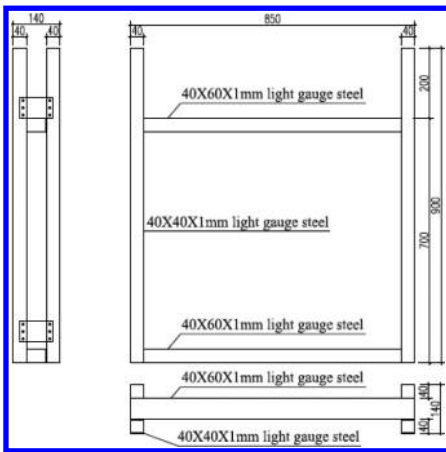


Figure 1. Light gauge steel wall framework.

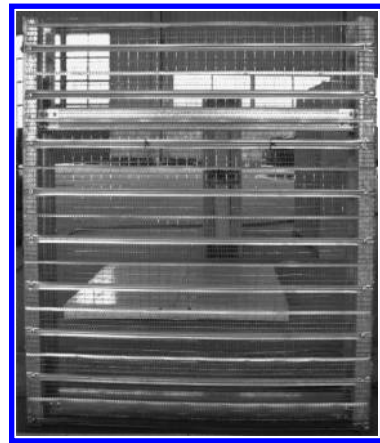


Figure 3. Wall framework with ribbed mesh.



Figure 2. Wall framework with steel mesh.

3 TEST RESULTS AND ANALYSIS

3.1 Influence of water-cement ratio on the shrinkage performance of foamed concrete

In order to study the influence of different water-cement ratios on the shrinkage of foamed concrete, foamed concretes respectively with water-cement ratio of 0.3, 0.35, 0.4, 0.45, and 0.5 are prepared and their dry density is 800 kg/m^3 . See Table 1 for the mix proportion. See Figure 4 for the shrinkage values of foamed concretes with different water-cement ratios at different age.

According to Figure 4, foamed concrete specimens of different water-cement ratios show shrinkage of different degree; as the hydration process of binding material continues, the shrinkage values are increasing. During the hydration process, solid particles are increasing in size after hydration and

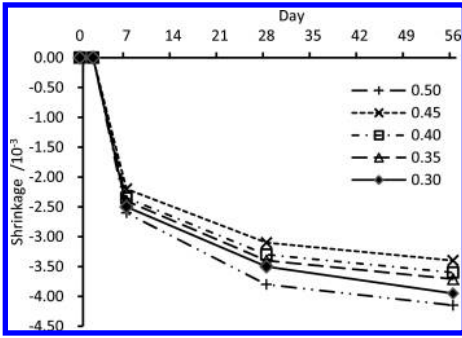


Figure 4. Shrinkage of foamed concrete under different water-cement ratios.

thus become close together, the framework intensity of foamed concrete is increasing, and meanwhile the liquid volume is decreasing, the solid and liquid volume after hydration is decreasing, and the gas volume is rising.

When the water-cement ratio is between 0.3 and 0.45, the smaller the ratio is, the bigger the shrinkage will be. the reason is that in the framework of foamed concrete, as the water in binding material produces a great number of gelling capillaries, the smaller the water-cement ratio, the less the free water in the system, and the internal relative humidity due to hydration of the binding materials decreases, resulting in dehydration in capillaries or decline of the liquid level, so that the lower the humidity, the bigger the tension of capillaries. when the water-cement ratio is 0.5, the shrinkage of foamed concrete becomes more serious instead and the shrinkage is 3.8 mm/m at the 28th day; while when the water-cement ratios is 0.3, the shrinkage is 3.5 mm/m at the 28th day. According to the cement hydration theory, when the water-cement ratio is bigger than 0.5, cement particles may be fully hydrated, and their own desiccation and shrinkage goes unnoticed compared to air shrinkage; as a result, the shrinkage value is very small. When the water-cement ratio is smaller than 0.3 (theoretical water requirement), cement mortar looks hydro-penic, the ratio of solid to liquid volume increases, and the volume of cement particles after hydration may gradually offset the decline in liquid volume, and thus the shrinkage decreases instead.

The growth rate of shrinkage of foamed concrete with different water-cement ratios is greater within the first 7 days than other periods, and it reduces after the 56th day. The hydration rate of cement within the first 7 days is great. The internal and external moisture gradient of specimens in the early phase is relatively big and the air shrinkage is relatively high, which are the reasons why foamed concrete shrinkage is rapid in the first 7 days.

3.2 Influence of fiber on the shrinkage performance of foamed concrete

In order to study the influence of different fiber content on the shrinkage of foamed concrete, formed concretes of dry density of 800 kg/m³ and with fiber content (relative to cement) of 0%, 0.3%, 0.6%, and 1.0% are prepared. See Table 1 for the mix proportion. See Figure 5 for the shrinkage values of foamed concretes with different fiber content at different age.

With the dosage of cement shown in Table 1, the water-cement ratio is set at 0.375 and the fiber content at 0–1.0%. As is shown in the Figure 5, with the increasing of the fiber content, the shrinkage at the 7th, 28th, and 56th day presents the trend of decreasing; compared to foamed concrete without fiber, the shrinkage decreases by 25% and 30% respectively at the 28th and 56th day when the fiber content is 1.0%. Fibers are distributed randomly in foamed concrete and a great quantity of hydration products attach to fibers to restrict the shrinkage. With the increase of fiber content, fibers' restrictions to foamed concrete are intensifying and the shrinkage value is becoming smaller. However, too high fiber content is not beneficial to the uniform mixing between foams and mortar. When it is over 0.6%, fibers may hang over agitating vanes during mixing and formwork inner walls when pouring. Therefore, the fiber content should be less than 0.6%.

3.3 Influence of lightweight aggregate on the shrinkage performance of foamed concrete

In order to study the influence of different lightweight aggregate content on the shrinkage of foamed concrete, formed concretes with haydite content of 0%, 20%, and 30% are prepared. See Table 1 for the mix proportion. See Figure 6 for the shrinkage values of foamed concretes with different haydite content at different age.

With the increase of the haydite content, the shrinkage of specimens shows gradual decline

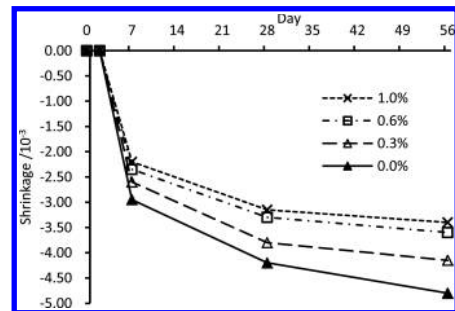


Figure 5. Shrinkage of foamed concrete under different fiber content.

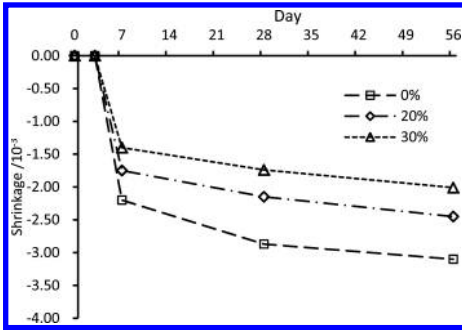


Figure 6. Shrinkage of foamed concrete under different haydite content.

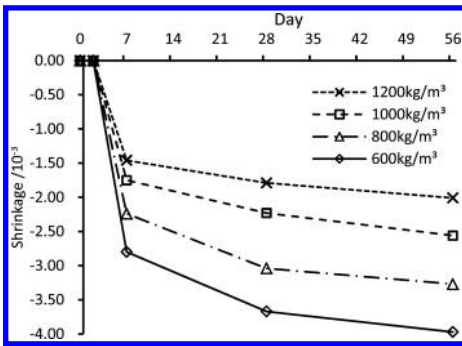


Figure 7. Shrinkage of foamed concrete under different dry density.

in Figure 6; when the content increases from 0% to 30%, the shrinkage drops from 3.3 to 2.6, the shrinkage drops to 1.4. This is because haydite performs well in volume stability and can replace foamed concrete is ovolumetrically to result in corresponding decline of specimen shrinkage. When the content is high, particles touch each other to form a framework which plays a supporting role to restrict shrinkage. Therefore, the higher the content, the more obvious the shrinkage decreases.

3.4 Influence of dry density on the shrinkage performance of foamed concrete

In order to study the influence of dry density on foamed concrete, formed concretes with dry density respectively of 600, 800, 1000, and 1200 kg/m³ are prepared. See Table 1 for the mix proportion. See Figure 7 for the shrinkage values of foamed concretes with different dry densities at different age.

In Figure 7, the dry density shows a linear relationship with shrinkage. The shrinkage decreases with the increase of the dry density while the shrinkage rate present a downtrend, which is because as

the hydration of binding materials continues, the solid volume is increasing, particles contact closely each other so that the framework strength of the foamed concrete increases, the foamed concrete of large apparent dry density has its strength higher than that of small apparent dry density in the same phase and becomes more powerful in shrinkage resistance. Foamed concrete show rapid shrinkage in the early phase, which is mainly because of the loss of volume with the decrease of water content due to hydration of binding materials.

3.5 Influence of different detailing requirements on light gauge steel and foamed concrete wall cracks

In order to study the influence of different detailing requirements on light gauge steel and foamed concrete wall cracks, wall specimens without any measure and with $\Phi 1.2@25 \times 25$, $\Phi 2.8@50 \times 50$, $\Phi 2.0@100 \times 100$, and high-ribbed formwork are respectively prepared and specimens 5-3 and 5-4 are installed with corner meshes at the vertical light gauge steel.

The following regular conclusions are obtained through comparative observation of the wall cracks of the five specimens (Fig. 8):

1. Specimen 5-1, as the control sample for which no measures are taken to restrict cracks, shows long and wide cracks 7 days later upon curing, most of which are short-term ones mainly caused by foamed concrete shrinkage. The adhesive strength between steel tubes and foamed concrete is poor, resulting in cracks on the concrete near steel tubes going in the same direction as the steel tubes.

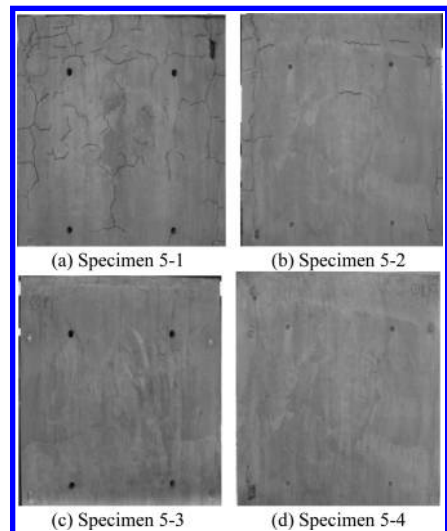


Figure 8. Influence of different structure measures on light gauge steel and foamed concrete wall cracks.

2. Specimen 5-2 is provided with a $\Phi 1.2@25 \times 25$ steel mesh, of which the cracks are greatly fewer than 5-1. For corner mesh is not taken for steel tubes, there are still obvious cracks in the position of the steel tubes.
3. The diameter of the steel mesh for 5-3 and 5-4 is bigger than that for 5-1 and thus the mesh is much bigger, and corner meshes are provided outside steel tubes; as a result, no cracks are discovered in the first 28 days and only a few short and thin ones are found after a long time.
4. Specimen 5-5 is provided with high-ribbed formwork, which is more ideal for crack control. What's more, such high-ribbed formworks are bonded to the outside of steel tubes so that corner meshes are not necessary. However fibers may hang over foamed concretes when pouring.

To sum up, Specimen 5-1 shows obvious cracks in the first 28 days, of which the length and width develop over time; the other 4 show no obvious cracks in the first 28 days, and only a few tiny ones are observed after 90 days, which are short and wide no greater than 0.1 mm. Tests show that it is very helpful to control light gauge steel and foamed concrete wall cracks by providing steel mesh or high-ribbed formwork at both sides of the wall's light gauge steel framework. Specimens 5-1 and 5-2 show serious cracks near steel tubes while 5-3, 5-4 and 5-5 which are covered with corner meshes or high-ribbed formwork show no obvious ones near the steel tubes, which means corner meshes can effectively control cracks on the contact surface of steel tubes and foamed concrete.

3.6 Influence of different curing measures on light gauge steel and foamed concrete wall cracks

In order to study the influence of different curing measures on light gauge steel and foamed concrete wall cracks, curing by watering and covering with straw and by watering and covering with plastic film and curing for 7, 10, and 14 days are respectively designed for comparative study.

The following conclusions are obtained through comparative observation of the wall cracks under these curing methods and curing time:

1. In terms of curing method, Specimens 6-3, 6-4 and 6-5 cured by watering and covering with film can more guarantee the water supply required by hydration during the curing period than those by watering and covering with straw; besides, moistures in wall surface cannot be easily evaporated and the air shrinkage and cracks in the earlier phase are avoided. Viewed from the construction convenience, it is more efficient to cure by covering with a film than with straws and it is easier to operate as well.

2. In terms of curing time, Specimen 6-5 with a longer curing period has fewer cracks than 6-3, which is because as the curing time prolongs, the cement in foamed concrete will be hydrated more sufficiently. For all earlier cracks happens during curing, the total shrinkage is reduced.

4 CONCLUSION

The following conclusions are obtained according to foamed concrete shrinkage tests, and wall crack tests by adding detailing measure and curing measures:

1. The most important cause of light gauge steel and foamed concrete wall cracks is the shrinkage of foamed concrete. It is of critical importance to reduction of wall shrinkage cracks by optimizing the mix proportion from the point of materials.
2. Providing the liquidity of foamed concrete required by construction is met, it is effective to reduce the shrinkage of foamed concrete by reducing the water-cement ratio and cement content, and adding lightweight aggregate and fiber.
3. It is beneficial for wall crack control by providing steel mesh or ribbed mesh at both sides of light gauge steel wall framework, and installing corner meshes on the vertical steel tubes at the wall external corners.
4. It is helpful to reduce wall cracks through curing by watering and covering with film for over 10 days.

REFERENCES

- [1] Yan, Z.J. & He, Y.J. 2013. *Cast-in-situ Foamed Concrete Composite Wall Technology*. Beijing: Chemistry Industry Press.
- [2] Tang, M. & Xu, L.X. 2013. *Foamed Concrete and Its Engineering Application*. Beijing: China Architecture & Building Press.
- [3] He, S.N. & Zhu X.Y. 2011. Study on Foamed Concrete Crack Control Without any Load. *New Building Materials* (10): 001–004.
- [4] Zhang, G.Y. & Chen Y.P. 2013. Study on modification of foamed concrete shrinkage performance. *New Building Materials*.(4):72–74.
- [5] Jiang, J. & Lu, Z.Y. 2013. Study on influence of additives on foamed concrete shrinkage performance. *Concrete* (8): 047–050.
- [6] Hu, S.K. & Li, Y.Q. 2010. Study on the influence of foam parameters on foamed concrete performance. *Wall Materials Innovation & Energy Saving in Buildings* (5): 028–031.
- [7] Ma, Y.P. & Li, G.Y. 2012. Influence of performance density and polypropylene fiber on foamed concrete shrinkage and cracking. *Materials Review* 26 (3): 121–125.

Study on the rutting resistance mechanism of Lucobit modifier

Ye Mao Zhang

Jiang Su Provincial Communication Planning and Design Institute Co., Ltd., Nanjing, P.R. China
Key Laboratory for Special Area Highway Engineering of Ministry of Education, Chang'an University,
Xi'an, Shanxi, China

Kun Wang & Guang Wei Hu

Jiang Su Provincial Communication Planning and Design Institute Co., Ltd., Nanjing, P.R. China

ABSTRACT: To research the rutting resistance mechanism of Lucobit, the text respectively studies the modified technology, the influence on asphalt and the percentage of impacting on asphalt. Results show that the softening point increases and the penetration decreases with the increase of Lucobit content. The 5°C ductility improves a little yet cannot meet the requirement. The rutting resistance of asphalt mixture with 7% Lucobit improves two grades. The percentage of Lucobit impacting on asphalt is higher than the other two modifiers. So Lucobit modifier improves the pavement performance of asphalt mixture by the double effect on asphalt and aggregate.

Keywords: pavement engineering; Lucobit modifier; rutting resistance mechanism

1 INTRODUCTION

Rutting is a common phenomenon in the damage of asphalt pavement. Compared with the crack and flushing, the damage of rutting is bigger which will influence road smoothness, cut down the whole strength of the pavement structure and surface layer, reduce the sliding resistance of pavement and even influence the safety of the high-speed driving for water accumulation in the rutting. Also it may affect the operation stability of vehicles while they overtake or change lanes. Thus, the problem of rutting is urgent necessary to be solved.

In order to improve the anti-rutting ability of highway asphalt, the high temperature strength and stability of the asphalt mixture must be increased. Currently the most universal method of road workers is mainly adopted the SBS modified asphalt, high viscosity asphalt and other reinforcement materials (such as polyester fiber, PR modifier, etc.) to improve the anti-rutting performance of asphalt mixture except for mixture gradation optimization. European countries attach great importance on improving the resistance to permanent deformation by adding the modifier to mixture. Modifying agent has been widely used in various levels of road, including a number of important bridge and tunnel pavement. Such as France uses PR, PLAST. S, Germany uses Lufu8000, Domix, DUROFLEX, etc., the United States uses SEAM modifier.

The Lucobit modified agent is developed and applied for patent by German Basifu chemical industry group in 1966. The company of Lucobit has exclusive rights to produce a kind of polymer which is made up of the mixture of high quality polyethylene copolymer and a special kind of asphalt (ECB). Research shows that the pavement performance of asphalt mixture with Lucobit modified is better than SBS modified asphalt mixture.

Lucobit modifier is a new material and new technology in the field of pavement engineering. Li Liu etc. [1] researched the pavement performance of Lucobit asphalt mixture. Results show that the pavement performance of Lucobit asphalt mixture has a little improving. Jumei Chen etc. [2,3] researched the rutting resistance performance of Lucobit asphalt mixture. They thought that Lucobit can effectively treat and reduce rut disease. The improvement mechanism is whether the improving performance of the asphalt, the aggregate or the two with Lucobit still needs to be studied. Thus, correlation analysis was studied in this paper.

2 MATERIALS AND METHODS

2.1 Modified technology

Lucobit modified by wet process: At the temperature of 160°C±5°C, Lucobit modified asphalt is

made under the condition of using colloid mill grinding 120 min at a speed of 6000 r/min. The technological process of modified by wet process is shown in Figure 1.

Studies have shown that Lufu8000 and PR rutting resistance agent are not suitable for wet method modification [4]. So the modification of them is modified with the dry process.

According to dry process of waste rubber powder and the modification mechanism, the modifier is directly put into the mixing pot, and then the asphalt is sprayed.

The indoor mixing includes three steps. The modifier with hot aggregate are sprayed into the pot dry mixing (time determined by tests) and then put into asphalt wet mixing. Finally, the mineral powder is sprayed and mixing evenly.

The location mixing process of modified asphalt mixture is very simple. It is same to the common asphalt mixture. Hot aggregate and modifier are cast for dry mixing in the same time. Then asphalt is cast for wet mixing. Finally mineral powder is added until mixing evenly. Dry method process is shown in Figure 2.

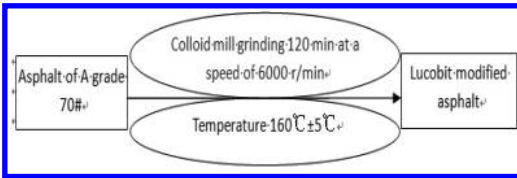


Figure 1. Lucobit modified asphalt modified by wet process flow.

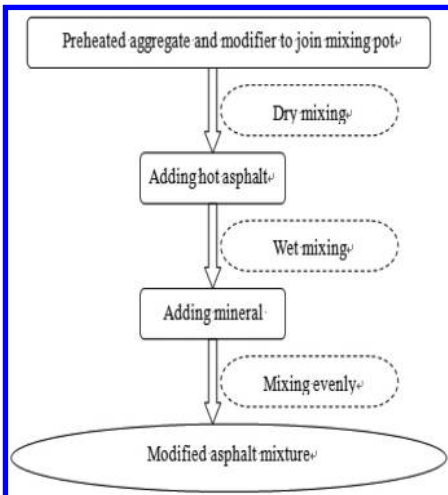


Figure 2. Dry method modification process.

2.2 The influence analysis method of Lucobit modifier on asphalt performance

To analysis the modified mechanism of Lucobit, different dosage (3%, 5% and 7%) of Lucobit are sprayed into the asphalt of A grade 70#. Three indicators of asphalt are tested.

$G^*/\sin \delta$ was defined as rutting factor by America SHRP. $G^*/\sin \delta$ is ruled ($G^*/\sin \delta \geq 1.0$ kPa) at the maximum design temperature. The bigger of $G^*/\sin \delta$ is, the better of the ability of high temperature resistance to permanent deformation. This experiment uses the Dynamic Shear Rheometer (DSR). Test frequency is 10 rad/s. Asphalt of A grade 70# is provided by Nanjing refinery. The dosage of Lucobit is 7% of the quality of asphalt.

2.3 Test method and ratio calculation of the percentage of modifier impacting on the asphalt

To research the effect principle of modifier more scientific, test method of the centrifuge extraction is adopted to obtain the approximate percentage of different kinds of modifier [5, 6]. To reduce the test error, the compatibility of modifier and trichloro ethylene needs to be verified before the test designing. Three kinds of modifier are put into trichloro ethylene. Proper stirring with a glass rod and experience half an hour, no obvious change of modifier is found. It is concluded that three kinds of modifier are not soluble to trichloro ethylene in directly. Test method is followed below.

- According to the mineral aggregate gradation, the dosage of aggregate (m_2) is weighed. The dosage of asphalt (m_3) is determined by asphalt-aggregate ratio. The dosage of modifier (m_4) is respectively determined by the proportion of asphalt mixture (m_1). The accurate value is 0.1 grams.
- The aggregate is heated to 170°C to 180°C and then the modifier is directly sprayed into mixing equipment and made dry mixing. Hot asphalt is added to mix 40 seconds to 50 seconds after 10 seconds to 15 seconds. According to the gradation of asphalt mixture, the same proportion of mineral powder (m_5) is added to mix until no grey material mixing evenly.
- The mixing asphalt mixture with modifier is put into the beaker. Trichloroethylene solvent is injected into the beaker until submerging the mixture after the temperature dropped to below 100°C. Proper stirring with a glass rod is made the asphalt dissolve completely.

- d. The mixture and liquor are poured into a centrifugal separator. The beaker and the glass rod are washed using a small amount of solvent and poured into the centrifugal separator.
- e. Start the centrifuge and gradually increase the speed to 3000 r/min. Asphalt solution is injected into the returnable bottle through the outlet. Stop injection after no outflow. Add new solvent with the same dosage to the hole of up cover and repeat the above operation several times after 3 minutes to 5 minutes until the flow of fluid is clear light yellow.
- f. Remove the above cover and circular filter paper. Evaporate drying in the kitchen ventilation or room temperature air. Then dry in the oven of $105^{\circ}\text{C}\pm 5^{\circ}\text{C}$. Weigh the quality. The gaining weight (m_3') is a part of mineral powder. Other mineral powder was leaked into the extraction liquid.
- g. The steps of measuring mineral powder quality in extraction liquid using the combustion method are as follows:
1. Pour the leaching liquor in returnable bottle into the measuring cylinder and ration accurately to mL (V_0).
 2. Fully stir extraction liquid. Take out 10 ml (V_1) into the crucible. Heat the liquor to be dark black on the hot bath. Set the high temperature furnace ($500\sim 600^{\circ}\text{C}$) firing residue. Remove the crucible cooling.
 3. Pour ammonium carbonate saturated solution into the crucible in the light of 5 ml per 1 g residue ratio. Put it into the oven of $105^{\circ}\text{C}\pm 5^{\circ}\text{C}$ for drying after an hour.
 4. Take out the crucible and cool it in the dryer. Weigh the quality of residue (m_6) and be accurate to 1 mg. Calculated the quality of mineral powder (m_5'') in the extraction liquid with the corresponding proportion.

Remove the aggregate in the container carefully and evaporate it to dry in the fume hood or indoor air. Put it into the 105°C oven for drying (usually four hour). Then put it into the big dryer cooling to room temperature. Weigh the quality of aggregate (m_2') in the container after drying.

Percentage of modifier to asphalt:

$$m_a = \frac{m_1 - m_2 - m_3 - m_5}{m_4} \times 100\% \quad (1)$$

- m_a —Percentage of modifier to asphalt, %;
 m_1 —Quality of asphalt mixture, g;
 m_2 —Quality of aggregate left in containers after drying, g;
 m_3 —Quality of asphalt in mixture, g;

- m_4 —Total quality of modifier, g;
 m_5 —Quality of mineral powder, g.

3 RESULTS AND DISCUSSIONS

3.1 Tests of three indicators on asphalt

Different kinds of asphalt were tested. Tests results of penetration are shown in Table 1.

Different kinds of asphalt were tested. Tests results of softening point are shown in Table 2.

Different kinds of asphalt were tested. Tests results of softening point are shown in Table 3.

Table 1, Table 2 and Table 3 show that the penetration decrease and softening point increase with the increase of Lucobit. The increasing of softening point indicates that the viscosity of bitumen is increasing which is in favour of the stickiness with aggregate. High temperature stability and the ability to resist deformation increase. The 5°C ductility

Table 1. Test results of asphalt penetration.

Asphalt type	Penetration/100 g, 25°C, 5 s			Average /0.1 mm
A grade 70#	71.6	71.8	69.7	71
3% Lucobit modified	59.3	59.9	59.7	60
5% Lucobit modified	53.8	53.1	52.9	53
7% Lucobit modified	46	46.4	44.8	46

Table 2. Test results of asphalt softening point.

Asphalt type	Softening point ($^{\circ}\text{C}$)		average ($^{\circ}\text{C}$)
A grade 70#	48.0	48.0	48.0
3% Lucobit modified	50.2	51.0	50.5
5% Lucobit modified	57.2	57.4	57.3
7% Lucobit modified	62.4	63.3	62.9

Table 3. Test results of asphalt ductility.

Test item	Test number	70# Lucobit asphalt			
		70#	Lucobit asphalt		
5°C ductility (cm), 5 cm/min	1	0	3%	5%	7%
	2	0	6	4.8	6.7
	3	0	6.1	4.9	7.1
	Average	0	6.9	6.1	6.9
15°C ductility (cm), 5 cm/min	1	>100	>100	>100	>100
	2	>100	>100	>100	>100
	3	>100	>100	>100	>100
	Average	>100	>100	>100	>100

of Lucobit asphalt has a little increasing while all of them cannot meet the requirement of SBS modified asphalt. The reason is that the composition of Lucobit contains some EVA. The EVA does not belong to the SBS modified asphalt. 5°C ductility of EVA and PE class (III) are not required by the specification.

3.2 Tests of rutting resistance factor on asphalt

A grade 70# asphalt was tested on the high temperature performance. Test results of DSR are shown in Table 4.

Lucobit modified asphalt was tested on the high temperature performance. Test results of DSR are shown in Table 4 and Table 5.

Table 4 and Table 5 show that $G^*/\sin \delta$ improves two levels when asphalt of A grade 70# is added to Lucobit. It indicates that Lucobit modification plays a positive role in improving the high temperature rutting resistance of asphalt mixture.

3.3 Tests of the proportion of modifier on the asphalt

According to AC-13C graded mixture three kinds of modified materials about 1280 g are respectively weighed including aggregate 1200 g, asphalt of A grade 70# 60 g, modifier 10 g and mineral powder 10 g. According to the test methods and steps of 2.3.1, tests are carried out. Test results shows in Table 6.

Table 6 shows that the percentages of three kinds of modified materials are different. The effect of percentage of Lucobit modifier to asphalt is higher than PR and Lufu8000.

Table 4. DSR Test results of A grade 70# asphalt.

Temperature (°C)	64	70
<i>Asphalt of A grade 70#</i>		
G^*/KPa	1.742	0.985
$\delta(^{\circ})$	87.01	87.27
$G^*/\sin \delta$	1.744	0.986

Table 5. DSR test results of Lucobit modified asphalt.

Temperature (°C)	76	82
<i>Asphalt of Lucobit modified</i>		
G^*/KPa	1.122	0.864
$\delta(^{\circ})$	86.27	86.97
$G^*/\sin \delta$	1.124	0.865

Table 6. Test results of percentage of modifier to asphalt.

Modifier types	Test number	Lucobit	PR	Lufu8000
m_1/g	1	1280.3	1279.8	1279.9
	2	1280.1	1280.1	1280.2
m_2'/g	1	1203.8	1203.8	1204.4
	2	1203.3	1204.3	1204.9
m_3/g	1	60	60	60
	2	60	60	60
m_3'/g	1	10	10	10
	2	10	10	10
m_4/g	1	10	10	10
	2	10	10	10
$m_d/\%$	1	55	50	45
	2	58	48	43

3.4 Rutting resistance mechanism of Lucobit

The modification of asphalt is a physical blending process [7, 8]. The sufficient mixing of modifier and asphalt is a basic prerequisite to improve the performance of asphalt. On this basis, the light component of asphalt is adsorbed by modifier and swells. The swelling of the modifier and the rest components of asphalt interact and form a new structure system. So the performance of the asphalt obtains improvement. In the process of grinding and the stabilizer or the action of catalyst, chain scission and crosslinking reaction happens. Then some mesh structure forms. So the viscosity and storage stability of modified asphalt is improved [9,10].

The components of 80% Lucobit are 2-butyl acrylate and vinyl polymer. Lucobit sets the advantages of both. Not only has excellent chemical stability, but also mechanical properties, tensile strength, weathering performance, creep resistance and impact resistance has greatly improved.

4 CONCLUSIONS

1. The softening point increases and the penetration decreases with the increase of Lucobit content. The 5°C ductility improves a little yet cannot meet the requirement.
2. The method of tests is adopted to analyze the percentage of different modifier to asphalt. Percentage of different modifier to asphalt is compared. The percentage of Lucobit impacting on asphalt is higher than the other two modifiers.
3. Influence rule of aggregate and asphalt for modifier is researched. The modification mechanism

of modifier is also analyzed. Lucobit modifier improves the pavement performance of asphalt mixture by the double effect on asphalt and aggregate.

REFERENCES

- [1] Liu L., Chen J.M. etc. Experiment study on the pavement performance of asphalt mixture with Lucobit 1210A [J] *Journal of China & Foreign Highway*, 2012(32):290.
- [2] Chen J.M. On the Use of Lucobit Asphalt Mixture in Rut Disease Treatment [J]. *Value Engineering*, 2014.
- [3] Kong Z.G. New type of modified asphalt additives Lucobit 1210A [J] *Traffic World*, 2008:104.
- [4] Zhao X.J. Research on the Materials and Pavement Performance with High Modulus Asphalt Concrete [D] Xi'an Chang'an University, 2009.
- [5] Hui B. Research on Technical Performance of Anti-rutting Additive Modified Asphalt Mixture [D] Chang'an University, 2009.
- [6] Corté J., Brosseaud Y., Simoncelli J., Caroff G. Investigation of rutting of asphalt surface layers: influence of binder and axle loading configuration. *Transport Res Rec*, 1994:28.
- [7] Zhou Y. Study on pavement performance of SAMPAVE crack structure layer material [D] Xi'an Chang'an University, 2007.
- [8] Zhou Y., Chen S., Chen H., Zhang K. Design method of SAMPAVE asphalt mixture. Beijing: The 10th International Conference of Chinese Transportation Professionals, 2010. p. 3890.
- [9] Tan Y., Shi K., etc. Research on the Impact of Asphalt Character on Stress Absorbing Layer Performance [J]. *Journal of Highway and Transportation Research and Development*, 2009:2-4.
- [10] Li Fu-pu, Shen Jin-an. The match and harmonization of polymer modified asphalt [J]. *The science and technology of pavement traffic*, 1999, 16(3):1-5.

Performance analysis and optimization of fuze TPV power supply

Chun Hua Yu, Xing Lin Qi & Min Gao

Mechanical Engineering College, Shijiazhuang, P.R. China

ABSTRACT: In order to improve the performance of fuze TPV power supply and promote fuze TPV power supply to move from theory to practice, the paper, proceeding from tactic demand of general fuze power supply, analyzed main performance that fuze TPV power supply should reach and put forward the way to optimize in accordance with the expression formula of the main performance. The analysis indicates that fuze TPV power supply's generation power and the rate of false cap's temperature rise have great effect on the performance of power supply. By optimizing the selection of false cap's material, design of power supply structure and control of heat transfer process, the main performance of fuze TPV power supply can be improved, thus pointing out the direction to the further study of fuze TPV power supply.

Keywords: performance analysis; optimization; TPV; fuze; power supply

1 INTRODUCTION

The TPV (ThermoPhotoVoltaic) generation technology, which converts thermal radiant energy to electric energy directly, was first put forward by an American named H. Kolm (Kolm 1956). In 1970s and 1980s, American military had once conducted demonstration and study on applying TPV technology to field generator (Guazzoni & Kittl 1974) and underwater unmanned vehicle generator (Holmquist & Wong 1995). However, the TPV technology then was not practical due to the extremely low efficiency of photoelectric conversion. In the mid-1990s, the TPV cell made up of GaSb was produced on a large scale, until then, TPV technology was further studied and began to move to practice. In 2008, the application of TPV technology to ammunition was first put forward by American ARDEC. They conducted many experiments about this, through which TRL6 (Technology Readiness Level 6) was achieved (Pereira & Janow 2009). In 2009, Pereira et al. (Amabile & Dratler 2009) in ARDEC put forward the concept of hybrid power system for fuze of ammunition, in which the TPV technology was utilized. Though studies on TPV technology are growing vigorously, only Pereira et al. has conducted researches on the application of it to fuze until now. However, the results haven't been published. To improve the performance of fuze TPV power supply, and promote fuze TPV power supply to move from theory to practice, the paper analyzed the performance that fuze TPV power supply should have and searches for proper method according to the tactical needs.

2 STRUCTURE AND FUNCTION OF FUZE TPV POWER SUPPLY

The basic structure of fuze TPV power supply is shown by the half-section view in [Figure 1](#).

The part marked with "1" in [Figure 1](#) is a false cap of fuze located at the head of a projectile. When a projectile is travelling at supersonic speed, the false cap is heated (Zhang & Pan 2003.), which causes its temperature to rise, thus forming a steady-state temperature field at last. The temperature of the false cap's stagnation point is the highest anytime, and the further the distance is between the stagnation point and the point else on false cap, the lower the temperature is. The inner surface and outer surface of the false cap both radiate energy outward, which is called thermal radiation.

The part marked with "3" in [Figure 1](#) is a TPV cell, a semi-conductor PN junction with two electrodes in essence. The semi-conductor PN junction can absorb photons and generate free charges. With the build-in electric field of PN junction, these charges move to the two electrodes of device and are collected by electrodes, thus forming current to drive external load. The minimum energy of a photon that the TPV cell can absorb and utilize is called bandgap (Antonio, et al. 2003).

The part marked with "2" in [Figure 1](#) is a filter. Because of the interference of light, the filter can transmit some bands of radiant spectrum, whereas other bands will be reflected. In the fuze TPV power supply, the filter stops photons whose energy are lower than the bandgap from reaching the TPV cell, for these photons not only cannot

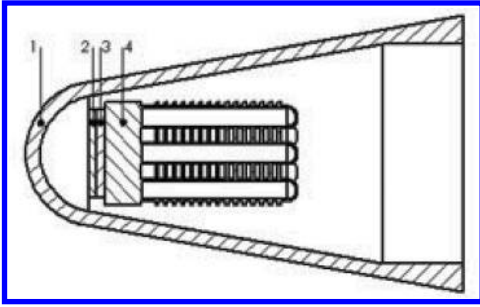


Figure 1. Fuze TPV power supply.

excite free charges, but will heat TPV cell, lowering its generation efficiency.

The part marked with “4” in Figure 1 is heat sink. In fact, the filter isn’t so perfect that some invalid photons still transmit through it, which results in its temperature rise. What’s more, the generation process of the TPV cell will also release some heat. If all these heat cannot be transferred, the temperature of the TPV cell will rise quickly, which will lower generation power and efficiency, or even result in irreversible damage (Antonio, et al. 2003). The heat sink can slower the temperature rise by quickening the process of heat transfer.

3 ANALYSES OF TACTICAL DEMAND OF FUZE TPV POWER SUPPLY

The fuze power supply needs to satisfy some tactical demands (Li & Zhi 1996). Taken the characteristics of TPV power supply into account, the fuze TPV power supply needs to meet tactical demands as follows.

1. Power Requirement.

The power of fuze power supply must meet working demand of fuze’s circuit. With the circuit becoming highly-integrated, the power consumption of fuze is becoming increasingly low (power consumption of electronic time fuze can be lower than 1 W). Even though this is a reality, electricity generation power is a main indicator measuring fuze’s power supply, and fuze TPV power supply is no exception.

2. Working Time Requirement.

Fuze power supply can only be used once. Different fuzes have different requirements of power supply’s working time. Firing towards ground requires the working time of power supply to last longer than fuze’s flying time, while firing towards air requires the working time of power supply to be longer than fuze’s autodestructive time. Fuze TPV power supply makes use of thermal radiation of false cap to generate

power, and its working time is only limited by the lifespan of TPV cell. As the fuze keeps flying, the temperature of TPV cell will get higher and higher. If none heat dissipation measures are taken, excessive temperature will pose irreversible damage to TPV cell, which results inability to work.

3. Activation Time Requirement.

Activation time of power supply refers to the time from activated moment (activation mechanism begin to work) to the moment when the output power reaching nominal value under specified load condition. Activation time should be shorter than the flying time of warhead covering minimum attack distance. As for electronic time fuze, the shorter activation time is, the better, or timing accuracy and dispersion will be affected. All in all, the shorter activation time is the better. The activation time of fuze TPV power supply depends on the rate of false cap’s temperature rise.

4 PROPERTIES CHARACTERIZATION AND OPTIMIZATION OF FUZE TPV POWER SUPPLY

4.1 Properties characterization

According to the analysis of last section, three factors that have the greatest effect on fuze TPV power supply’s performance are its generating power, temperature of TPV cell and rate of false cap’s temperature rise. Because the temperature of TPV cell has also effect on generating power, so the generating power of the power supply and the rate of false cap’s temperature rise were chosen to characterize the performance of fuze TPV power supply.

4.1.1 Generating power of the fuze TPV power supply

Electricity generating power varies with load. To characterize its load-carrying capability, TPV cell’s short-circuit current, open-circuit voltage and fill factor can be used.

Short-circuit current I_{SC} refers to the current passing through the TPV cell when its anode and cathode are connected. It’s also the maximum current that the power supply can output. It can be expressed by the following formula (Antonio, et al. 2003).

$$I_{SC} = \int_{\lambda} SR_{ext}(\lambda) f(\lambda) d\lambda = \int_{\lambda} SR_{ext}(\lambda) \frac{\epsilon c_1 V_F \lambda^{-4}}{hc(e^{c_2/\lambda T_c} - 1)} d\lambda \quad (1)$$

In the formula, $SR_{ext}(\lambda)$ represents external spectral response, which refers to normalized

short-circuit current gained from single wavelength light. $SR_{ext}(\lambda)$ is only relevant to the material that TPV cell is made of. $f(\lambda)$ represents photon flux and ε represents emissivity of the false cap's inner surface. V_F is the view factor of the false cap upon the TPV cell, which refers to the amount of radiation given off by the inner surface of the false cap that reaches the surface of TPV cell. T_c represents the inner surface temperature of the false cap and c, h, c_1, c_2 represent the speed of light in vacuum, Planck constant, First Planck constant and Second Planck constant respectively.

Open-circuit voltage V_{oc} refers to the supply voltage when the external circuit is open, which is also the maximum voltage the power supply can output. It can be expressed by the following formula (Antonio, et al. 2003):

$$V_{OC} = \frac{E_G(0)}{q} - \frac{kT_c}{q} \ln \frac{BT_c^\zeta}{I_{SC}} \quad (2)$$

In the formula, $E_G(0)$ is the bandgap of TPV cell when the temperature is 0 K, the unit of which is eV. $E_G(0)$ is only related to the material that TPV cell is made of. q represents elementary charge, k represents Boltzmann Constant, T_c is the temperature of TPV cell and B, ζ are constants irrelevant to temperature.

Fill factor FF is used to characterize the extent of effect that output current has on output voltage. The higher FF is, the less effect that output current has on output voltage, and the better performance that the power supply has. FF can be expressed by the following formula (Antonio, et al. 2003):

$$FF = \frac{V_{OC} - (kq/T_c) \ln(qV_{OC}/kT_c + 0.72)}{V_{OC} + kq/T_c} \quad (3)$$

The maximum electricity generating power of the fuze TPV power supply is:

$$P_{max} = I_{SC} \cdot V_{OC} \cdot FF \quad (4)$$

4.1.2 Temperature rising rate of the false cap

The false cap's temperature rising process is superposition of two one-dimensional inverse heat conduction processes. One process is that after absorbing aerodynamic heat, the outer surface transfer the heat to the inside and the other is the heat transferring process from the false cap's head to its tail, for the temperature of the false cap's head is higher than that of the tail. According to analytical solution of one-dimensional inverse heat conduction, temperature rising rate can be expressed by Fourier Number Fo . The formula is as follows (Xu & Wang 2011):

$$v_t = \frac{Fo}{\tau} = \frac{a}{\delta^2} = \frac{\lambda}{\rho C_p \delta^2} \quad (5)$$

In the formula, a represents thermal diffusivity. δ is the length in the direction of heat transferring. According to that, δ_i and δ_l are used to represent the thickness and the length of false cap. λ, ρ, C_p respectively represents thermal conductivity, density and specific heat of the material making up the false cap. τ is the heat conduction time.

4.2 Optimization method

According to the above analysis, parameters affecting the performance of fuze TPV power supply are emissivity of inner surface ε , view factor of TPV cell V_F , temperature of inner surface T_c , temperature of TPV cell T_e , thermal conductivity of false cap λ , density of false cap ρ , specific heat C_p , thickness of false cap δ_i and length of false cap δ_l , among which $\varepsilon, \lambda, \rho, C_p$ belong to false cap's physical parameters, δ_i, δ_l, V_F belong to structural parameters of power supply and T_c, T_e belong to procedure parameters. Therefore, performance optimization of the fuze TPV power supply can be conducted from three aspects, which are the material selection of false cap, structure design of power supply, and process control of the heat transfer.

4.2.1 Material selection of false cap

Apart from meeting the requirements of mechanical strength and aerodynamic performance, it would be better to choose material of high emissivity, high thermal conductivity, low density and low specific heat.

According to formulae (1) to (4), the increase of emissivity of false cap will bring about the increase in false cap's heat radiation intensity, thus resulting in the increase of short-circuit current I_{SC} , open-circuit voltage V_{oc} and fill factor FF , which will finally improve load-carrying capability of fuze TPV power supply. According to formula (5), high thermal conductivity, low density and low specific heat will help to improve the rate of temperature rise v_t of false cap's inner surface, then fastening the power supply activation

If the above mentioned four parameters cannot be optimized simultaneously, it would be better to choose material of high thermal conductivity, low density and low specific heat, and then spray a coating of high emissivity on the false cap's inner surface.

4.2.2 Structure design of power supply

Apart from meeting the requirements of mechanical strength, aerodynamic performance and volume, it's better to make the thickness of the false cap as thin and short as possible, false cap's nose as

blunt as possible. TPV cell should be located near the nose of the false cap.

According to formula (5), the thinner and shorter the false cap is, that is, the smaller δ_i , δ_o are, the greater the false cap's inner surface temperature rise rate v_i is, and then the faster the power supply can be activated. If the false cap cannot be shortened, a two-section false cap can be adopted. In the two-section false cap, the nose is made up of material of high emissivity, high thermal conductivity, low density and low specific heat, whereas the tail is made up of material that is completely opposite and the two parts are bonded by high-temperature adhesive. The material making up the tail is of low thermal conductivity, so that heat can only be transferred in false cap's nose, which means the length of the false cap is shortened equivalently. The shortened length cannot only improve the speed of power supply activation, but the temperature of false cap's nose.

The blunter the false cap's nose is, or the closer the TPV cell to the nose of the false cap, the bigger the view factor is, which is beneficial to short-circuit current, open-circuit voltage and fill factor. However, the blunter the nose of the false cap is, the bigger the air drag is, which will result in the decrease in aerodynamic heat flux. Therefore, the situation needs a comprehensive consideration.

4.2.3 Process control of the heat transfer

The inner surface temperature of the false cap is the result of dynamic equilibrium between the absorbed aerodynamic heat and the lost heat through radiation and convection. The temperature of false cap's nose will be increased by absorbing more heat and dissipating less heat. When the false cap is flying at a certain speed, aerodynamic heat flux can be improved evidently by reducing radius of false cap's nose making its nose sharper. What's more, air drag will be decrease, making the reduction of flight speed less quick. So, the method is practical, for aerodynamic heat is very sensitive to flight speed. However, the method also needs overall consideration for radiating area and view factor will be reduced. Dissipating less heat can be achieved by spraying coating of low emissivity on false cap's outer surface and inner surface of false cap tail, or by using the two-section false cap mentioned before.

On the contrary, lowering the temperature of TPV cell can be achieved by dissipating more heat and absorbing less heat. Fuze is an inclosed cavity, so heat cannot be transferred to the outside, but it can be moved from the high-temperature nose to the low-temperature tail by adopting some measures, for example, the method of heat sink or phase change to absorb heat. There is no use utilizing forced convection like electric fan. Not only the temperature will not be lowered, but the con-

vection heating intensity of the TPV cell in false cap's nose will increase. Absorbing less heat can be achieved by using a filter before the TPV cell (as is shown in Fig. 1), through which the bands that can't be use by TPV cell will be reflected. Or it can also be achieved by placing the TPV cell in an inclosed container, all of whose sides are opaque except the side that is against the TPV cell. Theoretically, the heat absorbed by TPV cell can be reduced, for there is no convection and radiation is suppressed as much as possible.

5 CONCLUSION

According to the tactical demands of common fuze and characteristics of TPV power supply, the paper proposed three factors that affect the performance of fuze TPV power supply most significantly, which are electricity generating power, temperature of TPV cell and temperature rise rate of false cap. Based on the analyses of performance formulae of the three factors, the paper proposed optimizing fuze TPV power supply from three aspects, which are the material selection of false cap, the structure design of power supply and the process control of heat transfer. The proposal points out the right direction in the further study of fuze TPV power supply. As to the specific rules regarding the effect that false cap material, power supply structure and heat transfer process have on fuze TPV power supply need to be further studied.

REFERENCES

- Amabile, K. & Dratler, R. 2009. An Overview of Novel Power Sources for Advanced Munitions. Picatinny Arsenal, NJ: US Army Armament Research, Development and Engineering Center.
- Antonio, L. & Steven, H. 2003. Handbook of Photovoltaic Science and Engineering. *John Wiley & Sons, Limited*.
- Guazzoni, G. & Kittl, E. 1974. Cylindrical Erbium Oxide Radiator Structures for Thermophotovoltaic Generators. *ECOM R&D Tech. Rep. 4249*.
- Holmquist, G. & Wong, E. 1995. Waldman C. Laboratory Development TPV Generator. *Proc. Second NREL Conference on Thermophotovoltaic Generation of Electricity*, 358.
- Kolm, H.H. 1956. Solar-battery power source quarterly progress report solid state research. Massachusetts, USA.
- Li. & Zhi. 1956. Radio Fuze and Electronic Time Fuze. Weapon Industry Press.
- Pereira, C.M. & Janow, C. 2009. Munitions energy system.
- Xu. & Wang. 2011. Engineering Heat Transfer. China Electric Power Press.
- Zhang. & Pan. 2003. Aerodynamic Heat and Thermal Protection of Hypersonic. National Defence Industry Press.

The monitoring research on process of heat and moisture transfer in active layer of permafrost

Ming Li Zhang

*State Key Laboratory Frozen Soil Engineering, Cold and Arid Region Environmental and Engineering Institute, Chinese Academy of Sciences, Lanzhou, Gansu, China
University of Chinese Academy of Sciences, Beijing, China*

Zhi Wen

State Key Laboratory Frozen Soil Engineering, Cold and Arid Region Environmental and Engineering Institute, Chinese Academy of Sciences, Lanzhou, Gansu, China

Ke Xue

*State Key Laboratory Frozen Soil Engineering, Cold and Arid Region Environmental and Engineering Institute, Chinese Academy of Sciences, Lanzhou, Gansu, China
University of Chinese Academy of Sciences, Beijing, China*

ABSTRACT: The thermal regime in permafrost region has been well developed, while it is insufficient in the dynamic law of soil moisture. Based on observed data of monitoring section in Beiluhe, the features of soil moisture-heat migration and the hydrothermal coupling mechanism are analyzed. The monitoring results show that the soil water content decreases as the temperature lowering while the freezing process in the autumn and cooling process in winter. The effects of temperature and moisture boundary on surface decrease with depth, so did the fluctuations of temperature and moisture. In the meantime, the content and migration of soil water have a significant impact on the freezing and thawing process. The unfrozen water content accounts for about 50% of the initial water content in winter. Water migrated to freezing front during soil freezing, which leads to soil frost heave and threatens the upper structure stability.

Keywords: permafrost; active layer; moisture migration; unfrozen water content

1 INTRODUCTION

Due to environmental disturbances and human activity, the climate has been changing in Qinghai-Tibet Plateau, such as climate warming (Li et al. 1996), precipitation increasing (Zhu et al. 2011), ground temperature rising. That is to say, the heat and water conditions are changing. The changing of moisture and thermal condition will result in the changes of hydrological and ecological features (Li et al. 1996, Zhao et al. 2000), affect the freeze-thaw process of active layers (Wu et al. 2003), and lead to serious frost heaving damage (Jin et al. 2011).

Theoretical analyzing, the interaction law of temperature and moisture is necessary to understand the mechanism of frost and thawing, guide and govern engineering diseases in civil engineering and environmental engineering. The thermal regime in permafrost region has been well developed since 1850s, while it is insufficient in

the research of the dynamic law of soil moisture. There are series of models to predict the thermal-moisture migration, such as hydrodynamics model (Harlan 1973, Taylor & Luthin 1978), segregated potential model (Konrad 1980), thermal-moisture-stress coupled model (Guo & Miao 1998, Mao et al. 2003), rigid ice model (Gorelik et al. 1998, Sheng et al. 1995) and so on. However, the natural field is so complicated that calculation models can not exactly represent the reality. So the calculation models have not been applied in the engineering.

We have monitored the surface layer moisture and temperature in Beiluhe Observation and Research Station on Frozen Soil Engineering and Environment. Based on the observation datasets, the heat and water process in permafrost regions were analyzed. The migration patterns, the features of soil moisture-heat migration and the hydro-thermal coupling mechanisms were analyzed.

2 MATERIAL AND METHOD

The observation field site selected for this study locates between Fenghuoshan and Kekexili in QTP with an elevation of 4620 m. In this site, the terrain is gently rolling and low mounds alternate with depressions. The ground vegetation coverage rate is commonly 70% ~ 80%. The active layer mainly consists of silty soils and fine sandy soils. The type of frozen soil is ice-rich permafrost with the thickness of 1–4 m ice-rich soil with a volumetric ice content of 50% ~ 80%. The recorded meteorological data show that the annual temperature ranges from $-37.7\text{ }^{\circ}\text{C}$ to $23.2\text{ }^{\circ}\text{C}$. The average annual temperature is $3.8\text{ }^{\circ}\text{C}$ with annual average rainfall of 290.9 mm and natural permafrost table is 2.5–3 m. In order to monitor thermal and moisture regime of the natural site, 5TM soil thermal and moisture probes and TP02 temperature probes were drilled in the natural ground.

3 RESULTS AND ANALYSIS

3.1 Temperature analysis

Active layer lies above permafrost which is the interface for heat and moisture transferring between permafrost and atmosphere. The temperature mainly varies with air temperature, solar radiation, soil constitution and precipitation, which leads to the changing of ice content, unfrozen water content, thermal conductivity and heat capacity. Regardless of the effect of soil particle surface energy and salt on freezing temperature, we assume that the freezing temperature of water in the soil is $0\text{ }^{\circ}\text{C}$. Figure 1 shows temperature varies with time within active layer at different depths. It can be seen that the depth of permafrost table is more than 2.2 m and the actual value should be 2.6–3.0 m.

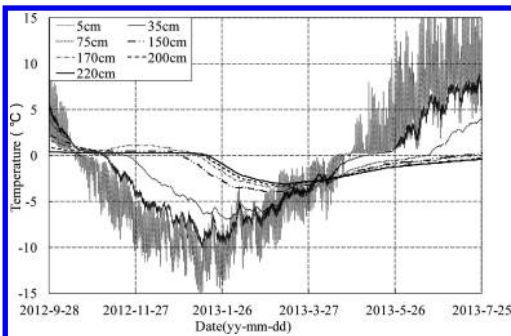


Figure 1. Variation curves of temperature within active layer at different depths.

Each measured point experiences four stage: freezing in autumn, cooling in winter, melting process in summer and the temperature rise in spring during the frozen-thaw cycle. Take the 5 cm measured point for example. The natural ground started to freeze since late October and the entire active layer finished the freezing process at late December. The freezing process lasts for 60 days and the freezing rate is about 4.5 centimeter per day. Then active layer comes into temperature-fall period which lasts for 40 days. From early February to late April, temperature of soil starts to rise until early May when the surface starts to melt.

The variation of temperature at different depth approximates the cosine law distribution and the variation period is approximate equivalent. However, the response time decays and extent decreases with depth. The temperature fluctuation gradually decreases and the initial freezing time and melting time begin to delay with depth.

3.2 Unfrozen water content analysis

Frozen soil consists of soil particle, unfrozen water, air and ice. Water in frozen soil exists in the form of solid ice, water vapor and liquid water. For the convenience of narration, the volumetric water content was described as unfrozen water content in frozen soil, and described as the total water content in melted soil. Figure 2 gives a relationship between soil water content and time at depth of 5–220 cm in the process of monitoring. As we can see:

1. Water content in the melting stage was significantly higher than that of freezing process, and the surface moisture content fluctuates intensely. The moisture content fluctuation of shallow soil is probably associated with short-term precipitation in summer. At the same time, the strong radiation, the evaporation and high wind speed in the plateau intensified the fluctuations.

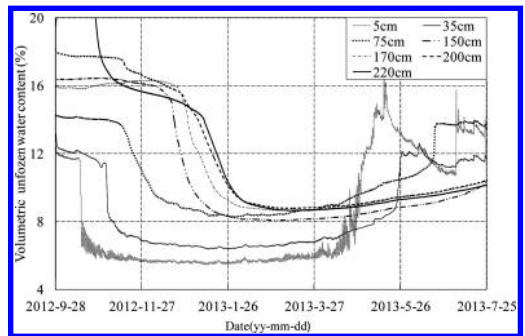


Figure 2. Variation curves of unfrozen-volumetric water content within active layer at different depth.

- In the winter cooling process and the summer melting process, the water content increases with depth. The primary cause leading to the distribution is that the soil temperature increases with depth in winter and the unfrozen water increases with the temperature in the negative temperature zone. In summer melting process, surface liquid from precipitation and ice melting infiltrates under the action of gravity which leads to the increasing of water content with depth.
- Soil hydraulic conductivity is extremely small in cooling process in winter and warming process in winter and the volume of migration is relatively small. In winter, free water near the soil matrix particles freezes at first. Then the free water far from particle surface freezes. Finally, the hydration water freezes. Hydration water has higher surface energy compared with free water. The soil from monitoring site is silty clay which tends to have larger specific surface area and surface energy. So there is also unfrozen water at very low temperature. The volume of moisture migration is relatively large under the action of gravity and irregular and periodic precipitation in summer and early autumn. From the middle of autumn, large quantities of unfrozen water migrate from unfrozen zone to the freezing front and the volume of migration is relatively large and the ground temperature tends to decrease.

3.3 Coupled heat and moisture analysis

Freeze-thaw process is an interrelated process with heat transfer, moisture migration and phase change. The change of moisture field changes the distribution of water content, which makes the heat capacity and heat transfer coefficient dynamic in a time dependent situation. Meanwhile, the change of temperature field will cause the change of water-physical properties (Zhou et al. 1982, Yang. 2003). Figure 3(a), (b) and (c) show the relationship between temperature and unfrozen-volumetric water content at 25 cm, 75 cm and 200 cm. it can be seen:

- The distribution of temperature and unfrozen water content at different depth approximates the cosine law and the variation period is approximating equivalent. Water content increased with a rise of temperature in spring and summer. However, the condition is the opposite in autumn and winter and unfrozen water content is bigger than spring and summer.
- Soil temperature and freeze-thaw process significantly affected by water content. Due to the

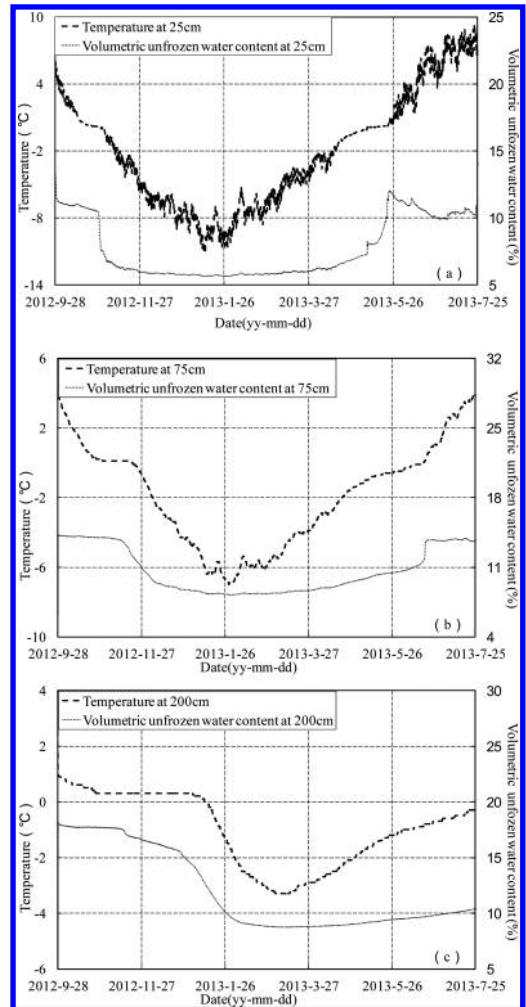


Figure 3. Variation curves of temperature and unfrozen-volumetric water content at various soil depths.

heat capacity of liquid water is 2 times of water ice, and 3–5 times larger than the soil matrix, it can absorb or release more heat. The existence of soil moisture is like a thermal resistance in freezing front during the water phase change. It will decrease temperature gradient imposed by external environment, lag the freeze and melt processes and greatly affect the distribution of heat in the soil. In the freezing process, the degree of soil saturation in frozen zone is low, water will gradually migrate from the unfrozen zone to freezing front and freeze. Large quantities of liquid free water freezes in the freezing early period, and the soil moisture changes dramatically. In this process, the freezing front is moving ceaselessly and the total water

content increased too, the total water content that deducting the ice content is the monitoring unfrozen water content.

3. There is a close relationship between soil freezing temperature and initial moisture content. Even if the temperature is very low, there still exists plenty of unfrozen water. The water that did not attend phase change accounts for about 50% of the initial water content in winter.

4 DISCUSSIONS

Macroscopically speaking, hydro-thermal process of permafrost is the process of hydrothermal coupling process. The moisture migration mainly includes the liquid convection and gaseous water migration in silt and clay. In the earth's surface that covered well with plants, gas moisture migration quantity is small, which can be neglected. For bare land, sand, gravel soil, and large pore engineering, migration of vaporous water occupies a large proportion, which should be considered.

It is very complicated in the process of water flow and heat transport including ice and water phase change in porous media. There remains plenty of unfrozen at subzero temperatures and the amount of unfrozen water decreases with the temperature. Understanding the unfrozen water flowing through frozen ground is important in investigations of water redistribution, mechanical stability and frost heaving. Moisture migration driving force is the first factor. Then equations include the effects of thermal conductivity, latent heat of phase change and the seepage should be established.

5 CONCLUSIONS

The freeze-thaw process and the dynamics of soil moisture were analyzed with the measured data of temperature and moisture within the active layer at Beiluhe Observation and Research Station on Frozen Soil Engineering and Environment in Qinghai-Tibet Plateau from September 27, 2012 to July 25, 2012. Both freezing and thawing processes, migration patterns and moisture-heat coupling mechanism of permafrost is revealed. We get the following conclusions:

1. Temperature and unfrozen water content at different depth approximates the cosine law distribution and the variation period is approximate equivalent. The degree of similarity gradually decreases with depth and the initial freezing time delayed with the depth of soil increasing.

2. The effects of temperature and moisture boundary on surface decreased with the depth, so did the fluctuations of temperature and moisture. Soil temperature and freeze-thaw process significantly affected by water content within the active layer. The existing of water will decrease temperature gradient imposed by external environment, lag the freeze and melt processes and greatly affect the distribution of heat in the soil.
3. There is a close relationship between soil freezing temperature and initial moisture content. Even if the temperature is very low, there still exists plenty of unfrozen water. The water that did not attend phase change accounts for about 50% of the initial water content in winter. Water migrated to freezing front during soil freezing, which leads to soil frost heave and threatens the upper structure stability. In the process of numerical simulation should select suitable soil freezing characteristic curve, determine the practical freezing temperature and water phase transformation ratio transition range to ensure the reliability of numerical calculation.

ACKNOWLEDGEMENTS

The research project was supported by the Science and Technology Project of State Grid Corporation of China, SGJSJS (2010)935-936, the 100 Talent Young Scientists Project granted to Dr. Zhi Wen, National Key Basic Research Program of China (No. 2012CB02610601), and the Program for Innovative Research Group of National Natural Science Foundation of China (Grant No. 41121061).

REFERENCES

- Fremond, M., Mikkola, M. 1991. Thermo-dynamical modeling of freezing soil. *Proceedings of 6th international symposium on Ground Freezing*: 17-24.
- Guo, L. & Miao, T.D. 1998. Thermodynamic model of heat-moisture migration in saturated freezing soil. *Chinese Journal of Geotechnical Engineering* 20(5):87-91.
- Gorelik, J.B., Kolunin, V.S. & Reshetnikov, A.K. 1998. rigid-ice model and stationary growth of ice. *The 7th International Permafrost Conference [C]*. Canada: Laval University:327-333.
- Harlan, R.L. 1973. An analysis of coupled heat- fluid transport in partially frozen soil. *Water Resources Research* (9):1314-1323.
- Jin, H.J., Wang, S.L. Yu Q.H., Wu, Q.B. & Wei, Z. 2011. Regionalization and assessment of environmental geological conditions of frozen soils along the Qinghai-Tibet Engineering Corridor. *Journal of Glaciology and Geocryology* 33(4):846-850.
- Konrad, J.M. & Morgenstern, N.R. 1980. A mechanistic theory of ice formation in fine grained soils. *Canadian Geotechnical Journal* (17):473-486.

- Li, S.X., Cheng, G.D. & Guo, D.X. 1996. The future thermal regime of numerical simulating permafrost on Qinghai-Xizang (Tibet) Plateau, China, under climate warming. *Science in China (Series D)* 39(4):434–441.
- Li, S.X., Nan, Z.T., Zhao, L. 2002. Impact of freezing and thawing on energy exchange between the system and environment. *Journal of Glaciology and Geocryology* 24(2): 109–115.
- Mao, X.S., Hu, C.S., Dou, M.J. & Hou, Z.J. 2003. Dynamic observation and analysis of moisture and temperature field coupling process in freezing soil. *Journal of Glaciology and Geocryology* 25(1):55–59.
- Sheng, D.C., Axelsson, K. & Knutsson, S. 1995. Frost heave due to ice lens formation in frozen soils. *Nordic Hydrology* (26):125–146.
- Taylor, G.S. & Luthin, J.N. 1978. A model for coupled heat and moisture transfer during freezing. *Canadian Geotechnical Journal* (15):548–555.
- Wu, Q.B., Shen, Y.P. & Shi, B. 2003. Relationship between frozen soil together with its water-heat process and ecological environment in the Tibetan Plateau. *Journal of Glaciology and Geocryology* (25): 250–255.
- Yang, S.X. 1987. A simulation of water and heat transfer during soil freezing. *Journal of Tsinghua University (Philosophy and Social Sciences)*(3):20–27.
- Zhao, L., Cheng, G.D., Li, S.X. 2000. The freezing and thawing process of permafrost active layer in Wudaoliang of Qinghai-Tibet Plateau. *Chinese Science Bulletin* (45): 1205–1210.
- Zhou, Y.W. & Guo, D.X. 1982. Principal characteristics of permafrost in China. *Journal of Glaciology and Geocryology* 4(1): 1–19.
- Zhu, Z.R., Li, Y. & Xue, C.X. 2011. Changing tendency of precipitation in permafrost regions along Qinghai-Tibet railway during last thirty years. *Journal of Glaciology and Geocryology* 33(4):846–850.

Triple objective evaluation model of green building based on whole life-cycle

Qing Lan Han & Xiao Lin Kong

Central South University, Changsha, China

ABSTRACT: To overcome some green building evaluating issues such as the limitation of current evaluation indicators setting, the complexity of the indicator subdivision and the difficulty of obtaining data, according to the requirements of sustainable development, from the perspective of the whole life-cycle, the paper discusses the environment, economy and society should be considered in setting green building evaluation indicators, constructs a triple objective evaluation system, and determines the weight of indicators. On this basis, the paper establishes an evaluation model of the triple objective. To scientifically balance the relationship of the triple objective, we introduce the coordination degree evaluation for previous results. Thus the two components constitute a comprehensive evaluation model. Finally, the paper selects building cases for application and verifies the indicator system and evaluation model scientific and feasible.

Keywords: green building; whole life-cycle; indicator system; evaluation model

1 INTRODUCTION

The concept of green building appeared in the 1960s. During the last 20 years, developed countries represented by America, Canada, Britain and Japan have researched green building deeply, and established their own appropriate green building evaluation systems, such as the LEED™ of America (1995), GB-Tool of Canada (1996), CABEBEE of Japan and NABERS of Australia (2003), in which the LEED™ of America has the greatest influence. LEED™ system carries out the evaluation through five aspects: sustainable building sites, water use, building energy and atmosphere, materials and resources, indoor air quality, and divides the buildings into 4 certification level by the total score; Canada GB-Tool divides evaluation indicators into resources efficiency, environmental impact, indoor environmental quality, service quality, economy, management before using and community traffic, and the evaluation clause may be changed in the terms of the actual construction, so it is relatively flexible and adaptable; Japan CASBEE system firstly proposes quantitative evaluation indicator-BEE (Building Environmental Efficiency), $BEE = Q/L$, Q is the quality and performance of building environment, L is the load and external environment of the building.

In the 1980s, concept of green building was introduced domestic. In September 2001, the Ministry of Construction made the first “China Ecological

House Technology Assessment System”, whose evaluation indicators were divided into five areas equally to LEED. In December 2003, the Olympic construction research group published GOBAS (Green Building Assessment system), its indicators were divided into Q and L learning from Japan CASBEE, in which Q means the construction quality and service levels, L means the ecological and environmental impact. In March 2006, the state promulgated the “Green Building Assessment Standard”, which brought public buildings inside the scope of evaluation, this standard fully learned advanced experience of foreign countries, and combined with environmental requirements to set the indicators from six areas: land saving, water saving, energy saving, materials saving, indoor environmental quality, operations management (residential buildings) and whole life-cycle overall performance (public buildings); then broke down the indicators in each category, including controls, general term and preferences, finally declared the buildings with one-star, two-star and three-star based on the actual scores. Up to December 2013, there were 1260 building projects got green building markings.

Throughout the current domestic and international green building evaluation systems, only GB-Tool system contained economic evaluation, but it only stayed at the concept level lack of specific indicators and calculation methods; though foreign evaluation systems are relatively perfect,

as domestic resources, environment and economic situation differ greatly, and many index segments don't have the reference, therefore how to set indicators are different; the current evaluation standards apply only to the residential and public buildings those have large consumption of resources, not are universal; in addition, complex sub-indicators, additional indicators increased difficulty of its operation and reduced the use of evaluation standards. View of this, from the perspective of whole life-cycle, based on the green evaluation, the paper introduces economic evaluation; combined with environmental quality of domestic construction to subdivision specific evaluation indicators, then sets weight to build triple objective evaluation system of green building; on this basis, in terms of the principles of complex systems and coordination subject, establishes comprehensive evaluation model covering comprehensive evaluation and coordination degree evaluation; finally, combines with the application cases to verify the research result scientific and feasible.

2 THE BUILD OF GREEN BUILDING EVALUATION SYSTEM BASED ON WHOLE LIFE-CYCLE

2.1 Build basis of indicator system

Perspective of the whole life-cycle is to view the whole process from pre-plan to demolition as a whole. We divide it into four stages covering planning and design, construction, management and operation, and demolition recycling. From the perspective of the whole life-cycle, green building is no longer a single individual, but an environmental-social-economic complex. Therefore, the goal of green building design needs to account environmental, economic and social aspects, to meet

triple goal of environmental protection, economic efficiency and social satisfaction, to create sustainable value. The triple objective evaluation needs to reflect environment, economy and society of green building completely.

2.1.1 Environmental assessment indicators

The environment of green building is to minimize energy consumption and reduce environmental impact. Environmental assessment should follow the current standards, and take the whole life-cycle control requirements into account by adding "long-term environmental value" to land, water, materials and energy saving. So we choose sustainable sites, materials saving, energy conservation and energy use, water saving and long-term environmental value to set indicators. Setting subdivide indicators refers to LEED system and domestic current standard, and combines with the comprehensive, comparable, measurable principles.

2.1.2 Economic assessment indicators

Economy only in GB-Tool is explicitly listed as an evaluation index, but since not the core index, only been given 10% weight, so didn't give specific quantitative benchmarks and scoring method. During recent years, the state has a preliminary study on the economic evaluation. Referring to relative papers, we select the incremental cost-effectiveness NPV (*SE*) and the incremental cost-effectiveness ratio (*CE*) two quantitative indicators. Two indicators are calculated as follows:

$$SE = NPV_S - NPV_C \quad (1)$$

$$CE = S/C \quad (2)$$

Among them, (1) NPV_S is the present value of the whole life-cycle incremental benefit, NPV_C is

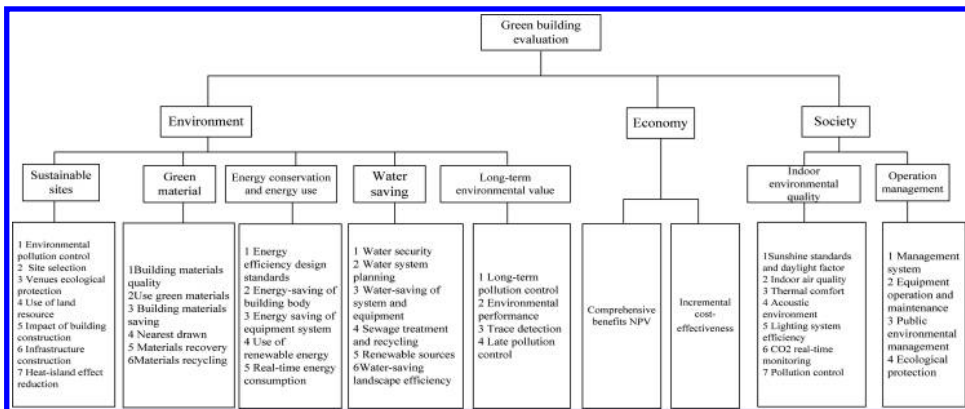


Figure 1. Green building triple objective evaluation hierarchy.

the present value of the whole life-cycle incremental cost; (2) C means the increase in costs of green buildings to achieve environment and livability relative to ordinary buildings, S means the cost savings.

2.1.3 Social assessment indicators

From the social point of view, the ultimate goal is to serve for users to satisfy their healthy and comfortable requirements. Combined with the current domestic construction environment, choose indoor environmental quality and operation management two indicators. Indoor environmental quality continues to be subdivided into seven areas based on the using demand: sunshine standard and daylight factor, indoor air quality, thermal comfort, acoustic environment, lighting systems, CO₂ real-time monitoring and control of pollutants; operation

management is mainly to evaluate later management and maintenance, selecting management rule, equipment operation and maintenance, public environment management and ecological protection to reflect the ongoing management of the whole life-cycle.

2.2 Triple objective evaluation hierarchy of green building

According to comprehensive, systematic, comparable and measurable principles, first level indicators of environment, economy and society correspond to green building triple objectives, the second and third level indicators are set in terms of the preceding build basis, then we build a triple objective evaluation hierarchy shown in Figure 1.

Table 1. Triple objective evaluation system of green building.

Item	Indicator	Weight
<i>Environment</i>		
Sustainable sites 22.5%	Venues ecological protection	0.0788
	Use of land resource	0.0562
	Infrastructure construction	0.0338
	Impact of building construction	0.0337
	Heat-island effect	0.0225
Green material 22.5%	Use green materials	0.0900
	Building materials saving	0.0450
	Materials recovery	0.0450
	Nearest drawn	0.0225
	Materials recycling	0.0225
Energy conservation and energy use 22.5%	Energy-saving of building body	0.0675
	Energy saving of equipment system	0.0675
	Use of renewable energy	0.0450
	Real-time energy consumption	0.0450
	Water system planning	0.0563
Water-saving	Water-saving landscape efficiency	0.0338
	Water-saving of system and equipment	0.0562
Water-saving 22.5%	Renewable sources	0.0450
	Sewage treatment and recycling	0.0337
	Trace detection	0.0600
Long-term environmental value 10%	Late pollution control	0.0400
<i>Economy</i>		
Comprehensive benefits NPV 50%		0.5000
Incremental cost-effectiveness 50%		0.5000
<i>Society</i>		
Indoor environmental quality 60%	CO ₂ real-time monitoring	0.1500
	Thermal comfort	0.1200
	Acoustic environment	0.1200
	Lighting system efficiency	0.1200
	Pollution control	0.0900
Operation management 40%	Equipment operation and maintenance	0.1400
	Public environmental management	0.1400
	Ecological protection	0.1200

2.3 The set of indicators' weight

The paper selects experts' advice and AHP to determine the indicators' weight. First level indicators' weight is 100% for the triple objective is important equally. Second level indicators' weight is set through experts' advice and the third according to AHP. Then we obtain the triple objective evaluation system of green building (Table 1).

3 THE TRIPLE OBJECTIVE EVALUATION MODEL OF GREEN BUILDING

According to complex system theory, the triple objective evaluation of green building can be seen as a complex system of environment, economy and society. This paper introduces coordination evaluation to measure the balance of triple objectives, so that the composite system maximizes their synergy.

3.1 Comprehensive evaluation

According to the principle of composite system, green building assessment can be defined as: P (Triple objective evaluation) = (environment P1, economy P2, society P3), specific calculation process is as follows:

First step is to determine the initial value of segment indicators of each target. Quantitative indicators are directly calculated, qualitative indicators are divided into five grades: "excellent-5" "good-4" "medium-3" "poor-2" "poorer-1";

Second step is to carry out the dimensionless of initial value. Quantitative indicators use the following formula:

$$y = (i - i_L) / (i_H - i_L) \times 4 + 1$$

where y is dimensionless index, i is indicator's initial value of the evaluated green building, i_L is

indicator's lowest value of all same buildings, i_H is the highest value.

Third step is to determine the evaluation value of each object (S_i). We use the weighted geometric mean method to get S_i . The indicators' weights are listed in Table 1.

Final step is to calculate the comprehensive evaluation value (Z). We think the triple objective is equally important, so use simple geometric mean method to get Z .

$$Z = \sqrt[3]{(S_1 \times S_2 \times S_3)} \tag{3}$$

Specific results are described in Table 2.

3.2 Coordination evaluation

Coordination applying to green building evaluation is to reflect equilibrium state of the triple objective of a point or a stage of the whole life-cycle. We choose standard deviation coefficient method to calculate the coordination evaluation value. The calculation process is as follows.

Taking the environmental and economic objectives for instance, their evaluation value are S_1 and S_2 , to calculate the standard deviation coefficient of the two as follows:

$$C_{1,2} = 4S_1S_2 / (S_1 + S_2)^2$$

Similarly:

$$C_{1,i} = 4S_1S_i / (S_1 + S_i)^2 \tag{4}$$

Note: $C_{1,i}$ is the coordination of any two targets.

$$C = \sqrt[3]{(C_{1,2} \times C_{1,3} \times C_{2,3})} \tag{5}$$

Note: C is the coordination degree of triple objectives. $0 \leq C \leq 1$, the larger the value, the better

Table 2. The explanation of comprehensive evaluation results.

Z	1	(1, 3)	3	(3, 5)	5
Comprehensive evaluation result	Lowest level	Below average	Average	Above average	Highest level

Table 3. Coordination degree of the green building triple objective.

C	[0, 0.55)	[0.55, 0.80)	[0.80, 0.93)	[0.93, 0.95)	[0.95, 0.97)	[0.97, 0.99)	[0.99, 1]
Coordination degree	Extreme disorder	Serious imbalance	Imbalance	Verge of disorder	Basic coordination	Coordination	Very coordination

Table 4. Results of triple objective evaluation of the three projects.

Green building	Environment S_1	Economy S_2	Society S_3	Z	Coordination evaluation				
					$C_{1,2}$	$C_{2,3}$	$C_{1,3}$	C	F
A	3.5090	2.8800	3.5000	3.2829	0.9908	0.9906	0.9999	0.9938	3.2625
B	3.6359	3.0000	3.9800	3.5146	0.9908	0.9803	0.9980	0.9897	3.4784
C	4.0046	3.0000	4.6500	3.8228	0.9795	0.9535	0.9944	0.9757	3.7299

the coordination degree. The classification standard of the coordination is as shown in Table 3.

3.3 The model of triple objective evaluation

On the basis of comprehensive assessment, the paper introduces the coordination concept to adjust it, and gets an integrated model of triple objective evaluation of green building:

$$F = \sqrt[3]{S_1 \times S_2 \times S_3} \times \sqrt[3]{C_{1,2} \times C_{2,3} \times C_{1,3}} \quad (6)$$

4 APPLICATION CASE

This paper selected three green building projects A, B, C identified by the current assessment standard. Then we apply the triple objective evaluation system and model to the projects, and verify the system and model scientific and feasible.

4.1 Project overview

Project A covers an area of 8681 square meters and a total construction area of about 40,000 square meters. It has received the three-star marking.

Project B has a total investment of 27 million, the land area is 3620 square meters, and construction area is 19,920 square meters. This project received two-star marking in 2009.

Project C covers land area of 16,000 square meters, total construction area is nearly 60,000 square meters, and volume rate is 3.6. This project received one-star marking in 2009.

4.2 Triple objective evaluation

We used the triple objective evaluation system to assess those three projects. Qualitative indicators' calculation accorded to the five levels of "excellent, good, medium, poor, poorer", and then continued to calculate the model value in accordance with the former calculation step. Final calculation results are shown in Table 4.

4.3 Result analysis

As can be seen from the comprehensive evaluation: (i) Triple objective evaluation system is consistent

with the current standard, the higher the star marking, the higher evaluation scores; (ii) Three projects' performance is significantly above average in the environmental and social aspects, but the economic performance is only at the average level, which needs more attention; (iii) The comprehensive evaluation score of the three-star building is at average level, although two-star and one-star projects are above average, there is still much room for improvement.

As can be seen from the coordination degree evaluation: (i) The coordination degree of project A is the highest, which performances as "very coordinated"; Project B and C only performance as "coordinate"; (ii) The coordination degree is contrary with the projects' comprehensive evaluation results, although the three-star project A has poor performance overall, but its coordination degree is worth learning; due to economic or social and environmental goals is not an effective balance, the coordination degree of buildings is impacted seriously.

5 CONCLUSION

Based on the analysis of existing green building evaluation standards at home and abroad, in accordance with sustainable development requirement, from the perspective of the whole life-cycle, the paper proposes a triple objective evaluation system covering environment, economy and society assessment, determines the weight of each indicator by expert advice and AHP, and constructs a triple objective evaluation model composed by comprehensive and coordination evaluation. The model could evaluate the coordination degree of triple objective while provides an assessment on environmental, economic and social aspects, fully reflects the environment, economy and society of green building, makes up the defect of current evaluation standard. Finally, the paper selects specific application cases and verifies the indicator system and evaluation model scientific and feasible.

ACKNOWLEDGEMENTS

This paper is supported by the Central South University Graduate Innovation Fund under grants No. 72150050415.

REFERENCES

- Chan H.W. & Qian Q.K. 2009. The market for green building in developed Asian cities-The perspectives of building designers. *Energy Policy* 37(8): 3061–3070.
- Ding G.K.C. 2008. Sustainable construction—The role of environmental assessment tools. *Journal of Environmental Management* 86(3): 451–464.
- GB/T 50378-2006. Green Building Evaluation Standard. Beijing: China Building Industry Press.
- Jing Chen. & Zhe Tian. 2011. Research on Incremental Cost and Benefit of Green Building Life-cycle. *Engineering Management Journal*.
- LEED™: Leadership in Energy & Environmental Design Building Rating System. U.S. Green Building Institute, 2003.
- LiuQin Chen. 2011. Discussion on Green Building Evaluation System. *Construction Economy*, June 2011.
- Mei S.N. 2002. China Ecological Residential Technology Assessment Manual. Beijing: China Building Industry Press.
- One Hundred Cases of China Latest Green Building. 2011. Beijing: China Building Industry Press.
- Rajesh Kumar Singh. 2012. An overview of sustainability assessment methodologies. *Ecological Indicators*.
- Sen Cao. & Cong Dong. 2012. Green Building Life-cycle Cost Benefit Evaluation. *Journal of Tsinghua University*.
- Wen S.B. & H.X. Xue. 2005. Triple Performance Evaluation Model of Enterprise Based on Scientific Development Concept. *Accounting Research*.
- Yan P.Z. & Hao Hu. 2006. Research on Economy Evaluation of Ecological Building Project. *Construction* 28(3): 203–204.

High-tech cabling system applied in green building

Fang Fang

Network Engineering and Research Center, South China University of Technology, Guangzhou, China

Xiao Feng Yu

The Siemon Company, Guangzhou, China

ABSTRACT: This paper describes the basic characteristics of green buildings. From the advanced network system design, high-density patch panel design, and intelligent infrastructure management, introduces the new ideas and the new methods of green building cabling system design. We can use high-tech cabling technology to promote green building more intelligent, energy conservation, and pollution reduction, achieve green building innovation and prosperity through the development of intelligent buildings.

Keywords: green building; cabling system; saving; design

1 CHARACTERISTICS OF GREEN BUILDING

1.1 *Green building*

In general, green building is the architectural design, construction, use, fully consider the environmental requirements, the building closely with other technologies combine to effectively meet a variety of useful functions in the same time, users can benefit physical and mental health, and create jobs and living space structure in line with environmental requirements. [1]

1. Ecology: In the design and construction process, people respect ecological laws, protect the ecological environment. The technique of green building is to protect the ecology, ecological adaptation, do not pollute the environment.
2. Affinity: Green buildings combined with modern civilization and the natural affinity to modern technological means to achieve long-term goals of ecological environmental protection.
3. Health: Green buildings using green building materials, to meet the health of the living environment, protect the health needs of the occupants.
4. Advancement: Green buildings contain a number of professional high-tech applications. Green building preferred to use many advanced technologies, reflects it's broad, integrated and advanced.
5. Developmental: Green buildings use a lot of intelligent systems, systems to increase or update devices have advanced scalability and flexibility. [1]

1.2 *Design of green building*

Green building and traditional architectural design compared to an increase in energy-saving high-efficiency target layout and design elements without damaging the environment, reduce air-conditioning and artificial lighting to create a pleasant, green environment.

The performances of the whole process of green building design are: to determine the green building goals; green technology initiatives choice; technical and economic integrated program; construction, management, and other work. [2]

2 CABLING SYSTEM IS THE FOUNDATION OF INTELLIGENT GREEN BUILDINGS

Cabling system is a modular, high flexibility of information transmission channel within a building or between buildings. It allows the device through voice, data equipment, switching equipment and a variety of control devices and information management systems together, but also to communicate with external cabling devices connected to the network. [3]

Integrated cabling application features:

- **Compatibility:** completely independent, integrated cabling system itself can be applied to a variety of application systems. Integrated cabling to voice, data and monitor equipment line through unified planning and design, integrated into a set of standard cabling.
- **Openness:** integrated cabling uses the open architecture, a variety of international current

standards, and to support all communication protocol.

- Flexibility: integrated cabling with a standard transmission cables and related links, hardware modular design.
- Reliability: integrated cabling uses the high quality materials constitute a set of high standards of information transmission channel. Every channel using special equipment testing link impedance and attenuation to ensure its electrical properties.

With its cabling system compatibility, openness, flexibility, reliability, and economy of advanced features, became the basis of data transmission in green building construction, so that the relationship between the various subsystems buildings more clearly and tightly. Intelligent cabling can be achieved for green building's construction and operational management, resource sharing, remote monitoring. Cabling level directly affects the level of green architecture. [4]

3 GREEN BUILDING'S CABLING SYSTEM DESIGN

3.1 *Advanced network system*

Use advanced infrastructure designed to meet green building future mission requirements decades of continuous development. Design must be forward-looking.

Currently, Class 7/F grade cable is the highest performance in the market, cabling systems, and 7 A class/FA class standards also about to launch, which fully meet the bandwidth requirements of the latest 10 Gbps copper network speeds and higher speeds in the future. These high-bandwidth cabling system is fully compatible with older technology. [5]

Lower performance cabling will be greater spending. Reduce the use of those materials need to be replaced over time will greatly encourage users to install more high-performance cabling system. For example, installing Category 5e systems will mean in the future need to replace all 10GBase-T applications to the desktop. Installation Category 6 systems will need to be adjusted when the number of channels.

Both the above circumstances are likely due to the material waste and the contracting officer need another home for "green" rating adversely affected. Reducing the need for removal and reinstallation of the cable, the same can be achieved savings of copper, aluminum and other metals, and other natural resources results. In the long run, Gigabit solution has a higher actual cost.

3.2 *High-density patch panel design*

High-density modular rack system is specifically designed to meet the high-density mounting and design. High-density patch panel system provides a robust, modular, multi-cable rack mount design, optimize network performance and manageability. It allows the user to configure the system according to the actual space and application requirements. It is also the flexibility to change or modify the configuration easily and quickly with the development and evolution of the network.

Choosing high-density pre-connected cabling product greatly reduce cabling space. Cabling systems for energy-saving design reduces energy consumption significantly, and this is an important direction for future cabling system.

3.3 *Intelligent infrastructure management*

Management also needs intelligent, space-saving is saving. Sophisticated management and software implementation of the data center infrastructure management, the purpose is to save energy.

Intelligent infrastructure management, in addition to checking the cabling channel through real-time to reduce the energy consumption of the cooling aspect, but also can reduce the power being used network equipment needs. When the design has a central region of the cabling, the intelligent infrastructure management system ensures that the entire switch ports using, as far as possible without reducing the number of switch ports, to reduce the power requirement of the device. Smart cabling system can access the network cable to the unused switch ports, without the need for an additional switch, which can save energy, thereby further saving cooling costs.

3.4 *Design of green data center*

The control center of green buildings can be designed according to the data center standards. Data centers need to have: strong access network, dynamically scalable infrastructure, and green energy room environment.

The idea of green data center includes energy saving and environmental protection. In considering ways to achieve green data center, people's attention for the cable infrastructure is not enough. Because the electrical devices, cooling systems and computer hardware are direct energy consumptions, so they always have a higher green configuration. However, the choices of cable media types and quantities, and transmission of energy consumption, will impact the data center environment.

The green data center should choose cabling products meet environmental requirements. Even

for a long time in the wiring closet will not be volatile toxic gases. Cabling system cable to achieve the following objectives:

- The normal transmission in a certain period of time at high temperatures.
- To prevent the spread of fire along the cable and produce toxic gases.
- Avoid corrosive gas damaged computer equipment connection.

Best solution is to choose flame-retardant, low smoke cable. [6]

3.5 Other cabling system design

LEED (Leadership in Energy and Environmental Design) certification, by the USGBC (USA Green Building Council) initiated, is internationally recognized as the most advanced and the most practical green building certification marking system. The following Siemon's products are introduced as an example.

1. Shielding Technology

Shielded cabling system performance brings longer life, with a small diameter, better utilization of the pipeline, cable more difficult to heat and other green energy-saving features.

2. Copper trunking cable assemblies

Siemon's TERA copper trunking cable assemblies provide an efficient and cost effective alternative to individual field-terminated components. Combining factory terminated and tested TERA outlets and fully shielded Siemon category 7 A TERA cable, Siemon TERA trunking cable assemblies offer industry leading performance to 10 Gb/s and beyond. Standard configurations also help maintain consistent cable layout, facilitate efficient move, add and change and significantly reduce scrap versus typical field installation. Combined modular design makes trunking cable the most "green" copper installation mode. [5]

3. Optical fiber technology

On fiber optic cabling, Siemon plug and play modules products and cable assemblies. Compact and lightweight plug and play modules and Razor Core cable with 12-fiber MTP connector adapter optimized space management, reducing the pipeline utilization. [5]

Siemon module is the industry's smallest low-loss 0.35 dB, which is the industry's low-loss single

plug and play solution that can support Gigabit applications in the 300 m length of 4 channel modules connected. [5]

Siemon innovative LC jumpers using sliding sheath blade design allows users to very easily plug in high-density environments; Siemon using a patent-pending design allows the fiber to change the rotation of the latch will not damage joints and fiber polarity; and a single hose, cable outer diameter finer cable duct designed to reduce congestion and improve air flow and make it easier for cable management. [7]

Recently, Siemon has launched a new XGLO Razor Core fiber backbone, which has significant fine diameter, allowing users to get an average of 50% compared to traditional space-saving components. This reduces the filling rate of the groove, thereby reducing the restriction of the pipe, having a better airflow. All of these features are to support higher density, improves efficiency and reduces costs. [7]

4 SUMMARY

In this paper, we focus on high-tech cabling system can be applied in green building, discussed the implementation method. Green building cabling system is complex system engineering. Design and installation of environmental protection and energy saving high-tech integrated cabling system, to the economic operation of the green building has a long-term and far-reaching influence.

REFERENCES

- [1] Likui, Yu. Intelligent Building and Sustainable Development. 2010: 6-7.
- [2] Yanwen, Yang. The Green Building Design Approach: a Comprehensive Process Explored in the Case of Taikoohui. South Architecture, 2013: 69.
- [3] <http://www.qianjia.com/special/cabling-system/Subject110>.
- [4] <http://www.qianjia.com/special/cabling-system/cs-2014004>.
- [5] The Siemon Company. Cabling infrastructure and green building action. Intelligent Building & City Information. 2010. 3 No. 160: 51.
- [6] Jinhua, Zhong & Liwei, Zhu & Caobo & Qigang, Ding. Next-generation green data center planning and design. Publishing house of Electronics Industry. 2011: 393-394.
- [7] <http://www.siemon.com>.

Research and prospect on durability of reinforced concrete structures

Q.L. Li, X. Wang, Z.Z. Li & J.F. Li

School of Civil Engineering, Hebei University of Science and Technology, Shijiazhuang, Hebei, China

X.M. Yang

Baoding Institute of Architecture Design Co., Ltd., Baoding, Hebei, China

Y.G. Han

Beijing Guohua Properties Co., Ltd., Beijing, China

ABSTRACT: The research of durability of RC structure has an important significance and can not be ignored. There is a direct relationship between the decrease of durability and the reduction of reliability and service life. The current research is reflected through discussing the relationship between damage mechanism and reliability, and some reasonable improvement measures are made. Finally, the prospect of the study in this field is put forward.

Keywords: reinforced concrete structures; durability; damage mechanism; reliability; service life

1 INTRODUCTION

In engineering construction, combined with the advantages between tensile resistance of steel and compressive resistance of concrete, RC structures have become the most widely used forms. Also, it must satisfy the requirements for safety, applicability and durability. Durability refers to the ability that component can keep applicability and security during design working life under certain circumstances and conditions of maintenance and use. In using process, due to the characteristics of material itself and application environment, the material suffers various corrosion and damage leading to the reduction of durability and reliability. So the actual life of structure is shorter than design life which causes great economic loss (Jin & Zhao 2002).

Durability problems have become increasingly prominent (Gong & Zhao 2000a, Yang 2007). Concrete carbonization, freeze-thaw damage, steel corrosion, etc. have become the main factors affecting the durability of RC structures. Some scholars have made study from material, component and structure and gotten the following conclusions (Wei et al. 2003): In most cases, performance deterioration of RC structures is not, or not directly caused by mechanical factors, but the effect of natural environment, application environment and physical and chemical action inside the material. Jinxin Gong & Guofan Zhao have reviewed the research status about reliability analysis related

to durability from five aspects (Gong & Zhao 2000b): (1) structural reliability analysis method considering the change of resistance at any time, (2) structural reliability analysis under corrosion environment, (3) reliability assessment of existing structures, (4) best maintenance decision of existing structures, (5) economical optimization design considering durability.

The implementation on high durability and long service life of RC structures is in accordance with energy conservation and emission reduction and sustainable development in the present society. Through the study on durability, on the one hand, the durability and the residual life of existing buildings can be scientifically assessed and predicted to choose the correct approach. On the other hand, the new project can be designed on durability to improve the level of design and construction quality and to ensure the normal operation of RC structures in the whole lifetime. So, it is significant to deep research the durability.

2 INFLUENCING FACTORS ON THE DURABILITY OF REINFORCED CONCRETE

2.1 *Steel corrosion*

Concrete contains $\text{Ca}(\text{OH})_2$, KOH and NaOH with the pH value from 12.5 to 13.5. The surface of steel is surrounded by a “passive film”—oxide film ($\gamma\text{Fe}_2\text{O}_3$). With the carbonation of concrete, pH

value decreases. When it decreases to about 11.5, passive film will be active and when it decreases to 9~10, passive film is completely destroyed. In the use environment, the phenomenon of steel corrosion occurs slowly.

The penetrating ability to oxide film of Cl^- is strong. When the concentration of free Cl^- in solution of concrete holes surrounding steel surface exceeds a certain value, even in the high alkalinity environment whose pH is greater than 11, the passive film will be destroyed by Cl^- , leading to steel's depassivation (Kong 2012). Corrosion of depassive steel is an electrochemical process. There is a potential difference in the steel surface forming corrosion cell. When water exists needed by electrochemical reaction and ion diffusion, steel corrosion occurs.

The corrosion product's volume increases of about 3 to 6 times the original, causing concrete cracking, delamination and flaking. Thus, it also provides access to the intrusion of water and Cl^- , accelerating corrosion.

2.2 Concrete carbonation

Concrete carbonation is a slow process. CO_2 in air interacts with alkaline materials in cement paste to lower the pH of concrete from 12.5~13.5 to about 8.3, especially with $\text{Ca}(\text{OH})_2$. It destroys the passive film surrounding steel surface, bringing adverse impact on steel corrosion. At the same time, the crystal water of hydration products are released along with carbonization process, bringing irreversible shrinkage to concrete. If carbonation shrinkage carries out under constraint, concrete cracks often come into being, thus it aggravates carbonization process. Carbonation would make concrete brittle and decrease ductility (Ye 2011).

Other acid gases such as SO_2 can also make concrete neutral, but the effect is generally limited to the concrete surface.

2.3 Freezing and thawing of concrete

Destructive effects of freeze-thaw cycle of concrete includes two aspects: heaving cracking and surface corrosion. Water freezes in the capillary pores of concrete, generating a stress greater than the tensile strength of concrete and then heaving cracking of concrete which declines concrete's mechanical properties as elastic modulus, compress. In general, cracks and spalling can be seen on its surface in freeze-thaw damage of concrete.

Freeze-thaw damage of concrete has been studied earlier and more deeply. From 1940, United States, the former Soviet Union, Europe, Japan began the research on mechanism of freeze-thaw damage, and put forward several failure mechanism: water

segregation and stratification theory, water pressure theory, osmotic pressure theory, water filling coefficient theory, critical water-saturated value theory, phenomenology theory (Li & Wang 2009).

2.4 Alkali-aggregate reaction

The common alkali-aggregate reaction is mainly ASR. ASR occurs around reactive aggregate particle and produces alkali-silica. The product absorbs moisture and expands. The expansion pressure can reach 7 MPa, which is enough to crack the concrete to its surface. Alkali-aggregate reaction actually depends on alkali content in concrete. The higher the content is, the more likely the reaction is.

3 MEASURES TO IMPROVE THE DURABILITY OF RC STRUCTURES

Finding the measures to improve the durability of RC structures and growth the service life of structure should be proceed from the factors that affect durability.

3.1 Using high performance concrete

FHWA defines that high-performance concrete is more durable and higher on strength than ordinary concrete. High-performance concrete has good frost resistance, high density, low permeability that can decrease the penetration of chloride ions and reduce the corrosion rate of steel. In the design of concrete mix proportion, less cement and lower water-cement ratio reduce the heat generated by the reaction of hydration and the effect of temperature cracking. So this can effectively weaken the influence brought by corrosive substances to steel through these cracks. Strict control of alkali content in the concrete aggregate to inhibit alkali-aggregate reaction is necessary.

3.2 Using protective materials on steel

Steel corrosion caused by chloride is the most important factor for structure damage and durability loss. Epoxy-coated rebar (Liu 2006), plastic spraying (resin) steel, galvanized steel (Liu 2006) and rebar rust inhibitor (Liu et al. 2008) are all able to enhance steel durability on resistance to chloride. Among them rust inhibitor is the most cost-effective.

3.3 Using concrete surface coating

Surface coating paint (epoxy resin, polyurethane, etc.) has the advantages of good stability, good sealing, long protection period and convenient

construction. Permeable coating has double protection to concrete of physical isolation and chemical isolation.

In addition to the above measures, strictly controlling the thickness of protective layer, strengthening early curing of concrete, improve the structure environment and improving the use environment of structure, etc. can also improve the durability of structure.

4 STUDIES ON DURABILITY

The above study is according to durability mechanism of material level. Durability research of RC structures also involves load effect on durability, durability design of the proposed structure, durability assessment of the existing structures and prediction of residual life.

4.1 *Load effect on durability*

Research progress of load effect on steel corrosion are introduced in two factors (Liu 2014): (1) load acting alone, (2) coupling effect of load and other factors.

When RC members are under sustained load alone, the steel corrosion rate is higher and time is shorter than them without load. It is related to cracks. The bigger the component loads, the greater the steel stress is and the more severe the corrosion is. When component bears fatigue load, the corrosion influence on steel is greater than bearing sustained load.

In RC components, steel corrosion is closely related to working environment and loads. The environment and loads are different, the coupling effects are different. When bearing loads, component corrosion rate followed by a slow to fast is: air environment, freshwater environment, saline environment. In the case of corrosive environment and loads, deterioration development process is not the simple superposition of deterioration caused by single factor, but the coupling caused. Coupling of environmental corrosion and loads accelerates the development of steel strain and make a significant reduction in carrying capacity.

But, some scholars come to different conclusions. ElMaaddawy holds that the size of load has no effect on the general corrosion rate of steel. Malumbela thinks that effect by sustained load on steel corrosion in RC structures is very small.

4.2 *Durability assessment and residual life prediction*

Durability assessment and prediction of residual life are based on ensuring structural reliability.

Structural reliability can directly reflect the impact on structural safety for the lack of structural durability, and the current structure design standard is established and revised on the basis of reliability theory. So, researching durability in reliability is a significant respect to structural durability analysis and design and an important part to reliability research in the whole process of life of structure.

For the assessment of durability, the following are the current methods: (1) comprehensively considering the various factors affecting durability, and making durability assessment through weighting process to damage index for durability, (2) fuzzy comprehensive evaluation method put forward by means of fuzzy mathematics (Gong & Wu 2012.), (3) durability evaluation method based on reliability, etc.. The key of structural life prediction is to determine the end of life standard which is the structural life assessment criteria. Scholars recognize the structure life from different angles, therefore, the definition of structural life state is different. For the study of life prediction, at present the main theories are: (1) Carbonation life theory. This theory assumes that the change law of carbonation depth and protective layer of concrete obeys normal distribution, establishing a relationship of steel corrosion rate and age and getting life prediction model of component. (2) Cracking life theory. This theory takes concrete cracks in the steel surface caused by corrosion as a failure criterion to predicting the life of structural members. (3) Using statistical theory for reliability. It takes resistance as time-varying random variable and load as random variable or random process to analyze the reliability of resistance attenuation structure and predict the life of structural members through reliability index variation function (Wei et al. 2003).

4.3 *Durability design of the proposed structure*

At present, a number of structural measures for the design of RC structures considering durability are provided in china, such as the maximum water-cement ratio, the minimum concrete strength, the minimum cement content, the maximum alkali content and the maximum chloride ion content, etc.. In addition, the minimum thickness of protective layer on concrete members are made detailed provisions. The analysis of reliability is only at the component level. For the existing structures, it can not yet fully reflect the nature of reliability of the whole structure.

5 PROSPECT

1. Continue the study on durability of the material level. Now, there is little research on the

mechanical properties of concrete after carbonation and on the change of material mechanical properties of concrete after Cl⁻ erosion. In terms of steel bar, there is also little research on change in material properties of concrete and steel after taking appropriate measures to the corroded RC structures.

2. The existing research results on mechanism of concrete structure durability are obtained under the level of material and component in different environments. The study of structure level has just started, mainly on durability design of the proposed structure and durability assessment and life prediction of the existing structure. The research needs to be focused on structure level, so as to link the research results with practical project better.
3. At present, the reliability analysis method of existing structure is based on field test of material strength and section size of component without considering change of material properties over time in the corrosive environment. It needs further exploring.
4. Researches on steel corrosion are mostly in the condition of no load or sustained load. Much more researches need to be done under conditions of variable load, fatigue load and coupling effect of load and other factors, especially fatigue load.

REFERENCES

- Gong, Jinxin & Zhao, Guofan. 2000a. State of the art of durability research of reinforced concrete structures. *Industrial Construction* 30(5): 1–5.
- Gong, Jinxin & Zhao, Guofan. 2000b. State of the art of reliability analysis of deteriorating reinforced concrete structure. *Industrial Construction* 30(5): 5–8.
- Gong, Yufa & Wu, Rumei. 2012. Reinforced concrete structure durability evaluation based on fuzzy comprehensive assessment. *Industrial Construction* 42(Supplement): 513–515.
- Jin, Weiliang & Zhao, Yuxi. 2002. State of the art on durability of concrete structures. *Journal of Zhejiang University (Engineering Science)* 36(4): 371–380.
- Kong, Yuqin. 2012. Summary of steel corrosion in reinforced concrete. *Scientific & Technical Information of Gansu* 41(5): 137–138.
- Li, Wei & Wang, Fengqiang. 2009. Preliminary discussion on the freeze-thaw damage mechanisms of concrete and prevention measures. *Science & Technology Information* (23): 57.
- Liu, Hao et al. 2014. Research progress on effect of loading on steel corrosion in concrete. *Concrete* (4): 9–12.
- Liu, Ruping. 2006. *Research on improving durability of reinforced concrete structure*. Wuhan: China Academy of Machinery Science & technology.
- Liu, Zhiyong et al. 2008. Maintenance and improvement of durability of reinforced concrete using migrating corrosion inhibitors. *Journal of the Chinese Ceramic Society* 36(10): 1494–1500.
- Wei, Jun et al. 2003. Recent studies and development directions of the durability of concrete structure. *Low Temperature Architecture Technology* (2): 1–4.
- Yang, Guangyun. 2007. Present situation of research into the durability of concrete structure. *Shanxi Architecture* 33(10): 133–134.
- Ye, Shucai. 2011. State of the art of durability research of reinforced concrete. *Anhui Architecture* (2): 141.

The research of selection of construction site of project based on grey correlation degree

Yan Ming Lv

College of Architecture and Urban-Rural Planning, Sichuan Agricultural University, P.R. China

Yi Wei

College of Civil Engineering, Sichuan Agricultural University, P.R. China

Lu Yun Zhang

College of Architecture and Urban-Rural Planning, Sichuan Agricultural University, P.R. China

ABSTRACT: The main research objective is selection of construction site of project. The main factors effecting how to choose construction site of project are introduced for modelling. The model on selection of construction site of project is built, based on decision-making grey correlation degree. In order that the optimal construction site is determined, several schemes need to be compared and analyzed carefully. With regard to decision-making system with small sample, poor data information and uncertainty, decision-making grey correlation degree excel in this kind of problem, avoiding the significant financial losses brought to corporations due to irrational decision.

Keywords: grey correlation degree; engineering project; selection of construction site

1 INTRODUCTION

The stages of investment decision in project is the crucial one of the planning and control of project cost. Whether it is good or not is a direct decisive factor of the success of project. And what the project investor face primarily is how to choose the location of project, therefore correct choice of location plays a significant role in investment decision of project, which means it becomes the crucial part of investment decision of project.

There are several factors taken into account when we choose and examine the locations of investment in project, such as national economy development, market's requirement forecasting, resource condition of society, investment strategy, use value or function and investment costs. Since all these factors differ in different regions or even different blocks of the same region, more often than not investors tends to merely focus on one relatively important indication like investment strategy for example. Hence one single mistake in decision-making would be a catastrophic disaster for companies or enterprises on account of partial idea and solutions when making decision.

Decision-making method can be classified as fuzzy mathematics decision method, maximizing difference deciding principle, decision-making

grey correlation degree and so on. In regard with decision-making system with small sample, poor data information and uncertainty, decision-making grey correlation degree has been more widely adopted in decision-making. When it comes to the choice and decision of region, the method, grey correlation degree, is applied in this text to provide investors with an efficient approach to choose the construction site of project.

2 THE BUILDUP OF MODEL ON SELECTION OF CONSTRUCTION SITE OF PROJECT

If there are n -schemes denoted by $Y = \{y_1, y_2, \dots, y_m\}$ and m -evaluation indicators denoted by x_{ij} ($i = 1, 2, 3 \dots n; j = 1, 2, 3 \dots m$) to choose construction site, meanwhile assume that the i 'th scheme with the j 'th index denoted by x_{ij} ($i = 1, 2, 3 \dots n; j = 1, 2, 3 \dots m$) index, then the matrix, $Z = (x_{ij}) m \times n$ is made up of indicators with the number of $m \times n$ from n -schemes. The matrix consists of sets of indicators on selection of construction site of project, whose data needs to be added to the matrix first.

2.1 The estimation on sets of optimal indicators

Set $F^* = [j_1^*, j_2^*, \dots, j_n^*]$

In the previous formula, j_k^* ($k = 1, 2, \dots, n$) represents the optimal value of k 'th target for all possible cases. If what is best for the program when the indicator reaches the maximum, then the maximum would be our ideal choice in this case. But what if the minimum works, remember all we need to examine is what produce the most ideal outcome. We may also choose the one, which is universally acknowledged. When choosing the optimal value, not only do we look for the one happening sooner than the other, but we also need to reckon the feasibility before making the final decision in that an unrealistic goal is unlikely to fulfill or to make a correct answer.

After selecting the optimal indicator, the matrix D is constructed. See Equation 1 below:

$$D = \begin{bmatrix} j_1^* & j_2^* & \dots & j_n^* \\ j_1^1 & j_2^1 & \dots & j_n^1 \\ \vdots & \vdots & & \vdots \\ j_1^m & j_2^m & \dots & j_n^m \end{bmatrix} \quad (1)$$

In the formula, j_k^1 means that the raw value of the i 'th scheme with k 'th indicator.

2.2 The normalizing processing of indicators

Since there are different dimensions and various orders of magnitude between evaluation indexes, it is inaccurate to compare them directly. Thereby it is imperative to get original index value gone through normalizing processing in order to guarantee the objectivity of the results of assessment.

It could be established that the internal of k 'th index could be set as $[j_{k1}, j_{k2}]$. Specifically j_{k1} is the minimum of k 'th index in every possible plan, and j_{k2} is the maximum of k 'th index in every possible plan. Then the formula of k 'th index with every evaluation could be deduced as Equation 2 below:

$$C_k^j = \frac{j_k^i - j_{k1}^1}{j_{k2}^1 - j_{k1}^1} \quad i = 1, 2, \dots, m; k = 1, 2, \dots, n \quad (2)$$

Moreover, C_k^j is a dimensionless quantity value, $C_k^j \in (0,1)$.

In that case, D is converted into matrix C . See Equation 3 below:

$$C = \begin{bmatrix} C_1^* & C_2^* & \dots & C_n^* \\ C_1^1 & C_2^1 & \dots & C_n^1 \\ \vdots & \vdots & & \vdots \\ C_1^m & C_2^m & \dots & C_n^m \end{bmatrix} \quad (3)$$

2.3 The associated matrix inferred from the correlation coefficient

According to theory of grey system, the referential sequence and comparative sequence could be set up respectively as $\{C^*\} = [C_1^*, C_2^*, \dots, C_n^*]$ and $\{C\} = [C_1^i, C_2^i, \dots, C_n^i]$. Applying the correlating-analysis method, the correlation coefficient of k 'th index of i 'th plan could be calculated as Equation 4.

$$\xi_i(k) = \frac{\min_i |C_k^* - C_k^j| + \xi \max_i |C_k^* - C_k^j|}{|C_k^* - C_k^j| + \xi \max_i |C_k^* - C_k^j|} \quad (4)$$

As shown in formula, $\rho \in [0,1]$ and $\xi = 0.5$ in general.

With the correlation coefficient, $\xi_i(k)$ ($i = 1, 2, \dots, m; k = 1, 2, \dots, n$), the associated matrix, $(E_{ik})_{m \times n}$ has been constructed successfully.

2.4 Weight calculated

Weight calculated of index can be divided into two categories: the first kind is called the method of Subjective weight, which Delphi method and the analytic hierarchy process is representative of. The other is summarized as objective weight method, which is made up of Principal Component Analysis and entropy weight method. This text Delphi method has been adopted in particular to determine weight of index for the following two reasons: on one hand, objective weight method is impossible to work because of lack of objective data and it is even more meaningless to combine objective weight method with the method of Subjective weight, considering that the accuracy of Weight calculated can be affected by introducing the method of Subjective weight which is already deficient in some way for error. On the other hand, experienced experts have an excellent understanding of weight of index which plays a role in influencing the decision process, when investment decision-making happens. The following procedures of Delphi method are:

① After index system is selected, each weight of index would be determined by several experts.

Before the matrix of evaluation index system is settled, judgment is reached to examine m -index with the help of z -expert. See Equation 5 below:

$$X = \begin{bmatrix} x_{11} & x_{12} & \dots & x_{1m} \\ x_{21} & x_{22} & \dots & x_{2m} \\ \vdots & \vdots & & \vdots \\ x_{z1} & x_{z2} & \dots & x_{zm} \end{bmatrix} \quad (5)$$

② Take the average of weight of index, fixed by different specialists.

Vector A of weight of index from the matrix of evaluation index system can be computed as Equation 6.

$$A = \left[\begin{array}{c} \frac{x_{11} + x_{21} + \dots + x_{n1}}{z}, \frac{x_{12} + x_{22} + \dots + x_{n2}}{z} \\ \dots, \frac{x_{1m} + x_{2m} + \dots + x_{nm}}{z} \end{array} \right] \quad (6)$$

2.5 Comprehensive evaluation results

Given that systematic research on research method has been conducted, the matrix of grey correlation aimed at choosing the construction site of project is bound to be calculated as Equation 7.

$$E - (E_{ik})_{m \times n} \quad (7)$$

The vector of weight equals:

$$A = \left[\begin{array}{c} \frac{x_{11} + x_{21} + \dots + x_{n1}}{z}, \frac{x_{12} + x_{22} + \dots + x_{n2}}{z} \\ \dots, \frac{x_{1m} + x_{2m} + \dots + x_{nm}}{z} \end{array} \right]$$

Accordingly, comprehensive evaluation results can be deduced as Equation 8

$$r_i = \sum_{k=1}^m A_k \times \zeta_i(k) \quad (8)$$

Whether the construction site is great or not depends on the magnitude of r_i . In terms of results of evaluation, the final discussion is listed as the follow:

- ① There is the correlation between the availability of program and the magnitude of r_i in that the score of program can be enhanced with the increase in magnitude of r_i .
- ② Only when $r_i = \max\{r_1, r_2, \dots, r_n\}$, the optimal case is found.
- ③ The sequence of the program from best to worst is consistent with the descending order of r_i .

It is pretty helpful for investors to apply the method of weighted grey correlation to selecting the multi-target investment places, thus avoiding the tremendous economic loss during construction process due to irrational decision-making.

First lines of paragraphs are indented 5 mm (0.2") except for paragraphs after a heading or a blank line (First paragraph tag).

3 THE EMPIRICAL STUDY OF SELECTION OF CONSTRUCTION SITE OF PROJECT

3.1 The general situation on geographic position of project

In light of the expansion of company, a new branch is the inevitable outcome voted by the most members of the company. After comparing and cross referencing every city in China, four construction sites located in Beijing, Tianjin, Shenyang and Chongqing have advantages over the other. But which city is the most likely one to be chosen as the ultimate site to found up a new branch company? Here are five indexes of evaluation we need to consider before we rank them from the top to the bottom. There is national economy development, market's requirement forecasting, resource condition of society, investment strategy, investment costs (see Table 1).

3.2 The weight of index system

This text, Delphi method has been adopted to determine Weight of five indexes. The figures of weight of five indexes are firstly introduced separately by eight experts. Then the final number is calculated as the mean of weight of the same index by all experts (see Table 2).

3.3 The application of model

In order to carry out the discussion in terms of the optimal case of selecting the construction site for the company, the theory of grey correlation degree weighted is applied to selecting the scheme on the construction site of project.

The relevance matrix of selecting the construction site for the company can be calculated as Equation 9.

$$(E_{ik})_{m \times n} = \begin{bmatrix} 0.33 & 0.43 & 0.60 & 1.00 \\ 0.33 & 0.43 & 0.75 & 1.00 \\ 1.00 & 0.60 & 0.33 & 0.43 \\ 1.00 & 0.50 & 0.33 & 0.67 \\ 0.33 & 0.43 & 0.60 & 1.00 \end{bmatrix} \quad (9)$$

There are five indexes of evaluation in the matrix which are national economy development, market's requirement forecasting, resource condition of society, investment strategy, investment costs from the top row to the bottom row. Moreover, there are four cities from the left column to right column, which represent Beijing, Tianjin, Shenyang and Chongqing respectively.

Table 1. The scores from experts on index system of construction site of project.

Region	National economy development	Market's requirement forecasting	Resource condition of society	Investment strategy	Investment costs
Beijing	60	65	90	95	70
Tianjin	70	75	85	85	75
Shenyang	80	90	75	75	80
Chongqing	90	95	80	90	85

Table 2. The weight from experts on index system of construction site of project.

Expert	National economy development	Market's requirement forecasting	Resource condition of society	Investment strategy	Investment costs
Expert 1	0.1	0.15	0.12	0.45	0.18
Expert 2	0.09	0.2	0.15	0.4	0.16
Expert 3	0.1	0.21	0.1	0.42	0.17
Expert 4	0.09	0.22	0.13	0.38	0.18
Expert 5	0.1	0.24	0.1	0.37	0.19
Expert 6	0.12	0.2	0.12	0.35	0.21
Expert 7	0.13	0.23	0.12	0.34	0.18
Expert 8	0.14	0.22	0.11	0.36	0.17

Determinant weight of this company can be calculated as Equation 10.

$$A_k = [0.11, 0.21, 0.12, 0.38, 0.18] \quad (10)$$

Hence, the results of assessment comprehensive see Equation 11.

$$r_i = \sum_{k=1}^m A_k \times \xi_i(k) = [0.67, 0.48, 0.50, 0.81] \quad (11)$$

For clarification, there are the figures of grey correlation degree weighted which stand for Beijing, Tianjin, Shenyang and Chongqing respectively from the left column to right column.

Due to $r_2 < r_3 < r_1 < r_4$, the preference for new branch company should go in sequence Chongqing, Beijing, Shenyang and Tianjin from the best scenario to the worst. Obviously, Chongqing is our optimal choice for branching out in a new city.

4 CONCLUSION

According to the research on selecting the construction site of project, the conclusions highly based on grey system models are summarized in below as

① Since how to select and decide the construction site of project clearly falls into the category of

grey system, it is in our best interests to introduce grey system models to conduct an independent study on the decision-making process in that it is so rational that it avoids or alleviates the significant financial losses.

② The most critical steps of applying gray relational grade theory to decision-making would be to adopt the approach to calculating index weight appropriately. What is more, Delphi method is a good way to work out the problem on index weight to avoid error accumulation effect when it comes to the circumstances where there is so limited objective data.

REFERENCES

- [1] Hong Ren. The planning and control of costs [M]. Beijing: Higher Education Press. 2004.
- [2] Xue-Qing Wang. The planning and control of costs [M]. Beijing: China building industry press. 2011.
- [3] Ju-long Deng. The Control Problem of Grey Systems [J]. Systems & Control Letter. 1982, 1(5): 288–294.
- [4] Dong Du. Modern comprehensive evaluation method and Classic Case [M]. Beijing: Tsinghua University Press. 2008.
- [5] Si-Feng Liu. The grey system theory and application [M]. Beijing: Science press. 2012.

The research on developing eco-tourism in natural reserves in China

Jian Bo He & Zhen Wang

Jiangxi Science and Technology Normal University, Nanchang, Jiangxi, China

ABSTRACT: With the rapid development of tourism and changes of tourist demand, the status of eco-tourism in tourism continuously improved. Because of natural reserve's unique tourism resources, it is going to join the tourism resource development. How to deal with the relationship between the natural reserve tourism resources development and protection has become a problem to be solved. In this paper, based on the definition of natural reserve, analyzed the problems existing in development of eco-tourism of the current reserve, put forward a series of measures, in order to promote the sustainable development of natural reserve eco-tourism.

Keywords: tourism; ecological tourism; natural reserve; tourism resources; sustainable development

1 INTRODUCTION

With the rise of people's living standards and development of economy, science and technology, people gradually turn from the traditional mass tourism to a higher level of tourist way-eco-tourism. Eco-tourism develops quite rapidly and has become the most ideal and the most promising form of tourism in the contemporary world, and has the important status in the development of national economy. It is a hot topic of contemporary society. Eco-tourism, as a good form of sustainable tourism development, its status in tourism industry of the world constantly has improved in many countries and regions, and it has very rapid development momentum.

Natural reserve plays an important role in improving ecological system, urban water conservation, biodiversity conservation, etc. It has excellent ecological environment, beautiful natural scenery, rich flora and fauna resources, deep historical and cultural background. Its development and construction are closely related with the social and economic development and human life. Developing eco-tourism in natural reserves can improve the ecological protection consciousness of humans, effectively promote the harmonious development of society, economy, culture in ecological tourist destination.

2 THE BASIC CONCEPT OF NATURAL RESERVE AND ITS DEVELOPING SITUATION IN CHINA

Natural reserve is also called "natural exclusively protected areas" (sanctuary), natural protected

area, etc. The law of the People's Republic of China on natural reserves defines natural reserve as the representative of the natural eco-system, natural concentrated distribution area of rare and endangered species of wild fauna and flora species, and has special significance to natural sites such as protection of land, land or sea water, a certain area shall be in accordance with the special protection and management of the area.

Natural reserve is a general term, according to the protection of the main object to differentiate, can be divided into 3 kinds: biological species, eco-system types and natural relics reserve; According to the properties of the sanctuary, they can be divided into 4 classes: scientific reserve, national park (scenic area), administrative zones and resource management reserve. Irrespective of the type of the reserve, and its overall request give priority to protection on the condition that it does not affect the environment under the premise of the scientific research, education, production and tourism activities so as to make its ecological, social and economic benefits fully displayed.

The natural reserve construction of our country began in 1956. State forestry department in 1956 formulated a draft about the protection of natural reserve. In the same year, the first natural reserve with modern significance-Dinghushan natural reserve has been established in Zhaoqing, Guangdong Province, China. By the end of 2013, the number of natural reserves in China has reached 2697. Among them, the number of state-level natural reserves reached more than 407.

3 THE MAIN PROBLEMS EXISTING IN DEVELOPMENT OF ECO-TOURISM IN NATURAL RESERVES

In recent years, the deterioration of ecological environment problems appeared around natural reserves. However, there are many reasons for it such as reduced precipitation, excessive use of water resources, vegetation destruction, the excessive farming development, etc. Rationally develop and save ecological resources, solve a series of ecological environment problems existing in the development of natural reserve are the problems to be solved urgently.

3.1 *Serious environmental pollution*

With the development of the eco-tourism of natural reserve, the environmental capacities of natural reserves have been overwhelmed, protected area fragile eco-systems have been fatal blow, the natural environment has been seriously polluted. With the rapid development of urban construction, some scenic areas and suburban get hit. For economic purpose, some scenic spots have shown great passion for construction of hotels, restaurants, blindly expanding tourist areas. With the increase of population in China, people's demands for land for farming and animal husbandry increase. This results in the decrease of soil productive potential. Soil water content, organic matter and other nutrients are in decline. The deterioration of physical and chemical properties of soil finally results in land desertification.

3.2 *Blindly develop and use tourism resources*

In the development of tourism resources of natural reserves, in order to pursue the economic benefits of eco-tourism, the in-depth research, comprehensive scientific argumentation, evaluation and planning are in short. Especially for new tourist areas, in order to pursue economic profits, the developers blindly to explore without any necessary argument with overall planning. Focusing on developing while ignoring protection results in damage and waste of many valuable and non-renewable tourism resources. In order to develop tourism industry, many natural reserves start to construct a lot of tourism facilities like piers, dams, islands, etc., which divides the whole ecological system, prevents wetland degradation, decreases the diversity of animal and plant species, interferes the habitation environment animals and plants as well as decreases the quantity of animals and plants.

3.3 *The lack of environmental protection consciousness for tourists and local residents*

The starting point of natural reserves to develop ecological tourism is to let visitors to be close to natural, protect natural, and hence with a good ecological education and ecological experience. Ecological tourists and local residents should have a strong ecological consciousness and environmental awareness. However, many local residents lack enough understanding of ecological tourism, ecological consciousness and consciousness of environmental protection. Thus, the tourism investors and operators there will inevitably pay much attention on economic significance and political achievements while ignoring the sustainable development of resources and social benefits during the process of developing ecological tourism.

4 THE STRATEGIES FOR ECO-TOURISM DEVELOPMENT IN NATURAL RESERVES

4.1 *To strengthen the control of environmental pollution and maintain the balance of eco-system*

We should work comprehensively on improvement of rivers into the lake and thoroughly clear up the river reaches which has been seriously filled with silt. We should plant the vegetation in both sides of river ways, build up sewage interception gutter, restore ecological environment, construct ecological protection forests and build ecological landscape belt. Meanwhile, we should also improve the water quality of rivers into the lake, protect the surrounding ecological environment and purifies the exogenous pollutants which can affect water quality before entering into lakes and reservoirs.

4.2 *Ecologically protect and restore the lakeside zone*

Develop eco-tourism of natural reserve, keep the area's unique natural ecological system tend to be the natural landscape, maintain ecological balance and coordinated development of internal system of different animal and plant species. All these will play important role in protecting biodiversity, storing flood-water for use in a drought, regulating climate, controlling soil erosion and promote degradation of environmental pollution. We should build up different auxiliary facilities on the basis of not destroying the original ecological system. Thus, ecological protection, ecological tourism and ecological environment education can be combined organically to realize the rational development of

natural resources and the improvement of ecological environment.

4.3 *Improve tourism planning and develop resources orderly and rationally*

Planning and designing must be conducted when developing eco-tourism in natural reserves. The developers and operators should reasonably plan functional zones, protect the Core Zone, develop Experimental Zone, Buffer Zone and core area. Core Zone is the core of protection zone which is the best-preserved area of primordial eco-system as well as the best shelter for plants and animals. We should adhere to the principle of sustainable utilization, practically protect the biodiversity, and strictly protect the core area which cannot be open to tourists. In Experimental Zone, the scientific research and production can be carried out. While in the tourist areas, the tourist activities can be done. In order to give full play to its functions of in protection, tourism, education, scientific research and production, the natural reserves should divide the functional areas reasonably according to their actual conditions. In the Buffer Zone, adjacent area between two paths should satisfy the minimum area for nest building of birds. The place between paths should not form a closed area, and should be extended to the Core Zone radially. In the dense area of tourism activities, in order to reduce the influence of tourism activities on the species in the area, the shortest distance between tourist path and birds should be the nearest distance in which tourists can be close to while without interfering species. In addition, in the distribution of reed zone, what can affect creatures in the area are mainly water activities. The planning of waterways should be in accordance with the planning of tourist paths and in the mean time, the scale of water activities must be strictly controlled.

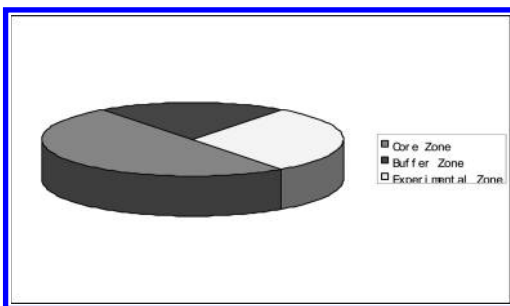


Figure 1. The division of functional zones in natural reserves.

4.4 *Control environmental capacity in tourist areas and take on protective exploitation*

To develop ecological tourism, the natural reserves should strictly control the number of tourists. Because of the fragility of tourism resources and limitation of tourist facilities, the tourist activities in natural reserves must be in moderation, or the ecological resources would be damaged and tourist reception quality cannot be assured. Thus, natural reserves must formulate reasonable tourism capacity and take on protective exploitation in the operation. In addition to realize the sustainable development of tourism resources increasing person's environmental knowledge, improving their environmental consciousness are also the main purpose of developing eco-tourism in natural reserves. The protective exploitation of eco-tourism in natural reserves will not only generate certain economic benefits for natural reserve, but also remind the public know the value of its existence and consciously be involved in the protective exploitation work of natural reserve.

4.5 *Intensify propaganda dynamics and improve the environmental protection consciousness of tourists*

The government should take various forms to ecological education for tourists, constantly improve the tourist ecological consciousness. Fully considering the environmental capacity and environmental carrying capacity of natural reserves should be done before formulating a long-term program. Control the tourist flow and reasonably distribute tourist income can make eco-tourism a tourism type of sustainable development. We should extensively use mass media, carry out various kinds of promotional events, popularize knowledge of natural conservation and improve the public's awareness of the natural protection and management. What's more, we should improve the environmental information release system, broaden the channels for public participation, give full play to the supervision and guiding role of news media and. In protected areas and its surrounding villages, we should also carry out community environmental education, transform the mode of mass production of local community and lead community mass to the path of sustainable development.

5 CONCLUSION

In recent years, tourist market is booming, and development of eco-tourism in natural reserves has received extensive attention of the society from all walks of life. With advocating and developing of

eco-tourism and improvement of education level of tourists, great changes have taken place in tourism market demands. The development of eco-tourism is satisfying modern people's demands for high quality tourism. Make full use of the advantages of natural reserve in ecological resources and develop ecological tourism projects with cultural connotation is a rare opportunity to develop ecological tourism. Through implementation of reasonable planning, we must unify development and protection, enrich the types of products of eco-tourism resources, promote the overall image of tourism destinations and increase tourism economy continuously. In the coming future, the eco-tourism in natural reserves will become a new bright spot in tourism development.

ACKNOWLEDGEMENT

This work was financially supported by 2012 Scientific Research Program of Jiangxi Science & Technology Normal University (KY2012SY10), 2011 Jiangxi Provincial Art Science Program (YG2011079).

REFERENCES

Clem Tisdell, Clevo Wilson. 2002. Ecotourism for the survival of sea turtles and other wildlife. *Biodiversity and Conservation*, (11).

- Elby M. and Morgan N.J. 1996. Reconstructing place image: a case study of its role in destination market research, *Tourism Management*, 17(4).
- Erich Hoyt. 2005. Sustainable Ecotourism on Atlantic Islands, with Special Reference to Whale Watching, Marine Protected Areas and Sanctuaries for Cetaceans. *Biology and Environment: Proceedings of the Royal Irish Academy*, 105B (3).
- Griffiths, Michael and Carel P. Van Schaik. 1993. The impact of human traffic on the abundance and activity periods of Sumatran Rain Forest Wildlife. *Conservation Biology*, 7(3).
- Jacobson, Susan K. and Alfredo Figueroa Lopez. 1994. Biological Impacts of Ecotourism: Tourists and Nesting Turtles in Tortuguero National Park, Costa Rica. *Wildlife Society Bulletin*, 22(3).
- Laarman J.G. and Durst P.B. 1987. Nature travel and tropical forests. *FREI Working Paper Series*. Southeastern Center for Forest Economics Research, North Carolina State University, Raleigh.
- Masberg B.A. 1999. A case analysis of strategies in ecotourism development. *Aquatic Ecosystem Health and Management* (2).
- Millman A. and Pizam A. 1995. The Role of Awareness and Familiarity with a Destination: The Central Florida Case, *Journal of Travel Research*, 33(3).
- Orams M. 1995. Using interpretation to manage nature-based tourism. *Journal of Sustainable Tourism*, 4(2).
- Stephen Wearing. 1999. John Neil. Ecotourism: Impacts, Potential and Possibilities. *Butterworth Heinemann*, Oxford.
- Tasos Hovards, Kostas Poirazidis. 2006. Evaluation of the Environmentalist Dimension of Ecotourism at the Dadia Forest Reserve (Greece). *Environ Manage.* (38).

Numerical analysis of CFG pile arrangement by FLAC

Li Hua Zhang & Hai Bo Liu

Department of Civil Engineering, North China Institute of Science and Technology,
The East of Beijing, Yanjiao, China

Qian Xu

Department of Security Engineering, North China Institute of Science and Technology,
The East of Beijing, Yanjiao, China

ABSTRACT: Based on the actual project, numerical calculation of three working conditions of “two short-one long arrangement”, “two long-two short alternative arrangement” and “three long-two short alternative symmetrical arrangement” from CFG pile have been respectively done using finite difference program FLAC in this paper, then we tried to find out the law of the three stake arrangement way on force as well as on bottom vertical displacement. Though the calculation and analysis, it can be seen that, the third condition-“three long-two short alternative symmetrical arrangement” is the soundest way, the symmetrical arrangement of long pillar and short pillar on each side, the shorter one in middle has obvious effect on overall deformation and common stress between pillars.

1 INTRODUCTION

CFG pile (i.e., Pile is a high bond strength pile which is mixed cement, fly-ash, rubble, stone chips, sand and mixtures with water) is a Foundation treatment of Composite Foundation which is composed of pile and soil between piles and cushions. Along with the construction of continuous development, pile composite Foundation as an effective means of Foundation treatment in an increasingly wide range in civil engineering. In recent years, the research of CFG pile of Different length has become a hot issue Because CFG pile meet Engineering Safety stability with a wider range of economic. Therefore, in most cases there is no need to make all the CFG pile with the same length. However, the Arrangement of different length CFG pile of is always controversial^[1-5].

Combing with the concrete engineering, this paper attempts to adopt numerical simulation of this problem with the preliminary study by finite-difference procedure of FLAC^[6-8].

2 BRIEF INTRODUCTION OF PROJECT

2.1 Main conditions of proposed building

The proposed building named Tianyang city phase III is built by Four Season Real Estate Co Ltd in Qingdao, designed by BeiJing Victory Star Architectural & Civil Engineering Design Co Ltd. and located on South of Yifeng Street Road and the west side of HW Road in Yanjiao Development Zone. The main building as shown in Table 1.

Due to the natural ground bearing capacity can not meet the design requirements, the need take Foundation treatment. Commissioned by the construction unit, Ch-Geotechnical Engineering Ltd in Hebei using Composite Foundation of CFG pile process the building.

2.2 The design of engineering geology and subgrade treatment

According to the Geotechnical Engineering investigation reports under exploration Institute under

Table 1. Main situations of proposed building.

Building and structure name	Ground layer	Underground layer	Length * width (m)	Total height (m)	Foundation forms	Foundation embedded depth (m)	Structure type
Tianyang	26	2	90.00 × 15.20	74.8	Raft foundation	7.00	Shear wall

Table 2. Parameters of soil.

Project	Mechanical parameters				
	Cohesion $C (Pa)$	Angle of internal friction $\varphi (^{\circ})$	Gravity $\gamma (kN \cdot m^{-3})$	Elastic modulus $E (Pa)$	Poisson ratio ν
Soil	20000	10	17	1.0e6	0.30

Table 3. Parameter of foundation treatment's design.

Capacity characteristic value of the composite foundation	Project ± 0.000	Base elevation (m)	Elevation of pile top (m)	Diameter	Pile spacing	Area replacement ratio 0.0710	Effective length (m)	Pile material strength
≥ 570 kpa	27.70	-7.40	-7.76	450 mm	1.50 m \times 1.50 m		29.5 8.0	C30 C30

Nonferrous geological prospecting Bureau of Chengde exploration Institute in North China, Characteristics of soil layers are shown in Table 2.

Combined with the standard calculation, we get the foundation treatment design more reasonable. Foundation treatment design of specific parameters are shown in Table 3.

3 NUMERICAL ANALYSIS

3.1 The first condition (one long-two short)

First of all, we take the condition of two short-long piles, schematic is shown in Figure 1.

This numerical procedures adopted internationally FLAC, because the FLAC program, inside the pile element, more suitable for solving geotechnical problems. This study simulate the soil by Mohr Coulomb constitutive model. For taking fully into account the influence of boundary conditions on the results, the model get 20 m in the horizontal direction, divided into 40 mesh and vertical access 40 m, divided into 80 mesh with 0.5 M thickness cushion. In order to study the bottom of the pile displacement variation, monitoring points is established at the bottom three piles. So that we can more easily get vertical displacement curve at any time.

Calculation of soil mechanical parameters are shown in Table 2, Piles and cushions the mechanical parameters are shown in Table 4 and numerical results are shown in Figures 2-5.

By Figure 2 shows, the bearing on this way of two short and a long pile is basic reasonable, because it is symmetric structure arrangement, therefore in short pile height, the length of column joint deformation, joint bearing, which meet

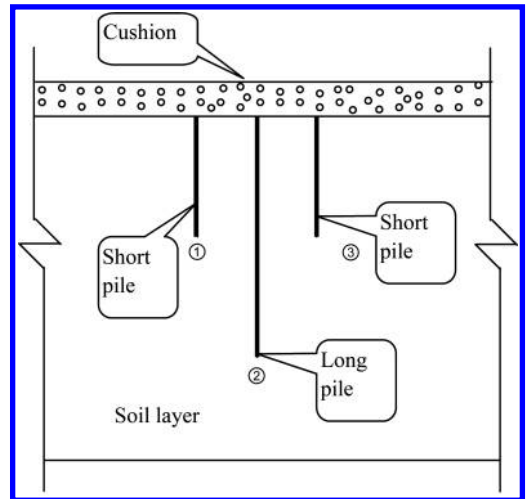


Figure 1. The schematic of two long-two short piles.

the requirement of shallow subsidence, meanwhile the long pile increase the stability of the system. From Figures 3-5 shows, because the fundamental advantages of CFG pile is a common force between pile and soil, the joint deformation, this also proved the point, the three pile length is different, but the vertical deformation is nearly the same, however, the speed of deformation has some differences, the curve slope is slightly different.

3.2 The second condition (two long-two short)

The second conditions, we take two long and two short interval symmetrical arrangement, the loading and other information completely same with

Table 4. Mechanical parameters of pile and cushion.

Project	Mechanical parameters				
	Cohesion C (Pa)	Angle of internal friction φ (°)	Gravity γ ($kN \cdot m^{-3}$)	Elastic modulus E (Pa)	Poisson ratio ν
Cushion	0	33	20	1.0e7	0.25
CFG Pile	C30			3e10	0.2

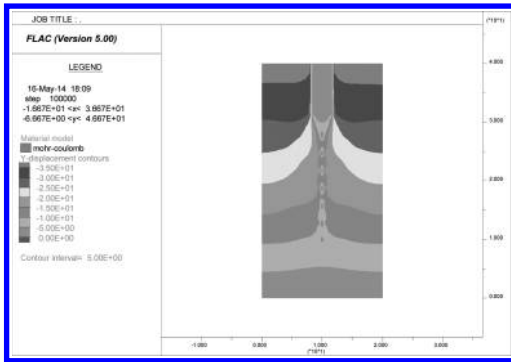


Figure 2. Two short and a long in Y direction displacement nephogram.

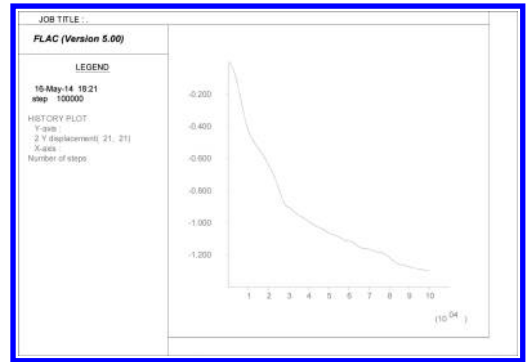


Figure 4. Two short and a long in ② vertical displacement of the pile bottom.

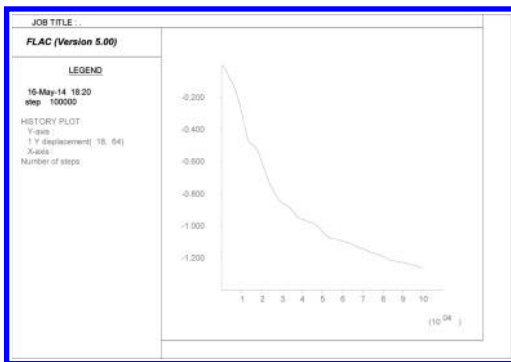


Figure 3. Two short and a long in ① vertical displacement of the pile bottom.

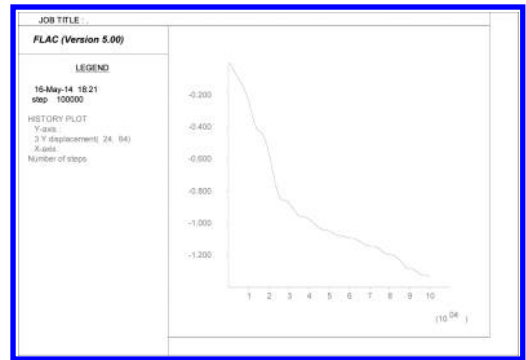


Figure 5. Two short and a long in ③ vertical displacement of the pile bottom.

the first conditions, schematic diagram is shown in Figure 6.

The results of numerical simulation is shown in Figures 7–11.

Because of the length of pile arrangement is not symmetrical, the far left side is the long pile, the far right side is the short column is shown in Figure 7, the Y direction displacement nephogram is also asymmetric, this will cause the uneven settlement of composite foundation, therefore, this method cloth pile should be banned.

The Figure 8 shows the curve of vertical displacement of ① pile, because of it is short pile and the position in the middle of the left and right two long pile, so the vertical displacement change faster at the beginning, and slow in the late, which is the result of long pile squeezing soil between piles on both sides; Figure 9, Figure 11 shows the curve of vertical displacement of ② and ④ pile, the internal and external conditions are same of the piles, therefore the deformation curve showing the same consistency; Figure 10 shows the curve of vertical

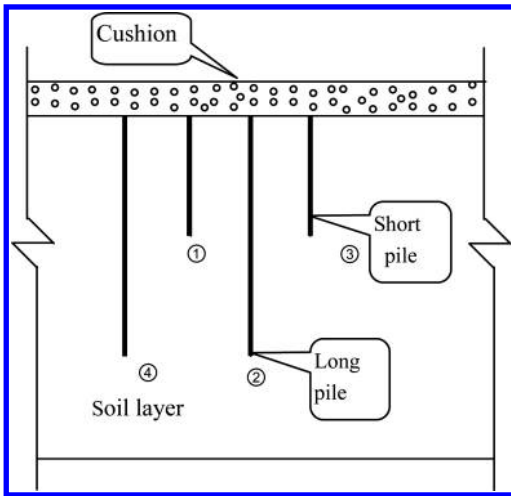


Figure 6. Two long-two short shown.

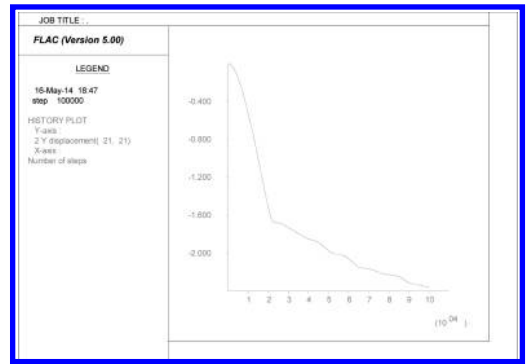


Figure 9. Two long and two short interval symmetrical arrangement in ① vertical displacement of the pile bottom.

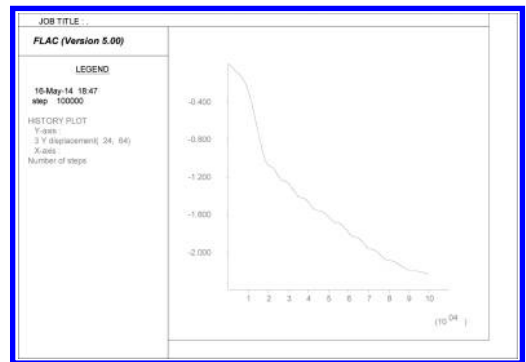


Figure 10. Two long and two short interval symmetrical arrangement in ② vertical displacement of the pile bottom.

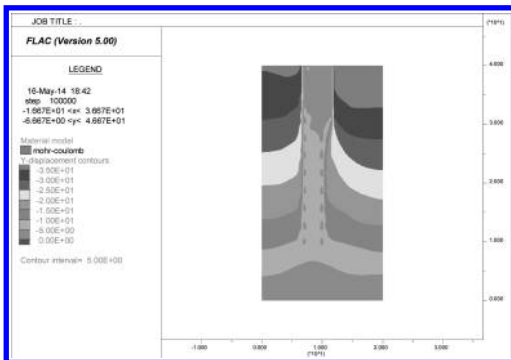


Figure 7. Two long and two short interval symmetrical arrangement in Y direction displacement nephogram.

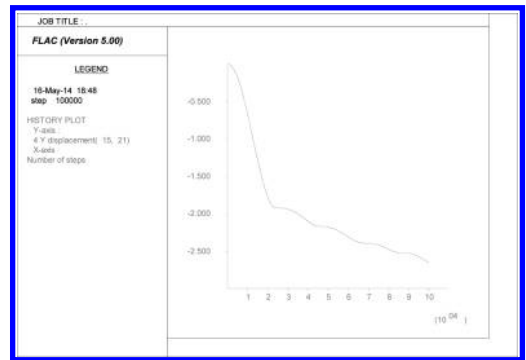


Figure 11. Two long and two short interval symmetrical arrangement in ③ vertical displacement of the pile bottom.

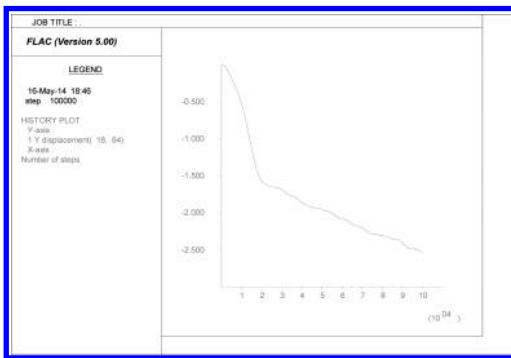


Figure 8. Two long and two short interval symmetrical arrangement in ④ vertical displacement of the pile bottom.

displacement of ③ pile which is the far right short pile, because of the short pile does not have long as protection and extrusion on the right side, so the vertical curve do not has obvious adjustment and deformation rate keep basically constant.

3.3 *The third condition (three long and two short interval symmetrical arrangement)*

The third conditions, we take three long and two short interval symmetrical arrangement, the loading and other information completely same with

the first and second conditions, schematic diagram is shown in [Figure 12](#).

The results of numerical simulation is shown in [Figures 13–18](#).

By [Figures 12–17](#) shows, the three long and two short interval symmetrical arrangement both verti-

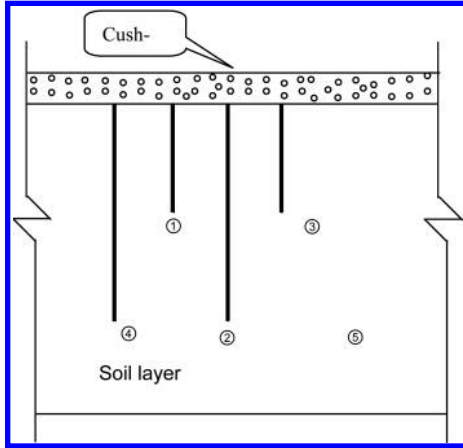


Figure 12. Three long and two short shown.

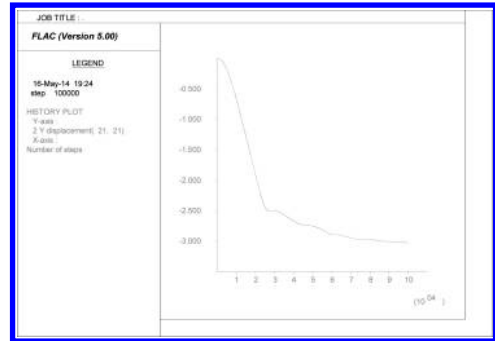


Figure 15. Three long and two short interval symmetrical arrangement in ② vertical displacement of the pile bottom.

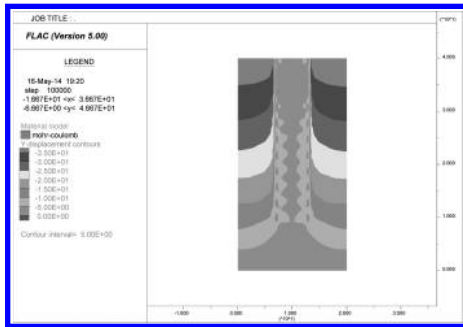


Figure 13. Three long and two short interval symmetrical arrangement in Y direction displacement nephogram.

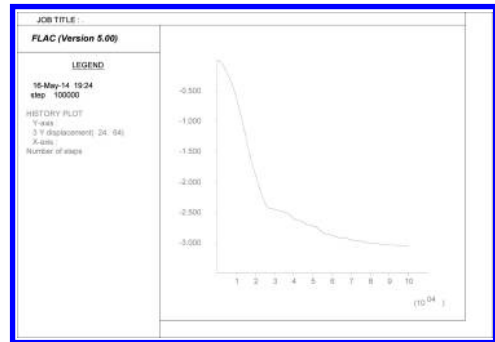


Figure 16. Three long and two short interval symmetrical arrangement in ③ vertical displacement of the pile bottom.

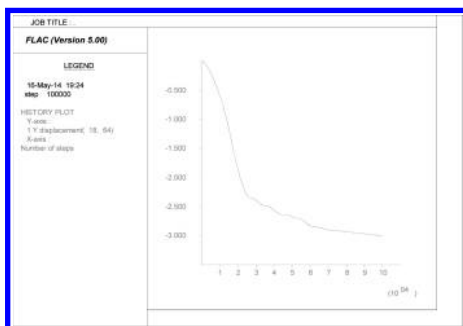


Figure 14. Three long-two short interval symmetrical arrangement in ① vertical displacement of the pile bottom.

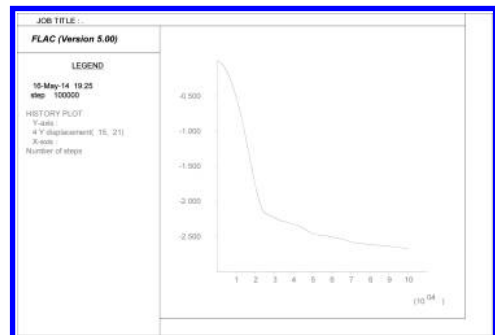


Figure 17. Three long and two short interval symmetrical arrangement in ④ vertical displacement of the pile bottom.

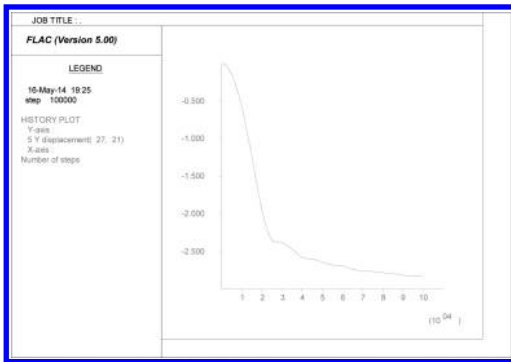


Figure 18. Three long and two short interval symmetrical arrangement in ⑤ vertical displacement of the pile bottom.

cal from the Y direction displacement, or vertical displacement of long-short piles in the pile bottom has shown a certain degree of rationality, pile and soil between piles can work together better, deformation of the pile bottom presents certain on molding, long pile in two side, short pile in the middle is the most ideal way of pile.

4 CONCLUSION

From the above 3 performance calculations, the piles arrangement of CFG lengths of the piles is important, and it has a direct impact on the deformation and displacement of the piles, and the first of the situation due to the shorter stud on the outside, the piling between the compression performance is not very good and among piles of soil areas have defect in common force. The second situation due to the dissymmetrical, therefore also in terms of deformation exhibited a lot of asymmetry. The three conditions are the most ideal situation, long

pile on the both sides and a short column in the middle, this interval symmetric layout is not only in the force, but in the deformed control, disguised laws have also demonstrated a predictable consistency.

ACKNOWLEDGEMENTS

This paper was supported by the National Natural Science Foundation of China (51178185), the Foundation of NCIST (2011B046).

REFERENCES

- [1] Lee C.J., Charles W.W. Development of Down drag on Piles and Pile Groups in Consolidating Soil [J]. Journal of Geotechnical and Geoenvironmental Engineering, 2004, 9:905–9141.
- [2] Bengt H. Fellenius, Results From Long-Term Measurement in Piles of Drag Load and Down drag [J]. Canadian Geotechnical Journal, 2006, 43(4): 409–4301.
- [3] Cesar Sagaseta & Andrew J. Whittle. Prediction of Ground Movements due to Pile Driving In Clay, Journal of Geotechnical and Geoenvironmental Engineering, VOI. 127, No. 1, January-2001.
- [4] H.G. Poulos, E.H. Davis. Pile Foundation Analysis and Design. By John Wiley 3: & Sons. Inc. 1980.
- [5] Kelly J.M. Aseismic Base Isolation Review and Bibliography, Solidyn. Earthquakeeng. 1986, 5:202–216.
- [6] British Standard Institute. British Standard BS8006: code of practice for strengthened Preinforced soils and other fills [S]. London: [s. n.], 1995.
- [7] K. Madsen, H.B. Nielsen, O. Tingleff, Methods for Non-linear Least Squares Problems (2nd Edition), 2004.
- [8] Cheung Y.K., Zienkiewicz O.C. Plates and Tanks on Elastic Foundation—An Application of Finite Element Method. Jour. of Solids and Structures. Vol. 1, 1965, 451–461.

Measures to improve residential sound insulation property in severe cold region

Qiu Ling Zheng

Jilin Jianzhu University, Changchun, China

ABSTRACT: In recent years the continuous decline of acoustic environment satisfaction in residential buildings is one of city dwellers' greatest concerns. This paper analyzes causes for poor sound insulation performance, proposed measures to improve sound insulation performance of residential combined with the construction characteristics of severe cold region, in order to improve the residential sound quality to ensure occupant comfort.

Keywords: severe cold region; city residential buildings; airborne sound insulation; impact sound insulation

1 INTRODUCTION

For nearly 10 years China is in the midst of great economic development with rapid urbanization which causes nearly half the population living in cities and towns, therefore built around a set of collective housing. Noise nuisance has become the hot social concern for that the continuous decline of acoustic environment satisfaction. Urban residents complaints about noise pollution in our country mainly focuses on disturbances of Noise to the residential environment such as they complain about Residential area environmental noise exceed the standard and poor Residential sound insulation ability.

In severe cold area in China, the temperature is low in winter with long duration. Take Changchun city as an example, the actual heating period in 2012–2013 is 174 days which accounts for 47% of the annual number of days^[1]. The main activities in severe cold area in winter are indoors, so the residential sound environment greatly affects comfort of life. Therefore effectively improve the ability of sound insulation of the residence can improve acoustic quality to ensure occupant comfort.

2 REASONS OF POOR RESIDENTIAL SOUND INSULATION

2.1 Outdoor environmental noise degradation

According to the data provided by “2012 national economic and social development statistical bulletin”, among the 316 monitoring city, city sound environment best quality of city area accounts for 3.5%, better accounted for 75.9%, mild pollution accounted for 20.3%, moderate pollution accounted for 0.3%^[2]. Compared with 2011, acoustic environment quality of the city fell by 1.6% in 2012, the whole city regional acoustic environment is poor (see Table 1), noise condition needs to be improved.

City regional noise comes from traffic noise, construction noise, industrial noise and life noise, in which the traffic noise has greatest impact.

In particular, the number of motor vehicle surges in the city, traffic is increasingly busy. Meanwhile, the ship and the port city of aviation noise cannot be ignored. These have led to the gradual development of traffic noise dimensional direction. Traffic

Table 1. Urban areas from 2008 to 2012 acoustic environment monitoring statistics.

Year	The number of monitoring cities	Best quality	Better quality	Light pollution	Moderate pollution
2008	392	7.9%	63.8%	27.0%	1.3%
2009	327	4.9%	70.0%	23.9%	1.2%
2010	331	6.3%	67.4%	25.4%	0.9%
2011	316	5.1%	72.8%	21.5%	0.6%
2012	316	3.5%	75.9%	20.3%	0.3%

noise greatly influenced the acoustic environment around residential areas, especially in the street residents.

2.2 *Both indoor noise sources and noise intensity are increasing*

With people's living standards being improved, more and more machines and equipment are adopted in residential construction, which contributed to the increasing number of noise sources. Also the popularity of high sound equipment, piano and other instruments among ordinary families has brought the residential indoor sound to a higher level. Moreover, many of the low-frequency noise is difficult to insulate, such as lift noise, engine room equipment noise (including noise produced by water pumps, heating pumps, and so on) etc., which has laid an increasingly serious impact on the residents, thus people tend to ask more about the insulation of residential buildings.

2.3 *Building construction*

The short supply of land has resulted in the emergence of a large number of high-rise buildings, which has also accelerated the development of architectural industrialization. As high-rise building requires reducing its weight, traditional brick wall has become obsolete and the use of lightweight structures and molding plate are recommended. Currently the construction material of residential wall is mostly light block, but its smaller mass area ratio has determined that the insulation ability of the wall is far from the national sound insulation requirements, neither can it meets people's increasing asks for quiet.

3 MEASURES TO IMPROVE THE RESIDENTIAL SOUND INSULATION PROPERTY IN COLD AREA

While designing for residents in cold areas, heat preservation in winter should be taken into consideration, the building body coefficient needs to be smaller. Combining architectural features of cold area with reasonable residential acoustic design can not only improve the acoustic quality of housing, but also increase the effect of residential insulation.

3.1 *Measures to improve the airborne sound insulation ability of the wall*

The sound insulation property of airborne sound exists in party wall, exterior wall, and party floor and between rooms of two adjacent families is

an important indicator of evaluating the indoor environment privacy. Party wall can commendably insulate the interference from noises including voices, TV stereo sound and other noise between neighbors, while the exterior walls can insulate the environmental noise from outside.

3.1.1 *Architectural layout design*

In the architectural design of houses, in order to reduce the disturbance to sleep, it is a priority to pay attention to the tranquility of the bedroom. Bedroom should be arranged on the backside towards noise sources, and should not be arranged adjacent to bathroom or elevator; on condition that the elevator was adjacent to the bedroom, measures should be taken to insulate and damp, if conditions permit, the wall can be made into double wall so as to effectively reduce noise; locate the kitchen, bathroom in a centralized way, up and down aligned; based on the actual situation in cold area, set an enclosed balcony, which is equivalent to one more layer of windows, to insulate noise as well as preserve heat and improve indoor temperature.

3.1.2 *Structural design*

Structure designed to be in harmony with the architectural design, the design must consciously arranged in the shear wall at the household, can effectively improve the insulation performance of the wall.

3.1.3 *Exterior window*

Exterior window is not only the weak part of residential buildings Thermal insulation, but also the weak part of sound insulation. For many residential buildings designs, there is a misunderstanding of blindly pursuit of lighting effects, resulting in relatively large window-wall ratio, or use large glass walls instead of solid walls. In fact, sound insulation and thermal effects of this kind of residential buildings are needed to be improved. Take Changchun City as an example, most residential buildings uses double glazing Exterior windows, double glazing has closer spacing, so the low-frequency sound insulation capability is poor.

It is suggested that the Exterior window should use triple-glazed windows, window frames select PVC-U steel profiles window and the chamber needs four-chamber, while strengthening the machining accuracy of the Exterior window, reduce the gap, strengthening confine ability and window-wall ratio is tightly controlled^[3].

For residential buildings which have higher sound insulation requirements or busy street residential buildings can use the no-open sound insulation windows with a separate ventilation system designed to meet the requirements of residential

buildings ventilation. Pay special attention to deal with the gap holes in the construction process, preventing sound leakage.

3.1.4 Wall

Lightweight wall can use multi-layered composite, double-wall separation. Sheet stacking elastic connections to improve its ability to cut off the air sound. But pay attention to the details of the deal, such as through the wall of the pipeline, to do acoustic treatment to avoid sound leakage which can cause significant decrease of wall sound insulation capabilities.

3.2 The measures to improve the ability of floor impact sound isolation

Compare with airborne sound, impact sound propagation in buildings is relatively complex, isolated impact sound materials developed slowly. Although the impact sound can be effectively isolated by some measures, but the impact sound isolation is the weak link of noise isolation in residential buildings construction for but it is expensive. Most current residential buildings use cast-in-place reinforced concrete floor, the reinforced concrete floor has high rigidity, but Poor vibration damping effect.

3.2.1 The low-temperature floor radiant heating

In severe cold areas, indoor heating uses low-temperature radiant floor heating (Fig. 1), will greatly enhance the ability of the floor impact sound isolation. Low-temperature Radiation floor heating is comfortable, environmental and evenly-heated,

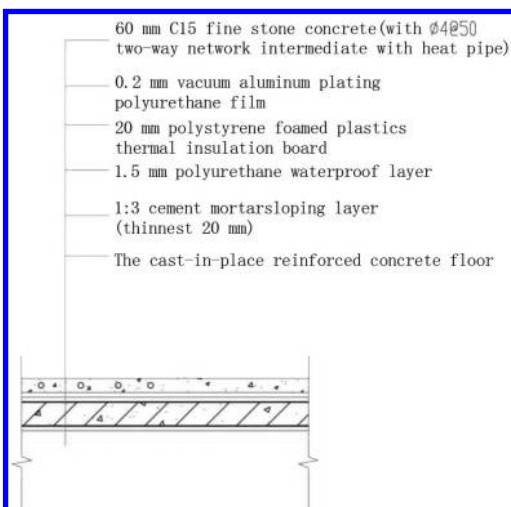


Figure 1. Radiant floor heating structure.

which is loved by cold area residents. Compared with the general residential buildings floors, this kind of buildings add reinforced concrete floor of insulation to the structural layer, laid heating pipes, increased the thickness of the structure. Although it is not in the strict sense of the floating floor, but sound insulation capacity also increased^[4].

3.2.2 Floating floor method

For the reinforced concrete floor, the effective method to improve the impact sound insulation ability is a floating floor method. Floating floor method spread a layer damping pad on top of the structural floor, and then pouring concrete on top to form elastic sandwich structure. Impact sound insulation can improve 18~22 dB. Damping pad type floating floor can meet the requirements of the international standard of sound insulation, with ideal sound insulation effect. This structural method is under complex construction compare with the traditional concrete floor. Especially the seams along the wall around shall be strictly treated prevent the formation of sound bridge. Because of its high cost. Floating floor method is suitable for use in the high-end residential products.

3.2.3 Pavement elastic ground material

Combining with the decorated ground, it is easy to solve the problem of floor sound and effective measures in the concrete floor shop outfit elastic ground material. Such as wooden floor decking (solid wood floor or composite floor), elastic rubber (plastics) floor of thickness in more than 3 mm, can reduce the energy of impact floor, decrease the vibration of the floor slab. The improvement of Weighted impact sound is greater than 5 dB. It is better especially in the residential indoor concreting on the ground, which lay of real wood floor board with the keel to improve sound insulation effect.

3.2.4 Acoustic ceiling

For high floors residential buildings. Acoustic ceiling can be set under the floor to make the cavity which is formed between the ceiling and floor to reduce the sound radiation of air inside from floor to the bedroom. Acoustic ceiling must be sealed and adopt flexible connection between ceiling and floor. Acoustic ceiling improve quantity of about 10 dB for the crash.

3.3 Strengthen the legislation and supervision

Nowadays there are increasingly strong demands for reducing noise, improving the acoustic environment because that disputes which were caused by Residential sound insulation.

The relevant government departments have already felt the importance of residential sound

insulation problems, on August 18, 2010 promulgated new revision of Code for design of sound insulation of civil buildings (GB50118-2010), and implemented starting in June 1, 2011. The minimum requirements of residential building bedrooms, living room (Hall) partition wall, splitting floor airborne sound insulation performance increased by approximately 5–7 dB^[5] compare with the original specification (GBJ118 88).

The local government also introduced a number of laws and regulations, to strengthen the control of noise. Beijing City Hall promulgated the “The noise pollution prevention and control law of Beijing” in January 1, 2007, the norms stipulated in the new residential sales, must announce the sound insulation status, urged the developers to gradually improve housing sound insulation quality. In addition, China has implemented the laws, regulations and standards of many restrictions to control noise.

But we should also see that, due to various reasons sound insulation effect is not a testing content in The housing acceptance part. When the sound insulation problem appears, developers Often Use the excuse that checks and accept qualification from project complete to prevaricate households. Therefore, we suggested taking the residential sound insulation as the residential quality acceptance criteria; accept the supervision and administration of the departments in charge of construction industry.

4 CONCLUSION

The acoustical environment forms after the completion of the construction. It is difficult to improve after the residents live in, and rebuilding has huge investment accompanied with bad effect. Developers must strict compliance with national laws, regulations, to ensure the quality management and quality control from the beginning of the decision-making, planning, concrete design, construction, until the final project approval. To provide a good residential sound environment for residents. Only in this way, we can create an elegant, quiet, comfortable environment for the residents.

REFERENCES

- Changchun heating ends for that Heating period accounted for nearly half of a year. [EB/OL] http://native.cn/city/201304/t20130415_512362838.shtml.
- Code for design of sound insulation of civil buildings GB 50118-2010[S]. China Architecture Industry Press, 2010.
- Lu Xiaodong & Zhu Peisheng. Preliminary study on residential sound insulation quality of Dalian area. [C]. The proceedings of The 11th National vibration and Noise Control Engineering Conference, 194–197.
- National economy and society developed statistical bulletin 2008–2012.
- Wang Hongtao & Jiang Yong. 2008. Study on the use of plastic external window in severe cold area[J]. China construction metal structure. 2008(4):31–37.

Equivalent solid-web beam method for steel truss based on the energy principle

Zai Hua Zhang

Steel Structural Institute of Civil Engineering College, Hunan University, Changsha, Hunan, P.R. China
Civil Engineering College, Hunan City University, Yiyang, Hunan, P.R. China

Xing Ping Shu

Steel Structural Institute of Civil Engineering College, Hunan University, Changsha, Hunan, P.R. China

Mei Li He

Civil Engineering College, Hunan City University, Yiyang, Hunan, P.R. China

ABSTRACT: During the analysis of complex structure including steel truss, the equivalent continuous model of steel truss is usually adopted for its high computational efficiency. The equivalent method commonly used is the equal deformation method and equal flexural rigidity method. Based on the consideration of equal height and equal strain energy, a equivalent solid-web method is put forward in this paper. According to the configurations of steel truss structure, the determine process of section parameter of the equivalent beam is presented in detail. Finally, the effectiveness of the model is verified by means of a comparative analysis of a project example.

Keywords: equivalent solid-web beam; steel truss; energy principle

1 INTRODUCTION

Owing to the characteristic of big stiffness, light weight and material savings, steel truss structure has been widely used in construction works, such as bridge structure, floor system with large span, etc. Although these structures can be modeled by truss elements in any finite element package at present, an equivalent continuum approach is beneficial in many ways: the input of the geometry is much simpler, the computer model is much cheaper and less time-intensive by the reduction of nodes and members required to accurately model the structure. These advantages are valid especially during the preliminary design phase where the determination of the global dimensions has priority over the concern of structural detailing.

There are several methods for the confirmation of the equivalent continuous model (D.B. McCallen, 1988). Of all analysis methods, there are two main ideas (Brian Giltner, 2000):

- The equivalent model of the beam is calculated based on the deflection of the loaded truss (equal deformation method).
- The equivalent stiffness I of the continuous beam model is calculated based on the truss cross-sectional area using parallel axis theorem ($I + Ad^2$) (equal flexural rigidity method).

In this paper, according to the configurations of steel truss structure, an equivalent solid-web beam method is put forward, Based on the comparative analysis of a project example, the effectiveness of the model was verified.

2 EQUIVALENT SOLID WEB BEAM METHOD BASED ON THE ENERGY PRINCIPLE

2.1 Basal principle

A truss consists of a group of members which are assumed to be connected at their joints with frictionless hinges. When the external loads are applied to the joints, each member of the truss is considered only to the bear axial force, while the main internal forces of a solid web beam include bending moment and shear force. According to the basic principle of energy, the strain energy of truss structure and solid-web beam can be expressed respectively as

$$U_{truss} = \sum_i \frac{N_i^2 L_i}{2EA_i} \quad (1)$$

$$U_{beam} = \int_0^l \frac{(M + Qx)^2}{2EI} dx + \frac{Q^2 l}{2GA_{s,eq}} \quad (2)$$

where, N_i, L_i, A_i are the axial force, length and cross-sectional area of each member of truss respectively, and M, Q, I, A_s are the bending moment, shear force, inertia moment of cross-section and web area of solid-web beam respectively.

Given that the steel truss and corresponding equivalent beam have the same span and section-height, the axial forces of each member for truss can be expressed as the function of internal forces of equivalent beam (M, Q). According to the principle of energy equivalence, we can get the corresponding section parameter of the equivalent solid-web beam.

2.2 The equivalent beam of typical steel truss

Figure 1 shows the basic unit of a kind of typical steel truss, and the correspondent equivalent beam segment is also illuminated. The section parameter of equivalent beam can be obtained according to above mentioned method.

The truss forces shown in Figure 1 are obtained by making the appropriate sections through the discrete unit and the equivalent beam segment. The strain energy of both discrete units, U_d , and the equivalent beam segment, U_e , can be defined (eqs.1 and 2). For U_d we make a summation over all bars i in the isolated unit.

$$U_d = \sum_i \frac{N_i^2 L_i}{2EA_i} = \frac{M^2 l}{2h^2 EA_1} + \frac{(M+Ql)^2 l}{2h^2 EA_1} + \left(\frac{T}{\sin \alpha}\right)^2 \frac{L}{2EA_3} + \frac{T^2 h}{2EA_2} \quad (3)$$

$$U_e = \int_0^l \frac{(M+Qx)^2}{2EI_{eq}} dx + \frac{Q^2 l}{2GA_{s,eq}} = \frac{M^2 l}{2EI_{eq}} + \frac{MTl^2}{2EI_{eq}} + \frac{T^2 l^3}{6EI_{eq}} + \frac{T^2 l}{2GA_{s,eq}} \quad (4)$$

where, EI_{eq} is the equivalent flexural rigidity, $GA_{s,eq}$ is the equivalent shear stiffness.

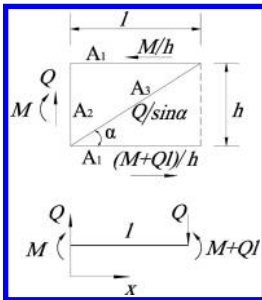


Figure 1. Unit of truss beam and the equivalent beam segment.

Energy equivalence results in $U_d = U_e$. By equating corresponding terms, in M^2 and Q^2 , in the equation (1) and (2), we get:

$$EI_{eq} = \frac{1}{2} EA_1 h^2 \quad (5)$$

$$\frac{1}{GA_{s,eq}} = \frac{l^3 (A_2 + A_3 h^3 / l^3)}{EA_2 A_3 l h^2} + \frac{l^2}{3EA_1 h^2} \quad (6)$$

If a normal force N acts on the neutral axis of the equivalent beam segment, we can derive an equivalent axial stiffness for the truss beam in an analogous way. Because of the vertical equilibrium, the normal force will not induce any force in the diagonal bar nor in the vertical batten bar. The induced forces in the longitudinal bars are for the upper and bottom bar respectively:

$$N_u = N_b = \frac{1}{2} N \quad (7)$$

According to energy equivalence, we can get the equivalent axial tensile (compressive) stiffness:

$$EA_{eq} = 2EA_1 \quad (8)$$

According to equation (5), (6) and (8), and the principle of equivalent section height, we can get the section parameter of equivalent beam.

3 APPLICATION EXAMPLE

An example problem is presented to validate the accuracy of this equivalent solid web beam. Figure 2 shows a kind of assembly steel frame (Z.H. Zhang, 2014). It can be seen that the floor beam of such a frame structure is a typical steel truss. We can take the truss for an example to validate the accuracy of above mentioned method.



Figure 2. Unit of truss beam and the equivalent beam segment.

In this assembly frame structure, the actual details of the typical truss beam are shown in Figure 3. Table 1 shows the dimensions and material properties of steel truss in detail. According to the principle of energy method (mentioned above), it can be equivalent to a corresponding solid-web steel beam: H-beam $450 \times 160 \times 6$.

Figure 4 shows the actual analytical model and equivalent model of the steel truss structure based on sap2000. By compare of the mid-span deflection under the same loading levels, the equivalent performance of these two kinds of analytical model can be checked. Table 2 shows the result of such a comparison, and it can be seen that the force-displacement curves of these two models agree well with each other, they are of good equivalence.

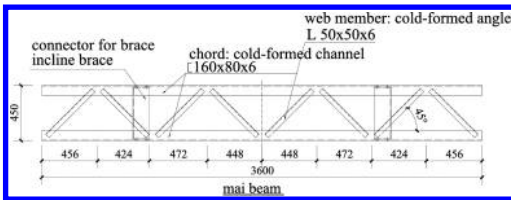


Figure 3. The detail of the typical truss of the assembly steel frame.

Table 1. The cross section of main component of the steel truss.

Sectional dimension	
Chord of truss	Cold-formed channel steel: $160 \times 80 \times 6$
Web member of truss	Hot-rolled angle steel: $2L50 \times 6$
Web member of truss	$2.06 \times 10^5 \text{ N/mm}^2$
Shear modulus	$7.92 \times 10^4 \text{ N/mm}^2$

Note: The layout of the typical truss refers to Figure 3.

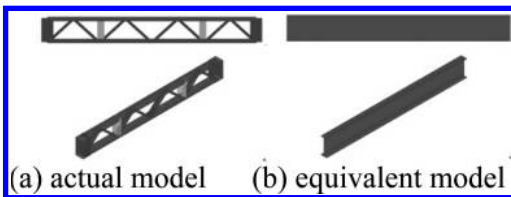


Figure 4. The actual and equivalent model of truss beam.

Table 2. Mid-span deflection contrast of equivalent model and actual model.

Load on the beam (kN/m)	Deflection of middle span (mm)	
	Actual model	Equivalent mode
10	1.3	1.2
20	2.5	2.3
30	3.7	3.5
40	4.9	4.6
50	6.1	5.7
60	7.3	6.9
70	8.5	8.0
80	9.7	9.2
90	10.9	10.3
100	12.2	11.4

4 CONCLUSION

Based on consideration of the same height, the same span and the equivalence of strain energy, an equivalent solid-web beam analysis method is put forward to simplify the analysis of steel truss structures. A preliminary validation of such a simplified method has been carried out, by means of a comparison between the simplified model and the actual model of a typical steel truss in an assembly steel frame. The comparison result shows a satisfactory agreement between these two methods, and it can be used in the analysis of practical engineering.

ACKNOWLEDGEMENTS

The research work was supported by the Natural Science Fund of Education Department of Hunan province (Grant No. 14C0212, 11C0245).

REFERENCES

- Brian Giltner, Aslam Kassimali, Equivalent Beam Method For Trusses [J], Practice Periodical on Structural Design and Construction, Vol. 5, No. 2, May, 2000, 70–77.
- McCallen D.B., K.M. Romstad, A Continuum Model for the Nonlinear Analysis of Beamlike Lattice Structures [J], Computers & Structures, 29, (1988), No. 2, 177–197.
- Zhang Z.H., X.P. Shu, Analysis on the Technology Characteristic of a New Kind of Assembly Steel Frame System [J], International Journal of Engineering and Technology, Vol. 6, No. 6, pp. 471–475, 2014.

A realization method of massive log management system for crime forensics

Hai-Yan Chen

Department of Computer Science and Technology, East China University of Political Science and Law, Shanghai, China

ABSTRACT: As the important source of evidence, log becomes the necessary event of inquiring evidences in the crime. With the popularity of all kinds of internet usage, there are more and more logs, and it is another difficulty how to analysis and find the massive log in the collection of evidence. In this paper, in view of the traditional relational database limitations and defects in the processing of massive logs, projecting and achieving a realization method of management system based on Hadoop and NoSQL, which provides a function in the collected information, searching and storing forever.

Keywords: massive log; crime forensics; Hadoop; management system

1 INTRODUCTION

With the wide spread of electronic commerce, social networking sites, video website, network application, the data is also becoming more and more huge for recording these, and even reaching TB or PB, so we call it “massive log”, which is a kind of “Big Data”. It is a hard problem that collects the data effectively, hold and search. In view of the great mass of evidence in computer crime forensics log function in [2], the design of an efficient real-time massive log stored query system is very necessary.

Traditional database fail to meet the high-intensity need because of the conforming restrict. And Google comes up the BigTable system, which lead to a series of database NoSQL. They have the same characteristic that reading and writing is based on Key-Value, but at the same time they lack of the function that operate multiply research and multiples analysis. And in the other hand, Hadoop use the MapReduce to speed up data research. However the limitation of cache mechanism, the productiveness is very low for not supporting a number of data collections largely.

2 THE ARCHITECTURE OF MASSIVE LOG MANAGEMENT SYSTEM

We design the system consisted by five parts: the central control cluster, massive log collection cluster, massive log retrieval cluster, massive log storage cluster and high speed Ethernet connection

module. The fundamental problem to solve is massive log collection quickly, research and distributed storage. The DBDMS system architecture is shown in Figure 1.

The Central Control Cluster works as the management controller in the whole system, it deals with tasks like acquiring user requests and doing the retrieval, keeping real-time monitoring of all parts and handling exceptions, triggering, canceling and updating tasks for certain clusters, optimizing the allocation of network connection resources, etc. The Massive log Collection Cluster have its process as execution units, it simultaneously opens several concurrent data collection modules on several machines to promote the data collection efficiency of the whole system. The Massive log Retrieval Cluster is the interactive interface between the whole system and its users. It submits

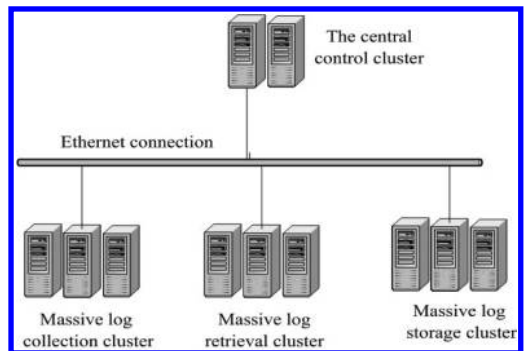


Figure 1. System architecture.

queries to the Central Control Cluster by the system custom queries or commands. The Massive log storage cluster where electronic evidence is saved permanently is conducive to sorting mass data and promoting the query efficiency.

3 THE CORE ALGORITHM OF MASSIVE LOG MANAGEMENT SYSTEM

Step 1. User submits query to the Data Retriever Cluster.

Step 2. The central control cluster gets the user request information from the massive log retrieval cluster; tries to quickly locate the target cluster.

Step 3. The central control cluster first searches the index in its cache, if there is some index information about the target cluster block, query commands will be sent directly to it, then the central control cluster will Listen and wait for the return of the target data; if there is not, parsing and re generating the optimal query conditions, and encapsulating the query command and the target cluster information, broadcasting to a massive log permanent storage cluster. Normally the Central Control Cluster divides the query term into: condition query, including relational arithmetic and logic arithmetic, Grouping Query, including grouping according to a certain element or calculation results from certain aggregate functions, and Fuzzy Query, including query

according to some special relation of a certain element.

Step 4. Massive log storage cluster retrieves its own database according to the query terms, if succeeds, returns the results to the central control cluster, otherwise it returns the failure message.

Step 5. The query result will be returned back from the central control cluster to the massive log retrieval cluster, and then to the user, the specific process of the algorithm is shown in Figure 2.

4 EXPERIMENTAL RESULTS AND ANALYSIS

Figure 3 shows the data retrieval efficiency in a period of time. Taking the data from 2014.03.01 to 2014.03.02 as an example, a total of 530386937 log record is stored, the relationship between the retrieval efficiency and time is basically linear growth, at around 200 s to return the retrieval results, the retrieval efficiency of the massive log

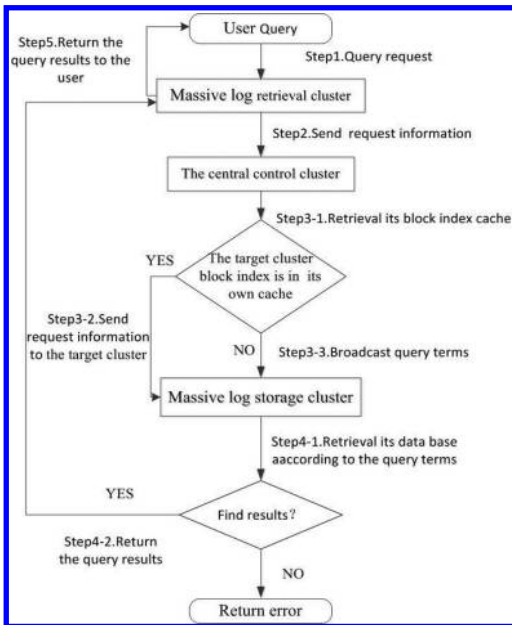


Figure 2. System data query algorithm.

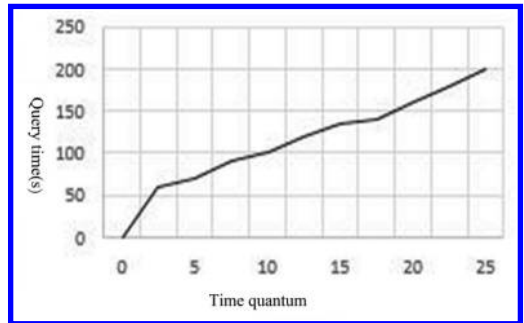


Figure 3. The relationship between time quantum and the retrieval efficiency.

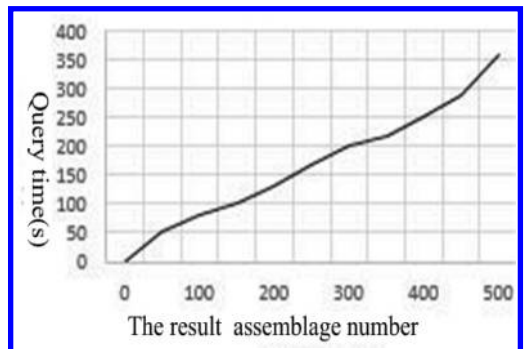


Figure 4. The result set and the retrieval efficiency relationship.

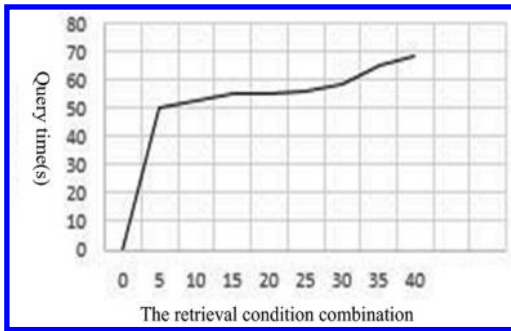


Figure 5. The retrieval efficiency and retrieval conditions combination.

management system is much higher than the traditional relationship database.

Figure 4 shows the result set and the retrieval efficiency relationship. Testing conditions continue to front, the more the number of visible collection, retrieval time is long, block index to find the corresponding more complex and more time-consuming.

Figure 5 shows the relationship between retrieval efficiency and retrieval conditions combination. Testing conditions continue to front, it is visible that with the retrieval condition is more and more complex, the retrieval efficiency increased slightly, but the margin is not large.

Experimental results show that the database system has its unique advantage in processing massive log retrieval and the retrieval efficiency is obviously superior to the traditional relational database.

5 SUMMARY

The realization method of massive log management system for crime forensics can significantly improve the storage and retrieval efficiency, but if the result set quantity is too large, the retrieval efficiency is reduced obviously, which needs to be further studied.

ACKNOWLEDGEMENTS

The corresponding author of this paper is CHEN Hai-Yan. This paper is supported by Projects of the National Social Science Fund (No.06BFX051); Shanghai university training and selection of outstanding young teachers in special research fund (No.hzf05046)

REFERENCES

- [1] Cao Xu. Design and implementation of log analysis platform based on the Hadoop's massive search. Zhejiang: Zhejiang Sci-Tech University, 2013.
- [2] Wang Ling, Hua Lin Qian. The computer forensics technology and its development [J]. Journal of software, 2003, (09):136-145.
- [3] BigTable:A Distributed Storage System for Structured Data. <http://download.csdn.net/source/979362>. 2009.
- [4] Christian von der Weth, Anwitaman Datta. Multiterm Keyword Search in NoSQL Systems. Digital Object Identifier, 2012:34-42.
- [5] Chen He, Derek Weitzel, David Swanson, Ying Lu. HOG: Distributed Hadoop MapReduce on the Grid. High Performance Computing, Networking, Storage and Analysis (SCC), 2012 SC Companion, 2012:1276-1283.

Research on the comprehensive evaluation of cuplok scaffolding

Yong Rui Chen, Lai Jun Liu, Wei Gang Sun, Lin Shen & Ping Qiao Yu

School of Highway, Chang'an University, Xi'an, Shaanxi, China

ABSTRACT: To evaluate the safety and stability of cuplok scaffolding, the comprehensive evaluation method is put forward. Firstly, 9 normal monitoring subjects are chosen as the evaluation indexes and the data related to index is extracted from a series of cuplok scaffoldings. Then the principal component analysis method is introduced to analyze the correlation between each index and create the comprehensive evaluation method of cuplok scaffolding. Finally, taking Xi'an City Xin Jiamiao overpass as an example, 24 different cuplok scaffolding designs of the same span are analyzed through eigenvalue analysis, buckling analysis and static analysis by Midas/Civil. Then the method is verified through the data extracted from the analysis. The results show that the application of principal component analysis in cuplok scaffolding safety evaluation can reflect the importance of each evaluation index and the actual measured safe state of cuplok scaffolding, and is feasible. The method has a strong practicability and is expected to provide theoretical guidance for safety analysis and evaluation of cuplok scaffolding.

Keywords: bridge engineering; safety assessment; principal component analysis; cuplok scaffolding; safe state

1 INTRODUCTION

The amount of bridges grows 10 thousands per year in China, which has reached hundreds of thousands at present. And the cast-in-situ concrete box girder is widely used in city over-pass. The cuplok scaffolding is the most widely used formwork support system in cast-in-place construction in domestic, which has characteristic of strong carrying capacity, simple structure, convenient assembly^[1]. But in recent years, many collapse accidents caused by instability of cuplok scaffolding occurred in domestic, which result in heavy casualties and huge economic losses^[2]. So the comprehensive evaluation of stability in cuplok scaffolding in construction process is critically important.

At present, the research of cuplok scaffolding is proceeded in four aspects: the calculation and analysis method^[3-5], the main factors affecting carrying capacity^[2], the technology of safety monitoring^[6,7], the reliability evaluation^[8].

The simulation of nodes and diagonal brace is one of the most important focus in the calculation of cuplok scaffolding. The rigidity of nodes has significant effect on the carrying capacity of scaffolding, and the difference of rigidity can cause uneven stress^[5,8]. The carrying capacity would be deducted along with the loose of node in scaffolding with no lateral restraint; but in rigid scaffolding with enough cross bracing, the loose of node has little influence on capacity of

scaffolding^[4]. The node of cuplok scaffolding is semi-rigid^[9], and this character can be simplified simulated in FE model through discounting the flexural rigidity of horizontal bar which restrain the vertical bar^[10]. Besides, the capacity of cuplok scaffolding has relation to structural factors, initial imperfection of bars, construction quality and site loads^[8]. Cross bracing can obviously improve the capacity of cuplok scaffolding^[11]; for cuplok scaffoldings with different vertical and horizontal ranges between tubes, different distance between ground and bottom horizontal tube, investigation about its geometric imperfection and node rigidity could be put forward in order to simulate the uncertainty of random event, such as the imperfection of tubes, through statistic method^[8]. And then the statistic data about resistance of cuplok scaffolding would be received, based on which the reliability of scaffolding can be evaluated. Verified by the experiment, the 3D precise model considering uncertainty factors such as the sleeve joints, semi-rigid nodes, grounding pole eccentricity and geometric imperfection can accurately predict the stress state of scaffolding^[12]. Besides, for the safety and stability of scaffolding during concrete construction, the stress, bending moment, node displacement, foundation settlement, vibration characteristics of cuplok scaffolding are necessary to be monitored^[6,13], and it would be warning if the monitoring data is above the preset threshold value^[14].

Most studies referred above are focus on influence factors of the bearing capacity, method of calculation and prediction and its experimental verification. The results of these studies has promoted the development of the basic theory about safety control technology of cuplok scaffolding, but in the fields of safety evaluation, these studies are mostly focused on individual index and lacking in comprehensive evaluation method^[8]. Although three are studies evaluating the reliability through probabilistic method, but they are lack of practical because of large statistic work. Meanwhile, the previous studies paid more attention on the prediction of the bearing capacity of scaffolding and slighted the evaluation of the safe state on-site; in recent years, some scholars proposed to bring the monitoring of the actual bearing condition into the safety control of cuplok scaffolding^[6,13], but there is no comprehensive evaluation method is put forward. Given those factors, aimed at the comprehensive evaluation method of safe state, on the basis of the stress and structural characteristics and the feasibility of the construction on-site monitoring, 9 normal monitoring subject used to characterize the working condition of cuplok scaffolding are put forward as its safe state evaluation indexes. And the Principal Component Analysis (PCA) is introduced to safe state evaluation of cuplok scaffolding for the first time, and a comprehensive evaluation method is obtained, which make the evaluation results more systematic, holistic and scientific.

1 SAFE STATE EVALUATION METHOD OF CUPLOK SCAFFOLDING

1.1 Index extraction

Safe state is a qualitative concept, and the safe state evaluation is to quantify it through several indexes extracted from the monitoring data and finite element analysis result under the construction loads. Due to the large amount of components, it is hard to monitor condition of all components, but the real safe state must be fully reflected. So the selection of evaluation index about cuplok scaffolding should be easy to be measured, systematically covered most aspects, objective and sensitive, and represented clearly. In view of this, the paper selected 9 normal monitoring subjects of cuplok scaffolding as indexes to evaluate its safe state.

1. The frequency of first order modal shape (f)
When the vibration frequency is close to the natural frequency, resonance occurs. The natural frequency of vibration can reflect the integral rigidity and stability of cuplok scaffolding.

2. First-order buckling mode coefficient (ω)
First-order buckling mode coefficient ω reflects the reserve size of carrying capacity of scaffolding. The greater value of omega, the larger size of the reserve capacity of the scaffolding.

$$\omega = \frac{F_{ex}}{F}$$

where F_{ex} is the ultimate bearing capacity of scaffolding, F is the load acting on the scaffolding.

3. Maximum axial force of vertical tubes (F_{Vmax})
Vertical tubes are the major components to bearing construction loads. The main internal force of vertical tube is axial force. The maximum axial force of vertical tubes (F_{Vmax}) is used to reflect of axial stress safe state of of vertical tubes.
4. Maximum bending moment of vertical tubes (M_{Vmax})
The major stress state of vertical tubes is axial force. But because of the semi-rigid character of nodes, when the uneven settlement of foundation or local deformation of scaffolding occurs, the vertical tube is constrained by horizontal tubes it contacted, so that bending moment exists in vertical tube. The maximum bending moment of vertical tubes is selected to reflect the most unfavorable bending state of vertical tubes and the rigidity of node.
5. Maximum axial pressure force in horizontal tubes (F_{Hmax-})
Ordinarily, the axial force in horizontal tubes are very small. But when local deformation exists, axial force takes place in horizontal tubes because of interactional constraint. Axial forces in horizontal tube include axial tensile force and axial pressure. The axial pressure is always caused by lateral displacement of nodes. The maximum axial pressure force can be chosen to reflect the most unfavorable state column stability in horizontal tubes.
6. Maximum axial tensile force in horizontal tubes (F_{Hmax+})
The displacement of nodes would cause axial tensile force in horizontal tubes. The maximum axile tensile force could be chosen to reflect the most unfavorable tensile state in horizontal tubes.
7. Maximum bending moment in horizontal tubes (M_{Hmax})
Bending moment in horizontal tubes has the same cause with which in vertical tubes. The higher of MH, the greater of deformation, possibility of unstability in scaffolding, the less of capacity of scaffolding. The maximum bending moment in horizontal tubes could be chosen to indicate the most unfavorable bending state and the rigid of nodes.

8. Maximum horizontal displacement of nodes (H_{max})

Node displacement is the most intuitionistic parameter to reflect deformation in cuplok scaffolding. The larger of the horizontal displacement, the worse of the local stability around the nodes. So the maximum horizontal displacement is available to reflect the most unfavorable condition for the local stability of cuplok scaffolding.

9. Maximum vertical displacement of nodes (V_{max})

Vertical displacement has closely relationship with foundation settlement, rigid of nodes and tightness of socket extension. The greater of the vertical displacement of nodes, the worse of local stability and security. So maximum vertical displacement of nodes is chosen to reflect the most unfavorable condition of local stability in cuplok scaffolding.

Safe state evaluation should choose the most unfavorable state of the indexes selected. So all internal force and displacement indexes are maximum value in monitoring. In on-site test, multiple sensors are arranged on the key section in scaffolding, and then the index value can be chosen from these sensors tested.

The safe state evaluation index system is shown in Figure 1.

1.2 Evaluation method

Principal Component Analysis (PCA) is recognized in 1901 by the father of the statistical Karl Pearson to discuss non-random variables. Multi indexes Principal Component Analysis (PCA) can convert many original indexes which are relative to each other into relatively small number, independent and comprehensive indexes without damage or loss less original information as far as possible, so as to achieve the purpose of simplified^[15].

As a basic mathematical analysis method, principal component analysis, which is a kind of ordinary

methods of multivariate analysis, is widely applied in demography, quantitative geography, molecular dynamics simulation, mathematical modeling and mathematical analysis. As the number of monitoring indexes are relatively large, in order to evaluate the safe state systematically and integrally without losing the basic information of each original index, so PCA is introduced in this article.

The main procedures that principal component analysis method realize are as follows:

1. Create the sample observations matrix X

$$X = \begin{pmatrix} x_{11} & \cdots & x_{p1} \\ \vdots & \ddots & \vdots \\ x_{1n} & \cdots & x_{pn} \end{pmatrix} \quad (1)$$

2. Convert X into standardized matrix Y :

$$Y = \begin{pmatrix} y_{11} & \cdots & y_{p1} \\ \vdots & \ddots & \vdots \\ y_{1n} & \cdots & y_{pn} \end{pmatrix}$$

$$y_{ij} = \frac{x_{ij} - \bar{x}_i}{\sqrt{S_{ij}}}, (i = 1, 2, \dots, p); \bar{x}_i = \sum_{j=1}^n x_{ij};$$

$$(i = 1, 2, \dots, p; j = 1, 2, \dots, n);$$

$$S_{ij} = \frac{1}{n-1} \sum_{k=1}^n (x_{ik} - \bar{x}_i)(x_{kj} - \bar{x}_j) \quad (2)$$

3. Calculate the sample correlation matrix R :

$$R = \begin{pmatrix} r_{11} & \cdots & r_{p1} \\ \vdots & \ddots & \vdots \\ r_{1n} & \cdots & r_{pn} \end{pmatrix} \quad (3)$$

$$r_{ij} = \frac{1}{n-1} \sum_{k=1}^n y_{ij} y_{ik} = \frac{1}{n-1} \sum_{k=1}^n \frac{(x_{ij} - \bar{x}_i)(x_{ik} - \bar{x}_k)}{S_j S_k};$$

S_j is the standard deviation of each sample index.

4. Calculate the eigenvalue and eigenvector of R . Convert R to eigenmatrix M through orthogonal transformation

$$M = Q'RQ = \begin{pmatrix} \lambda_1 & & & \\ & \lambda_2 & & \\ & & \ddots & \\ & & & \lambda_p \end{pmatrix} \quad (4)$$

$\lambda_1, \lambda_2, \dots, \lambda_n$ are eigenvalue of matrix R .

Suppose set the eigenvalues from big to small as $\lambda_1 \geq \lambda_2 \geq \dots \geq \lambda_n > 0$, each column vectors $\zeta_j = (\zeta_{1j}, \zeta_{2j}, \dots, \zeta_{pj})^T, (j = 1, 2, \dots, p)$ of Q is the normalized eigenvector corresponding to λ_j .

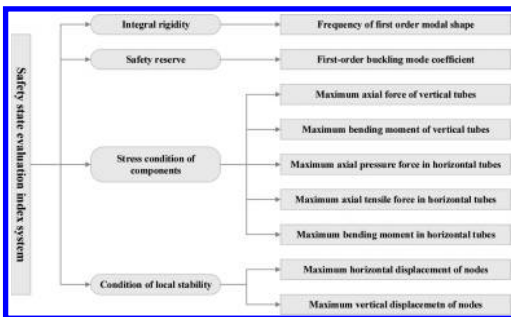


Figure 1. Safe state evaluation index system of cuplok scaffolding.

5. Creation of principal components

The function of PCA is expressing information included in p indexes with k principal components ($k < p$) through dimension reduction technique, and making comprehensive evaluation. k is determined by cumulative contribution rate η .

$$\eta = \frac{\sum_{j=1}^k \lambda_j}{\sum_{j=1}^p \lambda_j} \quad (5)$$

λ_j ($j = 1, 2, \dots, p$) are set from big to small, principal components F_1, F_2, \dots, F_k are obtained when $\eta \geq 0.85$.

2 EXAMPLE VERIFICATION

2.1 Erection plan of cuplok scaffoldings

Take Xinjiamiao elevated overpass in Xi'an as a validation instance for the safe state evaluation method of cuplok scaffolding. The superstructure of this bridge is (24.5 + 4 × 30) m, single box, 3 room prestressed continuous cast-in-site box girder. The beam is 1.7 m high, the roof plate is 13 m wide and the bottom plate is 9 m wide. Select the 5 span (30 m) as the research object. Getting large sample data tested on-site is difficult, meanwhile, the correctness of the method can't be proved if the sample size is too little. In order to solve the contradictions above, based on the cross selected, according to different vertical tubes spacing, horizontal pole interval, free length of the top vertical tubes, the height of bottom horizontal tubes and stiffness of nodes, a total of 24 set of erection plan (shown in Table 1) are given out. Eigenvalue analysis, buckling analysis and static analysis of mechanism of each plan are calculated through FEM program MIDAS/CIVIL. According to the calculation result and nine indicators proposed, relevant data is extracted to verify this comprehensive evaluation method. The preconditions of the simulated calculation is as follows:

1. The construction load on each top of cuplok scaffolding is same, which is 1.2 times the weight of concrete box girder.
2. There are X-bracing in four sides of scaffolding and cross sections. The interval between cross sections with X-bracing is 4.5–4.8 m. The leg of X-bracing is about 45° tilt.
3. In FEM model, the tubes are simulated by girder element. The semi-rigid node is simulated by releasing the constraint on both end of tubes. The released constraint of vertical tubes is 10%, and the horizontal tube is 30%.

Table 1. Parameters of each cuplok scaffolding plan.

Plan	Z	X & Y	L	H	Rigidity
P_1	0.9	0.9	0.3	0.3	R
P_2	0.9	0.9	0.3	0.3	S
P_3	0.9	0.9	0.3	0.6	R
P_4	0.9	0.9	0.3	0.6	S
P_5	0.9	0.9	0.6	0.3	R
P_6	0.9	0.9	0.6	0.3	S
P_7	0.9	0.9	0.6	0.6	R
P_8	0.9	0.9	0.6	0.6	S
P_9	1.2	1.2	0.3	0.3	R
P_{10}	1.2	1.2	0.3	0.3	S
P_{11}	1.2	1.2	0.3	0.6	R
P_{12}	1.2	1.2	0.3	0.6	S
P_{13}	1.2	1.2	0.6	0.3	R
P_{14}	1.2	1.2	0.6	0.3	S
P_{15}	1.2	1.2	0.6	0.6	R
P_{16}	1.2	1.2	0.6	0.6	S
P_{17}	1.2	0.9	0.3	0.3	R
P_{18}	1.2	0.9	0.3	0.3	S
P_{19}	0.9	1.2	0.3	0.3	R
P_{20}	0.9	1.2	0.3	0.3	S
P_{21}	0.9	1.2	0.6	0.6	R
P_{22}	0.9	1.2	0.6	0.6	S
P_{23}	1.2	0.9	0.6	0.6	R
P_{24}	1.2	0.9	0.6	0.6	S

* Z, the step of horizontal tubes; X&Y, the internal space between vertical tubes; L, the free length of top vertical tubes; H, the height of bottom horizontal tubes; R, rigid; S, semi-rigid; the unit is m .

4. In order to simulate the uneven settlement, suppose that there are 11 mm settlement in the midspan which is according to the maximum settlement on-site tested.^[14] The settlement of other position is distributed according to cosine curve.

2.2 Data of sample

According to the results calculated by Midas/Civil of each plan, f , ω , M_{Vmax} , F_{Vmax} , M_{Hmax} , F_{Hmax} , F_{Hmax}^+ , H_{max} , V_{max} are extracted, which are shown in Table 2.

2.3 Data processing

According to equation (2), standardized data is obtained through the standardized calculation from data in Table 2, which is shown in Table 3.

According to equation (3), the relevant coefficient matrix is obtained by correlation analysis from data in Table 2.

As is shown in the correlation coefficient matrix, f is positively related to ω . In the case of other

Table 2. Data of sample.

Plan	f	ω	$M_{V_{max}}$ (kN·m)	$F_{V_{max}}$ (kN)	$M_{H_{max}}$ (kN·m)	$F_{H_{max}}^+$ (kN)	$F_{H_{max}}^-$ (kN)	H_{max} (mm)	V_{max} (mm)
P_1	5.19	6.41	1.11	-73.45	0.45	21.10	-19.68	2.11	11.91
P_2	3.79	3.89	1.01	-71.02	0.25	22.92	-20.48	2.11	11.90
P_3	4.01	4.79	0.48	-63.74	0.26	26.01	-19.46	2.39	11.97
P_4	3.12	3.59	0.44	-62.53	0.12	27.35	-20.25	2.50	11.90
P_5	5.14	4.47	1.11	-73.46	0.45	21.10	-19.68	1.93	11.89
P_6	4.35	3.25	1.01	-71.04	0.25	22.92	-20.48	2.11	11.90
P_7	3.99	4.47	0.48	-63.76	0.26	26.01	-19.46	2.39	11.87
P_8	3.08	3.25	0.43	-62.55	0.12	27.35	-20.25	2.50	11.90
P_9	4.30	2.75	1.25	-83.78	0.50	28.63	-12.93	2.51	14.00
P_{10}	3.04	1.64	1.11	-81.52	0.28	30.88	-12.77	2.68	13.99
P_{11}	3.46	2.53	0.54	-75.77	0.25	34.54	-12.54	3.04	14.14
P_{12}	2.62	1.58	0.48	-74.90	0.14	35.48	-12.43	3.11	14.12
P_{13}	4.27	1.93	1.25	-83.80	0.50	28.63	-12.93	2.51	14.00
P_{14}	3.02	1.35	1.11	-81.53	0.28	30.88	-12.77	2.68	13.99
P_{15}	3.43	1.93	0.54	-75.79	0.25	34.54	-12.54	3.04	14.14
P_{16}	2.60	1.36	0.48	-74.91	0.14	35.48	-12.43	3.11	14.13
P_{17}	4.78	5.40	1.07	-78.62	0.48	20.03	-28.49	1.96	11.78
P_{18}	3.48	3.34	0.97	-75.91	0.27	21.96	-29.00	1.95	11.80
P_{19}	4.42	6.45	1.18	-64.13	0.43	23.70	-22.30	2.05	11.86
P_{20}	3.12	3.69	1.01	-62.74	0.24	24.89	-22.52	2.18	11.85
P_{21}	3.42	3.75	0.48	-57.59	0.22	27.20	-22.11	2.44	11.72
P_{22}	2.59	2.58	0.41	-57.09	0.12	27.72	-22.31	2.50	11.93
P_{23}	3.79	4.06	0.47	-67.48	0.27	23.88	-28.14	2.50	11.86
P_{24}	2.90	2.92	0.43	-66.07	0.13	25.44	-28.64	2.64	11.88

* Tensile force shown in Table 2 is positive; pressure is negative.

conditions unchanged, the scaffolding with high capacity has higher rigidity; f positively related to $M_{V_{max}}$ and $M_{H_{max}}$, and f has highest correlation with $M_{H_{max}}$. Tubes in cuplok scaffolding with high rigidity may sustain heavier bending moment. f has negative relevance with $F_{V_{max}}$, $F_{H_{max}}^+$, $F_{H_{max}}^-$. The more rigid scaffolding has stronger load redistribution ability, so that the axial forces of tube in which is relatively smaller. f has negative relevance with H_{max} , V_{max} . Displacement of nodes are relatively smaller in scaffoldings with higher rigidity.

ω is positively related to $M_{V_{max}}$, $M_{H_{max}}$, that means scaffolding with higher bending moment will has higher ultimate bearing capacity. Under the condition of equal settlement and local deformation, higher bending moment means stronger rigidity, in other hand, stronger bearing capacity. ω is negatively related to $F_{H_{max}}^+$, $F_{H_{max}}^-$, H_{max} , V_{max} . Under the same construction load, the scaffolding with higher axial force and displacement may has weaker ultimate bearing capacity. The value of $F_{H_{max}}^+$, $F_{H_{max}}^-$, H_{max} , V_{max} are related to the uneven settlement and local deformation. The more serious of uneven settlement and local deformation, the greater value of $F_{H_{max}}^+$, $F_{H_{max}}^-$, H_{max} , V_{max} , and

the weaker ultimate bearing capacity of cuplok scaffolding.

$M_{V_{max}}$ has obviously negative correlation with $F_{V_{max}}$. Under the condition of equal construction load, the bigger axial force of local vertical tubes, the less constraint of vertical tubes, so the smaller of bending moment in vertical tubes.

$F_{V_{max}}$ has obviously negative correlation with $M_{H_{max}}$, $F_{H_{max}}^+$, $F_{H_{max}}^-$, V_{max} . Under the condition of equal construction load, larger bending moment and axial force in horizontal tubes indicate that the horizontal tubes have stronger constraint on vertical tubes around, and the scaffolding has stronger load distribution capacity. So axial force in vertical is relatively small. The axial force in vertical tubes with vertical displacement is relatively weaker because of load redistribution caused by constraint from horizontal tubes.

$M_{H_{max}}$ has obviously negative correlation with $M_{V_{max}}$. The bending moment transmitted through semi-rigid nodes. So $M_{H_{max}}$ get bigger along with the increase of $M_{V_{max}}$.

Solve the eigenvalue and its contribution, accumulated contribution from correlation coefficient matrix.

Table 3. Standardized data of indexes.

Plan	f	ω	M_{Vmax}	F_{Vmax}	M_{Hmax}	F_{Hmax}^+	F_{Hmax}^-	H_{max}	V_{max}
P_1	1.98	2.07	0.99	-0.31	1.37	-1.27	-0.06	-0.95	-0.65
P_2	0.16	0.34	0.68	-0.01	-0.20	-0.88	-0.20	-0.95	-0.66
P_3	0.45	0.96	-0.94	0.90	-0.16	-0.22	-0.02	-0.18	-0.60
P_4	-0.70	0.14	-1.07	1.05	-1.24	0.07	-0.16	0.12	-0.66
P_5	1.91	0.74	0.99	-0.31	1.37	-1.27	-0.06	-1.44	-0.67
P_6	0.89	-0.10	0.68	-0.01	-0.20	-0.88	-0.20	-0.94	-0.66
P_7	0.42	0.74	-0.94	0.89	-0.16	-0.22	-0.02	-0.18	-0.69
P_8	-0.76	-0.10	-1.07	1.05	-1.26	0.07	-0.16	0.12	-0.66
P_9	0.83	-0.44	1.43	-1.59	1.76	0.34	1.14	0.15	1.32
P_{10}	-0.81	-1.20	0.98	-1.31	0.01	0.83	1.16	0.62	1.31
P_{11}	-0.26	-0.59	-0.74	-0.60	-0.24	1.61	1.20	1.59	1.45
P_{12}	-1.35	-1.24	-0.93	-0.49	-1.09	1.81	1.22	1.80	1.44
P_{13}	0.79	-1.00	1.43	-1.59	1.76	0.34	1.14	0.15	1.32
P_{14}	-0.83	-1.40	0.98	-1.31	0.01	0.83	1.16	0.62	1.31
P_{15}	-0.30	-1.00	-0.74	-0.60	-0.24	1.61	1.20	1.59	1.45
P_{16}	-1.38	-1.40	-0.93	-0.49	-1.09	1.81	1.22	1.80	1.44
P_{17}	1.45	1.38	0.87	-0.95	1.61	-1.50	-1.61	-1.36	-0.78
P_{18}	-0.24	-0.03	0.57	-0.61	-0.07	-1.09	-1.70	-1.39	-0.76
P_{19}	0.98	2.10	1.20	0.85	1.24	-0.71	-0.52	-1.11	-0.70
P_{20}	-0.70	0.21	0.67	1.02	-0.32	-0.46	-0.56	-0.75	-0.71
P_{21}	-0.31	0.25	-0.93	1.66	-0.42	0.04	-0.49	-0.05	-0.83
P_{22}	-1.39	-0.56	-1.14	1.72	-1.21	0.15	-0.52	0.12	-0.63
P_{23}	0.16	0.46	-0.95	0.43	-0.07	-0.68	-1.55	0.13	-0.70
P_{24}	-0.99	-0.32	-1.09	0.61	-1.16	-0.34	-1.64	0.49	-0.68

Table 4. The correlation coefficient matrix for indexes.

	f	ω	M_{Vmax}	F_{Vmax}	M_{Hmax}	F_{Hmax}^+	F_{Hmax}^-	H_{max}	V_{max}
f	1.000	0.708	0.590	-0.229	0.847	-0.657	-0.179	-0.667	-0.307
ω	0.708	1.000	0.195	0.383	0.428	-0.786	-0.585	-0.746	-0.747
M_{Vmax}	0.590	0.195	1.000	-0.604	0.809	-0.387	0.104	-0.531	0.105
F_{Vmax}	-0.229	0.383	-0.604	1.000	-0.536	-0.242	-0.497	-0.180	-0.705
M_{Hmax}	0.847	0.428	0.809	-0.536	1.000	-0.416	0.044	-0.488	0.056
F_{Hmax}^+	-0.657	-0.786	-0.387	-0.242	-0.416	1.000	0.779	0.956	0.844
F_{Hmax}^-	-0.179	-0.585	0.104	-0.497	0.044	0.779	1.000	0.651	0.865
H_{max}	-0.667	-0.746	-0.531	-0.180	-0.488	0.956	0.651	1.000	0.768
V_{max}	-0.307	-0.747	0.105	-0.705	0.056	0.844	0.865	0.768	1.000

According to Table 5, $\sum_{i=1}^{k=2} \lambda_i = 87.28\%$, in the light of principles of principal components selection: $\eta \geq 0.85$, 2 principal components F_1, F_2 is obtained.

$$F_1 = -0.748f - 0.884\omega - 0.412M_{Vmax} - 0.253F_{Vmax} - 0.516M_{Hmax} + 0.974F_{Hmax}^+ + 0.72F_{Hmax}^- + 0.953H_{max} + 0.817V_{max}$$

$$F_2 = 0.524f - 0.096\omega + 0.812M_{Vmax} - 0.883F_{Vmax} + 0.808M_{Hmax} + 0.059F_{Hmax}^+ + 0.517F_{Hmax}^- - 0.06H_{max} + 0.566V_{max}$$

According to Table 6, result are given as follows:

The contribution rate of first principal component F_1 is as high as 54.27%, which mainly contains $F_{Hmax}^+, F_{Hmax}^-, \omega, H_{max}, V_{max}$. Large local deformation or uneven settlement, will lead to a larger axial force is generated in horizontal bar around so the horizontal bar axial force is an important index of safe state evaluation bowl frame. Bowl for many times statically indeterminate structure, bar through the semi-rigid nodes connected to stand. Under ideal security status, bowl rack

Table 5. Eigenvalue and its contribution.

Principal component	Eigenvalue	Contribution (%)	Accumulating contribution (%)
F_1	4.884	54.27	54.27
F_2	2.97	33.01	87.28
F_3	0.593	6.59	93.87
F_4	0.296	3.29	97.15
F_5	0.133	1.48	98.63
F_6	0.088	0.98	99.61
F_7	0.022	0.24	99.85
F_8	0.013	0.14	99.99
F_9	0.001	0.02	100

Table 6. Eigenvectors of principal components.

Index	F_1	F_2
f	-0.748	0.524
ω	-0.884	-0.096
M_{Vmax}	-0.412	0.812
F_{Vmax}	-0.253	-0.883
M_{Hmax}	-0.516	0.808
F_{Hmax}^+	0.974	0.059
F_{Hmax}^-	0.72	0.517
H_{max}	0.953	-0.06
V_{max}	0.817	0.566

displacement of node does not occur, but in the actual work, inevitably produce certain bowl frame node displacement, mainly due to three aspects: first, poling uneven settlement of foundation; Second, the vertical compression rod extension point gap; Third, the bar near the large deformation. Can be seen from the above three causes, regardless of the reason why to choose a node displacement of more than a certain value when its amount of displacement could lead to local instability. So the maximum horizontal displacement and vertical displacement of nodes is an important index of local stability evaluation bowl frame. First order buckling mode coefficient of omega is bowl with an ultimate bearing capacity than the current work load, characterization of safe state of bowl frame carrying capacity reserve capacity, the greater the value of omega, bowl rack capacity reserve.

The contribution rate of the second principal components F_2 is 33.01%, which is far greater than the third component F_3 (6.59%). F_2 mainly reflect indexes including M_{Vmax} , M_{Hmax} , F_{Vmax} . Under ideal working conditions, cuplok scaffolding and the foundation are rigid enough. Load transmit to foundation through vertical tubes, and displacement of nodes would not take place. So there is no

bending moment in horizontal tubes. But actually displacement of nodes exists because of settlement, the compressure of gap between extension socket of vertical tubes and buckling deformation of tubes. As a result of the constraint from semi-rigid nodes, bending moment appears in tubes when nodes move. Under the condition that load and the rigidity are fixed, node displacement is positively related to bending moment in tubes around node. So bending moment is an important index to evaluate local stability of cuplok scaffolding. Axial pressure of vertical tubes is the most major work form of cuplok scaffolding under normal work condition. Generally axial pressure is far less than the limit of compressive strength, but instability of compressive bar may occur. So in view of this consideration, the second principal component contains axis pressure of vertical tubes, and it has clear meaning.

2.4 The comprehensive evaluation of cuplok scaffolding

According to Table 5, the contribution ratio of the two principal components is $\lambda_{F_1} = 54.27\%$, $\lambda_{F_2} = 33.01\%$. Then the formula to calculate the evaluation score of each scaffolding is as follows:

$$F = 0.5427F_1 + 0.3301F_2 \quad (6)$$

Substitute data from Table 2 into equation (6), the comprehensive score F for each scaffolding can be obtained, as is shown in Table 7.

The grading of evaluation standard is shown in Table 8.

Through analysis of comprehensive evaluation score in Table 7, the evaluation result can be obtained shown as follows:

1. Between 24 cuplok scaffoldings, the highest score is $F_{P_{16}} = 53.76$ he, and the lowest score is $F_{P_{23}} = 32.00$. The distribution of scores is obviously. bowl with an erection schemes, the set-up plan can be 24 size is divided into three regions the score distribution can be divided into 3 areas: $A_1 \sim A_3$. A_1 has high scores, including plan $P_9 \sim P_{16}$, score range is 52.07 ~ 53.76; A_2 includes plan $P_1 \sim P_8$, score range is 36.03 ~ 37.44; A_3 includes plan $P_{17} \sim P_{24}$, shooting range of 32.00 ~ 32.00.
2. The 1.2 m × 1.2 m arrangement on horizontal plane is adopted in A_1 ; 0.9 m × 0.9 m in A_2 ; 0.9 m × 1.2 m or 1.2 m × 0.9 m in A_3 . According to the distribution of evaluation scores, space between vertical tubes and step between horizontal tubes had a significant influence on the safe state evaluation score.
3. Take A_1 for example, $F_{P_{15}} = 52.08 > F_{P_9} = 51.22$. It means that scaffoldings with longer free length of bottom vertical tubes get higher

Table 7. Comprehensive evaluation score of each cuplok scaffolding.

Order	Plan	F
1	P_{16}	53.76
2	P_{12}	53.63
3	P_{14}	53.52
4	P_{10}	53.36
5	P_{15}	53.05
6	P_{11}	52.72
7	P_{13}	52.5
8	P_{19}	52.07
9	P_6	37.44
10	P_2	37.23
11	P_5	37.03
12	P_8	36.82
13	P_4	36.63
14	P_7	36.14
15	P_1	36.12
16	P_3	36.03
17	P_{18}	34.23
18	P_{22}	34
19	P_{20}	33.88
20	P_{17}	33.26
21	P_{21}	33.09
22	P_{24}	32.84
23	P_{19}	32.18
24	P_{23}	32

Table 8. Safe state comprehensive evaluation standard.

Grade	Well	Ordinary	Poor	Bad
F	<32	32-42	42-52	>52

evaluation score. $F_{P_{13}} = 51.64 > F_{P_9} = 51.22$, means that scaffoldings with longer free length of top vertical tubes get higher evaluation score. $FP_{15} = 52.08 > FP_{13} = 51.64$, the longer the sweeping bar, the higher the score; $F_{P_{10}} = 52.44 > F_{P_9} = 51.22$, $F_{P_{12}} = 52.63 > F_{P_{11}} = 51.77$, $F_{P_{14}} = 52.59 > F_{P_{13}} = 51.64$, $F_{P_{16}} = 52.76 > F_{P_{15}} = 52.08$, suggest that scaffoldings with semi-rigid nodes get lower evaluation score than scaffoldings with rigid nodes.

- The cuplok scaffoldings in area A_3 get lower score than scaffoldings in area A_1 and A_2 , but scaffoldings in area A_3 have relatively lower intensity of tube distribution than scaffoldings in A_1 . Through the analysis, that is mainly because cross bracing in A_3 has smaller tilt angle than it in A_1 . This difference improved the bearing capacity. Thus it suggests that bracing decorate has significant influence on bearing capacity of cuplok scaffolding.

- Comprehensive evaluation results show that maximum axial pressure of vertical tubes and maximum axial force in horizontal tubes have great influence on evaluation results, especially the is largest pressure to bowl with an comprehensive evaluation result is bigger, especially the maximum axial pressure of vertical tubes. It's mainly because the vertical tubes are major bearing components in cuplok scaffolding. So in the practical monitoring, the plan should arrange enough axial force measuring points and enough measuring frequency, in order to ensure its safety.

In the view that the results above agree with results evaluated by relevant experiment and standard, this comprehensive evaluation method can effectively evaluate integral safe state of cuplok scaffolding, and has certain theoretical guidance and reference for the evaluation research of cuplok scaffolding.

3 CONCLUSION

- Aiming at the safe state evaluation of cuplok scaffolding, 9 evaluation indexes are put forward in this paper, and the Principal Component Analysis (PCA) is introduced into this paper. Then a new comprehensive safe state evaluation method is obtained. Through example validation, the valuation result is explicit and reasonable.
- According to safe state comprehensive evaluation results, cuplok scaffoldings with larger space between tubes, free length of top and bottom vertical tubes get higher score. Cuplok scaffoldings with weak node rigidity get lower score. The safe state of cuplok scaffolding with high score is worse than which with low score.
- Evaluation method proposed in this paper has widely feasibility. After index adjustment and optimization, the comprehensive evaluation method can be applied to the erection scheme optimization, the economic comparison and other engineering fields.

REFERENCES

- X. Kegui, H. Xun, S. Yong, J. Tongle. Experimental Study on the Bearing Capacity of Full-Scale Cuplok Steel Tubular Supporting Frame. Construction Technology, 2010, 12: 021.
- N. Xie, G. Wang. Study on Load-Carrying Capacity of Super High Supports for Formwork. Engineering Mechanics, 2008: S1.
- T. Chandrangsu, K.J. Rasmussen. Structural Modeling of Support Scaffold Systems. Journal of Constructional Steel Research. 2011, 67 (5): 866-875.

- [4] U. Prabhakaran, R. Beale, M. Godley. Analysis of Scaffolds with Connections Containing Looseness. *Computers & Structures*. 2011, 89 (21): 1944–1955.
- [5] W. Xu, L. Chunyang. Influence Analysis of Bowl Connection Stiffness on the Stress of Cuplok Scaffolding. In: *The 19th national academic conference of bridge China Shanghai*, 2010: 6.
- [6] S. Xinhua, S. Pengxu, L. Laijun. Study on Monitoring Techniques of Cuplok Scaffolding. *Journal of Highway and transportation (application and technology)*. 2012 (11): 256–259.
- [7] X. Nan. In-Situ Test of Working State of High Formwork Supports During Concrete Placement. *Engineering Mechanics*. 2011 (S1): 85–89.
- [8] T. Chandrangu, K.J. Rasmussen. Investigation of Geometric Imperfections and Joint Stiffness of Support Scaffold Systems. *Journal of Constructional Steel Research*. 2011, 67 (4): 576–584.
- [9] L. Li, Z. Kangzhe, Z. Shoufei. Research on the Mechanical Character of Node in Cuplok Scaffolding. *Sichuan Building Science*. 2012 (03): 336–339.
- [10] C. Yonghong, C. Hui, Y. Wei. Treatment of Joints of Member Bars in Finite Element Analysis of Bowl-Shape-Fastener Scaffolding. *Construction Technology*. 2004 (02): 14–37.
- [11] D. Yongcan, M. Baozhong, Y. Na, L. Laijun. Factors Influenced the Safety of Cuplok Scaffolding. *Journal of Highway and transportation (application and technology)*. 2011 (11): 184–187.
- [12] H. Zhang, T. Chandrangu, K. Rasmussen. Probabilistic Study of the Strength of Steel Scaffold Systems. *Structural Safety*. 2010, 32 (6): 393–401.
- [13] Y.R. Chen, L.J. Liu, Y.C. Duan. Study on Safety Control of Costs and Application. *Advanced Materials Research*. 2013, 671: 2057–2062.
- [14] Y. Chen. Study on the Cuplok Steel Tubular Scaffolding Design and Construction Monitoring [D]. Chang'an University. 2011.
- [15] S. Wold, K. Esbensen, P. Geladi. Principal Component Analysis. *Chemometrics and intelligent laboratory systems*. 1987, 2 (1): 37–52.

Active control of structural vertical-vibration based on electromagnetic levitation technique

C. Xia & D.B. Fu

Fuzhou Planning Design and Research Institute, Fuzhou, China

S.K. Liu

Engineering Research Center of Maglev Technology, National University of Defense Technology, Changsha, China

ABSTRACT: This paper proposes a vertical-isolation device based on electromagnetic levitation technique, which is mainly composed of armature, electromagnet, coil winding and displacement sensors. The new device has a favorably capability in active control of vertical vibration, compared to the traditional vertical-isolation devices. The configuration department and operational principle of the device are firstly introduced. Then, the motion equation of Magnetically Levitated Isolation System (MLIS) is developed, and the active control methods of current are described. Finally, seismic response of a MLIS of typical frame column is numerical analyzed. The results show that the isolation device is able to greatly reduce the seismic responses of frame column. Meanwhile, the ordinary copper wire and insulation material are satisfied to the demands of the device on current.

Keywords: vertical-isolation device; magnetic levitation; active control; motion equation

In the past two decades, research efforts have been devoted to investigating the vertical-isolation technique of engineering structures and their application to the real structures. Several vertical-isolation devices which are composed of a series of basic components, like helical spring (Parvin and Ma 2001), air spring (Sugahara, Y. et al. 2007), and disk spring (Zhao, Y. M. 2008), have been developed. However, majority of these isolation devices belong to passive control. Due to the inherent uncertainty and randomness of earthquake, the performance of isolation devices, to a great extent, depend on their design parameters and character of earthquake. Therefore, it is necessary to study the active control technique of structural vertical-isolation devices.

Magnetic levitation technique is an emerging intelligent technique which integrating electromagnetism, electronic technique, control theory, and signal processing. The vibration control based magnetic levitation technique is to minimize the structural vibration with the virtue of magnetic force (Xia, C. et al. 2014). According to the source of magnetic force, the magnetic levitation technique is primarily categorized into permanent-magnet levitation, electromagnetic levitation, and hybrid magnetic levitation. The

later two techniques are widely applied in vibration control due to their favorably capability in active control (Bitterly, J. G. 1998; Bica, L. 2006; Ledezma-Ramirez, D. F. et al. 2012). Ahn et al. (1999) proposed a hybrid-type active vibration system that uses electromagnetic and pneumatic force. Mizuno et al. (2006) developed an active vibration isolation system using zero-power magnetic suspension. Emdadul Hoque et al. (2011) proposed a module-type three-degree-of-freedom vibration isolation system using modified zero-power control. However, the existent references have seldom referred to the application of magnetic levitation techniques in vibration control of building structures.

As such, this paper develops a new vertical-isolation device based on electromagnetic levitation technique. Compared to traditional vertical-isolation devices, the new vertical-isolation device have a favorably capability in active control of vertical vibration. In this study, the configuration department and operational principle of the vertical-isolation device are firstly introduced. Then, the motion equations and control algorithms of isolation system are developed. Finally, the seismic response of a MLIS of typical frame column is numerically analyzed.

1 VERTICAL-ISOLATION DEVICE BASED ON ELECTROMAGNETIC LEVITATION TECHNIQUE

1.1 Configuration department

Figure 1 is the vertical-isolation device based on electromagnetic levitation technique. The vertical-isolation device is mainly composed of armature, electromagnet, coiling and displacement sensors. The electromagnets are set on the upper side of armature, and fixed on the base through the supports. The armatures are placed on the top of base. The frame columns of superstructure are fixed on the armature. The displacement sensors are installed in electromagnets and armatures to measure the distances between the electromagnets and armatures for controlling the levitation force.

1.2 Operational principle

The operational principle of the vertical-isolation device is to control the structural vibration by adjusting the electromagnetic attraction. When the structure is subjected to random disturbance, the suspend gap between electromagnet and armature will change, which will lead to the balance between electromagnetic attraction and gravity broke. The purpose of active control is to minimize unbalance force by adjusting the electromagnetic attraction. The detail operational principles of the vertical-isolation device are described as follows.

In daily state (i.e. no earthquakes occur), the superstructure and armature are placed on the top of base. The device is not work.

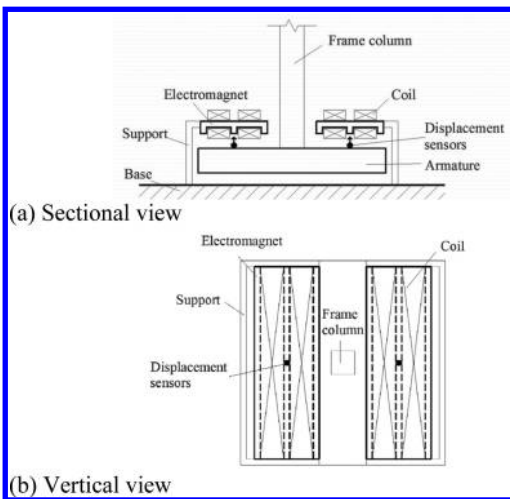


Figure 1. Vertical-isolation device based on electromagnetic levitation technique.

When the earthquakes occur, the earthquake warning signal is received by isolation device, the isolation device starts working, and the structure is levitated. When the earthquake waves arrive the structural base, the levitation force are controlled by real-time adjusting the current based on the suspend gap measured by displacement sensors. When the earthquake disappears, the isolation device complete working, and the superstructure and armature return to the top of base.

2 MOTION EQUATION OF ISOLATION SYSTEM

Figure 2 is the analysis model of isolation system based on electromagnet levitation technique.

According to the D'Alembert principle, the motion equation of isolation system is expressed by:

$$m\ddot{x}(t) + F(t) - mg = m\ddot{x}_g(t) \quad (1)$$

in which

$$F(t) = \frac{\mu_0 SN^2 [I(t)]^2}{4[x(t)]^2} \quad (2)$$

where $F(t)$ is the levitation force, m is the total mass of superstructure and armature; g is the acceleration of gravity (9.81 m/s^2); $x(t)$ is the suspend gap between electromagnets and suspensions; $\ddot{x}_g(t)$ is the absolutely ground acceleration in the vertical direction; μ_0 is the air permeability ($4\pi \times 10^{-7} \text{ H/m}$); S is the total area of magnetic pole; N is the number of turns; and $I(t)$ is the coil current, which can be formulated as:

$$\Delta U = RI + \frac{\mu_0 SN^2}{2x} \frac{dI}{dt} - \frac{\mu_0 SN^2 I}{2x^2} \frac{dx}{dt} \quad (3)$$

where ΔU is the control voltage; and R is the coil impedance.

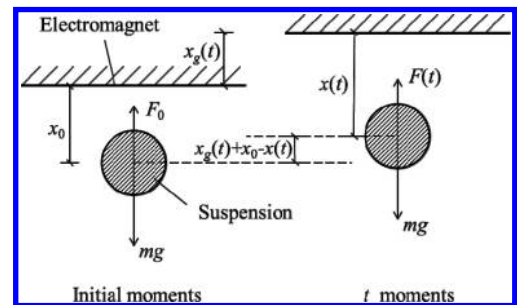


Figure 2. Analysis model of isolation system based on electromagnet levitation technique.

It is noted that the motion equation of isolation system in the initial moment can be described as

$$mg = F_0 = \frac{\mu_0 SN^2 I_0^2}{4x_0^2} \quad (4)$$

where F_0 is the initial levitation force; I_0 is the initial current, and x_0 is the initial suspend gap.

It is seen that the basic equations of vertical-isolation system based on electromagnetic levitation can be developed by uniting out Eqn. (1) to Eqn. (4).

3 ACTIVE CONTROL METHOD

The Eqn. (1) is a nonlinear equation. Therefore, a linearized motion equation of isolation model is constructed by using first order approximation of Taylor expansion. i.e.

$$m\ddot{x}(t) - \frac{\mu_0 SN^2 I_0^2}{2x_0^3} x(t) + \frac{\mu_0 SN^2 I_0}{2x_0^2} I(t) = m\ddot{x}_g(t) \quad (5)$$

The displacement stiffness $k_{xx} = -(\mu_0 SN^2 I_0^2 / 2x_0^3)$ and the current stiffness $k_{xi} = \mu_0 SN^2 I_0 / 2x_0^2$ are defined. Therefore, the Eqn. (5) can be rewritten as:

$$m\ddot{x}(t) + k_{xx}x(t) + k_{xi}I(t) = m\ddot{x}_g(t) \quad (6)$$

It is seen from Eqn. (6) that the vibration of suspension is related to ground motion time history, current time history, initial suspend gap, and initial current. When $x(t) = x_0 + x_g(t)$, the suspension is able to avoid vibrating. In this case, the Eqn. (5) is expressed as:

$$k_{xx}x(t) + k_{xi}I(t) = mg \quad (7)$$

$$I(t) = \frac{x_g(t) + x_0}{x_0} I_0 \quad (8)$$

It is seen from Eqn. (8) that the suspension is able to avoid vibrating by real-time controlling the current when the vibration excitation is known. However, the current is not able to real-time adjust according to the vibration excitation because the vibration excitation is unknown in actual situation. Therefore, the control algorithm of current is a key problem.

In order to minimize the vibration responses of suspension, several excellent control algorithms of magnetically levitated system would be chosen. So far, a lot of control algorithms of magnetic levitation system are developed, such as classical control algorithm (PID control, cascade control, feedforward

control), modern control algorithm (robust control, predictive control, variable structure control), and intelligent control algorithm (fuzzy control, expert control and neural network control).

4 SIMULATION ANALYSIS

A magnetically levitated system of typical frame column is chosen to analyze seismic response. The vertical load mg is 500 kN. The type of steel for electromagnet and armature is 1008#. The copper coil is wound in the electromagnet. The corresponding parameters of isolation system are: $S = 1.5 \text{ m} \times 0.1 \text{ m}$, $N = 500$, $x_0 = 50 \text{ mm}$, and $I_0 = 230.39 \text{ A}$.

The Elcentro Wave is chosen as the input excitant. The maximum value of acceleration is set as $0.65 \times 200 = 130 \text{ cm/s}^2$, according to the requirement for 8 degree protected earthquake intensity. The displacement time history, as shown in Figure 3, is obtained by the used of quadratic integral to the acceleration time history and cubic correction method.

In this study, a control method based on force balance is employed to control the vertical vibration of frame column (Xu. J.Q. 2012). The control force F_{con} is:

$$F_{\text{con}} = k_1(x - x_0) + k_2\dot{x} + F_d + F_0 \quad (9)$$

where k_1 and k_2 are the control parameters which need to set manually; and F_d is the interference force, which is equal to $m\ddot{x}_g(t)$ in the current situation.

The time interval of current control is set as 0.2 ms, and $k_1 = k_2 = 0$. Figure 4 is the control results of current time history. It is found that the maximum value of current output is 253.8 A. It shows that the ordinary copper wire and insulation material are satisfied to the demand of the device on current. Figure 5 is the absolutely acceleration

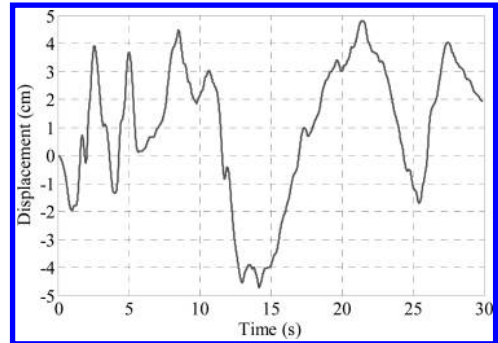


Figure 3. Vertical displacement time history of Elcentro wave.

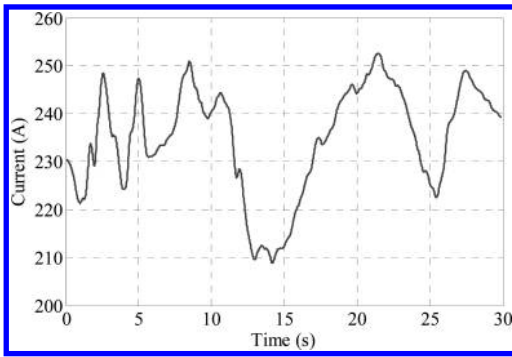


Figure 4. Current time history.

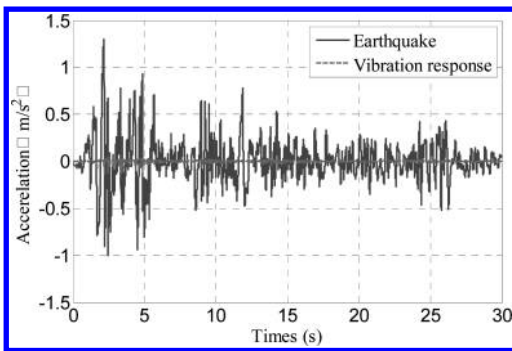


Figure 5. Vertical vibration response of frame column.

response of frame column. It is found that the maximum value of vertical acceleration is 13.4 cm/s^2 , which is 10.3% of the maximum value of earthquake wave (130 cm/s^2). It shows that the responses the isolation device is able to greatly reduce the seismic response of frame column.

5 CONCLUSIONS

In this paper, a vertical-isolation device based on magnetic levitation technique is designed. The motion equation of magnetically levitated system is developed, and the control algorithms of magnetically levitated system are described. The simulation analysis of a typical frame column is implemented. The result can be substantially summarized as follows:

1. The maximum value of vibration response is 10.3% of the maximum value of earthquake wave when a control method based on force balance is used. It is shown that the isolation device is able to greatly reduce the seismic response of frame column.

2. The maximum value of current output is 253.8A, which indicates that the ordinary copper wire and insulation material are satisfied to the demand of the device on current.

It is feasible to isolate the structural vertical vibration with the aid of electromagnet levitation technique. With high requirement of structural vibration control and rapid development of magnetic levitation technique, the magnetic levitation technique would be widely applied in vibration control of engineering structure.

REFERENCES

- Ahn, K.G., Pahk, H.J., Jung, M.Y., et al. 1999. A hybrid-type active vibration isolation system using neural networks. *Journal of Sound and Vibration* 192(4): 793–805.
- Bica, I. 2006. Advances in magnetorheological suspension: Production and properties. *Journal of Industrial and Engineering Chemistry* 12(4): 501–515.
- Bitterly, J.G. 1998. Flywheel technology: past, present, and 21st century projections. *Aerospace and Electronic Systems Magazine in IEEE*, 13: 13–16.
- Emdadul Hoque, D.M., Mizuno, T., Ishino, Y., et al. 2011. A three-axis vibration isolation system using modified zero-power controller with parallel mechanism technique. *Mechatronics* 21(6): 1055–1062.
- Kashiwazaki, A., Mita, R., Enomoto, T., et al. 2000. Three-dimensional base isolation system equipped with hydraulic mechanism. *Transactions of the Japan Society of Mechanical Engineers* 66: 2616–2621.
- Ledezma-Ramirez, D.F., Ferguson, N.S. & Brennan, M.J. 2012. An experimental switchable stiffness device for shock isolation. *Journal of Sound and Vibration* 331(23): 4987–5001.
- Mizuno, T., Takasaki, M., Kishita, D. et al. 2007. Vibration isolation system combining zero-power magnetic suspension with springs. *Control Engineering Practice* 15(2): 187–196.
- Morishita, M., Inoue, K. & Fujita, T. 2004. Development of three-dimensional seismic isolation systems for fast reactor application. *Journal of Japan Association for Earthquake Engineering* 4(3): 305–310.
- Parvin, A. & Ma, Z. 2001. The use of helical spring and fluid damper isolation systems for bridge structures subjected to vertical ground acceleration. *Electronic Journal of Structural Engineering* 1(2): 98–110.
- Sugahara, Y., Takigami, T. & Sampei, M. 2007. Suppressing vertical vibration in railway vehicles through primary suspension damping force control. *Journal of system design and dynamics* 1(2): 224–235.
- Xia, C., Fu, D.B. & Huang, B. 2014. Application of magnetic levitation technique in structural vibration control. *Earthquake Engineering and Engineering Dynamic* 34(1): 211–216. (in Chinese).
- Xu, J.Q. 2010. Magnetic suspension control method based on force balance. *Electric Machines and Control Application* 37(11): 20–23 (in Chinese).
- Zhao, Y.M., Su, J. Y., Zhou, X. Y., et al. 2008. Shaking table test and numerical analysis of vertical-isolated building model with combined disk spring bearing. *Journal of Building Structures* 29(6): 99–106 (in Chinese).

Remedy chromium ions contaminated soil by electrolysis method

Zhong Qiang Zhang, Zheng Gao, Na Liu, Yi Wei He, Zhen Wu, Ben Hui Lin,
Jia Ling Chen & Run Ye Ma

Department of Applied Chemistry, Hengshui University, Hengshui, P.R. China

ABSTRACT: The soil contaminated severely by chromium ions has been remedied by electrolysis method. The experiment showed that the mass of cathode graphite electrode increased with the increase of electrolysis time. It revealed that chromium ions in soil had been absorbed on the negative graphite electrode. The content of chromium ions in soil samples had been decreased to 19.45% at 20 mA current after 13 hours electrolysis. The result showed that the electrolysis method was effective to remedy chromium ions contaminated soil by decreasing content of chromium ions in soil. The good effect of soil remediation has been achieved on chromium ions contaminated soil.

Keywords: chromium; contaminated soil; electrochemistry; remedy

1 INTRODUCTION

Soil is not only one of the major natural resources for human beings, but also an important part of human ecological environment. With the development of industrial city, increase the city pollution and the number of agricultural chemical substances, the heavy metal ions polluted soil is increasingly serious^[1]. Data show that: the agricultural land area of heavy metal ions pollution is about 25 million square meters, and the heavy metal ions contaminated food is up to 12 million tons in China each year. The environmental monitoring system of the Agriculture Ministry of China has found that the contaminated agricultural products in farmland area exceeds 20% the total area, and among them the proportion of standard of heavy metal ions pollution of soil and crops are exceeded 80% from soil survey for 24 provinces/cities, 320 serious contaminated area and 82.23 million acres of field^[2]. The national survey of soil pollution survey in China released: The contaminated soil exceeds 16.1% of total land area of investigation (63 million square kilometers). The contaminated soil in the south was heavier than the north of China. The contaminated soil in Yangtze River Delta, Pearl River Delta, Northeast China and other old industrial areas were prominent, and a large range of the heavy metal ions contaminated soil exceeding the standard was found in southwest and south central area of China.

Chromium compounds especially Cr (VI) is one of important heavy metal ions pollutants. It is highly toxic to plants and animals^[3-5]. Human

would cause skin allergies, skin and mucosa ulcer perforation, erosive rhinitis and nasal septum perforation after chromium contacting. If a high dose of chromium ions was taken in, people were not only damaged on the oral, esophageal and gastrointestinal organs, but also kidney of human would be damaged when part of chromium compounds was absorbed into the blood. Therefore, chromium compounds is a strong toxic effect on human health^[6].

Electrokinetic remediation technology is known as “green remediation technology” because of its high efficiency, no two pollution, saving energy, and in situ remediation characteristics. When the electrode was inserted into the contaminated soil or groundwater, an electric field is formed by applying the direct current. The heavy metal ions in soil directed movement under the action of the electric field near the electrode, was enriched and absorbed on the negative electrode, and the contaminants was separated from soil^[7]. The migration mechanism of electrokinetic remediation of heavy metal ions contaminated soils included three modes such as electrodialysis, electromigration and electrophoresis^[8].

2 EXPERIMENTAL

2.1 *Materials and instruments*

All chemicals and reagents were used as received from commercial sources without further purification. Graphite electrode (made by myself). J1201-2 low voltage power supply (Shanghai Teaching

Instrument Factory). ZX38A/11 DC/AC resistance box (Shanghai Optical Instrument Factory). DH6-9023 Electric oven (Jintan City Guowang Experimental Instrument Factory). FA2204B Electronic balance (Shanghai Precision Instrument Factory). Current meter (Yueqing City Ying Electrical Appliance Co., Ltd.).

2.2 Process of experiment

2.2.1 Determination of moisture in graphite electrodes

A graphite electrode was put into electric oven at 105–120°C for a few minutes, then put into dryer to cool for 30 minutes, and weight the graphite electrode after it removed from the dryer. Repeated the above procedure until the sample electrode achieved constant weight. Seen from the data in Figure 1, along with the increase of drying time, the mass of graphite electrode tended to be a constant. When the graphite electrode was drier over 780 minutes, the mass was almost a fixed value. The final mass of the sample graphite electrode is 110.2663 g. It is the electrode real mass.

2.2.2 Removing the original metal ion in soil

The sample soil was sieved by 60 mesh sieve and weighted 8 kg exactly, then added 1883 mL distilled water in it. Two graphite electrode was respectively put into the soil as anode and cathode when the soil was fully soaked. The graphite electrodes were close contact with the soil, and the horizontal distance between two graphite electrodes was 20 cm.

The experimental device was installed according to the Figure 2. It maintained 12V voltage, and kept a constant current (20 mA) by regulating resistance box. After 1 hour, the cathode electrode was removed, gently rinsed with distilled water, and put into electric oven. The cathode electrode was dried at 105–120°C for 20–40 minutes, and then put into

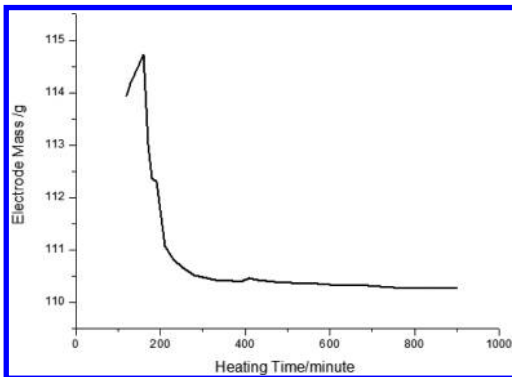


Figure 1. Determination of moisture in graphite electrodes.

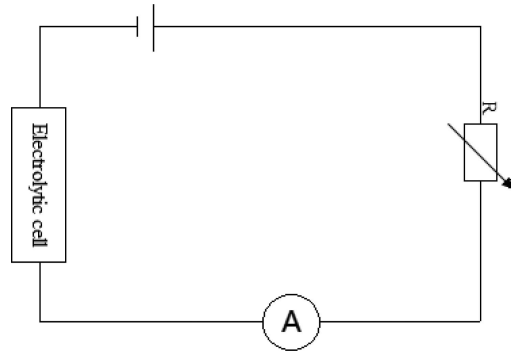


Figure 2. Experimental circuit diagram.

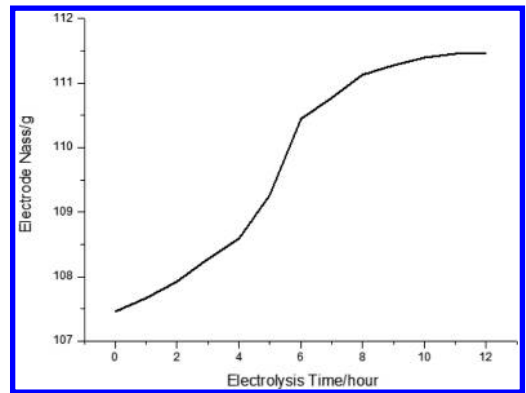


Figure 3. Change of cathode electrode mass with the increase of the electrolysis time.

the dryer to cool for 30 minutes and weighted. The above operations were repeated until the mass of cathode electrode achieved a constant value. The metal ions in the soil discharged continuously on the cathode graphite electrode, and deposited on it, so as to achieve the purpose to purify soil.

As shown in Figure 3, the mass of cathode electrode gradually increased along with the increase of the electrolysis time. The mass of cathode electrode tended to be a constant when the electrolysis time was up to 10 hours. It reached the maximum value 111.4794 g when the electrolysis time was 12 hours. The mass of sample soil is 110.2663 g, so the total mass of metal ions in sample soil is 0.1516 g/kg.

2.2.3 Remedy chromium ions from contaminated soil by electrolysis method

Another similar graphite electrode was treated as 2.2.1 processing. Its weight is 106.5113 g. The maximum chromium ions concentration is 300 mg/kg in the dry land according to “Chinese

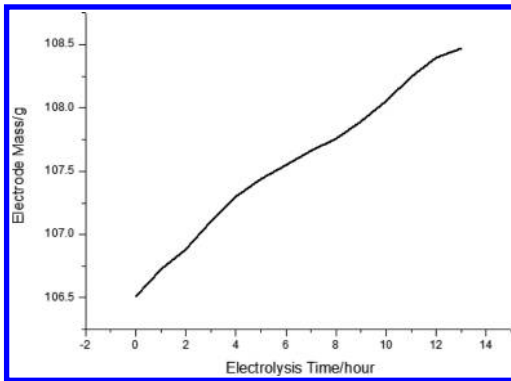


Figure 4. Change of cathode electrode mass in the electrolysis process.

environment quality standard in soil^[9]. $11.5465 \text{ g Cr}_2(\text{SO}_4)_3 \cdot 6\text{H}_2\text{O}$ was dissolved in 300 mL water. The concentration of chromium ions is 300 mg/kg in sample soil that had been treated in 2.2.2 procedure after the solution was sprayed evenly into the soil. Then a proper amount of distilled water was added to the soil. The electrode and another graphite electrode were placed in the electrolytic cell, and then the electrolysis circuit was connected as Figure 2.

As shown in Figure 4, the mass of cathode electrode was gradually increasing along with the increase of the electrolysis time, and the chromium ions discharged at the cathode and deposited in it as elementary substance. The mass of electrode is 108.4686 g after 13 hours electrolysis.

The mass of precipitation of chromium: $108.4686 - 106.5113 = 1.9573 \text{ g}$

The mass of chromium sulfate was converted: $[1.9573 \div (52.00 \times 2)] \times 500.31 = 9.4159 \text{ g}$

The percent of precipitation of chromium sulfate: $(9.4159 \div 11.5465) \times 100\% = 81.55\%$

So, the chromium ions in soil samples was reduced to 19.45% after 13 hours electrolysis.

3 CONCLUSION

Chromium ions contaminated soil was remedied by electrolysis method with graphite electrode in this paper. The experiments shows that the mass of cathode electrode was gradually increasing along with the increase of the electrolysis time, and the

chromium ions discharged on the negative cathode and deposited in it. The chromium ions in soil decreased to 19.45% at 20 mA current after 13 hours electrolysis. Good remediation result was achieved at chromium contaminated soil. In addition, it was operation simple, convenient, easy to obtain the required equipment, to treat heavy metal ions contaminated soil by electrolysis methods. The heave metals ions pollutants turning to elementary substance and soil is easy separated between each other, and heavy metal elementary substance can be used as a resource re-use, too. The purpose of environmental governance would be achieved.

ACKNOWLEDGEMENTS

Science and technology plan project of Hebei Province (No. 13211116).

REFERENCES

- [1] Ze Yi Zhou. Heavy metal pollution and control in China vegetable [J]. The resources and ecological environment of dynamic network, 1999, 10(3):21–27.
- [2] Qi Xing Zhou, Yu Fang Song. Principles and methods of remediation of contaminated soils [M]. Beijing Science Press. 2004.
- [3] Yi Bo He. Remediation progress on technology of heavy metal contaminated soil [J]. Guangzhou environmental chemical, 2006, 21(4):26–27.
- [4] XueJun Quan, Huai Qin Tan, You Cai Zhao, et al. Detoxification of chromium slag by chromate resistant bacteria [J]. Journal of Hazardous Materials, 2006, 137:836–841.
- [5] Ting Quan Pei, Liao Wang, Shan Zhong, et al. The soil Cr pollution characteristics and treatment analysis on typical simple landfill of chromium residue [J]. Journal of environmental engineering, 2008, 2(7): 994–999.
- [6] Qi Xing Zhou. Soil quality guidelines related to combined pollution of chromium and phenol in agricultural environments [J]. Human and Ecological Risk Assessment, 1996, 2:591–607.
- [7] Xia, Zhou. Remediation of heavy metal contaminated soil solutions [J]. Guangdong agricultural science, 2010, 12:158–160.
- [8] Cheng Li Chen, Min Liao. Research on heavy metal contaminated soil remediation technology progress [J]. Guangdong Trace Elements Science, 2004, 11(10): 1–2.
- [9] 《The environmental quality standards to soil》 (GB 15618–1995).

Statistical analysis of urban mass transit accidents and safety countermeasures study

Yan Rong Fu & Ya Dong Meng

College of Automobile and Transportation, Tianjin University of Technology and Education, Tianjin, China

ABSTRACT: Urban mass transit safety is one of the key fields of current research at home and abroad. Urban mass transit accidents can not only cause a large number of casualties, but also cause economic loss and large area of traffic jam. Therefore, urban mass transit safety management has important theoretical and realistic significances. Statistical analysis of urban mass transit accidents with casualties in recent ten years was done in this paper. Characters of urban mass transit accidents were summarized, reasons for accidents were analyzed. Suggestions and relatively advanced urban mass transit safety management methods were given to provide the bases and references for accident prevention and safety management.

Keywords: urban mass transit safety; statistical analysis; countermeasures study

1 INTRODUCTION

Urban mass transit safety problem has drawn high attention from governments and all walks of life all around the world, and has been incorporated into the national security strategy of the category. Establishing a perfect safety management system, improving the ability of urban mass transit system against major accidents and disasters, and ensuring the safety of rail transit have become a primary problem in rail transit construction and operation^[1].

Urban mass transit accidents happen frequently with various types, increased number of casualties, serious economic loss and big social influence in China in recent years. Although accidents happened with uncertainty and contingency, but the common characteristics and inherent law of the accidents were summarized through the statistical analysis of all the urban mass transit accidents happened from 2003 to the end of 2013. This will provide the bases and references for accident prevention and safety management in the future.

There's no authority statistics department to do the related statistics of urban mass transit accidents in China at the moment. Accidents with casualties have higher risk level and larger sphere of influence in all types of accidents. They are more serious and representative at the same time. The collected accidents happened in the construction and operation of urban mass transit in domestic with casualties from 2003 to the end of 2013, totally 77 cases happened in 19 cities, including Beijing, Shanghai, Guangzhou and Shenzhen. The

cases in this paper are mainly from the public news reports, comprehensive news websites and the city subway company websites.

2 STATISTICS ANALYSIS OF ACCIDENTS

Numerous accidents were analyzed comprehensively mainly from the accidents area distribution, annual distribution, casualties, types and so on. The development trend, prone areas, prone types and severity of accidents were obtained, which explained the necessity and urgency of effectively conducting the accident prevention and safety management^[2]. Thus finding reasons for accidents scientifically, comprehensively and objectively, and then do a good job in the prevention and control of the accidents specifically.

2.1 *Accidents areas distribution*

Statistical analysis of the urban mass transit accidents with casualties in recent ten years was done. Area distribution is as shown in [Figure 1](#). The statistical result shows that, the collected accidents were distributed in 19 cities, mainly including Shanghai, Beijing, Shenzhen, Guangzhou and Nanjing, in which urban mass transit was developed earlier or developed rapidly in recent years. The frequency of accidents was high in the earlier developed cities mainly because of experience lack of construction, operation and management, and lack of referential experiences from other cities in the early stage of development. Meanwhile the

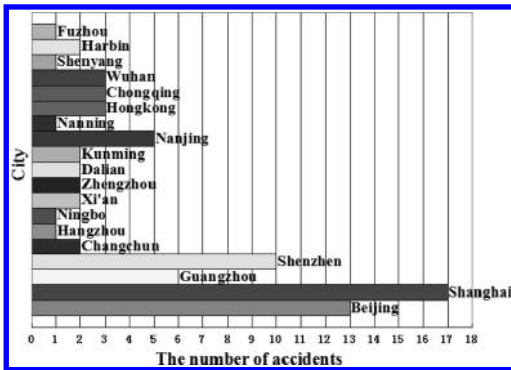


Figure 1. Areas distribution of urban mass transit accidents.

level of domestic technology was limited. Except for the lack of experience, less attention and bad management were also important reasons for the high frequency of accidents in rapidly developed cities.

2.2 Accidents annual distribution

Statistical analysis of the urban mass transit accidents with casualties in recent ten years was done. Annual distribution is as shown in Figure 2. The statistical result shows that, with the rapid development of urban mass transit in China, more and more cities built urban mass transit. At the same time, accidents with casualties were more and more, and the probability of accidents was increasing year by year, it reached the maximum in 2013. In recent years, more and more cities realized that urban mass transit played a large role in urban development, and sped up the construction of urban mass transit. There were some issues happened in the process of construction and operation, such as caught up the deadline, ignored details, nonstandard management, undemanding regulations, unclear responsibilities, poor staff training and so on. They were also main reasons for accidents.

2.3 The number of accident casualties

Statistical analysis of the urban mass transit accidents with casualties in recent ten years was done. The number of casualties is as shown in Figures 3 and 4. The statistical result shows that, with the rapid development of urban mass transit, the number of deaths in the accident tend to increase slowly. But there is a big change in the number of injuries. The numbers of injuries were more than 300 in 2009 and 2011 because of the major accident of railway. Through the analysis of accident

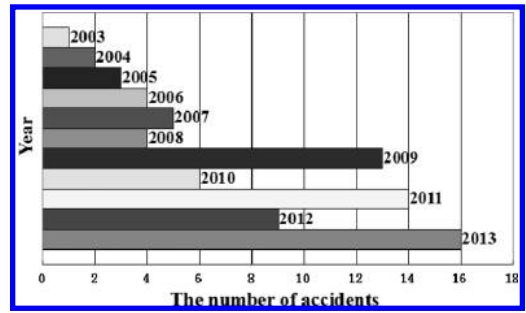


Figure 2. Annual distribution of urban mass transit accidents.

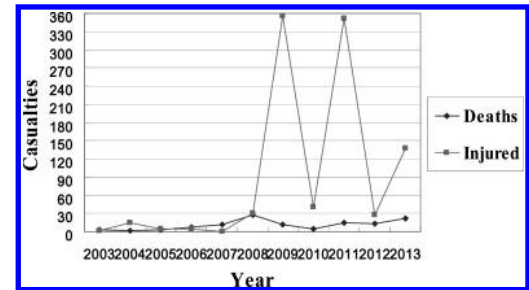


Figure 3. Urban mass transit accidents casualties.

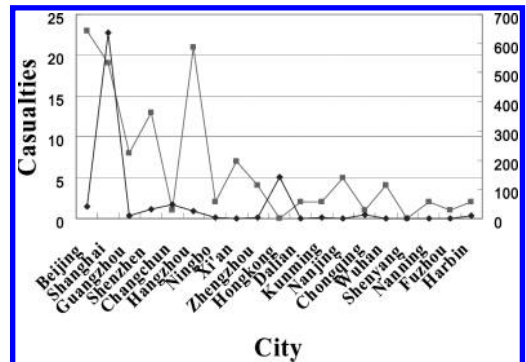


Figure 4. Urban mass transit accidents casualties in different area.

numbers, whether the regional distribution or the annual distribution, it shows that the severity of urban mass transit accidents is rising.

2.4 Accident types

Statistical analysis of the urban mass transit accidents with casualties in recent ten years was done. The number of casualties is as shown in Figure 5. The statistical result shows that, in all the accidents, engineering accidents accounted for more than

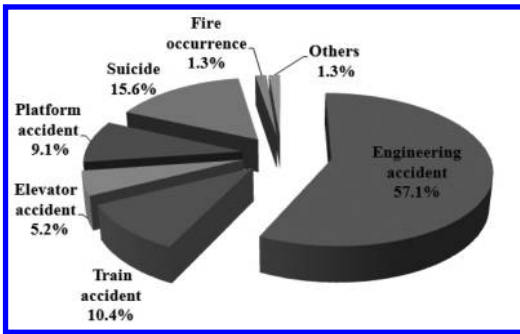


Figure 5. Urban mass transit accidents types.

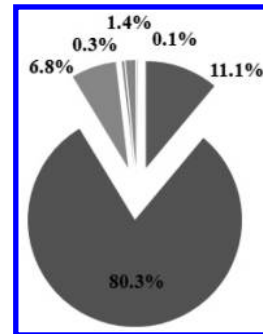


Figure 7. The proportion of injured in all urban mass transit accident types.

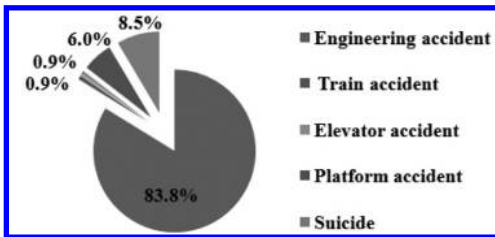


Figure 6. The proportion of deaths in all urban mass transit accident types.

half; the second was the suicide, accounted for 19%. Compared with foreign countries, fire occurrence cycle is longer and frequency is lower in China. Urban mass transit terrorist attacks are almost zero. Figure 6 and Figure 7 show that, in all types of urban mass transit accidents, there is the largest number of deaths in engineering accident, then the suicide; while there is the largest number of injuries in train accident, then the engineering accident.

Due to the late beginning of urban mass transit in China, lack of experience made engineering accidents the highest occurrence probability and the deadliest type of accidents. There were other reasons as well, including deficient survey of hydrology, geology and underground pipelines, insufficient predictive ability, imperfect emergency plan, rush deadlines and nonstandard management. Therefore, the prevention and safety management of engineering accidents are of uppermost priority in the management of urban mass transit safety.

Urban mass transit becomes the backbone of public transport due to the characteristics of large capacity and high density. Because of this, train accident becomes the highest occurrence probability and the deadliest type of accident. Therefore, prevention and safety management of train accident is the focus of operation and management for urban mass transit.

With the development of the society, the pace of life in the city speeds up, and the suicide becomes an

extremely complicated social phenomenon because of all the stress from emotion, family, health, interpersonal relationship, work and so on, which also makes the suicide in urban mass transit is on the rise. This kind of accident is unpredictable and has the characteristic of high mortality.

3 COUNTERMEASURES AND SUGGESTIONS FOR THE MANAGEMENT OF URBAN MASS TRANSIT

3.1 Establish complete safety management system

Provide direction to establish and implement safety management system by definite security policy and regulations. Achieve the goal of safe operation by developing, implementing and maintaining a safety management system, including applying efficient safety management procedures, and giving responsibility for operation staff.

3.2 Implement safety production responsibilities

According to the principle of “longitudinal to the end, transverse to the edge”, the relevant enterprises, departments, and subordinate groups must sign the SAFE PRODUCTION AND MAINTAINING STEADY LIABILITY AGREEMENT, and implement safety production responsibilities in accordance with the principle of “local management”. The safety supervision director is responsible for regional safety, and carries out the regional hazard remediation work.

3.3 Pay high attention to technical reform

Pay high attention to technical reform, pursue the full implementation engineering of removing hidden dangers, continuously improve the technical level of equipment and the reliability of vehicles.

3.4 Use operation information management system

Use a fully-fledged information management system, integrate and rebuild the system combined with local characteristics to provide a firm protection for accurate operation and safety management.

3.5 Strengthen emergency management drills

Further refine the emergency management system. The emergency action plan involves the establishment of emergency organizations at all levels, early warning mechanisms, emergency response, recovery measures, etc. Striving to improve emergency security work all-around and different level. Strengthen complicated emergency solving ability, constitute the program of emergency, and conduct the related drilling strictly, which involving the station fire, fracture of the steel rail, train rescue and so on.

4 CONCLUSIONS

Since the history of urban mass transit in China is very short. Compared with other developed countries, it is relatively backward for the safety problems study and the Security system construction. There are some outstanding problems existing in China domestic urban mass transit: lack experience of planning, design, construction and operation; each sides cannot be coordinated; low standard; relevant laws and regulations is not sound; safety facilities and equipments are imperfect; inadequate investment; safety supervision management system, accident prevention system and emergency

treatment mechanism are not sound; populace safety consciousness is weak and so on.

In order to strengthen the safety management of urban mass transit, we should strengthen daily safety training for the staff and passengers, improve the operating environment, create a good atmosphere, improve the safety management laws and policies, strengthen scientific management and safety management, establish and improve the long-term mechanism of urban mass transit safety supervision and management, enhance safety capacity for urban mass transit operation, improve the capacity for emergency rescue and relief work. In a word, it is primary to establish a urban mass transit security system which is fit for our country.

ACKNOWLEDGEMENTS

The corresponding author of this paper is Yanrong Fu. This paper is supported by Tianjin High School Science & Technology Fund Planning Project, 20120426.

REFERENCES

- Dongsheng, Xie, Mingyang, Wang & Hao, Lu, 2010. Accidents Statistics and Analysis of Subway Engineering. *EACSP 2010 (Beijing)*:205–209.
- Jingjing, Chen. 2010. Analysis on Grave Accidents and Disasters in Urban Rail Tran-sit Operation. *Urban Mass Transit* 5(5):41–45.
- Xiaoyu, Zheng, Su, Liu & Qi, Zhang, 2012. Research on the Safety and Reliability of Urban Mass Transit Operation Based on the Statistical Analysis of Accidents. *Safety and Environmental Engineering* 1(1):90–94.

Study of minimum base shear on design seismic code

Johnny Setiawan

Parahyangan Catholic University, Indonesia

Iswandi Imran

Civil Engineering, Bandung Insitute of Technology, Indonesia

ABSTRACT: As the world move to the accomplishment of Performance Based Engineering philosophies in seismic design of civil engineering structures, many modern seismic design codes adopt seismic design provisions of IBC 2012/ASCE 7-10. As compared to the previous version, several major modifications have been included in the ASCE 7-10. The code now requires a minimum base shear in analysis.

This paper aims to study the differences in the results of analysis with “minimum base shear” provision and without “minimum base shear” provision with Respons Spectrum Analysis (RSA), Linear Time History Analysis and Non Linear Time History Analysis (NLTHA).

A comparative study shows that ASCE 7-10 with “minimum base shear” provision can ensure performance level as expected, rather than “without minimum base shear” provision give poor performance level, especially in high-rise building classification. Concern the “minimum base shear” provision of the ASCE 7-10 will make structural design become uneconomical was not proven because it doesn't have a significant impact on the result, especially for building with low-rise building classification.

Keywords: minimum base shear; Respons Spectrum Analysis (RSA); Non Linear Time History Analysis (NLTHA); ASCE 7-10

1 INTRODUCTION

Many country adopted seismic design provisions of ASCE 7-10. As compared to the previous version, several major modifications have been included in the ASCE 7-10. The code now requires a minimum base shear in analysis.

It is found that the responses of tall buildings have very complex behavior during earthquake action. It is common for the response of a tall building to strong ground shaking to be heavily influenced by complex dynamic behavior, including the impacts of higher modes. Minimum base shear parameter make analysis more conservative.

Three buildings with classification low-rise, medium-rise and high-rise are analyzed with “minimum base shear” provision and without “minimum base shear” provision with Respons Spectrum Analysis (RSA), Linear Time History Analysis and Non Linear Time History Analysis (NLTHA).

Analytical evaluation of acceptance criteria for buildings designed using nonlinear response history analyses in accordance with ASCE 7-10. Design criteria in these standards present different means to determine design demands, depending on the number of ground motion records used in analysis. In this paper 5 ground motion records

are used, the most common approach presently adopted by structural engineers, the maximum of the values for each demand parameter is evaluated against limiting acceptance criteria that include strength and nonlinear deformation capacities.

2 DESCRIPTION OF ANALYSIS METHODS AND ACCEPTANCE CRITERIA

2.1 *The seismic response coefficient*

According to ASCE7-10, minimum base shear determined in accordance seismic response coefficient.

$$V = C_s W \quad (1)$$

The seismic response coefficient, C_s , shall be determined in accordance with:

$$C_s = \frac{S_{DS}}{\left(\frac{R}{I_e}\right)} \quad (2)$$

where

S_{DS} = the design spectral response acceleration parameter in the short period range as determined

R = the response modification factor
 I_e = the importance factor.

The value of C_s computed in accordance with (2) need not exceed the following:

$$C_s = \frac{S_{D1}}{T \left(\frac{R}{I_e} \right)} \quad (3)$$

C_s shall not be less than

$$C_s = 0,044 S_{DS} I_e \geq 0,01 \quad (4)$$

In addition, for structures located where S_1 is equal to or greater than 0.6 g, C_s shall not be less than:

$$C_s = \frac{0,5 S_1}{\left(\frac{R}{I_e} \right)} \quad (5)$$

where

S_{D1} = the design spectral response acceleration parameter at a period of 1.0 s

T = the fundamental period of the structure(s)

S_1 = the mapped maximum considered earthquake spectral response acceleration parameter.

2.2 Analysis procedure

2.2.1 Equivalent static analysis

All design against seismic loads must consider the dynamic nature of the load. However, for simple regular structures, analysis by equivalent linear static methods is often sufficient.

This is permitted in most codes of practice for regular, low- to medium-rise buildings. It begins with an estimation of base shear load and its distribution on each story calculated by using formulas given in the code. Equivalent static analysis can therefore work well for low to medium-rise buildings without significant coupled lateral-torsional modes, in which only the first mode in each direction is considered.

2.2.2 Response spectrum method

The representation of the maximum response of idealized single degree of freedom system having certain period and damping, during earthquake ground motions. The maximum response plotted against of undamped natural period and for various damping values and can be expressed in terms of maximum absolute accelerations, maximum relative velocity of maximum relative displacements.

Where a design response spectrum is required by this standard and site-specific ground motion procedures are not used, the design response spectrum curve shall be developed as indicated in Figure 1.

2.2.3 Time history method

It is an analysis of the dynamic response of the structure at each increment of time, when its base is subjected to a specific ground motion time history. Selected ground motions can be different than target response spectrum determined from seismic hazard analysis. Therefore, records are scaled by single factor scales to have their mean spectral accelerations complied with target spectrum. The seismic resistance design codes recommend the selection of at least three or seven ground motion records, for the time-history analysis purposes, which shall be compatible to the design spectrum.

2.3 Performance evaluation based

The structural performance evaluation describes the principles for assessment whether a structural design satisfies the target performance level of the

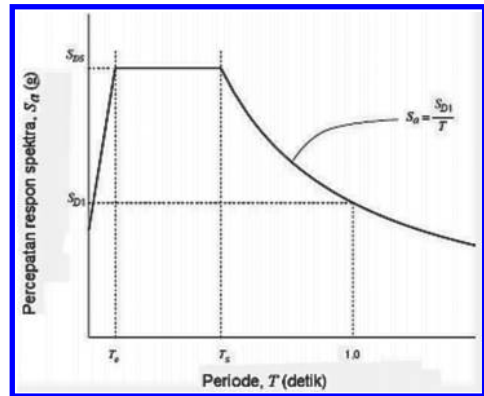


Figure 1. Design Response Spectrum (ASCE 7-10).

Table 1. Performance evaluation based on inter-story drift ratio (ATC-40).

Interstory drift limit	Performance level			
	IO	DC	LS	SS
Max total drift	0.01	0.01–0.02	0.02	0.03 Vi/Pi
Min inelastic drift	0.005	0.005–0.015	No limit	No limit

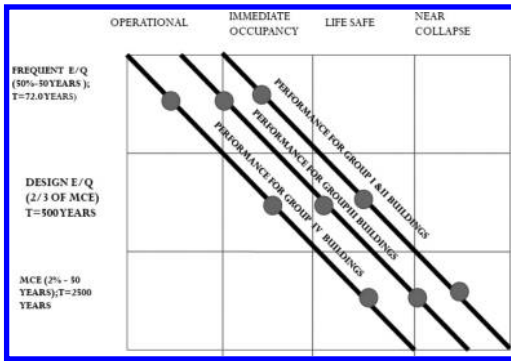


Figure 2. Performance levels (FEMA 303/NEHRP 1997).

building, which are common for every types of building structures.

Performance evaluation based on inter-story drift ratio (ATC-40) in Table 1. Performance evaluation based on structural component criteria (FEMA 356). FEMA 303/NEHRP 1997 recommended an assessment Figure 2.

3 METHODOLOGY

3.1 Model description

The pertaining structure of 10, 20 and 50 stories office building with the general form of plan shown in Figure 3. The height of typical floors are 4 meter. Base plan dimension in X 4 grid each 8 meter, and in Y 7 grid each 8 meter.

This paper aims to study the differences in the results of analysis with “minimum base shear” provision and without “minimum base shear” provision with Respons Spectrum Analysis (RSA), Linear Time History Analysis and Non Linear Time History Analysis (NLTHA).

3.2 Design response spectrum

Design response spectrum is required by this standard and site-specific ground motion procedures are not used, the design response spectrum curve shall be developed as in Figure 4.

3.3 Selection of ground motion records for time-history analysis

The seismic resistance design codes recommend the selection of at least three or seven ground motion records, for the time-history analysis purposes, which shall be compatible to the design spectrum.

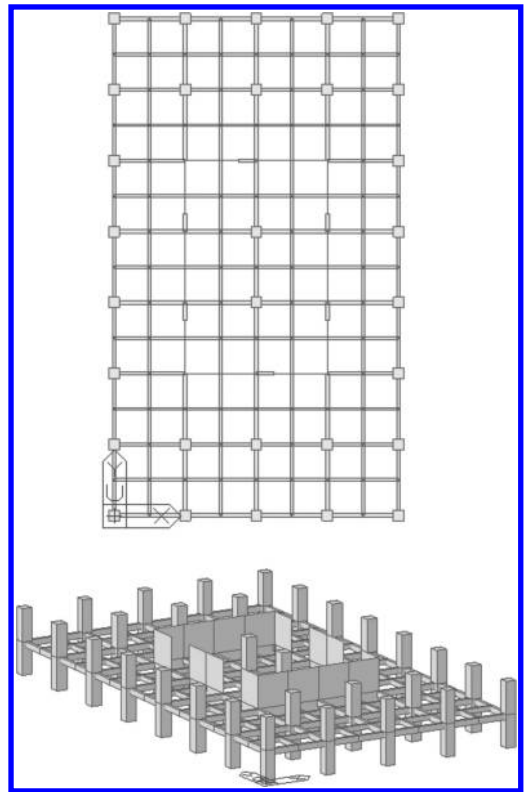


Figure 3. Layout model.

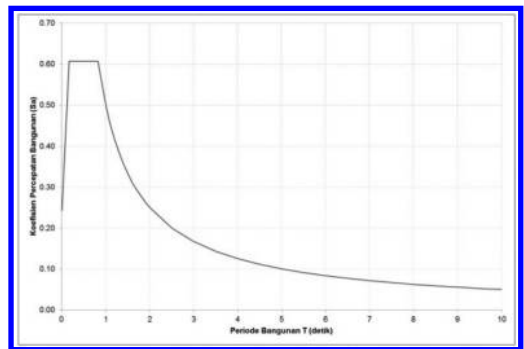


Figure 4. Response spectrum design.

A set of five ground motion records, as used in this paper, has selected from the PEER Strong Ground Motion Database. The selected ground motion records were recorded on firm soil, with no marks of directivity effects. The list of records is presented in Table 2.

Figure 5 and Figure 6 shows Scaled Spectrum and Scaled Ground Acceleration.

Table 2. PGA from the *Pacific Earthquake Engineering Research Center (PEER)*.

No	NGA	Event	Year	Station	Mag	Scale factor
1	179	Imperial Valley-06	1979	El Centro Array #4	6.53	0.9703
2	1605	Duzce-Turkey	1999	Duzce	7.14	0.6933
3	12	Kern County (Taft)	1952	LA-Hollywood	7.36	6.0771
4	1063	Northridge-01	1994	Rinaldi Sta	6.69	0.6679
5	–	Flores-Indonesia	1992	Maumere	7.80	0.6309

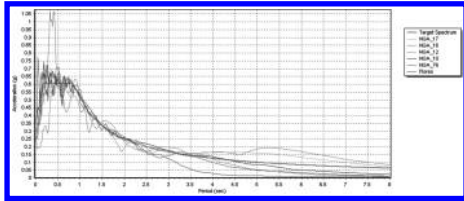


Figure 5. Target spectrum and scaled spectrum of selected ground motions.

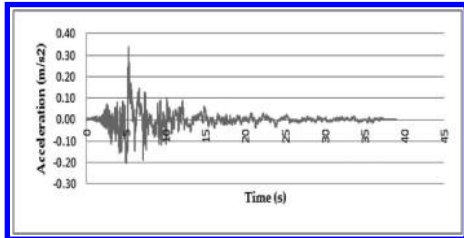


Figure 6. Scaled ground acceleration.

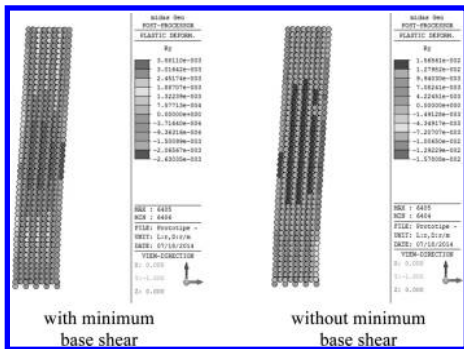


Figure 7. Prototype 50 story-element deformation.

4 RESULT

Analysis and design high-rise building “with minimum base shear” and “without minimum base shear” provision can provide good design result, but analysis “with minimum base shear” and “without minimum base shear” give different result in level performance as Figure 7–Figure 11.

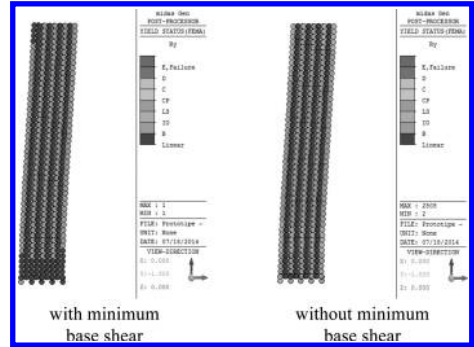


Figure 8. Prototype 50 story-yield status (FEMA).

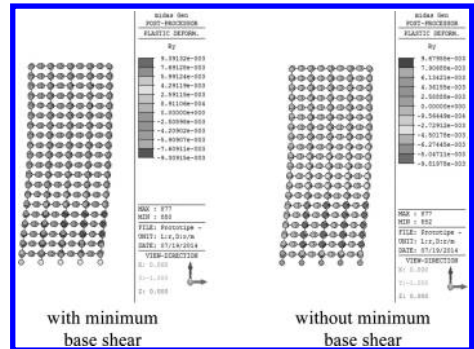


Figure 9. Prototype 20 story-element deformation.

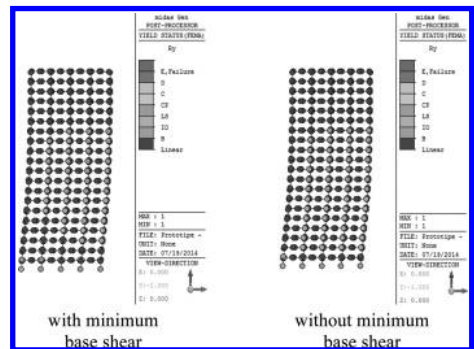


Figure 10. Prototype 20 story-yield status (FEMA).

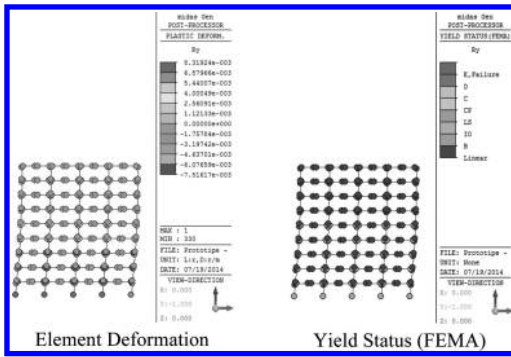


Figure 11. Prototype 10 story.

5 CONCLUSION

Analysis and design high-rise building “with minimum base shear” and “without minimum base shear” provision can provide good design result, but with “minimum base shear” provision can ensure good performance level as expected, rather than “without minimum base shear” provision give poor performance level.

For performance levels according to story drift ratios give good result as expected, Immediate Occupancy (IO) to Damage Control (DO), while analysis “without minimum base shear” give poor performance level, Life Safety (LS) to Structural Stability (SS). For performance levels according to structural component, “without minimum base shear” provision cause a lot of structural elements at the level Collapse Prevention (CP).

REFERENCES

- [1] ASCE 7-10. (2010). “Minimum Design Loads for Buildings and Other Structures”, American Society of Civil Engineers, Virginia.
- [2] ATC 40, (1996). *Seismic Evaluation and Retrofit of Concrete Buildings*, Volume 1, California, USA.
- [3] Andrew Fry J., Hooper J., Klemencic R. (2009). “PEER Design Case Study Building #1”.
- [4] Deierlein, G.G., A. Liel and C.B. Haselton, “Performance Assessment Through Nonlinear Time History Analysis”, EERI Technical Seminar.
- [5] FEMA 303, (1997). NEHRP Recommended Provisions for Seismic Regulations for New Buildings and Other Structures. Washington, D.C.
- [6] FEMA 356 (2000). Prestandard And Commentary For The Seismic Rehabilitation Of Buildings. Washington, D.C.
- [7] FEMA 368 (2000). NEHRP Recommended Provisions for Seismic Regulations for New Buildings and Other Structures. Part 1: Provisions and Part 2: Commentary. Building Seismic Safety Council. Washington D.C.
- [8] FEMA 450 (2003). NEHRP Recommended Provisions For Seismic Regulations for New Buildings and Other Structures. Part 1: Provisions and Part 2: Commentary. Building Seismic Safety Council. Washington D.C.
- [9] FEMA 451 (2006). NEHRP Recommended Provisions: Design Examples.
- [10] FEMA 451B (2007). NEHRP Recommended Provisions For for New Buildings and Other Structures: Training and Instruction Materials.
- [11] Los Angeles Tall Building Structural Design Council (2008). “An Alternative Procedure for Seismic Analysis and Design of Tall Buildings Located in the Los Angeles Region”.
- [12] MIDAS Information Technology Co., Ltd., 2013, “Midas/Gen User’s Guide”, MIDASoft, Inc., Livonia, USA.
- [13] MIDAS Information Technology Co., Ltd., 2013, “Analysis Manual, MIDASoft, Inc.”, Livonia, USA.
- [14] Park, R., and T. Paulay. (1974). “Reinforced Concrete Structures”, John Wiley and Sons, New York.
- [15] The PEER Center. (2010). “Guidelines for Performance-Based Seismic Design of Tall Buildings”.
- [16] The PEER Center. (2011). “Users Manual for the PEER Ground Motion Database Web Application”, The Pacific Earthquake Engineering Research Center, University of California, Berkeley.
- [17] Wilford M., Whittaker A., Klemencic R. (2008). “Recommendations for the Seismic Design of High-rise Buildings”, CTBUH.

Study of roadway layout in the σ_{HV} type in-situ stress field

Peng Lv & Xun Xi

School of Civil and Environmental Engineering, University of Science and Technology Beijing, Beijing, China

Li-Li Shao

School of Resources and Safety Engineering, China University of Mining and Technology, Beijing, China

Zheng-Xin Zhang

Jiaojia Gold Ore Mine of Shandong Gold Ore Mining Company Ltd., China

ABSTRACT: Through collecting the measured in-situ stress data from six deep mines, the in-stress fields of these deep mines are analyzed. The results show that with the depth of mining increasing, the vertical stress increases as the intermediate principal stress. The roadway layout cannot be based on the principle of maximum horizontal stress in σ_{HV} in-situ stress field ($\sigma_H > \sigma_v > \sigma_h$). Through analyzing the three-dimensional stress state of the circular roadway based on the generalized plane theory and the stress coordinate transformation, the influencing factors of the surrounding rocks stress are discussed. Numerical investigation by the software FLAC^{3D} were conducted on the distribution of plastic zone and the stress and displacement state of surrounding rocks in roadways with different directions. The results show that when the angle between the direction of roadway axis and the maximum principal stress is at $(\sin^{-1} \sqrt{(\sigma_v - \sigma_h)/(\sigma_H - \sigma_h)} - 30^\circ, \sin^{-1} \sqrt{(\sigma_v - \sigma_h)/(\sigma_H - \sigma_h)})$, the state of the surrounding rocks in roadway is optimal.

Keywords: in-situ stress; roadway layout; FLAC^{3D}

1 INTRODUCTION

In-situ stress is natural stress in the formation of the earth, which is the main force that leads to deformation and destruction. When designing a mine, to gain a better knowledge of in-situ stress for specific project area is vital for a reasonable display of the whole mine (Cai 2002). The in-situ stress varies with the change of depth. It shows big differences for in-situ stress in shallow and deep part. GaiYi and his colleagues founded the concept of critical depth. For the part above the critical depth, the horizontal stress is larger than vertical stress. And the part under the critical depth, the horizontal stress is smaller than vertical stress. However, the critical depth is various in different countries. In South Africa, it is 500 m; in the USA, it is 1000 m; in Greenland, it is 200 m (Chen 1990). And for China, there is no standard statistics to give the scale of critical depth. However, in some mines such as Huafeng coal mine and Panxi coal mine, the survey results have shown the situation that the horizontal stress is larger than vertical stress (Wei et al. 2013, Kang et al. 2007).

Decades ago, English and Australian scholars proposed the maximum principle stress theory to

design and support roadways. They put forward that in-situ stress has minimum influences to stability of roadways when the roadway direction is parallel to the maximum principle stress. Dong pointed out that the theory cannot give right direction of roadways when the vertical stress is larger than maximum horizontal stress (Dong 2000). Sun and his colleagues put forward that when the vertical stress is the medium principle stress, the roadway direction has an angle to the maximum horizontal stress, but they didn't give any relative explanation or the range of the angle (Sun 2010).

2 THE TYPE OF IN-SITU STRESS OF CHINA MINES

There are three types of in-situ stresses on the basis of numerical relation between horizontal stress and vertical stress. The in-situ stresses are as following:

$$\sigma_H \text{ type: } \sigma_H > \sigma_h > \sigma_v$$

$$\sigma_{HV} \text{ type: } \sigma_H > \sigma_v > \sigma_h$$

$$\sigma_v \text{ type: } \sigma_v > \sigma_H > \sigma_h$$

Table 1. Statistics of in-situ stress from some mines.

Series	Mine	Depth of measure point/m	Total number of measure points	Percentage and number of σ_H type measure points	Percentage and number of σ_{HV} type measure points	Percentage and number of σ_V type measure points
1	Linglong Gold Mine	250–970	18	4,22.2%	14,77.8%	0,0
2	Jinchuan Mine II	580–790	10	1,10.0%	9,90.0%	0,0
3	Xuzhou mining area	810–1176	14	6,42.9%	8,57.1%	0,0
4	Huainan mining area	500–1000	19	2,10.5%	16,84.2%	1,5.3%
5	Jincheng mining area	135–488	62	20,32.2%	37,59.7%	5,8.1%
6	Xinwen mining area	790–1220	9	0,0	7,77.8%	2,32.2%

In shallow crust, vertical stress is usually the minimum principle stress, and occasionally, it is the medium principle stress, and rarely, it is the maximum principle stress. With the increasing depth of excavation, the in-situ stress changes obviously. The in-situ stress layout situation in our mines is gained through the analysis of the statistics from some of the main mining communities (Cai et al. 2010, Cai et al. 1999, Zhang et al. 2012, Liu et al. 2012, Kang et al. 2009, Kang et al. 2007).

By analyzing the data from Table 1, it is obvious that with the mining depth increasing, the vertical stress has become the medium principle stress and even the maximum principle stress. In deep mining areas, σ_{HV} type has become main in-situ stress type to some degree. And σ_V type can only be seen in some special mine areas.

3 ANALYSIS OF 3-DIMENSIONAL ROADWAY STRESS STATE

Figure 1 shows the situation when roadway axial direction is not parallel to the direction of the maximum principle stress.

The original stress of the roadway under this situation is gained by stress transformation formula:

$$\begin{aligned}
 \sigma_{x'} &= \sigma_1 \sin^2 \alpha + \sigma_3 \cos^2 \alpha \\
 \sigma_{y'} &= \sigma_2 \\
 \sigma_{z'} &= \sigma_1 \cos^2 \alpha + \sigma_3 \sin^2 \alpha \\
 \tau_{x'y'} &= 0 \\
 \tau_{y'z'} &= 0 \\
 \tau_{x'z'} &= 0.5 \sin 2\alpha (\sigma_3 - \sigma_1)
 \end{aligned}
 \tag{1}$$

On the basis of method for generalized 2-dimensional problems, this issue can be seen as the combination of narrow-sense problem and double shear problem. The side pressure coefficient and shear stress have become key factor, which influences the roadway stress state. When

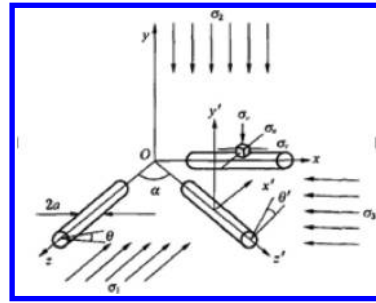


Figure 1. Roadway layout and force schematic diagram.

side pressure coefficient λ is 1, $\sigma_{x'} = \sigma_{y'}$. And then get $\alpha = \sin^{-1} \sqrt{(\sigma_2 - \sigma_3) / (\sigma_1 - \sigma_3)}$. The shear stress $\tau_{x'y'}$ increases when the angle α increases from 0 to 45°. It reaches its ultimate limit when $\alpha = 45^\circ$. And this value decreases with the increasing of angle α from 45° to 90°, and when α is 90°, it is 0. Due to the fuzziness of the influence of side pressure coefficient and shear stress to the roadway stress state, the stress state of surrounding rock cannot reach its optimum situation when simply define the side pressure coefficient as 1 and shear stress as 0. The author tries to give the optimum direction of roadways under 3-dimensional stress through theoretical analysis and numerical simulation.

4 LAYOUT OF ROADWAY UNDER IN-SITU STRESS OF σ_{HV} TYPE

When the in-situ stress is of σ_{HV} type, the angle of the direction of roadway to maximum horizontal stress direction is $\alpha = \sin^{-1} \sqrt{(\sigma_2 - \sigma_3) / (\sigma_1 - \sigma_3)}$ and the side pressure coefficient is 1. But the shear stress must be taken into consideration, so the optimum direction of roadway to the direction of maximum horizontal stress should be a certain angle.

In this part, Mohr-Coulomb round roadway excavation model is set up through FLAC^{3D}, a kind

of numerical simulation software. The regular pattern of optimum layout of roadway under σ_{HV} type in-situ stress is gained through the analysis of the distribution of elastic-plastic area and combining the 3-dimensional stress state of round roadways.

4.1 Numerical calculation model and parameters

FLAC^{3D} has become one of the most important tool in calculating rock mechanics problems since it was introduced by ITASCA company (Peng 2008). Mohr-Coulomb model is suitable for analyzing mechanical behavior of normal soil and rocks.

The numerical analysis model (Fig. 2) is 100 m in height, 100 m in width and 100 m in length. And it is divided into 19200 cubic units. The boundary of model is fixed. A round roadway of 5 m diameter is excavated. Set the maximum unbalanced force as 50 when calculation stops. In order to simulate the stress state and the influence by shear stress of roadway surrounding rock in deep strata under high stress, the stress state of rock mass underground is set as $\sigma_1 = 30$ Mpa, $\sigma_2 = 25$ Mpa, $\sigma_3 = 10$ Mpa (Table 2).

4.2 Simulation results and analysis

The boundary of the model is fixed. The elastic-plastic area distribution of roadways is a very important parameter which describes the stability of surrounding rocks. The simulation results of elastic-plastic area (Fig. 3) are gained when the angle of the roadway axial direction to the maximum horizontal stress varies from 0 to 90°.

By analyzing the simulation results, with the increasing of α from 0 to 60°, the plastic areas move from the four corners to roof and floor. Generally, the area of plastic is small when the angle is 30° and 45° and reaches its ultimate value when the angle is 60°. When the angle continue increases,

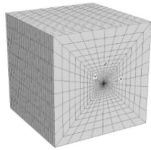


Figure 2. Numerical analysis model.

the area of plastic in roof and floor decreases and the area increases in the two walls of roadways. When the angle increases from 0 to 90°, the side pressure coefficient increases. The number $\lambda < 1$, when the angle is in the range of 0 to 60°; $\lambda = 1$, when the angle is 60°; $\lambda > 1$, when the range is 60° to 90°. The tangential stress increases from 0 when the angle increases from 0 to 45° and reaches the maximum value when the angle is 45°. And this value

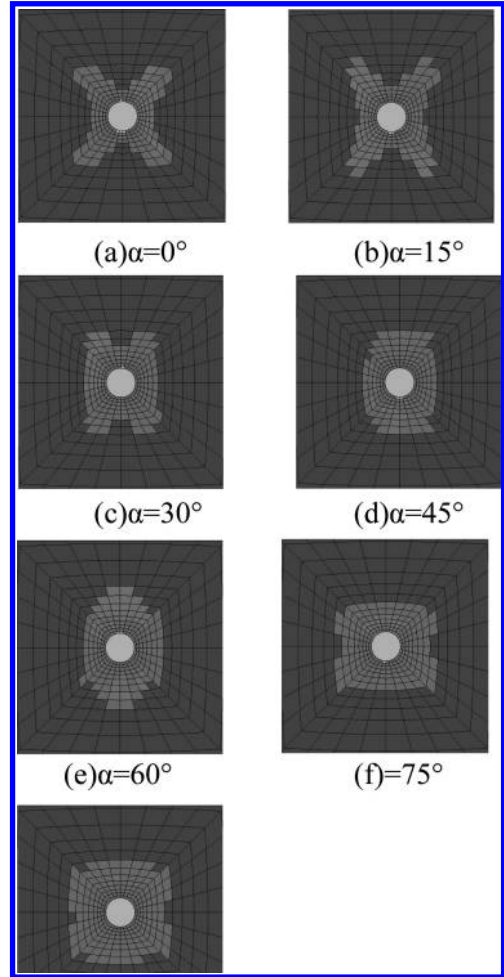


Figure 3. Simulation results of elastic-plastic area.

Table 2. Parameters of rock.

Density/ (kg · m ⁻³)	Bulk modulus/ GPa	Shear modulus/ GPa	Internal friction angle/(°)	Cohesion/ MPa	Tensile strength/ MPa
2500	2	1	30	2	2

decreases to 0 with the angle increases from 45° to 90°. Through overall consideration of plastic area and fracture area, it is obvious that the elastic-plastic states are better than other situation when the angle is 30°, 45° and 60°.

In other words, it reaches its optimum state when side pressure coefficient λ is close to 1 and less than 1 and the angle α is close to and less than $\sin^{-1} \sqrt{\sigma_V - \sigma_h} / \sigma_H - \sigma_h$.

This result is correspond to 2-dimension problems in which the side pressure coefficient λ is close to and less than 1 when the stress state of surrounding rocks is optimum. The author conducted several groups of simulation under different principle stresses and get the same results.

Obviously, the shear stress will influence the distribution of elastic-plastic areas in surrounding rocks. This is reflected in the situation that plastic area is not homogeneous when side pressure coefficient λ is 1. The influence of side pressure coefficient to the plastic area of surrounding rocks is much more obvious. The area is small when λ is close to and less than 1. So in order to get the optimum stress state of roadway under σ_{HV} type in-situ stress, the angle of roadway axial direction to maximum horizontal stress should falls in the range $(\sin^{-1} \sqrt{\sigma_V - \sigma_h} / \sigma_H - \sigma_h - 30^\circ, \sin^{-1} \sqrt{\sigma_V - \sigma_h} / \sigma_H - \sigma_h)$.

5 CONCLUSIONS

1. Currently, there are three types of in-situ stresses in the mines in our country which are σ_H type, σ_{HV} type and σ_h type. In those deep mines, the vertical stress is often the medium principle stress. To some degree, σ_{HV} type in-situ stress is the main in-situ stress type. And σ_V type can be seen in some specific mines.
2. With the increasing depth of mining, the vertical stress increases and gradually becomes the medium principle stress. The maximum horizontal stress principle is not suitable for the layout of roadways under σ_{HV} type in-situ stress.
3. Through the analysis of generalized plane strain theory and the transformation of stress coordinates under 3-dimensional stress state and numerical simulation with FLAC^{3D}, the plastic area of roadways under σ_{HV} type in-situ stress is small when the side pressure coefficient is close to and less than 1. The angle of roadway axial direction

to the maximum horizontal stress should falls in the range $(\sin^{-1} \sqrt{\sigma_V - \sigma_h} / \sigma_H - \sigma_h - 30^\circ, \sin^{-1} \sqrt{\sigma_V - \sigma_h} / \sigma_H - \sigma_h)$, which makes the layout of roadways better.

ACKNOWLEDGEMENT

This research work is supported by national technical task “The ‘12nd five year’ National key technology research and development program” (No. 2013BAB02B08).

REFERENCES

- Cai, M.F. 2002. *Rock mechanics and engineering*. Beijing: Science Press.
- Cai, M.F. et al, 1999. In-situ Stress Measurement at deep position of Jinchuan gold mine and distribution law of in-situ stress field in mine area. *Chinese journal of rock mechanics and engineering* 18(4): 414–418.
- Cai, M.F. et al. 2010. In-situ Stress Measurement at deep position of Linglong gold mine And Distribution Law Of In-situ Stress Field In Mine Area. *Chinese Journal of rock mechanics and engineering* 29(2): 227–233.
- Dong, F.T. 2000. The problem of the maximal horizontal geo-stress theory. *Rock bolt support* 3: 1–5.
- Chen P.N. 1990. *The assembly stress test data for the world*. Beijing: Seismological Press.
- Kang, H.P. et al. 2007. Research and application of in-situ stress measurement in deep mines. *Chinese journal of rock mechanics and engineering* 26(5): 929–933.
- Kang, H.P. et al. 2007. Research and application of in-situ stress measurement in deep mines. *Chinese journal of rock mechanics and engineering* 26(5): 926–933.
- Kang, H.P. et al. 2009. Research On In-situ Stress field in Jincheng Mining Area And Its Application. *Chinese journal of rock mechanics and engineering* 28(1): 1–8.
- Liu, Q.S. et al. 2012. Characteristics of in-situ stress field for deep levels in Huainan coal mine. *Rock and soil mechanics* 33(7): 2089–2096.
- Peng, W.B. 2008. *FLAC^{3D} practical tutorial*. Beijing: Mechanical Industry Press.
- Sun, Y.F. 2010. Effects of in-situ horizontal stress on stability of surrounding rock roadway. *Journal of china coal society* 35(6): 891–895.
- Wei L.G. et al. 2013. Technology of Once Blasting Large Cross Section Roadway Heading and Surrounding Rock Control in Over 1000 m Deep Underground Mine. *Coal science and technology* 41(2): 5–8.
- Zhang, G.F. 2012. In-situ stress measurements and analysis of action of geological structures of deep coal mines in Xuzhou. *Chinese journal of geotechnical engineering* 34(12): 2318–2324.

Study on the design of urban public facilities—take Hefei as an example

Bao Zhang & Bei Nan Hu

College of Architecture and Art, Hefei University of Technology, Hefei, Anhui, China

ABSTRACT: As a provincial capital with a history of over two thousand years, Hefei is surrounded by mountains and trees. It's a cordial and pleasant city, and it is changing day by day. With the rapid development of the process of the city, the construction of urban public facility in Hefei is entering a new phase. The paper will explore the public facilities in Hefei and make predictions for the future development trend from four main urban public facilities categories that are square, road, information and park facilities through cases analysis.

Keywords: industrial design; urban public facilities; Hefei

1 INTRODUCTION

Since ancient times, urban public facilities are essential equipment in people's public activities. In 1960s, urban public facilities first appeared in Europe as "Environment Facility" and it can be literally translated into "street furniture"^[1] or "city furniture"^[2]. Urban facilities, including street lamps, chairs, trash cans, bus stations, shop kiosks, telephone booths, signs, billboards, road guardrails and so on, are most used, most widespread and most closely connected with the crowd facilities products in cities^[3]. Divided according to use function, urban public facilities can be divided into two major categories. That is function and decoration facilities. With the deepening of urban functions, the variety and quantity of urban public facilities will become more and more. At the same time of increase in the number, the design value also increases apparently. As the provincial capital of Anhui, Hefei has a more than two thousand years history. Hefei is landscapes encircled and tree-lined, and its forest coverage is more than 40%. With the process of urban high-speed development, the construction of Hefei city public facilities also entered a new stage. The construction of urban public facilities of Hefei are also entering a new stage. The first generation "Hui wind newsstand" raised the curtain on majestic story, and the popular facilities product will put the story to a climax. This paper will explore the public facilities in Hefei and make predictions for the future development trend from four main urban public facilities categories that are square, road, information and park facilities through cases analysis.

2 STUDY ON THE DESIGN OF CITY SQUARE FACILITIES IN HEFEI

First of all, this paper studies Hefei train station square. Hefei Platform 1, Platform 2, station square and the waiting room were completed and opened in 1951 and the waiting room could accommodate more than 260 passengers. At that time, the station square of Hefei old train station still started with fundamental functions, such as stay, wait and so on. The materials of public facilities were mainly relatively cheap and durable cement and stone. There were no many other facilities and ad posters except wooden flagpoles, basic greening and a small number of stone benches. In order to meet the needs of the position and the function of Hefei, the new railway station in the early 80s improved greatly both form scale and function. The station square became crowded during the day and became splendid in the night. The materials of square ground mainly were marble and granite, which provided a lot of space for stay and wait, and the public facilities were relatively completed. Trash cans, signs, green barriers, chairs, ads, LED signs all had arrangement. But public facilities lacked structure characteristics and most were bought casually. Besides, function and performance is the only measurement, and the specificity of the visual and regional culture were little involved. During this period, the facilities of station square should be in the early stage of starting to think about design. Nowadays, station square is rebuilding completely and both image and function will improve greatly when completed and it both as the characteristics of transportation and assembly.

In addition, the design of city hall square is also representative. The city hall square of Hefei belongs to typical assembly city square, and it is the political center and it is the trade, finance and transportation network center of Hefei as well. The city square of Hefei, covering an area of 50000 square meters, began to construct in March 2000 and officially opened on May 1, 2001. The layout highlights “one point three axis”. “Cultural axis”, “technical axis” and “S natural axis”, which reflect characteristics of Hefei, organically combined into a central square—half is humanity and half is relaxation. There are many public facilities, such as pool, music fountain and sketches and so on. With the construction of station BRT, the traffic function of city square had been greatly improved. Numerous commercial squares in Hefei, for examples, Xintiandi plaza, Wal-mart square and Yintai plaza, are attached squares of commercial stores. Compared with others, the area of the square is small. But it attracts people through detail-oriented designs and cool-hunting effects. Facilities have various kind, chic shape, superior color, and the sculpture of streets, light posts of advertisements, deal of external wall, landscape decoration and lighting effects all are integrative designed.

3 STUDY ON THE DESIGN OF CITY ROAD IN HEFEI

With the development of city constructions, the road facilities of Hefei has been established in the early years of new China. It could be found the features of road facilities at that time from old photos. Modeling design, taking function as lead, reflected the thick solid feel. The surface of the facilities had plane decoration, which used the coating color as the main technique to distinguish. Although the earliest bus stop still used the design of waterproof cloth, its size was reasonable and its function was well. Generally speaking, the kinds of road facilities were very rare, and the green tree, basic traffic facilities, street lamp and bus stop are the all kinds of road facilities. Many people still concern about the Four Arched overbridged (now has been removed) which had been built in 1985. The intersection of Yangtze River middle road and Huizhou Avenue is one of prosperous sections. Van Lane overbridge, commonly known as Four Arched overbridge and ever stood here, is the first pedestrian bridge after reform and opening in Hefei. When the Four Arched overbridge was just built, many citizens went to there to visit and to take photos for memory. The Four Arched overbridge can be said to public facilities in the modern structure, material and form first appeared

in Hefei, and it is the milestone of Hefei public facilities.

Walking street is a rebound to dwindling vibrant street life. It not only is one of beautifying environment, but also it is the important means to promote the prosperity of business activities. Cultural and commercial walking street in Hefei Huaihe road, located in the center of the city, is the famous commercial street and the old street of humanities ceremony in history. The renovation project of Huaihe road which started in 1993 is the best line of transformation of old city. The modified walking street in 1998 becomes shopping, travel, culture, relax and catering an all-in-one modern cultural and commercial walking street. The public facilities of walking street include sculpted landscape, advertisement light box, sale kiosks, and chairs and so on. It has various kinds and different shapes, which is closely related with city characters of Hefei and has remarkable design and excellent making and it really becomes the window of the demonstration site. At the same time, it can study design rules from analyzing the bus waiting room and road police which are the representatives of road facilities. For example, because of heavy vehicles, big traffic, traffic jam during the rush hour and so on, the facilities of Yangtze River bus stop in the center area of Hefei has a long standing kiosk and the standing area is bigger as well. It uses ceiling design on structure, and uses stainless steel keel to shape. It is aluminum-plastic plate in outer space, and uses stainless steel square tube to connect with the ground at the bottom, and the middle of it is sunlamp to light in advertising light box. This bus station should be set public facilities for short rest to decrease the irritated mood when waiting for bus. Wuhu road is landscape road of Hefei, which is located near Baohe Park and Provincial library. It uses ceiling mental structure, but it will be more concise if it used black square tube as stanchion and the ceiling was liner shapes. There are many people on Wuhu road station during holiday and rush hours, so it should be set chairs at Wuhu road station in order to provide convenience for people.

4 STUDY ON THE CHANGES OF URBAN PARK FACILITIES IN HEFEI

Park is available to the public for touring, viewing, having a rest, carrying out scientific culture activities and exercise and other activities. And it has perfect facilities and good public green space. It also can improve ecology of city, prevent fires and take refuges. Hefei is a green ecological city. Up to now, the green land area of botanical garden in Hefei is 9085.5 hectares. The rate of

the city reached 40.2% and green coverage rate reached 5%, and the per capita public green area is 12.5 square meters. Statistics in 2013 show that the total of various kinds of parks in Hefei urban area reached 536. The Swan Lake Park and the Jade Lake Park belongs to the typical representatives of the comprehensive parks.

Swan Lake Park is located in the cultural district, officially opened to citizens free of charge in 2004. Except the artificial lake whose area is 1000 mu, the lake includes a man-made beach which is a “gold coast” and is 600 meters in length, shallow water recreation areas with cobblestones, all kinds of sculptures, gardens and facilities. Allusions related with water and sleek lines are the main designs of campus facilities. All kinds of facilities are created and constructed under the same theme, so under the premise that the function is good, the overall aesthetics and coordination degree of the Swan Lake Park are very high, and it was deeply loved by people.

The Jade Lake Park is located in Hefei economic-technological development area of University City, and Anhui University looked across the park, towards Hefei University of Technology. It is a key project of Hefei in 2006. Park covers an area of around two thousand mu, and 947 mu is the lake's area. The terrain slopes gently, and it both has the water and all kinds of trees. The natural scenery is beautiful. This area is divided into four zones which breaks the symmetrical uniform traditional layout and identifies the design concept of “humanity, ecology and landscape”. Besides, it uses many landscape elements, such as, mountain, water, city, forest and so on. It emphasis on the unity of the harmony between human and nature. Although it is artificial, it is like made by nature. The quiet style of the Jade Lake Park is also reflected in the campus facilities. Most use natural materials to create the ancient atmosphere. At the same time, it embodies the modern methods of gardening which combines Chinese classical methods through the deliberation of aesthetics and the composition of materials.

Figures, photographs, etc. can be in black/white or full color, but will be produced in the book in black/white only. Paste copies of the same size onto the typescript where you want them to appear in the text. Do not place them sideways on a page; however if this cannot be avoided, no other text (except the figure caption) should appear on that page. Figures, etc. should not be centered, but placed against the left margin. Leave about two lines of space between the actual text and figure (including caption). Never place any text next to a figure. Leave this space blank. The most convenient place for placing figures is at the top or bottom of the page. Avoid placing text between figures

as readers might not notice the text. Keep in mind that everything will be reduced to 75%. Therefore, 9 point should be the minimum size of the lettering. Lines should preferably be 0.2 mm (0.1”) thick. Keep figures as simple as possible. Avoid excessive notes and designations. Study on Urban Information Facilities' Change of Hefei

5 STUDY ON THE TREND OF URBAN PUBLIC FACILITIES IN HEFEI

The design of urban public facilities in Hefei is changing with each passing day. Whether it is a new technology innovation, popularization of new materials, implementation of a new plan, or the new urban fashion, Hefei which is the star of Anhui is going forward rapidly in fast channel. The development principles of urban public facilities of Hefei should comply with the following trend: it can show local characteristics, and meet the multiple needs of residents and tourists, meanwhile, it can embody the concept of low-carbon environment.

Regional culture has always been the most spirited social factor. Despite some typical cases mentioned above, it also can be easily found that the international style in urban area of Hefei. The same products and facilities increase to large numbers in urban communities, which are thrived in thousand times with no spread. As a big cultural province from ancient to modern time, Anhui explored the essence of regional culture, traditional culture and modern culture of Hefei, and decorated our life through the public facilities by the clever extraction of stylists. The numerous material and symbols in unique regional culture which is one of three characteristics of Anhui are waiting for the eyes of designers. The historical legends, cultural relics, traditional arts and diet, local customs and so on are also waiting for the designer to represent backgrounds. The marriage of the strategic layout in modern culture and regional metropolis will produce new sparks. Urban public facilities of Hefei should also be connected with the principles of saving and low-carbon environment. It not only can achieve environmental protection of “object” through materials, structure, process and so on, but also it can achieve environmental protection of “precise” through the use of facilities, experience of education, recycle and so on to make the whole life cycle of production, consumption and recycle be in good environmental state. At the same time, public facilities of Hefei should pay more attention to the new features which conform to automobile and digital ages. We should insist “people-oriented” rather than “car-oriented” in order to provide a friendly and orderly environment for

Hefei resident. Finally, urban public facilities' development of Hefei must put old man's general designs at a right height and invest heavily. General facilities are relatively weak at present, and taking care of all ages of society, offering them convenience and comfort also reflect the great love urban public facilities of Hefei.

6 CONCLUSION

Urban public facilities design connects with urban residents, city characteristics and many other factors. All these factors together drive it develop.

This paper studies on urban public facilities' design of Hefei, trying to look for pattern from the design change of representative products to explore the design road in the future.

REFERENCES

- [1] Christopher Alexander. 1979. *The Timeless Way of Building*: 155–193. New York: Oxford University Press.
- [2] Edmund Bacon. 1967. *Design of Cities*. Thames & Hudson.
- [3] Kevin Lynch. 1960. *The Image of the City*. MIT Press.

The application of conditional probability among Step-Stress Accelerated Life Testing

Heng Hui Guo, Chuan Ri Li, Kai Shan Wang & Yue Chan Pang
School of Reliability and Systems Engineering, Beihang University, Beijing, China

ABSTRACT: Due to the phenomenon that slow degradation exists in usage of material, accelerated life testing is needed to predict the lifetime of high reliability material. Step-Stress Accelerated Life Testing (SSALT) is currently most popular among the quantitative accelerated testing. Based on the character that the failures of each stress step are survived after all of the previous stress steps, this paper given a method to set and dispose data analysis of SSALT by employing conditional probability. Under the circumstance that the lifetime obeys Weibull distribution, a mathematical model to solve the conditional probability density function was established and the acceleration efficiency comparison results of step-down test and step-up test under different conditions were given. By stepwise analysis of failure and survival data, a likelihood function of selected acceleration model parameters of related material on the basis of conditional probability was established. Finally, an example of a product under electrical stress with Type-I Censored data, which is based on the inverse power law model, is given to estimate the parameters.

Keywords: conditional probability; acceleration efficiency; acceleration model parameters

1 INTRODUCTION

For a long time, the quantitative assessment of the high-reliability and long-life product has always been a technical problem in the field of reliability engineering. With the rapid development of science and technology and constantly improvement of the level of reliability, this problem is increasingly outstanding. For products of high reliability and long life, it mainly through accelerated life testing to evaluate lifetime. The Accelerated Life Testing (ALT) was employed to find out the life characteristic of long-life and high-reliability product. Among all the accelerated life testing methods, SSALT (step-up or step-down) is considered to be an important research direction because of its relative mature theory, the smaller sample size it required, quickly failed specimen saving test cost and time in a larger extent [1]. In the SSALT all specimen under testing have experienced the effects of all the previous stress steps, which means that all of the failures besides the first step occurs in the condition of they are survived after all of the previous steps. If the product's life obeys certain distribution under each different stress levels, the effect of the stresses may resulting in different test time in type-II censored ALT. For the product whose life obeys two-parameter Weibull distribution, many scholars believe that the acceleration efficiency of step-down test is higher than step-up

test, who have done qualitative analysis and Monte Carlo simulation to illustrate the conclusion [7–10]. However, it still lack the clear proof in theoretically. Though the analysis of SSALT is more complex than Constant Stress Accelerated Life Test (CSALT), the purpose of all the analysis is to calculate the equivalent material parameters or other relevant parameters. For Arrhenius model $\theta = A \exp(Ea/k \times s)$ which selects temperature as the considered stress, the key parameter is the equivalent activation energy of material. How to combine with the Physics of Failure (PoF) model with statistical analysis method is the research direction of test results processing. Nelson put forward a method of Maximum Likelihood Estimation (MLE) to deal with SSALT under the precise that cumulative damage cannot be neglected [5,6]. Sometimes, due to objective restrictions, it may cannot get the failure data accurately under a certain stress, which is called interval data. Interval data are used to be a common form of product life data in engineering [3]. A method of parameter estimation of interval data when the products are conducted under CSALT and lifetime obeys Weibull distribution is given in [11].

By analyzing the whole process, if we can separate each steps, it can solve many practical problems employing stepwise analysis, such as dealing with precise time data and interval data. Using conditional probability, it can solve these problems

excellently. The presented method gives a form of conditional probability, which can transfer the cumulative damage problem, existing in SSALT to a mathematic problem. It provides an easier method to compare the acceleration efficiency of step-up ALT and step-down ALT. By analyzing the failures and survivals of each steps respectively, it provides a method to establish the maximum likelihood function of acceleration model parameters.

2 ASSUMPTIONS AND THEORETICAL ANALYSIS

N samples are selected to conduct type-I or type-II censored SSALT under accelerated stresses $s_1, s_2 \dots s_k$. The number of failures under every steps are $n_1, n_2 \dots n_k$ and the test durations are $\tau_1, \tau_2, \dots, \tau_k$ respectively. So the number of survivals after the m -th step is $N - \sum_{i=1}^m n_i$. The acceleration factor among s_i and s_j is $AF_{i,j}$, which is a known function associated with the selected acceleration model. The equivalent test time at the beginning of the i -th step is $tt_i = \sum_{m=1}^{i-1} AF_{m,i} \times \tau_m$. Following assumptions are made prior to the analysis:

1. The failure mechanism of the products under usage condition and accelerated stresses is same, and the lives obey the two-parameter Weibull distribution;
The pdf under s_i is $f_i(t, \theta_i) = \beta / \theta_i (t / \theta_i)^{\beta-1} e^{-(t / \theta_i)^\beta}$, where θ_i = characteristic life under s_i , β = shape parameter.
2. The form of acceleration model under a certain kind of stress is known;
3. The remaining life of specimens depends only on the current cumulative fraction failed and current stress, regardless of the accumulation mode [4].

Generally speaking, there are two cases of data occurring when conducting the SSALT.

Case (1): The exact time of failure can be obtained, the j -th failure time under the i -th stress respect to the start time of the i -th step is t_{ij} . They are $t_{1,1} t_{1,2} \dots t_{1,n_1}, t_{2,1} t_{2,2} \dots t_{2,n_2}, \dots t_{k,1} t_{k,2} \dots t_{k,n_k}$. For type-II censored test, $t_{1,n_1} = \tau_1, t_{2,n_2} = \tau_2 \dots t_{k,n_k} = \tau_k$.

Case (2): The data obtained is interval-censored data when conducting the type-I censored test. So the equivalent failure time interval is $tt_i \sim tt_i + \tau_i$.

Under the SSALT, only the failure time under s_1 are life data, as $tt_i=0$. All of other failures occur in the condition of accumulated damage. And the life characteristic θ_i is determined by acceleration model, for Arrhenius model $\theta_i = A \times e^{x/s_i}$; for Inverse power law model $\theta_i = A \times s_i^{-x}$ etc. Where x is the parameter need to be estimated, s denotes stress level. All of the steps can be considered to be independent except the accumulated damage at the

beginning of the steps. According to the assumption (1), the pdf under different stresses can be represented as follows respectively:

$$f_i(t, \theta_i), 0 \leq i \leq k, 0 \leq t \leq \tau_k \quad (1)$$

Due to the existence of cumulative damage, all of the failures occur after τ_1 on condition that the samples under testing are survived after the previous stress steps.

Under the case (1), supposing that $\Delta \rightarrow 0^+$, the conditional probability of the j -th failure under the i -th step can be denoted as:

$$\begin{aligned} p_{ij} &= P(tt_i + t_{ij} < X < tt_i + t_{ij} + \Delta | X > tt_i) \\ &= \frac{P(tt_i + t_{ij} < X < tt_i + t_{ij} + \Delta)}{P(X > tt_i)} \quad \begin{matrix} 0 \leq t_{ij} \leq \tau_i \\ \text{for } 1 \leq j \leq n_i \end{matrix} \\ &= \frac{\int_{tt_i+t_{ij}}^{tt_i+t_{ij}+\Delta} f_i(t, \theta_i) dt}{\int_{tt_i}^{+\infty} f_i(t, \theta_i) dt} \propto \frac{f_i(tt_i + t_{ij}, \theta_i)}{\int_{tt_i}^{+\infty} f_i(t, \theta_i) dt} \quad 1 \leq i \leq k \end{aligned} \quad (2)$$

Under the case (2), the conditional probability that the failure occurs under s_i can be denoted as:

$$\begin{aligned} p_i &= P(tt_i < X < tt_i + \tau_i | X > tt_i) \\ &= \frac{P(tt_i < X < tt_i + \tau_i)}{P(X > tt_i)} = \frac{\int_{tt_i}^{tt_i+\tau_i} f_i(t, \theta_i) dt}{\int_{tt_i}^{+\infty} f_i(t, \theta_i) dt} \end{aligned} \quad (3)$$

The probability of the products which survive after τ_i in condition of surviving after tt_i is:

$$\begin{aligned} R_i &= P(t > tt_i + \tau_i | t > tt_i) \\ &= \frac{P(t > tt_i + \tau_i)}{P(t > tt_i)} = \frac{\int_{tt_i+\tau_i}^{+\infty} f_i(t, \theta_i) dt}{\int_{tt_i}^{+\infty} f_i(t, \theta_i) dt} \end{aligned} \quad (4)$$

3 THE COMPARISON OF THE ACCELERATION EFFICIENCY

A SSALT was conducted under temperature stresses T1 and T2. According to Equation 2, the conditional pdf of life under the two stresses can be represented as follows respectively:

Under the first step:

$$f_i(t) = \frac{\beta}{\theta_1} \left(\frac{t}{\theta_1} \right)^{\beta-1} e^{-\left(\frac{t}{\theta_1} \right)^\beta} \quad (5)$$

Under the second step:

$$f_2(t) = \frac{\beta}{\theta_2} \left(\frac{t_1 \times AF_{1,2} + t}{\theta_2} \right)^{\beta-1} e^{-\left(\frac{t_1 \times AF_{1,2} + t}{\theta_2} \right)^\beta + \left(\frac{t_1 \times AF_{1,2}}{\theta_2} \right)^\beta} \quad (6)$$

where, $AF_{1,2} = \theta_2/\theta_1$. If the numbers of failure are n_1 and n_2 respectively, the moment estimations of the failure probability are $q_1 = n_1/n$ and $q_2 = n_2/(n - n_1)$. The expectation of tests' duration are τ_1 and τ_2 . The following equations can be obtained.

Under the first step: $\int_0^{\tau_1} f_1(t) dt = q_1$, as $1 - e^{-\left(\frac{\tau_1}{\theta_1}\right)^\beta} = q_1$, so $\tau_1 = \theta_1 \times (-\ln(1 - q_1))^{1/\beta}$;

Under the second step:

$$\int_0^{\tau_2} \frac{\beta}{\theta_2} \left(\frac{\tau_1 \times AF_{1,2} + t}{\theta_2} \right)^{\beta-1} e^{-\left(\frac{\tau_1 \times AF_{1,2} + t}{\theta_2} \right)^\beta + \left(\frac{\tau_1 \times AF_{1,2}}{\theta_2} \right)^\beta} dt = q_2, \text{ as } e^{-\left(\frac{\tau_1 \times AF_{1,2} + \tau_2}{\theta_2} \right)^\beta} = e^{-\left(\frac{\tau_1 \times AF_{1,2}}{\theta_2} \right)^\beta + \ln(1 - q_2)}, \text{ so}$$

$$\tau_2 = \left(\left(\frac{\tau_1 \times AF_{1,2}}{\theta_2} \right)^\beta - \ln(1 - q_2) \right)^{1/\beta} * \theta_2 - \tau_1 \times AF_{1,2}.$$

The total duration is:

$$\begin{aligned} \tau_1 + \tau_2 &= \theta_1 (-\ln(1 - q_1))^{1/\beta} \\ &+ \left(\left(\frac{\tau_1 \times AF_{1,2}}{\theta_2} \right)^\beta - \ln(1 - q_2) \right)^{1/\beta} \\ &\times \theta_2 - \tau_1 \times AF_{1,2} = \theta_1 \times (-\ln(1 - q_1))^{1/\beta} \\ &- \theta_1 \times (-\ln(1 - q_1))^{1/\beta} \times AF_{1,2} \\ &+ \left(\left(\frac{\theta_1 \times (-\ln(1 - q_1))^{1/\beta} \times AF_{1,2}}{\theta_2} \right)^\beta - \ln(1 - q_2) \right)^{1/\beta} \theta_2 \end{aligned} \quad (7)$$

Because $AF = \theta_1/\theta_2$, the following formula can be rewritten as:

$$\begin{aligned} \tau_1 + \tau_2 &= \theta_1 \times (-\ln(1 - q_1))^{1/\beta} + \theta_2 \\ &\times \left[(-\ln(1 - q_1) - \ln(1 - q_2))^{1/\beta} - (-\ln(1 - q_1))^{1/\beta} \right] \end{aligned} \quad (8)$$

The target function of the optimization problem is to obtain the minimum total test time. If $(-\ln(1 - q_1))^{1/\beta} > (-\ln(1 - q_1) - \ln(1 - q_2))^{1/\beta} -$

$(-\ln(1 - q_1))^{1/\beta}$, $\theta_1 < \theta_2$ is set to get the minimum $t_1 + t_2$, otherwise, $\theta_1 > \theta_2$ is set to achieve this. Let $B = (-\ln(1 - q_1))^{1/\beta} - [(-\ln(1 - q_1) - \ln(1 - q_2))^{1/\beta} - (-\ln(1 - q_1))^{1/\beta}]$, considering the special circumstance when $q_1 = q_2 = q$, there is $B = (2 - 2^{1/\beta}) \times (-\ln(1 - q))^{1/\beta}$ which depends on the value of shape parameter β . The following three cases are discussed.

Case I: Assuming that $\beta = 1$, then the following result can be obtained: $B = (2 - 2^{1/1}) \times (-\ln(1 - q))^{1/1} = 0$. The total test time is independent of stresses order. Namely, if the products' life obeys exponential distribution, the acceleration efficiency is the same.

Case II: Assuming that $\beta > 1$, then the following result can be obtained: $B = (2 - 2^{1/\beta}) \times (-\ln(1 - q))^{1/\beta} > 0$. $\theta_1 < \theta_2$ is set to obtain the minimum time, there is $T_1 > T_2$, namely, step-down-stress ALT is more efficient than step-up-stress ALT.

Case III: Assuming that $\beta < 1$, then the following result can be obtained: $B = (2 - 2^{1/\beta}) \times (-\ln(1 - q))^{1/\beta} > 0$. $\theta_1 > \theta_2$ is set to obtain the minimum time, there is $T_1 < T_2$, namely, step-up-stress ALT is more efficient than step-down-stress ALT.

4 THE MLE OF ACCELERATION MODEL PARAMETERS

4.1 Theoretical analysis

Analyzing the whole process step by step, considering the number of failures and survivals, there are $N - \sum_{m=1}^i n_m$ samples tested under s_p , with the number of survivals is $N - \sum_{m=1}^i n_m$.

Under the case (1), the likelihood function can be written as:

$$L \propto \prod_{i=1}^k \prod_{j=1}^{n_i} p_{ij} * R_i^{N - \sum_{m=1}^i n_m} \quad (9)$$

Under the case (2), the likelihood function can be denoted as:

$$L \propto \prod_{i=1}^k p_i^{n_i} * R_i^{N - \sum_{m=1}^i n_m} \quad (10)$$

The equation is selected based on the type of test data. And then the life characteristic θ_i under different stress levels are combined with acceleration model to calculate the acceleration model parameters by MLE.

4.2 Data analysis with accurate failure time

According to historical data, the lifetime of this type of diodes obeys Weibull distribution. The

Table 1. Type-I censored test data.

Stress level s_i (V)	38	41	44	47
Time τ_i (h)	1000	600	250	125
Failure time t_{ij} (h)	336	168	144	48
	600	312	164	66
	888	408	184	84
	—	524	240	102

sample size is $N = 120$. The samples are conducted with

Type-I censored SSALT under voltage stress. The test data are shown in Table 1 [2].

According to Equation 2, the conditional probability of the j -th failure under the i -th step is:

$$p_{ij} = \frac{f_i(t_i + t_{ij}, \theta_i)}{\int_{t_i}^{+\infty} f_i(t, \theta_i) dt} = \frac{\beta \left(\frac{t_i + t_{ij}}{\theta_i} \right)^{\beta-1} e^{-\left(\frac{t_i + t_{ij}}{\theta_i} \right)^\beta}}{e^{-\left(\frac{t_i}{\theta_i} \right)^\beta}} = \frac{\beta \left(\frac{t_i + t_{ij}}{\theta_i} \right)^{\beta-1} e^{-\left(\frac{t_i + t_{ij}}{\theta_i} \right)^\beta}}{\theta_i \left(\frac{t_i}{\theta_i} \right)^\beta},$$

the conditional probability of being survived after the i -th step is:

$$R_i = \frac{\int_{t_i + \tau_i}^{+\infty} f_i(t, \theta_i) dt}{\int_{t_i}^{+\infty} f_i(t, \theta_i) dt} = \frac{e^{-\left(\frac{t_i + \tau_i}{\theta_i} \right)^\beta}}{e^{-\left(\frac{t_i}{\theta_i} \right)^\beta}} = e^{-\left(\frac{t_i + \tau_i}{\theta_i} \right)^\beta + \left(\frac{t_i}{\theta_i} \right)^\beta}.$$

For voltage stress, the acceleration model is Inverse power law model $\theta_i = A \times s_i^x$. According to Equation 9, the likelihood function is:

$$L \propto \prod_{i=1}^4 \prod_{j=1}^{n_i} p_{ij} * R_i(t)^{N - \sum_{m=1}^i n_m} = \left(\frac{\beta}{\theta_4} \right)^3 \prod_{j=1}^3 \left(\frac{t_{1j}}{\theta_1} \right)^{\beta-1} e^{-\sum_{j=1}^3 \left(\frac{t_{1j}}{\theta_1} \right)^\beta} * e^{-117 * \left(\frac{1000}{\theta_1} \right)^\beta},$$

$$* \dots * \left(\frac{\beta}{\theta_4} \right)^4 \prod_{j=1}^4 \left(\frac{t_{4j}}{\theta_1} \right)^{\beta-1} e^{-\sum_{j=1}^4 \left(\frac{t_{4j} + t_{4j}}{\theta_4} \right)^\beta} * e^{-4 * \left(\frac{t_{4j}}{\theta_4} \right)^\beta}$$

$$* e^{-105 * \left(\frac{t_{4j} + 125}{\theta_4} \right)^\beta} * e^{-\left(\frac{t_{4j}}{\theta_4} \right)^\beta}$$

By MLE with the use of Matlab, the corresponding parameters' estimates are: $\hat{A} = 4.8818 \times 10^{14}$, $\hat{x} = -6.7453$. So the acceleration model of the diode under voltage stress is: $\zeta^x = 4.8818 \times 10^{14} * S^{-6.7453}$, where ζ = characteristic life (h), S = stress level (V).

5 CONCLUSION

ALT is a test method that to find out the life characteristic of high reliability material, and it has far-reaching significance to the development of product quality. The presented method provides an application of conditional probability among SSALT. As we all know all of the pieces in step-stress ALT are tested on condition that they are survived after all of the previous stress steps. According to this character, this paper analyzed and compared the acceleration efficient of step-down ALT with step-up ALT on the basis of conditional relationship. If the Shape parameter is bigger than 1, step-down-stress ALT is more efficient than step-up-stress ALT, and vice versa. And then, it give a new method to estimate the selected acceleration model parameters by analyzing the data of failures and survivals under each stress step of SSALT.

REFERENCES

- [1] Chen Wenhua, Yang Fan, Liu Junjun, et al. 2012. Theory and Method for Simulation Evaluation of Accelerated Life Test Plan under Step-stress. Journal of Mechanical Engineering 48(22): 176–188.
- [2] Guo Jun. 1998. Implementation and Discussion of Step-stress Accelerated Life Testing. Applied Probability and Statistics 4(3): 327–330.
- [3] Qiu Leipin. 2007. Accelerated Life Test Study Based on Generalized Exponential Distribution with Interval Data Thesis. Zhejiang University.
- [4] Mao Shi-song, Wang Ling-ling. 1997. Accelerated Life Testing. Beijing: Science Press.
- [5] Nelson W B. 1980. Accelerated Life Testing Step-Stress Models and Data Analyses. Transactions of Reliability 29(2): 103–108.
- [6] Nelson W B. 2004. Accelerated Testing-Statistical Models, Test Plans and Data Analysis. New Jersey: John Wiley & Sons Inc.
- [7] Wang Ronghua, Sha Naijun, Gu Beiqing ect. 2012. Comparison Analysis of Efficiency for Step-Down and Step-Up Stress Accelerated Life Testing. IEEE Transactions on Reliability 61(2).
- [8] Xu Guang, Wang Ronghua. 2008. Efficiency analysis of the step-down-stress accelerated life testing. Journal of Shanghai Normal University (Natural Sciences) 37(5):468–478.
- [9] Zhang Chun-hua, Chen Xun, Wen Xi-sen. 2005. Step-down-stress Accelerated Life Testing-Methodology. Acta Armamentarii 26(5): 661–665.
- [10] Zhang Chun-hua, Chen Xun, Wen Xi-sen. 2005. Step-down-stress Accelerated Life Testing-Statistical Analysis. Acta Armamentarii 26(5): 666–669.
- [11] Zheng Ming, Yang Yi, Zheng Yu. 2003. Estimating Parameters in Weibull Distribution by Grouped Data. Appl. Math. J. Chinese Univ. Ser. A 18(3): 303–310.

Effect of band drain spacing on the improvement of hydraulic filled ultra-soft soil foundation

Ai Hua Liang, Zhi Jun Chen & Jian Yu

Key Laboratory of Port Geotechnical Engineering of the Ministry of Communication, CCCC Tianjin Port Engineering Institute Co., Ltd., Tianjin, China

ABSTRACT: A spacing of 0.7 m–1.3 m among band drains, as recommended in the Specification, is adopted to improve the hydraulic filled ultra-soft soil foundation by vacuum preloading technique, but its improved vane shear strength is about 12 kPa, far below the design or expectation, proven by the statistics from many projects countrywide. In this paper, a series of field tests was conducted in the Tianjin Harbor Industrial Area with 0.4-m, 0.5-m and 0.6-m spacings, separately among band drains, to improve the hydraulic filled ultra-soft soil foundation. It is showed that the improvement result is sensitive to the band drain spacing on the aspects of soil characters, soil strength and degree of consolidation. It is feasible to adopt a band spacing far smaller than the recommended one in the Specification to improvement the hydraulic filled ultra-soft soil; and the smaller band drain spacing can be used to effectively improve the strength of hydraulic filled ultra-soft soil foundation. In this test, a 40-cm band spacing was adopted and its 60-d vane shear strength was up to 26.4 kPa.

Keywords: band drain spacing; vacuum preloading technique; hydraulic filled ultra-soft soil; foundation improvement effect

1 INTRODUCTION

In the drainage consolidation method used to improve the saturated soft clay, the arrangement and spacing of the plastic band drain are important factors to affect the consolidation time^[1]. As specified by Sub-clause 4.3.4 in “Technical Specification for Vacuum Preloading Technique to Improve Soft Soils” (JTS 147-2-2009), “the band drain spacing should be 0.7 m–1.3 m, and a larger value should be adopted for the highly-sensitive clay”^[2].

Based on the engineering information from Dalian Port, Huanghua Port, Qingdao Port and Tianjin Port, the band drain spacing of 0.7 m–1.3 m recommended by the Specification has been adopted to improve the foundation of hydraulic ultra-soft soil. But after improvement by vacuum preloading technique for 3~5 months, the average vane shear strength was just about 12 kPa^[3], far below the design requirement or expectation. It has always been a challenge to effectively improve the improvement strength of hydraulic filled ultra-soft soil foundation.

To solve the above challenge, we tried to adopt a band drain spacing of 0.4 m–0.6 m rather than the one recommended in Specification in field tests so as to learn about the effect of smaller band drain spacing on improvement of hydraulic filled ultra-soft soil foundation.

2 FIELD TESTS

2.1 Soil characters

The test area is located in Tianjin Harbor Industrial Area, covering an improvement area of 1800 m². This area is covered by newly hydraulic filled soil, whose top soil is basically fluid mud of about 4 m in depth. Before the test design, in-situ soil sampling and laboratory soil tests were conducted for the test area. Thin-walled soil sampler was adopted to collect 80 soil samples, and the maximum depth of soil sampling was 3.5 m. The test results of laboratory soil samples are detailed in [Table 1](#).

The initial average of moisture content is greater than 85%, the vane shear strength is 2.0 kPa and the clay particles content is 56% in improvement area. So the soil is the typical ultra-soft cohesive soil^[3].

2.2 Test methods

The test area is divided into Area B1, Area B2 and Area B3 with each area of 600 m². Conventional vacuum preloading method was adopted and the improvement sketch is shown in [Figure 1](#). For Areas B1, B2 and B3, the band drain spacing was 60 cm, 50 cm and 40 cm separately, with an installation depth of 3.5 m, and the drainage plate is square arranged. A filter tube was laid between every two

Table 1. Laboratory experiment results of soils before improvement.

Item	Moisture content $w/\%$	Wet density ρ $/(g \cdot cm^{-3})$	Clay particles content (<0.005 mm) %	Void ratio e	Liquid limit w_L /%	Plasticity index I_p	Liquidity index I_L	Vane shear strength /kPa
Max	104.0	1.69	60	2.9	50.4	27.2	3.5	3.0
Min	73.2	1.45	52	1.5	40.5	20.1	1.5	0.7
Average	86.9	1.53	56	2.3	45.0	23.4	2.7	2.0

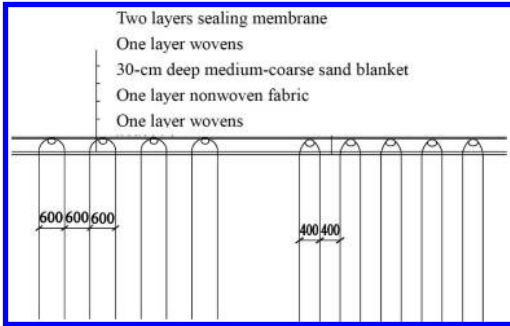


Figure 1. Sketch of conventional vacuum preloading.

rows of band drains which were connected to the filter tube directly. A 30-cm deep drainage blanket of yellow sand was laid and two layers of sealing membrane were laid at one time. Two jetting pumps were shared by these three areas. It was required that the vacuum degree in band drains should be maintained above 80 kPa for 60 d.

3 ANALYSIS OF MONITORING, INSPECTION AND IMPROVEMENT OF TEST AREA

In order to study the improvement result with different band drain spacings, pore-water pressure and ground surface settlement in the process of improvement was monitored. In addition, the in-situ soil sampling for soil analysis and vane shear tests were conducted for the pre-improvement, improvement in process and post-improvement stages.

3.1 Pore-water pressure observation

The pore-water pressure meters were all embedded at the central position of 4 band drains. The analysis of pore-water pressure dissipation and degree of consolidation calculated according to the pore-water pressure dissipation are shown in Table 2.

Table 2. Pore-water water pressure dissipation and calculated value of degree of consolidation in improvement area.

Improvement area	B1	B2	B3
Pore-water pressure dissipation value/kPa	35.7	65	73.7
Degree of consolidation/%	52.6	80.2	91.3

It is shown that the pore-water pressure dissipation is related to the change of band drain spacing. The pore-water pressure dissipation value and the calculated degree of consolidation of foundation soil increase as the band drain spacing decreases. Pore-water pressure dissipation of Area B1 with a 60-cm band drain spacing was only 35.7 kPa, which was very common for the hydraulic filled ultra-soft soil foundation improvement by vacuum preloading technique. The pore-water pressure dissipation of Area B3 and Area B2 with 40-cm and 50-cm band drain spacings was close to the dissipation value of ordinary foundation improvement by vacuum preloading technique.

3.2 Calculation of surface settlement and degree of consolidation

The estimated values of surface settlement and degree of consolidation (hyperbola method^[4]) are detailed in Table 3.

It is shown that the estimated degree of consolidation reduces as the band drain spacing increases. Moreover, the smaller a band drain spacing is, the earlier a required degree of consolidation can reach in the improvement area.

3.3 Change of moisture content and vane shear strength in pre- and post-improvement stages

The average values of the change of moisture content in pre- and post-improvement are detailed in Table 4. In-situ vane shear strength of pre- and post-improvement stage, at 20-d and 40-d after preloading are detailed in Table 5.

Table 3. Surface settlement and degree of consolidation of test area.

Area	Inserting plate settlement (mm)	Preloading settlement (mm)	Total settlement (mm)	Final settlement (mm)	Degree of consolidation (%)
B1 (60 cm)	134.0	682.0	816	1066.2	76.5
B2 (50 cm)	210.0	691.0	901	1038	86.8
B3 (40 cm)	312.0	675.3	987.3	1023.8	96.4

Table 4. Average values of vane shear strength of each area in pre- and post-improvement stages.

Reinforced area	Moisture content (%)		Ratio variation (%)
	Pre-improvement	Post-improvement	
B1	82.97	46.15	44.4
B2	84.05	45.3	46.1
B3	85.01	43.43	48.9

Table 5. Comparison of moisture contents of pre- and post-improvement.

Time duration/d	Area B1/kPa	Area B2/kPa	Area B3/kPa
Before improvement	2.3	2.8	2.5
20	4.8	11.5	13.8
40	7.1	17.7	21.4
60	13.0	21.6	26.4

According to Table 4, after 60-d improvement, the moisture content of foundation reduces greatly. The moisture content reduces as the band drain spacing decreases.

According to the comparison between pre-improvement and post-improvement stages in Table 5, the vane shear strength of Area B1~B3 increases greatly. So a small band drain spacing can rapidly increase the strength of hydraulic filled ultra-soft soil. The growth of vane shear strength increases as the band drain spacing decreases. If the band drain spacing is 60 m, vane shear strength reaches 13 kPa at 60 d. This value is close to the statistic of post-improvement vane shear with a band drain spacing recommended in the Specification, adopted for hydraulic filled ultra-soil in recent years. Therefore, during the improvement of hydraulic filled ultra-soil foundation, the band drain spacing smaller than 60 cm should be selected as much as possible. The adoption of 40-cm and 50-cm band

drain spacing increased the improvement strength of soil mass significantly. As shown in Area B3, with a 40-cm spacing, the vane shear strength was up to 26.4 kPa at 60-d.

Comparison between Table 4 and Table 5 shows that the difference of vane shear strength is great though the difference of moisture contents among the three areas after improvement is small. This indicates that there is a moisture content sensitive range, i.e. in this range, the minor reduction of moisture content can result in a significant strength increase.

3.4 Effect of band drain spacing on the improvement

In the test area, the 40-cm, 50-cm, and 60-cm band drain spacings were adopted. From the aspects of soil characters, soil strength and degree of consolidation, the foundation improvement is sensitive to the band drain spacing. As the band drain spacing decreases, the foundation improvement result becomes better obviously.

As a kind of disturbed soil, the newly hydraulic filled ultra-soft soil has no obvious formed soil skeleton. As a result, the smear effect^[4] generated by band drain installation poses no obvious effect on the improvement. Therefore, a band drain spacing far smaller than recommended one in the Specification may be adopted to improve the hydraulic filled ultra-soft soil foundation so as to improve the foundation improvement effect.

4 CONCLUSIONS

The following conclusions are drawn through the vacuum preloading tests with different band drain spacing:

1. In the test areas with 0.4-m, 0.5-m, and 0.6-m band drain spacings, it is shown that the foundation improvement is sensitive to the spacing on the aspects of soil variation, soil strength and degree of consolidation. It is feasible to adopt a band drain spacing far smaller than the recommended one in the Specification to improve the hydraulic filled ultra-soft soil foundation.

2. The smaller band drain spacing can effectively improve the foundation strength of hydraulic filled ultra-soft soil. In these tests, a 40-cm band drain spacing was adopted, which resulted in a 60-d vane shear strength of 26.4 kPa.

REFERENCES

- [1] GONG Xiao-nan. Foundation treatment manual [M]. 2nd ed., Beijing: China Building Industry Press, 2008. (in Chinese).
- [2] JTS 147-2-2009 Technical Specification for Vacuum Preloading Technique to Improve Soft Soils [S]. 2009. (in Chinese).
- [3] YE Guo-liang, Guo Shu-jun and Zhu Yao-ting. Analysis on engineering property of ultra-soft soil [J]. China Harbour Engineering, 2010(5): 1–9. (in Chinese).
- [4] Gao Zhi-yi. Analysis on mechanics of vacuum preloading method [J]. Chinese Journal of Geotechnical Engineering, 1989, 11(4): 11–23. (in Chinese).

Analysis on the influence of the thickness of external insulation layer of building envelope on building energy consumption in Sunan Region

Xiao Ping Feng & Xin Liu

Environment and Civil Engineering, Jiangnan University, Wuxi, Jiangsu Province, China

ABSTRACT: Taking an analysis object of hotel model with an area of about 6,000 m² as example, this paper analyzes the influence of the thickness of external insulation layer of building envelope on building energy consumption by making use of the BECS energy-saving analysis software. The results show that energy-saving reconstruction can not only reduce energy consumption of existing buildings, but also create good economic benefit, and improve the indoor comfortableness as well.

Keywords: Sunan Region; building envelope; energy-saving and insulation

1 INTRODUCTION

The building envelope is an important part of building energy conservation. Energy loss caused by heat conduction and air infiltration of building envelope is the main factor affecting energy conservation. Strengthening the thermal insulation of building envelope is the key to achieve the requirements of energy conservation. Energy-saving reconstruction of existing buildings is realized mainly through adopting thermal insulation measures. Among them, for external windows, the main measure is to add window layer, or reconstruct windows into two-layer or hollow windows. For exterior wall and roof, the main measure is to adopt external thermal insulation system. The insulation thickness of external wall has a large influence on the energy-saving effect. Taking certain existing office building in Wuxi area as example, this paper conducts simulation analysis on thermal insulation effect of its external wall, roof and external window by BECS software for building energy-saving design.

2 ANALYSIS MODEL

This office building is of 8-layer composite structure, with a floorage of 6,900 m², building height of 28.45 m, window to wall ratio of 0.03 for east orientation, 0.08 for west orientation, 0.28 for south orientation, 0.18 for north orientation and shape coefficient of 0.22. Its standard floor plan is as shown in Figure 1.

3 CONSIDERATIONS FOR ENERGY-SAVING RECONSTRUCTION

3.1 External wall

External wall can be classified into external insulated wall of single material and external insulated wall of composite material according to different insulation methods. External insulated wall with single insulation material adopts high-strength and light-weight insulate on material as wall materials. Composite insulated wall can be classified into outer insulated external wall,



Figure 1. Standard floor plan of certain office building.

inner insulated external wall and sandwich insulated external wall according to various making method. Study on energy saving of building envelope mainly considers study on outer insulation of external wall.

3.2 Roof

Roof insulation mainly adopts insulation material as insulation layer to increase roof insulation resistance. The insulation effect varies depending on the material and thickness of insulation layer. From analysis in aspect of energy-saving effect or economy, it is better to select extruded polystyrene board as insulation material. Roof insulation can not only reduce heat loss in winter, but also reduce temperature inside attic. The current roof structures are usually made into flat roof. It usually adopts flat roof of solid material, or uses the making method of flat roof of natural energy.

3.3 Window

Because the insulation performance of windows is the worst in building envelope, increasing the effect of energy saving of building external window is the important link for the improvement of the building energy-saving level. In the design of energy-saving windows, laminated glass is mostly adopted to increase air buffer of low thermal conductivity and improve the thermal resistance performance.

4 BUILDING ENERGY CONSUMPTION ANALYSIS AFTER ENERGY-SAVING RECONSTRUCTION OF BUILDING ENVELOPE

The insulation structure method is imported into BECS energy-saving design software to conduct building energy consumption analysis on energy-saving reconstruction of external wall, external window and roof.

In the premise of no change of thermal insulation materials, the building energy consumption is calculated after reconstruction through increasing thickness of insulation layer for external wall and roof, through selecting external windows with different heat transfer in case of external wall reconstruction. Compare it with the energy consumption of reference building with energy-saving rate reaching 50%, calculate the annual cooling and heat consumption per unit area of the building, and thus analyze the energy-saving potential of different reconstructed structure types of the

office building. The analysis results are shown in Table 1, Table 2, Table 3 and Figure 2, Figure 3 and Figure 4.

It can be seen from the figure that the decreasing trend of annual cooling and heat consumption of

Table 1. Relationship between external wall insulation layer thickness and annual cooling and heat consumption per unit area (extruded polystyrene board insulation).

Thickness (mm)	Annual cooling and heat consumption of per unit area (KWh/m ²)
40	92.28
60	91.23
80	90.58
100	90.17
120	89.87
140	89.63
160	89.47
180	89.33
200	89.22

Table 2. Relationship between roof insulation layer thickness and annual cooling and heat consumption per unit area.

Thickness (mm)	Heat transfer coefficient (W/m ² ·k)	Annual cooling and heat consumption of per unit area (KWh/m ²)
40	0.713	108.98
60	0.511	108.38
80	0.398	108.04
100	0.326	107.82
120	0.276	107.67
140	0.239	107.56
160	0.211	107.47
180	0.189	107.40
200	0.171	107.35

Table 3. Relationship between window heat transfer coefficient and annual energy consumption per unit area.

Heat transfer coefficient (W/m ² ·k)	Annual cooling and heat consumption of per unit area (KWh/m ²)
0.8	96.32
0.9	96.45
1.0	96.59
1.1	96.72
1.2	96.86

5 STRUCTURE METHOD OF ENERGY-SAVING RECONSTRUCTION SCHEME

See Table 4.

Table 4. Structure method before and after reconstruction.

Structural material (mm)	Before (mm)	After reconstruction (mm)
Cement mortar surface layer	20	20
Extruded polystyrene board		•(150)
Cement mortar bonding layer		20
Crushed stone, gravel concrete	40	40
Reinforced concrete	120	120
Lime mortar	20	20
Cement mortar surface layer	20	20
Extruded polystyrene board		•(100)
Cement mortar bonding layer		20
Concrete perforated brick	200	200
Lime mortar	20	20
Cement mortar surface layer	20	20
Extruded polystyrene board		•(100)
Cement mortar bonding layer		20
Reinforced concrete	200	200
Lime mortar	20	20
Cement mortar Surface layer	20	20
Extruded polystyrene board		•(100)
Cement mortar bonding layer		20
Reinforced concrete	120	120
Cement mortar surface layer	20	20

Note: “•” means insulation materials used in the scheme.

6 CONCLUSION

1. There is certain energy-saving potential through energy-saving reconstruction of building envelope.
2. Design of building envelop can save energy and create favorable economic benefit.
3. Energy-saving reconstruction of building is the need of conservation-oriented society and conforms to the development direction of society.

REFERENCES

- [1] Feng Ya, Yang Hong and Chen Qigao. Study on Thermal Insulation of Energy-saving Building in the South. *New Construction Materials*, 1999 (4): 20–22.
- [2] Xue Zhifeng, et. al. *Energy Efficient Building Technology and Application* [M]. Beijing: China Architecture Industry Press, 2005.
- [3] Tang Lin. Structure Principle of Wall Outer Thermal Insulation Energy Saving and Its Application in Engineering [J]. *Residential Technology*, 2006 (12): 18–21.

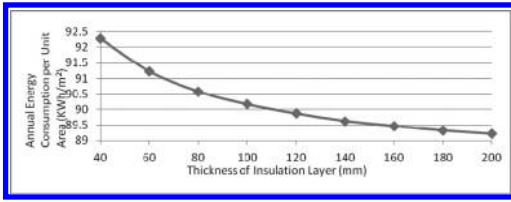


Figure 2. Relationship between external wall insulation layer thickness and annual cooling and heat consumption per unit area.

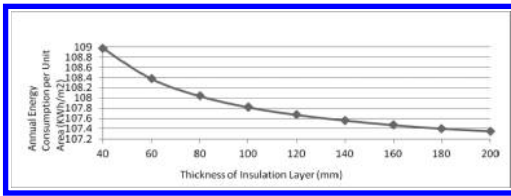


Figure 3. Relationship between roof insulation layer thickness and annual cooling and heat consumption per unit area.

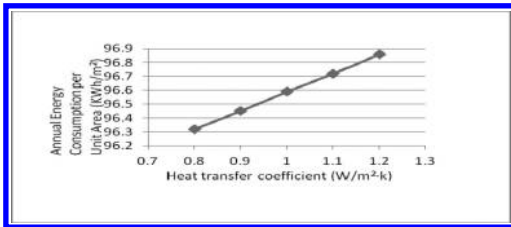


Figure 4. Relationship between window heat transfer coefficient and annual cooling and heat consumption per unit area.

building per unit area appears very steep at first then becomes stable when only the external wall thickness or roof insulation layer thickness is changed while other two factors remain unchanged. It is known that continuously increasing the insulation thickness during the stable period is not economical through analysis of economic factors. Then, the external wall with insulation thickness of 100 mm and roof with insulation thickness of 150 mm is selected. We can see from Figure 4 that the effect is better when heat transfer coefficient of external window is 0.8. If energy-saving reconstruction of the office building is comprehensively conducted in three aspects, its energy-saving rate can reach 64.58%.

An analysis of influence factors of income payment in developing countries

Lei Zhang

Department of Investigation, Jiangsu Police Institute, Nanjing, China

ABSTRACT: Based on the panel data from 2000 to 2011 of 41 developing countries, this paper discusses the influence factors of income payment in sub-project of current account perspective. It finds that the per capita GDP, foreign direct investment, the profit from foreign direct investment, employee compensation and carbon emissions have significantly positive correlation to income payment, while the power consumption amount and population density on the significant negative correlation relationship. The paper also analyses the residual graph from cross section.

Keywords: developing countries; income payment; panel data

1 INTRODUCTION

With the quick development of world economic trade liberalization and regional economic integration, the international division of labor in the world is becoming fiercely competitive. At this moment, competing for similar products in overseas export markets and absorption of factor mobility appear very important. In particular, the trade of goods and services is an important indicator of long-term economic trends for developing countries, which also reflects the core competitiveness of the international division of labor system. From 1980 to 2010, China's balance of trade continued to expand. The ratio of current account surplus to GDP rose from 0.09% to 4.01%. Respectively, this ratio was 10.11% and 9.31% in 2007 and 2008. The large scale of China's current account balance benefits from the strength of China's foreign trade after reform and opening up. But the current account of Brazil and India is being at a low level. Why is there such a performance? It must be analyzed from the sub-item of the current account. Current account consists of the trade in goods and services, income and transfer payments. As there are a good many references for trade in goods and services, the research about this is relatively explore mature in developing countries. And the share of transfer payments is very low. Therefore, we focus on the determinants of income account in the developing world.

2 MODEL SPECIFICATION, VARIABLE SELECTION AND DATA DESCRIPTION

2.1 Model specification

In order to investigate the factors influencing income payment in developing countries, this paper uses panel data model for empirical analysis. The panel data regression model can be expressed as:

$$Y_{it} = \alpha + \beta_{it}X_{it} + \delta_i + \gamma_t + \varepsilon_{it} \quad (1)$$

$i = 1, \dots, N; t = 1, \dots, T$

In this model, Y_{it} is the explained variable, α is the constant term, X_{it} is the observed values of explanatory variables. Random errors are assumed to be independent and identical distributed.

2.2 Variable selection

1. IP: Income payment. Income payment is the explained variables. It is the current account of international payments balance. Income payment mainly reflects the labor and capital flow occurs in the international foreign exchange expenditures.
2. CGDP: Real Gross Domestic Product per Capita, current price.
3. TCG: Technical cooperation grants. Technical cooperation grant is fund to encourage and support the technical innovation of domestic enterprises. And it includes the international

exchange and cooperation between government and non-government.

4. PRF: Profit remittance on foreign direct investment. Because of different capital regulation and foreign exchange settlement, the foreign direct investment profit remittance would be directly related to exchange rate system.
5. FDI: Foreign direct investment. Foreign direct investment is one of the most important indexes of economic development prospects. In general, the foreign direct investment is the side of a rapidly expanding economy.
6. PCF: Private capital flow. Private capital flow is different from FDI. It is more speculative and liquidity. Private capital occupy a larger share in the international arbitrage market. And it is more concerned about the short-term speculative gains.
7. WR: Workers' remittances and compensation. It is the total price paid which is the labor in a country received.
8. EPC: Electric power consumption. Electricity power consumption is positively correlated to economic growth. The index is selected in this paper to analyze the impact of economy grows way on international factor expenditure.
9. CO₂: CO₂ emissions. CO₂ emissions is one of the most important indexes to reflect the economy grows way. This paper selects the index to analyze the effects of environmental pollution on international factor expenditure.
10. PD: Population density. In the condition of labor flowing, the number of population density greater the economic development better.

2.3 Data description

In this paper, the CGDP index data originates from the database of Pennsylvania University. Other indicators data originate from the World Bank Development Indicators Database WDI2011. The variables described in Table 1.

3 THE EMPIRICAL RESULTS

3.1 Variable unit root test

This paper uses a panel data model. The cross section is 41, the time section is 20 years. Levin, Llin & Chu (2002) unit root test method is used to test the stability of variables. The test results are shown in Table 2. From Table 2 we can get the conclusion that the explained variable IP and nine explanatory variables were significantly stable through the Levin, Llin & Chu (2002) unit root test method.

3.2 The regression results

We used statistical software Eviews to regress the panel data. Random effects model is finally selected according to the Houseman test. Regression results showed that there are seven variables passed significant test. The R2 of random model is 0.97.

1. CGDP: Real Gross Domestic Product per Capita, current price
CGDP is positively related to income payment. Income payment would increase by 0.57 units while CGDP increases 1 unit. the elements of spending increased by 0.52 units. In general, there are more opportunities for people to achieve self-value and make more profit in rapid economic growth. So an increase in CGDP will promote the inflow of foreign capital and labor, and then lead to income payment increase.
2. PRF: Profit remittance on foreign direct investment
PRF is positively related to income payment. Income payment would increase by 0.16 units while PRF increases 1 unit. The impact of PRF on income payment is through exchange settlement. For example, an American firm who foreign direct invest in China earn profits which settle of balances in RMB. If it needs to pay profit to the parent company, banks with

Table 1. Data description.

Variable	Mean	Maximum	Minimum	Standard deviation	JB test	Probability
IP	21.02	25.08	16.03	2.13	17.95	0.00
CGDP	8.48	9.98	6.48	0.81	18.91	0.00
TCG	18.32	20.83	13.30	1.41	101.46	0.00
PRF	20.19	24.50	12.79	2.20	11.87	0.00
FDI	20.55	25.80	14.71	2.28	10.45	0.01
PCF	20.51	25.81	14.71	2.33	12.58	0.00
WR	20.11	24.38	14.40	2.16	12.49	0.00
EPC	23.12	28.75	6.52	3.54	1538.6	0.00
CO ₂	10.25	15.69	4.63	2.50	8.85	0.01
PD	4.11	5.94	1.71	1.06	9.15	0.01

Table 2. Unit root test.

Variable	Statistical values	Probability	Conclusion
IP	-52.89	0.00	Stable
CGDP	-5.19	0.00	Stable
TCG	-16.51	0.00	Stable
PRF	-13.40	0.00	Stable
FDI	-20.94	0.00	Stable
PCF	-12.79	0.00	Stable
WR	-24.42	0.00	Stable
EPC	-317.91	0.00	Stable
CO ₂	-137.39	0.00	Stable
PD	-6.08	0.00	Stable

Table 3. The regression results of panel data.

	Fe		Re	
	Coefficient	T value	Coefficient	T value
IP				
CGDP	0.57***	7.94	0.518***	7.88
TCG	-0.03	-0.64	-0.03	-0.67
PRF	0.16***	6.25	0.16***	6.61
FDI	0.12***	3.33	0.13***	3.76
PCF	0.03	1.09	0.04	1.24
WR	0.06**	2.16	0.05**	2.06
EPC	-0.06***	-2.70	-0.06***	-2.80
CO ₂	0.52***	12.19	0.52***	13.11
PD	-0.16***	-3.05	-0.17***	-3.89
Constant	5.84***	5.68	6.09***	6.18
Adjust R ²	0.90		0.97	
DW	1.17		1.36	

Notes: *, ** and *** were expressed past the test at the level of 10%, 5% and 1% level.

exchange qualified in China need to release dollars from RMB. In fact, Profit remittance on foreign direct investment is the money host country paid to foreign country. It is the factor payment of host country.

3. FDI: Foreign direct investment

FDI is positively related to income payment. Income payment would increase by 0.12 units while FDI increases 1 unit. From a practical standpoint of the world economic development, the economic growth of developing countries depends on investment and export, the contribution of the consumer is small. This is mainly because the economic level of developing countries is relatively low, consumption demand is insufficient. Lacking of funds and local investment to promote economic development is a widespread phenomenon in developing countries. Foreign direct investment has become an important contribution of economic

growth. Foreign direct investment has a variety of effects on international factors payment. But it must be noted that some local governments blindly introduce foreign capital, even directly open the door to foreign investment through local government land policy. Some foreign capital leave our high-speed growth of GDP, serious pollution of the environment, super cheap labor wages, but take away huge wealth which is rightfully to the majority of the people.

4. WR: Workers' remittances and compensation

WR is positively related to income payment. Income payment would increase by 0.06 units while WR increases 1 unit. Workers' remittances and compensation is labor costs. It is one of the most important indicators of the competitiveness of enterprises. In generally, the lower employee pay reduces the cost of enterprise, so the core competitiveness will be enhanced. By contrast, the higher workers' remittances and compensation will significantly decelerate the growth of export, which make the country to be in an inferior position in the similar products competition market. And the residents are more likely to consume import goods. It shows that, employee salary increases will lead to a reduction in exports, increase imports. It means that the higher workers' remittances and compensation will increase imports and income payment.

5. EPC: Electric power consumption

WR is negatively related to income payment. Income payment would decrease by 0.06 units while WR increases 1 unit. Electric power is not only the economic resources, but also an important guarantee for social development. But if the electric power consumption is growing, it is an extensive mode of economic development. From the development of the world industry history, one of the penalties of extensive mode of economic development is low value-added feature in the incorporate divides the work for globalization industry. At the same time, extensive mode of economic development would prove temporary beneficial. Growth of electric power consumption enhances the product competitive advantage by reduce labor and capital costs in the world similar products market. So the foreign labor and capital inflows cut down, which make imports and income payment decrees.

6. CO₂: CO₂ emissions

CO₂ emissions is positively related to income payment. Income payment would increase by 0.52 units while CO₂ emissions increases 1 unit. Domestic and foreign enterprises are the CO₂ emission body. Now more and more scholars pay attention to the environmental pollution problem of Multi-National Corporation. The regression results here show that there is serious

environment pollution in host country made by Multi-National Corporation. From the domestic enterprise point of view, serious environment pollution will make them loss competitiveness in strict quality censorship regulations of foreign market. And domestic consumers favor pollution-free products. This will increase imports and income payment.

7. PD: Population density

PD is negatively related to income payment. Income payment would decrease by 0.16 units while PD increases 1 unit. First of all, the amount of the population tolerance in a region is limited. Excessive population produces surplus labor, which will reduce cost of labor and capital. These will help to upgraded corporate core competitiveness. So the imports and income payment decrease. Secondly, the increasing of population density will elbow out the inflow of foreign labor, which apparently helps to reduce income payment.

4 CONCLUSION

This paper analyzes the factors influencing income payment based on the panel data of 41 developing countries from 2000 to 2011. The empirical results show that the per capita GDP, foreign direct investment, foreign direct investment profits, employee compensation and CO₂ emissions are significant positive correlated to income payment in developing countries, while power consumption and population density are significant negative correlated to income payment. So developing countries should try to change the way of economic development and lie special emphasis on environmental protection, which can not only reduce the loss of national wealth, but also can improve the domestic factor income and promote economic growth. In addition, openness makes international factors payment increase, which obviously widen the current account deficit gap.

ACKNOWLEDGMENT

Supported by a Project Funded by the Priority Academic Program Development of Jiangsu Higher Education Institutions (No. 137, 2011).

REFERENCES

- [1] Peter Gammeltoft, Remittances and Other Financial Flows to Developing Countries, *International Migration*, Vol. 40 (5) SI 2/2002: 182–211.
- [2] Amelia Santos-Paulino and A.P. Thirlwall, the Impact of Trade Liberalisation on Exports, Imports and the Balance of Payments of Developing Countries, *The Economic Journal*, 114 (February), F50–F72.
- [3] Graham Bird, The International Monetary Fund and developing countries: a review of the evidence and policy options, *International Organization*, Summer 1996, 477–511.
- [4] Calderon, Chong and Loayza, Determinants of Current Account Deficits in Developing Countries, *Policy Research Working Paper*, July 2000, 1–42.
- [5] Calderon, Chong and Loayza, Are African Current Account Deficits Different? Stylized Facts, Transitory Shocks, and Decomposition Analysis, *IMF Working Paper*, January 2001, 1–40.
- [6] Atish R. Ghosh and Jonathan D. Ostry, The Current Account in Developing Countries: A Perspective from the Consumption-Smoothing Approach, *The World Bank Economic Review*, Vol. 9, No. 2 (May, 1995), pp. 305–333.
- [7] Jorge E. Roldos, Tariffs, Investment and the Current Account, *International Economic Review*, Vol. 32, No. 1 (Feb., 1991), pp. 175–194.
- [8] Sebastian Edwards, Thirty Years of Current Account Imbalances, Current Account Reversals, and Sudden Stops, *IMF Staff Papers*, Vol. 51, IMF Fourth Annual Research Conference (2004), pp. 1–49.
- [9] Giovanni Lombardo, Price Rigidity, the Mark-up, and the Dynamics of the Current Account, *The Canadian Journal of Economics*, Vol. 35, No. 3(Aug., 2002), pp. 531–555.
- [10] Gian Maria Milesi-Ferretti and Assaf Razin, Current Account Reversals and Currency Crises: Empirical Regularities, *NBER Working Paper*, June 1998, 1–54.
- [11] Menzie Chinn and Eswar S. Prasad, Medium-Term Determinants of Current Accounts in Industrial and Developing Countries: An Empirical Exploration, *NBER Working Paper*, March 2000, 1–44.

The authenticity of the images: “The real emotion”—reflection on the movies “Under the Hawthorn Tree” and “Avatar”

Hong Mei Lu

Art and Design School, Wuhan University of Technology, Wuhan, P.R. China

ABSTRACT: From the analysis of the realistic movie “Under the Hawthorn Tree” and the science fiction film “Avatar”, this paper conclude that the image authenticity include not only the physical reality, but also the real emotion. Moreover, the real emotion is the foundation and core of the image creation. The true feeling of image is the image reality that transcend the material level and get to the psychological level. The true feeling of image is the cultural authenticity that possess the broader senses and universal values. Only basing on the authenticity of emotion, can the image be excellent image.

Keywords: true image; true feelings; Under the Hawthorn Tree; Avatar

Chinese movie “Under the Hawthorn Tree” and American 3D IMAX film “Avatar” respectively show the differences between eastern and western cultures. As opinions vary, no unanimous conclusion can be drawn. The various opinions mainly come from one movie is produced in the east and show the past life, the other is from the west and express the future. Then, about the point for understanding the meaning of images—the authenticity of the images is not only the physical reality, and it should include the real emotion, that is the foundation and the core for image creation. Image of the true feeling is beyond the material level, rise to the psychological level of image reality, it is a more broad significance and universal value of cultural authenticity.

Nowadays, with rapid development of digital imaging technology, the human beings not only can record the real life, but also build a parallel virtual image world. To a certain extent, the world have more freedom to realize and control the image. However, due to the subjective and objective technology involved, the audience mostly can't identify the film images is real or virtual, which part is reliable, and which part is deceptive. So, people began to think and debate about the authenticity of the images.

But, here, what I want to discuss is not the image authenticity based on real world problems, but the image to the people's psychological and emotional experience of the reality, from either real or virtual contemporary image to seek a common point—the real emotion. Two kinds of image movie “Under the Hawthorn Tree” and “Avatar” just represent the real and virtual, domestic and foreign respectively.

But the two film both express real, vivid, and touching feelings.

1 “UNDER THE HAWTHORN TREE” AND PURE LOVE

Director Zhang Yimou's movie “Under the Hawthorn Tree” adapted from a documentary novel. With the documentary style, film tells the love story between girl who named “Jing Chiu” and the boy with nickname of “The Third” in 1970 years. Although the film story is plain, but bring the audience mind moved by the pure, selfless love. These pure and beautiful loves raise a sympathetic response in different ages. At the impetuous era, the film has a very profound practical significance. “In fact, the story itself is very common, same as the text of the novel and the writing, be not at all surprising. But we can find that the story of pure love and eternal love something far more important than it symbolizes. The love, the need of the real life, that's why this story is so shocked.” [1]

The content of the film comes fully from a real story, even the hero and heroine's name are true. From the point of the image authenticity, it can be said that this is almost an entire image real work. But the fact is, the most impression on the audiences is not the film authenticity, but the “purest love story of all”. “It restores the real life state of the educated youth, to a certain extent, has presented a rich and vivid history for us, giving them space to imagine a strong emotional impact with the history.” [2] So, the emotional experience and empathy effect is the film's flash point.

2 “AVATAR” AND THE ORIGINAL ECOLOGICAL BEAUTY

The movie “Avatar” uses an advanced digital image technology. It takes ten years to build an American classic commercial film, tells the science fiction story of the future: As the Earth’s resource depletion, human plunder resources in the Pandora planet. Different from the documentary style “under the Hawthorn Tree”, “Avatar” creates a beautiful planet Pandora in the universe. Overlooking the earth, the scene of the story and the content are entirely fictional, which doesn’t exist in the real world. “The film shows only the digital information in the computer. The digital information manufacturing is a visual spectacle, but a huge reality lies, a duplicate image world and cannot find the basis from the reality.” [3] But, from the emotional level, the film and the real world of human emotion and value judgments are interlinked, and it is also the western films in addition to pure visual enjoyment, but also can be recognized around the audience emotional premise. Investigating its reason, “Whether the image authenticity exists or not, what the people support, as the judgment standard, is due to whether the people can observe with the naked eye and experience it, then established the ‘concept of community’”. [4] In the movie, the concept of “community”, it contains the common love to the goodness, cherishing the love and hate for the destruction of the environment and exploitation. So from the emotional point of view, the spirit content of the film is very real. “Everything here will make people addict, everything is such harmonious and perfect, making people feel that this is the real star. When it is subjected to the threat and destruction from the earth, the audience can’t help produce a mood. It is the anger, the most direct cause of the sense of reality is the emotion generated from digital images. Neither the computer generated NA’VI people nor planet Pandora exists, but the effect is so perfect and realistic when appearing on the screen, so it completely conquers all the audience’s eyes and mind.” [3] “It is actually very simple, just the fusion communication of love and conscience “. [5] In fact, this kind of communication is not only between Earth and NA’VI people on the movie, but also the audience and film can interact.

“The movie is nothing but for the sake of a cross—through the present complex, arrived into a simple world, even if the virtual world only exists in the mind, it makes people feel happy.” [6] “Under the Hawthorn Tree” praises pure love, and “Avatar” defends the original ecology. Both let the

audience feel a kind of pure beauty. I think this is the common point of the two films, and the most important touches our hearts.

3 THE SIGNIFICANCE OF IMAGE EMOTIONAL TRUTH

In fact, whether the real or virtual image, the creation and development of images are indispensable. The famous contemporary photographer and digital animation artist, Miu Xiaochun once said, “Both the photography, realistic images and virtual images are important to me, because this kind of virtual is entirely from my own imagination and dreams, more or less.” [7] And what I want to say is: good image works, whether real or virtual, have one thing in common, that is the image of good condensation of the writers from a universal value of emotion, thus to resonate in the heart of the audiences.

To make a long story short, no matter how powerful the technical strength is, there is such a thing as all image produced in the reality basis and core—true feelings. Whether the image is happy or sad, good or evil, beautiful or ugly, clear or chaos, real or virtual, if it contains the depths of the human soul and the true feelings, as praise for the pursuit of beauty; Whip and fight against the war, violence, exploitation, oppression, cheat all the ugly, alienation, distortion, then on the emotional level, image has authenticity, and even can be said, this is an eternal meaning of images from real.

REFERENCES

- [1] Jiang Ke. Acura pure: Thoughts about Novel “*Under the Hawthorn Tree*” in the [J]. Youth writer (Sino-foreign Literary Version). 2010 (6).
- [2] Hu Sha. *The Elegy and Beautiful Love Under the Hawthorn Tree—“Under the Hawthorn Tree” Love Ethics [J]*. Journal of Huazhong Normal University (Humanities and Social Sciences Edition). 2010 (1).
- [3] Qin Xiaolin. *Digital Image Real [J]*. Northwest Art. 2010 (2): 51–53.
- [4] Huang Wen Da. *About the Image Authenticity [J]*. Social Science. 2007 (11).
- [5] Ni Xiang Bao. *How Can We Reduce the Influence by “Avatar” [J]*. Journal of Zhejiang University of Media and Communications. 2010 (4).
- [6] Shao Ling. *What Makes us think constantly of [N]*. 2010.2.26. Wen Wei Po, Culture News, Culture View.
- [7] Miu Xiao Chun. *The Power of the Images [J]*. Oriental Arts. 2010 (13).

Methods and measures of project cost implementation and control on all the stages of engineering project

Jian Xin Li

Sichuan College of Architecture Technology, Deyang City, Sichuan Province, China

ABSTRACT: In consideration with features of the corresponding stage of construction cost, the paper analyzes the methods and measures to control the construction cost in corresponding stage and proposes some suggestions, putting forward that control, implementation and management of the project cost should be run through the whole process of construction projects and attaching great importance to every link of construction cost. Only in this way, can the final construction cost management be ensured reasonable and systematic.

Keywords: construction cost; implement; control; methods and measures

1 BASIC CONCEPTS OF PROJECT COST

Project cost management is a pointer to the whole process of engineering project construction, the full range, multi-level use of technology, economic and legal means of management, through the project construction process cost forecasting, optimization, control, analysis, supervision, investment efficiency to maximize the optimal allocation of resources and construction projects. The total cost of construction project cost is the completion of a project is required to spend [1].

2 BASIC PRINCIPLES OF PROJECT COST VALUATION

Cost is the lowest economic limit of construction engineering project cost valuation is a specific function, is completed in a specific place and time of building products, engineering cost should be higher than the cost, this is the single building product price decision. Our country "Bidding Law" also stipulates lower bid not cost bidders. So the cost is the lowest economic limit project cost valuation, it has also been effective protection in the law.

An important task in the current project cost management is to completely abandon the legal effect of ration, give full play to the regulatory role of the market, change the amount of "quantity one price", the "separation of quantity and price", realize the price mechanism based on market the formation of project cost.

The design phase should be the focus of project cost control and management, according to the analysis of the western countries, the design cost is only

equivalent to the entire process of construction cost is below 1%, the influence degree which is less than 1% of the cost of the project cost accounts for more than 75%. In the field of engineering construction, engineering design and project cost control is not closely linked is a universal phenomenon, think design is just a design personnel responsibility, cost control is the cost of personnel responsibilities, resulting in the design of generally pay more attention to product safety and practical design, advanced technology, emphasizing the design value, do not pay enough attention to the economy design of products [2]. Therefore, to ensure that the design work can fully weigh the formation of a more reasonable design in four aspects of safety, function, standard and economy, it is necessary to the project design phase of the project cost control and management to do the following work.

3 BASIC CHARACTERISTICS AND PROJECT COST CONTROL

As a commodity, construction products have a long construction period, more procedures, resource consumption, influence factors, such as valuation of complex, reflected in the project cost management is the performance characteristics of multi subject, stage, dynamic, system.

3.1 *The project cost and control the implementation of multi subject*

Many of the main project cost management object is the project cost, but the subject of engineering cost management, not only refers to the project

legal person, including the competent department of the government, industry associations, cost consulting agencies, contractors, design units are also the subject of the engineering cost management. The competent department of the government promulgated laws and regulations, industry associations on the project cost management in the implementation of the technical guidance, the two sides according to the engineering cost implementation behavior are around the project cost of construction cost management, which has much subjectivity obviously.

3.2 *The project cost and control the implementation stage*

A construction project in general to go through the project decision, engineering design, construction bidding, construction, completion and acceptance stage, the corresponding the engineering cost documents including investment estimation, preliminary design and construction drawing budget estimates, bidding price, settlement and the completion of project accounts etc.. One is project cost management content is dynamic in each stage of project construction. For example: in the project decision-making stage, project cost management the goal is to prepare a reliable estimate of investment, in order to ensure the validity of decision; in the construction bidding stage, is to make the tender and can reflect the changes in the market and technical level; in the construction stage, is the prerequisite to meet the quality and schedule as much as possible under the control of engineering cost in order to improve the efficiency of investment. The goal is to prepare a reliable estimate of investment, in order to ensure the validity of decision; in the construction bidding stage, is to make the tender and can reflect the changes in the market and technical level; in the construction stage, is the prerequisite to meet the quality and schedule as much as possible under the control of engineering cost in order to improve the efficiency of investment.

Two is the construction cost is also dynamic. During the construction, there are many uncertain factors, such as the price level, social factors, natural conditions, are dynamic in nature, so it has the dynamic engineering cost management. During the construction, there are many uncertain factors, such as the price level, social factors, natural conditions, are dynamic in nature, so it has the dynamic engineering cost management.

3.3 *The engineering cost management system*

Project investment estimation, cost of preliminary design, construction drawing budget, pre tender, the contract price, settlement and the completion

of project accounts the system of project cost management. Only to the study of the project cost management as a system, in principle, viewpoint and method of system engineering to the implementation of the project cost management, to the overall implementation of effective management, realize the maximum efficiency of investment [3].

4 DIFFERENT STAGES OF THE PROJECT CONSTRUCTION COST AND CONTROL THE IMPLEMENTATION METHODS AND MEASURES

4.1 *The project decision-making stage*

The project cost decision-making phase of the project implementation and control of project to do have a definite object in view. In the reasonable cost of implementation and control target, we will be based on the main factors influencing the decision-making phase of the project cost control, one by one. We need to adopt the correct methods and accurate information, the objective to calculate project cost, good staff for the project decision, which makes the decision-making phase of the project construction cost control and implementation achieved satisfactory results.

4.2 *Feasibility study for project*

The feasibility study refers to the investment decision, the advanced technology of the proposed project and applicability, economic rationality and validity, as well as the construction the comprehensive analysis of the necessity and feasibility, so that whether the project should invest and how to invest and conclusive opinions, and provide reliable scientific basis for project investment decision-making. To select the optimal construction scheme. The construction scheme is good not only to consider the cost of project construction, but also consider the completion of operations costs.

Including the selection of reasonable and economic construction. Die; selection of advanced and applicable, economic and reasonable technology process and production method; the correct choice of the main process equipment; select the appropriate construction area and site.

4.3 *Select the accurate data, the correct method of preparation of investment*

Engineering cost estimate value corresponding to the decision-making phase of the project is estimated investment amount, it is an important part of the project pre construction preparation of project proposal and feasibility study report, is one of the important basis of project

decision-making. Investment estimation accuracy not only affects the quality and economic feasibility evaluation of research results, but also directly related to the preparation of the next stage of design and construction drawing budget estimates, the construction project financing scheme has direct influence. Therefore, the project cost comprehensively and accurately estimate the construction project, is an important task in the feasibility study and the decision-making stage cost management, mainly from the choice of cost data accurately and the use of correct estimation method to be realized.

4.4 *Reasonable financing strategy, reduce the cost of capital*

Financing structure and source of funding the project directly affects the construction project cost, thereby affecting the project decision. Mainly from the following aspects consider: determining capital requirements, choose reasonable financing modes, select the source of funds, as far as possible to reduce the cost of capital, the risk of investment.

4.5 *The design phase of the project includes the following two stages*

The stage of preliminary design and construction drawing stage. The preliminary design phase of the project the project cost is the cost of preliminary design project; project cost in construction drawing design stage is the corresponding construction drawing budget. Both the budget and construction drawing budget project preliminary design, which is based on the project feasibility study on the project in the design of further improve and deepen. The total cost should be controlled in the range of estimated investment of the project total investment value allowed by the floating inner. The budget documents is an important basis for future bidding bidding, construction stage, the payment of specific costs. We should actively and timely involved in the project design, to meet the project functional, practical, advanced at the same time, the economy is also considered. Let the design always with the economy even as one, design optimization, cost control.

The construction phase is the concrete implementation stage of the project investment, investment cost is the most concentrated stage. A contract price should be strictly according to the contract The same price, and do a good job in the period of the data record and audit work. The project cost in this stage corresponds to the settlement price. The project cost in this stage corresponds to the settlement price.

A complete, effective data is the objective, real, credible conclusion assurance, data collection,

collation and the construction process is smooth. An important guarantee for the. In addition to various types of the national norm, standard extraction cost, cost information and relevant document, data also includes reporting, engineering drawings, bidding documents, tender documents, bid clarification supplementary documents, BOQ, construction contract, engineering change notice, the construction organization design, project acceptance, the procurement contract equipment and material, various supplemental agreement, process contact list, meeting minutes and other geological investigation, the above all kinds of data to a personal registration, sorting and classification management. The work of early do the fully implemented in the actual construction, and the expenses are well documented, lay the foundation for the future engineering settlement [4].

The main equipment and bulk materials cost occupies a very important position in engineering cost, is also an important link to control cost. Mainly in the following aspects of work:

1. The large equipment orders, procurement of bulk materials must adhere to tender;
2. The small small quantities of materials procurement to adhere than quality than price, than the credibility of the three principles;
3. In strict accordance with the construction, the design requirements to prevent shoddy work, strictly the quality pass;
4. To strengthen the quantitative management, according to the quota content material, perfect material warehouse management system.

Engineering change, contract visa is another important factor of project cost in construction stage, is one of the main reasons to break easily investment control target. So it is important to strengthen the engineering change, contract management is to ensure a visa, investment control measures to achieve the goal of. Mainly include:

1. The engineering change should be identified as soon as possible and inform the relevant departments;
2. The strict implementation of change, visa approval procedures, to which the occurrence of engineering quantity and the contents of the audit, analysis, comparison;
3. And resolutely put an end to increase the expenses caused by the tender documents and contracts are not perfect.

After finishing the project, in project completion and acceptance stage, this stage is the final stage of the project cost, the cost is the project completion settlement, to please the qualified related units, organizations for acceptance. Focus on covert project review, concealed engineering quantity have

signed the owner's engineer and engineer confirmed can get settlement. The project on the outside the contract must have the approval process handover certificate. Change to occur during the construction cost to each audit, completion settlement.

5 CONCLUSIONS AND RECOMMENDATIONS

With the basic construction of our country's continuous development and engineering cost system continue to improve, implementation, the project cost control methods and measures, more and more comprehensive and effective. In this paper, according to the characteristics of each stage of engineering cost of construction project, the project cost control methods and measures. Application and put forward some suggestions, the whole process of thought control, implementation and management of engineering cost should be run through the project construction, for each one of the links should attach great importance to, only in

this way, in order to ensure the rationality of cost management system, the final cost. In addition, to the post evaluation has been completed, compared the various stages of construction cost, analysis of the data, find out the reasons of cost changes, the implementation of measures taken by the summary of cost control, timely feedback, accumulate experience for future project cost work.

REFERENCES

- [1] D.L Luo. Determination and control of domestic & international construction project cost [M]. Beijing: Chemical Industry Press, 2008.
- [2] W.Z Kui. The construction project cost management [M]. Xi'an: Xi'an map publishing Pres, 2000: 5-10.
- [3] W Xu, J.W Li. The civil engineering project management [M]. Shanghai: Tongji University press, 2000: 1-6.
- [4] W.P Wang, J.H Li. A highway construction project cost control thinking [J]. Shanxi architecture, 2012, 38(15): 260-261.

A subgrade stability analysis method based on the strain monitoring information

Yi Ming Xiang, Wan Xue Long, Gui Xiang Ling & Bin Du

Guizhou Communications Planning Survey and Design Institute Co., Ltd., Guiyang, China
National and Local United Engineering Laboratory of Mountain Traffic Disaster Prevention and Control Technology, Guiyang, China

ABSTRACT: Since the resilient modulus can well reflect the overall subgrade conditions, it scientifically determines the subgrade stability. Based on the multi-layer elastic system theory, there is an inherent relationship between subgrade resilient modulus and strain of base top surface, and the strain of base top surface can be monitored in real-time and accurately. By using BP neural network algorithm as an inversion method, the mathematical inversion model of subgrade resilient modulus is established, in which the strain of base top surface in the characteristic cross-section is taken as an input variable and subgrade resilient modulus is considered as an output variable.

Keywords: subgrade resilient modulus; flexural tensile strain of base top surface; BP neural network; parameter inversion

1 INTRODUCTION

1.1 Background

Immediate factors affecting subgrade resilient modulus are soil, water content and degree of compaction, while indirect factor is road work environment. Recent studies have shown that subgrade water content, wet and dry types and degree of compaction have an exponential relationship to resilient modulus (Cui 2007, Cheng & Hou 2010), so the use of resilient modulus can better reflect the overall engineering status of the subgrade, and scientifically determine the subgrade steady state. The decrease of subgrade strength is early signs of subgrade deformation and rupture, so that it is necessary to monitor the subgrade strength, and seek effective techniques for real-time dynamic monitoring subgrade resilient modulus, which has important practical value and significance.

1.2 Research method

Taking into account the inherent relationship between subgrade resilient modulus and strain of base top surface, the strain of base top surface can be monitored in real-time and accurately. Based on the elastic layered system theory, the mathematical inversion model of subgrade resilient modulus is established by using BP neural network algorithm, in which the strain of base top surface is taken as an input variable and subgrade resilient modulus

is considered as an output variable. The proposed method is validated by an actual road subgrade example.

2 PARAMETER INVERSION METHOD OF BP NEURAL NETWORK

2.1 Pavement structure calculation parameters

The stress and strain of pavement structure are analyzed by using BISAR3.0 software based on SHELL design method. According to the multi-layer elastic continuous system theory under the double-circle vertical loads, the semi-rigid asphalt pavement from a test section of the national highway 102 from Changchun city to Dehui city in Jilin Province of China is analyzed, model parameters of each pavement structure layer are shown in [Table 1](#), and the mechanical model of pavement structural analysis is shown in [Figure 1](#).

According to China's "Specifications for design of highway asphalt pavement" (JTG D50-2006), the pavement structure is calculated by reference to the interfacial complete continuity in asphalt pavement, the style of double rounds uniform load, standard axle load of 100 KN, loading pressure $p = 0.7$ MPa, and equivalent circle radius of circular uniform distributed load $\delta = 10.65$ cm. Let Y-axis direction is the direction of the road cross-section, Z-axis is in the center line between double-circle uniformly distributed loads, as shown

Table 1. Calculation parameters of pavement structure.

Structure layer	Thickness (cm)	Resilient modulus (MPa)	Poisson ratio
Asphalt concrete pavement	11	1400	0.25
Lime fly-ash base course	34	1500	0.25
Two ashes-soil subbase	20	750	0.30
Fill subgrade	-	15~200	0.35

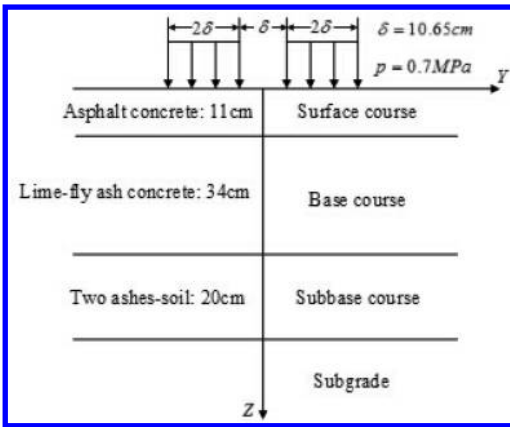


Figure 1. Mechanical model of pavement structure analysis.

in Figure 1. In order to facilitate the comparison of calculation results, the position of circle center is taken as the calculated point. With the change of subgrade resilient modulus under traffic loads, the change of strain on the base top surface in the road cross-section direction (Y-axis) is calculated and analyzed.

2.2 Influence of subgrade rebound module on the stress of pavement structure

Through studying the change of subgrade rebound modulus in the northwest, north and northeast china with the seasons, a great number of literatures show that the range of subgrade rebound modulus was about 15~200 MPa in the course of the year. Therefore, in order to comparative study of the influence of subgrade rebound modulus on the stress of pavement structure, the subgrade Rebound Modulus of 15~200 MPa are chosen in increments of 5 MPa to analyze pavement structural mechanics, which is a total of 38 cases. Finally, flexural tensile strain values of base top surface are

got under different subgrade resilient modulus, as shown in Table 2.

In the training samples, the subgrade resilient modulus are as the output samples, and the flexural tensile strain of base top surface are as the input samples after the sample data are normalized. It is worth noting that after the completion of neural network training, the monitoring data of flexural tensile strain of base top surface should be normalized, then the normalized data are fed into neural network, when the monitoring data of flexural tensile strain of base top surface is used to calculate subgrade resilient modulus. Ultimately, the calculated results of subgrade resilient modulus are achieved after the anti-normalization of the output data.

2.3 Normalization of neural network training samples

In the neural network modeling, the neurons in the hidden layer use the Sigmoid function or the hyperbolic tangent function. This kind of S type excitation function is generally in the range (0, 1) or (-1, 1), while the neurons in the output layer use a linear activation function (Purelin), whose range is $[-\infty, +\infty]$, so that the magnitude of the input values and the output values of training samples may vary greatly. Therefore, the sample data needs to be normalized before network learning, and the

Table 2. Flexural tensile strain values of base top surface under different subgrade resilient modulus.

Subgrade resilient modulus (MPa)	Flexural tensile strain of base top surface ($\mu\epsilon$)	Subgrade resilient modulus (MPa)	Flexural tensile strain of base top surface ($\mu\epsilon$)
15	-105.2	110	-53.8696
20	-98.5252	115	-52.8279
25	-92.908	120	-51.8433
30	-88.1054	125	-50.9109
35	-83.944	130	-50.0262
40	-80.297	135	-49.1854
45	-77.0693	140	-48.385
50	-74.1883	145	-47.6218
55	-71.5975	150	-46.8931
60	-69.2523	155	-46.1964
65	-67.1169	160	-45.5295
70	-65.1625	165	-44.8903
75	-63.3651	170	-44.2769
80	-61.7053	175	-43.6877
85	-60.1665	180	-43.1211
90	-58.7349	185	-42.5758
95	-57.3988	190	-42.0504
100	-56.1481	195	-41.5438
105	-54.9742	200	-41.055

processed sample data is the range of [0, 1] or [-1, 1], so as to ensure that the data is in the same magnitude, and the neural network has sufficient input sensitivity and good fitting to the training samples, thereby improving the efficiency of the neural network training. The processing method of normalization is as follows:

$$x_i' = \frac{2(x_i - x_{\min})}{x_{\max} - x_{\min}} - 1 \quad (1)$$

where, x_i is the i -th original data value of the sample data, x_i' is the normalized value, and x_{\max} and x_{\min} are the maximum and minimum values in the sample data respectively. In the training sample, subgrade resilient modulus as the output sample and the flexural tensile strain of base top surface as input samples are normalized separately, thus the calculated results are as shown in Table 3.

It is worth noting that after the completion of the neural network training, in use of the monitoring data of strain of base top surface to calculate subgrade resilient modulus, the monitoring data of strain of base top surface should be normalized, and then the normalized data will be entered into the neural network to be computed. Finally, the calculated results of subgrade resilient modulus are achieved through the anti-normalization of the output data according to equation (2).

$$y_i = \frac{1}{2}(y_i' + 1) + 1 \quad (2)$$

Table 3. Input and output samples after normalization.

Output data	Input data	Output data	Input data
-1	-1	0.0270	0.6004
-0.9459	-0.7919	0.0811	0.6329
-0.8919	-0.6167	0.1351	0.6636
-0.8378	-0.4670	0.1892	0.6927
-0.7838	-0.3373	0.2432	0.7203
-0.7297	-0.2235	0.2973	0.7465
-0.6757	-0.1229	0.3514	0.7715
-0.6216	-0.0331	0.4054	0.7953
-0.5676	0.0477	0.4595	0.8180
-0.5135	0.1208	0.5135	0.8397
-0.4595	0.1874	0.5676	0.8605
-0.4054	0.2483	0.6216	0.8804
-0.3514	0.3044	0.6757	0.8995
-0.2973	0.3561	0.7297	0.9179
-0.2432	0.4041	0.7838	0.9356
-0.1892	0.4488	0.8378	0.9526
-0.1351	0.4904	0.8919	0.9690
-0.0811	0.5294	0.9459	0.9848
-0.0270	0.5660	1	1

where, the subgrade resilient modulus are obtained by calculation after anti-normalization of y_i , $y_i' \in [-1, 1]$ is the neural network output.

2.4 Determination of neural network topology

The three layer neural network topology of 1-3-1 is selected, namely one input point, three hidden nodes and one output node. The transfer function of hidden layer is a hyperbolic tangent function, the transfer function of the output layer is the linear function (Purelin), and the learning algorithm is the Levenberg Marquardt algorithm. The flexural tensile strain of each measuring point is as the network input, and the subgrade resilient modulus is as the network output. When iteration times are to 985, the fitting error of neural network reaches 10^{-5} , and the entire network training time is 6 s.

2.5 Prediction accuracy of neural network

In order to test the prediction accuracy of neural network, seasonal measurement of soil resilient modulus of a highway in Jilin province is studied in the literatures (Tan 2005, Wu 2005), and the measured subgrade resilience modulus with the seasons in a year are shown in Table 4. The corresponding

Table 4. Subgrade resilient modulus change with month.

Month	Subgrade resilient modulus (MPa)	Month	Subgrade resilient modulus (MPa)
1	185.6	7	32.4
2	188.9	8	30.5
3	52.1	9	43.7
4	40.2	10	46.8
5	17.2	11	38.0
6	28.3	12	187.8

Table 5. Prediction accuracy of neural network.

Month	Desired output (MPa)	Predicted output (MPa)	Relative error
1	185.6	188.52	1.57
2	188.9	186.57	-1.24
3	52.1	54.12	3.88
4	40.2	38.35	-4.61
5	17.2	16.77	-2.50
6	28.3	27.30	-3.54
7	32.4	34.22	5.62
8	30.5	31.83	4.36
9	43.7	45.53	4.18
10	46.8	44.63	-4.64
11	38.0	39.09	2.87
12	187.8	180.68	-3.79

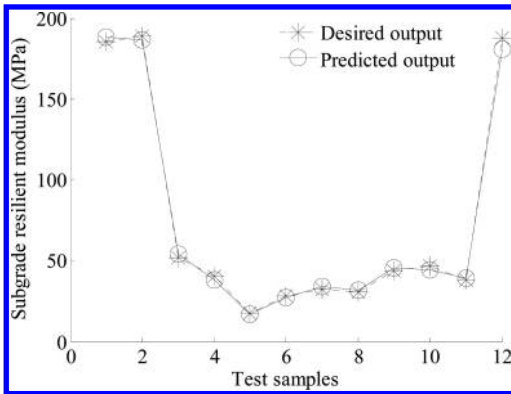


Figure 2. Accuracy test results of neural network.

calculation data of strain of base top surface are entered into the trained neural network in order to get the corresponding subgrade resilience modulus. The calculation results and the relative error of neural network are as shown in Table 5 and Figure 2.

3 CONCLUSIONS

Based on the multi-layer elastic system theory and the SHELL design method, the pavement structure layer is regarded as ideal elastic system, and the subgrade resilient modulus are substituted into the SHELL design method. The relationship between the flexural tensile strain of base top surface and the subgrade resilient modulus is calculated by software BISAR3.0, in which the real-time evaluation of subgrade stability is achieved by monitoring the flexural tensile strain of base top surface. In order to achieve subgrade resilience modulus through the calculation of strain of base top surface, the nonlinear mapping relationship between

the strain of strain of base top surface and subgrade resilient modulus is fitted by using BP neural network algorithm. Conclusions as a result, we draw the following conclusions:

1. The subgrade resilient modulus as a variable is substituted into the pavement mechanics model, so that the strain of base top surface can be calculated with different subgrade resilient moduli. In order to complete real-time dynamic monitoring of the subgrade resilient modulus by monitoring strain of base top surface.
2. The results of pavement structure mechanics calculation example show that, BP neural network algorithm can accurately fit the nonlinear mapping relationship between the strain of base top surface and subgrade resilient modulus, and the maximum relative error between the neural network curve fitting results and the test samples is 4.8%. The subgrade resilient modulus is obtained by calculating the strain of base top surface, and this method has advantages of high calculation speed and reliable outcomes. When the fitting error of BP neural network can reaches 10^{-5} , the network training time is 6 s.

REFERENCES

Cui Lingqiu. The characteristic and determination method of highway subgrade modulus in china's northeast [D]. Xi'an: Chang'an University, 2007 (In Chinese).

Cheng Peifeng & Hou Enchuang. The variation characteristics and prediction road subgrade strength in Harbin city [J]. Journal of China & Foreign Highway, 2010, 30 (1): 57-59 (In Chinese).

Tan Qiping. Study on influencing factors and their relationship of subgrade resilient modulus [D]. Xi'an: Chang'an University, 2005 (In Chinese).

Wu Hongjuan. Influence analysis of subgrade resilient modulus on pavement design [D]. Xi'an: Chang'an University, 2005 (In Chinese).

Research on differential settlement control standard of road subgrade in seasonal frozen area

Yi Ming Xiang, Wan Xue Long, Gui Xiang Ling & Bin Du

Guizhou Communications Planning Survey and Design Institute Co., Ltd., Guiyang, China
National and Local United Engineering Laboratory of Mountain Traffic Disaster Prevention and Control Technology, Guiyang, China

ABSTRACT: The stress analysis model of asphalt pavement structural was established using the finite element method when subgrade uneven settlement deformation occurred. Through analyzing pavement mechanical response under different conditions of differential settlement, the differential settlement control standard of road subgrade in the seasonal frozen area is determined. The result show that: based on the subgrade overall stability requirements, the variable slope rate of 0.12% and subgrade differential settlement of 1.5 cm can be taken as the lower limit of settlement control standards; when considering the flexural strength of pavement materials, the variable slope rate of 0.57% and subgrade differential settlement of 7 cm can be taken as the high limit of settlement control standards. The differential settlement control standard is divided into five levels: safer, safe, dangerous, more dangerous, and very dangerous.

Keywords: seasonal frozen area; subgrade additional stress; differential settlement control standard; finite element method

1 INTRODUCTION

The uneven deformation of subgrade which caused by seasonal freezing and thawing has already become one of the important reason for the early damage of subgrade and pavement of seasonal frozen area. Since the subgrade and pavement can be seen as a whole, the uneven deformation of subgrade can lead to the difference settlement of subgrade, as a result the uneven deformation of pavement will happen and the pavement layer will also generate additional thawing stress, when the uneven deformation exceeds the limit value, the pavement layer will be damaged because of the additional stress and the pavement load exceed the allowable tension stress of pavement materials. The strength and stability of the subgrade are the basic conditions to guarantee the normal used of the road, whether the subgrade is stable mainly features on the deformation size of subgrade settlement. So we need to establish the control standard of uneven settlement, then we can use it to control the uneven settlement of the subgrade and guarantee safety driving. In this paper, we take the properties and design parameters of the first-class highway between Chang Chun and De Hui along the Jing-Ha highway as the basic to establish the

mechanic model of the pavement layer. Through the research the mechanical response of pavement layer in different uneven settlement conditions to determine the control standard of the subgrade and pavement uneven settlement in seasonal frozen areas.

2 ESTABLISH THE ANALYSIS MODEL

2.1 *The basic assumption of the model*

In this paper, we take the pavement layer as the research object. Under the subgrade deformation of thawing and sinking, in the finite model element we take the uneven settlement of subgrade top caused by the uneven subgrade deformation of thawing and sinking as the load condition acts on the top surface of embankment (Huang & Ling 2005, Zheng et al. 2005). Analysis the stress characteristics of pavement structure under the uneven settlement deformation. In the calculation the assumptions we used are as follows:

1. The structure and settlement of the subgrade are symmetric; take half of the pavement into calculation.
2. The pavement layers are elastic materials which are continuous and isotropic, mechanical

properties are represented by modulus (E) and poisson ratio (μ).

3. The pavement layers are continuous in vertical, every layer doesn't have void phenomenon; the asphalt surface and the base are continuous.
4. The effect of temperature change isn't been taken into consideration, only analysis the additional thawing stress.

2.2 Material parameters

The finite model element is established basing on the practical conditions of the first-class highway between Chang Chun and De Hui along the Jing-Ha highway. To simplify calculation, in the analysis we use the surface layer, base and sub-base as the pavement structure system, reference the Specifications for Design of Highway, the design parameter values of the pavement are shown at Table 1. Take safety and practical conditions into consideration, the modulus value choose the average of the upper value and the limited value are regulated by the Specifications for Design of Highway, at the same time, take the material aging and water damage etc disadvantage factors into consideration, the tensible strength value of every structure layers choose the limited value.

2.3 Bound and initial conditions

The deformation principle of frozen soil and observation data showed that the uneven settlement of pavement will generate reversed arch

deformation the settlement of embankment lookalike a bending basin, at the cross-section directions of the subgrade the settlement of center subgrade is bigger than the sides, the settlement model of subgrade is shown at Figure 1. The settlement deformation curve can be fitted by quadratic parabola or cosine curve, in this paper we use the quadratic parabola to simulate the settlement deformation curve when we calculate the additional stress of the asphalt pavement (Wang et al. 2006, Ji 2005).

$$\delta = \delta_{\max} \left(1 - \frac{x^2}{B^2} \right) \quad (1)$$

δ_{\max} : The largest difference settlement of the subgrade.

x : The distance between any point and the center of the subgrade.

y : The difference settlement between any point in the curve and the top of the subgrade.

B : the width of the top subgrade. Origin of coordinates locates at the viatic centerline.

We take the pavement structure layers as the research object when we do the analysis of the pavement structure mechanic response. So we simplify the model as showed in Figure 2. The surface of the pavement and the sides that are explore to air don't have any constrains. The pavement center has the constrain of x direction and vertical direction doesn't have any constrains. The radius of the subgrade settlement is the half of the pavement width, the longitudinal axis of the settlement curve is the center line of the model.

Table 1. Calculation parameters of pavement structure.

Material types	Material	Thickness/cm	Resilient modulus/MPa	Poisson ratio/ μ	Tensile stress/MPa
Surfave layer	Asphalt concrete	11	1400	0.25	0.8
Base	Lime-fly ash concrete	34	1500	0.25	0.5
Subbase	Lime-fly ash soil	20	750	0.25	0.2

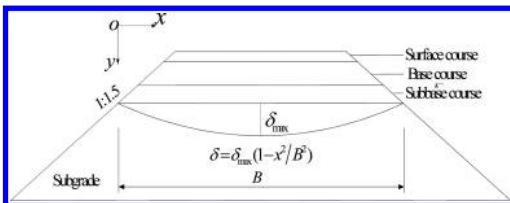


Figure 1. Settlement deformation of subgrade.

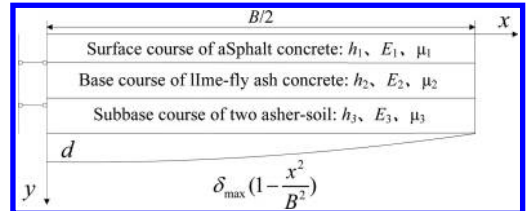


Figure 2. Pavement structure calculation model.

3 THE MECHANICAL RESPONSE OF THE PAVEMENT STRUCTURE UNEVEN SETTLEMENT

3.1 Mechanical analysis of the pavement material tension cleft failure

The finite element analysis showed that when the settlement at the range of from 1 to 10 cm, the stress of the pavement structure will be changed. The calculation result is showed at Table 2 and Figure 3.

From the Figure 3 we can see that uneven settlement has obvious effect on the additional stress of the pavement structure layers. As the uneven settlement increased the horizontal compression of the bottom surface is linearly increased and the horizontal tensile stress of the subgrade bottom surface is also linearly increased, but horizontal compression increases slowly.

From Table 2 we can see that when the settlement is 7 mm, the tensile stress of the subgrade

Table 2. Additional stress calculation of pavement structure.

Uneven settlement/cm	Tensile stress of surface layer/MPa	Tensile stress of base/MPa	Tensile stress of subbase/MPa
1	-0.0489	-0.00214	0.02923
2	-0.09779	-0.00428	0.05846
3	-0.14669	-0.00642	0.0877
4	-0.19558	-0.00856	0.11693
5	-0.24448	-0.0107	0.14616
6	-0.29337	-0.01284	0.17539
7	-0.34227	-0.01498	0.20463
8	-0.39116	-0.01711	0.23386
9	-0.44006	-0.01925	0.26309
10	-0.48895	-0.02139	0.29232

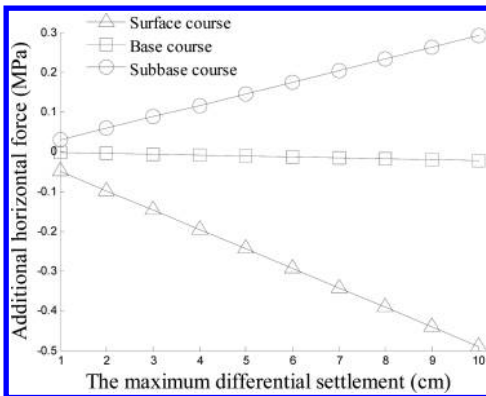


Figure 3. Additional stress of pavement structure.

bottom surface is 0.20463 Mpa, which exceeds the tensile strength 0.2 Mpa and the subgrade will be damaged. Take the traffic loads and material aging, water damage etc disadvantaged factors into consideration, as the time increases the tensile strength will decrease greatly, so the material parameters should choose the limited one, but it still has the chance that can't reflect the practical conditions, so it is reliable to choose 4 mm as the uneven settlement, so when the subgrade damaged because uneven settlement deformation the largest uneven settlement is 7 mm, half of the subgrade width is 12.25 m and the ratio of alter gradient is 0.57%.

3.2 Analysis of the pavement material fatigue failure response

The Specifications for Design of Highway regulates that the fatigue failure strength of asphalt pavement structure layer is characterized by allowable tensile stress of the pavement material. When the additional tensile stress generated by asphalt pavement structure layer bigger than the allowable tensile stress of the pavement material the pavement will be damaged (Gao 2009)

$$\sigma_R = \sigma_{sp} / K_s \quad (2)$$

σ_R : allowable tensile stress of the material.

σ_{sp} : cleavage strength of the material.

K_s : tensile strength structure coefficient.

For the asphalt concrete surface

$$K_s = 0.09 A_a \cdot N_e^{0.22} / A_c \quad (3)$$

For the inorganic binder stabilized base course

$$K_s = 0.35 N_e^{0.11} / A_c \quad (4)$$

A_c : high classification coefficient, high way and first-class road choose 1.0, secondary road choose 1.1.

A_a : asphalt mixture grading factor, fine and medium grain asphalt concrete choose 1.0, coarse grain choose 1.1.

N_e : cumulative equivalent axle in the period of design.

Based on the design structure parameters of the first-class highway between Chang Chun and De Hui along the Jing-Ha highway the calculated allowable tensile stress of the asphalt surface is 0.2 Mpa and the allowable tensile stress of the basement is 0.08 Mpa. From the Table 2 we can see that when the uneven settlement become 3 mm the additional stress of the basement is 0.88 Mpa, which exceeds the allowable tensile stress 0.08 Mpa

and the basement will generate tension crack failure, then some fractures will appear in the asphalt surface. So, if we take the material fatigue property into consideration we should put the uneven settlement of 3 cm and the ratio of alter gradient 0.24% as the control standard.

4 THE CONTROL STANDARD AND CLASSIFICATION OF UNEVEN SETTLEMENT

4.1 Control index of uneven settlement

There are many factors that can influence the uneven settlement, so it's hard to describe the deformation curve. Reference the scientific research achievement of home and abroad, we choose ratio of alter gradient as the control standard of subgrade uneven settlement. The definition of ratio of alter gradient is that (Zhang 2009):

1. The settlement of subgrade center is δ_z , and the settlement of subgrade sides is δ_b .
2. Half of the subgrade width is $B/2$
3. The horizontal uneven settlement of subgrade is $\Delta\delta = \delta_z - \delta_b$, and the ratio of alter gradient is $\Delta_i = (2\Delta\delta / B) \times 100\%$.

4.2 Control standard of uneven settlement

Take the ultimate tensile strength and the fatigue properties into comprehensive consideration, choose 0.5 as the corresponding weight.

$$\Delta_{\text{容}} = 0.57\% \times 0.5 + 0.24 \times 0.5 = 0.41\% \quad (5)$$

$$S_{\text{容}} = 7 \times 0.5 + 3 \times 0.5 = 5 \text{ cm} \quad (6)$$

Take uneven settlement 5 cm and the ratio of alter gradient 0.41% as the control standard. Considerate the stability requirement of frozen soil subgrade, the observation and research results of Wu Ziwang (1988) showed that when the variation range is less than 1 cm the subgrade is stable, when the variation range is 3 cm–4 cm, the subgrade is damaged. And the research of Zhang Dongqing (2008) also thinks that the allowable uneven settlement of semi-rigid subgrade pavement is 1–2 cm. So, considerate the complexity of highway hazard

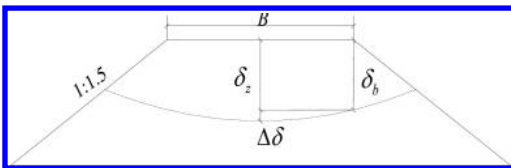


Figure 4. Settlement deformation of pavement surface.

Table 3. Control standard of pavement uneven settlement.

Differential settlement rating	The maximum allowable differential settlement (cm)	The maximum variable slope rate (%)
Safe	<1.5	<0.12
Relatively safe	1.5~3	0.12~0.24
Relatively dangerous	3~5	0.24~0.41
Dangerous	5~7	0.41~0.57
Extremely dangerous	>7	>0.57

in seasonal frozen areas, we take 1.5 cm as the uneven settlement control standard and the ratio of alter gradient is 0.12%.

4.3 Classification of subgrade uneven settlement

Through the analysis we can see that if we considerate ultimate failure the uneven settlement is 7 cm; if we considerate the fatigue properties of subgrade structure material the settlement is 3 cm; Take the ultimate tensile strength and the fatigue properties into comprehensive consideration, the settlement is 5 cm, considerate the stability of the requirement of subgrade the settlement is 1.5 cm. So we put 1.5 cm and 0.12% as the limited value and take 7 cm and 0.57% as the upper value, we divide the classification of subgrade uneven settlement into five different levels, they are: safe, relatively safe, relatively dangerous, dangerous and extremely dangerous.

5 CONCLUSIONS

1. Through the analysis of the pavement structure mechanic response we can see that if we considerate ultimate failure the uneven settlement is 7 cm and the ratio of alter gradient is 0.57%.;if we considerate the fatigue properties of subgrade structure material the settlement is 3 cm and the ratio of alter gradient is 24%; Take the ultimate tensile strength and the fatigue properties into comprehensive consideration, the settlement is 5 cm and the the ratio of alter gradient is 0.41%.
2. Put forward that when we considerate the stability requirement of the subgrade, we put 1.5 cm and 0.12% as the limited value and take 7 cm and 0.57% as the upper value, we divide the classification of subgrade uneven settlement into five different levels, they are: safe, relatively safe, relatively dangerous, dangerous, extremely dangerous.

REFERENCES

- Gao Zhiwei. Study on active control of settlement difference between target based on Mountain Expressway [D]. Xi'an: Chang'an University, 2009 (In Chinese).
- Huang Qinlong, Ling Jianming, Qian Jin-song. Influence of pavement under discrepant deformation after construction between existing subgrade and that to be widened [J]. Journal of Tongji University (Natural Science), 2005, 33 (6): 759–762 (In Chinese).
- Ji Yangbeibei. Study on the design method of asphalt pavement structure in Permafrost Regions [D]. Xi'an: Chang'an University, 2005 (In Chinese).
- Wang Shuangjie, Huang Xiaoming, Hou Shuguang. Numerical Analyses of Pavement Deformation and Stress in Permafrost Regions [J]. Journal of Glaciology and Geocryology, 2006, 28 (2): 217–222 (In Chinese).
- Wu Ziwang, Cheng Guodong, Zhu Linnan, etc. Permafrost subgrade engineering [M]. Lanzhou: Lanzhou University Press, 1988 (In Chinese).
- Zhang Dongqing. Research on diseases and prevention measures of seasonal frozen subgrade [D]. Changchun: Jilin University, 2008 (In Chinese).
- Zhang Yongqing. Study on the characteristics and control measures of differential settlement of Highway Subgrade in Mountainous Region [D]. Xi'an: Chang'an University, 2009 (In Chinese).
- Zheng Yuefeng, Xu Feilong, Xie Jingbao, Ling Jianming. Design of river and creek treatment based on control of uncoordinated deformation in road engineering [J]. Journal of Tongji University (Natural Science), 2005, 33 (4): 466–470 (In Chinese).

Analyzing the influential elements of FLAC strength reduction method of slope safety factor determined

Jing Luo Cai

Taiyuan University of Technology, Shanxi, China
 North China Institute of Technology, Beijing, China

Ze Chuan Ye, Guan Li & Li Hua Zhang

North China Institute of Technology, Beijing, China

ABSTRACT: Safety factor determined many ways in which Fast Lagrangian Analysis (FLAC method) to determine the safety factor is one of the most widely used. After all, it is based on numerical simulation technology. Therefore, this method will be a lot of numerical factors. In this paper, a typical exam ACADS based. This paper from the boundaries and the grid density to safety factor do a little preliminary research. The results showed that the grid density on the slope safety factor greater impact; and if the calculated slip surface as long as the boundaries within the boundaries of the safety factor is not too sensitive.

Keywords: FLAC; strength reduction method; slope; safety factor; influential elements

1 INTRODUCTION

Fast Lagrangian Analysis (FLAC France) to determine the safety factor is used widely because FLAC program built SolveFos solver, thus making use of the method to solve the slope safety factor is relatively easy, once successful, not repeated reduction calculation. Furthermore, FLAC powerful post-processing capabilities are unmatched by other programs, it is easy to track key points displacement, velocity and stress variation with time [1–3]. However, due to the rise of the real strength reduction was 10 years, affecting the program calculates the stability factor of many factors, so many people are skeptical, this paper analyzes the mesh density and boundary on slope stability factor affected.

2 BASIC PRINCIPLE OF STRENGTH REDUCTION

The strength reduction techniques and numerical simulation methods are combined in a given evaluation index, by adjusting reduction factor for slope stability analysis, and seek the minimum slope stability safety factor. The basic principle is to soil strength indicator cohesion and internal friction

angle c is divided by a reduction factor values simultaneously F :

$$\left. \begin{aligned} c' &= \frac{c}{F} \\ \tan \phi' &= \frac{\tan \phi}{F} \\ F &= \frac{\alpha}{F} I_1 + \sqrt{J_2} = \frac{k}{F} \end{aligned} \right\} \quad (1)$$

The formula, α , k can be expressed as:

$$\left. \begin{aligned} \alpha &= \frac{\sin \phi}{\sqrt{3}(\sqrt{3} \cos \theta_s - \sin \theta_s \sin \phi)} \\ k &= \frac{\sqrt{3} \cos \phi}{\sqrt{3} \cos \theta_s - \sin \theta_s \sin \phi} \end{aligned} \right\} \quad (2)$$

By equation (1) to obtain a new set of as a material new parameters for numerical calculation, when the soil slope conforms to a given critical failure state determination conditions, the corresponding F is called a minimum safety factor of slope. Where, are the stress tensor and the first invariant of the stress tensor second invariant bias, different α , k and c , are constants related to different α , k represents the type of the plane Yuan, Zha Shangyi, ZhengYing-ren, DENG Wei-dong et al article in detail and derivation.

3 ENGINEERING EXAMPLE

In 1987, the Australian Computer Applications Society (ACADS) used in Australia slope stability analysis program to conduct a survey. The survey questions designed to assess a total of ten small five questions sent to 120 units calculated invitation. Because of this large-scale survey, so the results obtained are more reliable. This example uses ACADS examination questions 1 (C), this study is a non-homogeneous soil, slope body contains three layers of soil, section dimensions shown in Figure 1, the layers of soil mechanical parameters in Table 1, the final recommendation answer assessment questions safety factor of 1.39.

4 FAST LAGRANGIAN ANALYSIS METHOD TO DETERMINE THE SLOPE STABILITY FACTOR

4.1 Calculation model

Calculation of the horizontal coordinate system used for the X-axis, the Y-axis vertical direction, according to Figure 1, the horizontal distance of 50 m, the vertical distance of 20 m; using Mohr-Coulomb constitutive model; as axial deformation can be ignored, therefore, this calculation is plane strain problem; boundary conditions: left and right side of the boundary constraints for the X-direction, the bottom for X & Y bidirectional constraint.

Table 1. Physical and mechanical properties of soil.

Mechanical parameters	C (kPa)	φ (°)	ρ (kg·m ⁻³)	E (kPa)	ν
Materials 1	0.0	38.0	1950	1.0e4	0.25
Materials 2	5.3	23.0	1950	1.0e4	0.25
Materials 3	7.2	20.0	1950	1.0e4	0.25

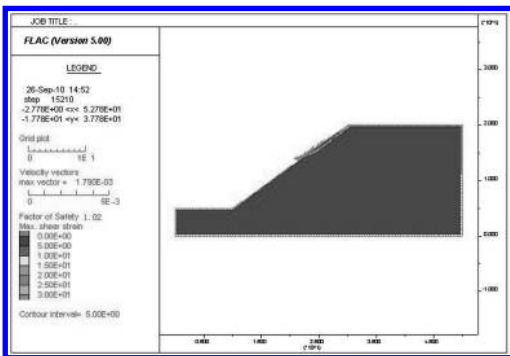


Figure 1. X direction grid number 102, the safety factor, shear strain, velocity vector.

4.2 Different mesh density impact analysis on slope stability factor

For this example, we use the X axis direction to control the basis of the number of grids, Y axis direction, the number of grids will change with the X-axis and corresponding changes in the number of grids. The number of X-axis grid was divided 102, 56, 26, 16 months. Get number of different grid safety factor, shear strain, velocity vector shown in Figure 2, Figure 3, Figure 4, Figure 5.

Figure 2, Figure 3, Figure 4, Figure 5, with the reduction in the number grid, and the shear strain rate vector contour and did not change (mainly concentrated in the top of the hill), which shows how the number of grid position on the slip surface has little effect; but get gradually approaching the recommended safety factor of safety factor of 1.39. When the X-axis grid number is 102, this time to get the safety factor of 1.02, the value and the recommended answer 26.62% of error, showing larger error; And when the X-axis grid number is 16, this time resulting safety factor of 1.36, the value is only 2.16% and the recommended answers errors, the safety factor calculations and errors are summarized in Table 2.

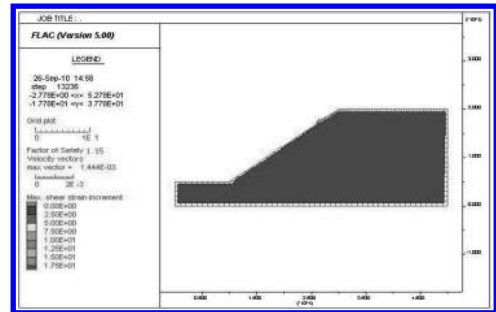


Figure 2. X direction grid number 56, the safety factor, shear strain, velocity vector.

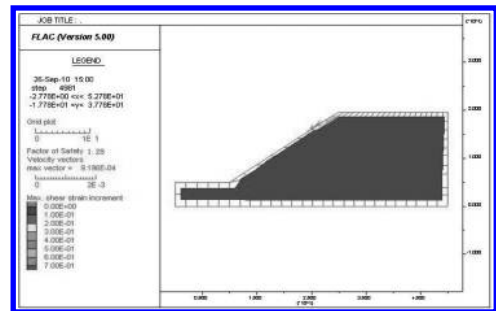


Figure 3. X direction grid number 26, the safety factor, shear strain, velocity vector.

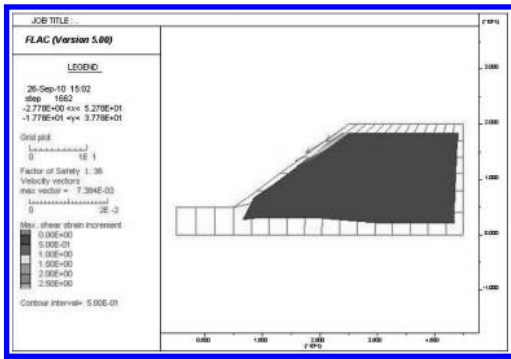


Figure 4. X direction grid number 26, the safety factor, shear strain, velocity vector.

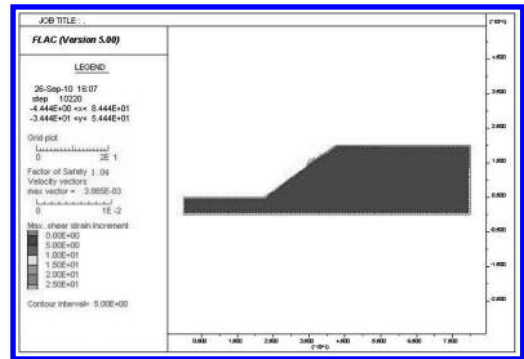


Figure 6. Boundaries X direction grid number 102, the safety factor, shear strain, velocity vector.

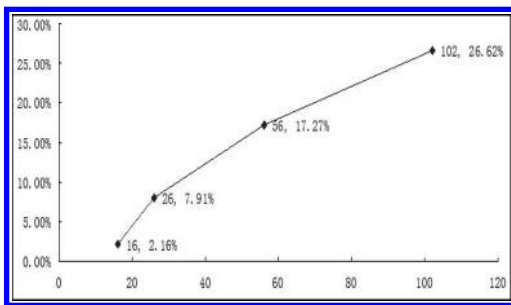


Figure 5. The relationship between the grid number and the deviation.

Table 2. Factor of safety results and deviation.

The number of X-axis grid	102	56	26	16
Safety factor	1.02	1.15	1.28	1.36
Error %	26.62	17.27	7.91	2.16

Table 2 can clearly found that with the increase of the number of grids, the calculated safety factor decreases, the error is gradually increasing. But it must be noted that the safety factor is reduced as the number of computational grid increases is not linear, in my calculation, the number continues to decrease when the grid when this study establish an accurate model of non-uniform slope would be very difficult because it is difficult to accurately determine when layer separation.

4.3 Different boundary impact analysis on slope stability factor

For example this model, according to Zhang Lu Yu boundaries, ZhengYing-ren, who's

recommendation that the distance between the left edge to the foot of the slope 1.5 H (H is the slope height), top of the hill to the right boundary a distance equal to 2.5 H.

According to the above conditions, when the X-axis grid number is 102, after a safety factor calculated is 1.04 (Fig. 6), and in Figure 2 which does not extend boundaries of the results obtained (1.02) is very close, error has only 1.92%, while the number of the X-axis grid are calculated, respectively 56, 26, 16, errors were 1.17%, 1.25%, 1.34%, and the shear strain increment position and distribution of cloud nor change significantly. This shows that, in FLAC, the calculated slip surface as long as the boundary within the scope of the selection boundary for strength reduction has little effect on the calculation results.

5 CONCLUSIONS AND PROSPECTS

Finite difference grid for determining the number of slope safety factor to a certain extent, because the Fast Lagrangian Analysis (FLAC France), after all, is based on the numerical simulation technology, and any numerical simulation techniques rely on the grid, its the results should naturally be the impact of mesh density; and if the calculated slip surface as long as the boundary within the scope of the selection boundary for strength reduction has little effect on the calculation results.

From the engineering point of view, strength reduction only provides an evaluation index, only a preliminary analysis of the slope. But note that the numerical simulation is not a "master key", today's geotechnical community has basically formed a consensus, numerical simulation techniques are essential, but can not completely rely on, otherwise there is a "trade-off" is suspected.

ACKNOWLEDGEMENTS

The corresponding author of this paper is Cai Jing Luo. Project supported by the National Natural Science Foundation of China (51178185).

REFERENCES

- [1] Liu Hai-bo, Liu Yu-li, Lin Da-cha. Discussion on the strength reduction FEM method of the applicability on the basis of Bishop Method of soil slope [J]. Highway, 2010, 3(5):15–18.
- [2] Liu Hai-bo, Qi Hong-wei, Lin Da-chao. Discussion on two kinds of strength reduction methods applicability of determining the slope stability factor [J]. Journal of Earthquake Engineering and Engineering Vibration, 2010, 30(5):11–15.
- [3] Chen Yu-min, Xu Ding-ping. Foundation and Project of FLAC/FLAC3D. BEIJING: China Water Conservancy and Hydropower Press, 2009.

Chaos behaviors of a class of constant-length substitutions and the hyperspace systems

Wei Wang

Information Technology College, Jilin Agricultural University, Changchun, China

Xiao Gang Zhu

The Institute of Changchun Engineering Technology, Changchun, China

ABSTRACT: Research on dynamical system has penetrated into many fields of engineering technology. In this paper, we investigated dynamical properties for non-primitive substitution and the set-valued maps induced by the substitution. We gave a sufficient condition for the hyperspace systems induced by non-primitive substitution don't have distributional chaotic pairs.

Keywords: chaos; constant-length substitution; hyperspace system

1 INTRODUCTION

In the fields of engineering technology, many practical problems related to the chaos phenomenon, such as the change of river water quality prediction of air pollutants concentration, accurate prediction and so on.

To define the distribution of chaotic [1] involved in this dissertation are as follows:

Let (X, f) be a compact system, and d is a topological measurement of X . If there is $Y \subset X$, so that for any different $x, y \in Y$, we have

1. there is an $\varepsilon > 0$, so that

$$F(f, x, y, \varepsilon) = \liminf_{n \rightarrow \infty} \frac{1}{n} \# \{i \mid d(f^i(x), f^i(y)) < \varepsilon, 0 \leq i < n\} = 0,$$

2. for all $t > 0$,

$$F^*(f, x, y, t) = \liminf_{n \rightarrow \infty} \frac{1}{n} \# \{i \mid d(f^i(x), f^i(y)) < t, 0 \leq i < n\} = 1,$$

Then we call Y is a distribution chaotic set of f . If f has an uncountable distribution chaotic set, it is distribution chaotic.

In recent years, it has made some achievements on the study of the distribution of chaos. In [2], it studies the time series of dissolved oxygen in the Lianshui river basin analysis of chaos theory, phase space reconstruction and embedding theory based on the calculation of Lyapunov index, the attractor

dimension and the largest complexity of river water quality system. In [3], it applies the Matlab technology platform and the segmented three Hermite interpolation based on wavelet denoising, using phase space reconstruction was used to construct the neural network model to forecast the time series. In [4], it proves that Short term prediction of river water quality change is feasible, and the application of chaotic phase space model of linear prediction model, the prediction results of water quality management and control of Lianshui Lake Basin has a certain reference value.

2 CONSTANT-LENGTH SUBSTITUTIONS AND SET-VALUED MAPS

Let $S = \{0, 1\}$, $\Sigma_2 = \{x = x_0x_1 \dots \mid x_i \in S, i = 0, 1, \dots\}$, $\rho: \Sigma_2 \times \Sigma_2 \rightarrow \mathbb{R}$ denoted by:
 for all $x = x_0x_1 \dots, y = y_0y_1 \in \Sigma_2$,

$$\rho(x, y) = \sum_{n=0}^{\infty} \frac{|x_n - y_n|}{2^n},$$

Then ρ is a measure on Σ_2 . We all the metric space (Σ_2, ρ) (with two symbols) one-sided symbolic space, or the symbol space.

Definition 2.1 [6] Let η be a constant-length substitution on the symbol space Σ_2 , whose definition is:

$$\eta(0) = a = a_0a_1 \dots a_{n-1},$$

$$\eta(1) = b = b_0b_1 \dots b_{n-1},$$

and is satisfies:

1. $a_0 = 0$,
 2. there is an $i > 0$, so that $a_i = 1$,
- Then there is a fixed point of η in Σ_2 beginning with 0, which is denoted by u .
- Let X_η be the closure of the orbit of u under the action of σ , denoted by

$$X_\eta = \overline{orb(u, \sigma)} = \overline{\{u, \sigma(u), \sigma^2(u), \dots\}}.$$

Then we call the subsystem (X_η, f) the substitution system induced by η .

Let $f = \sigma|_{X_\eta}$, then the restriction mapping $f : X_\eta \rightarrow X_\eta$ is a subshift of σ , and we call it a subshift induced by the substitution η .

Definition 2.2 If the substitution η satisfies $0 \prec \eta(1)$, then η is primitive. Otherwise, η is non-primitive.

Next, we suppose that f is a subshift induced by η , and satisfies the follow conditions:

(C) there are different $s_1, s_2, t \in \{0, 1, \dots, n-1\}$, so that $a_{s_1} \neq b_{s_1}, a_{s_2} \neq b_{s_2}$ and $a_t = b_t$.

Definition 2.3 Let (X, J) be a topological space, $P(x)$ is the family of all non-empty subsets of X and G_1, G_2, \dots, G_n are n non-empty open subsets of X . Put

$$B(G_1, G_2, \dots, G_n) = \left\{ U \in P(x); U \subset \bigcup_{i=1}^n G_i, \text{ 且 } U \cap G_i \neq \Phi, 1 \leq i \leq n \right\}$$

Then all the sets with form

$$B(G_1, G_2, \dots, G_n)$$

make up a topological basis of $P(x)$, we call them Vietoris topology, and call the topological space $(P(X), J_v)$ the hyperspace of (X, J) .

In this paper, we study the family of all closed sets of (X, J) :

$$K(X) = \{K \in P(X); K \text{ is a non-empty compact subset}\}.$$

Definition 2.4 [7] For all $A, B \in K(X)$, let

$$\rho(A, B) = \sup_{x \in A} d(x, B) = \sup_{x \in A} \inf_{y \in B} d(x, y),$$

we call it the Hausdorff separation of A, B .

Call

$$H(A, B) = \max\{\rho(A, B), \rho(B, A)\} = \max\{\sup_{x \in A} \inf_{y \in B} d(x, y), \sup_{y \in B} \inf_{x \in A} d(y, x)\}$$

a Hausdorff measure of $K(X)$.

Let $f : X \rightarrow X$ be a continuous map of X and $\bar{f} : K(X) \rightarrow K(X)$, defined by

$$\bar{f}(A) = \{f(a) : a \in A \subset X\},$$

We call \bar{f} is a set-valued map of $K(X)$, and $(K(X), H, \bar{f})$ is the hyperspace system induced by (X, d, f) .

Next, we suppose η is a non-primitive substitution with constant-length, and ρ_1 is a measure of $\Sigma_2([6])$. (X_η, f) is a substitution system induced by η , and $(K(X_\eta), \bar{f})$ is the hyperspace system.

3 HYPERSPACE SYSTEM AND CHAOS

Theorem 3.1 If η satisfies condition (C), then the hyperspace system $(K(X_\eta), \bar{f})$ has no distribution chaotic pairs.

Proof According to Theorem 3.3 of [3], we see f has no distribution chaotic pairs. That is to say, for all $x_1, x_2 \in X_\eta$, $\varepsilon > 0$, the following formula always holds up

$$\lim_{n \rightarrow \infty} \frac{1}{n} \#\{i \mid \rho_1(f^i(x_1), f^i(x_2)) < \varepsilon, 0 \leq i \leq n-1\} = 1 \quad (4.1)$$

So, for $x_1, x_2 \in X_\eta$ and $\varepsilon > 0$, there is some $N > 0$, so that if $n > N$, $\rho_1(f^i(x_1), f^i(x_2)) < \varepsilon$, i.e.

$$\liminf_{i \rightarrow \infty} \rho_1(f^i(x_1), f^i(x_2)) = 0.$$

For arbitrary $A, B \in K(X_\eta)$, and according to the arbitrariness of $x_1, x_2 \in X_\eta$, we see as $i \rightarrow 0$,

$$\rho(\bar{f}^i(A), \bar{f}^i(B)) = \sup_{x \in A} \inf_{y \in B} \rho_1(f^i(x), f^i(y)) \rightarrow 0,$$

and

$$\rho(\bar{f}^i(B), \bar{f}^i(A)) = \sup_{y \in B} \inf_{x \in A} \rho_1(f^i(y), f^i(x)) \rightarrow 0.$$

Then, according to the definition of [7], as $i \rightarrow 0$,

$$H(\bar{f}^i(A), \bar{f}^i(B)) = \max\{\rho(\bar{f}^i(A), \bar{f}^i(B)), \rho(\bar{f}^i(B), \bar{f}^i(A))\} \rightarrow 0.$$

So for all $\varepsilon > 0$,

$$F(\bar{f}, A, B, \varepsilon) = \liminf_{n \rightarrow \infty} \frac{1}{n} \#\{i \mid H(\bar{f}^i(A), \bar{f}^i(B)) < \varepsilon, 0 \leq i < n\} = 0,$$

and for all $t > 0$,

$$F(\bar{f}, A, B, t) = \limsup_{n \rightarrow \infty} \frac{1}{n} \# \left\{ i \mid H(\bar{f}^i(A), \bar{f}^i(B)) < t, 0 \leq i < n \right\} = 0.$$

According to the definition of distribution chaotic pair, $\{A, B\}$ is not the distribution chaotic pair. For the arbitrariness of A, B , we draw the conclusion that $(K(X_\eta), \bar{f})$ has no distribution chaotic pairs.

ACKNOWLEDGEMENTS

This work was financially supported by the scientific research foundation of Jilin Agricultural University (201310), the Education Department of Jilin province "12th Five-Year Plan" science and technology research projects (2014, No 468), the project development plan of science and technology of Jilin Province (20140204045 NY) and the project development plan of science and technology of Jilin Province (20130522110 JH).

REFERENCES

[1] Balibrea F, Smítal J, Štefánková M. 2005. The three versions of distributional chaos. *Chaos, Solitons & Fractals*, 23:1581–1583.

[2] Xu Min, Zeng Guangming, Xie Gengxin. 2003. Preliminary research on the application of chaos theory to dissolved oxygen prediction. *Acta Scientiae Circumstantiae*, 23(6):776–780.

[3] Liao G.F, Wang W, Fan Q.J. 2009. A class of non-primitive substitutions and chaos. *Chinese J Contemp Math*, 30(2):133–138.

[4] Zhu Yuan, Huang Sheng. 2013. Chaotic prediction of air pollutants based on Wavelet and BP neural network. *Journal of Southwest university of science and technology*, 28(3):24–27.

[5] Xu Min, Zeng Guangming, Su Xiaokang. 2004. A Preliminary Study on Application of Chaos Theory to Prediction of River Water Quality. *Environmental Science and Technology*, 27(1):51–55.

[6] Zhou Zuoling. *Symbol dynamical systems*. 1997. Shanghai: Shanghai Scientific and Technological Education Publishing House.

[7] Ma Xianfeng. 2006. *Discrete dynamical systems for some hyperspaces*. Jilin University, PHD Dissertation.

[8] Liao Gongfu, Wang Lidong, Fan Qinjie. 2013. *Mapping iteration and chaotic dynamical system*. Beijing: Science Press.

Simulation tool application of energy consumption unit in sustainable residential building evaluation

Yuan Su & Yue Fan

Architecture and Fine Art School, Dalian University of Technology, Dalian City, Liaoning Province, China

ABSTRACT: Sustainable residential building refers to reduce the loss of resources, reduce pollution, protect the environment, create a healthy and comfortable living environment, realizes the construction and operation cost minimum during various stages of the life cycle. Energy consumption unit predicting is used as an important evaluation standard to master the energy operation and energy conservation management. This paper is to expound the concept of sustainable buildings and focuses its research on the simulation tool application of energy consumption unit in sustainable residential building. Following the conception of sustainable development and the simulation tool of predicting, sustainable residential building has been designed and came into being and it is provided with a building form which can realize its aim.

Keywords: sustainable residential building; energy consumption unit; CO₂ emissions; energy conservation

1 INTRODUCTION

1.1 *Background*

Global warming is the rising average temperature of Earth's atmosphere and oceans since the late 19th century and its projected continuation. Many studies have pointed out that human activities have contributed to a number of the observed changes in the climate. This contribution has principally been through the burning of fossil fuels, which has led to an increase in the concentration of GHG in the atmosphere. It is an issue to avoid the critical situation caused by the rapid change of climate and to secure sustainability.

United Nations Framework Convention on Climate Change Third Conference of the Parties (COP3) was held in Kyoto, and the Kyoto Protocol which defined the reduction of greenhouse gas including carbon dioxide from the 1990 level in 2012 after 2008 was adopted in December, 1997. The total amount of GHG emissions during the period of 2008 to 2012 should cut down a ratio of 6% reduction. The Japanese government announced on 23rd September, 2009 that Japan will aim to reduce GHG emissions by 25% by 2020 compared to the 1990 level [1–3].

1.2 *Necessity for sustainable residential building in China*

The CO₂ emissions of China have succeeded in a 74% reduction in 2009 from 1978 which was

the peak. The achievements were a result of the environment policy, such as energy saving law, the official announcement and execution of the five-year plan, and the trial of Green GDP. Till 2009, CO₂ emissions by GDP in China are 10 times more than in Japan, and the reduction of CO₂ emissions target in 2020 is to cut down 40% of the emissions from 2005.

At present China construction energy consumption is much lower than the level of the western developed countries. The reasons were summarized that not for low energy consumption, high efficiency, good technology content, strong energy conservation consciousness, but for that the level of economic development and living conditions were low compared with western developed countries. From the statistics analysis, it seems that China didn't need to develop the energy-efficient building and green building at once.

However, energy consumption of buildings in China will be far more than the average value in western developed countries in the near future because of the construction develops, such as the construction number, the construction area and the current construction speed. Therefore, it is urgent to pay close attention to the resource utilization and the development of energy conservation of residential buildings. In prior researches, various works have been reported about definition and evaluation on sustainable buildings in Japan.

2 SUSTAINABLE RESIDENTIAL BUILDING

2.1 Definition

The concept of “sustainable residence building” is definite by the Japanese Ministry of Economy and Trade and Industry (METI) and “create life value residential development technology research group” in 2000. It is the research project named “resource recycling residential technology development project” formally. It is considered the residential building should meet as followings: durability; sustainable; reducing energy consumption and effective utilization of energy residential system in the whole life cycle. [4]

2.2 Steps towards sustainable residential building

“Sustainable building” has been raised around for many years. It contains the following main components: 1) Improving economic efficiency, 2) Protecting and restoring ecological systems, 3) Enhancing the well-being of all people. Sustainable residential building refers to the natural resources recycling and reducing, energy efficient optimization combination, living environment, health and safety, ecosystem balance operation residential, the main point is the resource, energy recycling of various stages of the life cycle of the sustainable building.

3 ENERGY CONSUMPTION UNIT

3.1 Basic unit of energy consumption

Basic unit management is prescribed as an evaluation standard of energy consumption by Energy Conservation Law method in Japan. The concept of energy consumption unit has been mentioned and developed in previous research by professor Ojima [5–8]. Energy consumption unit is judged by the amount of actual energy consumed per floor area, and it may be said that consumption efficiency is high when this value is low. Energy consumption

in numerator is a total amount, which is calculated by converting respectively the usage amount of fuel such as oil and gas, steam and electricity into thermal energy, J (Joule). Finally, they are converted into the equivalent value of crude oil which is named as primary energy. It is easy to compare the characteristics of energy consumption between other similar buildings by using energy consumption unit. The usage will also lead to improvements in formulation of energy conservation related measures by detailed examination of energy consumption unit for different facilities, different sectors and different areas.

3.2 Predicting energy consumption

Based on the research on attribute evaluation of energy consumption unit by Ojima lab [9], peak load can be predicted using energy consumption unit of the different periods once the equipment capacity is decided. Consumed energy amount of different periods can also be predicted using monthly and annual energy consumption unit. The flow of prediction of energy consumption amount using energy consumption unit is shown in Figure 1. However, since there are various buildings’ energy consumption units, selection of a suitable standard energy consumption unit is important. Moreover, it is necessary to correct energy consumption unit because energy consumed changes by aging etc.

Building load calculation program and further technique of predicting energy consumption is shown in Figure 2. The route A of energy consumption prediction matches to the running hours of the equipment and the peak load. Thus, secondary energy amount of consumption can be calculated by multiplication of these directly. However, equipment operates with part load usually, so the energy consumption unit operation differs from rated efficiency, thus it is necessary to make efficiency correction in that case. For example, part-load operation time of the equipment can be converted into the equivalent amount as a full

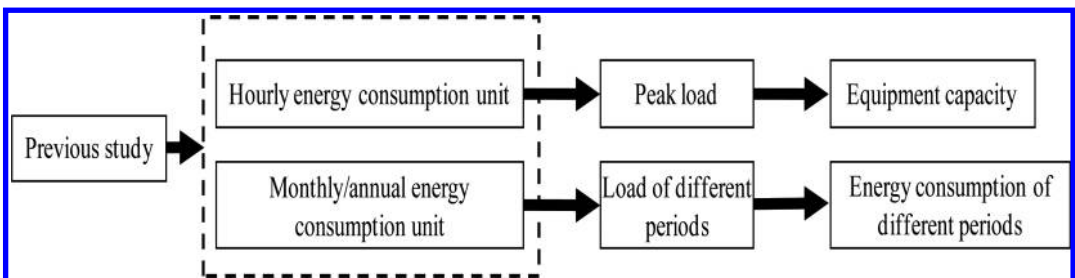


Figure 1. Flow of prediction of energy consumption amount.

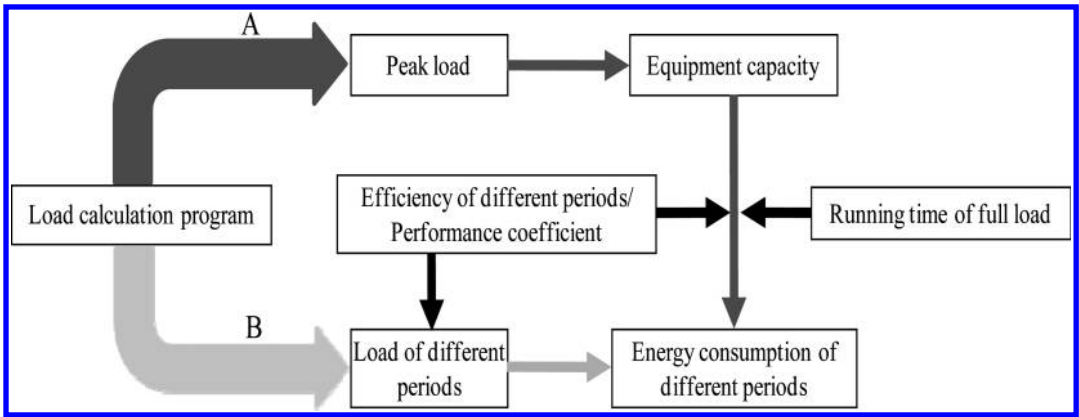


Figure 2. Load calculation program and further technique of predicting energy consumption.

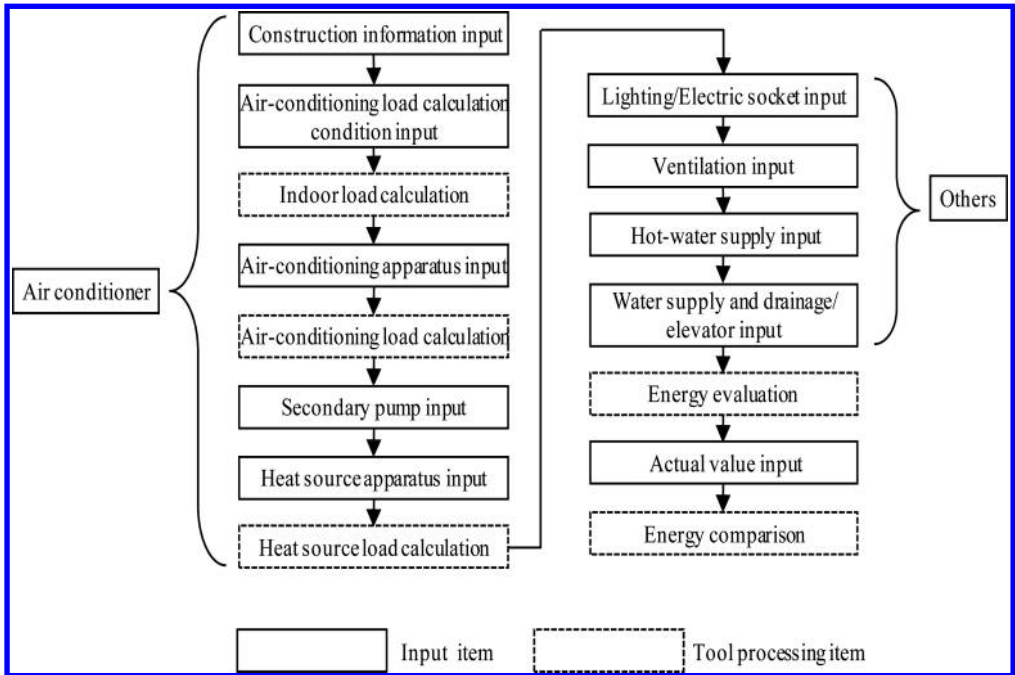


Figure 3. Simulation tool of energy consumption unit for buildings.

load time. This method is called full load equivalent running-hours methods.

The route B of energy consumption is calculated by the load of different periods first, and then the secondary primary energy consumption can be calculated by efficiency of different periods or performance coefficient. Various kinds of load calculation programs are developed recently, and thus the dynamic heat load during the period can be calculated. The method of calculating energy

consumption by paying attention to such a load pattern is called load pattern method.

4 SIMULATION TOOL APPLICATION OF ENERGY CONSUMPTION UNIT

Hayakawa et al developed a simulation tool of energy consumption unit for office buildings. The paper described the simulation tool to evaluate

energy management level of buildings for business use. The annual energy consumption can be easily estimated for various types of buildings whose input parameters are related with building services and end-use conditions [10–11].

In this tool, energy consumption point was considered as eight classifications such as air-conditioning apparatus, pump, heat source apparatus, lighting, electric sockets, ventilation, hot-water supply, water supply and drainage/elevators. Figure 3 shows the program flow of energy unit management tool. Along with this flow, input, calculation, evaluation, and actual value comparison are performed.

First, construction information, the air-conditioning area ratio and indoor load calculation conditions, a floor use calendar, the number of staying-in-the-room staffs, hour-of-use of lighting and an electric socket are inputted and an indoor load calculation is performed. Next, after carrying out the zone definitions of floors with the same air-conditioning conditions, air-conditioning load calculation is performed when inputting the air-conditioning system, the numbers of air-conditioners, the amount of fresh air, etc. Following this, heat source load was calculated after inputting data of secondary pump and heat source apparatus, for instance, heat source kind, numbers, an operation priority, etc. Here to, the calculation was related as air-conditioners.

In addition to air conditioners, electricity consumption of lighting is calculated by capacity multiply numbers and using time. Electricity consumption of electric socket are calculated automatically from load factor (the amount of real consumption divided by installed capacity), or manual operation. Other consumption is calculated by the regression analysis of actual recorded data. If a calculated result is displayed, the result can be compared with the actual value of energy consumed.

5 CONCLUSIONS

In this paper, the introduced concept of sustainable residential buildings from Japan has been stated. The background and characteristic of sustainable residential buildings and methodology of measurement and calculation of energy consumption unit has been described. The evaluation on energy consumption of sustainable residential buildings is examined using simulation tool. As a result, the energy consumption can be calculated and compared by the regression analysis of actual recorded data.

ACKNOWLEDGMENT

We express our deepest gratitude to the “Program for New Century Excellent Talents in University” (NCET-11-0049), “General Project of Science Research from Department of Education of Liaoning Province (L2013017), “Scientific Research Foundation for Doctors from Liaoning Province” (20141021), “Scientific Research Foundation for Doctors from Dalian University of Technology” (DUT12RC(3)90), for the financial assistance provided to support this research.

REFERENCES

- [1] The Kyoto Protocol was adopted in Kyoto, Japan, on 11 December 1997.
- [2] Framework Convention on Climate Change, UNFCCC, <http://unfccc.int/2860.php>, 2012. 2.
- [3] The twelfth session of the Conference of the Parties to the Climate Change Convention (COP 12), in Nairobi from 6 to 17 November 2006.
- [4] Homepage of Ministry of Education, Culture, Sports, Science and Technology, 2012. 1.
- [5] Toshio Ojima et al, Evaluation on the attribute of energy consumption unit, Jess project room Ltd. and Tokyo gas Ltd., 2005. 2.
- [6] Satoshi Hayakawa, Hiromi Komine: An analysis of energy consumption unit in buildings for business use, Part 1 In case of office buildings, Journal of Environment Engineering, No. 578, pp. 85–90, 2004. 4.
- [7] Satoshi Hayakawa, Hiromi Komine: An analysis of energy consumption unit in buildings for business use, Part 2 In case of department stores, Journal of Environment Engineering, AIJ, No. 600, pp. 67–73, 2006. 2.
- [8] Junqiao Han, Toshio Ojima: Prediction of energy consumption based on the floor utilization of general merchandising store, Journal of Environment Engineering, AIJ, No. 580, pp. 77–84, 2004. 6.
- [9] Toshio Ojima Lab, Research on attributes evaluation of an energy consumption unit, JES project room, February 2005.
- [10] Satoshi Hayakawa, Hiromi Komine, Tatsuo Inooka, et al: Development of the simulation tool for energy management of buildings for business use, Part 1 Simulation tool of energy consumption rate for office buildings, Journal of Environment Engineering, AIJ, No. 616, pp. 91–98, 2007. 6.
- [11] Kosuke Satoh, Hiromi Komine, Tatsuo Inooka, et al: Development of the simulation tool for energy management of buildings for business use, Part 2 Expansion of target type of building and enhancement of calculation function, Journal of Environment Engineering, AIJ, No. 630, pp. 1045–1052, 2008. 8.

Analysis of civil construction based on systems engineering theory

Wen Bi Xue

Xi'an University of Architecture and Technology, Xi'an, China
Chang'an University, Xi'an, China

Mao Sheng Yang

Xi'an University of Architecture and Technology, Xi'an, China

ABSTRACT: Systems engineering theory has penetrated into all kinds of engineering and technology. From the perspective of systems engineering, this paper analyze the structure, function, reliability etc. of civil construction, and propose methods of its reliability improvement and dynamic adjustment. The conclusion is that civil construction is a complex system and its successful implementation must be under the guiding of systems engineering theory.

Keywords: civil construction; systems engineering; structure; function; reliability; dynamic adjustment; information feedback adjustment

With the continuous development of systems engineering theory, it has penetrated into all kinds of engineering and technology. Civil construction technology is an important part of natural sciences and its successful implementation must be under the guiding of systems engineering theory. The successful ancient Dayu works and Dujiangyan project, in our opinion, are all outstanding application of systems engineering in civil engineering technology. In modern civil construction organization, the significance of systems engineering is more enormous. In this paper, system engineering theory is used to analyze the process of civil construction, reflecting its huge role.

1 THE STRUCTURE AND FUNCTION OF CIVIL CONSTRUCTION

1.1 *The structure of civil construction*

Systems theory suggests that the structure of the system be composed of elements and relationships between elements. It is described as follows:

$$S = (E, R).$$

In this formula, E represents elements which compose the system; R represents relationships between the elements.^[1]

Thus, the civil construction can be seen as a system which is the combination of personnel, equipment, and technology, with certain relationship between

these elements. It has the function to complete the construction of civil engineering building. It should be noted here is that the elements of the system can be further divided into smaller subsets, for example, personnel can be divided into management personnel, construction personnel etc. And construction personnel can be further divided into carpentry team, reinforced work team, bricklayer team and so on. In addition, elements collection and relationships collections both are indispensable in a system. Personnel, equipment and technology without any relation do not have the function of building up project successfully.

1.2 *The function of civil construction*

Systems theory suggests that general system function is receiving input, processing and transforming, and outputting.^[1] Thus the general function of civil construction system is inputting labor, materials, equipment, water, electricity, energy, and information (of the owner, construction team and supervising organization), through processing and transforming, outputting building.

The improvement of system function depends on high efficiency of processing and transformation. That is, fixed inputs, outputs are more, faster, better; or certain output, less input. The key is to adjust the relationship between elements. To improve the construction system functions, it is necessary to improve relations between personnel, equipment, and technology. It can be classified into two types:

A. Relationship between subsystems

Usually different people operate different equipment and the professional efficiency is different. Different devices should use different techniques, such as sliding form in high-rise building construction technology, tensioner and anchor in post-tensioned prestressed tensioning, and heavy lifting equipment in prefabricated assembly technology in bridge engineering.^[2]

B. Relationship between elements of the subsystem

In construction system, to adjust relationship between elements of subsystem means to coordinate relationships between people, or between equipment, or between techniques. For example, project manager should pay attention to difference in salary and labor intensity to avoid a huge wage unfair between workers and consequent interpersonal disharmony. Equipment should also comply with construction characteristics, such as, the advanced equipment should be used in the most important part of construction, and inferior equipment used in the less important part. Just as Chinese saying “good steel should be used wisely.” So superior lifting crane should be used in main building to make full use of its lifting capacity, and small construction crane can be used to in podium of the building and get its flexibility and rapidness. In construction technology various techniques should coordinate with each other; otherwise it will lead to poor quality of construction, and even complete failure. For example, in post-tensioned construction technology which is used in production of prestressed concrete, tendon profile must be reserved previously.

2 SUBCONTRACT IN CIVIL CONSTRUCTION ORGANIZATION

Systems theory suggests that the optimization of overall system do not require all elements of system are optimal, because optimization of elements does not mean optimization of the entirety. Sometimes, in order to achieve optimum of the whole, some partial interests are to be curbed even sacrificed. Using this theory in the civil construction, we may subcontract unskillful works to other professional construction team, rather than do every part of whole project. For example, with absence of advanced drilling equipment, construction organization should subcontract foundation work to other specialized company and concentrate mostly on the construction of upper part of the main building. Although on the surface a little profit is lost in foundation work, construction organization can take advantage of their strengths in carrying out the upper construction in the long run, because the subcontractor (specialized

foundation construction sector) will certainly give play to their strong points in this area, reducing the duration of project and ensure the quality of construction, which is also beneficial to main contractor and construction companies will eventually achieve an optimal overall efficiency.

3 THE RELIABILITY OF CIVIL CONSTRUCTION SYSTEM

3.1 Reliability analysis of civil construction system

Reliability of system can be defined as the probability that the system will perform in a satisfactory manner for a given period of time when used under specified operating conditions.^[3] So the reliability of construction organization system refers to the probability to complete the project safely ensuring quality and schedule (removing irresistible reasons) at the same time. Only systems of high reliability can obtain good economic results, win in the market and achieve success, so construction organization must improve its reliability to obtain good profit and sustainable development.

In modern construction technology, the most widely used construction technique is construction flow process in which the whole construction process of the proposed project is divided into a number of different construction processes, each construction team are brought into construction in accordance with procedures and complete construction tasks successively. The advantage of construction flow process is successive construction, reasonable schedule, and guaranteed quality. However, these features also determine that the construction system is a typical series model.^[4] In a series model all components must operate in a satisfactory manner if the system is to function properly. Its reliability will decrease greatly if reliability of subsystem decreases.

Reliability of series model can be calculated by the following formula:

$$P = \prod_{i=1}^n p_i$$

Here, p_i represents the reliability of various subsystems.

On the analogy of this, the reliability of civil construction depends on reliability of every process of construction. The failure of one process will cause the failure of entire construction system. That is, the quality of the output of the system—building is not reliable. So reliability of every part of the project, such as foundation works, steel works, concrete works, flooring

works embellishment works and so on should all be under control.

3.2 *Methods to improve the reliability of construction system*

There are a variety of ways to improve system reliability such as elaborate design, best components selection, redundancy technology, appropriate repair, reduction of rated capacity, improvement of the environment, etc.^[5] In construction system, in order to increase the reliability of the system and ensure the construction quality, there are also a lot of methods. Weight-increasing method is a common one. That is, in order to improve the overall reliability of the whole system, we tend to treat the construction procedure differently. For example, in concrete works, which is a very important part of construction, the schedule will be slowed down, extending time of concrete vibrating and curing. Another example is that the speed of construction of key node of beam and column will be reduced in order to ensure construction quality. That is, the weight of important process is increased. On the contrary, in the construction of some less important parts, the pace of the project will be slightly accelerated under the premise that the quality of the project will be guaranteed.

In addition, the reliability of construction system is different in different time. For example, reliability of construction during the daytime is higher than that in the night; and it is lower in winter than in other seasons. To ensure system reliability in different times, the redundant design approach is used. For instance, increasing investment in human resources or material in the winter construction, or extending concrete curing time etc.

It should be noted that advanced construction equipment is the basis of system successful operation, and there is a method called superior element selection method. Although in construction system, management and coordination is very important, but the “software” must be based on reliable “hardware”. “One can’t make bricks without straw”, when the construction organization is lack of necessary advanced equipment, efficient management cannot create efficient construction system.

4 DYNAMIC IMPROVEMENT OF CONSTRUCTION SYSTEM

The construction organization system is a dynamic system. Although civil construction has the fixed site and system function is played in the same place, which looks like static, in fact, this system

is a dynamic system and its product (buildings) is updated continuously and its state parameters change constantly.

A good construction system should be flexible and improving the construction plan in time according to environmental conditions, in order to guarantee that the entire construction system is always under optimum situation. System theory points out: the change of system is absolute, constancy is relative.^[5] And what we need to control is the direction that the system changes. The most common problem in the process of construction is construction schedule variance and the best way to control it is the feedback mechanism, which need guidance of closed-loop system theory. In order to ensure quality and planned speed of construction, the construction schedule should be adjusted timely according to accurate information. Timely, efficient, and detailed construction information recording is the base of effective feedback. So the project supervision and gang master should make construction record every day, and report to the project management promptly. It is best to use computer software to input the process construction information, including records of construction quality and schedule, to adjust system effectively.

The civil construction organization is a hierarchical system.^[6] In general, project manager command gang masters, and gang masters command workers. Usually front-line workers report the project progress and quality information to the gang master, and gang master report to the project manager. This is a normal hierarchical system, on which information feedback is based. But abnormal hierarchical system is also essential. Under some special circumstances, when problems arise, the front-line worker can promptly report to the senior person in charge of the project to ensure the construction safety. So the abnormal hierarchical system is necessary complement of normal system and the combination of the two systems make the feedback more effective.

5 CONCLUSIONS

Construction is the foundation of national economy development. The output of the construction organization system—buildings, possesses the characteristics which is different from other products: fixed space, huge body, huge consumption of material and energy. Once completed, it can’t be completely change.^[6] These features require the construction organization must ensure high quality, otherwise the consequences be unbearable. Civil engineering construction

is of long cycle, more open-air work and poor security. It is full of complexity and comprehensiveness, pursuing overall benefit maximization. These characteristics determine that system theory is needed to guide the civil engineering construction.

It is believed that in the future, science progress and technology innovation will bring revolutionary progress to civil construction. The system engineering theory, which emphasize scientific coordination, comprehensive and systematic is the guiding ideology of the future construction. With the maturation and continuous expansion of application of system engineering theory, it will make further guidance in design and construction of civil engineering and will promote the development of China's construction greatly in the future.

REFERENCES

- [1] Sun Dongchuan & Lin Fuyong. System Engineering Introduction (the second edition) [M], Beijing: Tsinghua University Press. 2009.
- [2] Zheng Tianwang & Li Jianfeng. the Civil Engineering Construction Technology [M], Beijing: China Electric Power Press. 2005.
- [3] Brian Wilson. Systems: Concepts, Methodologies, and Application [M], New York: John Wiley & Sons. 1990.
- [4] Deng Tiejun. Research on the theory and method of reliability in structural engineering construction system [D], Changsha: Hunan university. 2007.
- [5] Wang Yingluo. Systems Engineering (third Edition) [M], Higher Education Press. 2007.
- [6] Frederick E. Gould. Construction Project Management (Professional Edition) [M], Beijing: Tsinghua University press. 2004.

The ventilation of traditional veranda style architecture in Haikou

Ying Wang, Xiao Chen & Yong Ping Wang

Department of Architecture, Nanjing Tech University, China

ABSTRACT: The veranda style architecture built by overseas is one of the characteristics of Haikou city. In this paper, the traditional veranda style buildings in Haikou, including dwellings and arcade buildings with local building components and materials, are introduced. While analysis on its architecture space and ventilation is also made. From the ventilation mode of the veranda buildings, it proves out that climate is an important relatively stable environmental factor, which has a profound impact on architectural form and geographical features. For geographical buildings, the most important issue is to adapt to the local climate. Actually, it is the local geographic environment and climatic conditions which had brought up the original ecological features of directly.

Keywords: ventilation; veranda style architecture; arcade building

1 INTRODUCTION

1.1 Climatic characteristics

Haikou city locates in the north of Hainan Island, at an latitude of 19°57'04"N to 20°05'11"N, a longitude of 110°10'18" E to 110°23'05"E, where is to the south of Qiongzhou Strait, facing Guangdong province across the sea. As located in northern margin of low-latitudes tropics, it belongs to the tropical Marine climate. The climate characteristic here is: warm and dry in spring, hot and rainy in summer, frequent typhoons and storms in autumn, and sometimes cold in winter for cold air invasion.

In Haikou, the annual sunshine time is long, with a strong radiation energy. The annual sunshine hours here are 2000 or more; and the solar radiation can be up to 120000 calories. The annual average temperature is 23.8°C, with a highest temperature around 28°C, and the lowest one about 18°C. The annual average precipitation is 1664 mm, and the average annual evaporation is 1834 mm. The annual average wind speed is 3.4 m/s, mainly in south-east wind. Therefore, in building thermal category, Haikou belongs to the hot summer and warm winter area.

1.2 Historical reasons

Due to the unique geographical environment, coupled with bad social environment like political unrest or difficult life, in history, there were a large number of people in Hainan across the ocean, making their lives in Vietnam, Thailand, Malaysia, Singapore and other South Asian

countries. Haikou had become one of the biggest hometowns for overseas Chinese in Hainan. At the end of 19th Century to early 20th Century, some early overseas, who had successfully established a certain economic base in the host country, came back home and started to purchase land for building new houses. For the curiosity and worship of foreign psychology and advanced concepts, they tried to imitate South Pacific culture by constructing houses in similar style. As a result, many traditional buildings with veranda, had appeared inside Haikou city. Some of them are still preserved today, recalling that period of history.

2 SPATIAL ANALYSIS

Veranda style Architecture, also called Colonial Architecture, is considered to be the architectural style created by European settlers in global colonial expansion, combined with European architectural forms and indigenous traditional building materials. This architectural form, of which the the main function is shade shelter, was quickly accepted by people in hot, rainy areas. It was soon widely used in South Asia and Southeast Asian countries, including India. With the colonial expansion, veranda style architecture also gradually spreaded to South China where the climatic condition is similar.

Veranda is characterized by the overlying roof, colonnade supporting eaves in front of the entrance. In order to adapt to the hot and rainy climate in Hainan, a semi-closed or semi-open space is created for shading both sunshine and rain, and also for ventilation. It is the transition between indoor and

outdoor, and also can be used as the expansion and extension of living space or traffic space.

2.1 Veranda style dwellings

Most of the veranda style dwelling preserved in Haikou were built by overseas. They were usually built in downtown area with dense population and land-use restriction. Therefore, the layout of the buildings was always compact. The colonial veranda style was learned to apply on architectural modeling.

However, the traditional Chinese style was also reflected on interior layout and detailed decorations.

For example shown in Figure 1, it is a residential building built in Haikou city in 1920s by a Singapore overseas. The house faces south, with traditional three-Bay layout width of 10.6 m and a depth of 12.6 m. 2.4 m-wide galleries were arranged on both north and south sides. The stair lead to 2nd floor is located inside the south gallery.

2.2 Arcade building

Arcade building is an important veranda architecture type in tropical and subtropical regions. It is used for both residential and commercial functions.^[1] The First arcade building in Haikou was built in 1849, which appears an Eurasian mixed feature.

Arcade Building is formed to cater the small-scale diversified needs of handicraft industry and the individual business, with a series of contiguous gable walls close together. The layout is compact,

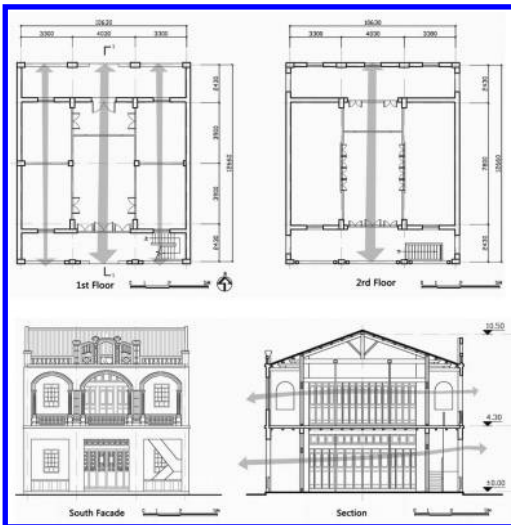


Figure 1. The typical example of veranda style dwellings in Haikou.

forming a continuous dynamic commercial fundamental scene. Most of the arcade Building that facing the streets are usually 2-storey, while a few of them are 3-storey, with a width of 4–6 m and a depth of 10–20 m. From the outdoor space into the interior space, there is a space sequence of “bright-gray-dim-bright-dim” or “bright-gray-dark.”^[2]

This kind of high density layouts makes full use of the block hinterland of the streets. This kind of layout model not only elongates the distance between the streets, but also reduces the width of each facades that takes up, making limited street length to accommodate more shops.

3 BUILDING COMPONENTS AND MATERIALS

3.1 Building structure

The brick timberwork and reinforced concrete technology in Hainan were far-reaching impact by western building technology in early 20th Century.

Many traditional veranda buildings have independent gable walls, with purlines shelved on the brick wall, rafters placed on the purlines, and the tiles directly padded on the rafters. The building roof form is sloping roof. There are mainly two structures as the following:

1. Structure of brick and wood

This technology of structure is brick combined with wooden beams, wooden floor, wooden staircases and wooden roof (shown in Fig. 2). It is especially suitable for the small width of arcade building. Wooden beams are set on the load-bearing walls, with the wood floor laid on it.

This new brick wood construction usually has two or three floors; the construction of vertical has fundamentally changed the traditional layout of a one-story courtyard system.



Figure 2. The wooden roof constructions inside a veranda building.

2. Reinforced concrete structure

The technology of reinforced concrete was imported to Hainan in the early 20th Century. The beam column system is generally divided into main beam and secondary beam in reinforced concrete. The main beams were set on the column; while the secondary beam were set on the main beams. Reinforced concrete floor slabs were paved on secondary beams. In Large rooms, transverse brick columns generally set with a distance of about 2 meters. In order to save money, sometimes wooden floor were used to instead of the reinforced concrete floor.

However, the reinforced concrete was not used widely at that time. On one hand, the reinforced concrete technology relied on steel, cement and other materials imported from abroad; on the other hand, many wealthy overseas Chinese were still prefer to use Chinese traditional structure like wooden floor, wooden walls, wooden partition in their Western-style houses. Of course, the new structure must have new material to adapt. The new building materials were mainly cement, steel, colored glass, iron, expensive wood (black salt, etc) in this period. These materials mostly needed to import from abroad, so the building costs was very expensive.

3.2 Materials and processes

Under the influence of Southeast Asia colonial style, revolutionary changes have taken place in building materials selection. Overseas Chinese in Southeast Asia contacted with the advanced Western system in reinforced concrete structures, they put this structural system back to Hainan when they return. New structures brought new architectural forms like Colonnade, parapet and gallery over the main hall. And reinforced concrete was creatively used in decorative components, producing prefabricated decorative elements which were durable with larger sizes.^[3]

In the process, the arcade building also combines two distinct process characteristics from East and West. The process is prefabricated concrete technology and traditional gray plastic technology in Hainan.

1. Western prefabricated concrete technology

Prefabricated concrete technology is widely used in the arcade building in the 20th Century. Its main materials are imported cement (red mud), sand, steel, wood, and so on. The arch is molded by the concrete, while others are molded by bricks. Railings, parapets and other components are use prefabricated parts and then assembled at the scene. There are many finished parts transport directly from Southeast Asia.



Figure 3. The pediments of a arcade building with ash plastic and prefabricated decorative components on it.

2. Local traditional ash plastic technology

The veranda buildings in Haikou were usually punishable by ash plastic technique on the pediments, the columns, the pillars, etc (shown in Fig. 3). The main material of ash plastic technology is plaster that is constitute in flax, oyster shells and cooked seaweed. Sometimes glutinous rice paste, brown sugar water are added into it, stirring and beating. Ash plastic is molded by the plaster, the minerals toner can be add in the plaster. The surface can be painted when the plaster is semi-dry. Compared to the brick and stone, ash plastic technology has great plasticity.^[4]

4 VENTILATION ANALYSIS

4.1 The exterior wall insulation properties and the selection of materials

The heat absorption of exterior wall is determined by its surface color and texture. Aside from the direct solar radiation. It is also affected by the reflected radiation of the wall nearby. Therefore, the exterior wall in tropical and subtropical region requires to reduce both the direct and reflected radiation. The exterior wall of Haikou veranda building, unlike the white walls of southern traditional architecture, is built with greenish-blue bricks, plastering slurry or hair treatment on the surface. It is reasonable from a physical point: greenish-blue brick wall absorbs more direct solar radiation than white painted wall, but reflects less radiation to others.

In Haikou, ash plastic process is the most common decoration in traditional houses. Its processing technique and materials are used basically the same as ash plastic in traditional buildings: paper-reinforced ash and grass ash are used as the main raw material, shaped on the wire, tiles or bamboo skeletons. The difference is, the ash plastic decoration on veranda buildings is usually not painted, but brushed directly with the grass ash of 3:1 ratio of ash and sand. The

white grass ash reflects heat more easily, making the wall surface temperature about 6°C lower than brick wall, effecting a better insulation.

4.2 Indoor micro climate environments

It is passive energy saving to control air conditioning and adjust the micro-climatic conditions by making full use of a variety of courtyards. It is very important to create a good ventilated environment by using open indoor space, increase the indoor air circulation, so as to improve the indoor environment of damp and hot. So organization internal ventilation. In veranda buildings, courtyard, patio and corridor combination of ventilation system were designed to organize ventilation, promote indoor and outdoor air convection, and accelerate the dissemination of the indoor heat,^[5] just as it is shown in Figure 4.

In Haikou, veranda buildings, through the entry ventilation system formed by small yard, patio and lanes, thermal and moisture problems are solved. The narrow and long layout, using small courtyards type stretched out the practice of hot wind, even in the case of hot and no wind, as the roof and patio temperature rising above, the formation of the upper and lower convection can effectively adjust indoor climate. Using the method of air-flow regulation, through the wind pressure and hot pressing promote the air convection.

4.3 The relationship of the bottom door, bump balcony and hot pressing ventilation

From the indoor microclimate analysis, the role of the bottom door should not be neglected to thermal pressing ventilation. Although the traditional veranda houses can still organize ventilation after

closed the door, but the effect of the thermal pressing ventilations when the door and balcony door open is better. Therefore, during visiting Arcade Building Street have found that there are lower door and threshold set in the entrance of first floor. Residents usually open the door, close the lower door and threshold. It makes good effect to keep the air fresh and play a security role.

On the facade of the arcade building, there are bump balconys or verandahs in early styles. It is a swap space for the indoor and outdoor temperature. Otherwise, the sunlight will be directly through the windows into the lobby. The temperature of lobby will be higher. It will become a source of heat. It is bad for the residents which are living in the lobby. To enlarge the interior space later, the bump balconies are gradually abolished, the external walls are flushed with columns of the arcade building. The blinds are used to reduce the direct sunshine.^[6]

5 CONCLUSION

It is the best embodiment that heat insulation, ventilation and heat dissipation, avoiding the wet, against typhoon, blocking dust of veranda building functions is to adapt to the tropical, subtropical humid climate, and improve the environment of sidewalk, asylum street building entrance. The characteristic of traditional veranda buildings is tall and slim, obscured and transparent, diversified and compatible, realistic but also changed; it reflects architectural culture in Southeast Asia. The Haikou arcade Streets not only show us Haikou residents daily activities, such as shopping, dining, leisure, communion; while its architectural has a certain reference on modern architectural design.

REFERENCES

- [1] Clifton Barton. Trust and Credit: Some Observations Regarding Business Strategies of Overseas Chinese Traders in South Vietnam [J]. Singapore: Maruzen Asia, 1983.
- [2] The arcade in Guangzhou and the protection of arcade Street [D]. Master's thesis of Xi'an University of Architecture and Technology, 2003.
- [3] Yu Chen. Arcade shape in modern cities and buildings [D]. Master's thesis of Chongqing University, 2006.
- [4] Lin Lin, Yan Sun. The arcade plane type and spatial distribution of Guangdong [J]. Southern Building, 2004.
- [5] Yuanding Lu. Lingnan Humanities, Character, Building [M]. Beijing: China Building Industry Press, 2005.
- [6] Hao Xie, Xiaolin Liu, Lunlin Zang. Discussion the shade combine with the art on high-rise buildings [J]. Industrial buildings, 2002.

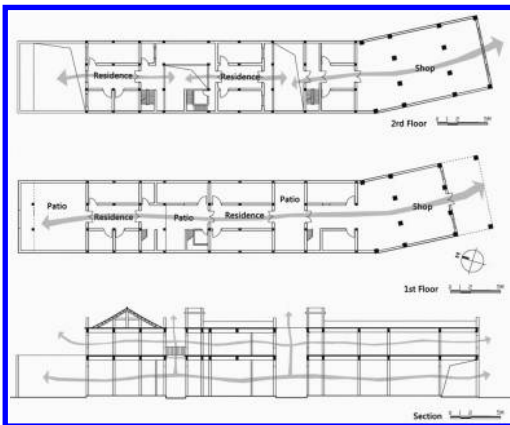


Figure 4. The layout and ventilation schematic diagram of an arcade building in Haikou.

Evaluation of compressive strength of hardening concrete containing high calcium fly ash

Wei Jie Fan & Xiao Yong Wang

Department of Architectural Engineering, College of Engineering, Kangwon National University, Chuncheon, Korea

ABSTRACT: High-calcium Fly Ash (FH) is widely used as mineral admixtures in concrete industry. In this paper, a hydration model is proposed to describe the hydration of high-calcium fly ash blended-cement. This model takes into account the hydration reaction of cement, the chemical reaction of fly ash, and reaction of free CaO in fly ash. Using the proposed model, the development of compressive strength of FH blended concrete is predicted using the amount of Calcium Silicate Hydrate (CSH). The agreement between simulation and experimental results proves that the new model is quite effective.

Keywords: high-calcium fly ash; concrete; hydration; model; compressive strength

1 INTRODUCTION

Mineral admixtures such as silica fume, fly ash, and slag is widely used in concrete. There are two general classes of fly ash can be defined: low-calcium fly ash (FL: CaO content is less than 10%) and high-calcium fly ash (FH: CaO is greater than 10%) [1]. Most investigators reported that adding fly ash to concrete could effectively improve the properties of hardened concrete. Investigations also show that the addition of fly ash can affect the fluidity of fresh concrete [2], porosity, and development of compressive strength [2].

Modeling of hydration of cement based materials is very useful to evaluate the age dependent properties of concrete. In 1997, Tomosawa [3] put forward a model of Portland cement hydration. It is a kinetic model. Park [4] improved Tomosawa's model by considering microstructure development. In 2010, Wang [5] introduced a new model for low calcium fly ash blended concrete.

On the other hand, Papadakis [1] proposed a simplified scheme that describes the activity of silica fume, FL and FH. But, it is a chemical-based steady-state model, not a kinetic model. So in this paper, a kinetic model is proposed to predict the evolution of chemical and volumetric compositions of high-calcium fly ash-cement blends. High-calcium fly ash has pozzolanic and hydraulic properties. It means that FH can consume Ca(OH)₂ (CH) produced from hydrate (CSH). Using the amount of CSH, the development of the compressive strength can be predicted.

2 ESTABLISH HYDRATION MODEL OF CEMENT-FH BLENDS

2.1 Model of cement hydration

The basic hydration equation for cement hydration can be described in the following Eq. (1), which was originally created by Tomosawa [3]:

$$\frac{d\alpha}{dt} = \frac{3C_{w\infty}}{(v+w)r_0\rho_c} \times \frac{1}{\left(\frac{1}{k_d} - \frac{r_0}{D_e}\right) + \frac{r_0}{D_e}(1-\alpha)^{-1} + \frac{1}{k_r}(1-\alpha)^{-2}} \quad (1)$$

where α = hydration degree of cement particle; v = stoichiometric ratio by the mass of water to mineral; w = physically bound water; ρ_c = density of cement; k_d = reaction coefficient in a dormant period; r_0 = radius of cement particles; D_e = effective diffusion coefficient of water; k_r = coefficient of reaction rate for each mineral component; and $C_{w\infty}$ = abundance concentration of water at the outer region of gel.

Eq. (1) is valid in the case of w/c is in high level. But, in fact, during the hydration process, water will be consumed. And the surface of cement particle contacting with water will decrease. Then the relative hydration rate will decrease. The modification of Eq. (1) can be expressed as

$$\left(\frac{d\alpha}{dt}\right)' = \frac{3\rho_w(S_w/S_0)}{\left(\frac{1}{k_d} - \frac{r_0}{D_e}\right) + \frac{r_0}{D_e}(1-\alpha)^{-1} + \frac{1}{k_r}(1-\alpha)^{-2}} \times \frac{w_0 - (v+w)\alpha C_e}{(v+w)r_0\rho_c w_0} \quad (2)$$

In Eq. (2), the cement particles are assumed to be spherical and of uniform size with an average radius of r_0 , ρ_w = density of water w_0 is the water mass; the item $((w_0 - (v+w)\alpha C_e)/w_0)$ considers the decrease of the available capillary water for cement hydration, C_e = cement mass; S_w = effective surface area of the cement particles in contact with water, and S_0 = total surface area if the surface area develops unconstrained.

The value k_d is described as follows

$$k_d = \frac{B}{\alpha^{1.5}} + C\alpha^3 \quad (3)$$

where B and C are reaction coefficients of cement in the initial dormant period.

The effective diffusion coefficient of water (D_e) is affected by the tortuosity of the gel pore as well as the radius of the gel pore in hydrate. This phenomenon can be expressed as a function of the degree of hydration and is expressed as

$$D_e = D_{e0} \ln\left(\frac{1}{\alpha}\right) \quad (4)$$

D_{e0} = value of hydration degree (α) equal to $1/e$.

2.2 Model of FH reaction in cement-FH blends

The addition of FH has both physical and chemical effects on the hydration of cement. The physical effect includes a retardation effect and heterogeneous nucleation. The chemical aspect is the pozzolanic and cementitious activity of fly ash. Compared with the physical effect, the chemical effect has a dominant influence on the long-term properties of FH-concrete [5–6].

The reaction of high calcium fly ash is assumed to consist of three processes, i.e. initial dormant process, phase boundary reaction process, and diffusion process. In FH, only glass phase will react, and the hydration equation of the active (glass) part in FH can be written as follows

$$\frac{d\alpha_{glass}}{dt} = \frac{3C_{free}\rho_w m_{CH}(t) \times 1/v_{FH} r_{0FH} \rho_{FH} P}{\left(\frac{1}{k_{dFH}} - \frac{r_{0FH}}{D_{eFH}}\right) + \frac{r_{0FH}}{D_{eFH}}(1-\alpha_{glass})^{-1} + \frac{1}{k_{rFH}}(1-\alpha_{glass})^{-2}} \quad (5a)$$

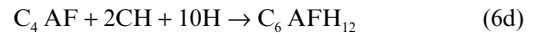
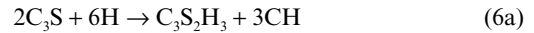
$$k_{dFH} = \frac{B_{FH}}{\alpha_{glass}^{1.5}} + C_{FH}\alpha_{glass}^3 \quad (5b)$$

$$D_{eFH} = D_{e0FH} \ln\left(\frac{1}{\alpha_{glass}}\right) \quad (5c)$$

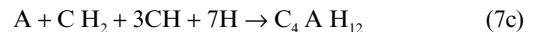
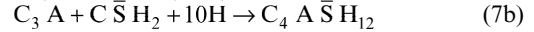
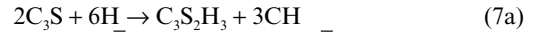
where P = quality of the FH in mixing proportion; v_{FH} = stoichiometry ratio by mass of CH to FH; r_{0FH} = radius of the FH particle; ρ_{FH} = density of fly ash, k_{dFH} = reaction rate coefficients in the dormant period; B_{FH} and C_{FH} are coefficients; D_{e0FH} = initial diffusion coefficient; $m_{CH}(t)$ = calcium hydroxide content; k_{rFH} = reaction rate coefficient. As shown in equation (5a); because FH is a cementitious material, the reaction of FH relates with calcium hydroxide and capillary water.

2.3 Phase volume fractions of cement-FH blends

Papadakis [1] proposed that the chemical reactions of the mineral components of Portland cement can be expressed as follows:



And the chemical reactions of the mineral components of FH can be expressed as follows:



The Portland cement and FH can be analyzed in terms of oxides: total CaO (C), SiO₂ (S), Al₂O₃ (A), Fe₂O₃ (F), SO₃ (\bar{S}). Let us denote $f_{i,c}$ and $f_{i,p}$ as the weight fractions of the constituent i ($i = C, CF, S, A, F, \bar{S}$) in the cement and FH, respectively. In FH, only the glass phase can react. γ_A and γ_S are the weight fraction of the oxide S and A in the pozzolan. Using the molar weights of reactants and products, the amounts of the produced compounds Calcium Hydroxide (CH) and Calcium Silicate Hydrate (CSH) can be calculated as follows:

$$CH = RCH_{CE}\alpha Ce - \{(1.851\gamma_S f_{S,p} + 2.182\gamma_A f_{A,p}) - 1.321(f_{C,p} - 0.7f_{\bar{S},p})\}\alpha_{glass}^P \quad (8a)$$

$$CSH = 2.85(f_{S,c} \times \alpha \times Ce + \gamma_S f_{S,p} \times \alpha_{glass} \times P) \quad (8b)$$

In Eq. (8a), RCH_{CE} = mass of produced calcium hydroxide from the hydration of cement.

3 EVALUATION OF COMPRESSIVE STRENGTH

To verify the proposed model, experimental results from Papadakis [1] are used. The physical and chemical characteristics of the cement and FH are given in Table 1.

Table 1. Physical and chemical characteristics of cement and FH.

	Cement	Pulverized FH
<i>Physical properties</i>		
BET specific surface (m ² /g)	1.3	6.2
Particle mean diameter (μm)	14.0	12.6
Density (kg/m ³)	3130	2660
<i>Mineralogical characteristics</i>		
Insoluble residue (%)	0.14	30.88
Glass phase content (%)	–	50
<i>Chemical analysis (%)</i>		
SiO ₂	20.10	39.21
Al ₂ O ₃	4.25	16.22
Fe ₂ O ₃	3.49	6.58
CaO	63.20	22.78
SO ₃	2.88	4.30
LOI	0.86	2.10

Table 2. Absolute and relative mixture proportions for mortar specimens.

Specimens	Control	FHA1	FHA2	FHA3
C	154.6	154.6	154.6	154.6
W	257.4	257.4	257.4	257.4
P	0.0	51.5	102.9	154.4
A	1544	1492	1441	1389
W/C	0.5	0.5	0.5	0.5
A/C	3.0	2.9	2.8	2.7

C, W, P, A: kg of cement, water, FH and aggregate, respectively, per cubic meter of total mortar volume; W/C, P/C, A/C: the water-cement and aggregate-cement ratio, respectively.

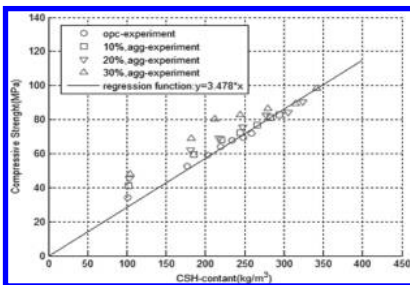


Figure 1. Compressive strength of concrete as a function of calculated CSH content.

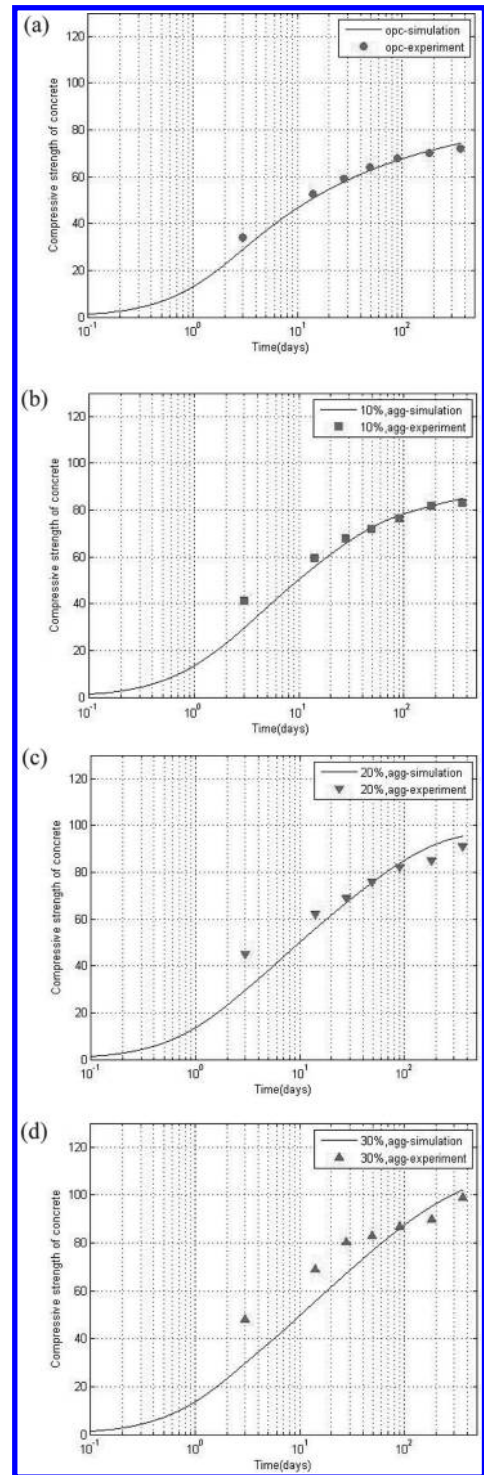


Figure 2. Evaluation of compressive strength of FH concrete.

In the control specimen, the water-cement ratio (W/C) was 0.5 and the aggregate-cement ratio (A/C) was 3. FH to replace volume of aggregate, three contents of FH were selected: 10%, 20%, and 30% addition to the cement weight giving specimens FHA1, FHA2, and FHA3, respectively. The mixture proportions are given in Table 2.

The specimens were prisms of $40 \times 40 \times 160$ mm, cured under lime-saturated water at 20°C , and tested for compressive strength at the ages of 3, 14, 28, 49, 91, 182, and 364 days.

3.1 *The relationship between compressive strengths and calculated CSH amounts*

Using proposed hydration model, we can calculate CSH contents. Figure 1 presents the compressive strength of FH blended concrete as a function of calculated CSH contents. As shown in Figure 1, for concrete with different FH contents and different ages, a single linear relationship exists between the compressive strengths and calculated CSH amounts.

Using the gradient of line shown in Figure 1, we can evaluate the development of compressive strength of FH-cement blends. Figure 2 shows the comparison between experiment results and simulation results of compressive strength of mortars. We can clearly find that good agreement between predicted value and experimental value. In the early-age, the simulation value is slightly lower than the experimental value.

Maybe because of the nucleation effects of FH [6], we do not consider this effect in the modeling.

4 CONCLUSIONS

The paper presents a kinetic hydration model of cement-FH blends. The reaction of FH is divided

into three processes, i.e. initial dormant process, phase boundary reaction process, and diffusion process. The amounts of Calcium Silicate Hydrate (CSH) are predicted considering the contributions from cement hydration and FH reaction. Furthermore, the development of compressive strength of FH-concrete is evaluated using CSH contents. The simulation results agree with experimental results.

REFERENCES

- [1] Vagelis G. Papadakis, Effect of fly ash on Portland cement systems: Part II. High-calcium fly ash, Cement and Concrete Research, Volume 30, Issue 10, October 2000, Pages 1647–1654.
- [2] Wei Sun, Handong Yan, Binggen Zhan, Analysis of mechanism on water-reducing effect of fine ground slag, high-calcium fly ash, and low-calcium fly ash, Cement and Concrete Research, Volume 33, Issue 8, 2003, Pages 1119–1125.
- [3] Tomosawa, F., "Development of a Kinetic Model for Hydration of Cement," Proceedings of the 10th International Congress Chemistry of Cement, V. II, F.S. Glasser and H. Justnes, eds., Gothenburg, 1997, 8 pp.
- [4] Park, K.-B., Noguchib, T., and Plawsky, J., "Modeling of Hydration Reaction using Neural Network to Predict the Average Properties of Cement Paste," Cement and Concrete Research, V. 35, 2005, pp. 1676–1684.
- [5] Wang, X.-Y., Lee, H.-S., and Park, K.-B., "Simulation of Low-Calcium Fly Ash Blended Cement Hydration," Materials Journal, Volume 106, Issue 2, March 1, 2009, Pages 167–175.
- [6] wang xiao-yong, lee han-seung, Modeling the hydration of concrete incorporating fly ash or slag, Cement and Concrete Research, volume 40, 2010, pages 984–996.

Experiment validation of gravity feed liquid cooling evaporator simulation

Qing Jiang Liu, Xiao Jie Ma, Shi Yuan Chen, Fang Han & Ren Qing Zhan

Refrigeration and Air Conditioning Department, Mechanic Institute, Tianjin Commercial University, Tianjin, China

Tianjin Key Laboratory of Refrigeration Technology, Tianjin University of Commerce, Tianjin, China

ABSTRACT: In order to the small gravity feed liquid system cold storage optimization, it is analyzed that the evaporator area in gravity feed liquid system is how to influence the efficiency of the system. The visual basic software is used to simulation. The influence of heat transfer coefficient, heat transfer temperature difference and refrigerating capacity is simulated with the change of the evaporator area of the refrigeration system. Through the experiment validation, the feasibility of the application software is determined.

Keywords: cold storage; gravity feed liquid refrigeration system; area of evaporator

1 INTRODUCTION

The small cold storage using gravity for liquid cooling is an efficient refrigeration system. In this paper, the computer simulation technology is used to optimize the evaporator.

2 THEORETICAL ANALYSIS AND SIMULATION CALCULATION

2.1 Mathematical mode

As a result of the two-phase flow heat transfer calculation is relatively complex, in order to simplify the calculation, the mathematical model of recycling evaporator is the following basic assumptions:

1. The refrigerant in the tube and the air outside the tube is one-dimensional, steady-state flow;
2. The air state parameters of the evaporator inlet are uniformly distributed;
3. Neglect the axial heat transfer, heat transfer only in diameter direction;
4. The flow velocity of the refrigerant is same in each channel, and it is the average flow velocity.
5. The frost layer on the surface of the evaporator surface is evenly distributed
6. All non-condensable gas is in the evaporator.

This experiment adopts the mean logarithmic temperature difference method to do the

heat exchanger. The heat transfer equation is following:

$$Q = KA\Delta t_m \quad (1)$$

Thermal equilibrium equation is following:

$$\begin{aligned} \phi &= q_{m1} \cdot c_1 \cdot (t_1' - t_1'') \\ &= q_{m2} \cdot c_2 \cdot (t_2' - t_2'') \end{aligned} \quad (2)$$

Heat transfer coefficient K is

$$K = \left[\frac{a_{of}}{a_i \cdot \alpha_i} + r_i + r_w + r_s + \frac{1}{\alpha_{a^*e}} \right]^{-1} \quad (3)$$

Q —Transfer heat, W;

a_i —Refrigerant exothermic coefficient, W/(m²·K);

a_{of}, a_i —the evaporator per meter length of the total surface area, Internal surface area, m²;

α_{a^*e} —Air side equivalent heat coefficient, W/(m²·K);

r_i —On the internal surface of the tube fouling resistance, m²·K/W;

r_w —Fin side fouling resistance, m²·K/W;

r_s —Tube wall heat conduction thermal resistance, m²·K/W.

Heat transfer temperature difference is the power of refrigeration system to enhance heat transfer. In the case of other conditions unchanged, the bigger system heat transfer temperature difference is, the bigger refrigerating capacity. The calculating

formula for heat transfer temperature difference is as following:

$$\Delta t_m = \frac{t_{a1} - t_{a2}}{\ln \frac{t_{a1} - t_0}{t_{a2} - t_0}} \quad (4)$$

t_{a1}, t_{a2} —Dry bulb temperature of the air in and out of the evaporator, °C;

t_0 —The refrigerant evaporation temperature in the evaporator °C.

The heat transfer coefficient of finned tube bundle of the lateral air can be calculated as follows:

$$\alpha_{of} = c \frac{\lambda}{b} \text{Re}_f^n \left(\frac{d_0}{b}\right)^{-0.54} \left(\frac{h}{b}\right)^{-0.14} \quad (5)$$

$$\text{Re} = \frac{ub}{\nu} \quad (6)$$

c, n —coefficient, $c = 0.203, n = 0.65$;

b —spacing of fins, m;

d_0 —pipe diameter, m; h —fin height, m;

u —air velocity in the narrow tube section, m/s;

ν —kinematic viscosity coefficient of air, m^2/s ;

μ —dynamic viscosity of air, $\text{pa} \cdot \text{s}$;

λ —the thermal conductivity of air, $\text{W}/(\text{m} \cdot \text{k})$.

2.2 Simulation software

According to the above mathematical model, the calculation software is developed with Visual Basic. The software can be set parameters in the simulation.

In the process of simulation experiment, the working condition of temperature is, respectively, chosen as: 0°C, -3°C, -6°C, -9°C, -12°C, -15°C, -18°C, -21°C, -24°C. The original area of evaporator is $F = 25^2$. This paper is to study the evaporator heat transfer performance in the area of 0.9F, 0.85F, 0.8F, 0.75F, 0.7F. Therefore, need

to separately simulate the evaporator heat transfer coefficient and the heat transfer temperature difference. The effect of the refrigeration efficiency in different evaporator area and working conditions is of comparative study. The results are shown in the Figures 3 and 4.

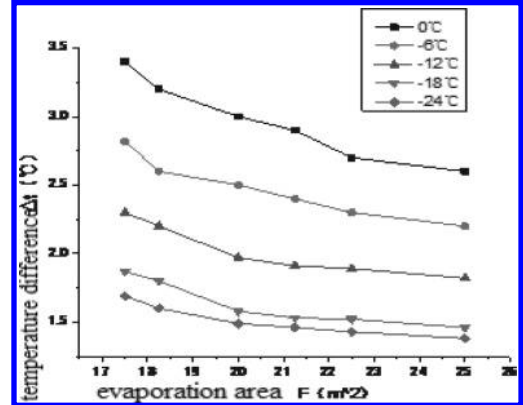


Figure 2. Relation between evaporator area and temperature difference.

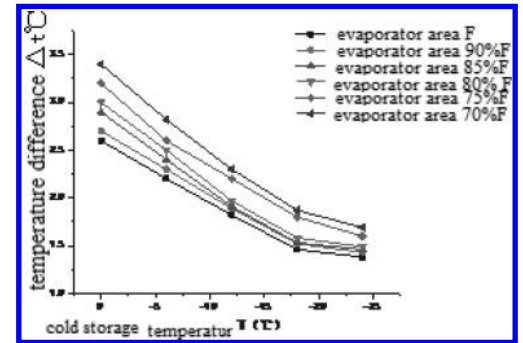


Figure 3. Relation between cold storage temperature and temperature difference.

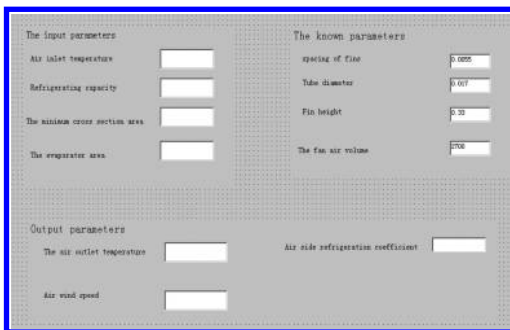


Figure 1. Simulation interface.

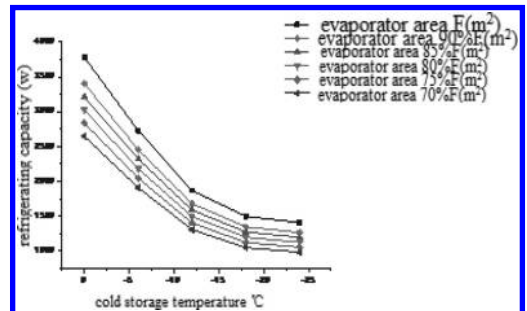


Figure 4. Relation between cold storage temperature and refrigerating capacity.

With the decrease of the evaporation area, the heat transfer coefficient and heat transfer temperature difference of the air side is increased. With the decrease of the evaporator area, it can improve the efficiency of refrigeration. With the evaporator area decrease, its refrigerating capacity will also decline and extend the time of cold storage to the expected temperature. Therefore, a modest area is taken, not only increases the evaporator heat transfer coefficient and heat transfer temperature difference, but also conforms to the requirements of project specification.

Under the experimental temperature 0°C, -6°C, 12°C-18°C, -24°C, as the cold storage temperature drops, the heat transfer temperature difference will be small. The refrigerating capacity decreases with the reduction of area of evaporator and the cold storage temperature decreases. Under 70% evaporator area in -24°C temperature condition, the refrigerating capacity is less than 1000 w and unable to meet the requirements of refrigeration. Therefore, we will choose the 75% evaporator area as the future experiment evaporator.

3 EXPERIMENTAL ANALYSIS

3.1 Experimental apparatus

Experiment system as shown in Figure 5.

The experiment uses air-cooled condensing compressor unit and forced ventilation finned tube evaporator, the main parts includes: closed rolling rotor compressor, air cooled condenser, high pressure reservoir, outside the balanced thermal expansion valve, manual expansion valve, a gas-liquid separator, forced convection type evaporator, etc.

A finned tube evaporator was used in this system, its structure as shown in Figure 6.

The direction of flow of refrigerant in the evaporator is perpendicular to the air. The heat exchange area of the evaporator is $F = 25 \text{ m}^2$.

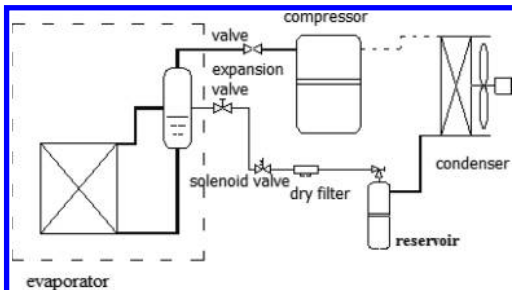


Figure 5. Gravity for liquid cooling system schematic diagram.

3.2 Comparison of experiment and simulation

The evaporator experimental value and simulation value comparison, under 75%F evaporator area, is as follows.

From Figures 7 and 8, you can see that with the decrease of the cold storage temperature, the

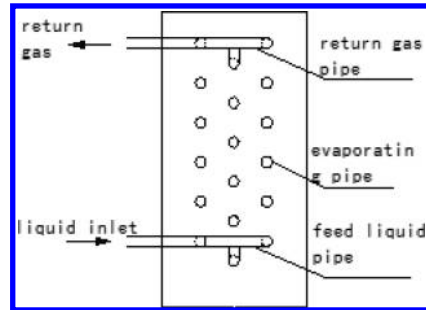


Figure 6. Evaporator structure of the gravity liquid supply system.

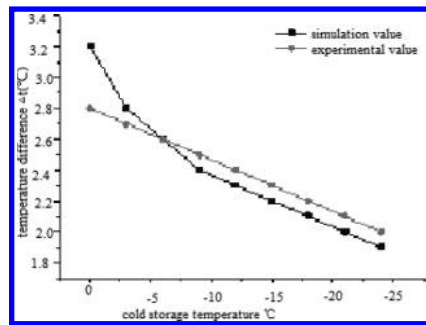


Figure 7. Evaporator experimental value and simulation value of temperature difference and cold storage temperature contrast, under 75%F evaporator area (the liquid height 700 mm).

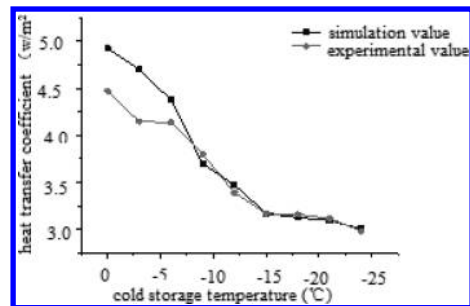


Figure 8. Evaporator experimental value and simulation value of heat transfer coefficient and cold storage temperature contrast, under 75%F evaporator area (the liquid height 700 mm).

evaporator experimental value and simulation value of heat transfer coefficient and heat transfer temperature difference is decreased. The difference value of the temperature difference and the refrigerating capacity on evaporator experimental value and simulation value of heat transfer coefficient is $\pm 0.2^{\circ}\text{C}$ and $\pm 2 (\text{w}/\text{m}^2)$.

In conclusion, this experimental value and simulation value overall trend is consistent and the relative error is smaller. Therefore, the simulation values believed to be correct and effective. The simulation software is a reference value for the research and design of gravity feed liquid system application.

3.3 Evaporator area 75%F and 100%F experimental value comparison

From Figures 9, 10 and 11, when cold storage temperature is below -6°C , as the evaporation area

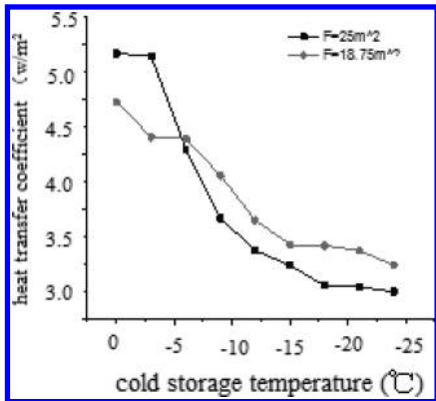


Figure 9. The heat transfer coefficient under different evaporation area (the liquid height is $H = 700 \text{ mm}$).

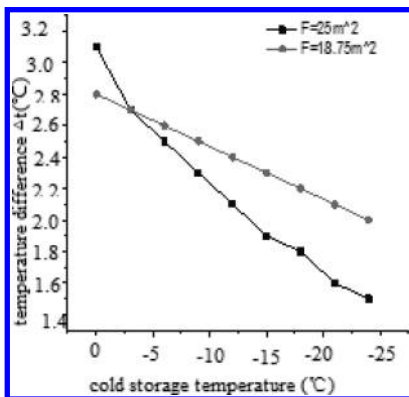


Figure 10. Heat transfer coefficient under different evaporation area (the liquid height is $H = 700 \text{ mm}$).

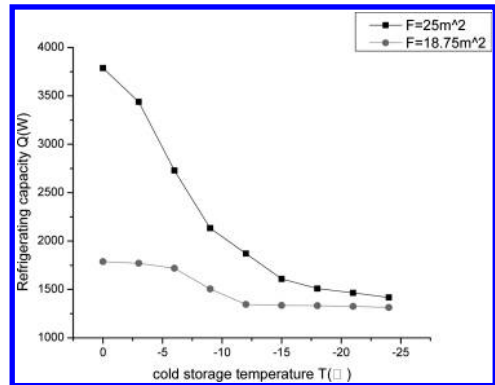


Figure 11. Refrigerating capacity under different evaporation area (the liquid height is $H = 700 \text{ mm}$).

is decreased, the heat transfer temperature difference and the heat transfer coefficient is increased. Though the refrigerating capacity is decreased, the decrease degree of the refrigerating capacity is lower with the evaporator area decrease. By reducing the area of evaporator, therefore, to increase the efficiency of the gravity feed liquid cooling system is feasible.

4 CONCLUSION

In a gravity feed liquid cooling system, the decrease of the evaporator area of evaporator can increase the heat transfer temperature difference and heat transfer coefficient, while making the capacity decreases slightly. But the refrigerating capacity of 75%F evaporator can reach the original evaporator refrigerating capacity of more than 93%. This experimental value and simulation value overall trend is consistent and the relative error is smaller. It is testified that simulation software is valuable for the research and design. Also it is found that the reduction of 25% evaporator area can make the system work best below the condition of -18°C cold storage temperature. This is very important in the practical engineering.

REFERENCES

- [1] Qingjiang Liu, Fang Han. Study on the effect of the evaporator area on the heat transfer performance in the gravity feed liquid refrigeration system. Applied Mechanics and Materials, 2013(11):58–60.
- [2] Li xing: Theoretical and Experimental Study on the Performance of the Gravity Feeding Refrigeration System Used in Refrigerated Warehouse [D]. Tianjin: Tianjin university of commercial, 2008.

Pricing and strategies of carbon emissions trading based on shadow price theory

S.Q. Li, X.Y. Wu, S.P. Hu & X. Sun

Tianjin University of Finance and Economics, Tianjin, China

ABSTRACT: As a market economic policy of carbon reduction, carbon emissions permit trading has been highly focused recent years. The paper built a shadow price model of carbon emissions based on the shadow price theory, and discussed the formation mechanism of shadow price of carbon emissions from the government and the company perspectives. The results show that the initial price of carbon emissions permit trading should be fixed by its shadow price, which means that the profit of product by per carbon, while the price in secondary market should be fixed by considering the unit cost and profit of carbon emission. At last, the paper provided some strategies for the development of carbon emission trading in China.

Keywords: carbon emissions; trading pricing; shadow price

1 INTRODUCTION

With the increase in global temperature, the environmental problems caused by the emission of greenhouse gases have recently become the focus of the world. Under the “Kyoto Protocol”, the emission permits of greenhouse gas (in particular, carbon dioxide), as a scarce resource in each country, has a possible commercial value and the possibility of trading. China, a developing and main carbon emission country, has promised to reduce 40%–50% of carbon emissions by 2020. To achieve the great goal, the successful emission schemes would be the powerful way to reduce the carbon emission (Wang 2013). However, the lack of effective carbon trading market and complete legal infrastructure are the obstacles to the trading success (Lo 2012). Some researchers pointed out that the main reason leading to inefficient market is the imperfect pricing mechanisms (Wang & Zhao 2010), such as the methods of pricing and the government intervention. Bernard et al. analyzed the strategic competition between Russia and developing countries by dynamic game theory (Bernard 2008). Kirat and Ahamada studied the impact of the European Union emission trading scheme on the electricity sector (Kirat & Ahamada 2011). However, the studied of carbon trading in China is still less; given this, the paper built a shadow price model of carbon emissions based on the shadow price theory, and discussed the formation mechanism of shadow price of carbon emissions from the government and the company perspectives. The findings would provide some proposals for China’s emerging carbon emissions trading.

2 METHODS

As the application of linear programming in the computation, Shadow price is introduced by Kantorovich who is mathematician and mathematical economists of the former Soviet Union (Kantorovich 1960). This theory reflects the price of the optimal allocation of resources, and then it was improved by Samuelson to reflect the price of the best use of resources. Aucamp and Steinberg defined the shadow price of a resource as the variable rate of optimal objective function value that is brought by incremental unit-resource (Aucamp & Steinberg 1982).

They believe that commodity prices are decided by the last unit of production, which is marginal cost of production other than the average cost of the commodity. The following mathematical formula will express the shadow price theory more vividly:

$$\begin{aligned} \max z &= \sum_{j=1}^n c_j x_j \\ \left\{ \begin{array}{l} s.t. \sum_{j=1}^n a_{ij} x_j \leq b_i \\ x_j \geq 0, i = 1, 2, \dots, m \end{array} \right. \end{aligned} \quad (1)$$

The dual model is:

$$\begin{aligned} \min \sum_{i=1}^m b_i y_i \\ \left\{ \begin{array}{l} s.t. \sum_{i=1}^m a_{ij} y_i \geq c_j \\ y_i \geq 0, j = 1, 2, \dots, n \end{array} \right. \end{aligned} \quad (2)$$

the shadow price of the type i of resources p_i is defined as the formula (3), which means that the right partial derivatives of the optimal objective function z^* on the resource b_i .

$$p_i = \frac{\partial z^*}{\partial b_i^+}, \quad i = 1, 2, \dots, m \quad (3)$$

And the final shadow price is calculated from formula (2):

$$p_i = \min \{ y_i^{*1}, y_i^{*2}, \dots, y_i^{*k} \} \quad (4)$$

Carbon emission permits for trade of is based on the concept of the “cap and trade system” which was proposed last century. The general way is: according to available information and a certain standard, the government assesses the environmental capacity of some areas to meet the maximum allowable carbon emissions then divides it into a number of shares which refer to carbon emission permits. On the primary market of carbon emission, the government allocates the initial sale of emission permits of carbon by free allocation, auction or sale. Companies who get the carbon emission permits can control the permits based on their own situation. In the secondary market companies can buy or sell their emission permits of carbon. Put it in layman’s terms, if the company can not complete their own targets of emission reduction, they have the right to buy a certain number of the quotas or emissions permits from other companies who have excesses quotas or emission permits to complete their own emission permits of carbon. Thus the emission permits for trade of carbon market is formed.

In emission trading, according to the amount of carbon emissions, companies may decide to buy or sell their own carbon emissions permits. When the price of an emission permit is above the marginal cost, the companies tend to control the pollution by themselves. On the other hand, they may choose to buy some shares of emission permits. Through the sale or auction of emissions permits, if the emission permits are allowed in the trading in the market, companies can reach their carbon emissions goals changing from the negative to the positive.

Above all, the price of the carbon emission trading is decided by the marginal control cost, and it’s reasonable to be interpreted as the shadow price of the carbon emission.

3 MODEL CONSTRUCT

According to the theory of shadow price, when a resource is in the best allocation, its marginal output value is the shadow price which can be calculated by the linear programming. The essence of

the shadow price reflects the price of optimal using the resource. In the carbon emission exchanges, the shadow price is the incremental benefit from each unit of carbon emission. Besides it is the valuation of contribution brought by emission permit as a resource in production, other than actual market price. To simplify the study problem and analysis, we only study on carbon emission of a company of an area, and then make the following assumptions:

Assumption 1: there are N ($N \geq 2$) carbon emission corporations, and the total carbon emission is C_t , the initial allocation of carbon emission of each corporation is C_{i0} , and the initial price is p_i .

Assumption 2: the carbon emission of each corporation C_{ti} is directly proportional to its output Q_i , so $Q_i = \alpha_i C_{ti}$.

Assumption 3: without consideration of technical progress, in other some suggestions for the development of carbon emissions trading in China are proposed control I_i . The negative linear relationship was shown between I_i and α_i , $\alpha_i = \varepsilon - \eta I_i$.

Assumption 4: the unit cost of production is c_i , and the unit profit of product is M_i .

Assumption 5: During the operation, company’s demand of emission permit is non-zero.

Assumption 6: All companies must purchase emissions permit, in addition no more emission fees are charged.

In the above assumptions, $i=1,2,\dots,N$.

Under the above assumptions, when we define the initial pricing of emission permits, all companies’ profit maximization can be used as bases. Thus the objective function and constraints can be expressed as:

$$\begin{aligned} \max M &= \sum_{i=1}^N (M_i \times Q_i) = \sum_{i=1}^N \left[M_i \times \left(\frac{C_{ti}}{\alpha_i} \right) \right] \\ &= \sum_{i=1}^N \left[\left(\frac{M_i}{\alpha_i} \right) \times C_{ti} \right] \\ s.t. \quad &\sum_{i=1}^N C_{ti} \leq C_t \end{aligned} \quad (5)$$

4 DISCUSSION

4.1 The initial pricing of carbon emission trading

For solving the model, the paper introduced the Lagrange multiplier λ and established the Lagrange equation:

$$L = \sum_{i=1}^N \left[\left(\frac{M_i}{\alpha_i} \right) \times C_{ti} \right] + \lambda \times \left(C_t - \sum_{i=1}^N C_{ti} \right) \quad (6)$$

The first-order condition of equation (6) is:

$$\frac{\partial L}{\partial C} = \frac{M_i}{\alpha_i} - \lambda = 0 \quad (7)$$

So

$$\lambda = \frac{M_i}{\alpha_i} \quad (8)$$

According to the assumptions, α_i is the unit carbon emission of product, and M_i is the unit profit of product, so λ is the unit permit of carbon emission. λ expresses the price of emission permit as optimal allocation in one area and the marginal revenue of carbon emission rights, rather than the market price of carbon emission rights. According to the shadow price theory, the λ would be the shadow price of carbon emission rights. When the market price of carbon emission rights is lower than the shadow price, unit cost is under the unit benefit of using the emission permits of carbon, thus the social benefit would be growth by expansion of production. Otherwise we have to reduce production. So when carbon emission rights are allocated by sale, the Government defines the initial price as p_i ; $p_i = M_i/\alpha_i$.

4.2 The formation mechanism of shadow price for carbon emissions

When emission permits are initially allocated as a form of payment by the Government, as a viable resource, the environment is protected by corporations. The view point on carbon emission rights from a corporate perspective would be that they have to buy emission permits to carry out carbon emissions. According to the above assumptions, we make a separate analysis of a certain corporations in an area mentioned in the assumptions, the profit function and constraints are:

$$\begin{aligned} \max \quad & M = M_1 \times Q_1 = kQ_1 - c_1Q_1 - I_1 \\ \text{s.t.} \quad & \alpha_1Q_1 = (\varepsilon - \eta I_1) \times Q_1 \leq C_{10} \end{aligned} \quad (9)$$

k is the unit income of product.

Solved by Lagrange equation:

$$\lambda_1 = \frac{k - c_1}{\alpha_1} = \frac{k - c_1}{\varepsilon - \eta I_1} \quad (10)$$

According to the above result, the Lagrange multiplier λ_1 is a corporation's shadow price of, the carbon emission rights. In other words, when the company has an extra unit emission permit, if the marginal revenue is more than shadow price λ_1 , it would want to purchase the emission permit to expand the production in the carbon emission trading market. On the contrary, the corporation will sell a certain amount of carbon emission to

get the income. In the same way, you can reach the result of other company in this area.

The shadow price of carbon emissions cannot be equal to the market price, the later is a given number which is relatively stable, but the former is the optimal result of resource allocation with the changing of business conditions and resource usage. The relationship between the shadow price, carbon emission α_i and the cost of product c_j is negative correlation. The relationship between the shadow price and investment of control carbon emission is a positive correlation. In other words, the higher a unit carbon emission costs are, the less the company holds the quota of carbon emission, or the higher product costs are, the lower the unit profit is. All these circumstances will raise the shadow price of carbon emissions, so the corporation would like to curb pollution by themselves in order to maximize profits. On the other hand, the more a company spends in order to curb pollution by them, the more permits of carbon emission a corporation wants to purchase, thus the shadow price will be raised.

5 STRATEGIES FOR THE DEVELOPMENT OF CARBON EMISSION TRADING IN CHINA

5.1 Clarified the property ownership of the carbon emissions in law

To clarify the property ownership of the carbon emissions in law is a prerequisite of the carbon emissions trading. From the above constraints of model we can see that, companies only obtain the required share of carbon emission. If the carbon emission of a company is unfettered, the shadow price of carbon emissions will be insignificant. Each company will not benefit from economizing the use of carbon emissions, or lost of benefit because of the waste of carbon emissions. Therefore, to clarify the property ownership of the carbon emissions in law, is one of the necessary conditions that shadow price of carbon emission can play important role in reducing the negative impact on the environment. In addition, the shadow price will reflect the marker condition of carbon emission trading.

5.2 Nurturing and developing a good market system for carbon emissions trading

Only under the most perfect of carbon emissions trading market conditions will the shadow price fully play its role. Specifically, we need to make the following efforts on building the carbon emissions trading market system. Improving the relative laws and regulations of carbon emission carbon emissions trading must be carried out under the framework of the law. As an additional administrative

measure of Market-oriented allocation of resources, through the improvement of relevant legislation, to ensure that carbon emission trading rules to follow. With the increase of trading, more and more problems are exposed; at the same time, we should improve the penalty measures to companies with excess carbon emissions. Establishing and improving the rational trading rules to prevent unfair competition or monopolies of carbon emission among companies, then the shadow price of carbon emissions can not be put to full use. In order to create a fair and transparent trade environment by strengthening supervision of local environmental authorities, developing an advanced monitoring facilities and effective monitoring teams, establishing strict regulatory measures to effectively manage, control and supervise the operation of the carbon trading market. Establish the rational standards and methods of monitoring carbon emissions, otherwise the action of illegal emissions, excess emissions will affect the trader's enthusiasm involved in the transaction, the role of shadow prices will be greatly reduced.

5.3 *To regulate the initial allocation of carbon emission, to diversify trading and financial product*

In the perfect and free carbon emissions permit trading, the initial allocation of carbon emissions must follow the strict market rules from the beginning. It should adopt the measure of enterprise purchase such as public auction or sale, rather than free allocation. This paper uses the shadow price theory, to discuss the initial allocation pricing of carbon emission rights made by the government, however, the shadow price of carbon emission can not be equated to the market price. Although theoretically it is very reasonable and feasible that unit price of using resource is decided by shadow price, actually it is very difficult to define the marginal cost or marginal benefit. Therefore, we have to introduce the option theory for further study on the initial allocation of carbon emission. We need to gain experience to accelerate the innovation of financial derivatives of emission permits of carbon. We should diversify financial derivatives in the form of China carbon trading market, including the emission permits of carbon and its' financial derivatives such as Options and futures, Investment or speculation.

5.4 *The introduction of modern technology into the carbon emissions permit trading and strengthen the construction of the communication facilities*

Firstly using modern technology to establish an information platform of carbon emissions permit trading to provide the information of supply

and demand, marketing services and intermediary services, reducing the "rent-seeking" caused by information asymmetry, improving the transparency of transactions and reducing the cost of emission permits of carbon. If the cost of searching is too high, it will restrict the amount of trade to a certain extent. At that time, you cannot find the perfect market and the real shadow price. Secondly the establishment of information network system will improve the traders' monitoring capability in the carbon emissions permit trading. Construct the environmental monitoring network in the whole country to provide protection for trading. Establish and improve the carbon emissions monitoring system to constantly monitor the company's carbon emission. Therefore the information asymmetry between emitters and supervisor can be eliminated.

6 CONCLUSION

China will achieve the target to reduce 40%–45% of carbon emissions by 2020, there is a great potential on the emission permits of carbon. As a market-based control policy for carbon emission, carbon emissions permit trading is in its infancy. In determining the initial price of emission permits of carbon, Government should consider the earning per unit and carbon emissions per unit; in purchasing the emission permits of carbon, company should consider the carbon emissions per unit, unit cost of production and cost of control carbon emissions. Furthermore, the emission permit of carbon needs to be further explored in theory and practice, especially reference to the legal, marketing, finance and information technology.

REFERENCES

- Aucamp, D.C., & Steinberg, D.I. 1982. The computation of shadow prices in linear programming. *Journal of the Operational Research Society*, 557–565.
- Bernard, A., & Haurie, A., Vielle, M., & Viguier, L. (2008). A two-level dynamic game of carbon emission trading between Russia, China, and Annex B countries. *Journal of Economic Dynamics and Control*, 32(6), 1830–1856.
- Kantorovich, L.V. 1960. Mathematical methods of organizing and planning production. *Management Science*, 6(4), 366–422.
- Kirat, D., & Ahamada, I. (2011). The impact of the European Union emission trading scheme on the electricity-generation sector. *Energy Economics*, 33(5), 995–1003.
- Lo, A.Y. 2012. Carbon emissions trading in China. *Nature Climate Change*, 2(11), 765–766.
- Wang, Q. 2013. China has the capacity to lead in carbon trading. *Nature*, 493, 273.
- Wang X.H. & Zhao B. 2010. The dilemma and crack of the carbon trading in China. *Theoretical exploration*, 3:66–69. (in Chinese).

Reliability distribution of traction system for rolling stock

Shi Jia Liu & Yang Lu

Locomotive and Car Research Institute, China Academy of Railway Sciences, Beijing, China

ABSTRACT: This paper studies the selection and application of reliability distribution method for rolling stock. Based on reliability models, it uses score distribution method to distribute indexes of subsystems, and it uses fuzzy AHP and equal distribution method to distribute indexes of components. By interpolating with software, it calculates the distribution indexes to satisfy the logic relation of components and simplify the calculation process at the same time. The idea is also suitable for similar complex system to distribute reliability.

Keywords: traction system; reliability model; score distribution method; fuzzy analytic hierarchy process; equal distribution method

1 INTRODUCTION

According to certain principles and methods, system reliability is a process that reliability indexes are distributed to subsystems and components from top to bottom, from entirety to portion. It is also a process taking advantage of the labor, material and financial resources properly. Reliability distribution is generally used in demonstration stage and initial design stage aiming to implement the reliability index and define the components for the designers, so that systems or components will meet the required reliability eventually.

There are several methods of reliability distribution, such as equal distribution method, score distribution method, redistribution method, relative fault rate and relative fault probability distribution method, distribution method considering importance and complexity etc. Different products should choose different distribution methods, based on the reliability data, different design stages, different objectives and constraints. In addition, it is difficult to distribute properly at once time, so it requires to adjust and repeat distribution in lack of reliability data.

2 RELIABILITY DISTRIBUTION

2.1 The reliability distribution of traction subsystem

Reliability modeling is the base for the reliability distribution, and it is also the premise of reliability analysis and design. Task reliability block diagram represents the logic relation among the units of products, and can be used to calculate

the reliability parameters. It is the most common reliability models. Traction system consists of two subsystems: high voltage electrical subsystem and traction device subsystem. The two subsystems are connected in series, as shown in Figure 1.

It is the most convenient method to distribute fault rate of the traction subsystems by the specialist scoring method. In order to response to the real situation objectively, the reference standard of distribution factor for scoring is shown in Table 1.

The score of distribution factor ranges from 1 point to 9 point. The higher score means the fault rate of subsystem is higher. Assuming the reliability index of system is λ_s , the reliability index of subsystem is λ_i :

$$\lambda_i = c_i \cdot \lambda_s \tag{1}$$

In formula (1), $i = 1, 2, \dots, n$ is the number of subsystems, c_i is the coefficient of subsystem i .

$$c_i = \omega_i / \omega \tag{2}$$

In formula (2), ω_i is the score of subsystem i , ω is the score of system.

$$\omega_i = \prod_{j=1}^4 r_{ij} \tag{3}$$



Figure 1. Task reliability block diagram of traction system.

In formula (3), r_{ij} is the score of subsystem i and factor j ; $j = 1$ is complexity; $j = 2$ is importance; $j = 3$ is technology maturity; $j = 4$ is work environment.

$$\omega = \sum_{i=1}^n \omega_i \quad (4)$$

In formula (4), $i = 1, 2, \dots, n$ is the number of subsystems.

Table 1. Reference standard of distribution factor for scoring.

Distribution factor	Reference standard for scoring
Complexity	By considering the number of components, the difficulty of detection and control etc; The more complex the products, the greater the distribution fault rate, the higher the score.
Importance	By considering the series or parallel connection of reliability model, redundancy, the influence caused to system after products going wrong, etc; The more important the products, the smaller the distribution fault rate, the lower the score.
Technology maturity	By considering the technology to produce the products, fault condition of similar products, etc; The more mature the products, the smaller the distribution fault rate, the lower the score.
Work environment	By considering the installation position of products, work environment, etc; The better the environment, the smaller the distribution fault rate, the lower the score.

If the reliability index of traction system—the average fault rate of major fault is 0.2 (1/million km), the distribution result of subsystems is shown in Table 2.

2.2 The reliability distribution of traction first level components

As an example of traction device subsystem, this part illustrates the reliability distribution of the first level components. First, build the task reliability model. All of the first level components use the redundancy design. The system can continue to work with single component damage, but it may cause reduction of power or speed to rolling stock. The task reliability block diagram of traction device subsystem is shown in Figure 2.

In order to show formulas conveniently, the reliability block diagram is simplified into six parts, as shown in Figure 3.

The reliability model of traction device subsystem is a hybrid model with series and parallel connection. By combing the fuzzy analytic hierarchy process and equal distribution method, analysis factors are divided into three layers from top to bottom. The top layer is the target, it expresses the goal of designers which is the fault rate distribution of traction device subsystem. The bottom layer is the available scheme, this is distribution fault rate of each first level component (module). The middle layer is element, it expresses the element of the overall goal. It can also be formed by multiple layers. Complexity, importance and technology maturity are used as distribution elements. The work environment of traction device subsystem is similar, so the influence of environment will not be consideration. The connection between layers means the relation between each element of higher and lower layers. The hierarchy structure model is shown in Figure 4.

Table 2. Distribution result of traction subsystems.

Subsystem	r_{11}	r_{12}	r_{13}	r_{14}	ω_i	c_i	λ_i
High voltage electrical subsystem	3	5	6	5	450	0.3191	0.0638
Traction device subsystem	8	5	8	3	960	0.6809	0.1362
Total					1410	1	0.2



Figure 2. Task reliability block diagram of traction device subsystem.

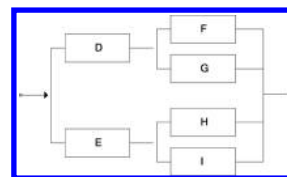


Figure 3. Simplified task reliability block diagram of traction device subsystem.

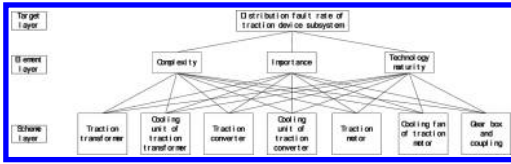


Figure 4. Hierarchy structure model of traction device subsystem for fault rate distribution.

Table 3. Comparison scale and its description.

Comparison scale	Importance of degree	Illustration
1	Factor <i>i</i> and factor <i>j</i> are equally important	2, 4, 6, 8 and the reciprocal of each number have the similar meanings
3	Factor <i>i</i> is slightly important than factor <i>j</i>	
5	Factor <i>i</i> is obviously important than factor <i>j</i>	
7	Factor <i>i</i> is strongly important than factor <i>j</i>	
9	Factor <i>i</i> is extremely important than factor <i>j</i>	

For the same layer factors, judgment matrixes are constructed by paired comparison method and 1 to 9 comparison scale. The paired comparison method makes quantitative judgment by comparing relative importance of each two factors. The relation among factors also requires to be given by experts according to the relative elements and experience. 1 to 9 comparison scale is shown in Table 3. (2, 4, 6, 8 means that the importance of degree is between the up and the low comparison scales.)

The fuzzy judgment matrix *A* is constructed with all the comparison results. Each element of the matrix expresses the influence degree of different factors from the higher layer. *A* is an *n*-dimensional matrix $A = [a_{ij}]_{n \times n}$, *n* is the number of factors which is being analyzed. The elements of judgment matrix satisfy the following relations:

$$a_{ij} = 1/a_{ji}, \quad a_{ii} = 1$$

λ_{max} is the maximum characteristic root of judgment matrix *A*. The weight vector is obtained by calculating the feature vector of λ_{max} and normalizing the feature vector. The elements of ω indicate the relative importance proportion of each factor, that is the weight of each factor.

Structure the judgment matrix of element layer to target layer for traction device subsystem.

$$\begin{bmatrix} 1 & 2 & 1/2 \\ 1/2 & 1 & 1/3 \\ 2 & 3 & 1 \end{bmatrix}$$

By calculating, the maximum characteristic root is $\lambda_{max} = 3.0092$, and the weight vector is

$$\omega^{(2)} = (0.2970, 0.1634, 0.5396)^T$$

For the rationality of weight, it can be inspected by checking the consistency of judgment matrix. *RI* is the average random consistency index of judgment matrix, the values of *RI* is shown in Table 4.

The consistency index is $CI = (\lambda_{max} - n) / (n - 1) = 0.0046$, the consistency rate is $CR = CI / RI = 0.0079$. When $CR < 0.1$, it can be explained that the judgment matrix has a good consistency, at the same time, the weight is distributed properly.

It is similar to the judgment matrix of scheme layer to element layer, that is the first level components (modules) of traction device subsystem to complexity, importance and technology maturity.

$$\begin{bmatrix} 1 & 1/3 & 1/5 & 1/2 & 1/6 & 2 & 1/3 \\ 3 & 1 & 1/3 & 2 & 1/4 & 4 & 1 \\ 5 & 3 & 1 & 4 & 1/2 & 6 & 3 \\ 2 & 1/2 & 1/4 & 1 & 1/5 & 3 & 1/2 \\ 6 & 4 & 2 & 5 & 1 & 7 & 4 \\ 1/2 & 1/4 & 1/6 & 1/3 & 1/7 & 1 & 1/4 \\ 3 & 1 & 1/3 & 2 & 1/4 & 4 & 1 \end{bmatrix}$$

$$\begin{bmatrix} 1 & 1/3 & 1/2 & 1/3 & 1/2 & 1/3 & 1/2 \\ 3 & 1 & 2 & 1 & 2 & 1 & 2 \\ 2 & 1/2 & 1 & 1/2 & 1 & 1/2 & 1 \\ 3 & 1 & 2 & 1 & 2 & 1 & 2 \\ 2 & 1/2 & 1 & 1/2 & 1 & 1/2 & 1 \\ 3 & 1 & 2 & 1 & 2 & 1 & 2 \\ 2 & 1/2 & 1 & 1/2 & 1 & 1/2 & 1 \end{bmatrix}$$

Table 4. The values of *RI*.

<i>n</i>	1	2	3	4	5	6	7	8	9
<i>RI</i>	0	0	0.58	0.90	1.12	1.24	1.32	1.41	1.45

1	1/2	1/3	1/2	1/6	4	1/3
2	1	1/2	1	1/5	5	1/2
3	2	1	2	1/4	6	1
2	1	1/2	1	1/5	5	1/2
6	5	4	5	1	9	4
1/4	1/5	1/6	1/5	1/9	1	1/6
3	2	1	2	1/4	6	1

The calculation result is shown in Table 5.

From the Table 5, the consistency rates are all less than 0.1, so the result can be accepted. The combination weight vector of scheme layer to target layer is:

$$\omega = (0.0551, 0.1164, 0.1750, 0.0878, 0.3604, 0.0562, 0.1330)^T$$

The combination weight vector expresses the distribution proportion of fault rate, which is different component (module) in reliability model of traction device subsystem. Traction motor module is distributed the largest fault rate.

The average fault rate of major faults for traction device subsystem is 0.1362 (1/million km) as shown in Table 2. In the reliability model of traction device subsystem, the first level components (modules) are all obeyed exponential lifetime distribution. Assuming the fault rate of each component (module) is $\omega\lambda$, the value of t is 1 million kilometers, and the distribution result satisfies the index requirement. Put fault rate into the mission reliability mathematical model of traction device subsystem.

$$R_D = R_E = R_{transformer} \cdot R_{cooling\ unit\ of\ transformer} = e^{-0.1715 \cdot \lambda}$$

Table 5. Calculation result of scheme layer to element layer for traction device subsystem.

Number k	1	2	3
$\omega_k^{(3)}$	0.0466	0.0610	0.0580
	0.1134	0.2058	0.0910
	0.2548	0.1072	0.1516
	0.0712	0.2058	0.0910
	0.3684	0.1072	0.4326
	0.0322	0.2058	0.0241
	0.1134	0.1072	0.1516
Maximum characteristic root	7.1828	7.0152	7.2136
$CI_k^{(3)}$	0.0305	0.0025	0.0356
$CR_k^{(3)}$	0.0231	0.0019	0.0270

Table 6. Distribution result of the first level components for traction device subsystem.

First level components	ω_i	$\omega_i\lambda$	λ_i
Traction transformer	0.0551	0.0469	0.0469
Cooling unit of traction transformer	0.1164	0.0990	0.0990
Traction converter	0.1750	0.1489	0.1489
Cooling unit of traction converter	0.0878	0.0747	0.0747
Traction motor	0.3604	0.3066	0.0766
Cooling fan of traction motor	0.0562	0.0478	0.0239
Gear box and coupling	0.1330	0.1131	0.0283

$$R_F = R_G = R_H = R_I = R_{converter} \cdot R_{cooling\ unit\ of\ converter} \cdot R_{motor} \cdot R_{cooling\ fan\ of\ motor} \cdot R_{gear\ box\ and\ coupling} = e^{-0.8285 \cdot \lambda}$$

$$R_{traction\ device\ subsystem} = 1 - \left\{ 1 - R_D \cdot \left[1 - (1 - R_F)(1 - R_G) \right] \right\} \cdot \left\{ 1 - R_E \cdot \left[1 - (1 - R_H)(1 - R_I) \right] \right\} = 1 - \left\{ 1 - R_D \cdot \left[1 - (1 - R_F)^2 \right] \right\}^2 = e^{-0.1362}$$

The equation is obtained by bringing in the distribution weight of each component (module):

$$1 - \left\{ 1 - e^{-0.1715 \cdot \lambda} \cdot \left[1 - (1 - e^{-0.8285 \cdot \lambda})^2 \right] \right\}^2 = e^{-0.1362}$$

The solution of equation is calculated by interpolating with software $\lambda = 0.8507$. According to the reliability model, the distribution result of the first level components (modules) is obtained. Because the modules of traction motor, the cooling fans of motor, gear box and coupling are made up by several components with series connection, (such as: the motor of car 1 is made up by 4 traction motors with series connection in car 1.) the fault rate of each component is obtained according to the number of components and equal distribution method. Then, the final result of the first level components (modules) is shown in Table 6.

From Table 6, distribution fault rate of traction converter is the largest one than other fault rate of the first level components in traction device subsystem. The order of successively reducing distribution fault rate of rest parts is: Cooling unit of traction transformer, Traction motor, Cooling unit of traction converter, Traction transformer, Gear box and coupling, Cooling fans of traction motor.

3 CONCLUSION

Reliability distribution result provides the basis for product design, reliability test and reliability evaluation. Therefore, it is very important to select the appropriate distribution method, and to consider the comprehensive distribution elements for the different characteristics products. This paper studies the selection and application of reliability distribution method for rolling stock traction system, the similar complex systems could apply the same method. Firstly, build the appropriate reliability model, then select the distribution method according to the series or parallel connection, at the same time, ensure the subsystems and components obey exponential lifetime distribution.

Usually, all of the subsystems are connected in series from the system. In the situation of clearing the influence of distribution factors to subsystems, scoring distribution is the easiest method for subsystem distribution. For the distribution of subsystem, reliability model is usually hybrid model, and there are multiple components. The result of each component (module) can be obtained by using the fuzzy AHP, comparing each two factors of element layer and scheme layer, and bringing the weight of distribution in reliability mathematical model. To the modules, which are consisted of the same parts connected in series or parallel, they are

distributed by equal distribution method. Because of the mathematical model of hybrid model is more complex, it can be simplified by using interpolation with software, at the same time, it satisfied the logic relation of components (modules).

REFERENCES

- [1] Shengkui Zeng. Reliability Design and Analysis [M]. Beijing: National Defense Industry Press, 2011:37–38.
- [2] Aiming Liu. Research and Application of Reliability Design Technology for Rail Vehicle Door System [D]. Nanjing: Nanjing University of Science and Technology, 2008.
- [3] Chaozhong Zhang, Xiaoli Bai, Qifu Luo. The Reliability Allocation Method of A Measuring Equipment Based on Fuzzy AHP [J]. Machinery Design & Manufacture, 2010, (6): 219–220.
- [4] Yuling Wang, Fangyi Li, Jianfeng Li, Jian Chen. Fuzzy Analysis Hierarchy Process Method of System Reliability Allocation [J]. Machinery Design & Manufacture, 2008, (2): 13–15.
- [5] Jinan Lei, Liang Wang, Liang Zhang. The Application of Fuzzy AHP Evaluation in the Reliability Analysis of Mechanical Equipment [J]. Machinery, 2007, 34(5):14–16.
- [6] Ximing Dong. Reliability, Availability, Maintainability and Safety of Rail Train [M]. Beijing: China Railway Publishing House, 2009: 73–74.

Study on the problems and countermeasures of Urban Utility Tunnel construction

Jiang Hang Wu & Da Zhi Wu

Zhejiang Sci-Tech University, Hangzhou, China

ABSTRACT: Urban Utility Tunnel (UUT) is one of the most important structures in the development of underground space, and has many advantages compared with traditional pipe laying method, but the development speed is very slowly in China at present. The main factors restraining the popularization of UUT construction were fully analyzed in this paper, and the countermeasures can be used to promote the development of UUT were also pointed out. The relevant achievements can provide useful references for the departments of planning, policymaking, and management.

Keywords: existing problem; countermeasure; Urban Utility Tunnel construction

1 INTRODUCTION

With the growing development of China's economy and the improving level of urbanization, people's requirement of the municipal pipeline has been increasing. Both types and quantities are beyond the maximal capacity of the existing facilities, leading to a common phenomenon—recurrent opening the road for reconstruction, which not only wastes labor and money and affects the regular urban transportation, but also is an extreme waste of the limited underground space. At present, it is a widespread choice of many developed international cities to build Urban Utility Tunnel (UUT), which is similar to a huge bag collecting all kinds of municipal pipelines while still leaving a corridor for maintenance workers. Also, all facilities like water drainage, fire protection, electrical power, monitoring equipment,

ventilation and illumination are included. Figure 1 is typical section of a UUT.

Compared with the traditional layout of conduits, the UUT has many advantages, but its construction speed is very slowly. To promote the development of UUT, the main factors restraining the popularization have been analyzed and the measures can be used have been pointed out.

2 MAIN FACTORS RESTRAINING THE POPULARIZATION OF UUT IN CHINA

2.1 The existence of underground conduits

The underground conduits in old town are concentrated and complicated, intertwining with each other. A small adjustment will affect the whole system. In addition, the number of departments, areas of expertise and surrounding residents and enterprises and public institutions involved is incredibly large. It will be a really painstaking and complicated task once the construction begins.

2.2 Large investments VS slow returns

The UUT construction is a project that requires huge amount of front-end investment without direct financial return in a short term, which also greatly affects whether the project can be popularized and implemented extensively. As for enterprises or governments, whether the UUT should be constructed yet depends on the fund. The problem of UUT construction is longer the construction



Figure.1. Typical section of the UUT.

technique concerning with the construction standard of today's world but the profit and returns in the recouping period.

Kunming is a pioneer in the field of market-oriented management of UUT. It is really a tough exploration as the huge investment and slow recovering benefits leads to a stalemate. It is reported that the load value taken by Kunming Pipe Network as the construction unit, which is only for the UUT in Caiyun Road and Guangfu Road, reaches up to one billion RMB. The average investment per mile is beyond thirty million, while the subsequent management and maintenance fee is up to millions RMB each year [1]. UUT is a prohibitive project without direct return on investment for a majority of enterprises in China.

2.3 The imperfection of legal system

A well-established and sound legal system is an indemnificatory foundation for better promotion and efficient operation of UUT. At present, the legal system in mainland China is incomplete, however, Taiwan has already established an advanced legal system which plays a decisive role. Since the promulgation of UUT Act on June 14th, 2000, Taiwan has issued a series of regulations of UUT, such as Procedures of UUT Construction and Appropriation allocation and Rules for Implementation of the Law on UUT in 2001, Procedures of Management and Employment of Utility Fund in 2002, The Design Standard of UUT Project in 2003, all of which form a standard operational procedures [2].

However, this kind of rules and regulations are not so universal in mainland China. Shanghai issued Construction Standard of UUT in Shanghai Expo Site (GD/TJ08-2017-2007) [3], which is merely directed toward Shanghai Expo Site. There are only a few relevant rules or regulations like Provisions of Overall Plan for UUT, Procedures of Shanghai Municipality on the Administration of Road Stringing, Regulations on Hangzhou Municipality on Administration of Underground Utilities and Procedures of Chongqing Municipality on the Administration of Plan for Utility Project, etc. Yet these rules and regulations just simply illustrate the laying condition and different types of the utilities integrated without further mentioning the specific problems of engineering and technology, investment and financing, management and maintenance, public using and charges, etc, which shows that the legislation of UUT construction in mainland China is still at an early stage of exploration, lacking uniform national standard of legal system. The deficiency in legal system has greatly impeded the popularization of UUT in mainland China.

2.4 Difficulties in management

The traditional independent construction model determines the relative independence of its management mode, that is, the main unity of construction undertake the management and maintenance of the utilities, which results in a good many abuses. E.g. it adds to difficulties for future management and maintenance by changing the program at will or evading management. All these abuses of traditional direct paving make it more difficult for further management. It provides a great challenge for relative departments transforming from self-contained mode to centralized management. Whether each department will subject themselves to the control and arrangement of a certain one and whether this certain department can conduct a rational and scientific management of all utilities come as a big problem. Besides, our country has neither directly made special legislation for managing UUT construction nor established uniform managerial standard and system, even without specific administrative departments regulating the management and operation UUT orderly and effectively.

2.5 Ideological misunderstanding points

The front-end investment of UUT is definitely much higher than that of independent paving. According to statistics, the average construction costs of UUT in Japan, Taipei and Shanghai are (calculated in RMB) ¥500,000/m, ¥130,000/m, ¥100,000/m respectively. Many people then think it is uneconomic while costing too much, but actually we should not only take the construction cost into consideration but also assess the overall benefits according to the practice. Take the west region of Zhong Guan-cun as an example [4], suppose the lengths of both the pipeline and UUT are 1900 and the given period is 50 years, the comparison of construction cost of the two modes are showed in Table 1.

Although the direct cost of utility almost doubles that of the traditional mode, the general effect of UUT with its life span is affirmative considering all kinds of external costs. Also, it can bring up sound economic and social benefits.

Table 1. Comparison of the costs of traditional direct paving and UUT. Unit: million Yuan

	Direct cost	External cost	Sum
Traditional direct paving	31.2662	127.634	158.9002
UUT	63.8	404.043	101.4655

3 SEVERAL MEASURES TO PROMOTE THE UUT CONSTRUCTION

3.1 *To gradually establish a complete set of legal system of UUT construction*

Promulgation of a complete legal system is the foundation of promoting utility tunnel, but the domestic legislation is still at an early stage. We should draw on advanced experiences from home and abroad, like Special Measures of Utility Tunnel Construction of Japan and Regulations of Urban Utility Tunnel of Taiwan, etc.

The author suggests the specific legal system can be established on two levels: first, make national-level utility tunnel regulations; second, make local-level utility tunnel regulations. The first one can be divided into two aspects, that is, politic legislation and technological legislation. The politic legislation should clarify the utility tunnel's attribution and ownership to confirm the main building unit and management mode and compartmentalize the rights and obligations of pipeline institutions, while the technological legislation should formulate specific standard and specifications for all kinds of designs (such as layout design, structure design, pipeline design, disaster-prevention design, etc.), construction methods (such as construction technology, construction process, construction safety, etc.), inspection and acceptance (such as inspection methods, acceptance indexes, etc.) and materials and equipment (such as construction materials, supervising systems, ventilation systems, power systems, drainage systems, communication systems, labeling systems and ground facilities, etc.). The content of the local-level utility tunnel regulations should be specified on the basis of the one of national-level, at variance with different places and situations.

3.2 *To innovate the investment, construction and operation mechanism of UUT*

With the reform of China's urban infrastructure's investment and financing system, the traditional direct paving ways like BOT, PPP, etc. are no longer the best options. Making a general survey of financing modes around the world, a fund for utility tunnel construction has been relatively mature. Taiwan is such a successful example.

Utility tunnel construction requires a big investment and a high cost of operation and maintenance. Thus, a reasonable construction mode is in great need. According to different sources of the fund, it can be divided into "government funded" construction mode, "government and enterprises jointly funded" construction mode and "franchising" construction mode. Generally, the government

and enterprises jointly funded construction mode is more widespread. Considering market economic development, China should adopt the jointly funded mode (such as the traditional volume method, i.e. sharing the fund according to the volume.) while supported by the government subsidies. Meanwhile, the sharing ratio should be kept low and the pipeline companies' affordability should fully be taken into consideration [5].

3.3 *To gradually legalize the charging fee standard*

The management department of utility tunnel should confer with relative departments and standardize the charging fee as well as improve the price system to balance the interests, coordinate the conflicts among all parties and finalize the form of law to ensure the management of utility tunnel. The following principles can be regarded as a reference while pricing: (1) Stick to the price policy of public utilities, (2) Who benefits then who pays, (3) Compensate for the cost, (4) Decentralize decision-making and pricing accordingly, (5) Proceed step-by-step, (6) Make overall plans and taking all factors into consideration [6].

3.4 *To establish a specific UUT management department*

In daily operation and management, many departments are involved so that it is hard to coordinate the interests of all parties, due to which, the development of utility tunnel is restricted. Therefore, the fragmental management system that "who owns who manages" must be broken and a unified management performed by a specific department should be established. Main responsibilities of this new department can be seen in 3 stages: it is responsible for collecting and raising excavation costs and unifying procedures and filing when starting the construction; responsible for monitoring the project quality and the business operations of the investments during the construction period; responsible for signing contracts with the professional companies on the matter of inspection, maintenance, management, etc. when finishing the construction, to maximum the benefit of utility tunnel construction [6]. In addition, the department should be entitled with certain rights such as overall management, approval authority, execution and penalty by law.

3.5 *To establish an underground pipeline information sharing platform*

At present, the information of underground pipeline is recoded and preserved by paper, such

as drawings, diagrams, etc., which would lead to material information loss, inconvenience of inquiring and low efficiency. For those cities with or without an information-sharing platform, it is necessary to integrate the utility information and build a functional system to restore, supervise, analyze, account, inquiry, output and update the underground utility information. Moreover, the realization of electronic administration relies on the help of Internet, sensors, GIS and other advanced technologies to provide the channel to inquiry electronic maps and other image data [7]. In this way it will follow the convenience of urban plan, urban construction, good underground space development, and the improved resilience to handle emergencies.

3.6 *To comprehensively considerate the development of subway, tunnel, basement and other underground space*

At present, we live in a period when our country is exploring underground space actively, especially the utility tunnel. It is recommended to integrate the UUT plan with other related underground space plans. When constructing underground space in deferent regions, we should build several short utility tunnels at the same time and connect each other then a huge utility tunnel project covering a whole region and even a whole city would come into shape. It is also recommended to transform the underground space construction to the utility tunnel construction as soon as possible, which can avoid surface construction damages and traffic accidents caused by early underground projects, conserve the underground space, and reduce the capital investment and the utility tunnel construction costs.

3.7 *To convoke special sessions and organize department-related discussions regularly*

Relative departments should convoke special sessions on utility tunnel regularly and organize all-round communication effectively. Through

analyzing the above methods of planning, implementing, managing, we can learn lessons and build more scientific, effective, systematic and perfect utility tunnel process with Chinese characteristics.

4 CONCLUSIONS

At present, China is still in the preliminary process of urban utility tunnel construction, facing with many problems. For example, many laws and regulations need improving, more construction mode needs exploring and new management system needs innovating, etc. However, according to the development at home and abroad, the integrated construction of utility tunnel is an inevitable trend. Therefore, grasping the situation and seizing the opportunity to develop the urban utility tunnel construction based on our national condition will become one of the most important ways of building resource-saving and environment-friendly cities.

ACKNOWLEDGEMENTS

This paper is funded by National Natural Science Foundation of China under contract No. 51108421.

REFERENCES

- [1] Xu Xiaojun. 23/05/2012. http://news.163.com/12/0523/09/8269/LQKV00014_AEE.
- [2] Hou Wenjun, Jiang Haijun, Sun Wei, Song Lili. 2005. Municipal Engineering Technology, Vol. 23(2005), p. 229–232.
- [3] Wang Hengdong, Xue Weichen. 2009. Special Structures, Vol. 26(2009), p. 102–104.
- [4] Guan Xin. 2009. Building Economy, Vol. 29(2009), p. 42–45.
- [5] Yang Yiting. 2013. Journal of Shenyang Jianzhu University (Social Science), Vol. 15(2013), p. 286–289.
- [6] Shen Rong. 2008. Water & Wastewater Engineering, Vol. 34(2008), p. 105–107.
- [7] Wang Jiangbo, Dai Shenzhi, Gou Aiping. 2011. Urban Planning International, Vol. 26(2011), p. 87–94.

Application study of green building technology in universities and colleges in cold regions

Ju Qiu & Li Bin Xia

Jilin Jianzhu University, Changchun, China

ABSTRACT: With the expansion of the scale of universities and colleges in China, university and college buildings have become a major source of energy consumption. Due to the special climate of universities and colleges in cold regions, the issue of energy consumption becomes more prominent. Therefore, this paper mainly studies the issue of rational use of green building technology, to reduce the building energy consumption of teaching buildings, research buildings, administration buildings, teacher and student apartments, gymnasium, cafeteria and other buildings, and improve the utilization of campus resources.

Keywords: cold regions; universities and colleges; energy consumption; green building technology

1 RESEARCH BACKGROUND

As is stipulated in Specialized Planning of Building Energy Conservation in 12th Five-Year Plan, it is required to implement the scale advance of green buildings and build in universities and colleges concentrated green buildings demonstration area mainly dominated by green buildings. Domestic universities and colleges have responded positively to the country's call in new campus construction and renovation projects, and actively promoted the use of a variety of green building technologies. The universities and colleges in cold regions, due to climate factor, should take into account heating, insulation and other issues more in campus construction; therefore, they are characterized by high energy consumption with the demand for more energy. In this context, it is of great importance to apply green building technology in colleges and university in cold regions.

2 CONCEPT OF GREEN BUILDING TECHNOLOGY

What is green building technology? The buildings with the application of this technology have a healthy and comfortable indoor environment, and achieves coordination, integration and coexistence with natural environment, play a role in protecting natural environment at every stage of their life cycle to a certain degree, and coordinate the relations between people and natural environment.^[1]

3 CLIMATIC FEATURES OF COLD REGIONS

Cold regions are most notable for their unique climate, which can be regarded as a basic feature as well. The main climatic feature of most cold regions can be mainly found in winter, so people will often associate these regions with snow, coldness, darkness and winter together. In winter, the cities in cold region has five climate characteristics: the outdoor temperature is generally lower than 0°C; daylight and sunshine time is short; winter precipitation is often dominated by the form of snow; longer duration of these three climatic features above; significant season change.

4 APPLICATION STUDY OF GREEN BUILDING TECHNOLOGY IN UNIVERSITIES AND COLLEGES IN COLD REGIONS

According to different purposes and uses, green building technologies can be divided into land conservation, energy conservation, water conservation, renewable energy use, indoor and outdoor physical environment control and waste resources processing and so on. In view of the unbalanced development of the green building technology and the actual level of research, this paper only studies the application of energy-saving technology, water-saving technology, solar energy utilization technology of green building in the construction of universities and colleges in cold regions.

4.1 *Energy-saving technology*

Due to the long duration of cold winter in China's cold regions, the universities and colleges in cold regions requires heating for a number of days with more energy consumption accordingly. Under such harsh climatic conditions, it is of special significance to improve campus building insulation and improve the thermal efficiency of heating facilities, in order to improve indoor thermal environment in college and universities in cold regions in winter, and achieves saving of heating energy. As for any building, the peripheral structure of buildings is the first and most important part of cold insulation. Therefore, in universities and colleges in cold regions, energy saving in external envelope structure of buildings is especially important. The so-called external envelope structure mainly refers to the external walls, windows and roof sections of the buildings. Thus, energy saving in the external envelope structure of university and college buildings covers the selection of external wall materials, the development of external wall insulation ways, selection of windows and glass, choice of roof insulation forms.

First of all, in external envelope structure design in university and college buildings in cold regions, it is very important to choose wall materials of a good thermal performance and of relatively cheap price in the selection of wall materials choice. It is recommended to choose appropriate new energy-saving wall materials based on campus culture and history, main architectural style, and surrounding environment. For example, we can make use of load-bearing materials and efficient insulation material (such as rock wool board or polystyrene board, etc.) to build a compound wall since this type of wall meets the requirements of energy saving, land saving, waste recycling, insulation, heat insulation, light weight and high strength in the construction of university and college buildings in cold regions.

Secondly, when it comes to the methods of external thermal insulation of external wall, the external wall insulation method with larger advantage can be adopted. Because university and college buildings accommodate a large number of people every day, security is always given top priority. In comparison to internal thermal insulation of external wall, external thermal insulation of external wall helps increase the stability of the building and extends its life with great assurance of security. In addition, this approach can basically eliminate heat "thermal bridge" effect, save winter heating costs, save energy on campus; it can improve wall dampness in winter, improve insulation capacity; it is conducive to the stability of room temperature, especially in the bedroom, and it can improve *t* students' quality of life.

Currently, the majority of universities and colleges in cold regions adopt centralized heating, which is an important measure to both achieve energy conservation and improve environment. With the continuous development of universities and colleges, unit energy consumption keeps going up with an increasing amount of carbon dioxide emissions. Therefore, as for universities and colleges in cold regions, the adoption of centralized heating and use of advanced technology to reduce energy consumption, increase efficiency and reduce carbon dioxide, sulfur dioxide and dust emissions will help improve the global environment. Meanwhile, the central heating is a measure for the conservation of construction land. Without central heating, it is necessary for universities and colleges to build different specifications of boiler rooms and coal storage fields, thus demanding much more land; on the contrary, the implementation of central heating can achieve land saving.

Besides, in view of the actual situation and the economic strength of the universities and colleges in cold regions, air conditioning and ventilation adopts natural ventilation and mainly makes use of the building's natural ventilation. It mainly plays a role in two aspects: improvement of thermal comfort and indoor air quality. In summer, the use of natural ventilation for passive cooling can reduce air conditioning energy and prevent the occurrence of sick "building syndrome"; in winter, the natural ventilation under a reasonable degree of control can help get rid of excess moisture and contaminants in the room, so as to reduce heating energy consumption.

4.2 *Water-saving technology*

Universities and colleges, the workplace of teachers and a place for the education of college students, have a huge daily demand for water. Especially the universities and colleges in cold regions, due to the special geographical climate, have greater demand for water. However, as our country is one of the world's countries short of water, water resource is becoming increasingly tense. In this context, as for universities and colleges in cold regions, water-saving technology is also a very important technology.

Water conservation has two layers of meanings: one is water saving in the usual sense; the other is a reasonable use of water. In other words, water conservation is the improvement of water use efficiency in a reasonable and economical ways, the careful management and civilized use of water resources, so that the limited water resources can meet the needs of economic and social development. That is to say, we should achieve good benefits when we save valuable water resources.^[2]

The university and college buildings in the cold winter should adopt water-saving equipments and appliances, including faucets, toilet flushing devices, water pipes and other equipments. Among them, faucet is a water apparatus applied throughout the classroom buildings, canteens, dormitories, gymnasium, library and other buildings, and a water apparatus for cleaning and hands and face washing with the largest amount of users and the widest application in universities and colleges in cold regions. It is most closely related to teachers and students and its performance has the largest impact on water conservation effect. Therefore, automatic faucet with little flow of water can be applied in the classroom buildings, dining halls and other public areas, to simply meet the function of hands washing, and reduce water consumption appropriately. Toilet flushing device is the key to the water conservation in university and college buildings because plenty of water is used for toilet flushing in university and college buildings in cold regions. It is equally advisable to apply automatic faucets to achieve water conservation.

Meanwhile, the use of rainwater is an important way. Rainwater has always been discharged into the sewer as wastewater. However, rainwater is different from neither drinking water nor sewage water, and it needs special processing to make the best use of everything. Now rainwater is more used as a source of reclaimed water. It is not easy to control the rainwater flow or collect it. The university and college buildings can adopt materials of good water permeability with the equipment of water storage devices to collect and store rainwater as reclaimed water.

4.3 Use of solar energy technology

With the improvement of scientific and cultural level, the development and utilization of new energy sources, especially natural resource like solar energy, has become the main method of energy efficiency in buildings. In the universities and colleges in cold regions in our country, the

use of solar energy can be seen everywhere and it can be broadly divided into solar hot water and solar power generation. For example, students can make use of solar hot heaters for heating water in the bathroom. If there is enough solar energy, the heater can directly heat the water for everyone to use. In rainy days or days with less sunlight, when the heated solar water temperature is still below the water temperature for bath, students can choose auxiliary heating to ensure that their daily use of hot water is not affected in whatever weather conditions. This practice can greatly reduce energy consumption on campus. In addition, more and more universities and colleges in cold regions choose to make use of solar lights. Technically, it is basically power-free to turn on night lights with sunlight energy absorbed by the solar panels.

5 CONCLUSION

In face of a deteriorating environment and increasing depletion of energy today, green building technology has become an important technology in the construction industry. By adopting more reasonable green building technologies and constructing comfortable green buildings, the universities and colleges in cold regions can not only enhance the campus image and improve the quality of life on campus, but also contribute to and set a good example for energy saving and environmental protection. Therefore, for universities and colleges in cold regions, green building technology is not just a construction tool and instrument, but also the power source to push forward the development of the universities and colleges.

REFERENCES

- [1] Building Science [2007] 205. Green building technology rules evaluation [S]. Beijing: China Architectural Press, 2007.
- [2] Huang Fengzhu. Water saving technology in Sichuan building [J]. Building Science Research, 2006 (10).

Research on the influence of lean of bridge piers on continuous rigid frame bridge

Wen Zong Ying

Chongqing Communication Construction Group, Chongqing, China

ABSTRACT: Errors must exist in the construction of long span bridge. And the construction errors inevitably influence the performance of bridge structure. So it is necessary to study the influence of construction error on bridge structure. This paper, focusing on continuous rigid frame bridge based on real multi-span continuous rigid frame bridges as engineering background, simulates the construction errors of lean of bridge piers using FEM to analyze its influences on the internal force, stress and displacement of the continuous rigid frame bridge, and then evaluates the influences of such errors on continuous rigid frame bridge in construction.

Keywords: section size; continuous rigid frame bridge; construction error; influence

1 INTRODUCTION

The construction process of long-span bridge is quite complex, and is influenced by various uncertain factors, which may lead to deviation between the actual state of bridge structure and the theoretical calculation analysis. And the existence of the construction error is one of those factors. This paper mainly analyzes the influence of pier leaning on the bridge structure^{[1][2]}.

Based on a prestressed concrete continuous rigid frame bridge constructed in a certain expressway, the influence of pier leaning on the internal forces, the stress and displacement of long span continuous rigid frame bridge are studied by using finite element analysis software Dr Bridge. Based on the simulation, the influence of the error in the height of the main girder section on similar bridges is evaluated^{[3][4]}. The paper can provide assistance and monitoring for the construction of the bridge, which helps the smooth construction of the bridge.

2 METHOD

2.1 The background of the related project

In this paper, in accordance with the design drawing, Dr Bridge, a professional software for bridge, is adopted to establish the bridge finite element models of the whole bridge structure of the normal state, which is shown in Figure 1.

For the convenience of elaboration, the state in which the piers are normal is referred to as the normal state. The state in which the piers are inclined is called the leaning state.

3 THE INFLUENCE OF PIER LEANING ON THE BRIDGE STRUCTURE

After the closure of the full bridge, prestressed tensioning is carried out, and then bridge deck pavement is constructed, thus forming a bridge. The finished state of the bridge is the initial state of the bridge structure. In order to make clear the influence of pier leaning on the finished continuous rigid frame bridge, the paper analyzes the influence of pier leaning on pier No. 2 as well as the internal force, stress and displacement of the bridge's girder.

3.1 Influence analysis of the finished state of the bridge

In the paper, the influence of bridge pier No. 2 is analyzed, including its influence on internal force, stress and displacement effect. Above has shown that fold stage tilted pier of 3, 4, 5 # pier can be

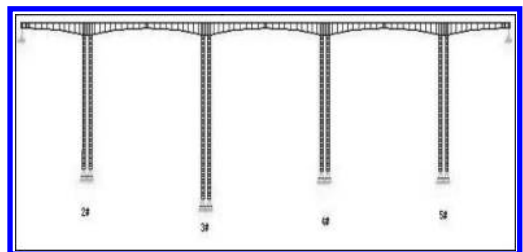


Figure 1. The finite element model of the bridge under the normal state.

ignored, the influence of the finite element calculation results show that the bridge into phase 2 pier tilt to the No. 3, 4, and 5 pier and girder, it does not, there would not be in detail. It has been shown by finite element analysis that the influence of pier leaning on piers No. 3, 4 and 5 can be omitted in the closure state, which will not be stated in detail in the paper.

3.2 Influence analysis on the internal force of pier

① Influence analysis on the axial force of pier No. 2
The axial forces of pier No. 2 under the normal and pier leaning states are shown in Figures 2 and 3.

It can be seen from the Figures 2 and 3 that the difference value between the axial forces in the two different states is about 1000 kN, thus the influence of pier leaning on the axial force of pier 2 is little, which can be neglected.

② Influence analysis on the shear force of pier No. 2
The shear forces of pier No. 2 under the normal and pier leaning states are shown in Figures 4 and 5.

According to the Figures 4 and 5, the influence of pier leaning on the shear force of pier No. 2 is significant, and the shear force in the pier leaning state increases obviously. In the left limbs of pier No.2, the shear forces under the

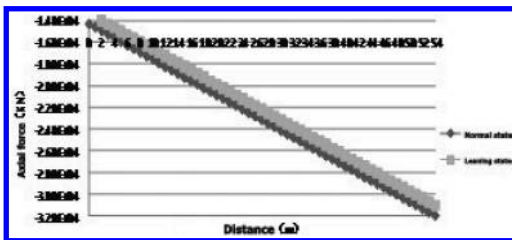


Figure 2. The comparison of the axial forces of pier No. 2 at its left rib under the normal and pier leaning states.

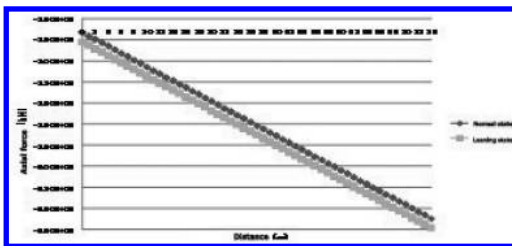


Figure 3. The comparison of the axial forces of pier No. 2 at its right rib under the normal and pier leaning states.

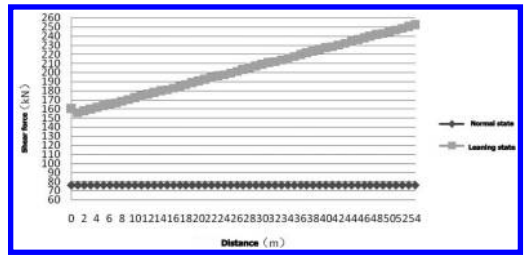


Figure 4. The comparison of the shear forces of pier No. 2 at its left rib under the normal and pier leaning states.

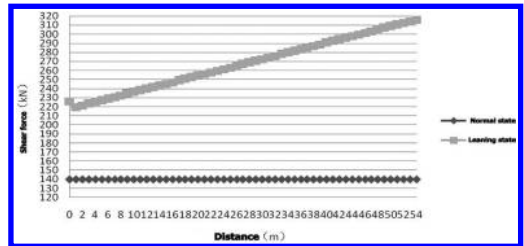


Figure 5. The comparison of the shear forces of pier No. 2 at its right rib under the normal and pier leaning states.

normal state of bridge pier remains the same, which is 76.1 kN; while the shear forces under the pier leaning state change approximately in a linear way from 160 kN at the top of the pier to 252 kN at the bottom. The shear force in the pier leaning state is 3.3 times of that in the normal state. In the right limbs of pier No. 2, the shear forces under the normal state of bridge pier remains the same, which is 139.9 kN; while the shear forces under the pier leaning state change approximately in a linear way from 226 kN at the top of the pier to 316 kN at the bottom. The shear force in the pier leaning state is 1.4 times of that in the normal state.

③ Influence analysis on the moment of pier No. 2
The moments of pier No. 2 under the normal and pier leaning states are shown as in Figures 6 and 7.

According to the Figures 6 and 7, in the finished state of the bridge, the influence of pier leaning on the moment of pier No. 2 is significant, and the moment in the pier leaning state increases obviously. In the left limbs of pier No. 2, the moment under the normal state of bridge pier change approximately in a linear way from $-2351 \text{ kN} \cdot \text{m}$ at the top of the pier to $1759 \text{ kN} \cdot \text{m}$ at the bottom; while the moment under the pier leaning state change approximately in a non-linear way from $-4341 \text{ kN} \cdot \text{m}$ at

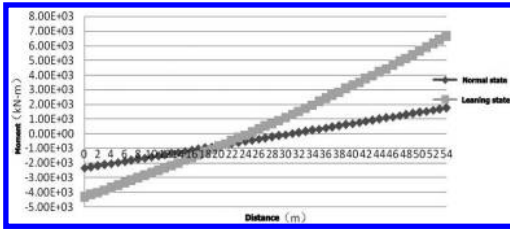


Figure 6. The comparison of the moments of pier No. 2 at its left rib under the normal and pier leaning states.

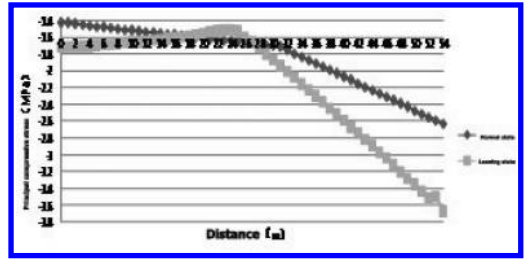


Figure 8. The comparison of the principal compressive stress of pier No. 2 at its left rib under the normal and pier leaning states.

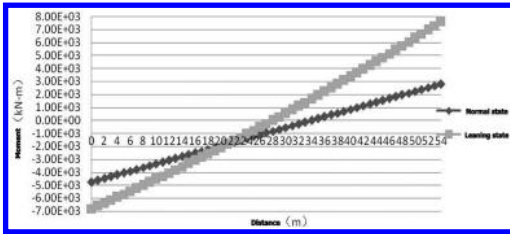


Figure 7. The comparison of the moments of pier No. 2 at its right rib under the normal and pier leaning states.

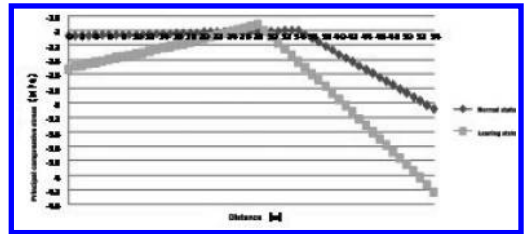


Figure 9. The comparison of the principal compressive stress of pier No. 2 at its right rib under the normal and pier leaning states.

the top of the pier to $6630 \text{ kN}\cdot\text{m}$ at the bottom. The moment in the pier leaning state is 3.77 times of that in the normal state. In the right limbs of pier No. 2, the moment under the normal state of bridge pier change approximately in a linear way from $-4755 \text{ kN}\cdot\text{m}$ at the top of the pier to $2801 \text{ kN}\cdot\text{m}$ at the bottom; while the moment under the pier leaning state change approximately in a non-linear way from $-6816 \text{ kN}\cdot\text{m}$ at the top of the pier to $7603 \text{ kN}\cdot\text{m}$ at the bottom. The positive moment in the pier leaning state is 2.71 times of that in the normal state, while the negative moment in the pier leaning state is 1.43 times of that in the normal state. However, the maximal moment position in both the positive and negative moment area are the same, which is in the top or the bottom of the pier.

3.3 Influence analysis on the stress of pier

This section selects both the principal tensile and compressive stress of the pier as indicators for stress analysis. In both the normal and pier leaning states, the principal tensile stress of pier No. 2 can be regarded as zero, which will not be elaborated in the paper. And its principal compressive stress diagram is shown in Figures 8 and 9.

According to the Figures 8 and 9, in the finished state of the bridge, the influence of pier leaning on the principal tensile stress of pier No. 2 is significant, and the principal tensile stress in the pier leaning state increases obviously. In the left limbs

of pier No. 2, the principal tensile stress under the normal state of bridge pier changes in a broken-line way from -1.43 MPa at the top of the pier to -2.63 MPa at the bottom; while the principal tensile stress under the pier leaning state changes approximately in a broken-line way from -1.72 MPa at the top of the pier to -3.67 MPa at the bottom. The principal tensile stress in the pier leaning state is 1.4 times of that in the normal state. In the right limbs of pier No. 2, the principal tensile stress under the normal state of bridge pier changes in a broken-line way from -2.07 MPa at the top of the pier to -3.08 MPa at the bottom; while the principal tensile stress under the pier leaning state also changes in a broken-line way from -2.53 MPa at the top of the pier to -4.23 MPa at the bottom. The principal tensile stress in the pier leaning state is 1.37 times of that in the normal state. However, the maximal tensile stress position in both the two states is the same, which is in the top or the bottom of the pier.

3.4 Influence analysis of the finished state of the girder

The finished state of a bridge is the initial completed construction state of a bridge, and it is necessary to analyze the stress in such a state. This section mainly investigates the influence of pier

leaning on the main girder of the bridge, including internal force, stress and displacement. It has been shown in the above content that the influence of pier leaning in the closure state on the girder on pier No. 3, 4 and 5 can be neglected. And finite element calculation results show that in the finished state of a bridge, pier leaning barely has any influence on the girder on pier No. 3, 4 and 5, and its influences on the axial force, bending moment, principal tensile, compressive stress and the vertical displacement as well as the shear forces in the area besides the top of the girder on pier No. 2 can all be neglected, while it has certain influences on the shear forces on the top of the pier, and has significant influences on the horizontal displacement of the girder on pier No. 2. In the following, some analysis results are shown in the figures. For the convenience of this paper, the bridge is divided into left and right parts according to its mid-span section.

4 INFLUENCE EVALUATION ON PIER LEANING

This section mainly evaluates the influence of pier leaning on the bridge from 3 aspects, namely internal force, stress and linearity [5][6].

4.1 Influence evaluation on the internal force of pier leaning

It can be seen from the above that the influence of pier leaning on the axial force of the pier can be neglected. The maximal axial force of pier No. 2 during the construction and usage processes in which pier leaning occurs is $3.71e + 04$ kN, and that in the normal state is $3.64e + 04$ kN. The difference value between the two is 700 kN, and the relative difference is 1.9%. As security reserves in engineering design is relatively high, thus the influence of pier leaning on the axial force of the pier will not be in this paper; the influence of pier leaning on the internal force of main girder are negligible, which will not be elaborated in the paper; and this section focuses on the influences of pier leaning on the shear force and bending moment.

① Influence evaluation on shear force

The maximal shear force of pier No. 2 during the construction and usage processes in which pier leaning occurs is 345 kN, and that in the normal state is 500 kN. The difference value between the two is 155 kN, and the relative difference is 45%. As bridge piers are eccentric compression members in engineering and its the shear force usually small, bridge pier in the engineering design by shear force is small, no

special anti-shear design has been conducted in the design process, and only ordinary steel is reinforced in the structure. According to highway reinforced concrete and prestressed concrete bridge and culvert design specifications [51]: if the structure meets the requirements in rule 7-1, no calculation related to the shear bearing capacity of the oblique section needs to be carried out. And the structure is reinforced by steel according to the following inequality $\gamma_0 V_d \leq (0.5 \times 10^{-3}) \alpha_2 f_{td} b h_0$. In order to prevent the occurrence of large cracks, the section size of the pier should satisfy the inequality that $\gamma_0 V_d \leq (0.51 \times 10^{-3}) \sqrt{f_{cu,k}} b h_0$. In this case, the section size of the pier meets the above requirements.

In this case, the shear bearing capacity of the bridge pier is carried by the concrete and stirrup, which is calculated according to the inequality $\gamma_0 V_d = V_u \leq \alpha_1 \alpha_2 \alpha_3 (0.45 \times 10^{-3}) b h_0 \sqrt{(2 + 0.6p)} \rho_{sv} f_{sv} \sqrt{f_{cu,k}}$. The calculated maximal shear bearing capacity of the pier is bigger than 10000 kN, which is far bigger than the actual the maximum shear of pier. And the importance coefficient this bridge structure is 1.1, so the bridge pier can withstand the shear force.

② Influence evaluation on moment

The maximal moment of pier No. 2 during the construction and usage processes in which pier leaning occurs is 9.31×103 kN·m, and that in the normal state is 5.35×103 kN·m. The difference value between the two is 3.96×103 kN·m, and the relative difference is 74%. In this case, the maximal moment of the steel bar calculated according to the inequality

$$\gamma_0 M_d \leq f_{cd} b x (h_0 - x/2) + f_{sd} A_s (h - a_s)$$

is bigger than 2.60×104 kN·m, which is two times of the moment bore by the pier when pier leaning occurs. And the importance coefficient this bridge structure is 1.1, so the bridge pier can withstand the shear force.

4.2 Influence evaluation on stress

The stress in a structure affects the safety and usage of the structure. Based on the comparison between maximum principal tensile and compressive forces, in the construction and use processes of the bridge in which pier leaning occurs as well as those calculated in the actual state, the influence of the internal force is evaluated.

It can be known from above that the influence of pier leaning on the principal compressive stress of piers is significant, and it increases obviously, while the principal tensile stress is very small, which can be regarded as 0 mpa. In the

construction and usage processes, the maximum principal compressive stress is 4.23 MPa, and that in the normal state is 3.08 MPa, the different value between them is 1.15 MPa, and relative difference is 37%. While the piers is casted by C40 concrete of which the design value of compressive strength is 18.4 MPa, and tensile strength is 1.65 Mpa. The maximum principal compressive stress is 4.3 times of the design value of compressive strength; therefore bridge pier can withstand the stress of bridge.

4.3 Influence evaluation on linearity

The line shape of a bridge influences its aesthetics, driving comfort and even of the durability of the bridge. The influence evaluation on the linearity of a bridge is conducted through the comparisons between horizontal and vertical displacements of the pier in the construction and usage processes as well as in the normal state.

It can be known from the above that the influence of pier leaning on the displacement of pier No. 2 is obvious. The maximal horizontal displacement in the pier leaning state is 2 times of that in the normal state, and the vertical displacement decreases. Thus pier leaning has significant influence on the displacement of pier No. 2, while barely has any influences on other piers or linearity of the bridge^[7-9].

REFERENCES

- Fan Lichu. The bridge engineering [M]. Beijing: China Communications Press, 2001.7.
- Gu Anbang, Zhang Yongshui. Construction of the bridge to monitor and control [M]. Beijing: Mechanical Industry Press, 2005.
- Hao Chao. Large span steel cable-stayed bridge construction error adjustment method [J]. Journal of Zhejiang University, 2003,5 (3), 310-313.
- Hohenbichler M, Rackwitz R. Sensitivities and importance measures in structural reliability [J]. Civil Eng. System, 1986(3):203-209.
- Karamchandani A, Cornell C.A. Sensitivity estimation within first and second reliability methods [J]. Structure. Safety, 1992 (11), 97-105.
- Polhill, R.M. 1982. *Crotalaria in Africa and Madagascar*. Rotterdam: Balkema.
- Tang Pan, Liu Airong. Effect of bridge construction stage of internal forces of continuous rigid frame bridge [J]. Journal of Guangzhou University, 2009, 12(6), 76-78.
- The people's Republic of China Ministry of transportation. JTJ/JT F50-2011 highway technical specifications of culvert construction [S]. Beijing: China Communications Press, 2004.
- Wang Jinfeng, Liu Bin. High pier and long-span continuous rigid frame bridge structure characteristics and construction control of [J], Chinese harbour construction, 2005, 6 (3), 40-43.
- Zhou Junjie. Long span curved continuous rigid frame bridge construction error factors analysis [J]. Shanxi architecture, 2011, 6 (17), 93-95.

The channel investigation of BIM technology localization

En Tian Qie, Yong Li & Yuan Yuan Jiao

Wuhan University of Science and Technology, Wuhan, China

Chang Tao Wang

China Construction, Seventh Engineering of Five Corporation, Yichang, China

ABSTRACT: BIM technology, as a technology of computer application, has a revolutionary significance. In this paper, we present a localization channel that BIM technology should be popularized in construction unit at first, by analyzing the localization capability of each participating unit, namely, owner, design, construction, supervision, operation and maintenance. In addition, we propose some BIM localization programs, such as specialized BIM technology company should be established, design unit and construction unit should cooperate with the BIM company, construction unit should expand BIM business, and so on.

Keywords: BIM technology; construction unit; localization

1 INTRODUCTION

BIM (Building Information Modeling) is mentioned several times in “*The Development Program of Construction Industry Informatization for 2011–2015*” (referred to as the “Outline”), which was issued by the Ministry of Housing and Urban-Rural Development in 2011, and its overall objective clearly states: there are a series of goals to be completed in the period of “The Twelfth Five-year Plan”, such as basically achieving the popularization of building enterprise information systems, accelerating the application of new technologies in engineering, e.g. BIM technology and network-based collaborative work, promoting informatization standard of the construction, advancing the industrialization with independent intellectual property, to form a group of construction enterprises reaching the international advanced level. Besides, its specific objectives and development priorities also pointed out: that, survey and design enterprises should promote the establishment and application of the collaborative design system of BIM technology, and explore the BIM three-dimensional design in the design phase; construction enterprises should enhance the level of integration application of enterprise and project management information system, and promote the research and application of BIM during the construction phase. We can see that, the “Outline” provides a good opportunity for construction enterprises to popularize BIM.

BIM technology originated from foreign, which is another computer application technology following the CAD (Computer-Aided Design), and its basic idea is that: Architectural Design on computer is an operation of the components with attribute information, instead of point, line, surface and other basic elements. With the further development of BIM technology in foreign countries, the concepts and technologies of BIM are also introduced to our country, and a series of research that can promote BIM localization is already underway, such as popularizing BIM concept, developing localized BIM software, exploring the localization application of BIM technology, formulating BIM standards, etc.

2 THE VALUE OF BIM TECHNOLOGY

2.1 3D rendering and display

The visualization of BIM model can clearly demonstrate complex shape and space, and the rendering based on secondary development can give people a real feeling and direct visual impact, which is convenience for communication, discussion, decision-making in the process of project design, construction and operation.

2.2 Rapid calculation and improving accuracy

Due to the high fineness of the data of BIM model, it can quickly provide data information

that is needed by each pipeline installation, which can effectively improve the efficiency of construction management.

2.3 *Precise planning and avoiding the waste*

We can quickly obtain the basic engineering data by BIM technology, which provides effective support for the construction unit to make resource plan, and greatly reduces the waste of resources in logistics and store.

2.4 *Virtual construction and effective collaboration*

4D simulation techniques based on BIM platform can carry on virtual construction, and compare the construction plans at any time. Government, owners, design unit, construction unit, supervision unit, procurement unit, and operation, can share and exchange information on the BIM platform.

2.5 *Collision detection and reducing rework*

BIM collision detection technology can optimize the space and piping arrangement at the early stage of the construction, and reduce the possibility of mistakes and rework during the construction phase.

2.6 *Conflict coordination and decision support*

BIM database can be shared in various departments, besides, engineering information can be aggregated, split, and contrast, based on the component type, which can guarantee to provide timely and accurate engineering data for decision-makers in terms of cost, schedule, safety, quality management, etc.

In summary, BIM technology can bring great impact on owners, design unit, construction unit, supervision unit, operations unit and other units, for research BIM technology, so it makes sense to research the popularity of BIM technology in construction units.

3 THE ANALYSIS OF BIM TECHNOLOGY LOCALIZATION

3.1 *The problems of BIM technology localization*

3.1.1 *The barriers of data exchange*

Currently, the lack of exchange software or exchange format among widely used architectural software leads the data can't be shared. Take the data input from the PKPM software to the Revit structure software in structure design for example,

because the PKPM structural model can't be directly imported into the Revit, the information of section size calculated by the PKPM structural can only be entered into Revit structure by hand, and the efficiency of information transmission is very low. Further, there is a series of other data sharing barriers, such as the data of high version software can't be used by the low version, the same data can't be shared by two or more computers, and so on.

3.1.2 *The lack of professional and technical personnel*

BIM technology in China is in the primary stage of development, so very few people are equipped with BIM work experience. Moreover, the practitioners are accustomed to the existing work pattern, and the staffs with a lot of business are more reluctant to learn BIM technology. Besides, it will be high-cost to hire BIM experts and buy the BIM software, which makes participation units are reluctant to use BIM technology.

3.1.3 *The difficulties of learn BIM software*

Learning BIM software is a long process. Particularly, in the current situation that BIM technology is not very mature, the BIM cases that can be used for reference are rarely, and the compatibility of BIM software is very poor, which causes great inconvenience to learning BIM software.

3.2 *The BIM localization capability of participation units*

3.2.1 *Construction unit*

Construction unit, known as project owner, is the investment entity or investors of the construction project. Its main assignment is proposing construction planning, and providing construction land and funds for construction. According to "*The guide of American owner using BIM*", the owner can use BIM to complete eight things, namely, data research, performance testing, system control, space tracking, asset management, maintenance management, state records, and scene forecast. The owner in our country mainly uses BIM to manage asset and coordinate the relationship between the design, construction, operation and maintenance. According to the domestic and overseas owner's work content, we can conclude that: the main task of the owner is to control and manage the whole building, instead of engaging in specific engineering technology; owner knows very little of professional knowledge and BIM technology, and their ability is far less than setting up the model with BIM software. In addition, the current owners do not realize that themselves are the

biggest beneficiaries of BIM technology, and are very passive to use BIM technology. Therefore, the construction unit is of great resistance to promote BIM localization.

3.2.2 The design unit

Although the characteristics of BIM technology, such as visualization, two-dimensional drawing, synergy, and automatic measurement, greatly reduce the workload of the designers and builders, the design unit can't be the main driving force of BIM technology localization. There are four main reasons: First, the design unit participates in the project construction for a short time, and will be basically out of the building lifecycle after the design completed; Second, the BIM technology is in the promotion phase at present, design unit are reluctant to provide downstream units with a precise, complex and high-cost BIM models for free in the absence of the owner's support; Third, due to the lack of domestic core design modeling software, most of the design institutes use the way that collaboration with foreign BIM companies to promote BIM technology, and lost a way to explore BIM localization. Fourth, in the era of CAD, designers and engineers mostly carry out individual work, however, BIM technology emphasizes teamwork, and sudden change in the habit of thinking is difficult to for staff to adapt. In summary, the design unit can't effectively promote BIM technology localization.

3.2.3 The supervision unit

The comprehensive strength of promotion BIM technology of supervision unit is relatively weak. Persons engaging in supervision work are mostly old or inexperienced, and have difficulty in learning BIM technology; Supervision Company is unlikely to provide financial for developing a localized BIM software serving supervision, and supervision unit in our country using BIM technology in its supervision work is also very rare, as shown in Figure 1. In short, according to human, material and financial resources, it is difficult for supervision unit to have a good performance in the development of BIM technology.

3.2.4 The operation and maintenance unit

Operation and maintenance management, as a stage of building lifecycle, refers to the maintenance and management of the construction. The operation and maintenance unit requires very little information extracted from the BIM model, and their work content determines that it is necessary for the unit to build the whole building model, therefore, the possibility of the operation and maintenance unit using BIM technology is also very small, as shown in Figure 1.

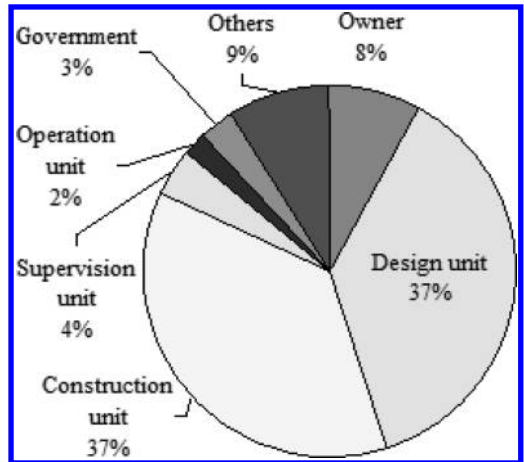


Figure 1. Ratio of each participation unit using BIM.

3.2.5 The construction unit

Construction, as one of the main stage of the building lifecycle, accounts for about 70 percent of the construction costs, and has a direct relationship with quality, safety and ongoing maintenance costs of the building. BIM technology just can facilitate these core issues. Take the Collision Detection in BIM technology as an example, construction unit re-establishes the BIM model based on the two-dimensional drawing that has been designed by design institute, and then construction, the effect is that: greatly reducing rework, improving construction efficiency, saving material and labor costs, easy management, and at least saving half of the cost in total. Therefore, the construction unit is willing to use BIM technology for improving construction efficiency, cost savings, and meticulous management.

In the process of promotion BIM technology, it is most appropriate to support the construction unit among the owner, design unit, construction unit, supervision unit, operation unit, and maintenance unit, as shown in Table 1. First, in these five units, BIM software developer first completes the development of localization software about construction, which provides a prerequisite for construction companies using localized BIM software. Secondly, the construction unit has abundant capital, which can provide capital guarantee for the development and application of localized BIM technology software. Third, the technical staff of construction unit has plenty of motivation to learn BIM technology, which differs from the Design Institute that rejects the three-dimensional BIM technology, and also differs from supervision, owner, operation and maintenance that fully don't understand BIM technology. Fourth, BIM

Table 1. Analysis of the channel of BIM localization.

Channel of BIM location	A	B	C	D	E
Software	3	4	5	2	1
Consciousness	3	4	5	2	1
Manpower	3	4	5	2	1
Finance	5	3	4	2	1
Enthusiasm	3	5	5	2	1
Total	17	20	24	12	6

The letters A, B, C, D, E represent owner, design unit, construction unit, supervision unit, operation and maintenance unit. And 5 is the highest ranking and the corresponding fraction, 1 is the lowest ranking and the corresponding fraction, etc.

technology brings different economic benefits for design, construction, and supervision, it can improve efficiency, reduce rework, save material, and significantly save cost for the construction side. Finally, the construction unit has a certain technical strength to set up BIM team.

3.3 *The specific measures of BIM technology localization*

3.3.1 *Forming specialized BIM technology company*

At present, the main units using BIM technology are design, construction, and consulting, participation units can't take the motivation of BIM application, technology and benefit together effectively. If we establish BIM technology company, it will integrate the three factors to maximize the advantages of BIM technology. The reasons are as follows.

First, BIM technology company can provide leasing services of the BIM family library for design unit, construction unit, and component manufacturers. Currently, in the process of using BIM technology to set up model, a crucial issue is the lack of BIM library family. BIM technology company can provide these services for them and other units after they building a large BIM family library.

Second, BIM technology company can provide value-added services of BIM model to operating unit. If BIM model is treated as a product, it will have a lot of value-added space. BIM technology company can retain BIM model, and cooperate with software developers, then reprocesses the BIM model to be an intelligent operation and maintenance building system and sells it to operational units.

Third, BIM technology company can provide consulting services for software development companies. The development of high performance BIM software requires combining the knowledge

of software programming and architecture, however, software developers often lack professional knowledge of architecture. So, BIM technology company can provide consulting services about architectural knowledge for software developers in the development of BIM software.

3.3.2 *Design unit and construction unit cooperating with BIM consulting company*

If design unit and construction unit cooperate with BIM consulting company, BIM consulting company can provide a series of suggestions and trainings about BIM for them. The design unit and construction unit can carry out a serious of business based on BIM technology, at the same time, it can also promote the development of BIM technology, which will achieve a win-win situation between them. However, the BIM consulting companies are rarely in our country, and it is difficult for design unit and construction unit to find a strong BIM consulting company, so, this strategy can be effectively implemented after the BIM developing to a certain stage.

3.3.3 *Construction unit expanding BIM outsourcing*

Firstly, construction unit should set up a small BIM team. Secondly, the unit provides regular training for them, and encourages them engaging in BIM technology outsourcing business. Nevertheless, using this method to implement BIM technology in construction project may be difficult, because the strength of small construction units is limited.

4 CONCLUSION

BIM technology, from being presented to being applied, has lasted more than ten years of development in our country, there are still many problems to be solved. However, according to the rapid pace of its development at present, we can predict that BIM technology will play an important role in building informatization, and bring a new revolution for Chinese construction industry. Therefore, the government, software development, developers, design unit, construction unit, and so on, should work together to promote localized BIM concept and technology. We believe that the arrival of the era of BIM is just a matter of time.

REFERENCES

- Amarnath, C.B. & Anil Sawhney J. 2011. Uma Maheswari Cloud Computing to Enhance Collaboration. *Coordination and Communication in the Construction Industry.*

- Arayici Y. & P. Coates & L. Koskela & M. Kagioglou & C. Usher & K. O'Reilly. 2011. Technology adoption in the BIM implementation for lean architectural practice. *Automation in construction*, 20(2).
- Jianhua Cheng & Hui Wang. 2012. The application and promotion of BIM technology in project management. *Construction Technology*. 41:18–21.
- Johnson & Weisheng Lu & Yi Peng & Qiping Shen & Heng Li. 2013. Generic Model for Measuring Benefits of BIM as a Learning Tool in Construction Tasks. *Journal of construction engineering and management*, 139(2).
- Kristen Barlish & Kenneth Sullivan. 2012. How to measure the benefits of BIM-A case study approach *Automation in construction*.
- Marnath, C.B. & Anil Sawhney J. & Uma Maheswari, 2011. Cloud Computing to Enhance Collaboration. Coordination and Communication in the Construction Industry.
- Paola Sanguinetti & Sherif Abdelmohsen & JaeMin Lee & JinKook Lee & Hugo Sheward & Chuck Eastman. 2012. General system architecture for BIM: An integrated approach for design and analysis. *Advanced engineering informatics*, 26(2).
- Sijie Zhang & Jochen Teizer & Jin-Kook Lee & Charles M. Eastman & Manu Venugopal. 2013. Building Information Modeling (BIM) and Safety: Automatic Safety Checking of Construction Models and Schedules. *Automation in construction*, 29(Jan.).
- Weisheng Lu & Yi Peng & Qiping Shen & Heng Li. 2013. Generic Model for Measuring Benefits of BIM as a Learning Tool in Construction Tasks. *Journal of construction engineering and management EISCI*, 139(2).

The architectural style characteristics of Enshi Tujia Diaojiolou from Peng

Ying Hong

Mass Media and the College of Art and Design, Wuhan Institute of East Lake, Wuhan, China

ABSTRACT: Diaojiolou Enshi Tujia people living places, generally built close to the mountains, communities fall distribution, well-proportioned, majestic, both symmetrical beauty double hanging form, also has the harmonious beauty into the mountainous environment, the outstanding representative of a Tujia architecture and sculpture art, taking Xuanen County of Enshi Prefecture Peng Diaojiolou example, from the construction of the main structure, building materials, decorative aspects to analysis the main architectural style of Enshi Tujia Diaojiolou characteristics.

Keywords: Peng; Tujia Diaojiolou; building

1 INTRODUCTION

Western Hubei Tujia traditional houses mainly located in Hubei Tujia and Miao Autonomous Prefecture in Enshi Tujia Diaojiolou houses, this region is located in the Wuling Mountain in Wushan and the two mountain, surrounded by mountains, arable land is not much, so in order to minimize the total cultivated area, residents only build houses in the gentle slopes of the mountain, or slightly more. After Wen long evolution, formed the Ganlan style form. Tujia Architecture—Diaojiolou, is each national minority bar style building is the most unique, Yishanbangshui, in the light of its general trend and build, with anti-virus snake beast invasion, dry and ventilated, high utilization rate, is an important part of Tujia culture. In Xuanen County, Enshi Prefecture, ShaDao Gou Zhen Liang he Cun Peng Jia Zhai has thrown the preservation of the integrity of the hanging leg buildings, is a typical Western Hubei Tujia settlement location and typical Tujia copycat.

2 FOLLOWING THE PENGJIA VILLAGE

Xuanen County of Hubei Province, Enshi Tujia and Miao Autonomous Prefecture Pengjia village ancient Diaojiolou group has hundred years history, set the Tujia Diaojiolou physical beauty, space level outline beauty in one, is the national Ministry of housing and urban rural development, the State Cultural Relics Bureau released the fourth batch of “China history and culture of the village”, one of the 20 folk cultural ecological protection zone is

also the Enshi Tujia and Miao Autonomous Prefecture named.

Diaojiolou old stilt, pavilion, porch column. Located in the Wulingshan mountains foothill Peng Jia Zhai, Hubei province is located in the Enshi Tujia and Miao Autonomous Prefecture of Xuanen County, southwest of Sha Dao Gou zhen. Whole village 45 families a total of more than 250 people, is the Department of Tujia nationality. The Peng moved here from Hunan, as the Peng Tujia settlements.

Pengjia village beautiful mountains and rivers, unusual topography, an exquisite scenery, blew. In the village houses a total of 23 buildings. Each self-contained, size ranging from hundreds to hundreds of square meters. Generally in next two dark three Bay as the house to house, niche for wing. Pengjia village Yishanbangshui the century old building, with a distinctive Tujia architectural art and culture atmosphere (Fig. 1).



Figure 1. Pengjia village on stilts.

3 TUJIA DIAOJIAO BUILDING STYLE

Towards things, well location. Diaojiaolou for Tujia people living places, Diaojiaolou usually semi erect, half rely on land landscape; most of the mountain and build, a tiger sat shape, “Zuo Qinglong, right white tiger, the former Suzaku, after basaltic” as the best game; pay attention to building orientation, or sit West to East, or sitting East to west.

Diaojiao Lou is Ganlan style architecture. The middle of the prototype, both sides for the Rao, for living, cooking. In a suspending part, usually around the floor upstairs corridor, the corridor is also equipped with railings. In a suspending part, usually around the floor upstairs corridor, the corridor is also equipped with railings.

Wood tiles material alone. Tujia Diaojiaolou mostly wooden structure, grey, lattice windows, eaves hanging vacant, wooden armrests. About the people in the wooden walls inside and out with tung oil, clean and bright.

Technical beautification, overall coordination. In order to prevent thieves, Diaojiaolou housing around the stone, mud brick walls. Zheng is in front of dam, dam outside the wall there is a character in the left door. Around the house are bamboo, trees and landscape tree. However, because of taboo and “funeral”, “escape” homophonic, unlucky, so no mulberry, not a peach. Tujia Diaojiaolou grilles embossed, engraved, carving, carving delicate, content rich and colorful.

3.1 *Enshi Tujia Diaojiaolou structural characteristics*

The Pengjia village as the representative of the folk have a single hanging type, double hanging type, two layer, three layer hanging hanging, flat lifting type and a hanging type, almost all styles diaojiaolou. Diaojiaolou built in slope, height of lateral and built a house (the house), the lower house (room), called building two room vertical force into a small courtyard, or the three force into the courtyard house. The house is three Bay, on two floors, three column five ride (not landing pillars) or five column eight is arranged in the middle of the main room, riding, both sides is divided into inside and outside two, for the bedroom, outside as Kang wu. “A lot of people in the fire is still well preserved. If aguest, sitting beside the fire, smoke a home grown tobacco, while on the chat.”

On the hanging feet (columns) of high and low, built by the to pography, downstairs or captive animals, or piled straw, or used for toilet. The two floor is flush with the ground, the house is built, form a corridor, viewing, can enjoy the cool air, drying clothes (Fig. 2).



Figure 2. Diaojiao building structure.

3.2 *Enshi Diaojiao building materials characteristics*

Previous by general with thatched roofs or fir skin, useful also slate covered roof, Diaojiaolou multi-purpose clay tile, and the position ofstress, so the construction of the Tujia Diaojiao Lou is a major event in the life of Tujia people. First, to prepare a wood, Tujia people call it “of Castle Peak”, is generally used in baseball or gum, because “father”, “purple” is a homonym for “spring”, “sub”, auspicious, mean spring to the sons, Wang; the second step is the processing of beam and column material, Tujia people for the “big”, they in the beam’s gossip, Tai Chi, lotus seed pattern; third processes named “fan”, is the processing of Liang Zhu connected tenon, lined wooden fan; the fourth step is to “LiWu vertical column”, is a very important step. The owner to choose a lucky day, please the neighbors for help, to sacrifice before the beam beam, then they make concerted efforts will be a row of wooden fan is up, then, firecrackers Qiming, next door neighbours send gift. After LiWu Jian column is nail rafter angle, Geva, loading siding. Rich people but also on the roof decoration to the days with engeaved dragons and Phoenix in the corridor under the eaves, hole.

3.3 *Enshi Tujia Diaojiao building decorative features*

Interior decoration of Enshi Tujia Diaojiaolou, mainly in the door, windows, beam, Fang, stigma, Chu, Qin Fang, roof, roof decoration, especially the Diaojiaolou pane decorative art form, is an important symbol to measure the level of construction technology. The other varieties, such as the lattice type, chain type, corrugated, sculptures, thin greasy, content rich and colorful, some status symbol, or pray for good fortune, and some performance of farming, some reflection of life education, some children, some records of customs. Birds and animals, flowers and birds, insects and fish dance competition, myths and legends, true to



Figure 3. Diaojiao building decoration.

life likeness, deliberate deeply. In order to reduce the structural rigidity, monotonous feeling, in the roof, cornice, frieze cover, stigma, pick a variety of beam and column are carved figures, flowers, landscapes, animal, and stories, myths and legends and other contents of the line shape of the pattern (Fig. 3). Greatly enriched the content of Tujia Diaojiao building decoration. And the roof of the decorative as times change shape is also has the very big change, at the beginning of the overlying a piece of tile, simple design, the main emphasis on practicality, medium-term common pattern is

a triangle, a late stage, ridge crest development to a prosperous stage, more added some auspicious, connotation for aspects, such as “Fu”, “Shou” and different shape, but also the emergence of many styles of pattern, observational and uniqueness are strengthened.

4 CONCLUSION

In 2009, in the two He Kou Cun Peng Jia Zhai, was named as the “China historical and cultural village”. Simplicity is also with modern civilization and harmony, people’s life idea, is with the development of the times and constantly changing. Peng people through television, network and go out to work, modern life that should be white ceramic tile, cement and big sofa. Their consciousness, the national characteristics of the old house, has not been able to represent new life now. So, Peng has Diaojiaolou group, also have satellite Tianguo, solar water heater, electric wire pole and thickly dotted line. How to absorb the modern civilization, and let the Pengjia village Diaojiao Lou characteristics to the protection and inheritance, is facing the reputation in outside of the ancient village project.

REFERENCES

- [1] Peng Fei, Gong Xiaofang, Ceng Fanpu, “value evaluation and protection of traditional houses in Western Hubei Tujia Diaojiao building group Pengjia village as an example”, the construction of small towns, 2011 February.
- [2] Li Baihao, Yang Jie, “function, forms and culture of Hubei vernacular architecture”, Buddha in building, 2007.
- [3] Zhou Chuan, “traditional folk art aesthetic characteristics of Western Hubei Tujia”, Journal of Chongqing Jianzhu University, 2008.

The calculation methods of property of the parallel composite isolation system

Hua Yan & Feng Mei Pi

Faculty of Civil Engineering and Architecture, Langfang Teachers University, Langfang, Hebei Province, China

ABSTRACT: This paper mainly studies the calculation methods of property of the parallel composite isolation system. According to the restoring force curve of composite seismic-insolated structure, predominant period, stiffness coefficient, and horizontal earthquake coefficient maximum, making charts, then getting the base shear coefficient of the correspond structure from the charts directly, you can know the earthquake effect on the structures and determine the seismic intensity of composite isolation system on the base of amax.

Keywords: parallel composite isolation the chart base shear coefficient

1 INTRODUCTION

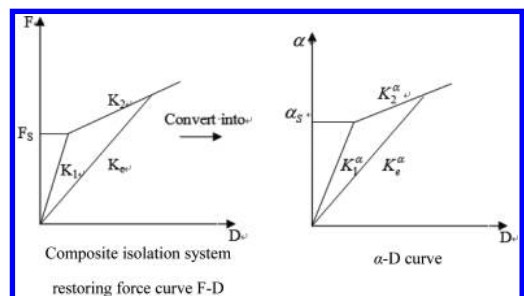
The Parallel Composite Isolator is connected in parallel by Laminated Rubber Bearing and friction-sliding bearing. In the system, Laminated Rubber Bearing provides Centripetal force for the system; friction-sliding bearing hysteretic energy dissipation, which has a good capacity of dissipating energy. The Composite Isolator has the advantages of the above two Composite Isolators, and at the same time it can improve the shortcomings of a single isolation bearings, moreover, it will greatly enhance the earthquake resistant capability of building structure, which is a simple, economic, effective isolation bearing and has a wide application. When using the parallel composite isolator, the gravity load of the superstructure can be undertaken by both Laminated Rubber Bearing and friction-sliding bearing. The remarkable advantages includes that, firstly, decreasing the numbers of the LRB and increasing natural vibration period; secondly, reducing yield shear force and increasing damping; thirdly, reducing the cost.

2 RESEARCH METHOD

As the parallel composite isolation bearing bracket using two different forms, especially after entering the non-linear structure, the seismic response of the structure is not easy to determine, and this study is relatively small home and abroad, so designers can not design a good grasp of the seismic capacity of such a structure, and they can not estimate isolation effect of composite isolation before they start to design, which will bring

big inconvenience to the wide application of this structure. The main contents of this paper are under parallel composite isolation system, based on composite isolation restoring force curve, in the case of the basic parameters of a given shear yielding base isolated structure, making charts, graphs can be directly obtained from the corresponding base shear coefficient structure, from which we can know the earthquake effect that the building suffers from, and determine the Seismic intensity values this Composite isolation system can resist.

3 CONVERSION FROM COMPOSITE ISOLATION EQUIVALENT LINEAR HYSTERESIS CURVE F-D CURVE TO α -D CURVE



F—Composite Isolation System Base Shearing Force
 F_S —Composite Isolation System Yield Shear Force
 D—Displacement of Isolation System

α —Shear Coefficient
 α_s —Yield Shear Force Coefficient
 K_1 —Stiffness of the isolation layer when not slip.
 The stiffness is the sum of Horizontal stiffness rubber bearings and Sliding friction bearing horizontal stiffness
 K_2 —Stiffness of the isolation after isolation layer slip.
 The stiffness is rubber bearings Horizontal stiffness
 K_s —Equivalent Stiffness
 K_1^α —Stiffness of the isolation layer when not slip after conversion
 K_s^α —Isolation layer slip stiffness after conversion
 K_c^α —Equivalent stiffness after conversion.

4 MATLAB IMPLEMENTATION PROCESS

```

%x is friction pressure ratio
%as is yield shear coefficient
%u is silp bearing frictian coefficient
%Ds is isolation layer yield displacement
%K1a is first stiffness of laminated rubber bearing under  $\alpha$ -D coordinate
%B is equal to the ratio of the first stiffness and second stiffness
%K2a is the second stiffness of laminated rubber bearing under  $\alpha$ -D coordinate
%T is site predominant period
%D is isolating system displacement
%Kea is equivalent stiffness under  $\alpha$ -D coordinate
%Te is equivalent self vibration period
%E is equivalent damping ratio
%a is structure base shear coefficient
%N1 is slope adjustment coefficient in plummeted area
%r is attenuation index when the curve deline
%N2 is damping adjustment coefficient
%amax is maximum earthquake effect coefficient

x = 0.3,u = 0.1,Ds = 10,B = 0.25,T = 0.65;
as = x*u;
K1a = as/Ds;
K2a = B*K1a;
D = [];Kea = [];Te = [];E = [];a = [];N1 = [];r = [];N2 = [];amax = [];
for i = 2:500
    D(i) = 0;
    D(i) = D(i-1)+1;
if D(i) <= Ds
    Kea(i) = as/Ds;
    else Kea(i) = (as+K2a*(D(i)-Ds))/D(i);
    end
    Te(i) = 2*(1/(Kea(i)*10e+2))^(1/2);
    E(i) = 2/pi*as*(D(i)-Ds)/(D(i)^2*Kea(i));
    if E(i) <= 0.05
        E(i) = 0.05;
    else E(i) = 2/pi*as*(D(i)-Ds)/(D(i)^2*Kea(i));
    end
  
```

```

a(i) = Kea(i)*D(i);
N1(i) = 0.02+(0.05-E(i))/8;
if N1(i) < 0
    N1(i) = 0;
else N1(i) = 0.02+(0.05-E(i))/8;
end;N1(i);
r(i) = 0.9+(0.05-E(i))/(0.5+5*E(i));
N2(i) = 1+(0.05-E(i))/(0.06+1.7*E(i));
if N2(i) < 0.55
    N2(i) = 0.55;
else N2(i) = 1+(0.05-E(i))/(0.06+1.7*E(i));
end;N2(i);
if Te(i) <= 0.1
    amax(i) = a(i)/(10*(N2-0.45)*Te(i)+0.45);
elseif Te(i) > 0.1 & Te(i) < T
    amax(i) = a(i)/N2(i);
elseif Te(i) >= T & Te(i) < 5*T
    amax(i) = a(i)/((T/Te(i))^r(i)*N2(i));
elseif Te(i) >= 5*T
    amax(i) = a(i)/(N2(i)*0.2^r(i)-N1(i)*(Te(i)-5*T));
end;
plot3(D(i),a(i),amax(i));
grid on;
hold on;
fprintf('as(%f),Ds(%f),K1a(%f),B(%f),K2a(%f),D(%f),Kea(%f),Te(%f),E(%f),a(%f),N1(%f),r(%f),N2(%f),T(%f)=%f.\n',as,Ds,K1a,B,K2a,D(i),Kea(i),Te(i),E(i),a(i),N1(i),r(i),N2(i),T,amax(i));
end.
  
```

5 APPLICATION

For determined parallel Composite Isolation, we know the parameters of each bearing condition, according to these parameters; we can get base shear coefficient corresponding structure from the chart directly. And you can know the Seismic structure suffered from the earthquake and you can determine seismic intensity that a composite isolation system can resist according to α_{\max} .

An office building whose total weight is 24,500 tons, using parallel Composite Isolation. The Parallel composite isolation is composed of general laminated rubber isolator and friction-sliding bearings. Its coefficient of friction $\mu = 0.1$, $\lambda = 0.2$, yield displacement of the isolation $D_s = 10$ mm. Design earthquake grouping II, II sites $T_g = 0.4$ s, $k_2 = 96722$ N/mm, $k_1 = F_s/D_s$. Check the seismic intensity the structure can resist.

$$\text{By } K_1 = \frac{F_s}{D_s} = \frac{\alpha_s * G}{10} = \frac{\lambda * \mu * G}{10} = 490000 \text{ N/mm}$$

$$\text{By the formula (3-4) } \beta = \frac{K_2}{K_1} = 0.2$$

By the formula (3-2) $K_1^\alpha = \frac{K_1}{G} = \frac{\lambda^* \mu^* G}{G^* D_s} = 0.002$

And $\lambda = 0.2$, $\mu = 0.1$, $T_g = 0.4$, $D_s = 10$ mm.

Corresponding table is when $\lambda = 0.2$, $\mu = 0.1$, $K_{\alpha}^1 = 0.002$, $\beta = 0.2$, $T_g = 0.4$, $D_s = 10$ mm:

D (mm)	K_{α}^c	α	T_{eq}	ξ	α_{max}
1	0.001	0.001	2.00	0.05	0.0426
10	0.002	0.02	1.414	0.05	0.0623
20	0.0012	0.024	1.826	0.2653	0.1360
30	0.000933	0.028	2.070	0.3032	0.1739
40	0.000800	0.032	2.236	0.2984	0.1983
50	0.000720	0.036	2.357	0.2829	0.2213
60	0.000667	0.040	2.449	0.2653	0.2434
70	0.000629	0.044	2.523	0.2480	0.2648
80	0.000600	0.048	2.582	0.2321	0.2857
90	0.000578	0.052	2.631	0.2176	0.3061
100	0.000560	0.056	2.673	0.2046	0.3269
110	0.000545	0.060	2.708	0.1929	0.3486
120	0.000533	0.064	2.739	0.1824	0.3701
130	0.000523	0.068	2.765	0.1728	0.3914
140	0.000514	0.072	2.789	0.1642	0.4125
150	0.000507	0.076	2.810	0.1564	0.4333
160	0.000500	0.080	2.828	0.1492	0.4538
170	0.000494	0.084	2.845	0.1427	0.4741
180	0.000489	0.088	2.860	0.1366	0.4942
190	0.000484	0.092	2.874	0.1311	0.5140
200	0.000480	0.096	2.887	0.1260	0.5336
210	0.000476	0.100	2.898	0.1213	0.5529
220	0.000473	0.104	2.909	0.1169	0.5721
230	0.000470	0.108	2.919	0.1128	0.5910
240	0.000467	0.112	2.928	0.1089	0.6097
250	0.000464	0.116	2.936	0.1054	0.6282
260	0.000462	0.120	2.944	0.1020	0.6465
270	0.000459	0.124	2.951	0.0989	0.6646
280	0.000457	0.128	2.958	0.0959	0.6826
290	0.000455	0.132	2.964	0.0931	0.7004
300	0.000453	0.136	2.970	0.0905	0.7180
310	0.000452	0.140	2.976	0.0880	0.7354
320	0.000450	0.144	2.981	0.0857	0.7527
330	0.000448	0.148	2.986	0.0834	0.7698
340	0.000447	0.152	2.991	0.0813	0.7868
350	0.000446	0.156	2.996	0.0793	0.8037

When the laminated rubber fabricated using a rubber pad having a diameter of 400 mm, the shear deformation of 50%, i.e., displacement of the isolation layer is 200 mm, the coefficient corresponding to the isolation layer is about 0.1 Shear, Maximum of seismic influence coefficient is 0.53, Seismic intensity of 7 degrees is a rare case.

REFERENCES

- [1] Xue Suduo, Zhouqian. SMA—The design and performance of rubber bearing isolation [J]. Beijing: World Earthquake Engineering, 2003, 19(4):34–38.
- [2] Fanjian, Tang Jiayang. Earthquake response analysis of sliding structure [J]. Earthquake Engineering, 2001(3):27–31.
- [3] Yang Shubiao. Research on isolation performance of masonry parallel composite isolation system [J]. Industrial Construction, 2000, 30(12): 15–17.
- [4] Yang Shubiao. Simplified calculation of Composite isolation seismic response [J]. World Earthquake Engineering, 2001, 17(2): 65–69.

Gas-pressure sintered Si_3N_4 fabricated by ceramics injection molding

Xian Feng Yang, Jiang Hong Yang, Xie Wen Xu, Ming Ming Wang

College of Physics and Electronics Science, Changsha University of Science and Technology, Changsha, P.R. China

Zhi Peng Xie

State Key Laboratory of New Ceramics and Fine Processing, College of Materials Science, Tsinghua University, Beijing, P.R. China

ABSTRACT: Ceramic injection molding technique was applied in preparing the gas-pressure sintered Si_3N_4 . In this study, flowability of the feedstock, debinding rate, and microstructure of evolution during production were explored. The results showed that when the solid loading was lower than 50% and surfactants addition was up to 6%, the flowability was fit for injection molding. The dedinding process was mainly controlled by debinding temperature and time. When the debinding temperature was 40°C and debinding time reached 4 hours, about 35% wax was solvent debinded and the thermal debinding could be carried out. The mechanical properties was excellent and the hardness reached 1650 GPa, and fracture toughness $7.2 \text{ MPa} \cdot \text{m}^{1/2}$.

Keywords: ceramics injection molding; Si_3N_4 ceramic; gas-pressure sintered

1 INTRODUCTION

Silicon nitride ceramics has been widely applied in the fields of bearing, turbines of engine and parts for high temperature. Compared with the other kinds of oxide ceramics like alumina and zirconia ceramics, Si_3N_4 ceramics showed lower thermal expansion coefficient, higher strength retain at higher temperature, perfect corrosion resistance and lower density^[1]. Several kinds of silicon nitride ceramics including pressureless sintered, gas pressure sintered and reaction bonded sintered existed in the engineering field, in which gas pressure sintered Si_3N_4 showed best mechanical properties^[2].

In the production of Si_3N_4 ceramics, molding technique was one of the processing steps determining the production costs. Compared with the traditional molding techniques like slip casting, cold isostatic pressing and dry pressing, ceramics injection molding showed the advantages of high efficiency, high surface quality and dimension accuracy. So the combination of ceramic injection molding and gas pressure sintered techniques was preferred for the high performance and lower manufacturing costs^[3].

Although ceramic injection molding has been successfully used in oxide ceramics production, it has not been widespread in silicon nitride. The prime cause lied in the difficulties in the preparing of low viscosity and higher solid load feedstock,

especially for the sub-micron Si_3N_4 powder. The fundamental research on debinding rate, control of debinding defects and microstructure evolve during debinding was lack^[4].

In this study, the feedstock with good flowability was prepared. The relationship between debinding rate and debinding time was explored. The microstructure evolution during production and mechanical properties of sintered ceramics were characterized.

2 EXPERIMENTS AND CHARACTERIZATION

The silicon nitride ceramic powder used in this study with median diameter (d_{50}) of $0.34 \mu\text{m}$ was prepared in the labotary. Polypropylene (PP), Polyethylene (PE), wax (PP:PE:Wax = 10:10:80) was used as the organic binder for the feedstock. Additionally, Stearic ic acid (SA, Shantou Xilong Chemical Factory, China) was used as surfactant.

The feedstock was prepared by mixing Si_3N_4 powder with organic binder on the double roller at 165°C for 1 hour. Then the feedstock was crushed into particles smaller than 3 mm. Balls with diameters of 13 mm were prepared on the injection molding machine (JPH30, Hengli Plastic Machinery CO., Ltd, China). Injection temperature was 155°C -175°C -185°C -190°C from inlet to nozzle.

These balls were used for solvent debinding, thermal debinding and gas pressure sintering. The solvent debinded body was thermal debinded in vacuum furnace to 900°C, and then sintered in gas pressure sintering furnace to 1795°C for 3 hours with N₂ pressure of 8 MPa.

Injection molded samples were immersed in the kerosene at the constant temperature. Five samples were tested to get the mean value of the fraction of binder removed at different debinding time. The fraction of binder removed was calculated by equation (1):

$$W = \frac{m_i - m_d}{m_i \times v} \quad (1)$$

where W is the fraction of binder removed; m_i and m_d is the weight of initial green body and dried debinded samples. v is the initial weight fraction of water soluble binder in the injection molded sample. It was assumed that wax did not evaporate or degradation in mixing and injection molding. The debinded samples were dried at 40°C for 48 hours. The weight of the sample was tested by electronic balance with accuracy of 0.1 mg. The microstructure of the green body was observed by scanning electronic microscope (LEO 1530, Germany). The rheological behavior of the mixtures was characterized with a capillary rheometry (Instron model 3211, England).

3 RESULTS AND DISCUSSION

3.1 Effect of solid loading and stearic acid on the rheological properties of the feedstock

Figure 1 shows the shear viscosity of the feedstock with different solid loading. When the solid loading

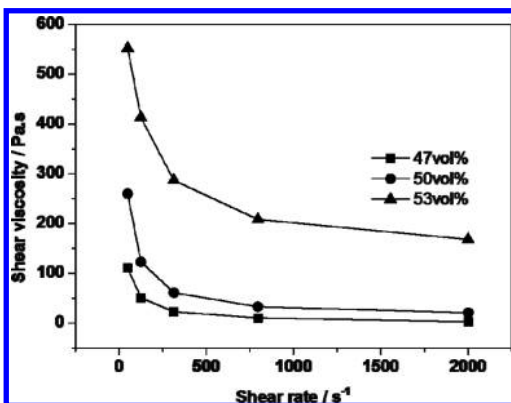


Figure 1. Shear viscosity of the feedstock with different solid loading.

was lower than 50%, the shear viscosity was lower than 100 Pa.s when the shear rate was 1000 s⁻¹, which means that the feedstock was fit for injection molding. When the solid loading was up to 53%, the flowability of the feedstock was dramatically decreased, and the defects will be not avoided during injection molding^[5].

Figure 2 shows the influence of stearic acid on the rheology of the feedstock. It was shown that when the addition of stearic acid was reduced to 2%, the shear viscosity increased obviously. For the ultra fine silicon nitride powder, stearic acid played the role of modifying the compatibility between organic binder and powder surface. Enough surfactant was beneficial for reducing the particle agglomeration, which means the lower viscosity could be obtained at higher solid loading. While feedstock with less surfactants will lead to the deteriorated flowability and inhomogeneous in the binder and powder distribution, which will eventually result in defects during dedinding and sintering^[6].

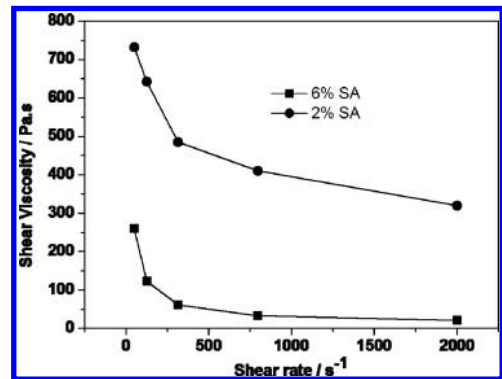


Figure 2. Influence of stearic acid on the rheology of the feed stock (solid loading = 50%).

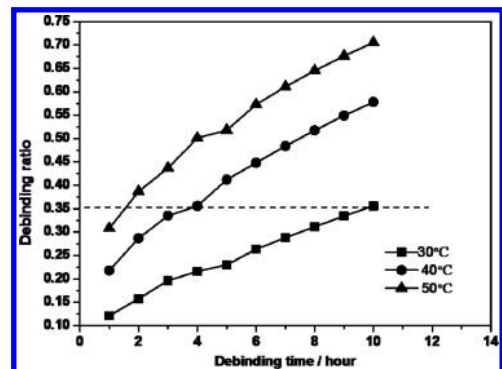


Figure 3. Debinding ratio at different debinding time and temperature.

3.2 Effects of temperature on the debinding ratio

Figure 3 shows the debinding ratio at different debinding time and temperature. It was shown that higher debinding temperature was helpful to

increase the debinding rate. It was because that the debinding mechanism was the diffusion of wax in the debinding medium. High temperature could promote the molecular vibration and the debinding coefficient was increased. According to the related debinding dynamic analysis, the debinding process was controlled by the dissolution of the wax at the debinding interface in the first stage. With the debinding depth's increasing, the controlling step was transferred to the diffusion of wax in the connected pores in the debinded outer layer. On the other hand, longer enough debinding time was necessary because the next thermal debinding could only be carried out when enough wax was solvent debinded for the connection of connected pore nets in the green body. It was pointed out that connected pore nets could be formed when more than 35% wax was debinded during solvent debinding (shown by the line in the Fig. 3)^[7].

3.3 Microstructure evolution and mechanical properties

Figure 4 shows the microstructure evolution during the injecting molding, solvent debinding, thermal debinding and sintering. It was shown that the Si_3N_4 powder was coated by the organic binder and no pores appeared on the fracture surface, and several kinds of organic binders melted and blended together and could not be identified (Fig. 4a). While the fiber like binder composition was observed on the fracture surface of the solvent debinded body, which was the residual polymer binder. And most wax was dissolved during solvent debinding. After thermal debinding, the residual polymer binder degraded and evaporated from the brown body, and only the Si_3N_4 particles were left. After gas pressure sintering, densification was finished and the typical needle-like Si_3N_4 grains were observed.

Table 1 showed that the density of the sintered body was 3.2 g/cm^3 , and hardness 1650 GPa ,

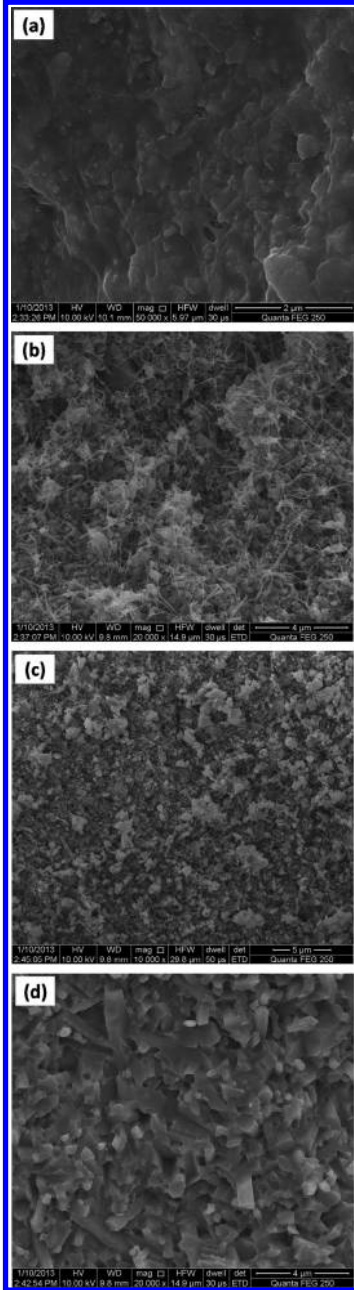


Figure 4. SEM photograph of green body (a), solvent debinded body (b), brown body (c) and sintered part (d).

Table 1. Properties of the ceramic body during debinding and sintering.

	Density (g/cm^3)	Shrinkage (%)	Hardness (HV, GPa)	Fracture toughness ($\text{MPa}\cdot\text{m}^{1/2}$)
Green body	–	–	–	–
Solvent debinded body	1.73	0	–	–
Brown body	1.69	10.4	–	–
Sintered body	3.23	20.5	1650	7.2

Fracture toughness $7.2 \text{ MPa} \cdot \text{m}^{1/2}$, which could be fit for Si_3N_4 ceramic bearings and other advanced structure parts. The entirely shrinkage from green body to sintered body was 20.5%.

4 SUMMARY

Si_3N_4 ceramics was fabricated by ceramic injection molding. When the solid loading was lower than 50% and surfactants addition was up to 6%, the flowability was good for injection molding. The dedinding process was mainly controlled by debinding temperature and debinding time. When the debinding temperature was 40°C and debinding time reached 4 hours, about 35% wax was solvent debinded and the thermal debinding could be carried out. The mechanical properties was excellent and the hardness reached 1650 GPa, and fracture toughness $7.2 \text{ MPa} \cdot \text{m}^{1/2}$.

ACKNOWLEDGEMENT

This work was financially supported by the National Nature Science Foundation of China (NSFC 51102024).

REFERENCES

- [1] Longjie Zhoua, Yong Huang, Zhipeng Xie, et al. Preparation of Si_3N_4 ceramics with high strength and high reliability via a processing strategy, *Journal of the European Ceramic Society*, 22(2002)1347–1355.
- [2] M.H. Bocanegra Bernal, B. Matovic, Mechanical properties of silicon nitride-based ceramics and its use in structural applications at high temperatures, *Materials Science and Engineering A*, 527(2010) 1314–1338.
- [3] M.H. Bocanegra-Bernal, B. Matovic, Dense and near-net-shape fabrication of Si_3N_4 ceramics, *Materials Science and Engineering A*, 500(2009)130–149.
- [4] A.J. Millan, M.I. Nieto, R. Moreno, Aqueous injection moulding of silicon nitride, *Journal of the European Ceramic Society*, 20(2000)2661–2666.
- [5] Mutsuddy B.C. Influence of powder characteristics on rheology of ceramic injectionmolding mixtures. *Proceedings of the British Ceramic Society*, 33(1983)117–137.
- [6] Song J.H and Evans J.R.G. The effect of undispersed agglomerates on the relative viscosity of ceramic molding suspensions. *Journal of Materials Science Letter*, 13(1994)1642–1644.
- [7] Xianfeng Yang, Zhipeng Xie, Guanwei Liu and Yong Huang. Dynamics of water debinding in ceramic injection molding. *Advances in Applied Ceramics*, 108(2009)295–300.

Green SCC design algorithm and its performance

C.L. Hwang, Y. Risdianto, C.T. Chen, M.G. Tesfamariam, H.T. Phuoc & A.H. Limongan
National Taiwan University of Science and Technology, Taipei, Taiwan, P.R. China

B.L.A. Tuan
Cantho University, Cantho, Vietnam

ABSTRACT: Self-Consolidating Concrete (SCC) is a mixture that can be compacted into every corner of formwork without vibrating compaction. The method for achieving self-consolidating involves not only deformability of mortar, but also resistance to segregation between coarse aggregate and mortar when the fresh concrete flows through reinforcing bars. Many projects have been done using SCC with Densified Mixture Design Algorithm (DMDA) method in Taiwan. In this study, the method can create high density with low water and cement content to achieve the high cement strength efficiency. The stability can be controlled when the water cement content ratio is higher than 0.42, water content is around 160 kg/m³ and cement content is less than $f^{\prime}c/20$ by using Rice Husk Ash (RHA). And then the physical density, flowability, and homogeneity can be achieved. Fresh properties of concrete in this study shows excellent flowability and passing ability without bleeding or segregation. In 28 days after casting, the compressive strength and splitting tensile concretes shows good result, this indicate that the SCC had good strength performance.

Keywords: self-consolidating concrete; densified mixture design algorithm; fresh properties; strength performance

1 INTRODUCTION

Self-Consolidating Concrete (SCC), a new kind of concrete with excellent deformability and segregation resistance, was first developed in Japan 1986. It is special type of concrete that can be consolidated into the heavily reinforced structures and fill the corner of formworks without requiring any internal or external mechanical vibration and compaction during the placing process [Gesoglu, 2012; Guneyisi, 2013].

In recent years many researchers have established SCC by using Supplementary Cementitious Materials (SCM) like: fly ash, blast furnace slag, rice husk ash, etc. The SCM can improve the various properties in fresh and hardened state of concrete. SCC in general contains a large amount of powder materials, a superplasticizer and/or viscosity modifying admixtures. High powder content is often supplemented by mineral admixtures that could increase the slump of concrete mixture without increasing its cost. The use of Fly Ash (FA) and Rice Husk Ash (RHA) in this study also reduces the demand for cement, fine fillers and sand which are required in SCC [Khurana, 2001]. Furthermore, there are several advantages to using SCC, such as maintaining and improving durability

properties, environmental benefits related to the disposal of waste materials and reducing carbon dioxide emissions. Up to now, little research has been taken to investigate the use of RHA and FA as supplementary material in Vietnam and Taiwan. For example, in 2005 Bui et al. published a paper in which they burnt Vietnam RHA in an incinerator for RHA production and studied the particle size effect on the strength of RHA blended gap-graded Portland cement concrete [Hwang, 2011].

2 EXPERIMENTAL WORK

2.1 Materials

Crushed coarse aggregate (12.5 mm maximum size, density 2.5–2.7 and absorption capacity < 3%) and natural sand (modulus of fineness 2.7–3.2, density 2.5–2.7 and absorption capacity < 3%) were provided from local quarries. ASTM C150 type I cement from Taiwan Cement Company, ASTM C618 class F fly ash from Taiwan Power Plant, and RHA collected from Saigon Ve Wong Co., Ltd., Ho Chi Minh city, Vietnam were used as binders in this research. The mixing water was local tap water. Type-G superplasticizer, having 43% solid content with specific gravity

of 1.18, was used to achieve the desired workability for all concrete mixtures. All materials conform to the related ASTM standards.

2.2 Procedures of the proposed mixture design

DMDA was developed by Professor Hwang and has been successfully applied to many projects in Taiwan, including its use in the construction of Taipei 101, the world's tallest building [Tu, 2006]. The major difference from other mixture design algorithms is that instead of partial replacement of cement, DMDA incorporating fly ash is used to fill the void of aggregates and hence increase the density of the aggregate system. The purpose of such action is to reduce the cement paste content for design properties such as workability, strength, and durability. As a result, besides physically acting as filler, fly ash and rice husk ash act chemically as pozzolanic material.

The weight ratio α_{\max} of blended fly ash and sand can be expressed as the Equation 1:

$$\alpha_{\max} = \frac{W_F}{(W_F + W_S)} \quad (1)$$

where W_F and W_S = the weight of fly ash and sand, kilograms per cubic meter, respectively. Then, the blended fly ash and sand mixture at a fixed ratio of α_{\max} is used to fill the void within coarse aggregates. Using a similar filling process, the maximum dry, loose density of blended aggregates can be obtained from the plot of blended fly ash/sand mixture and coarse aggregate. The weight ratio β_{\max} at the maximum dry, loose density can be expressed as the Equation 2:

$$\beta_{\max} = \frac{(W_F + W_S)}{(W_F + W_S + W_A)} \quad (2)$$

where W_A = the weight of coarse aggregate, kilograms per cubic meter. At the point of maximum density, the aggregate structure of fly ash, sand and coarse aggregate is assumed to be completely packed using the hand-dry rodding method in accordance with the ASTM C29 standard. From this, the void (V_v) among aggregates can be calculated and the minimum cement paste (V_p) can be estimated as Equation 3. When considering the V_p for real concrete production, it is necessary to multiply a coefficient (N) to account for a lubricated layer ($V_L = S \cdot t$) on the surface of the aggregate (S) in order to achieve the workability of concrete.

$$V_p = V_v + S \cdot t = N \cdot V_v = N \cdot (1 - (W/\gamma)) \quad (3)$$

where S = the surface area of aggregates, square meter; t = the thickness of lubricating paste on the

surface of aggregate, micrometer; V_v = the smallest void among aggregates, cubic meter; W_i = the weight of aggregate, kilogram per cubic meter; and γ_i = the density of aggregate, kilogram per cubic meter. Due to the difficulty in measuring $S \cdot t$, it is suggested for convenience's sake that various $N \cdot V_v$ coefficients be tested to obtain the required workability, in this study $N = 1.3$. Thus the w/b ratio is calculated as following:

$$w/b = \frac{W + SP}{C + W_F + W_{RHA}} \quad (4)$$

where S = superplasticizer, kilogram per cubic meter; C = cement content, kilogram per cubic meter; W_{RHA} = rice husk ash content, kilogram per cubic meter; and W_F = fly ash content, kilogram per cubic meter. The amount of RHA in Equation 4 is around 11% of the weight of cement. The dosage of SP was determined through previous experience and the workability of the concrete from a trial batch. The result of each concrete mixture is shown in Table 1 on sample code D3513.

Another sample (sample code A3500) was designed and prepared according to ACI method in order to compare and see the difference. The ACI 211.1 standard practice for normal weight concrete mix proportion design was used.

2.3 Testing programs

Concrete was made with natural coarse and fine aggregate. Water-to-binder ratio (w/b) 0.35 was chosen to test effect on the properties of concrete. Concrete was mixed in a laboratory pan mixer. Firstly, Portland cement, FA, and RHA were mixed with water followed by the addition of the natural sand. Finally, superplasticizer (SP) was added to control slump of fresh concrete.

The unit weight and slump test results shown in Table 2. Slump and slump flow spread of fresh state were controlled to meet the high flowing concrete requirement of 255–265 mm and 700 mm, respectively. The passing ability test of fresh concrete of this study was done by J-ring test based on the European standard as a guideline. J-ring test, an extension of the slump flow test, is used to measure flow spread and passing ability. The test

Table 1. Mixture proportion of SCC.

Sample code	Mixture proportion (kg/m ³)						
	Cement	RHA	FA	Water	SP	Sand	Stone
A3500	457	–	–	160	3.5	923	829
D3513	227	25	215	164	5.8	1009	731

Table 2. Flowability test.

Sample code	Unit weight (kg/m ³)	Slump test			T ₅₀ (sec)
		Slump (mm)	Slump flow (mm)	Flow time (sec)	
A3500	2361	255	700	35	5
D3513	2339	265	700	35	5

Table 3. Passing ability and viscosity tests.

Sample code	V-funnel (sec)	J-ring test		
		Passing ability (mm)	Flow spread (mm)	T _{50j} (sec)
A3500	9	13	520	8
D3513	11	5	695	6

result shown in Table 3 indicates the passing ability of concrete ranged from 520 mm to 695 mm. The result of J-ring T_{50j} also confirms the same conclusion as the slump flow test of T₅₀ (viscosity).

The concrete cylinders with dimension of 100 mm in diameter and 200 mm in height were used for the compressive strength. The specimens were cured in saturated limewater at temperature 28±2 °C. The compressive strength test was done according to ASTM C39.

3 RESULTS AND DISCUSSION

3.1 Compressive strength test

Compressive strength, one of the most important mechanical properties of concrete, reflects the overall performance and is a major indicator of general quality control of hardened concrete through service life of the structure. Factors influencing the strength of concrete are the types and quality of materials, the mixture proportion, the construction methods, the curing condition, and the test method.

The result of compressive strength is shown in Figure 1. At 28 days compressive strength of D3513 concrete was 37.5% and the 56 days compressive strength was 22.7% lower than A3500 concrete specimen because A3500 contain 201.3% cement higher than D3513.

3.2 Splitting tensile strength test

Splitting tensile test may explain the mechanical behaviour especially on the brittleness of concrete.

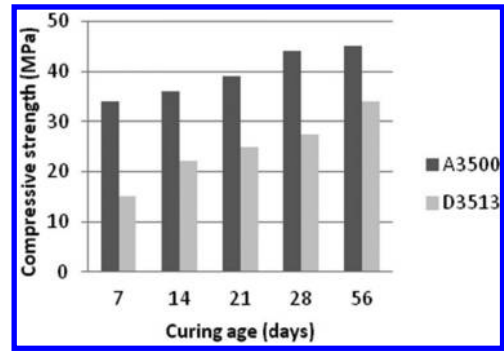


Figure 1. Compressive strength test values of SCC.

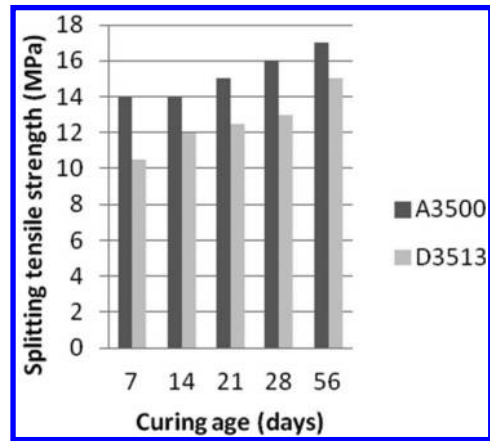


Figure 2. Splitting tensile strength test values of SCC.

Figure 2 show the splitting tensile strength of two specimens, concrete D3513 to be more brittle than A3500 concrete. For normal weight concrete, the aggregate is generally stronger than the matrix. When concrete is subjected to a tensile stress, cracks will typically propagate in the matrix or along the-matrix-aggregate interface. In addition, propagating cracks may be counteracted by aggregate particles, resulting in the meandering and branching of cracks. For D3513 concrete, however, the crack propagation will more typically go through the interface of aggregate and thus cause a more abrupt collapse of the concrete. This may explain why lighter weight is more brittle than heavier weight of concrete [Zhang, 1991].

4 CONCLUSIONS

DMDA method can create the optimum physical density of concrete. By having the optimum packing

density, concrete can present the high cement efficiency and compressive strength and its support towards the green concrete. As a SCC, DMDA concrete in this study demonstrate the excellent flowability without bleeding and segregation.

REFERENCES

- Gesoglu, M., et al. 2012. Recycling ground granulated blast furnace slag as cold bonded artificial aggregate partially used in self-compacting concrete. *Journal of hazardous materials*: 352–358.
- Guneyisi, E.; Gesoglu, M.; Algin, Z. 2013. Performance of self-compacting concrete (SCC) with high-volume supplementary cementitious materials (SCMs). *Eco-Efficient Concrete*: 198–217.
- Hwang, C.L.; Bui, B.L.A.; Chen, C.T. 2011. Effect of rice husk ash on the strength and durability characteristics of concrete. *Construction and building materials* (25): 3768–3772.
- Hwang, C.L.; Hung, M.F. 2005. Durability design and performance of self-consolidating lightweight concrete. *Construction and building materials* (19): 619–626.
- Khurana, R. & Saccone, R. 2001. Fly ash in self-compacting concrete, fly ash, silica fume, slag and natural pozzolan in concrete. In Malhotra V.M. (ed.), *ACI SP-199*: 259–274.
- Tu, T.Y.; Chen, Y.Y.; Hwang, C.L. 2006. Properties of recycled aggregates. *Cement and concrete research* (36): 943–950.
- Zhang, M.H. & Gjorv, O.E. 1991. Mechanical properties of high-strength lightweight concrete. *ACI materials journal*: 240–247.

Free and forced vibration of rectangular plates using the finite difference method

Yousef S. Al Rjoub & Osama Abdeljaber

Civil Engineering Department, Jordan University of Science and Technology, Irbid, Jordan

ABSTRACT: This paper presents a finite difference method to solve free and forced vibration problems of rectangular plates with differing boundary conditions. The natural frequencies are obtained from the peaks of the free vibration response in the frequency domain by exciting the plate with an initial displacement. The free vibration response in the time domain is calculated using the finite difference method. This is then converted to the frequency domain using Fourier transform. In this paper, the plate is subjected to various dynamic loadings, namely, a step function, rectangular and triangular loads, and a sinusoidal harmonic loading. The present results are compared to analytical and numerical solutions available in the literature. The results obtained are in good agreement with those of exact and numerical results available in the literature.

Keywords: dynamic loadings; finite difference method; natural frequency; plate

1 INTRODUCTION

Plate elements are being used increasingly in various fields of engineering, especially in aerospace, mechanical, civil, and hydraulic structures. The analysis of free and forced vibration of rectangular plates is highly significant in the performance of such structures. As a result, much research has been conducted to determine the dynamic plate behavior. Leissa [1, 2] presents comprehensive and accurate analytical results of the free vibration of rectangular plates with differing boundary conditions. Twenty-two cases are considered, based on the possible combinations of clamped, simply-supported, and free-edge conditions. An exact solution is obtained for six cases having two opposite sides simply-supported. The remaining 15 cases are analyzed using the Ritz method, with 36 terms containing the products of beam functions. An approximate solution for the free vibration of rectangular plates using the Rayleigh-Ritz method has been obtained by several researchers [3–9]. Other researchers [10–12] used a finite element method. Eftehari and Jafari [13] presented a combined application of the Ritz and Differential Quadrature (DQ) methods to solve the free and forced vibration of rectangular plates with differing boundary conditions. Yang, et al. [14] used the finite difference method to obtain the complex natural frequencies for linear free vibration, bifurcation, and chaos for forced nonlinear vibration of an axially moving plate. Gupta, et al. [15] presented the forced vibration of a non-homogeneous simply-supported-free-simply-supported-

free rectangular plate of variable thickness. An approximate formula is obtained to estimate the maximum deflection of a rectangular plate subject to uniform harmonic loading. Wang and Xu [16] used Discrete Singular Convolution (DSC) to analyze the free vibration of beams, annular plates, and rectangular plates with free boundary edges. This method is examined using eight examples of free vibration of beams, annular plates, and rectangular plates with differing boundary conditions. Ducechi, et al. [17] used the Von Karman equations to analyze the nonlinear vibration of thin rectangular plates. The eigenmodes of a fully clamped plate are calculated based on a fast converging solution strategy. The nonlinear dynamic of the first two modes, both in the free and forced regimes, is taken into consideration. A closed form solution of the natural frequencies and the corresponding mode shapes of thin plates with any type of boundary condition is obtained by Xing and Liu [18], using a dual method. A closed form solution for the free vibrations of rectangular Mindlin plates with any boundary condition is proposed by Xing and Liu [19], using a new two-eigenfunctions theory. The proposed theory is obtained by reformulating the three classical eigenvalue differential equations of a Mindlin plate. Then, separation of variables is used to solve the two differential equations, which are identical to those of Kirchhoff plate theory, [20]. Werfalli and Karoud [21] studied the free vibration of thin, isotropic rectangular plates with various edge conditions using a Galerkin-based finite element method. A closed form solution for the free

vibration of rectangular thin plates with three edge conditions, namely fully simply-supported, fully clamped, and two opposite edges simply supported and the other two edges clamped, is obtained by Wu, et al. [22], using Bessel functions. Njoku, et al. [23] used the peculiar shape functions of the Taylor series, along with Galerkin's method, to determine the natural frequencies of a fully clamped, isotropic, thin rectangular plate. An analytical solution of the free vibration of a completely simply supported rectangular Kirchhoff plate is obtained by Bahrami, et al. [24], using a wave propagation approach. Jain, et al. [25] studied the free vibration of rectangular plates having parabolically varying thickness, with two simply-supported parallel edge conditions, based on the classical theory of plates. The Frobenius method is used to solve the equation of motion. As a result of the product of an infinite series and a function satisfying the boundary conditions at two simply supported parallel edges, the deflection of the plate is obtained accordingly. Numayr, et al. [26] used the finite difference method to solve the free vibration of composite plates with differing boundary conditions. In their study, the effects of shear deformation and rotary inertia are included. Yeh, et al. [27] analyzed the free vibrations of clamped and simply-supported rectangular thin plates using the finite difference and differential transformation methods. The order of the differential transformation, the number of sub-domain spaces, the variable conditions, and the type of initial condition are used as investigative parameters.

It is clear from the previously outlined literature that the dynamic behavior of rectangular plate subjected to impact loading is very important. In this paper, an attempt to understand the dynamic behavior of rectangular plates with differing boundary conditions using the finite difference method to perform dynamic analysis is made. In this paper, Fourier transform is used to convert the free vibration response from the time domain, obtained by the finite difference method, to the frequency domain, thereby obtaining the natural frequencies. In the forced vibration case, the rectangular plate is subjected to various impact loadings, such as, constant force, rectangular, triangular, and sinusoidal harmonic. The natural frequencies are obtained for plates with differing boundary conditions and are compared to exact and numerical results available in the literature. The dynamic response in the forced vibration regime is studied.

2 MATHEMATICAL MODEL OF A PLATE

Consider an isotropic, elastic, rectangular Kirchhoff plate of thickness h , lengths a and b in

the x - and y -directions, respectively, as shown in Figure 1. The plate has mass density ρ , Young's modulus E , Poisson's ratio ν , and flexural rigidity $D = Eh^3/12(1-\nu^2)$. The differential equation of motion for forced vibration is given by [20] as:

$$D \left[\frac{\partial^4 w(x,y,t)}{\partial x^4} + 2 \frac{\partial^4 w(x,y,t)}{\partial x^2 \partial y^2} + \frac{\partial^4 w(x,y,t)}{\partial y^4} \right] + \rho h \frac{\partial^2 w(x,y,t)}{\partial t^2} = p(x,y,t) \quad (1)$$

where $w(x,y,t)$, and $p(x,y,t)$ are the transverse deflection of the plate and the dynamic loadings applied, respectively.

Four types of dynamic loadings are considered, namely, a step function of infinite duration, a rectangular load of finite ($t_d = 0.1$ sec) duration, a triangular load of finite ($t_d = 0.1$ sec) duration, and a sinusoidal harmonic loading of finite duration ($t_d = 0.1$ sec), Figure 2.

In this study, a plate with six different boundary conditions are considered, namely, SSSS, SCSS, SCSC, CCCC, CCCS, and CCSS, where S refer to a simply-supported edge and C to clamped edge.

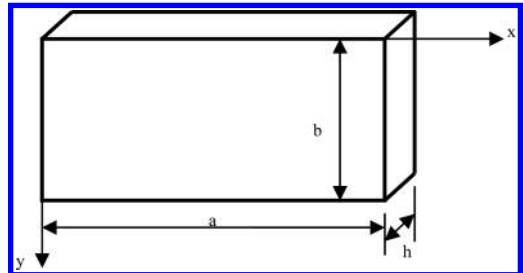


Figure 1. Thin rectangular plate geometry and coordinate system.

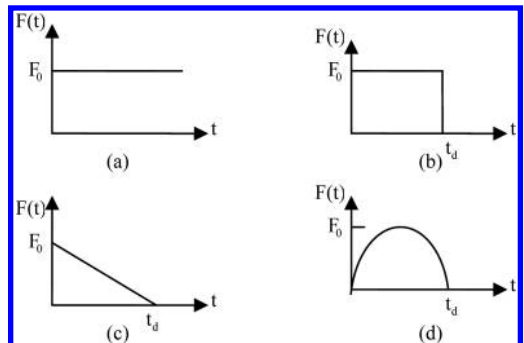


Figure 2. Dynamic loading functions (a) constant, (b) rectangular, (c) triangular, (d) sinusoidal.

The boundary conditions for simply-supported edge can be written as,

$$w(x,y,t) = \frac{\partial^2 w(x,y,t)}{\partial x^2} + \nu \frac{\partial^2 w(x,y,t)}{\partial y^2} = 0 \text{ at } x=0 \text{ or } a,$$

$$w(x,y,t) = \frac{\partial^2 w(x,y,t)}{\partial y^2} + \nu \frac{\partial^2 w(x,y,t)}{\partial x^2} = 0 \text{ at } y=0 \text{ or } b.$$

and for a clamped edge as,

$$w(x,y,t) = \frac{\partial w(x,y,t)}{\partial x} = 0 \text{ at } x=0 \text{ or } a,$$

$$w(x,y,t) = \frac{\partial w(x,y,t)}{\partial y} = 0 \text{ at } y=0 \text{ or } b.$$

Equation (1) can be written in a finite difference form, Figure 3, as:

$$\left(20 + \frac{\rho h \Delta^4}{D \Delta t^2} \right) w(i,j,t) - 8w(i,j-1,t) - 8w(i,j+1,t) - 8w(i-1,j,t) - 8w(i+1,j,t) + 2w(i-1,j-1,t) + 2w(i-1,j+1,t) + 2w(i+1,j-1,t) + 2w(i+1,j+1,t) + w(i,j+2,t) + w(i,j-2,t) + w(i+2,j,t) + w(i-2,j,t) = \frac{\Delta^4}{D} \left[\begin{matrix} p(i,j,t) \\ + \frac{2\rho h}{\Delta t^2} w(i,j,t-1) \\ - \frac{\rho h}{\Delta t^2} w(i,j,t-2) \end{matrix} \right] \quad (2)$$

where Δ is the size of the square mesh which is assumed to be equal to 0.02 m in this study, Δt is the time interval (0.001 sec), t is the time in sec, and

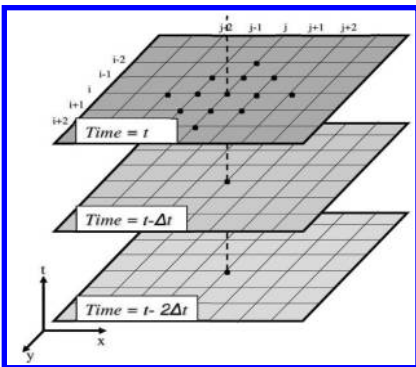


Figure 3. Plate meshes numbering in x-, y-, and t-coordinates.

i and j are the node numbers in the x- and y-directions, respectively.

The free vibration of the plate is obtained by setting the external loads to zero. For all plates considered in this study, the plate is excited by an initial displacement at point $(a/4, b/4)$, as shown in Figure 4. The deflection at point $(3a/4, 3b/4)$ is calculated using the finite difference method. Fourier transform is then used to convert the response from the time domain to the frequency domain. The natural frequencies are measured from the peaks of the curve, see Figure 5. To demonstrate the forced vibration cases, equation (2) is used to calculate the deflection at the central point (i, j) of the plate due to the various dynamic loadings, by representing that equation as:

$$w(i,j,t) = \frac{\text{LHS}}{\text{RHS}} \quad (3)$$

where LHS is the left hand side of equation (2), and RHS is right hand side of the same equation.

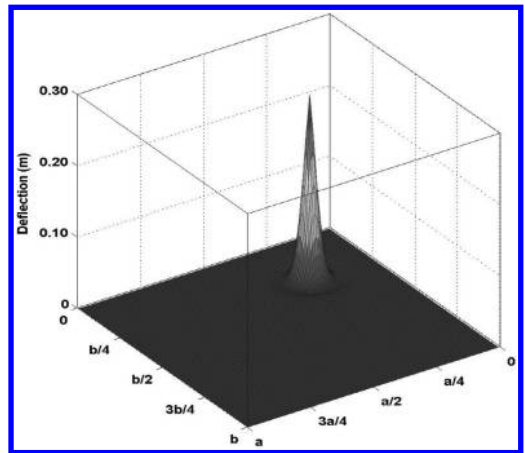


Figure 4. Initially displaced plate.

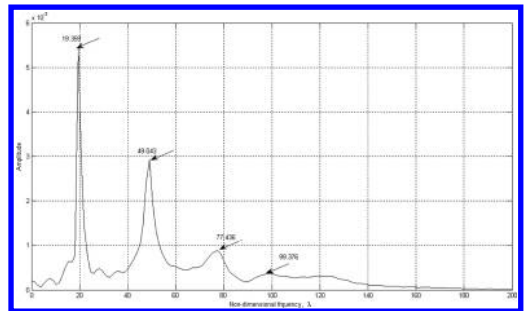


Figure 5. Calculation of the non-dimensional frequency using Fourier transform, for an SSSS plate.

For each time step, 0.001 sec, the deflection is computed by equation (3), and the corresponding response due to each dynamic loading is obtained. It should be mentioned here that a Matlab program titled “Free and forced vibration of plates” was written to demonstrate the present results.

3 RESULTS AND DISCUSSION

To demonstrate the free and forced vibrations, the material properties used in this study are as follows: concrete Young’s modulus, $E = 30 \times 10^9 \text{ N/m}^2$; Poisson’s ratio, $\nu = 0.3$; mass density, $\rho = 2800 \text{ kg/m}^3$; and plate thickness, $h = 0.1 \text{ m}$. Tables 1–3 shows the first four non-dimensional frequency parameters, $\lambda = \omega a^2 \sqrt{\rho/D}$, for rectangular plates with different values of a/b , namely, 2/3, 1, and 1.5, and various boundary conditions, namely, SSSS, SCSS, and SCSC, respectively, calculated by the present

Table 1. Natural frequency parameter for SSSS plates.

Aspect ratio a/b	Mode number	Present solution	Exact ref. [1, 2]	Ritz and DQ ref. [13]
2/3	1	14.337	14.256	N.A.
	2	27.371	27.416	
	3	44.315	43.865	
	4	48.226	49.348	
1	1	19.359	19.739	19.739
	2	49.043	49.348	49.348
	3	49.043	49.348	49.348
	4	78.207	78.957	78.957
1.5	1	32.258	32.076	N.A.
	2	61.584	61.685	
	3	99.709	98.696	
	4	108.509	111.033	

Table 2. Natural frequency parameter for SCSS plates.

Aspect ratio a/b	Mode number	Present solution	Exact ref. [1, 2]	Ritz and DQ ref. [13]
2/3	1	15.641	15.578	N.A.
	2	30.612	31.072	
	3	44.415	44.564	
	4	53.438	55.393	
1	1	23.461	23.646	23.646
	2	50.832	51.674	51.674
	3	58.652	58.646	58.646
	4	84.719	86.135	86.135
1.5	1	42.697	42.528	N.A.
	2	67.978	69.003	
	3	115.613	116.267	
	4	118.726	120.996	

Table 3. Natural frequency parameter for SCSC plates.

Aspect ratio a/b	Mode number	Present solution	Exact ref. [1, 2]	Ritz and DQ ref. [13]
2/3	1	16.428	17.373	N.A.
	2	34.390	35.345	
	3	44.466	45.429	
	4	59.857	62.054	
1	1	27.371	28.951	28.951
	2	53.266	54.743	54.743
	3	67.857	69.327	69.327
	4	91.235	94.585	94.585
1.5	1	54.273	56.348	N.A.
	2	76.722	78.984	
	3	121.560	123.172	
	4	141.078	146.268	

Table 4. Natural frequency parameter for CCCC plates.

Aspect ratio a/b	Mode number	Present solution	Exact ref. [1, 2]	Ritz and DQ ref. [13]
2/3	1	16.428	17.373	N.A.
	2	34.390	35.345	
	3	44.466	45.429	
	4	59.857	62.054	
1	1	27.371	28.951	28.951
	2	53.266	54.743	54.743
	3	67.857	69.327	69.327
	4	91.235	94.585	94.585
1.5	1	54.273	56.348	N.A.
	2	76.722	78.984	
	3	121.560	123.172	
	4	141.078	146.268	

finite difference method and compared to the exact solution of Leissa [1, 2] and the numerical solution of Eftehari and Jafari [13]. It is clear from the results that the present finite difference method agrees well with those of the exact solution [1, 2] and the numerical solution [13].

Tables 4–6 also shows the first four non-dimensional frequency parameters, $\lambda = \omega a^2 \sqrt{\rho/D}$, for CCCC, CCCS, and CCSS rectangular plates, respectively, with aspect ratio values of 2/3, 1, and 1.5, calculated by the present finite difference method and compared to the numerical solutions of Leissa [1, 2] and those of Eftehari and Jafari [13]. Again, the present finite difference method results agree well with those of the numerical solution obtained by [1, 2] and those of [13]. It should be mentioned here that the non-dimensional frequency parameter for a/b values of 2/3, and 1.5 is not available in [13].

Table 5. Natural frequency parameter for CCCS plates.

Aspect ratio a/b	Mode number	Present solution	Ritz ref. [1, 2]	Ritz and DQ ref. [13]
2/3	1	25.412	25.861	N.A.
	2	37.797	38.102	
	3	61.255	60.325	
	4	64.366	65.516	
1	1	31.281	31.829	31.826
	2	62.552	63.347	63.331
	3	71.686	71.084	71.076
	4	99.056	100.830	100.792
1.5	1	47.339	48.167	N.A.
	2	84.437	85.507	
	3	125.036	123.990	
	4	145.230	143.990	

Table 6. Natural frequency parameter for CCSS plates.

Aspect ratio a/b	Mode number	Present solution	Ritz ref. [1, 2]	Ritz and DQ ref. [13]
2/3	1	19.550	19.952	N.A.
	2	33.887	34.024	
	3	54.742	54.370	
	4	56.045	57.517	
1	1	27.371	27.056	27.054
	2	59.955	60.544	60.544
	3	61.258	60.791	60.794
	4	91.237	92.865	92.853
1.5	1	43.989	44.893	N.A.
	2	76.246	76.554	
	3	123.167	122.330	
	4	126.098	129.410	

The proposed finite difference method is examined for the forced vibration analysis of rectangular plates subjected to various dynamic loadings, namely, constant force, rectangular force with time of duration, $t_d = 0.1$ sec, triangular force with time of duration, $t_d = 0.1$ sec, and sinusoidal pulse with time of duration, $t_d = 0.1$ sec, and frequency of 20 rad/sec. The amplitude of all dynamic loadings is assumed to be 20 kN with time step, $\Delta t = 0.001$ sec. Figures 6–11 show the central displacement of a square plate with various boundary conditions, namely, SSSS, SCSS, SCSC, CCCC, CCCS, and CCSS, respectively. It is clear from the results that the central displacement has a sudden jump at $t_d = 0.1$ sec for rectangular, triangular, and sinusoidal loadings. The central displacements for the case of a rectangular load are higher than those due to sinusoidal and triangular loadings at all times, regardless of the boundary conditions.

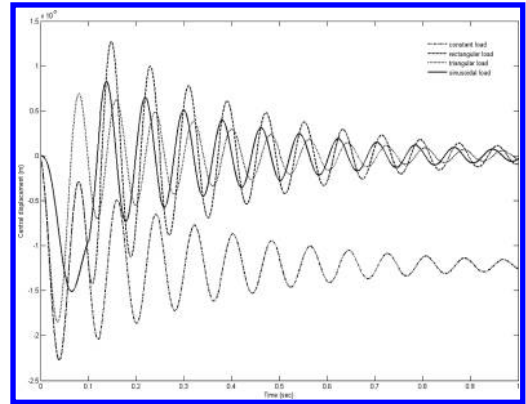


Figure 6. Central displacement versus time for an SSSS plate for various dynamic loadings.

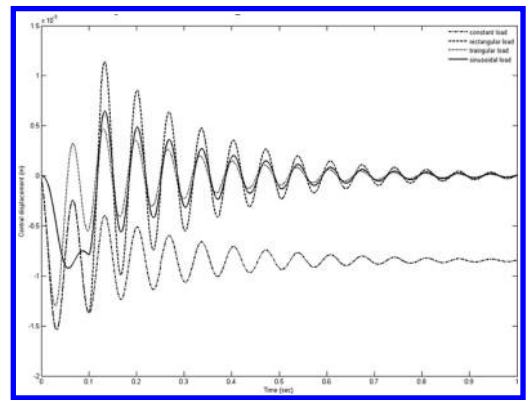


Figure 7. Central displacement versus time for an SCSS plate for various dynamic loadings.

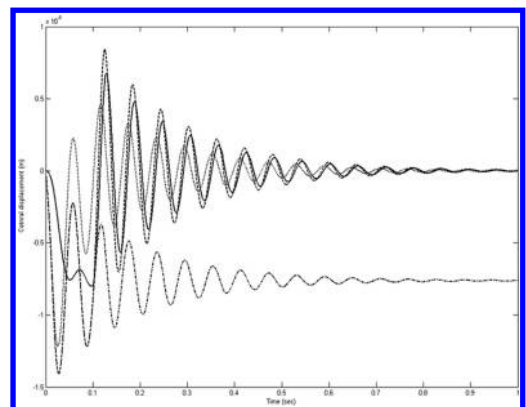


Figure 8. Central displacement versus time for an SCSC plate for various dynamic loadings.

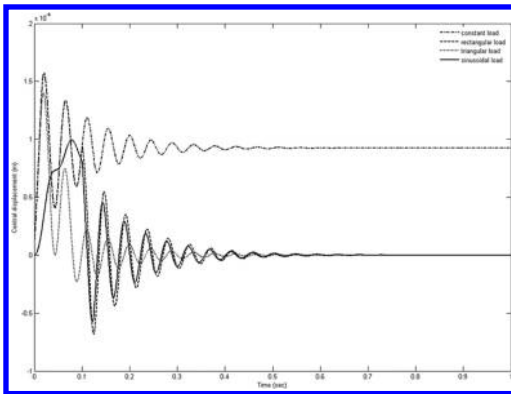


Figure 9. Central displacement versus time for an CCCC plate for various dynamic loadings.

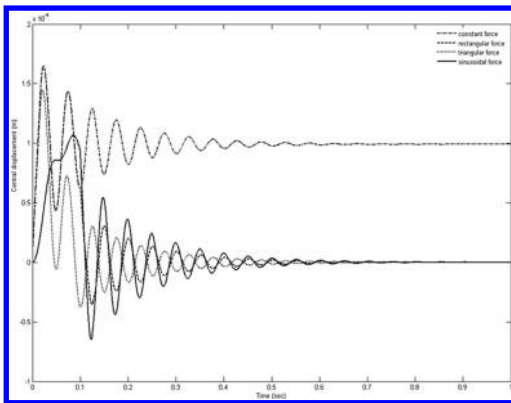


Figure 10. Central displacement versus time for an CCCS plate for various dynamic loadings.

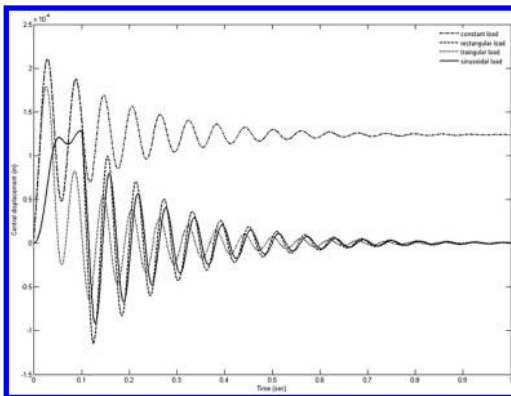


Figure 11. Central displacement versus time for an CCSS plate for various dynamic loadings.

The response for all plates will go to zero, except for the case of constant load. By comparing the results of Figure 6 with those of Figure 9, one sees that the rate of convergence of the response to zero for SSSS plates is slower than that of CCCC plates. The central displacements of plates having two opposite simply supported edges, namely, SSSS, SCSS, and SCSC is higher than those of plates not having two opposite simply supported edges, namely, CCCC, CCCS, and CCSS, compare Figures 6–8 with Figures 9–11.

4 CONCLUSIONS

In this paper, the free and forced vibration of rectangular plates is studied using the finite difference method. Six different cases of rectangular plates are considered based on their boundary conditions. Fourier transform is used to convert the time response obtained by the finite difference method to the frequency domain for an initially displaced plate. The corresponding natural frequencies of the rectangular plates are obtained. The dynamic behavior of rectangular plates is studied in this paper by subjecting them to various dynamic loadings. The results obtained in this study are in good agreement with exact and numerical results available in the literature.

REFERENCES

- [1] A.W. Leissa, "Vibration of Plates, Washington," NASA SP-160, US Government Printing Office, 1969.
- [2] A.W. Leissa, "The free vibration of rectangular plates," Journal of Sound and Vibration, vol. 31, no.3, pp. 257–293, 1973.
- [3] A.W. Leissa, "The historical bases of the Rayleigh and Ritz methods," J. Sound Vib., vol. 287, pp. 961–978, 2005.
- [4] S. Ilanko, "Comments on the historical bases of the Rayleigh and Ritz methods," J. Sound Vib., vol. 319, pp. 731–733, 2009.
- [5] D. Young, "Vibration of rectangular plates by the Ritz method," ASME J. Appl. Mech., vol. 17, pp. 448–453, 1950.
- [6] S.F. Bassily, S.M. Dickinson, "On the use of beam functions for problems of plates involving free edges," ASME J. Appl. Mech., vol. 42, pp. 858–864, 1975.
- [7] R.B. Bhat, "Natural frequencies of rectangular plates using characteristic orthogonal polynomials in Rayleigh-Ritz method," J. Sound Vib., vol. 102, pp. 493–499, 1985.
- [8] K.M. Liew, K.Y. Lam, "A set of orthogonal plate functions for vibration analysis of regular polygonal plates," ASME J. Vib. Acoust., vol. 113, pp. 182–186, 1991.

- [9] C.W. Lim, K.M. Liew, "Vibrations of perforated plates with rounded corners," *J. Eng. Mech.*, vol. 121, no. 2, pp. 203–213, 1995.
- [10] A.Y.T. Leung, J.K.W. Chan, "Fourier p-element for analysis of beams and plates," *J. Sound Vib.*, vol. 212, no. 1, pp. 179–185, 1998.
- [11] O.C. Zienkiewicz, R.L. Taylor, "The Finite Element Method," vol. 1, McGraw-Hill, New York, 1989.
- [12] J.N. Reddy, "An Introduction to the Finite Element Method," second ed., McGraw-Hill, New York, 1993.
- [13] S.A. Eftekhari, A.A. Jafari, "A mixed method for free and forced vibration of rectangular plates," *Applied Mathematical Modelling*, vol. 36, pp. 2814–2831, 2012.
- [14] X.D. Yang, W. Zhang, L.Q. Chen, M.H. Yao, "Dynamical analysis of axially moving plate by finite difference method," *Nonlinear Dynamics*, vol. 67, pp. 997–1006, 2012.
- [15] A.K. Gupta, M. Saini, S. Singh and R. Kumar, "Forced vibrations of non-homogeneous rectangular plate of linearly varying thickness," *Journal of Vibration and Control*, vol. 12, pp. 1–9, 2012.
- [16] X. Wang, S. Xu, "Free vibration analysis of beams and rectangular plates with free edges by the discrete singular convolution," *Journal of Sound and Vibration*, vol. 329, pp. 1780–1792, 2010.
- [17] M. Ducceschi, C. Touzé, S. Bilbao, and C.J. Webb, "Nonlinear dynamics of rectangular plates: investigation of modal interaction in free and forced vibrations," *Acta Mechanica*, vol. 225, pp. 213–232, 2014.
- [18] Y. Xing, B. Liu, "New exact solutions for free vibrations of rectangular thin plates by symplectic dual method," *Acta Mech Sin.*, vol. 25, pp. 265–270, 2009.
- [19] Y. Xing, B. Liu, "Closed form solutions for free vibrations of rectangular Mindlin plates," *Acta Mech Sin.*, vol. 25, pp. 689–698, 2009.
- [20] S.P. Timoshenko, S. Woinowsky-Krieger, "Theory of Plates and Shells," McGraw-Hill, New York, 1959.
- [21] N.M. Werfalli, A.A. Karoud, "Free Vibration Analysis of Rectangular Plates Using Galerkin-Based Finite Element Method," *International Journal of Mechanical Engineering*, vol. 2, no. 2, pp. 59–67.
- [22] J.H. Wu, A.Q. Liu, and H.L. Chen, "Exact Solutions for Free-Vibration Analysis of Rectangular Plates Using Bessel Functions," *Journal of Applied Mechanics*, vol. 74, pp. 1247–1251, 2007.
- [23] K.O. Njoku, J.C. Ezeh, O.M. Ibearugbulem, L.O. Ettu, and L. Anyaogu, "Free vibration analysis of thin rectangular isotropic CCCC plate using Taylor series formulated shape function in Galerkin's method," *Academic Research International*, vol. 4, no. 4, pp. 126–132, 2013.
- [24] M.N. Bahrami, M. Loghmani, and M. Pooyanfar, "Analytical Solution for Free Vibration of Rectangular Kirchhoff Plate from Wave Approach," *World Academy of Science, Engineering and Technology*, vol. 39, pp. 221–223, 2008.
- [25] Jain, R. Kbishan, and S.R. Soni. "Free vibrations of rectangular plates of parabolically varying thickness," *Indi. J. Pure Appl. Math.*, vol. 4, pp. 267–277, 1973.
- [26] K.S. Numayr, R.H. Haddad, and M.A. Haddad. "Free vibration of composite plates using the finite difference method," *Thin-walled structures*, vol. 42, no. 3, pp. 399–414, 2004.
- [27] Y.L. Yeh, M.J. Jang, and C.C. Wang, "Analyzing the free vibrations of a plate using finite difference and differential transformation method," *Applied mathematics and computation*, vol. 178, no. 2, pp. 493–501, 2006.

Tensile properties and water absorption of Recycle Polypropylene (rPP)/Oil Palm Empty Fruit Bunch (OPEFB) composites: The effect of Maleic Anhydride-g-Polypropylene (MAPP) addition

Halimatuddahlia Nasution

Department of Chemical Engineering, Faculty of Engineering, Universitas Sumatera Utara, Medan, Indonesia

ABSTRACT: The effects of Maleic Anhydride (MAPP) as compatibilizer on tensile properties and water absorption of Recycle Polypropylene (rPP)/Oil Palm Empty Bunch Fruit (OPEFB) composites were investigated. Several contents of MAPP viz. 2, 4, 6, 8 wt.% were prepared. Corresponding rPP/OPEFB composite without MAPP addition was also made for comparison. The OPEFB composition was fixed at 30 wt.%, while rPP was 70 wt.% and reduced correspondingly on the addition of MAPP. Composites were prepared in extruder with temperature of 190 °C. Results indicated an improvement in tensile strength and elongation at break were obtained on the addition of MAPP up to 6 wt.%. It was also revealed that the water absorption was significantly decreased as the MAPP was increased up to 6%. However, the addition of 8 wt.% MAPP was found to reduce these properties. Scanning electron microscopy (SEM) images from the tensile fracture surface supported that the improvement on interface region between matrix and filler have occurred.

Keywords: Recycle Polypropylene; Oil Palm Empty Fruit Bunch; Maleic Anhydride-g-Polypropylene; tensile strength; water absorption

1 INTRODUCTION

Production of plastic waste in Indonesia was ranked as the second producer of domestic waste that is equal to 5.4 million ton per year. Based on statistical data of domestic Indonesian waste, the amount of plastic waste that is 14% of the total waste production in Indonesia [1]. It comprises mostly plastics used in food packaging such as PET, PVC, LDPE, HDE, and PP. One of the most popular plastic packaging is plastic cup for sparkling beverages which is made from PP. Since Incineration method is not a good solution because it raises the pollutions, the only alternative left for easy disposal of this huge plastic waste is recycling to obtain value added products. Therefore, it is a promising way of use recycle PP (rPP) as matrix to obtain composite and a perfect choice due to its low cost and the resulting protection of environment. Plastic recycling is a process which basically comprises the following steps: collection, separation, cleaning and pelletizing. Adhikary [2] and Bhaskar [3] have published studies dealing with rPP composites.

On the other hand, in general the use of fillers in composites aim to reduce costs, provide color, strengthen or reinforce composite materials. As a filler, natural fibers have several advantages

compared to inorganic fillers such as lower density, renewability, improvement in the mechanical properties, increase in range of applications, biodegradability, greater deformability, enhanced energy recovery and relatively lower cost [4]. Several studies of natural fibers used as filler in composites such as jute, kenaf, banana, and bamboo [5–8] has been done. One of natural fibers which can be potentially used is fiber of Empty Fruit Bunch Palm Oil (EFBPO). The utilization of fiber of EFBPO as fillers had been studied using thermoplastic matrix [9–11].

However, the interfacial adhesion between natural fiber and thermoplastics is usually very weak due to the high interfacial tension. This leads to undesirable properties of the composites. The process of modifying interfacial properties of an incompatible polymer blend leading to the creation of polymer blend is called compatibilization [12]. Physical compatibilization is a modification of polymeric structure to enhance miscibility, control of crystallization as a means to lock-in developed morphology and addition of compatibilizing agents [13]. Maleic Anhydride-g-Polypropylene (MAPP) is the most common compatibilizer/coupling agent which is expected to give good compatibility between the natural fiber and the thermoplastic by formation of stronger linkages in the interfaces and reducing

filler-matrix surface tension. Some researchers have published studies dealing with MAPP addition on composites [10, 14–16].

In the present study the effect of MAPP addition on tensile properties and water absorption of rPP/OPEFB composites were investigated.

2 EXPERIMENTAL

To carry out this experiment, fixed quantities of rPP, EPOFB, and calculated quantities of MAPP were measured. In the formulations where the MAPP had added, the rPP mass was reduced correspondingly thus, the total proportion of the rPP and the MAPP was 70%. The composition of the systems are shown in Table 1. The mixture was fed into extruder machine, and processed at temperature of 190 °C. Composites were then compression molded using hot press at 190 °C. In hot press, composites were preheat for 5 minutes and followed by 5 minutes compression time at the same temperature. The specimens were allowed to cool under pressure for another 5 minutes.

Tensile tests were carried out according to ASTM D638 using a Universal Testing Machine GOTECH AL-7000M. One mm thick dumbbell specimens were cut from the moulded sheets with a dumbbell cutter. The tensile test was performed at constant rate (20 mm/min) at room temperature. The results were quoted based on the average value of five specimens for each system.

For water absorption test, small blocks of 1 × 5 × 5 cm were cut from the sheet and oven dried at 103 ± 2°C to determine dry weights. The blocks were immersed in distilled water at room temperature and weighed after 2, 4, 6, 12 and 24 hours of soaking to determine their wet weights. Prior to weighed, specimens were wiped with tissue to make sure all their surfaces dried. Water absorption was calculated according to Equation (1).

$$\text{water absorption(\%)} = \frac{w - w_0}{w_0} \times 100\% \quad (1)$$

where: w and w_0 indicate wet weight and dry weight of the specimens (g), respectively.

Table 1. Formulation of rPP/EPOFB composite.

Sample	EPOFB wt.%	rPP wt%	MAPP wt.%
1.	30	70	0
2.	30	68	2
3.	30	66	4
4.	30	64	6
5.	30	62	8

3 RESULTS AND DISCUSSION

3.1 The effect of MAPP addition on the tensile strength and elongation at break of rPP/OPEFB composites

The effect of MAPP addition on tensile strength of rPP/OPEFB composites are shown in Figure 1. It was found that the addition of MAPP until 6 wt (%) resulted in an increase of tensile strength.

The lowest tensile strength of composite without the addition of MAPP could be attributed to the poor interfacial interaction between the polymeric matrix and filler, not allowing efficient stress transfer between the two phases of the material. Poor interfacial bonding causes partially separated micro-spaces between the filler particles and the polymer matrix, this causes stress propagation when tensile stress is loaded and induce increased brittleness [15]. This leads to undesirable tensile resistance of the composite.

Nevertheless, the addition of compatibilizer (MAPP) has improved interfacial bonding between the filler and the matrix and improved the tensile strength. The application of the MAPP as compatibilizer increased hydrophobicity of the composites. Other investigations noted, the increase in the tensile strength of the composites on addition of MAPP was caused by maleic anhydride from the MAPP molecule which reacts with the hydroxyl groups (–OH) of cellulose or hemicellulose, the two main constituents in OPEFB [11]. The reaction of the hydrophilic –OH groups from the filler and the acid anhydride groups from MAPP, forming ester linkages. Here, the anhydride moieties of functionalized polyolefin compatibilizer entered into esterification reaction with the surface hydroxyl groups of OPEFB. Upon the esterification reaction, the polyolefin backbone chain of the compatibilizer was exposed on the surface of OPEFB. It is believed that these exposed polyolefin chains diffused into the PP

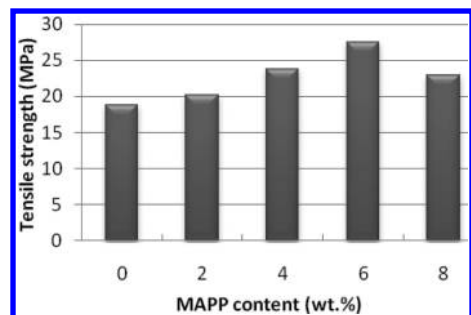


Figure 1. Plot of tensile strength versus MAPP content for rPP/OPEFB composites.

matrix phase and entangled with rPP molecules during processing creating a bridge at the interface between the OPEFB and the rPP matrix [2]. As was noticed above, further increase in the MAPP up to 6 wt.% has significantly increased the tensile strength of the composites. Fuqua and Ulven [17] have investigated the different MAPP loading (0, 5 and 10 wt.%) effects on tensile properties of corn chaff fiber reinforced PP composites. It was found that 5 wt.% MAPP yielded the optimum value for the composites in term of tensile strength.

However, the tensile strength reduction observed with 8 wt.% MAPP content. It could be attributed to a plasticizing effect exerted by MAPP on the composites since it is possible that MAPP has a lower molecular weight compared to the matrix PP [11].

The effect of MAPP additions on the elongation at break of RPP/OPEFB composites are showed in Figure 2.

An examination of Figure 2 reveals that the elongation at break of rPP/OPEFB composites were significantly improved as content of MAPP increase until 6 wt.%. This could be related to improvement adhesion between OPEFB fiber and rPP. Without addition of MAPP, the elongation at break of composite shows the lowest value. This could be attributed to the lack adhesion on filler-matrix interface. On the addition of MAPP, as in the case of tensile strength, improving the adhesion between OPEFB and rPP has enhanced the elongation at break. At high MAPP content (8 wt.%), decreases on elongation at break were however observed for the rPP/OPEFB composite. This could be related to the migration of too much of the compatibilizer around the fibers, causing self entanglement among the compatibilizers rather than the polymer matrix, resulting in slippage [11].

3.2 The effect of MAPP addition on water absorption of rPP/OPEFB composites

Figure 3 shows the effect of MAPP addition on water absorption of rPP/OPEFB composites.

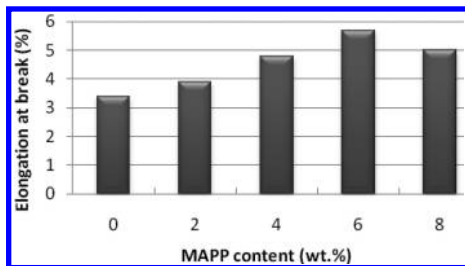


Figure 2. Plot of elongation at break versus MAPP content for rPP/OPEFB composites.

It shows the water absorption was decreased due to the addition of compatibilizer (MAPP) to the rPP/OPEFB composites.

The current composite consists of hydrophilic (OPEFB) and hydrophobic (rPP) parts. The hydrophilicity of cellulose and hemicellulose within the OPEFB is the main cause of water absorption. They contain numerous hydroxyl groups (-OH) and carboxyl groups (-COOH) which had tendency to interact with water molecules via hydrogen bonding. Under water immersion, the water molecules resided in the unfilled pores and voids in the composites, and formed hydrogen bonds with the components of cellulose and hemicellulose. On the addition of MAPP, the anhydride moieties in the MAPP reacted with the surface hydroxyl groups of OPEFB (ester linkage). Therefore, application of the MAPP decreased the surface tension in composites and it caused the hydrophilic part less accessible for the water molecules due to good encapsulation of the OPEFB by the hydrophobic part as well as decreased number of hydroxyl groups in the OPEFB part. Similar to our findings, Chinomso et al [11] who studied OPEFB Filled HDPE reported that the amount of water absorbed was found to decrease with increase in MAPP content.

However, the composites containing 8 wt.% MAPP exhibited slightly higher water absorption compared with the composites with 6 wt.% MAPP. It is possible that unreacted MAPP increased the hydrophilicity of the composites since the MAPP contains a low content of polar groups in contrast to the non-polar rPP matrix.

3.3 Morphology

Microstructure of the fractured surface for rPP/OPEFB composite specimens tested in tensile is examined using Scanning Electron Microscopy (SEM). Images of the composites without and with compatibilizer (MAPP) are shown in Figures 4a and 4b, subsequently, in 1000× magnification.

Figure 4a shows there was fiber pull out leaving holes behind on uncompatibilized rPP/OPEFB composite. It is clearly indicating weak interfacial region and damage mainly occurred along the loose and weak interface between OPEFB fiber and rPP matrix. As mention before, the hydrophilic nature of OPEFB fiber filled hydrophobic rPP is believed to be responsible for the poor interfacial adhesion between OPEFB and rPP. This image has become evidence the low value tensile strength and high degree of water absorption of composite. However, as seen on Figure 4b, the presence of MAPP in rPP/EPOFB composite reduced the holes turned more difficult fiber pull-out during brittle fracture. The surface of fiber displayed a rough morphology confirming

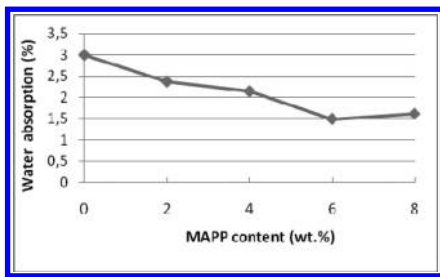


Figure 3. Plot of water absorption versus MAPP content for rPP/OPEFB composites.

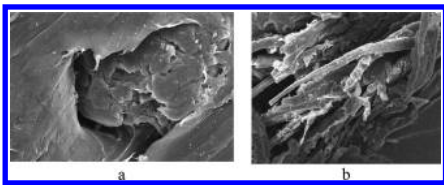


Figure 4. SEM micrographs of fractured surfaces of composites rPP/EPOFB. a) without MAPP addition; b) with MAPP addition (6 wt.%).

its effect on promoting adhesion in the interfacial region, indicating stress transfer from the matrix to the fiber, resulting in enhanced tensile in response to stress. Interface bonding between the fillers and the matrix is the key to transfer the stress from the matrix into the fillers across the interface [11].

4 CONCLUSION

Tensile strength and elongation at break of Oil Palm Empty Fruit Bunch (OPEFB) fiber filled Recycle Polypropylene (rPP) have shown improvement with increasing of Maleic Anhydride g-Polypropylene (MAPP) up to 6 wt.% content. The addition of MAPP into rPP/OPEFB composites was found to significantly improve surface adhesion between filler and matrix. SEM images of the fractured surfaces confirmed that an addition of the MAPP compatibilizer improved the interfacial bonding between the rPP and the OPEFB fiber for the rPP based composites.

REFERENCES

[1] Information on <http://www.antaranews.com/berita/417287/produksi-sampah-plastik-indonesia-54-juta-ton-per-tahun>. Selasa, 4 Februari 2014.
 [2] Adhikary, K.B. 2008. Wood flour recycled polymer composite panels as building materials. Thesis.

Chemical and Process Engineering, University of Canterbury
 [3] Bhaskar, J. Haq, S. Pandey, A.K. & Srivastava, N. 2012. Evaluation of properties of propylene-pine wood Plastic composite *J. Mater. Environ. Sci.* 3(3): 605–612
 [4] Bos, H. 2004. The Potential of Flax Fibres as Reinforcement for Composite Materials, Thesis. University Press Facilities, Eindhoven, the Netherlands
 [5] Verma, B.B. 2009. Continuous jute fibre reinforced laminated paper composite and reinforcement-fibre free paper laminate. *Bull. Mater. Sci.* 32: 589–595.
 [6] Akil, H.M. Omar, M.F. Mazuki, A.A.M. Safiee, S. Ishak, Z.A. & Abu Bakar, M.A. 2011. Kenaf fiber reinforced composites. *A Review, Materials and Design* 32: 4107–4121.
 [7] Ghosh, R. Reena, G. Krishna, R.A. & Raju, L. 2011. Effect of fibre volume fraction on the tensile strength of banana fibre reinforced vinyl ester resin composites. *International Journal Of Advanced Engineering Sciences And Technologies* 4: 089–091.
 [8] Ochi, S. 2012. Tensile properties of bamboo fiber reinforced biodegradable plastics. *International Journal of Composite Materials* 2: 1–4.
 [9] Khalid, M. Ratnam, C.T. Chuah, T.G., Ali, S. & Choong T.S.Y. 2006. Comparative study of polypropylene composites reinforced with oil palm empty fruit bunch fiber and oil palm derived cellulose. *Elsevier Materials & Design* 29: 173–178.
 [10] Khalid, M. Ali, S. Abdullah, L.C. Ratnam, C.T. & Choong T.S.Y. 2006. Effect of MAPP as coupling agent on the mechanical properties of palm fiber empty fruit bunch and cellulose polypropylene biocomposites. *International Journal of Engineering and Technology* 3(1): 79–84.
 [11] Chinomso, M. Ewulonu. & Igwe, I.O. 2012. Properties of oil palm empty fruit bunch fibre filled high density polyethylene. *International Journal of Engineering and Technology* 3(6): 458–471.
 [12] Utracki, L.A. (1990). *Polymer Alloys and Blends: Thermodynamics and Rheology*. New York: Hanser Publications.
 [13] Xanthos, M. (1988). Interfacial Agents for Multiphase Polymer Systems: Recent Advances. *Polym. Eng. Sci.* 28(21), 1392–1340.
 [14] Kim, H.S. Lee, B.H. Choi, S.W. Kim, S & Kim, H.J. 2007. The effect of types of maleic anhydride-grafted polypropylene (MAPP) on the interfacial adhesion properties of bio-flour-filled polypropylene composites. *Composites: Part A* 38(6): 1473–1482.
 [15] Marti-Ferrer, F. Vilaplana, F. Ribes-Greus, A. Benedito-Borrás, A. & Sanz-Box, C. 2006. Flour rice husk as filler in block copolymer polypropylene: Effect of different coupling agents. *Journal of Applied Polymer Science* 99(4): 1823–1831.
 [16] Rosa, S.M.L. Santos, E.F. Ferreira, C.A. & Nachtiga, S.M.B. 2009. Studies on the Properties Rice-Husk-Filled-PP Composites—Effect of Maleated PP. *Materials Research* 12(3), 333–338.
 [17] Fuqua, M.A. & Ulven, C.A. 2008. Preparation and Characterization of Polypropylene Composites Reinforced with Modified Lignocellulosic Corn Fiber, The Canadian Society for Bioengineering.

Evaluation of structural stability for beam made of submarine structural steels (SM 400, SM 490) at high temperature

In-Kyu Kwon

Department of Fire Protection Engineering, Kangwon National University, South Korea

Oh-Sang Kweon, Heung-Youl Kim & Seung-Un Chae

Fire Research Center, Korea Institute of Civil Engineering and Building Technology, South Korea

ABSTRACT: Submarine structural steels have been developed to improve the weakness, weldability and have the same structural property as an ordinary structural steels such as SS 400, SS 490 has. These are used for major structural members such as column and beam. However, the fire resistance performance of them was not clarified to the variations of lengths. Because the fire resistance was evaluated by fire test and the result derived from the test have been used to all structural beams regardless the variance of lengths, boundary conditions, and sizes of section. In this study, to demonstrate structural stability at high temperature and suggest the proper fire resistance performance of them, the analytic method was applied using mechanical properties at high temperature and related theoretical processes such as a heat transfer and a stress analysis.

Keywords: submarine structural steels; beam; fire resistance; structural stability at high temperature; stress

1 INTRODUCTION

Structural stability of beam in a compartment where a fire is taken place is very important, for it can produce the secondary stress dependent on heat. If the beam expands, the adjacent columns are likely to generate a new bending moment and if the beam shrinks by the action of suppression, the beam would be loaded a new compression. These structural behaviors make the beam to lose its structural stability and the deflection may be increased gradually. Therefore, to protect the weakness of structural stability for beams in high temperature, the fire protective materials should be applied onto the surface. However, the thickness of fire protective materials derived from fire test is allowed to all beams regardless the size of section, lengths, and boundary conditions. In this study, to know the structural stability according to variance of lengths of H-section beam made of SM 490, an analytic method was done using mechanical properties with a heat transfer theory and a stress analysis. After evaluation of structural stability of the beam made of SM 490, the results are compared to those of SM 400.

2 STRUCTURAL BEHAVIOR AND ANALYTIC CONDITIONS OF BEAM

Beam is one of the major structural element in steel framed building. The role of it is transferring

the applied load toward column and load bearing wall. Therefore, if there is a fire within a compartment, the beam begins to expand and sag, and load bearing capacity is going down gradually. These structural behaviors at high temperature depend on boundary condition, and lengths. However, the fire resistant of beam would be evaluated by fire test using a horizontal furnace and a specimen having 4100 mm in length, H-400 × 200 × 8 × 13, and simple beam with a loading under a standard fire curve. Contrary to the fire test of the beam, the real situations of each building are totally different from the test conditions. In this study, to analyze the structural stability of beam according to variance of lengths, the following conditions are applied and expressed in Table 1. To calculate the maximum load that is allowed to the beam,

Table 1. Conditions of analysis.

Sorts	Contents	Remarks
Size	H-400 × 200 × 8 × 13	Section area is 84.2 cm ²
Sorts of steels	SM 490	
Lengths (mm)	4100, 4400, 4700	
Boundary condition	Simple beam	
Fire source	Standard fire curve	KS F 2257-1

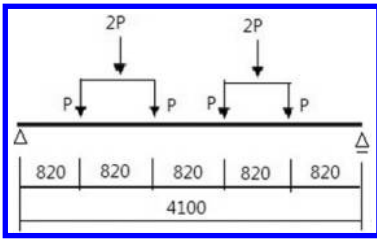


Figure 1. Loading diagram for a simple beam.

Table 2. Expansion coefficients of SM 490.

Sorts	Temperature	Regression equation (E-03/°C)	Remarks
SM 490	$T \leq 140 \text{ }^\circ\text{C}$	$0.082T - 2.65$	$R^2 = 0.98$
	$140 < T \leq 730 \text{ }^\circ\text{C}$	$0.01T + 7.89$	$R^2 = 0.93$
	$730 < T \leq 870 \text{ }^\circ\text{C}$	$-0.02T + 30.7$	$R^2 = 0.97$
	$870 \text{ }^\circ\text{C} < T$	$0.009T + 3.50$	$R^2 = 0.98$

Table 3. Specific heat of three kinds of SM 490 steel at high temperatures.

Sorts	Temperature	Regression equation (J/gK)	Remarks
SM 490	$T \leq 610 \text{ }^\circ\text{C}$	$0.0008T + 0.38$	$R^2 = 0.94$
	$610 < T \leq 710 \text{ }^\circ\text{C}$	$0.006T - 2.78$	$R^2 = 1$
	$710 < T \leq 810 \text{ }^\circ\text{C}$	$-0.004T + 3.97$	$R^2 = 1$
	$810 \text{ }^\circ\text{C} < T$	$0.0007T + 0.62$	$R^2 = 1$

Table 4. Mechanical properties of SM 490 at high temperatures.

Sorts	Properties	Temperature	Regression equation
SM 490	Yield strength	$T \leq 200 \text{ }^\circ\text{C}$	Cold value (315 MPa)
		$200 \text{ }^\circ\text{C} < T$	$-0.41T + 396.58$
	Elastic modulus	$T \leq 200 \text{ }^\circ\text{C}$	Cold value (210 GPa)
		$200 \text{ }^\circ\text{C} < T$	$-0.26T + 261.28$

the conditions for the 4100 mm in length is like to Figure 1.

Mechanical and thermal properties of SM 490 used in the analysis are shown in the Table 2 ~ Table 4.

3 ANALYSIS OF STRUCTURAL STABILITY OF H-SECTION BEAM AT HIGH TEMPERATURE

To get the fire resistance performance of H-section beam by an analytical method, the calculation of

Table 5. Structural property features of beam.

Length of beam (mm)	Bending stress (MPa)	Maximum moment	Magnitude of P (kN)	Maximum deflection (mm)
4100	142.7	2.46P	69	4135260P/EI
4400	132.95	2.76P	57	7365013P/EI
4700	124.47	3.06P	48	10422535P/EI

surface temperature is needed at first step. The surface temperature history according to a standard fire curve defined in KS F 2257-1 can be calculated using specific heat, density of steel, and etc.

Structural features according to lengths are shown in the Table 5. An interval between the points is 820 mm and the end of each beam has a different length.

4 RESULTS OF STRUCTURAL STABILITY FROM ANALYSIS

The results are shown in Figure 2. In the figure, the history of increasing temperature for SM 490 is compared with that of SM 400. In the whole, the tendency of increasing pattern between two structural steels is very similar and there was no a big temperature difference.

The result from expanded length by an expansion coefficient is shown in Figure 3. Each expanded length showed a similar increasing tendency until 700 °C. However, from 700 °C to 900 °C the result from SM 490 revealed larger expanded length than that of the SM 400. It was considered that the difference was depended on the each expansion coefficient of steel.

Maximum load according to surface temperature of each length are shown in Figure 4. The difference of maximum load between 4400 mm and 4100 mm was almost 82% and that between 4700 mm and 4100 mm was 70%. Therefore, to apply the same fire protective materials derived from a standard fire test using 4100 mm in length is not appropriate to longer length of beam. To compensate the difference of maximum load in high temperature range, an additional fire protective measure should be considered.

The deflections among three beams are shown in Figure 5. In the figure, the magnitude of each deflection was big as the length of beam is bigger. By this result, when the length of beam is getting longer than that was done in the fire test, another measure should be enforced to maintain the fire safety of the building.

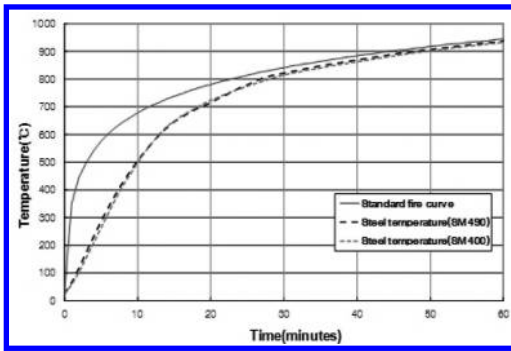


Figure 2. Surface temperature rising versus times.

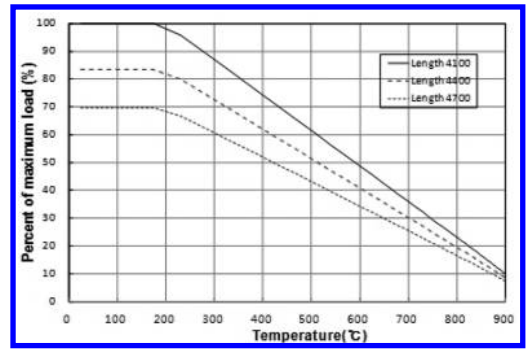


Figure 4. Maximum load versus steel temperatures.

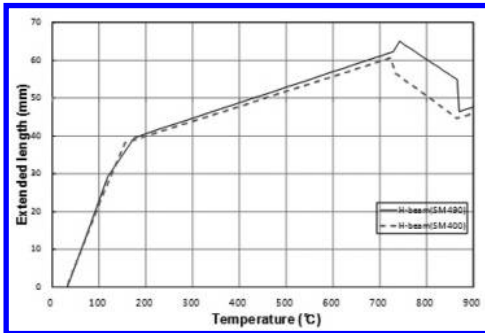


Figure 3. Expanded length versus steel temperatures.

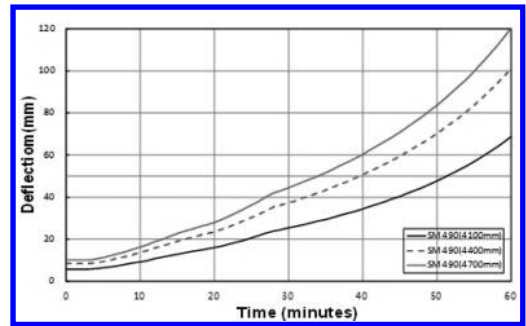


Figure 5. Deflection versus times.

5 DISCUSSIONS

Fire resistance of structural beam is dependent not only on the structural conditions but structural level. Especially, the level of yield strength plays a key role in structural performance at high temperature. Therefore, it is essential to know the structural properties in high temperature to evaluate the structural stability in fire situation. In real construction site, the length of structural beam can be diverse to meet the requirement of an architectural design aspect. But, the fire resistance of each structural beam is deemed to be satisfied when the minimum fire protective materials approved by fire authority is applied. After analysis using structural properties at high temperature and related theories, this is not reasonable and as the length of beam is longer than that of approved, the fire protective materials should be applied more to sustain the structural stability in high temperature.

6 CONCLUSIONS

When the structural beam made of SM 490 exposes to fire condition, the fire resistance performance

will be decreased gradually. This study was done for evaluation of structural stability according to lengths of the beam by an analytic method and got the followings;

1. The expanded length of beam made of SM 490 versus an increased steel surface temperature is very similar to that of SM 400. But the difference was only shown after 700°C and this can be considered as a not serious result.
2. Fire resistance performance is decreased as the length of beam made of SM 490 is longer and the maximum load in 4400, 4700 mm in length are shown 82%, 70% of 4100 mm, respectively. Therefore, to compensate for the structural stability of 4400, 4700 mm, an additional fire protective material should be needed.
3. The increased values of deflection versus increased surface temperature were shown.

ACKNOWLEDGEMENT

This study has been conducted by the relevant study to “Structures have more than 3 hour fire-resistance rating and smoke control-evacuation in fire” project, a major project of KICT.

REFERENCES

- Kwon, I.K. 2009. Development of analytic program for calculation of fire resistant performance on steel structures, *Journal of the Regional Association of Architectural Institute of Korea*, Vol. 11, No. 3: 201–208.
- Korean Standard Association. 2002. KS D 0026 Method of elevated temperature tensile test for steels and heat-resisting alloys, Seoul, Korea.
- Park, S.Y. Kim, H.Y. and K.P. Hong. 2010. Analytic study on the fire resistance of the asymmetric H-section slim floor beam concerning the load ratio, *Journal of Architectural Institute of Korea*, Vol. 26, No. 9: 55–62.
- Yin, Y.Z. and Wang, Y.C. 2004. A numerical study of large deflection behaviour of restrained steel beams at elevated temperatures, *Journal of Constructional Steel Research* 60: 1029–1047.

Design and making of conformal cooling system for cycle time reduction in curvature and complex shape mold component

Manat Hearunyakij & Sathaporn Chatakorn

Department of Mechanical Engineering Technology, College of Industrial Technology, King Mongkut's University of Technology North Bangkok, Bangkok, Thailand

ABSTRACT: Commonly, conventional cooling system of a plastic injection mold consisted of a drilled set of interconnected cooling channels. These cooling channels frequently provide non-uniform cooling, resulting in long cooling time and part warpage. Aim of the research work was to design conformal cooling system for improve mold insert which cannot build cooling system inside. Typical plastic rinsing spray, core insert of plastic injection mold has small dimension and complex shape design. P20 powder metal is used for DMLS process and coolant for mold cooling system is oil. The technique 3D scanning is used for part model creating. Rhinoceros 4.0 and Moldex3D R11.0 computer programs are applied for cooling system design and plastic flow analysis. The results from plastic injection experimental, cycle time can reduce 35.0 seconds compare with conventional cooling method.

Keywords: conformal cooling; DMLS; cooling time; plastic flow analysis

1 INTRODUCTION

Plastic injection molding process has been widely used in mass production of high quality plastic parts with various complex shapes. The process consists of three crucial stages which are filling stage, packing stage and cooling stage [1]. Among these three stages, the cooling stage takes about 65%–70% of each cycle time [2]. During cooling stage, heat of molten plastic was taken by cooling system until it reached ejection temperature [3]. Therefore, the cooling stage is very important to the production of plastic injection parts. Generally, the cooling system of a plastic injection mold required a straight drill to create coolant flow lines [4]. Hence conventional plastic injection mold is always straight coolant flow line and circular cross section cooling channel only. This kind of cooling system caused not only defects in molded parts such as warpage due to non-uniform shrinkage but also increased the cooling time [4], [5].

For cooling system design, main factors which affect cooling efficiency are:

- Diameter (\varnothing) and perimeter of Cooling channel
- Coolant velocity
- Distance between cavity surface to cooling channel
- Distance between cooling channels.

From many studies, it was found that the conformal cooling can reduce cycle time by approximately 20% compared with conventional cooling [6], [7].

However, method to create conformal cooling system is more complicated than that of conventional cooling system which consisted of straight drill holes [8]. For conformal cooling system, DMLS (Direct Metal Laser Sintering) technique is used to make injection mold inserts. The advantages of this technique were to create cooling channels with different cross sectional shapes such as circular, oval, rectangular, etc. Furthermore, DMLS can be used to create coolant flow line along with shape of plastic part [9].

Aims of this research work were to reduce cycle time of plastic injection mold which have small dimension and complex shape component. Conformal cooling design and DMLS technique were used for decrease limitation of conventional cooling method.

2 METHODOLOGY

In this research, 3D optical scanning technique was used for part modelling preparation in the initial step. From this technique, it provided part modelling which is STL (Stereolithography) file type. After that, the part modelling was created into part surface modelling. Plastic injection mold including mold base, feeding and cooling system were designed in Rhinoceros 4.0 computer program. Finite element model preparation of plastic part and injection mold system were created in Moldex 3D R11.0 which is computer program for

plastic flow analysis. Moldex 3D R11.0 was used for analysis of plastic flow behavior in every stage of plastic injection process such as filling, packing and cooling stage in the order of cooling efficiency comparison between conformal and conventional cooling. The results from computer simulation were used for decision of mold insert with conformal cooling system fabricating.

2.1 Plastic injection process analysis

Plastic injection part in this research is rinsing spray which consists of curvature shape configuration as shown in Figure 1. The rinsing spray has also water flow channel inside which has curve design. The plastic injection mold for this part has mainly 2 components which are used for water flow channel creating as shown in Figure 2 (Part No. 1 and 2). Basically these components have to move by mechanic or hydraulic system during injection process. For this case, component No. 1 is split out from mold impression by mechanic system but component No. 2 is split out by hand outside



Figure 1. Typical plastic part.

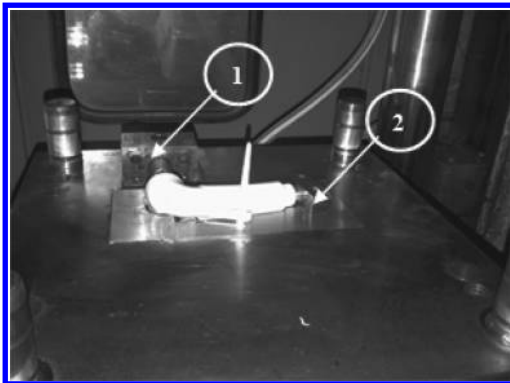


Figure 2. Injection mold for rinsing spray.



Figure 3. Sub insert for rinsing spray injection mold.

the mold after injection process cycle finishing by the reason of mold size limitation and part order quantity.

Sub insert for rinsing spray injection mold is illustrated in Figure 3. The configuration of this component is curvature design and small dimension. The biggest and smallest diameter of this component is approximately 12.0 and 8.0 mm. Length of this component is approximately 125.0 mm. Hence it is very difficult to create cooling system inside this component by conventional method. The problem that occurred during injection process is heat accumulation in this component. It is causes of cycle time increasing and part warpage problem. The cooling time is necessary to increase more than normal for solving shrinking and warpage problem.

3 THEORY

3.1 Energy conservation [10]

For the cooling stage of plastic injection molding, a three-dimensional, cyclic, transient heat conduction problem with convective boundary conditions on the cooling channel and mold base surfaces is involved. The heat transfer equation is governed by a three-dimensional Poisson equation,

$$\rho C_p \frac{\partial T}{\partial t} = k \left(\frac{\partial^2 T}{\partial x^2} + \frac{\partial^2 T}{\partial y^2} + \frac{\partial^2 T}{\partial z^2} \right) \quad (1)$$

where T is the temperature, t is the time, x , y , and z are the Cartesian coordinates, ρ is the density, C_p the specific heat, k is the thermal conductivity. Equation (1) holds for both mold base and plastic part with modification on thermal properties.

3.2 Initial condition

The initial mold temperature is assumed to be equal to the coolant temperature. The initial part temperature distribution is received from the analysis results at the end of filling (EOF) and packing (EOP) stages.

$$T(0, \vec{r}) = \begin{cases} T_c, & \text{for } \vec{r} \in \Omega_m \\ T_p(\vec{r}), & \text{for } \vec{r} \in \Omega_p \end{cases} \quad (2)$$

3.3 Boundary condition

Heat from the molten plastic part is released by the coolant flowing in cooling channel as well as the ambient air surrounding the exterior surfaces of the mold base through a heat convection mechanism. For this research, the effect of thermal radiation is disregarded. The conditions defined over the boundary surfaces and interfaces of the mold are specified as,

$$\text{for } t \geq 0, \quad -k_m \frac{\partial T}{\partial n} = h(T - T_0) \quad (3)$$

where n is the normal direction of mold boundary. On the exterior surfaces of the mold base Γ_m :

$$h = h_{air}, T_0 = T_{air} \quad \text{for } \vec{r} \in \Gamma_m \quad (4)$$

On the cooling channel surfaces Γ_c :

$$h = h_c, T_0 = T_c \quad \text{for } \vec{r} \in \Gamma_c \quad (5)$$

When h_c and h_{air} are heat transfer coefficients of coolant and air.

4 PLASTIC FLOW ANALYSIS

4.1 Conformal cooling system design

In this research, the conformal cooling system was designed for sub insert component as shown in Figure 3. Pattern of cooling line is spiral as shown in Figure 4.

In spiral cooling system, the coolant flow from the bottom to the top of the spiral pattern. The temperature of the coolant increased as it flows through the spiral channel, while the melt gradually cooled down to some degree due to heat transfer from the melt to the coolant. Cooling channel cross section was designed as a freeform shape in the order to coolant flow area increasing. The distance between cooling channel and outer surface of sub insert is approximately 3.0 mm and

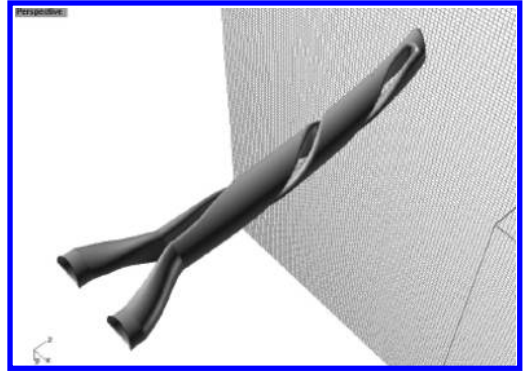


Figure 4. Spiral cooling type for mold sub insert.

cooling channel diameters at the inlet and outlet are equally 10.0 mm.

4.2 Finite element model preparation

Rhinoceros 4.0 which is computer program was used for part model, feeding and cooling system creating. After that all of plastic injection mold system and components were created into solid mesh model in Moldex3D R11.0. Mesh size of part model is approximately 0.8 mm due to part model thickness. The flow chart of finite element model preparation in this research is shown in Figure 5.

4.3 Plastic flow analysis

The computer program which used for analysis of plastic flow behavior and cooling efficiency is Moldex 3D R11.0. By the injection conditions are set as below and Figure 6 illustrates PVT diagram of the material.

Material properties

- Melt temperature = 220 °C
- Ejection temperature = 100 °C
- Freeze temperature = 120 °C
- Plastic density = 1.06 g/cm³
- Melt flow index 220,5 = 17 g/10 min

Injection condition setting

- Filling time = 2.5 sec
- Packing time = 6.0 sec
- Plastic injection volume = 42.77 cm³
- Maximum injection pressure = 155 MPa
- Cooling time = 80 sec
- Coolant type = Oil
- Initial coolant temperature = 70 °C

The results of computer simulation shows that cooling time reduced from 199.67 sec to 121.64 sec when compare between conventional and conformal

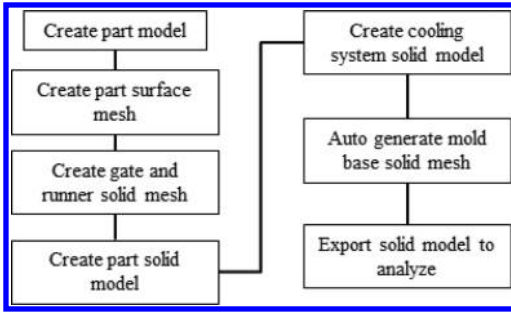


Figure 5. Flow chart of FEM preparation.

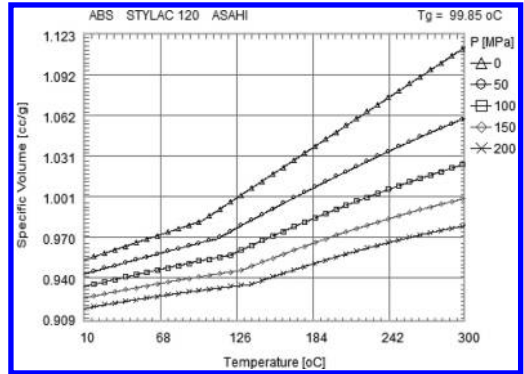


Figure 7. PVT diagram of ABS (Stylac 120).

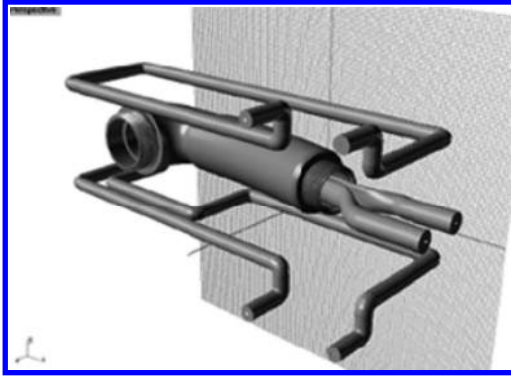


Figure 6. Part and cooling system model.

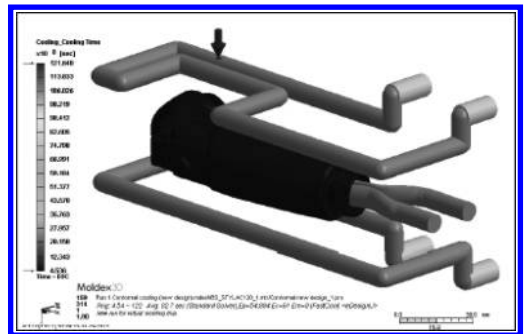


Figure 8. Cooling time at EOC result.

cooling. The average part cooling temperature at the end of cooling stage (EOC) reduced from 110.56 °C to 86.59 °C due to conformal cooling system designs for sub insert. Furthermore computer simulation shows result of part warpage total displacement that reduced from 2.85 mm to 1.39 mm.

5 MOLD INSERT FABRICATION AND EXPERIMENT

5.1 Mold insert fabrication

The technique that used for sub insert with conformal cooling system fabrication is Direct Metal Laser Sintering (DMLS) process as mention above. The DMLS machine is illustrated in Figure 8. The powder metal for sub insert fabrication is steel grade P20. Figure 10 illustrates sub insert with conformal cooling system from DMLS process.

5.2 Plastic injection process experiment

Injection machine was chosen for experiment is NISSEI injection machine size 150 tons. The



Figure 9. DMLS machine.

coolant temperature of conformal cooling system was controlled with mold temperature controller. Quantity of plastic injection part in this experiment is equally 100 Pcs. After the injection process experiment, plastic injections part were measured



Figure 10. Sub insert from DMLS process.



Figure 11. Rinsing spray product.

and assembled with other plastic components as shown in Figure 11 for operation testing.

The results from plastic injection experiment show that cycle time reduce approximately 35.0 sec according to computer simulation. Conformal cooling provided lower temperature at sub insert more than conventional method. Hence cycle time of injection mold with conformal cooling can be decreased. For product testing result, plastic injection parts could assembly with other components and passed the dimension checking process.

6 CONCLUSION

The aims of this research work were to decrease limitation of conventional cooling method and reduce cycle time of plastic injection process. Conformal cooling design can solving problems of limitation from conventional cooling method such as mold component with small, curvature and

complex shape. The design of coolant flow line type such as spiral or parallel type should consider with dimension and part shape. From the simulation result, conformal cooling not only decreases cooling time but also part warpage problem due to decreasing of temperature differentiation between mold insert, core and cavity plate.

ACKNOWLEDGEMENT

This work was supported by Thai-German Institute (TGI) for laser sintering machine and Coretech system (Thailand) for Moldex3D R11.0 computer program.

REFERENCES

- [1] Lin, J.C. 2002. Optimum cooling system design of a free-form injection mold using an Adductive network. *Journal of Materials Processing Technology*, Volume 120, 15 Jan 2002, Issues 1–3: 226–236.
- [2] Park. H.S and Pham. H.N. 2009. Design of conformal cooling channels for an automotive part, *International Journal of Automotive Technology*, Volume 10, No. 1: 87–93.
- [3] Tang. S.H, Kong. Y.M, Sapuan. S.M, Samin. R, Sulaiman. S. 2006. Design and thermal analysis of plastic injection mould, *Journal of Materials Processing Technology*, Volume 171.: 259–267.
- [4] Sánchez. R, Aisa. J, Martínez. A, Mercado. D. 2012. On the relationship between cooling setup and warpage in injection molding, *Measurement*, Volume 45, June 2012, 1051–1056.
- [5] Kovács. J.G, Sikló. B. 2011. Investigation of cooling effect at corners in injection molding, *International Communications in Heat and Mass Transfer*, Volume 38, Issues 10: 1330–1334.
- [6] Hassan. H, Regnier. N, Ce'dric Le Bot, Defaye. 2010. G, 3D study of cooling system effect on the heat transfer during polymer injection molding. *International Journal of Thermal Sciences*, Volume 49, Issues 1: 161–169.
- [7] Rannar. L-E, Glad. A, Gustafson. C-G. 2007. Efficient cooling with tool inserts manufactured by electron beam melting, *Rapid Prototyping Journal*: 128–135.
- [8] Altaf. K, Raghavan. V.R, Rani. A.M.A. 2011. Comparative thermal analysis of circular and profiled cooling channels for injection mold tools, *Journal of applied science*, Volume 11, Issues 11: 2068–2071.
- [9] Mayer. S, Optimised mould temperature control procedure using DMLS. EOS GmbH Electro Optical Systems, www.eos.info.
- [10] Yan-Chen Chiou, Ya-Yuen Chou, Hsien-Sen Chiu,, Chau-Kai Yu, Chia-Hsiang Hsu, *Integrated true 3D simulation of rapid heat cycle molding process*. CoreTech System Co., Ltd., www.moldex3d.com.

Study on the space layout of rural residents in Fusong county of Jilin Province

Rui Qing Qie

Department of Land Resource Management, Jilin Agricultural University, Changchun, China

ABSTRACT: We determined weight of indicators by means of AHP (Analytical Hierarchy Process) and applying the geographical spatial analysis of GIS according to six evolution indicators and physical condition and location factor, which classified rural residents in Fusong county to four levels including high potential development region, middle potential development region, low potential development region, not suitable for development region.

Keywords: rural settlements; spatial distribution and optimization; Fusong county

1 INTRODUCTION

With the construction of new socialist countryside, the rural settlements and county planning has accumulated many successful experiences, there are also some problems and deviation mainly in the absence of specific measure for local conditions and classification regulation principle, and the link with the relevant planning is not close enough^[1]. According to the characteristics of temporal and spatial distribution of settlements in Fusong county, we construct evaluation index system of rural residential comprehensive development strength, combine the evaluation result with the regional development planning and optimize the layout of residential land in order to provide reference for the planning of rural residents in other areas of Jilin Province.

2 STUDY AREA AND RESEARCH METHODS

2.1 The general situation of research area

Fusong county is located in the southeast of Jilin Province, the upper reaches of the Songhua River, northwest of Changbai Mountain, the northeast of Baishan City, longitude 127°–128° 06' 01', latitude 41° 42'–42° 49'. It borders with Huadian City and Dunhua City bounded by Songhua River in the north, borders with Linjiang City and South Korean Nationality Autonomous County in the south, neighbor on Antu county and Democratic People's Republic of Korea. It is 125 km long from north to south and 87 kilometers wide.

Table 1. Classification indicators value and weight of comprehensive development potential of rural residential area in research area.

System	Indexes	Level 1 (3 points)	Level 2 (2 points)	Level 3 (1 points)	Level 4 (0 points)	Weight
Natural condition	Slope (°)	0–6	6–15	15–25	>25	0.0881
	Distance from the river (m)	500–1000	1000–1500	1500–2000	<500 or >2000	0.1508
Location condition	Residential area (hm ²)	>10	5–10	1–5	<1	0.1827
	Distance from motorway exit (m)	<1000	1000–2000	2000–3000	>3000	0.2272
	Distance from train station (m)	1000–2000	2000–3000	3000–4000	<1000 or >4000	0.1121
	Distance from the town (m)	<1000	1000–2000	2000–3000	>3000	0.2391

2.2 Data sources and processing

Data sources: The current land use map of Fusong County in 2011, Fusong County 1:5 million topographic map, The overall planning of land use in Fusong County (2006–2020), Fusong statistical yearbook (2011). Data processing: we extraction rural residential data from land use status map of Fusong County, generate Shape file format by GIS software.

2.3 The establishment of evaluation index system

The index mainly includes topography, body of water and residence area in natural conditions^[2,3]. Consider the gradient of 25 degrees, the distance of 500 m and 2500 m waters as residential land natural condition critical value. The indexes in the location are chosen including the train station distance, distance to motorway exit and the distance of the town. Determine the index weight value by Hierarchy analysis software Yaahp 5.5 shown as [Table 1](#).

Table 2. Settlement distribution at different slope levels of Fusong county.

Slope	Slope level	Residential area/hm ²	Ratio/%
0°–6°	I	5118.34	76.13
6°–15°	II	1450.04	21.57
15°–25°	III	137.46	2.04
>25°	IV	17.54	0.26
Total		6723.38	100.00

Table 3. Settlement area in river buffers.

Distance/m	Residential area/hm ²	Ratio/%
500–1000	1458.72	21.70
1000–1500	776.22	11.55
1500–2000	424.23	6.31
<500 or >2000	4064.21	60.45
Total	6723.38	100.00

Table 5. Settlement area in road and railway buffers.

Road distance (m)	Residential area (hm ²)	Ratio (%)	Railway distance (m)	Residential area (hm ²)	Ratio (%)
<1000	1750.29	26.03	1000–2000	329.17	4.90
1000–2000	911.76	13.56	2000–3000	532.27	7.92
2000–3000	921.74	13.71	3000–4000	814.54	12.12
>3000	3139.59	46.70	<1000或>4000	5047.40	75.07
Total	6723.38	100.00	Total	6723.38	100.00

3 ANALYSIS ON DISTRIBUTION CHARACTERISTICS OF SPATIAL RESIDENTS

3.1 Different slope of rural settlements distribution analysis

We make statistic on the attribute table according to the classification criterion of slope by GIS software, then the distribution of different slope residential was shown as [Table 2](#).

3.2 Analysis of rural residents nearby rivers condition

Make buffer analysis based on the linear river surface layer to 500 m interval buffer distance, then classify to four levels including 500–1000 m, 1000–1500 m, 1500–2000, less than 500 m or more than 2000 m. At last, make overlay analysis with the layers and the settlements distribution layer to get the relationship between residential distribution and far and near distance to the river. The results was shown as [Table 3](#).

3.3 Analysis of rural residential area

According to the land use map of Fusong County in 2011, first we make the residential area classification which detail is shown as [Table 4](#).

3.4 Analysis of rural settlements in the external traffic conditions

Make buffer analysis based on the linear road layer^[4], then classify to four levels including less than 1000,

Table 4. Settlement distribution at different slope levels of Fusong county.

The scale of residential (hm ²)	Residential area (hm ²)	Ratio (%)
>10	5274.37	78.45
5–10	663.85	9.87
1–5	596.32	8.87
<1	188.84	2.81
Total	6723.38	100.00

Table 6. Settlement area in river buffers.

Distance (m)	Residential area (hm ²)	Ratio (%)
<1000	729.72	10.85
1000–2000	290.44	4.32
2000–3000	386.00	5.74
>3000	5317.22	79.09
Total	6723.38	100.00

1000–2000 m, 2000–3000, and more than 3000 m. Make buffer analysis based on the railway layer, then classify to four levels including 1000–2000 m, 2000–3000, and 3000–4000 and less than 1000 or more than 4000 m. At last, make overlay analysis with the two layers to get the rural residents of Fusong county traffic condition shown as Table 5.

Make buffer analysis based on the town layer, then classify to four levels including less than 1000, 1000–2000 m, 2000–3000, and more than 3000 m. At last, make overlay analysis with the result layers and the settlements distribution to get distribution of settlements and town near and far distance shown as Table 6.

4 THE RESULTS OF COMPREHENSIVE POTENTIAL

We study on quantitative analysis of each evaluation factor with analysis of the distribution characteristics and combine the influence degree of each index for residential development^[5]. A scientific evaluation can be gotten by the available calculation formula (1).

$$\begin{cases} S = 0 & V_k = 0 \\ S = \sum_{\gamma=1}^N W_k \cdot v_k & V_k \neq 0 \end{cases} \quad (1)$$

S—the score of comprehensive development potential of rural residential
 n—Evaluation factor
 W_k—The weight of the k factor
 V_k—The quantitative values of the k factor.

We can divide residence areas into 4 different levels according to Table 7, thus we will find that 77.02% of Fusong County residential land are low potential development area and unsuitable development potential area.

5 DISCUSSION AND CONCLUSION

We determined weight of indicators by means of Analytical Hierarchy Process and applying the geographical spatial analysis of GIS according to six

Table 7. Evaluation results of comprehensive development potential of rural residential area in research area.

Evaluation level	Value	Residential area (hm ²)	The percentage (%)
High development potential area	1.68–2.46	607.94	9.04
Middle development potential area	1.11–1.68	936.94	13.94
Low development potential area	0.57–1.11	2489.31	37.02
Unsuitable development potential area	0.00–0.57	2689.19	40.00

evolution indicators from physical condition and location aspect, which classified rural residents in Fusong county to four levels including high potential development region, middle potential development region, low potential development region, not suitable for development region.

Rural residential is the main source of the urban construction land index, to promote rural resources re integration, we need strengthen the rural infrastructure construction, land transfer and scientific planning and space orderly layout. Residential layout optimization can alleviate the need for construction land, reducing the number of new construction land, conducive to state farmland protection and food security, help protect the environment, and promote the process of urbanization and new rural construction.

REFERENCES

- [1] Su G.H., Chen F.Z., Zhengx Q., et al. Analysis of Dynamic Evolution Mechanism of Rural Settlements Land Expansion in the Progress of Urbanization [J]. Journal of Anhui Ash. Sci, 2009, 37(19):9075–9077, 9083.
- [2] Andrew J. Hansen, Daniel G. Brown. Land-use change in rural America: Rates, drivers, and consequences[J] Ecological Applications, 2005, 15(6):1 849–1 850.
- [3] Carmen C.F., Elena G.I. Determinants of residential land use conversion and sprawl at the rural-urban fringe [J]. American Agricultural Economics Association, 2004, 86(4):889–904.
- [4] Li X., Meng Q.X., Li Y. Research on intensive utilization potential of rural residential areas-taking Change city in Henan province as an example [J]. Journal of Northwest A & F University (Natural Science Edition), 2011, 39(5):51–58, 64.
- [5] Jiang G.H., Zhang F.R., Tan X.J. Spatial structure adjustment of rural residential land in Pinggu district, Beijing [J]. Transactions of the Chinese Society of Agricultural Engineering, 2008, 24(11):69–75.

On the emotional orientation of surface architecture

Hui Ma

Art and Design Academy of Jilin Jianzhu University, Changchun, China

ABSTRACT: As a certain stage of architectural style development, surface architecture refers to the architecture that has the tendency of surface design. The organization structure of architectural surface design of surface architecture has the characteristics of interweaving, penetrability and replication. The interweaving promotes the entanglement and connection of form and consciousness. The penetrability guides the thinking and imagination of environment and artistic conception. The replication accumulates and spreads the experienced moods and emotions. From the perspective of emotional design, this paper examines the emotional characteristics of surface architecture and the environmental experience of instinct level, behavior level and rethink level of the emotional architectural design driven by the surface.

Keywords: surface architecture; emotional design; interweaving; penetrability; replication

1 INTRODUCTION

The explanation of surface in *Ci Hai* is the outermost layer of cells of plant. Wikipedia gives three definitions. On plants, surface is a layer of cells on the surface of the leaves and buds. On vertebrates, surface is the outer layer of skin. On invertebrates, surface is the outer layer of the cell. In the book of *Surface*, the philosopher Avrun Stroll understands it as the “physical surface”, “abstract surface” and “the abstract surface of physicalism” on the physical layer. According to this, we can understand the architectural surface as “the external interface of architecture which has material, texture and color visual characteristics with two-dimensional attribute”, “the surface of architecture which has its own structure and the shrouded and decorative function for the building and is independent of building”, and “the main body of the building in which the architectural structure and system are integrative”. As a certain stage of the architectural style development, the surface architecture is expressed and highlighted through surface by architectural design in the minimalist architecture and it refers to the architecture that has the tendency of surface design. The color, texture, structure relations and material attributes of surface architecture are aroused through visual sense and tactile sense.

“Twelfth five-year” social science research project of the education department in Jilin province (Ji UNESCO co word [2012] No. 463th) “The emotional orientation research of the texture in surface architecture”.

The understanding and feeling achieved through experience about the form and content of architectural surface make the surface architecture has clear emotional orientation.

In accordance with the way that construction and main body feel and maintain the relationship, the emotional design can be divided into three levels: the instinct level, behavior level and rethink level design. Instinct level focuses on the external form and the intuitive reaction of the space. Behavior level pays attention to the simple, convenient, comfortable, smooth, durable and saving characteristics in the process of behavior. Rethink level concerns our attitude towards life and the meaning of our life. In the environment, the surface architecture is showed in a variety of external forms and presents some characteristics which can be communicated, experienced and perceived. These characteristics are the bridge and medium of surface architecture form, structure and main body feelings.

2 THE INTERWEAVING OF SURFACE

When some texture organization structure of surface architecture presents the crisscross, uneven, interlocked and rough smooth interlaced changes, at the same time, with the characteristics of the explicit form, the related reaction about the emotion occurs, then the characteristics that the surface organization structure interweaves and changes with the psychological feelings are called the interweaving of surface. Interweaving drives the emotions and feelings through the form, stimulates the brain to store,

understand, organize and reconstruct the information, promotes the entanglement and connection of form and consciousness and reaches the effect that to create a rich emotional experience site.

The transparent church designed by Belgian designer Gijs Van Vaerenbergh (combination of Belgian architect Pieterjan Gijs and Arnout Van Vaerenbergh) in Limburg province of Belgium (as shown in Fig. 1) is a 10 meters high building with special structure and has 100 layers that are built with 2000 pieces steel discs. The steel discs form the beautiful interlaced effect through lapping. When the light casting, the mysterious mesh-shaped enclosure is built by construction and light and shadow. The uncertainty of the boundary of enclosure and the stretch of light and shadow make the space more blurred and mysterious. In this atmosphere, the main building and god also seems to have some connection and the possible of conversation due to the existence of the medium. As the building, 2000 pieces steel discs not only connect the external and internal space of the building, but also connect the external real space with the image of spiritual world.

The design of the transparent church mobilizes the design mechanism of instinct level and performs very well on the rhythm and the relation between unreality and reality of the instinct level materials, but the thinking and image caused on the rethink level make construction has profound connotation and special quality.

3 THE PENETRABILITY OF SURFACE

Surface architecture often uses the virtual and real combination method formed by the arrangement and organization of building materials to perform the relationship between entity and vanity directly or indirectly, or directly through the surface materials to reach the effect of visual penetration and extension of thought. Surface materials and environment together constitute the unique effect with the visual penetrability. The visual penetrability will go through the boundary of materials and guide the audience and the behavioral agent to continue thinking and imaging the environment and artistic conception, such characteristics are called the penetrability of surface architecture. The penetrability helps interface to complete the function and constructs the artistic conception and the rhythm that the design wants to convey to let the imaginary space run arbitrarily. This is the so-called things have end and meaning is infinite. The penetrability can also mobilize other sense organs of the body like the sense of smell and hearing to build the atmosphere of the environment together.

The Derwent river bank public corridor GASP project (Glenorchy Art and Sculpture Park) (as shown in Fig. 2) designed by Australian architectural studio Room 11 is a community Park which



Figure 1. The transparent church in Belgium (Source: internet).



Figure 2. Derwent river bank public corridor GASP project (Source: internet).

includes Art center, activity space for children and the public exhibition hall. The building is located in beautiful coastal area and the core content of the design is a public corridor and architecture which was built along the Glenorchy Derwent. How to integrate the background of the seashore of the building with the building is the key to the success or failure of the architectural design. The overall planning is divided into three phases. One of the main part is the exhibition hall which is near the coastal area. The architectural design of the exhibition hall is composed of concrete and red glass, this forms the architectural features with distinctive surface. The using of the red glass makes the construction has the very good visual penetrability. Walking in the exhibition building, we can have a panoramic view of the beautiful seashore landscape. The winding skyline is casting on the glass and forms special landscape. The red rendering makes the building enveloped in the evening glow and this sends out the thick art atmosphere. The whole environment is full of charm due to the permeability characteristic of glass materials. Visitors can not only view the landscape and enjoy the cool, but also can feel the subtle changes of the weather, the flying seabirds and the sound of sea waves.

Architects break down barriers of the interface communication with the aid of penetrability of architectural surface materials and make the building inside and outside become a community. The powerful screen effects from visual sense and auditory participation and experience touch the direct multiple perception of instinct level. The quiet view and admire and rich environmental experience are the perfect interpretation of the instinct level of emotional design.

4 THE REPLICATION OF SURFACE

Replication is the most obvious characteristic of material language of surface architecture. Its characteristics are that the materials of architectural surface can regard the fragment of architectural form as the texture unit and reproduce it through a certain pattern and shape, then to form a kind of organized and orderly formal system. The unit itself which can be reproduced exists the diversity of model and the whole unit has the possibility of unlimited replication and the ductility of sustained growth. Theoretically, such unit which has the characteristics of material properties can cover any size surface of architecture and has the characteristics that can be grown.

Take the Tales Pavilion designed by Italian designer Luca Nichetto in Lido, Chaoyang in

Beijing for example (as shown in Fig. 3). This is an unique building. This building which is good at telling stories is popular with high emotional design investment. The designer uses magic technique to cover the whole exhibition hall with more than 1200 copper pipes. These copper pipes in the hands of the designer turn into forceful “grass” and with the change of time these “copper grass” will change colors on their own initiative like natural grass with the signs of life. On the processing of architectural surface, the designer lines each copper pipe and makes the architectural surface form uniform with replication. Although the unit form is simple, the restriction of rules makes it no longer an individual copper pipe but the “shape” of architectural surface, thus a kind of continuous and extended surface architecture characteristic without center which is obtained through repetition is presented. The results of 1200 times repetition make the copper pipe has special biological characteristics, so the appearance characteristics of the “grass” are more intense with the bending processing on the top and the repeated visual effect and psychological mapping are generated in the process of repetition. The emotions and moods experienced by the main body are accumulated and continue to be spread with the simple and constant repetition. The sites are also filled with a large amount of simple atmosphere. Such atmosphere will continue to play a role in the process of behavior experience.



Figure 3. The Tales Pavilion in Beijing (source: internet).

5 CONCLUSION

From the perspective of emotional design, this paper states the interweaving, penetrability and replication characteristics of surface architecture. Through three actual cases, the paper explains the function of the specific characteristics in the surface architectural design and how to use the surface design to mobilize the senses and to guide the in-depth experience of the emotional design in instinct level, behavior level and cognition level.

REFERENCES

- [1] Huima, 2012 (03). The Study of Emotional Design and Its Spatial Characteristics [J]. Trends in Building Materials Research.
- [2] Chen Juan, Mo Tianwei. 2008 (05). From Architectural Surface to Surface Architecture [J]. New Architecture.
- [3] Written by [U.S.] Donald Norman. Translated by Fu QiuFang, Cheng Jinsan. Emotional design [M]. Beijing Electron Industry Press, 2005 (05).
- [4] Written by [Denmark] S.E. Rasmussen. Translated by Liu Yafen. Experiencing Architecture [M]. Beijing Intellectual Property Publishing House, 2003 (02).

Effect of refrigerant charge and TXV opening on the performance of air-source heat pump water heater

Zhi Hua Wang

School of Energy and Power Engineering, Xi'an Jiaotong University, Xi'an, Shanxi, China

ABSTRACT: This paper describes the experiment carried out to analyze the effects of improper refrigerant charge and incorrect TXV (Thermal Expansion Valve) opening on the air-source heat pump water heater using R134A. The performance of the system were measured in combinations of four refrigerant charges of 70%, 85%, 100% and 115% of the optimal value and three TXV opening of 30%, 45% and 60% of full opening at ambient temperature of 20D/15W (dry-bulb temperature/wet-bulb temperature). The results showed that the maximum COP was nearly 33%, 31.9% and 4.4% higher than that of 70%, 85% and 115% of the optimal refrigerant charge at 60% TXV opening, respectively. And it was found that the increase in TXV opening can enhance COP when water temperature exceeded 30°C.

Keywords: heat pump; water heater; refrigerant charge; TXV opening

1 INTRODUCTION

The Air-Source Heat Pump Water Heater (ASHPWH) system has been drawn extensive attention for its high efficiency, energy-saving recently [1] and [2]. However, incorrect opening of expansion valve and improper refrigerant charge will deteriorate the system performance.

Improving the ASHPWH system performance, reliability, and its environmental impact has been also an ongoing concern. Many studies have been undertaken in an attempt to overcome this weakness of the air-source heat pump.

Baek et al. [3] studied that the control methods of the gas-cooler pressure in a CO₂ heat pump by varying the refrigerant charge, compressor frequency, EEV opening, and outdoor fan speed at various outdoor temperatures. Palmiter et al. [4] investigated the effect of airflow and refrigerant charge on the seasonal performance of an air-source heat pump using R410A. Kang et al. [5] optimized an avionic cooling system using R236fa by varying the refrigerant charge and the expansion valve opening. The effects of refrigerant charge on the performance of the water-to-water heat pump using R407C were measured by applying the capillary tube and the EEV as an expansion device under various charging conditions [6].

Previous studies indicated that improper refrigerant charge and incorrect opening of expansion valve would penalize the performance of heat pump. However, their results are mostly limited to air conditioners, very few tests have been performed

with the ASHPWH system, the principle of which is similar, but there are some great differences in condensing temperature, compressor discharge temperature and compression ratio compared with heat pump air-conditioning. Therefore, it is essential for studying the effect of improper refrigerant charge and incorrect TXV opening on the thermal performance of the ASHPWH system.

The main objectives of this study are to provide experimental data on the performance of a ASHPWH system which uses environmentally friendly refrigerant of R410A and to investigate the system optimization with respect to the variation of refrigerant charge amount, TXV opening at ambient temperature of 20D/15W when 120 L water is heated from 15 to 55°C.

2 EXPERIMENTAL SETUP AND PERFORMANCE CALCULATION

2.1 System description

A schematic diagram of the experimental setup to measure the performance of the ASHPWH system by varying the refrigerant charge and opening of expansion valve at ambient temperature of 20D/15W was illustrated in Figure 1. The discharged R134A refrigerant from the compressor unit flows into condenser which wraps around outer of the water tank, and reject the heat to cold water, and then flows through the filter-drier. The dried and filtered R134A refrigerant throttled by the TXV enters the evaporator, in which R134A

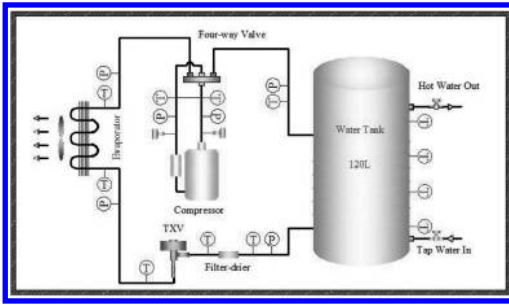


Figure 1. The schematic of air source heat pump water heater system.



Figure 2. Experimental set up air source heat pump.

absorbs heat from air, finally, the superheat R134A enters the compressor unit that accomplish a cycle.

2.2 Experimental setup

Figure 2 shows the experimental set up for air-source heat pump water heater system. This test rig was consisted mainly of rotary compressor, evaporator, TXV and condenser. The experimental setup used the Mitsubishi RB174GHAC type rotary compressor which swept volume was $17.4 \text{ cm}^3/\text{r}$, built-in overload protection device (which were on/off in 0.15 MPa and 0.25 MPa in suction and discharge pressure) with rated power supply of 380 V, 50 Hz, and rated power of 600W. Finned-tube heat exchangers was used as the evaporator, which was made of copper tubes with aluminum fins and outer diameters. The condenser was made up of a smooth copper tube ($\text{Ø}9.52 \times 0.5$, length $4.6 \times 104 \text{ mm}$), which was wound into a spiral shape around the water tank. The curvature radius of the coil was 0.16 m. TXV was used and the capacity of the thermal storage tank was 120 L. In this experimental system, R134A was used as the working fluid.

Table 1. Main characteristics of the plant instrumentation.

Measured variable	Measurement device	Calibration range	Calibrated accuracy
Temperature (°C)	Platinum resistance	-100~150 °C	$\pm 0.1 \text{ }^\circ\text{C}$
Temperature (°C)	T-type thermocouple	-50~150 °C	$\pm 0.2 \text{ }^\circ\text{C}$
Pressure (MPa)	Pressure transducer	0~6	$\pm 1\% \text{ FS}$
Power (kW)	Power meter	0.01~24.00	$\pm 0.01\%$ of full scale
Weight (Kg)	High-precision electronic scale	0~20	$\pm 0.1 \text{ g}$

The experiment was carried out in enthalpy difference laboratory which was consisted of adiabatic indoor and outdoor rooms. In order to estimate the performance of the system, the temperature and pressure of the refrigerant were measured and the instruments were located in the test rig that was shown in Figure 1, such as the inlet and outlet of the compressor and so on. Platinum resistance temperature sensor and T-type thermocouple were installed to measure water temperature and refrigerant temperature. All the temperature sensors were well calibrated in a controlled temperature bath using standard precision mercury glass thermometers. The error of the pressure transducer was less than $\pm 1\% \text{ FS}$ (6 MPa). Table 1 summarizes the main characteristics of the plant instrumentation.

3 RESULTS AND DISCUSSION

Experiment using the experimental ASHPWH on the heating performance under various refrigerant charge and TXV opening were carried out, and the experimental data were collected only after adequately prepared to ensure measuring stability and accuracy.

3.1 Effect of refrigerant charge on the system performance

In order to characterize energy efficiency of this ASHPWH system, the value of the system COP was used. Figure 3 has been drawn to show the variations of COP according to the refrigerant charge and TXV opening. The operating conditions for the ASHPWH system were shown in Table 2. It should be noted that the refrigerant charge and TXV opening had many adjustments before the experiment was carried out to avoid the condenser

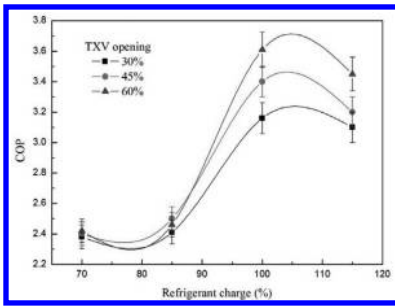


Figure 3. Effect of refrigerant charge on COP at various TXV opening.

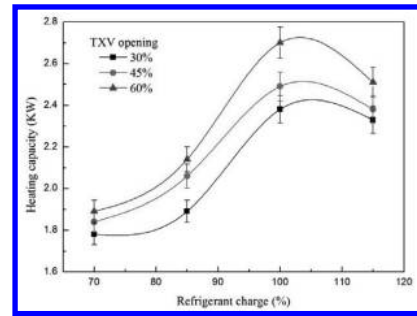


Figure 4. Effect of refrigerant charge on heating capacity at various TXV opening.

Table 2. Operating conditions for ASHPWH system.

Ambient temperature (°C)	Water temperature (°C)	Refrigerant charge (%)	TXV opening (%)
20D/15 W	15 to 55	70	30
			45
			60
		85	30
			45
			60
	100	100	30
			45
			60

pressure was too high which activated the pressure switch and safety shut down of the compressor, and to ensure the smooth running of the experiment.

As can be seen from Figure 3, with the refrigerant charge increased, there were similar tendency of COP under the various TXV opening, the system COP increased to a point and then tended to decrease, and there was a maximum COP. The system showed the maximum COP which was around 3.6 at the optimal refrigerant charge when the TXV opening was 60%. This can be explained that the mass flow rate of refrigerant was very low when the refrigerant charge was insufficient and TXV opening was small, which resulted in longer heating time and large power consumer. But it has small influence on the performance of the system when refrigerant charge over the optimal value. And it was nearly 33%, 31.9% and 4.4% higher than that of 70%, 85% and 115% of the optimal refrigerant charge at 60% TXV opening, respectively. Besides that, the COP of the system was about 5.5% and 12.2% higher than that of 45% and 30% TXV opening respectively at the 70% of the optimal refrigerant charge.

The effect of refrigerant charge and TXV opening on the heating capacity is illustrated in Figure 4.

Similar variation pattern to that shown in Figure 3 can be seen. The increase of the system heating capacity slowed down when it increased to a certain value, it increased from 1.9 kW to 2.68 kW first if refrigerant charge increased from 70% to 100% and then decreased to 2.4 kW if refrigerant charge increased from 100% to 115% at the 60% TXV opening. It was obvious seen that the maximum was around 2.3 kW at the optimal refrigerant, which was 9.5% and 14.2% higher than that of 45% and 30% TXV opening. As seen, the heating capacity of the experimental ASHPWH was reduced slowly at 60% TXV opening when the refrigerant charge exceeded optimal value.

3.2 Effect of water temperature on COP

Figure 5 shows the COP of the system with respect to water temperature under various TXV opening. It obvious that there were huge differences among TXV opening was 30%, 45% and 60%. The COP increases quickly in the earlier stage of the water temperature. Moreover it descended linearly from around 5.8 to 2 when water temperature exceeded 20 °C at 45% and 60% TXV opening. This was because with the condenser temperature increasing, the compression ratio and the irreversibility increased and led to the system performance deviated from the optimal working condition. However, compared with two controls which were mentioned above, the maximum COP at TXV 30% opening was only about two thirds of 60% TXV opening. This illustrated that the TXV opening had great influence on the COP of the system. It was worthy point out that the COP curves of TXV opening was 45% and 60% had a cross-point when the water temperature was around 30 °C, and the COP of 45% TXV opening was higher than that of 60% TXV opening at the left-side of the point, but in contrast at the right-side of the point. Because there was a large temperature difference between water and refrigerant that caused higher heat

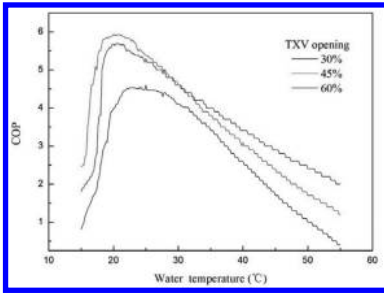


Figure 5. Effect of water temperature on COP at various TXV opening.

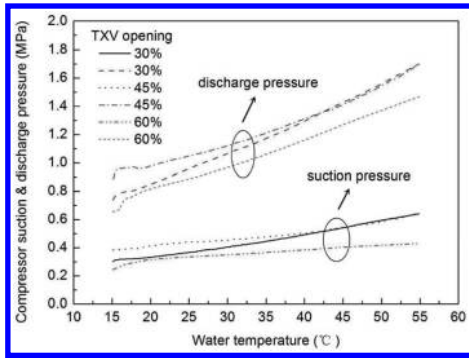


Figure 6. Effect of water temperature on compressor discharge and suction pressures at various TXV opening.

transfer rare, but as the temperature difference decreased, it resulted in performance of the system reduced. As the condenser temperature increase, more refrigerant volume was required to be sent to the high pressure side [7]. So we can increase the TXV opening to enhance COP of the system when water temperature exceeded 30°C.

3.3 Effect of water temperature on the compressor suction and discharge pressure

Figure 6 indicates the measured variation profiles of compressor discharge pressure and suction pressure during the water temperature was from 15°C to 55°C when the refrigerant charge was the optimal value at various TXV opening. The compressor discharge and suction pressures decreased with the TXV opening increased at a certain water temperature. This was because increasing TXV opening resulted in refrigerant volume increasing. As it can be seen in Figure 6, the compressor discharge and suction pressures increased with the increasing water temperature, and the discharge pressures variation for the system responded to a nearly straight linear function of the water

temperature but the compressor suction pressures varies relatively smoothly. It has been determined that the compressor ratio of the system increases with rising water temperature and more compressor power was required, which caused the COP of system decreased. It was found that the compressor discharge and suction pressure of the 30% and 45% TXV opening were almost the same but the 60% TXV opening had risen relatively slowly when the water temperature exceeded around 43°C. This illustrated that TXV opening more significant impact on the system performance at high water temperature. It was worth noting that the compressor discharge and suction pressure were unstable during startup, which contributed to refrigerant migration characteristics, in other words, during startup process, a large quantity of refrigerant left the evaporator and entered the accumulator and condenser, the refrigerant in the accumulator gradually evaporated and moved to other components, but the evaporator was starving that resulted in suction pressure dropped rapidly, and the condenser was opposite, all of these caused suction and discharge pressure fluctuations and then they were gradually stable.

4 CONCLUSIONS

This paper reports an experimental investigation on the dynamic performance of an air-source heat pump water heater. The effect of operating parameters on the system performance were analyzed and the conclusions are as follows:

1. Improper refrigerant charge and incorrect TXV opening have significant impact on system performance, the maximum COP was nearly 33%, 31.9% and 4.4% higher than that of 70%, 85% and 115% of the optimal refrigerant charge at 60% TXV opening, respectively.
2. The effect of refrigerant charge and TXV opening on the heating capacity were similar to COP. The system heating capacity increased from 1.9 KW to 2.68 KW first when refrigerant charge increased from 70% to 100% and then decreased from to 2.4 KW when it increased from 100% to 115% at the 60% TXV opening. It shows that less the optimal refrigerant charge had a greater influence on the performance of ASHPWH system than over the optimal value.
3. TXV opening more significant on COP at high water temperature, there was a cross-point in COP curves between 45% and 60% TXV opening when the water temperature was around 30°C. This result suggested that increasing the TXV opening can enhance the COP of the system when water temperature exceeded 30°C. Besides, TXV opening was increased can also

decrease the compressor ratio at high water temperature.

REFERENCES

- [1] K.J. Chua, S.K. Chou, W.M. Yang, Advances in heat pump systems: a review, *Appl Energy*. 87 (2010) 3611–3624.
- [2] T.T. Chow, G. Pei, K.F. Fong, M. He, Modeling and application of direct-expansion solar-assisted heat pump for water heating in subtropical Hong Kong, *Appl Energy*. 87 (2010) 643–649.
- [3] C. Baek, J. Heo, J. Jung, H. Cho, Y. Kim, Optimal control of the gas-cooler pressure of a CO₂ heat pump using EEV opening and outdoor fan speed in the cooling mode, *Int J Refrig*. 36 (2013) 1276–1284.
- [4] L. Palmiter, J.H. Kim, performance of an air-source heat pump using R-410A, *Energ Buildings*. 43 (2011) 1802–1810.
- [5] H. Kang, J. Heo, Y. Kim, Performance characteristics of a vapor compression cooling cycle adopting a closed-loop air-circulation system for avionic reconnaissance equipment, *Int J Refrig*. 35 (2012) 785–794.
- [6] J. Choi, Y. Kim, Influence of the expansion device on the performance of a heat pump using R407C under a range of charging conditions, *Int J Refrig*. 27 (2001) 378–384.
- [7] M. Kim, M.S. Kim, J.D. Chung, Transient thermal behavior of a water heater system driven by a heat pump, *Int J Refrig*. 27 (2004) 415–421.

Research on the urban plans of Xi'an (1950–1952)

Yi Xiao

School of Architecture, Xi'an University of Architecture and Technology, Xi'an, China
School of Architecture, Henan University of Science and Technology, Luoyang, China

Yun Ying Ren

School of Architecture, Xi'an University of Architecture and Technology, Xi'an, China

ABSTRACT: Xi'an is not only a famous ancient city but also a representative industrial city in our modern history after 1949. During the Recovery Period of National Economy, from 1949 to 1952, three urban plans of Xi'an that guided the construction of Xi'an were made to promote the development of Xi'an and prepare for the large-scale industrial constructions. As the examples of this period, 1950, 1951 and 1952 Master Plans of Xi'an are representative. This paper analyses the three urban plans of Xi'an from the perspectives of the historical background, formulation of the plan, content, implementation and actual influence to the urban construction accordingly. Then on the basis of the urban planning theory and implement, this paper presents the characteristics of urban planning of Xi'an during the Recovery Period of National Economy.

Keywords: Xi'an; the Recovery Period of National Economy; Master Plan; the Soviet Union

1 INTRODUCTION

Xi'an is not only a famous ancient city but also a representative industrial city in our modern history after 1949. During the Recovery Period of National Economy, from 1949 to 1952, three master plans of Xi'an that guided the construction of Xi'an city were made to promote the development of Xi'an and prepare for the large-scale industrial constructions. As the examples of this period, 1950, 1951 and 1952 Master Plans of Xi'an are representative. The paper analyses the three master plans of Xi'an from the perspectives of the historical background, formulation of the plan, content, implementation and actual influence to the urban construction accordingly.

2 1950 MASTER PLAN

2.1 Background

During the Recovery Period of National Economy in early 1950, in order to meeting the needs of economic construction on a large-scale immediately, Fang Zhongru, the deputy mayor of Xi'an, proposed to draw up urban construction plan and instructed government department concerned to do it. In November 1950, Xi'an government drew up Xi'an Construction Plan (1951–1965) that was submitted to the Second Session of the Second

Xi'an Municipal People's Congress. Then it was discussed and adopted [1]. In this plan, designated function of Xi'an city was designated as the light-industry city, the logistic hub in northwest, and the ancient cultural tourist city. The city was divided to several functional districts on the basis of function division, such as industrial district, commercial district, ordinary residential district, institutes and colleges district and mixed-use district. Meanwhile, special urban planning administrative department, Xi'an Construction and Planning Commission, was established. Zhang Fengbo, the deputy mayor of Xi'an, is a chairman of committee and in charge of organizing to make the construction plan [2].

2.2 Content

In second half of the 1950, 1950 Xi'an Master Plan was completed that was the first planning of Xi'an after 1949 under the leadership of the Xi'an Construction and Planning Commission. The main contents are as follows.

The urban development strategy adopted 'Organic decentralization'. The expanding direction for urban development was to the west. The new town was built in the western suburbs of old city, also known as the Ming city. The area of new town is larger than the area of old city. The city space layout extended from east to west. The new town centre was located at the area between

the eastern of the North Hancheng Road and the western of Tumen. The road network of the new town adopted the mixture of grid roads and radiated roads. The urban population of the city was forecasted to grow to 1.25 million [2].

The new urban spatial layout was formed. Xi'an municipal administration center was located at Xicang in the old city. The northwest regional administration center was located at the new town. To coordinate the development balance between the old city and new town, the area between the old city and new town would to become an economic center that was the economic link between them. As the center of the city, the business center is located at Xishao Gate. Outside the East Gate of the old city, the urban built-up area would be preserved and served as the industrial and residential mixed-use district. On the north side of the new town, the area along the railway was served as the transportation district. Industrial districts were interlaced with residential districts in the new town for the organic combination of urban functions. Green belt lied on the periphery of the urban land. Urban form is similar to the rectangle. The length of urban form from east to west is longer than the length from north to south. On the periphery of the city, higher education district was located at the southeastern. Warehouse district was located at the northwestern. Two small airports were set respectively the north and the east by south. All of them formed the new urban structure.

The Xi'an city had six typical functional districts, such as flour industrial district, mechanical industrial district, commercial district, central business district, the industrial and residential mixed-use district and institutes and colleges district. In every district, the production (working/teaching) district was adjacent to residential district for the staff going on duty and coming off duty conveniently. The road network planning followed the original grid pattern and extended outward. This plan had altered the symmetric layout pattern of old city.

2.3 *Approval of urban plan*

1950 Xi'an Master Plan was discussed and adopted by Xi'an Construction and Planning Commission in early 1951. Then Xi'an Construction Plan (1951–1965) and 1950 Xi'an Master Plan were submitted to the Northwest Military and Administrative Committee and its subordinate the Northwest Finance and Economic Committee. After the briefing and the reviewing, Xi'an Construction Plan (1951–1965) and 1950 Xi'an Master Plan was asked to submit to Beijing by Xi'an Construction and Planning Commission. In June 1951, Financial and Economic Committee that was subordinated to Government Administration Council of the Central

People's Government examined the plan in the debriefing and made extensive notes on the plan. They considered that the plan still needed further study and readjustments and proposed amendments and addenda to the plan. Before the accomplishment of the master plan, Xi'an was allowed to go according to the submitted plan [3].

2.4 *Planning implementation*

This plan instructed the preliminary construction of the industrial district in the western suburbs in 1951. It has played a positive role in guiding the urban construction at that time and laid the foundation for the large-scale economic constructions during the First Five-year Plan Period. The E'fang Road, Laodong Road, West Weiyang Road and East Weiyang Road were all built in accordance with the plan [2]. They marked the beginning of the development of Xi'an urban spatial structure after 1949.

3 1951 MASTER PLAN

3.1 *Content*

In June 1951, aiming at the existence question of the 1950 Master Plan, Xi'an Construction and Planning Committee modified it again and formulated the second master plan, 1951 Xi'an Master Plan, according to all aspects of the views and requirements in the debriefing. This plan firstly increased 30 square kilometers of urban land. Then it adjusted the layout of industrial district and residential district. It made residential district close to industrial district by interlaced and mixed layout method for the staff go on duty and come off duty conveniently.

3.2 *Planning implementation*

The roads and factories of Xi'an were constructed in accordance with the plan later on. The arms industry and local industry in the western suburbs were built in good order, such as No. 3507 Factory, No. 604 Factory, Xin Xibei Printing Plant, Xi'an Pharmaceutical Factory, No. 544 Factory etc [2]. The interlaced and mixed layout of the industrial district and residential district in Xin Xibei Printing Plant was in accordance with this plan.

4 1952 MASTER PLAN

4.1 *Background*

The last two (1950 and 1951) master plans of Xi'an were greatly influenced by modern urban

planning theories. However, with the recovery of the national economy, urban construction resumed and developed in 1952. The nationwide urban planning also resumed at the same time. The First Urban Construction Symposium was held by the Financial and Economic Commission of the Central People's Government Council in Beijing, September 1–9, 1952. The urban planning theory of the Soviet Union was introduced. 1952 Xi'an Urban Planning was influenced by the theory of the Soviet Union. Based on the first two urban planning, 1952 Xi'an Master Plan had made the adjustments considerably.

4.2 Content

1952 Xi'an Master Plan terminated the urban spatial development strategy of the expansion of Xi'an city to the west. Urban center was located at the area between Xihua Gate and the bell tower. The urban space was developed outward around the old city. The new pattern of urban spatial structure was formed. The institutes and colleges district in the south and airports in the north and east outside the city were preserved. The interlaced layout of industrial district and residential district was cancelled. The concentrated layout of industrial district was adopted. The urban size was reduced. Following the original grid pattern of Chang'an and Ming city and extending outward on the basis of the old city road, the road network planning had altered the symmetric layout pattern of the old city. The north and south street of the old city and its extension was considered as the urban central axis. Moreover, the slant roads were situated in the southeast and southwest. The urban sprawl stretched out in the direction of east, west and south around the old city. The north of the old city was not considered as the main developing direction, because it was conditioned by the Han Chang'an ruins and railway crossing. It's performed as the local industry, warehouse and worker residential district and the urban land bank for the future [2].

4.3 Planning implementation

According to the layout of this plan, a lot of industrial projects were implemented in 1952. Baqiao Thermal Power Plant was built in the eastern suburbs east of the Chan River. The Xi'an Textile Mill and Renmin Flour Mill were built in the western suburbs that formed warehouse district. Shanxi Posts & Telecommunications School, Xi'an Normal College, Northwest Russian College, Northwest Finance and Cadre School, Northwest Labour Union Cadre School, Husbandry and Veterinary School, Youth League School, Shanxi

Normal College were built in the southern suburbs that formed the institutes and colleges district.

5 PLANNING EVALUATION

5.1 Background

The Central Committee of the Communist Party of China asked the urban planning of the major industrial city was designed by the Central Minister of Construction Engineering in September 1953 [4]. Therefore, the Xi'an overall urban planning (1953–1972) was completed in 1954. However, the basic principles of the last three (1950, 1951 and 1952) plans were inherited by the Xi'an overall urban planning (1953–1972), such as the development pattern of urban space and the road network.

In a word, there had been three master plans of Xi'an from 1950 to 1952. The first two were instructed by experts and scholars at home and made according to the western urban planning theory and Japanese experiences without the technical and economic datum of Xi'an. They have showed the ideas that the city should give priority to the big city and done the full research and the consideration to the conservation of the old city in the plans. However, there are some questions. The utilization of urban land and urban functional districts were not defined clearly. The benefits from taking full advantage of the old city were not realized.

In 1952 Xi'an Master Plan, influenced gradually by the Soviet model, the urban planning emphasized the dependence on the old city and tended to develop the new town around the old city. The choice of this urban renewal mode was closely related to the political situation at home and abroad and the urgent needs of the development at that time. To some extent, this urban renewal mode promoted the city's economic and social development. However, its drawbacks are becoming obvious too. With the large-scale development of the urban infrastructure, they are manifested in the serious damage to the ancient city's outlook and deterioration of traffic conditions in overloaded city center.

6 CONCLUSIONS

6.1 The influences of multiple theories

After 1949, the urban planning started out with the establishment of the related administration and the formulation of the urban planning spontaneously in our country. With the stability of the political situation and the establishment of the urban planning administration, each city carried

out the preparation and compilation of the urban master plan immediately in 1950. At that time, for the lack of urban planning experts and urban construction datum of Xi'an, the references of the Xi'an master plans mainly were on the basis of the western urban planning theory and Japanese experiences. The Xi'an master plans are the modern urban planning influenced by western urban planning theory. The issues on the development of urban space, urban functional districts and the conservation of the old city were considered in the planning. Then with the help of the Soviet Union experts, the method and procedure of urban planning compilation were influenced gradually by the Soviet Union urban planning theory, technology and method.

6.2 *Planning implementation*

The urban master plan only puts forward the ideas and proposals for the construction of the future during this period, because related examination and approval system and institutions were not set up. Therefore, these ideas remained firmly on the drawing board.

However, three Xi'an Master Plans were reasonable proposals based on those modern planning documents. The 1950 Xi'an Master Plan was discussed and adopted by The Second Session of the Second Xi'an Municipal People's Congress. It was submitted to the Northwest Military and Administrative Committee and its subordinate the Northwest Finance and Economic Committee. Then the Financial and Economic Committee in

Beijing allowed to go according to this submitted plan. Therefore these ideas about the layout of urban functional development had played a guiding role in the construction and been implemented partly, such as roads, municipal construction and the location and construction of the residential quarters and factories. All these prepared for the large-scale urban construction of Xi'an in the Five-year Plan Period.

ACKNOWLEDGEMENTS

This work was financially supported by Specialized Research Plan of Shanxi Provincial Office of Education (11JK0213) and National Natural Science Foundation Project (51178370).

REFERENCES

- [1] Xi'an Chorography Office. Xi'an Chorography (Vol. 5) [M]. Xi'an: Xi'an Press, 1996 (In Chinese).
- [2] Xi'an Chorography Office. Xi'an Chorography (Vol. 2) [M]. Xi'an: Xi'an Press, 1996 (In Chinese).
- [3] Xiutao Peng. A Study on them History of City Planning for Chinese New Modern Industrial City-Centered on the 156 Soviet-aided Key Projects [D]. Wuhan: Wuhan University of Technology, 2006 (In Chinese).
- [4] Yibin Li. Initiation and Development of Urban Planning in the Initial Stage of the People's Republic of China (1949-1957) [D]. Chengdu: Sichuan University, 2005 (In Chinese).

Integrating sustainability into design planning

Rui Jie Lu

Tongji University, Shanghai, China

ABSTRACT: The adverse effects of the dual differentiation of idea and technology in sustainable building design in contemporary China are analyzed in this paper. By discussing the feasibility, a solution which makes the sustainable strategies as one of the main architectural generation logic is proposed. As a result, the architectural energy consumption would be reduced, and the significance of sustainable in architecture would be recognized again.

Keywords: sustainability; architectural design; idea; technology

1 THE CURRENT SITUATION IN SUSTAINABLE BUILDING DESIGN

It is difficult to build an overall architectural quality organically, because of the dual differentiation of idea and technology in sustainable building design in contemporary China. As Otto Frei (2005), Professor of University of Stuttgart, said, “Something that is beautiful is not necessarily ethical too. Beauty is not equal to goodness.” In architecture, if beauty corresponds to the pure concept, goodness is the combination of subjective concept and objective technology (Guo Yimin, 2013). However, it is the dual differentiation of idea and technology that leads to a phenomenon that “beauty can be cruel and ugliness can be good.” In this situation, the excellent technology would not always produce the excellent architecture. On the contrary, the improper or excessive use of energy-saving technology might result in a huge consumption of energy, and the abuse of technology might even cause the stop of thinking about the nature of architecture. Obviously, when we talk about the architectural sustainability we should concern not only the physical performance of a building but also the relationship between technology and form, which could help us think about the nature of architecture.

To sum up, this paper would discuss three problems which exist in sustainable architectural design in contemporary China, namely, regarding the sustainable building as a special architectural style, ignoring the impact of sustainability on architectural form design, and equating sustainable building design to calculation or technological display.

1.1 *Regarding the sustainable building as a special architectural style*

The sustainable building tends to be regarded as a special architectural style, due to the dual differentiation of idea and technology. The artistically and individualistically inclined thinking and the peculiar commercial selling point in contemporary consumer society in China make form as the main focus by some architects. As a consequence, the sustainable building is considered as a special architectural style, and this makes some architects unable to apply their common professional knowledge in sustainable building design. For instance, as recently as 2001, Peter Eisenman (2001) said, “To talk to me about sustainability is like talking to me about giving birth. Am I against giving birth? No. But would I like to spend my time doing it? Not really. I’d rather go to a baseball game.” It seems that Peter Eisenman equated the sustainable issue with deconstructivism, and he thought they were contradictory with each other (Hao Lin, 2003).

In fact, the sustainable building is not a certain style. To be specific, the ultimate goal of architectural design is to create form, and this process needs to follow certain logic, such as site context, functional requirements, aesthetics requirements, energy-saving requirements and so on. Sustainability is one of the key points and one of the logic to influence the form generation.

1.2 *Ignoring the impact of sustainability on architectural form design*

The lack of interaction between sustainability and design tends to afford the building a deceptive appearance. In other words, some architects produce false sustainable appearance for buildings

by simply ignoring the impact of sustainability on form generation in the primary design stage and then adding some energy-saving equipment or techniques to the form at the end of the design process. The appearance of such a building does not build on an energy-saving foundation logically, which would cause troubles in design process and would also result in a huge waste of energy in daily use.

1.3 *Equating sustainable building design to calculation or technological display*

Another extreme situation in sustainable building design is that the pursuit of the minimal energy consumption and the display of the maximum available technology utilization and the most advanced sustainable technology use. The reason for this phenomenon is that the interaction between idea and technology is absent, and the technology becomes the only focus in design process. Some architects simply equate the sustainable building design to calculation or technological display. On the one hand, they ignore the complexity of the form. On the other hand, they neglect the fact that the sustainability is only one of the factors affecting the design process. In other words, the optimization of the energy consumption does not virtually mean the energy-saving and the reasonability of space and form. It is inevitable that the excessive pursuit of the energy optimization and the display of technological means will lead a great loss of interactions between design and sustainability.

2 INTEGRATING SUSTAINABILITY INTO DESIGN PROCESS

Because of the dual differentiation, the architectural form and the energy-efficient technology could not always get the equivalent attention at the same time. Sustainability, unlike site's context, architectural function and aesthetics, fails to influence design strategies in architectural form generation process. However, this does not necessarily mean that the sustainability does not have such ability. The lack of enough researches on the methods of integrating sustainability into design process may be one of the main reasons to the above problem. Therefore, It is reasonable to discuss the methods of integrating sustainability into design process from the following two aspects.

2.1 *Regarding sustainability as one of the design logic*

The dual differentiation of sustainability and architectural form design may cause many adverse

consequences. On the one hand, focusing on the materialization of concept while ignoring the sustainability would lead to a huge waste of energy in future utilization. On the other hand, taking the routinely energy-saving calculation as the whole consideration of sustainable building design would cause the degradation of the sensitivity of architecture. Nowadays, the requirements for energy efficiency and for the fast pace of construction call for a design method which could reach a balance between sustainability and architectural form.

The behavior of design does exist in energy-saving projects. According to David P. Billington's view (1985) about the relationship between technology and science, energy-saving method belongs to technology which is the artifact based on human intention. It means that the energy-efficient project is not all about the dull calculation; the creationary behavior which is closely related to human intention exists in it.

Energy-saving project could be set free from the calculation and be regarded as important as concept or intention by design thinking. It could become one of the factors determining the design process. In other words, design makes energy efficiency and other constraints as integrity which exerts influences on the form design together. Therefore, sustainable design is not equivalent to calculation and selection; it is a creational process which integrating the subjective intention and the objective constraints as a whole. It changes the limited and closed calculation and selection process into an infinite and open design process. This openness not only turns the one-way process into a two-way interaction between concept and sustainability but also expands the scope of design. That is to say, it integrates technical sustainability into concept, so that the scope of creation could be expanded.

The result of the common architectural design is the combination of the architect's intentions and the site condition, the function and other requirements. Besides, the additional constraints of the sustainable building design contain climate, topography and other local environmental factors. And then the extra value of the sustainable design exists in the aesthetic issue.

2.2 *Using solution-based design thinking and focusing on the core concept to coordinate and enhance the relationship between form and sustainability*

The sustainability as part of design concept is the main focus in this paper, which could be realized by using design thinking.

Firstly, being a solution-oriented way of thinking, design thinking is closely related to the local

environment and culture, and it could avoid excessive use of energy efficient technologies. To be specific, when designing sustainable architecture, architects may return to their common way of thinking. That is to say, design is a process of finding, analyzing and solving problems which are closely related to local climate, topography, function and other constraints. By using design thinking, the building would be more harmonious with local environment and culture.

Secondly, as a solution-focused thinking, design thinking could take sustainability as one of the design constraints which have the ability to influence and determine the ultimate form of architecture. Thus, sustainability and other requirements could work as integrity in form design process. In other words, because there are a lot of internal and external constraints in design process, architects are well advised to come up with comprehensive and balanced solutions to meet various requirements. The design thinking would relate the sustainability with other constraints together in the early design stage, so that architects could refer and consider all of them comprehensively at the same time, and reach a balanced solution by repeatedly coordinating their relationships. As a consequence, the sustainability could become one of the main factors to influence and determine the form design. That is to say, the ultimate form is not a simple addition of separate techniques; rather, it has a strong relationship with the sustainability and other constraints.

Thirdly, architecture could be designed around a clear principle, so that sustainability and other constraints would be logically and organically expressed in the final form of a building. If there is no clear principle to guide the design, the process and the strategy might be chaotic logically, and the result might look like a collage of separate fragments, since the technique does not have the ability to guide the design all by itself. In other words, the realization of the concept, instead of the technology, is the core of design. That is the reason why

the clear initial concept would be the clue and the structural foundation for the development and the result of design. In architectural design process, energy-saving technology, together with other techniques, could be arranged around a core concept, and then they could better influence the form design and be organized as an organic entire system in the final form.

3 CONCLUSIONS

This research plays a positive role in avoiding the dual differentiation of concept and technology in sustainable building design in contemporary China. By raising the awareness of design in sustainable building projects and providing a method of integrating sustainable strategies into architectural design process, architects could not only effectively prevent the unnecessary energy consumption in architecture due to the mismatching of the above two aspects but also have the opportunity to rethink the sustainability as one of the architectural basic issue.

Project supported by the National Natural Science Foundation of China (Grant No.: 51378353).

REFERENCES

- Billington, D.P. 1985. *The tower and the bridge: the new art of structural engineering*. Princeton: Princeton University Press.
- Guo, Yimin. 2013. Technical approach to represent tradition. *Time + Architecture* (5): 16–25.
- Hao, Lin. 2003. Architecture in transition and sustainable aesthetics. *Symposium of Architectural Society of China*: 107–113.
- Hawthorne, Christopher. 2001. An interview with Peter Eisenman by Metropolis Magazine.
- Otto, Frei. 2005. *Complete works: lightweight construction, natural design*. Berlin: Birkhaeuser.

The research on the impact of external traffic organization of HOPSCA on urban space

Quan Hua Hou

School of Architecture, Chang'an University, Xi'an, China
School of Highway, Chang'an University, Xi'an, China

Wen Hui Wang

School of Architecture, Chang'an University, Xi'an, China

ABSTRACT: Authors of the paper take the external traffic organization and urban public space of Wanda Plaza in Xi'an Lijiacun for the study, through investigation and analysis to go on a study of the impact of the external traffic organization of HOPSCA on urban public space. For the inspiration of the design and planning.

Keywords: HOPSCA; external traffic; urban public space; Wanda Plaza

1 INTRODUCTION

HOPSCA as a multi-functional complex building system plays a important role in the modern city with increasing importance. This dynamic open system actively involved in the city's environment, it is not only the place for people's activities, but also the link between architectures and cities.

Generally speaking, HOPSCA is always in the city's gold location with high intensity of traffic. While the lack of consideration of the reasonable transition planning between city and building may result in perfect function but disordered external space of HOPSCA. How to establish a reasonable relationship between the external traffic organization of HOPSCA and urban public space has become an issue that cannot be ignored when we talk about city problems.

Therefore, the authors take the combination of Wanda Plaza in Xi'an to do a deep study on the relationship between external traffic organization of HOPSCA and urban public space and to identify the reason as well as to propose solutions to rationalize the issue on this basis finally, which will make the HOPSCA blend with urban space better and establish a mutual motivation.

2 SITUATION ANALYSIS

Wanda Plaza in Lijiacun covers an area of 48,400 m², total building area of approximately 345,700 m², floor area ratio of about 5.99, apartment building area of 168,000 m², five high-rise apartments, com-

mercial building area of 177,700 m². It is one of the representative of Wanda "Third HOPSCA Generation". It is also the member of "Lijiacun District" for mid-range consumer. Wanda brand appeal to consumers large and the current operating is in good condition. Because of its brand awareness and reputation, the business environment surrounding the project can play a leading role to improve the appearance of the city (Fig. 1).

2.1 Current situation of external traffic organization

2.1.1 Dynamic traffic organization

1. Walking traffic organization

Walk flow lines is mainly plane of the organization, no three-dimensional flow line organization. Pedestrian traffic system is in conjunction with urban design that people and vehicles are separated from each other. The main entrance of plaza is enlarged to connect with the city on



Figure 1. The location of Wanda Plaza.

walking system. Walking traffic is mainly considered the inner commercial street.

2. Vehicular traffic organization

The base was isolated into a rectangle with Yanta Road, Lijiacun Road, Changsheng Street and Wanda road. It makes it easier to organize the external traffic flow of vehicles. The underground car park has two entrances on west and north, which are located in Changsheng Street and Lijiacun road. Wanda Road connected Yanta Road and Changsheng Street to meet the needs of cargo transportation and business hotel logistics as well as residential traffic organization, which must avoid the city road (Fig. 2).

3. Public transport organization

Around the base it has 12 bus lines and the planned Metro Line 4 go through under the east. there there is a bus station and a taxi stop around the base, which is located in Yanta Road. And a taxi drop-off stop located in Lijiacun Road.

2.1.2 Static traffic organization

With the rapid warming of realty industry and urban renewal in recent years, the space capacity of city center rapidly improving. The increasing structure area has led to increasing human traffic, and the requirement of parking spaces is also greatly increasing. However, due to the central area cannot take up a block of ground as a large public parking block and most of the buildings don't set up any underground parking garage, or even if there were one, but only available to employees to use, many motor vehicles and bicycles have to occupy road space or plaza space for parking, thus greatly reducing the capacity of city roads. In addition, the lack of city road space is a common problem while the popularity of the cars making this problem more severe. The growth of road is far below the growth of vehicle in the amount, and the traffic congestion situation inevitably appears.

2.2 Current situation of external public space

2.2.1 Space the basic structure

Wanda Plaza external public space mainly refers to the public space except for the shopping center, the entertainment center and the hotel apartment, in addition to meeting the function of building inside,



Figure 2. The entrance of underground parking.

but also an important part of urban public living space. Form and function including: sidewalks, driveway, entrance of plaza and walking street.

2.2.2 Activities on space

Through investigating people's social activities on external public space, we found that the number of people staying on the entrance square reached about 36%, 10% of which are stall merchants, and the rest is the number of walking outdoor or waiting. Compared the number of people on the square and on the commercial walking street, it's found that the number of people staying in the walking street is more (may be affected by the weather).

3 THE IMPACT OF EXTERNAL TRAFFIC ORGANIZATION ON PUBLIC SPACE

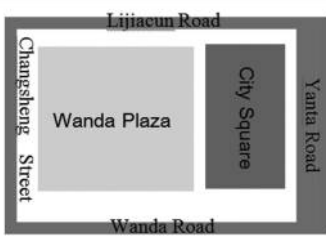
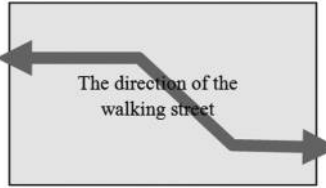
3.1 Impact on the spatial form of public space

1. Due to the limited area and the volume ratio of Wanda Plaza, it is combined with its traffic organization to build the external public space. There's not too much decoration of entrance and directly connected with the plaza.
2. Space is mostly take roads and commercial facade for interface, taking standards of the scale of traffic and parking design to ensure unobstructed traffic, while paying the expense of walking space. Due to the lack of three-dimensional organization of traffic of people and vehicles, the connection of two parts that divided by Yanta Road is cut. With the lack of attraction on both sides and the lack of effective public space guidance, the entire base was in isolation, which is not harmonious with the urban space and lacking of continuity.

3.2 Impact on the accessibility of public space

Wanda Plaza is surrounded by a relatively good public transport links. Investigation shows that 51% of people choose public transportation that has become the first choice of people to travel, and the time spent basically all within 30 mintes. People who select to walk or non-motorized to travel spend the least time at an average of only about 15 min (Fig. 3). On the view of satisfaction level of transport, more than half of the respondents think it is very convenient and relatively easy, in which that the date of bus is slightly lower than other modes. there is a large space for building public transportation system. From the point of HOPSCA itself, the closeness of external public space and urban walking traffic system determines the extent of public space attraction [5]. Wanda Shopping Mall as an example, the public space along with the Yanta Road is more attractive

Table 1. The composition of external space of Wanda Plaza.

Spatial Composition	Space Features	Space Schematic
City Square	City Square has a area of 2000-3000m ² , generally located near the main entrance of the shopping center walking street. These will not only play a role of transport hub and trade center, but also provides the city a public space for communication and activities. City Square act as a "point" role in the whole space.	
Commercial Street	Wanda Plaza forms a commercial street of indoor space. The commercial street is designed an enlarged nodes in the main intersection turning, such as indoor walking street in the circular atrium and so on. The role of commercial street in the whole space act as a "line" sewing through the spaces.	

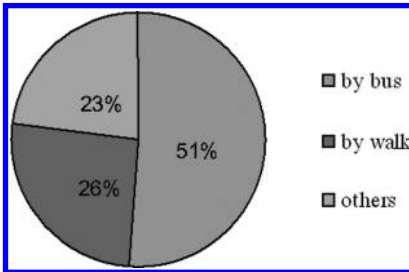


Figure 3. The proportion of travel mode.

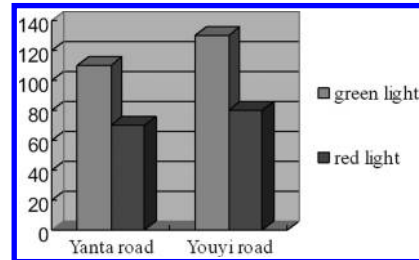


Figure 5. The time of traffic light on the cross.

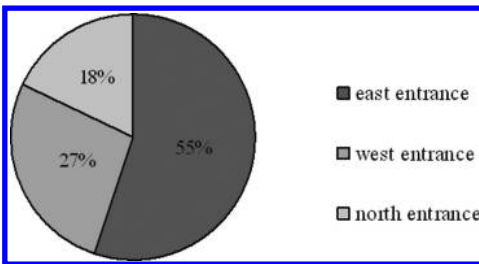


Figure 4. The proportion of entrance flow.

than three other entrances of commercial walking street. By observing the number of people from both two entrances of north and south, it can be found that the number was much higher in eastern entrance, which shows that entrances open on city traffic road can attract more people (Fig. 4).

3.3 The impact on the safety of the public space

Wanda Plaza has a huge gathering of people, but it seems that the designers did not give much thought

to solve problems of how to evacuate the crowd outside the building.

1. The wide broad motorized transport poses a security threat to people's travel.
For example, the large cross on south caused difficulties for walking, pedestrians that wants to go to the other side often need to pay 2-3 times to wait for the traffic lights (Fig. 5).
2. Lack of communication with other blocks
If pedestrians want to walk through Yanta Road, they have to go south to the cross for about 200 m, but there is no crosswalk or overpass, which leads some people to take risks, such as jaywalking, that will cause danger.
3. The construction of subway makes a block of chaotic on traffic.
4. The entrance of motor vehicle is too close to the main entrance of the building, which is the lacking of buffering.
5. The lack of humanization of transport facilities is
For example, although the external public space designed with obstacle-free facilities, but they

are often occupied by vehicle or other obstruction, so it is nominal.

3.4 *The impact on function of public space*

The public space based on line-shape implies a function of movement. Compared with the entrance, about 80% of respondents prefer to stay in the walking street. But because of the interference of the city traffic, it attracted a block of people to stay. Pedestrians tend to occur at the space center, but people sitting and chatting tend to be attracted to the edge of space. Thus walking traffic space and open space has been divided naturally, in which way that will not affect walking traffic while providing a relatively safe and open space.

From the perspective of the richness of activities, the main outdoor activities may occur at entrance square. The activities of main entrance is simple, which is mostly constituted by walking, and closely connected with the city walking system; walking commercial street make up the shortage of pure walking space, and ensures traffic requirement while providing chances of a rest.

4 SUGGESTIONS TO MAKE IT RATIONAL

4.1 *Conduct a full investigation and analysis*

Efficiency in modern society makes extraordinary sense, but “fast” always leads to the ignorance of “quality.” Preliminary research analysis plays an unusual role in the design, environmental analysis, traffic forecasts and calculation of the flow of people will need to take full consideration in the design, which can make the project rule-based. If there is no reasonably adequate investigation, any design is castles in the air.

4.2 *Consider the impact of traffic design on city*

1. Combine the HOPSCA with public transportation

HOPSCA is often considered as a part of urban public traffic system, assume the functions originally belonged to the city. It does this work by forming a transport system with the city subway, underground walking system, overhead lines, buses and light rail, which greatly increase the traffic capacity of the city center streets, ease the ground pressure and improve the urban traffic conditions.

2. Implement traffic diversion and improve walking system

Implementation of traffic diversion is one of the effective way to solve the traffic problems, the gist is to separate the different nature of the traffic flow as much as possible to reduce the cross between Vehicle traffic flow and walking traffic

flow, relief the impact on the city roads, including traffic diversion and construction of three-dimensional plane traffic.

3. Design rational parking space

The utilization of road for parking space will cause the loss of urban public space and traffic congestion. It will be recognized that to use the top of the building or underground space may solve the parking problem. But also pay attention to the rational and orderly evacuation of traffic and external interface to avoid unreasonable burdens caused by heavier traffic system.

4.3 *Facilities in place*

Pay attention to management in the project after the implementation. Specify the appropriate measures under different environment and circumstances, such as holidays, etc. and increase its guiding role of the landscape and accessible facilities to ensure the orderly conduct of traffic.

5 CONCLUSION

Lijiacun Wanda Plaza greatly enhances the vitality of the block, but the unfavorable external space traffic organization disrupts the order of urban public space. By the investigation of Wanda Plaza in Lijiacun, the research analyzed the impact of external traffic organization on urban public space, and found that the current HOPSCAs' external transport has a close relationship with urban public space and proposed some suggestions to make it rational. The designers of HOPSCA should always grasp the coordination between the urban public space and the external traffic of HOPSCA, through three-dimensional traffic, optimizing parking and other strategies to achieve this goal.

REFERENCES

- Di, J. 2009. The research for the intervenient property of the public space in HOPSCA. *Xi'an Architecture and Technology University*: 61–67, Xi'an.
- Guxin, L. 2005. The research and practice of urban complex development. Nanjing. Southeast University Press.
- Jianjun, W. & Wei, S. 2012. Initial Exploration on Traffic Impact Analysis of HOPSCA. 2013(1). *Traffic & Transportation*: 46–49. Shanghai.
- Weiwei, B. 2012. Study on urban complex external space design. *Northwest Agriculture and Forestry University*: 6–14, Xi'an.
- Yulian, L. & Zhengfan, H. 2006. Environmental psychology. Beijing: China Building Industry Press.
- Zhen W. 2008. “MIX”-Research of contemporary urban building complex. *Tongji University*, Shanghai.

An analysis on the social benefit of combining charities with road race events—with the 2011 Beijing Marathon as a case

Qing Song Zhu

Institute of Physical Education, Hechi University, Yizhou, Guangxi, China

ABSTRACT: This paper analyzes the social benefit of combining nonprofit organizations with city Marathon events by the case analysis method, aiming to enable more event operators to understand the value of this new operating mode and provide better services for the events. Moreover, through the stage of the road race events, the operators can attract NGO's participation with the injection of the public service element to establish a participation platform for national welfare, promote the development of charity and achieve a win-win situation.

Keywords: charity; Beijing Marathon; event; benefit

1 INTRODUCTION

In 2011, China Olympic Road Running Co., Ltd. (CORR)—the event operator of Beijing Marathon introduced the new operating mode of “running for charity” into China to promote the event rank among the first-class international road running around the world, and helped to develop the market of China road running as well as improve the system of road running.

The combination of sports events and charities is the necessary trend of the sustainable development of China sports industry. The new type of charity cooperation mode explored by 2011 Beijing Marathon created the platform of “running for charity” and improved its brand value while enhancing the competitive level. The mutual integration of event and charity increases the brand asset of the event, making all participators to pay closely attention to the society and care about others while challenging themselves, to support the development of Marathon event and charity with their actions. Therefore, the combination of sports events and charities has profound significance on not only the sports undertaking but also the charity undertaking of China.

2 START-UP OF SPORTS CHARITY IN CHINA

In 2005, China's top ten Lawrence champion committee and China Charity Federation (CCF) initiated the champion fund project aiming to help vulnerable group. This is the only sports charity

fund organization under the CCF, indicating the official start-up of China sports charities.

In this year, China's sports circle participated in a number of charitable activities. For example, the State General Administration of Sports donated RMB387,000 to the disaster area in the Southeast tsunamis; Huang Yubin, deputy director of the National Gymnastics Center, and Teng Haibing, champion of the Athens Olympic Games, took the lead in donating RMB1,100 respectively and thereby brought along other athletes; the National Center of table tennis and badminton donated all the collected fund of RMB2 million by holding benefit match; the team with Shenxue and Zhao Hongbo as representatives in the Winter Project Management Center donated their one-month salary; during the “Chinese Love Action Evening Party” held in Beijing, Wang Yifu, Wang Junxia, Deng Yaping, Guo Jingjing and other sports stars gave non-benefit performance and donated for the disaster area on the stage. Liu Xiang, who is called the champion of “sport charity” in China, not only donated his racing suits, running shoes, autobiography books and remuneration, but also donated more than RMB500,000 in his own name and attended dozens of charity activities when the Southeast Asia suffered from tsunamis.

3 THE EMERGENCE OF THE “RUNNING FOR CHARITY” SPORT CHARITY MODE IN CHINA

Marathon is a very popular long-distance running project internationally. In many developed countries,

when mentioning Marathon, many people firstly think that it looks like a Happy Carnival with public service as the purpose. The combination of sport charity and event abroad has already established a certain scale and operating mode, as well as perfect organization building and system. Whereas a precedent was set in China in 2011.

London Marathon is one of the top 11 global gold standard Marathons granted by IAAF. Through 30-years of development, it has grown to be a traditional Marathon jointly attended by about 40 categories and 60 charitable organizations. Nearly 90% out of the 40,000 athletes attending the 2011 London Marathon are from the collected enrollment by various charitable organizations, the idea of “Running for Charity” has rooted in people’s heart through the event and become the representative part for promoting London Marathon.

In 2011, Beijing Marathon, together with the charity operating organization of London Marathon, began the exploration in the establishment of strategic cooperation relationship with overseas charity operating organization and firstly introduced the “Running for Charity” sport charity new mode in China, building a sport platform for the demonstration and propagation of charitable organizations, i.e. for athletes to spread public service culture among the general public through solicit contributions and propaganda, and for more people to understand and pay closely attention to and even participate in the public service organization. In addition, through the combination with charity and the injection of more intension at the spiritual level in Marathon, athletes not only complete a match but also make contributions for charity and public service.

On Oct. 16, 2011, when Beijing Marathon started at the Tiananmen Square and thousands of people stood at the both sides of road cheering for athletes, many people found a special team wearing propagating shirts printed with charitable organizations and slogans, who were the athletes representatives from 13 charitable organizations at home and abroad and made the first stage pose in Beijing Marathon, indicating the beginning of public service in Beijing Marathon from then on.

4 ANALYSIS ON THE SOCIAL BENEFIT OF 13 CHARITABLE ORGANIZATIONS’ PARTICIPATION IN BEIJING MARATHON

“Running for Charity” was a highlight and characteristic feature of 2011 Beijing Marathon, with participators of 13 charitable organizations, including national public service organizations such as China Greenery Fund, China Women Development

Fund, China Youth Development Fund, civil public service organizations such as Natural Friends, and religious public service organizations such as Hebei Jinde Charity Fund, as well as large-sized international charitable organizations such as Children with Cancer UK, Cancer Research UK, Alzheimer’s Society, ensuring the variety of type and proposition of charitable organizations.

In addition, 2011 Beijing Marathon paid more attention to national participation compared with the past. For example, the organizing committee extended the closing time for another one hour, newly added family running project for children to feel the charm of sports personally, set the reward for non-professional Chinese athletes, i.e. the male and female who won the first to fifth were offered the opportunity of attending overseas Marathon organized by Beijing Marathon Organizing Committee and one set of Adidas sports equipment free of charge, encouraging and enhancing the participation degree of non-professional Marathon athletes of the public. The course of 2011 Beijing Marathon was also relocated from original Olympic Sport Center to the central celebrating square of Beijing Olympic Park.

4.1 *With marathon as the carrier and participative behavior to spread public service idea, will be helpful to the formation of national charity consciousness*

Firstly, 13 charitable organizations attending the 2011 Beijing Marathon “Running for Charity” owned their special page on the official website of Beijing Marathon, where people could click to enter and understand the details of these organizations and the charity projects cooperated with the event. This was propaganda at one side. Because the participators were enrolled via the official website of Beijing Marathon, such propaganda at least covered the group, whereas the final participators for the 2011 Beijing Marathon reached to 400,000 people.

Secondly, the 13 charitable organizations set up their own team to attend the Marathon event in terms of the specified quota, spread public service culture and idea by the way of raising money and propaganda, for more people to understand and pay closely attention to charitable organizations and participate in the public service activities, thus the arena became a wide platform for them to propaganda and raise money. For example, China Greenery Fund defined the theme of the public service long-distance running as “2011 Running for Charity—Protecting the Mount Gaoligong in Yunnan”, the participating slogan of Save the Children was “Running for every child’s healthy growth”, while the proposition of the China Youth

Development Foundation (CYDF) was “Running for the happy sport of the Hope Project” etc.. Furthermore, since the public service activity was online dated August 15th., 2011, the highest record of personal raising money has reached RMB2,592. On Oct. 10th., 2011, two alumni from University of Science and Technology of China realized three Put Options and finally competed a donation of RMB300,000.

Public service organizations, through the participation in Marathon and injection of public service element, with Marathon as the carrier, build a sport charity platform for them to display and propaganda, and spread their own idea and target of public service to the public, and build a participation platform for national public service and also arouse wide attention of the society.

4.2 *With the help of public service, enrich the intension of marathon and benefit the enhancement of the society's soft strength*

With the globalization of economy, sport events also enter the era of globalization. More and more cities would like to improve their reputation and influence via large events. Currently, the most popular in domestic is the city international Marathon, with similar meaning and purpose and no more innovation. The increasing Marathon events show that China's Marathon has entered a new stage. Therefore, Marathon is not only the cradle of training excellent athletes but also undertakes more massive social responsibility.

In 2011, Beijing Marathon took risk of exploring the cooperation mode of sport event and charity to combine the intension of them, making the public meaning of Beijing Marathon “Running for Health” and the public effect of “Running for Charity” become the essence. For this, Beijing marathon kept standing out among those city's marathon events in China.

The combination of Beijing Marathon and charity work break through the traditional sport event modes, enrich the meaning of the event, and integrat humanistic concept and the elements of harmonious development into the event. It realizes a win-win situation, that not only enlarging the brand equity and influence of the event, developing the event, but also supporting the development of the charity work. For those competitors, when they challenge themselves in the event, they are showing their care to the society and others at the same time. Their running in the marathon means the participation in the charity. They run for charity, and run for hope. This kind of events have the side effect of planting the charity seeds among people, and put public element into the host cities. As time passes, the seeds will sprout, blossom and bear fruit, the

public service element will flow among cities, the personal cultivation will be shaped, the city's image will be bolstered, and the soft power of society will be enhanced at the end.

4.3 *Build a fitness and charity platform for national public, improve the public quality, create a good social morality*

Fitness was an eternal theme in the long history of Beijing Marathon. In 2011, Beijing Marathon revolutionized its operating mode. The cooperation between the event and some charitable organizations let Beijing marathon become the model and focus among Chinese city's marathon events. 400,000 participants was the maximum entering number of the event over the years. Those thirteen charitable organizations that cooperated with Beijing marathon were seriously selected by the organization committee. Their slogans presented the support both for competition and charity, showed the ideal combination with Beijing marathon.

Once upon a time, the public joined the marathon for fitness. Now, the participation of marathon has a deeper meaning beyond fitness, charity. So, 2011 Beijing marathon provided the public a double meaning platform. For the participants, they could kill tow birds with one stone, exercising themselves, and helping others. It would stimulate the enthusiasm of the public participation, and then expanded the scale of Beijing marathon and improved its influence. Health consciousness and public charity understanding were spread at the same time.

The public service element in 2011 Beijing marathon popularized the knowledge of combination between sport fitness and public service to the participants and even the whole people. It could benefit both the body and mind for a person, Improve the public quality, and create a good social morality.

4.4 *Public services combine with marathon spirit, promoting social harmony*

Public services activities are a series of behaviors that contribute to society, do something free for the society based on what one could do, show one's grateful heart to others, and provide services and help for disadvantaged groups. For example, China Children and Teenagers' Fund (CCTF) invited its cooperative enterprise, Jiayi company, to set up a competition team for their project “Action to Eliminate Infant Anemia” in 2011. The project aims to Provide “Caring Nutrition Packages” to the parents of children the ages 6-to-36 months old. Each RMB100 donation could provide a child “Caring Nutrition Packages” for three years.

Marathon is one kind of sport activities, and it itself presents the “Marathon” spirit. Marathon is not only for those professional athletes, but a kind of form of public fitness. Beijing marathon, after 30 years, has grown up as a big sport event for the whole people, motivating more and more people to take physical training and run for healthy life.

Public services spread love and civilization, help to set up a harmony society and promote society progress. For those who join public service activities, they do their part to make contributions to society, enrich their life experience, and improve their mental state. And for service objects, public services are good for them to widen their social circle, improve their confidence in other people and the society, make them easier to be a social being, increase their sense of belonging. Marathon events promote the development of the national fitness, carry forward the Olympic spirit, and provide the development of people. Therefore, the combination of charity and marathon, is the integration between public philosophy and marathon spirit. It will benefit the society harmony and human progress.

5 CONCLUSION

1. It was a succeed for the first combination of 2011 Beijing marathon and charity. It promoted the development of Chinese charity work, and also enlarged the event brand equity and influence, realized a win-win situation. At the same time, it made a sample and reference platform for other large-scale sport events and city's marathons.
2. The social benefit of combining charity with road race events is always delayed. Events organizers should focus on the long-term benefits, but not only current economic benefits.

Furthermore, the road race events should undertake some social responsibility besides sport. Only such events will become more and more popular. And such sport activities are fit for the society development, are belonged to the whole people.

3. Sport charity is popular in foreign countries. In Chinese, it is still on the start stage, and the sport charity activities are still in extensive and simple forms, mainly the personal donation from some sports stars. The sport charity strength is weak, and seldom public are conscious of sport charity. The public service activities combined with marathon events are common in foreign countries. In China, Beijing marathon in 2011 was the first test about it. This start had a kind feedback in any way, and should insist such operating mode in the future and make it better and better. To make further integration between public sport and public charity, the marathon events will be not only the public sport parties, but the happy carnivals for people to participate the public services.

REFERENCES

- [1] Hou Keke & Wang Yusi. Sports Charity in China [N]. *Guangming Daily*, 2006, 1 (005).
- [2] Charity was first introduced in 2011 Beijing marathon, 13 public service organizations participated in the competition [EB/OL]. <http://www.ccafc.org.cn.2011,10,18/2012,7,10>.
- [3] Sina Sports. Running for Charity ... love for 2011 Beijing Hyundai Beijing marathon [EB/OL]. <http://sports.sina.com.cn.2011,10,09/2012,7,10>.
- [4] Zhou You & Fang Chenghua. On the Social Function of Sports Charity [J]. *Journal of Jilin Institute of Physical Education*, 2011, 27(3):32–33.
- [5] Bai Liang & Song Zongpei. Research on Charity Activities in American Sports. [J]. *The Sports Culture Tribune*, 2010, 11:37–40.

The social effects of traditional sports in the Yifan Festival of Molao people

Zong Feng Huang

Institute of Physical Education, Hechi University, Yizhou, Guangxi, China

Yong Liang Yang

Institute of Physical Education, Guangxi Normal University, Guilin, Guangxi, China

ABSTRACT: This article will study the social effects of the traditional sports in Yifan Festival of Molao people by sourcing related documents, using questionnaires, interviewing experts etc., and extracting the folk Yifan Festival in the Wus in Heng'an village of Dongmen town, the Yins in Zhongshi village of Dongmen town, the Luos in Mazhai village of Long'an county, the Xies in Siba's new residential quarters, Luocheng Molao people autonomous county, Guangxi region in China, as well as taking the 2009, first Yifan Culture Festival in Luocheng as examples. It is found that the actively operation of traditional sports in this festival has achieved glaring results, mainly represented in four aspects: firstly, it can maintain the stability and promote the harmony in society; secondly, it can reinforce the cohesion among peoples and the development and sustenance of ethnic groups; thirdly, it can put forward the growth in tourism and economy of the ethnic region; finally, it can accelerate the spiritual building of the new Socialist Countryside.

Keywords: Molao people; Yifan Festival; traditional Molao sports; effect

1 INTRODUCTION

With the legalization of traditional festivals in China, the development and expansion of traditional folk cultures have been scheduled on the government agenda. The Yifan Festival of Molao people is their most ceremonious festival, enlisted in the first batch of China's non-material cultural heritages in June, 2006, together with the Spring Festival, Qingming Festival, Dragon Boat Festival and Mid-autumn's Day etc. It is rich in cultural connotations and functions as the best platform of the ethnic culture. Along with the improvement of science and technology, the activities of the festival have changed significantly: apart from the simplified sacrifice, it also add performance, antiphonal singing, economic exchange, dragon dance, lion dance and traditional sports competitions. Among all the above, traditional sports is the major part of the celebration. The intensive promotion of traditional sports in Yifan Festival is in purpose of extending the popularity of the traditional sports in Molao people's residential regions, furthering the extension its influence, genuinely benefiting the people by providing health and happiness for them.

2 THE OVERALL SITUATION OF HISTORY AND CULTURE

2.1 *The Molao traditional festival—Yifan Festival*

The traditional festivals of Molao people include Yifan Festival, Chunshe Festival, Honor of the local Gods—Powang—Festival, Anlong Festival, Hillside Hiking Festival, Molao's traditional New Year, and festival of protecting the seeds. Yifan Festival stands out to be the most important one. The word "Yifan", in the ethnic people's perception, means gratitude and celebration of the harvest. It has always been loaded with the people's brilliant wishes towards the coming year: fine weather, good harvest, family security and productive and healthy livestock. With an 800-year history, Yifan festival is a traditional one indigenous to Molao people.

2.2 *Brief introduction of traditional Molao sports*

The traditional Molao sports is a traditional cultural form that has been highlighted in and separated from its ethnic culture, and it is an important part of the latter. It derived from the people's

Table 1. Analyses of prize winning in national minorities game themed on Yifan Festival.

Activities	Time	Venue	Race name	Prize
Bamboo ball	1998	Guangxi. PRC	9th Regional Minorities Game	First prize
Bamboo ball	1999	Beijing. PRC	6th National Minorities Game	First prize
Zongzi scrape	1991	Guangxi. PRC	4th National Minorities Game	First prize
Dragon ball capture	2010	Guangxi. PRC	12th Regional Minorities Game	Second prize

custom, production and daily life. It is an indispensable activity that facilitates the people to keep fit, communicate with each other, optimize their life. It is created by the people during their daily labor in different periods in history out of the needs of survival and production. It is closely linked with the social and spiritual life of the people, and becomes an indispensable part of their life^[1].

Since 1983, experts on culture and sports have excavated many activities themed on Yifan Festival, for example, there are 45 kinds of activities: zongzi scrape, bamboo ball, beacon ball, phoenix's egg protection, dragon ball capture, sparkler scrape, Molao's three chess, cockfight, etc. And some of them have won first and second prizes in Guangxi Regional Minorities Game and National Minorities Game (as showed in Table 1), influencing regions around China.

3 THE SOCIAL EFFECTS OF TRADITIONAL SPORTS IN THE YIFAN FESTIVAL OF MOLAO PEOPLE

3.1 Maintain the social stability and harmony

3.1.1 Resolve contradictions in family

Many of the sports performances and activities held in Yifan Festival require members of family or extended family to participate together. For example, Zhulian Ball, also called "couple zhulian ball, requires its competitors to be a couple according to the rule. It used to link a couple with its special "sickle base", which was replaced by a rope nowadays. The couple should be united and cooperative so that they could win the game. Suppose they are inconsonant and conflicting, they won't even move and the game can't go on. So that the couple should work with each other for a mutual goal in order to win the game. As the prover goes,

"harmony in a family brings wealth." The traditional sports serve to resolve some small contradictions and conflicts between couples in their daily life, prompting harmony in families, building favorable atmosphere such as mutual trust and love, solidarity and cooperation, and co-creation of happy life among family members. The whole society consists of numberless families. When every family realizes harmony, the whole society will be sure to obtain the good atmosphere.

3.1.2 Remit contradictions among villages

There are usually contradictions among villages triggered by land, roads and buffalo pastures. Participating the traditional sports games in Yifan Festival can remit these contradictions. Many of the traditional games in Yifan festival divided the teams based on "Dong" or small stations, for example: bamboo ball, zongzi scrape and dragon ball capture. In bamboo ball games, the attackers and the defenders will be tied together by a rope, suppressing each other. This group of players may be friends or ex-enemies in life. No matter how large their distance used to be, in this game, which is almost like a playful game, they get close to each other when trying to suppress each other. The venues function as a place where they resolve contradictions and further the friendship. In addition, when a village holds Yifan Festival, it will invite its neighbour to take part in the activities, in which the villages cooperate with each other and have great fun together. They can remit the contradictions during the very entertaining and interesting games. It is unanimously agreed that holding Yifan Festival, especially traditional sports has a better effect on conciliating their conflicts than holding meditations.

3.1.3 Enrich the spare life of villages and decline misbehaviors like gather-gambling

According to the local people, During Yifan Festival, gather-gambling has declined. Also, neighbors come together to join the celebration, as they get along with each other more often, they establish brotherhood, consequently, the social conflicts have declined. The secretary of Zhongshi village, Dongmen Town said, "the major work of us are to guard stability and increase the earnings of our villages. Particularly during festivals, we pay heed to arranging more activities, and arranging for those returning home. There is a large population in our village, among them are 2000 who leave for working in cities. If these young men muddle around in cities, we will have to handle their problems if any." The above have fully expressed that the Molao people's traditional sports in Yifan Festival can enrich the spare life of villages and decline misbehaviors such as gather-gambling. As a result, to hold more

traditional cultural and sports activities in traditional festivals exerts an optimistic effect on guarding social stability and building social harmony.

3.2 *Enhance cohesion and sustainability of the people*

In the folk Yifan Festival, the players are organized in the basis of “dong”, which means a tribe. The head of “dong”, authority of the people, preside over Yifan Festival. He handle all the affairs and take the responsibility of maintaining stability and solidarity in the people. There is a holy task to be accomplished in Yifan Festival: selecting the next head. In the past, every family would bring ickers and zongzi in sacrifice for gods in the festival. After the sacrifice, they will distribute the oblation among the villages. The surplus will be spread on the ground. And the villages would have to grab the oblation, whoever gets the most will be the next head. Today, the experts on cultures and sports have researched and analyzed many traditional sports games in Yifan Festival that are tightly connected with the above-mentioned phenomenon. They include zongzi scrape, dragon ball capture, bamboo ball and zhulian ball. They alter the simple zongzi and icker grab into the now interesting traditional sports games, in which the winner will be the head.

Besides, in the large-scale Luo Cheng Molao people’s Yifan Culture Festival, zongzi scrape, dragon ball capture, bamboo ball and zhulian ball are organized in the basis of village and town. In the activities, the players participate and entertain together, enhancing their coordination and cooperation, strengthening their mutual trust and friendship, intensifying cohesion between individuals, between small and large groups, and enhancing the sustainability of the people consequently.

3.3 *Promote the development of ethnic tourism and economy*

Luo Cheng is a key object in China’s help-the-poor project, facing still significant difficulties in stability and development. The town is abundant in touring resources: fascinating natural scene, unique cultural sites, history-honored ethnic custom, ornamental, healthy and entertaining traditional sports ... Such advantageous cultural environment has attracted visitors from all around the world: litterateurs, archaeologists, experts on folklore and travel enthusiasts. The tourists can enjoy a feast of historic cultural sites and attractive scenery, as well as take part in traditional sports activities featured on fitness, entertainment and adventure. The association of the dynamic sports activities and the static cultural and natural scene satisfies the psychological needs of modern tourists,

expands the development space and adds to the appealing power of local tourism. According to incomplete statistics, the various scenic spots over Luo Cheng have welcomed over 10,000 tourists during November 28th to 29th, 2009.

3.4 *Accelerate the spiritual building of the new Socialist Countryside*

The building of the new Socialist Countryside generally requires “productivity development, well-off life, rural civilization, neat environment, and democratic administration.” The ten words are rich in their contents, containing material, spiritual and political civilization. These three requirements are inseparably interconnected with each other, whose core is the all-round improvement of man. With the development of modern society, the Molao people have also witnessed an improvement in their material aspect of life, and at the same time demand a higher level in the spiritual aspect. The spiritual building of Molao people relatively lags behind the material development. Holding traditional sports activities in Yifan Festival can just make up for this lag.

3.4.1 *Comparison on the appreciation of folks towards different events in Yifan Festival*

According to Table 2, 62.5% of the questioned are those who appreciate performances of traditional sports, which guarantees the interests of folks in implementing traditional sports activities. Also, it is noticed that the most favored event in Yifan Festival is the performance of traditional sports. It can be concluded that the implement of traditional sports has won the appreciation of a large number of folks.

3.4.2 *The survey on Molao people’s watching the traditional sports activities*

According to Table 3, 174 out of 188 who are surveyed have watched traditional sports activities and performances, with a percentage of 92.5%.

Table 2. The appreciation of folks towards different events in Yifan Festival (n = 180).

Activities	Number of folks who appreciate	Percentage
Yifan sacrificial ceremony	50	26%
Performance of traditional sports	120	62.5%
Ethnic art exhibition	56	29.2%
Travel cultural activities	70	36.5%
Yifan gourmet festival	85	44.3%
Special thousand banquet	90	46.9%

Table 3. The survey on Molao people's watching the traditional sports activities.

Frequency	Number	Percentage
Have watched	174	92.5% (n = 188)
Often watch	151	80.3% (n = 174)
Occasionally watch	23	12.0% (n = 174)
Never watch	14	7.4% (n = 188)

Table 4. The reflections of Molao folks on watching their additional sports activities in Yifan Festival (n = 174).

Levels of reflection	Number	Percentage
Fun, exciting, pleasant	148	85.1%
The gong and drums are impressive, inspiring	122	70.1%
Will continue to watch	157	90.2%
Try to participate in person	139	79.8%
No feelings	17	9.8%

Among them, 151 people often watch the activities, 23 people occasionally watch them, holding the ratios of 80.3% and 12% respectively, which explains that the majority of folks concern about the traditional sports games and performances in Yifan Festival.

3.4.3 *The reflections of Molao folks on watching the traditional sports activities in Yifan Festival*

According to Table 4, in the 174 people who have watched the traditional sports games and performances, 85.1% think the games are fun, exciting and pleasant; 70.1% replies that the gong and drums, which are used to encourage the participators are very impressive and inspiring; 90.2%, an overwhelming majority said they will continue to watch the games; only 9.8% of them think they are boring.

It can be seen that Molao people's traditional sports activities are very popular with folk, and can create fitness and happiness for them. It is an undeniable responsibility of the administration of custom affairs to take advantage of Yifan Festival to popularize the ethnic sports and meet the needs of the people.

4 CONCLUSION

Yifan Festival is indigenous to Molao people of China, except for the hindrance in the Cultural Revolution, it has always been carried on and provoked enthusiastic responses. No matter it is held by folks or government, in the festival, the people have took active part in the activities and brought about positive influences. The traditional sports of Molao people render on the people infinite delight, fitness and happiness. In accordance with the responses given by local folks: the degree of appreciation, frequency of watching and the reflections after watching, traditional sports on the background of Yifan Festival enrich the spare life of the folks, stimulates the building of refined, scientific, and healthy lifestyle, and evokes enterprising, cheerful and uprising mental states. It has really enhanced the spiritual level of the people, and keeps on satisfying their spiritual demands that increase in a daily basis.

REFERENCES

- [1] Brief History of Molao People [M], Guahngxi Nationalities Publishing House, 1983:14-16.
- [2] Cui Lequan, A Glance on the Leisurely Mode of Ancient People EJ], Sports and History, 2000, (2).
- [3] Zheng Yingjie, The progress of Traditional Sports and Mountain Village Civilization around Hunan Province, Hubei Province, Chongqing and Guizhou Province, Beijing Normal University Academic Journal, 2000, (4).
- [4] Wang Tianjun, The Prospect and Strategies of Developing Tourism based on Ethnic Sports, Guangzhou Physical Culture College Academic Journal, 2000, (2).
- [5] The Xinhua News Agency, The CPC Central Committee and State Council on further construction of a new socialist countryside views, [z], 2006-2-21.
- [6] Lu Yuanzhen, The Hope Lies in The Revival of Oriental Sports—on Transforming the Chinese Ethnic Sports Meeting into Oriental Games, [J], Sports Culture Guide, 2003,9:16-19.
- [7] Song Yan, Putting Forward the Ethnic Culture, and Serve For Folks of all Peoples. [A], Exploration, Innovation, and Objectivity—Collection of Research and Practice in Qinghai Province During the 11th Five-year Plan, [C] 2011.06.
- [8] Chengbo, Suhang, Plan and Uphold Ethnic Cultures, The Northeast Windows, 2012, 02.

Contractor's claims management evaluation

Li Min Jia & Sha Lu

School of Economics and Management, China Three Gorges University, Yichang, Hubei, China

ABSTRACT: Existing literature on claims are focused on one aspect of claims management, there is little literature to study how to evaluate contractor's claims management. By analyzing the content of claims management and the process of claims to build the indicators system to evaluate contractor's claims management, it can reflect the level of contractor's claims management, and establish a new gray correlation degree and TOPSIS evaluation model. Using new evaluation model constructed to empirical analysis, the result shows that the new comprehensive model could reasonably evaluate the contractor's claims management.

Keywords: claims management; gray correlation degree; TOPSIS model; contractor

1 INTRODUCTION

Construction has the features of large investment, long construction period, complex topographic and geologic conditions, large construction difficulty, complex technology and there are many risks and unforeseen factors in the process of performing the contract, which leads to a lot of changes and claims. Therefore, construction contractors should do their best to claims management. It is important to know their own claims management problems and shortages, particularly important to know their comprehensive ability of claim management compared to other similar contractors. Most literature about claims management is focus on an angle of claim management to carry out research, few articles to study claims management evaluation. Lixia Zhang use fuzzy comprehensive evaluation model to evaluate the ability of the contractor's claims [1], there is a large correlation between the evaluation indicators, and include external factors, such as contractor's technical capability, financial capability and it so on, but they have no direct relation to claims management.

Evaluating contractor's claims management involves a number of factors, it is a multiple indicators preferred process, so introduce a multiple attribute decision making method to evaluate object. TOPSIS can reflect the overall similarity of the ideal solution among alternatives by way of the function curve, so structure relative closeness functions. TOPSIS is an effective multiple attribute decision making method, widely used in project evaluation, investment decision-making, optimal plan choosing, but the model itself is based on the original data, when the information in limited circumstances, use sample data to analyze can't

guarantee the correctness of decision results difficult [2]. However, In the process of claims management project evaluation, due to the information to evaluate the merits of the measure object is incomplete, coupled with human and other factors, so comprehensive comparison with the "gray" feature. Grey correlation analysis and TOPSIS method, a new decision-making model that combined with the advantages of gray correlation degree and TOPSIS model analysis problem more comprehensive and objective [3]. Traditional TOPSIS model in practical applications prone to cause problem of reverse order. This article use improved TOPSIS model can solve this problem [4]. This article put forward evaluation model based on gray correlation analysis and improved TOPSIS model to evaluate contractor's comprehensive claims management capabilities.

Combined content and procedures of claims management to build a comprehensive claims management evaluation indicators system. Choosing four branch offices of a large water conservancy and hydropower construction enterprise as the object of study, by the comprehensive evaluation model proposed in this article come through what degree can various indicators influence claims management f , and the final ranking of four branch offices' claims management, so they can mutual know their gap or advantage.

2 CONFIRM THE EVALUATION INDICATORS OF CONTRACTOR'S CLAIMS MANAGEMENT

In project management, the tasks of claims management are claims and counterclaims [5]. Claims tasks include forecasting the opportunity

Table 1. Contractor's claim management evaluation indicators system.

Target layer	Decomposed layer	Index layer
Claim management evaluation	Claim chance's seeking	Analysis contract terms $F1$ Investigate event $F2$ Submit claim intention $F3$
	Internal processing of claim	Collect claim evidence $F4$ Calculate the value of claim $F5$ Formulate claim strategy $F6$ Submit claim report $F7$
	Claim's settlement	Claim negotiation $F8$ Claim dispute resolved $F9$
	Counterclaim	Analysis three states $F10$ Analysis report claim $F11$ Submit counterclaim report $F12$

to claiming and finding opportunities when construct project, and management work in the process of resolving claims and handling claims dispute. Counterclaims include counterattack and prevent the other party claims. In practice, there is little claim the proprietor lodge to contractor, so simplify counterclaim management indicators. This article based on the constituent elements of claims management and combined with the processing of claims event to design 3 first class indicators and 9 second class indicators of claims and 4 second class indicators of counterclaims, and establish a comprehensive evaluation indicators system of contractor's claims management.

3 BUILD CONTRACTOR'S CLAIMS MANAGEMENT EVALUATION MODEL

Assuming the evaluation object of project claim management $C = (C_1, C_2, \dots, C_m)$, Evaluation index $F = (F_1, F_2, \dots, F_m)$, the Matrix of original data $X = (x_{ij})_{m \times n}$, x_{ij} means the attribute value of evaluation object i when its indicator is j , $i \in m, j \in n$.

3.1 Determine the indicators weights

There are subjective weighting method and objective weighting method to decide weight, this article adopt entropy weight method belong to objective weighting method in entropy method, that the entropy weight method is mature, so do not specifically introduced. Weight vector is $w = (w_1, w_2, \dots, w_i)$.

3.2 Set up improved evaluation model

Traditional TOPSIS model has the problem that it can reverse order sometime. This article adopt modified TOPSIS model to overcome this problem

and build gray correlation degree and modified TOPSIS comprehensive evaluation model. Steps are as follows.

3.2.1 Establish the improved evaluation model

Firstly, standardize the original data matrix, which is the biggest difference from traditional TOPSIS in modeling process. Standardize the data.

$$\begin{aligned}
 1) \ y_{ij} &= \frac{x_{ij} - \min_{1 \leq i \leq m} x_{ij}}{\max_{1 \leq i \leq m} x_{ij} - \min_{1 \leq i \leq m} x_{ij}}, \quad j = (1, 2, \dots, n) \\
 2) \ y_{ij} &= \frac{\max_{1 \leq i \leq m} x_{ij} - x_{ij}}{\max_{1 \leq i \leq m} x_{ij} - \min_{1 \leq i \leq m} x_{ij}}, \quad j = (1, 2, \dots, n) \quad (1)
 \end{aligned}$$

1) to benefit-type indicator, 2) to cost-type indicator, that ensures the maximum value is 1, the minimum value is 0. The matrix after standardization process. $Y = (y_{ij})_{m \times n}$.

3.2.2 Calculate the distance evaluation object to ideal solution and negative solution

As ideal solution Y^+ (the set of all ideal solution) is 1, negative ideal solution Y^- (the set of all negative ideal solution) is 0, the distance evaluation object to ideal solution and negative solution is d_i^+ and d_i^- .

$$d_i^+ = \sqrt{\sum_{j=1}^n w_{ij} (y_{ij} - 1)^2} \quad (2)$$

$$d_i^- = \sqrt{\sum_{j=1}^n w_{ij} (y_{ij} - 0)^2} = \sqrt{\sum_{j=1}^n w_{ij} y_{ij}^2} \quad (3)$$

3.2.3 Determine the weighting standard matrix of gray correlation degree

Standard matrix got from equation (1) multiplied by index weight got from entropy weight method,

the result is standard matrix Z that gray correlation degree calculation required. $Z = W^*Y$.

3.2.4 Calculate gray correlation coefficient of object with ideal object and negative ideal object

Firstly, calculate gray correlation coefficient of object i and the ideal object about indicator j .

$$r_{ij}^+ = \frac{m + \xi M}{\Delta_{ij} + \xi M}, \xi \in (0,1) \quad (4)$$

$\Delta_{ij} = |z_{0j}^+ - z_{ij}^+|$, $m = \min_i \min_j \Delta_{ij}$, $M = \max_i \max_j \Delta_{ij}$, ξ is distinguish coefficient, generally take 0.5, z_{0j}^+ is the biggest value of z_{ij}^+ .

Calculate gray correlation coefficient of object i and the ideal object.

$$r_i^+ = \frac{1}{n} \sum_{j=1}^n r_{ij}^+, (i = 1, 2, \dots, m) \quad (5)$$

Secondly, calculate gray correlation coefficient of object i and the negative ideal object about indicator j .

$$r_{ij}^- = \frac{m + \xi M}{\Delta_{ij} + \xi M}, \xi \in (0,1) \quad (6)$$

$\Delta_{ij} = |z_{0j}^- - z_{ij}^-|$, $m = \min_i \min_j \Delta_{ij}$, $M = \max_i \max_j \Delta_{ij}$, ξ is distinguish coefficient, generally take 0.5, z_{0j}^- is the least value z_{ij}^- of.

Calculate gray correlation coefficient of object i and the negative ideal object.

$$r_i^- = \frac{1}{n} \sum_{j=1}^n r_{ij}^-, (i = 1, 2, \dots, m) \quad (7)$$

3.2.5 Calculate relative closeness degree

Applies dimensionless method to handle distance and gray correlation coefficient got from above steps.

$$\varphi_i = \Phi_i / \max_{1 \leq i \leq m} \Phi_i \quad (8)$$

Φ_i stands for d_i^+ , d_i^- , r_i^+ , r_i^- , φ_i is $(d_i^+)_{new}$, $(d_i^-)_{new}$, $(r_i^+)_{new}$, $(r_i^-)_{new}$, stands for value after the dimensionless.

The larger the value of $(d_i^-)_{new}$ and $(r_i^+)_{new}$, the closer to the ideal solution, the smaller the value of $(d_i^+)_{new}$ and $(r_i^-)_{new}$, the closer to the negative ideal solution.

$$S_i^+ = a_1(d_i^-)_{new} + a_2(r_i^+)_{new}, (i = 1, 2, \dots, m) \quad (9)$$

$$S_i^- = a_1(d_i^+)_{new} + a_2(r_i^-)_{new}, (i = 1, 2, \dots, m) \quad (10)$$

a_1 and a_2 can react the degree of the preference evaluator to position and shape, they are positive numbers, and the sum of the two is 1. The larger a_1 is, the stronger preference evaluator to distance, the stronger a_2 , the stronger preference evaluator to shape. S_i^+ synthetically reflects the closeness of solution and ideal solution, the bigger the value is, the better the object, and S_i^- reflects the degree that object away from the ideal solution, the smaller the value, the better the object.

New close degree based on Euclidean distance and new gray correlation degree can reflect the positional relationship and the similarity of the data curve between the object and the ideal solution and negative ideal solution. Calculate the relative closeness degree of object i .

$$T_i^* = \frac{S_i^+}{S_i^- + S_i^+}, (i = 1, 2, \dots, m) \quad (11)$$

The bigger the value of new close degree, the better the evaluation object.

4 EMPIRICAL STUDY OF CONTRACTOR'S CLAIMS MANAGEMENT EVALUATION

This article selects 4 branch of large water conservancy and hydropower project construction enterprise as the research object, please the relevant project manager, chief of the contract, chief Engineer and their like who are familiar with claims management score with 12 evaluation indicators of claims management with excellent (8–10 points), good (7–8 points), medium (6–7 points), and poor (6 points or less). Average score of 4 objects' each evaluation indicator as shown in [Table 2](#).

4.1 Calculate the weight of indicators

The evaluation indicators weight by entropy weight method, as shown in [Table 3](#).

The above table shows the formulate claim strategy, investigate event and calculate the value of claim make up a larger share of the weight, and that indicates these indicators have a great relationship with claims management level.

4.2 Calculate the distance

Due to the selected data through expert scoring, they are efficiency indicators. Establish a standardized matrix, by [equation \(1\)](#) can make sure all the ideal solution is 1, all negative solution is 0. According to the formula (2) (3) can calculate the Euclidean distance between the evaluation object and the ideal solution and negative ideal solution.

Table 2. The original data of experts scoring.

Branch office	F1	F2	F3	F4	F5	F6	F7	F8	F9	F10	F11	F12
C1	7	8.2	8	7.5	7.4	7.6	7.2	9	7.2	7.5	8.3	7.1
C2	6.5	7.5	7.8	8	8.9	8.9	7.4	7.5	8.3	7.4	7.6	7.5
C3	8.2	6.7	7.4	6.9	6.9	6.2	6.9	8.3	6.8	7.9	7.2	7.8
C4	7.1	6.1	8.5	7.3	7.5	6.9	7.8	7.1	7.5	7.8	7.9	7.1

Table 3. Indicators, weight and rank.

Indicators	F1	F2	F3	F4	F5	F6	F7	F8	F9	F10	F11	F12
Weight	0.1	0.171	0.034	0.039	0.125	0.246	0.027	0.115	0.074	0.01	0.037	0.022
Ranking	5	2	9	7	3	1	10	4	6	12	8	11

$$D^+ = (d_1^+, d_2^+, d_3^+, d_4^+) = (0.522, 0.489, 0.828, 0.767)$$

$$D^- = (d_1^-, d_2^-, d_3^-, d_4^-) = (0.660, 0.768, 0.438, 0.380)$$

4.3 Calculate gray correlation degree

According to the formula (4)–(7) can calculate the grey correlation degree of each evaluation object with ideal solution and negative ideal solution.

$$R^+ = (0.819, 0.855, 0.736, 0.742)$$

$$R^- = (0.775, 0.765, 0.889, 0.855)$$

4.4 Dimensionless distance and gray correlation degree

According to the formula (8) can obtain the result as shown below.

$$(D^+)_{new} = (0.631, 0.591, 1.000, 0.926)$$

$$(D^-)_{new} = (0.860, 1.000, 0.570, 0.495)$$

$$(R^+)_{new} = (0.958, 1.000, 0.860, 0.867)$$

$$(R^-)_{new} = (0.871, 0.860, 1.000, 0.961)$$

According to the formula (9) and (10), make $\alpha_1 = \alpha_2 = 0.5$, combine distance and correlation.

$$S^+ = 0.5(D^-)_{new} + 0.5(R^+)_{new} \\ = (0.909, 1.000, 0.715, 0.681)$$

$$S^- = 0.5(D^+)_{new} + 0.5(R^-)_{new} \\ = (0.751, 0.725, 1.000, 0.944)$$

4.5 Calculate relative closeness degree

According to the formula (12) can get closeness degree set of contractors.

$$T^* = (0.548, 0.580, 0.417, 0.419)$$

Ranking as the size of closeness degree, the greater the closeness degree, the better evaluation object's claims management. So that the evaluation object 2 have the best comprehensive claims management level and evaluation object 3 need to promote its claims management. Evaluation object 2 obtain the top score at calculate the value of claim and formulate claim strategy that have the biggest impact to claims management, by calculating the comprehensive evaluation model, the relative closeness degree get the highest score, that indicate its comprehensive claims management is the best.

5 CONCLUSION

In this article, gray correlation degree is combined with improved TOPSIS model, we have built a new evaluation model to evaluate the claims management of contractors. Constructing 12 evaluation index systems which about the claims management of contractors to reflect the various aspects of claim management comprehensively. By the way, analyzed the data collected by Entropy weight method, concluded that there are three indicators have a greater impact on the evaluation of claim management, they are formulate claim strategy, investigate event and calculate the value respectively. By the evaluation model of claims management conducting an empirical analysis, and come to a conclusion that the claims management of con-

tractor 2 is best, which reflects the actual situation effectively. This suggests that the new gray correlation degree and TOPSIS evaluation model which adapt to evaluate the contractor's claims management comprehensive ability evaluation, the result is reasonable. Through claims management evaluation can help the contractor understand their own claims management situation, recognize the advantages and disadvantages and make the claims management work well.

REFERENCES

- [1] Lixia, Zhang & Fuxiang, Wei. 2007. Comprehensive evaluation research about the claims ability of contractors. *Statistics and Decision* 05: 157–158.
- [2] Yanbin, Li & Xinyi, Yu, Zhijie. The risk assessment research about gray correlation degree and TOPSIS method photovoltaic project. *Power System Technology* 06: 1514–1519.
- [3] Xiaodong, Sun & Jiao, Yue. 2005. Decision Method Based on Grey Correlation and TOPSIS. *China Management Science* 04: 63–68.
- [4] Junmin, Wei & Baoqing, Hu. 2013. The land remediation Reasonable evaluation based on improved TOPSIS. *Resource Sciences* 07: 1407–1414.
- [5] Hu, Cheng. 2008. *Construction project management and contract claims*. Nanjing: Southeast University Press.

Matrix transfer method of the curved-wall type tunnel lining structure calculation

Jing Yin & Rong Gui Deng

Department of Geotechnical Engineering, Southwest Jiaotong University, Chengdu, Sichuan, China
State Key Laboratory of Hydraulics and Mountain River Engineering, Sichuan University, Chengdu, Sichuan, China

Zhi Bin Zhong & Pan Wang

Department of Geotechnical Engineering, Southwest Jiaotong University, Chengdu, Sichuan, China

Min Hu

Sichuan Jiaoda Engineering Testing Consulting Co., Ltd., Chengdu, Sichuan, China

ABSTRACT: In the curved wall taken on “linear” micro segment of the tunnel lining section, according to the straight beam deflection initial parameter equation to establish straight beam transfer field matrix. Consider tunnel lining axis force and axial displacement factor to modify the straight beam transfer field matrix, and through coordinate transformation matrix to connect various “linear” micro section, transfer field matrix expression of the curved-wall type tunnel lining structure is deduced, using the boundary conditions to solve internal force and displacement of the curved-wall tunnel lining. Through example calculation, the method of this article used is of high precision and simple, can provide a approach to analyze the reliable force and displacement of the curved-wall tunnel lining structural design.

Keywords: matrix transfer method; curved-wall type tunnel lining; field matrix; internal force; displacement

1 INTRODUCTION

When tunnel lining is under greater surrounding rock pressure on the vertical and horizontal directions, often using curved-wall type tunnel lining^[1]. At present the analysis calculation of the internal force of tunnel lining often adopt load structure method and layer structure method^[2,3]. The layer structure method considered the interaction of structure and surrounding strata, can more realistically simulate the structural internal force of the underground structure and deformation of surrounding strata under every single construction Step. But due to the complexity of the surrounding strata and the interaction between formation and structure, layer structure method is in the development stage, in many engineering applications, just as a supplementary means^[4,5]. Load structure method based on the mechanics principle, not considering the interaction of the structure and the formation. In load structure method, often using force method and displacement method which are only applicable to solve the problems that calculation diagram is relatively rough, the number of unknowns is not too much in structure analysis^[6].

When the load of the tunnel lining structure is no longer symmetrical, plus the role of anchor cable, the number of unknowns are too much, then with the traditional method of tunnel mechanics, the calculation has certain difficulty. Therefore, the paper proposes a matrix transfer method of the curved-wall type tunnel lining structure.

Matrix transfer method is a structural analysis method between force method and displacement method. Because the calculation process is multiple multiplication of a series of lower order matrices, it is a kind of high precision and simple method, through programming, can obtain accurate results. At present, some scholars applied the transfer matrix method to concrete structure analysis. Literature^[7] detailed discusses the application of matrix transfer method in a variety of engineering structures; In Literature^[8], the matrix calculation method of anti-slide pile is deduced by using the initial parameter method; Literature^[9-13] put the matrix transfer method used in structural analysis of the curved bridge; Literature^[14] put the matrix transfer method used in the static analysis of steel bridge structure, four kinds of representative bridge are chosen as the research object, and

to solve the internal forces and displacements respectively;^[15] by combining the finite segment method and the matrix transfer method of multi body system dynamics discrete time, formed the matrix transfer method of finite segment discrete time of the nonlinear beam.

The basic idea of the transfer matrix algorithm of the curved-wall type tunnel lining is to straighten the curved micro-segment. In the curved wall taken on “linear” micro-segment of the tunnel lining section, and according to the straight beam deflection initial parameter equation to establish transfer field matrix, finally through the coordinate transmitting matrix to connect every micro-segment, using the boundary conditions to solve the internal force and displacement of the curved-wall type tunnel lining.

2 THE MATRIX TRANSFER OF CURVED-WALL TYPE TUNNEL LINING STRUCTURE

Using the differential relation of displacement y , rotation ϕ , bending M , shear F , load density q and beam stiffness EI , the differential equation normal form of the beam deflection curve is obtained:

$$\frac{d^4 y}{dx^4} = \frac{q}{EI} \quad (1)$$

Take a beam element to analyze, as shown in Figure 1.

Combined with the boundary conditions on $i-1$:

$$\begin{cases} y(0) = y_{i-1} \\ y'(0) = \phi_{i-1} \\ -EIy''(0) = M_{i-1} \\ -EIy'''(0) = F_{i-1} \end{cases} \quad (2)$$

Initial parameter equation of deflection curve of the straight beam element can be obtained:

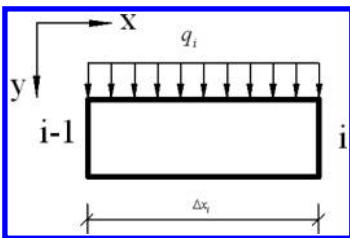


Figure 1. Schematic view of beam element.

$$y_i = \frac{q_{i-1}}{24E_i I_i} \Delta x_i^4 - \frac{F_{i-1}}{6E_i I_i} \Delta x_i^3 - \frac{M_{i-1}}{2E_i I_i} \Delta x_i^2 + \phi_{i-1} \Delta x_i + y_{i-1} \quad (3)$$

Using the differential relation of displacement y , rotation ϕ , bending M , shear F , load density q , can get the transfer field matrix (4) of the straight beam:

$$\begin{bmatrix} q_i \\ F_i \\ M_i \\ \phi_i \\ y_i \end{bmatrix} = \begin{bmatrix} \frac{q_i}{q_{i-1}} & 0 & 0 & 0 & 0 \\ -\Delta x_i & 1 & 0 & 0 & 0 \\ -\frac{\Delta x_i^2}{2} & \Delta x_i & 1 & 0 & 0 \\ \frac{\Delta x_i^3}{6E_i I_i} & -\frac{\Delta x_i^2}{2E_i I_i} & -\frac{\Delta x_i}{E_i I_i} & 1 & 0 \\ \frac{\Delta x_i^4}{24E_i I_i} & -\frac{\Delta x_i^3}{6E_i I_i} & -\frac{\Delta x_i^2}{2E_i I_i} & \Delta x_i & 1 \end{bmatrix} \begin{bmatrix} q_{i-1} \\ F_{i-1} \\ M_{i-1} \\ \phi_{i-1} \\ y_{i-1} \end{bmatrix} \quad (4)$$

In the calculation of the curved-wall type tunnel lining structure, the impact of axial force (while the pressure is positive) also should be considered, and the displacement calculated by (4) is just the radial displacement of the curved-wall type tunnel lining structure, still need to calculate the axial displacement w_i . After considering the axial force and axial displacement, (4) can be modified to (5):

$$\begin{bmatrix} q'_i \\ F'_i \\ N'_i \\ M'_i \\ \phi'_i \\ y'_i \\ w'_i \end{bmatrix} = \begin{bmatrix} \frac{q_i}{q_{i-1}} & 0 & 0 & 0 & 0 & 0 & 0 \\ -\Delta x_i & 1 & 0 & 0 & 0 & 0 & 0 \\ 0 & 0 & 1 & 0 & 0 & 0 & 0 \\ -\frac{\Delta x_i^2}{2} & \Delta x_i & 0 & 1 & 0 & 0 & 0 \\ \frac{\Delta x_i^3}{6E_i I_i} & -\frac{\Delta x_i^2}{2E_i I_i} & 0 & -\frac{\Delta x_i}{E_i I_i} & 1 & 0 & 0 \\ \frac{\Delta x_i^4}{24E_i I_i} & -\frac{\Delta x_i^3}{6E_i I_i} & 0 & -\frac{\Delta x_i^2}{2E_i I_i} & \Delta x_i & 1 & 0 \\ 0 & 0 & -\frac{\Delta x_i}{E_i A_i} & 0 & 0 & 0 & 1 \end{bmatrix} \begin{bmatrix} q_{i-1} \\ F_{i-1} \\ N_{i-1} \\ M_{i-1} \\ \phi_{i-1} \\ y_{i-1} \\ w_{i-1} \end{bmatrix} \quad (5)$$

(5) is the transfer equation of a straight beam micro-segment. In order to connect the two micro-segment which is not in the same line, based on the coordinate transformation matrix, it's main purpose is to put the displacements (radial and

axial displacement) and internal forces (shear and axial) of a micro-segment before to transfer to the next micro-segment, to continue moving forward.

As shown in Figure 2, boundary condition of $i-1$ is used to calculate the displacement and internal force of i , $i-1$ to i and i to $i+1$ are not in a straight line, so shear and axial forces need to convert using the coordinate transformation matrix. (6) shows the conversion of displacement, shear, and axial force of node i .

D_i , Z_i are the element transfer matrix and the coordinate transformation matrix, therefore, transfer field matrix of the curved-wall type tunnel lining structure as (9).

$$\begin{bmatrix} q_i \\ F_i \\ N_i \\ M_i \\ \phi_i \\ y_i \\ w_i \end{bmatrix} = \begin{bmatrix} 1 & 0 & 0 & 0 & 0 & 0 & 0 \\ 0 & \cos(\Delta\theta_i) & \sin(\Delta\theta_i) & 0 & 0 & 0 & 0 \\ 0 & -\sin(\Delta\theta_i) & \cos(\Delta\theta_i) & 0 & 0 & 0 & 0 \\ 0 & 0 & 0 & 1 & 0 & 0 & 0 \\ 0 & 0 & 0 & 0 & 1 & 0 & 0 \\ 0 & 0 & 0 & 0 & 0 & \cos(\Delta\theta_i) & \sin(\Delta\theta_i) \\ 0 & 0 & 0 & 0 & 0 & -\sin(\Delta\theta_i) & \cos(\Delta\theta_i) \end{bmatrix} \begin{bmatrix} q'_i \\ F'_i \\ N'_i \\ M'_i \\ \phi'_i \\ y'_i \\ w'_i \end{bmatrix} \quad (6)$$

Letbe:

$$Z_i = \begin{bmatrix} 1 & 0 & 0 & 0 & 0 & 0 & 0 \\ 0 & \cos(\Delta\theta_i) & \sin(\Delta\theta_i) & 0 & 0 & 0 & 0 \\ 0 & -\sin(\Delta\theta_i) & \cos(\Delta\theta_i) & 0 & 0 & 0 & 0 \\ 0 & 0 & 0 & 1 & 0 & 0 & 0 \\ 0 & 0 & 0 & 0 & 1 & 0 & 0 \\ 0 & 0 & 0 & 0 & 0 & \cos(\Delta\theta_i) & \sin(\Delta\theta_i) \\ 0 & 0 & 0 & 0 & 0 & -\sin(\Delta\theta_i) & \cos(\Delta\theta_i) \end{bmatrix} \quad (7)$$

$$D_i = \begin{bmatrix} \frac{q_i}{E_i I_i} & 0 & 0 & 0 & 0 & 0 & 0 \\ \frac{q_{i-1}}{E_i I_i} & 1 & 0 & 0 & 0 & 0 & 0 \\ -\Delta x_i & 0 & 1 & 0 & 0 & 0 & 0 \\ 0 & 0 & 0 & 1 & 0 & 0 & 0 \\ -\frac{\Delta x_i^2}{2} & \Delta x_i & 0 & 1 & 0 & 0 & 0 \\ \frac{\Delta x_i^3}{6E_i I_i} & -\frac{\Delta x_i^2}{2E_i I_i} & 0 & -\frac{\Delta x_i}{E_i I_i} & 1 & 0 & 0 \\ \frac{\Delta x_i^4}{24E_i I_i} & -\frac{\Delta x_i^3}{6E_i I_i} & 0 & -\frac{\Delta x_i^2}{2E_i I_i} & \Delta x_i & 1 & 0 \\ 0 & 0 & -\frac{\Delta x_i}{E_i I_i} & 0 & 0 & 0 & 1 \end{bmatrix} \quad (8)$$

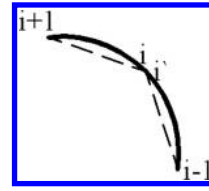


Figure 2. Schematic view of relationships between two micro section.

$$\begin{bmatrix} q_i \\ F_i \\ N_i \\ M_i \\ \phi_i \\ y_i \\ w_i \end{bmatrix}^T = Z_i D_i \begin{bmatrix} q_{i-1} \\ F_{i-1} \\ N_{i-1} \\ M_{i-1} \\ \phi_{i-1} \\ y_{i-1} \\ w_{i-1} \end{bmatrix}^T \quad (9)$$

3 THE BOUNDARY CONDITIONS OF CURVED-WALL TYPE TUNNEL LINING

The connection of both ends of micro-segment is established by (9), as long as divided enough micro-sections, and know all of the internal forces and displacements of one section, can calculate the internal forces and displacements of the entire curved-wall type tunnel lining structure using (9). Therefore, it is necessary to using the boundary conditions to solve out the internal forces and displacements of one section. The boundary conditions of curved-wall type tunnel lining are mainly concentrated in two corners, similar to pile calculation, transfer matrixes of the two corner can be pressed by (10).

$$D = \prod_{i=1}^n Z_i D_i = Z_n D_n Z_{n-1} D_{n-1} \cdots Z_2 D_2 Z_1 D_1 \quad (10)$$

After obtained the transfer matrix D , then can get the relation (11) between internal forces and displacements of the two wall corners of tunnel lining. Because the horizontal distribution force is known, in the remaining 12 quantities, as long as know that any of 6, can according to formula (11) to solve the remaining 6.

$$\begin{bmatrix} q_{n+1} \\ F_n \\ N_n \\ M_n \\ \phi_n \\ y_n \\ w_n \end{bmatrix}^T = D \begin{bmatrix} q_1 \\ F_0 \\ N_0 \\ M_0 \\ \phi_0 \\ y_0 \\ w_0 \end{bmatrix}^T \quad (11)$$

4 INSTANCE OF LINING CALCULATION

In order to facilitate verification the correctness of using matrix method to calculate the curved-wall type tunnel lining and program corresponding to the calculation, also for the convenience of contrast, the instance of here don't calculate the

entire lining structure, but calculate an arc with both ends fixed which under the action of horizontal distribution force. Which, radius $r = 5$ m, central angle $w = 90^\circ$, width $b = 0.6$ m, thickness $h = 0.6$ m, elastic modulus $E = 25.5$ Gpa, moment of inertia $I = 0.0108$ m⁴, sectional area $a = 0.36$ m², horizontal distribution force perpendicular to the arc $q = 500$ kN/m.

Transfer matrix between the two endpoints can be obtained by the formula (10):

$$D = \begin{bmatrix} 1 & 0 & 0 & 0 & 0 & 0 & 0 \\ -4.999 & -1.306e-15 & 1.000 & 0 & 0 & 0 & 0 \\ 5.001 & -1.000 & -1.306e-15 & 0 & 0 & 0 & 0 \\ -25.00 & 5.001 & 4.997 & 1.000 & 0 & 0 & 0 \\ 2.591e-4 & -9.079e-5 & -5.179e-05 & -2.852e-05 & 1.000 & 0 & 0 \\ 4.864e-4 & -2.267e-4 & -9.776e-05 & -9.076e-05 & 4.997 & -1.306e-15 & 1.000 \\ -1.624e-4 & 9.790e-05 & 3.186e-05 & 5.184e-05 & -5.001 & -1.000 & -1.306e-15 \end{bmatrix}$$

Using the boundary conditions can be obtained:

$$\begin{bmatrix} q_{n+1} & F_n & N_n & M_n & 0 & 0 & 0 \end{bmatrix}^T = D \begin{bmatrix} 500 & F_0 & N_0 & M_0 & 0 & 0 & 0 \end{bmatrix}^T$$

Inserting **D** in upper formula:

$$\begin{bmatrix} 0 \\ 0 \\ 0 \end{bmatrix} = \begin{bmatrix} 2.591e-4 & -9.079e-05 & -5.179e-05 & -2.852e-05 \\ 4.864e-4 & -2.267e-4 & -9.776e-05 & -9.076e-05 \\ -1.624e-4 & 9.790e-05 & 3.186e-05 & 5.184e-05 \end{bmatrix} \begin{bmatrix} 500 \\ F_0 \\ N_0 \\ M_0 \end{bmatrix}$$

Using the above expression can solve the force and displacement of the internal section, then can get the internal force and displacement of arbitrary cross-section using transfer matrix (9). Results as shown in **Figures 4–8**.

As structure and load are symmetrical, so the shear force is antisymmetric, axial force, bending moment and displacement are symmetrical. Provisions axial displacement along the forward

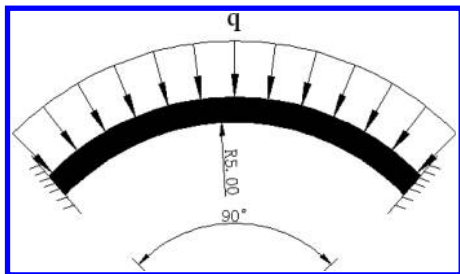


Figure 3. Schematic view of the calculation example.

direction of the calculation is positive in the calculation, the axial displacement is positive, and vice versa, negative, causing the axial displacement diagram is antisymmetric, actually it is symmetrical.

As can be seen from **Figures 4–8**, the calculation results and the corresponding boundary conditions are consistent, and the relationship between internal force and displacement is coordinated, then can prove the matrix transfer formula of arc

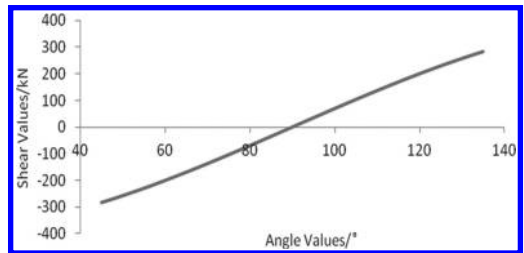


Figure 4. Shear diagram.

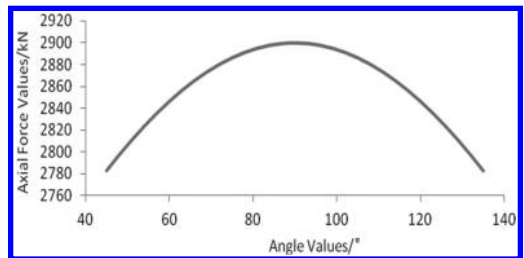


Figure 5. Axial force diagram.

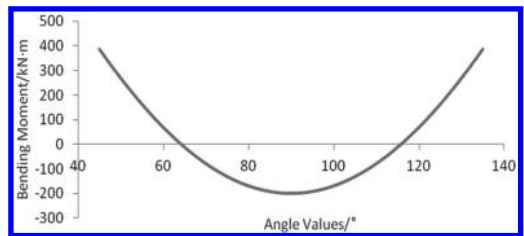


Figure 6. Bending moment diagram.

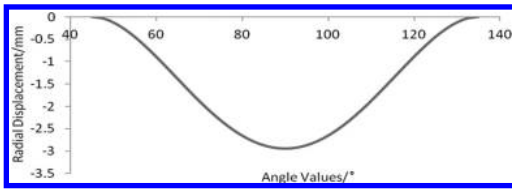


Figure 7. Radial displacement diagram.

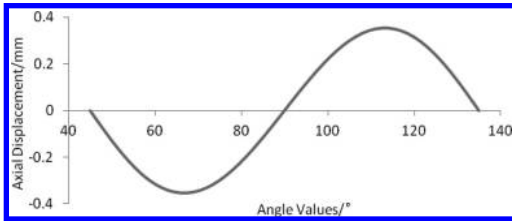


Figure 8. Axial displacement diagram.

lining and program composition that this paper derived are correct.

5 CONCLUSION

1. The actual calculation of the arc segment taken from the curved-wall type tunnel lining structure shows that the matrix transfer formula proposed in this paper is correct.
2. For the static calculation of the curved-wall type tunnel lining, using the matrix transfer method is a very desirable approach. This method avoids the abandonment error when using finite element method for solving equations and ill-posed problems which is easy to occur in the coefficient matrix of the linear equations.
3. Compared with finite element method, this method is easy for data preparation, take up less memory, short operation time, and program composition is far simpler than the finite element method, especially suitable for engineers and technicians to apply on the microcomputer.

FOUNDATION ITEM: This research is supported by Research Fund for the Doctoral Program of Higher Education (20120184110023) and

Engineering Foundation of State Key Laboratory of Hydraulics and Mountain River (1208).

REFERENCES

- [1] Wang Cheng. Tunneling Engineering[M]. Beijing: China Communications Press, 2009.
- [2] Ministry of Transport of the People's Republic of China. JTG D70-2004 Design Specification of Highway Tunnel[S]. Beijing: China Communications Press, 2004.
- [3] Ministry of railway of the People's Republic of China. TB10003-2005 Design Specification of Railway Tunnel[S]. Beijing: China Railway Publishing House, 2006.
- [4] Zhao Shangyi, Zheng Yingren, Song Yakun, ect. An Analysis of the Design Method of Underground Tunnel Linings[J]. Journal of Logistical Engineering University, 2007, 23(4):29-33.
- [5] Luo Yanjian. The existing problems of railway tunnel structure design theory and method[J]. World Tunnel, 1997, (5):8-12.
- [6] Li Liankun. Structural mechanics[M]. Beijing: Higher Education Press, 2004.
- [7] Liu Qingtan, Ni Guorong. The Transfer Matrix Method in Structural Analysis[M]. Beijing: China Railway Publishing House, 1997.
- [8] The Second Survey and Design Institute Ministry of Railways. Anti-slide Pile Design and Calculation[M]. Beijing: China Railway Publishing House, 1983, 3.
- [9] Wang Fumin. Curved Girder Bridge Transfer Matrix Design Method and Engineering Application Practice[M]. Beijing: China Railway Publishing House, 2009, 3.
- [10] Qu Erren, Liu Xiaowu, Yi Yunkun, ect. Transfer Matrix Method Applied to Structural Analysis of Curve Bridge[J]. Journal of Hefei university of Technology. 1999, 22(6):73-79.
- [11] Li Qingning. The transfer matrix method of bar elements with variable cross-section[J]. Journal of Xi'an University of Architecture & Technology, 1997, 33(1):18-22.
- [12] Chen Shengping, Hu Shengsong. Transmission Matrix Method for Continuous Beam[J]. Journal of Hubei Polytechnic University, 1998, (13):173-175.
- [13] Li Huisheng. Using the transfer matrix method to calculate the internal force and deformation of the curved beam[J]. Bridge Construction, 1991, 1(3):65-66.
- [14] Zhang Jie. Research on Application of Transfer Matrix Method in Structural Analysis of Steel Bridges[D]. Hohai University. 2005.
- [15] He Bin. Study on Transfer Matrix Method for Multibody System Dynamics and Its Application in Launch Dynamics[D]. Nanjing University of Science and Technology. 2006.

The use of virtual water trade in water resources optimization in Minqin

Jian Min Han, Meng Liu & Yan Chen

College of Humanity, Gansu Agricultural University, Lanzhou, Gansu, China

ABSTRACT: In this paper, the method for calculating the virtual water content of crop products, livestock and poultry products was presented which based on the explaining of the concept of virtual water and virtual water trade and the actual situation of Minqin. It helped us determine the types of agricultural and animal husbandry that was suitable for Minqin. It could provide a certain basis for water resources optimal allocation and the adjustment of industrial structure, and make contributions to improving environment and increasing farmers' income and economic output.

Keywords: virtual water; virtual water trade; Minqin; water resources optimization

In a closed and conservative economic society, a country or a region could only rely on their own resources to achieve its development goals. However, in an open economic society, a country or a region could import goods produced by other countries or regions, and export goods produced by the rich local resources to achieve its development goals. To measure the amount of water resources invisible transfer caused by merchandise trade, it urgently needed an appropriate concept or a tool. The concept "virtual water" was just to meet this demand. And virtual water really played an important role in improving the efficiency of the global water resources allocation.

1 THE CONCEPT OF VIRTUAL WATER AND VIRTUAL WATER TRADE

Virtual water was the water resources needed in the process of goods and services production. The introduction of virtual water provided a possible way to alleviate the water shortage problem for water shortage nations or regions; that is to say, they could buy some grain from international market to ensure water resources and food safety.

Virtual water trade was that the nations or regions lack of water resources achieved water and food security by buying water intensive agricultural products from nations or regions which are rich of water. From the perspective of system, virtual water trade used systematic thinking method to search for the various influencing factors associated with the problem and search for strategies to solve regional internal problems outside the scope of them, and

solved the shortage of water resources and food security by advocating virtual water trade—which meant exporting high efficiency but low water consumption products and importing food products that couldn't be produced by themselves because of water shortage. Consequently virtual water trade had major strategic significance in water shortage countries or regions, and it obtained the application in some countries and regions, such as Jordan, Israel, Japan and so on.

For water shortage Minqin, it could alleviate the pressure of water resources shortage by developing virtual water trade—import goods requiring a large number of water resources in the process of production and export goods requiring a little water, and improve the ecological environment and increasing the farmers' income and economic output.

2 THE BASIC SITUATION OF WATER RESOURCES ALLOCATION IN MINQIN, GANSU

2.1 *The basic situation of Minqin*

Minqin (38°3'—39°27'N., 101°49'—104°12'E.) lies in the west of Gansu, the lower reaches of Shiyang River on the north side of the eastern end of the Hexi Corridor, surrounded by Tengeryn and Badan Jilin desert to the east. The county area is vast, and its terrain dips from southwest to northeast. The topography is mainly high plains, also includes low mountains and basins, the desert landforms significant. It covers an area of 15,900 square km. Among them, sand dune and Gobi desert account for over 85%, but the county only account for less than 9%.

Water resources supply in Minqin mainly included four parts: atmospheric precipitation, surface water, ground water and trans-basin diversion. The surface water and groundwater is the main for Minqin, but the precipitation amount was very little, and the interannual change is big, and the average annual of it is 110 mm mainly on summer. The only surface water available was the Shiyang River in Minqin. The total quantity of water available was only 304 million m³, including 137.3 million m³ of available groundwater and 167 million m³ of exploitable groundwater.

Minqin was an irrigation agriculture county, which mainly produces grain crops, meanwhile abounded with melon. At present, the county had built 10 commodity base, including grain and oil, cotton, melon seeds, muskmelon, beet, fruit, vegetables, livestock and poultry, medicinal materials, small grains and so on. In general, the primary industry agriculture accounted for the major proportion, the development speed of the second and third industry became faster than agriculture, having already started to show the promotion on the development of the national economy. The national economy maintained a rapid, healthy development momentum.

2.2 *The realistic basis of implementing virtual water trade in Minqin*

According to the comparative analysis between plant area and water consumption (Table 1) of different crops of Minqin in 2007, grain crops was high water consumption, but the pepper, melon and vegetables in Greenhouse of economic crops still consumed a lot of water. Through different crops plant areas weighted average, the water consumption of grain crops was 530 m³/mu, economic crops was 420 m³/mu, and forage grass was 400 m³/mu. Without considering part cultivated land reduction, the saving water consumption for

the adjustment of agricultural planting structure was about 2 million m³, compared with the ratio of grain crops, forage and economic crops in 2007, and the quantity relative to Minqin whose total water demand was 772 million m³, the amount of over-exploitation of groundwater was 522 million m³, was a drop in the bucket, so to speak, the policy had no effects.

In 2006, the plant area of grain crops of Minqin was 300,600 Mu, and the grain output was 180.5 million kg. It obtained income 267 million yuan, and net income was 142 million yuan. It consumed 160 million m³ water which accounted for 24% of the total water requirement of the year according to the water consumption of grain crops—530 m³/mu. And the output value was 1.67 yuan per cubic meter, and net income was 0.88 yuan. Yet, the cost of 60 million m³ water that pumped into Minqin by Jingtaichuan pumping irrigation project was 72 million yuan every year. According to this cost, the total cost of 160 million m³ water was 192 million yuan, which was 50 million more than the net income—142 million yuan. That is to say, the costs of grain production had already been more than the profits. The annual average output stabilized at about 160 million kg, while the quantities of commodity grain were 73 million kg which consumed 64.7 million m³water. In terms of the transformation between water and food, transferring 73 million kg commodity grain from Minqin was equivalent to transfer 64.7 million m³ water from Minqin which was water shortage. The output value was 108 million yuan. It also meant that it was not enough to give 72 million offered by the national water diversion project to other county. But it almost could buy and transport 73 million kg food from Henan with the money^[2]. According to the field experimental results in 2002, Dr. Yang Zhen of Lanzhou University calculated the virtual water content equivalent to the grains imported and the resulting economic benefits by simulation. Simulation results showed that transferring 1/3 grain output was equivalent to transferring 0.51 × 10⁸ m³ water; transferring 1/2 grain output was equivalent to transferring 0.77 × 10⁸ m³ water; transferring the total grain output was equivalent to transferring 1.54 × 10⁸ m³ water. The increase of GDP value respectively was 61.84%, 92.76% and 185.52%. These data showed that, virtual water trade of Minqin played a significant role in promoting its economic development^[3].

In this special area, it was an enormous waste of water resources to produce food with precious water resources to transfer to other localities. So we transformed industrial structure into animal husbandry, industry and the third industry by implementing virtual water trade. The transformation mainly could be realized by implementing

Table 1. The water consumption of different crops in Minqin county^[1] (m³/mu).

Crops	Water consumption
Wheat	490
Film mulching corn	480
Wheat maize intercropping system	730
Film sunflower	360
Fennel	370
Seed-watermelon	400
Film pepper	530
Broad irrigation cotton	360
Drip irrigation cotton	245
Greenhouse vegetables	410

virtual water trade; meanwhile, it was the best way to solve the crisis of water resources.

3 THE CALCULATION OF VIRTUAL WATER CONTENT IN CROP PRODUCTS AND LIVESTOCK AND POULTRY PRODUCTS OF MINQIN

3.1 The calculation of virtual water content of crop products

3.1.1 The calculation formula of virtual water content in general crop products

The water that crop products need mainly depends on a variety of complex factors, such as species, regional physical geography condition, irrigation conditions and management style. So the estimation of virtual water content is only a rough approximation of a specific location. According to the general method, the formula of virtual water content of a crop product shows as follows.

$$SWD[n,c] = \frac{CWR[n,c]}{CY[n,c]} \quad (1)$$

In this formula, $SWD[n,c]$ is the virtual water content (m^3/kg) of unit weight of crop c in region n ; $CWR[n,c]$ is unit water requirement (m^3/hm^2) of crop c in region n ; $CY[n,c]$ is specific yield (kg/hm^2) of crop c in region n .

3.1.2 The calculation formula of virtual water content in crop products of Minqin

According to the actual situation, the main crop products were wheat, corn, cotton, oil, fennel and vegetables. Based on industry water quota of Wuwei and the actual crop yield in 2009, the calculation formula of their virtual water content showed as follows.

3.1.2.1 The virtual water content of wheat

$$SWD[wheat] = \frac{CWR[wheat]}{CY[wheat]} = \frac{6000}{7240.686} = 0.8287(m^3/kg)$$

3.1.2.2 The virtual water content of corn

$$SWD[corn] = \frac{CWR[corn]}{CY[corn]} = \frac{7500}{9625.294} = 0.7792(m^3/kg)$$

3.1.2.3 The virtual water content of cotton

$$SWD[cotton] = \frac{CWR[cotton]}{CY[cotton]} = \frac{4500}{1573.114} = 2.8606(m^3/kg)$$

3.1.2.4 The virtual water content of oil

$$SWD[oil] = \frac{CWR[oil]}{CY[oil]} = \frac{5100}{5327.145} = 0.9574(m^3/kg)$$

3.1.2.5 The virtual water content of fennel

$$SWD[fennel] = \frac{CWR[fennel]}{CY[fennel]} = \frac{5100}{4275.035} = 1.193(m^3/kg)$$

3.1.2.6 The virtual water content of vegetable

$$SWD[vegetable] = \frac{CWR[vegetable]}{CY[vegetable]} = \frac{6900}{42963.284} = 0.1606(m^3/kg)$$

Water consumption of per unit area and per unit area yield was shown in Table 2, based on the statistical data of 2009 in Minqin.

The results showed that among the six crop products of Minqin in 2009, the virtual water content of per unit of cotton ($2.8606 m^3/kg$) was the biggest; fennel took the second place; oil, corn, wheat were medium, and vegetable was the least. It illustrated that the amount of water consumption of producing or consuming agricultural products was too big, but the benefits were small.

3.2 The calculation of virtual water content of livestock and poultry products

3.2.1 The calculation of virtual water content in general livestock and poultry products

The virtual water content of livestock and poultry products in their living bodies is its total water consumption in the whole life cycle, including the virtual water content of food consumption, the consumption of drinking water, the water

Table 2. Crop irrigation Quota of Minqin^[4].

Crop classification	Crop name	Irrigation volume (m^3/hm^2)	Output (kg/hm^2)
Grain crops	Wheat	6000	7240.686
	Corn	7500	9625.294
Economic crops	Cotton	4500	1573.114
	Oil	5100	5327.145
	Fennel	5100	4275.035
Other crops	Vegetable	6900	42963.284
	Forage grass	3600	10500

consumption of service facilities and manure. So the virtual water content of live animals is composed of 4 parts.

$$VWC_a[e,a] = VWC_{food}[e,a] + VWC_{drink}[e,a] + VWC_{serv}[e,a] - VWC_{excreta}[e,a] \quad (2)$$

In the formula (2), VWC_a is the virtual water content (unit: m^3/kg) of the animal a for exporting in nation or region e ; VWC_{food} , VWC_{drink} , WC_{serv} and $VWC_{excreta}$ is respectively the virtual water content (unit: m^3/kg) of feeding, drinking water, service facilities and manure^[5].

3.2.1.1 The calculation of the virtual water content of feeding

$$VWC_{food}[e,a] = \frac{\int_{birth}^{slaughter} \left\{ q_{mixing}[e,a] + \sum_{c=1}^n SWD[e,c] \times C[e,a,c] \right\} dt}{W_a[e,a]} \quad (3)$$

In this formula, $q_{mixing}[e,a]$ is the water consumption (m^3/d) of mixing feed of the animal a for exporting in region e ; $C[e,a,c]$ is the quantity (kg/d) of the consumption of crops c for animal a in region e ; $SWD[e,c]$ is the virtual water content (m^3/kg) of crop c in region e ; $W_a[e,a]$ is the average slaughter weight (kg) of live animal a in region e .

3.2.1.2 The calculation of the virtual water content of drinking water

$$VWC_{drink}[e,a] = \frac{\int_{birth}^{slaughter} q_d[e,a] dt}{W_a[e,a]} \quad (4)$$

In this formula, $q_d[e,a]$ is the water consumption (m^3/d) of the animal a for exporting in region e ; $W_a[e,a]$ is the average slaughter weight (kg) of live animal a in region e .

3.2.1.3 The calculation of the virtual water content of service facilities

$$VWC_{serv}[e,a] = \frac{\int_{birth}^{slaughter} q_{serv}[e,a] dt}{W_a[e,a]} \quad (5)$$

In this formula, $q_{serv}[e,a]$ is the water consumption (m^3/d) of the service facilities for animal a in region e ; $W_a[e,a]$ is the average slaughter weight (kg) of live animal a in region e .

According to the specific situation of Minqin, livestock and poultry products such as cattle, sheep, pig, and chicken were fed in backyard farms and transaction, so it didn't form dimensions. So the calculation of virtual water content of service facilities was only the half of drinking water.

3.2.1.4 The calculation of the virtual water content of manure

Statistics showed that the annual amount of animal manure was about $17.3 \times 10^8 t$, among which the cow dung was $10.7 \times 10^8 t$, pig manure was $2.7 \times 10^8 t$, sheep manure was $3.4 \times 10^8 t$ and poultry dung was $1.8 \times 10^8 t$. Nitrogen and phosphorus in the manure were $1.60 \times 10^7 t$ and $3.63 \times 10^6 t$, which was equivalent to 78.9% and 57.4%^[6] of the amount of fertilizer used in China. For a pig farm having an annual slaughter capacity of 10,000 head of pig, the average amount of daily manure emissions was 17.5t, in which nitrogen and phosphorus was respectively 105 kg and 70 kg. For a chicken farm having 10,000 chickens, the average amount of daily manure emissions was 1.5t, in which nitrogen and phosphorus was respectively 24.45 kg and 23.1 kg^[7]. Long-term using farmyard manure not only could improve soil properties, but also had a significant effect on increasing crop yield and improving crop quality. So it was an ideal fertilizer to develop ecological agriculture.

In the vast rural areas in Minqin, farmers widely adopted returning manure to field directly, returning fermentation to field, producing the organic

Table 3. The amount of livestock and poultry manure^[8] Unit: $kg/head \cdot day$; $g/a \cdot day$.

Items	Days of age/d	Food consumption	Manure emissions	Urine emissions	The total waste discharge
Mature beef	900	5 (mixed feed) + 40 (grass) + 30 (water)	20	25	45
Sheep	360	0.5 (mixed feed) + 3 (grass) + 5 (water)	1.25	2.75	4
Sow	270	5 (mixed feed) + 13 (water)	3.6	4.5	8.1
Boar	270	5 (mixed feed) + 13 (water)	2.6	5.2	7.5
Commercial pig	135	3 (mixed feed) + 13 (water)	1.75	5.75	7.5
Table poultry		0.125 (mixed feed) + 0.3 (water)	0.05-0.1		0.05-0.1
Layer		0.13 (mixed feed) + 0.3 (water)	0.11		0.11

** Some feed intake of livestock and poultry was calculated according to investigation and water quota.

and inorganic compound fertilizer and other methods to highly utilize animal manure in agricultural production. Therefore, the virtual water content in animal manure used as farmyard manure was left in the locality. This was objective, realistic and existent.

3.2.1.5 The reference of the calculation of the amount of food and water consumption of chickens and pigs

The average water consumption of one table poultry in different weeks of age was shown in Table 4.

According to 8 weeks, the average amount of daily water consumption of one chicken in its life cycle was 3.9 litres (0.0039 m³).

The average amount of daily food consumption of one chicken in different weeks of age was that one week was 11 g. It could be seen from the above rule that the amount of daily food consumption of chicken in 11~20 days of age was the days of age times 2 plus 5 g; the amount of 21~30 days of age was the days of age times 2 plus 7 g; the amount of 31~40 days of age was the days of age times 2 plus 9 g. According to 8 weeks, the average amount of

daily food consumption of every chicken in its life cycle was 56.4 g (0.0564 kg).

3.2.1.6 The coefficient of the virtual water content of livestock and poultry manure
According to the amount of livestock and poultry dung and urine, feed intake, water consumption and current situation of Minqin, this paper estimated the coefficient of the virtual water content of livestock and poultry manure. The coefficient was that feed intake absorption rate of pig, chicken, cattle and sheep was respectively 55%, 75%, 40% and 55%; the discharge rate of feces was respectively 45%, 25%, 60% and 45%. The coefficient of virtual water content of livestock and poultry manure was shown as follows.

$$\begin{aligned} \text{Pig, Sheep: } VWC_{\text{excreta}}[e,a] &= (VWC_{\text{food}}[e,a] + VWC_{\text{drink}}[e,a]) \times 45\% \\ \text{Cattle: } VWC_{\text{excreta}}[e,a] &= (VWC_{\text{food}}[e,a] + VWC_{\text{drink}}[e,a]) \times 60\% \\ \text{Chicken: } VWC_{\text{excreta}}[e,a] &= (VWC_{\text{food}}[e,a] + VWC_{\text{drink}}[e,a]) \times 25\% \end{aligned}$$

Table 4. The average of water consumption of every table poultry in different weeks of age.

Weeks of age	The amount of daily water supply (Litre)
1	3.8
2	10.2
3	20.8
4	27.2
5	33.3
6	39
7	42.8
8	45

3.2.2 The calculation of virtual water content of pig, cattle, chicken and sheep in Minqin

The formula of virtual water specific content of mixed feed in region *e* was $SWD[e,c] = CWR[e,c]/CY[e,c]$.

In this formula, $CWR[e,c]$ was the water requirement (m³/hm²) of crop *c* in region *e*; $CY[e,c]$ was specific yield (kg/hm²) of crop *c*.

According to the above formula, the virtual water content of mixed feed of Minqin in 2007 could be figured out. $SWD[\text{mixed feed}] = CWR[\text{mixed feed}]/CY[\text{mixed feed}] = 7000/8661 = 0.8082 (m^3/kg)$.

Table 5. The amount of food consumption and the average weight of pigs in each stage.

Weeks of age	Weight (kg)	Daily feed consumption (kg/head)	Cumulative intake (kg/head)	Feed efficiency	Cumulative feed efficiency
2	3	0.18	1.26	1	/
4	8	0.45	6.3	1.24	0.77
6	14	0.76	16.9	1.57	1.12
8	21	1.1	32.3	1.82	1.4
10	30	1.4	51.8	2.27	1.64
12	40	1.75	77	2.43	1.84
14	52	2.03	107.5	2.7	2.02
16	64	2.33	140.1	2.94	2.16
18	76	2.6	176.5	3.17	2.32
20	88	2.85	216.4	3.28	2.46
22	100	3.0	258.4	3.4	2.58

Table 6. Rural livestock (poultry) classification and water consumption quota table.

Classification	The unit of quota	Water consumption quota
Large livestock (including cattle, horses, donkey and mule)	m ³ /head·day	0.030
Pig	m ³ /head·day	0.013
Sheep	m ³ /a·day	0.005
Poultry	m ³ /a·day	0.0004

The unit amount of irrigation was 7000 m³/hm²; the ratio of per unit yield of wheat and corn was 4:6.

The formula of virtual water content of forage grass in region e was $SWD[e,c] = CWR[e,c]/CY[e,c]$.

In this formula, $CWR[e,c]$ was the water requirement (m³/hm²) of forage grass c in region e ; $CY[e,c]$ was specific yield (kg/hm²) of forage grass c .

According to the above formula, the virtual water content of forage grass of Minqin in 2007 could be figured out. The average output of forage grass in Minqin was 2500 kg/mu (37500 kg/hm²), so $SWD[grass] = CWR[grass]/CY[grass] = 3600/37500 = 0.096(m^3/kg)$.

3.2.2.1 The calculation of virtual water content of pig in Minqin

In 2007, the slaughter amount of pig of Minqin was 107,000 head, producing meat 7490 tons. In the calculation, there was no other classification. The paper calculated the average intake and water consumption by weeks of age in accordance with the growth cycle. The ratio of the amount of mixed feed and water consumption for feed mixing was 5:1. The average weight of slaughter of pig calculated in accordance with The 2008 Gansu Rural Yearbook (printed by Gansu Xin Tong Printing Co., Ltd., 2008.10 P496).

$$\begin{aligned}
 VWC_{pig}[pig] &= VWC_{food}[pig] + VWC_{drink}[pig] \\
 &+ VWC_{serv}[pig] - VWC_{excreta}[pig] \\
 &+ \frac{\int_{birth}^{slaughter} \{q_m[pig]\}}{Wp[p]} \\
 &+ \frac{\sum_{c=1}^n SWD[mixed] \times C[pig, mixed] dt}{Wp[p]} \\
 &+ \frac{\int_{birth}^{slaughter} q_d[pig] dt}{Wp[p]} + \frac{\int_{birth}^{slaughter} q_{serv}[pig] dt}{Wp[p]} \\
 &- VWC_{excreta}[p]
 \end{aligned} \tag{6}$$

$$VWC_{food}[pig] = (0.4 \times 135 + 0.8082 \times 1.675 \times 135) / 75 = 3.1567(m^3/kg).$$

According to known data, we could calculate the results. $VWC_{pig}[pig]$ was 1.856 m³/kg.

3.2.2.2 The calculation of virtual water content of cattle in Minqin
Cattle feed was comprised of mixed feed and forage grass, so $VWC_{food}[cattle] = VWC_{mixed feed}[cattle] + VWC_{grass}[cattle]$. The feed of cattle was 20% mixed feed and 80% forage grass, so $\sum_{c=1}^n SWD[cattle] = SWD[mixed feed] \times 20\% + SWD[grass] \times 80\%$.

There were 66,000 head of cattle, and 52,000 head were draft cattle in Minqin in 2007. In the calculation, there was no other classification. According to the growth cycle, the paper calculated the average intake and water consumption in three periods. The ratio of the amount of mixed feed and water consumption for feed mixing was 5:1. The average weight of slaughter of draft cattle calculated in accordance with the 2008 Gansu Rural Yearbook (printed by Gansu Xin Tong Printing Co., Ltd., 2008.10 P496). Cattle slaughter and meat production were calculated according to production scale factor—0.6.

$$\begin{aligned}
 VWC_{cattle} &= VWC_{mixed feed}[cattle] \\
 &+ VWC_{grass}[cattle] + VWC_{drink}[cattle] \\
 &+ VWC_{serv}[cattle] - VWC_{excreta}[cattle] \\
 &= \frac{\int_{birth}^{slaughter} \{qm[c] + \sum_{c=1}^n \{SWD[mixed]\}}{Wc[c]} \\
 &\times C[c, m] \times 20\% + SWD[g] \times C[c, g] \times 80\% \} dt}{Wc[c]} \\
 &+ \frac{\int_{birth}^{slaughter} q_{drink}[c] dt}{Wc[c]} + \frac{\int_{birth}^{slaughter} q_{serv}[c] dt}{Wc[c]} \\
 &- VWC_{excreta}[cattle]
 \end{aligned} \tag{7}$$

$$VWC_{mixed feed}[cattle] = 17.569 (m^3/kg).$$

According to known data, we could calculate the results. $VWC_{cattle}[cattle]$ was 7.095 m³/kg.

Table 7. The virtual water content of livestock and poultry products^[9] Unit: m³/kg.

Items	Pork	Beef	Mutton	Chicken
The virtual water content	3.24	19.99	18.01	3.50
The virtual water content of Minqin	3.1567	17.569	14.8565	3.1745

3.2.2.3 The calculation of virtual water content of chicken in Minqin

$$\begin{aligned}
 VWC_{chicken}[chicken] &= VWC_{food}[chicken] \\
 &+ VWC_{drink}[chicken] + VWC_{serv}[chicken] \\
 &- VWC_{excreta}[chicken] \\
 &+ \frac{\int_{birth}^{slaughter} \{qm[ch]\}}{Wch[ch]} \\
 &+ \frac{\sum_{c=1}^n SWD[mixed] \times C[chicken, m] dt}{Wch[ch]} \\
 &+ \frac{\int_{birth}^{slaughter} q_d[chicken] dt}{Wch[ch]} + \frac{\int_{birth}^{slaughter} q_{serv}[chicken] dt}{Wch[ch]} \\
 &- VWC_{excreta}[chicken]
 \end{aligned} \tag{8}$$

$$VWC_{food}[chicken] + VWC_{drink}[chicken] + VWC_{serv}[chicken] = 3.1745 \text{ (m}^3/\text{kg)}.$$

According to known data, we could calculate the results. $VWC_{chicken}[chicken]$ was 2.3822 m³/kg.

3.2.2.4 The calculation of virtual water content of sheep in Minqin

Sheep feed was comprised of mixed feed and forage grass, so $VWC_{food}[sheep] = VWC_{mixed\ feed}[sheep] + VWC_{grass}[sheep]$. The feed of sheep need was 20% mixed feed and 80% forage grass, so $\sum_{c=1}^n SWD[sheep] = SWD[mixed\ feed] \times 20\% + SWD[grass] \times 80\%$. The slaughter amount of sheep of Minqin in 2007 was 380,000 head, producing mutton 5700 tons. In the calculation, there was no other classification. In accordance with the growth cycle, the paper calculated the average intake and water consumption in three periods. The ratio of the amount of mixed feed and water consumption for feed mixing was 5:1. The average weight of slaughter of sheep calculates in accordance with the 2008 Gansu Rural Yearbook (printed by Gansu Xin Tong Printing Co., Ltd., 2008.10. P496).

$$\begin{aligned}
 VWC_{sheep}[sheep] &= VWC_{mixed\ feed}[sheep] \\
 &+ VWC_{grass}[sheep] + VWC_{drink}[sheep] \\
 &+ VWC_{serve}[sheep] - VWC_{excreta}[sheep] \\
 &+ \frac{\int_{birth}^{slaughter} \{qm[s] + \sum_{c=1}^n \{SWD[m]\}}{Ws[s]} \\
 &= \frac{\times c[s, m] \times 20\% + SWD[g] \times c[s, g] \times 80\% \} dt}{Ws[s]} \\
 &+ \frac{\int_{birth}^{slaughter} q_{drink}[s] dt}{Ws[s]} + \frac{\int_{birth}^{slaughter} q_{serv}[s] dt}{Ws[s]} \\
 &- VWC_{excreta}[s]
 \end{aligned} \tag{9}$$

$$VWC_{mixed\ feed}[sheep] + VWC_{grass}[sheep] + VWC_{drink}[sheep] + VWC_{serv}[sheep] = 14.8565 \text{ (m}^3/\text{kg)}.$$

According to known data, we could calculate the results. $VWC_{sheep}[sheep]$ was 7.8310 m³/kg.

3.3 Confirmation

The calculation of the virtual water content of livestock and poultry products was rather complicated. There was no statistical data, and the survey data had its limitation. So this study checked the accuracy of the calculation of the virtual water content of livestock and poultry products, consulting the research achievements of virtual water content of livestock and poultry products in some Chinese provinces and cities which were carried out by Chapagain A.K, Hoekstra A.Y and other scholars. In this study, the virtual water content of livestock and poultry products of Minqin was close to the corresponding research achievements. And it was normal and reasonable that the virtual water content of livestock and poultry products of Minqin which was in the arid area was lower than the national average.

4 THE COMPARISON OF VIRTUAL WATER CONTENT BETWEEN AGRICULTURAL PRODUCTS AND LIVESTOCK AND POULTRY PRODUCTS OF MINQIN

This paper calculated the virtual water content of agricultural products and livestock and poultry products of Minqin.

The calculation formula of unit water value was as follows.

$$UWW[i, j, c] = P[i, j, c] / VWL[i, j, c].$$

Table 8. The unit water value of main grain crop products of Minqin.

Main products	Unit virtual water content (m ³ /kg)	Unit price (yuan/kg)	Unit water value (yuan/m ³)
Wheat	0.8287	2.30	2.775
Corn	0.7792	2.18	2.7977
Cotton	2.8606	8.24	2.8805
Oil	0.9574	9.0	9.4005
Fennel	1.193	4.5	3.7720
Vegetables	0.1606		
Beef	7.0950	40.0	5.642
Pork	1.850	18.0	9.729
Mutton	7.831	42.0	5.3633
Poultry (chicken)	2.3769	14.0	5.890

Table 9. Part of the livestock and poultry products production and sales in 2009 Unit: one.

Items	Pigs	Sheep	Chicken
The amount of livestock on hand	57333	823116	780000
Slaughter capacity	58730	759066	503000

In the formula, $UWV[i, j, c]$ was the unit water value of agricultural products; $P[i, j, c]$ was the price of unit agricultural product; $VWL[i, j, c]$ was the virtual water content of agricultural products. Variable i represented a specific region, j represented a specific year, and c represented a specific product.

According to the market price of main grain crops products and the virtual water content of unit mass of Gansu in December 2011, the paper concluded the measure of unit water value.

Because there was no statistical data of the private trade in food and livestock products, and the survey data had its limitation, the paper obtained a trend data through conducting an interview investigation in part of sheep farms and chicken farms with a certain scale in Minqin. The data showed that more than 45–60% of the sheep, chicken, and eggs were sold to outside the county, more than 65–90% of the chicken and pig feed came from more than ten large-scale feed manufacturers, such as New Hope Group, Dabeinong Technology Group, Chia Tai Group and so on. These partly corroborated that feed grains came from other areas, and most of livestock and poultry products sold to other counties.

5 CONCLUSION

1. The average unit water value for livestock and poultry products was two times more than that of agricultural products (oil except).
2. Livestock and poultry products were of low water consumption but high value, however, the main agricultural products were of high water consumption and low value.
3. The value of consuming 1 unit of water resources to produce 1 unit livestock and poultry product was equivalent to produce more than 2 unit agricultural products. In other words, producing 1 unit livestock and poultry product could save more than half of water resources than producing 1 unit agricultural product. Therefore, it will be the optimal choice to replace agricultural products with livestock and poultry products especially foreign trade grain products for Minqin in the optimal allocation of water resources.
4. In the process of agricultural structure adjustment in Minqin, reducing production areas of wheat, corn, cotton, fennel and other crops, and energetically developing herbivorous livestock industry and livestock products trade will be the inevitable direction for improving ecological environment and increasing farmers' income and economic output.

REFERENCES

- [1] Peng, J. 2009. Review and discussion on utilization of agricultural waste resources in China. *Ecology and Environmental Sciences* 18 (2): 794–798.
- [2] Su, J.Y. & Li, Y.Y. & Luan, D.M. 2005. The effect of zymin in reducing environmental pollution for livestock and poultry manure. *Feed China* (16):35–36.
- [3] Sun, Y.F. & Feng, C.X. & Li, Y.Q. 2009. The calculation and application of straw feed intake of cattle. *Henan Journal of Animal Husbandry and Veterinary Medicine* 30(5):12–13.
- [4] Han, Y.P. & Lei, H.J. 2011. *Study on Regional Development Based on the Virtual Water*. Beijing: China Water Power Press.
- [5] Liao, S.C. 2009. *Study on the Water Resources Crisis in Minqin* (MS., Gansu Agricultural University, China).
- [6] Liao, S.C. & Han, J.M. 2008. Exploration and discussion on water crisis in Minqin county. *Guangdong Agricultural Sciences* (5):123–126.
- [7] Chai, X.M. 2007. The countermeasures for water resources and ecological environment in Minqin. *Information of Agricultural Science and Technology* (10):211–214.
- [8] Bureau of Statistics of Minqin County. National Economic and Social Development Statistical Data Collection during 2006–2009. China.

Study on model and design of old-age residence

Lei Li Li

Jilin Jianzhu University, Changchun, Jilin, P.R. China

Yue Li

Baishan Planning Bureau, Baishan, Jilin, P.R. China

ABSTRACT: In this paper, under the conditions of China has entered the aging society, analyzed of the characteristics of China's aging population. And from the social level, the corporate level, consumer level describes the significance of the study, clear research objectives. On this basis, domestic and foreign senior housing patterns were studied, and the old house has been built has been designed to resolve, provide a reference model for future senior housing choice and design.

Keywords: old-age residence; pattern; design elements

1 BACKGROUND AND SIGNIFICANCE

1.1 Background

The usual international practice is that people over the age of 65 are counted as the elderly, When the total population aged 65 accounted for more than 7%, the population aged type is called. China's aging population is very alarming rate, experts predict that by 2040, China's elderly people aged 65 will reach about 400 million people, about 26% of the total population, China is facing severe challenges of population aging.

1.2 Significance of the study

1.2.1 Based on the social level

Aging of the population as a problem of social development can not be avoided, it is highly likely the Chinese society and economy have a strong impact and shock, triggering social and major economic restructuring, state, society, enterprises and individuals will have to pay a considerable costs and cost. Because of this, the study population aging, population aging is one of the very important issue of this century China.

1.2.2 Based on the enterprise level

With the advent of an aging society, the elderly, more and more elderly housing demand growing, this is a sunrise industry, the real estate business has opened up a unique development path.

1.2.3 Based on the consumer level

Housing for the elderly, not just shelter in place, the elderly after leaving the job, most of the time

is spent in the homes and communities, so research comfortable and convenient apartments for the elderly from residential and community environment for career career transition to retirement for the elderly is very important.

2 MODES IN ELDERLY RESIDENTIAL DOMESTIC AND FOREIGN

2.1 Domestic elderly residential business model

At present, Chinese old-age residence mainly include elderly residential housing, apartments for the elderly, nursing homes, daycare center.

2.1.1 Elderly residential housing

This kind of housing is Specifically for older people living in line with the characteristics of residential aged physical mentality. In older houses, there are age-residential living alone, living with children age-dwelling, older residential neighborhood type.

2.1.2 Apartments for the elderly

C his kind of housing is Specifically for older people to live together, in line with the mentality of old physical features apartment-style old house, with food, sanitation, culture and entertainment, health care service system is the integrated management of housing types.

2.1.3 Nursing homes

Social pension services are designed for older people with dignity and hospitality settings, with a living life, culture and entertainment, health care and many other services.

2.1.4 *Daycare center*

Designed for short-term reception elderly community care services hosting service establishments with daily life, culture and entertainment, health care and many other services and facilities, daycare and boarding can be divided into two kinds.

2.2 *Foreign elderly residential business model*

In recent years, some developed Western countries began looking for a way to lighten the burden on the country, but also to adapt to the needs of smaller households facility. Many countries are actively seeking measures between facilities between care and family care. For example:

Residential building patterns of older Americans, there are three main types: stand-alone senior housing; Assembling elderly residential; elderly residential care type.

Sweden has a good social welfare system, its housing policies to help the elderly live independently as the goal, but the elderly do its utmost to meet their long-term residence in a familiar place and the environment will.

3 CASE STUDY AT HOME AND ABROAD

3.1 *Case study abroad senior housing*

3.1.1 *Florida "Sun City Center" project*

Florida "Sun City Center" elderly community is one of the most famous in the world community ripe old age, one of the most typical of older communities nation's best, "The whole community features area clear, has six residential communities, communities share a supermarket, medical institutions, post offices, banks and churches," the property type is tailored for the elderly: "Sun City Center" (as McMansions), "The King's Hall" (for the townhouse), "Lake Tower" (as a secondary care apartments and home care agencies), "Aston courtyard garden" (to hire an independent living apartment), "freedom Square" (as a secondary care apartments and home care agencies). Currently, Sun City has become a well-known American brand development elderly community.

Sun City for the architectural planning of the elderly: accessibility design emphasizes easy and safe. Community-based housing to low-rise buildings, arranged in all areas of accessibility walking trails, accessible slip ramp, set the low key, high outlet; highly oriented space to deal with the perception of memory decline in the elderly: a sense of direction, traffic safety, road accessibility arrangements are made, the implementation of strict people and vehicles.

Community facilities for the elderly, emphasizing health. Built hospitals and elderly care centers; mental health centers; older libraries, community exchange hall.

Rich club sports: indoor and outdoor swimming pools, lawn bowling, tennis, chess and card room, bowling alley, dance hall, gymnasium everything.

3.1.2 *Learn from America sun city center project*

1. Large-scale development of suburban development approach, to the lowest bidder, which will help build large-scale facilities, improve community quality, reduce overall development costs;
2. Phased development, facilities construction phases, to avoid wasting money, maintain a good pace of development;
3. Facilities Management socialization, before completion of the development of a unified community management, both to ensure the professional standards of community service, and brand benefits, and also allows the community to get sustainable development, to maximize profits;
4. Brand chain business model, developers in the Sun City development business model developed, this development model will have a choice of other cities in the United States, and follows the same project name, in order to facilitate brand building.

3.2 *Domestic elderly residential case study*

3.2.1 *Beijing Oriental Sun City*

Beijing Oriental Sun City is located in Shunyi District, Beijing Chaobai River 7,000 acres of vast woodland; planning area of nearly 2,340,000 square meters, total construction area of 700,000 square meters, can accommodate a total of more than 20,000 people; architectural forms McMansions, conjoined villas, apartments point, plate apartments and apartments corridor, an area of 78 716 square meters a month.

1. Plan features:

Ribbon arrangement, borrowed scenery maximization: Community Bangshui built, surrounded by 7,000 acres of greenbelt. Three groups banded tile, to ensure that each group maximum contact area and the landscape;

Group designed, functional independence: As the project phases are large body mass, a longer period, the use of group design, landscape features internal support, and do not rely on;

Foreign groups are closed, opening up: the elderly need more security, therefore, tour groups are the central core enclosed landscape layout, space for outside groups effectively cut off; older people eager to communicate, so the

internal arrangement of a large number of open exchange space.

2. Supporting features:

Providing a full range of supporting life of the elderly, improve life, health, entertainment, leisure, communication and other facilities, with a medical center, old cultural and educational centers, elderly fitness and recreation center, a conference center, shopping centers, domestic service centers, a total of 70,000 square meters of commercial city. Communications package includes anti-skid steel road barrier-free design brick, floor apartment can accommodate a stretcher to all medical elevator, weak community built with advanced management center with emergency assistance call system, life service systems, information delivery system (convergence and broadband fiber), the community also has a green belt with a coded public health and safety within their installed facilities connected with community call intelligent security systems.

3.2.2 *Learn from beijing oriental sun city project*

1. A healthy natural environment: Community water systems and green environment to create outstanding.

In the water system design aspects, the community as a whole is located on top of a golf course, the ratio of water to reach 3 to 5 percent; in green design aspects, there are 100,000 trees surrounding hills, community greening rate of 80% in the air environment to create a community of negative oxygen ions in the air up to 2000 the average content/cubic meters, the living environment has reached convalescence level.

2. Humanized planning and design: barrier-free design, size, environmental design, fully meet the convenience of older persons live, exchange requirements.

Accessible design, specially designed for the elderly; four-story apartment located elevator and barrier free ramps; ground slip handle, wall embedded handrails, Yang wipe round the corner; indoors emergency call and electronic security systems; bedroom fully consider the orientation, lighting and ventilation; toilet not far away from the bedroom with a slip handrails; sockets, switches are correspondingly reduced height; Proximity Lock replacement rotary key; using bright colors, enhancing the environment identifiability.

Type design have focused on the elderly eager to communicate: Some villas located a double living room; Chinese traditional concept of children living with their parents: large multi-bedroom apartment; elderly people in need of care, and some units designed rooms nanny.

Environment designed to facilitate communication, to break the closed, promote exchanges; big clubs become older mutual exchange activities mainly space; garden design emphasizes interactivity: in the garden district have opened up a small platform as the randomness of the exchange space, easy to elderly chat.

3. The public buildings tailored for older: building community hospitals, recreation centers, universities for the elderly, self farms and so on.

The main building includes nearly 50,000 square meters of grand public buildings located in the community center, community center, sports center, resort hotel, commercial center and hotel apartments, four plates based, cultural, entertainment, commercial, medical, health body, leisure and other functions in one.

4 SUMMARY

In summary, elderly housing should focus on people-centered family care, trying to explore the emotional and from the traditional mode of modern life balance, to build a people-oriented “family housing.”

It will allow people to enjoy the warmth of a perfect life tradition intertwined with modern civilization. Family housing is leading a new living concept, the formation of new consumer behavior.

REFERENCES

- [1] Tang Li. Aging on residential areas in public places and facilities requirements [J]. South Building, 1999 (3):22-24.
- [2] Wengxiao Min. Generations living residential design Study [J]. Residential Technology, 2000 (3):72-75.
- [3] Mayer, Christopher and Katerina Simons, 1994. Reverse Mortgages and the Liquidity of Housing Wealth [J]. Journal of the American Real Estate and Urban Economics Association, Vo. 122, No. 2, 235-255.

Practice of new regionalism—taking “Design of Business Street at Zhuang Yuan Road along Xishui Bahe” for example

Yi Yang & Meng Xuan Zhang

School of Architecture and Urban Planning, Huazhong University of Science and Technology, Wuhan, Hubei, P.R. China

Qi Huang

College of Architecture and Urban Planning, Tongji University, Shanghai, P.R. China

ABSTRACT: Every era should have its character. The characteristics that we are looking for should not only have the common connotations and signs of this era, but also the imprinting that can rock people’s heart. From this viewpoint, the appearance of neo-regionalism is a very good trend in architectural field, which merges well the quintessence of modernism and regionalism, responds to modern architecture, and contributes to context transmission.

Keywords: neo-regionalism; Xishui Bahe; business street design

1 THE ERA THAT WE LIVE IN AND NEO-REGIONALISM

Usually, the architectural style and economic development level of an era reflect its characteristic; for an example, palaces and residences in the feudal society of China is the achievements of materialization in the angle of architecture after the feudal hierarchy goes deep into people’s lives. Therefore, something like existence of quadrangles is not only the continuation of cultural life of last era, but also moreover the media that connects people outside the quadrangles and “history”. In contrast, the inexhaustible new architectural types have more fashionable criteria, with lower admittance thresholds; there is the practice of standardization of architectures due to their product implementation as well as the continuous trying of experimental projects. However, facing the more welcomed world with more freedom, we hesitate over and over again—in the deluge of information, what choices are the truly correct ones? What kind of architecture is the one that can not only satisfy eyes of people that are seeking the beauty, but also comfort the lonely deep heart of people after they smile? Some shortcomings such as the aridity of architectural emotion and lacking of sense of places, prevail everywhere like the popularity of fast-food culture. When the development of architectures with modernism comes into a changing era, facing the innovative architectural styles, how we can define ourselves in the times when

architectures get typed, stereotyped and product-implemented?

The appearance of new regionalism is the outcome of this background. It is different from the standardization and stereotype and it focuses on the understanding of regional context. It is also different from architecture of vernacularism; it is not the spontaneously produced expression of architectural type of “residence” through the combination of climate, culture, community and handicraft arts, but a kind of tendency about the common cultural summarization and interpretation in a region. New regionalism, as its name suggests, is the new development after combining regionalism and presentism; its fundamental element lies in that it considers both the comparatively-iconic regional culture with and the comparatively-common global culture, but it doesn’t have preference to either party. Thus, the starting point of new regionalism design is not to show up its novelty and supereminence, comparing to the universal aesthetics; on the contrary, the design is merged with the thinking that modernism has on the location and region and it releases and satisfies the native complex of people as possible as it can.

2 OVERVIEW OF PROJECT BACKGROUND

Xishui County is located in south of Dabie Mountain, east of Hubei Province, the north bank of the middle reaches of Yangtze River,

which is subordinate to Huanggang City. It is in the Yangtze River development zone of Jiujiang, Huangshi and Wuhan; and Yangtze River channel, Liujie highway and Shanghai-Chengdu expressway cross its territory in parallel; Huangshi Yangtze River Bridge crosses over Sanhua Town of Xishui County, with 20 minutes drive to the county; Beijing Kowloon railway crosses the territory of Xishui County with passenger terminal and cargo terminal, which establishes the all-round transportation network including railway, highway and waterway. Xushui is a well-known historical and cultural county; thereinto, Yao Minggong (1583–1644)—prime minister of Ming Dynasty, Chen Hang (1785–1862)—the number one scholar of Qing Dynasty, and Wen Yiduo (1899–1946)—a fighter of democracy, lived or grew here once.

15 towns (farms) and 1 provincial economic development zone are subordinate to Xishui County, and Bahe Town is west gate of Xishui. The south of Bahe Town faces Ezhou across the river, its west is connected with Huangzhou First Bridge, its east neighbors the Orchid Creek of Spring Town and its north adjoins the Zhuwa Town. Bahe Town is the significant part of “Two Circles and One Band” strategy of Hubei Province and it is determined as the one of “Key Towns along River” in the mentioned planning. The route of Zhuangyuan Road in Bahe Town is located in its administrative central zone, neighboring to provincial road in Gezhou Bay and adjoining to Wangtian Lake Tourist Landscape Area. According to the direction of the mentioned planning, the total land area of this lot is 30 hectares, which is a commercial land.

In the solution design of Zhuangyuan Road, we consider that Zhuangyuan Road is the main road to Wangtian Lake Tourist Landscape Area as well as the place where tourists have the first expression about Bahe Town; therefore, the orientation of Zhuangyuan Road must have the dualism, which means that we need to not only build up a energetic political & cultural center of Bahe Town and establish the landscape corridor of Wangtian Lake Landscape Area, but also create the characteristic commercial & residential axis line to enrich the cultural activities of residents. In order to leave the city to the residents as possible as it can, there is less than 30% building density in the final solution design; that is to say, in the land with area of 15 hectares, the total land area is about 45,000 square meters and the floor area is almost 230,000 square meters.

3 ARCHITECTURAL DESIGN

The first well-known representative figure in Bahe is Yao Minggong, the Prime Minister of Ming

Dynasty, therefore, the style of the first phrase development will be determined as features of Ming Dynasty, and the next 2 phrase development are style of Qing Dynasty and style of the Republican of China respectively. We consider that Zhuangyuan Road is the main road to Wangtian Lake Tourist Landscape Area as well as the place where tourists have the first expression about Bahe Town, thus, we will set up the characteristic archways at every intersection in the solution design as the beginning & end of space. It is mainly about the commercial development in the first phrase; both sides of the road will be dwindled 10 meters to make the sidewalk. 2 rows of commercial-residential buildings will be built in the lot beside both sides of road; the row facing the street has 4 storey and the row behind the street has 6 storey. In that case, both sides of the business street have 3 frontages; 2 of them are facing the inside pedestrian street and the last one is facing the outside main road of city. The abundance of street frontage is equal to that it enhances the quality requirements of our detail design, because the more places that people feel, the more architectural experience that we need to leave to tourists. About design of the size of the pedestrian street, the most touched part is the architectural detail with the similar size of people's body, besides the creating of whole atmosphere of street.

In the solution design of the first phrase, we all think about carefully the ideas of Ming Dynasty style from shapes & structures to details. One of the most distinct characteristics in Ming's architectures is that the requirements about shapes & structures of architectures are stricter than in Song Dynasty. At the early stage of Ming Dynasty, the hierarchy about the residences gets strict; and the gable and hip roof, double eave roof, big arch or sunk panel is allowed to be used in building residences of officials. All these restrictions were for the civilians in Song Dynasty; but in Ming Dynasty, it was also for government officials. Considering requirements that except royal members in Ming Dynasty, the gable and hip roof is not allowed to be used in building the residences of civilians, but only “2 mansions” (overhanging gable roof and flush gable roof), in the architectural design of first phrase development of Zhuangyuan Road, the roof shapes of architectures are amended on the basis of overhanging gable roof; through inserting horse-head walls between every 2 stores, it will make every store have style of overhanging gable roof as well as the flavor of modernity.

In the detail design of architectures, we also use much the carpentry of Ming Dynasty; we not only decorate carefully the windows and doors with frontage, but also learn from the features of

Ming's architectures—exquisite workmanship, sophisticated decoration, delicate and elegant carving & painting. In the second floor with the street frontage, we all design the balconies for long-distance overlooking; this kind of design not only is good for enlarging the floor area, but also embodies plentifully the architectural features of Ming Dynasty in the aspect of handling pillars, diaphragm plates and moldings. Specifically speaking, in this design, the mean-diameter blade length ratio of the pillar is basically 1:12; in that case, to a great extent, it is different from 1:8 or 1:10 of architectures of Tang Dynasty; moreover, more complicated paintings of tangled flowers are utilized in the carving decoration, which is different from that “wands and Goulan” style was utilized in building balustrades in the architectures of Tang Dynasty.

Although this kind of design prefers to use symbols and symbolism to express the feeling, which is possibly judged like that it is with more lyricism, romance and popularity, but lack of reason, the architectures of democratism declare that behind the combination of kinds of architectural elements, actually the space shapes & structures reflected by cultural system is hidden. Three lanes and seven alleys in Fuzhou City, with nickname of “the museum of Ming & Qing's architectures” have traditional poetic imagery, which means that it keeps the quiet in a noisy neighbor; therein, the three lanes are Yijin Lane, Wenru Lane and Guanglu Lane; and they are famous respectively for water-side pavilions & stages, massive Confucian scholars and Guanglu presentation platform. Therefore, in design of the business street at Zhuangyuan Road, we also try to express the particularity of locations and places through the method of modernism. In the second and third phrase development, they are mainly about tourism business, restaurants, entertainment and residential service, and the width of the city road is reduced to 20 M from the previous 40 M. This kind of size measure is better for building the Lang type space. The design not only adds the garden-like relaxing space and central landscape band of the pedestrian street into the whole street, but also creates the atmosphere of the wine shop and club in the designs of stores through utilizing the details of shop fronts at the ground floor & wooden pillars of the open floor and adding the scene elements.

The seeds of capitalism have appeared since Ming Dynasty and the commodity economy started to boom vigorously. Due to the influence of this kind of thoughts, the geomancy started to gain a big development space. There was a saying about axis while locating the stores in Ming

Dynasty; that is to say, according to the regulations of geomancy, the frontage of stores is the best to follow along “Zi Wu axis” (locating in the north with south frontage), “Wu Zi axis” (locating in the south with north frontage), or “Qian Xun axis” (southeast) and “Gen Kun axis” (southwest) to do the arrangements. Besides following the above mentioned “frontage axis” method, there is another saying of “stores with frontage of river (water) or road and with hills above & with water below, will have more fortune.” In the first phrase architectural design of Bahe, 70% of architectural planning utilizes the “Gen Kun axis”, and other 30% architectures utilizes “Zi Wu axis” or “Wu Zi axis”. This kind of design planning not only satisfies well the requirements of locating design, but follows the geomancy of Ming Dynasty in the angle of culture, which is a kind of heritage in the name of culture.

The traditions never stop moving forward; moreover, the classical traditions will not become outdated. Whether the classical gardens of Suzhou become the foot-binding cloths or not, Mr. Pei Leoh Ming got it polished again successfully. Thus, utilizing the old traditions in the modern times; the modern designers should learn from the ancient arts and create their new modern values, which is the goal that they should pursue. Not all diversification of city lies on the richness of forms; the more important part is that how to embody the values of “being people-oriented”. Making the design rock the people's heart is the ultimate pursuit of architects.

REFERENCES

- [1] Lin Shenghua: Regionalism of Architectures and Architectural Design—Architectural Design of Huangyan Business Street Zone; March (2006).
- [2] Shi Bing: Design & Study of Pedestrian Commercial Street's Regionalism; University of Science & Technology of Suzhou (2010).
- [3] Yin Hang: Regain of Regionalism Design Strategy of Architectures; Shanxi Architectures 14th Period (2010).
- [4] Zhang Kexin: Design & Study of Pedestrian Commercial Street in the Old town of Xi'an Based on Cultural Characteristics; Xi'an University of Architecture and Technology (2009).
- [5] Zhang Jiaming: Analysis on How Does the Planning Design of City Business Street Embody the Regional Characteristics—Taking Design of the Commercial street in Canyons Resort, Qi ao Island, Zhuhai; Knowledge Economy; 2nd Period (2011).
- [6] Shi Bing: Design Analysis of Natural Regionalism in the Pedestrian Commercial Street; Fujian Construction Science 1st Period (2010).

The experimental study on mechanical properties of elephant grass stem

Xiao Liang, Bing Fang, Da Peng Ye & Hong Jun Hu

Fujian Agriculture and Forestry University, Fu Zhou, Fujian, P.R. China

ABSTRACT: To study the mechanical properties of the elephant grass stalks cutting parts. In order to get the maximum damage to the mechanical properties of stress, elastic modulus and other parameters. We use computer-controlled electronic universal testing machine test the bottom of the elephant grass in harvest period tension, compression and bending. Obtained under test conditions along the grain tensile, compression, bending stress-strain curves, test results show that: the bottom of the elephant grass stalk of stretching along the grain average of 106.5 MPa maximum tensile strength, elastic modulus of 997 MPa; compression parallel to grain average of the maximum compressive strength of 7.29 MPa, elastic modulus of 67 MPa; maximum flexural strength parallel to grain bending average of 32.7 MPa, elastic modulus of 381 MPa. Elephant grass failure stress parameters close to *Arundo donax*, much larger than the corn, wheat and other stalk destruction stress parameters, Mechanized harvesting of elephant grass should not be using the traditional grass cutter for cutting tools. Provide theoretical and basic technical parameters for cutting tools and cutting mode of elephant grass. For low power consumption and high efficiency elephant grass cutting machine's design has important guiding significance.

Keywords: elephant grass; mechanical properties; stress-strain curve; destruction stress parameters

1 INTRODUCTION

Energy generation projects can have significant environmental impacts. The growing demand for energy in recent decades has been met mainly by the increase in the use of fossil fuels, with large negative effects such as the increase in pollution and in carbon emissions. Bio-refineries, such as elephant grass, may represent a viable and sustainable alternative to replace the need for oil, coal, natural gas and other non-renewable energy sources, as they are able to convert biomass into chemicals, energy and other essential materials. Elephant-grass is one of high yield and quality grass, which can be used as training material, fuel for power generation, replaced fiber board, fuel ethanol. What's more, elephant-grass could be planted a wide range of soil, and also it is a good grass for soil and water conservation. Elephant-grass belonging to angiosperms is a tropical and subtropical plants. The most suitable temperature for elephant-grass growing is 25 to 35 degree. Elephant grass is tall, erect tufted, owning developed root system. And the height is generally 4–5 m, up to 7.08 m. Elephant grass is high yield plant, in the south of our country can be planted 300–500 *t/hm*, and can be harvested the consecutive years^{[1][2][3]}.

Elephant grass stem wood fiber as the energy and industrial raw materials is potential, the mechanical properties of the stem is very important for cutting,

such as, the bending properties of elephant grass stems influence the process of destruction^{[4][5][6][7]}. The aim of our study is to determine the influence of the sampling area in one stem on the mechanical properties of elephant stem. Tensile tests were carried out on fibers extracted from three distinct sampling areas on one elephant stem.

2 MATERIALS AND METHODS

2.1 Plant material

Elephant grass stalks were collected from fungus grass planting Center of Fujian Agriculture and Forestry University, Collecting the bottom of Elephant grass stalk different geographical locations. The bottom of stem water content is about 75%. Select the diameter range of 17 mm–23 mm for the test. Elephant grass harvest stubble height of about 30 mm–50 mm. The acquisition of 30 mm–200 mm from the ground a stalk for the collection of specimens. The test environment for the sample: temperature 16 °C, indoor relative humidity is 52%.

Material requirements: No obvious defects and damage. After the giant fungus grass back, stripping leaves, wipe clean. Specimen timber making reference to the state of physical and mechanical properties of the test method and the state of physical and mechanical properties of bamboo test methods^{[8][9]}.

2.2 Production of test materials

Leaves and nodes were removed and stalks were further gently scrubbed in tap water. Measuring the diameter of the Elephant grass stalk. According to the test method of physical and mechanical properties of wood and bamboo, making the test specimen. Tensile samples: 100 mm long, 15 mm wide and t mm thick, test effective middle part specifications 60 mm long, 2 mm wide and t mm thick, and both ends of the clamping portion arc smooth transition. As shown in Figure 2. Compression specimen: Sample was $30.0 * d * t$ (high * big end diameter * small end diameter). Both ends need sanded smooth. As shown in Figure 3. Bend specimens: 100 mm long, 15 mm wide and t mm thick. As shown in Figure 4.

2.3 Test equipment

SNAS microcomputer control electronic universal material testing machine. The use of the devices for tensile, compression and bending test, using cross lines chuck, disc plane special pressure head and three point bending test device for testing. The system consists of host machine, RG controller, computer control system of three parts, during trial operation can dynamically display the load value,



Figure 1. Elephant grass plant.

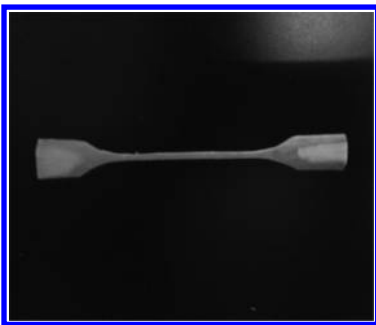


Figure 2. Tensile test specimen.



Figure 3. Compression test specimen.



Figure 4. Bend test specimens.

deformation, test speed and should test the stress-strain curve and the test results.

3 RESULTS AND DISCUSSION

3.1 Tensile stress and results analysis

Use Cross grain chuck clamp the upper and lower ends of the specimen, Tensile load, The loading rate was 3 mm/min . Tensile test specimens obtained stress-strain curve. Six groups and the tensile stress corresponding to the diameter of the sample-strain curve shown in Figure 5 course.

As can be seen from the graph, during the experiment after tensile stress reaching the fungus grass stalk maximum tensile strength. Elephant-grass stalk pulled off and a sharp decline in the instantaneous stress. Test measured the maximum tensile strength of elephant grass is 106.5 MPa, The minimum value is 70.9 MPa. The average tensile strength is 90.9 MPa. Tensile elastic modulus of 997 MPa.

3.2 Compression test and results analysis

The compression specimen is placed at flat indenter bearer plane, set the compression modu-

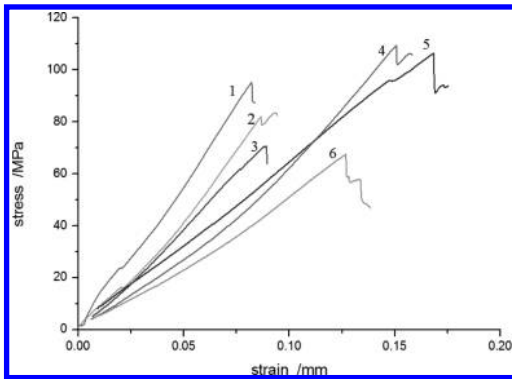


Figure 5. Tensile stress-strain curve.

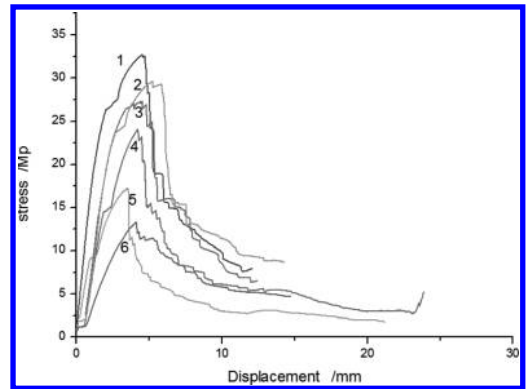


Figure 7. Bending stress-displacement curve.

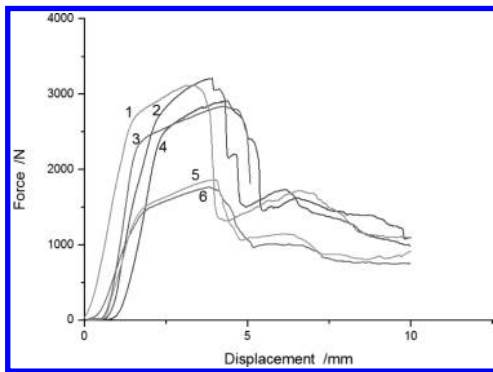


Figure 6. Compressive force-displacement curve.

ulus of elasticity material control process in the control of machine, applied compressive load, a speed of 3 mm/min, set the compression displacement is 1 mm, test specimens obtained compression stress-strain curve. Analysis of force-displacement curve data, obtain the test compression elastic modulus pieces. Elephant-grass test measured the maximum compressive strength (Compression failure stress). The maximum is 7.29 MPa, the minimum value is 6.05 MPa, the average value is 6.6 MPa. Compressive modulus of elasticity is 67 MPa.

3.3 Bending test and results analysis

Using three-point bending test method^[10], The sample for plate processing, selection of material elastic modulus in bending test control program, Define the corresponding cross-sectional area of the specimen Elephant-grass, Bending the span is 48 mm, the preload of 10 N (Ensure the pressure head closely contact with the sample). Bending stress loading speed 3 mm/min.

Figure 5 is the bending computer drawing the stress-displacement curve, bending stress exceeds maximum bending strength after the elephant grass stem fracture and Stress decreases. Test measured the largest bending strength (Bending stress). The maximum value is 32.7 MPa, the minimum value is 17.3 MPa, the average value is 25.98 MPa, bending modulus of elasticity 381 MPa.

4 CONCLUSION

1. The tensile, compression, bending test of stress-strain curve showed some nonlinear features. Tensile and bending test, the load exceeds elephant-grass maximum damage stress, The grass instantly destroyed (Tensile and bend breaking). Presents obvious brittle fracture resistance, compression test, the load exceeds the maximum compressive stress, Elephant-grass samples get into tight compression stage, stress reaches a certain value, until the specimen fracture.
2. Test measured the Elephant-grass stalk mechanical parameters: the maximum tensile strength of the elephant-grass stalk in harvesting period is 106.5 MPa. The tensile elastic modulus is 997 MPa; the maximum compressive strength of 7.29 MPa. The compressive modulus is 67 MPa; the maximum bending strength was 32.7 MPa, flexural modulus of elasticity of 381 MP.
3. Physical and mechanical properties of elephant-grass is close to bamboo grass (Moso bamboo tensile strength is 153.1 MPa, the compressive strength is 66.3 MPa, bending strength 152 MPa^[10]); Far more than corn (The longitudinal tensile strength of 90 MPa). Wheat (Longitudinal tensile strength of 21.2–31.2 MPa) Other physical and mechanical stalk parameters. So the elephant-grass mechanized harvesting

should not use the traditional cutting methods and cutting tools, so we need to develop suitable cutting tools for elephant grass.

ACKNOWLEDGEMENTS

The corresponding author of this paper is Ye Dapeng. This paper is supported by pennisetum. Sp mountain harvesting mechanized equipment technology integration research. JCJJ13005.

REFERENCES

- [1] Zheng Jinying, Chen Lifeng, Lin Zhanxi. The Analysis of JUNCAO Industrial Growth and Its Versatility. 2011, 27(1):304–308.
- [2] Li Zhiwen. The characteristics of elephant grass study as an energy source [J]. *Agricultural Engineering Technology*. 2013(6).
- [3] Liao Qingxi, Shu Caixia, Tian Boping. Research on the Cutting Process Based on High-speed Photography Technology for the *Arundo donax* L. [J] *Journal of huazhong agricultural university*. 2007, 03:415–418.
- [4] Liao Yitao, Liao Qingxi Tian Boping. Experimental research on the mechanical physical parameters of bottom stalk of the *Arundo donax* L. in harvesting period [J]. *Transactions of the Chinese Society of Agricultural Engineering*, 2007, 04:124–129.
- [5] Liu Qingting, Ou Yinggang, Qing Shangle. Study Progress on Mechanics Properties of Crop Stalks [J]. *Transactions of the Chinese Society for Agricultural Machinery*, 2007, 07:172–176.
- [6] Gao Mengxiang, Guo Kangquan, Yang Zhongping. Study on Mechanical Properties of Cornstalk [J]. *Transactions of the Chinese Society for Agricultural Machinery*, 2003, 04:47–49.
- [7] Kronbergs E. Mechanical strength testing of stalk materials and compacting energy evaluation [J]. *Industrial Crop and Products*, 2000, 11(2~3):211–216.
- [8] Chinese Academy of Forestry. GB/T1927-1943-91, People's Republic of China National Standard: National physical and mechanical properties of wood test methods [S]. *China Standards Review*, 1991.
- [9] Chinese Academy of Forestry. GB/T15780-1995. People's Republic of China National Standard: National physical and mechanical properties of Bamboo test methods [S]. *China Standards Review*, 1995.
- [10] Liu Qingting, Qu Yinggang, Yuan Naxing. Bending load induced failure forms of sugarcane stalks [J]. *Transactions of the Chinese Society of Agricultural Engineering*, 2004, 03:6–9.

Architecture value and protection strategy of fortress settlement: A case study from Zhaibochang ancient residential

Xiao Fang Bi

School of Architecture, South China University of Technology, Guangzhou, China
Henan Polytechnic University, Jiaozuo, China

Lu Wang

Henan Polytechnic University, Jiaozuo, China

Da Jun Xu

Jiaozuo Planning and Architectural Design Institute, Jiaozuo, China

ABSTRACT: Fortress ancient village has its unique origin and geographical characteristics in the Chinese traditional village, this article has a description of the fortress characteristics of the ancient village zhaibuchang. Analysis its unique spatial characters, and the traditional characteristics of the space form. The thick Wall and river have special value, this paper also sums up some diversity conservation tactics.

Keywords: architecture; nature conservation; building; manufacture

1 INTRODUCTION

Zhaibuchang ancient buildings is located in the fraternity County town 5 kilometers southeast of sujiazuo town in Henan province, which east 4 km away from the township government, west to WenBo Road, South to the Qinhe River Plain, north of Taihang, as shown in [Figure 1](#). As a typical fortress settlement, Zhaibuchang was located in Hanoi County in Ming Dynasty, and it belonged to Three Map County in the Qing Dynasty [1], In 1927 under the fraternity County so far.



Figure 1. Location of Zhaibuchang.

2 HISTORY AND PRESENT SITUATION

Zhaibuchang was built in the Ming Dynasty by Wang Taishun family. According to records of the Migrants policy of Zhu Yuanzhang, after Wang Migration to the village they propagated quickly, several generations, it had a big family, and established a business firm “TaiShun”. In The Kangxi and Qianlong’s, the business was bigger and bigger by the Wang family’s fourteen descendants, “Taishun” reputation is more.

In September 2000, Zhaibuchang has been approved as a key cultural relics protection units by Henan provincial government. The ancient buildings can also remains fully human history and reflect the Kangxi and Qianlang’s time.

Zhaibuchang Castle Village not only is big in scale, but also in the shape of the pavilion style buildings of Beijing’s quadrangles and China South’s, with the characteristics of the Northwest Henan place obvious, Which is a large quantity of construction quality, unique architectural style houses preserved in Henan province, Offers a great deal of physical evidence about residential, folklore and architectural technology in The Central Plains area in the Ming and Qing Dynasties. It has rich ornamental value on the construction craft [3], wood carving, stone carving and folk customs.



Figure 2. Residential status.

Now the ancient buildings have one Wang's ancestral hall and residential buildings more than 130 blocks. Most of them are Qian Long, Jia Qing, Dao Guang period, exception of a small number of the late Ming and early Qing Dynasty, Village wall and village river are preserved well, Each group of the courtyard has one door and two courtyards, as shown in Figure 2. Building structure is relatively fixed, each has its own merits and exquisite material, and modeling beautiful.

3 CHARACTERISTIC OF FORTRESS SETTLEMENT

3.1 Fortress settlement space layout

Settlement, “Hanshu·GouxuZhi” interpretation, “(the Yellow River water) to go, then fill silt fertilizers, the people plowing land, or long harmless, slightly built house, then into the settlement”, which refer to a place has many local population. Analysis the type of settlement should focus on the stability of the settlement, formed in a relatively long period of stable village houses.

The Central Plains area is the birthplace of our five thousand years of civilization of the Chinese nation. Which is the political, cultural center, since the establishment of the Han nationality in Yan-Huang emperor's. In the Central Plains region inhabited of the Han nationality area, formed the rural settlement characteristic, scattered in the vast central plains of China.

On the site selecting of Settlement, more emphasis on naturalism, combined with the natural landscape, integrate various cultural conditions, the pursuit of content rather than the form sense, looking for a change in the order of balance, changes of mountain, river, road. As shown in Figure 3, The spatial form of settlement, including space history humanities, irrigation water, defense function etc. The ancients said: “worthy of heaven, and earth,” reflects the optimization thought about natural environment, rising to the ancient “FengShui” concept, which using the principles of Yin Yang and the five elements to explain the nature, the person can have a living environment—cool in summer and warm in winter, enough drink

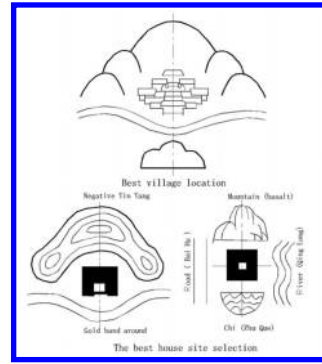


Figure 3. Feng Shui pattern.

water, safe flood control for defense. The pattern of FengShui is “Qinglong light, white tiger right, Suzaku former, genbu after” [4].

In order to protect the villagers Wang ancestors built the wall, the whole village surrounded by a thick wall like a castle. Zhaibuchang village slightly oblong, view the whole village from south, it like a turtle, in China traditional thought tortoise as “Sishen brake”, in charge of the northern treasure, is auspicious symbol of longevity. Basaltic (turtle) head south, north of the village of tail, several East-West streets and North-South alley constitute clear moire, the piece is made of yard, as shown in Figure 4.

3.2 Residential space shape

Zhaibuchang ancient dwellings distributed street at No. 2 street including the ninety building's, Over-looking the yard, communicated with the Academy, carved beams and columns, set things human aura, both the South and the North Building in one style, exquisite art, layout strict. The door carved couplets, stone lion, stone drum and other features.

Zhaibuchang traditional residential space form reflects the people's basic spatial shape. The courtyard is composed of yard, room, is a complex of patriarchal ethics, FengShui concepts.

3.3 The wall and the river

The wall is about 10 meters high, about 2.5 kilometers long around the village, rammed earth with stone out [4], After more than a hundred years of history, four old gates of the wall and twelve towers has been demolished, but the wall still stand as firm as a rock is well vicissitudes of life, showing the charm of tenacity and forceful, As shown in Figure 5.

The wall and the river was constructed from Xianfeng eleven years finished in Tongzhi seven years spring, As shown in Figure 6, dating back



Figure 4. Village turtle chart.

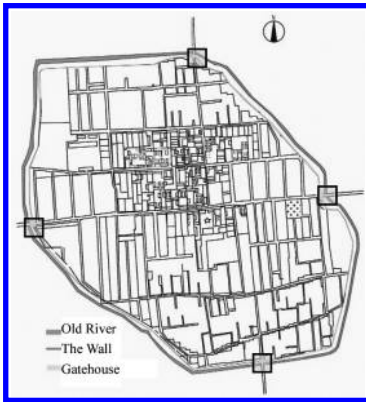


Figure 5. Map of wall and river.



Figure 6. The wall.

about one hundred and forty years of history. Jiang Taigong had Otsuge Uranainandesu future, said “Chang”, displayed Feng Shui of the place is very good, the future will be thriving and prosperous, as saying “Bu Chang”. In the Ming Hongwu years, because of the locust plague, people Reduced a lot in Huaiqing area, Zhu Yuanzhang had migrated some people from Shaanxi Hongdong to settle in Huaiqing, in

Tongzhi seven years, built the wall, the door, three villages composed together, collectively referred to as the “zhaibuchang”. The village gate with a large plaque about 1.5 meters length 0.75 meters high made of bluestone, respectively inscription is: “Na chun rong”, “Lan rong guang”, “Yi Qiu pulp”, “Ying die cui”. Four plaques mean the four seasons, the Taihang Mountain, the Yellow River, with superior geographical position.

4 PROTECTION AND UTILIZATION STRATEGY

Zhaibuchang village has a history nearly 300 years, its historical value is obviously, but because of disrepair, present condition is not well. Some problems are restricting the protection of ancient buildings, renovate and reuse.

4.1 Protection method of ancient buildings

In 1982, a perfect the people’s Republic of China cultural relics protection law enacted, incorporated into the heritage, heritage buildings to protect under the law. In 1992 published the people’s Republic of China Law on the protection of cultural relics, in 2000 revised the law. For the actual situation more accord with domestic and international charter and protection of modern cultural heritage theory practice [5], 2002 Chinese Bureau of cultural relics promulgated the China cultural relics protection criterion.

“Standard” stressed “protection is real, comprehensive preservation and continuation of the historical information and value”, “real”, “comprehensive” concept has the same meaning of “authenticity” and “integrity” in recent years the international charter and international society widely used. Emphasis on “protection of existing kind of undisturbed and historical information. Repair should be based on the existing valuable material as the main basis”, “all the protection measures must abide by the principle of not changing the original form of the cultural relics”.

Nowadays Wang’s descendants still live in the houses, repairing by themselves, but because of financial, material resources, they can’t do very well. The spatial pattern of the original building got great damage. In 2008 the government allocated a portion of funds for repair Zhaibuchang building, some new walls were built, the front the space of the ancestral hall is very cramped, serious damage to the space environment of the ancient village. The ancestral hall is often used as a space of rural settlement center, the hall become the cultural center of this village, which make the person produces psychological sense of belonging.

4.2 Means of protection can be executed

I have a few degrees to the village research and lead the students of our school Surveying and mapping the Fort, and talk about the village with Wang's later who more than 70 year old, the old man has a deep emotion with the ancient village. Year by year zhaibuchang building lost its original vitality, forgotten and destroyed. So the protection of ancient buildings be imperative, not only for the protection of ancient buildings, but also to protect the traditional culture of the region.

The spirit of integrity, authenticity protection strategy, diversity, sustainability. The protection of zhaibuchang need to set up a leading team, strengthen management, establish heritage management system, and person delegated to assume the responsibility of protecting the ancient buildings. It is Urgent to have a overall plan of the residential houses, drawing maps, Propaganda residential historical and cultural value. Made a foundation for the development of the tourism industry, strengthen the construction of hardware facilities. To focus on remediation of the streets, houses, residential environment clean and tidy. Increase the development of local traditional culture.

5 CONCLUSION

As a wonderful work in Central Plains, zhaibuchang settlement quietly hide private, intimate and familiar, comfortable and quiet, keep itself, inheritance of

traditional houses area feature. But some houses after long time of wind and rain, damaged many, is badly in need of repair. We are looking forward to Traditional folk culture and art with a history of the castle village can radiate new color.

ACKNOWLEDGEMENTS

The project was supported by National Natural Science Foundation and the State Key Laboratory of Subtropical Building Science, South China University of Technology, China (Project No. 51278196, 2012ZA02, 2014ZA05).

REFERENCES

- [1] Graph, namely Li, refer local zoning name specified in Ming and Qing dynasty. Gu Yanwu *RI Zhi Lu* volume twenty-two: change rural to city and change Li to graph.
- [2] P. Mensinga, J. Straube, C. Schumacher: Assessing the freeze-thaw resistance of clay brick for interior insulation retrofit projects, Proceedings of thermal performance of the exterior envelopes of whole buildings XI, Clearwater Beach, FL, USA (2010).
- [3] Yang Huancheng: Gorgeous and colorful Henan ancient architecture art, Cultural Relics of Central China, (1984).
- [4] Wang Qiheng: Research of Feng Shui Theory, Tianjin University press, (2007), p.38.
- [5] Cheng Jianjun: Guangzhou Guangxiao temple architecture research and protection engineering report, Beijing, China Architecture Industry Press, (2010).

Discussion of strata division of Bingmagou Formation in Yichuan of Yuxi region

Jie Zhu, De Shun Zheng & Shu Hui Zhu

School of Resources and Environment Engineering, Henan Polytechnic University, Jiaozuo, China

ABSTRACT: Bingmagou Formation of Mesoproterozoic erathem is rarely researched by scholars until now. The scope and area of Bingmagou Formation is too few. Maanshan Formation of wufo Group parallel unconformably onlaps Bingmagou Formation in Wananshan of Yichuan. Dengfeng Group of Archean is covered in angular unconformity by it. So it should be divided from the above and the lower strata, that the study of structural geology and sedimentary environment will be made well.

Keywords: Bingmagou Formation; Maanshan Formation; Dengfeng Group; division of strata

1 REGIONAL GEOLOGICAL CONDITIONS

Bingmagou Formation is firstly named by regional geological team of Henan (1964) in 1:0.2 Million Regional Geological Measurement Report of Linrufu Region. It exists in Bingmagou nearby of Yichuan in Henan. The outcrop of Bingmagou Formation here is 5 km from east to west, and 100–1000 m from south to north. Dengfeng Group of Archean is covered in unconformity by it, and Xionger Formation is partly covered in unconformity by it too^[1-2]. Maanshan Formation of wufo Group of mesoProterozoic erathem parallel unconformably onlaps it. The section of Bingmagou which is measured is in Wananshan of Lvdiian Yichuan. The outcrop of it is very little, and the thickness of it is unstable. From bottom to top the rock grain size of section is from crude to thin section. The distribution of gravel is from close to thin. A sedimentary cycle is formed by the mode of conglomerate—sandy conglomerate—sandstone-shale of silt, and secondary rhythm of sedimentary is so much. Parallel bedding and cross bedding could be noticed in sandy conglomerate and sandstone. A similar strata which was named Xiaobeigou Formation was found by Wangzhihong (1979) and the NO 2 geological team of Henan (1981) in Wangwushan of Jiyuan. The time and space and the lithology are considered similar by both regional geological team of Henan (1981) and Regional Geological Book of Henan Province (1989) later time. It should be considered as one Formation, which named by Bingmagou. The outcrop of Bingmagou Formation was found better in Wugang too. And the section of Bingmagou which was found recently is in Lushan. The four distribution of Bingmagou Formation mentioned

above formed one line on the whole. The orientation of them is from north west to south east. The sedimentary thickness becomes thinner along the above orientation. So the outcrop regions of Bingmagou Formation maybe one system of a same river^[3-4].

2 GENERAL SITUATION OF STRATA FEATURES OF BINGMAGOU FORMATION

In fact, Bingmagou Formation lies in a special horizon. By field measurement, we could found Maanshan Formation of wufo Group parallel unconformably onlaps Bingmagou Formation, and Dengfeng Group of Archean is covered in angular unconformity by it.

2.1 *Dengfeng Group of Archean which is under it*

The group was firstly named Taishan complex by Zhangbosheng (1951), then it was named Dengfeng complex again by Maxingyuan (1957) in Songshan region of Dengfeng. Later it was named more times again, and lastly, it was named Dengfeng Group unitly by both regional geological team of Henan (1981 a) and Bureau of geology and mineral resources of Henan (1989)^[1-2]. It was divided with Shipaihe, Guojiayao, Changyao, and Shitigou Formations from bottom to top. Bearing biotite plagioclase gneiss, biotite granulite, plagioclase-hornblend, phyllite, chlorite schist etc are its lithology mainly. Bottom was not seen, and Songshan Group of lower Proterozoic angular unconformity onlaps it. Migmatization of Gneiss series is serious which is on the bottom of Dengfeng Group.

Generally speaking it's the core of domal structure. The main lithology is plagioclase-hornblend. Schist which is sedimentary normally and low metamorphic consist of the top of Group, and flysch construction could be seen here. The Group lies in Dengfeng County, the lower part of horizon could be seen in Linshan of Jiyuan and Linzhou-Huixian of Taihang mountain area. The upper part of horizon could be seen better in Songshan region. The separatrix of Bingmagou Formation and Dengfeng Group of Archean found on field (Fig. 1).

2.2 *Maanshan Group of Mesoproterozoic erathem which is on top of it*

Wangyuelun, Wangzejiu etc (1959) named it with Maanshan quartzite firstly in Maanshan Foguang village of Yanshi county^[1-2]. The main lithology is quartz sandstone which including a little conglomerate and silty shale. On the bottom basal conglomerate could be seen. As the symbol, basal conglomerate parallel unconformably onlaps Bingmagou Formation, or unconformably onlaps Dengfeng Group or Songshan Group. The finish symbol on top is the end of quartz sandstone, and conformable contacts with shale of Puyu Formation. Xinji Formation of lower cambrian parallel unconformably onlaps Maanshan Formation in most region. It belongs to Wufoshan Group. Except to Maanshan Formation, Puyu Formation, Luotuopan Formation and Hejiazhai Formation consist of this Group from bottom to top. The separatrix of Bingmagou Formation and Maanshan Formation of wufu Group found on field (Fig. 2).

2.3 *The measured profile of Bingmagou Formation on the spot in Yichuan*

According to differences of lithology, color, texture and structure etc, the Formation were divided into



Figure 1. Separatrix of Bingmagou Formation and Dengfeng Group of Archean.



Figure 2. The separatrix of Bingmagou Formation and basal conglomerate of Maanshan Formation of wufu Group.

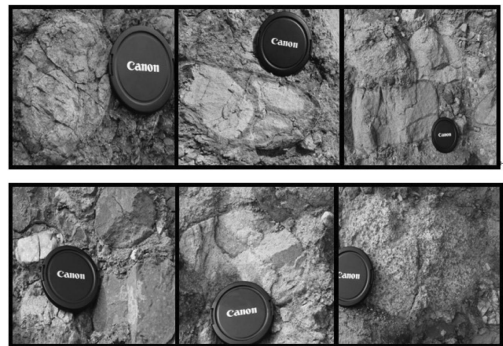


Figure 3. Metamorphic components.

2 Sections (103 beddings) by this paper temporarily, and the thickness is about 676 m.

The under section was divided into 11 beddings, and the thickness is about 69 m. Metamorphic crude conglomerate is the mainly lithology (Fig. 3). Gravel ingredients of conglomerate are complex, and the colors are various, for example yellow, brown, grey white, black etc^[5]. The size of gravel of conglomerate is various, the biggest diameter of them is about 40 cm, matrix supporting, basal cement, grading of conglomerate is poor, roundness is better relatively, texture maturity is better, and compositional maturity is poor. Conglomerate of this section is thick-bedded or huge thick-bedded, inclination of 30°, and inclination angle of 29°. Gneiss of Dengfeng Group is Under the section, inclination of 74°, inclination angle of 28°, the contact style is angular unconformity.

The upper section of Bingmagou Formation was divided into 93 beddings, and thickness is about 607 m. Secondary conglomerate and thin conglomerate are the mainly lithology in lower

part of this section, and thickness is about 179 m, gravel diameters are below 8 cm mostly. Grey green or purple or kelly boulder clay were seen from top of lower part to middle part of this section, tear mark is obvious. Sandstone, siltstone, mudstone could be seen from underpart to top in this section, and light green shale distributes in some beddings. Multiple sedimentary rhythm had developed here. Many kinds of beddings had grown here, for example, parallel bedding, wedge-shaped cross bedding, and tabular bedding etc. In addition, shear joint could be seen too^[5-6]. Different from the under section, the color of upper section is almost purple. Quartz sandstone is the mainly lithology according to thin section observation, and some cuttings and a little feldspar. Metamorphic components are included in sandstone, and the components are same as the conglomerate in bottom, so it had been carried from bottom of the section obviously.

3 STRATA EVOLUTION OF BINGMAGOU FORMATION

In April 1989, Bingmagou Formation was divided into Ruyang Group by the book of Regional geology of Henan Province. Regional geological team of Henan (1964) named this Formation. The outcrop of it is very little, and it is located in west of Songshan and Wangwushan region.

Bingmagou Formation was divided into Ruyang Group of middle Proterozoic from Table 1.

Table 1. Regional geology of Henan Province Ruyang, Luoyu Group and sinian system of middle and upper Proterozoic evolution table (partly).

Geoscience institute of Henan 1981	Regional geology of Henan province
<i>Sinian system</i>	<i>Sinian system</i>
Dongpo Formation	Luoquan Formation
Luoquan Formation	
Dongjia Formation	Dongjia Formation
Huanglianduo Formation	Huanglianduo Formation
<i>Luoyu group of qingbaikouan system</i>	<i>Luoyu group of upper proterozoic</i>
Luoyukou Formation	Luoyukou Formation
Sanjiaotang Formation	Sanjiaotang Formation
Cuizhuang Formation	Cuizhuang Formation
<i>Ruyang group of Jixian system</i>	<i>Ruyang group of middle proterozoic</i>
Beidajian Formation	Beidajian Formation
Baicaoping Formation	Baicaoping Formation
Yunmengshan Formation	Yunmengshan Formation
Xiaougoubei Formation	Bingmagou Formation

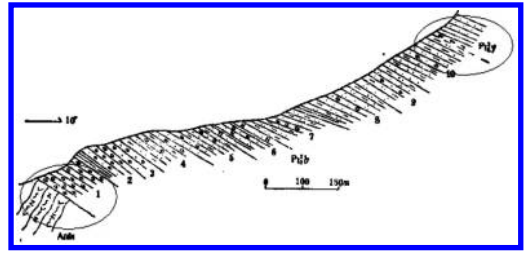


Figure 4. Profile of Bingmagou Formation Ruyang Group of Yichuan county in Regional geology of Henan Province.

Table 2. Rock strata of Henan province evolution table of Wufoshan group (partly).

Bureau of geological and mineral 1989		Rock strata of Henan Province	
€1	Xinji Formation	€1	Xinji Formation
Luoyu Group	Luoyukou Formation	Z	Hongling Formation
Pt3	Sanjiaotang Formation	Pt3	Hejiazhai Formation
	Cuizhuang Formation	Wufoshan Group	Luotuopan Formation
Ruyang Group	Beidajian Formation	Pt2	Puyu Formation
Pt2	Yunmengshan Formation		Maanshan Formation
	Bingmagou Formation	Pt2	Bingmagou Formation
Pt1	Songshan Group	Pt1	Songshan Group

From Figure 4, we can draw the conclusion that Yunmengshan Group parallel unconformably onlaps Bingmagou Formation, and Dengfeng Group of Archean is covered in angular unconformity by it^[2]. In the following book Rock strata of Henan Province, Dengfeng Group of Archean or Xionger Group of middle Proterozoic is covered in angular unconformity by Bingmagou Formation, and Yunmengshan or Maanshan Group parallel unconformably onlaps it.

From Table 2, we can see, Bingmagou Formation was still divided into Ruyang Group until 1989. But it was separated with Wufoshan Group in Rock strata of Henan Province, Maanshan Formation of wufo Group parallel unconformably onlaps Bingmagou Formation, and Songshan Group of Paleoproterozoic is covered in angular unconformity by it. We could not find strata of Songshan Group, but metamorphic rock of Dengfeng Group was found on the spot.

4 CONCLUSION

By the principle of division of strata, parallel or angular unconformably should not exist. So by the meaning of author, it's not proper that Bingmagou Formation was included in Ruyang Group in Regional geology of Henan Province^[7]. And because of parallel unconformably with Maanshan of Wufoshan Group, Bingmagou Formation was not divided into Wufoshan Group in fact. From Table 2, we can see that, it was not divided into Wufoshan Group, so it is right obviously. According to description of two books again, Dengfeng Group of Archean or Xionger Group of mesoProterozoic or Songshan Group of Paleoproterozoic was covered by Maanshan Formation in angular unconformity. So for Bingmagou Formation of Yichuan we should replace Songshan Group to Dengfeng Group in Table 2. All in all, because of parallel unconformably with Maanshan Formation and angular unconformity with Dengfeng Group, we should take Bingmagou Formation out upper and under strata. It is an independent strata for the whole mesoProterozoic erathem^[8-9].

In consideration of features of conglomerate and sandstone, as well as the special horizon of Bingmagou, so sedimentary environment analysis and dynamic mechanism as well as source analysis would be very essential and necessary. It will be a help to improve and perfect strata of Huabei in middle proterozoic.

REFERENCES

- [1] Bureau of Geology and mineral resources of Henan Province. *Rock strata of Henan Province* [M]. Wuhan: China university of geosciences press, 1997.
- [2] Bureau of Geology and mineral resources of Henan Province. *Regional geology of Henan Province* [M]. Beijing: Geological Press, 1989.
- [3] Yuanguo Zhang, Lei Chen, ChangleLiu. The Discovery of the Middle Proterozoic Bingmagou Formation in Lushan County, Henan Province, and its significance [J]. Geological Bulletin of China, 2011, 30(11): 1716-1720.
- [4] Xiu Hong, Hongrui Zhou, Ziqiang Wang etc. Sedimentary facies of the Mesoproterozoic Jixianian in western Henan Province [J]. Journal of Palaeogeography, 2008, 10(6):589-598.
- [5] Changxiu Yang, Shiyan Wang, Zhenhong Liu etc. Mesoarchean-Neoproterozoic Grey Gneiss in the Lushan Area, Henan Province[J]. Geological Review, 2008, 54(3):327-334.
- [6] Guowei Zhang, Zongqing Zhang, Yunpeng Dong. Nature of Main Tectono-Lithostratigraphic Units of the Qinling Orogen: Implications for the Tectonic Evolution [J]. Acta Petrologica Sinica, 1995, 11(2):101-114.
- [7] Xiaomin Zhu. *Sedimentary Petrology* [M]. Beijing: Petroleum Industry Press, 2008.
- [8] Yongjun Fan, Fusheng Wang. *Sedimentary rocks and sedimentary facies* [M]. Beijing: Petroleum Industry Press, 2009.
- [9] Youbin He, Wenguang Wang. *Sedimentary rocks and sedimentary facies* [M]. Beijing: Petroleum Industry Press, 2008.

Bon temples in Ding Qing of Qamdo

Han Wen Qi

College of Civil Engineering, Nanjing Tech University, Nanjing, Jiangsu, P.R. China

Xiao Meng Zong

College of Industrial Design and Artistic Design, Nanjing Tech University, Nanjing, Jiangsu, P.R. China

Yong Ping Wang

College of Architecture, Nanjing Tech University, Nanjing, Jiangsu, P.R. China

ABSTRACT: This paper focused on the monastery of Bonpo in Tibet, taking Qamdo country as an example, mainly analyzes its nature and characteristics, to let more and more people know about the original religions of Tibet.

Keywords: east of Tibet; bonpo monastery; construction status

1 SUMMARY OF TIBETAN BON RELIGION

As the primitive religion in Tibetan areas, Bon religion was initially originated from the ancient Tibetan and spread to Tubo later. Nowadays, the Bon religions are divided by scholars into the original Bon religion and Yong-Zhong Bon religion. The Yong-Zhong Bon religion is the main Bon religion existing in Tibetan, which fusion the doctrine in some of the original Bon religion and with strong local characteristics, closely related to the life of the Tibetan people. At the same time, the Bon religion is also an integral part of the multi-culture in Tibet. According to historical records, the ancestor of Bon religion was born in Zhang Zhong Wei Ma long ren (there are differences in academia and will not discussed here) [1]. It originated from the mysteries about the heaven, earth, moon, stars and mountains, the fear about the disaster, plague, disease, wind, rain, thunder and lightning, and the psychological fear and worship of nature. After a long time of accumulation, it gradually becomes a religion. Therefore, the Bon beliefs and culture is the crystallization of native Tibetan traditional culture, and its source can be traced back to ancient times of the Tibetan culture.

Bon religion is one of the oldest Tibetan religious, and its doctrine is permeated and influenced the art, the culture and the life of the Tibetan [2], the building is no exception. The formation, development, and the change process of architecture in Tibet follow the universal laws: from simple to

complex. Meanwhile, there existed many unique cultural phenomena in its long development period because of its special historical culture and geographical characteristics, and the architectural features changed at the same time. There are many historical information and architectural culture needed to be further researched. This paper mainly analyzed the Bon temples in Ding Qing rdzong of Qamdo.

2 DING QING MONASTERY

The full name of the monastery is sTeng chen dgon gYung drung bstan rgyas gling (Fig. 1). Ding Qing Monastery is located in the west of Ding Qing, about 800 meters away. It was founded in 1061 by Khyung dbus Shes rab rgyal mtshan [3]. About 150 monks studied in the temple in its heyday period. Most of the cultural relics were destroyed during the Cultural Revolution and the temple was reconstructed in 1985. There are five function groups: the Buddhist group, the political security group, the learning group, the financial management group and the protection of cultural relics group. The main artifact of the temple is a pair of Thangka.

The author learned that the history of the temple is roughly divided into two periods. The first period is built on Ding Qing village, and the temple in the village was basically ruined out (Fig. 2). However, it was important in this period from the wreckage of the walls. The temple face south with not very big scale, and its main entrances and exits

3 YUNG ZHONG BARI MONASTERY



Figure 1. The entrance to the temple.



Figure 2. Broken beam mount.

located in the southwest, through it was a square surrounding by 2 single verandah monks apartment. The structure of the apartment was rammed earth and wood-frame [4–5]. Square is the debate places for monks, adjacent to the north of the square is oratory and hall. The building was crumbling in it and from its carving exquisite architectural details and paintings; it is not difficult to speculate about the importance of the building at that time.

The second period is the temple moved to a hill neat Ding Qing village because of various historical reasons. Ding Qing temple is built down the hillside with the obvious characteristics of mountain lands, and it face south. From the south to the north, the slope gradually rises. The Mani stone pile was located in 200 meters, to north of the temple, on the east side of the pile is the main road. Pass-through the temple, buildings was on the both sides of this road and spread from east to west, most temple was civil structure and the height of the building is mostly 2–3 layers. Now the temple was host by the 27 generation living Buddha, called jiang cuo rob. Ding Qing temple education system mainly divides into four colleges: the Zha-Cang college, the Bian-Ming college, the Nei-Ming college and the Chan-Xiu college. The author happened to see a Buddhist activity in Ding Qing temple, and the activity lasted for a week. During that period, the monks must reciting scriptures and using zanba to make sacrifices for worship.

Yung Zhong Bari Monastery (Fig. 3) is under the administration of the Ding Qing villages, about 12 kilometers westward on the highway. The monastery situated on a hill and surrounded by a number of holy mountains [1]. This temple is founded by Yong Zhong Ping Cuo in 1434. Yong Zhong Bari temple covers an area of 4750 square meters, and construction area of 796 square meters. The temple is not a long existing architectural history, most of the cultural relics were destroyed during the Cultural Revolution and the temple was reconstructed in 1984.

The layout of the temple is reasonable, and the main hall of the temple can be seen when entered in the front door. There is a square in front of the hall and in the middle of the square is a white tower for the believers worship and Buddhism activity. According to local monks, the temple has the largest Mani stone pile in Ding Qing area. Yong Zhong Bari temple with celestial burial platform and the celestial burial platform is divided into two: one is for normal death, and the other is used for unfortunate death. Around the celestial burial platform, there are a lot of small stone package, and these stone package are buried children died when they were very young. There are also places for female monks, which is near the celestial burial platform. It's a branch of Yong Zhong Bari temple, and the normal supply was shouldered up the mountain by the male monks. The footprints of the legendary Zhen ba nan ka was here, and which was also seen by the author. However, the author is still skeptical for these myths and legends.

Above all, the construction scale of Yong Zhong Bari temple is not very large, and the material of the monastery is stone and wood. The architectural is 2–3 layers and the building is not very long. The application of modern materials on many buildings can be easily found. Many temples window has abandoned the original wooden window with aluminum alloy instead, which will produce the contradiction of an architectural language. The beauty of traditional architecture was from



Figure 3. The Buddha hall of the temple.

details, and the modeling of modern architecture is concise and lively to reflect the logic of space. The local component and traditional architecture in modern architecture are bound to cause the confusion of this logic, which were directly embodied by the architecture. From the perspective of building, the temple was not that importance in the characteristics of the building.

4 MIN JI MONASTERY

Min Ji temple located in Chalong village in Ding Qing of Qamdo, is the Qing dynasty architecture. The temple was founded by Lang jie wang jie and Mei jie gu xiu in 1842. The Buddha halls are toward south, with 2 floors. The temple is mainly enshrined the holy stupa for Lang wang zhen jie and the stupa has 5.6 meters high, and worship 128 small statues.

Min Ji temple is not larger than other temples in Ding Qing, and the temple only has one building. Its north was Buddha hall, and the south was living room for monks. They get together to take the shapes of an internal open courtyard. Min Ji temple covers an area of about 7000 square meters and the building area of 3800 square meters. The doorway of the temple faces west, and the temple is red and yellow, the wall is red and the roof is yellow. The building materials of the temple are the Tibetan traditional rammed earth wall and wooden beams, also used the material such as concrete and cement. The material of windows is aluminum alloy instead of traditional wood.

The debate place was set up in the west of the temple, and this is rare. Generally, the square of Bon temple used for debate is at the front of the Buddha hall. However, due to the narrow terrain, the debate square was built at west. In the middle of



Figure 4. The Bon mandala.

the square is the prayer flag. The pillars decoration and the color drawing on the wall are very delicate [5], and the painting on the columns and beams are mainly composed of cloud and animal. The roof is elegant (Fig. 4), which was composed of many different Bon mandala square boards, which can reflect the characteristics of the Bon religion.

REFERENCES

- [1] Cai, R., Dun, Z.: A Concise History of the Bon religion (China Tibetology publishing house, Beijing 2012).
- [2] Su, B.: Archaeological Studies on Monasteries of the Tibetan Buddhism (Wenwu publishing House, Beijing 1996).
- [3] Karmay, S.G., Nagano, Y.: A Survey of Bonpo Monasteries and Temples in Tibet and the Himalaya (Saujanya Publications, Delhi 2008).
- [4] Xu, Z.: An Introduction to Tibetan Traditional Architecture (China Building Industry Press, Beijing 2004).
- [5] Chen, Y.: Tibetan Architecture in China (China Building Industry Press, Beijing 2007).

Study on innovation of Chinese elements in modern interior design

Yi Feng Liu

Department of Art Design, Hunan Women's University, Hunan, Changsha, China

ABSTRACT: In the modern design field, the lack of Chinese design style and the overflow of new Chinese style are being criticized. In this paper, the orientation of Chinese elements is expounded, the abstraction and expression of Chinese elements in interior design are discussed, and the innovative integration between Chinese elements and interior design is studied. The focus of this study is to identify a reasonable corresponding point for heritage and development of Chinese elements under the cultural globalization context. The purpose is to promote the heritage of Chinese elements and communication with the Western culture in the design field.

Keywords: Chinese element; traditional culture; interior design; innovation

1 INTRODUCTION

The “non-independence” of the Chinese modern culture and the lack of a traditional native culture in China are evident. Distinctive and strong regional culture features have disappeared in most Chinese cities, and Chinese elements filled with the spirit of traditional culture in Chinese art designs, especially in interior design, are inadequate [1]. The relationship of Chinese elements and modern art design has been substantially examined, but little has been reported on the innovation of Chinese elements in interior design similar to the current paper [2–4]. Heritage and innovation of Chinese elements in modern interior design, that is, the continuation and development of Chinese traditional culture, are discussed in the final analysis. As the influence of China in the world continually increases, a new design concept and style filled with Chinese elements has gained worldwide attention. Thus, we should not only add Chinese elements in interior design, but also innovate in the theories and methods of design on the basis of the traditional culture.

2 ORIENTATION OF CHINESE ELEMENT

The so-called “Chinese elements” refer to any entity that gradually forms through the fusion, evolution, and development of the Chinese nation. These elements are created and inherited by the Chinese people, as well as reflect the humanistic spirit and folk psychology and the cultural achievement of Chinese characteristics [5]. Chinese elements in interior design are dimensions of visual aspects

in China, which include two aspects, namely, the material culture elements and the spiritual culture elements. At the core of the spirit of Chinese elements are three tenets of Buddhism, Confucianism, and Taoism, which include the Confucian spirit of benevolence, Tao following of natural rules, wisdom and compassion in Buddhism, and the combination of these religions. These definitions, as the core connotations of Chinese element symbols, accumulate in the subconscious of Chinese people and become common traits of nationality within communities, such as religion, ethics, custom, science, and art. Thus, Chinese elements are considered a spiritual system, which can generate various ideas and express diverse cultural symbols.

3 ABSTRACTION OF CHINESE ELEMENTS ON INTERIOR DESIGN

Philosophic thinking and literary thoughts can be integrated into Chinese traditional aesthetic ideology, which influence the aesthetic value orientation of the Chinese nation. The thoughts of Laozi lay the foundation of Chinese aesthetic ideology. Literati and scholars over the years have developed an integrated system of modern Chinese aesthetic ideology by conducting a series of studies, such as exploration, analysis, organization, induction, and conclusion. Chinese traditional aesthetics emphasizes overall harmony. Thus, we should follow the principle of overall planning in interior design and focus on creating a whole atmosphere.

Chinese characters in the form of stroke have been honored as “the most beautiful” characters in the world. The design idea, which combines

Chinese character graphic elements with interior decoration, continues to propagate its belief on a large scale in recent years. The symbols of elements have become the most recognizable symbols of Chinese culture. They can be used to assist decoration language to enhance its effectiveness. This representation method in interior design is more likely to be accepted and mastered by interior designers.

A schematic diagram of the chairs in the form of Chinese characters is presented in Figure 1. Figure 1 shows that the structure and form of the characters are similar to the basic structure of a chair. The designer designs the chair in the form of Chinese characters using this characteristic. These characters are recreated without meaning and pronunciation to match the characteristics of modern furniture and to comprise the most basic strokes of Chinese characters. A schematic diagram of the commodity shelf, Chinese character “见”, is illustrated in Figure 2. Figure 2 shows that a designer comes up with two Chinese characters “见” in identical forms using the basic principle of the furniture design, and can form a space between two vertical surfaces. According to the characteristics of the font, the horizontal strokes in the middle



Figure 1. A schematic diagram of the chairs in the form of Chinese characters.



Figure 2. A schematic diagram of the commodity shelf, Chinese character “见”.



Figure 3. A schematic diagram of the table lamp with Chinese characters.



Figure 4. A schematic diagram of the table ware of Chinese characters design.

of Chinese characters “见” have become the barrier of the cabinet. Combined with the structure of the auxiliary, Chinese characters have new functions. Small home decoration items play an important role in the presentation of theme and the creation of atmosphere for interior design, as shown in Figure 3 and Figure 4.

4 INNOVATION OF CHINESE ELEMENTS IN INTERIOR DESIGN

The development of cultures all over the world is based on their integration and influence on each other. No culture is stuck in the past, has an independent existence, and is unaffected by any foreign ideas. In the course of human development, different cultures not only collide and conflict with each other, but also communicate with each other. The mutual absorption and integration between Chinese traditional culture and Western culture is the essential approach to the innovation in interior design. This so-called “mix and match” approach has appropriately quoted other national and ethnic cultural elements and achieved a sensory

balance and leap. However, how “mix and match” is measured should be considered. Blindly rejecting a foreign culture is a one-sided tactic. Thus, being blind to foreign culture is negative not only to their own value created by the conflict, but also to our local culture created by the positive effects of the contrary. We should discard the dross, keep the essential, and obtain a better understanding of the cultural backgrounds of the selected elements. Meaningless decorative packing should be avoided. We should realize the coordination of materials and colors, and avoid excessive abruptness.

Abstract composition is a means of pondering and designing patterns that are full of rationality and logical inferences. Three-dimensional forms comprise abstract forms for abstract composition, such as shape and color, which can completely or almost not reproduce a concrete object. Perceptual abstract in the East has its own unique feature that draws itself closer to the abstract between the similar and the dissimilar, other than the rational abstract spirit in the West. Numerous similarities in integrity, symmetry, balance, simplicity, and generalization exist between Chinese visual elements and the modern graphic style.

The constructional drawing of Suzhou Museum designed by I.M. Pei is shown in Figure 5. Figure 5 demonstrates that the architecture designed by I.M. Pei actually merges with the traditional mechanism of Suzhou City. He abstracts the most beautiful Chinese elements that are full of concentrated taste in the Chinese garden. The design builds the integral atmosphere of the landscape in accordance with the spirit of the place, and thereby completes the abstract representations of artistic conception. The design inspiration for the roof of the museum comes from the Suzhou traditional top view, which includes Qiaoqiao cornices and nuanced architectural details. However, a new roof is reinterpreted and has evolved into a new geometric effect. The modern steel structure is extensively used in architectural construction, and has replaced the wood materials of the Suzhou traditional architecture.



Figure 5. A constructional drawing of Suzhou Museum designed by I.M. Pei.



Figure 6. A constructional drawing of the new exhibition hall of the Nantong Museum garden designed by Liangyong Wu.

The roof, which consists of geometric shapes, not only inherits the crisscross mansard roof of the ancient buildings in Suzhou, but also breaks through the shackles of Chinese traditional architecture “big roof” in the light, fully reflecting the idea of “the application of light on the design”.

A constructional drawing of the new exhibition hall of the Nantong Museum garden designed by Liangyong Wu is shown in Figure 6. Figure 6 illustrates that Liangyong Wu melts the ancient Chinese gardens with the modern museum at an organic whole, combines national features with scientific contents, and adopts design styles in the form of scattered points, multiple axes, and landscapes. Moreover, the designer cleverly combines the original buildings with modern pavilion-style buildings. This design idea is referred to as perfect “abstract inheritance”. This museum contains numerous trees and flowers, rare birds, and animals, which correspond to indoor display. All types of landscape facilities are likewise used to intersperse the museum. Thus, these designs can create an elegant, sophisticated, and relaxed atmosphere.

5 SUMMARY

Chinese interior design is essentially based on the characteristics of the Chinese traditional culture. The future of interior design in China is based on the creative inheritance and development of the traditional design style. Multicultural coexistence and global cultural exchange have become the characteristics of contemporary society. Thus, we should equally focus on the absorption of foreign cultures, Chinese traditional culture inheritance, and development. The only route to modern Chinese interior design is to creatively combine various elements in different cultures and form the interior design, which originate from but exceed tradition.

ACKNOWLEDGEMENTS

The corresponding author of this paper is Yifeng Liu. This paper is supported by Scientific Research Fund of Hunan Provincial Education Department of China (No. 14C0592) and Scientific Research Fund of Hunan Women's University of China (No. HNNY12YBKT004).

REFERENCES

- [1] Yang Chen: Literature and Art Forum Vol. 6 (2010), p. 61.
- [2] Li Tao, ZhouJing: 3rd International Conference on Green Building, Materials and Civil Engineering (GBMCE) (2013), p. 649.
- [3] Wuying Chen, Tianlu Fang: 2012 International Conference on Civil, Architectural and Hydraulic Engineering (ICCAHE) (2012), p. 276.
- [4] Huan Feng, Chang Xiao: 2012 International Conference of Green Building Materials and Energy-Saving Construction (GBMEC) (2012), p. 75.
- [5] Rongxin Tan: Literature and Art Studies Vol. 12 (2013), p. 72.

Adult picture book creation with mixed media—using a story of “Weirdness” as an example

Rui Lin Lin

Department of Commercial Design, Chienkuo Technology University, Changhua City, Taiwan

ABSTRACT: This study performed a creative design of an adult picture book based on a piece of city news as a graduation project of a design curriculum, through the cross-school team teaching method with two professional design teachers and team cooperation and learning of the research subjects, the students from the Department of Commercial Design of a Technology University. The story was adopted from a case of a girl named Bai who wanted to get married which once shocked the society in Taiwan. The nimble and mysterious characteristics of a cat were used with the slightly turbid blue tone to imply the female title role’s unsociable personality and miserable experiences. Then a paranormal event led to a series of stories which made the male title role suffer physically and mentally and struggle. The hand drawings were combined with the computer graphics skills to achieve aesthetics of the delicate images.

Keywords: mixed media; picture book creation; image processing

1 INTRODUCTION

In this study, before the picture book was created, current related data were collected, summarized, and analyzed. Finally, a piece of city news was chosen as the material for the plot. The news piece was about a case of a girl named Bai trying to get married in 1997 in Taiwan. The mysterious characteristic of a cat was used to show the female title role’s bad interpersonal relations due to gene mutation, which led to the miserable fate of being killed.

The male leading role, out of curiosity, participated in an occult game with a joking attitude. Unexpectedly, the game caused a series of ghost events. The melancholy blue tone was used to present the male leading role’s painful struggling and conflicts, physically and mentally, increasing the attraction of this picture book.

2 LITERATURE REVIEW

2.1 *Animal characteristics*

Family viverridae is a small or middle sized carnivore with a long and pointed head, a long body, and short legs. Usually there are stripes or spots on its body and scent gland near its anus. When facing enemies, it sprays fluid with a strong smell. It also leaves smells for the purpose of communication. Some animals’ scent glands are used as sources for perfumes or drug ingredients. Family viverridae is usually active at night. Its actions are secret and can hardly be observed [2].

Currently there exist 19 genera and 35 species of family viverridae, mainly in South West Europe, South Asia, East Indies, Africa, and Madagascar, with the dentition formula of 3/3, 1/1, 3–4/3–4, 1–2/1–2. They usually rest in forests and on grasslands. In daytime, they may hide in ground holes or bushes. They are nocturnal animals and eat small vertebrates, insects, fruits, and roots. Sometimes they also eat carrions. They act alone, with the average activity distance of 500 m per day and average activity range of 0.83 km² per month. Usually they have 2–5 newborns at one birth. They are weaned at 4–4.5 months. When reared in pens, their average lifespan is 10 years and 6 months [2].

2.2 *Types of drug abuse and crimes*

In late 60 s, under the influences of the social customs of madness and hippies, actions such as sniffing thinners or organic sorbents such as methylbenzene had become common. After sniffing, there will be illusions and senses of ease and happiness. Related games were then developed and became popular among teenagers.

There are various types of games, including (1) recreational games: they are short games, usually introduced by friends or senior schoolmates, such as smoking and drinking. The more they are banned, the more teenagers want to try them. They can be stopped through abstinence and environment adjustment; (2) delinquent juvenile games: some juveniles already have a lot of problems

before using drugs, such as making bad friends. These juveniles' behaviors may become more rampant after drug abuse. These juveniles run away from reality through a sense of intoxication caused by drugs. It is rather difficult to treat them; and (3) dependent games: the dependency of human bodies on organic solvents has not yet proved currently. Even though stopping using these drugs does not lead to addiction, mental dependency may still cause deep sinking and eventually death. It is difficult to treat these users [4].

2.3 *Media and colors*

Creators must be quite familiar with and understand tools and media for painting in order to achieve creative aesthetics using the best way of presenting situations through images. Generally, for hand drawings, depiction lines are drawn with pencils and color pencils, which can also be used for shading and coloring. There are pencil leads of different hardness corresponding to different depths and luster. Color pencils can be categorized into water color pencils and dry ones. They can be used to color with water [9][10].

Markers are water or oil soluble. Basically, they are ink-based painting tools, between dry media and water media. There are thick and thin markers, transparent and opaque markers. They don't penetrate surfaces and can be applied flexibly. Concentrations of ink can be adjusted by adding water, for the purpose of creating gradient effects [3][8].

3 RESEARCH METHODS

3.1 *Creative thinking*

Thinking is also the process of reorganizing information from environments or concepts stored in knowledge systems. While thinking, the most commonly used symbols are mental images and languages. Thinking includes many aspects. Symbols used in thinking also have special meanings. The nature of thinking is autistic. A type of thinking is called directed thinking. It is about resolving some issues or creating something new. In other words, it is to resolve a problem using information from environments and concepts of thinking [6].

Mental images are another type of symbols of thinking. When people use them to think, they are doing visual thinking. These images are abstract objects related to substances in past experiences instead of substances themselves. For many people, thinking possesses the nature of language and literature activities and is a form of an internal language [7].

3.2 *Creative thinking methods*

Creativity is often defined as the ability to create novel things, ideals, or results. However, showing novelty or uniqueness may not be a form of creativity. Creativity must be measured based on some proper standards. Creativity is related to personality, education, and culture [1].

To understand the process of creativity, it is necessary to know the contradictions such as that this process is unique but also general, it is about using existing knowledge but also about resisting influences of existing knowledge, it is to put in a lot of efforts to come up with a solution to a problem but it can also obstruct generation of ideas, and reducing attention and motivation is helpful in generating creativity [5].

4 DESIGN RESULTS

4.1 *Image creation*

A nimble cat which loved to stay in the dark and could go anywhere it wanted to go was used to symbolize the female title role who was lonely due to her shy personality and gene mutation and was kidnapped on her way home after school and was unfortunately killed. The hues used for the images were turbid blue, giving a creeping feeling. The title of the book was "The Spirit Behind", indicating a sprit was hiding behind (Fig. 1).

4.2 *Content of the picture book*

July 16th: The summer vacation began. Gao Jun suggested to play the game of dish fairy in the deserted blockhouse behind the school to do something exciting. These people were so boring. But I was one of the boring people. The vines hanging on inside the blockhouse were horrible. It was dark inside. I didn't know where they found those tools, but when everything was in position, the set did look like something. After reading the spell Gao Jun found through Google search, the disk actually started to move! It had to be Gao Jun trying to deceive us! (pp. 1~2)

July 27th: After the game of dish fairy we played last time, I had been having the same dream over and over. In that dream, a girl kept on talking to me. But I couldn't see her face. Based on the rear view, she was beautiful. Every time when I wanted to grab her from behind, I woke up. Would it be something I foresaw? Would love be coming knocking at my door? Haha! August 2th: I was sweating out of fear, for I finally saw her face! I couldn't get those horrible two-colored eyes out of my mind. They were so weird and ferocious. August 7th: The dream seemed to stop. When staying in the

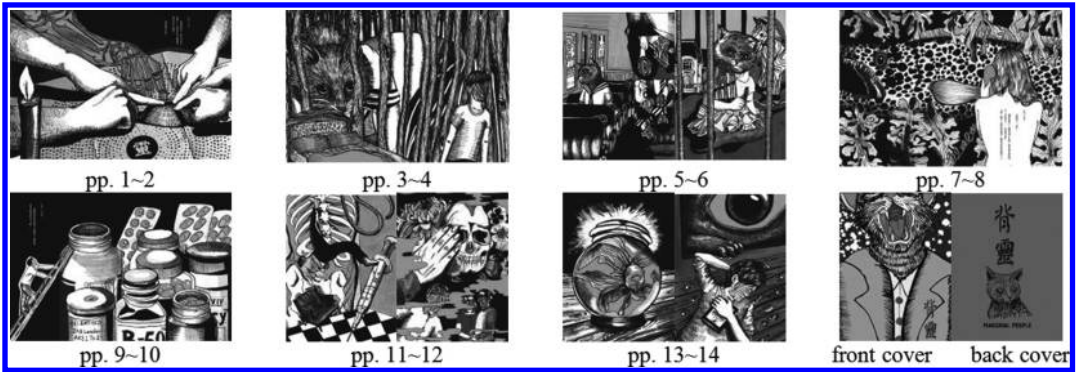


Figure 1. Images from the picture book.

room, I always felt that someone was watching me. I told my brothers and they thought I was crazy. (pp. 3~4)

August 11th: Today, a couple who seemed quite rich came to my doorstep. They cried and said their baby Xiao Xi, whom had been raised by them since as a child was killed. Her soul was wondering around out there and drawn by a game of dish fairy once. She got along with me well in the dreams and she liked me. She appeared in their dreamed and expressed her wish for marrying me. They even brought a huge cash gift. Couldn't this be the latest fraud? I don't want to say no more about what happened today. It was so ridiculous! August 14th: The couple showed up again. I had no idea how they got my address. That was so weird. They said that, due to gene mutation, the eyes of Xiao Xi had two colors. She had been lonely in school because of her strange eyes and quiet personality. One day on her way home, she was kidnapped and killed. The killer was a criminal with a previous conviction of psychological issues. He asked for ransom, a lot of money. However, before he got the money, he killed her and cut her body into pieces due to his unstable mental state. This couple wanted me to think about this. I felt sorry for them when I thought about what they had said. But it is just too ridiculous for me to marry a ghost! If they keep on bothering me like this, I will call the police. (pp. 5~6)

August 19th: I had dreamed about Xiao Xi for days. She was deserted in the ocean and kept on crying. It was so horrible. I was sweating again out of fear. It gave me the creeps when I thought about the dreams. As long as I fell into asleep, I dreamed about her. I was going out of my mind. (pp. 7~8) August 25th: I started to look for drugs which could make me excited so that I wouldn't want to sleep. It would be fine if I didn't sleep, right? (pp. 9~10)

September 9th: A few days ago, Gao Jun invited me to go to a bar to relax for a little while. It had

been a long time since the last time I did that. He also gave me some drugs. He called them "health supplements" from a friend. After injecting this kind of drugs, I felt like I was flying. I loved that feeling. All the annoying things seemed to go away. I was in love with that feeling. I am running out of money this month. I need to save some for the drugs. September 15th: My parents came to see me and found that I was using drugs. They were so mad! Gao Jun was arrested for on a charge of selling drugs. My parents forced me to break drug dependence. I was lucky that I was completely addicted. I don't know what I was thinking back then. It is not too late to stop now. (pp. 11~12)

September 21th: The dream was gone. Now I still need periodical treatment for I still have some addiction to drugs. My friend gave me a goldfish with a pair of two-colored eyes as a gift. I put it in my room as a symbol of a new beginning. Watching it swimming in the water makes me feel calm. However, its eyes and the emotions showing in its eyes are so familiar. I can't remember where I saw eyes like these. Forget it! It is just me being suspicious! (pp. 13~14)

5 CONCLUSIONS

The discussions regarding the picture book of this study and the proposed suggestions are summarized below.

1. Attractive plot of the picture book: The material and the plot of the picture book were attractive to readers, offering them a space for imagination.
2. Visualization of the plot: The way the images were created made the story more authentic. The internal feelings and mental side of the characters which were difficult to express were successfully presented to readers.

3. Combination of hand drawings and computer graphics skills: The advantages of hand drawing and computer graphing were well integrated and applied to the image designs and creative ideas of the picture book, making the book more attractive.
4. Technology innovation and design aesthetics: The well utilization of mixed media made the picture book creative work more complete. The image processing of the digital content also helped to present technology innovation and design aesthetics.

REFERENCES

- [1] Gao, B.Q. Teaching Theory: Ideals and Practices, Wunan Publishing Co., Ltd., Taipei (2007).
- [2] Editorial Committee, Encyclopedia of Vertebrates, National Institute for Compilation and Translation, Taipei (2004).
- [3] Lin, J.C. Teaching Theory, Wunan Publishing Co., Ltd., Taipei (2006).
- [4] Chang, J. Devils' Rules: From Campus Bullying to Killing Families for Plunder, Nuggets Culture, Taipei (2011).
- [5] O'Quin, K., Besemer, S.P. Creative Products, Encyclopedia of Creativity (Second Edition), (2011), pp. 273–281.
- [6] Chen, L.A. Theories and Practices of Creative Thinking Teaching, Psychological Publishing Co., Ltd., Taipei (2008).
- [7] Zheng, L.Y. Cognitive Psychology, Wunan Publishing Co., Ltd., Taipei (2006).
- [8] Xing, M.Y. Creation Skills with Mixed Media, Cube Culture Inc., Taipei (2012).
- [9] Xu, X.J. Computer Graphics Skills for Photoshop: Practices of Line Sketching and Coloring, Grand Tech information Co., Ltd., Taipei (2011).
- [10] Xu, Y.Y. Color Pencils, San Min Book Inc., Taipei (2003).

Adult picture book creation with mixed media—using a story of the case of the disappearing bodies as an example

Rui Lin Lin

Department of Commercial Design, Chienkuo Technology University, Changhua City, Taiwan

ABSTRACT: This study adopted the cross-school team teaching method with two professional design teachers to guide the students from the Department of Commercial Design of a Technology University to cooperate as a team in their graduate design project. The subject chosen by the team was an adult picture book with the story inspired by the murder of three young men from the city news. The tarsier was used as a metaphor of a talented young man who killed his friends and classmates of 10 years because of his extreme personality and deviant behaviors. Although eventually the young man could not escape the net of justice, the pain of the four families would never be fully healed. During the process of the creation, the teachers and the students had made discussions and modifications constantly to make the images more delicate and the story more complete.

Keywords: mixed media; picture book creation; image processing

1 INTRODUCTION

This study collected, organized, summarized, and analyzed the current related picture book creation materials. The plot of the picture book was based on city news story which one shocked Taiwan. It was adapted from the murder of three young men in 1990. The main character was designed as a tarsier, with physical and psychological characteristics implying the slyness, shrewdness, and unstable emotions of the criminal who set a trap to kill his good friends and classmates.

The story was lamentable. Although eventually the criminal was caught and trialed, still four people were dead, and four families were broken. How could the victims' and the killer's families face the society and people's judgments?

2 LITERATURE REVIEW

2.1 *Animal characteristics*

Currently, there are still one genus and five species of family *tarsiidae* existing. They live mainly in Sulawesi, Borneo, Philippines, and some nearby islands. Their main characters are small bodies and large eyes. The diameter of their eyes is about 1.6 cm. Their heads are round and they can turn their heads almost 360 degrees. Their noses are short with some hair by the edges but hairless in the middle, necks are short, ears are long and hairless, tails are thin, long, and almost hairless with

only a little hair on the ends, forelimbs are long, hind legs are long, and fingers and toes are long and with pads at the ends for easy grabbing and holding. Only the nails of the second and third toes of their hind legs are unguis for carding hair. All the other nails are flat. Their teeth formula is $2/1, 1/1, 3/3, 3/3$ [3].

Lengths of tarsiers including head and body are about 8.5–16 cm, lengths of their tails are about 13.5–27.5 cm, and they weight about 80–165 g. Colors of their backs are from gray brown to dark brown, while their abdomens are slate. They live on the islands of the Philippines. According to their ecological habits, they mainly stay in secondary forests and shrubberies. But they many also show up in primeval forests and mangrove forests. Their activities are mainly on trees. They are nimble and can jump from one tree to another freely. They can jump 5–6 m long. The average jumping distance is 1.4 m. Once in a while, they go down on the ground where they also move by jumping. On the ground, they can jump about 1.2–1.7 m long and 0.6 m high. They mainly eat insects as food. Sometimes, they also eat crustaceans and lizards. They do activities alone or in pairs. They are territorial animals which mark their territories with urine and secretions. Every year, there are two reproductive peaks. Their estrus cycle is about 25–28 days, and gestation is about 136 days. Usually one offspring is produced at one birth. Weight of offspring is 20–31 g. At birth, their eyes are open and they already have hair. They can crawl right after being born, can

jump after a month, and can catch insects for food when they are 42 days old. Soon they are weaned and their weights reach adults' weights. If reared in pens, their life-span is 13 years and 5 months. They are rare species [4].

3 CRIMINAL MINDS AND BEHAVIORS

Committing a crime is a wrong behavior. There is a complex psychological process behind it. Every criminal has a specific course of life and unique psychological qualities. Normal people becoming criminals and the formation of criminal personalities of criminals are associated with specific environments, especially childhood family environments.

In reality, many criminals are similar to those in films in temperament, thoughts, and concepts. Through analyses and comparisons, it can be found that one of their common characteristics is evil in their minds. In order to satisfy their various psychological needs, they wouldn't hesitate to violate their consciences. And this is the source of evil [2].

4 MEDIA AND COLORS

Before creation, it is important to first understand painting materials, clearly distinguish essential characteristics of peripheral equipments, and get familiar with basic skills of pencil drawing, in order to apply the most suitable methods during creation. Generally, pencils and color pencils can be used in learning to depict outlines, create shadow, and color. When necessary, some color mixing skills can be applied as well. There are pencil leads of different hardness corresponding to different depths and luster. Color pencils can be categorized into water color pencils and dry ones. They can be used to color with water [7][8].

Markers are water or oil soluble. Basically, they are ink-based painting tools, between dry media and water media. There are thick and thin markers, transparent and opaque markers. They don't penetrate surfaces and can be applied flexibly. Concentrations of ink can be adjusted by adding water, for the purpose of creating gradient effects [5].

5 RESEARCH METHODS

5.1 *The content of instructional design*

An experienced instructional designer pays special attention to precision and professionalism of curriculums. Curriculum design and instructional design have something in common. Curriculum

design covers objectives, purposes, goals, teaching materials, learning experiences, and evaluation methods. A good instructional designer must consider all these factors and their interactions.

When teachers perform instructional design, it is important to consider learners' characteristics, teaching goals, teaching methods and strategies, teaching and evaluation, in order to create systematic structures for their teaching plans. The levels of instructional design can be combined with teaching forms [6].

6 REFLECTIVE TEACHING

Teachers' reflective teaching is an important issue in educational innovation and has a great influence on improvements in teaching quality. Reflective thinking originates from the needs to resolve doubts and look for any possible solutions. It is a type of willingness of individuals to perform frequent self-evaluation and development.

Reflective thinking is a part of the process of constructing cognition. It integrates characteristics of appraisers and critics, showing individual and unique capability of appreciation. It is like with art works which are demonstrated and criticized. Teachers' reflective thinking is about appreciation and evaluation, which are closely related, of their teaching behaviors [1].

7 DESIGN RESULTS

7.1 *Image creation*

This study performed the art creation of a picture book with mixed media including pencils, color pencils, markers, and ink. The story was adopted from the murder of three young men which once shocked Taiwan in 1990. The leading character was designed as a tarsier, a primate, symbolizing a smart but mysterious young man who killed three good friends and classmates of 10 years because of his weird personality (Fig. 1).

8 CONTENT OF THE PICTURE BOOK

February 18th: It was the day of the field trip. I'd spent the whole day with Kai Xiang, Yan Ru, and Yun Ting, my best friends. It was cold. The sky was gray. But I was very happy. (pp. 1~2)

December 24th: Today I got a full score on the pop quiz in the class today. It was a piece of cake to me. Nothing can defeat me. (pp. 3~6)

May 12th: I went to Taipei for work and had been all by myself there for a long time. I had been excited all day because they told me they were

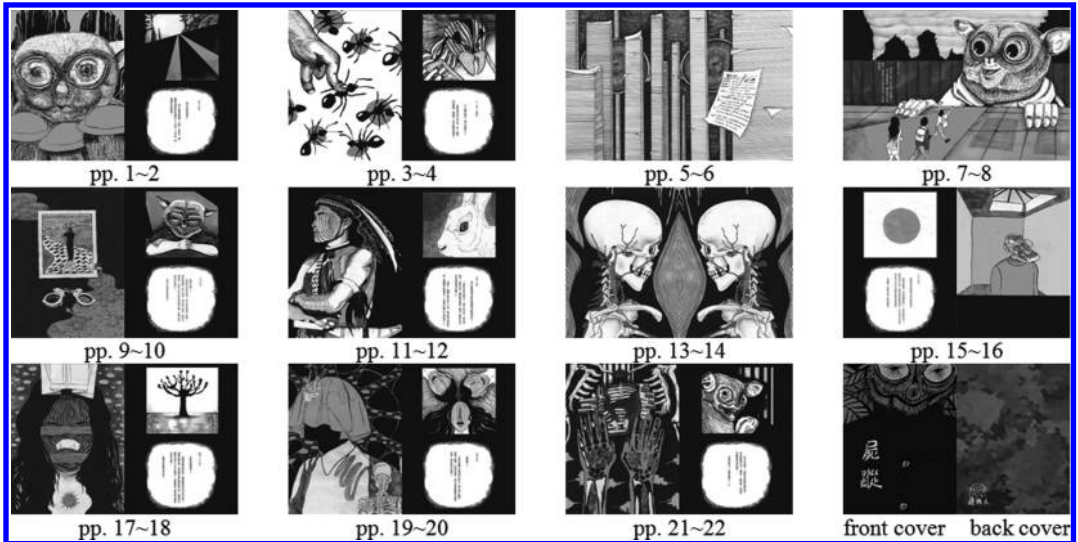


Figure 1. Images from the picture book.

coming to visit me in Taipei. I planned a perfect trip and expected their arrival. (pp. 7~8)

June 5th: They disappeared. I was questioned in the police station. The police said I killed them. They asked me where they were. (pp. 9~10)

January 18th: The police received a report with information possibly related to Kai Xiang and Yan Ru. "When I was in the mountains, I saw a white rabbit, a snow white rabbit. Its glittering eyes caught my attention, so I ran toward it." One aborigine told the police, "it stopped by a rotted board. It was like the rabbit was sent to guide me there. I moved the board and I was shocked. There were two dead bodies which had been sleeping there for quite some time." (pp. 11~14)

January 19th: The families of Kai Xiang and Yan Ru went to the police station to identify the bodies. Kai Xiang's mother started to cry right after seeing the body. That was her son. Although the face was no longer recognizable, she recognized the shoes. The limited edition shoes were purchased in Japan and brought back as the birthday gift for her son. How ironic! The shoes became the key to solve the case. (pp. 15~16)

April 28th: Yun Ting was found as well. I thought her body was well hidden. I brought her to a place by the Dansue River for the nightscape. I let her sleep there. I sealed her eyes, mouth, and nose with tapes. And I buried her clothes somewhere about 10 m away. This way, she wouldn't call for help even after she died. She was supposed to belong to me forever. (pp. 17~18)

May 6th: I was arrested. I killed them because they didn't want to follow my plan for the trip.

I killed them, but I didn't commit any crime. I simply wanted to own them. I really didn't commit any crime. The police told me that the court in the human world could not execute me, but the one in the nether world could. I shivered and turned around, seeing them right behind me. I told the police, "I am ready!" (pp. 19~22).

9 CONCLUSIONS

The discussions regarding the picture book of this study and the proposed suggestions are summarized below.

1. Plot of the adapted story: The story was inspired by a horrible case from the city news. It was an attractive story, making readers want to know what happened. By the end of the story, some advices regarding crime prevention were proposed, so that readers can learn about how to prevent criminal minds. There were educational messages delivered through entertainment.
2. Creating atmosphere of the story: The smart leading character's ill behavior due to his twisted personality finally led to an ending of harming others and himself. It was a pity. The atmosphere of the images of this picture book changed with the scenes. It was very creative and could completely show the value of the story.
3. Combination of hand drawing and computer graphics: Hand drawing created warm feelings for the images, while computer graphics added unique feelings to the images. With both skills properly combined, the picture book creation

was even more delicate and exquisite, and more attractive to readers.

4. Aesthetics with technology innovation: With the down-to-earth feeling of the paper quality, the integration computer graphics, the color combinations, the image processing, the creation of atmosphere, and the composition to deliver deep messages through simple words, formed the aesthetics of technology innovation for this picture book.

REFERENCES

- [1] Gao, B.Q. *Teaching Theory: Ideals and Practices*, Wunan Publishing Co., Ltd., Taipei (2007).
- [2] Tibor, B., Charlotte, G., Jan, T. On the Relation between Cognitive and Biological Modelling of Criminal Behaviour, *Computers in Human Behavior*, vol. 27, Issue 5, September (2011), pp. 1593–1611.
- [3] Editorial Committee, *Encyclopedia of Vertebrates*, National Institute for Compilation and Translation, Taipei (2004).
- [4] Rahman, J.M., Cuddy, S.M., Watson, F.G.R. Tarsier and ICMS: two approaches to framework development, *Mathematics and Computers in Simulation*, vol. 64, Issues 3–4, 11, February (2004), pp. 339–350.
- [5] Xing, M.Y. *Creation Skills with Mixed Media*, Cube Culture Inc., Taipei (2012).
- [6] Zhang, Q.B. *Teaching Theories and Practices*, Wu Nan Book Inc., Taipei (2009).
- [7] Jin, R.L. *Color Design*, Top Team, Taipei (2011).
- [8] Xu, Y.Y. *Color Pencils*, San Min Book Inc., Taipei (2003).

Adult picture book creation with mixed media—using a story of a crime of passion as an example

Rui Lin Lin

Department of Commercial Design, Chienkuo Technology University, Changhua City, Taiwan

ABSTRACT: This study adopted the cross-school team teaching method with two professional design teachers, one from a school in central Taiwan and the other in southern Taiwan, to guide the students from the Department of Commercial Design of a Technology University in the team graduation design. The topic selected by the students' team was an adult picture book. The plot was inspired by a true story from city news about a crime of passion with the victim being eaten. The expression with a character of a crane's head and a human's body was adopted to present the horrible event of a man killing his lover out of hatred from love, eating her dead body, and eventually getting caught and punished by the law. During the process of creation, the teachers and the students had continuously discussed and modified the work, to make the images more delicate and the plot smoother. The students first create the images through hand-drawing. Then the images were colored with mixed media. Eventually, computer graphics software was used on image modification, special effects, retouch, and layout arrangement, to improve the quality of the picture book and increase market sales.

Keywords: mixed media; picture book creation; image processing

1 INTRODUCTION

Where does a creative idea for a picture book come from? A creator can hardly create something new continuously if he sees inspiration as something totally unexpected and waits for inspiration to come to his mind. In fact, creativity and aesthetics share the same principles. Although they are both perceptual, there are still some rules to follow. Adult picture books are different from children's books in the aspect of creation. There are fewer limitations. Issues can be related to races and various cultures.

Adult picture books can create values of combining literature and art. And their features of novelty and recreation can stimulate the publication market to go for something new. Readers' tastes are also influenced. One special example is Jimmy, who has been leading the trend of picture books and made picture books no longer for children only. Especially, the affection-oriented trend of design established by picture books has directly facilitated the aesthetics in daily lives. Highly praised adult picture books have been gradually published and sold in more diversified forms, creating new business opportunities for designing and verifying the features of the times under the influences of the post-modern culture [2].

2 LITERATURE REVIEW

2.1 *Animal characteristics*

Red-crowned cranes (*crus japonensis*) are usually 140 cm long and very tall, the tallest among all types of cranes. Their beaks, feet, and the areas between heads and throats are black. Behind their heads there is a red area. And the areas behind their eyes are white, while feathers on their tails are black. All the rest parts are white. They can be found in north-east Asia, east Siberia, Mongolia, and north Japan. And they spend winters in Korea, north-east China, and Japan.

Red-crowned cranes usually roost in wide mountain valleys with wetlands, grass-covered lands, or grassy marshes. Because of their tall heights, they can find and avoid their natural enemies. They eat small rats, frogs, large insects, seeds of plants, sprouts, and leaves. When flying, they flap their wings powerfully, with their necks and feet straightened. And they glide. When they fly in large numbers, they fly in a V formation or in an oblique line. When migrating, they follow fixed routes [7].

3 CRIMINAL MINDS AND BEHAVIORS

Committing a crime is a wrong behavior. There is a complex psychological process behind it. Every

criminal has a specific life track and some unique mental qualities. A crime is like a sharp knife, cutting the society to create a cross section, revealing the truest and cruelest side of the society.

How to face crimes and prevent crimes are the severe tests judicial authorities have to take. And the general public shall all participate in resolving this issue. Some crimes are often closely related to extreme cognitive styles of people involved which make them feel the crimes are something they have to do. However, results are in fact bad for both themselves and their victims. One false step can bring everlasting grief [1].

4 MEDIA AND COLORS

A pencil drawing is made of drawing elements including lines, strokes, and shading. With good lines and proper strokes, outlines of an object can be depicted precisely with quality and 3D visual effect. Lines and strokes can present different types of 3D spaces. And with various shading, quality, sense of quantity, sense of space, and changes in lighting can be expressed more objectively and authentically. Color pencil look like pencils in appearance. However, color pencils are with rich colors and can be used to draw lines with various colors.

There are two types of color pencils, water-based and oil-based. When using water-based color pencils, water can be added as a solvent to create works with more changes. Markers can create sense of transparency. When coloring the same area over and over, the color in that area becomes darker. New colors can be created by mixing different colors. With these features, 3D visual effects, lighting, and shading of objects can be enhanced. Colors of color ink are very bright and transparent, bringing a sense of crystal clearness and moistness. When different colors are overlapped, a new color is created. This feature can be used in drawing. It is especially useful to show dazzling colors and aesthetics of blended water colors [5].

5 RESEARCH METHODS

5.1 *Creative thinking teaching*

This study adopted the creative thinking teaching method to develop the students' ability of creative thinking. Therefore, during the teachers' teaching of the adult picture book, the students were treated as the subjects. A supportive environment was provided, along with some creative thinking strategies, to inspire the students' interest for learning. The students were allowed to express

their opinions. And different opinions could be accepted. Through exchanging ideas and thoughts, creative thinking could be inspired [3].

6 PROBLEM BASED TEACHING

This study adopted the problem-based teaching method to inspire the students to apply high-level thinking to problem solving. The purpose was to transform various important concepts and principles into all kinds of questions. By asking questions, the teachers guided the students during the learning related to the creation of the picture book. The problem-based teaching method is a teaching method with a teacher guiding his students through systematic steps to find a problem, think about the problem, and resolve the problem step by step, in order to increase the students' knowledge, enrich their life experiences, and develop their abilities to think and to resolve problems [4].

7 ADAPTIVE TEACHING

This study applied the adaptive teaching method based on the individual differences of the students, in order to inspire their active learning spirit, so that they could truly understand what they'd learned, be willing to act, and therefore their potential could be developed. This method is an individualized teaching method of encouraging students to perform self-learning under the guidance of their teachers. When applying this method, teachers can adopt proper skills and procedures to reduce their students' loading or mistakes in information processing, to maintain the students' learning motivation and to increase their willingness to learn, as well as to teach them to resolve learning difficulties with resources around them, breaking bottlenecks [6].

8 DESIGN RESULTS

8.1 *Image creation*

In order to create a special feeling for readers, all the images of this picture book were drawn with delicate lines, with the visual image of a crane's head on a human body. Parts of the images were colored blood red, implying that the love changed and eventually led to the crime of passion and even the horrible man-eating event. The color red was used to present the story with color aberration. Finally the images went through digital processing using the computer graphics software and output with partial glazing. Because the horrible story was

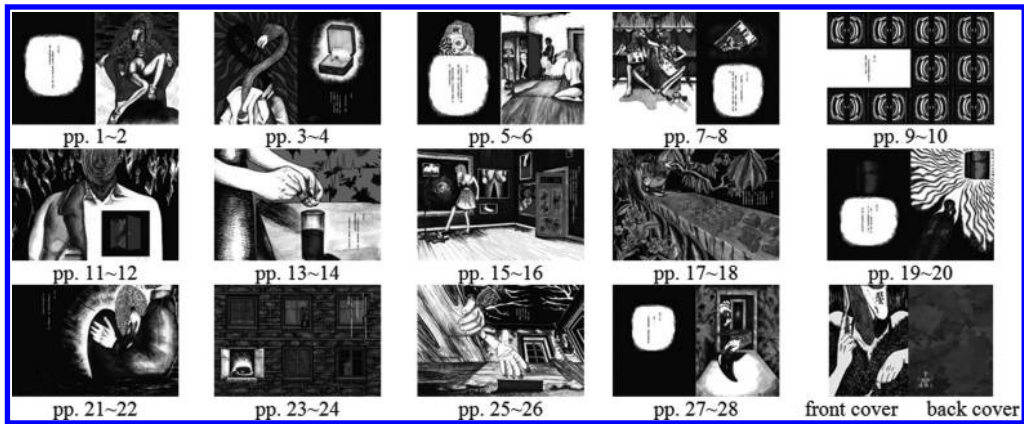


Figure 1. Images from the picture book.

about the leading lady who could not stand the pain of the break-up killing her boyfriend and eating his body, the picture book was named “Satiation”, referring to a physical and mental state of never being satiate even when full. After coloring, digital processing, and layout, the picture book was completed, as shown below (Fig. 1).

9 CONTENT OF THE PICTURE BOOK

February 14th: I am a lucky woman. I have everything, a beautiful look, wisdom, money, and a boyfriend who loves me ... (pp. 1~2). March 4th: We promised each other to stay in love forever. Today, I found a small box in Jing An’s drawer, there was a very beautiful diamond ring inside. Finally, he is going to realize his promise! (pp. 3~4). March 20th: Recently, Jing An has treated me differently. He has been cold ... I haven’t heard the words “I love you” from him for a long time. I think he is avoiding me. But I have given everything, my body, my money, and my heart, to you ... (pp. 5~6). March 27th: Have I been sleeping for 3 days? It feels like my head is going to explode. Did we break up? Is it a dream? It has to be a dream ... He’s supposed to be in love with me forever. I am so perfect. Everybody loves me! It is not possible ... (pp. 7~8). April 2th: Is Jing An’s heart different from mine? I love him, and he loves me, right? (pp. 9~12). April 4th: Today, Jing An came to my place. He said he was thirsty. I got him a cup of his favorite juice. Jing An slept next to me. He slept so well! He hadn’t been like that for a long time ... (pp. 13~14). April 5th: There was blood everywhere. I’d spent a lot of efforts to clean up the mess. Jing An has mysophobia. Jing An’s heart is the same as mine. I am sorry.

I misunderstood you. You must have been seduced by that bad woman, you must have been ... you must ... I know you still love me ... (pp. 15~16). April 6th: I made some soup in the morning, with the hands which had touched me gently once. I named the soup “Holding Hands”. It’s kind of funny. Jing An’s chest is delicious. It’s soft and flexible. I used to sleep on his cheek every night (pp. 17~18). April 8th: Jing An ... Is it cold in the fridge? Hold on, just a moment. We will be together forever. I am sorry, you know I have a small appetite (pp. 19~20). April 18th: On that day, I finally found her, found the woman who seduced Jing An (pp. 21~22). April 20th: Jing An and I are together in one body now. We can be together forever. I feel so lucky, and so does Jing An (pp. 23~24). April 29th: I was eating something with red liquid. The police broke into my place after receiving a report. I looked at them dully with a spoon in my hand. Wait! I just need to finish these. The police found my diary hidden in the crack of the floor, with the details of the crime inside (pp. 23~24).

10 CONCLUSIONS

The animal, crane, mating for life, was used to imply that, in the human world, marriage and relationships should be respected. However, the man ceased to be faithful, resulting in the extreme behavior of the woman. Eventually, curses come home to root. People should learn from this story. Creation of the atmosphere of the story: The plot was inspired by a true story from city news about a crime of passion with the victim being eaten. To show the emotions between the lovers, in the beginning parts of the image were colored carmine, the color of sweetness. Then when the affair

led to the crime of passion, the color used was blood red. The color was even a little bit turbid. And the atmosphere of the story about the crime was created.

Aesthetics created with technology innovation: Mixed media were used for the hand drawings. And then image processing was performed with the drawings using the computer graphics software. The true story from city news about a crime of passion with the victim being eaten was perfectly presented. And the book also included some content of the criminal mind and behavioral analyses to help readers understand and alert them. It is hoped that the aesthetics of this picture book created with technology innovation can increase readers' motivation to buy this book.

REFERENCES

- [1] Tibor, B., Charlotte, G., Jan, T. On the Relation between Cognitive and Biological Modelling of Criminal Behaviour, *Computers in Human Behavior*, vol. 27, Issue 5, September (2011), pp. 1593–1611.
- [2] Chen, C.P. The Research of Picture Books at Present Taiwan—The literature picture books published from 1998 to 2006 in Taiwan, Master Dissertation, Department of Industrial Design, Huafan University (2007).
- [3] Chiu, F.C. Fit between Future Thinking and Future Orientation on Creative Imagination, *Thinking Skills and Creativity*, vol. 7, Issue 3, December (2012), pp. 234–244.
- [4] Gallardo, J.R.R., Santiago, C., Juan, J.G.A., Arturo, V. Assessing Student Workload in Problem Based Learning: Relationships among teaching method, student workload and achievement. A case study in Natural Sciences, *Teaching and Teacher Education*, vol. 27, Issue 3, April (2011), pp. 619–627.
- [5] Xing, M.Y. *Creation Skills with Mixed Media*, Cube Culture Inc., Taipei (2012).
- [6] Elizabeth, S. Opportunities to Develop Adaptive Teaching Expertise during Supervisory Conferences, *Teaching and Teacher Education*, vol. 28, Issue 5, July (2012), pp. 768–779.
- [7] Wang, Z.Q., Fu, J.C., Hao, C., Chen, Z. The Spatial-Temporal Pattern Changes of the Red Crowned Crane (*Grus Japonensis*) Population in Zhalong NNR and the Related Driving Forces, *Acta Ecologica Sinica*, vol. 29, Issue 6, November (2009), pp. 351–356.

Adult picture book creation with mixed media—using a story of “Forfeiting Lives” as an example

Rui Lin Lin

Department of Commercial Design, Chienkuo Technology University, Changhua City, Taiwan

ABSTRACT: The research subjects of this study were the students from the Department of Commercial Design of a Technology University teamed up for cooperative learning. Two professional design teachers guided the students’ graduation design work through the cross-school team teaching method. The team of students created an adult picture book based on a piece of city news with creative design. The plot was adapted from a true story of a poison gas killer which once shocked Taiwan. An aardwolf with cruel and savage nature was used as a metaphor. The color of turbid green implied the deviant behavior of the criminal who originally had an innocent personality but eventually committed a horrible serial-killing crime. Although the criminal eventually could not escape from the punishment of the law, the tragedy already happened. The plot was very touching and provided food for thought.

Keywords: mixed media; picture book creation; image processing

1 INTRODUCTION

It requires a good and creative idea to create a picture book which can satisfy readers. Content with excellent pictures and literary compositions can help with sales in the market. Especially, when picture books are no longer for children, creators can choose adult themes to increase topicalities and ductibilities of stories. Adult picture books can show richer contents and deliver deeper emotions, psychological states, and behaviors of characters, which make these books more complete. Thus, good and creative materials and ideas become very important.

2 LITERATURE REVIEW

2.1 *Animal characteristics*

Before the creative design was performed, this study first collected, organized, summarized, and analyzed information and materials regarding themes for picture books and selected a piece of city news as the core of the story. The story was based on the 1976 case in Taiwan of a poison gas killer. And the criminal was designed with the look of an aardwolf, which is cruel and savage in nature and is an opportunist in the natural world. It often waits for an opportunity to pick up prey or carrion left by lions to save its own strength. Its voice is changeable, sometimes like human laughter. It can communicate using various voices. Its weird

voice creates an image of nervous and crazy quality. In the picture book, turbid green was applied to present the criminal’s psychological states and behaviors [3].

3 CRIMINAL MINDS AND BEHAVIORS

Both criminals and regular people are research subjects of criminal psychology. Crimes can be considered as embodied behaviors of humans’ hidden dark sides. Crimes are caused by personality, various problems or factors in the environment, and their interactions. Committing a crime is a wrong behavior. There is a complex psychological process behind it. Every criminal has a specific course of life and unique psychological qualities [5].

4 MEDIA AND COLORS

Before starting, creators should get familiar with painting tools and materials so that they can choose the most suitable ways for hand drawings. Generally, pencils and color pencils can be used to depict lines, create shadows, and color for drawings. If necessary, they can be both used for the same drawing. There are pencil leads of different hardness corresponding to different depths and luster. Color pencils can be categorized into water color pencils and dry ones. They can be used to color with water [9].

Markers are water or oil soluble. Basically, they are ink-based painting tools, between dry media and water media. There are thick and thin markers, transparent and opaque markers. They don't penetrate surfaces and can be applied flexibly. Concentrations of ink can be adjusted by adding water, for the purpose of creating gradient effects [7].

5 RESEARCH METHODS

5.1 *Creative thinking*

When humans think, they can create mind images based on their will. However, degrees differ from one person to another. There are some rules or restrictions along with problems around us. Yet, they also provide directions for thinking. How to find a problem and how to see a problem are more important than how to solve a problem. Finding problems is helpful for not only scientific creative thinking but also thinking in arts and daily life. Creative thinking is unique and novel. It has to be different from traditional and habitual thinking [4][6].

6 CREATIVE THINKING TEACHING

Creative thinking teaching is a flexible teaching method of thinking and problem solving with timely encouragement from teachers. It can inspire students' motivation of creation, encourage their performances in creation, and facilitate development of their creative talents. In the process of teaching, teachers should follow the principles of cultivating creativity to arrange reasonable and efficient teaching scenarios with proper attitudes. Through diversified and vigorous course contents, teaching activities, and learning environments, students can be stimulated to think while learning. This teaching method can help students to develop the creative thinking ability of making something out of nothing and making something new out of something [1][2].

7 PROBLEM BASED TEACHING

Problem based teaching is to inspire students to apply high-level thinking to solve problems, with the purpose of transforming various important concepts, theories, and principles into different types of problems and guiding students through learning activities using the method of asking questions. Teachers' job in problem based teaching is to come up with questions to encourage exploration and provide students structures for learning,

in order to facilitate their interest in learning and discovery and growth in knowledge [8].

8 DESIGN RESULTS

8.1 *Image creation*

This study used an aardwolf with cruel and savage nature to imply a criminal who was abused in his childhood, developed some very wrong concepts and ill behaviors, eventually killed some people in a very cruel way, and made money out of his murders. The images were in turbid green with some changes in color tones to present various mental states of the criminal in different situations. The book was named "Forfeiting Lives", meaning the criminal had killed a lot of people cruelly, forfeiting their lives (Fig. 1).

9 CONTENT OF THE PICTURE BOOK

June 23th: The wooden wall is already rotten. There is a strong musty smell. My mother holds me tightly, hiding her head behind me so she doesn't have to face anyone. The photo of the family was thrown away on the ground, as dirty as stinking shoes. I love my mother, but I have two mothers (pp. 1-2). July 8th: "Go to hell, you filthy bastard." "I will teach you a lesson, son of the bitch." "You discuss me." "Stop. Shut up. Shut up now." All the curses go through my brain like thin needles. I wish you all disappear (pp. 3-4). September 20th: This is the first woman in my life. Her hair is medium, and she is down-to-earth. There is often a gentle smile on her face. It's unavoidable for a couple to fight. It's unavoidable to hit you. It's unavoidable to kill you. I pat you on the head. There is blood everywhere on the ground. My hands, my eyes, and the moon are ensanguined. You look the most beautiful when you are asleep (pp. 5-10). September 24th: I need a new companion. I leap with joy on my way to the heaven on earth. At night, the neon lights are brighter than the clear sky. The lady's beautiful dance steps dazzle my eyes. Then she walks toward me. Her name is Xiao Ru. I take her to the corner. The fragrance from her hair, her red lips, her waist-length hair, and her attractive body ... she's the one. I want her to be my woman (pp. 11-14). December 18th: Xiao Ru does not belong to me only. I return home early because my business trip finished earlier than expected. When I open the door, I smell betrayal. That woman and another guy lie on my bed. That is my bed. That's too much. I cut off the power and walk toward them, who are still sleeping. I direct the electricity to go through their whole bodies can feel the

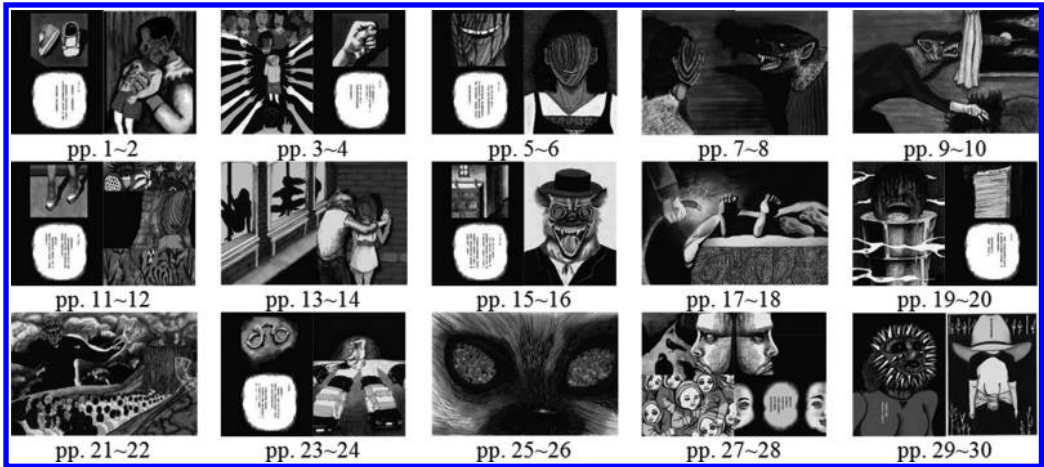


Figure 1. Images from the picture book.

“electric shock” once again. The burning smell irritates my nose. The sound of electricity comforts my emotions. A smile raises the corner of my shaking mouth (pp. 15–18). February 10th: With a series of made-up lies regarding the national treasure, I get rich merchants’ attention and lure them into the poison gas iron bucket to “kill them with poison gas” and steal their huge fortune. “Making money is so easy, as easy as killing people.” (pp. 19–22). June 4th: You are surrounded! The wailing of sirens is harsh to the year. I’ve killed too many people and am now a wanted criminal. I cannot fight back against so many police officers. My sentence is death. This society created me. On the execution ground, I petition for a chance to repent my sins of killing those people. But, how many have I killed? Let me count, 2, 3, 4, 23, 50 ... (pp. 23–30).

10 CONCLUSIONS

The cruel nature of the animal, an aardwolf, was used as a metaphor of the criminal’s inhumane behaviors of cheating people out of money and killing people through improper measures, making one’s hackles rise. The discussions regarding the picture book of this study and the proposed suggestions are summarized below.

11 DISCUSSIONS

1. Attractiveness of the theme: According to the theory of criminal psychology, readers can release accumulated resentful emotions through a criminal’s behaviors. Their hidden desire can

be satisfied by experiencing crimes through a criminal’s behaviors. This is why this picture book can arouse readers’ curiosity.

2. Authenticity of the created situations: The creators used exquisite and vivid images to deliver the message of the treacherous criminal using the weakness of humanity, greed, to make up lies to make easy money and commit serial killings, showing the key points of the story adequately.
3. Hand drawings and computer graphics processing: Hand drawing skills added warmth to the images, while computer graphics skills added senses of technology to them. Using these two types of skills together made the picture book creation more sophisticated with aesthetics.
4. Aesthetics of creation and innovation: The creators had the capability of creation and innovation for the picture book. The story was based on a social event which once shocked Taiwan. According to the results of the exhibitions and sales of the product, this picture book is indeed loved by a huge variety of readers.

12 SUGGESTIONS

1. Exquisiteness of the literary compositions: More interludes which can reveal more situations should be included in the writing of the story content, so that the picture book can present the criminal’s true feelings and thoughts through more scenes, further enriching the content with more depth.
2. Story scene design: Changes of scenes in this picture book must be logical, and with proper text for additional explanation, the images can

present the story to readers in a more authentic way.

3. Entangled contradictory attitude: Criminals usually kill people in situations where they believe there is no other choice. Or some criminals may commit willful murders. These psychological complexes are hard to understand. It is suggested that the creators of the picture book can add more content regarding this aspect.
4. Marketing channel planning: During the trial sale period of the actual product of this picture book, there were a lot of positive feedbacks. It is suggested to proceed with follow-up marketing channel planning and arrangement, so that the design achievement of this innovative product can be shared to readers who love adult picture books.

REFERENCES

- [1] Einav, A.U., Miriam A., Developing the Skills of Critical and Creative Thinking by Probability Teaching, *Procedia-social and behavioral sciences*, vol. 15 (2011), pp. 1087–1091.
- [2] Gao, B.Q. *Teaching Theory: Ideals and Practices*, Wunan Publishing Co., Ltd., Taipei (2007).
- [3] Editorial Committee, *Encyclopedia of Vertebrates*, National Institute for Compilation and Translation, Taipei (2004).
- [4] Chiu, F.C. Fit between Future Thinking and Future Orientation on Creative Imagination, *Thinking Skills and Creativity*, vol. 7, Issue 3, December (2012), pp. 234–244.
- [5] Chang, J. *Devils' Rules: From Campus Bullying to Killing Families for Plunder*, Nuggets Culture, Taipei (2011).
- [6] Zheng, L.Y. *Cognitive Psychology*, Wunan Publishing Co., Ltd., Taipei (2006).
- [7] Xing, M.Y. *Creation Skills with Mixed Media*, Cube Culture Inc., Taipei (2012).
- [8] Rao, R.V., Savsani, V.J., Vakharia, D.P. Teaching-Learning-Based Optimization: An optimization method for continuous non-linear large scale problems, *Information Sciences*, vol. 183, Issue 1, 15 January (2012), pp. 1–15.
- [9] Xu, Y.Y. *Color Pencils*, San Min Book Inc., Taipei (2003).

Research on Chinese rural public security evaluation system based on fishbone diagram analysis—a case study of South Dagang district for the first partition

Ming Sun & Shao Yu Wang

School of Architecture, Harbin Institute of Technology, Harbin, China

ABSTRACT: The paper introduces Environmental Carrying Capacity (ECC) theory into rural public safety research. According to its index system construction principles, article selects 5 primary index, and 10 secondary indexes, and establish rural public safe index system based on fishbone diagram analysis method. With the help of SPSS software, the use of Principal Component Analysis (PCA), the rural public security system are calculated by using PCA and their capacity are ranked. The key components affecting rural public risk are found out, which provides a good reference for risk alleviation. The result shows that there are big differences in the risk level of public safety in these areas; the components of Infrastructure and land carrying capacity are the most important factors affecting rural public risk, and increasing investment in infrastructure & effective use of idle land, can better improve the carrying capacity of villages and towns public safety.

Keywords: rural public security; fishbone diagram; Principal Component Analysis (PCA); safe system

1 INTRODUCTION

Currently, with an increased risk of mountain flood disasters such as collapse, landslide, debris flow, all kinds of natural and man-made disasters still are at higher risk. Disaster sudden and unpredictability are more prominent gradually. Rural areas development are relative lag than urban, its safety control level is low. The increasingly serious natural disasters impact on rural land, rural residents are less able to withstand these disasters. It make rural Public Security (PS) problem be one of the important influence factors in rural economic and social development (Wu Fan, 2013). However, our research today is less about public safety in rural areas and there are very few studies of public safety system frame. Therefore, it is the inevitable trend of future development to research the system establishment (Wang Jian et al., 2005). Through the establishment of public safety evaluation system, based on South dagang district for the first partition a example, the evaluation results are sorted, and paper put forwards the corresponding planning measures to improve the ability of rural prevent and fight natural adversities.

2 OVERVIEW

South Dagang District (SDD) was formerly known as south dagang farm in hebei province. In

2007 it changed its name to cangzhou bohái new area south dagang industrial park, enjoy the country agricultural reclamation policy. A partition is located in northeast of bohái bay in the west bank, east bohái sea, longs to the warm temperate semi-humid continental monsoon climate, annual average temperature is 12.1°C, Total area is 9093.03 hectares, population has 16000 people, and cultivated land areas are 54000 acre; Ground water is salty, with short of freshwater resources, most of the land is saline-alkali land, and little irrigated land, so all crop have a lot of weather dependence (National Bureau of Statistics of China, 2013).

Nowadays, A partition 15 villages have no preparation of disaster prevention and mitigation planning, flood control planning and fire fighting planning, and villages etc. The rural development are in disordered state with great disaster vulnerability. In terms of land carrying capacity, it has less construction land per capita, idle lands are not sow, land have severe salinization. Supporting infrastructure is backwardness. Village sewage and garbage disposal is still in its original state, it make villagers' production and life to bring great health security hidden danger. Some villages have been many migrant workers leaving the empty nest elderly or children, will be not enough to deal with public safety emergencies, causing unnecessary damage and loss of life from public safety planning and management.

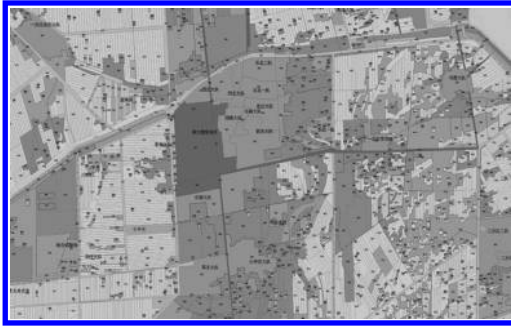


Figure 1. Nan Dagang villages construction land status.

Figure 1 shows the south dagang villages construction land status chart.

3 ESTABLISHMENT OF EVALUATION

Rural PS events mainly include natural disasters, accidents disasters, public health and social security events, etc. Rural environmental capacity include rural resources endowment, ecological environment and infrastructure for ECC of the rural population and economic and social activities. Land, population, environment and infrastructure is the main component they jointly formed the rural security system [3]. Establishment of the evaluation index should be based on existing and potential natural disasters and rural PS and other public safety factors. In fully considering the influence factors of the regional ECC, select index from the land, security, population, infrastructure and social economic conditions and so on. This study references Zhu Zhengwei public safety evaluation index, with the help of fishbone diagram analysis, and considers actual situation of villages and towns public safety finally finds an important index of affecting rural security (Fig. 2).

Among them, the social ECC, security guarantee capability, land, capability are three major factors of supporting indicators for PS. Population and infrastructure and idle land are the three main factors of pressure index for public safety.

4 PRINCIPAL COMPONENT ANALYSIS

4.1 Index standardization

PCA is a recombination index method by using the ideas of dimension reduction, on the premise of keeping unchanged primary index information. With reference to text and graphic file, such as Cngzhou city yearbook (2013), the south dagang

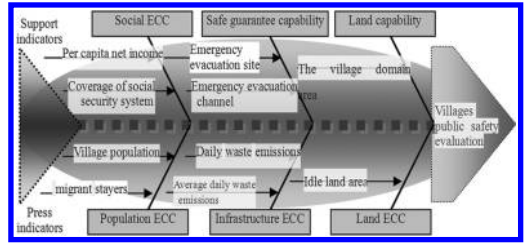


Figure 2. The rural public safety evaluation index system.

district master plan (2012–2030) and the village upgrade planning in south dagang a partition (2013–2030), the paper is combined with field investigation, takes related data statistic to index system (Fig. 1), standardizes statistical indicators data:

$$z_{ij} = \frac{x_{ij} - \bar{x}_j}{s_j}, \quad i = 1, 2, \dots, n; \quad j = 1, 2, \dots, p \quad (1)$$

$$\bar{x}_j = \frac{1}{n} \sum_{j=1}^n x_{ij}, \quad s_j = \sqrt{\frac{1}{n-1} \sum (x_{ij} - \bar{x}_j)^2} \quad (2)$$

4.2 Factor analysis

Factor analysis data based on SPSS factor process. The KMO value is close to 1, means the strength of the correlation between variables, the original variables is more suitable for factor analysis. Sig of Bartlett phericity test value is less than 0.05 significant level, the more there is relationship between variables. The results can meet the requirements of factor analysis, and further complete the principal component analysis Table 1 shows that total variance explained (Table 1).

Table 1 shows that the first four initial characteristic root is greater than 1, and the cumulative percentage is above 80%. Beauce of Table 2 variable does not missing, the extracting principal component number $m = 4$, it obtains the initial characteristic root: $\lambda_1 = 3.408$, $\lambda_2 = 2.073$, $\lambda_3 = 1.809$, $\lambda_4 = 1.099$; Principal component contribution rate: $r_1 = 0.3408$, $r_2 = 0.2073$, $r_3 = 0.1809$, $r_4 = 0.1099$. Selection of four principal component is more appropriate.

4.3 PCA score analysis

Through the four columns of data in the initial factor loading matrix, eigenvector matrix are obtained. Combination of standardized data, the villages eigenvector principal component values Z_i ($i = 1, 2, 3, 4$) is concluded. Table 2 shows the villages

Table 1. Characteristic value and total variance explained.

Component	The initial eigenvalue			Extraction squares sum			Rotate the squares sum		
	Total	Variance/ %	Accumulation/ %	Total	Variance/ %	Accumulation/ %	Total	Variance/ %	Accumulation/ %
1	3.408	34.081	34.081	3.408	34.081	34.081	2.932	29.321	29.321
2	2.073	20.731	54.812	2.073	20.731	54.812	2.101	21.006	50.326
3	1.809	18.089	72.901	1.809	18.089	72.901	1.856	18.556	68.882
4	1.099	10.986	83.887	1.099	10.986	83.887	1.500	15.005	83.887
5	0.735	7.355	91.242						
6	0.330	3.296	94.537						
7	0.249	2.492	97.029						
8	0.137	1.372	98.401						
9	0.109	1.087	99.488						
10	0.051	0.512	100.000						

Table 2. The villages public safety carrying capacity and sorting in 2012.

Indicator	PC1	PC2	PC3	PC4
Z score: the village domain area (h m ²)	-0.21599	0.813255	0.265969	-0.24424
Z score: idle land area (m ²)	-0.18512	0.679058	-0.1098	0.639915
Z score: village daily waste emissions (t)	0.872469	-0.26846	-0.0825	-0.02875
Z score: village daily sewage emissions (m ³ /d)	0.93823	0.022038	-0.03461	-0.03976
Z score: village emergency evacuation site (m ²)	-0.03928	0.906909	-0.0159	0.137037
Z score: village emergency evacuation passage (m)	0.025135	-0.0293	-0.07914	0.977756
Z score: per capita net income (cny)	-0.15792	-0.07959	0.942954	0.039402
Z score: the coverage of social security system (%)	0.034075	0.243132	0.819284	-0.18396
Z score: gross population (person)	0.917965	-0.11913	-0.25205	0.100344
Z score (migrant stayers (person))	0.582006	-0.05028	0.366565	-0.09312

public safety carrying capacity and sorting in 2012 (Table 2).

4.4 Interpretation of result

Table 2 shows that village principal components Z1 includes daily sewage emissions, gross population, daily waste emissions, migrant stayers. Principal component Z1 mainly explain the four indicators, can be named as PS infrastructure and population bearing capacity factor. Village principal components Z2 includes emergency evacuation site, the village domain area, idle land area, namely land carrying factor. Principal component Z3 contains the per capita net income and social security coverage, can be called as public safety factor. There are village emergency evacuation channels and idle land area in Principal component Z4 while can be named as public safety propylaea. These four factors, especially the first two factors will strengthen the rural public safety in large extent. Table 3 shows that principal component generated

rotating component matrix according to the new name (Table 3).

The results are shown in Table 2. There are large difference between the carrying capacity of village public safety. The bearing capacity of the village associated with distance downtown location. The closer villages distance SDD, the stronger their safety capacity are. West zhuang village and southwest zhuang village are close to the district government. The two village public safety bearing capacity are stronger than any other villages, with strong economic strength, infrastructure, population and land carrying capacity. This is because seat of district government have larger PS investment proportion, high land utilization ratio, and perfect PS infrastructure, these will help the surrounding villages resource sharing and mutual cooperation.

Yan Jia Jang Ji village, East Zhuang village and MaYing village should strengthen the PS foundation design, and improve the bearing capacity. Villages should strengthen the village land, especially the use of idle land, minimize to reduce land

Table 3. Rotating component matrices.

Indicator	PC1	PC2	PC3	PC4
Z score: the village domain area (h m ²)	-0.21599	0.813255	0.265969	-0.24424
Z score: idle land area (m ²)	-0.18512	0.679058	-0.1098	0.639915
Z score: village daily waste emissions (t)	0.872469	-0.26846	-0.0825	-0.02875
Z score: village daily sewage emissions (m ³ /d)	0.93823	0.022038	-0.03461	-0.03976
Z score: village emergency evacuation site (m ²)	-0.03928	0.906909	-0.0159	0.137037
Z score: village emergency evacuation passage (m)	0.025135	-0.0293	-0.07914	0.977756
Z score: per capita net income (cny)	-0.15792	-0.07959	0.942954	0.039402
Z score: the coverage of social security system (%)	0.034075	0.243132	0.819284	-0.18396
Z score: gross population (person)	0.917965	-0.11913	-0.25205	0.100344
Z score (migrant stayers (person))	0.582006	-0.05028	0.366565	-0.09312

salinization, drought, and enhance land bearing capacity of public safety.

5 RESULTS AND DISCUSSIONS

5.1 Public safety planning countermeasures

We should realize the preparation of village public safety planning work as soon as possible, set up SDD—Partition—Villages trinity disaster prevention and mitigation planning system, implement the rural and urban safety resources sharing, promote regional response to PS events.

1. Perfecting the villages comprehensive disaster prevention and mitigation planning. The village should strengthen safety capacity building, improve the system mechanism of disaster prevention, perfect natural disaster emergency plan and organize rehearsals, enhance the construction of early warning information release ability. The local government needs to increase more support of public safety response capacity in order to protect serious natural disasters area. Planning schemes make full use of the swags as fire pool, village wheat field as an emergency shelter, integrate surrounding idle land, and, strengthen the ecological capacity.
2. Partition comprehensive disaster prevention plan partition 1, which has fewer basic infrastructure, disaster prevention and mitigation, is not effective means to face public safety emergencies, must comprehensively arrange overall disaster prevention resources and the strength. Through the dangerous house renovation project, most of them had improved, but there were some dangerous house, lack of emergency shelter, lower road hardening rate, impeded emergency evacuation channel. Therefore, plan should improve the village built, especially disaster prevention performance of crowded places, major construction projects and lifeline engi-

neering, and promote safety schools & hospitals, engineering construction. Scheme should strengthen the protection governance of ponds, dilapidated reservoirs reinforcement, and ecological environment treatment in disaster area, increase project investment such as the dangerous house renovation, emergency water source, rural drinking water safety.

3. Whole SDD public security facilities planning. To coordinate area linkage ability construction of disaster prevention and mitigation, schemes should optimize development planning and upgrade industrial structure promote fortification standards of village buildings and public facilities of, strengthen the administrative zones infrastructure disaster relief capacity building in the transportation, communications, radio and television, electric power, gas supply, water supply and drainage pipe network, schools, and hospitals, make effective use of the existing place such as primary school, secondary school, park, stadium wheat field, idle land, build comprehensive public safety new model.

5.2 Management strategies

1. The PS information management. To improve the level of information management, effective use information resources of all types and at all levels, expand access to information channels and means, improve the level of information processing and analysis. Establishing database of villages and towns comprehensive disaster prevention and mitigation, perfect the disaster information dynamic update mechanism, improve the security of information system standards, to ensure the safety of disaster prevention and mitigation information. To strengthen rural information sharing ability of disaster prevention and reduction, and improve the village south dagang, partition, disaster prevention and mitigation information

integration, intelligent processing and service level, strengthen the village disaster prevention and mitigation with partition, south dagang related departments interconnectivity, exchange information sharing and collaborative services. The existing resources, make full use of the villages and towns combined with technologies such as radio, television and mobile information terminal equipment.

2. Public safety risk management. The scheme is designed to perfect the measures of reducing disaster risk, establish risk sharing mechanism of the PS, accelerate the disaster investigation and evaluation system. According to investigation, villages need carry out PS risk and disaster reduction survey, update the current ability, and set up PS database, an integrated disaster risk evaluation index and evaluation system. The plan promoted the development of the integrated natural disaster risk assessment method. To establish natural disaster evaluation system, and constantly improve the risk assessment, emergency assessment, loss assessment, social impact assessment and performance evaluation level, villages and local governments need to be continuously perfect the comprehensive assessment mechanism of natural disasters.

6 CONCLUSIONS

In recent years, rural public safety policies have become increasingly more ambitious under the pressure of high natural disaster risk and governmental initiatives for the support of disaster prevention and mitigation. On the one hand, disasters result in costs for the public administration; on the other hand, local scale programs represent an important element for the transition towards a more sustainable safe paradigm. Rural safe programs can be effectively employed as a mean to accelerate this process if they are correctly designed (Sun, Yu et al., 2013; Li, D.R. 2013).

According to current situation of environment bearing capacity, the research presented involved the analysis and research of rural public safety planning system, focusing on the improvement of environmental carrying capacity with high efficiency public security index evaluation frame. The developed rural public safe system helps attaining the balance between town and environmental comfort.

In addition, rural public safe system has been embedded with the principal component analysis for optimizing natural risk management. Villages exhibits the improvement and the potential for public security evaluation. In future work, rural public security evaluation frame will be further tuned to its maximum efficiency. Future research could focus on individual villages, conducting longitudinal studies that look at all relevant natural disk factors, and socio-economic variables.

ACKNOWLEDGEMENTS

The presented study is part of a research project which is funded by China Postdoctoral Science Foundation (Grant No. 2014M551247); Project also supported by the National Natural Science Foundation of China (Grant No. 71372091). This works is also supported by the Fundamental Research Funds for the Central Universities of China (Grant No. DL13CB15).

REFERENCES

- Cheng, X.H., Wang, Z.N., 2012. Preliminary Study on Theoretical Model of Rural Meteorological Disaster Prevention System. *Journal of Catastrophology* 27, 117–121.
- Li, D.R., 2013. National comprehensive disaster reduction and risk management information system integration. *China's disaster reduction* 6, 18–20.
- National Bureau of Statistics of China 2013. *Cangzhou statistical yearbook*. Beijing: China statistics press, 24–73.
- Sun, Y., Li, X.G., Yao, X.D., 2012. Tianjin district land comprehensive carrying capacity research. *Urban development research* 9, 107–109.
- Wang, J., Sun, T.H., Li, P.J., 2005. Studies on the environmental bearing capacity. *Journal of applied ecology* 4, 68–72.
- Wu, F. 2013. Study on natural disaster emergency management of local government in China. (Master Thesis) Yunnan university of finance and economics, Kunming China.
- Yang, L., 2008. Research on the three gorges reservoir area of small towns environmental bearing capacity of quantitative. (Master Thesis) Chongqing university, Chongqing China.
- Zhu, Z.W., Xiao, Q.Y., 2006. International public safety evaluation system: theory and application prospect. *Journal of public management* 3(1):27–33.

Predict of loss of fuel during the road reconstruction in Indonesia

Dewa Ketut Sudarsana

Student in Doctoral Civil Engineering Program, University of Brawijaya, Malang, Indonesia
Lecturer, University of Udayana, Jimbaran, Indonesia

Harnen Sulistio, Achmad Wicaksono & Ludfi Djakfar

Lecturer, Department of Civil Engineering, Faculty of Engineering, University of Brawijaya, Malang, East Java, Indonesia

ABSTRACT: National Roads in Indonesia are still in substandard in order continues to be reconstructed to establish connectivity Trans National and supports the Trans Asian. During the reconstruction period has negative impacts such as loss of road user costs, loss of fuel energy, and the environment. Prediction model of the fuel loss has not been studied. National road reconstruction project in Bali, Indonesia is used as a case study. Analysis of fuel consumption refers to the guidelines of Highways Pd-T-15-2005-B, which adapts from HDM IV, 2000. Characteristics traffic during reconstruction, predicted based on the traffic characteristics on pre reconstruction condition by multiplying the adjustment factor F_q for traffic volume, F_v for speed and F_d for the degree of saturation. Average fuel loss on each road link is predicted to 144.6 liters/day. Loss of fuel during duration schedule for completing each road reconstruction predictability of 11,128 to 55,772 liters, and the loss of fuel for the 6 the link road studied is 164,075 liters.

Keywords: road reconstruction; negative impact; loss of fuel; predict

1 INTRODUCTION

In order to establish connectivity Trans Asian, Indonesian National roads are sub-standard condition still continues to do the reconstruction. During the reconstruction period has negative impact on road users and the environment. In Negara-Pekutatan road reconstruction in Bali province in fiscal year 2013 founded the capacity of the road decreased by 32%, the vehicle's speed at peak hours down from 40 km/h to 35 km/hour, the traffic volume decreases to 18% [4]. The decline of the performance traffic characteristics resulting in the loss of road users cost. Research on the loss of the road users cost during the implementation of the National road reconstruction project in the province of Bali fiscal year 2012 founded 1.37% of the contract of physical value per day [5]. Fuel consumption cost is a component of the road users cost. In Indonesia, Predicted loss of fuel during road reconstruction cannot be done. Prediction of a loss of fuel has not been conducted, so that needs to be studied.

2 MATERIALS AND METHODS

Location of the research conducted by the Executive of the National Road Office, or "Balai Pelaksana Jalan Nasional (BPJN) VIII", province of

Bali, Indonesia. Case studies are the National road reconstruction project, 2-lane 2-way, urban and interurban, for fiscal year 2013. The link road be studied are presented in Table 1. Descriptive and statistical analysis used in this analysis [1]. This paper specifically analyzes predicted a loss of fuel during the road reconstruction.

The formulation of fuel consumption, refer to the guidelines of Vehicle Operating Cost (VOC) Pd-T-15-2005-B by Department of Public Works [3]. These guidelines are adapted some equations and parameters of HDM IV in 2000. Analyzes traffic performance using Indonesian Highway Capacity Manual (IHCM) 1997 guidelines [2]. The framework of the analysis phase is presented in Figure 1.

Table 1. Name and length of link road.

No cases	Name of link road
S7	Cekik-Batas Kota Negara
S8	Antosari-Batas Kota Tabanan
S9	Kota Singaraja dan Kubutambahan
S10	Batas Kota Singaraja-Kubutambahan
S11	Jimbaran-Uluwatu
S12	Denpasar-Tuban

Source: [6].

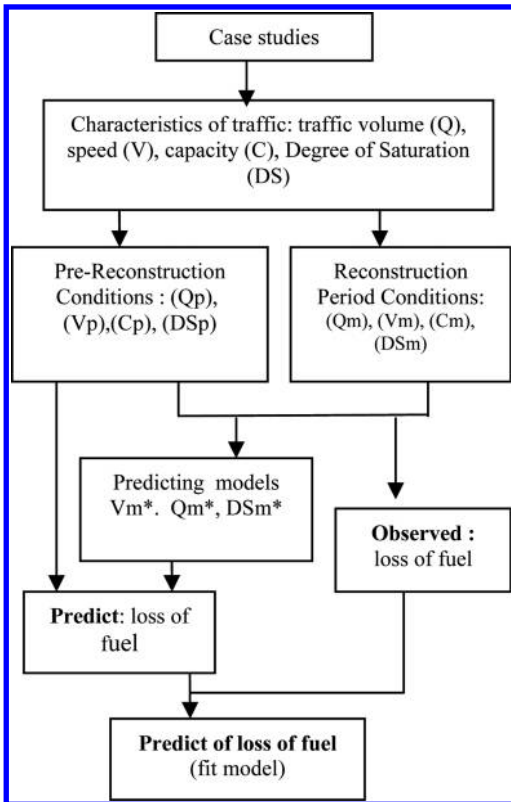


Figure 1. Framework of analysis.

3 DATA AND ANALYSIS

The characteristics of traffic related to the prediction of fuel consumption are the volume (Q), speed (V) and the Degree of Saturation (DS). DS is the ratio between the volumes (Q) with a capacity (C). The capacity of urban road can be determined in equation (1) [2].

$$C = C_o \times FC_w \times FC_{sp} \times FC_{sf} \times FC_c \quad (1)$$

where:

- C = actual capacity (pcu/h)
- C_o = capacity of the ideal conditions (pcu/h)
- FC_w = road width adjustment factors
- FC_{sp} = separator adjustment factor
- FC_{sf} = side friction adjustment factor
- FC_c = city size adjustment factor.

Traffic characteristics on pre reconstruction denoted by p, so it can be written Q_p, V_p, DS_p. During the reconstruction period is denoted by m, so it can be written Q_m, V_m, DS_m. Average of traffic characteristic values for 6 link roads case study, denoted by r, so that the pre reconstruction

conditions can be written Q_{pr}, V_{pr} and DS_{pr}, while during reconstruction are Q_{mr}, V_{mr} and DS_{mr}. The graph in Figure 2 it can be seen the average of the volume value of Q_{pr} and Q_{mr}. Figure 3 is a graph of the speed average value of V_{pr} and V_{mr}, and Figure 4 is a graph of the degree of saturation average value of DS_{pr} and DS_{mr}.

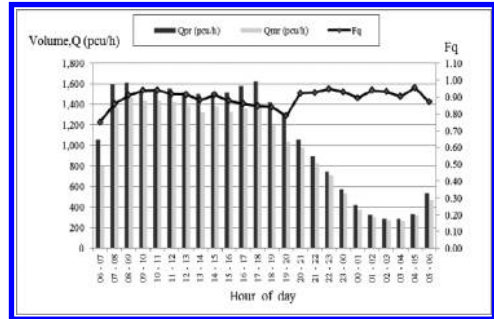


Figure 2. Average traffic volume Q_{pr} (pcu/h), Q_{mr} (pcu/h) and the volume adjustment factor F_q, by hour of day.

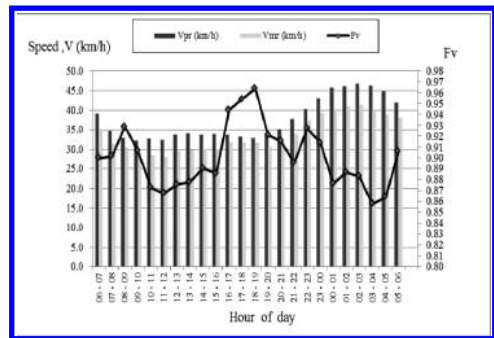


Figure 3. Average speed V_{pr} (km/h), V_{mr} (km/h) and the speed adjustment factor F_v, by hour of day.

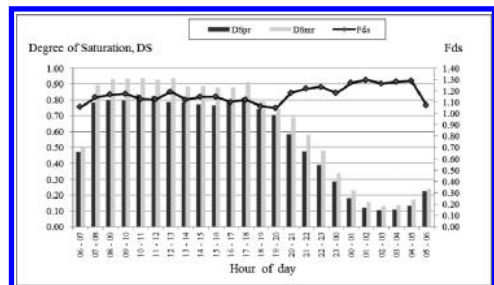


Figure 4. Average degree of saturation DS_{pr}, DS_{mr} and degree of saturation adjustment factor F_{ds}, by hour of day.

3.1 Traffic volume Q_p - Q_m relationship

The average traffic volume on pre reconstruction (Q_{pr}) with during reconstruction (Q_{mr}) relationship can be seen in Figure 2 and can be determined as in equation (2).

$$\begin{aligned} Q_{mr} &= Q_{pr} \times F_q \\ \text{Or} \\ F_q &= Q_{pr}/Q_{mr} \end{aligned} \quad (2)$$

where:

F_q = traffic volume adjustment factors'

F_q values are presented in Figure 2.

Based on the F_q values, then the traffic volume during reconstruction (Q_m^*) can be predicted as in equation (3).

$$Q_m^* = Q_p \times F_q \quad (3)$$

3.2 Speed V_p - V_m relationship

The average of vehicle speed on pre reconstruction (V_{pr}) with during reconstruction (V_{mr}) relationship can be seen in Figure 3 and can be determined as in equation (4)

$$\begin{aligned} V_{mr} &= V_{pr} \times F_v \\ \text{Or} \\ F_v &= V_{mr}/V_{pr} \end{aligned} \quad (4)$$

where:

F_v = speed adjustment factor.

The value of the speed factor F_v is presented in Figure 3. Based on F_v values it can be predicted the speed on during reconstruction (V_m^*) as in equation (5).

$$V_m^* = V_p \times F_v \quad (5)$$

where:

V_m^* = prediction of speed during reconstruction (km/h)

V_p = speed of pre reconstruction (km/h)

F_v = speed adjustment factor.

3.3 Degree of Saturation DS_p - DS_m relationship

The average degree of saturation on pre reconstruction (DS_{pr}) with during reconstruction (DS_{mr}) relationship can be seen in Figure 4 and can be formulated as in equation (6).

$$\begin{aligned} DS_{mr} &= DS_{pr} \times F_{ds} \\ \text{Or} \\ F_{ds} &= DS_{mr}/DS_{pr} \end{aligned} \quad (6)$$

where:

F_{ds} = degree of saturation adjustment factor.

The adjustment factor of degree of saturation F_{ds} values is presented in Figure 4. Based on the F_{ds} values, then the degree of saturation of during reconstruction (DS_m^*) can be formulated as in equation (7).

$$DS_m^* = DS_p \times F_{ds} \quad (7)$$

where:

DS_m^* = prediction of degree of saturation on during reconstruction

DS_p = degree of Saturation on pre reconstruction

F_{ds} = adjustment factor of the degree of saturation, see Figure 4.

3.4 Fuel consumption

The fuel consumption for each vehicle can be calculated by equation (8) [3].

$$\begin{aligned} KBBM_i &= (\alpha + \beta_1/V_R + \beta_2 \times V_R^2 + \beta_3 \times R_R + \beta_4 \\ &\times F_R + \beta_5 \times F_R^2 + \beta_6 \times DT_R + \beta_7 \times A_R \\ &+ \beta_8 \times SA + \beta_9 \times BK + \beta_{10} \times BK \\ &\times A_R + \beta_{11} \times BK \times SA)/1000 \end{aligned} \quad (8)$$

where:

α = constant

$\beta_1 \dots \beta_{11}$ = parameter coefficients

V_R = average of speed

R_R = average of road ramp up

F_R = average sloop down the road

DT_R = degree of average curve road

A_R = average of acceleration

SA = standard deviation of acceleration

BK = weight vehicles

i = type of vehicle.

A_R is average of acceleration can be calculated by equation (9):

$$A_R = 0.0128 \times DS \quad (9)$$

Standard deviation of acceleration (SA) is determined from the equation (10):

$$SA = SA \max (1.04/(1+ e^{(a_0 + a_1) \cdot DS}) \quad (10)$$

where:

$SA \max = 0.75$ (m/s²) (default).

a_0, a_1 : $a_0 = 5.14$; $a_1 = -8.26$ (default).

3.5 Prediction of the loss of fuel model

Loss or increase of fuel consumption ($KBBM$) can be determined from the difference in fuel consumption on during reconstruction ($KBBM_m$) reduced by the fuel consumption on pre reconstruction ($KBBM_p$), and can be formulated as in equation (11).

Table 2. Loss of fuel (liters/day).

Link road	Qp (pcu/day)	LoF*	LoF	LoF/LoF*
S7	29,806	46.4	52.5	1.13
S8	26,322	74.0	75.0	1.01
S9	27,720	120.0	114.2	0.95
S10	20,663	59.8	61.5	1.03
S11	44,935	229.2	232.4	1.01
S12	67,920	338.0	335.9	0.99
Average	36,228	144.6	145.3	1.02

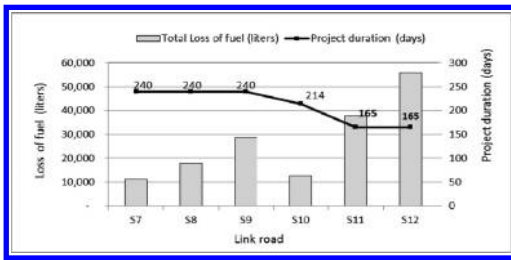


Figure 5. Loss of fuel on link road.

$$KBBM = KBBMm = KBBMp \quad (11)$$

By substituting the traffic characteristics on pre reconstruction (Q_p , V_p , DS_p) and the model prediction of the reconstruction (Q_m^* , V_m^* , DS_m^*), into the equation (8), (9), (10) and (11), then KBBM prediction equation obtained as in equation (12).

$$KBBM = \left\{ \beta_1 \frac{(1 - F_v)}{(V_p \cdot F_v)} + \beta_2 \cdot F_v^2 \right. \\ \left. \frac{(V_p - 1)^2 + 0.128 (\beta_7 + \beta_{10} \cdot BK)}{(F_{ds} - 1) + 0.78 (\beta_8 + \beta_{11} \times BK)} \right. \\ \left. \frac{1/(1 + e^{(-3.1540) \cdot F_{ds} \cdot DS_p}) - 1/}{(1 + e^{(-3.1540) \cdot DS_p})} \right\} / 1000 \quad (12)$$

3.6 Analysis of loss of fuel

The loss of fuel per day by using predictive models (LoF^*) and loss of fuel with observational (LoF) is presented in Table 2. The average of LoF^* prediction found was 144.6 liters/day, while the average of loss of fuel by observed was 145.3 liters/day. In Table 2 also presented the ratio between LoF with LoF^* ($RLoF = LoF/LoF^*$). Average ratio $RLoF$

found was 1.02 (there is a 2% difference). It can be said that the model prediction equation (12) is the fit model. The total loss of fuel prediction each link road for the scheduled duration of the project D (days) is presented in Figure 5. The total loss of fuel each link road ranged from 11,128 to 55,772 liters, and the total loss for the 6 link roads is 164,075 liters.

4 CONCLUSION

The characteristics of traffic during road reconstruction correlates with the prediction of a loss of fuel such as volume, speed and degree of saturation can be predicted based on the traffic characteristics on pre reconstruction by multiplying the volume adjustment factor F_q , the speed adjustment factor F_v and degree of saturation adjustment factor F_{ds} . The results of a loss of fuel using the prediction model compared with the observed, differences were found 2% only, it can be said that the prediction model has the fit model. An average of a loss of fuel by prediction on each road link was found as 144.6 liters/day. Total of losses of fuel prediction during reconstruction by 6 link roads is 164.075 liters.

REFERENCES

- [1] Bhattacharyya, G.K. and Johnson, R.A., 1977. Statistical Concepts and Methods. John Wiley and Sons.
- [2] DPU (Departemen Pekerjaan Umum). 1997. Manual Kapsitas Jalan di Indonesia (MKJI).
- [3] DPU (Departemen Pekerjaan Umum). 2005. Pedoman Perhitungan Biaya Operasi Kendaraan, Nomor: Pd.T-15-2005-B, Puslitbang Prasarana Transportasi.
- [4] Sudarsana Dewa Ketut, Harnen Sulistio, A Wicaksono dan Ludfi Djakfar. 2013. Kajian Kinerja Jalan Akibat Adanya Zona Kerja (Work Zone). Prosiding The 16th FSTPT International Symposium, UMS Surakarta, 1–3 Nov 2013.
- [5] Sudarsana Dewa Ketut, Sulistio Harnen, Wicaksono Achmad and Djakfar Ludfi, 2014. The Analysis Of Work Zone Road User Costs Due To The Delay Completion Of The Road Maintenance Project. Adv. in Nat. Appl. Sci., 8(3): 103–108.
- [6] Sudarsana Dewa Ketut. 2014. Model Kerugian Penggunaan Jalan Pada Masa Pelaksanaan Proyek Rekonstruksi Jalan. Draft Naskah Disertasi, Program Doktor Teknik Sipil, Fakultas Teknik, Universitas Brawijaya Malang.

Optimizing transportation system planning design for campus in severe cold climates

Yu Zhang

School of Architecture, Harbin Institute of Technology, China

Zi Guang Chen

School of Architecture and Engineering, Heilongjiang University, China

ABSTRACT: Authors of papers to proceedings have to analyze the transportation characteristics in campus in severe cold climates. In order to ensure the unique characteristics and propose a proper planning design methodology, all the papers have to be prepared strictly according to the investigation and monitoring data in selected campus. Standing from the point of architectural design, the planning strategy had been proposed in this paper could be guide to improve the safety, efficiency and reasonability.

Keywords: severe cold climates; green campus; transportation system; planning design

1 INTRODUCTION

In the campus locates in severe cold region, the transportation is suffered by the slippery road and strong wind and snow environment in winter time which lasts over 4 months. Therefore, the severe climate reduced the transportation efficiency and caused the problem such as traffic inconvenience and campus environment decline. How to reduce the effect of the severe climate and how to utilize the specific natural resources in urban area in severe cold region and to create green transportation environment in campus is a topic needed to be thought and discussed urgently.

2 RELATED CONCEPTION

Present article aimed at transportation system in campus locates in severe cold region, through the analysis of the utilization characteristics; the reasonable design principles for transportation system would be proposed and could be used as guide for architectural design of the campus in severe cold climates. The related conception includes:

2.1 *Campus in severe cold climates*

The characteristics of severe cold climates can be summarized into long winter time with extreme cold weather and heavy snowfall, short summer time, four distinctive seasons. In China, the three provinces including Heilongjiang, Jilin, Liaoning in northeast region and some part in northeast of Inner-Mongolia are typical severe cold climate

region. The campus in these regions is suffered by the local cold weather, the difficulty of communication, transportation and education activities are increased a lot in winter time.

2.2 *Green campus*

It refers to the campus which is developed in a sustainable way and utilize the all the resources and opportunities to improve the built environment for all the people in the campus. Present article is focused on the transportation planning in campus in severe cold climates and discussed the issues about energy conservation, low carbon emission, the quality of thermal, wind environment and air. The aim of present article is try to improve the convenience, safety and comfortable of campus in severe cold climates.

2.3 *Transportation system in campus*

Present article divides the transportation system into two types: fast traffic transportation system refers to the vehicle traffic while slow traffic transportation system refers to bicycle and pedestrian traffic.

3 UTILIZATION CHARACTERIZATION OF TRANSPORTATION SYSTEM IN CAMPUS IN SEVERE COLD CLIMATES

The transportation mode in a campus relates to the factors such as scale, function, local climate and geography situation of the campus. Actually, the

Table 1. Climate information of 4 cities in China.

City	Latitude (degree)	Length of day time (hour)	Lowest temperature in winter (OC)	Highest temperature in summer (OC)
Harbin	N45.1	8 h40 m	-7-18	14-25
Beijing	N39.5	9 h16 m	-5-5	18-29
Shanghai	N30.4	10 h8 m	4-12	21-28
Guangzhou	N22.3	10 h44 m	13-21	24-31

Source: www.tianqi.com.

pedestrian mode is the best transportation mode in campus because of the low carbon emission and the scale of the campus. But for campus in severe cold climates, bicycle and pedestrian should be the main transportation mode and complementary with vehicle. In spring and summer, bicycle and pedestrian would be adopted more than in autumn and winter because of the cold weather. The vehicle is usually used by teachers and people outside the universities, in campus it should be limited the utilization of vehicle and reduce the influence to the pedestrian safety in campus.

3.1 Characterization of transportation system of campus in severe cold climates

1. Harsh pedestrian conditions with snowy and windy environment

The biggest obstacle for walking in the campus in winter time is the severe weather that cold wind with snow declines the comfortable level. Thus both the teachers and students would reduce the willing and time to go out, hence the environment is desolate in winter and campus life is seriously impacted.

Four cities had been selected to make the comparison (Table 1). From the data we can know that Harbin locates in northeast part of China which is the typical severe cold region while Beijing has the similar heating time but the temperature is much higher than Harbin. In winter time, the cold period is much longer and environment is more serious.

2. Slippery road with low-security

In winter, there is snow and ice cover on the road which makes the transportation in campus low efficiency and causes the safe risk because of the automotive brakes and slips. In the meanwhile, the slippery causes huge disturbance for walking and bicycle and declines the security for teachers and students.

3. Transportation needs longer response time in winter

In winter, people moves slower because of the thick clothes. White snow covers the campus, snow blew by the wind, vapor come out from mouth, all of these factors makes disrupts the



Figure 1. Three places selected for the investigation in HIT.

vision of people. In addition, the hearing ability is disrupted by thick clothes and accessories. Thus people needs much longer time to response the traffic information and the efficiency of transportation is reclined.

4. Weaker light environment with short length of daytime

In cold climate region, the length of day is shorter than night. In northeast part of China, sunset time is around 4 pm, in some high latitude area, the sky get dark around 3 pm. In winter time, the lighting environment is poor while it's getting colder after sunset since lack of solar radiation. The result is in the first class in the morning and the final class in the afternoon, the environment is dark and cold. On one hand, the weather increased the difficulty of transportation and interrupt the normal activities in campus. The enthusiasm of outside activities is declined a lot.

3.2 Transportation characterization in campus in severe cold climates

An investigation is made in first campus of Harbin Institute of Technology. Three important transportation nodes (Fig. 1) includes: main entrance area, Fayuan Street and square of faculty of Science had been selected and to be investigated the transportation information in the period of

Table 2. Transportation mode comparison in campus in severe cold climates (times/person. hour).

Place	Traffic mode	10–11 am		6–7 pm	
		Winter	Summer	Winter	Summer
Place A Campus main entrance	Vehicle	96	153	78	139
	Bicycle/motorcycle	6	25	3	39
	Walking	113	255	179	399
	Total quantity	215	433	260	577
Place B Fayuan street	Vehicle	72	136	51	89
	Bicycle/motorcycle	77	89	33	56
	Walking	569	1017	158	369
	Total quantity	718	1242	242	514
Place C Square in front of faculty of science	Vehicle	36	47	50	68
	Bicycle/motorcycle	22	52	18	33
	Walking	343	468	112	234
	Total quantity	526	567	170	335

Data is investigated.

10–11 am and 6–7 pm. The investigation was made on 15th November 2013 and 28th May 2014. The traffic flow refers to double directions traffic and been divided into walking, bicycle/motorcycle and vehicle. The data collected (Table 2) through this investigation could be analyzed and help us to propose the design strategy for campus design in severe cold climates. The transportation characterization of campus in cold climates could be summarized as the following points:

1. Compared with summer, in fixed traffic node, the traffic flow is much less (ignore the quantity variance among different transportation mode), it's caused by the short length of daytime in winter and it's already totally dark around 5 pm therefore people reduce the outdoor activities. From the data we can know that even in the peak time of lessons around 10 am, traffic flow is lower in winter. So the cold weather influences a lot to human activity.
2. There are big differences of the transportation mode between winter and summer. Campus is the area with high proportion of bicycle/motorcycle but the data shows that the proportion of vehicle increased a lot while the proportion of bicycle/motorcycle and walking decreased a lot. It's because the windy and snowy weather and the resistance of slippery road.
3. In different traffic nodes but in the same time, there is big difference of traffic flow quantity and traffic mode since people would reduce the outdoor activity and ignore unessential transportation demand.

In conclusion, although the transportation quantity is reduced in winter, the transportation plays an important role in operation of the campus.

4 PLANNING REQUIREMENTS OF TRANSPORTATION SYSTEM IN CAMPUS IN SEVERE COLD CLIMATES

On the base of analysis of problems and characteristics of transportation system in campus in cold climates, the planning requirements could be summarized as following points:

4.1 Shortest path

Slow traffic system refers to non-motor vehicle traffic should in the campus should avoid of circumambulation but connecting the living area with teaching area and sports area. There should be shortest path passing through the greening area and square to meet the demand of fast arriving in winter.

4.2 Improving safety and antiskid performance

Ensuring the traffic safety is the primacy principle for transportation while antiskid is the main requirement for reducing safety risk. Through choosing the proper texture of the material, timely cleaning and strengthen the management of transportation system, the antiskid performance could be improved.

4.3 Wind protective and comfortable

Adopting wind protective measures could help to improve the comfort level especially for slow traffic system in campus. By leading, weakening and drawing the wind, wind environment of the road could be improved and have an effect on the guiding and promotion for non-vehicle transportation.

4.4 *Avoiding disturbing from different traffic mode*

Separating pedestrians and vehicles system is the guarantee for improving comfort of slow traffic system, in the same time, each traffic mode would improve the efficiency since avoiding disturbing.

5 PLANNING STRATEGY FOR TRANSPORTATION SYSTEM IN CAMPUS IN SEVERE COLD CLIMATES

Synthesizes the current transportation problem, climate characteristics, available technic conditions, economic factors with the initial functional demands of campus in severe cold climates, the planning strategy for transportation system had been proposed as following points:

5.1 *Compound road network with fast and slow traffic system*

For road network design, we should avoid of single traffic mode and pedestrian and vehicle mixing, but compound the pedestrian slow traffic system with vehicle fast traffic system synthetically. By adopting the functional space division, combining the geography condition, greening and terrace difference, the fast and slow traffic systems could be separated and combined with the consideration of continuity and accessibility.

For example, in design for new campus of Northeast Petroleum University (Fig. 2), fast



Figure 2. Campus planning for Northeast Petroleum University.

traffic system is fixed in periphery while there is antiskid pavement and greening area connected with slow system which is safe, comfortable and high accessibility. The pedestrian path and bicycle road had been broaden with variation floor covering and landscape sketches to encourage people to choose pedestrian traffic mode and reduce vehicle traffic, furthermore, to fulfill the aim of low carbon emission and creative more opportunities for outdoor communication.

5.2 *Suitable scale of road and building*

Suitable length of the road and scale of the building along the street could be an adjustment for wind and sunshine and improve the surrounding environment. Inside the campus, the height of the building along the street should not be too high because low height could decline the speed of wind and weaken the wind together with plants surrounding. On the other hand, low height building with slop roof could help more solar radiation to reach on the road and speed up the melt of snow and ice.

For example, in campus design of Yingkou University (Fig. 3), dormitory building adopted the low height and slope roof help to improve the wind environment of the enclosed pedestrian area. The suitable scale of building and length makes road can absorb more solar radiation in daytime.

5.3 *Road interface help to relieving uncomfortable feeling*

We should arrange greening plants and landscape sketches in different density by taking consideration of the original geography condition. In cold climate region, pine and cypress together with shrub in different height planted along the street could play the role as climate barrier in winter to improve micro-climate and create a quiet environment. In the direction of main wind in winter, thick shrubs



Figure 3. Campus design for Yingkou University.



Figure 4. Photo in Northeast University.

could be planted to slow down the speed of wind as the shield of severe environment. Planting the tall trees could make the road absorb more solar radiation in winter.

For example, in campus design for Northeast University, deciduous species and evergreen species, trees and shrubs with lawn are used harmoniously (Fig. 4) to protect sunshine in summer and wind in winter to create a quiet and comfortable micro-climate in campus.

5.4 *Antiskid detailed design for road*

The pavement material for roads with good water permeability and antiskid performance could be used because the rough surface of the material could meet the antiskid demand in winter. In the same time, the colorful and various pavement materials could be recognized easily in campus which is covered by white snow and used to improve the vitality of transportation system. In the campus with height difference, the slope of the

road should be eliminated and used antiskid measures on the surface.

5.5 *Three-dimensional and multi-functional transportation*

In campus design, the form of the buildings, geography conditions should be utilized to construct a three-dimensional transportation system which could help to avoid of severe climate factors and to build diversified transportation environment. In the meanwhile, it could relieve the traffic congestion in rush hour for the classes. By adopting the three-dimensional traffic space, the comfort and safe traffic requirement could be met, together with the utilization of buildings, geography, landscape, the characteristics of severe cold climate could be pursued interests and avoid risks to create an multi-functional transportation system in campus with distinctive local features.

REFERENCES

- [1] Hongyuan Mei, *Cold Region Architecture*, Beijing: China Architecture & Building Press, 2012, ISBN: 9787112143399.
- [2] Jessie Hui Wang, Changqing An, Jiahai Yang, A study of traffic, user behavior and pricing policies in a large campus network, *Computer Communications* 34 (2011) 1922–1931.
- [3] Hongwei Tan, Shuqin Chen, Qian Shi, Lingling Wang, Development of green campus in China, *Journal of Cleaner Production* 64 (2014) 646–653.
- [4] Robert J. Koester, James Eflin, John Vann, Greening of the campus: a whole-systems approach, *Journal of Cleaner Production* 14 (2006) 769–779.

Research advances and engineering application of energy pile system

Chao Yang, Zhi Rong Zhu, Guo Liang Dai & Wei Ming Gong

School of Civil Engineering, Southeast University, Nanjing, Jiangsu Province, China

ABSTRACT: Energy pile system is a new type of ground-source heat pump system. Heat was exchanged between energy pile system and the soil by building pile foundation for carrier and closed-loop tubes. Energy pile system uses geothermal energy, combining heat exchanger and pile, which will not only reduce the significant costs and maintenance costs, but also contribute to the environmental protection and energy-saving emission reduction. Based on a large number of literature, the research results of technical background, mechanism, engineering application at home and abroad of energy pile system were summarized. The study results show that the trends in development of renewable energy is necessary. With the deepening of relative research, the development of energy pile system will be faster by virtue of its unique advantages.

Keywords: energy pile system; geothermal energy; mechanism; engineering application

1 INTRODUCTION

Preene M and Powrie W (2009) found that the interaction with depth of several kilometers was required by traditional geothermal energy systems, and the hydrothermal produced by huge heat energy here could drive a turbine to generate electricity. However, the enormous cost of the system was only for large-scale applications. In recent years, great progress has been made in the field of shallow geothermal energy systems. Katzenbach R et al. (2007) found that these systems were more potential than conventional systems in terms of sustainability, flexibility and economy. Shallow geothermal energy was based on the principle that foundation could be used as the thermal energy, that was the natural potential and thermal storage capabilities could be used.

In ground source heat pump systems, the common tubes of underground heat exchanger were horizontal and vertical buried tubes. Currently, the dominant form in engineering applications of geothermal heat exchanger was vertical buried tubes. Diao nairen and Fang zhaohong (2006) found that the vertical buried tubes geothermal heat exchanger took a less area and had stable performance characteristics, but its higher drilling costs reduced the economic suitability of ground source heat pump system compared with traditional air conditioning systems. It was suggested that the idea of energy piles was to overcome these obstacles. Energy piles was a new ground heat exchanger and was also known as pile tube geothermal heat exchanger. Hamada Y et al. (2007) found that the

plastic heat exchanger tubes of ground source heat pump system was buried in the concrete pile of buildings in construction and was combined with the building structure. Underlying infrastructure to meet the capacity requirements, the most common applications of these systems for energy efficient space heating and cooling for residential and commercial buildings of all sizes have been achieved at the same time. The area and the initial investment of system using geothermal heat exchanger with tubes in pile could be reduced, and it was becoming a new hot spot for ground source heat pump systems research and applications.

This paper introduced the working principle of energy pile system, response of pile to heat exchange and heat tubes of heat exchanger and discussed the considerations of design energy pile system. The classical engineering applications of energy pile system was introduced on the basis of these technical background at home and abroad. Finally, the prospects of the technology in China was analyzed by review of the technology in China's domestic market needs and relevant policies and regulations.

2 TECHNICAL BACKGROUND

2.1 Working principle of energy pile system

Energy pile system was a kind of heat pump technology with carrier of pile and low temperature heat source of soil. It used the characteristics of the soil with relatively stable temperature, relying on a small number of power-driven compressor,

heat transfer between system and the earth could be achieved by circulating fluid (pure water or anti-freeze with water as the main ingredient) flowing in a closed underground. Heat was stored in the summer and absorbed in the winter from the soil so that heat energy could be recycled in winter and summer, by sending wind with the floor or ceiling, in order to achieve the heating and cooling requirements. It had energy efficient, environmentally friendly, etc. which conventional air conditioning system didn't have, was a advanced technology to adapt conservation-oriented society and circular economy.

The working mechanism of the energy pile system was that heat was transferred from one area to another area by circulating fluid. Hepbasli A (2002, 2003) considered that: the operation of the heat exchanger would cause the heat and moisture around the soil simultaneous flowing, the heat transferring was mainly caused by heat conduction and a certain level of moisture migration. Rees et al. (2000, 2009) found that heat should be transferred from molecule to molecule. Heat transferring in porous media could be induced through the following mechanism: thermal convection, conduction and heat transfer caused by state of water changes. Brandl H (2006) confirmed these related processes involved condensation, ion exchange and freeze-thaw cycles. These processes could be considered as heat exchange among fluid, between concrete and soil.

2.2 *Response of energy pile in heat exchange process*

Pahud D and Hubbuch M (2007) and Hamada Y et al. (2007) found that the reported field test of the energy pile system was only related to thermodynamic aspects and heating or cooling behavior of the system currently. Laloui et al. (2006) observed thermal and geotechnical characteristics of the energy piles and found that the axial force was as twice as to the load at pile top under thermal cycling conditions, the heat effect at the pile tip was most obvious when temperature was up to about 15 degrees. Bourne-Webb et al. [13] first studied geotechnical properties of pile affected by the heating and cooling processes. The results showed that heat exchange had almost no effect on the geotechnical properties of the pile. An ideal model was also proposed to explain response of pile to heat load by field tests on energy piles of Lambeth College.

2.3 *Pile tube heat exchanger and form of buried tube*

The traditional vertical tubes system would cause additional costs of drilling and tubes burying,

while energy pile could be described as a new form of ground heat exchanger. Therefore, energy pile ground source heat pump system was also a ground source heat pump system.

An important difference between energy pile heat exchanger and traditional vertical borehole heat exchanger was backfill materials. Li xinguo et al. (2004) found that energy pile heat exchanger needed to bury plastic tubes heat exchanger in the pile foundation of building, and the backfill material was cement concrete. because heat transfer performance of concrete was superior to that of other drilling backfill material. Therefore, heat transfer effect of energy pile heat exchanger was better than drilled borehole heat exchangers with ordinary backfill material. In addition, as the concrete had better compactness, making the tubes and pile foundation, pile foundation and the earth in close contact, could reduce contact resistance, enhance cycle working fluid heat the soil and the earth. Due to the large pile spacing, the thermal interference between the tubes could be greatly reduced, and working conditions of underground heat exchanger was more stable.

There was two main forms of buried tubes in energy piles: one was that heat exchange tubes was preplaced in the steel framework of the piles and buried to the base of the building together as pouring concrete. Another one was that heat exchange tubes was fixed in precast hollow steel cage of foundation in advance. Then it was transferred to the pile well with the reinforcement cage together. The main form of building foundation construction was bored pile, therefore, the application of the second form would be more extensive, and the pile diameter and buried depth of latter was larger than that of the former.

2.4 *Considerations of energy pile system design*

The design of energy pile system was not much different from the ground source heat with other forms of tubes, but special attention must be paid to the system design as following:

1. PE tubes firmly fixed on the steel cage was very critical in the whole production process. The structure of reinforcement cage should be strong enough to protect tubes being damaged. The tubes should always be kept vertical and centered in placement and promotion process, which was conducive to the peripheral resistance and concrete conduit to enrich relatively uniform flow when the pressure piles, without hanging cage or other abnormal failure.
2. Based on the heat balance of the underground heat exchanger, the length of tubes could be determined by smaller load values when the cooling load was greater different from the

heating load. Once the pile diameter and pile length was determined, the number of piles with tubes was also determined. When the energy pile with tubes could not meet the necessary requirements of cooling and heating load, the number of piles should not increase to increase cooling and heating load. Other forms of buried tubes or other supporting measures to increase the cooling tower and boiler was prior.

3. Settlement of pile was a problem of pile tubes system. For high-rise buildings, the tubes would be pulled off or the whole system was down due to great tension load caused by large settlement. Chong zhi and Tang zhiwei (2007) found that the quality of construction and reasonable choice of pile diameter, pile length and aspect ratio should be paid more attention in the construction.
4. Geothermal characteristics of the soil was very important to optimize the parameters of the system.
5. The relevant information was limited.

3 ENGINEERING APPLICATIONS OF ENERGY PILE SYSTEMS IN FOREIGN COUNTRIES

3.1 Energy pile system in Austria, Switzerland and Germany

Austria, Switzerland and Germany were pioneer countries to study the technology in recent decades. Extensive use of energy pile system had become characteristic of Austria. The total number and the annual growing number of energy piles in Austria from 1984 to 2004 were shown in Figure 1. Lainzer tunnel in central of Vienna area was a typical example. A lot of bored piles were used in Lainzer tunnel, where one was set to energy pile in third piles there. Brandl H (2009) found that the absorption energy of the system was not only for heating and cooling of railway stations and other administrative buildings, but also for preventing the freeze-thaw of damage bridges.

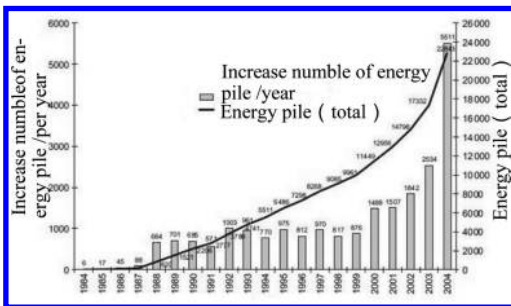


Figure 1. Number of energy pile in Austria.

Boennec O (2008) reported two well-known examples using energy pile system of Swiss Federal Institute of Technology in Lausanne and Dock Midfield Airport in Switzerland shown Figure 2. Ebnöther A (2008) reported that there were 440 piles set in Dock Midfield airport, among which were 300 energy piles for heating and cooling. Performance evaluation found that the heat pump and energy pile system could provide 85% of its annual heating needs (about 2700 MWh/year), conventional refrigeration systems could meet the annual cooling demand (when approximately 1200 MW/year).

Laloui L et al. (2006) reported that the energy pile system was used in the Frankfurt main tower with height of 200 m and some commercial projects in Germany. This foundation of building was made up of 213 piles, of which 112 pile with length of 30 meters were energy piles. Fisch M N and Himmler R found that 200 energy piles were used in the international Solar Energy Center in Berlin, seasonal heat storage could meet 20% of heating requirements and 100% of cooling requirements. The German Federal Government was willing to adopt this new technology and actively promote the development of ground source heat pump market. Sanner B et al. (1996) suggested this alternative energy to achieve economically sustainable using should be considered heating and cooling operation.

3.2 Energy pile system in the United Kingdom and Japan

Energy pile is a relatively new technology in the UK, a large number of studies were researched by many domestic scholars. The Keble College and Lambeth College of Oxford university were the classical project. The first project using energy piles in Britain began in 2001. the technology in the project was from Austria, located Keble College, Oxford. Heat exchange tubes were set up all standard and drilling bitten piles. No problem happened



Figure 2. Dock Midfield Airport.

on the system since running. The initial design of energy pile distribution was shown in Figure 3.

Yashihiro et al. (2007) reported a field test performance of space heat of an energy pile system, the system was applied to a pile foundation of the actual construction, and the heat operation vision chart of the building was shown in Figure 4. The building was completed in October 2000 in Sapporo (Hokkaido, Japan in the western city), including office and residential functions, The underground heat transfer fees was reduced by using friction piles installed a space heating and cooling systems. It was found that the average coefficient of the heat transfer operation was up to 3.9 by long-term measurements of space heat transfer operation, and quarterly energy could be reduced up to 23.2% compared with the conventional air conditioning system.

3.3 Energy pile system in other countries

There was some large ground source energy pile systems in the United States, such as Stockton College. The project was built in the early 1990s

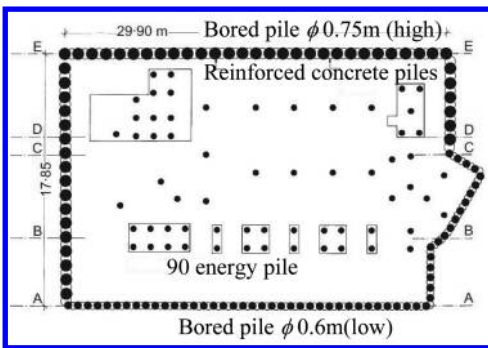


Figure 3. Energy pile distribution of Keble collage.

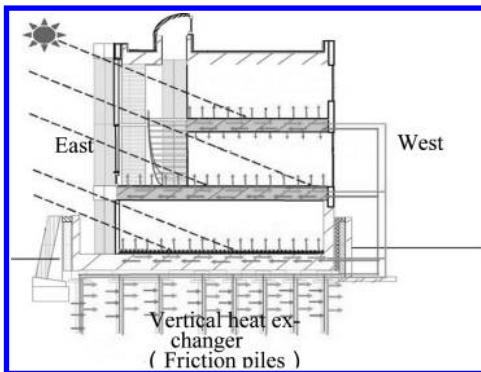


Figure 4. Heat operation of building with energy pile.

and considered to be the world's largest single-season heat underground facilities at that time. Epstein C M (1998) and RSC found that the electricity and gas consumption were reduced by 25% and 70% by using this system, and the system had significance for the whole College's carbon dioxide emissions reducing by 13%. Rybach L (2000) and Yari M and Javani N (2006) reported that Netherlands, Belgium, France, Poland, Sweden, Norway, Canada, Iran and other countries had also adopted the ground source heat pump technology, but progress in energy piles had not been reported.

4 RESEARCH ADVANCES AND ENGINEERING APPLICATION OF ENERGY PILE SYSTEM IN CHINA

4.1 Classical engineering application of energy pile systems in China

Energy pile system was used as cold and heat sources in Expo Axis of Shanghai World Expo project. Yu mingjian et al. (2010) found that the project was a permanent venue and the life of underground tubes was consistent with architecture, combining structural pile layout features and large base area of 130000 m², the use of piles buried way could save investment and achieve better economy.

Huatai Securities Plaza located in Nanjing Hexi CBD core area was the benchmark building of financial agglomeration area in Jiangsu Province. 2275 energy piles with a total amount of 350,000 m was used in ground heat exchanger system. After the completion of the project, 662 tons of standard coal could be saved and 1,721 tons of CO₂ emissions could be reduced per year. It was the landmark project with the maximum number of domestic energy piles and the overall largest, and its technology which put tube outside the cage down to the end of energy pile was domestic initiative.

Tianjin Hang Lung Plaza was listed as a key construction project in Tianjin in 2008. Tongfang ground source heat pump and energy pile technology was first used in the project. The initial investment costs was reduced due to high efficiency of heat transferring, reducing the construction of the underground heat exchangers and the use of the floor area under the building, which land resources was saved greatly.

In addition, ground source heat pump central air conditioning system was also used in Hubei Mobile 3G center building. Energy pile system with 142 double-U and the effective depth of 30 m was used in the ground source heat pump central air-conditioning system. Chong zhi and Tang zhiwei (2007) reported that energy pile system with pile

tubes construction depth of 50 m was also used in clubhouse project in Wenzhou city, Zhejiang province. Only 72 piles could be buried and could not meet the needs of the heat exchanger, therefore, 20 heat exchanger well with depth of 100 m was set on the north side of building. Zhang qin et al. (2007) reported that energy pile system engineering was used Landsea International Block Located in Nanjing.

Currently, energy pile was not universal in the domestic ground source heat pump project in china. On the one hand, the technology had not been fully promoted and a broad social awareness building energy had not yet formed. On the other hand, construction technology of energy pile also needed to be improved. The domestic self-developed technology was used in many energy pile. These projects not only saved energy for the state and society, but also pointed out a new direction for the application of energy piles in China.

4.2 Prospects of energy pile system in China

In China, the total building energy consumption accounts for about 25% of the terminal community energy consumption, where heating air conditioning energy consumption accounts for more than 50% of the total building energy consumption. Therefore, the achievement of economic growth with less energy input is an urgent task of economic and social sustainable development.

Since the late 1990s, it made great progress on research and application of ground source heat pump technology in China. The theoretical and experimental research was very active with engineering applications increasing every year. A series of related policies and regulations had been launched with the rapid development of the domestic ground source heat pump market. The cooperation agreement on the use of geothermal energy was signed by Chinese Ministry of Science and Technology and the U.S. Department of Energy in November 8, 1997, and it was also as the cooperation protocols in the development and using field of energy efficiency and renewable energy technologies of two governments. The People's Republic of China Renewable Energy Law was promulgated in 2005. Beijing had also developed a "Guidance on the development of heat pump systems". The project with source heat pump system could be given some financial aid in the guidance.

In summary, the promulgation of relevant policies and regulations meant the trend of renewable energy to replace conventional energy sources. To vigorously accelerate the development of renewable energy is one main way to construction of a conservation-oriented society and the development of recycling economy proposed by China, and is

an important way of energy saving in "Eleventh five-Year" period.

5 CONCLUSION

This paper describes the technical background, work mechanism and engineering applications at home and abroad of the energy pile. At present the energy pile system as a new technology of ground source heat pump system completely met the needs of sustainable development strategies under background of promoting conservation and energy-saving society, which could be also used as a way to cope with climate challenges and achieve energy saving. The ground source heat pump system would be used more widely under the growing market demand and encouraging to promote policies and regulations. Energy pile as a ground source heat pump technology with low costs and no additional land would also acquire a huge development.

ACKNOWLEDGEMENTS

The authors appreciate the support of the Major State Basic Research Development Program of China (973 program) (No. 2013CB036304).

REFERENCES

- Boennec O. Shallow ground energy systems [J]. Proceedings of the Institution of Civil Engineers-Energy, 2008, 161(2): 57-61.
- Bourne-Webb P., Amatya B., Soga K., Amis T., Davidson C., Payne P. Energy pile test at Lambeth College, London: geotechnical and thermodynamic aspects of pile response to heat cycles [J]. Geotechnique, 2009, 59(3): 237-248.
- Brandl H. Energy foundations and other thermo-active ground structures [J]. Geotechnique, 2006, 56(2): 81-122.
- Chong zhi, Tang zhiwei. Energy pile geothermal heat pump system and its application [J]. Renewable resources, 2007, 25(2): 94-96. (in Chinese).
- Diao nairan, Fang zhaohong. Ground-coupled heat pump technology [M]. Beijing: High Education Press, 2006. (in chinese).
- Ebnöther A. Energy piles: the European experience [C]. GeoDrilling 2008, HakaGerodur, 2008.
- Epstein C.M. Impact of groundwater flow on the Stockton geothermal well field [C]. Proc 2nd Stockton International Geothermal Conference. Pomona, 1998.
- Fisch M.N., Himmler R. International Solar Center Berlin-a comprehensive energy design [C]. Building performance congress, Germany, 2005.
- Hamada Y., Saitoh H., Nakamura M., Kubota H., Oehifuji K. Field Performance of an energy Pile system for space heating [J]. Engineering and Buildings, 2007, 39: 517-524.

- Hamada, Y., Saitoh, H., Nakamura, M., Kubota, H. & Ochifuji, K. Field performance of an energy pile system for space heating [J]. *Energy and Buildings*, 2007, 39(5): 517–524.
- Hepbasli A., Akdemir O., Hancioglu E. Experimental study of a closed loop vertical ground source heat pump system [J]. *Energy Conversion and Management*, 2003, 44(4): 527–48.
- Hepbasli A. Performance evaluation of a vertical ground-source heat pump system in Izmir [J]. *International Journal of Energy Research*, 2002, 26(13): 1121–39.
- Katzenbach R., Clauss F., Waberseck T. Geothermal energy-sustainable and efficient energy supply and storage in urban areas [C]. *The sixth China urban housing conference*, Beijing, China, 2007.
- Laloui, L., Nuth, M. & Vulliet, L. Experimental and numerical investigations of the behaviour of a heat exchanger pile [C]. *Int. J. Numer. Anal. Methods Geomech*, 2006, 30(8): 763–781.
- Li xinguo, Xue yuwei, Zhao jun et al. Experimental study and economic analysis of three underground heat exchanger[C]. *National Machinery Industry Power Technology Information Network 2004 Annual Conference*, 2004: 75–79. (in Chinese).
- Pahud D., Hubbuch M. Measured thermal performance of the energy pile system of the Dock Midfield at Zurich Airport [C]. *Proceedings European Geothermal Congress 2007, Germany*, 2007: 1–7.
- Preene M., Powrie W. Ground energy systems: from analysis to geotechnical design [J]. *Geotechnique*, 2009, 59(3): 261–71.
- Rees S.W., Adjali M.H., Zhou Z., Davies M., Thomas H.R. Ground heat transfer effects on the thermal performance of earth-contact structures [J]. *Renewable & Sustainable Energy Reviews*, 2000, 4(3): 213–65.
- RSC. Energy studies at the Richard Stockton College of New Jersey. 2009.
- Rybach L., Sanner B. Ground-source heat pump systems, the European experience [J]. *Geo-Heat Center Bulletin*, 2000: 16–26.
- Sanner B., Hopkirk, R.J., Kabus F., Ritter W., Rybach L. Practical experiences in Europe of the combination of geothermal energy and heat pumps [C]. *Proc 5th IEA Conference on Heat Pumping Technologies*, 1996, 1: 111–25.
- Thomas H.R., Rees S.W. Measured and simulated heat transfer to foundation soils [J]. *Geotechnique*, 2009, 59(4):365–75.
- Yari M., Javani N. Performance assessment of a horizontal-coil geothermal heat pump [J]. *International Journal of Energy Research*, 2007, 31(3): 288–99.
- Yu mingjian, Wang hao, Ni dan. Underground Space Development of Shanghai Expo Park Expo Axis [J]. *Shanghai Architecture and Technology*, 2010, 2: 5–7. (in Chinese).
- Zhang qin, Yuan dongli, Cheng hongtao. Design of Ground Source Heat Pump Air Conditioning System for Nanjing Landsea 1–6 [J]. *Engineering Experience*, 2007, 5: 35–37. (in Chinese).

Investment efficiency analysis on installing coal ash system in power plants

Feng Dai, Jiao Fan & Yong Lan Xu

School of Business and Management, North China Electric Power University, Beijing, China

ABSTRACT: Coal ash is the main solid waste emission of power plant. Recently the sales rate of coal ash stays at a low level, unsold coal ash require for disposal which will cost highly and pollute the environment seriously. Referring to the technical and economic evaluation about installing grinding system on Pan Mountain Power Plant, the paper discussed the investment efficiency and the feasibility of coal ash classification usage. The results proved that installing grinding system could reduce disposal amount sharply and increase the utilization rate to bring great economic and environmental benefits.

Keywords: coal ash; grinding system; classification usage; techno-economic analysis

1 INTRODUCTION

Coal ash is the inevitable output of thermal power. The coal ash emission amount around the world keep increasing year by year, but the utilization rate still maintains a low level. The developed countries, such as the United States and the Europe, have attached great importance to the comprehensive utilization of coal ash since 1960s. The applications become more and more extensive. The average utilization rate of the European coal combustion products association (ECOBA) member countries is about 48%. According to the American Coal Ash Association (ACAA) statistics, the utilization rate of coal ash in America rose from less than 20% in 1966 to 60% in 2007. Japan, as the world's largest importer country of coal, with a small land and strict environmental demands, started research and industrialization early on coal ash. Nowadays the utilization rate has exceeded 85%^[1-3]. In comparison, India's annual coal ash emission was more than 100 million tons, but its utilization rate was less than 20%.

The comprehensive utilization rate of coal ash in china has increased from 35% in 1994 to 68% in 2011. In 2011, the coal ash production amount reached up to 540 million tons and 367 million tons was used up. However, recently the way to deal with the coal ash is limited to directly selling. Because of the simple production operation and limited chain extension, there seldom have deep processing project, which causing a large pressure on the capacity of the ash field. At the time, the transportation costs, ash field construction costs and the environmental protection costs also bring

great challenges for the generation companies. By the mean of grinding system, the coal ash could be classified into several types, such as I level, II level and III level, which can get huge economic benefits. It also significantly reduces the disposal amount of coal ash by increasing the sales rate, reducing the land occupation amount and relieving the environmental pressure.

2 THE CHARACTERISTIC OF COAL ASH

Referring to the physical properties such as Square-hole sieve allowance, ignition loss and others, the coal ash could be classified into three types, including I level, II level and III level ash according to the GB1596-91 standard. The physical properties and classification standard are shown in Table 1 and Table 2.^[4-5]

Coal ash could be used for construction, back-filling, agriculture and producing building material, such as cement, brick, block, aerated concrete, ceramsite and etc. it also could applies for recycling to extract useful materials. Different usage has

Table 1. The physical properties of coal ash.

	Density g/cm ³	Dense degree %	Weight of screen residue %	
			80 um	40 um
Range	1.9~2.9	25.6~47.0	0.6~77.8	13.4~97.3
Average	2.1	36.5	22.2	59.8

Table 2. The physical classification of coal ash.

Category	4.5*10 ² mm square hole sieve allowance	Ignition loss
I level	<12%	<5%
II level	<20%	<8%
III level	<45%	<15%

different demand for the ash fitness. For example, the dam construction must use I level ash, ensuring the good cement liquidity, uniform distribution and solid body. Superfine coal ash can be mixed to 40% in the cement, which bring great economic benefit. Crude ash could be used to fill road, make aerated concrete block and etc. Therefore, the coal ash processing companies should strive to develop the comprehensive utilization and high processed products, preliminary forming the coal ash “pretreating—high processing—new material” chain, gradually stepping into high processing track of the solid waste.

3 THE INVESTMENT EFFICIENCY ANALYSIS ON INSTALLING COAL ASH GRINDING SYSTEM

3.1 Project background

Pan mountain power plant is in Tianjin, it is 90 kilometer from Beijing to the west and 75 kilometer from Tangshan to the east. It is located in power grid load center. With 1200 MW installed capacity, it generate 6.5525 billion KWh. The company has two sets of 40 t/h sorting equipment and ash field. Its annual coal ash emission amount reach up to 600 thousand tons. Relying on the geographical advantage, the solid waste sales condition was good, the sales rate in 2010 reach up to 95.34%.

3.2 Efficiency evaluation process

The technical and economic evaluation process of coal ash grinding system can be divided into six steps:

1. Making investment estimation. According to the equipment selection and market price, we can figure out the total investment.
2. Making costs estimation. Incremental method was adopted for the technical and economic evaluation of renovation project, so we can ignore the repeated costs which exist no matter the renovation project happened. Assuming the total cost for maintaining the existing management mode is 0, we can figure out the depreciation cost, maintenance costs, wages and welfare, expenditure

- on power and financial costs and other expenses after installing the grinding system.
3. Making the revenue estimate. It also adopt incremental method. We should separately estimate the coal ash sales amount and price under the situation of maintaining the existing mode or installing grinding system.
4. Making incremental cash flow statement. Combined with the collected data, we can figure out cash inflows, cash outflows and net cash flow, finally forming the incremental cash flow statement with the yes-no method.
5. Figuring out the technical and economic indexes. According to the incremental cash flow statement from step 4, we can figure out the indexes, including investment payback period, net present value and else.
6. Making comprehensive evaluation. We can provide the evaluation result referring to the above technical and economic indexes.

The specific evaluation process is illustrated in Figure 1.

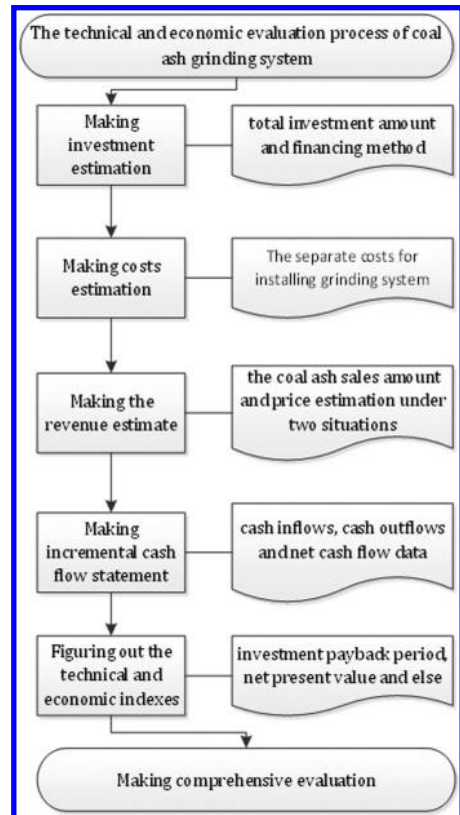


Figure 1. Evaluation process for installing ash grinding system.

3.3 Empirical analysis

Pan Mountain power plant prepare to choose open mill grinding system with 30 t/h output. Based on the existing ash field and classification system, the grinding system take the crude ash after classification as resource [6-8]. Combined with the equipment selection and market price, the investment amount is about 6.1 million. The company adopt loan with an annual rate of 5% as the financing method.

1. Sales amount and revenue

After the system was put into operation, according to the full load running 4000 hours, it can provide an annual 120 thousand tons of I level coal ash. In order to simplify the calculation process, we assume the sales rate as 100%. In 2013, the coal ash output amount was about 464.5 thousand tons and the average price was about 43.4 yuan per tons. It contains 1.1 thousand tons I level ash classified by the current classification system, which benefit 82.9 thousand yuan.

According to the current I level grey price 75.4 yuan/t, after installing the grinding system, the I level ash output reach up to 121.1 thousand tons and get 9.3109 thousand yuan income. The remaining ash still sell at the price of 43.4 yuan/t. finally we

can get the total revenue is about 23.8392 million. The detail about revenue is illustrated in Table 3.

2. Annual total cost

The fixed asset investment is about 8 million yuan. the depreciation adopt average life method, the depreciation years are 20 and the residual value rate is 4%. Time value should be considered, we set the annual loan rate at 5%, the business tax rate at 3% and the education tax and additional rate at 11%. The annual interest cost set as 400 thousand. We assume that there are 5 workers with annual salary of 50 thousand. The system operating with full load would consume 2550 thousand KWh, we set the electricity price as 0.4 yuan/KWh. Equipment maintenance cost set as 2.5% of the original value and the income tax rate set as 25%. The separate cost calculation are shown in the following Table 4.

3. The incremental NPV

Combined by the revenue and cost data under two situation, we can figure out the net cash flow and get the final incremental cash flow statement. It is shown in Table 5.

We can figure out the dynamic investment pay-back period is 9.42 years. The evaluation results show that the incremental net present value is

Table 3. The revenue under two situation (thousand yuan).

Items	Current system	Install grinding system
I level ash amount (thousand tons)	1.1	121.1
I level ash price (yuan/ton)	75.4	75.4
I level ash revenue (thousand yuan)	82.9	9130.9
Ordinary ash amount (thousand tons)		33.89
Ordinary ash price (yuan/ton)	43.4	43.4
Ordinary ash revenue (thousand yuan)		14708.26
Total revenue (thousand yuan)	20160	23839.2

Table 4. The separate costs data (thousand yuan).

	Education tax and additional	Annual financial cost	Salary	Fuel	Equipment maintenance	Depreciation	Annual income tax
Cost	793.5	400	300	1020	150	384	5150

Table 5. Incremental cash flow statement (thousand yuan).

Years	0	1	2	3	4	5	6	7	8	9	10	11-20
Incremental cash flow	-8000	1230	1230	1230	1230	1230	1230	1230	1230	1230	1230	-
Incremental cash flow present value		1230	1120	1010	921.56	838	762	692	629	572	520	-
Accumulative total		-6770	-5650	-4640	-3716.5	-2880	-2120	-1420	-800	-220	300	-
Incremental NPV	2253											

2.253 million yuan and the investment payback period is 9.42 years. It prove that installing grinding system on pan mountain power plant is economic and reasonable. This project has good profitability and anti-risk ability.

4 CONCLUSION

Nowadays the utilization rate of the coal ash around the world stay at a low level and it is limited to simple usage. The paper give out the different economic value of different level ash. It comes to the conclusion that installing grinding system can promote the economic efficiency through the investment evaluation. In the term of economy, coal ash grinding system further promote the utilization rate and make a contribution to the development of coal ash chain. In the term of environmental protection, it relieve the pressure on the ash field and save more land. Therefore the installing grinding system has obvious environmental benefits and social benefits.

REFERENCES

- [1] Tang Yuxiang. Comparative Research on Sino-Japanese Fly Ash Comprehensive Utilization[J]. Journal of Anhui Agriculture Science. 2010, 38(36): 20852–20877.
- [2] RenQian. Analysis of fly ash characteristics and evaluation on its recycling utilization[D]. Beijing: Southwest Jiaotong University: 2009.
- [3] Zhang Hui. The Analysis of Economic and Social Benefits on Installing Coal Ash Grinding System at the Power Plant[J]. value engineering, 2013, 33(2): 55–56.
- [4] Chen L. Flue Gas Desulfurization by Products Additions to Acid Soil: Alfalfa Productivity and Environment quality [J]. Environmental Pollution, 2001, 114 (2): 161–168.
- [5] Zhang Gang, Gui Herong. Stuely on the Chemical Oxygen Demand (COD) reduction of min-ing wastewater by modified fly ash [J]. 2nd International Conference on Asian-European Environmental Technology and KnowledgeTransfer. 2008.
- [6] Zhang Qian, Liang Jie, etc. Comprehensive Utilization of Fly Ash [J]. Guangzhou Chemical Industry. 2013, 41(14): 6–9.
- [7] Aear A. C, Yueel H, Culfaz A. The Synthesis and Sodium-silver Iron Exchange of Sodalites [J]. Chemical Engineering Communications, 2003, 190(8):861–882.
- [8] Yoshitaka Ishikawa, Takashi Kiga. Aiming to Interchange Effective Use of CCP Technology in Asian Countries:Setting up the Committee on Advancing the Effective Use of CCP Technology in JOCAL[J]. International Ash Utilization Symposia. 2009.

Exploration on the ecology dominant development pattern along the Changshuang road

Li Min Bai

Jilin Jianzhu University, Changchun, Jilin, China

ABSTRACT: This paper regards the area along Changshuang road as the research object and explores the development form and pattern of the area along the linear traffic. Thinking practice planning object as a starting point, the author puts forward the research method of the hierarchical and regional urban form and establishes the objective mode of the development form which is mainly dominated by ecology about the research object. The form and development pattern along the Changshuang road area are integrated by segmented pattern and integral pattern. Finally the author points out that the urban form research should pay more attention to the specific form and pattern research of urban local area and that the form and pattern and the planning and control on concrete operated level should be linked in order to guide the planning practice and management on the meso-level and micro-level directly.

Keywords: ecology; along the road; development form and pattern; Changshuang road

1 INTRODUCTION

Since the 1990s, more and more domestic scholars realize the importance of urban form research for the sustainable development of urban health, so the study of urban form is also wide. Regarding the area along the Changshuang road as the research object (As shown in Fig. 1), this paper explores the specific development form and pattern of urban local area or suburban area along the linear traffic in depth. Such development form and pattern is dominated by ecology and regards the urban sustainable development as the goal. It will segment the research object, then choose the development

form and pattern according to its ecological characteristics and finally put forward the whole development pattern of the research object.

2 GENERAL SITUATION ALONG THE CHANGSHUANG ROAD

Changshuang road is the main road to contact the Shuangyang district of Weixing city in Changchun province with the center of Changchun. Changchun is the capital of Jilin province, is located in the northeast plain of China and north-central region of Jilin province. Shuangyang district is located in the southeast of Changchun city, is a municipal district (Weixing city) of Changchun and there are 37 kilometers from the center of Changchun. The position of the area along Changshuang road which is the research object in this paper is within the range of hinterland along the Changshuang road between the center of Changchun and the Shuangyang district of Weixing city. The research object along the Changshuang road is 31 kilometers long. The elastic border control is used on both sides and there is no specific width limit.

Due to the different ecological resources advantages, the natural ecology and industrial distribution along the Changshuang road appear sectional features. The area from Changchun to Sheling is low mountains and hills district where the Dahei mountain is regarded as the resource characteristics. The range of hinterland covers the thick trees and then forms the spectacular forest landscape.

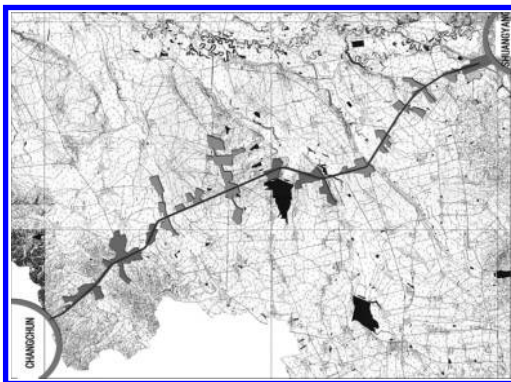


Figure 1. Diagrammatic drawing of the area along the Changshuang road.

The main industry is tourism, the tourism lands like Changchun Jing Yue Tan national forest park, Changchun movie wonderland and a large number of private resorts are all in this area. The area from Sheling to Shuangyang regards the river valley plain which is formed in the ShuangYangHe flowing area as the main resource characteristics. The main industry is agriculture and industry. The agriculture is given priority to rice fields and the spectacular paddy landscape is formed along the way. The industry is mainly in the industrial concentration district of Shuangyingzi town along the Changshuang road.

About the layout of residential areas, there are two big towns along the Changshuang road: Sheling town and Shuangyingzi town. The two towns stride the Changshuang road and present the nodular development. Other rural residential areas present scattered state and distribute linearly along the spontaneous network traffic.

The basic conditions of natural ecological landscape resources along the Changshuang road are superior. But due to lacking of effective control in the long-term development, the spread and development of large amount of private resorts (Changchun—Sheling) occupy and damage forest resources, influence the continuity and traffic of landscape along the road and challenge the ecological function of Dahei mountain. At the same time, the scattered layout of residential areas is harmful to the land consolidation and will damage the environment and landscape seriously. The development and form of industrial concentration district needs to be controlled urgently (the current pattern diagram is shown in Fig. 2).

Based on a new development strategy of Changchun, Shuangyang district is in the strategic position in the future development. As the main road to connect the central city with the Weixing city and due to the radiating and driving effect of central cities, the land along the Changshuang will spread and expand to both sides along the traffic artery. The ecological function which is the important ecological barrier of the Changchun development of Dahei mountain hinterland along the Changshuang road will face challenges. So seeking a kind of

sustainable development form and pattern that the ecology and economy are balanced becomes the urgent matter.

3 THE WHOLE DEVELOPMENT FORM AND PATTERN OF THE AREA ALONG THE CHANGSHUANG ROAD

3.1 *Ecology factors—the whole development mode of the combination of city and natural evolution*

According to the natural ecological conditions, the area along the Changshuang road can be divided into Dahei mountain natural ecological conservation district and ShuangYangHe river valley plains. Fully on the basis of the original natural conditions, the research object will be divided into two sub-zone. They are Sheling zone—low mountains and hills section, Shuangyingzi section—valley plain section. The urban planning and land development of two zones should combine with the natural characteristics of this region and adopt the whole development pattern.

3.2 *Traffic factors—the “string bead type” development pattern along the Changshuang road*

The relationship between urban traffic and urban form is the relation of “trunk” and “shape”. The urban expansion is along the direction of traffic axis with high efficiency, this reflects the basic rule that the economic development should stretch along the direction of the least resistance. The areas around the traffic node are often the most easy to develop. In the city, the node with relatively superior traffic condition and high accessibility is concentrated on the space and then the city will present the characteristics that near the transport facilities.

To avoid the extension and rapid development of urban land along the Changshuang road axis, the TOD development mode is suggested to be used for reference. That is to use the attracted effect of the traffic hub for various urban activities and contact the traffic infrastructure construction with the urban development to form a kind of development pattern with the combination of points and lines. Combining the forward planning that the fast rail line 3 will extend to Shuangyang district, the further integration of land development along Changshuang road is proposed. From the point of view that the natural conservation and urban development are planned synchronously, a new development plan should be established. Several “growth poles” should be located along the Changshuang road (light railway station combines

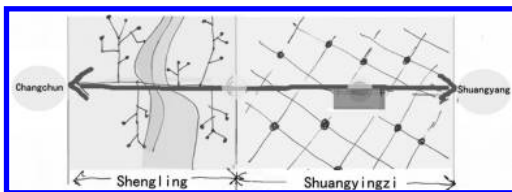


Figure 2. Diagrammatic drawing of the current development pattern of Changshuang road.

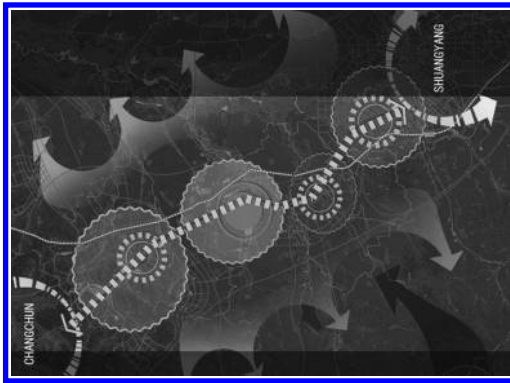


Figure 3. The “string bead type” form and pattern.

with towns). In accordance with TOD mode (As shown in Fig. 3), land development should combine with the rail transit station to ensure the green open space between the “growth poles”, to avoid the land spread and growth and to control the scale of urban construction.

4 EACH SECTION DEVELOPMENT PATTERN OF THE AREA ALONG THE CHANGSHUANG ROAD

4.1 The development pattern of sheling section

4.1.1 “Zoning protection, zoning construction” under the condition of ecological protection

The Dahei mountain area is divided into core reserve, prospective reserve and ecological sensitive area. The core reserve is the Jing Yue Tan forest park. The development and construction of the core reserve is forbidden except the necessary research facilities. Combining with ecological construction and industrial structure adjustment, the existing countries and residential areas can be moved outward gradually. The prospective reserve is mainly the area where the vegetation that has significant effects on the ecological environment in this area grow well like the existing natural forests, natural secondary forest and plantation outside of the legal reserve. The prospective reserve should strengthen the vegetation restoration in the ecological fragile zone and forbid the large-scale development and construction. The ecological sensitive area is the ecological fragile area where has large amount of human activities and serious water and soil loss such as the existing farmland, wasteland and abandoned lands of mines. The construction intensity and scale of development and construction in the ecological sensitive area must be determined reasonably. The protection

and development goals of Dahei mountain should be realized according to the zoning protection and zoning construction.

4.1.2 Industrial development and distribution pattern

The main industry of Sheling is tourism. The distribution of tourism land should adopt the form and pattern of Paris Marne-la-Vallee new town: “bunch of grapes shape” discrete spatial layout form. Marne-la-Vallee new town pillows Marne in the north, leans on the forest in the south, reaches the foot of the platform in the west and approaches the big Maureen river valley in the east. The terrain in the area is undulate and the river wriggles cross. For the sake of the natural space, the construction land on the prior development axis is divided into several relatively independent city groups. Through the rail transit, they connect with the highways and are separated by the north-south green space, and then the “bunch of grapes shape” discrete layout form is formed.

4.2 The development pattern of Shuangyingzi section

4.2.1 Industrial development and distribution pattern

The natural features of river valley plain in Shuangyingzi section gave birth to the fertile farmland, so the agriculture becomes the main industry. The distribution should pay attention to the protection of ShuangYangHe river system. The farmland boundary control should not occupy the necessary land of river system and water conservation. At the same time, the state of farmland matrix should not be crushed by artificial construction plaques and the scale and integrity should be guaranteed. Also, the agricultural sightseeing tourism resources should be developed with the help of vast paddy landscape. Combining the Dahei mountain tourism resources with the tourism of Shuangyang, the tourism industrial chain is formed and the functions of tourist route of Changshuang road are further performed.

The villages and towns industrial concentration district of Shuangyingzi section is the secondary industry which is developed by the features and advantages of Shaungyang sika deer resource. Under the condition of general double phenomena that the economic interests is driven and the current domestic agricultural land resources are occupied, the industrial land still has the trend to be expanded. Without the limitation of natural conditions, the plain characteristic land of Shuangyingzi section is easy to be extended. To prevent the spread with the low efficiency, the boundary of the growth of industrial land (development scale) should be

controlled in the planning. According to the UGB control method (UGB policy is an effective way for America to solve urban spread and to protect natural land, from the perspective of the boundary of the natural evolution, it determines the boundary of the urban development clearly through the detailed survey of natural geography and ecology, the land out of the boundary is strict protection area where the development is not allowed), the natural conservation boundary should be confirmed through the survey of natural geography and ecology. At the same time, in order to control the growth boundary effectively, the corresponding annual allowed development capacity should be formulated and the compact development of construction land should be guided.

4.2.2 The layout and planning control of rural residential areas

Most of the plain characteristic residential areas in Shuangyingzi section along the Changshuang road are dotted. The network layout is connected through the country road system. Also part of residential areas are distributed along the network road. Considering the characteristics that the city construction in plain area is easy to connect with each other, rural land-use planning should adopt the land intensive way to improve the efficiency of land-use. The scattered residential areas should be integrated effectively and distributed compactly to prevent the excessive spread of the construction land. The layout of villages and towns along the Changshuang road hinterland should focus on the node of the network road and with the help of traffic advantages to prevent the continuous arrangement along the road and to protect the continuous natural space of farmland. This makes each artificial living groups scatter in the area like pearls and forms the living habitation which has the country pastoral style outside of Changchun city.

5 THE INTEGRATION OF THE WHOLE AND SECTIONAL DEVELOPMENT FORM AND PATTERN OF CHANGSHUANG ROAD

The area along the Changshuang road is integrated according to the hierarchical and zoning research form, comprehensive form characteristics (As shown in Fig. 4).

Regarding the combination of “string bead type” the whole development pattern and the villages and towns as TOD node.

Combining with the whole urban development method of the natural evolution: Dahei mountain protection area puts forward the development pattern of “zoning protection, zoning construction”. The paddy agriculture that regards ShuangYangHe

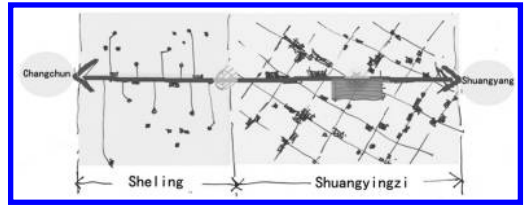


Figure 4. Diagrammatic drawing of the development pattern and form of Changshuang road.

as the main resource characteristics pays attention to the water conservation protection of ShuangYangHe.

Industrial distribution: The tourism is the leading industry. The “bunch of grapes type” distribution technique is put forward about the disordered and extended development current situation of resorts along the road. Combining with the ecology to develop and construct moderately. About the industrial land, the UGB policy should be adopted to limit its border.

Rural residential areas regard the “traffic network” link node as the main construction land to carry the intensive construction and save land resources.

6 CONCLUSION

The purpose of the exploration mode is not to describe the spatial content and form of the ultimate ideal state that the urban spatial development want to reach, it is not a kind of specific spatial structure and spatial form, it is a principle and it is the spatial development strategy in a sense. In addition, the best and general urban form is not existing in the world. About the choice of urban spatial form in the urban planning, there is no paranoid ideas existed in some superior form. The key lies in whether the selected urban spatial form fits with local specific conditions and the principle of the sustainable development. The significance of this paper is to put forward the specific development form and pattern of local area in urban and the paper hopes there are some inspirations to the study of the urban form and pattern.

REFERENCES

- Cui Gonghao, Wujin. 2005. Spatial structure features and development of urban fringe area in China—take Nanjing for example. *Journal of geographical sciences* (2).
- Duanjin. Research on the urban form and the spatial strategy. *Urban planning*, 2003 (2).
- Gukai. 2001. The theory and method of urban form—explore the comprehensive and rational research framework. *The urban planning*, (12).

Research on the green space system planning of Changchun and Eco-city construction

Li Min Bai

Jilin Jianzhu University, Changchun, Jilin, China

ABSTRACT: As the important mode of the sustainable development, the Eco-city construction has become an important subject in planning field in recent years. This paper first analyzes the connotation of the Eco-city. Starting from the practical cases of Eco-city construction and combining with the planning characteristics and history of Changchun green space system, the paper puts forward the green space system which is the important life support system for urban and the planning principles and methods which should be followed when creating the Eco-city.

Keywords: Eco-city; green space system planning; Changchun; the sustainable development

1 INTRODUCTION

The concept of Eco-city is put forward in the process of “MAB” planning research which was initiated by the UNESCO in the 1970s and this marks the transformation of human society from industrial civilization to ecological civilization. The concept of “Eco-city” regards the fighting of the environmental pollution and the pursuing of beautiful natural environment as the starting points. With the progress and development of society and the science and technology, the concept and connotation are also expanding. At present, practical activities of Eco-city have been spread all over the world and these cities embody the concept of the ecology and the sustainable development in some aspects according to their own characteristics.

2 THE PRACTICAL SUCCESSFUL CASES OF ECO-CITY CONSTRUCTION

2.1 *The Berkeley, California in united*

The “urban ecology” organization led by Register who is the advocate of American Eco-city has carried on the effective practice of Eco-city construction since 1975 on the west coast of the coastal city—Berkeley in the United States. After 20 years efforts, a typical Eco-city with the characteristics of both city and township was built up in Berkeley (as shown in Fig. 1). Its idea and practice have the broad influence around the world. Berkeley Eco-city practice pays attention to the natural characteristics, determines that the center service radius is 400 meters and the sub center is 200 meters according

to the walking scale, develops around the center and encourages land mixed use and high-density development. Creating low speed street system, deploying the bus lines, advocating walk instead of driving, delaying and trying to stop the construction of fast lane, inheriting and protecting the historical culture, restoring the abandoned channel and planting fruit trees along the street are all energy use rules. Through these rules, the structure of energy utilization should be improved, the green residence which uses the solar energy should be con optimization for city which uses the wind power generator (the world’s largest wind power plant), solar energy and geothermal energy should be provided.

2.2 *The Curitiba in Brazil*

Curitiba which is located in southern of Brazil is considered to be the city which is nearly the



Figure 1. Eco-city vista in Berkeley.



Figure 2. Eco-city landscape in Curitiba, Brazil.

“Eco-city” in the world (as shown in Fig. 2). After 20 years practice, the development mode of its transit oriented is proved to have good sustainability and praised by the international community widely, at the same time, it is also the learning model of Eco-city construction for developing countries.

The comprehensive planning of urban planning college in Curitiba puts forward the innovative land utilization and management methods with the comprehensive development of land and traffic. Five cities in strategic axis should present linear growth and develop with the commercial district and dwelling district with high density to absorb the rapid increase population. The urban planning should set flood control and increase green space. City should set the economical comprehensive bus system and the express bus transit lines along the five axes to reach 45% rates of taking bus and then to reduce traffic jam.

3 THE GREEN SPACE SYSTEM PLANNING OF CHANGCHUN

3.1 General situation of city development in Changchun

Changchun is located in the hinterland of China northeast Songliao plain where the terrain is flat and open, the natural conditions are unique, the ecological environment is good, the afforestation coverage in the city reaches 39% and the reputation of “forest city” is given. Changchun regards the construction of forest city as the goal. Under the guidance of planning, the external ecosystem of city is improved constantly. In the city, the green system becomes networking and walking system. The ecological parks, city parks, street green space and residential green space are connected organically through river system and roads in order to form the green corridor across the city. The urban

function facilities like living, working, traffic and strolling about or having a rest are scattered in the green to guide urban residents to close green and water, constitute the “green city” that human and the natural environment dependent each other closely and thus to shape the habitable living space that “city in the forest, people in the green” for urban residents.

3.2 Historical characteristics of green space system planning in Changchun

The south of Changchun is surrounded by mountains and waters and the natural ecological wetland with serried river system is in the north, this provides superior conditions for the construction of urban green space system. From the city featured resources, the urban planning of puppet “Hsinking” regards the green open space as framework, the urban function division is reasonable and adopts the ideal park mode. This lays the foundation for today city pattern of Changchun. Since 1980, regarding the enhancing of urban ecological quality as a starting point, the natural ecological environment elements like river, lake and topography should be made full use to built the ecological system with the characteristics of Changchun city. Since 2003, regarding the creating of the “green city” as the goal, the urban green space system should be optimized, the construction of greenbelt around the city, river system greening and ecological corridors should be strengthened, the green space system should be optimized and the green space should be created. For many years, Changchun gradually becomes a modern international city which has the “transparent, sparse and clear, grand and open” characteristics and styles.

In Changchun urban green space system special planning which is Completed in 2008, the green space system planning in the urban area is the space layout of “three sources”, “five areas”, “six wedges”, “ten belts” and “nets”. The starting point of layout is the concept of generalized green space. The surroundings are forest parks (as shown in Fig. 3), water resource protection areas, mountain villages and farmlands which are the main body of the green space ecological structure. Those express the overall concept of natural ecological environment planning in the whole region. The green space system planning layout and pattern in the center of urban are summarized as “one ridge”, “one chain”, “two rings”, “gardens” and “nets”. Taking the central city as the core, it is mainly to complete that the green space covers the entire city. The existing features of natural landscape and historic culture should be expressed fully. The construction of urban public green space should be paid more attention. Taking the Yitong River green space as



Figure 3. The Jing Yue Tan forest park in Changchun.



Figure 4. The Jing Yue Tan forest park in Changchun.

the mapping center, the key is to enhance the green space landscape construction of the main road, strengthen and beautify the important landscape nodes, adjust the structure and layout of land use reasonably in order to achieve the optimum combination of ecological, economic and social benefits.

3.3 Changchun green space system planning under the concept of Eco-city

Based on the regional ecology of Jilin province, Changchun wide-area ecological framework is constructed in order to plan and build the “one ridge, two rivers, four areas” city regional ecological architecture. “One ridge” refers to the Dahei Mountain. In the planning, the planting area should be increased gradually, the management of soil and water loss and the green of barren mountain should be strengthened and the ecological function of soil and water conservation should be enhanced constantly. “Two rivers” refers to the Songhua River and Dongliiao River. In the planning, the protection of main water catchment area of two water systems should be strengthened and the emissions of pollutants should be managed and restricted. “Four areas” refers to the eastern low mountains and hills ecological construction district, the central terrace plain green industrial ecological construction district, the central city ecological construction district and the western lakes plain farming ecological construction district within the scope of urban region.

Considering the development needs of economy and society of the city and the protection requirements of ecological environment, the city regional ecological framework should be built in order to form “one ridge, two rings, three reservoirs, eight wedges” ecological landscape structure. “One ridge” means Dahei Mountains. “Two rings” means the ring road green belt near region and expressway green belt around the city. “Three reservoirs” refers to the three river reservoirs with

the function of water source. It includes Yinmahe River and Shitoukoumen reservoir, Yitong River and Xinlicheng reservoir and Xinkai River and Taipingchi reservoir. “Eight wedges” refers to the eight wedge-shaped open green spaces which are introduced into the central city with the combination of traffic and municipal corridors.

The important ecological green spaces around city like water system, wetland and mountains should be protected and controlled. Four country parks should be set. They are the west lake park, Fufengshan geological park, Yitong river wetland park and the northeast wetland park in Changchun (as shown in Fig. 4).

4 PLANNING PRINCIPLES AND METHODS OF ECO-CITY GREEN SPACE SYSTEM PLANNING

4.1 *The operability of planning objects is the premise to realize the Eco-city*

Eco-city construction should set clear goals and should regard the concrete and feasible content and project as support. The possibility for realizing these goals is very strong. It is also need to have outstanding key construction projects. The Eco-city construction should pay attention to the design of the target at the beginning. Facing the complicated urban ecological problems, the designer should begin from small places. The design of target should be specific and practical and can be directly used to guide practice.

4.2 *Optimizing the functional action of ecological property in the urban fringe*

The environmental texture is respected and the historical context is inherited in order to construct the spatial structural system with urban characteristics. Changchun urban green space

system planning must make full use of the natural conditions and give full play to the existing features of natural landscape and historic culture in Changchun. Regarding the Yitong river basin spatial system as the composition center, the landscape style with connotation of plains should be created and the city characteristics should be built. Through the using of the continuous and opening and closing urban open space sequence with the characteristics of natural geography, topography, history, culture and urban nature, the urban spatial structure which regards the urban green space system as guide also should be built. To seek new integration mode, emphasize the close integration of distribution scale of park green space and recreation and leisure of residents and highlight the creation of external space and pocket green space through grasping the characteristics from the overall structure and form. Changchun features round square should be kept and the construction with level characteristics of urban green space system planning should be developed.

4.3 *The development of circular economy is the key to the success of Eco-city*

The development of circular economy is the important support to realize the ecologicalization of urban economic system and also is the key to the success of Eco-city construction. The key of the Eco-city construction is to introduce the recycled production and consumption model into the process of Eco-city construction. For example, since the early 1990s the Eco-city construction which regards the reducing of waste and the realizing of the circular society as the main content in Kyushu, Japan puts forward the idea that “the wastes arising from the industry might be used for other industries, the overall waste emissions should be zero”. The Whyalla of Australia makes the construction principles of the guarantee of traditional energy, the energy substitution, the sustainable use of water resource and the reuse of waste water and solves the problems of energy and resources of the city.

4.4 *Public participation is an important part of the eco-city construction*

Successful Eco-city construction encouraged the widest public participation. No matter from the setting of planning and formulation, the process of actual construction or the subsequent supervision and monitoring, there are specific measures to ensure the participation of the public. The managers of Eco-city construction should make planning with citizens actively and work with some action

teams, especially the teams related to the environment. The teams can become partners in some specific projects and they are relatively independent at the same time. The wide public participation is an important part of the success of the Eco-city construction.

5 CONCLUSION

Planning should improve the ecology and guide the healthy city life. Urban green space system planning researches the stereo network structural system of Eco-city, stroll and rest and the landscape greenbelt which are formed by the combination of points, lines, and faces with the connection of ring, belt, line, net and wedge. type, scale, characteristics and structural layout of all kinds of city greenbelt should be deployed synthetically and arranged overall. From the angle of constructing the sustainable development city, higher urban green space construction goals should be required and the spacial layout planning of urban green space system should be carried on reasonably. To promote the urban sustainable development through increasing the urban biological diversity and landscape diversity, protecting and improving the urban ecological environment, expressing the ecological benefits of urban green space and optimizing the urban living environment. The urban planning workers in Changchun should always take the harmony of human and nature as the basic requirement of city development and should continuously carry out it to the planning. Through the planning and practice, the city natural elements should be protected, the urban ecological security should be maintained, the combination of artificial and natural living environment should be created and the ecological quality of urban life should be improved effectively. Then the city can move towards the road of Eco-city construction.

REFERENCES

- Li Hao. The “China model” of the Eco-city planning and construction. *Research on urban development*. 2013 (12).
- Lv Jing, Quan Zhen. Research on Changchun green space system planning and urban characteristics construction. *Journal of Jilin Institute of Architecture & Civil Engineering*, 2010 (8).
- Wan Hongyan, 2004. Eco-city Paradigm Research. *Master thesis of Beijing Normal University*.
- Yin Hongyan. The development mode of foreign Eco-city. *Foreign cities*. 2008 (12).
- Yin Shimei, 2004. To the Eco-city: Research on the urban green space planning system.

The thinking of industrial heritage protection and reuse under the background of urban renewal

Li Min Bai

Jilin Jianzhu University, Changchun, Jilin, China

ABSTRACT: In the post-industrial age, more and more urban development enters into the stage of urban renewal. The industrial heritage which is remained in the industrial age faces the realistic problems of the protection and reuse. Taking Shanghai and Changchun industrial heritage protection practice as example, this paper summarizes several models of industrial heritage update and puts forward several methods of industrial heritage protection planning.

Keywords: industrial heritage protection; urban renewal; industrial architecture

1 INTRODUCTION

With the rapid development of industrial technology and social economy, industrial structure and land-use structure of industrial city face the corresponding reform and adjustment, so a large number of industrial heritages produce. Industrial heritage is an important part of cultural heritage and is a sign of times development. It bears the peculiar historical and cultural connotation and has the unique value that can not be ignored. In the Nizhny Tagil Charter, the TICCIH defines the industrial heritage as the industrial civilization remains which have the historical, technological, social, architectural or scientific value. These remains include architecture, machinery, plant, factory, mine field for mineral separation and smelting, warehouse, the sites of energy production, transmission and utilization, transportation and infrastructure and the social activities that are related to the industry like residence, religion and educational facilities.

2 THE PRACTICE OF INDUSTRIAL HERITAGE PROTECTION AND REUSE IN CHINA

2.1 *The practice of Shanghai industrial heritage protection*

From the perspective of the use condition of outstanding modern industrial architecture, some tries and ideas of reuse driven by the government and enterprises have emerged, such as the Mengqing garden (the former Shanghai brewery) (As shown in Fig. 1), the Creek art center (the former warehouse group of FuXin flour factory), the Old

millfun 1933 (the former Municipal butchery) and the 2577 Chuangyi compound (the former Shanghai mechanical bureau/Longhua gunpowder plant) (As shown in Fig. 2). More and more outstanding industrial architectures will move towards the



Figure 1. Shanghai Mengqing garden.



Figure 2. Shanghai Mengqing garden.

positive and dynamic protection and reuse from the idle and declining state and also a large number of general industrial architectures highlight their value in the aspect of history and culture, urban style and features and the sustainable development afresh through the appropriate reuse. Especially in recent years, the accumulation areas of creative industries born naturally in the renovation of old cities and the adjustment of industrial structure provide a kind of new idea and opportunity for the protection and reuse of industrial architecture in Shanghai. Many accumulation areas of creative industries in Shanghai were born in the old factories and warehouses. These old factories and warehouses which sprout the creative industries at the earliest like Tianzifang in Taikang road and Moganshan road 50 now have become a city scenery line. In addition, the Shanghai sculpture space (the former cold-rolled workshop of 10th steel factory in Shanghai), Xujiahui green new landscape (the former greater China rubber factory chimney), “Jinjin apartment” in Pudong Jinqiao (the former idle plant), the “Motel 168” (the former old factory of Yanan pharmaceutical factory) and other old factory reconstruction open the situation of the combination of many forms like the cultural facilities, landscape construction, apartment for the single, economical chain hotels and the industrial architecture reuse. Also with the tourism development of industrial heritage, Shanghai industrial architecture reuse presents the diversified tendency with recreation. Investigating its reason, city structure, the adjustment of layout and the improvement of the quality of city function are big background of the reuse and development of global industrial architecture (community) and its accumulation areas. From the angle of city development, these industrial lands are one of the main factors that can provide opportunities for development. Using and developing a large number of vacant industrial lands, there is no need to remove residences and a mass of financial and material resources can be saved. The industrial lands after the comprehensive redevelopment have special historical space atmosphere. This not only can attract the tourists and promote the consumption in this region, but also can solve the re-employment problem of local laid-off workers through a certain proportional service. Such relatively low price and good location make the cities of every country turn their attention to the development of industrial lands. Hoping this can drive the development and revitalization of urban economy of post-industrial society.

2.2 *The practice of Changchun industrial heritage protection*

Vanke Hills in Changchun project's former address is the Diesel Engine Plant and it is the first industrial architecture renovation project. Here has made



Figure 3. Changchun Vanke Hills 1948 club.

Chinese first tank and marine diesel engine and has glorious red memories. According to the land context and the urban cultural inheritance, the Vanke Hills which is transformed in accordance with the Ruhr in Germany retains the spiritual fortress of the old Diesel Engine Plant. The original transport tracks, water tower, the red brick walls and iron gates in the park make people in Changchun relive the glory of past. About the Vanke Hills project, the first requirement is the buildings should avoid the trees and to keep part of the pines, cypresses, poplars and willows that have the same age with Diesel Engine Plant, the second is to keep some old workshops and the third is to set up a museum and to keep the history of here.

The building elevation of Vanke Hills is simple and rational German style. Some of the industrial former site architectures are kept and repaired in community. Modern architecture is mixed with the red brick walls, rusty steel plates and other old industrial materials. The old factory buildings with Russian style near the street record the red years in the 1950s. Vanke keeps it perfectly and builds it into the business street with both history and fashion sense which is named “Changchun 1948”. 1948 club (As shown in Fig. 3) is the building that the original factory structure is reserved and local parts are constructed afresh and it is regarded as the fitness club for the community. The business street keeps the memory of history which includes the wooden beams workshop and club. In the entrance, the whole wall will be the transplant of old building and the unique architectural shape and five-pointed star of those years are kept. This fully embodies the time aesthetic connotation. The distinctive long wooden beams buildings of the old factory are retained and combined with the modern new buildings.

3 THE REUSE MODEL OF INDUSTRIAL HERITAGE

3.1 *Cultural creative industry*

Cultural creative industry is the important direction of city development in the future. Through the renovation and reuse of the existing valuable

industrial factory buildings, it is possible to attract artists to found studios and then to establish the art market. This can make it become the activity center of artistic creation and exchange with the outside world and a new cultural environment is opened up. Through the creation of the cultural atmosphere, the industrial heritage accumulation area becomes the urban places with the characteristic of landmark. For example, the main buildings of the “798” art park which is located in the Dashanzi area in the northeast of Beijing Chaoyang district are designed and built by the former east German experts in the 1950s and retain the maximum architectural structure of original German Bauhaus design style. In the late 1990s, professors of CAFA rented part of the factory buildings here as art field. This sets a certain tone for the later organization of cultural creative industry.

3.2 Industrial heritage tourism

Maintaining the original environmental atmosphere of industrial estate, basically retaining the original appearance of factory building facilities, even lasting certain production function and keeping the factory operation are the vivid display of industrial civilization. On the basis of these, adding new service facilities to satisfy the new function of industrial heritage tourism services and then the industrial tourism projects can be carried out. The classic case of the model is center shopping district which is located in the Oberhausen. The first iron foundry in Ruhr industrial base was established in 1758. Later in order to solve the unemployment problem produced by the factory closures in the De-industrialization, Oberhausen explores a road for revitalization. Combining the shopping tour with the industrial heritage tourism, a large shopping center is established in the abandoned former address of factory according to the concept of Moore shopping district, at the same time, an industrial museum is also opened up and a giant gasholder is retained. In addition, there are also the matched cafes, food courts, tennis center and civic center. These attract the weekend visitors from the Netherlands to here to go shopping, take a leisurely life and a vacation.

3.3 Museum and exhibition hall

Renovating the industrial architectures of industrial heritage into the buildings for show like museum and exhibition hall is the most common update model of industrial heritage protection. The model uses the characteristics of large span, capacious space and enough daylight of industrial architecture. For example, the predecessor of the Tate Gallery in London (As shown in Fig. 4) is the



Figure 4. The Tate Gallery in London.



Figure 5. Zhongshan Shipyard Park.

bank power station which was built in 1947 and was forced to close.

The Tate Gallery retains the original state of the due to the rising crude oil prices and the replacement power plant furthest and only renovates the turbine room as the exhibition space. It makes full use of capacious space characteristics of the industrial architecture and meets the needs of the exhibition space of modern art.

3.4 Public open space for tour and rest

This model is to renovate the entire factory site into the park to provide unique outdoor activities places of industrial landscape for the masses. Retaining the chimney and water tower which has strong industrial information symbol and regarding them as the landscape elements in the park. For example, the Shipyard park which is renovated from the Zhongshan Yuezhong Shipyard retains the original banyans, revetments and plants and makes use of the chimney and gantry crane to show the combination of industrial aesthetics and natural ecology with modern landscape sketch (As shown in Fig. 5). The original industrial land has pollution problems more or less, so the development

cost is larger. Therefore, using the industrial land with pollution reasonably and building urban public open space or a variety of theme parks through the appropriate ecological restoration are the most distinctive, economical and effective long-term ideal behavior.

4 THE PLANNING AND DESIGN OF INDUSTRIAL HERITAGE UPDATE

4.1 *Remaining original appearance, updating parts*

To conduct the integrated reserve for the industrial heritage, to reinterpret the industrial landscape through the limited new elements and to update and renovate the function transformation which is focused on the interior of the buildings and facilities. Keeping the whole factory structure on design should be paid attention. Partial renovation and update of industrial buildings and facilities are conducted within the environment of the old industry. The broken industrial remains are unified and integrated through new design elements and landscape system.

4.2 *Remaining the essence, blending old and new*

About the essence part of industrial remains, the structural retention should be made. It is mainly the display retention or renovated as the public service facilities. Through the ecological rehabilitation, the surrounding environment is largely different from the original industrial environment. To retain parts of industrial remains and industrial landscape and to build new urban functions or natural landscape on the rest. Getting in touch or making contrast with the old industry to achieve the effect of blending old and new.

4.3 *Creating new images, inheriting peculiarities*

After the demolition of old buildings and the clear of site contamination, the new urban function and urban space are shaped again. The field trace of industrial wasteland is replaced by the target of new image completely.

Industrial heritage witnesses the development of a certain industry of a country or a region. It carries a lot of real information that reflects the industrial history and can let people make scientific and reasonable judgment about the economic society, industrial technology, the level of production and a series of industrial activities at that time. It is important data for the study of the history of a certain industry and urbanization process, it can provide important materials for historical research and has important historical significance. Industrial heritage has the physical and spiritual double value and it is the carrier of industrial culture and an important part of cultural heritage. It has the vital significance for the completely cognition of the evolution and inheritance of industrial culture.

5 CONCLUSION

Industrial history is a part of modern civilization. People often have a kind of special emotion about the industrial architecture of historical heritage, because the specific historical symbols can evoke the memory of people for the special years. The protection and reuse of industrial architecture is beneficial to enshrine memory and to continue the urban context. At present, Chinese industrial heritage protection lacks unified policies and regulations and some regions lack the planning and design with standardization and specialization. Industrial heritage protection and update need to cause enough attention and to play its important value in the urban development.

REFERENCES

- Hou Tingting. 2012. Research on the update strategy of Liuzhou industrial heritage protection under the perspective of cultural ecology. *Postgraduate thesis of Guilin University of Technology*.
- Jin Zhiqiang, Liu Bo. The Community renovation of urban industrial heritage. *Chinese & Overseas Architecture*, 2008 (01): 144–147.
- Yang Xun. 2009. Research on the reuse of industrial heritage in urban renewal, [*Master degree thesis*]. *Chongqing: Chongqing University*.

Influence factors analysis of sulfate attack for cement concrete

Yan-Cong Zhang

Key Laboratory of Highway Construction and Maintenance Technology in Loess Region,
Ministry of Transport, P.R. China

Shanxi Key Laboratory of Highway Construction and Maintenance Technology in Loess Region,
Shanxi Transportation Research Institute, Taiyuan, P.R. China

Ling-Ling Gao

Department of Road and Bridge Engineering, Shanxi Conservancy Technical College, Yuncheng, P.R. China

ABSTRACT: The reason of sulfate attack of concrete was analyzed from Aft damage, $CaSO_4 \cdot 2H_2O$ damage, Mg^{2+} damage and thaumasite damage. Then the effect of performance of concrete itself, corrosion solution, the environment and working conditions on sulfate corrosion of concrete was determined.

Keywords: cement concrete; sulfate attack; influence factors

1 INTRODUCTION

In recent years, highways, bridges, utilities and other engineering were found problems with sulfate attack of concrete, seriously affecting the quality of concrete structures. With the construction of a large number of infrastructure projects, concrete and reinforced concrete works facing huge potential risk by sulfate attack destroyed in a complex groundwater environment.

According to the resultant invasion and destruction of material and type of different hydration products, sulfate cement concrete erosion damage is generally divided into the following types: expansion Aft destruction, $CaSO_4 \cdot 2H_2O$ expansion of destruction, Mg^{2+} erosion and thaumasite type corrosion.

Factors cement concrete sulfate attack of many reasons both concrete aspects of their physical and mechanical properties, but also with the SO_4^{2-} work environment, such as Cl^- , Na^+ , Ca^{2+} , Mg^{2+} , and other content and pH of the solution is closely related, but also with concrete working conditions and ambient conditions such as stress, moisture migration, alternating wet and dry, freeze-thaw cycles, water erosion, and many other factors. To sum up can be divided into four areas: the performance of the concrete itself, erosion solution, the environment and working conditions.

2 THE EFFECT OF CONCRETE ITSELF ON SULFATE ATTACK

Concrete own performance is one of the important reasons for resistance to sulfate attack, and

its own factors include cement mineral composition, amount of mixed materials, but also includes water-cement ratio of concrete admixtures and dense and so on.

2.1 The effect of cement mineral composition on sulfate attack

Different cement in concrete, its resistance to sulfate attack is different. This capability is largely dependent on the mineral composition of the cement clinker content of the mineral composition and relative, and in particular the content of C_3A and C_3S . Because C_3A hydration resulting hydrated calcium aluminate is an essential component of the formation Aft. And C_3S hydration is an essential component of $Ca(OH)_2$ generated by the formation of gypsum, reducing the relative content of C_3A and C_3S correspondingly reduces the likelihood Aft and gypsum formation, so as to effectively improve the ability of anti-concrete sulfate attack.

2.2 The effect of admixtures on sulfate attack

Reasonable incorporation of fly ash, slag, silica fume and other active admixture for concrete sulfate resistance is important to improve the ability of the concrete [1] [2]. In general, the higher the amount of mixed materials, the stronger its resistance was. After the first concrete admixture incorporation activity and the content of C_3A and C_3S can be effectively reduced; secondly, active mixed with the cement hydration products $Ca(OH)_2$ hydration reaction occurs again, thus preventing further erosion of plaster from a certain extent.

Studies have shown that: the sodium concentration of 5%, a pH environment under 3, fly ash content of 40% compared to 20% sulfate resistance improved significantly. But high volume fly ash concrete in wet junction due to salt crystallization prone to surface erosion. When the slag volume reached 60% in order to help improve the sulfate resistance of concrete; while 5% silica fume content perform better than 10%.

2.3 The effect of mix proportion on sulfate attack

Concrete water-cement ratio is larger, the mortar, the greater porosity than the smaller cement. The greater the chance of SO_4^{2-} , Na^+ , Ca^{2+} , Mg^{2+} entering the interior concrete react, the number of micro-cracks and crack the more external ion diffusion rate and the internal rate of precipitation of salts will accelerate the destruction of sulfate attack speed will accelerate.

Reasonable mix can effectively improve the density of concrete, reducing its porosity [3]. Thus, the erosion was harder to penetrate inside the pores of concrete, the sulphate reducing erosion. Another would be a reasonable mix prompted improve the strength of concrete, so the rational design of concrete mix is very necessary.

3 THE EFFECT OF EROSION SOLUTION ON SULFATE ATTACK

Effects of erosion sulfate solution on the concrete erosion include the SO_4^{2-} concentration, the Cl^- concentration and temperature of the solution and the PH value of the solution.

3.1 The effect of SO_4^{2-} concentration on sulfate attack

Erosion solution concentration especially the SO_4^{2-} concentration and temperature have a significant impact on the concrete sulfate attack. Studies have shown that: When small SO_4^{2-} concentrations, erosion product to Aft based; whereas at high concentrations, erosion, gypsum-based products; while the concentration in the middle value, gypsum and ettringite will produce.

Temperature erosion of the solution is different, different speeds concrete sulfate attack. Tests showed that: As the temperature increases, the speed of erosion accelerated. In addition, when a relatively low temperature, corrosion product is not ettringite and gypsum, but $CaCO_3 \cdot CaSiO_3 \cdot CaSO_4 \cdot 15H_2O$, which can result from the concrete to the concrete whole collapsing, causing the concrete unforeseen overall damage.

3.2 The effect of Cl^- concentration on sulfate attack

Because Cl^- permeability greater than SO_4^{2-} [4], when and coexistence, on the surface of concrete, the cement hydration sulphoaluminate reacts first with SO_4^{2-} ; while inside the concrete, the first hydration sulfur Cl^- and aluminum calcium reacts tricosan calcium aluminate $3CaO \cdot Al_2O_3 \cdot 3CaCl_2 \cdot 3H_2O$, thus effectively reducing the possible Aft formation. Therefore, the presence of sulfate attack will ease the situation.

3.3 The effect of solution PH on sulfate attack

With the change in erosion solution PH value, sulfate attack reaction also constantly changing. Studies have shown that: when $12 < PH < 12.5$, $Ca(OH)_2$ and $C-H-S$ begin to dissolve, while Aft crystallization; When $10.6 < PH < 11.6$, $CaSO_4 \cdot 2H_2O$ crystallization; when $PH < 10.6$, Aft begins to decompose; when $PH < 8.8$, even if mixed sulfate attack super plasticizer concrete admixture and activity are inevitable.

4 THE EFFECT OF WORKING CONDITIONS ON SULFATE ATTACK

Concrete working conditions have a more significant impact on its resistance to sulfate attack. Working conditions include: flushing water conservancy, the stress state.

In general, compression concrete structures sulfate corrosion resistance than the flexural, torsion members better. Compressive stress concrete structures balanced tensile stress tensile failure of concrete from a certain extent, indirectly increase the tensile strength of concrete. And withstand bending tensile stress of the concrete will not have this feature. Water Resources Research sulphate resistance of concrete erosion is still inconclusive. Generally it believed that the stress generated by accelerating the development of erosion cracks sulfate attack generated a new round of sulphate accelerated erosion.

5 THE EFFECT OF ENVIRONMENTAL CONDITIONS ON SULFATE ATTACK

Impact of environmental conditions on the concrete sulfate attack is more complex, including: freeze-thaw cycles, moisture migration, alternating wet and dry and so on.

When the concrete in freeze-thaw cycle status, the concrete structure gradually become loose, the intensity will be gradually reduced, while the impermeability of concrete gradually decline into

the internal resistance of concrete that will be reduced infiltration rate will be increased significantly, thus accelerating the damage.

Moisture migration of the solution has a certain effect on the extent of concrete sulfate attack. Reaction with moisture migration needed to continue to be brought into the gap, while the cement hydration products while continuing to drain away, this weak alkaline environment to promote concentration essentially unchanged, the gap that is constantly eroded product produced. Tests showed that [5]: 5% sodium sulfate solution, when the reaction reached equilibrium with a third participate in the reaction, and the only fifth reacted in a 2% solution. Therefore, if the concrete in flowing water, the extent of damage is intensified.

Alternating wet and dry will also accelerate the rate of sulfate attack of concrete []. The reason is that: only when the concentration of the erosion, and the solution reaches a certain dose, the crystals will precipitate, Aft Expansion damage will occur. And alternating wet and dry the solution to accelerate the evaporation of moisture, and an indirect increase in the concentration of the solution, thus accelerating the crystallization of gypsum, prompting Aft type failure of the concrete occurs.

ACKNOWLEDGEMENTS

This research was supported by Shanxi province communications department Science and

Technology Project (2013-1-10), and Shanxi natural science foundation project (2013011027-1).

REFERENCES

- [1] Jeong Jin-Hoon, Dan G., Zollinger P.E. (2006). "Finite-element modeling and calibration of temperature prediction of hydrating Portland cement concrete pavements." *Journal of Materials in Civil Engineering, ASCE*, 18(3): 317-324.
- [2] William G.D., Joe P.M. (1999). "Experimental Verification of Rigid Pavement Joint Load Transfer Modeling with Ever FE." *Transportation Research Record: Journal of the Transportation Research Board*, 1684/1999: 81-89.
- [3] Yao Jialiang, Hu Keyi, Yuan Jianbo (2012). "Mechanical Performance of Interface between Cement Concrete Pavement and Lean Concrete Base Treated with Different Bond-breaking Layers." *Journal of Highway and Transportation Research and Development*. 29 (2):7-12.
- [4] Zhang Ruizhuo, Ling Tianqing, Yuan Ming (2011). "Influence of Asphalt Semi-rigid Base Modules on Pavement Structural Stress." *Journal of Chongqing Jiaotong University (Nature Science)*. 30 (4):755-758.
- [5] Zhao Yanqing, Wang Guozhong, Wang Zhichao (2010). "Cracking Analysis of Asphalt Pavement Based on Dynamic Modulus." *Journal of Human University (Natural Sciences)*. 37 (7):7-11.

Experimental study on cementation strength of unsaturated granite residual soil

L.S. Tang

*School of Earth Sciences and Geological Engineering, Sun Yat-Sen University, Guangzhou, Guangdong, China
Guangdong Province Key Laboratory of Geological Processes and Mineral Resources, Guangzhou, Guangdong, China*

H.T. Sang

*School of Engineering, Sun Yat-Sen University, Guangzhou, Guangdong, China
Guangdong Province Key Laboratory of Geological Processes and Mineral Resources, Guangzhou, Guangdong, China*

X.B. Deng, Z.G. Luo & H.K. Chen

School of Earth Sciences and Geological Engineering, Sun Yat-Sen University, Guangzhou, Guangdong, China

ABSTRACT: The matrix suction widely used in unsaturated soil theory, not representing the interaction between soil particles, is not in conformity with the effective stress principle of soil. The concept of intergranular suction is an important theory, of which structure suction is the characterization of tensile stress between soil particle, embodying the structure characteristic of unsaturated soil. Cementation strength, as an important part of variable structure suction, plays a critical role in the structure strength of unsaturated granite residual soil. While maintaining the original structure of soil and water content, the decreasing part of soil strength caused by the removal of cementing material is just the cementation strength because of the lost of the corresponding cementation. On the basis of the thought, 3 groups of soil samples are picked up in the northeast of Guangzhou city, whose basic physical and mechanical properties are tested, and whose grain size composition analysis is carried on by sieving method combined with laser particle size analyzer, then the native of the 3 groups of soil sample is determined. The relationship between cementation strength and relative contents of free iron are obtained through penetration test, direct shear test and cementation content analysis test, then cementation strength corresponding 100% relative contents of free iron is calculated by binomial regression analysing the experimental data, at last calculation formula and theory model of cementation strength for unsaturated granite residual soil is established, where the absolute content of free iron and water content as the dependent and cementation strength as independent variables. The experiment results and research show that the ratio of cementation strength in unsaturated granite residual soil to shear strength is more than half of the overall strength of soil, and the cementation strength having positive correlation with cementation content, has negative correlation with water content, but the impact of cementation content on cementation strength is greater than water content.

Keywords: granite residual soil; variable structure suction; cementation strength experiment; calculation formula of cementation strength

1 INTRODUCTION

Suction theory is the core of the unsaturated soil mechanics theory as well as the difficulty. The matrix suction of the soil reflecting water absorbing capacity, which is widespread used currently, representing the interaction between soil particle and pore water rather than the interaction between soil particles, is not in conformity with the principle of effective stress of soil. To get rid of this

dilemma, domestic researchers tried to explore the mechanical properties of unsaturated soil from new perspective, such as generalized suction^[1], absorbed suction^[2], structure suction^[3], suction stress^[4], tension suction^[5] and liquid bridge force^[6]. T.S. Tang, etc put forward the concept of intergranular suction (including wet suction and structure suction) on the study basis of the gas-liquid interface soil capillarity around the unsaturated soil particles, surface tension and the structural strength, pointed out

that the existing effective stress principle and shear strength theory of unsaturated soil in the study of unsaturated soil nature cannot succeed, there are two essential reasons: (1) mistakenly believe that the matrix suction is equivalent to wet suction; (2) it is failed to realise that the suction of unsaturated soil is composed of wet suction and structure suction. Structural characteristics of unsaturated soils are usually obvious, so structure suction should not be ignored due to the structural of soil in the study of unsaturated soil mechanics characteristics, especially the particularity in unsaturated soil such as loess, red clay and expansive soil. The structure suction proposed by the author is the characterization of tensile stress between soil particle, mainly includes the cementation force, dipole force, magnetic force, surface force (electric double layer suction) and ion—electrostatic force, etc., is influenced by soil water content, the particle composition and arrangement, the chemistry of pore solution, etc., but the degree of each force affected varies. According to the fact that whether structure suction is affected by the change of water content, the structure suction can be divided into intrinsic structure suction and variable structure suction^[3].

Cementing material and soil particle surface between the chemical potential is foundation of cementation strength. Cementing material can be separated from the pore water under the action of cementation interface chemical force, and then crystallization or adsorption on the surface of soil particles, which can produce bonding force between particles. When saturation of soil is reduced, namely when the moisture is lost or the concentration of the pore solution is increased, minerals in the cement makes the cementation strength between the soil particles increases gradually by crystallization or deposition, which makes a gradual increase in intensity of soil. When soil moisture recover what one has previously lost or lose what one has previously recovered, cementing force will also experience from large to small or change from small to big, the whole process is reversible. Only when the nature or the chemical composition of the pore solution is changed, can the reversible dynamic balance be broken, thus entered a new reversible dynamic balance. Thus, the constitutive relation between bonding force and the degree of saturation is determined by the water, -soil chemistry, which is an important part of the variable structure suction.

Granite residual soil, a kind of typical red clay in southern China, has a strong structural. A group of scholars's research, such as CHENG^[7], shows that the granite residual soil particles is mainly connected in the form of point contact by cementation of free iron oxide^[8], which makes the structure of the soil have a certain strength. But after the

removal of free iron, the structure strength will disappear or weaken, then shear strength is reduced. Therefore it can be believed that the change of the soil strength is derived from the degradation of cementation strength caused by the loss of cementing material, namely the decrease of soil strength is the cementation strength caused by the corresponding removal of cementation, whose value is equal to the difference of soil strength before and after lossing of cementing material, such relationship as follows:

$$p_s = \tau_0 - \tau_f \quad (1)$$

where p_s is cementation strength, τ_0 is soil's shear strength before losing the cementing material, τ_f is soil's shear strength after losing the cementing material.

Above is the theoretical basis and core of this paper, which is also the difficulty. Considering there exists lots of closed pore in the granite red soil, when infiltrating wash in penetrating fluid, because of the limitations of contact area, especially the cementation in closed pores has no seepage to wash, so chemical reaction is incomplete in the process of infiltrating washing, at the same time in order to keep the original structure of soil samples, and soil samples can not be scattered grinding fine soil particle to increase the contact area with hydrochloric acid, therefore some part of the cementing material residues is left over in soil samples, and therefore it cannot be simply thought the cementation strength of the soil sample could be determined by measuring the mechanical properties of the cemented soil samples before and after lossing cementing material. But it should be noted that although cementing material cannot be completely removed, soil sample shear strength changes with the gradual loss of cementing material, and there exists one-to-one corresponding relations between them, so the cementation strength of the soil sample after removing completely the cementing material can be deduced according to the shear strength of soil sample corresponding to the different removal degree of cementing material, on the basis of which the cementation strength of the soil sample can be calculated.

2 SPECIMEN PREPARATION

According to the regional geological data of Guangdong Province, there is Yanshanian stage 2 intrusive granite exposed widely, partial inclusion of rock mass of Yanshanian stage 4 in the north-east of Guangzhou city. Thus, Yantang, Plum garden and Cencun in the northeast of Guangzhou city are selected in this experiment as a sampling

Table 1. Basic physical and mechanical properties of soil samples.

Soil sample	MHY	YT	CC
Water content (%)	29.56	24.19	21.53
Wet density (g/cm ³)	2.10	1.95	2.16
Dry density (g/cm ³)	1.63	1.57	1.78
Void ratio (<i>e</i>)	0.79	0.87	0.60
Cohesion (kPa)	21.37	28.13	19.94
Internal friction angle (°)	21.96	23.12	28.58

settings (respectively number of MHY, CC and YT), where regional rocks are Yanshanian stage 2 granite. Samples are selected in three fresh profile of typical granite residual soil, sampling depth controlled in 1.2~3.0 m, to facilitate comparison, which are in gravel layer, sand layer and homogeneous layer respectively.

Grain size composition analysis is conducted by sieving method combined with laser particle size analyzer. grain size composition analysis with 0.075 mm diameter as experimental watershed, the screening method is used to analysis particles whose size greater than 0.075 mm, and laser granularity instrument is used to analysis particles whose size less than 0.075 mm. Classified by the mass fraction of the particles whose size greater than 2 mm, soil sample MHY is confirmed for sandy sticky clay, soil sample CC for gravel sticky clay, soil sample YT for cohesive soil. In order to better understand the basic physical and mechanical properties of the soil, at the same time provide a reference and contrast for the later strength test, the basic physical and mechanical indexes of the soil sample are tested, and the test results are shown in Table 1. Table 1 illustrates that the shear strength of soil sample CC is higher, followed by soil sample YT, soil samples MHY lowest, which may be closely related with water content of soil samples.

3 EXPERIMENT PROCESS AND METHOD

The experiment focuses on the analysis the change of soil samples' strength before and after the removal of cementation, therefore, the test of removal cementation is the key to the research, cementing material is dissolved with penetration test combined with vacuum pump, and then the cementation strength of the soil sample after completely removing cementation can be deduced according to the change of shear strength of soil samples corresponding to the different removal degree of cementation, on the basis of which the cementation strength of soil samples can be calculated.

3.1 Total process of experiment

When tested, the three kinds of samples were divided into 6 groups, one group of which (no. I) is used as a contrast, the rest are used respectively for penetration test (no. II~VI). Penetrating fluid is 3 mol/L HCL, and penetration time is controlled respectively for 2, 4, 6, 8 and 10 days, penetration process shown in Figure 1. Penetrating fluid head is 1 m, vacuum at 0.6 bar. The original water content of soil samples is recovered after the completion of permeability (drying and wetting it over and over again at low temperature, and let stand for 24 hours, error control in the plus or minus 3%), and the shear strength (τ_0 , τ_f) and iron content of soils are measured.

The test results of II~VI and I are compared, then different iron content in the corresponding shear strength difference (that is the cementation strength) are available, and characteristic curve of the cementing strength changing with cement content are drew, on the foundation of which the relation and the curve of free iron oxide content and the corresponding soil shear strength is explored.

3.2 Shear strength test

Shear strength test is taken by ZJ-2 Strain-controlled direct shear apparatus for quick shear test. To more intuitively reflect the change of soils' intensity values, facilitating subsequent calculations, this test directly read of peak intensity of direct shear test, and additional vertical load is 100 kPa, instrument correction coefficient 1.76.

3.3 Cementation content analysis test

Atomic absorption spectrometer (ASS) is applied in this test. Samples must be crushed to 200 mesh before test, then are weighed 0.2 g and 0.4 g by electronic scales. 8 mL aqua regia (2 mL nitric acid, 6 mL hydrochloric acid), 3 mL hydrofluoric acid are added into 0.2 g sample, and aqua regia and hydrofluoric acid are double in the 0.4 g sample, shaken well, placed on the electric heating plate heated dissolving a certain time until all aqua regia and hydrofluoric acid are evaporated to dryness, to

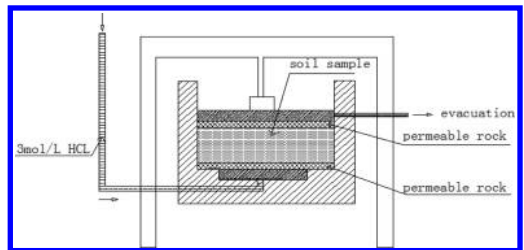


Figure 1. Penetration test schematic diagram.

maintain 150°C for 2 hours, got rid of SiF₄, plus nitric acid of 5% to dissolve the crystal half an hour appropriately using waste heat, finally placed to 100 mL than plug pipe and stand still. Samples are tested by flame AAS method, the standard solution of Fe: 1 mg/L, 2 mg/L, 3 mg/L, 4 mg/L, 5 mg/L.

4 EXPERIMENTAL RESULTS

After infiltrated wash in penetrating fluid of hydrochloric acid, the shear strength of samples are decreased while maintaining the same original

structure of soil and water content, the difference of soils' shear strength is equal to the cementation strength value in corresponding with the removal cementation in the penetration test. The test results are in Table 2.

Through penetration test, total iron content in the soil samples also will reduce accordingly, test results in Table 3. Existing research shows that In the granite residual soil of Guangdong Region, free iron accounted for the proportion of the total iron content is higher, the ratio between 70%~80%, the higher weathering degree, the higher the ratio; the opposite is small^[9]. The soil samples from Yantang (YT),

Table 2. Cementation strength in corresponding with the removal cementation material in different penetrating time.

Soil samples	Penetrating time (d)	Cementation strength in corresponding with the removal cementation (kPa)					
		Accumulated amount			Amount of different period		
		MHY	CC	YT	MHY	CC	YT
II	2	0.74	0.93	0.69	0.74	0.93	0.69
III	4	2.17	2.79	2.03	1.43	1.86	1.49
IV	6	3.57	4.61	3.18	1.40	1.82	1.15
V	8	4.75	6.12	4.34	1.18	1.51	1.16
VI	10	5.32	6.84	4.97	0.57	0.72	0.63

Table 3. Total iron content before and after removing cementation.

Soil samples	Penetrating time (d)	Total iron content (%)		
		MHY	CC	YT
I	0	3.2821	3.4263	3.1609
II	2	3.1807	3.3224	3.0732
III	4	2.8769	3.0183	2.8195
IV	6	2.6999	2.8423	2.6509
V	8	2.5751	2.7161	2.5307
VI	10	2.4954	2.6355	2.4577

Table 4. Relative contents of free iron* in soil samples before and after removing cementation.

Soil samples	Penetrating time (d)	Accumulated amount (%)			Amount of different period (%)		
		MHY	CC	YT	MHY	CC	YT
I	0	0	0	0	0	0	0
II	2	4.12	4.33	3.47	4.12	4.33	3.47
III	4	16.46	17.01	13.50	12.34	12.68	10.03
IV	6	23.65	24.35	20.17	7.19	7.34	6.67
V	8	28.72	29.61	24.92	5.07	5.26	4.75
VI	10	31.96	32.97	27.81	3.24	3.36	2.89

*Annotation: Relative content is the percentage of the change of free iron and the original content of free iron in the soil.

cohesive soil, has the highest soil weathering degree, the soil samples from Plum garden (MHY), sandy sticky clay, the second, and the soil samples from Cen Cencun (CC), cohesive soil, has the minimum weathering degree. Based on the different weathering degree of the soil samples, the test determines the free iron in the soil sample YT accounts for the ratio of total iron content is 80%, soil sample MHY 75%, and soil sample CC 70%. Thus, the changes of free iron content can be calculated before and after the test, and the results are shown in Table 4.

With simultaneous Table 2 and Table 4, the relationship between cementation strength and relative contents of free iron can be obtained, as shown in Figure 2. At the same time in order to have cementation strength corresponding all free iron, Binomial regression analysis is carried out on the data of Figure 2, and relationship formulas between each cementation strength and relative contents of free iron of three kinds of soil samples are obtained, as shown in Table 5, then cementation strength corresponding 100% relative contents of free iron can be calculated by corresponding formula. According to Table 5, cementation strength corresponding all free iron is 35.77 kPa, 43.00 kPa and 40.04 kPa

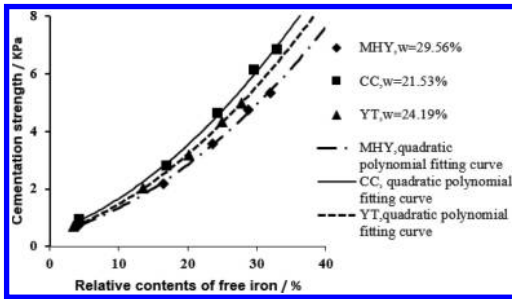


Figure 2. Relation curve and prediction analysis between cementation strength and relative contents of free iron.

Table 5. Test results analysis.

Soil sample	Relationship between cementation strength and relative contents of free iron	Correlation coefficient	Cementation strength corresponding 100% relative contents of free iron	Peak intensity of direct shear	Ratio
MHY	$p_c = 0.0029w_c^2 + 0.0636w_c + 0.4099$	$R^2 = 0.98$	35.77 kPa	60.73 kPa	58.90%
CC	$p_c = 0.0034w_c^2 + 0.0853w_c + 0.4696$	$R^2 = 0.97$	43.00 kPa	74.41 kPa	57.79%
YT	$p_c = 0.0032w_c^2 + 0.0765w_c + 0.3898$	$R^2 = 0.97$	40.04 kPa	68.86 kPa	58.15%

*Annotation: p_c is cementation strength, kPa; w_c is relative content of free iron, %.

respectively, soil sample MHY highest, followed by soil sample CC, soil sample YT minimum. The ratio of three bond strength to their shear strength is roughly equal, about 58%, more than half of the overall strength of soil, which demonstrate that cementation is of great significance on the strength of granite red soil. With goethite cemented kaolin as the object, from the number and strength of bond hydrogen, C.B. CHENG^[10] have measured cementation strength of kaolinite in the natural state, whose theoretical value is 39.9 kPa, which can match well with the experiment results. This prove the test results are reliable, and the test method has a certain guiding significance.

5 CALCULATION FORMULA OF GRANITE RESIDUAL SOIL'S CEMENTATION STRENGTH

According to the Figure 2, relative content of free iron oxide could be converted to absolute content, thus the corresponding relation of the absolute content of free iron under different water content and cementing strength may be established. At the same time due to the incomplete removal of free iron, test results can't fully display all the change law of cementation strength, so in order to improve the accuracy of the regression analysis. According to the relationship formulas in Table 5 between cementation strength and relative contents of free iron, the cementing strength could be calculated respectively when the relative contents of free iron is 40%, 50%, 60%, 70%, 80%, 90% and 100%, and the relative content of free iron is converted to the absolute content, through binary regression analysis, cementation strength calculation formula can be established, where free iron absolute content and water content as the independent variable, bond strength as the dependent variable.

$$p_c = 16.5346w_c - 0.3675w_w + 3.6862, R^2 = 0.95 \quad (2)$$

where p_c is cementation strength, kPa; w_c is the absolute content of free iron, %; w_w is water content, %; R^2 is correlation coefficient.

At this point, a formula is established in this study which can intuitively reflect relationship between the water content, free iron content and cementation strength. In the application of this formula, only need to measure to measure soil moisture content and free iron content, the cementing strength of the unsaturated clay granite can be more quickly and accurately calculated, which provides a new angle for theory research and practical engineering application of unsaturated soil suction. Although the water content and free iron content determines the cementing strength together by a Formula (2), the effect of free iron content on the cementation strength is greater than water content.

It should be noted that Cementing strength affected by water content and free iron content, is also affected by other factors such as temperature, PH^[11], whose affection mainly reflected on the coefficients and constant, so the cementation strength formula should have the following form:

$$p_c = K_1 w_c + K_2 w_w + K_3 \quad (3)$$

This is also the model of theory formula of cementation strength, where K_1 , K_2 and K_3 are related to such factors as the temperature and PH.

6 CONCLUSION

1. Cementation strength is an important part of variable structure suction in the unsaturated granite residual soil. While maintaining the original structure of soil and water content, the decreasing part of soil strength caused by the removal of cementing material is the cementation strength because of the lost of the corresponding cementation.
2. Granite residual soil particles connect each other mainly by cementation of free iron oxide in the form of point contact. The ratio of cementation strength to shear strength is more than half of the overall strength of soil, which demonstrate that cementation is of great significance on the strength of granite red soil.
3. This paper established calculation formula and theory model of cementation strength for unsaturated granite residual soil, where the absolute content of free iron and water content as the dependent and cementation strength as independent variables, which show that the cementation strength having positive correlation with cementation content, has negative correlation with water content, and the impact of

cementation content on cementation strength is greater than water content.

ACKNOWLEDGEMENTS

The research work was supported by the National Natural Science Foundation of China (Grant No. 40872205), Specialized Research Fund for the Doctoral Program of Higher Education (No. 2012017111.0031), Guangdong Natural Science Foundation (No. 07003738), and Science and Technology Planning Project of Guangdong Province, China (No. 2008B0.30303009).

The first author: Liansheng TANG, professor, doctoral adviser, E-mail: eestls@mail.sysu.edu.cn.

Corresponding author: Haitao SANG, doctoral candidate, E-mail: 772192033@qq.com.

REFERENCES

- [1] Shen Z.J., 1996, Generalized suction and unified deformation theory for unsaturated soils, *Chinese Journal of Geotechnical Engineering*, 18, 1–9.
- [2] Tang L.S., Wang S.J., 2000, Absorbed suction and principle of effective stress in unsaturated soils, *Chinese Journal of Geotechnical Engineering*, 22, 83–88.
- [3] Tang L.S., 2000, Structure suction and principle of general effective stress in unsaturated soils. *Acta Scientiarum Naturalium Universitatis Sunyatseni*, 39, 95–100.
- [4] Lu, N., Likos, W.J., 2006, Suction stress characteristic curve for unsaturated soils, *Journal of Geotechnical and Geoenvironmental Engineering*, 132, 131–142.
- [5] Luan M.T., Li S.Q., Yang Q., 2006, Matric suction and tension suction of unsaturated soils, *Chinese Journal of Geotechnical Engineering*, 28, 863–868.
- [6] Zhang Z., Liu F.Y., Zhang, G.P., etc., 2013, Microscopic hydraulic behavior from the interactions between uneven-sized wet particles and liquid bridge, *Journal of Hydraulic Engineering*, 44, 810–817.
- [7] Cheng C.B., Xu C.W., 1986, Property of the cementing material and its influence on mechanical characteristics for residual soil from granite, *Rock and Soil Mechanics*, 7, 61–66.
- [8] Zhang X.W., Kong L.W., Wang J., 2013, Experimental study of SEM-EDS for cementation bond characteristics of Zhanjiang clay *Rock and Soil Mechanics*, 34, 195–203.
- [9] Wu N.S., 2005, A study on characteristics and some engineering problems of granite residual soil with structural nature, Nanjin, Nanjing Forestry University.
- [10] Cheng C.B., Chen Q., Liu S.J., etc., 1998, Microscopic study on cementation strength in soils, *Journal of Huazhong Agricultural University*, 17, 143–149.
- [11] Kong L.W., Luo H.X., 1993, Effect of the conversion in form of free iron oxide on the engineering property of the red clay, *Rock and Soil Mechanics*, 14, 25–39.

Application and experiment research on diaphragm wall foundation in bridge engineering

Lei Wang, Wei Ming Gong & Guo Liang Dai

School of Civil Engineering, Southeast University, Nanjing, Jiangsu Province, China

He Guo

China Urban Construction Design and Research Institute, Beijing, China

ABSTRACT: The diaphragm wall used for deep foundation in bridge foundation construction is a new attempt in China. Its force mechanism is very complex, and there are very few situ test data about this new form of bridge foundation. In order to study the deformation behavior of diaphragm wall, the field measurement was carried out in Yanhe bridge in Yanan city. The horizontal and vertical displacements of the diaphragm wall were tested in this measurement. The construction situation and process were introduced at great length. The key technology about the joint of the diaphragm wall was presented. The result indicated that the diaphragm wall used for bridge foundation could bear the vertical and horizontal load effectively, and the displacement was controlled in the design scope.

Keywords: bridge abutment; diaphragm wall foundation; field experiment; displacement

1 INTRODUCTION

The diaphragm wall was invented in the first half of the 20th century, at that time it was used for waterproofing or retaining structure. It was introduced into China at the late 1950s. At the present stage, diaphragm walls were widely used in civil engineering such as excavation engineering, metro station, bridge engineering, basement engineering and so on. But in these engineering, most of the diaphragm walls were used just for supporting or temporary structures. When the main structures were finished, the diaphragm walls were useless and were removed. This caused a huge waste. So, recently the diaphragm walls started to be used for load bearing wall in high-rise building or underground substation, and when the main structures were finished the diaphragm walls were preserved permanently and bear the upper load. This method achieved remarkable economic effect.

However, in bridge construction engineering, most of the diaphragm walls were only used for supporting or temporary structures in China. There were many long-span bridges which adopted the diaphragm walls engineering, such as the 4th Nanjing Changjiang River Bridge, Huangpu Zhujiang River Bridge, Wuhan Yangluo Changjiang River Bridge, Runyang Changjiang River Bridge and so on. The sizes of the diaphragm walls in these bridges were very large.

For example, the plan view size of the diaphragm wall in the 4th Nanjing Changjiang River Bridge was 82 m × 59 m, with the depth was 40~50 m. Although these diaphragm walls were very large, their main functions were as temporary structures to retain water and soil press. The design generally did not consider their carrying capacity. This method of work was not economic.

Compared with China, Japan did more diaphragm walls in civil engineering especially in the fields of bridge constructions. Japanese different method of work was that the diaphragm wall was used for lower part of bridge foundation which was called diaphragm wall foundation to bear the upper load. In China, the first method of work like this was an over line bridge in state road 209 line in Shanxi Province. In this paper we would introduce the second diaphragm wall foundation in Yanhe River Bridge in Shaanxi Province. Both of the two bridges were in the northwest of China. This area was Chinese loess area. Loess had the good orthostatic characteristics. The horizontal bearing capacity of the bridge foundation was the control target in this area. Connecting the single diaphragm wall into closed diaphragm wall foundation with structural connector could obtain large horizontal bearing capacity. The common used types of closed diaphragm walls foundation were in [Figure 1](#). The internal space of the closed diaphragm wall foundation could be filled by soil or concrete.

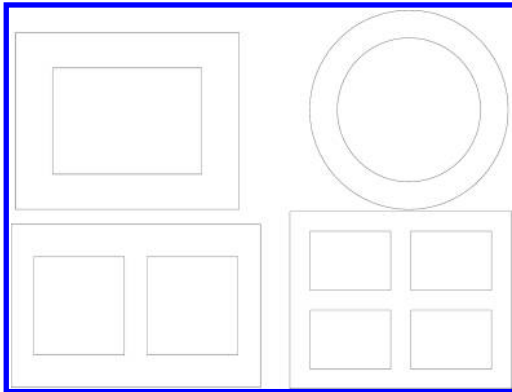


Figure 1. Common used types of closed diaphragm wall foundation.

In this paper, we would introduce the second diaphragm wall foundation in Yanhe River Bridge in detail. The construction method and step were summarized. The vertical and horizontal displacements of the diaphragm wall were given. The deformation regularity was analyzed. The results showed that the diaphragm wall foundation could control its deformation effectively. The displacements were suitable for the design requirements. The diaphragm wall foundation will be widely used in bridge construction in China.

2 ENGINEERING BACKGROUND

Yanhe River Bridge was built in 1958. It was a three-span stone arch bridge with clear span of 30 m, with full-length of 120 m and the height of the arch is 6.6 m. More than 50 years of application, there were some problems appeared in the bridge. It already could not satisfy the current traffic demand and use. So, the local government decided to widen and strengthen the old bridge. Yan'an was a famous holy land of revolution. Yanhe River Bridge located at the middle of Baota Hill and Qingliang Hill. It was the landmark building of this revolution scenic area. In order to retain the status of main structure and outlook style of the bridge, the new bridge was the same structure and outlook with old bridge, which was a three-span stone arch bridge with clear span 30 m. The site actual picture of Yanhe River Bridge was shown in Figure 2.

The old bridge foundation was gravity type u-shaped abutment foundation. If the new bridge foundation used the same foundation style with the old one, there need deep foundation excavation. The bridge is located at the downtown area and closed to the underground business district, it



Figure 2. The site actual picture of Yanhe River Bridge.

Table 1. The soil parameters.

Soil layer number	Allowable bearing capacity (Kpa)	Frictional resistance of pile (Kpa)	Standard penetration test
Thick pellet soil ②	200	100	11.7
Silty soil ②-1	100	15	4.3
<i>Sandstone ④</i>			
Strong weathered	500	130	
Weak weathered	1200		

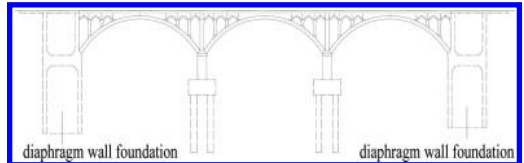


Figure 3. The layout elevation of the new bridge.

was very strict for the excavation support. So the diaphragm wall was used as excavation support. In the loess region the soil had promising future due to its advantages such as small water content, high strength, low underground water level, easy construction into the groove, self-standing, short project execution time, without mud protection and so on. The soil prospecting parameters were shown in Table 1. These conditions were extremely advantageous to use diaphragm wall. The closed diaphragm wall had a larger contact area with the surrounding soils to get greater wholeness. It had great horizontal stiffness and was able to withstand larger vertical load and horizontal load. From what had been discussed above, there had the feasibility and economy obviously to use the diaphragm wall as supporting structure, at the same time as the bridge foundation. The layout elevation of the new bridge was shown in Figure 3. The plane dimensions of the diaphragm wall founda-

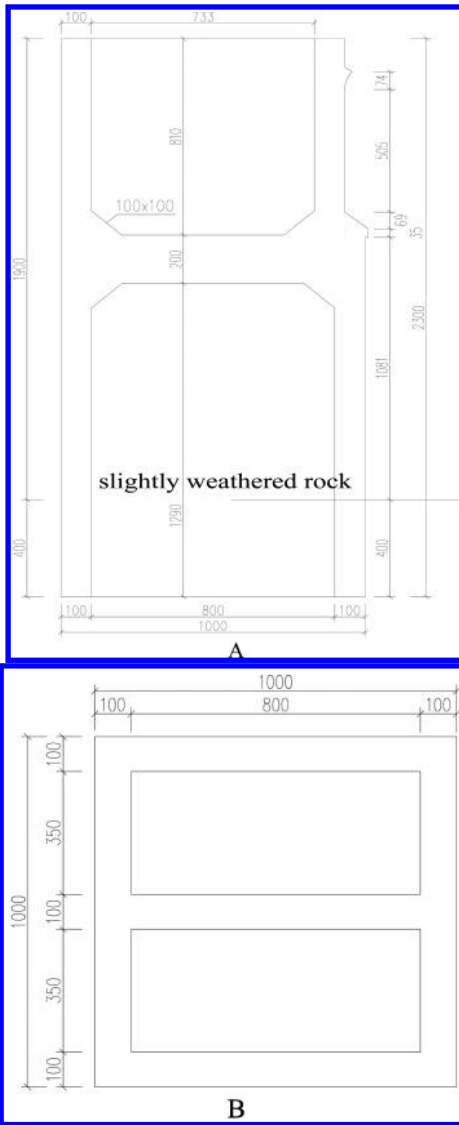


Figure 4. The layout plan of the diaphragm wall foundation.

tion were 10 m × 10 m with the thickness was 1 m. Dimensions and design of the foundation are indicated in the layout (Fig. 4).

3 CONSTRUCTION METHODS AND STEPS

Using the good self-standing feature of the loess, half of the diaphragm wall foundation was constructed first liked “E” glyph. Then another half of

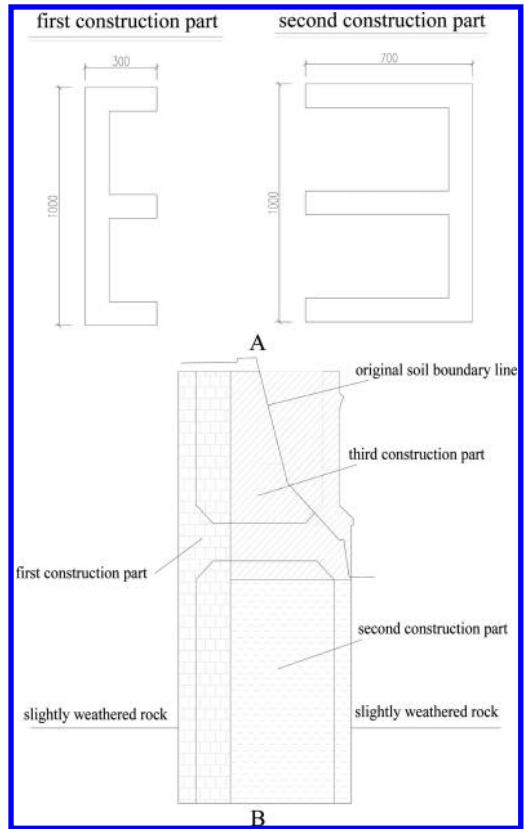


Figure 5. The sketch diagram of construction steps.

the diaphragm wall foundation was constructed. The construction method adopted binding reinforcement and pouring concrete in situ after the soil was excavated. The sketch diagram of construction steps were shown in Figure 5. From Figure 5, we could see the diaphragm wall closed to the soil was constructed as supporting structure to resist the soil pressure at first. After the diaphragm wall reached the design strength, the soil was excavated, the excavation depth was 4 m below the slightly weathered rock. Then the second part of diaphragm wall and the cross beam were constructed. Finally, the third part of diaphragm wall on top of the cross beam was constructed and the soil was backfilled the same as the original.

The actual pictures of construction process were shown in Figure 6. Figure 6 was explained in detail as follow: A was the first half of the diaphragm wall foundation liked “E” glyph. B indicated the excavation depth was 4 m below the slightly weathered rock. C and D were the actual pictures of binding reinforcement and pouring concrete for another half part of the diaphragm wall below the

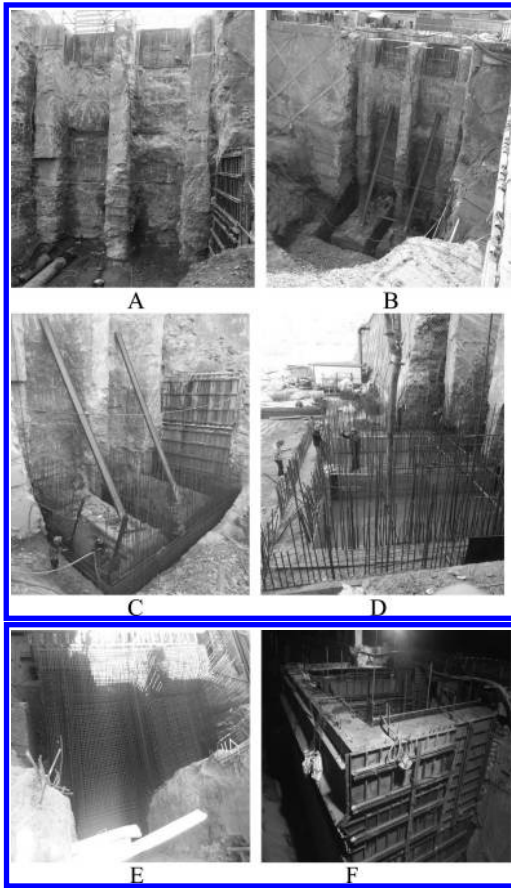


Figure 6. The actual pictures of construction process.

cross beam. When all the diaphragm wall foundation was finished after pouring concrete, it was shown in F.

In this project, the joint construction of the diaphragm wall is one of the most key technologies. There are two kinds of construction technology for joint: flexible joint and rigid joint. When the diaphragm wall is just for supporting structure, the flexible joint can satisfy the requirements of soil retaining and permeability. This diaphragm wall foundation was as part of the main bridge structure to be permanent underground foundation. This diaphragm wall foundation in addition to meet the requirements of permeability and retaining, also require the strong shear capacity. Such so, the rigid joint was used in this project. The construction drawing design of the rigid joint was shown in Figure 7. The bonding steel plate could withstand the shear force of the joint seam caused by two parts of the diaphragm wall foundation. This bonding steel plate could cause the two

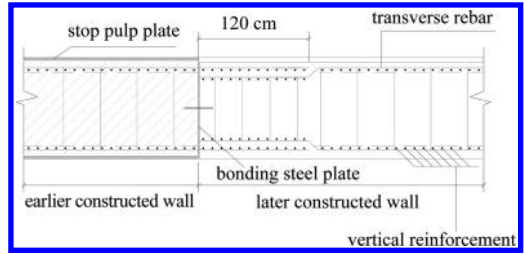


Figure 7. The construction drawing design of the rigid joint.

parts of diaphragm wall shared the vertical load of the upper structure together and coordinated the uneven settlement. At the same time, this bonding steel plate had good water sealing performance.

4 FIELD EXPERIMENT ON HORIZONTAL AND VERTICAL DISPLACEMENTS

The horizontal and vertical displacements are the control factors for this bridge foundation design. So when the bridge foundation was constructed, the horizontal and vertical displacements of the diaphragm wall foundation were tested at the same time. The horizontal and vertical displacements were measured by total station and sliding micrometer respectively. The horizontal displacement curve changed with time was shown in Figure 8. Figure 8 showed that the horizontal displacement was increased as the time changed. There were seemed 3 growing trend stages in the curve. During the early 20 days the horizontal displacement was increased sharply. That was because the excavation was digging to the design elevation during this period of time. During the period of the next month, the horizontal displacement curve had a gentler gradient and had some fluctuations or undulating. This was caused by the construction process which the concrete was poured, especially the filling concrete in the void of the diaphragm wall foundation had a great influence on the horizontal displacement. The third stage was from 7 May to 29 May, when the main bridge arch was built on the diaphragm wall foundation. This indicated that the main bridge arch could cause the diaphragm wall foundation had a great horizontal displacement. It also provided that the diaphragm wall foundation bear huge horizontal load caused by the main bridge arch.

The vertical displacement curve changed with time was shown in Figure 9. The vertical displacement was increased as the time changed. The curve seemed the same variation tendency with the horizontal displacement curve. From Figure 8

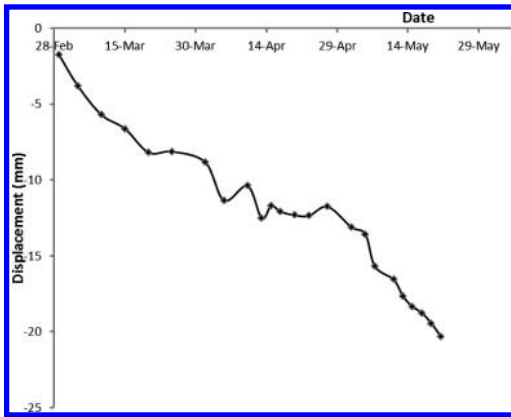


Figure 8. The horizontal displacement curve.

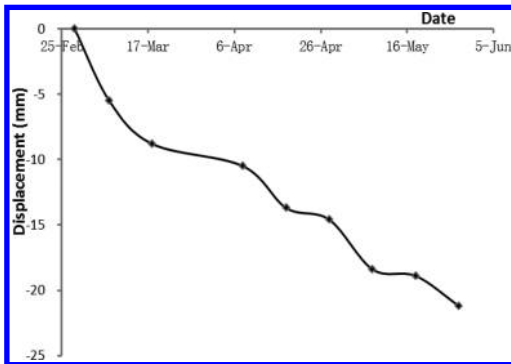


Figure 9. The vertical displacement curve.

and Figure 9, it could be indicated that both the maximum horizontal displacement and vertical displacement were no more than 25 mm. The displacement did not reach the alarm value of design. The diaphragm wall foundation could bear both the horizontal and vertical load to control the displacement under the design allowable value.

5 CONCLUSION

The second engineering practice which made the diaphragm wall foundation as part of main structure of bridge foundation in China was introduced in this paper. The construction method and procedures of the diaphragm wall foundation were introduced in detail. The key point of construction—the construction method of the joint of the diaphragm wall foundation were presented. Combined with the practical engineering Yanhe Bridge, the design control index of horizontal and vertical displacements were tested in construction

site. The test result showed that both the horizontal and vertical displacements were no more than 25 mm. The diaphragm wall foundation could bear both the horizontal and vertical load to control the displacement under the design allowable value.

In our country, the design and construction levels of diaphragm wall foundation were behind Japan, Europe and other developed countries. Especially in the bridge construction project, although the diaphragm wall foundation was often used, more of them were used as supporting structure. The supporting structure was temporary. When the main structure was completed, the supporting structure was thrown out of use. This will undoubtedly cause a huge waste of resources. Yanhe Bridge engineering practice had been setting a good example for how to use the diaphragm wall foundation to be main part of the bridge structure. The newly built Yanhe Bridge had been opened to traffic successfully on August 1, 2013. At present, the bridge is running in good condition. We believe that the diaphragm wall foundation will be wildly used in Chinese bridge construction.

ACKNOWLEDGMENTS

This research was sponsored by the China Urban Construction Design & Research Institute and Yanan city construction bureau. Senior engineer Guo, professor Gong and Dai gave a lot of supporting for this project. The authors appreciate the support of special project of important science and technology of transport of ministry of transport in twelfth five year plan period (No. 2011318494160).

REFERENCES

- Chen Song, Xing Peilin, Ye Jiawan. Analysis on design method of super-deep foundation pit diaphragm wall as the main structure [J] Building Structure, 2012, 42(9):48–51.
- Chen Xiao-dong, Gong Wei-ming, Meng Fan-chao, Li Tao. Test on vertical bearing behavior of shaft diaphragm wall foundation. [J] Chinese Journal of Geotechnical Engineering, 2007, 11(29):1665–1669.
- Dai Guo-liang, Gong, Wei-ming, Li, Hui, Zhou, Xiang-qin. Load-transferring Method of Closed diaphragm Wall Foundation [J]. Journal of Civil, Architectural & Environmental Engineering, 2011(33):96–99.
- Duan Chao jing, Xu Wei, Xu Chao ran. Construction Technology of Super-deep Diaphragm Wall of Fourth Nanjing Changjiang River Bridge. [J] Construction Technology, 2010, 39(2):39–42.
- Guo hui guang, Sun wei, Xu wei. Gigantic slurry wall-analysis of load-bearing properties in construction section of circular slurry wall. [J] Building construction, 2004, 3(26):188–190.

- Song Zhang, Cheng Qian-gong, Gong Wei-ming, Chen Xiao-dong. In-situ static vertical loading test on rectangular diaphragm wall in loess subgrade. [J] *Rock and Soil Mechanics*, 2008, 10(29):2713–2718.
- Tian Xin, Yao Zhi-an, Fang Hui. Construction Techniques for Excavation and Lining of North Anchorage Foundation Pit of Suspension Bridge of Huangpu Bridge over Zhujiang River in Guangzhou, [J] *Bridge construction*, 2008, 6:49–52.
- Xiong Xiao-bo, Sun Jun, Xu Wei. Construction Technology of North Anchor Foundation Pit of Runyang Bridge [J] *Construction Technology*, 2003, 8(32):4–6.
- Xu An-jun, Wang Jian-hua, Ding Yong-chun. Diaphragm construction technology for deep excavation of South Tibet Station of Shanghai Metro [J]. *Chinese Journal of Geotechnical Engineering*, 2007, 28(B11):1664–1672.
- Xu Zhonghua, Wang Jianhua, Wang Weidong. Deformation behavior of diaphragm walls in deep excavations in Shanghai [J]. *China civil engineering journal*, 2008, 41(8):81–86.
- Weng Qiping, Wang Weidong, Zhou Jianlong. Design of diaphragm wall of an ultra-deep cylindrical excavation constructed by top-down method [J] *Journal of Building Structures*, 2010, 31(5):188–194.

The influence of Shrinkage-Reducing Agent on the early-age shrinkage under the different curing system and mechanical properties of concrete

Qing Wei Fang, Jun Ying Lai, Xiao Qian Qian & Kai Dong

College of Civil Engineering and Architecture, Zhejiang University, Hangzhou, China

ABSTRACT: Concrete is currently the most widely construction materials. As is more and more complex construction condition, shrinkage and cracking are frequent phenomena. It is necessary to apply a variety of methods to solve the reduction of shrinkage and cracking of concrete. This study used a Shrinkage-Reducing Agent (SRA) to reduce the early-age shrinkage and to value the effect of the SRA on the mechanical properties, simulating the actual construction environment (focus on wind speed and sealed curing). Concrete was prepared with a JZ, a PCA and a SRA. The early-age shrinkage and the autogenous shrinkage of concrete is tested, by using concrete tester of CABR-NES/E non-contact shrinkage deformation. Also compressive strength, splitting tensile strength and flexural strength were determined, according to GB/T50081-2011. The results show that the SRA reduces some mechanical properties of concrete and the greater the wind speed, the greater the shrinkage of concrete. SRA can also help reduce the early-age shrinkage of the concrete at the different wind speed and in field applications, attaches great importance should be given to the sealed curing system, and as far as possible to avoid the wind.

Keywords: early-age shrinkage; autogenous shrinkage; wind speed; mechanical properties

1 INTRODUCTION

In recent years, the cracking phenomena of concrete have been quite severe, causing the direct or indirect economic losses to amazing degree. As we all know, the contraction deformation of the concrete under constraint conditions is mainly caused by the early shrinkage cracking, such as plastic shrinkage, drying shrinkage, temperature shrinkage, autogenous shrinkage, chemical reduction and uneven shrinkage and so on. When this constraint deformation caused by stress or strain is greater than the ultimate tensile strength and ultimate tensile strain of concrete, cracks will be produced.

At present, for the extensive use of C30 or C40 ordinary concrete in the field of civil engineering, the cracking has been most easily caused by the plastic shrinkage and the drying shrinkage. Therefore, the study of these two kinds of shrinkage and crack has become a focus in the field of civil engineering. To settle the problems in practical applications, various approaches have been proposed and followed: increased attention to early-wet curing practices that reduce evaporation or provide external water, optimization of the mixture proportions to increase the aggregate volume fraction, usage of internal curing using lightweight aggregates and applications of mixing admixtures (SRA) or fiber (such as polypropylene fiber) to improve

the plastic shrinkage crack resistance of concrete. Some researchers have employed expansive additives to counteract shrinkage.

Research on shrinkage reducing admixtures was first initiated during the 1980's in Japan and led to the development of the first generation of SRA [1–2]. Today, several various SRAs are commercially available, and although they do not exactly have the same chemical composition, they are similar in nature and all serve to reduce the surface tension of concrete's pore fluid [3]. During the past 30 years, various research studies [4–11] have been performed to evaluate the performance of SRAs and to quantify their shrinkage reduction capacity in concrete mixtures. It has been shown that by lowering the surface tension of pore fluid, SRA can reduce drying shrinkage of concrete by up to 50% [5, 10].

Some negative side effects have also been reported, in contrast to the significant advantages of SRA in improving the shrinkage performance of concrete. Namely, it has been observed that SRA reduces the rate of cement hydration and strength development in concrete.

Although extensive research has been performed on measuring the shrinkage and mechanical properties of concrete containing SRA, very few studies have looked at the effect of SRA on the shrinkage of concrete based on the construction environment

(this paper focuses on wind speed). This study provides testing support in order to further improve the shrinkage of concrete theory, at the same time, and the test is available for construction enterprises in the process of working to help reduce indirect cracks of concrete during construction. It has certain theoretical significance and engineering practical value.

2 MATERIALS, EXPERIMENTAL PROGRAM AND TEST METHODS

2.1 Materials

2.1.1 Cement

Portland cement (C) with a P.O 42.5 grade from Hangzhou Huawei Building Materials Co., Ltd was used. The physical properties and chemical compositions of the cement are presented in Table 1 and Table 2.

2.1.2 Fine aggregate

Natural sand was used as fine aggregate in this study. The properties of the fine aggregate are shown below: Fineness modulus is 2.5 and apparent density is $2.63 \text{ g} \cdot \text{cm}^{-3}$.

2.1.3 Coarse aggregate

The crushed quartzite stones were used as coarse aggregate in this study had 31.5 mm maximum size.

2.1.4 Chemical admixtures

In this study, SRA and a high-range water-reducing admixture from the Jiangsu SoBote New Materials Co., Ltd were employed. Table 3 displays the properties of the two admixtures including their designations, brand names (trade names), chemical names, color, and specific gravity.

2.2 Experimental program

To explore the effect of SRA on the early-age shrinkage at the different curing system and mechanical properties of concrete, different concrete mixtures were prepared. Table 4 displays the mixture proportions and Table 5 shows the design of curing environment.

2.3 Test methods

The concrete was mixed in a forced mixer. The slump test and the initial setting time was executed in line with GB/T50080-2011.

For the each of the mixtures, compressive strength and splitting tensile prisms were casted and tested at 3,7,14 and 28 days, respectively, using $100 \text{ mm} * 100 \text{ mm} * 100 \text{ mm}$ cubic moulds conforming to GB/T50081-2011. Concrete specimens ($100 \text{ mm} * 100 \text{ mm} * 400 \text{ mm}$) in accordance with GB/T50081-2011 were prepared to measure flexural strength after 3,7,14 and 28 days, respectively. After 1 day, all the specimens were demolded and

Table 1. Physical properties of cement.

	Setting (Time/min)		Flexural strength/Mpa		Compressive strength/Mpa	
	Initial	Final	3d	28d	3d	28d
Soundness						
Qualified	125	187	5.7	7.75	25.3	49.56

Table 2. Chemical compositions (by mass, %) of main materials.

Material	CaO	SiO ₂	Al ₂ O ₃	Fe ₂ O ₃	MgO	SO ₃	LOI	Total
Cement	55.9	21.0	10.5	4.5	3.3	21.0	1.5	

Table 3. Properties of chemical admixtures.

Admixture designations	Brand name	Chemical name	Color	Specific gravity
PCA	PCA-I	Polycarboxylate superplasticizer	Dark brown	$1.03 \text{ g} \cdot \text{cm}^{-3}$
SRA	SBT®-SRA (I)	Polyether type	Light yellow	$1.01 \text{ g} \cdot \text{cm}^{-3}$

Table 4. Mix proportion of concrete.

Code	Mix Proportion/(kg·m ⁻³)					SRA
	Cement	Water	Sand	Stone	PCA	
JZ	386	185	784	1150	0	0
PCA	386	185	784	1150	3.474	0
SRA	386	185	784	1150	3.474	5.79

Table 5. The design of curing environment.

Code	Curing environment
1	Temperature: 20°C, relative humidity 60 ± 5%, sealed
2	Temperature: 20°C, relative humidity 60 ± 5%, wind speed: 0.7 m/s
3	Temperature: 20°C, relative humidity 60 ± 5%, wind speed: 1.1 m/s

moist-cured at 20°C and 95% relative humidity until testing.

To value the early-age shrinkage of concrete, all the mixtures were sealed before the initial setting time to guarantee there being no drying shrinkage before measurement. At the initial setting time, all the specimens were opened, at the right point when the early-age shrinkage arose and the measurement began. Figure 1 exhibits the experimental equipment for shrinkage measurement in detail, by using concrete tester of CABR-NES/E non-contact shrinkage deformation from BOYUAN TECHNOLOGY Co., Ltd. The size of each specimen was 100 mm*100 mm *500 mm. 2 mm Teflon plate and two layers of plastic film were placed at the bottom of concrete prisms to decrease the frictional resistance respectively. Furthermore, Teflon plate and plastic film were also set around paste specimens to prevent the paste leakage when casting and vibrating. The Teflon plate was drawn off when the moment measurement started.

3 EXPERIMENTAL RESULTS AND DISCUSSION

3.1 The results of the properties of the fresh concrete

The test results for the fresh concrete with the different mixtures are showed in Table 6. As can be seen in Table 6, the addition of PCA-I leads to a remarkable increase in the slump and the initial setting time compared to the JZ, but the addition of PCA-I and SBT[®]-SRA (I) causes a slight increase

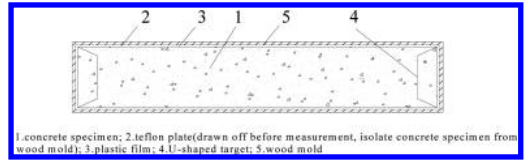


Figure 1. Full figures of concrete shrinkage measurement equipment.

Table 6. The properties of the fresh cement.

Code	The initial setting time (H:M)	The slump (mm)
JZ	4:12	25
PCA	6:30	130
SRA	7:18	140

in contrast to PCA. It should be noted that mentioned that another option could have been to maintain a constant PCA-I dosage and reduce the mixing water to obtain the desired workability when using SBT[®]-SRA (I) for these mixtures.

3.2 The results of the strength of concrete

The results of compressive strength, splitting tensile strength and flexural strength of concrete are showed in Figure 2–4.

It can be seen in Figure 2 that the 3d compressive strength of only mixed water-reducing agent decreased by about 9%, the 7d compressive strength reduced about 8.9%, the 14d compressive strength by about 7.9% and the 28d compressive strength reduced 3.8%, compared to the JZ; the 3d compressive strength of concrete with PCA-I and SBT[®]-SRA (I) reduced about 22.6%, the 7d compressive strength decreased by about 17.7%, the 14d by about 16.5% and the 28d compressive strength reduced about 13.5%, compared to the JZ.

From Figure 3, the 3d splitting tensile strength of only mixed water-reducing agent decreased by about 16.7%, the 7d splitting tensile reduced about 20.1%, the 14d splitting tensile by about 22.4% and the 28d splitting tensile strength reduced 4.50%, compared to the JZ; the 3d splitting tensile strength of concrete with PCA-I and SBT[®]-SRA (I) reduced about 49%, the 7d splitting tensile strength decreased by about 47%, the 14d by about 29% and the 28d splitting tensile strength reduced about 17.20%, compared to the JZ.

It can be found in Figure 4 that the 3d flexural strength of only mixed water-reducing agent decreased by about 8.7%, the 7d flexural strength

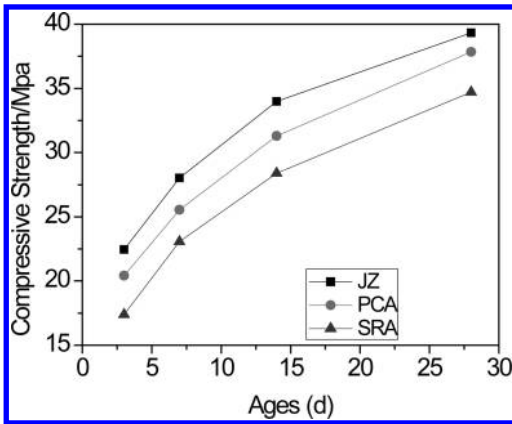


Figure 2. Effect on compressive strength of concrete with and without SRA.

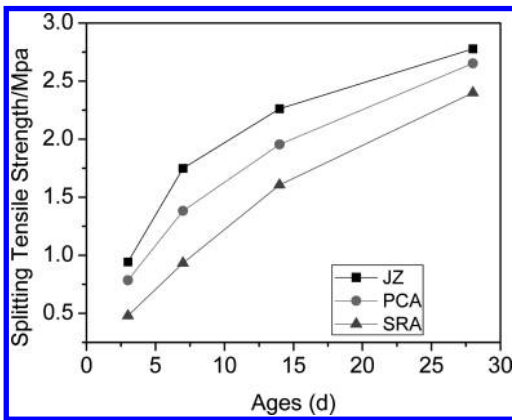


Figure 3. Effect on flexural strength of concrete with and without SRA.

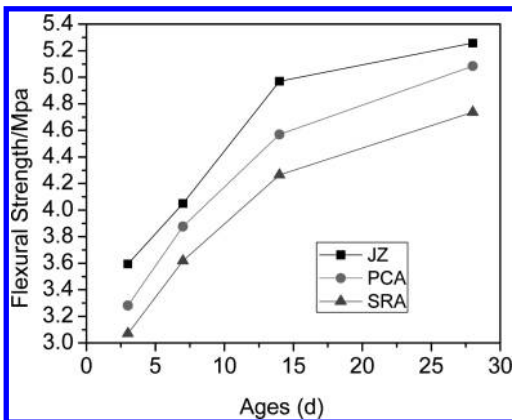


Figure 4. Effect on splitting tensile strength of concrete with and without SRA.

reduced about 4.3%, the 14d flexural strength by about 8.1% and the 28d flexural strength reduced 3.3%, compared to the JZ; the 3d flexural strength of concrete with PCA-I and SBT®-SRA (I) reduced about 14.5%, the 7d flexural strength decreased by about 10.2%, the 14d by about 14.2% and the 28d flexural strength reduced about 9.9%, compared to the JZ.

It is interesting that under the condition of the same water/binder ratio, the concrete with the water-reducing agent or the water-reducing agent and the shrinkage-reducing has an adverse influence on the development of the strength of the concrete. A large number of researchers [12–15] have found that the unit weight of concrete decreases and the air content of concrete increasing with the usage of the water-reducing agent or the shrinkage-reducing agent, indicating reduction in mechanical properties of concrete.

3.3 The results of the shrinkage of concrete

Starting from the initial setting time, the free shrinkage of sealed specimens after 120 hours is shown in Figure 5 and the shrinkage of concrete prisms with 0.7 m/s and 1.1 m/s wind speed is shown in Figure 6 and Figure 7.

From the free shrinkage in Figure 5 it can be noted that the shrinkage rate (the expansion rate) in about 7 hours after the initial setting time is extremely high, but then experiences a phase of relatively slow expansion. As is shown in Figure 5 and Figure 6, all the concrete shrinkage curves go through approximate linearly increasing, a phase of inflation instead of shrinkage, and then begin to shrink, but the shrinkage rate of concrete is quite small.

From the Figure 5 and 6, under the condition of the same mixture ratio and the different curing environment, the contraction of shrinkage-reducing

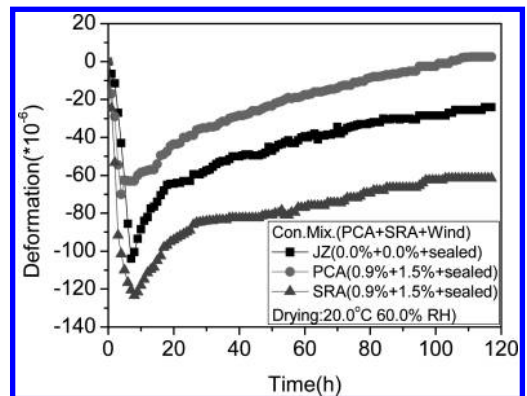


Figure 5. The free shrinkage of sealed specimens.

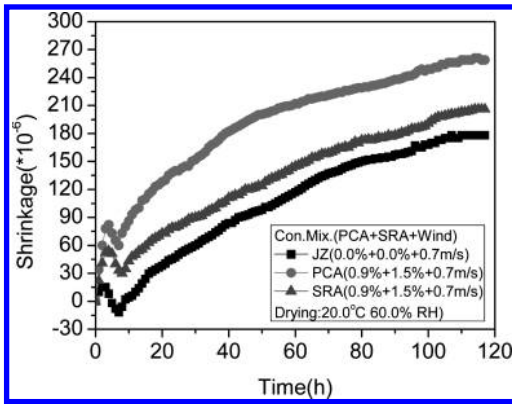


Figure 6. The early-age shrinkage of concrete with 0.7 m/s wind speed.

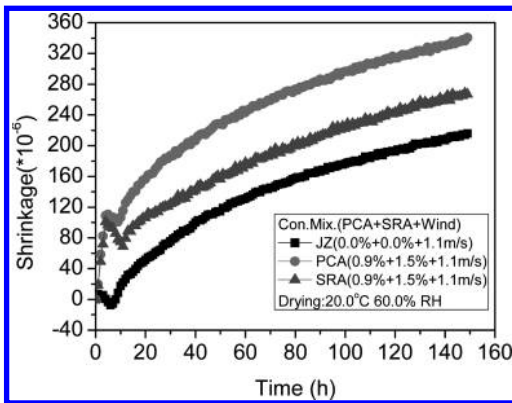


Figure 7. The early-age shrinkage of concrete with 1.1 m/s wind speed.

agent has a significant effect. From the values of the early-age shrinkage of concrete, it could be calculated that the early-age shrinkage rate of PCA was 1.46 times that of the JZ and 1.26 times that of the SRA in Figure 5, and the shrinkage rate of the PCA was 1.57 times that of the JZ and 1.27 times that of the SRA in Figure 6. The reasons for these may be as follows:

(1). In the case of the same water/binder ratio, when adding the water-reducing agent, because of its dispersive effect, the quantity of free water in the concrete increases, thus accelerating the evaporation of pore water and increasing the shrinkage of concrete; (2). After adding the shrinkage-reducing agent, because the shrinkage-reducing agent can reduce the surface tension of water in pores, the evaporation of water decreases compared with that of water-reducing agent, so the shrinkage

decreases compared with that of water-reducing agent, which however, still increases compared with the benchmark set. (3). In addition to reduction on the shrinkage by decreasing the surface tension of the pore solution in cement, SRA can lead to a concurrent reduction evaporation rates of cement paste, cement mortar or concrete, regardless of mixing SRA into fresh concrete or applying it onto the surface of cement based materials[16–19].

This study suggests that the shrinkage-reducing agent and water-reducing agent to reduce the shrinkage of concrete have showed good compatibility.

4 CONCLUSION

This paper has summarized the results of a study on the effects of SRA on the shrinkage under the different curing system and mechanical properties of concrete. The following conclusions can be drawn from the experimental results:

1. Under the same mixture proportions, concrete containing water-reducing agent or water-reducing agent and shrinkage-reducing agent exhibits a delay in setting time and a reduction in the compressive, flexural and splitting tensile strength.
2. The greater the wind speed, the greater the shrinkage of concrete. In field applications, attaches great importance should be given to the sealed curing system [20], and as far as possible to avoid the wind.
3. The shrinkage-reducing agent and water-reducing agent to reduce the shrinkage of concrete have showed good compatibility.

REFERENCES

- [1] Goto T., Sato T., Sakai K., Li M. 1985. Cement shrinkage reducing agent and cement composition. *US Patent #4547223, 1985, United States Patent and Trademark Office, www.uspto.gov.*
- [2] Sato T., Goto T., Sakai K., 1983. Mechanism for reducing drying shrinkage of hardened cement by organic additives. *Cement Association of Japan*:52–55.
- [3] Farshad R., Gaurav S. & Jason W., 2007. Interactions between shrinkage reducing admixtures (SRA) and cement paste's pore solution. *Cement and Concrete Research* 38(2008):606–615.
- [4] Tomita R., Simoyama Y. & Inoue K., 1986. Properties of hardened concrete impregnated with cement shrinkage reducing agent. *Cement Association of Japan*: 314–317.
- [5] Shoya M., Sugita S. & Sugawara T., 1990. Improvement of drying shrinkage and shrinkage cracking of concrete by special surfactants. *E. Vazquez (Ed.), Admixtures for Concrete*: 484–495.

- [6] Shah S.P., Karaguler M.E. & Sarigaphuti M., 1992. Effect of shrinkage reducing admixtures on restrained shrinkage cracking of concrete. *ACI Materials Journal* 89(3): 289–295.
- [7] Balogh A., 1996. New admixture combats concrete shrinkage. *Concrete Construction*: 546–551.
- [8] Folliard K.J. & Berke N.S., 1997. Properties of high performance concrete containing shrinkage reducing admixture. *Cement and Concrete Research* 27 (9):1357–1364.
- [9] Berke N.S., Dallaire M.P., Hicks M.C. & Kerkar A., 1997. New developments in shrinkage reducing admixtures. *V.M. Malhotra (Ed.), Proceedings of the Fifth CANMET/ACI International Conference on Superplasticizers and Other Chemical Admixtures in Concrete, ACISP-173, American Concrete Institute, Farmington Hills, Michigan:971–998.*
- [10] Nmai C., Tomita R., Hondo F. & Buffenbarger J., 1998. Shrinkage reducing admixtures. *Concrete International*:31–37.
- [11] Ribeiro A.B., Goncalves A. & Carrajola A., 2006. Effect of shrinkage reducing admixtures on the pore structure properties of mortars. *Materials and Structures* 39 (2): 159–166.
- [12] Nguyen Quangphu, Jiang Lihua, Liu Jiaping, Tian Qian & Do Tienquan, 2008. Influence of shrinkage-reducing admixture on drying and mechanical properties of high-performance concrete. *Water Science and Engineering* 1(4):67–74.
- [13] Kevin J. Folliard NeaL & S. Berke, 1997. Properties of high-performance concrete containing shrinkage-reducing admixture. *Cement and Concrete Research* 27(9):1357–1364.
- [14] Guolei, 2012. The development and property of compound shrinkage reducing admixture for concrete. *DaiLian, China:Dalian University of Technology.*
- [15] QiaoDun, 2010. Influence and mechanism of shrinkage reducing admixtures on shrinkage reducing of cement based materials. *ChongQing, China: College of Material Science and Engineering of Chongqing University.*
- [16] Kovler K & Jensen O.M, 2007. General concept and terminology. In Kovler K, Jensen OM, editors. RILEM report 41 Internal curing of concrete. RILEM Publications S.A.R.L.:5–13.
- [17] Bentz D.P, 2005. Curing with shrinkage-reducing admixtures beyond drying shrinkage reduction. *Concr Int* 27(10):55–60.
- [18] Qian J.S, Qiao D, Shi L, Dang Y, Wang Z & Li Y, 2009. Function and mechanism of shrinkage reducing agent coating concrete. *J Chin Ceram Soc* 37(12):140–146.
- [19] Bentz D.P, Geiker M.R & Hansen K.K. Shrinkage-reducing admixtures and earlyage desiccation in cement pastes and mortars. *Cem Concr Res* 2001(31):1075–1085.
- [20] Zhu Yaotai, 2005. Experimental Investigation and Theoretical Modeling on Early-age Shrinkage Cracking in Concrete. *HangZhou, ZheJiang, China: ZheJiang University.*

Value for money and its application for infrastructure investment projects

J. Ceselsky, J. Kucera, B. Vojvodikova, M. Ferko & Z. Proske

Faculty of Civil Engineering, VSB-Technical University of Ostrava, Ostrava, Czech Republic

ABSTRACT: Construction and reconstruction of settlements and individual municipalities, environmental management and the creation, deployment of the forces of production and building transport and technical equipment requires a large expenditure of material and human resources. That is why the economic aspects of the majority decision in these planes built in the foreground and are often decisive. Thereby but more serious is that the economic aspects of the settlement, the creation and function remain in their whole, unprocessed, and can not speak of a set of individual techniques and methods traditional indicators and experiments with new approaches. This is true both at the level of the national economy, and in their own urban designs. Still a few remain identified specific economic shaping patterns of settlement and the less it is possible to speak of their control. Also practical assessing economics of specific solutions are often used non-apt indicators in addition to economics usually identifies with the lowest acquisition cost or high-intensity land use with little regard for functional efficiency and little studied much higher operating and maintenance costs (Hrůza, 1977).

Keywords: investment; municipal engineering; value for money

1 SUSTAINABLE DEVELOPMENT OF SEAT AND INFRASTRUCTURE

The economic principle of “value of money” (Eng. value for money) represents a qualitatively different view of the preparation, realization and exploitation of a particular investment project than in the Czech Republic usual. From an investment perspective emphasizes the careful consideration of all aspects of the project lifecycle, not just the initial costs or benefits, but the sum of all costs and benefits over the standard required life.

Sustainable residential development is economically primarily qualitative development (Rynda, 2000). Involves the use of the seat, while watching the economic prosperity, but ultimately also leads to weakening of future generations, ie to degrade the seat in the physical or economic sense. Crucial role in the sustainable development of settlements have a particular investment in infrastructure.

Infrastructure is a set of conditions which ensure the functioning of the economy. Infrastructure is defined as “social overhead capital” and includes the necessary investments in the sector contingent upon economic development (Rektořík, Russ, 2012). In the most general sense is a set of interconnected structural elements, which can then keep the entire structure together. It follows that the different emphasis on infrastructure develop-

ment can influence the dynamics of the economy, both in local, regional and supra-regional and even international scale.

2 ECONOMICS OF INFRASTRUCTURE PROJECTS

General relationships in construction of municipal infrastructure primarily pursue economic goal. Right—whether laws, regulations, decrees, private contracts, etc.—are just a means to express the goals of economic development. Legal relations have to “serve” economic goals, not vice versa. This economic goal is not to be seen beyond the usual understanding of the term “economic”; should include the positive difference between the whole society benefits and costs of a project (environmental, social, safety, etc.), ie not only the positive difference between the initial income and expenditure captured from an accounting perspective. From this broader perspective, it is interpreted that concept and in international practice, particularly in the context of project tools used Cost-Benefit Analysis (“CBA”).

As part of the investment project, which is always expressed by three basic elements—activities, time and money—it therefore is to set and actual implementation of solutions in the most

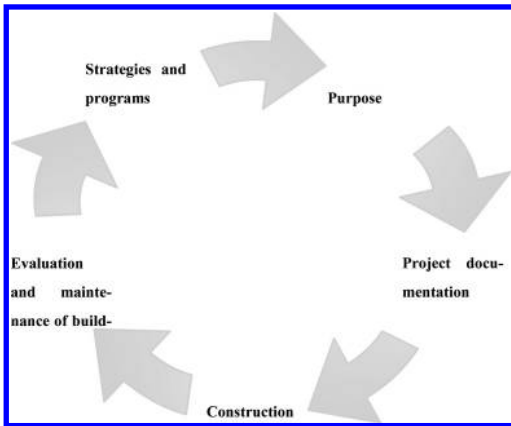


Figure 1. Project cycle of investment.

economically advantageous. Enforcement of economic objectives, which should serve relationship, here should be ensured at all stages of the project cycle roads (Fig. 1).

In the context of public investment is therefore necessary to ask the following basic questions and solve them within the economy of the investment project:

- Why the public sector invests?
- Who invests in the public sector?
- How and to what the public sector invests?
- How is the investment in favor of the public sector realized?
- What is the subject of public sector investment used/operated?

3 THE PRINCIPLE OF “VALUE FOR MONEY”

The basic term that in good international practice occurs in relation to the economy, public investment is “value for money”. Value for money can be defined as “the optimum combination of whole-life cost and quality of the investment that meets the reasonable needs of users.” In terms of dealing with taxpayers concept of “Value for Money” by National Audit Office, we can define as a Utility (U) obtained of each investment or the amount of money spent on each. Result investment—building object in itself forms two basic dimensions: E—financial and economic dimension and U—dimension of utility (Beran, Dlask, 2011):

$$f(E,U) \tag{1}$$

Like any commodity, can be applied to building object a business view and only maximize economic

yields and monitor independently evolving user effects (2) or maximize user interests and monitor an independently evolving economic effects (3):

$$\max g(E) \rightarrow h(U) \tag{2}$$

$$\max h(U) \rightarrow f(E) \tag{3}$$

Value for money is not only based on the minimum cost (economy) but also to maximize the efficiency and effectiveness (Principles 3E).

3E principles are expressed in EU law, particularly in the budgetary provisions, namely Article 27 EC Regulation 1605/2002 as the principles of sound financial management:

- Economy = means a use of public funds to ensure the set of tasks with the least expenditure of these funds, while maintaining adequate quality of the tasks;
- Effectiveness = means a use of public funds to ensure an optimum level of achievement of the objectives in carrying out certain tasks. Effectiveness is understood the degree of achievement of the objectives and the relationship between intended and actual impacts of the activity;
- Efficiency = means using public means which will give the greatest possible extent, quality and benefits of tasks performed in comparison with the amount of resources spent on their performance.

4 THE IMPORTANCE OF INVESTING IN MUNICIPAL INFRASTRUCTURE

During the decision-making process of investment in municipal infrastructure is crucial to take into account several crucial aspects (Vanier, Danylo, 1998):

- The important aspect is the size of the area (or importance) and type of area (or specifically residence) in which investments of municipal infrastructure should be located to,
- Also significant is the time horizon for investments to be prepared
- But always in terms of a set of realistic alternative solutions/investment.

Each investment should be initially evaluated and subsequently may be finally decided. In case of municipal infrastructure is always some kind of comprehensive system (the system of collective urbanized area, including subsystems conceived proportion to his needs). The investment into the system of collective urbanized area and implementation of such an investment is always a need to look at as a step forward “when there is no way back.” Evaluation of the current situation

are usually defined specific problems in the area, whether it is a problem in the individual sections of the technical infrastructure or problems coordinating the nature of the utility networks. Here again it is necessary to use appropriate alternative solutions (including assessment)—the solution must respect the developmental trends in the area. Of course it is necessary to analyze the wider relations and links in area, including an analysis of public space.

In the case of investment in municipal infrastructure analogy can not miss investment proposal to other “sectors” in the area. In the case of deficiencies, it is necessary to make an additional investment (recovery of public space—street, area, Regeneration of apartment houses, construction of new areas for recreation and others).

In connection with the importance of investment in municipal infrastructure is necessary to highlight the importance of planning activities, which defines the development of the municipal infrastructure and the development itself (town). Already during the creation of task planning documentation is necessary to respond to the municipal infrastructure to carry out research and analysis of the current state of municipal infrastructure in the area.

5 CONCLUSION

Sustainable development within settlements should be measured in its specific forms, ie the evaluation of long-term economic sustainability, which in monetary terms compared:

- existing urban solutions with any proposed changes (including statements loss of territory resulting from the proposed solution or an existing use using the positive and negative externalities);
- short-term costs and benefits for the investor, induced income and expenses in the long term (both in terms of operation and in terms of the evaluation).

Due to the fact that once again the dominant role in the development and building of settlements takes the public sector, it is necessary to include not only the comparison of income and expenditures, and the short-term and longer-term impacts, but also follow the principles of 3E.

If the creation of the final set of indicators of the economic pillars of sustainable development is successful and concise, will be used as a supporting argument for the selection of such spatial solutions that are economically sustainable, ie long-economically efficient with minimal negative externalities in economic terms

ACKNOWLEDGEMENT

The paper was written as part of the project task nr. TD020202 of Technology Agency of Czech Republic “Determination of the need for public investment in areas with an emphasis on effectiveness, efficiency and economy”.

REFERENCES

- Beran, V., Dlask, P., Schneiderová Heralová, R., Tománková, J. 2011. Management udržitelného rozvoje území 3. Prague: Česká technika—nakladatelství ČVUT.
- Glynn, J.J., Perkins, D.A. & Stewart, S. (Eds.). 1996. Achieving Value for Money. United Kingdom: WB Saunders.
- Hrůza, J. 1977. Slovník soudobého urbanismu. Prague: Odeon.
- Rektořík, J., Hlaváč, J. et al. 2012. Ekonomika a řízení odvětví technické infrastruktury, Prague: Ekopress.
- Uplatnění zásady „Hodnoty za peníze“ v investičním cyklu projektů dopravní infrastruktury, Studijní materiál pro seminář, 2011 [online]. [Cit. 14.7.2014]. Dostupné z: http://www.vzdelavanimkekvalite.cz/PDFs/Hodnota_za_penize.pdf.
- Vanier, D.J., & Danylo, N.H. 1998. Municipal infrastructure investment planning: asset management. In Innovations in Urban Infrastructure Seminar of the APWA International Public Works Congress (pp. 25–39).

Finite element analysis of beam from rolled IPN 160

O. Sucharda, J. Vasek & D. Mikolasek

Faculty of Civil Engineering, VSB-TU Ostrava, Czech Republic

ABSTRACT: The paper deals with a finite element analysis of a beam. Different approaches to creation of computational models exist within numerical calculation. The calculations are supported by an experiment. Beam, 2D and 3D models were used. The purpose of the paper is to assess the approaches to the modelling of steel beam. Steel beam has a profile IPN160. Two software applications were used for the finite element analysis. The algorithm for the linear analysis was developed in Matlab. The non-linear analysis was processed in ANSYS.

Keywords: finite element method; computational models; steel beam; load-deformation diagram

1 INTRODUCTION

Steel elements have been widely used in building structures. Steel parts of structures form often load-bearing components. An example might be supporting beams made from rolled sections which are placed next to ceilings, or a steel skeleton in a tier building. Attention has been paid to the steel structures for a rather long time. Now, the dimensioning is governed by standard EC (ČSN EN 1993-1-1). In order to calculate internal forces in rather complex structures, the preferred approach is the Finite Element Method (Rombach, G. 2007) which can use rod, 2D or 3D computational models. Civil engineering typically uses rod models for standard structures. There are, however, more complex structural solutions or details which need to be analysed carefully. The purpose of this paper is to evaluate different computational models used for a model beam which has been tested in a laboratory.

2 NUMERICAL ANALYSIS

The beam consists of a rolled section, IPN 160, S 235 grade. Its length is 1.2 m and it is loaded with a single load in the middle of the span. Span is $l = 0.9$ m. For geometry and shape of the beam see Figure 1.

In each variant, the elastic bearing capacity of the cross-section was calculated. Additional criteria were internal stress, deformation and material plastifying. Initial calculations in the numerical analysis were performed in MATLAB (MATLAB, 2014).

The algorithm developed in MATLAB is based on the Finite Element Method which uses beam/2D/3D finite elements. Calculations

in MATLAB assumes elastic behaviour of the material. The non-linear analysis was performed in ANSYS (ANSYS, 2007).

3 BEAM AND 2D COMPUTATIONAL MODELS

Beam models are not demanding in terms of calculation because the elastic bearing capacity of a steel rod which is loaded with a bending moment only can be calculated analytically. The limit force for the beam is big: $F_{\max} = 123.29$ kN. Because this is a rod model, the elastic limit bearing capacity is given by the normal stress σ_x in outermost fibres in the cross-section. If the normal stress exceeds the yield stress, the outermost fibres will become plastified. The maximum moment in the middle of a beam calculated using a rod model in MATLAB is $M = 27.74$ kNm.

If 2D finite elements are used, the model is more detailed. The calculation was performed in four

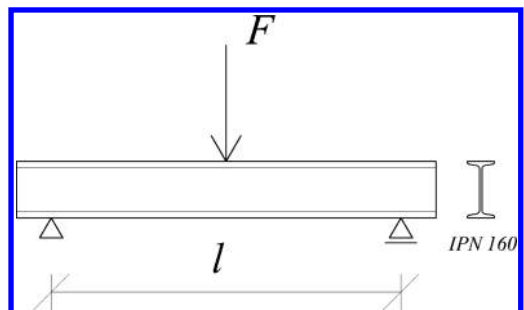


Figure 1. Model of a steel beam.

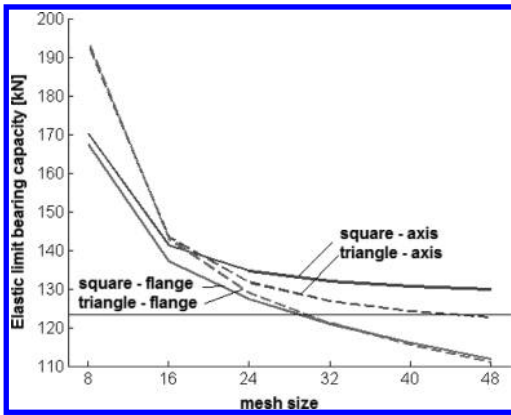


Figure 2. 2D model—FEM mesh size versus the elastic limit bearing capacity.

variants. Types of the finite elements and boundary conditions were different there. Following finite elements were used: a triangle element with one integration point and an isoparametric four-node finite element with four integration points. The difference in the boundary conditions was the position of the load and supports. In the first variant, the support and load were located on the beam axis. In the second variant, the load and supports were located at the lower/upper edge.

When using FEM in calculation, the mesh size plays an important role. For this reason, a parametric study was carried out in order to investigate the elastic limit bearing capacity versus the mesh size in a longitudinal direction. Considering the beam geometry, the mesh was divided longitudinally into 8, 16, 24, 32, 40 and 48 elements.

The load corresponds to the state when the outermost elements on the beam flange plastified. Figure 2 shows the limit load for each mesh size in the FEM mesh. The value of 123.29 kN is in line with results of the analytical solution. Calculations proved that the increasing mesh size in FEM decreases the elastic limit bearing capacity of the beam. The closest approximation in the analytical solution was obtained when the mesh was divided into 32 elements along the beam length.

The results also suggest that with the finer mesh size the calculated bearing capacity for the variant where the beam is supported in the middle is higher than that for the variant where the beam is supported at the beam flange.

4 3D COMPUTATIONAL MODELS

The beam was also analysed using a 3D computational model. The finite element was a four-node

tetrahedron with one integration point. The mesh is shown in Figure 3 and Figure 4.

In the 3D model, the load was distributed in nine nodes along the section width in the middle of the span. Similarly as with the 2D model, the dependence of the elastic limit bearing capacity on the mesh size was studied. The longitudinal segmentation was same as in the 2D model.

The cross-section consisted of 117 finite elements. Two variants of support locations were studied there. In the first variant, the supports were located in the beam axis, while the second variant had the supports in the beam flange.

Figure 4 shows the normal stress σ_x . The beam plastifying process is shown in a beam cross-section in Figure 5. The plastifying process started in the point of load.

The 3D model was also studied in variants with different mesh size. Results are shown in Figure 6. And again: the more finite elements were used in the mesh size, the lower bearing capacity was obtained. The reason is, probably, that less energy is needed to plastify a smaller finite element.

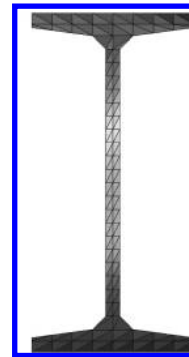


Figure 3. FEM mesh—a cross-section, IPN 160.

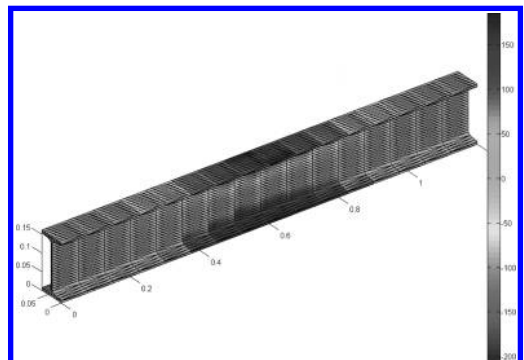


Figure 4. Stress σ_x [MPa] in the beam.

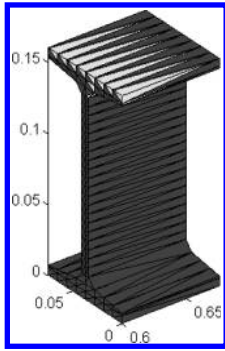


Figure 5. 3D model—a detail of a plastified area.

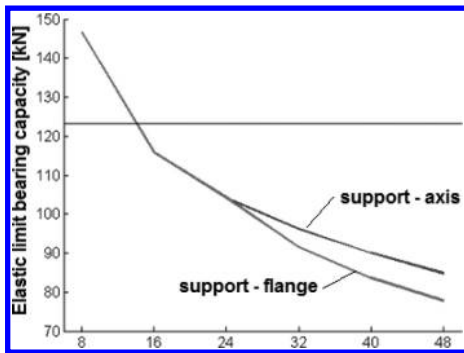


Figure 6. 3D model—a detail of a elastic limit bearing capacity and mesh size.

Another reason is that the total bearing capacity is lower. If compared with 2D models, the bearing capacity is considerably lower.

5 NON-LINEAR ANALYSIS

Numerical calculations were performed in ANSYS. This software can be used for non-linear analyses as well. A 3D computational model from finite volume elements was created for the analysis. For the model see Figure 7.

The calculation took non-linearities into account. The non-linearities were physical and/or geometric. In places where the boundary conditions existed the contact elements were used. Figure 8 and Figure 9 show deformation results of the calculation.

6 EXPERIMENTAL VERIFICATION

In order to support and validate the numerical computations, an experiment was carried out. The

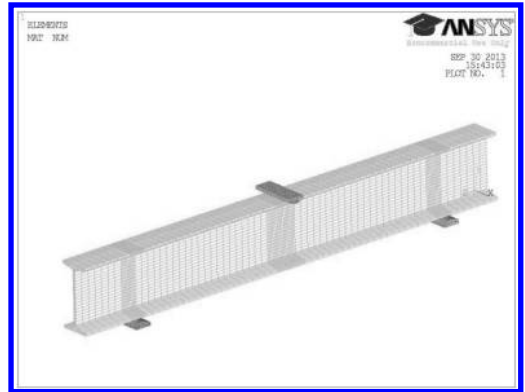


Figure 7. ANSYS—the FEM mesh in the model.

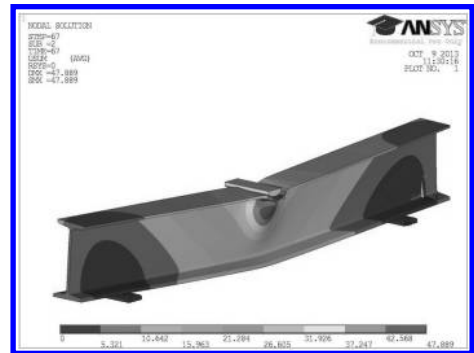


Figure 8. ANSYS—general deformation of the beam.

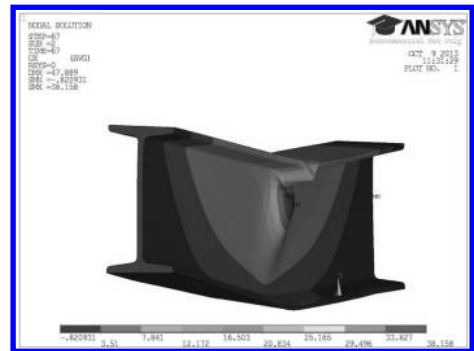


Figure 9. ANSYS—deformation in x-axis.

IPN steel profile was subject to a three-point bending test—see Figure 10. The purpose was to monitor the loading process, the principle of failure and load-deformation diagram which could be used for the numerical modelling. The test was carried out

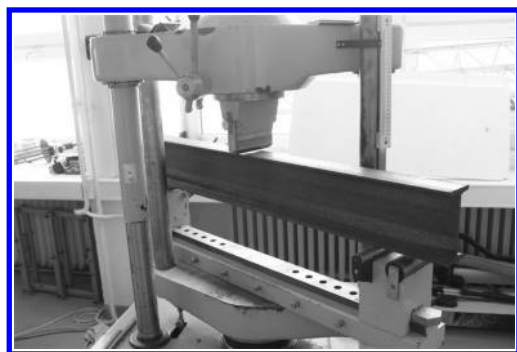


Figure 10. Three-point bending test on IPN 160—experiment.

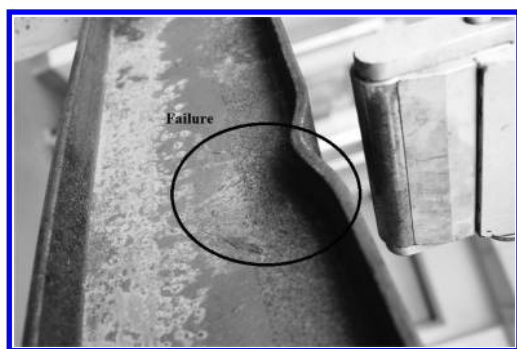


Figure 11. Failure in the beam—web buckling.

in the Laboratory of Building Materials, at VŠB—Technical University of Ostrava. The experiment was evaluated using the laboratory facilities.

The test has showed that the loading process consists of following phases. First, the press head touches the upper edge of the rolled IPN section. Then, the linear loading occurs. The first area where the material plastifies visibly is the upper beam flange straight under the press head and on the lower part of the lower beam flange. That area is less significant.

The beam is still under the load but the relation between the loading process and deformation is not linear anymore.

The increasing load does not plastify the beam flange anymore and more prominent imperfections appear in the web. Then, the wall start buckling and local plastifying occurs. See Figure 11. Because deformations were significant and the loading force was decline, the test was closed. The load-deformation diagram should consider also rigidity of the testing equipment as this influences the evaluation too.

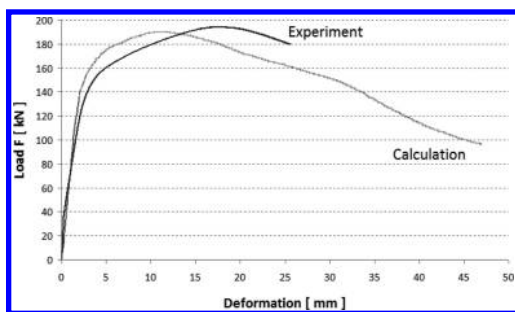


Figure 12. Load-deformation diagram.

7 CONCLUSION

The numerical calculations for a beam made from a rolled IPN 160 section have proved that in some cases the elastic bearing capacity is influenced by the number of finite elements and boundary conditions. The bearing capacity and sensitivity to the result evaluation appeared, in particular, in 3D models.

The 3D models have also shown that with more elements in the mesh, the model with supports along the beam axis is able to bear more than the beam supported at the beam flange. Similar dependences have been also shown in 2D models.

The IPN 160 section is regarded pursuant to ČSN EN 1993-1-1 (ČSN EN 1993-1-1) as the class I cross-section. With those cross-sections, a plastic joint can appear and the total bearing capacity increases by a plastic safety margin.

The safety margin for calculation can be obtained by comparing the load-deformation diagram and the non-linear analysis. See Figure 12. The reason is that the non-linear analysis included variable characteristics of steel.

The authors of this paper will focus their future work on the probabilistic methods, such as those mentioned in (Krejsa, M. et al. 2013) and (Křivý, V. & Marek, P. 2007), for calculations where random effects of input variables could be taken into account.

ACKNOWLEDGEMENT

The works were supported from sources for conceptual development of research, development and innovations for 2014 at the VŠB-Technical University of Ostrava which were granted by the Ministry of Education, Youths and Sports of the Czech Republic.

REFERENCES

- ANSYS. Release 11 documentation for ansys, SAS IP, INC., 2007.
- ČSN EN 1993-1-1. Eurocode 3: Design of steel structures—Part 1-1: General rules and rules for buildings. Praha: Český normalizační institut, 2006.
- Krejsa, M., Janas, P. & Čajka, R. 2013. Using DOPRO Method in Structural Reliability Assessment. In *ICMAM2012, Applied Mechanics and Materials*. Vol. 300–301, pp. 860–869 (10 p). ISBN 978-3-03785-651-2. DOI: 10.4028/[www.scientific.net/AMM.300–301.860](http://www.scientific.net/AMM.300-301.860).
- Křivý, V. & Marek, P. 2007. Probabilistic design of steel frame structures. *Stahlbau*, Vol. 76, Issue 1, Pages 12–20.
- MATLAB—The Language of Technical Computing. Software. [on-line]. <<http://matlab.com/>>. The MathWorks, Inc., Massachusetts, USA, 2014.
- Rombach, G. 2007. *Anwendung der Finite-Elemente-Methode im Betonbau*. 2. Auflage. Berlin: Ernst & Sohn. ISBN 978-3-433-01701-2.

Numerical modeling of rotary stiffness of joint for rails

O. Sucharda, D. Mikolasek, J. Brozovský & L. Zidek
Faculty of Civil Engineering, VSB-TU Ostrava, Czech Republic

ABSTRACT: The paper deals with modeling of rail joint and with determination of rotary stiffness of joint for the 49 E1 rail. The numerical modeling is combined with laboratory testing. The purpose of the works was to find out the rotary stiffness of a rail joint between the rails for rod models. FEM has been used for the numerical analysis of the rail joint. The computational model uses finite element method. The calculation takes into account constitutive and structural nonlinearities. Slippage between the elements is modeled using contact elements.

Keywords: finite element method; computational models; rotary stiffness; load-deformation diagram

1 INTRODUCTION

Structural layers (Plášek, O. 2012), (SŽDC 2008), (Esveld, C. 2001) in railway tracks (ČSN 73 6301, 1998) have been influenced by the undermining. Deformation in landscape typically results in failures and faults in transport structures which may, in turn, jeopardize traffic safety and continuity. Methods which have been used so far for analyses and design of transport route elements and for the entire transport route system (Plášek, O. 2003), (Kortiš, J. 2011) have certain limitations on underground territories.

(Noorzaei, J., Pour, PM. & Jaafar, MS., et al 2012) also deals with analyses of railway tracks. Such analyses are often combined with investigation into fatigue (Ringsberg, JW., Franklin, FJ., Josefson, BL., Kapoor, A. & Nielsen, JCO. 2005). It is also possible to use the modal analysis (Kortiš, J. 2011). The analysis of the rail joint is based on (Mikolášek, D. & Sucharda, O. 2013) which have been dealing with modeling of railways.

Several factors influence the stiffness of track superstructure (such as the seat of rail joints or performance of rail joints). In this case, a particular attention is paid to the influence of the rail joint stiffness on total stiffness of the segments which form together the railway superstructure.

The rail joint has been analyzed by a 3D computational model which consists of eight node finite elements, SOLID45, in ANSYS (ANSYS, 2007) which is a software application where both physical and geometrical non-linear analyses can be carried out. ANSYS is based on the Finite Element

Method (Zienkiewicz, O.C. 1972) and can be used for rather complex numerical models, the evidence being (Králik, J. & Šimonovič, M. 1993).

2 STRUCTURAL JOINT IN THE 49 E1 TRACK

The 49 E1 rails are connected every 25 m by means of different types of joints. This paper deals only with the rail joint type which is used in railway tracks in the Ostrava-Karviná Coal Colliery where the track superstructure has been suffering from undermining effects. This is a S joint—see the Figure 1 on the left. The rail joint is fixed to the rail by means of four bolts, Ø 24 mm. The surface of a rail joint should preferably match up with outer surfaces of the rail. The bolts are tightened up with a torque spanner up to 180–210 Nm.

The joint transfers the bending moment from one rail onto another. There is a purely contact connection with friction. Structural stiffness is influenced by slippage between the rail and rail joint. There are drilled holes Ø 32 mm in the rail and Ø 26 mm in the rail joint. The drilling in the rail is bigger so that the rail could dilate freely in case of length changes in the rail.

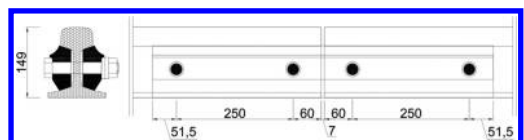


Figure 1. Geometry of the S joint for the 49 E1 rail.

3 LOADS AND MATERIAL PROPERTIES

In the numerical test, the rail-rail joint structure is loaded with numerical deformation. It has been decided to use numerical deformation because the numerical computation is more stable and because it is possible to calculate the ascending branch in the stress strain curve which would not be possible if a numerical test were used. In the physical test, the load was a short-lasting power load (the steel was loaded in a trial test with speed which has not influenced mechanical properties). The bolts used for fixing the rail joint were made of steel, 8.8 grade, dia. \varnothing 24 mm. The yield point was $f_y = 800$ MPa and the strength limit was $f_z = 880$ MPa. Table 1 describes the steel used in the rail joint, rail and bolts.

Two types of stress strain curves for steel were used in ANSYS for the numerical physical nonlinear calculation. See Figure 2. The stress strain curve had the yield point of 680 MPa and was defined as a multilinear curve. The connecting elements as well as the supporting underlying structure (the bearing surfaces and a loading wedge) were described by a bilinear stress strain curve. The multilinear stress strain curve was used to describe the material of the rail and rail joint. The reason for using a multilinear curve was that a plastifying process was expected, in particular, in the area of contact between the rail and rail joint and a contact stress played a more significant role there.

If the stress strain curve were more precise, the computed stress distribution could be more realistic

Table 1. Features of the steel used in the rail and rail joint, ANSYS.

Identification	Unit
E_x	210,000 [MPa]
μ	0.3 [-]
G_x	80,700 [MPa]

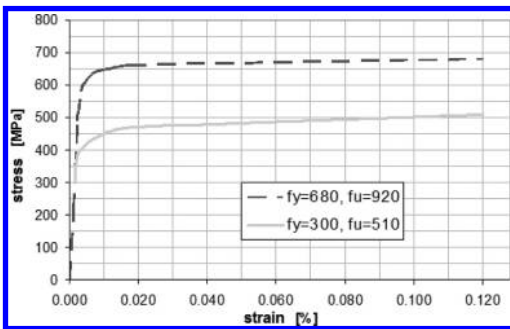


Figure 2. Stress strain curve for steel.

and the calculation process could converge better (the expected stiffness was higher if compared with than in a bilinear stress strain curve). Two different stress strain curves with the yield points of 300 MPa and 680 MPa were chosen for the rail joint only. The rail joint was calculated always with the yield point of 680 MPa. The strength of the steel in a rail was chosen differently from the numerical model described in (Plášek, O., 2012). There were two reasons for this. First, the rails were supplied in a rather high strength quality and the new value of the strength fits better the material used in the railway track under investigation. Second, more time was needed for the calculation—if the yield point is high, more deformations are allowed for physical nonlinearities and behavior of the railway tracks and joints can be analyzed for extensive deformation.

In order to describe behavior of a rotary semi-stiff joint between the 49 E1 rails, the numerical model modeled prestress in bolts which connects the both rails through two side rail joints. The prestress was chosen to be 0 N and 45 kN. This force is applied if the bolt is fastened with a torque spanner at 0 Nm and 210 Nm, respectively.

This is a theoretical value only. In reality, it depends on the contact between the segments (the rail joint and the rail) and on friction factors of each surface. This force was described in a numerical model using a factor of thermal expansion of the steel. For that type of the bolt and thermal expansion of the steel, the absolute difference in temperatures which creates tension in a bolt is 40°. Because of slippage on contact surfaces, the temperature was increased up to 320° in the numerical model. No verification was made in the physical test whether the fastening moment would create such tensile force in the bolt. It was assumed that the bolt was capable of such force. The prestress was applied in the bolts in order to



Figure 3. Measuring the rail and rail track in a laboratory.

find out the influence on the rotary stiffness of the joint. ANSYS considered following friction coefficients for steel: $\zeta_{12} = 0.12$ in the rail joint and rail, $\zeta_{14} = 0.14$ for the bolt and nut, and $\zeta_{125} = 0.125$ for the bolt, rail and rail joint.

Figure 3 shows the experimental measurement of the rail and rail joint. Dislocations in several points were monitored during the loading process. These were the points in the middle of the span on the upper and lower section of the rail. In one third of the structure, horizontal dislocation was measured.

4 NUMERICAL MODELS

The rail joint was calculated for two basic models: *A* and *B*. Figure 4 shows the first model of the *A* type. The chart shows the joint and its orientation during the load test. Figure 5 shows a detail of a finite element computational model of a rail and rail joint. The *A* model was tested numerically for two options. A_{+0} is without prestress in a bolt and both the rail and rail joint have the same yield point: $f_y = 680$ MPa. $A_{+0,1,300}$ is for a loose joint where the yield point for the rail is $f_{y,kolejnice} = 680$ MPa and



Figure 4. FEM calculation model a detail of a mesh in a rail and rail joint.

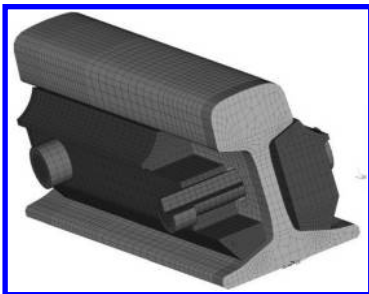


Figure 5. FEM calculation model a detail of a rail and rail joint.

that for the rail joint is $f_{y,spojka} = 300$ MPa. The both models were calculated for the same finite element grid with the contact stiffness being $FKN = 1$.

B is a numerical model only (in has not been tested in laboratory). It should help specifying the rotary stiffness for a model with a rather small volume (in order to solve less equations and to use symmetry of the task). The numerical model *B* was calculated for two load directions and for two tightening moments (where B_{+0} is tightened at $M_u = 0$ Nm and B_{+210} at $M_u = 210$ Nm). Two stress strain curves were considered for the rail joint (same as with the *A* type). The “+” in the lower index means that the load was applied onto the upper head of the rail. See Figure 6. Attention was also paid to the influence of normal stiffness of the contact elements on the rotary stiffness of the edge. Six variants of the *B* model were tested there.

B_{+0} (with the bending moment of $M_u = 0$ Nm) and B_{+210} (with the bending moment of $M_u = 210$ Nm) loaded the upper head of the rail. B_{-0} (with the bending moment of $M_u = 0$ Nm) and B_{-210} (with the bending moment of $M_u = 210$ Nm) were loaded on the lower flange of the rail (the rail moves up and the track head is drawn by the bending moment). The models were calculated for the same finite element mesh with the contact stiffness being $FKN = 1$. The yield point of the rail joint was $f_y = 680$ MPa.

$B_{+0,10}$ was a loose joint. The model was calculated for the same finite element mesh with the contact stiffness being $FKN = 10$. The yield point of the rail joint was $f_y = 680$ MPa.

$B_{+0,1,300}$ was a loose joint. The model was calculated for the same finite element mesh with the contact stiffness being $FKN = 1$. The yield point of the rail was $f_{y,kolejnice} = 680$ MPa and that of the rail joint was $f_{y,spojka} = 300$ MPa.

The models in ANSYS were created by 3D finite element—SOLID45. Each model was calculated as a physical nonlinear model with friction contacts. There were more than 420,000 degrees of freedom in the *A* model and more than 142,000 degrees of freedom in the *B* model (SOLID45 is a finite element with three degrees of freedom and three

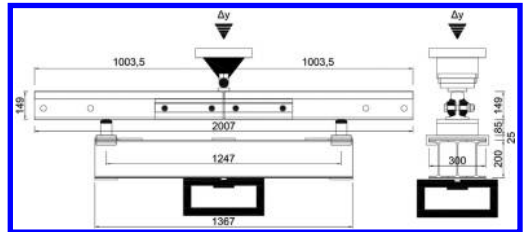


Figure 6. Physical test: the complete structure: the 49 E1 rail and S joint.

dislocations). The calculation took more than 24 hours for *A* and about 2 hours for *B*.

Below is the summary of the numerical models:

A type: both the numerical calculation and physical test

- typ_*A*₊₀ a loose joint, the head under load, $f_{y,spojka} = 680$ MPa, FKN = 1
- typ_*A*_{+0_1_300} a loose joint, the head under load, $f_{y,spojka} = 300$ MPa, FKN = 1

B type: the numerical testing only

- typ_*B*₊₀ a loose joint, the head under load, $f_{y,spojka} = 680$ MPa, FKN = 1
- typ_*B*₊₂₁₀ for the tightening, the head under load, $f_{y,spojka} = 680$ MPa, FKN = 1
- typ_*B*₋₀ a loose joint, the foot under load, $f_{y,spojka} = 680$ MPa, FKN = 1
- typ_*B*₋₂₁₀ for the tightening, the foot under load, $f_{y,spojka} = 680$ MPa, FKN = 1
- typ_*B*_{+0_10} a loose joint, the head under load, $f_{y,spojka} = 680$ MPa, FKN = 10
- typ_*B*_{+0_1_300} a loose joint, the head under load, $f_{y,spojka} = 300$ MPa, FKN = 1.

5 AN EXPERIMENTAL TEST OF A RAIL JOINT

The detail under testing had the geometry and load described in the *A* model. In this test, the bolts were tightened as in the real railway track. Two measurements in an elastic area were carried out. The real test was a verification test for the numerical model (the *A* type). A detail was loaded in an elastic area—cca. 3 mm from the central deflection. Then, it was loaded gradually. An increase in deformation in excess of 20 mm represented the complete plastifying process in a rail joint (for the yield point being $f_y = 680$ MPa for both the rail joint and rail). The rail joint is the softest part of the detail (its moment of inertia is below that of the rail).

Figure 4 and Figure 6 show the loading test in a press which is capable of producing as much as 1,000 kN. The tested structure was laid on a steel weldment consisting of three I-sections, 200. The sectors were welded to each other through steel plates, each 10 mm thick. A general-purpose backplate was placed on the welded sections. On both sides, the backplate supported the rail. There was 80 mm of free space for deflection.

The supporting structure from the I-sections was fixed into the lower part of the press. The upper mandrel was a steel cylinder, Ø 50 mm. It was pressed against a 20 mm thick bearing plate on the rail's upper head. The lower structure made from the welded I-sections was not perfectly stiff and its deformations were considered in defor-

mations procuded in a press. In the physical test, the deformation at the edges of the I-sections was deducted from global deformation in the middle of the rail which were measured at the press and measuring sensors.

6 RESULTS NUMERICAL CALCULATION

The numerical test was carried out in ANSYS using the FEM for both the entire structure of the joint (same boundary conditions and same geometry as with the physical test) and for the half numerical model of the joint. Several tightening moments and two values of the contact stiffness were tested. Two stress strain curves were considered (different yield point for the rail joint). In case of *B*, the load was applied in both directions on the axis of the main moment of inertia of the rail.

Equation 1 describes the rotary stiffness depending on the bending moment and rotation. This relation was used in order to describe the rotary stiffness of the rail joint.

$$K_{\varphi i} = \frac{M_i}{\varphi_i} [MNmrad^{-1}] \quad (1)$$

Dislocation of two points on the rail near the bolt and at the rail ends was determined in the numerical model. The dislocation of those points in the vertical axis and horizontal distance between the points were the basis for calculation of rotation in the rail joint. The values of the rotary stiffness were drawn in the diagram. The rotary stiffness for the physical test was determined similarly.

7 RESULTS—THE PHYSICAL TEST

The real test was carried out using a segment of a railway track which was operated in the Ostrava—Karviná Coal Colliery. Bolts in the joint were not



Figure 7. Deformed rail and rail joint after the experiment.

tightened up and the joint was tested as-is. The test provided information about mechanical and physical properties in the rail joint used in real railway tracks. As one piece only was tested, it is not possible to draw general conclusions on the basis of such results. It is, however, likely that the rail joints of the same type (the same rail and same rail joint) will behave and response similarly in other railway tracks which are in operation. Figure 7 shows deformation of the rail and rail joint in detail.

8 SUMMARY OF OBTAINED RESULTS

The numerical tests were calculated as physical non-linear tests for different stress strain curves and contact stiffness with different prestresses in bolts. Results of this calculation are very reliable. The tests, however, take much time and preparation of inputs and adjustment of the model as a whole are rather complicated. Figure 8 shows deformation of a rail/rail joint obtained in the numerical calculation.

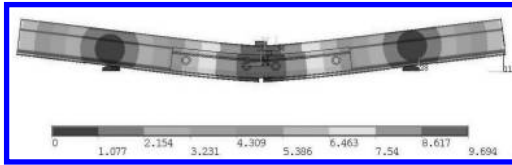


Figure 8. Deformed rail and rail joint: numerical calculation of typ_A₀.

The physical test of the rail joint was not too complicated in terms of needed facilities and equipment. It has been found out in the real test that the rotary stiffness of the joint is small (against the full cross-section of the rail). The rail is made from the steel, grade S235–S355 (no tensile test of the rail joint has been performed yet and no detail information is available now). Slippage of the contact surface reduces rather considerably the rotary stiffness of the joint and the joint become plastified.

Beginning with the moment of 36 kN for the yield point of steel up to 680 MPa, the 49 E1 rail is still in an elastic area. If the yield point exceeds 680 MPa, outer fibres start plastifying and with the yield point of 300 MPa the joint is fully plastified. To put it simply, the rail joint can be regarded as an articulated joint. In case of a rod model, the rotary stiffness resulting from numerical solutions or laboratory measurements can be used. This will describe behavior of the track superstructure in a more complex way. Figure 9 and Table 2 show the rotary stiffness.

The local peak of stress appears in pressure points between the track and rail joint. The extreme value is 925 MPa. This is a local value. In direct surroundings of that value, the stress drops to 627 MPa, reaching the yield point of steel.

Figure 9 shows the curves which describe the rotary stiffness depending on the bending moment and rotation. There are 2 numerical models, A and B, and the physical test—“realn7_tets”. The physical test is drawn in a full red line. It is clear from the curves that the best match for the measured value is the numerical models of the rail joint with the lower yield point—300 MPa.

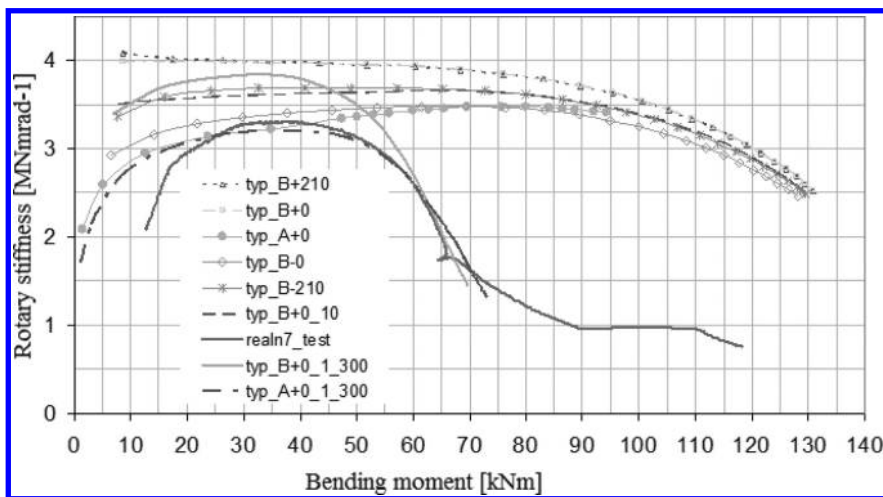


Figure 9. Rotary stiffness of the rail joint (the both halves).

Table 2. Rotary stiffness in the numerical models (a half of the rail joint).

Rotary stiffness ANSYS [MN mrad ⁻¹]	typ B ₊₀	typ B ₊₂₁₀	typ B ₋₀	typ B ₋₂₁₀	typ B _{+0,10}	typ B _{+0,1_300}	typ A ₊₀	typ A _{+0,1_300}
M ₂₀	8.1	8.2	6.2	6.8	7.02	7.02	5.25	5.52
M ₃₀	8	8	6.7	7.3	7.2	7.68	6.25	6.36
M ₄₀	7.9	7.9	6.8	7.4	7.25	7.56	6.4	6.34
M ₆₀	7.87	7.87	6.9	7.34	7.37	5.4	6.8	5.14
M ₈₀	7.7	7.7	6.8	7.2	7.2	→ 0	7	→ 0

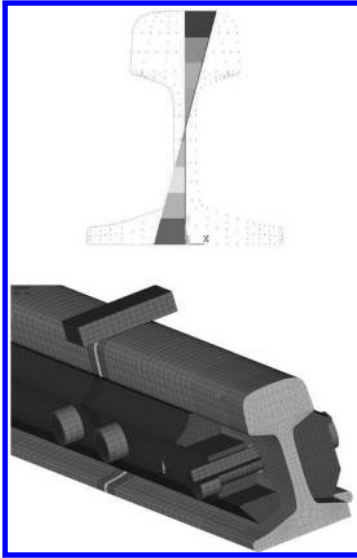


Figure 10. Detail of stress in the rail cross-section. Rail/rail joint grid.

Figure 10 shows the stress in the rail cross-section. The illustration on the right is a detail of the Finite Element mesh and rail joint components.

9 CONCLUSION

The physical test shows the real behavior of different rail times most reliably. Such test is, however, rather expensive and might be not so efficient as much time is needed for preparation and completion of the test. In some cases, the test cannot be performed because of restriction in technology processes or facilities. This is the reason why numerical modeling should be carried out—it supplements and optimizes the real measurement. (If a numerical model is well prepared, it is possible to find an optimum structural solution and test it. No several variants of structural details are needed and expensive measurement is eliminated).

Results obtained in the numerical modeling of the rail point are very similar for different input parameters and different for complexity of the model. It is, in particular, the rotary stiffness of the rail point which is very similar. The rotary stiffness obtained in a numerical model is sufficient and reliable, if compared with that measured in the test. The average value of the measured and calculated values of the rotary stiffness is ca. $K_{\phi, \text{průměr}} = 3.21$ MNmrad⁻¹. That rotary stiffness applies to the entire rail joint. It follows from the comparison of the numerical models and measurements that the both procedures are reliable and provide correct deformation and stiffness parameters of the joint. This means, the numerical modeling can be used for other types of the joints and structures. The physical measurement is still an important process for validation of behavior of structural details and components. Future works which will deal with this topic will consider influence of the modal analysis and dynamics as in (Kortiš, J. 2011.) and (Shabana, AA., Chamorro, R. & Rathod, C. 2008.). With such tasks it is also recommended to consider random influence of input variables and use the probabilistic method for calculation, such as (Krejsa, M. et al. 2013) or (Křivý, V. & Marek, P. 2007).

ACKNOWLEDGEMENT

The works were supported from sources for conceptual development of research, development and innovations for 2014 at the VŠB-Technical University of Ostrava which were granted by the Ministry of Education, Youths and Sports of the Czech Republic.

REFERENCES

- Ansyes, Release 11 Documentation For Ansyes, SAS IP, INC., 2007.
- ČSN 73 6301 Designing of railways. (In Czech). Praha: Český normalizační institut, 1998.
- Esveld, C. 2001. *Modern Railway Track*. Second Edition. Delft: MRT-Production, 2nd ed. 654 p. ISBN 90-800324-3-3.

- Kortiš, J. 2011. Estimation of Modal Parameters by using Operational Modal Analysis, *In Proceedings of the 5th International Conference on Dynamics of Civil Engineering and Transport Structures and Wind Engineering, DYN-WIND*, 30.05-02.06.2011, Jasná pod Chopkom, Žilina: University of Žilina, 978-80-554-0354-0.
- Králík, J. & Šimonovič, M. 1993. Elasto-plastic Analysis of Deformation Soil Body with 3D-Finite and Infinite Elements. In: *GEOMECHANICS '93*, IACMAG, Ostrava.
- Krejsa, M., Janas, P. & Čajka, R. 2013. Using DOProC Method in Structural Reliability Assessment. In *ICMAM2012, Applied Mechanics and Materials*. Vol. 300–301, pp. 860–869 (10 p). ISBN 978-3-03785-651-2. DOI: 10.4028/www.scientific.net/AMM.300-301.860.
- Křivý, V. & Marek, P. 2007. Probabilistic design of steel frame structures. *Stahlbau*, Vol. 76, Issue 1, Pages 12–20.
- Mikolášek, D. & Sucharda, O. 2013. Rotation stiffness of the rails connection type 49 E1 with connector S. (In Czech). *Stavební obzor*. Number 4/2013.
- Noorzaei, J., Pour, PM. & Jaafar, MS., et al. 2012. Numerical Simulation of Railway Track Supporting System Using Finite-Infinite and Thin Layer Elements Under Impulsive Loads. *Journal of Civil Engineering and Management*. Vol. 18, Iss. 2, p. 245–252. ISSN 1392–3730. DOI:10.3846/13923730.2012.671286.
- Plášek, O. 2003. Railway construction. Instructions to exercise. (In Czech). 2nd ed supplemented., Brno: CERM, s.r.o. Brno, 110 p. ISBN 80-7204-267-X.
- Plášek, O. 2012. Construction of rail superstructure. (In Czech). Document Pdf [online]. [cit. 2013-01-01]. Dostupný z WWW: <http://public.rfx.cz/Lienert/Upevn%ECn%ED.pdf>.
- Ringsberg, JW, Franklin, FJ., Josefsen, BL., Kapoor, A. & Nielsen, JCO. 2005. Fatigue evaluation of surface coated railway rails using shakedown theory, finite element calculations, and lab and field trials. *International Journal of Fatigue*. Vol. 27, Iss. 6, p. 680–694. ISSN 0142-1123. DOI: 10.1016/j.ijfatigue.2004.11.002.
- Shabana, AA., Chamorro, R. & Rathod, C. 2008. A multi-body system approach for finite-element modelling of rail flexibility in railroad vehicle applications. Proceedings of the Institution of Mechanical Engineers, Part K: *Journal of Multi-body Dynamics*. Vol. 222, Iss. 1, p. 1–15. ISSN 1464-4193. DOI: 10.1243/14644193JMBD117.
- SŽDC, 2008. *Prescription S3 superstructure*. Approved generálním director SŽDC 3.6.2008 under ref: 9675/08-OP effective July 1, 10th 2008. (In Czech).
- Zienkiewicz, O.C. 1971. *The Finite Element Methode in Engineering Science*. London: McGraw-Hill.

Research on the influence of section size error on height of main beam on continuous rigid frame bridge

Tong-Ling Wan

Puyang to Hebi Transportation Hall Highway Management Office of Henan Province, Henan, China

ABSTRACT: Errors must exist in the construction of long span bridge. And the construction errors inevitably influence the performance of bridge structure. So it is necessary to study the influence of construction error on bridge structure. This paper, focusing on continuous rigid frame bridge based on real multi-span continuous rigid frame bridges as engineering background, simulates the construction errors of ± 10 cm of the main beam using FEM to analyze its influences on the internal force, stress and displacement of the continuous rigid frame bridge, and then evaluates the influences of such errors on continuous rigid frame bridge in construction.

Keywords: section size; continuous rigid frame bridge; construction error; influence

1 INTRODUCTION

The construction process of long-span bridge is quite complex, and is influenced by various uncertain factors, which may lead to deviation between the actual state of bridge structure and the theoretical calculation analysis. And the existence of the construction error is one of those factors^{[1][2]}. As a construction error, there are barely any study related to the error in the height of the main girder section, and quantitative analysis, relevant data and documents regarding its impact on the bridge structure of concrete are very vague^{[3][4]}.

Based on a prestressed concrete continuous rigid frame bridge constructed in a certain expressway, the influence of the error in the height of the main girder section on the internal forces, the stress and displacement of long span continuous rigid frame bridge are studied by using finite element analysis software Dr Bridge. Based on the simulation, the influence of the error in the height of the main girder section on similar bridges is evaluated.

This study helps to understanding the influence of height error in girder cross section on bridge structure more clearly; it can provide a reference for the bridge detail optimization; and it can provide assistance and monitoring for the construction of the bridge, which helps the smooth construction of the bridge.

2 METHOD

2.1 *The background of the related project*

In this paper, the related bridge is located in a highway, and the bridge is a prestressed concrete

variable cross-section continuous rigid frame bridge, the lower structure is with double limb rectangular solid pier piers. Moreover, the bridge upper structure is (45 + 3 × 80 + 45 meters) prestressed concrete continuous rigid frame, which is composed by single box single chambers. Box girder root height is 4.7 meters, the height across the centre beam is 2.2 m, and it changes according to 2.0 parabolas. The box girder roof is 12.775 m wide and 0.3 m thick, its bottom is 7 m wide and the thickness changes from 0.32 m by 2.0 parabola to 0.8 m. The thickness of web plate are 0.7 m and 0.5 m respectively, within the thickness of top box girder roof is 0.4 m, bottom plate thickness is 1.1 m, and the web is 0.7 m thick.

2.2 *Settings on the change of section size*

There exist clear requirements on size error of the components of a bridge in construction process. According to the technical specification for construction of highway bridge (JTG TF50-2011)^[5], the allowed error of section size in height is +5 mm or -10 mm. The author found that, in many construction processes of long span continuous rigid frame bridges, size error existing in bridge girder cross section height exceeds the limits in the specification.

In order to better understand the influence of size error on structure, this paper assumes that the size error in the bridge girder cross section height amounts to ± 10 cm. By computing, the influence of size error is calculated.

In this paper, through the establishment of the bridge structure models of normal condition and high size deviation ± 10 cm girder bridge, the

impact of continuous rigid frame bridge girder size error on bridge structure are studied respectively from three aspects such as the internal force, stress and displacement.

2.3 Modeling and calculation

The cross section of the bridge is single box with single room, which is input according to design drawings. The cast-in-situ box girder is built according to the C55 concrete stated in the design drawings and C40 concrete is chose for piers. The longitudinal prestress steel is low relaxation steel wire of 15.24 mm in diameter and its the standard strength is 1860 Mpa. Ordinary steel, anchorage, corrugated pipe and other materials are selected according to the design drawings.

The division of the bridge is in accordance with the construction process by stages. Meanwhile, nodes are set at the controlling section of internal force, displacement mutation, section area to the location and setting the permanent and temporary supporting node. According to the design drawings and construction processes of the bridge, the whole bridge is divided into 584 units. Piers and girders are rigid connected. The bearing at the end side span is simulated by the vertical two-way bearing according to the actual situation.

This bridge takes the following loads into consideration: the self weight of the bridge, the concrete density of 26 kN/m^3 ; and the prestressed load are input in accordance with the information provided in the design drawings. The tension control stress of the main span prestressed anchor is $\sigma_{con} = 1339.2 \text{ Mpa}$; the pipeline's influence on the friction coefficient of each local deviation coefficient $K = 0.0015$; the relaxation coefficient of prestressed steel beam $\varepsilon = 0.30$, and the friction coefficient between the prestressed steel beam and pipe wall $\mu = 0.20$, the deformation of the anchorage devices $\gamma = 0.006 \text{ m}$. Concrete shrinkage and creep: considering creep and shrinkage of 10 years of which the processing method is to add a construction process of a decade into virtual construction stage; During construction, temporary load includes people, machinery and heap load; according to the temperature effect, the bridge is the temperature of the local actual situation is taken into consideration for the overall whole cooling temperature of $20 \text{ }^\circ\text{C}$. The bridge paving layer consists of 12 centimeters of C50 concrete waterproof layer and 10 cm of asphalt concrete. Thus, the 10 centimeters of asphalt concrete pavement layer is taken into consideration for nonlinear temperature effect. The live load considers vehicle load, regardless of the trailer load. As there is no sidewalk, no crowd load is considered.

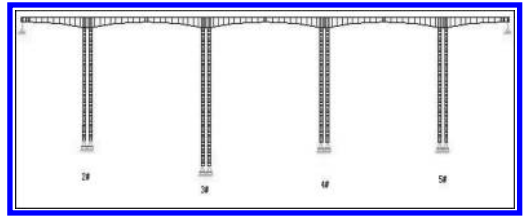


Figure 1. The finite element model of the bridge under the normal state.

In accordance with the design drawing, Dr Bridge, a bridge professional software, is adopted to establish the bridge finite element models of the whole bridge structure of the normal state, which is shown in Figure 1.

When size error exists in the height of bridge girder cross section, the state of the bridge is an abnormal one. Its modeling, the material, the cross section of unit input, and the division of construction stage, boundary conditions and load condition of input are in accordance with normal model.

For the convenience of elaboration, if the size is consistent with the design of the girder, such a state of the bridge is referred to as the normal state. The state of the bridge which girder height size varies within -10 cm is called state I, and the state which girder height size varies within -10 cm is called state II.

3 THE INFLUENCE OF THE SIZE ERROR IN THE MAIN GIRDER OF THE BRIDGE ON THE BRIDGE STRUCTURE

3.1 Internal force analysis of the main girder

This section mainly analyzes the influence of main girder size error on the internal force of the continuous rigid frame bridge^[6-9].

3.2 Main beam axial force

The axial force of the main girder under normal condition is compared with state I and II respectively, and the contrast figure is as follows.

It can be seen from Figure 2 and Figure 3: the tendencies of the axial forces are similar within all the states and coincide at their key points. Under the normal state and state I, the change of maximum axial force is not obvious, the maximum difference in the corresponding section is 151.5 kN , and relative deviation is within 1% ; Under the normal state and state II, the change of maximum axial force is also not obvious, the maximum difference in the corresponding section is 180.3 kN , and relative deviation is 1% . Therefore, it can be

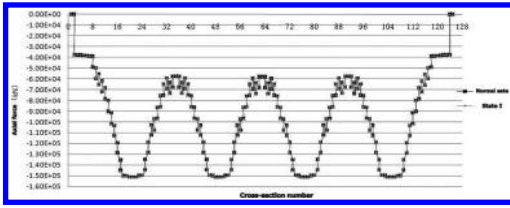


Figure 2. The comparison of the axial forces of the girder under the normal state and state I.

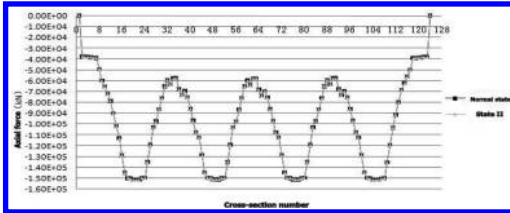


Figure 3. The comparison of the axial forces of the girder under the normal state and state II.

concluded that the girder axial force of main girder is little affected by the size deviation, which can be ignored.

3.3 Main beam shear force

In the bridge, the contrast of the girder shear force is shown in Figures 4 and 5.

It can be seen from Figure 4 and Figure 5: the tendencies of the shear forces are similar within all the states and coincide at their key points. Compared with the main girder shear with the normal condition, the maximum shear force in state I is reduced by 1%, the maximum difference in the corresponding section is ± 100.0 kN, and relative difference is within 2%; Under state II, girder shear maximum value is increased by 1%, the maximal shear difference for each corresponding section is 190.2 kN, relative deviation is 1%. Therefore, it can be concluded that the girder shear force of main girder is little affected by the size deviation, which can be ignored.

3.4 Main beam moments

The moments of the main girder under normal condition is compared with state I and II respectively, and the contrast figure is as follows.

It can be seen from Figure 6 and Figure 7: the tendencies of the moments are similar within all the states and coincide at their key points. Compared with the main girder shear with the normal condition, the maximum moment in state I is reduced

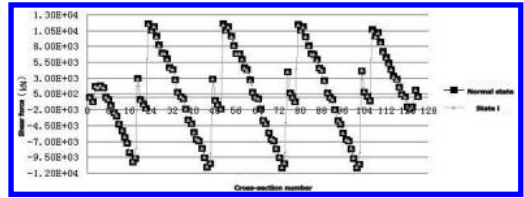


Figure 4. The comparison of the shear forces of the girder under the normal state and state I.

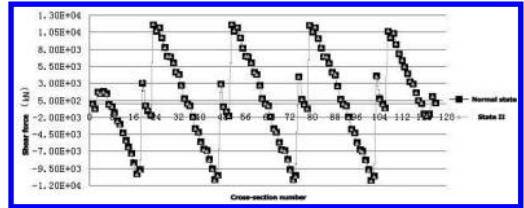


Figure 5. The comparison of the shear forces of the girder under the normal state and state II.

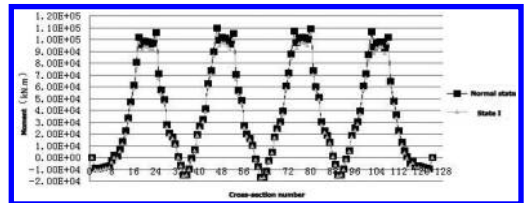


Figure 6. The comparison of the moments of the girder under the normal state and state I.

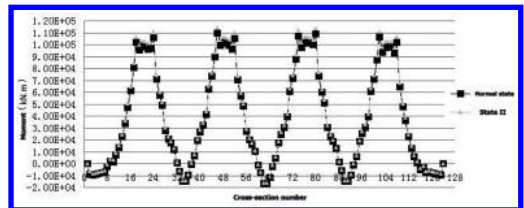


Figure 7. The comparison of the moments of the girder under the normal state and state II.

by 2500 kN·m, relative difference is within 4%; the maximum difference in the corresponding section is 2000–2800 kN·m, and relative difference is 3%–5%; Under state II, girder maximum moment is increased by 5000 kN·m, relative deviation is 5% the maximal difference for each corresponding section is 2400–5000 kN·m, relative deviation is 3%–5%. And the change in moment in most of the sections of the girder exceeds 1000 kN·m. Therefore, it can be concluded that the girder moment

of main girder is considerably affected by the size deviation, which cannot be ignored.

3.5 Main beam stress analysis

This section mainly analyzes the influence of the size error of ± 10 cm in girder height on the stress of the bridge structure.

In the constructed bridge, the principal tensile force at the top of the girder and the principal compressive force at the bottom of the girder are compared with those of the bridge in state I and II. For reading convenience, the bridge is shown in two figure separated from its mid-span section.

It can be obtained that under state I, the maximal increment of the principal compressive force amounts to 10%; under state II, maximal decrement of the principal compressive force amounts to 9.5%, thus the influence of the size error on the principal compressive force is quite little^[10].

3.6 Displacement influence analysis

This section mainly analyzes the influence of size error on the displacement of the bridge.

In the constructed bridge, the vertical displacement of the girder under different states is compared with each other.

It can be seen that the difference between the vertical displacements under different states amounts to 3 mm under the influence of the size error, which can be neglected.

4 INFLUENCE EVALUATION

This section mainly evaluates the influence of the size error in girder height within ± 10 cm on the internal force, stress and linearity of the continuous rigid frame bridge.

4.1 Internal force influence evaluation

Above research shows that the influence of the size error in girder height within ± 10 cm little affects the axial force and shear force in the girder.

4.2 Stress influence evaluation

Above research shows that the influence of the size error in girder height within ± 10 cm little affects the tensile, compressive force in the girder as well as the maximal compressive force.

4.3 Linearity influence evaluation

Above research shows that the influence of The size error in girder height within ± 10 cm on the displacement of girder is negligible.

5 CONCLUSIONS

In this paper, the influence of size error of ± 10 cm in girder height in continuous rigid frame bridge on the bridge structure is evaluated and the following main conclusions have been obtained.

The size error in girder height within ± 10 cm little affects the axial force and shear force, but have a certain influence of main girder bending moment, while the structure in the design of bridge structure safety reserve is higher, so the influence of the main girder height size error within ± 10 cm are negligible on bridge bending moment.

The size error in girder height within ± 10 cm little affects the tensile and compressive force in the girder, so the influence on the bridge can be neglected.

The size error in girder height within ± 10 cm little affects displacement of main girder. Therefore, the influence on the displacement can also be neglected.

Therefore, The size error in girder height within ± 10 cm will not affect the safe use of long span continuous rigid frame bridge.

REFERENCES

- Fan Lichu. The bridge engineering [M]. Beijing: China Communications Press, 2001.7.
- Gu Anbang, Zhang Yongshui. Construction of the bridge to monitor and control [M]. Beijing: Mechanical Industry Press, 2005.
- Hao Chao. Large span steel cable-stayed bridge construction error adjustment method [J]. Journal of Zhejiang University, 2003,5 (3), 310–313.
- Hohenbichler M, Rackwitz R. Sensitivities and importance measures in structural reliability [J]. Civil Eng. System, 1986 (3): 203–209.
- Karamchandani A, Cornell C.A. Sensitivity estimation within first and second reliability methods [J]. Structure. Safety, 1992 (11): 97–105.
- Ma Baolin. High pier and long-span continuous rigid frame bridge [M]. Beijing: China Communications Press, 2001.
- Tang Pan, Liu Airong. Effect of bridge construction stage of internal forces of continuous rigid frame bridge [J]. Journal of Guangzhou University, 2009, 12(6), 76–78.
- The people's Republic of China Ministry of transportation. JTJ/T F50-2011 highway technical specifications of culvert construction [S]. Beijing: China Communications Press, 2004.
- Wang Jinfeng, Liu Bin. High pier and long-span continuous rigid frame bridge structure characteristics and construction control [J]. Chinese harbour construction, 2005,6 (3), 40–43.
- Zhou Junjie. Long span curved continuous rigid frame bridge construction error factors analysis [J]. Shanxi architecture, 2011, 6 (17), 93–95.

Classification and discussion of fastening system of ballastless track

Jia Cong Huang & Cheng Hui Li

MOE Key Laboratory of High-Speed Railway, Southwest Jiaotong University, Chengdu, China

ABSTRACT: Fastening system is one of the most important component parts of the track structure, but it also the key-technology of the ballastless track structure. In order to ensure security driving and comfort riding for the passengers, fasteners is not only possess sufficient strength and buckle pressure, but needs the favorable elasticity and the rail height and gauge adjustment ability etc. In order to achieve the purpose of the economic rationality and security operations, it is considerable to choose the type of fasteners reasonably and bring to bear fasteners performance abundantly.

Keywords: high speed railway; ballastless track; fastening system; structure; function; classification; parameters

1 THE BASIC FUNCTION AND WORKING STATE OF FASTENING SYSTEM

The ballastless track of the high speed railway is consist of rail, fitting, sleeper, fasteners, ballast bed, turnout and other strengthen equipment. The track can guide the train running, sustain the pressure, and transmit it to the subgrade and other constructions.^[1]

Fastener is the key component of the track structure, whose role is to fix the correct position of the rail and to prevent longitudinal and lateral displacement of the rail, and it can provide suitable elasticity, the force will be transmitted to the rail sleeper or support the rail bed.

The role of the fastener is a combination the rail and sleeper track structure in ballast to sustain the train loads and vertical horizontal forces. As the train speed rising and requirement of heavy haul, the track structure advanced from ballast to ballastless, and the wooden pillow is also developed into concrete pillow. When designing the fastener, elasticity has been mainly premeditate, the maintainability and insulation have been fairish considered.

2 FASTENER TYPE OF BALLASTLESS TRACK IN HIGH-SPEED RAILWAY

2.1 *Fastener type of ballastless track in high-speed railway in domestic*

The high-speed railway fastening is consist of clip, component plate of spring foundation, which use the elastic fastener system. As the high-speed

railway developed, so many kinds of fastening systems have been developed in ballastless track., such as Japan, Germany, British, France and etc. The elastic-separation type bar-spring fastener has been used widely for ballastless track in domestic. The characteristics of the fasteners for the ballastless track in China are that the withholding component is the elastic structure. The fastener is fastened separately with two elastic layers. The elasticity is provided by the plate under the rail.

2.2 *The fastener category of the ballastless track in high speed railway*

According to the kind of clip, it can be separated into two kinds, including bar-spring and shrapnel. The bar-spring clip fastener mainly includes Vossloh by Germany, Pandrol by British and IV type, V type, WJ-7, WJ-8 fasteners by China; and the shrapnel fastener mainly includes the directly-connected fastener and the Nabla fastener by France.

According to the bearing way of horizontal force, it can be divided into two types, retaining shoulder-provided or not. The retaining shoulder-provided fastener needs to set rail slot in track slab or sleeper bearing the rail lateral force which is passed by rail. The other kinds of fasteners do not need to set the rail slot, and the rail lateral force which is beared by the anchor blot and the friction. The former representative of products include Vossloh-300 Fastener, WJ-8 Type Fastener; and the latter representative of products include the Directly-connected Fastener, Pandrol Fastener, Krupp ECF Fastener from Germany and the Bar-spring IV Type Fastener, WJ-7 Type Fastener from China.

According to the fastening methods, the fastener can be divided into the two types of bolts and no bolts. At present, in addition to Pandrol Fastener and the Bar-spring IV Type Fastener, other methods are used by the bolts.

According to the linking method with the ballast bed, the fastener separate into the integral fastener and the divided fastener. There are steel plate in divided fastener, and the rail is firmly fixed on the steel plate by the withhold pieces. There are no steel plates in divided fastener in general. Vossloh-300 Fastener, the Japan directly-connected IV fastener, the Nabla fastener by France, the Bar-spring IV Type Fastener and the WJ-8 Type Fastener by China are all the typical representative of the divided type fasteners.

According to the gauge controlling mode, it can be separated into level adjustment and step less adjustment. Japan's eight straight, straight 8K and our country's WJ-7 type fastener system are the stepless adjustment.

2.3 Common high-speed railway fastening systems in domestic and abroad

The ballastless track structure is widely used in new high-speed railway nowadays. It is widely used abroad is Germany Vossloh-300 Fastener and Krupp EFC Fastener, and the WJ-7, WJ-8 fasteners designed by ARS are also widely used in our country.

2.3.1 Vossloh fastener

The composition and the name of the fastener system is shown in Figure 1.

The architecture of Vossloh Fastener system is relatively simple, closely linked good elasticity and it also has large anti-climb resistance, long life and low maintenance. So it adjust to use in the ballastless track structure. This system is double-elastic structure, which is bottomed rail cushion and flexibility. There is no rail slot, and it is possible to adjust to the gauge using the gauge bezel. Not only did the gauge bezel have the ability of maintaining gauge, but it has the function of insulation effect. The static stiffness of the Vossloh 300 fastener is

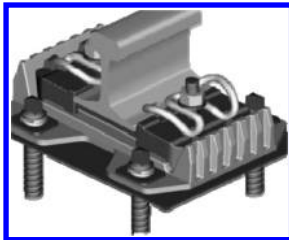


Figure 1. Vossloh-300a fastener.

20–30 kN/mm, the buckling pressure is greater than 18 kN, and the range of bar-spring is greater than 15 mm and the longitudinal anti-climbing ability of the rail is more than 9 kN.

At present, most of the lines in Beijing-Tianjin inter-city railway, Wuhan-Guangzhou high-speed railway and the whole lines of Beijing-Shanghai high-speed railway are all using the Vossloh 300 fasteners.

2.3.2 Japan direct-connected 4K and 8K fastening system

The ballastless track has been researched since 1960s in Japan, which is used direct-connected 4K and direct-connected 8K. In recently, it used the improved-direct-connected 4K and 8K fastening system.

The direct-connected 8K fastener system with the steel plate and the separated structure, which is using embedded plastic sleeves that replaced the metal sleeves. In order to adjust the gauge with moving the steel plate, the oval blot holes are open in the steel plate. The height can be regulate from 0 to 70 mm through the track pad, the steel plate and the adjustable pad, and the range of gauge is ± 10 mm. The direct-connected 4K fastening system is single elastic layer structure with no steel plate, and the shrapnel withhold the rail directly. When the bolt is not tightened, there is only the lower part of shrapnel withhold the rail; and when the bolt is tightened enough, the upper of it is also connected with the rail. At this time, the range of gauge is ± 6 mm, and the range of the height is from 0 to 10 mm.

The improved direct-connected 4K fastening system is utilized the tee hexagon bolts, spherical washer and double adjustable plate. And the range of the height adjustment of system is from 0 to 50 mm, the range of gauge is ± 10 mm.

2.3.3 Pandrol-fastclip fastening system

The fastclip fastening system is shown as Figure 2. The fastclip fastening system developed by Pandrol Company consist of the steel plate, plate plot, flat pad, insulating bush, W bar-spring, insulation gauge block, elastic plate and the insulation

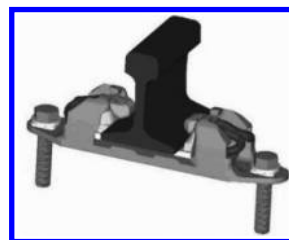


Figure 2. Pandrol fastener.

cushion. Through embedding the insulating bush and anchor bolts into the track slab and sleeper, the steel plate is fixed on it. In the upper of the steel plate is fastclip fastening system, and it used W bar-spring to withhold the rail, which is on bolts attachment. This method named self-locking fastening, through which the elliptical hole moving around to achieve the gauge adjustment.

To achieve the insulation of fastener system, the fastclip fastener system relies on the elastic plate under the rail, insulation gauge block insulating bush and the insulation cushion.^[2]

At present, most of the lines in Wuhan-Guangzhou and Hefei-Wuhan high-speed railway are using this type of fasteners.

2.3.4 High-speed railway fastening system in domestic

With the development and researching of bar-spring IV fastener, V fastener WJ-7 fastener and WJ-8 fastener besides applying the Vossloh 300 fastener and fastclip fastener. The type of bar-spring IV and V fasteners could run up to 250 km/h to meet the operational requirement of passenger dedicated lines which are used in ballast track. Embedded sleeper ballastless track and the slab ballastless track which adjust to use in the bridge, tunnel and the subgrade could run up to 250 km/h to meet the operational requirement of passenger and freight transport dedicated lines and 350 km/h for passenger dedicated line.^[3]

WJ-7 fastening system is shown as Figure 3. The Steel plate of the WJ-7 fastener was fastened to the track slab through the tight fit between anchor bolt and pre buried insulating sleeve.

At present, this kind of fastener is used in parts of the lines in Wuhan-Guangzhou high-speed railway and Shanghai-Nanjing inter-city railway.

WJ-8 fastening system is shown as Figure 4. The requirement of longitudinal resistance of the rail is the same as WJ-7 fastening system. The left and right adjustment is ± 5 mm, the gauge adjustment is ± 10 mm, and the rail height adjustment is 30 mm. The insulation pad which set up between the steel plate and the rail can buffer the shock from the rail

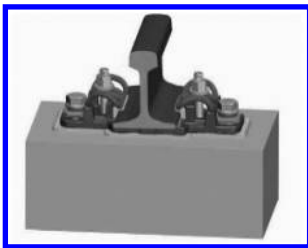


Figure 3. WJ-7 fastener.

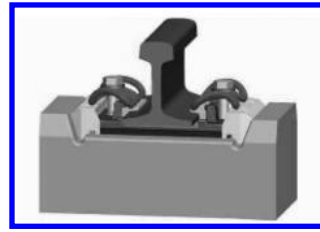


Figure 4. WJ-8 fastener.

to the steel plate. It also can improve the insulation performance of the fastening system.

3 KEY POINTS FOR DESIGN OF FASTENING OF BALLASTLESS TRACK

3.1 The design principle of rail fastener

Only to adjust through the fastener. Therefore, the fastener used in without a frantic jumble orbit needs to have ability to improve. Compared with a frantic jumble orbit, without a frantic jumble of track structure has strong stability and keeping the ability to track geometry. When the line under the condition of normal operation, the change of gauge is less, however, in consideration of concrete foundation construction error, fastener manufacturing tolerance and rail abrasion, it needs ability to adjust to left or right.

3.2 Rail fastener design points

3.2.1 Big resistance of avoiding climbing

Suitable resistance of avoiding climbing is the basis of keeping track stability. Before the opening of the new railway line, track bed design parameters of longitudinal resistance include High-speed rail line 14 kN/pillow (23.3 kN/m) and 200 km per hour cargo and passenger line 12 kN/pillow (20 kN/m). The measured values of the longitudinal resistance of the track bed includes PC pillow for 9.80 kN/pillow (17.20 kN/m) and PC pillow is 19.20 kN/pillow (33.68 kN/m). Obviously, anticlimb ballasted track fastener resistance is greater than the longitudinal resistance of the track bed to meet stability and seamless of rail line laying requirements.

3.2.2 Enough fastener pressure

The rail fastener must have sufficient pressure to ensure a reliable connection between the support and rail. The pressure should not result in the occurrence of rail longitudinal displacement along the bottom plate at the time of the rail bending and rotation, in another word, fastener longitudinal

resistance is greater than the longitudinal resistance of the track bed. The fastener pressure should not be so great, otherwise, it would be a sharp decline in fastener flexibility, impacting fasteners life. If the rail buckle pressure is a little bigger, the temperature telescopic rails will be less, because of the increasing of anti-climb resistance. Also, because of the increasing of track panel rigidity and resistance and energy of long curved rail swollen, stability of the seam line is extremely effective.

3.2.3 *Less components, less maintenances*

The modern railway track structure maintenance can only be carried out within a very short skylight, therefore it requires less maintenance for the rail fasteners. This requires the fastener components have sufficient strength, within a desired life cycle during the use of fastener components do not generate fatigue damage and significant residual deformation, as well as requiring fasteners have better performance at the same time, when fastener and elastic cushion produce wear and residual deformation, the decrease of fastener resistance is small and fastener bolts do not require tightening very often.

3.2.4 *Uniform stiffness and good smoothness*

Modern express railway requires consistent joint stiffness to make sure track elasticity is uniform and guarantee good running quality and passenger riding comfort. Compared with the ballasted railway, the ballastless track requires much better elasticity of the fasteners to minimize track vibration and ease impact between wheel and rail, because the ballastless track structure have removed the ballast layer that provides elasticity for the track.^[5] In a fairly long period of time, the uniformity and stability of fastener stiffness is often difficult to ensure which is limited to the production equipment and management capacity of our country.

3.2.5 *Good damping property*

Rail fastener with lower stiffness is an effective way to reduce force between wheel and rail, as well as vibration and noise. But lower stiffness easily affect the ability of fastener to constrain the rail track, especially the ability to prevent fastener turning outwards, which needs to achieve a balance between the two through the ingenious structural design. The elasticity of concrete sleeper track and ballastless track is mostly provided by fasteners. The stiffness of this kind of track is usually larger than wooden sleeper track.

Therefore it must reduce the stiffness of concrete foundation to make it as close as possible with the stiffness level of ballasted track. Theoretical and experimental results show that, it can be achieved by applying low stiffness rail pad, and the fastener vertical joint stiffness should be around 30 kN/mm, which is appropriate. In the meantime, the rail fastener with 20–40 kN/mm lateral stiffness is appropriate, which can reduce lateral force between wheel and rail. But insufficiency of lateral stiffness will cause gauge widening and out of gauge, which is not allowed in the operation.^[6]

3.2.6 *Good insulation property*

In order to ensure the absolute safety requirements of rail traffic, fastener should have good insulation property to guarantee the normal work of track circuit. The track slab and roadbed slab of the ballastless track, there are many fasteners on each slab as well as many reinforcing bars inside the slab.^[7] It is not like the ballasted track, which PC sleepers are laying solely by the ballast. Therefore, it is very necessary to increase the insulation resistance of ballastless track section, as well as the insulation prosperities of every set of fasteners and internal reinforcing bars of slabs. Especially it should prevent insulation resistance decrease when raining which may cause low ATC signal receiving level and arouse running safety problems. In general, insulation resistance of ballastless track fasteners should be above 100 M Ω .

REFERENCES

- [1] Lu Zuwen Ballastless Track for Passenger Dedicated Railway [M]. Beijing: China Railway Publishing House, 2006.
- [2] He Huawu Ballastless Track Technology [M]. Beijing: China Railway Publishing House, 2006.
- [3] Wang Qichang. Ballastless Track Fastening System [M]. Chengdu: Southwest Jiaotong University Press, 2006.
- [4] Zhao Guotang. High-Speed Railway Ballastless Track Structure [M]. Beijing: China Railway Publishing House, 2006.
- [5] TB 10082-2005, Code For Design Of Railway Track [S].
- [6] Lu Zuwen. Summary of High-Speed Railway Track Technology [J]. Journal of Railway Engineering Society, 2007(1): 53–54.
- [7] Xu Youding Key Points for Design of Ballastless Track Fastening of High-Speed Railway [J]. Journal of Railway Engineering Society, 2010(4): 40–43.

The compared study of flexible central buckles cable girder anchorage system of steel truss girder suspension bridge

Cheng-Dong Yang

Guizhou Expressway Group Co., Ltd., Guizhou, China

ABSTRACT: By taking an under-construction long span steel trussed girder suspension bridge as an example, the structure and institution method of the flexible central buckles are studied and compared in the paper. Then based on the FEM analysis of the anchor-box and auricular anchor plate cable-girder anchorage system using ANSYS, the stress distribution and stress transferring mechanism of the cable anchorage system are analyzed. Some useful conclusions are achieved, which may be a meaningful reference to choosing to the design of the flexible central buckles of the same steel trussed girder suspension bridge.

Keywords: steel truss girder suspension bridge; flexible central buckles; cable-girder anchorage system; finite element analysis and comparison

1 INTRODUCTION

The modern suspension bridge is a kind of flexible cable beam composite system, it is composed of main cable and stiffening girder, it is a very competitive bridge with large span capacity and beautiful structure model and other advantages. The main cable of suspension bridge is the main load-bearing component, it transfer the weight of stiffening girder, the two stage of dead load and live load to the main tower and foundation. The sling cable of suspension bridge is small to resist horizontal displacement effect because it is vertically arranged, when suspension bridge is under external loads, the longitudinal and transverse direction between the cable and the girder of suspension bridge will produce relative displacement, and slings will be tilted and local bending, the stress of the short slings in the center position of suspension main span is worse. In order to reduce the longitudinal expansion amount of stiffening girder, reduce the deflection of the main span, improve the bending and fatigue of the sling of the main span, the central buckle is set between the central position on the stiffening girder and the main cable^[1-4]. At present, the flexible central buckle is set on the lots of suspension bridge of the large span steel truss girder, the sling of the central buckle is reliably connected with the main cable and the stiffening girder through anchorage system of the ends of the beam of the anchor box or ear plate, because the load transfer of the end the beam is complex, the effect of stress concentration

of the ends of the beam is obvious and easy to have fatigue and strength failure^[5-8], the space finite element analysis must be carried out for the central buckle. In the paper, through the study of anchorage method the end of the girder, the finite element models of the two beam anchoring system of anchor box and ear plate are established, the law and stress distribution of each panel in anchorage system of sling and girder are studied, some valuable conclusions are obtained.

2 THE BRIDGE ENGINEERING SURVEY

The bridge is located on Dong Ting lake, it is the suspension bridge of Twin Towers and asymmetric double span steel truss stiffening girder, its main cable span distribution is 460 m+1480 m+491 m. The main cable rise span ratio is 1/10, its transverse spacing is 35.4 m.

The girder of the suspension bridge is combined with steel truss stiffening girder of combined type, the interaction of plate girder is considered. The steel truss beam of the suspension is consist of the main truss, the transverse truss, the bottom lateral bracing and the steel bridge deck system, the main truss mode is adopted in the node board technology of whole welding. The height is the main truss of the suspension bridge is 9 m, the length of the standard inter node is 16.8 m, the center distance of left and right chord of two pieces of the main truss is 35.4 m; the main truss of the suspension bridge is



Figure 1. Effects diagram of Dongting Lake bridge of Taiyue Highway.

the Warren Type Structure consisting of the top and the bottom chord and vertical and oblique chord; the main transverse truss is single truss structure consisting of the upper and the lower beam, the external oblique abdominal rod, the vertical and the medial oblique abdominal rod; the bottom lateral bracing is for the system of K. The steel bridge deck system is the orthotropic steel deck structure consisting of the bridge deck, U shaped stiffening ribs, longitudinal deck ribs, bridge deck transverse beam, the bridge deck transverse ribs and I-shaped longitudinal beam.

The braiding forms of the main cable of the suspension is for the Prefabricated Parallel Wire Strands (PPWS), the PPWS of small side and the main span are made of high strength galvanized steel wire of 175 shares, the PPWS of the big side span are made of high strength galvanized steel wire of 181 shares, the each share of high strength galvanized steel wire is 127 root, a diameter of each root is 5.35 mm, the nominal tensile strength 1860 MPa. According to the size of the force, the sling is divided into two kinds type, a kind type of sling is adopted to the wire rope of the 8×41 WS + IWR structure, diameter of 68 mm, nominal tensile strength 1870 MPa; another kind type of sling is adopted in the wire rope of the 8×55 SWS + IWR structure, diameter of 88 mm, nominal tensile strength 1960 MPa; the connection of the sling and the cable clamp is adopted with the straddle type, the connection of the sling and the steel truss girder is adopted with pin hinge.

The bridge tower of the suspension bridge is adopted in the portal frame, the foundation under the single pylon tower is set to the D280 pile of 40. Cross strait anchorage is set to gravity anchor of underground continuous wall foundation. The lateral resistant wind bearing is set in the bridge tower of the starting point, the vertical bearing and lateral resistant wind bearing are set in the bridge tower of end side and anchorage.

3 STUDY ON THE ANCHOR METHOD OF BEAM END OF FLEXIBLE CENTRAL BUCKLE

Along with the people deepening the understanding to the central buckle on the role in long-span suspension bridge, the following three central buckle connection is developed and formed: (1) the flexible central buckle, namely one and more pairs of inclined hangers are set in the stiffening girder cross to form longitudinal restraint of the main cable and beam; (2) the rigid central buckle, namely the stiffening girder is connected with the main cable by rigid triangular truss in the middle of the main span^[3]; (3) the cable and the beam are directly fixed connection. In the three kinds of connection, the flexible central buckle connecting is the weakest, the rigid central buckle joint is slightly, the connection that the cable and beam directly is fixed is the strongest effect. A few large span suspension bridge setting a central buckle that have been built in the domestic and abroad is listed in the Table 1.

As can be indicates from the above table, the rigid central buckle of the strong connection is set in the steel box stiffening girder suspension bridge, the flexible central buckle of the weaker connection is set in the steel truss stiffening girder suspension bridge. its reason is investigated, after the main cable and the stiffening girder is connected with the central buckle in the middle of the main span, it is equivalent to an increase of 1.5 rigid support^[9], the connected stiffness set central buckle is in general matching to the stiffness of the stiffening girder. Because the height of the stiffening girder of steel box beam is lower and its stiffness is relatively small, the strong connection is used between the main cable and the stiffening girder in order to better play its role in supporting, so the rigid central buckle is set generally; the height of the steel truss beam is more large with strong rigidity, a relatively weak central buckle can be arranged on the with connection of the main cable and the

Table 1. The general summary of long span suspension bridges with central buckles.

Bridge name	The main cable span (m)	The stiffening girder type	The central buckle type
The great belt bridge	535 + 1624 + 535	Three span continuous steel box girder	Rigid
The little belt bridge	240 + 600 + 240	Three span continuous steel box girder	Rigid
The Runyang Yangtze River bridge	470 + 1490 + 470	Single span two hinged girder	Rigid
The Si Du River bridge	114 + 900 + 208	Single span two hinged steel truss girder	Rigid
The South Seto great bridge	274 + 1100 + 274	Three span continuous steel truss girder	Flexibility
The North Seto great bridge	274 + 990 + 274	Three span continuous steel truss girder	Flexibility
The Zi Shui great bridge	200 + 856 + 190	Single span simply supported steel truss girder	Flexibility
The Ba Ling River great bridge	248 + 1088 + 228	Single span simply supported steel truss girder	Flexibility
The Ai Zhai great bridge	242 + 1176 + 116	Single span simply supported steel truss girder	Flexibility

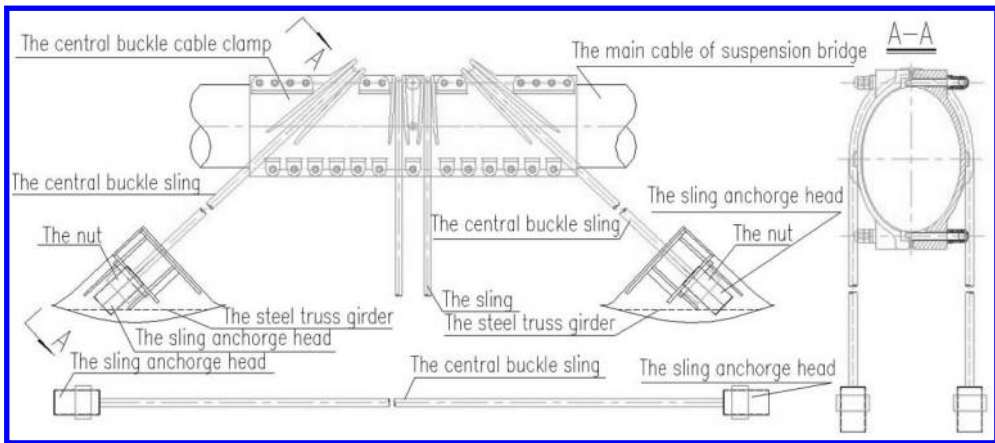


Figure 2. Scheme I: Structure of central buckles cable.

steel truss beam, so the flexible central buckle of simple structure can meet the requirements. It is indicated in study of Song Hui^[10], the influence of central buckle on single span suspension system stiffness is very small, that has a significant effect on vertical stiffness of two and three span continuous longitudinal vertical elastic constraint system. In addition, the optimal central buckle set scheme is selected needing to take various factors into consideration when designing, such as Si Du river bridge using of single span steel truss stiffening girder, because the it located on the road one-way Longitudinal Slope of 2.41%, the longitudinal displacement caused by automobile brake force is big, the rigid central buckle of strong connection effect was used in designing to the structural stress and working conditions of expansion joints and bearings.

Considering the girder of the suspension bridge is the steel truss of rigid greatly, the flexible central

buckle is set in the designing, namely 5 of wire rope sling is set in the middle span of the stiffening girder, it are symmetrically arranged on the middle span of both sides. The flexible central buckle system can be divided into three parts: the main cable end anchorage system, intermediate sling anchorage and stiffening girder end anchorage system.

The 8×55 SWS + IWR structure is used on the middle sling of central buckle, the steel wire rope diameter is 88 mm, nominal tensile strength is 1960 MPa; the straddle connection is used in the rope clip of the main cable, the bearing type hot cast anchor is adopt in the end of the steel truss girder; the anchor head comprises anchor cup and rut, its materials are made of 35CrMo alloy steel. Casting zinc copper alloy to fix the wire rope in the anchor cup, the error produced in manufacturing and installation is eliminated in setting the adjusting rut on anchor head (Fig. 2 and Fig. 3).

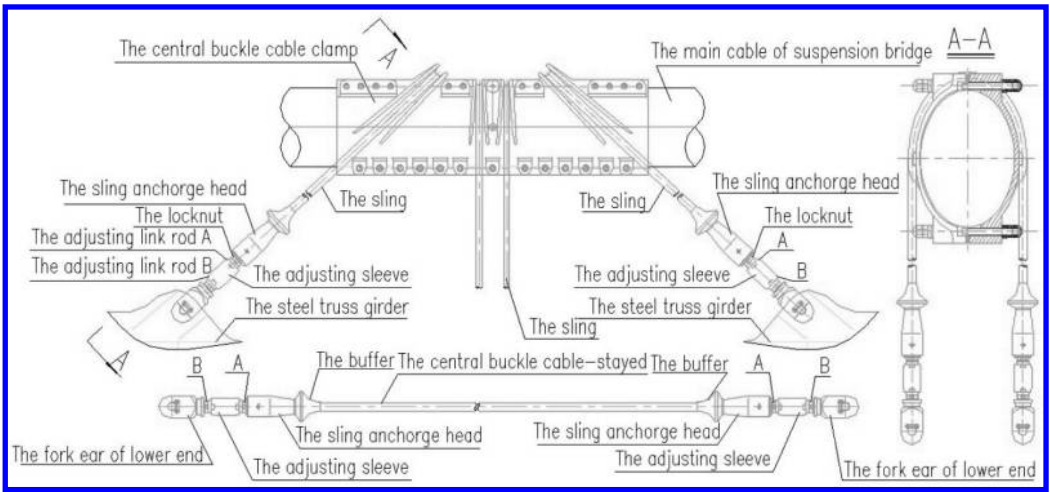


Figure 3. Scheme II: Structure of central buckles cable.

The anchor system of the main cable side of central buckle is composed of cable clamp of left and right involution, that is locked ring on the main cable in screw, the waterproof sealing rubber strip is filled in the joint block, the cable clamp is longitudinal extension to setting the grooves formed by the convex rib to hang the short oblique cord; the cable clamp designing length of central buckle is 3.38 m, the wall thickness is 45 mm, the material is for the low alloy steel castings of ZG20 Mn; in order to preventing the cable and cable relative slip between the cable clamp, 25 high strength screw were set to provide adequate confining stress on the cable clamp.

The two kinds of anchoring scheme of the beam end in central buckle is studied in the paper. The anchor structure of the anchor box (pressure) is set in the end of beam in the scheme I, that is welded along the central buckle sling axial with the whole node plate extending upward from the web of the top chord, upper and lower anchor plate, backing plate. Before and after the pressure plate and the stiffening rib, the bolt connection is adopted in the shim plate and the pressure plate; at the same time the diagonal stiffened plate is welded in the corresponding bearing plate position on both web sides (Fig. 4).

The anchor structure of the ear plate (pin hinge) is set at the end of the beam in the Scheme II, that is welded with ear plate of the upper chord web upward formation in the nodes and transverse stiffener welding; at the same time the two plate affixed have been arranged on both sides of the pin hole to reinforce the pin hole of ear plate (Fig. 5).

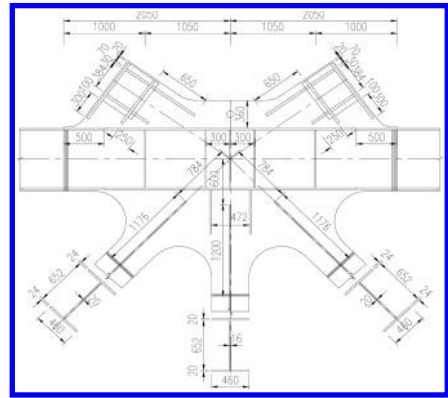


Figure 4. Scheme I: Structure of central buckles cable-girder anchorage joint plate (unit: mm).

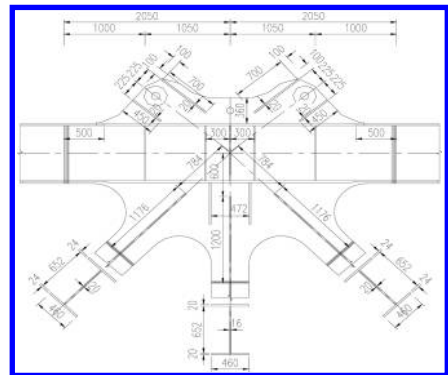


Figure 5. Scheme II: Structure of central buckles cable-girder anchorage joint plate (unit: mm).

4 THE LOCAL STRESS ANALYSIS OF THE GIRDER END ANCHORAGE SYSTEM OF ANCHOR BOX

Because the anchor structure of the end of beam of central buckle is complex, the general finite element program ANSYS is adopted to local space finite element analysis in the most unfavorable conditions. The stiffening girder of two pairs central buckle intersection position in the vicinity of the middle span of main truss is taken as the research object. In order to reducing the influence of the beam end anchoring system analysis results of central buckle on the boundary conditions, according to the Saint Venant's Principle calculation model 8.4 m a steel truss girder segment is taken each in the longitudinal in beam end anchoring position before and after of stayed-cable of the central buckle, considering the symmetry of the steel truss girder, it is taken to the half position of the bridge panel span in the horizontal, it is taken to whole steel truss beam in height direction.

The whole structure is considered to be a homogeneous elastic body in finite element calculation, the steel truss girder and steel anchor box are made of Q345qD steel, the material is isotropic, the yield limit is 345 MPa, the elastic modulus is 210×103 Mpa, Poisson's ratio is 0.3, the density is 7850 kg/m^3 . The maximum cable force of a single cable-stayed of central buckle is 1250 KN. When loading the diffusion effect of the backing plate to the cable force is considered, in accordance with the stress diffusion angle of 15° the cable force from anchor ring is brought to on the bearing plate torus after the expanding. The boundary conditions of calculating model is: all nodes of segment model of two side section in the longitudinal direction of the bridge are consolidated; in the cross direction of bridge, the symmetric constrain is applied on the transverse bridge deck width half section of the segment model of the box beam.

Because cable-stayed anchor head anchor tightly press on the backing plate under a huge cable force, the bolt connection is between backing plate and back bearing plate, there are a relationship not being welded but being pressed close between the three, which brings some difficulty to the finite element modeling. At present there are 3 kinds of methods to handle the connection: equivalent plate thickness^[12], nonlinear contact element method, solid element with nonlinear contact element, etc.. The contact problem to be a highly nonlinear behavior, lot of computational resource are needed, and by the current calculation theory limits the result is not easy to converge, so it is not convenient for engineering application; though the stress values calculated in the equivalent plate thickness method are

relatively large, its calculation theory is simple and it is easy to be mastered and be applied by engineering design personnel. The nonlinear contact problem between anchor box bearing plate and the anchor pad is dealt with equivalent thickness method in the paper.

When the models are established, the every chord of steel truss girder and orthotropic bridge decks are used 4 nodes elastic shell Shell63 unit of ANSYS to simulation; considering that the equivalent plate thickness is larger after anchor box bearing plate is calculated by the equivalent, it is used in 8 nodes elastic shell element shell 93 to simulate, shell 93 element is based on a thick shell theory and it is considered the influence of shearing deformation. When the finite element is analysis, the model is established in strict accordance with the truss members, bridge deck and the central buckle anchor plate and stiffener location and size, when meshing, the grid of anchor box near plate is conducted appropriate encryption, there are 51341 nodes and 53472 units in the finite calculation element model totally (Fig. 6 and Fig. 7).

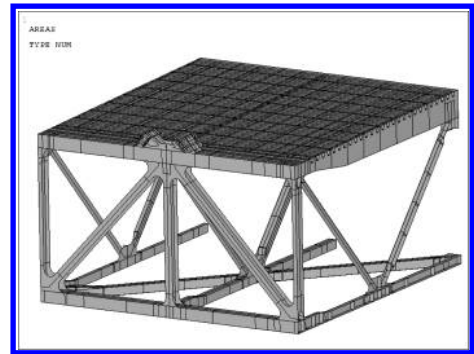


Figure 6. Scheme I: Global FEA model.

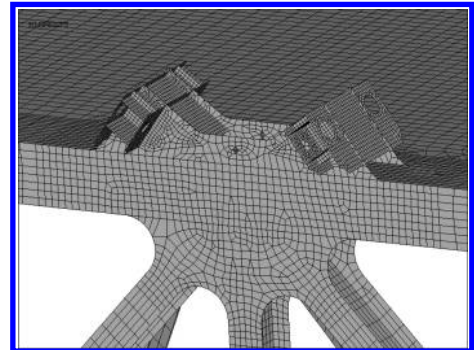


Figure 7. Scheme I: Partial FEA model of central buckles joint plate.

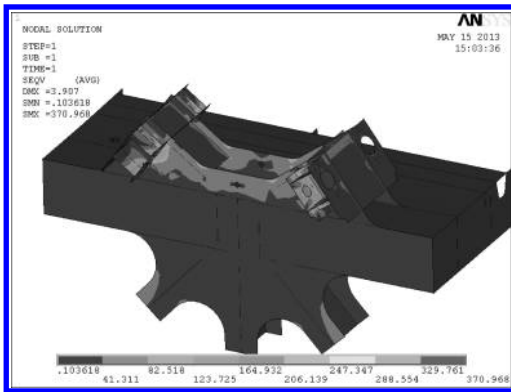


Figure 8. Scheme I: Partial FEA model of central buckles.

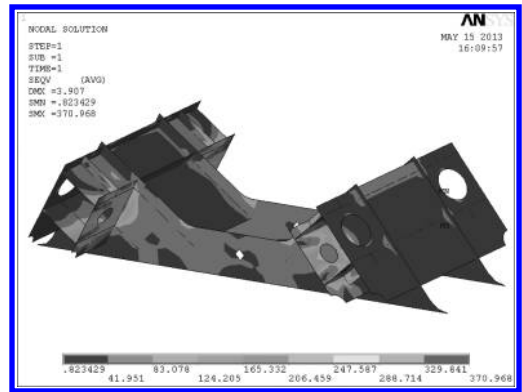


Figure 9. Scheme I: Mises stress of central buckles (Unit: Mpa).

Table 2. Scheme I: Mises stress numerical table of central buckle.

The position	Mises stress (MPa)	The maximum position
The anchoring plate	370.97	The Junction position with bearing press plate
The bearing press plate	341.57	The Junction position with anchoring plate
The node plate (not including the ear plate)	171.39	The Junction position with bearing press plate
The top chord	36.89	The Junction position with oblique web bar
The vertical web bar	29.54	The Junction position with top chord
The oblique web bar	54.8	The Junction position with node plate
The bridge deck	31.62	The position nearly central buckle
The transverse diaphragm	38.96	The U rib position nearly central buckle

Mises stress diagram of the anchorage zone of central buckle is shown in Figure 8 and Figure 9, Mises stress values of central buckle parts and near the main plate in the condition is shown in Table 2.

It can be shown from the above calculation results, the phenomenon of stress concentration in small range occur in the welding of anchorage system of beam end and bearing plate hole outside, the larger Mises stress occurs in the vicinity of the anchor plate and bearing plate junction, the value is for the 370.97 MPa. The rest of high stress area appears on the node board near the anchor plate location, the stress value is about for 170 MPa. The rest of the plate stress level is not high, keeping the following in the 100 MPa. The upper and lower anchoring plate of central buckle play the effective support to the bearing plate, the cable force spread the whole node plate through a weld between the bearing plate and anchoring plate and gusset plate, then spread to the entire steel truss beam. Because the anchoring system structure is complex and the welding seam is more, the stress concentration position is more else.

5 THE LOCAL STRESS ANALYSIS OF THE EAR PLATE GIRDER END ANCHORAGE SYSTEM

The ear plate cable beam anchorage method has been widely applied in the tradition steel box girder cable-stayed bridge, the force transmission reliability and structure rationality of the cable beam anchoring system is commonly verified in the results of the finite element simulation analysis and model test^[13-15]. But its application is seldom reported in flexible central buckle of steel truss suspension bridge. In the paper it is considered that the cable girder anchorage system is applied to the suspension bridge flexible central buckle, and the local stress analysis is done in the establishment of finite element calculation models to the system.

In addition to the central buckle cable anchorage structure made the appropriate changes in the scheme, the calculation model of completely consistent of scheme I is adopted in the rest of the scheme. Taking into account that there is the welding stick plate to reinforcement on both sides of the pin hole of the ear plate, the stick plate

zone is used in 8 nodes elastic thick shell element shell 93 in ANSYS simulation; when it is loaded, it is assumed that the sling force uniformly is applied on upper semicircular ring of the pin hole of the ear plate through a pin shaft. The calculation model is shown in Figure 10 to Figure 11, the model is discretized into 50471 nodes and 51733 units.

Mises stress diagram of the anchorage zone of central buckle is shown in Figure 12 and Figure 13, Mises stress values of central buckle parts and near the main plate in the condition is shown in Table 3.

It is shown from the above results that the maximum stress occurs near the pin hole in the ear plate,

but its spread quickly. The very small range of stress concentration appeared near the hole wall in contact with the pins shaft along the cable force direction, the maximum Mises stress is 237.17 MPa, the rest position stress is below 100 Mpa. The transmitting path of cable force of the system is: the cable force transfer the pin hinge connecting piece through the low end of the fork lifting lug, the pin hinge connecting piece is then transmitted to the anchorage ear plate, and the middle cable force transferred to the entire main truss through the upper chord web. Because the anchorage system has the advantages of simple structure, less so the weld, the stress transfer smoothly, the location of stress concentration is less.

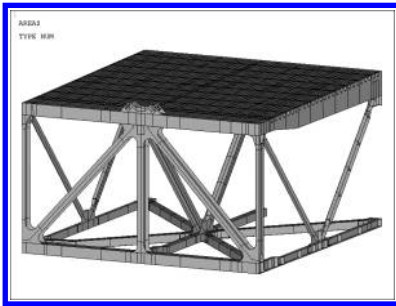


Figure 10. Scheme II: Global geometry model.

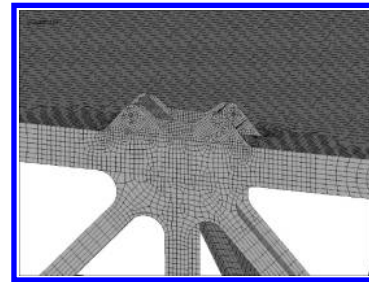


Figure 11. Scheme II: Partial FEA model of central buckles joint plate.

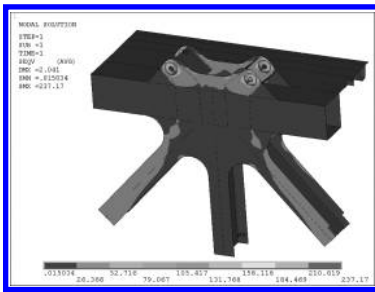


Figure 12. Scheme II: Partial mises stress of central buckles.

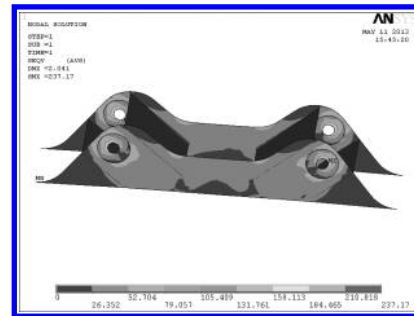


Figure 13. Scheme II: Mises stress of central buckles.

Table 3. Scheme II mises stress numerical table of central buckle.

Position	Mises stress (MPa)	The maximum position
Ear plate	237.17	Pin hole nearly
Ear plate stiffening plate	64.99	The junction with the ear plate
Node plate (not including the ear plate)	51.38	The junction with the oblique web bar
Top chord	29.5	The junction with the oblique web bar
The vertical web bar	31.7	The junction with the top chord
The oblique web bar	41.44	The junction with the node plate
The bridge deck	21.5	The position nearly central buckle
The transverse diaphragm	31.24	The U rib position nearly central buckle

6 CONCLUSION

Based on the construction of large span steel truss girder suspension bridge in the paper, the setting of central buckle of long-span suspension bridge is studied, the setting method and the stress transfer mechanism of the beam end anchoring system of the two flexible central buckle of the anchor box and ear plate are studied comparatively, the local space finite element calculation model of two anchoring system is established with the spatial element, the stress distribution of anchorage system is studied. The following conclusions can be obtained according to the above analysis:

1. The structure of anchor box anchorage system is complex, the plate number is more, each plate processing precision of welding seam and dimension is required higher. The path of stress transfer of the anchor method is complex, the its stress transfer mainly through the weld seam of the bearing plate, anchor plate and gusset plate, because of the structure space constraints, the weak area exists in middle span position of outside without web stiffening support, there are high stress level in the area, the stress concentration in the welding seam position is obvious, the stress diffusion is not conducive.
2. Because the ear plate anchorage system is simple structure, easy to manufacture, convenient to installation and maintenance, easy to late replacement. The stress value of each member in anchorage zone of ear plate anchorage system is the larger in the small range of the pin hole of the ear plate near, after it is strengthened in arranging the board on both sides in the pin hole of the ear plate, the stress in the rest position outside the pin hole spread quickly, the stress transmission is fluid.

In summary, when the central buckle is set in large span steel truss girder suspension bridge, the flexible central buckle can be given priority setting, and the ear plate anchorage system is used at the beam end. The stress concentration of the anchorage system is less and the stress extreme is the smaller, that is more suitable for the steel truss girder suspension bridge that the cable force is not too large and the space structure installed is limited than anchor box system central buckle.

Author for correspondence: Yang Chengdong;
E-mail:345241426@qq.com;Tel: 13984880498.

REFERENCES

- [1] Gao Jian, Liu Gao, Zeng Yu, Design of central buckles of Guizhou Baling River steel trussed suspension bridge. [C]// Proceedings of the national conference on bridge engineering. Beijing: China Communications Press, 2005:101–106.
- [2] Zhang Jinqun, QU Zhaole, Song Jianyong, Yang Yun. Overview of Multi-pylon Multi-span Suspension Bridge [J]. Journal of Highway and Transportation Research and Development, 2011, 9(28):30–45.
- [3] Wang Jun, Jing Hong-liang. Influence of Flexible Central Buckle on Dynamic Behavior of Long-Span Suspension Bridge [J]. Shang Highways, 2010, 4(0):35–38.
- [4] Viola JM, Syed S, CI Enance J. The New Tacoma Narrows Suspension Bridge: Construction Support and Engineering [C]// ASCE. Proceedings of the 2005 Structures Congress and the 2005 Forensic Engineering Symposium. New York: ASCE, 2005:1–12.
- [5] Li Xiao-zhen, Cai Jing, Qiang Shi-zhong. Studies on models of cable-girder anchorage for long-span cable-stayed bridges with steel box girder [J]. China Civil Engineering Journal, 2001, 37(3):73–79.
- [6] Li Zhan. The affect of characteristics of the vibration of cable for single-span simply supported steel truss suspension bridge from Central buckle[J]. Journal of Highway and Transportation Research and Development (Applied Technology Edition), 2010, 11(71):169–171.
- [7] Wang Hao, Li Ai-qun, Guo Tong. Multi-scale Finite Element Modeling Method on Supe-long span Suspension Bridges with Central Buckle [J]. China Journal of Highway and Transport, 2009, 06 (22): 60–66.
- [8] Wang Hao, Li Aiqun, Yang Yudong, et al Influence of Central Buckle on Dynamic Behavior of Long span Suspension Bridge [J]. China Journal of Highway and Transport, 2006, 19 (6): 49–53.
- [9] Shanghai Municipal Engineering Design Institute. The handbook of bridge design Engineers. [M]. Beijing: China Communications Press, 2007.
- [10] Song Hui, Lin Qia, Tang Maolin. Influence analysis of central buckle in suspension bridge on different suspension systems [J]. Engineering Science, 2010,12 (7):22–27.
- [11] Xu Xun, Qiang Shi-zhong, He Shuan-hai. Influence of central buckle on dynamic behavior and response of long-span suspension bridge under vehicle group excitation [J]. China Journal of Highway and Transport, 2008, 21(6):57–63. (in Chinese).
- [12] Yan Hai, Fan Li-chu. Research on nonlinear contact problem of cable-beam anchorage for long span cable stayed bridge [J]. China Journal of Highway and Transport, 2004, 17(2):46–49.
- [13] Liu Qingkuan, Qiang Shizhong, Zhang Qiang, et al. Structural analysis of ear-plate cable and beam anchorage for cable-stayed bridge [J]. China Journal of Highway and Transport, 2002, 15 (1):72–75.
- [14] Wei Xing, Qiang Shiz-hong. 3D analysis on anchorage zonebetween beam and cable in cable-stayed bridge [J]. China Railway Science, 2004, 25 (5):67–71.
- [15] Zhu Jinsong, Xiao Rucheng, Cao Yi-shan. Model Test on the Cable Anchorage of the Main Girder of the Hangzhou Bay Bridge [J].China Civil Engineering Journal. 2007, 40(1):49–53.

Study of greenway site selection based on cultural route: Research on grassland silk road (from Xanadu to Zhongdu)

Pan Zhou

College of Horticulture and Forestry Sciences, Huazhong Agricultural University, Wuhan, Hubei, China

Jia Yu Wu

College of Urban and Environmental Sciences, Peking University, Beijing, China

Xue Fei Wu

College of Horticulture and Forestry Sciences, Huazhong Agricultural University, Wuhan, Hubei, China

Yi Wei Huang

Taubman College of Architecture and Urban Planning, University of Michigan, Ann Arbor, Michigan, USA

ABSTRACT: Greenways are green networks with multi-functions and multi-objectives, and the cultural and heritage preservation aspect of Greenway system has become one of the most important research directions in the field. Cultural route, as a cutting edge concept in the world heritage research, concentrates on the overall value of background environment and relevant areas. Greenways with the emphasis on the cultural aspect strengthen the sense of identity and its historic value. The paper takes Grassland Silk Road (from Xanadu to Zhongdu) as an example, delimits the protection scope of this Cultural Route based on the specific sources and resistance plane via Minimal Cumulative Resistance (MCR) model. Moreover, the research determines the site selection and the service facility planning guide of Greenway through the analysis of heritage utilization. In summary, the research can provide a new approach for Cultural Route protection and Greenway utilization in the research field.

Keywords: Greenway; Cultural Route; the Grassland Silk Road; Cumulative Resistance (MCR) model

1 INTRODUCTION

On June 29, 2012, The Site of Xanadu was listed in the UNESCO World Heritage List at the 34th World Heritage Committee meeting. It was since 1988 that Xanadu had begun applying for World Cultural Heritage, as one of the third category of the national key cultural relics protection units announced by the State Council of China. Then it was added into the Preparatory Directory for World Cultural Heritages of China in 1996, and designated again in the Preparatory Directory reenacted by the state bureau of cultural relics in 2006. Finally, Xanadu was voted to be listed formally as a world heritage site in the World Heritage Committee meeting hold in Russia in June, 2012. However, it should be noted that it was via the associated application with the Site of Zhongdu (Zhangbei, Hebei Province) that Xanadu was included both in the Preparatory Directory in 1996 and the one reenacted in 2006. Although Zhongdu had no chance to be declared, its close connection

with Xanadu is beyond any doubt. Among the three post roads in Mongol-Yuan Period, the one between Xanadu and Zhongdu was formed firstly and used most frequently, which is a typical cultural route with abundant monuments and waters all around it. Unfortunately, the protection of this cultural route, which is located in the middle part of the farming-pastoral zone in Northern China with fragile ecology, is confronting severe challenges. Recently, it has suffered increasing ecological problems—desertification, grasslands-waters degradation, soil-water loss and soil salinization.

1.1 *Research review on Cultural Route*

As a hotspot problem in the heritage protection field, Cultural Routes research started at the expert meeting with the theme of “Routes as Part of our Cultural Routes” held in Spain in 1994. Then the ICOMOS International Scientific Committee on Cultural Routes (CIIC) was established for the research of Cultural Routes Heritage in 1998. In the

2005 version of Operational Guidelines for the Implementation of the World Heritage Convention (World Heritage Center, 2005), Cultural Route, as an important component of Heritage Routes, was included in World Heritage List. ICOMOS Charter on Cultural Routes (ICOMOS, 2008), enacted at the 16th ICOMOS meeting in 2008, illuminated its content, value and significance comprehensively and systematically. By this time, a relatively perfect theoretical system of Cultural Routes had formed as a new type of heritage recognized in the World Heritage field.

Many related research results were published involving review of the theoretical development and research (Liu, 2007), identification and introduction (Wang, Ruan, 2010; Angela, 2005), concept discrimination (Liu, 2006), value assessment (Ruan, Ding, 2008), and protection planning and management of Cultural Routes (Jing, 2005). However, it was not given insufficient attention about how to identify its protection area reasonably and scientifically. The delimitation of the protection and buffer area of heritages is not only the basement of heritages protection planning but also an important content of the heritage protection management assessment of the World Heritage Organization. The formation of Cultural Routes, as a special heritage type, is influenced by the surrounding natural geographical environment which determines the path and form directly (ICOMOS, 2008). Additionally, in order to protect the authenticity and integrity of the setting, an indispensable element of Cultural Routes, it is particularly important to delimit a setting scope clear and administrable. With both cross-cultural significance and dynamic character, Cultural Routes are huge in the spatial dimension as well as changing constantly with the dynamic regional environment on the time dimension, so that it is complex to delimit protection area of Cultural Routes.

1.2 *Research review on Greenway*

The thought of Greenway was derived from Parkway in the 18th century, and enriched by the thoughts of Greenbelt and Green Line in the late 19th century. The clear concept of Greenway was arisen in 1950s and developed as trails with the main objective of recreation from 1960s to early 1980s. Subsequently, the comprehensive Greenway was formed gradually with multiple targets, including biological conservation, environmental protection, historical protection, recreation and education. With the emergence of Greenway Movement, there were numerous research achievements on Greenway (Ahern, 1995) as the hot research area in various disciplines, such as environmental sciences (Ndubisi, 1995), urban planning

(Walmsley, 1995) and geography. These researches included ecological benefits of Greenway (Smith & Hellmund, 1993; Dawson, 1995), cultural heritage protection (Fabos, 1991; Lewis, 1964), leisure and recreation function (Shafer, et al., 2000; Tzolova, 1995), planning method of Greenway (Turner, 1995) and so on. While the original Greenway was mainly based on rivers (Furuseh & Altman, 1991), valleys (Yahner & Korostoff, 1995) or urban street landscape (Burel & Baudry, 1995), its multi-functionalization enabled Cultural Route (Wu, et al., 2013), green infrastructure (Walmsley, 2006) and Scenic byway as the basis of Greenway planning (Schrader, 1995). The research scales of Greenway involved region (Gobster, 1995), urban (Lindsey, 1999) and community.

Suitability analysis is a key planning method of the multifunctional Greenway (Zhu & Liu, 2006). Miller W, et al. (1998) achieved the comprehensive evaluation results of the suitability analysis of Greenway through overlaying three main functions, biological conservation, river corridor protection and recreation, in their research on the valley in Arizona, USA. Dawson KJ (Dawson, 1995) assessed the priority of regional Greenway networks in Georgia on the basis of inner value, outer value and stress degree. Conine et al. (2004) researched multiobjective urban Greenway planning suitability based on human requirement.

The common methods of land suitability evaluation contained entropy-right method (Wei & Wang, 2013), analytic hierarchy process (Zhou & Ren, 2011) and neural network model, which all belonged to the map superposition method or the combinative method based on logic rules. In these methods, however, there remained strong subjectivity in the process of factor weight ascertaining and rule making (Chen, et al., 2006). Moreover, they merely focused on the vertical process of landscape units by overlaying every ecological factor instead of concerning the horizontal process of landscape (Li et al., 2002). Minimal Cumulative Resistance (MCR) model played an important role in land suitability evaluation, which emphasized objectivity of evaluation results and horizontal process of landscape units with plenty of practice in various areas, including the ecological security pattern (Yu, 1999), natural conservation areas (Li & Liu, 2006) and urban land analysis (Liu et al., 2010). As a consequence, this paper explores to apply MCR model to the regional heritage protection and Greenway site selection on basis of the Grassland Silk Road (from Xanadu to Zhongdu).

1.3 *Research review on the Grassland Silk Road*

Among four ancient Silk Roads of China, the Grassland Silk Road is the earliest one which

Table 1. The comparison of Greenway and Cultural Route.

	Greenway	Cultural Route
Research area applied first	Landscape architecture, Ecology	World Heritage research
Researcher raising first	Whyte (1959)	The Expert Meeting on Routes as our Cultural Heritage, Madrid (1994)
Accrediting official agency	President's Commission on Americans Outdoors	ICOMOS
Research content	<ol style="list-style-type: none"> 1. Ecological protection; 2. Historical and cultural conservation; 3. Evaluation research on visual aesthetics; 4. Research on planning concept and method of comprehensive Greenway; 5. Research on the user experience; 6. Implement, management and relevant policies; 7. Construction and development of Greenway in the world. 	<ol style="list-style-type: none"> 1. Basic principles and methods of Cultural Route; 2. Assessment, protection, preservation, management and basic mechanisms of related knowledge development; 3. Basic principle and standard of reasonable utilization, authenticity, integrity; 4. The construction of national and international cooperation platform.
Similarity	<ol style="list-style-type: none"> 1. Functions of linear heritage protection; 2. Point-line-area combination in liner heritage; 3. Various types (classified based on objective and function, regional type, al.); 4. Methods of research and management. 	
Difference	<ol style="list-style-type: none"> 1. Different scales (Greenway is Multi-scale and Cultural Route is large scale); 2. Different emphasizes of heritage protection (Greenway is aimed for nature, economy, and culture equivalently while Cultural Route attaches absolute importance to the value of culture). 	

experienced the longest historical periods, spread over the vastest territory, and developed the most routes. Until Ming and Qing Dynasties, the Grassland Silk Road had been changing constantly and achieved its greatest prosperity during Yuan Dynasty. Unfortunately, it was gained insufficient attention. It was the Desert Silk Road as the main part of the Silk Road that China and Kazakhstan united to apply for World Cultural Heritage in 2014. Recently, the depth and width of the research on the Grassland Silk Road which mainly focused on historical changes and cultural and economic interaction, is far less than that of the other three Silk Roads. Therefore, this research on Grassland Silk Road (from Xanadu to Zhongdu) could not only be beneficial to improve public recognition, but also provide referable strategies of heritage protection and sustainable utilization after the Site of Xanadu was entitled as World Heritage.

2 METHOD AND MATERIAL

2.1 Protection scope analysis of Cultural Route

Wu et al. (2013) have concluded that the Grassland Silk Road (from Xanadu to Zhongdu) meets the standards of Cultural Route. As its constant evolution, currently, it is inexistence the Silk Road with clear and unique location. Hence, we focus on the key cultural heritages, identify relevant surrounding

area and delimit heritage protection area ultimately. Based on Minimal Cumulative Resistance (MCR) model, we define heritage sites as sources and attribute resistance plane to the setting around it.

2.1.1 Minimal Cumulative Resistance (MCR) model

MCR model, put forward originally by Knaapen in 1992, described the costing during the process species moving from source to destination. This model, however, in recent study, merely focuses on resistance coefficient and distance rather than source. In the suitability analysis on the heritage protection and recreation for Greenway, we define heritage sites and travelling resources as sources, and classify resistance coefficients of different land use based on the resistance of relevant expansion prevented by the setting. The expression modified is following,

$$MCR = k * f_{min} \sum_{j=n}^{i=m} D_{ij} * R_i$$

Thereinto, MCR is the value of minimal cumulative resistance plane, k is the modification coefficient. The higher the source is ranked, the larger the relevant area spreads. In turn, the lower-ranked source confronts a stronger resistance. f refers to the positive correlation between the minimal

Table 2. Greenway planning based on minimal cumulative resistance model.

Goal level		Index level		Factor level					
Site selection planning for Greenway based on MCR model	Heritage protection suitability analysis	Source: site	Value of K	0.6	0.7	0.8	0.9	1	
		Resistance factor	Level of source	World heritage	World heritage	National heritage	Provincial heritage	City and town heritage	Other heritage
			Resistance coefficient	0	10	30	60	100	
			Slope	<5°	5°–10°	10°–15°	15°–25°	>25°	
			Land use	Waters and forest	Grassland and boskage	Farmland	Bare area and wasteland	Towns and villages	
			Vegetation coverage	>65%	50%–60%	25%–50%	10%–25%	<10%	
			Waters and buffer	Water bodies	LLB < 400 m; RaSL < 100 m	LLB400–1000 m; RaSL100–300 m	LLB1000–2500 m; RaSL300–800 m	Others	
	Humidity coefficient	>0.24	0.22–0.24	0.20–0.22	0.18–0.20	<0.18			
	Recreation suitability analysis	Source: site	Value of K	0.6	0.7	0.8	0.9	1	
		Resistance factor	Level of source	First level	Second level	Third level	Fourth level	Fifth level	
			Resistance coefficient	0	10	30	60	100	
			First level road	<300 m	300–1000 m	1000 m–3000 m	3000–6000 m	>6000 m	
			Second level road		<500 m	500–1500 m	1500 m–3000 m	>3000 m	
			Towns	<500 m	500 m–1000 m	1000–3000 m	3000–8000 m	>8000 m	
Villages			–	<300 m	300–800 m	800 m–1500 m	>1500 m		

Note: World Heritages refer to Natural and Cultural heritages listed in the UNESCO World Heritage List. National heritages refer to the national key cultural relics protection units, National Scenic areas and National Nature Reserves. The provincial heritages refer to the provincial cultural relics protection units, Provincial Scenic Spots, and Provincial Nature Reserves. Town heritages refer to the town cultural relics protection units, Town Scenic Spots and Town Nature Reserves. Other heritages refer to those listed no protection units mentioned above. The resource of each rank corresponds to the site and scenic spot at the same level.

cumulative resistance of any pot in space and both the distance to all sites and the surface characteristic of landscape units. D_{ij} is the spatial distance between some site and some pot in natural area; R_j is the resistance coefficient of relevant expansion prevented by natural area.

There is a close relationship between the formation and development of the Grassland Silk Road (from Xanadu to Zhongdu) Cultural Route and natural environment. Sites are severely threatened by the harsh environment in the northern farming and pastoral area. In order to avoid sporadic protection, we explore to apply Greenway to the protection and utilization of Cultural Route via suitability analysis based on MCR model.

2.1.2 *Determination of source and resistance plane*

We define as sources the sites on this Cultural Route, which vary from World Heritage to Town-level units. Now that the affected and relevant area depends on the levels of these sites, we characterize them in five levels, apply them to MCR model respectively and select the minimum value of the superimposed results.

Currently, sites on the route have been damaged by environmental degradation and human disturbance intensification to varying degrees. So we purpose to remain heritage features in the relevant area based on heritage integrity, and simulate possible environmental threats to delimit the core area of heritage protection reasonably.

According to the environmental character of the study area, an assessment system of landscape process resistance is constructed based on factors including resistance coefficient, slope, land use, vegetation coverage, waters and humidity coefficient. Commonly, the protection scope might be smaller when the environmental threat is severer and the heritage protection is more difficult with the lower resistance coefficient, the steeper slope, the longer distance to waters and the arider climate. The resistance of each single factor is ranked in five levels based on the results of expert decision.

2.2 *Analysis on site selection of Greenway*

The Cultural Route heritage should involve and benefit local residents rather than remain conserved mechanically like a museum. The leisure and recreational function of Greenway could refresh Cultural Route effectively. Given that the service function essentially depends on the improvement of the traffic and infrastructure conditions, it is necessary to identify and rank recreation resources and determine resistance plane which impacts accessibility.

Different from sites, resources contain not only heritage items which can be utilized for recreation

but also involve tourist attractions at all levels. Similarly, given their various service scope, we rank these "sources" in five levels applied in MCR model and select the minimum value from the overlaid results. That is to say, when the level of tourist attraction and heritage is different, the higher level value should be selected. For instance, if one is both a town cultural relics protection unit and a 4 A-level tourist attraction, it should be identified as the second-level source.

Greenway accessibility and the condition of service facilities mainly depend on the distance from sources to roads and settlements at all levels. Roads are divided into the first-level (national roads and provincial roads) and the second-level roads (village roads and town roads). Settlements are ranked into towns and villages. According to the present condition of the study area, buffer areas at different levels are identified and resistant plane is formed.

3 RESULT

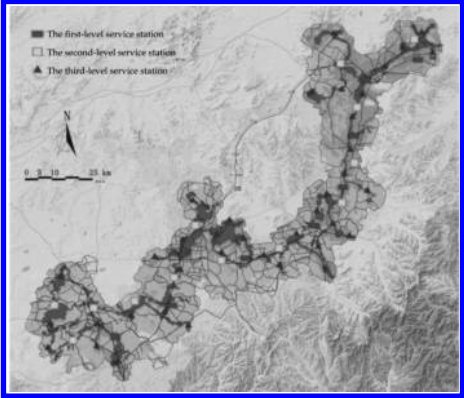
3.1 *Determination of protection scope of Cultural Route*

We calculate the minimal cumulative resistance plane through the cost-distance in ArcGIS, interpret and extract available data combined with histograms, and conclude the evaluation results of heritage protection for Greenway. As a result, the most suitable area is generally located in mountain forest and surrounded by waters with abundant vegetation. The better suitable area is mainly distributed in grassland and farmland with smooth terrain and the less suitable area primarily includes built-up area, bare land and some steep ground.

3.2 *Site selection and service facility planning for Greenway*

The final suitability evaluation result is concluded through the combination of the heritage protection evaluation result and the leisure and recreation evaluation result. From that point, the most suitable area of 616.0 square kilometers, mainly contains the buffer area of sites and waters with plenty of vegetation, which accounts for 8.7% of our research area. The more suitable area, primarily distributed around sites and waters with smooth terrain and good plants, covers 1855.0 square kilometers with the ratio of 26.2% of research area. The mid-level suitable area is mainly farmland and grassland with moderate vegetation, covering an area of 2732.9 square kilometers and accounting for 38.6%. The less suitable and unsuitable areas with poor vegetation are mainly situated in the dis-

Table 3. Construction requirements of service station at all levels.

Level	First-level service station	Second-level service station	Third-level service station
Area (m ²)	300–400	150–300	50–150
Service radius (km)	16	8	4
Situation	Located in exits of Greenway, especially those connected with provincial roads or accesses to towns	Located in branches of Greenway mainline, mainly combined with extant historical heritages	Located in entrances of historical heritages
Function	Mainly contains visitor centers (including transportation, bike rental, dinning and retail, public education, emergency medical help, toilet, watering points and the whole route model)	Mainly contains information office, receiving point for map and brochure, bike rental, emergency medical, toilet, watering points, alarm point	Mainly contains receiving point for map and brochure, toilet, watering points, alarm point
Attention	Utilize extant buildings and facilities	Coordinate with other stations at the same level	Coordinate with stations at two upper levels
Distribution map of service stations			

tricts with steep slope or far away from waters and transportation, whose area are respectively 1493.9 square kilometers and 382.3 square kilometers with the ratio of 20.1% and 5.4%.

In the study area, there is clear liner corridor in the northeast with highly suitable area, densely covered with rivers and lakes, such as Shandian River. It is difficult to select the site for Greenway in the southwestern part because of the discontinuous and patchy distribution. So we purpose to connect these sporadic areas through linking the closest districts. And then the site selection planning for Greenway is conducted, combined with existing natural and cultural resources on the basis of suitability analysis. Finally, the scope of site selection for Greenway is ascertained with dual functions of protection and exhibition. It connects 30 historical heritage sites from northeast to southwest in series and 12 natural landscapes. Its coverage area has moderate ecological conditions, mainly involving waters and the surrounding woodlands, grasslands and a few farmlands with good vegetation and smooth terrains. Moreover, the Greenway, with good recreation accessibility and service potential,

connects Zhangbei County, Guyuan County and Zhenglan Banner, and links National Highway 207, Zhangshi highway, Provincial Road 308 and 341, and numerous village roads.

Greenway service station mainly provides users with reception, recreation outdoor, public education, dinning, retail, safety services, maintenance and management. Commonly, service stations are ranked with different service facilities and different functional requirement. According to the current construction experience of Greenway and Urban Road Public Service Facilities Set Specifications DB11/T500-2007, we propose the site selection with the combination of construction requirements and site condition characters.

4 CONCLUSION

The purpose of this paper is to discuss site selection and planning method for Greenway based on Cultural Route, and the approach of the protection scope delimitation and utilization of Cultural Route by the way Greenway planned. Firstly, we

have applied the modified MCR model to the suitability analysis on Cultural Route and have achieved the protection scope with sites and resources as sources and the resistance coefficient ascertained by different land use.

Additionally, site selection for Greenway has been determined as well as the service facility planning guide based on the analysis. This study provides a new approach to protect Cultural Route and utilize the comprehensive Greenway in its original way.

5 DISCUSSION

5.1 *Data deficiency and inaccessibility*

It is different to conduct suitability analysis in China and western countries. In America, scientific data are accessible to fulfill communication and cooperation, which provides a reliable foundation for discussion, planning and research, thus the suitability analysis is widespread and comprehensive. On the contrary, in China, many adverse conditions impede relevant research, such as data deficiency. And in our study, these six evaluation factors selected could not completely represent the condition of Greenway planning in this area. There are three other factors are inaccessible, including wildlife habitat, vegetation types and ecological sensitive area. With the complete information from those three aspects, the research would have been improved to a great extent.

5.2 *Modification of MCR model*

The previous suitability evaluation researches merely focus on vertical ecological process, so that patchy suitable areas were usually formed rather than liner corridor spaces. MCR model could avert this phenomenon and takes both distance and resistance into account. However, the neglect of sources diversity might also result in other problems, such as resources waste in the protection process. In our study, we propose to resolve this problem through modifying MCR model and bringing in variable diversities of resources.

ACKNOWLEDGEMENT

We would like to express our sincere appreciation to Associate Professor Yan Du in the college of Horticulture and Forestry Sciences, Huazhong Agricultural University (HZAU) and members of landscape architecture heritage research group. This project would not have been possible without the input and assistance from the following individuals: Qiang Zhu (Peking University), Shuaike

Yin (Beijing Forestry University), Haichen Yan (HZAU), Danfeng Tao (HZAU).

REFERENCES

- Ahern, J. Greenways as a planning strategy [J]. *Landscape and urban planning*, 1995, 33(1): 131–155.
- Burel, F and Baudry, J. Social, aesthetic and ecological aspects of hedgerows in rural landscapes as a framework for greenways[J]. *Landscape and Urban Planning*, 1995, 33(1): 327–340.
- Chen, Y.F., Sun, D.Y., Lu, G.F. Application of catastrophe progression method in ecological suitability assessment: a case study on Zhenjiang new area[J]. *Journal of Ecological*, vol 26, 2006 (8): 2587–2593.
- Conine, A, Xiang W.N., Young J, et al. Planning for multi-purpose greenways in Concord, North Carolina[J]. *Landscape and Urban Planning*, 2004, 68(2): 271–287.
- Dawson, K.J. A comprehensive conservation strategy for Georgia's greenways[J]. *Landscape and Urban Planning*, 1995, 33(1): 27–43.
- Fabos, J.G. From parks to greenways into the 21st century[C]//*Proceedings from Selected Educational Sessions of the 1991 ASLA Annual Meeting*, Kansas City, MO. 1991.
- Furuseth, O.J., Altman R.E. Who's on the greenway: Socioeconomic, demographic, and locational characteristics of greenway users [J]. *Environmental Management*, 1991, 15(3): 329–336.
- Gobster, P.H. Perception and use of a metropolitan greenway system for recreation[J]. *Landscape and Urban Planning*, 1995, 33(1): 401–413.
- ICOMOS, Report on the Expert Meeting on Routes as our Cultural Heritage, Madrid, Spain, 1994, http://www.icomosci.org/CIHC/LJNESCO_CONVENTION.htm.
- ICOMOS. The ICOMOS Charter on Cultural Route [EB/OL]. http://www.international.icomos.org/charters/culturalroutes_e.pdf.
- Jing, F. UNESCO'S Efforts in Identifying the World Heritage Significance of the Silk Road[A]. *Proceeding of ICOMOS 15TH General Assembly and Scientific Symposium[M]*. World Publishing Corporation, 2005: 934–943.
- Lewis, P.H. Quality corridors for Wisconsin[J]. *Landscape Architecture*, 1964, 54(2): 100–107.
- Li, Ji-hong and Liu, Xue-hua. Research of Nature Reserve Zonation Based on The Least-cost Distance Model [J]. *Journal of Natural Resources*, 2006, 02: 217–224.
- Lindsey G. Use of urban greenways: insights from Indianapolis[J]. *Landscape and urban planning*, 1999, 45(2): 145–157.
- Liu, Xiao-fang. The Debate of Cultural Routes [J]. *Journal of Guilin Institute of Tourism*. 2006; (05): 622–5.
- Liu, Xiao-fang. Review of Studies on Cultural Routes [J]. *Journal of Guilin Institute of Tourism*. 2007; (06): 920–3.
- Liu, Xiao-fu, Su Jian-min and Zhang Lin-bo. Research on Applying Minimal Cumulative Resistance Model in Urban Land Ecological Suitability Assessment: As an example of Xiamen City [J]. *Acta Ecologica Sinica*, 2010, 02: 421–428.

- Li, W, Wang, Y, Jiang Y, et al. Spatial approaches to ecological regulation in urban areas: A case in Shenzhen[J]. *Acta Ecologica Sinica*, 2002, 23(9): 1823–1831.
- Ndubisi, F, DeMeo T, Ditto N.D. Environmentally sensitive areas: a template for developing greenway corridors [J]. *Landscape and Urban Planning*, 1995, 33(1): 159–177.
- Rojas, Angela. The Royal Road and Its Role in Organising Cuban Territory[A]. *Proceeding of ICOMOS 15TH General Assembly and Scientific Symposium*[M]. World Publishing Corporation, 2005: 1084–1089.
- Ruan, Yi-san and Ding Yuan. Value assessment, Cultural Route and The Grand Canal protection [J]. *China Ancient City*, 2008; (01): 38–43.
- Schrader C.C. Rural greenway planning: the role of streamland perception in landowner acceptance of land management strategies[J]. *Landscape and Urban Planning*, 1995, 33(1): 375–390.
- Shafer, C.S., Lee B.K., Turner S. A tale of three greenway trails: user perceptions related to quality of life[J]. *Landscape and Urban Planning*, 2000, 49(3): 163–178.
- Smith, D.S., Hellmund P.C. Ecology of greenways: design and function of linear conservation areas[M]. University of Minnesota press, 1993.
- Turner, T. Greenways, blueways, skyways and other ways to a better London[J]. *Landscape and Urban Planning*, 1995, 33(1): 269–282.
- Tzolova, G.V. An experiment in greenway analysis and assessment: the Danube River[J]. *Landscape and Urban Planning*, 1995, 33(1): 283–294.
- Walmsley, A. Greenways and the making of urban form [J]. *Landscape and Urban Planning*, 1995, 33(1): 81–127.
- Walmsley A. Greenways: multiplying and diversifying in the 21st century[J]. *Landscape and Urban Planning*, 2006, 76(1): 252–290.
- Wang, Jianbo, Ruan, Yisan. Study of the Great Canal Legacy system as Cultural Route [J]. *China Ancient City*, 2010; (09): 42–6.
- Wei, Hong-an and Wang Jie-yong. Assessment of Land Consolidation Suitability in Loess Hilly-gully Region in Yan'an City [J]. *Areal Research and Development*, 2013,03: 129–132.
- Whyte, W.H. Securing open space for urban American: conservation easements. Washington: Urban Land Institute, 1959. 69.
- World Heritage Center. 2005 Operational Guidelines for the Implementation of the World Heritage Convention. <http://whc.unesco.org/archive/opguide05-en.pdf>.
- Wu, Jia-yu, Zhou, Pan and Du, Yan. Greenway Planning Based on Cultural Route along Grassland of Silkroad from Xanadu to Zanadu [J]. *Urban Development Studies*, 2013,04:28–33.
- Yahner, T G, Korostoff N, Johnson T P, et al. Cultural landscapes and landscape ecology in contemporary greenway planning, design and management: a case study[J]. *Landscape and urban planning*, 1995, 33(1): 295–316.
- Ye, Xin-min, Jakhadai Chimeddorji. Xanada Research Anthology + Xanada Research Collected Works, Central University for Nationalities Press, 2003: 201–345.
- Yu, Kong-jian. Landscape Ecological Security Patterns in Biological Conservation[J]. *Acta Ecologica Sinica*, 1999,01:10–17.
- Zhou, Li and Ren Zhi-yuan. Evaluation of Natural Suitability for Human Living Environment: A Case Study of the Region of Guanzhong and Tianshui Based on GIS [J]. *Areal Research and Development*, 2011, 03: 128–133.
- Zhu, Qiang and Liu Hai-long. Review of Greenway Research [J]. *Urban Problems*, 2006, 05:11–16.

Gaussian model investigation in modeling of air pollution diffusion using Geographic Information System (GIS)

F. Sabbagh, A. Afshari, M. Hassanzadeh & S. Kaveh

Department of Civil Engineering, Ferdowsi University of Mashhad, Mashhad, Iran

M. Amiri

Azad University, Kashmar Branch, Kashmar, Iran

ABSTRACT: One of the most common and useful models that is used in air pollution models is Gaussian modeling. This model is very accurate in estimation of air pollution diffusion. In this study in a Gaussian model, in a lump source and certain time, variation of wind-sedimentation velocity and also its chemical reactions in a simple model has presented. With modeling the pollution diffusion in FORTRAN programming software, the results have introduced in ARC GIS software and the plan of pollution diffusion for the specific situation has been derived. For verifying the model and determining the accuracy of it, the previous studies have used.

Keywords: air pollution modeling; Gaussian model; Eulerian model; Geographical Information System (GIS)

1 INTRODUCTION

Today, air pollution effects on human and the surroundings are revealed to all. Many cases have been observed in a factory due to pollution diffusion from its chimney has been fined by the Environmental Protection Agency (EPA). During incidence of these problems, on one hand the public has concerns about air pollution. On the other hand industrialists objection, stating that the factory pollution not bring to the metropolitan areas and it will be safe. Therefor with checking the amount of pollution in the metropolitan areas, the factories could responding to concerns. In the air quality modeling, it is important that, is the pollution has diffused from a source at a certain distance, be in standard range or not? In other words, how much is the amount of air pollution at certain distance from the pollution source? Or in instantaneously nuclear explosions, the nuclear pollutions are released how far away, and how far must be declared as a crisis polluted area?

Gaussian model still has maintained its position in estimating atmospheric pollution and has been the basis of various software applications. Such studies on the application of Gaussian models in air pollution modeling software is ADMS software. In this model the Gaussian model has developed for study of managing local air quality and

chimneys environmental pollution. ADMS model routinely used by local labor in England to predict air quality. Another model that is used for predicting pollutant concentrations in urban conditions and in almost flat lands is TAPM. This model is a three-dimensional model, which has shown excellent results. Today Computational Fluid Dynamics (CFD), and Lagrangian transport equations are used for the weather forecasting models. EPAUS air quality models are also based on the Gaussian model. ISC is one of these models that is a sustainable Gaussian model for studying the industrial pollutant concentrations [2].

Before obtaining a numerical solution, problem begins by considering a coordinate system on the ground. This, enables the region that be meshed, defined in a local coordinate system and then define the equations for each desired point. To solve the problem the finite difference method was used and the desired model, which is an Eulerian model with a set of distribution and transport equations are presented [1]. This Eulerian model was presented with Marczuk [7] and Zannetti and Graziani [9] were developed it, and used it in distribution modeling [7, 8, and 9].

The purpose of this study was to evaluate and compare the results obtained by Gaussian model for the distribution of pollution in the atmosphere and to present the results in a GIS environment.

2 RESEARCH METHODOLOGY

Copy the Eulerian distribution model is defined as follow [1]:

$$\frac{\partial C_i}{\partial t} + V \rho \cdot \Delta C_i^\rho - \nabla \cdot (K_i \nabla C_i) = f_i \quad I = 1, 2, \dots, p \quad (1)$$

In which P is the number of air pollution samples, $C_i = C_i(X_1, X_2, X_3, t)$ indicates the i th pollution average. V is the wind velocity and K_i is distribution diagonal tensor. $f_i = f_i(C_1, C_2, \dots, C_p)$ represent the source [1]. The chemistry as a source of pollution has considered as a part of source:

$$f_i = E_i + R_i + P_i \quad (2)$$

In which E_i is direct emission of i th sample, R_i is the variation of concentration in i th sample in chemical reactions and P_i is removing rate by sedimentation. Chemical distribution in (X_1, X_2, X_3) position is determined with Gaussian model:

$$E_i = \frac{C_{i0}(2\pi)^{-3/2}}{\sigma_x \sigma_y \sigma_z} \exp \left\{ - \left[\left(\frac{X_1 - X_{10}}{\sqrt{2}\sigma_x} \right)^2 + \left(\frac{X_2 - X_{20}}{\sqrt{2}\sigma_y} \right)^2 + \left(\frac{X_3 - X_{30}}{\sqrt{2}\sigma_z} \right)^2 \right] \right\} \quad (3)$$

$\sigma_x, \sigma_y, \sigma_z$ are standard deviation of specific distribution of concentrations in the smoke column [1]. With solving the Eulerian distribution equation in 1 dimension state with considering the immediate source, in situation that wind speed and distribution confusion coefficient are constant, regardless of precipitation and atmospheric chemistry we can write:

$$C(x, y, z, t) = \frac{Q}{(2\pi)\sigma_x \sigma_y \sigma_z} \times e^{-\left(\frac{(x-x_0)u - (y-y_0)v - (u^2 + v^2)(t-t_0)}{2\sigma_x^2(u^2 + v^2)}\right)^2} + e^{-\left(\frac{(x-x_0)v - (y-y_0)u}{2\sigma_y^2(u^2 + v^2)}\right)^2} \left(e^{-\left(\frac{z - (z_0 + h)}{2\sigma_z^2} + e^{-\left(\frac{z - (z_0 + h) + 2H}{2\sigma_z^2}\right)} \right)} \right) \quad (4)$$

In this equation Q is emission source, $u, v,$ and w are the velocity parameters, h is the height of chimney, H is the height of mixing layer, t_0 is distribution time, $(X_0 + Y_0 + Z_0)$ are the source coordinates, h is effective height of chimney (the height of smoke rising and height of chimney).

As a rule in Gaussian model, it is suggested that the horizontal axis and wind direction has same direction and the coordinates of the starting point is at the base of the chimney. In above equation chemical reaction and precipitation are not considered. Therefore, these parameters are also categorized as a factor in equation (3).

$$P_i = \frac{v_{wi}}{h} c_i = -\frac{W_{ri}}{h} p_0 c_i \quad (5)$$

$$v_{wi} = W_{ri} p_0$$

In this equation, SO_2 pollutants is used as sample pollutants for atmospheric chemistry.

$$R_{SO_2} = \bar{\alpha}_{SO_2, SO_2} C_{SO_2} \quad (6)$$

$$\bar{\alpha}_{SO_2, SO_2} = -2 \frac{k_1 k_3}{k_2}$$

h is average depth of mixing, v_{wi} is the deposition velocity [1], $K_1, K_2, K_3,$ are kinematic parameters according to the following chemical equation [1].



$$\begin{aligned} v_{wSO_2} &= 0.28^{m/s} \\ \alpha_{SO_2, SO_2} &= -0.0012 \end{aligned}$$

The above equation has not solved, but the coefficient is presented which removes has applied.

$$\begin{aligned} R_{SO_2} &= -0.0012 * C \\ P_i &= \frac{-0.28}{h} * C \end{aligned} \quad (8)$$

And according to the average mixing layer height $h = 2000$ (m).

$$\begin{aligned} \alpha &= -(0.0012 + 0.00014) \\ \alpha &= -1.34 * 10^{-3} \end{aligned} \quad (9)$$

The concentrations have been considered as follow:

$$\begin{aligned} C^{n+1} &= C^n + \Delta t * \frac{\partial C}{\partial t} \\ C_1 &= C_0 + \alpha * t * C \end{aligned} \quad (10)$$

In this equation t is the time, C the concentration that achieved in a timeframe and α is removal coefficient. If the distribution time is start at 7.30 am, concentration at 8 am is equal to:

$$C_{at8} = C_{at7:30} + \alpha * t * C \quad (11)$$

Table 1. Atmospheric stability class [3].

Wind velocity on height of 10 m (m/s)	Daytime, incoming solar radiation			Night, cloudiness	
	Strong	Moderate	Weak	Clouded	Cloudless
<2	A	A-B	B	E	F
2-3	A-B	B	C	E	F
3-5	B	B-C	C	D	E
5-6	C	C-D	D	D	D
>6	C	D	D	D	D

Table 2. Diffusion coefficients for identifying σ_x σ_y σ_z [3].

Atmosphere stability class in accordance with Pasquill	$\sigma_x, \sigma_y (m)$	$\sigma_z (m)$
<i>Open country</i>		
A	$0.22x (1 + 0.0001x)^{-1/2}$	$0.2x$
B	$0.16x (1 + 0.0001x)^{-1/2}$	$0.12x$
C	$0.11x (1 + 0.0001x)^{-1/2}$	$0.08x (1 + 0.0002x)^{-1/2}$
D	$0.08x (1 + 0.0001x)^{-1/2}$	$0.06x (1 + 0.0015x)^{-1/2}$
E	$0.06x (1 + 0.0001x)^{-1/2}$	$0.03x (1 + 0.0003x)^{-1}$
F	$0.04x (1 + 0.0001x)^{-1/2}$	$0.16x (1 + 0.0003x)^{-1}$
<i>City</i>		
A-B	$0.32x (1 + 0.0004x)^{-1/2}$	$0.24x (1 + 0.01x)$
C	$0.22x (1 + 0.0004x)^{-1/2}$	$0.2x$
D	$0.16x (1 + 0.0004x)^{-1/2}$	$0.14x (1 + 0.0003x)^{-1/2}$
E-F	$0.11x (1 + 0.0004x)^{-1/2}$	$0.08x (1 + 0.0015x)^{-1/2}$

In this equation t is equal to 30 min and also C is the distributed concentration.

This equation can also be used later to obtain the concentrations shown in Table 1. In this case the wind speed can be changed in a of 30 minutes periods, and on the basis of it the concentration could be achieved.

3 REQUIRED INFORMATION IN MODELING

3.1 A—Information of emission source

1. Physical information about chimney such as height, location, and internal diameter
2. speed and temperature of the released gases
3. emission rate.

3.2 B—Meteorological Information

1. Average wind flow and its direction
2. Wind speed
3. The height of the mixing layer
4. The atmospheric air temperature
5. Classification of air stability

3.3 C—Topographic information (in this study determining the coefficients depends on the site located at the city or suburbs)

The equations and functions are modeled in FORTRAN programming software. The outputs is provided as ASCII file for entering to GIS environment.

4 RESULTS

After surveying the information about the pollution that distributed from an emission source, the results was presented as follow.

Pollution was distributed from 7:30 am in neutral weather situation. Speed and direction of wind was determined and surveyed until 13 o'clock. Figure 1 has presented the information that verified with the results of reference [1]. Then in Figure 2 the state of pollution distribution has been showed. Although the Gaussian model cannot determine the real amount of pollution but the process of variation considering the various parameters are fully documented.

As can be seen in Figure 1, the results of model have some errors. Considering that the errors

Table 3. Input information to Gaussian model with lumped source.

Information	Symbol	Example 1	Example 2	Example 3
Source		Lumped	Lumped	Lumped
Source intensity (g/s)	Qc	6.995	6.995	6.995
Source discharge (m ³ /h)	Flow	250000	250000	250000
Atmospheric stability class	Atmosphere	d	d	d
Diffusion time (s)	Time	1800	3600	5400
Time of pollution calculation (s)	Time	1800	3600	5400
Kind of city area	City	2	2	2
Source diffusion coordinates (m)	Ws	4000	4000	4000
	Ys	4000	4000	4000
	Zs	299	299	299
Height of pollution calculation (m)	Z	300.5	300.5	300.5
Height of mixed layer	Hm	4000	4000	4000
Diffusion temperature (k)	Ts	773	773	773
Area temperature (k)	Ta	299	299	299
Chimney height (m)	Hs	48.45	48.45	48.45
Chimney diameter (m)	ds	2.82	2.82	2.82
Reduce temperature rate versus height	$r = dt/dz$	1.5	1.5	1.5
Area length (m)	LB	5000	5000	5000
Angle between horizontal				
Axes and wind direction (degree)	B	45	45	45
Wind velocity in 10 meter height (m/s)	Vw	5.68	5.19	5.59

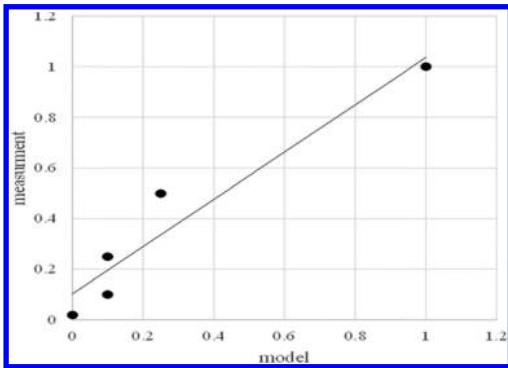


Figure 1. Verification of Gaussian model.

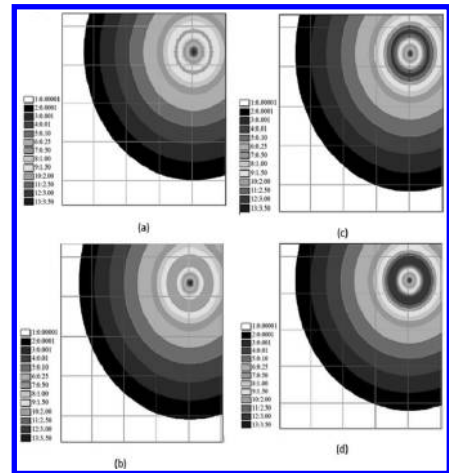


Figure 2. a) SO₂ concentration (g/m³) at 8 o'clock (30 min after starting the diffusion); b) SO₂ concentration at 8:30 (1 hour after starting the diffusion); c) SO₂ concentration at 9:30 (2 hour after starting the diffusion); d) SO₂ concentration at 11 o'clock (3:30 hour after starting the diffusion).

change linearly, Gaussian model can be adjusted with use of error equation.

For presenting the distributing of pollution, the results was presented at GIS environment. As can be seen in Figure 2 when go away from the source, concentration is increased and diffusion occurred.

Due to Figure 2 at the first, the pollution concentration increases in downstream of wind direction and bring to maximum of its amount. After that due to diffusion process, precipitation, and air chemical reactions, the concentration of pollution decrease with going away from source.

Results also show that during the time, the concentration increases and circuit more vast area. Considering above data the maximum concentration zone and the effect of various parameters on amount of diffusion, precipitation, and air chemical

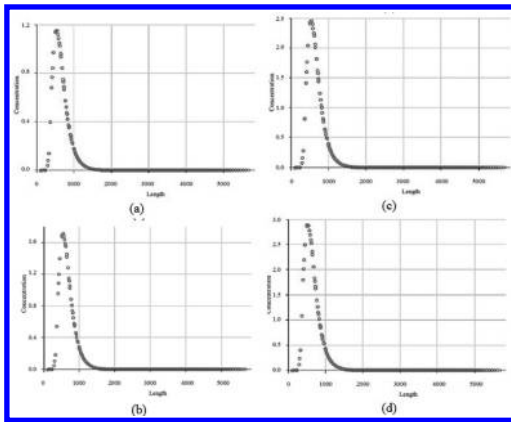


Figure 3. a) Concentration (g/m^3) and distance from emission source at 8 o'clock, b) 8:30, c) 9:30, d) 11.

reactions, in downstream of wind direction from the source could be determined. Finally with considering the air pollution in critical air situation in one area, with restriction of effective parameters or turning the source off in specific hours, improve the air quality in critical times. Figure 3 presents the maximum concentration of pollution in different times into the distance from the source in downstream of wind in a neutral condition.

As shown in this Figure, noted that the computation is performed in a neutral atmosphere, maximum distance formed in approximately 600 meters downstream of air pollution, but over time, the pollution concentration increases. After reaching to maximum level of pollution, diffusion will be based on atmospheric stability class and with distance from the source of pollution concentration is reduced. Based on the diffusion coefficients, concentration will reach its minimum at a certain distance it can be concluded that the air quality is not affected by the pollution source. It should be noted that, in a stable atmosphere, the diffusion happen farthest from the chimney.

To study the effect of environmental parameters on the pollution diffusion, source was removed from the circuit and diffusion rate in the downstream direction of wind is examined.

As shown in Figure 4, initially the pollution is removed from the source, amount of pollution increasing and will decrease after reaching its maximum. But with turning the source off as shown in Figure 4 (b) (Three hours after release) environmental pollution concentration, in terms of distribution and sedimentation from the area is gradually dropped out. If this test investigates in steady state survival rates of pollution in the area is far longer, but in an unstable atmosphere survival rates will be lower than the neutral condition. In critical times

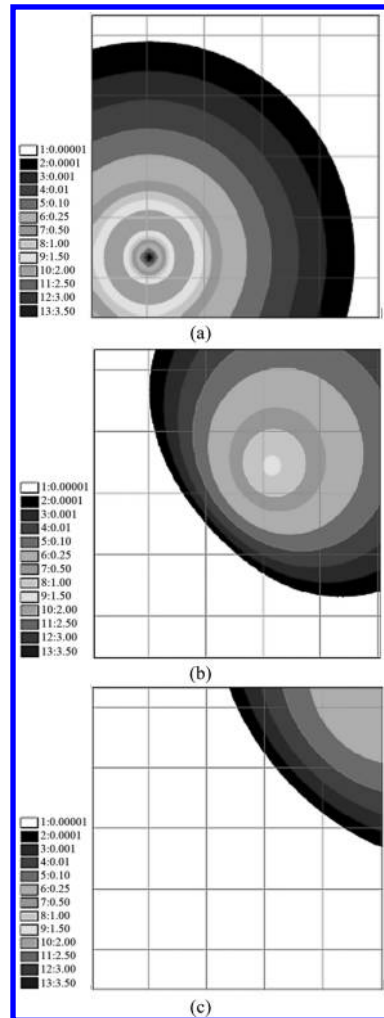


Figure 4. a) SO_2 concentration (g/m^3) at 8/30 (one hour after release); b) SO_2 concentration at 11/30 (three hours after release); c) SO_2 concentration at 13 hours (5:30 hours after release).

that contamination concentration exceeds the critical clean air with removing the source in special time air pollution concentration bring to standard. Figure 4 identifies the effect of removing source in reduction the pollution in the region.

5 CONCLUSIONS

Gaussian lumped model, expressed in this paper to estimate the pollution change with environmental parameters changing can present fairly accurate result. Geographic Information System GIS

can also utilize in environmental modeling. Also efficient management of the crisis control and the rapid transfer of information created. With increasing wind speed concentration of pollution reduced. Pollution rate in the area were much longer, but in an unstable atmosphere the persistence of neutral condition will be shorten. Gaussian model cannot help determine the true value of pollutant concentrations but the changes according to different parameters are fully documented.

REFERENCES

- [1] N. Sanin, G. Montero, "A finite difference model for air pollution simulation" *Advances in Engineering Software* 38 (2007) 358–365.
- [2] Kiely Gerard, "Environmental Engineering", Mc Graw Hill Publication Company 1997.
- [3] N.Kh. Arystanbekova, "Application of Gaussian plume models for air pollution simulation at instantaneous emissions", *Mathematics and Computers in Simulation* 67 (2004) 451–458.
- [4] Steven R. Hanna, Rex Britter, Pasquale Franzese, "A baseline urban dispersion model evaluated with Salt Lake City and Los Angeles tracer data" *Atmospheric Environment* 37 (2003) 5069–5082.
- [5] Bruno Sportisse, "Box models versus Eulerian models in air pollution modeling" *Atmospheric Environment* 35 (2001) 173–178.
- [6] Krzysztof Brzozowski, Wojciech Kotlarz "Modelling of air pollution on a military airfield" *Atmospheric Environment* 39 (2005) 6130–6139.
- [7] Marczuk, G.I. "Mathematical Modelling of the Natural Environment" PWN, Warszawa (in Polish), 1985.
- [8] Zannetti, P. "Air Pollution Modeling. Theories, Computational Methods and Available Software" Van Nostrand Reinhold, New York, 1990.
- [9] Zannetti P., Graziani G. "Survey of long range transport models. In: Computer methods and software for simulating environmental pollution and its adverse effects" *Environmental modeling, Vol. II*. Southampton: Computational Mechanics; 1994. p. 103–42.

A comparative analysis to prioritize renewable energy alternatives using Fuzzy Analytic Hierarchy Process

V. Baratzadeh, S. Kaveh, Y. Edrisian, F. Sabbagh & A. Afshari

Department of Civil Engineering, Ferdowsi University of Mashhad, Mashhad, Iran

ABSTRACT: Energy is a key element in modern life and it is important to establish long-term policies to provide a secure and bright future in our industry. Energies produced from natural resources such as wind, sunlight, rain and geothermal heat which are known as renewable energies have good environmental and economic prospective for all countries and Hence many policy-makers always are looking forward to select an alternative and it effects energy investments. In this paper trying to find a method to prioritize the selection among renewable energy alternatives based on a Fuzzy-AHP method. In this paper criterion such as reduction in harmful effects, cost and so forth was determined in order to find the most appropriate renewable energy alternative is for Iran.

Keywords: renewable energy; fuzzy logic; decision making; AHP

1 INTRODUCTION

Renewable energy sources have been important for humans since the beginning of civilization. Clean, domestic and renewable energy is commonly accepted as the key for future life. This is primarily because renewable energy resources have some advantages when compared to fossil fuels. Renewable energy sources are also often called alternative sources of energy. Renewable energy resources that use domestic resources have the potential to provide energy services with zero or almost zero emissions of both air pollutants and greenhouse gases. Main renewable energy resources are biomass energy, hydro energy, geothermal energy, solar energy, and wind energy [1].

When we try to select any alternative using some criteria, we have to take into account conflicting issues among the considered criteria. For example, two criteria that could be used in selecting a renewable energy alternative might be reliability and implementation cost. These are two conflicting criteria since an attempt to increase reliability possibly causes an increase in implementation cost. The selection among renewable energy alternatives is a multi-criteria problem with many conflicting criteria. We have to evaluate some alternatives by taking into account their advantages and disadvantages based on selection criteria. Hence, this problem should be solved by a multi-criteria method. These kinds of criteria make the evaluation process hard and vague. In many decision-making problems the decision maker's

(DM) judgments are not crisp, and it is relatively difficult for the decision maker to provide exact numerical values for the criteria or attributes. Therefore most of the evaluation parameters cannot be given as precisely and the evaluation data of the alternative energy policy's suitability for various subjective criteria and the weights of the criteria are usually expressed in linguistic terms by DMs. In order to model this kind of uncertainty in human preferences, fuzzy logic is applied very successfully. The fuzzy logic is a matter of the fuzzy set theory particularly used to dealing with imprecise information by using membership functions. Fuzzy set theory was formalized by Zadeh in 1965. In a classical set, an element belongs to, or does not belong to, a set whereas an element of a fuzzy set naturally belongs to the set with a membership value from the interval [0, 1].

In this paper fuzzy-AHP based multi-criteria decision-making procedures is suggested to determine the most appropriate renewable energy alternative for Iran. For this aim, 4 main and 17 Sub-criteria are considered and 5 different renewable energy alternatives are evaluated. As fuzzy based multi-criteria decision-making procedures, Fuzzy Analytic Hierarchical Process methodology (FAHP), proposed by Zeng et al. [2] is used in case of energy evaluation.

AHP, one of the most outstanding MCDM (multi-criteria decision-making) approaches, has been used to solve energy problems successfully such as Kagazyo et al. [3], Nagesha and Balachandra [4].

2 LITERATURE REVIEW

Energy investment decisions are inherently multi-objective in nature. MCDM methods can help governments to evaluate energy sector plans and policies. Recently some studies about MCDM have concentrated on energy problems.

Hamalainen and Karjalainen [5] used AHP to select the weights of criteria of Finland's energy policies. Keeney et al. [6] presented another application of MCDM methods in national energy policy. The system supported the state toward the formulation of a modern environment, since it incorporated the "new parameters" of the energy market, namely the liberalization and the climate change. The system was successfully applied in the 13 accession member states of the European Union. Haralambopoulos and Polatidis [7] described an applicable group decision-making framework for assisting with multi-criteria analysis in renewable energy projects, utilizing the PROMETHEE II outranking method to achieve group consensus in renewable energy projects. The proposed framework was tested in a case study concerning the exploitation of a geothermal resource, located in the island of Chios, Greece. Mavrotas et al. [8] presented an approach based on a mixed 0–1 multiple objective linear programming model and applied to the Greek electricity generation sector to identify the number and output of each type of power units needed to satisfy the expected electricity demand in the future. Mirasgedis and Diakoulaki [9] compared the external costs calculated for a number of power plants using different energy sources with the outcome of a multi-criteria analysis where environmental impacts were expressed in physical terms or on a qualitative scale. They identified similarities and disparities in the obtained rankings and clarified on the basis of the fundamental principles of the two approaches, external cost estimates and multi-criteria analysis. Although external costs did not accurately reflect the traditional value system of individual decision makers, they gave suitable price signals and thus helped in eliminating distortions of the current energy market.

In recent years, some studies have concentrated on fuzzy energy planning and fuzzy energy policy making. Cavallaro and Ciraolo [10] proposed a multi-criteria method in order to support the selection and evaluation of one or more of the solutions to make a preliminary assessment regarding the feasibility of installing some wind energy turbines in a site on the island of Salina in Italy. They compared the four wind turbine configurations using a multi-criteria methodology to rank the solutions, from the best to worst. Beccali et al. [11] made an application of the multi-criteria decision-

making methodology to assess an action plan for the diffusion of renewable energy technologies at regional scale. They also carried out a case study for the island of Sardinia. They used ELECTRE-III method under fuzzy environment. Borges and Antunes [12] presented an interactive approach to deal with fuzzy multiple objective linear programming problems based on the analysis of the decomposition of the parametric (weight) diagram into indifference regions corresponding to basic efficient solutions. The approach was illustrated to tackle uncertainty and imprecision associated with the coefficients of an input–output energy-economy planning model, aimed at providing decision support to decision makers in the analysis of the interactions between the energy system and the economy on a national level.

3 METHODOLOGY

3.1 AHP model criteria and alternatives

When the decision should be made based on various objectives and criteria the case would move from single-criterion decision-making process toward multi-criterion decision approach. To perform a multi-criteria analysis it is important to identify and precisely define the elements and after that start modeling and analysis one of the most efficient multi-criteria decision making techniques is AHP (Analytical Hierarchy Process) which is built on the basis of pair-wise comparison and helps decision-makers to evaluate different options based on various type of criteria. In this paper, because of uncertainty and range variation conditions governing the problem, methods of multi-criteria decision making in fuzzy and fuzzy numbers and calculations has been considered to solve this problem. The more human being involved in the problem or the system get more complex the fuzzy logic is more efficient to describe and solve the problem.

Alternative: selected alternatives for prioritization process.

Criteria: Characteristics or functional parameters that are effective in selection. Criteria may be quantitative or qualitative and quantitative criteria may be desirable as positive or negative.

Decision Matrix: usually decision-making matrix is used to formulate a multi-criteria problem.

Figure 1 depicts analytic hierarchy process and comparison of alternatives versus criteria. And alternative and criteria and their descriptions are shown in Table (1) and (2).

3.2 Problem solving algorithms and approach

A multi-criteria decision-making procedure proposed by Zeng et al. [6] is reconstructed to select

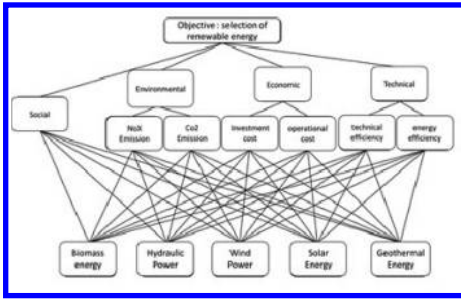


Figure 1. A hierarchy for selection of the most appropriate renewable energy alternative in Iran.

Table 1. Alternatives.

Energy alternatives	Symbol
Geothermal energy	A1
Solar energy	A2
Wind power	A3
Hydraulic power	A4
Biomass energy	A5

Table 2. Evaluation criteria.

criteria	Sub-criteria
Technological	Technical criteria can be divided into technical efficiency (C1) and energy efficiency (C2)
Economical	Economic criteria can be divided into investment costs (C3) and operational and maintenance cost (C4)
Environmental	Consideration of environmental criteria is in order to avoid contamination of the environment. For this purpose measuring pollutants each source of energy produce can be effective. In order to consider the importance of ecological effect of each pollutant the amount of CO ₂ (C5) and NO _x (C6) emission considered as sub-criteria
Social	Social criteria (C7) refers to popularity and application for domestic purposes. Could this kind of energy somehow be used for domestic purposes? In other words, how much energy is used in the residential areas or in the industry?

the most appropriate renewable energy alternative. In a typical AHP method, experts have to give a definite number within a [0–1] scale to the pair-wise comparison so that the priority vector can be computed. For instance, all forms of renewable

energy in terms of the criterion of “technical efficiency” of a pair-wise comparison matrix, are numbered. After that for the rest criteria, the pair-wise comparison of alternatives based on the criteria have to be done. Finally, the final calculations based on AHP method, alternatives are weighting and sorted in descending order, an alternative which has the most amount of weight in the final AHP calculation is selected as the best alternative. Regarding to the fuzzy conditions of the problem, fuzzy numbers and calculations applied in solving this problem.

3.3 Determination of fuzzy condition and calculations

For example, criteria pair-wise comparisons matrix and alternatives pair-wise comparison matrix for the criteria “technical efficiency” are shown in Table (3) and (4). Fuzzy terms means determination of variation scope for the changes of importance of a criteria. Figure 2 depicts scope changes values. Preference amount of entered data in the pair-wise

Table 3. Pair-wise comparison matrix.

	C1	C2	C3	C4	C5	C6	C7
C1		–S	–M	–VS	(–VS, –Ex)	–Ex	(–M, E)
C2			+M	–M	–S	–VS	+VS
C3				–S	–VS	–Ex	+M
C4					–M	–S	+VS
C5						–M	+Ex
C6							Ex
C7							

Table 4. Alternatives pair-wise comparison matrix for the criteria “technical efficiency”.

	A1	A2	A3	A4	A5
A1					
A2			–S	–VS	+M
A3				–M	+VS
A4					+Ex
A5					

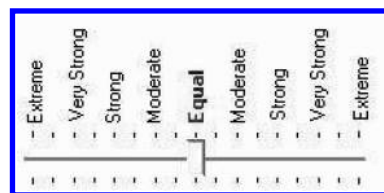


Figure 2. Scope variation for pair-wise comparison.

comparison matrix is done according to Figure 2. The values are consist of Very strong (VS), Strong (S), Moderate (M), Equal (E) and Extreme (Ex) if there is lower priority values, negative values (left) will be included.

Similarly, for other criteria, all alternatives are must be compared with pair-wise comparison matrix and prioritizing renewable energy alternatives will be dine based on final calculations in the study. Figure 3 depicts obtained Results from pair-wise comparison between criteria and alternatives.

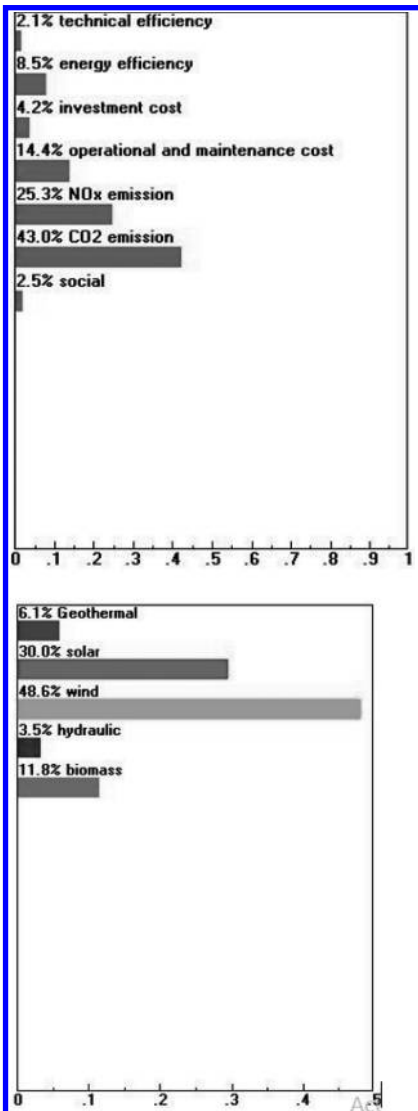


Figure 3. Final ranking of the calculations to prioritize the criteria and alternatives.

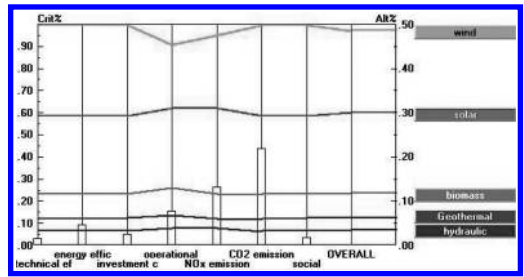


Figure 4. Sensitivity of alternative performance versus criteria.

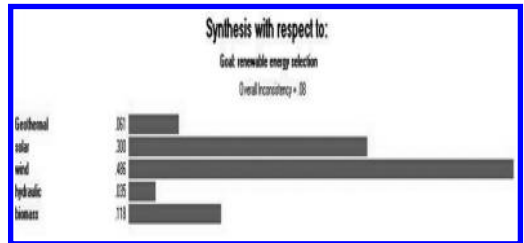


Figure 5. Final results of the calculations.

After weighing criteria, CO₂ emissions with the most points with 0.43 as the most important criterion for the assessment of renewable energy were identified. Criteria for NOx Emission, operational and maintenance costs, energy efficiency, investment cost, social and technical efficiency with respective weights of 0.253, 0.144, 0.085, 0.042, 0.025 and 0.021 were prioritized afterward. Pair-wise comparisons of energy alternatives versus the criteria indicates that wind energy point of 0.486 is the best renewable energy. Solar energy, biomass, geothermal and hydraulic weights 0.3, 0.118, 0.061, 0.035, respectively, were prioritized. Sensitivity of alternative performance measures and the final calculation results can be seen in Figures 4 and 5.

4 CONCLUSION

Energy is considered one of the most important factors in the generation of wealth and also a key factor to show the economic development. The importance of energy in economic development has been recognized almost universally; the historical data attest to a strong relationship between the availability of energy and economic activity. Iran have huge potential for the purposes of renewable energy. For this purpose, this study is based on the selection of the most appropriate renewable energy investment for Iran. In this paper, to make a deci-

sion for selecting the best renewable energy for Iran, fuzzy AHP. Most common renewable energy was identified, and with respect to the identified criteria to measure their priority, compare and ultimately prioritize with fuzzy Analytical Hierarchy Process model. The results of the method conveys that the alternative with the highest score is selected as the best alternative, as well as other alternatives are ranked in order of preference. All alternatives on all criteria within the pair-wise comparison matrix method, are weighted and compared with each other. After weighing criteria, CO₂ emissions rated 0.43 were identified as the most important criteria for the assessment of renewable energy. Emission criteria for NO_x, operational and maintenance costs, energy efficiency, investment cost, social and technical efficiency with respective weights of 0.253, 0.144, 0.085, 0.042, 0.025 and 0.021 were prioritized. Pair-wise comparison of energy alternatives versus defined criteria, indicates that wind energy points equal to 0.486 is selected as the best renewable energy. Solar energy, biomass, geothermal and hydraulic were prioritized in order of weight 0.3, 0.118, 0.061 and 0.035. The results of this prioritization among several renewable energy can be used for decision making in energy planning. Moreover prioritization of certain types of renewable energy plus geographical studies can be used for a geographical area for utilization of this type of energy in that. Exploitation of renewable energy sources prone areas, while maintaining or no damage to the environment can have an important role in optimizing energy planning.

REFERENCES

- [1] Kaygusuz K. Environmental impacts of energy utilisation and renewable energy policies in Turkey. *Energy Policy* 2002; 30:689–98.
- [2] Zeng J., an M., Smith N.J. Application of a fuzzy based decision making methodology to construction project risk assessment. *International Journal of Project Management* 2007; 25:589–600.
- [3] Kagazyo T., Kaneko K., Akai M., Hijikata K. Methodology and evaluation of priorities for energy and environmental research projects. *Energy* 1997; 22(2–3): 121–9.
- [4] Nagesha N., Balachandra P. Barriers to energy efficiency in small industry clusters: multi-criteria-based prioritization using the analytic hierarchy process. *Energy* 2006; 31(12):1633–47.
- [5] Hamalainen R.P., Karjalainen R. Decision support for risk analysis in energy policy. *European Journal of Operational Research* 1992; 56:172–83.
- [6] Keeney R.L., Renn O., Winterfeldt D.V. Structuring West Germany's energy objectives. *Energy Policy* 1987; 15:352–62.
- [7] Haralambopoulos D.A., Polatidis H. Renewable energy projects: structuring a multi-criteria group decision-making framework. *Renewable Energy* 2003; 28:961–73.
- [8] Mavrotas G., Diakoulaki D., Papayannakis L. An energy planning approach based on mixed 0–1 multiple objective linear programming. *International Transactions in Operational Research* 1999; 6:231–44.
- [9] Mirasgedis S., Diakoulaki D. Multi-criteria analysis vs. externalities assessment for the comparative evaluation of electricity generation systems. *European Journal of Operational Research* 1997; 102:364–79.
- [10] Cavallaro F., Ciraolo L. A multi-criteria approach to evaluate wind energy plants on an Italian island. *Energy Policy* 2005; 33:235–44.
- [11] Beccali M., Cellura M., Mistretta M. Decision-making in energy planning: application of the ELECTRE method at regional level for the diffusion of renewable energy technology. *Renewable Energy* 2003; 28:2063–87.
- [12] Borges A.R., Antunes CH. A fuzzy multiple objective decision support model for energy-economy planning. *European Journal of Operational Research* 2003; 145:304–16.

Construction of a green golf club buildings on undermined area

R. Cajka

Faculty of Civil Engineering Department, Department of Structures, VSB—Technical University of Ostrava, Ostrava, Czech Republic

P. Labudek, K. Burkovic & M. Cajka

ARMING Ltd., Ostrava, Czech Republic

ABSTRACT: According to the Czech Mining Act, mining companies are responsible to eliminate consequences of black coal excavation on the surface. An interesting example of reclamation of a site which was affected by undermining is the design and construction of a golf course. Structures in the golf club in Lipiny have been designed to resist mining effects which are still actively occurring. Undermining effects are eliminated by sliding joints between the foundation and subsoil. The sliding joints reduce efficiently friction forces and state of stress in superstructures. All the structures have been designed to resist the load of green roofs (roofs with grass) which fit well in the reclaimed site.

Keywords: foundation structure; undermined areas; soil—structure interaction; slide joints; crack elimination

1 INTRODUCTION

The natural golf course was created in the Czech Republic in the Moravian-Silesian Region in the Karviná Doly excavation territory between the Olše and Stonávka Rivers. This territory was affected by underground excavation of black coal. This is a protected coal deposit site where mining is still in process and related phenomena occur actively on the surface.

This situation had to be taken into account when designing the architectural, structural, technical and static solution to the structure. The architectonic solution of the site was prepared by

Petr Labudek. Other experts proposed the static solution.

2 LANDSCAPE RECLAMATION

According to the Mining Act, §31, Section 5 (Zákon č. 44/1988 Sb. 2012), each excavation company is obliged to remediate the site. This include reclamation of the site in line with special laws, incl. rehabilitation of land affected by the excavation. The excavation company is also obliged to monitor the site after end of operation. Land released during the excavation is reclaimed in line with the plan for developing, preparation and excavation of the site—see § 32 (Zákon č. 44/1988 Sb. 2012). Reclamation is general adaptation of the site and territories structures, the aim being to eliminate damage to the landscape.

Construction of the golf course was required to fulfill requirements for reclamation of the landscape in line with the Act No. 44/1988 Coll. on protection and use of raw materials (“Mining



Figure 1. The links with a driving range in the rear.

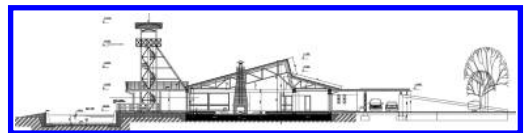


Figure 2. Cross-section of the main facility.



Figure 3. Back facilities.

Act”) (Zákon č. 44/1988 Sb. 2012). Before start of construction, it was necessary to reclaim the site in general. Originally, there had been housing development there but excavation of the coal destroyed that part of the city completely. The undermining caused the landscape to drop by several meters. Debris of demolished buildings were still on the site, and not all parts of the buildings were completely removed there. Reclamation consisted of a technical and biological parts. The technical reclamation included relaying of buried networks and supply of dump rock to form the landscape. Then, the biological reclamation was carried out: the dump rock was covered with soil and grass, bushes and trees were planted there. Rough landscaping started in 1998. Construction of the golf course started in the autumn 2009 and the whole of the golf site was completed in the summer 2011.

The construction of the golf site helped thus effectively and sensitively to reclaim the landscape in line with the Mining Act (Zákon č. 44/1988 Sb. 2012).

3 UNDERMINING EFFECTS

According to the binding opinion of the excavation company, OKD a.s., the construction was designed pursuant to ČSN 73 0039 (ČSN 73 0039 1989, 1991) to fulfil class III construction parameters. The deformation parameters are as follows:

- inclination $i_{\max} = 6.5 \cdot 10^{-3}$ rad
- horizontal deformation $\epsilon_{\max} = 4.0 \cdot 10^{-3}$ –
- radius of curve $R_{\min} = 20$ km

3.1 Method of foundation

The purpose of the load-carrying structure in terms of statics is to eliminate negative effects of the undermining. Landscape elongation, ϵ_{\max} , was eliminated considerably in the foundation structure. The foundation slab and base frame are

reinforced with concrete reinforcement. A rheological sliding joint is used there—see, for instance, (ČSN 73 0039 1989, 1991, Cajka & Manasek 2006, Cajka & Sekanina 2007, Cajka & Mateckova & Janulikova 2012 and Cajka 2013).

3.2 Steel structures and masonry

The steel structure is placed through joints on the foundation structure. Rectification is possible. Because the height of the structure is $h < 10$ m, inclination and curving of the landscape will not influence much internal forces inside the steel structure. In brick walls, minor failures may occur and additional repairs of plaster or additional leveling of floors might be necessary.

3.3 Distribution into dilatations units

Because the structure are located on the undermined territory and the site is regarded as a class III site (ČSN 73 0039 1989, 1991), they have to be divided into dilatation units with the maximum length of 30 m. Dilatation was calculated on the basis of estimated deformation of the undermined territory, location of centre of gravity and heights

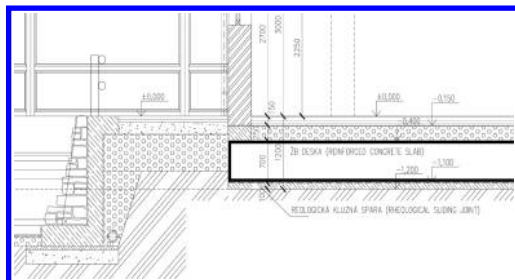


Figure 4. Composition of the sliding joint and cross-section of the foundation slab.

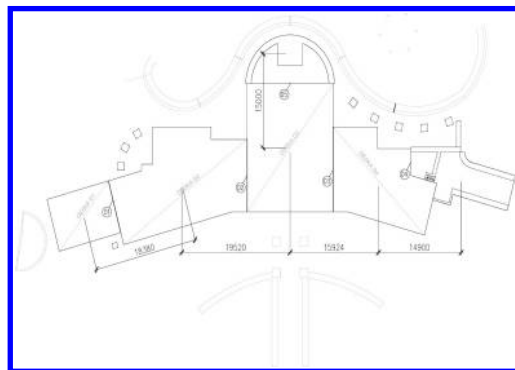


Figure 5. System of dilatation units.

of dilatation units pursuant to ČSN 73 0039 (ČSN 73 0039 1989, 1991).

4 FOUNDATIONS AND THE SLIDING JOINT

Under the sliding joint, series of rock has been consolidated. The rock consisted of gravel sub-base $E_{def} > 60$ kPa with the required rati $on E_{def2}/E_{def1}$ pursuant to ČSN 72 1006. For application of a rheological sliding joint, the sealing coat of concrete was cast on the gravel cushion.

The rheological sliding joint consists of a two layers of heavy modified asphalt belt (“NAIP”). The rheological sliding joint was covered with a cement finish in order to prevent the rheological sliding joint from being damaged by binding of the concrete reinforcement. The foundation structure was made from concrete, class C25/30 pursuant to EN 206-1 and reinforcing iron R10505 (S500), see Figure 6. The foundation was cast continuously, without creating undesirable working joints.

In order to design the sliding joint and to set internal forces in the structure correctly, it is essential to know the shear resistance of the asphalt belt for a specific rate of deformation (Cajka 2013). The shear resistance for the specific rate of horizontal deformation of landscape was specified by experiments in laboratories of the Faculty of Civil Engineering in VŠB—Technical University of Ostrava. Measurement results were used in calculation of internal forced in reinforced concrete foundation. The software was based on a finite element method—see (Cajka & Sekanina 2007 to Cajka 2013).

The subsoil in proposed paper is analyzed as three parametrical C_z , C_x and C_y , where C_z represents vertical resistance of the subsoil (Buchta &

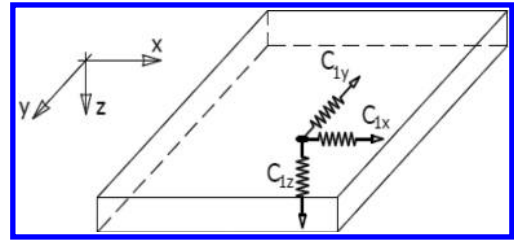


Figure 7. Scheme of parameters C_x , C_y and C_z .

Mynarcik 2014, Cajka 2002, Cajka & Manasek 2005), and C_x , C_y represent horizontal shear resistance of subsoil (Cajka & Mateckova & Janulikova 2012, Cajka 2013, Cajka 2013), Figure 7.

FEM was used to analyse the state of stress of the construction caused by a vertical load and settlement. For that purpose, a slab on elastic subsoil was analysed. For instance, see (Ahmad & Irons & Zienkiewicz 1970, Buchta & Mynarcik 2014, Cajka 2002, Cajka & Manasek 2005, Cajka & Krivy & Sekanina 2011, Cajka 2014, Hradil & Kalab & Knejzlik & Korinek & Salajka & Kanicky 2009, Hrubesova & Kalab 2005, Janulikova 2014 and Krivy 2012). All procedures based on numerical integration (Cajka & Buchta & Burkovic & Fojtik 2014) of an elastic half-space make it possible to solve efficiently the state of stress and contact stress which influence considerably fiction forces in subsoil. If using parallel programming methods (Frydrysek & Janco & Gondok 2013, Halvonik & Fillo 2013) it is possible to analyse, at the same time, non-linear behaviour of concrete structures (Kralik & Simonovic 1993), creation of cracks and general reliability of load-carrying structures.

If we know the maximum value of the tensile force or pressure force, for instance from the solution pursuant to ČSN 73 0039, it is possible to modify the previous equations and derive the relation for the constant friction parameter C_{1x} , resp. C_{1y} , see (Cajka & Manasek 2006, Cajka 2013).

$$C_{1x} = E_c \cdot A_c \cdot \left[\frac{1}{L} \cdot \operatorname{argcosh} \left(\frac{F_x + E_c \cdot A_c \cdot \epsilon_{\max}}{N_{x,\max} + E_c \cdot A_c \cdot \epsilon_{\max}} \right) \right]^2 \quad (1)$$

This method expresses the parameters of the contact functions within the static analysis, if FEM is used. If it is assumed that the friction parameters C_{1x} and C_{1y} are constant for the foundation structure, the distribution of the normal forces is not similar as if the method pursuant to ČSN 73 0039 (Cajka 2013) is used. For simple cases, however,



Figure 6. Reinforcement of concrete foundation slab.

this method is sufficient because the maximum values of the normal forces are not exceeded.

5 LOAD-CARRYING STRUCTURES

External walls and internal load-carrying structures are made of standard brick blocks placed on lime-cement mortar. A reinforced concrete ring beam was cast in site on the brick structure. The ring beam reinforces the brick structure of the building. Above windows, the ring beam is replaced with cast-in-situ head pieces. The head pieces transfer the load from trusses in the load-carrying steel structure of the roof.

In places without load-carrying walls, steel columns are used instead of the brick construction. The load-carrying steel structures are anchored into concrete by means chemical anchors which are applied into predrilled holes. Base plates and top plates are placed in cement mortar and anchored with bolts. Thanks to bolt connection between the steel elements, dilation and rectification is possible—this compensates excessive uneven subsidence of landscape by undermining (ČSN 73 0039).

In places with dilatation joints, there are oval holes in steel elements and trapezoid sheets. The



Figure 10. A driving range.

steel structure was made from steel S235, JR G2 (dead-melted steel) pursuant to EN 10025-2, „B“ class pursuant to ČSN 73 2601.

6 CONSTRUCTION OF A GREEN ROOF

For attractive appearance of the construction and sensitive harmony with the reclaimed landscape, it was decided to use a green roof. Steel frame girders are installed on the reinforced concrete ring beam and steel skeleton. The frame girder carry the load of the roof. The green roof cladding consists of a moisture stop, heat insulation, a waterproof foil, an inclined layer, a drainage layer and a humus layer with grass turfs.

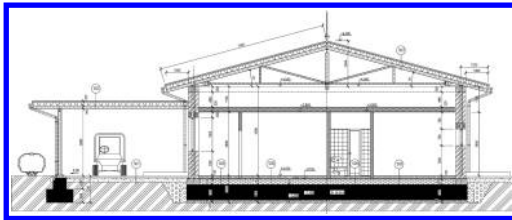


Figure 8. Back facilities—a cross-section.



Figure 9. Detail of a green roof.

7 CONCLUSION

Construction of a golf course is among solutions which improve attractiveness of the reclaimed territory which has suffered from extreme impacts of undermining (Zákon č. 44/1988 Sb. 2012, Davis & Rabinowitz 1956, Dostal & Kozubek & Markopolous et al., Florin 1959, Hyzl & Stehlik & Varas & Zdralek 2009, Janulikova & Stara 2013). The reclaimed landscape meets now requirements set forth for reclaimed territory in the Mining Act No. 44/1988 Coll., on protection and use of raw materials (Zákon č. 44/1988 Sb. 2012). The territory which would not be otherwise used, is now utilised as a sports centre for sports and leisure times activities for people living in this region.

In order to reduce the state of stress caused by the undermining, the sliding joints from melt-able insulate belts were used in the construction of facilities within the gold course. They include (Cajka & Manasek 2007, Cajka & Sekanina 2007, Cajka & Mateckova & Janulikova 2012, Cajka 2013, Kalab & Lednicka 2012). The design, static

solution and assessment of the state of stress of the structures were based on requirements of the standards (ČSN 73 0039 to ČSN EN 1997-1 73 1000 Eurokód 7/Eurocode 7), derived numerical methods (Ahmad & Irons & Zienkiewicz 1970 to Cajka & Manasek 2007, Cajka 2013 to Cajka 2014) and results of laboratory tests of materials used in the sliding joints conducted by the Department of Structures in the Faculty of Civil Engineering in VSB—Technical University of Ostrava (Cajka & Sekanina 2007 to Cajka 2013).

There were several reasons for choosing the green roof. The undermining results in movements of the dilatation units. If fragile materials—such as ceramic or concrete tiles—were used, damage to the roof cladding might occur. Thanks to the green roof, the structure possesses very good acoustic and thermal properties. Last but not least, it is attractive, considering the purpose and nature of the golf course. The proposed green roof improves general reclamation of the territory which had suffered from mining subsistence as it is clear from the attached photos. The construction of the Golf Club Lipiny was awarded the Special Environment Prize in the competition for the best construction in the Moravian-Silesian Region in 2011.

ACKNOWLEDGMENT

This outcome has been achieved with the financial support by the project “Conceptual development of science and research activities 2014” on the Faculty of Civil Engineering, VSB-TU Ostrava.

REFERENCES

Ahmad, S. & Irons, B.M. & Zienkiewicz O.C. 1970. Analysis of Thick and Thin Shell Structures by Curved Finite Elements. *International Journal for Numerical Methods in Engineering*, Vol. 2, No. 3, pp. 419–451.

Bednar, J. & Wald, F. & Vodicka, J. & Kohoutkova, A. 2013. Experiments on membrane action of composite floors with steel fibre reinforced concrete slab exposed to fire. *Fire Safety Journal*, Volume 59, Pages 111–121. ISSN: 03797112, DOI: 10.1016/j.firesaf.2013.04.008.

Brzobohaty, T. & Dostal, Z. & Kozubek, T. et al. Cholesky decomposition with fixing nodes to stable computation of a generalized inverse of the stiffness matrix of a floating structure. *International Journal For Numerical Methods in Engineering*, Vol. 88, Issue 5, pp 493–509. doi: 10.1002/nme.3187.

Buchta, V. & Mynarcik, P. 2014. Experimental testing of fiberconcrete foundation slab model. *Applied Mechanics and Materials*, Vols. 501–504, pp 291–294, doi:10.4028/www.scientific.net/AMM.501-504.291.

Cajka, R. & Buchta, V. & Burkovic, K. & Fojtik R. 2014. Experimental Soil—Concrete Plate Interaction Test and Numerical Models. *Key Engineering Materials*, Vols. 577–578, pp 33–36 Trans Tech Publications, Switzerland, doi:10.4028/www.scientific.net/KEM.577-578.33.

Cajka, R. & Krivy, V. & Sekanina, D. 2011. Design and Development of a Testing Device for Experimental Measurements of Foundation Slabs on the Subsoil. *Transactions of the VSB—Technical University of Ostrava, Construction Series, Volume XI, Issue 1*, VSB—TU Ostrava, ISSN 1804-4824 (Online). doi: 10.2478/v10160-011-0002-2.

Cajka, R. & Labudkova, J. 2014. Dependence of deformation of a plate on the subsoil in relation to the parameters of the 3D model. *International Journal of Mechanics*, Volume 8, Pages 208–215, ISSN: 1998–4448.

Cajka, R. & Manasek, P. 2005. Building Structures in Danger of Flooding. *LABSE Conference New Delhi, India, Role of Structural Engineers towards Reduction of Poverty*. New Delhi, India, pp. 551–558, ISBN 978-3-85748-111-6, WOS: 000245746100072.

Cajka, R. & Manasek, P. 2006. “Physical and Finite Element Shear Load Response Modelling of Viscoelasticity Materials”, in B.H.V. Topping, G. Montero, R. Montenegro, (Editors), “*Proceedings of the Eighth International Conference on Computational Structures Technology*”, Civil-Comp Press, Stirlingshire, UK, Paper 240, doi:10.4203/ccp.83.240.

Cajka, R. & Manasek, P. 2007. “Finite Element Analysis of a Structure with a Sliding Joint Affected by Deformation Loading”, in B.H.V. Topping, (Editor), “*Proceedings of the Eleventh International Conference on Civil, Structural and Environmental Engineering Computing*”, Civil-Comp Press, Stirlingshire, UK, Paper 18, doi:10.4203/ccp.86.18.

Cajka, R. & Mateckova, P. & Janulikova, M. 2012. Bitumen Sliding Joints for Friction Elimination in Footing Bottom. *Applied Mechanics and Materials*, Volume 188, pp. 247–252, Trans Tech Publications, Switzerland, ISSN: 1660-9336, ISBN: 978-303785452-5, DOI: 10.4028/www.scientific.net/AMM.188.247.

Cajka, R. & Mateckova, P. 2011. Temperature Distribution of Slide Joint in Reinforced Concrete Foundation Structures. 17th International Conference on Engineering Mechanics 2011, Svratka, May 09–12, 2011. *Engineering Mechanics*, pp. 95–98, ISBN 978-80-87012-33-8, WOS: 000313492700017.

Cajka, R. & Sekanina, D. 2007. “Angular Displacement of a Normal in the Foundation-Subsoil Contact Area”, in B.H.V. Topping, (Editor), “*Proceedings of the Eleventh International Conference on Civil, Structural and Environmental Engineering Computing*”, Civil-Comp Press, Stirlingshire, UK, Paper 19, doi:10.4203/ccp.86.19.

Cajka, R. 2002. Soil—structure interaction according to European standards (in Czech). *Transactions of the VSB—Technical University of Ostrava, Construction Series, Volume II, Issue 2*, ISBN 80-248-0397-6, ISSN 1213–1962.

Cajka, R. 2013. Accuracy of Stress Analysis Using Numerical Integration of Elastic Half-Space, *Applied Mechanics and Materials*, 300–301, pp. 1127–1135. Trans Tech Publications, Switzerland, ISSN: 16609336, ISBN: 978-303785651-2, DOI: 10.4028/www.scientific.net/AMM.300-301.1127.

- Cajka, R. 2013. Analysis of Stress in Half-space using Jacobian of Transformation and Gauss Numerical Integration. *Advanced Materials Research*, Vol. 818, pp 178–186, Trans Tech Publications, Switzerland, doi:10.4028/www.scientific.net/AMR.818.178.
- Cajka, R. 2013. Analytical derivation of friction parameters for FEM calculation of the state of stress in foundation structures on undermined territories. *Acta Montanistica Slovaca*, Volume 18, Issue 4, Pages 254–261, ISSN: 13351788.
- Cajka, R. 2013. Horizontal Friction Parameters in Soil—Structure Interaction Tasks. *Advanced Materials Research*, Vol. 818, pp 197–205, Trans Tech Publications, Switzerland, doi:10.4028/www.scientific.net/AMR.818.197.
- Cajka, R. 2014. Comparison of the calculated and experimentally measured values of settlement and stress state of concrete slab on subsoil. *Applied Mechanics and Materials*, 501–504, pp 867–876. Trans Tech Publications, Switzerland, ISSN: 16609336, ISBN: 978-303785651-2. doi:10.4028/www.scientific.net/AMM.501-504.867.
- Cihlarova, D. & Seidler, T. & Rezac, M. 2014. Roads problems on undermined areas in the moravian—silesian region. *Applied Mechanics and Materials*, Volume 505–506, Pages 477–480. ISSN: 16609336 ISBN: 978-303835006-4, DOI: 10.4028/www.scientific.net/AMM.505-506.477
- ČSN 73 0039. Navrhování objektů na poddolovaném území. Základní ustanovení. Design constructed facilities in mining subsidence areas. Basic requirements. 10/1989, a-06/1991.
- ČSN 73 1001. Zakládání staveb. Základová půda pod plošnými základy. Foundation of structures. Subsoil under shallow foundations. 8/1988, Z1 9/2009, zrušena 04/2010.
- ČSN EN 1992-1-1 (73 1201) Eurokód 2: Navrhování betonových konstrukcí—Část 1–1: Obecná pravidla a pravidla pro pozemní stavby. Eurocode 2: Design of concrete structures—Part 1–1: General rules and rules for buildings ČNI 11/2006.
- ČSN EN 1997-1 (73 1000) Eurokód 7: Navrhování geotechnických konstrukcí—Část 1: Obecná pravidla. Eurocode 7: Geotechnical design—Part 1: General rules, ČNI 9/2006.
- Davis, P. & Rabinowitz, P. 1956. Abscissas and Weights for Gaussian Quadratures of High Order. *Journal of Research of the National Bureau of Standards*, Vol. 56, No.1, January 1956, pp. 35–37.
- Dostal, Z. & Kozubek, T. & Markopolous, A., et al. A theoretically supported scalable TFETI algorithm for the solution of multibody 3D contact problems with friction. *Computer Methods in Applied Mechanics and Engineering*. Vol. 205, SI, pp. 110–120. doi:10.1016/j.cma.2011.02.015.
- Florin, V.A. 1959. *Osnovy mechaniki gruntov, Tom I. Gosstrojizdat*, Moskva, Leningrad.
- Frydrysek, K. & Janco, R. & Gondok, H. 2013. Solutions of Beams, Frames and 3D Structures on Elastic Foundation Using FEM. *International Journal of Mechanics*, Issue 4, Volume 7, pp. 362–369.
- Halvonik, J. & Fillo, L. 2013. The Maximum Punching Shear Resistance of Flat Slabs. *Procedia Engineering*, Volume 65, Pages 376–381, ISSN 1877–7058, doi.10.1016/j.proeng.2013.09.058.
- Hradil, P. & Kalab, Z. & Knejzlik, J. & Korinek, R. & Salajka, V. & Kanicky, V. 2009. Response of a Panel Building to Mining Induced Seismicity in Karvina Area (Czech Republic). *Acta Montanistica Slovaca*, Vol. 14, No. 2, pp. 143–151.
- Hrubesova, E. & Kalab, Z. 2005. Example of modeling of the mining induced seismicity impact on the building using numerical system Plaxis. *Impact of Human Activity on the Geological Environment—Proceedings of the International Symposium of the International Society for Rock Mechanics*, Eurock 2005, pp. 213–218.
- Hyzl, P. & Stehlik, D. & Varaus, M. & Zdralek, P. 2009. Experience with triaxial loading systems for the testing of road construction materials. *7th International RILEM Symposium on Advanced Testing and Characterisation of Bituminous Materials*, May 27–29, 2009 Rhodes, Greece, WOS:000280392100087.
- Janulikova, M. & Stara, M. 2013. Reducing the Shear Stress in the Footing Bottom of Concrete and Masonry Structures. *Procedia Engineering*, Volume 65, Pages 284–289, ISSN 1877–7058, doi: 10.1016/j.proeng.2013.09.044.
- Janulikova, M. 2014. Comparison of the shear resistance in the sliding joint between asphalt belts and modern PVC foils. *Applied Mechanics and Materials*, Volume 501–504, Pages 945–948, ISSN: 16627482, ISBN: 978–303835005-7, DOI: 10.4028/www.scientific.net/AMM.501-504.945.
- Kalab, Z. & Lednicka, M. & Korinek, R. & Hrubesova, E. 2012. Influence of local geological pattern on values of vibrations induced by road traffic. *Acta Geophysica*, 60 (2), pp. 426–437. ISSN: 1895-6572 (print version), ISSN: 1895-7455 (electronic version), doi: 10.2478/s11600-011-0076-3.
- Kalab, Z. & Lednicka, M. 2012. Foundation conditions of buildings in undermined areas: An example of evaluation. *Acta Geophysica*, 60 (2), pp. 399–409.
- Kohoutkova, A. & Broukalova, I. 2013. Optimization of fibre reinforced concrete structural members. *Procedia Engineering*, Volume 65, Pages 100–106. ISSN: 18777058, DOI: 10.1016/j.proeng.2013.09.018.
- Kralik, J. & Simonovic, M. 1993. Elasto-plastic analysis of deformation soil body with 3D-finite and infinite elements. *International Conference Geomechanics 93, Strata Mechanics/Numerical Methods/Water Jet Cutting/Mechanical Rock Disintegration*, Pages 229–232, Ostrava, Czech Republic, Sep 28–30, 1993.
- Krejsa, M & Janas, P & Yilmaz, I & Marschalko, M & Bouchal, T. 2013. The use of the direct optimized probabilistic calculation method in design of bolt reinforcement for underground and mining workings. *The Scientific World Journal*, Volume 2013, Article number 267593, ISSN: 1537744X, DOI: 10.1155/2013/267593.
- Krejsa, M. 2014. Probabilistic failure analysis of steel structures exposed to fatigue. *Key Engineering Materials*. Volume 577–578, Pages 101–104. ISSN 10139826, ISBN 978-303785830-1, DOI: 10.4028/www.scientific.net/KEM.577-578.101.
- Krivy V. 2012. Design of corrosion allowances on structures from weathering steel. *Procedia Engineering*, Volume 40, Pages 235–240, ISSN: 18777058, ISBN: 978-162748603-3, DOI: 10.1016/j.proeng.2012.07.086.

- Marschalko, M. & Treslin, L. 2009. Impact of underground mining to slope deformation genesis at Doubrava Ujala. *Acta Montanistica Slovaca*, 14 (3), pp. 232–240.
- Moravcik, M. & Kotula, P. & Bahleda, F. 2012. Experimental and FEM analysis of hybrid composite structures with GFRP elements. *Procedia Engineering*, Volume 40, Pages 268–273. ISSN: 18777058, ISBN: 978-162748603-3, DOI: 10.1016/j.proeng.2012.07.092.
- Mynarcik, P. 2013. Technology and Trends of Concrete Industrial Floors. *Procedia Engineering*, Volume 65, Pages 107–112, ISSN 1877-7058, doi: 10.1016/j.proeng.2013.09.019.
- Navratil, J & Zich, M. 2013. Long-term deflections of cantilever segmental bridges. *Baltic Journal of Road and Bridge Engineering*, Volume 8, Issue 3, Pages 190–195. ISSN: 1822427X, DOI: 10.3846/bjrbe.2013.24.
- Pinka, M. & Stolarik, M. & Fojtik, R. & Petrik, T. 2012. Experimental Seismic Measurement on the Testing Construction and the Analyze. *Transactions of the VSB—Technical University of Ostrava, Construction Series, Volume XII, Number 1/2012*, ISSN 1804-4824 (Online). doi: 10.2478/v10160-012-0006-6.
- Poulos, H.G. & Davis, E.H. 1974. *Elastic Solutions for Soil and Rock Mechanics*. New York John Wiley & Sons, Inc.
- Sekanina, D. & Cajka, R. 2008. Interaction between Prestressed Floor and Subsoil. (in Czech). *Transactions of the VSB—Technical University of Ostrava, Construction Series*, Volume IX, Issue 1, pp. 17–24, ISBN 978-80-248-2105-4.
- Stara, M. & Buchta, V. 2014. Experimental tests of pre-stressed masonry and numerical modeling of resultant deformations. *International Journal of Mechanics*, Volume 8, Issue 1, Pages 138–143, ISSN: 19984448.
- Sucharda, O. & Brozovsky, J. 2013. Bearing Capacity Analysis of Reinforced Concrete Beams. *International Journal of Mechanics*, Issue 3, Volume 7, pp. 192–200.
- Sucharda, O. & Brozovsky, J. 2013. Failure and plasticity conditions of concrete in the finite element analysis. *Applied Mechanics and Materials*, 367, pp. 165–168. DOI: 10.4028/www.scientific.net/AMM.367.165.
- Zákon č. 44/1988 Sb., o ochraně a využití nerostného bohatství (horní zákon), v platném znění, Parlament České republiky. 2012. (Act No. 44/1988 Coll. on protection and use of raw materials, the Mining Act, as amended).

Effect of the special environments on bond behavior of CFRP anchor

Wen-Rui Yang

School of Transportation, Wuhan University of Technology, Wuhan, China
Business School, Jiangxi University of Technology, Nanchang, China

Xiong-Jun He & Kai Zhang

School of Transportation, Wuhan University of Technology, Wuhan, China

Peng Zhang

Department of Civil and Architecture Engineering, Guangxi University of Science and Technology, Liuzhou, China

ABSTRACT: Effects of special environment on the basic mechanical properties of Carbon fiber (CFRP) anchor were studied by acidic, alkali, salt solutions and tensile test. Using of bond stress and slip linear regression method to forecast the slip value of different reinforcement diameter, different anchoring length under general environmental and acidic, alkali, salt solutions corrosion. Test and analysis results show that the tensile strength of CFRP and Epoxy mortar changes, the elastic modulus, elongation change little, the bond slip amount increased by more than 50%, bond performance relative to influence by the corrosion. With acid, salt corrosion as compared to a case, the bonding properties of CFRP anchor and epoxy mortar are more sensitive to alkali corrosion.

Keywords: Carbon fiber (CFRP) anchor; environmental effect; poll-out test; bond behaviour

1 INTRODUCTION

Most of geotechnical anchor engineering in the long-term corrosion, harsh environment, such as acid rain, coastal salt corrosion in China's large area. FRP composites have unique properties such as high strength-to-weight ratio, resistance to corrosion, and ease of installation in the field, which make them exceptionally attractive to a wide range of construction applications^[1]. Therefore, there is an urgent need to investigate the effects of long term degradation on the FRP-concrete interface in various representative environments.

Two methods used to study the performance of FRP bar under special environments: FRP bar direct exposure (such as direct exposure to the erosion solution), configure FRP bar in concrete to withstand environmental effect. Some research^{[2][3]} was used to study the FRP itself along with the change of environment change and produce performance, does not represent the FRP rebar and concrete after combined with practical engineering, the durable performance of the environmental impact and response. So the good performance of FRP reinforcement in the project of the actual, is more used is to make it puts FRP rebar in concrete subjected to environmental effects^{[4][5][6][7]}.

Therefore, as the actual research in geotechnical engineering work state, the paper consider two

main factors affecting the anchor bond properties of CFRP anchor: CFRP bar, epoxy mortar adhesive. At the same time, studied the corrosion resistance of the CFRP bar and epoxy mortar adhesive under special circumstances.

2 TESTING PROGRAM

LI Chen-chen (2013)^[8] studied on GFRP reinforced accelerated deterioration test by alkaline simulated concrete pore solution. Through the experiment of high concentration accelerated corrosion method, using the acid (H_2SO_4), alkali (NaOH), salt (NaCl) to soak in different times of CFRP anchor and epoxy mortar, and blocks to test the mechanical properties of CFRP bar and grouted medium epoxy mortar in different soaking time stage, studied the impact of acid, alkali, salt corrosion on the CFRP bar, the basic properties of epoxy mortar and the bond performance.

2.1 Test materials

CFRP anchor. This experiment uses the diameter of CFRP bar, 7 mm, which produced by Liuzhou OWM Machinery. The performance with rib reinforcement material is stronger, but the ribbed reinforcement anchor technology is not mature

enough, so the light round bar was studied by using this test; the end anchorage anchor tube material for steel 40Cr, diameter 14.4 mm, diameter 28 mm, length respectively using 245 mm, 300 mm, 350 mm, according to the contrast test of bond performance used by different anchorage length. The tensile strength of CFRP rod body is relatively high, in order to give full play to the advantage of the strength of the rod body, the rod body can bear large pulling force, required the sufficient adhesion strength of anchoring agent. On the basis of relevant literature research, selection epoxy resin adhesive with better bonding performance and high strength.

Corrosion test solution. Corrosion of components is a long period of evolution process, in order to achieve certain effect in the short term corrosion test stage, so used the high concentration of corrosion of acid and salt test with corrosion solution respectively by PH = 3(H_2SO_4), PH = 13(NaOH), 10% salt (NaCl). The corrosion resistance of PEVA material sheet soaked and sealed the surface of containers, lest the vessel suffered acid salt corrosion, impacting the solution concentration and the experimental result. Because the anchor corrosion resistance is low, coated with a layer of butter before immersion in the anchorage surface, avoid anchorage corrosion seriously affect the mechanical properties tests later.

Test method. High concentrations of the test, using the acid (H_2SO_4), alkali (NaOH), salt (NaCl) of three different corrosive medium for CFRP anchor and epoxy mortar test. Studied the appearance, weight and size and other physical properties in 0 d, 10 d, 20 d, 30 d, 40 d, 50 d, 60 d, 70 d, 80 d, 90 d, at the same time, tensile tests were carried out in 0 d, 60 d, 90 d, measured the strength, elastic modulus, elongation rate of basic mechanical properties and adhesive property. In the process of test, tested weekly ensure constant PH. Each set of three specimens, and according to the corrosion solution and days numbered bolt, block, such as Ac30-1, Al30-2, Sa30-3.

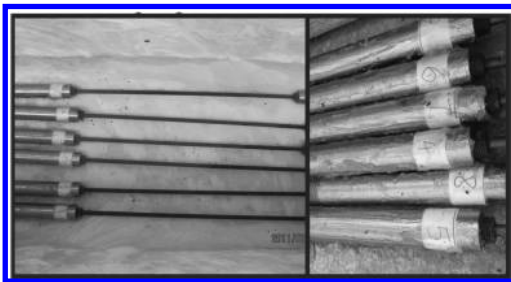


Figure 1. The CFRP anchor immersion corrosion.

Mechanical properties of the specimen test in electro-hydraulic servo universal testing machine, loading force method for load control, in the middle of the CFRP anchor specimen gage length symmetrical paste two strain gauge, external static resistance strain gauge; Bolt axial fixation, extensometer reading connected to computers. Then, bring to bear on the stability of a continuous load, until the specimen damage, every five KN read after loading strain and displacement values and amplify the meter reading, epoxy mortar test block every thirty KN readings.

2.2 Analysis of experiment result

The failure mode of the specimens, after corrosion and without corrosion, still appear debonding, breaking of the end clamp, splitting, but debonding is given priority to, shows that after corrosion bolt bonding performance affected by negative.

Variation of Physical Properties. Therefore, regardless of the material of the dissolution or medium permeability is both associated with diffusion performance, just dissolution in the corrosive medium permeability are polymer materials after internal and interact with them. Diffusion capacity and weight change after corrosion are connected with corrosive medium molecular size, gap materials in the rate of pore size distribution, affinity of corrosive medium and material.

Changes in physical properties of CFRP bolt. The changes in physical properties of CFRP bolt, showed little change of bolt diameter measurement, but the amount of weight change with corrosion age different is different: (1) the corrosion in the age of 30 d, 60 d, may be due to CFRP anchor corrosion, anchor weight decreases; (2) under the condition of corrosion in the age of 90 d, the corrosive medium may be seeping from the surface and make the internal anchor weight increase.

Epoxy mortar block. When the epoxy mortar specimens immersed in corrosion solution with a small amount of corrosion on the surface of a block, the weight loss of the specimens slightly; when taken out, test block is retained on the surface of water, the solution did not enter the internal block without the weight increase, density of visible inside the block is very good, block material adhesive performance is very good, Rubber cover tightly, the water is not easy to enter the sub.

2.3 Basic mechanical properties of specimen

By the tensile test after CFRP anchor acid, alkali, salt solution immersion, because the CFRP reinforcement compressive strength of resin is smaller, testing machine chuck and the member is not fully exposed, member tension clamp compressive stress

Table 1. Mechanical property loss of CFRP anchors after acid alkali and salt corrosion.

Corrosive medium	Corrosion time (d)	Change rate of tensile strength	Change rate of elastic modulus	Change rate of ductility
Acid solution	60	-6.35%	-2.76%	-5.06%
	90	-6.65%	-3.29%	-4.81%
Alkaline solution	60	-5.08%	-4.1%	-2.05%
	90	-9.24%	-4.25%	-5.26%
Saline solution	60	-7.62%	-3.68%	-5.97%
	90	-14.90%	-3.68%	-12.86%

Table 2. Mechanical properties of epoxy mortar block after acid alkali and salt corrosion.

Corrosive medium	Corrosion time (d)	Compressive strength (Mpa)		Elasticity modulus (Gpa)	
		Mean	Standard deviation	Mean	Standard deviation
Unconditioned	0	74.24	2.56	9135	25.3
Acid solution	60	73.38	6.96	9080	27.35
	90	72.43	0	8400	82.84
Alkaline solution	60	76.875	6.39931	9210	78.82
	90	79.955	0.685894	7830	40.42
Saline solution	60	74.54	1.89	8790	1.50
	90	78.47	0	8390	92.07

is very large, if the direct clamping head tension, often end crushing phenomenon before tensile failure. So, do not occur in tensile test end crushing phenomenon in order to ensure the test. This test uses a steel processing into the two ends of the anchorage.

CFRP anchor Failure form CFRP bolt tensile test after acid salt corrosion of 0 d, 60 d, 90 d, is similar to ordinary environment. Stress—strain curve is linear elastic changes until the bolt failure. Load to ultimate load of 60%–70%, heard the noise of the fiber stripping resins and part of the fibre fracture, then specimen began to destroy.

Epoxy mortar block Table 2 shows the mechanical properties of epoxy mortar test block after the acid, alkali, salt corrosion, Compressive strength and elasticity modulus of epoxy mortar test block decreases after acid corrosion, modulus of elasticity; with the increase of the number of days of corrosion increasing the intensity of epoxy mortar, elastic modulus decrease trend. Alkaline corrosion strength maximum 7.7%, 14.29% lower elastic modulus.

The mechanical properties of epoxy mortar test block of Table 5 gives the acid, alkali, salt corrosion, acid corrosion of epoxy mortar test block strength decreases, the elastic modulus decreases; Under the condition of alkali, salt corrosion, Increasing the intensity of epoxy mortar, elastic

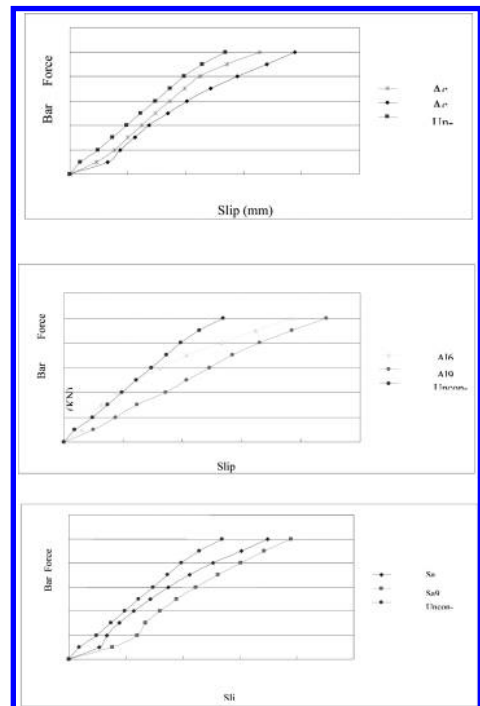


Figure 2. Two kinds of special environment and general environmental case load-slip curve.

modulus tended to reduce with the increase of corrosion time, the strength increase by 7.7%, the elastic modulus decreases by 14.29% after alkaline corrosion.

3 BOND PERFORMANCE ANALYSES

Determination of total displacement of anchor and CFRP rod elastic elongation by test, through two difference is a bolt slippage. Figure 2 graphs the CFRP bolt load-slip curve under acid, alkali, salt environment and general environment. The curve comparison: CFRP anchor load-slip more than the general environment, and increasing slippage with the increase of corrosion time. Account for the lower anchor bond properties of CFRP through acid, alkali, salt corrosion. Figure 2 show the slippage larger by alkali corrosion than the acid, salt corrosion, CFRP anchor by alkaline solution corrosion greater influence t than the acid, salt corrosion.

4 CONCLUSIONS

1. The physical properties of CFRP anchor and epoxy mortar block changed little after acid, alkali, salt corrosion: from the appearance point of view look from the appearance, after the corrosion of acid, alkali and salt solution, CFRP anchor and epoxy mortar block surface color and size are not obvious change, the weight gain rate and the weightlessness rate is small, the overall weight change is very small, the degree of corrosion is relatively low.
2. Long-term acid corrosion of epoxy mortar produced adverse effect, strength and elastic modulus showed a trend of decrease; Alkali, salt corrosion of epoxy mortar about significantly improve the compressive strength and elastic modulus decreased with increasing corrosion time, alkali, salt corrosion, with no negative impact on epoxy mortar, and the influence of alkali corrosion environment change is more sensitive to acid, salt corrosion.
3. Through CFRP anchor tensile test after acid, alkali, salt corrosion, tensile strength and elastic modulus, elongation decreased with increasing corrosion time, but reduce the value is smaller, corrosion medium did not cause significant damage to the CFRP anchor, CFRP anchor has good corrosion resistance.
4. Compared with acidic solution and salt solution, the CFRP anchor of alkali corrosion is relatively more sensitive. But on the whole, the

influence of acid, alkali and salt corrosion of GFRP bolt is not serious.

5. The interface of CFRP bar and epoxy resin is relatively weak, after acid, alkali, salt corrosion creating slippage is bigger, by the corrosion of bond slip increases more than 50%, had a greater influence on the bond properties relative. Explain the bonding performance of CFRP anchor down; Also more sensitive to alkali corrosion.

ACKNOWLEDGMENTS

This research is supported by the National Natural Science Foundation of China (Grant No. 51168006), the National Natural Science Foundation of China (Grant No 51178361), Liuzhou City, Guangxi Province, the research and development of Applied Technology Program (Grant No 2010020603), Research on aging performance of new carbon fiber pressure type anchor (Grant No JY3303).

REFERENCES

- [1] Nakaba K, Kenakubo T, Furuta T. Bond behavior between fiber-reinforced polymer laminates and concrete. *ACI Structural Journal*, 2001, 98(3):1-9.
- [2] F. Katsuki, T. Uomoto. Prediction of deterioration of FRP rods due to alkali attack. *Proceedings of the Second International RILEM Symposium (FRPRCS-2), Non-Metallic (FRP) Reinforcement for Concrete Structures*, London 1995: 83-89.
- [3] Fu Kai, Xue Wei-chen. Accelerated Aging Tests for Evaluations of Tensile Properties of GFRP Bars under Artificial Seawater Environment [J]. *Journal of Building Materials*, 2014, 17(1):35-41.
- [4] GangRao, H., and Barger, J. (2001). "Aging of bond between FRP and concrete cubes." *FRP composites in civil engineering*, Vol. II, J.-G. Teng, ed., Elsevier, 1569-1578.
- [5] Mohamed S. Sayed, Hossam Z. EL-Karmouty, Ghada D. Abd-Elhamid. Structural performance of circular columns confined by recycled GFRP stirrups and exposed to severe conditions. *Housing and Building National Research Center*. 2012. 1687-4048.
- [6] Fu Kai, Wang Wei, Xue Wei-chen. Accelerated aging test for evaluation of compressive properties of GFRP rebars under simulated concrete environment [J]. *Journal of Building Structure*. 2013, 34(1):117-122.
- [7] Mathieu Robert, Patrice Cousin, Brahim Benmokrane. Durability of GFRP reinforcing bars embedded in moist concrete. *Journal of Composites for Construction*, 2009, 13(2):66-73.
- [8] Li Chen-chen, Yu Ai-min, Wang Ying-lai. Durability of FRP Rebars in Alkaline Environment of Concrete [J]. *Building science*, 2013, 29(1):47-51.

Research on Tonga traditional houses adaptive to environment

S. Jin

School of Architecture and Urban Planning, Shenzhen University, Shenzhen, China

H. Huang

The Institute of Architecture Design and Research, Shenzhen University, Shenzhen, China

Z. Yang

Academy of Fine Arts, South China Normal University, Guangzhou, China

ABSTRACT: Tonga archipelago has special location and mild climate, and it affects local people and their architecture. Tonga traditional houses are so much about life. The goal of this paper is to study the interaction among geography, climate, culture and architecture by taking Tonga as an example. This paper analyzes the development process of Tonga traditional houses. It particularizes the different types of Tonga house forms. It presents the local craftship and the construction procedures of the traditional houses. And it proposes the main design consideration in terms of environmental adaptation.

Keywords: house form; environment; culture; Tonga

1 GEOGRAPHY AND CLIMATE

Tonga is an archipelago in the South Pacific Ocean. It consists of 171 islands, covers 748 sq km and supports a population of 104,227 people. (Fig. 1) (July 2001)

Tonga lies three degrees east of the International Date Line; therefore Tonga is the first country in the world to welcome each new day.

The islands of Tonga were formed on top of two parallel submarine ridges. Between the ridges is the trough. The deep water in the ocean east of the

ridges is known as the Tonga “deep”, which is one of the deepest parts of the ocean-floor.

Tonga has a favorable climate, which is warm, humid, and moderately wet throughout the year. The temperature and rainfall vary with the location.

The geography and position of Tonga within the Pacific affects its climate, and the climate affects Tongans culture and lifestyle. Tongan traditional house is the outcome of how people adapted to the environment.

2 HISTORY

Dutch navigators (Schouten and Le Maire) in 1616 were the first Europeans to sight the Tongan archipelago. Captain James Cook visited the islands 125 years later. To quote from him: “Tonga archipelago is the ‘Friendly Islands’ because of the gentle nature of Tonga people.”

Tonga was united into a Polynesian kingdom in 1845. It became a constitutional monarchy in 1875 and a British Protectorate in 1900. Tonga acquired its independence in 1970. It remains the only monarchy in the Pacific.

3 CULTURE AND LIFESTYLE

“In constituting and reconstituting the social world, human beings at the same time are involved in an

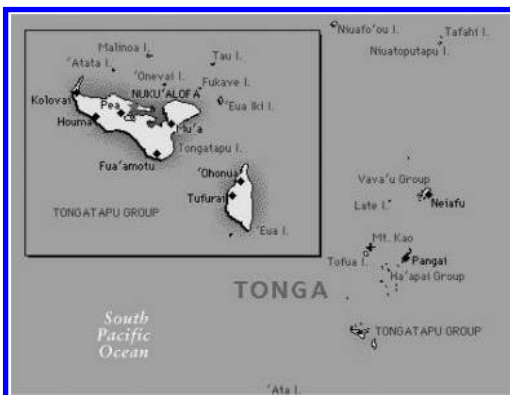


Figure 1. Tonga archipelago.
Source: <http://cn.bing.com/images>.

active interplay with nature, in which they both modify nature and themselves.” (Giddens, 1981)

Tongans are very social and enjoy outdoor activities. (Fig. 2) Rugby is the national sport. Men enjoy the competitions in volleyball, basketball, soccer, and tennis. Women play netball and field hockey. Movies and dances are also major recreation in larger villages. Families have picnics on the beach for special occasions.

Men traditionally build boats, canoes, and houses and are proficient in woodcarving. Women traditionally weave mats, baskets and leis, etc.

3.1 Breathing

Breathing is central to the Tongan culture and life-style. It is hardly to breathe within circular plan form; the Tongans split the circular floor plan and extend the space lengthwise in order to increase the use of space and create their breathing environment. (Fig. 3)

3.2 Family ranking system

Tonga has a very complex family ranking system. It involves two fundamental factors, sex and age. Of the two, sex is immutable, and may surpass age. The husband is considered the head of the immediate family, while the wife holds higher ranking.



Figure 2. Tongan daily life.
Source: <http://cn.bing.com/images>.

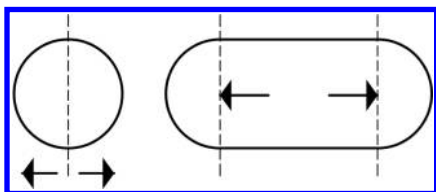


Figure 3. Extend the circular floor plan to ovoid floor plan.

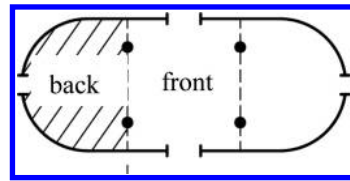


Figure 4. “Front” and “back” shows in the floor plan.

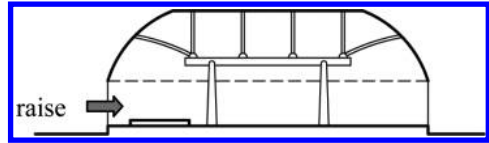


Figure 5. Raised elevation shows in the section.

Tongan family ranking system affects the layout of the houses. “A chief when sitting among his inferiors, a pile of mats is provided to raise him above the common level.” (Gifford, 1929)

It defines the interior space by giving it a “front” and “back” in the floor plan. (Fig. 4) It raises the elevation vertically in the section in order to manifest this important feature. (Fig. 5)

3.3 Privacy

Tonga houses are open to the environment due to the mild climate and Tonga lifestyle. Inside the house, the “front” and “back” areas define the domain privacy. And screens are also used to divide the different spaces on a temporary basis. Screens are made of local mat that can be removed during the day.

4 TONGAN TRADITIONAL ARCHITECTURE

“Architectural ideas are not so much about building, but about life.” (Kollar, 1983)

Tonga traditional house and its use deliver the message to the young generation about the formality, respectful behavior, and reverence etc.

The first house type with the single central post is described by Anderson (1983). “This form, with thatch walls used to be commonly used as a temporary dwelling house. (Fig. 6) Its gabled construction is much easier to construct than those houses that consist of two-post and a ridge beam off which the rafters fell to low side walls.”

An “A” shape house form with no posts on the two gable ends opened up the internal space. (Fig. 7) With the walls completely open, space flows from inside to outside. The “A” shape house

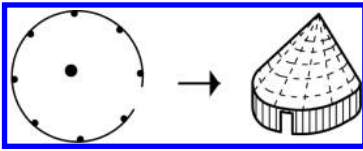


Figure 6. Single-central-post house form.

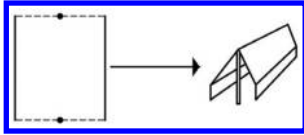


Figure 7. A-shape house form.

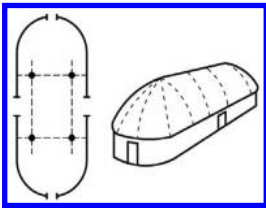


Figure 8. Four-post house form.

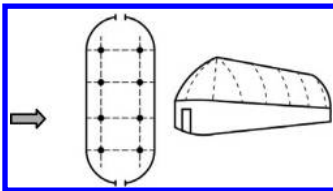


Figure 9. Multi-post house form.

form is believed to precede the two—post house form. (Fig. 8)

With the development of society, the two-post house form extended to the four-post house form, and then developed into multi-post house system, which repeats the spatial frame and has more indoor and outdoor functions. (Fig. 9) The Tonga house form has a gradual development progress.

“The house form is not simply the result of physical forces or any single causal factor, but is the consequence of a whole range of socio-cultural factors seen in their broadest terms. Form is in turn modified by climatic conditions and by methods of construction, materials available, and the technology.” (Rapoport, 1969)

Local materials are used in Tonga houses. Coconut leaves are for thatch roof and walls, which can breathe itself under the wind pressure. Coconut husk are used to make lashings, which can fasten the house elements together and decorate the

house. Local materials make local dwelling a pleasant place to live for inhabitant.

The thatch roof and walls are not only building materials, but also an insulator and filter. When the hot air rises inside the house, it can escapes through the air gaps between the thatches. And the low eaves line can cut off solar penetration.

“The indoor environment should be safe, appropriate for its purpose and pleasant to inhabit. There should be little to cause annoyance or distraction and work or pleasure. Activities should be unhindered physically or mentally. A suitable environment can contribute towards a person’s health, well-being and productivity.”—Cibs

Natural ventilation is always the major design consideration for Tongan houses. With the favorite mild tropical climate, Tongan outdoor lifestyle prefers more open-planning layout. Therefore, there is less segregation of areas inside the house.

With the constant development, Tonga house forms have many types. (Fig. 10) And the main differences among the house types are scale, materials, and ornamentations. The ornamentations demonstrate the house owner’s identity of the nobles. The level of decorative details and lashings shows the stratum of a king, noble and commoner. The house types may vary, but the principle of construction is the same.

After the owner decide to build a house, his family and friends start to collect all the materials.

Timbers are trimmed and roughed out near the place of felling. And then they are dried for the use of posts and rafters; they are stacked near the building site. Coconuts husk are used for lashings. The thatch roof is made from coconuts leaves. The ridge is covered with several layers of thatches. Small sticks help to secure the top with two coconut fronds.

They dig the hole in the ground on the site and put the small outside posts in place. The wooden



Figure 10. Tonga traditional houses.

band is placed at the joint of walls and roof. After the posts-structure is finished, the thatch roof is put on it to complete the main construction.

Small timbers are lashed at approximately 450 mm in between the outside posts. They are set into the ground hole and reach up to the wooden band. The thatches are tied to these small timbers in two layers. The first layer is started from the ground up to the wooden band, while the second layer is started from the top to the ground. Thatches overlap each other. The first layer is the inner layer; the second layer is the outer layer. Thatch walls are done after the outer layer attaches to the inner layer. Wall covering is constructed from small mats. Coconut leaves are braided together for covering mat. And it is also used for floor mat. The leaves-made mat is more comfortable than the solid floor. But the mat needs to be replaced every three to four years as the leaves decay.

5 CONCLUSION

Tonga is an archipelago in the South Pacific Ocean. It remains the only monarchy in the Pacific. Tongans lifestyle has been adapted to suit the favorable tropical climate. Tongans are very social and enjoy outdoor activities. Tonga traditional houses are

designed simple, flexible, and sustainable in order to satisfy their lifestyle. People take their own body as an instrument of measurement, using the traditional method to construct their own space. Natural ventilation and open space are the main design considerations for Tongans.

ACKNOWLEDGEMENTS

The corresponding author of this paper is Zhi Yang.

This paper is funded by: China Postdoctoral Science Foundation (2013M530459); 2014 Guangzhou Twelfth Five Years Plan of philosophical and social science program (14G21).

REFERENCES

- Anderson, Andrew. *Tonga: Apt Housing*. Auckland: Thesis at Auckland University. 1983.
- Giddens, A. *A Contemporary Critique of Historical Materialism*. Berkeley: University of California Press. 1981.
- Gifford, Edward. W. *Tongan Society*. Bernice P. Bishop Museum Bulletin 61. Honolulu, Hawaii, 1929.
- Rapoport, Amos. *House Form and Culture*. Prentice-Hall Inc. Englewood cliffs, New Jersey. 1969.

Innovative design of integrated facility for the aged based on green building concept

Yang Chen & Ying Liu

Harbin Institute of Technology, China

ABSTRACT: China has already entered into a rapid development period of population aging, then the demand for integrated nursing facilities and green buildings for aged people has becoming an urgent livelihood issue. Based on green building concept, this paper analyzes the current status and development tendency of the integrated nursing facilities for the aged, and studies on innovative design strategy to get safe, healthy, appropriate and effective facilities, with the purpose to promote construction quality and living quality for aged people.

Keywords: aging; green building concept; integrated nursing facility; innovative design

1 INTRODUCTION

With the rapid development of national economy and society progress, china has already entered a rapid stage of population aging. According to data released from the State Statistics Bureau, by the end of 2013 the total population of China is 1.36072 billion, among which the population of people elder than 60 is 202.43 million, with proportion of 14.9%, and the population of people elder than 65 is 131.61 million, with proportion of 9.7%. According to forecast, the aging population will be 3 billion by around 2023, the number will exceed 4 billion by around 2035, and the number will peak at 4.87 billion by 2053, at that time the aged share of total population is 34.87%. The rapid aging process and vast aging population are bound to exert an influence on the aged care pattern and aged facility service system, which makes the requirement for the integrated facilities more urgent. Nowadays, green building has becoming a consensus, and we should maximumly utilize resource to provide aged people with safe, healthy, appropriate and effective integrated facilities, this is not only an effective way for achieving energy conservation and environmental protection, but also the tasks and responsibilities for architects and planners.

2 GREEN BUILDING CONCEPT

Green building theory is the production of global ecology awareness, and also known as healthy building. It is a common view that green building will consume the minimum energy and resources,

and exert minimum influence on ecological environment in its whole life cycle. At the meantime, it provides healthy, comfort, effective environment for working and living, which makes people, architecture and nature in harmony together. The features represent as:

2.1 “Green” in the whole life cycle

The whole life cycle of green building includes planning, design, building, operation, reconstruction, and dismantle. In the whole cycle, green building alleviates the contradictions between environment and energy consumption, and provide healthy, comfort, energy saving and harmless space for people.

2.2 *Harmonious coexistence with natural environment*

Green building is the result of the combination of ecological technology and architecture. Starting from the local characteristics, we should set up the thought of “follow nature, back to nature”, through the landscape environment optimization design, try to keep the original plants and historical heritage. Using advanced energy system, renewable and clean energy resources, make the material energy recycle, to achieve harmonious coexistence between human and nature, and achieve sustainable development.

2.3 *Health and comfort of architecture space*

Green building fully meet people’s basic requirement for living space, from the design to consider the surrounding environment, architectural structure, color, style, energy-saving technologies, etc.,

to determine the suitable space scale, reasonable sunshine distance, healthy green plants, convenient the greenway system, effective connectivity between indoor to outdoor, security insurance, pollution reduction and quality promotion.

2.4 *Energy-saving technology*

Energy-saving technology is particularly important for green building. Researches on green building have utilized a variety of new type energy, such as solar energy, geothermal energy, wind energy, hydro-power, bioenergy, and new energy-saving materials and many other new technologies, new products.

Green building has becoming a global concerned topic, with certain theoretical basis, which provides new design strategy for integrated facilities for the aged.

3 STATUS ANALYSIS OF THE INTEGRATED FACILITY ARCHITECTURE FOR THE AGED

Integrated facility for the aged is constructed for the aged living, life care, health care and entertainment, such as nursing homes, is a kind of intensive architecture. To be specific, firstly medical care function, including medical treatment, rescue, and health care; secondly daily care function, including dining, living, walking, etc., basic life care; thirdly, spiritual support function, including psychological consultation and hospice; fourthly, cultural education function, including learning, teaching, and cultural communication; fifthly, ecological function, let people close to the nature. From the above, integrated facility need to be designed with technologies of energy saving, environmental protection, low-carbon, barrier free and advanced technology, to provide a green and intensive support system for the aged people.

Nowadays, China has make remarkable achievements in construction of integrated nursing facility, but there are also problems cannot be ignored. Through field investigation, it is found that the problem mainly includes the following aspects:

3.1 *Shortage of safety design*

Integrated nursing facilities are special architectures, safety design should be considered throughout the whole design process. But from investigation, it is found that part of nursing facilities lack of ramp way and blind way in design; some facilities haven't set up safety hand rail neither in hallway or living room, even stairs, or have hand rails with unreasonable design in height or shape; and some facilities exist height difference on ground, or have no

antiskid design on ground, or have unreasonable design on elevator settings, etc., these all increase the possibility of danger. Moreover, a few facilities lack of television monitoring and emergency call, and nearly all nursing facilities lack safety warning equipment for emergency, which greatly delay the emergency rescue.

3.2 *Poor living comfort*

Investigation shows that the construction standard of some integrated nursing facilities is at a relatively low level, and the comfort level of living environment is poor. The problem is embodied in: low construction standard for per bed, narrow living space, short sunshine duration, poor ventilation, and poor sound insulation, lack of leisure space and green space. Especially for nursing facilities in downtown, due to the restriction of high land cost, it is difficult to allocate enough public space. In addition, some facilities located in the suburbs are also lack of public space for communication, lack of effective area of green space, in spite of large-area yard, which cause the physical space insufficient for leisure activities.

3.3 *Lack of leisure space*

For the aged, the physical requirement is at a low level, what they really care is problem in spiritual world, such as spiritual sustenance and lonely life, which have great influence on the quality of their lives. At present, most of the nursing facilities focus on the service of physical supply, but neglect the leisure and spiritual demands of the aged, and always lack of leisure space, which debases quality of aged people's spiritual life, and also make it difficult to satisfy their emotional needs, to enjoy their retirement lives.

4 INNOVATIVE DESIGN STRATEGY FOR INTEGRATED NURSING FACILITY BASED ON GREEN BUILDING CONCEPT

4.1 *Green safety design: Intensify security assurance*

The first principle need to be considered for nursing facility design and planning is safety, therefore planning layout, architectural design and detail design should consider safety design, such as barrier-free design and handrail design. Concretely including the following aspects:

4.1.1 *Safety design for layout*

Considering the security and convenient for travel and activity of aged people, the separation

of pedestrian and vehicles should be introduced, and the traffic organization should guarantee that emergency vehicles can reach the entrance of any building, in addition to meet the requirements of firefighting, evacuation, transportation and so on. Moreover, there should be parking space for both motor vehicles and non-motor vehicles in the layout. There also should be accessible parking spaces dedicated for wheelchair users, near the main entrance of the building, accessible parking spaces should be clearly marked to strengthen prompt functions, and connected with the pedestrian path.

4.1.2 Safety design for key parts

The design from building entrance to vehicle road should consider the requirement of crawling, stopping, transferring for aged people, and should reserve enough buffer space. The specific term is that the height change between building entrance and road surface should not more than 500 mm, low height steps and ramp way should be introduced; the height of the steps should lower than 120 mm, the tread width should greater than 350 mm; and there should be handrail on the steps; ramp way should be skid proof, with gradient less than 1/12, and continuous length not more than 6 m. Such as the appropriate design of accessible ramp way in Golden Age nursing facility in Hangzhou, as shown in Figure 1.

The vertical transportation should adopt the way of combination of stairs and elevator. Considering for aged people, the stairs should be low height steps with handrail, and with step on the stair platform. The selection of elevator should accord with the relevant provisions, and should be equipped with safety handrail, monitoring and intercom system.

4.1.3 Safety design for details

The detail design focuses on the safety auxiliary measures, such as the safety handrail should

maintain the continuity, as shown in Figure 2; and the bathroom should be mounted with safety handrail, to increase the safety in use for aged people, as shown in Figure 3. Avoiding design with sharp corners as far as possible. There should be guidance system throughout the whole nursing facility, with properties of continuity, clearness and markedness.

4.2 Green environment design: Promote environmental comfort level

The main purpose of integrated nursing facility is to provide comfort living environment for aged people. The design contents refer to sound, brightness, temperature, air condition, humidity, color, cleanliness, natural environment, psychological pleasure and so on, all that related to comfort sensation. In this paper, it is divided into three aspects to discussed, as physical environment, spatial environment and cultural connotation.

4.2.1 Physical environment control

To maintain the comfort level of the room, physical parameters should be controlled at certain range, with corresponding technology. Under our



Figure 1. Appropriate design of accessible ramp way.



Figure 2. Continuous safety handrail in corridor.



Figure 3. Safety handrail on toilet.

research, it is found that parameters should be controlled within the following rang. The noise level below 45 dB, impact sounds below 75 dB. The room can maintain enough sunshine and ventilation in natural way, so facing south is the best choice, and facing north takes the second place. The temperature is better to be controlled within 18–25 in winter, and 23–28 in summer; and the optimal humidity is $50\% \pm 10\%$.

4.2.2 Spatial environment organization

It deals with the relationship between environment and architecture, concretely including wind environment and microclimate surrounding the architecture, and sunshine distance control between buildings, and application of green space and water. Such as the Guangrong nursing home in Shenyang, as shown in Figure 4, the landscape is well designed, and has formed suitable spatial scale, with pleasant microclimate leisure space.

4.2.3 Cultural connotation combination

Environment design should also emphasize cultural connotation combination, which could be done in physical ways, such as sculpture, plant or natural mountain and so on. And it makes environment to be smart and elegant, natural and harmonious.

4.3 Green culture design: Construct leisure space for communication

Aged nursing should be on basis of material life, and on purpose of satisfying the mental requirements, in measures of emotion communication and ideas exchange. This section will discuss the culture design for construction of leisure space.

4.3.1 Leisure space increase

Through the increasing of outdoor spaces for aged people communicating, to increases the

chances of engagement in the elderly, to meet the leisure requirement of aged people. The specific measures including: establishment of activity center, leisure club, outdoor rain gallery (Fig. 5) and so on.

4.3.2 Supporting facility improvement

Improving leisure facilities, including outdoor fitness facilities, recreation facilities, recreation room, chess tables and chairs, etc. In addition, environment art as the auxiliary facilities, including sketch, sculpture, lamps and lanterns, lotus pond, the elements need to be under unified style of the design and arrangement.

4.3.3 Activity enrichment

The leisure space can be used more efficiently, such as activities of daily care, daily learning, public benefit activities (Fig. 6), artistic performance, and so on. As a result, the aged people will not only enrich the their lives, but also obtain physical and mental pleasure, reflect the value of their lives.



Figure 5. The outdoor rain gallery.



Figure 4. Good combination of building group and landscape.



Figure 6. Group activity for aged people.

5 CONCLUSIONS

China has already entered into a rapid development period of population aging, then the demand for integrated nursing facilities and green buildings for aged people has becoming an urgent livelihood issue. This paper starting from the concept of green building, proposes innovative design strategy for integrated nursing facility for the aged, and strives to provide safe, convenient and comfortable nursing facility, in order to satisfy the multi-level requirements of aged people.

ACKNOWLEDGEMENT

The paper is supported by the National Natural Science Foundation of China (Project No.: 51308141).

REFERENCES

- [1] Zhang Ying (2014), The development direction of green ecological buildings, ShanXi Architecture.
- [2] Xiu Long & Ding Jianhua (2014), Thinking and practice on green building design, Architecture Technique.
- [3] Yang Anmu (2014), Discuss the Implementation Strategy and the Development Tendency of the Green Building Design, Urbanism and Architecture.
- [4] Quan Xin (2013), New Trend of Design for the Community Support for Old Age and the Aged Apartment in Recent Years of America, Architectural Journal.
- [5] Wang Su & Xia Jing (2013), Discussion on integrated aged community planning under the background of population aging, Development of Small Cities & Towns.
- [6] Guo Xu, et al. (2013), Design code for building of elderly facilities, Architecture & Building Press.

Simulation on visitor evacuation in large-space exhibition building

Ying Liu, Yang Chen & Qiao Chu Jiang

School of Architecture, Harbin Institute of Technology, Heilongjiang, China

ABSTRACT: The emerging art exhibitions and sales activities in large spaces exhibition buildings enriched citizen's after-hour life and brought very rich cultural life. Meanwhile the visitor crowds gathering in a rather close place during a short period of time also have potential risk. For understanding the evacuation performance of exhibition buildings, this paper used pedestrian simulation software Pathfinder to simulate the crowd movement in Iberian Contemporary Art Center in Beijing 798 Art Area. Based on the simulation experiments and results, we analyzed the building's weak link during evacuation process, brought forward plans for improvements and optimized the evacuation performance of this contemporary art center.

Keywords: pedestrian evacuation simulation; performance optimization; Contemporary Art Center

1 INTRODUCTION

In recent years, with the rapid development of marketing economy, all kinds of exhibitions and sales activities are becoming increasingly popular. Exhibition halls, galleries and art centers are constantly emerging in major cities of China mainland. Most of these exhibition buildings are one or two floor, with relatively close space and larger area (Wu & Chen 2011). Because most of the exhibition activities are held during a short period of time, which would result in inevitably crowd gathering. Once disasters like fire happened, visitors will be very hard to evacuate, and it will also bring severe damage of properties, death and injuries (Fu 2008). This paper investigate the evacuation performance of large-space exhibition building by pedestrian crowd simulation, taking Iberian Center for Contemporary Art in Beijing as an example, using software Pathfinder to simulate the crowd movement and congestion area, finally bring forward the optimization strategies for improving its evacuation performance.

Iberian Center for Contemporary Art is located in the 798 Art Area, Chaoyang District, Beijing. It was renovated by a group of old factory buildings, the total building area is 4000 square meters, The exposition area occupies 2,000 square meters, among which the main exhibition hall covers 1200 square meters according to the information on art China website. The ground floor has multiple functional spaces such as exhibition space, small theater, video archive, multi-media reading room, public education center, magazine editorial, academic lecturer hall, coffee bar and shop for art work, etc (Figs. 1 and 2). Iberian Center for



Figure 1. The exterior of Iberian Contemporary Art Center.

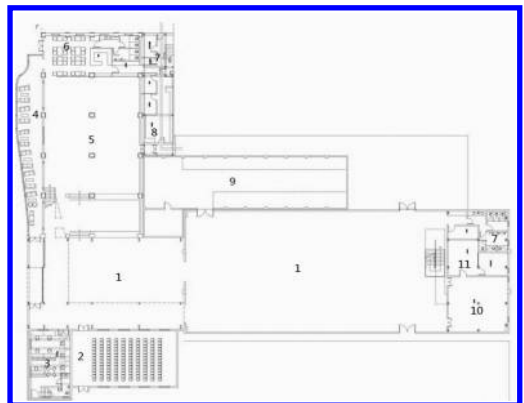


Figure 2. The ground floor plan of Iberian Contemporary Art Center.

Contemporary Art is another large art institution after Ullens Center for Contemporary Art, and it is now one of the largest and most powerful contemporary art institutions in China.

2 PEDESTRIAN EVACUATION SIMULATION

2.1 Simulation software

This study uses pedestrian simulation soft Pathfinder as the simulator, which is based on pedestrian movement and developed by Thunderhead engineering in the United States. It provides simulation design and execution with graphic user interface as well as three dimensional viewable result and analysis. It also could provide every single user a set of his/her own parameters including highest speed, exit choice, etc. The pedestrian movement pattern in Pathfinder includes both SFPE and Steering mode. The result from SFPE mode provides a reference calculation and could conduct much more complicated movement analysis (Xu & Wang 2012).

2.2 Parameter setup

The simulated model in Pathfinder is built by plans published on archigo website. The original building has two floors, but most of areas on the first floor are directly connected with the ground floor, only a small part has floor and used as reception area. Therefore, the building model mainly considers the visitors evacuation problems on the ground floor. There are 7 exits to the outside in total, which are located in exhibition space (2 exits), service area (2 exits), coffee bar (1 exit), small theater (1 exit) and video archive (1 exit) respectively.

There are 112 visitors in the simulation experiments, in which 50 visitors are in the small theater, 5 visitors in video archive, 9 visitors in coffee bar, 7 visitors in public education center, 6 visitors in multi-media reading room, 28 people in exhibition spaces, 2 people in magazine editorial and 2 in restrooms. All user patterns are randomly set, with half male and half female in the crowd. The shoulder widths of the crowds are from 38 cm to 45 cm. The maximum speed of the crowd is 1.5 m/s and minimum speed is 1.2 m/s. The pattern for crowd movement is Steering mode.

2.3 Evacuation process

The simulation scenario during evacuation process is shown in Figure 3, when 42 visitors out of 112 has been successfully evacuated out of the building.

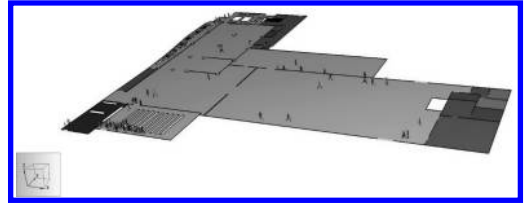


Figure 3. The simulation scenario during evacuation process.

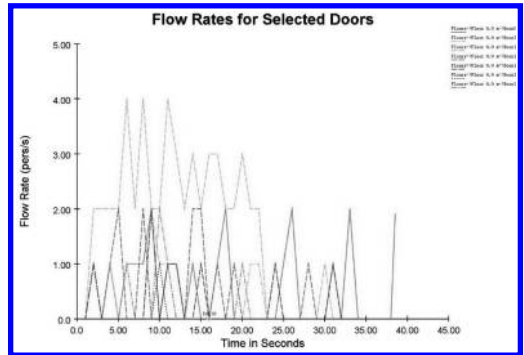


Figure 4. Flow rate for selected doors.

2.4 Simulated results

The simulated results show that 38.5 seconds are needed for total 112 visitors in the ground floor to evacuate out of the building. From the real-time simulation process it is obviously clear that visitors in the exhibition space spend longest time to get out, especially those who are spending time in the shops for art work, they need to walk out of the shop to find the nearest exit. Crowds in the small theater spend 22 seconds to evacuate. The ones with higher movement capability spend much lesser time than those who were slow to move. In the last 5 seconds in the simulation process, only one slow-moving visitor is still inside the building.

During the simulation process, flow rate for different doors vary a lot. Figure 4 shows the flow rate for several selected doors during the simulation process. The door for small theatre has the highest utilization and largest flow rate with its maximum peak value 4 persons per second. While the peak value of flow rate of two doors for exhibition space are 2 persons per second. The average flow rate peak values of other doors are 1 person per second, availabilities are relatively lower.

Exhibition spaces are chosen to modeling the number change of visitor crowd by time, in the first 15 seconds, number of occupants decrease dramatically, while from 15 to 38 seconds the number of occupants decrease in a much slower speed, after

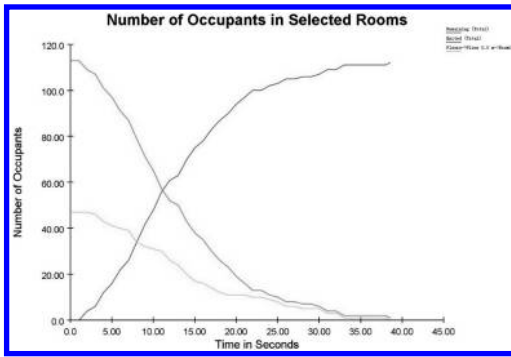


Figure 5. Number of occupants in selected rooms.

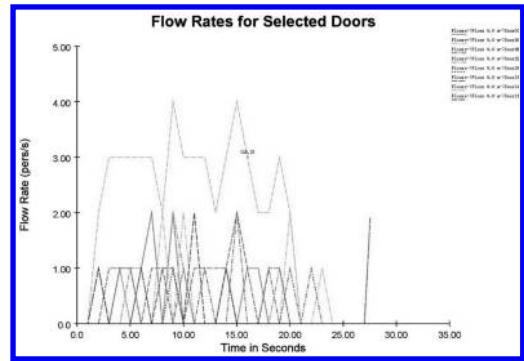


Figure 6. Flow rate for selected doors after optimization.

30 seconds the total number of occupants in the building is equal to the number in the exhibition spaces.

3 EVACUATION SIMULATION OPTIMIZATION

3.1 Optimization strategies

The above simulated results show that average flow rate in two exhibition spaces is not high, because the circulation routes to arrive these two gates are very long. Visitors in the shop have to come out to evacuate. For those who have movement capability problems, the whole process would cost 38 seconds. Another reason is the exhibition space is large, which makes visitors hard to decide which exit is the closest one, even though they located the exit clearly, it still takes a while to arrive at door. The longer decision making process and walking distance are major disadvantages in emergency escape. On the other hand, even though there is only one exit for the small theatre, but building area of the theatre is small and circulation is simple, crowds could arrive at the exit very easily. Therefore, a new exit for the shop is suggested as an optimization for improving visitor crowd evacuation performance.

3.2 Performance comparison

The total evacuation time improved significantly after optimization, from 38.5 seconds to 27.5 seconds. During the evacuation process, the newly increased exit has clear influence on the separation of crowd flow. The exit for the coffee bar close to theatre part barely has been used (Fig. 6). Current door can be subtracted or set up other functions under the condition that no functions would be compromised.

By comparing the average flow rate of exits before and after optimization, we can conclude

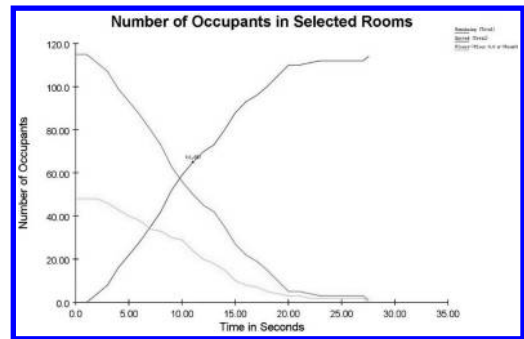


Figure 7. Number of occupants in selected rooms after optimization.

that average flow rate of exit on the north part of the exhibition space is decreased very obviously, the average flow rate of newly increased exit is almost the same as the south exit of exhibition space, which separate crowd flow very effectively.

Compare to the number of occupants in several selected rooms during the evacuation modeling process in exhibition spaces and the whole building in the original plan, before optimization visitor crowd decrease faster in the first 0–25 seconds, from 25–38 seconds only a few people still in the building and it takes them 13.5 seconds to find the exits; while after optimization total evacuation time decreases about 25%, the number of visitor crowd reduces extremely fast in the first 25 seconds, from 25 to 27 seconds only a few of visitors find the exit and it only takes them 7 second to fulfill the task (Fig. 7). The evacuation performance improved obviously after optimization.

4 CONCLUSION

Large exhibition buildings such as art centers are very easily cause crowd gathering in a short period

of time, therefore have relatively higher demands for fireproofing and evacuation performance. By modeling the pedestrian evacuation in Iberian Center for Contemporary Art, congestion and over long walking distance problems are found in exhibition spaces. While in the theatre and lecturer hall, the evacuation issues are relatively easy to solve as long as the circulation is reasonable and directions are clear. The simulation experiments and results show that in designing the plans for exhibition buildings, more attention should be paid on the number and location of exits for large area exhibition space, circulations in the interior should be easily recognizable and walking distance from any part of the interior space to the nearest exit should not be very long, considering visitors with poor movement capabilities should be able to evacuate safely on their own under emergency situations.

ACKNOWLEDGEMENTS

This work was financially supported by the National Natural Science Foundation of China

(NSFC), Grant No. 51308142, supported by “the Fundamental Research Funds for the Central Universities” (Grant No. HIT. NSRIF. 2014072 and 2013074, HIT. HSS. 201124). China Postdoctoral Science Foundation funded project.

REFERENCES

- FU Rong-sheng, The application of performance-based design on large space exhibition's evacuation, *Fire Science and Technology*, Vol. 27 (Supplement), Aug. 2008, p 112–115.
- Information on <http://www.archigo.com>.
- Information on http://art.china.cn/zixun/2010-01/16/content_3346869.htm.
- Wu Jing, Chen Bing, The evacuation problems in exhibition buildings, *Fire Science and Technology*, Vol. 30 (2), Feb. 2011, p 112–115.
- Xu Yan-qiu, Wang Zhen-dong, Study on evacuation simulation of fire ground based on pathfinder and FDS, *Journal of Safety Science and Technology*, Vol. 8 (2), Feb. 2012, p 50–54.

Investigation on bond-slip behavior between Shape Memory Alloy and concrete by finite element method

Di Cui

Research and Development Center of Civil Engineering Technology, Dalian University, Dalian, China

ABSTRACT: The bond between SMA and concrete is the basis for these two materials to work together. In order to study the bond-slip behavior between Shape Memory Alloy (SMA) and concrete, the SMA concrete pull-out specimens were simulated by finite element method. Then the variation of the bond force and the slip are analyzed. Results show that the numerical results agree well with the experimental results, which indicate the effectiveness of the bond-slip model.

Keywords: bond-slip behavior; Shape Memory Alloy; concrete; finite element method

1 INTRODUCTION

In recent years, some reinforced concrete structures in service always occurred durability damage, which makes improving the durability of traditional reinforcement structures become a hot issue. To solve this problem, some researchers use Shape Memory Alloy (SMA) to replace the steel reinforcements in concrete structures due to the unique characteristics of SMA. SMA as a functional material has two novel functions-shape memory effect and superelastic. Besides, shape memory alloy also has excellent physical and mechanical properties. Thus, a lot of research work has been carried out on SMA concrete structures (Sakai et al. 2003, Effendy et al. 2006, Liao et al. 2006, Kuang et al. 2008, Alam et al. 2009, Cui et al. 2010, Shin et al. 2010, Hu et al. 2011, Choi et al. 2013, Malagisi, et al. 2013, Abdulridha et al. 2013, Wang et al. 2011). Most of the work focuses on the self-rehabilitation of the concrete structure under the effect of SMA.

The bond between SMA and concrete is the basis for these two materials to work together. However, the interaction mechanism between SMA and concrete is not clear up to now and few corresponding research work has been carried out (Sun et al. 2013). Thus, it is necessary to conduct the research work on the bond-slip behavior between SMA and concrete. In this paper, the behaviors of SMA concrete pull-out specimens were simulated by using the finite element method.

2 SIMULATION OF BOND-SLIP BEHAVIOR BETWEEN SMA AND CONCRETE

2.1 Model of SMA concrete pullout test specimens

The size of the SMA concrete specimens is 150 mm × 150 mm × 150 mm, the concrete strength is C30, the diameter of SMA strands is 2 mm, the thickness of concrete cover is 75 mm, the embedded depth of SMA strands is 150 mm. Since the model is symmetrical, 1/4 of the specimen is taken for analyzing. Figure 1 shows the finite element model of the specimens.

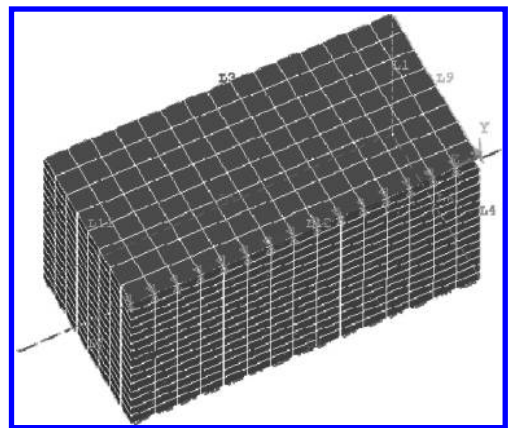


Figure 1. Model of SMA concrete pullout specimen.

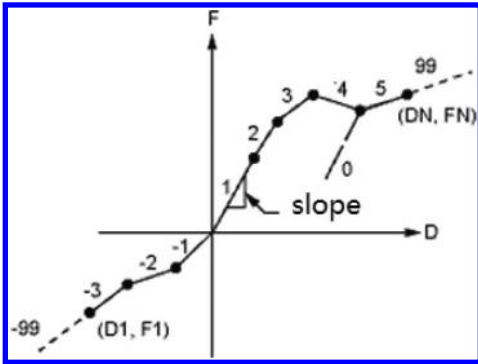


Figure 2. F-D relationship of nonlinear spring COMBIN39.

2.2 Material models

A separate model is employed in simulating the SMA concrete pullout specimens, i.e. SOLID65 is used to simulate the concrete and LINK8 is used to simulate SMA strands.

2.3 Connection units between SMA and concrete

In order to give an overall consideration on the interaction surfaces between SMA strands and concrete, the tangential nonlinear springs COMBIN39 (shown in Fig. 2) are set up by connecting the coincident nodes. In this way, the interaction of bond-slip behavior between SMA strands and concrete can be reflected by tangential interaction. In numerical simulation, F is the bond force between SMA strands and concrete; D , equaling to the above mentioned s , is the slip between SMA strands and concrete. The F-D curve is determined on the base of above established the bond-slip constitutive model between SMA and concrete. $F = \tau \cdot A$, τ is the bond stress between SMA strands and concrete, A is the area of a single unit on the surface between SMA strands and concrete. Besides, the values of the control point A, B, C and D are as follows: $\tau_1 = 1.27$ MPa, $\tau_2 = 2.92$ MPa, $\tau_4 = 1.57$ MPa; $s_1 = 2$ mm, $s_2 = 12.1$ mm, $s_3 = 25$ mm, $s_4 = 39$ mm.

3 RESULTS ANALYSIS

3.1 Bond force

The simulation results are given in Figure 3, which is agreed well with the experimental data (Sun et al. 2013), especially in the elastic stage and the rotational degumming stage.

In numerical simulation, mapping mesh method is used to mesh the concrete and the SMA strands. The unit length is 10 mm, thus 16 coincident nodes

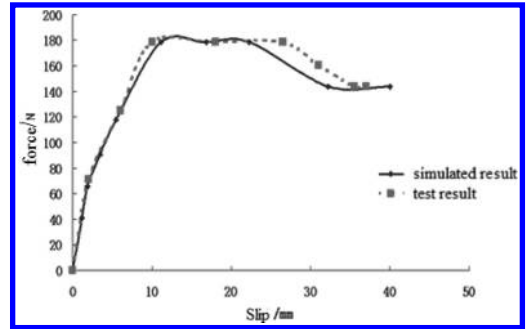


Figure 3. Relationship of bond force-slip.

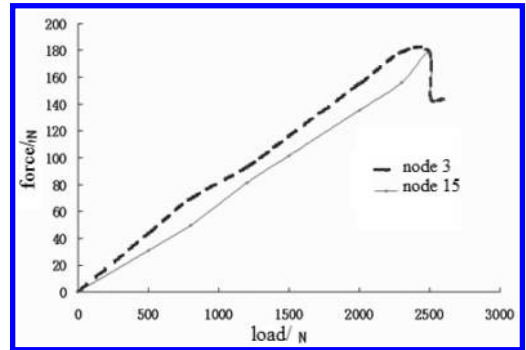


Figure 4. Relationship of load-bond force at different nodes.

of concrete and SMA strands will be generated. Define the loading end as the starting end, i.e. the location of Node 1 is set to 0. Consequently, Node 15, near to the free end, is 140 mm away from the loading end. Figure 4 shows the relationship between the bond force and the load of different nodes. It is found that the bond force increases with the increasing of the load. Compared with Node 3, Node 15 is close to the free end. When the bond force reaches the peak value, SMA strands is just pulled out. Therefore there is no decreasing stage for Node 15.

Figure 5 shows the bond force distribution within the bond region under different loads. From this figure, it can be seen that the bond force reaches maximum rapidly within a certain region near the loading end, and then it decreases with the increasing of the distance to the loading end. Moreover, with the increasing of the load, the bond force increases gradually. Meanwhile, the peak of the bond force does not offset to the free end though the load increase.

The variation situation of the bond force at the loading end is shown in Figure 6. It can be seen from this figure that the maximum of bonding force

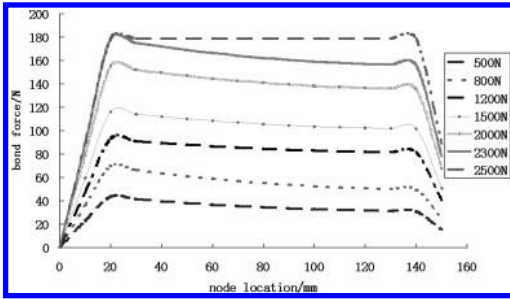


Figure 5. Bond force distribution in bond region.

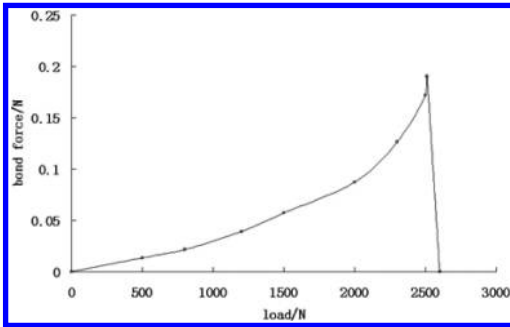


Figure 6. Bond force at the loading end.

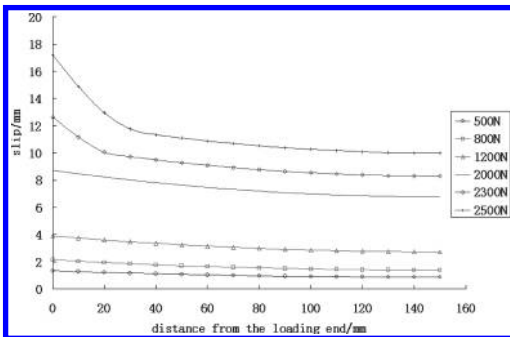


Figure 7. Slip distribution under different loads.

at the loading end is about 0.2 N which indicates that the bonding effect at the loading end is very small during the pullout process, i.e., the bond force almost does not work on the SMA strands.

3.2 Slip

Figure 7 shows the slip of different nodes along the embedded SMA strands under different loads. It can be seen that the slip decreases gradually from the loading end to the free end.

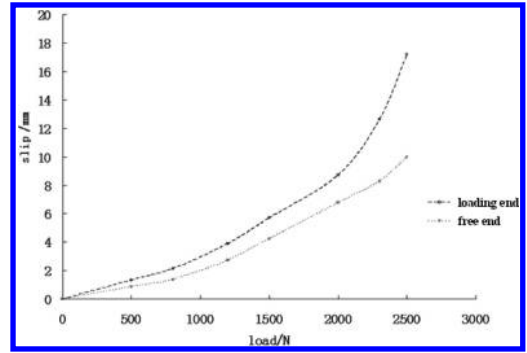


Figure 8. Relationship of slip-load at loading end and free end.

Moreover, the slip increases with the load increasing. During the pullout process, the embedded part of SMA strands will generate deformation. And the closer is to the free end, the smaller is the deformation. Thus, the slip near the loading end is larger than that near the free end.

The slips of the loading end and the free end are shown in Figure 8. From this figure, it is shown that the slip increases nonlinearly with the increasing of the load. In the pullout specimen, the stress of SMA strands close to the loading end is larger than that far from the loading end, thus the stress transferred to concrete is also large at the position near the loading end. Meanwhile, with the increasing of the load, the bond between SMA strands and concrete is destroyed. Therefore, the bond force no longer increases, but the slip continues to increase with the increasing of load. And the slip of the loading end increases more rapidly than that of the free end.

4 CONCLUSIONS

The bond-slip behavior of SMA concrete is investigated in this paper, and the main conclusions are drawn as follows:

1. Through studying the tensile properties of SMA strands, a simplified bilinear model was set up to reflect the relation between stress and strain of SMA strands.
2. Based on the existing study on bond-slip model relationship between SMA and concrete, a formula for calculating the bond stress was improved.
3. The bond-slip properties of pullout specimens are simulated by finite element method. The results show that the numerical results agree well with the experimental results, which illustrates the effectiveness of the bond-slip constitutive model proposed in this paper.

ACKNOWLEDGEMENTS

This work was supported by the National Natural Science Foundation of China (Grant No. 51378085, 51008040 and 11302034), the Scientific Research Fund of Liaoning Provincial Education Department (Grant No. L2013465) and the Open Research Fund of State Key Laboratory of Coastal and Offshore Engineering (Grant No. LP1114).

REFERENCES

- Abdulridha, A., Palermo, D., Foo, S. et al. 2013. Behavior and modeling of superelastic shape memory alloy reinforced concrete beams, *Engineering Structures* 4(49): 893–904.
- Alam, M.S., Nehdi, M. & Youssef M.A. 2009. Seismic performance of concrete frame structures reinforced with superelastic shape memory alloys. *Smart Structures and Systems* 5(5): 565–585.
- Choi, E., Chung, Y.S., Park, K. et al. 2013. Effect of steel wrapping jackets on the bond strength of concrete and the lateral performance of circular RC columns, *Engineering Structures* 48: 43–54.
- Cui, D., Li, H.N. & Song, G. 2010. Study on vibration control of concrete structures reinforced with superelastic shape memory alloy, ASCE, *Earth and Space*, March, Hawaii, USA.
- Cui, D., Song, G. & Li, H.N. 2010. Modeling of the electrical resistance of shape memory alloy wires. *Smart Materials and Structures* 19(5): 055019.
- Effendy, E., Liao, W.I., Song, G.B., et al. 2006. Seismic behavior of low-rise shearwall with SMA bars, *Earth and Space*, March, Houston, U.S.A.
- Hu, J., Choi, W.E. & Leon R.T. 2011. Design, analysis and application of innovative composite PR connections between steel beams and CFT columns. *Smart Materials and Structures*, 20(2): 025019.
- Kuang, Y., Ou, J. 2008. Self-repairing performance of concrete beams strengthened using superelastic SMA wires in combination with adhesives released from hollow fibers. *Smart Materials and Structures* 17(2): 025020.
- Malagisi, S., Marfia, S. & Sacco E. 2013. Modeling of smart concrete beams with Shape Memory Alloy actuators, *Convegno Nazionale IGF XXII* 1–3: 180–186.
- Sakai, Y., Kitagawa, Y., Fukuta, T. et al. 2003. Experimental study on enhancement of self-restoration of concrete beams using SMA wire, *Smart Structures and Materials*. International Society for Optics and Photonics: 178–186.
- Shin, M. & Andrawes B. 2010. Emergency repair of severely damaged reinforced concrete columns using active confinement with shape memory alloys, *Engineering Structures* 32: 656–664.
- Sun, L., Feng, Y.Z., Cui, D. 2013. Bond-slip constitutive relationship of N L.i-Ti alloy wire and concrete, *Journal of Liaoning Technical University (Natural Science Edition)* 32(3): 342–348. (in Chinese).

Study on architecture technology safety management

Shu Wang

Anhui Jianzhu University, Hefei, China

ABSTRACT: In this dissertation, first of all the severe situation of Chinese Architecture technology work safety is pointed out, as well as the main Problems, opportunities and challenges. Meantime the research status quo and developing tendency of management modes of Architecture technology, safety management theories and modes, and safety management theories and modes of Architecture technology are summarized. Moreover the basic connotations and essential requests are set forth, Basic connotations and essential requests are set forth. With theoretical foundations found out including theories of market economy, Corporation theory, Refined management and safety management. And then the game model of refined Architecture technology safety management, Economic benefit model of safety service charge are innovatively constructed, resolving the mechanism of refined Architecture technology safety management. Guaranteeing systems are established to ensure successful implementation. Leading system of safety education and training includes leading system of safety concept and training system of safety skills. Controlling system of safety Precaution and analysis includes real-monitoring system and systematic inquiring system; restricting system of safety obligation and institution includes restricting system of safety obligation and restricting System of safety institution. Optimizing system of safety environment status includes optimizing System of material environment status and optimizing system of humanistic environment status.

Keywords: architecture; safety; management

1 INTRODUCTION

With the high-speed and stable growth of national economy, the modernization processes of major cities constantly speed up in our country, the urban construction changes with each new day. The development of city cannot leave the construction of infrastructure, as part of infrastructure construction, the underground utilities engineering construction has also made the huge progress, this (Architecture technology was related technology that use excavated or does not excavate to underground utilities, pipeline and buried cable carried on to lay down a science of repair or replacement) the rapid growth has provided the turning point for the Architecture technology. In the past few years, the Architecture technology received the government in the promotions in many cities and party attaching great importance. In relevant authority vigorously under advocates, many cities actively use the Architecture technology to carry on the underground utilities construction, but with Architecture technology in the promotion in middle-and-small city, because the construction of management system falls behind the development of construction technique, exposed some issues in safety control.

2 ARCHITECTURE PROBLEMS IN SAFETY MANAGEMENT

2.1 *Long running make pipeline aging*

Cause a large number of accidents. At the same time, the aging condition of gas pipeline is a lack of comprehensive and profound understanding, the lack of reasonable measures and scientific management system, to improve the safety of pipeline operation.

2.2 *Lawless and brutal construction in pipeline make mechanical damage in city construction*

Such as no Environmental test and investigation situation unclear, this has led to a buried pipeline construction machinery directly damage, even lead to major catastrophic accidents.

2.3 *Lack of advance*

Science of leak detection and plugging technology, this cause leakage accident occurred. Great casualties and property losses, and can't adapt to the development of pipeline in the long run, and higher requirements.

2.4 *Question of personnel safety*

Management personnel's safety consciousness weak, Careless at work and the worker did not act in accordance with the relevant provisions. According to the rules, combined with technical quality is not high, this will lead to the relaxation of gas enterprise safety management, responsibility

2.5 *Regulatory problems*

The safety management and safety supervision is not strong enough. Because of the gas pipeline security Imperfect laws and regulations, combined with the competent department in charge of safety management and safety supervision by the administrative department of labor force Is insufficient, it can't from the design, construction, operation, inspection and acceptance of link effectively the safety of the gas pipeline in the pipe Reason and procuratorial supervision, the fuel gas enterprise security management of many problems and hidden danger can discover and solve in time, And accidents that have occurred in the unable to complete the investigation and handling of seriously, causing the cause of the accident, the responsibility Also don't know, the accident responsible without proper disposal.

3 THE PRINCIPLE OF ARCHITECTURE TECHNOLOGY AND SAFETY MANAGEMENT

3.1 *Non-humanized principle of safety education*

Safety management, the first, it is to increase the safety awareness of employees, let employees to consciously abide by rules of safe production of Safeguard their own lives. In enterprise's safety production, the implementation of the non-human education is a must and will Worker's physical and mental health and their family life, make them genuinely concerned their own safety and enterprise The safety in production, in order to realize from "want me safe" to "I want security" concept.

3.2 *Participation principle*

The modern safety management is based on the enterprise level 3 safety education, and more emphasis on the participation of employees. When in the implementation of mandatory safety measures at the same time, the staff of independent management is introduced into the safety management work, make all staff participation and effort. Only in this way, it's possible to achieve the goal of no harm.

3.3 *Principles of up and down*

In terms of the personal safety of employees, enterprise managers have unshirkable responsibility, and since by management And under the push, it is the first premise of enterprise safety management work thoroughly. So, shall be established by the contractor Is in command personally manager security committee, safety management meeting will be held on a regular basis, from the global guidance on the enterprise's safety management work. Only when the managers of a strong sense of responsibility and the enthusiasm of the staff effectively when has it been possible to achieve the goal of no harm.

3.4 *The principle of prevention first*

We should follow the principle of "safety first, prevention first". Because people's unsafe behavior and unsafe state of the content Constitute the potential unsafe factors, so must try to eliminate in advance. Especially in the safety management work Should be pointed out that must pay attention to matters of everyday, and pre-service training in order to enhance security of key position Knowledge, advance the security hidden danger in the bud, effectively prevent dangerous accidents.

3.5 *The principle of continuous improvement*

Safety management is a kind of dynamic management, after the existing safety problems solved, the new risk factors will produce, so safety management must adapt to changing circumstances, solve the new problems appear constantly, will be Enterprise security risk to a minimum.

3.6 *Connotation and characteristics of Refined Management*

The fine management based on the three connotation and characteristics Fine Management, Refined Management), from the perspective of the extensive Management is relative to the past. Fine management to establish scientific process as the core, emphasize the management process of quantification and accuracy, is more efficient, more economical, a modern enterprise management mode. Compared with extensive management, fine management has obvious advantages, mainly manifested in the following aspects.

3.7 *As the core to establish a scientific process*

In the past, China's long-term planned economy system, since the reform and opening up, China's gradual transition from planned economy to

market economy system, economic growth will increase steadily, and people's material demand, Chinese enterprises to grasp the good opportunity, is developing rapidly. Refinement, intensive enterprise management has also been referred to the agenda. So establish scientific internal management processes, and constantly improve enterprise management methods, has become the inevitable choice of the enterprise.

3.8 *Establish a digital management system for internal decision making*

Company advocated "use Numbers to talk". Under this condition, in order to rigorous attitude towards enterprise's production and operation activities as necessary. Enterprises engaged in Architecture technology on yield, quality, production cost, raw material prices, etc. Must have a digital basis for decision making. All kinds of detailed and accurate data, is to improve enterprise management level of assurance. Meet user requirements, etc., such as product is to through the various indicators. Therefore, relative to the extensive management to fine management in enterprise production and operation of large amounts of data analysis, understand the enterprise production and operation situation, make decisions in a timely manner.

3.9 *Enterprise financial management is the main line*

With the widely application of the fine management in coal mine enterprise, the enterprise's financial position is more and more attention, the enterprise production cost and material flow indicators, reflect the business situation become the important basis. Indexes of product quality, sales income are closely linked, so the enterprise can't in order to improve the quality and do not concern other indicators, also can't in order to reduce costs while ignoring safety input, but to give full consideration to index linkage mechanism, in guarantee under the premise of safety in production, improve the financial position of the coal mining enterprises.

4 THE UNDERSTANDING OF FINE MANAGEMENT AND GRASP

The enterprise of Architecture technology has its unique characteristics and management style, to Refined Management must be based on industry characteristics, enterprise actual, from the following several aspects of understanding and the understanding of the essence of fine management.

5 RECISION COLLABORATION

Enterprise from authority to the grassroots, from production to the secondary, tunnelling face to improve transportation system, from material supply to processing and sales, despite its clear department division of labor and functional division and division of work, but the unit, between process and link between the relationship in between is very tight, so the precision cooperation and collaboration is refined management, one of the important content of coal mining enterprises.

6 REFINING INDICATORS

In Architecture technology enterprise, the production task of each unit, security index, operation index, etc. Each index of evaluation is the important management means. Elaboration is for each unit of production and operation index positioning, decomposition, measuring the essence, location is must be based on each unit division of responsibilities, to determine degree of roles and responsibilities of each unit in the indicators, content of the project in order to make each unit index; Decomposition of refined is carried out in accordance with the index of determine the content of the project refinement, especially production conditions variability factors must be considered, according to the different conditions of each index decomposition; Estimates refers to the index calculation basis, the principles must be clear, resources, or data must be reliable and credible, calculation results and the actual error control in a certain area. Engaged in Architecture technology implementing fine management of enterprise, index calculation is very important, also is very difficult, need a lot of basic data, however, indicators of the degree of refinement is gradually refined with fine management implementation degree, precise, if give up because of this, it will never achieve the goal of fine management.

7 SEGMENTATION PROCESS

In the extensive management of coal enterprises, the concept of process is very dilute, is at best understood as a specific work of internal working procedures (such as coal mining enterprises to the work of drilling, charging blasting, the coal, supporting, and pick up slip, etc.). Fine management referred to in the process of division begins with enterprise's overall work, from the enterprise to the unit, to the team, according to the dominant process, auxiliary processes the nature of the process (or service), to involve all of the work, project

content, from big to small, from inside to outside for segmentation step by step, forming numerous small process, sub process, etc., and according to the order of completion time of ordering, at the same time, each working procedure work content, work standards, work efficiency, etc.

8 DETAILS OF THE MANAGEMENT

Detail management to the enterprises engaging in Architecture technology is mainly manifested in: one is prepare the rigour of the enterprise management system, implementation of seriousness, control rigor; Secondly, employee behavior, standardization, the standardization of operation consciousness; Three managers is people-oriented, standardized, scientific, management behavior; Four is enterprise management operation mechanism of systemic, effectiveness and efficiency; Five

is the enterprise management process programmed, standardized and accurate. And so on.

This paper is supported by 2012 Anhui province quality project (2012 jyxm393) support.

REFERENCES

- Hammer. W (2002). Handbook of System and Product Safety [M]. Englewood Cliffs. N.J. Prentie Hall.
- James S. Lumsden. (2012). Operations Safety Risk Management [J]. Managing Integration and Test Safety Risk, G.P. Singh. Safety and economy in civil structures. Minerals Metals Review. vol.
- Valcrie Sutherland Peter Makin and Charless Cox.(2000) The Management of Safety [M]. Printed and bound in Great Britain by Athenacum Press Gateshead, 234-256.
- Wdams Mark (2001). International Conference and Workshop on Reliability and Risk Management. September 15-18, 1998.

Research on properties of GCL in MSW land

Xiao Bo Xiong

State Key Laboratory of Geohazard Prevention and Geoenvironment Protection, Chengdu, China
School of Civil and Architecture Engineering, Nantong University, Nantong, China
Department of Geotechnical Engineering, Tongji University, Shanghai, China

ABSTRACT: With the acceleration of China's sustainable social and economic development and urbanization, the amount of municipal waste increase from 8 to 10 percent annually. At present, the sanitary landfill disposal is the main way of garbage disposal. The impervious barrier is the key to ensure that the landfills should not be the source of secondary pollution to the surrounding. A GCL is a factory-manufactured material which consisting of bentonite clay to form hydraulic barrier, supported by GT and GM held together by stitching, needling and many type of chemical adhesives. The waterproof mechanism of GCLs was studied. In this paper, hydraulic conductivity tests are performed to obtain seepage coefficient of GCLs, taking liquids such as distilled, deioned water and landfill leachate. At the two experimental conditions, the first condition is GCL by experiments under conditions of hydrate firstly and compress secondly, and the second condition is GCL by experiments under conditions of compress firstly and hydrate secondly. The results show that when at a low main stress, the initial velocity of deformation is very high, and the total hydrated thickness is big, with increasing of σ_w , the thickness of GCLs decreasing. The results show that cation valence, cation concentration and hydration ionic radius in hydration and permeation liquids have influences on hydraulic conductivity of GCLs.

Keywords: landfills; impervious barrier; GCLs; properties; experimental analysis

1 INTRODUCTION

With the acceleration of China's sustainable social and economic development and urbanization, the amount of municipal waste increase from 8 to 10 percent annually. Disposal methods of city garbage are: landfill, composting, incineration. Among them, the landfill including traditional landfill, sanitary landfill and secure landfill. At present, the sanitary landfill disposal is the main way of garbage disposal, and treatment of landfill leachate generated in the process is particularly crucial, if not handled properly, likely to cause harm to the environment of secondary pollution. The impervious barrier of cover system and lines system is the key to ensure that the landfills should not be the source of secondary pollution to the surrounding. Applications of geosynthetics, such as geomembrance, GCLs, geonet (GN), geocomposite (GC) and geofoam (GF), etc. They are used to all aspects of landfill as liners and covers. The leakage prevention structures were found designed improperly and leakages happened incidentally in landfills in China.

2 CURRENT STATUS AND PROSPECTS OF GCLS

The new type GCLs come out in 1987 at a Germany company. In 1989, GCLs was widely applied in sanitary landfills in USA. The national code for the new type liner material was taken to draw up which was finished in 1999 completely. There was limited information on GCL. For composite lined and geomembrane systems, the leak detection system flow rates were utilized. The average monthly flow rate for composite liners ranged from 0~32 l/hd for geomembrane and GCL systems. A GCL was installed on the bottom of a salinity-gradient solar pond in Texas in 1994.

Giroud (1989) developed a series important experience equations, Foote G.J., Benson C.H., Edil T.B., et al. (2001) developed a mathematical method to study the seepage problem within which solution penetration through the defect of geomembrane.

Young H.M et al. (2004) reviews the state of the science and practice on the infiltration rate through compacted clay liner. The hydraulic

conductivities for clay liners range from 1×10^{-9} cm s⁻¹ to 1×10^{-4} cm s⁻¹. The shape of defect and properties of the composite materials take much effect on the function of geosynthetics, Rowe R.K. (2005), Young H.M., Johnson B., Carson D, et al. (2004). During the construction stage and operation stage of MSW landfill, there are several factors to form cracks of the GM. In recent, the equity of construction of GM and GCLs is very poor in Chinese, thus, it is very necessary to do systematic research on the defect and its seepage characteristic.

GCL was introduced into China in the late 1990s. In 2001, Tianjin Xingrong Nonwovens Co., Ltd. successfully developed acupuncture and gluing GCL, GCL and gluing method was patented.

Xie Hai Jian, Ke Han, Chen Yun (2006) considered the landfill of organic pollutant concentrations over time, based on the problem of one-dimensional diffusion of organic pollutants in the composite liner were solved analytically. Qian Xuede Qian, Shi Jianyong, Guo Zhiping et al. (2004) have conducted in-depth research on the migration of contaminants through from clay liner system. Chen Yun-min, Xie Hai-jian, Ke Han, et al. (2006) on the establishment of a foundation in layered soil contamination in a one-dimensional diffusion model, to obtain analytical solution by separation of variables.

Shen Junfeng, Li Shengrong, He Shaohui, et al (2006) using self-expansion stress analyzer, the company under the U.S. CETCO saturated absorbent waterproof blanket expansion stress conditions were measured directly, the results showed that: Stable (1) stress analyzer performance measurement The results reproducible. (2) waterproof blanket swelling stress changes over time can be classified in three stages. ① (0 ~ 50h) rapidly increased stress, an increase of $7 \times 10^{-4} \sim 1 \times 10^{-3}$ MPa/h; ② (50 ~ 1730h) slowly increasing the stress, or $7.54 \times 10^{-6} \sim 2.02 \times 10^{-5}$ MPa/h; ③ (after 1730h) is smooth fluctuations in phase expansion stress that paragraph mean 0.0719 MPa, the maximum instantaneous 0.729 MPa.

Chen shengshui et al. (2006) introduced a new type of bentonite mats, by needling the GCL divided into small squares of about 1 cm², the bentonite is relatively fixed in a small box, in order to achieve blocked due bentonite on the lower geotextile slip between the accumulation of synthetic material or affect the stability of the purpose of its penetration. He Jun (2008), liner systems for various requirements of the specification, the amount of water entering the landfill on groundwater and numerical calculation of the cumulative amount

of inorganic contaminants through the liner at the bottom.

Yang Hui, Guo Xujing, Chen Gang (2009) to find the biochemical reaction mechanism on the basis of waste degradation, considering convection, dispersion, diffusion, adsorption and biodegradation of organic matter, such as the role of the establishment of a solute transport leachate convection—dispersion model, one-dimensional mathematical model and analytic solution.

Wang Baohui, Dong Huisi, Xu Zhaoming, et al. (2010) to simulate solute transport of pollutants in porous media theory, based on the research results summarized common migration model pollutant solutes in porous media at home and abroad, and a detailed description of traditional convection—diffusion equation model and its development.

Xu Chao et al. (2011) conducted interior shear test of GCLs, considered the role of tension and winding acupuncture fibers are the main factors controlling acupuncture internal shear strength of GCLs.

He Jun et al. (2011) explored the percolation of water and CaCl₂ solution when the GCL self-healing, the test results showed that when the hydration water and CaCl₂ solution GCL large differences in the amount of expansion, when tap water percolation time defect diameter of 11 mm, when the GCL is not completely healed, when using CaCl₂ do leachate can achieve self-healing defect hole diameter is reduced to 7 mm, that is, leachate ion content is too high would undermine the self-healing of GCL.

Xing Yuhang, Wang Hongyu, Peng Fei. (2012) discussed the research progress of hydraulic characteristics of the landfill liner system, focusing on alternative and impermeable layer from the cushioning material two aspects of the current setup hotspot landfill liner systems are summarized and discussed. Zhan LT, Guan C, Xie HJ, Chen YM (2014) discussed vertical migration of leachate pollutants in clayey soils beneath an uncontrolled landfill at Huainan, China.

Studies have shown that inorganic contaminants can basically diffusion through the geomembrane, and the geomembrane can be regarded as a complete barrier material, geomembrane defects are the main channel for leakage and migration of heavy metal ions penetrate through the composite liner.

The study shows that all the indexes and benefits from this technique are much better than those from the traditional anti-seepage technique (Table 1).

Table 1. Statistics of anti-seepage engineering for man-made lake with GCLs in China.

Province	Numbers	Area/m ²	Province	Numbers	Area/m ²
Neimenggu	1	25000	Yunnan	3	18220
Gansu	1	10000	Hubei	3	7280
Guangxi	1	20000	Guangdong	4	13240
Shanxi	1	6000	Anhui	6	18395
Tianjing	1	7000	Beijing	9	167398
Chongqing	1	15000	Jiangsu	22	77213
Hebei	1	50000	Zhejiang	28	138385
Jiangxi	2	7254	Shanghai	37	95907

3 THE BASIC PROPERTIES OF GCLS

A GCL is a factory-manufactured material which consisting of bentonite clay to form hydraulic barrier, supported by GT and GM held together by stitching, needling and many type of chemical adhesives. The four basic GCLs are: ① two layer of GT(GM) with bentonite and bonding agent; ② two layer of GT(GM) with bentonite and stitch fiber; ③ two layer of GT/GM with bentonite and mending fiber; ④ one layer of GT(GM) with bentonite, and so on.

Anti-seepage effectiveness of GCLs involves: (1) Hydraulic conductivity of GCLs; (2) Absorption ability of bentonite in GCLs during liquid permeation; (3) Internal shear strength of GCL while applied in practical engineering system.

The waterproof mechanism of GCLs is: The main component of bentonite is montmorillonite, montmorillonite can be divided into sodium bentonite and calcium bentonite according to the type and size of interlayer exchangeable cations. Bentonite can be divided into sodium bentonite and calcium bentonite and so on.

The radius of Na⁺ is bigger than that of Ca²⁺, charge is low, the sodium ions of sodium bentonite more easily to form dispersible granules after absorbing water. Sodium ions can absorb 5–6 times its own weight of water, the volume can be expanded to 15 times its own volume, after the sodium ions swelling to form a colloidal impermeable layer, by blocking the further spread of water molecules, so as to achieve the purpose of water.

GCL has a strong healing power, and this is an important reason for GCL which can be successfully applied to a variety of water projects. Generally, when the diameter of GCL impermeable composite materials is 15 cm, Which have defects (diameter <30 mm), it is possible to heal. Therefore, to select the quality sodium bentonite for GCLs firstly.

The swell stresses of a GCL, made by the CETCO Company, USA, were measured directly

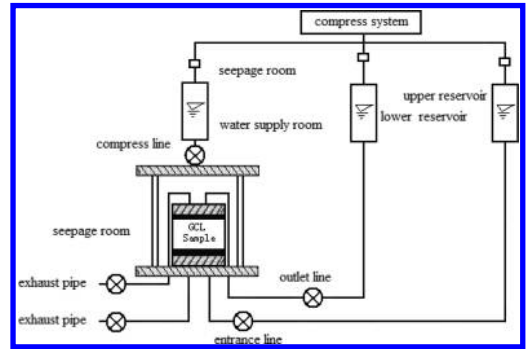


Figure 1. Seepage coefficient test apparatus.

using a custom-made swell stress instrument under water-sorbed saturation conditions. The results show that in the test process, the variation of the swell stress curve with time can be divided into three segments.

The seepage coefficient test apparatus is shown in Figure 1. At the two experimental conditions, if the vertical stress is less than 250 kPa, the seepage coefficient of GCL is approximate same.

If the vertical stress is more than 250 kPa, the seepage coefficient of GCL by experiments under conditions of hydrate firstly and compress secondly (The first condition: here, it is named cw1) is lower than the seepage coefficient of GCL by experiments under conditions of compress firstly and hydrate secondly (The second condition: here, it is named wc2), when in the condition (wc2), the thickness of GCLs is bigger than that of the condition (cw1), thus, the coefficient of seepage of GCL could increase very slow.

The results of hydrated swelling experiments of GCLs samples by main stress is list in Table 2, We know, firstly, because of the properties of water absorption of bentonite, the swelling deformation of GCLs increase very fast, till the thickness of GCLs to attain to the biggest. Under the series

Table 2. The experimental results of hydrated swelling of GCLs.

σ_w /kPa	M_{GCL} /kg/m ²	H_o /mm	H_c /mm	H_v /mm	w/%	E_B
50	5.49	6.86	6.28	7.71	102.2	2.46
150	5.34	6.88	5.87	6.53	92.5	1.99
300	5.46	6.85	5.47	5.86	70.2	1.73

main stress such as 50 kPa, 150 kPa and 300 kPa, the hydrated time list sequences as 8.3d, 6.0d, and 5.0d. When at a low main stress, the initial velocity of deformation is very high, and the total hydrated thickness is big, with increasing of σ_w , the thickness of GCLs decreasing, at the same time, the water content (w) and porosity ratio (n) decreasing (show in Table 2).

Xu Chao (2009) developed geosynthetics osmotic pressure tester (Geo-Syn) using it to conduct apenetration tests.

The results show that the effect was the cation of the ionic valence, in the same concentration, the free expansion of bentonite monovalent cations (Na^+ and K^+) solution is the largest, and the free expansion of the cations (Al^{3+}) solution is the minimum amount, When the divalent cations (Ca^{2+} and Zn^{2+}) in solution, the amount of free expansion is between the Na^+ (K^+) and the Ca^{2+} (Zn^{2+}).

4 DESIGN CALCULATOR-LEAKAGE RATE THROUGH GCLS

4.1 Statement of problem

This calculator computes the rate of leakage through defects in GCLs (Fig. 2). The typical thickness value of hydrated GCLs is from 5 to 10 mm, which depends on the compressive stress when during hydration. Evaluation in field, sponsored by USEPA (1991).

The rate of leakage through a GCL due to GCL is negligible compared to that leakage through defects in the GCLs, and only consider the leakage through from defects. When there is one defect in GCLs, firstly, the liquid first flows through from this defect, secondly, it passes the side several gap between the GCL and the low-permeability soil (Clay soil), and, finally it infiltrates in the low permeability soil.

Flow through from GCL to clay soil is interface flow, and is dependent on the quality of contact between the two components. Several contact conditions are shown as follows:

1. Good contact: relate to one installed GCL, with few wrinkles, a Clay soil layer was adequately compacted and has a smooth surface. Contact quality factor C_{q0} and $C_{q\infty}$ are list in Table 3.

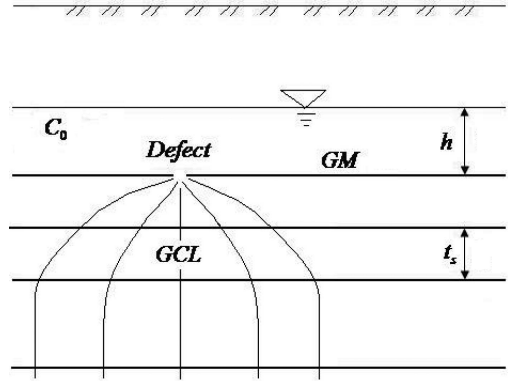


Figure 2. Chart of GM and GCL cross section.

Table 3. Contact quality factor (C_{q0} and $C_{q\infty}$).

C_{q0} (circular, square, rectangular)		$C_{q\infty}$ (infinite length)	
Good contact	Poor contact	Good contact	Poor contact
0.21	1.15	0.52	1.22

2. Poor contact: relate to a GCL that has been installed with a certain number of wrinkles, and/or placed on a low-permeability soil that has not been well compacted and does not appear smooth. Contact quality factor C_{q0} and $C_{q\infty}$ are list in Table 3.

Generally, there are two kinds of defects, such as installation defects and manufacturing defects. Classical GM may have about 0.5 to 1 (1 to 2 per hectare) pinholes per acre from manufacturing defects. The density of installation defects is a function of the quality of installation, testing, materials, surface preparation, equipment, and QA/QC program.

Research by Giroud and Bonaparte (1989) have shown that for installed GM liners, with exactly construction quality assurance, could have 1 to 2 defects per acre (4000 m²) with a ordinary defect diameter of 2 mm ($A_{defect} = 3.1 \times 10^{-6}$ m²). Typically, one defect of liners per acre (4000 m²) is considered with a defect ($A_{defect} = 0.1$ cm², $d = 3.5$ mm),

Table 4. Defect densities of different conditions.

Installation quality	Defect density (number per acre)	Frequency (percent)
Excellent	Up to 1	10
Good	1 to 4	40
Fair	4 to 10	40
Poor	10 to 20*	10

*Higher defect densities have been reported for older landfills with poor installation operations and materials; however, these high densities are not characteristic of modern practice.

for a conservative design a defect ($A_{\text{defect}} = 1 \text{ cm}^2$, $d = 11 \text{ mm}$) can be considered (In Table 4).

4.2 Solution of problem

Several shapes of GM defect:

Defect shape is circular, the diameter is d

$$\frac{Q}{A} = n \cdot 0.976 \cdot C_{qo} \cdot [1 + 0.1 \cdot (h/t_s)^{0.95}] \cdot D^{0.2} \cdot h^{0.9} \cdot k_s^{0.74}$$

Defect shape is square, the width is b

$$\frac{Q}{A} = n \cdot C_{qo} \cdot [1 + 0.1 \cdot (h/t_s)^{0.95}] \cdot b^{0.2} \cdot h^{0.9} \cdot k_s^{0.74}$$

Defect shape is rectangular, the width is b , and the length is B :

$$\frac{Q}{A} = n \cdot C_{qo} \cdot [1 + 0.1 \cdot (h/t_s)^{0.95}] \cdot b^{0.2} \cdot h^{0.9} \cdot k_s^{0.74} + n \cdot C_{qso} \cdot [1 + 0.2 \cdot (h/t_s)^{0.95}] \cdot (B - b)^{0.1} \cdot h^{0.45} \cdot k_s^{0.87}$$

Q —Leakage rate through the considered defect of GM (m^3/s);

Q^* —Leakage rate per unit length of defect of GM ($\text{m}^3/\text{s.m}$);

A —Considered area of GM (m^2);

n —Number of defects per considered area of GM (A);

C_o or C_{qso} —Index of contact quality;

h —Hydraulic head of GM anti-seepage system (m);

t_s —Thickness of the clay soil of the composite liner (m);

D —Diameter of circular defect (m);

b —Width of defect (m);

B —Length of rectangular defect (m).

Limitation of the equations presented:

- If the effect is circular, the value of defect diameter is range from 0.5 mm to 25 mm. In the case

of the defects (the shape is not circular), it is proposed to apply the limitations for the width of defect.

- The liquid head of GM anti-seepage system should be equal to 3 m, or less than 3 m.

4.3 Input values

4.3.1 Case 1: Geometry of circular defect

- Considered geomembrane area (A) is 4000 m^2 , $A = 4000 \text{ m}^2$;
- Hydraulic head on top of the geomembrane (m) is 0.29 m, $h = 0.29 \text{ m}$;
- Thickness of the low-permeability soil (m) is 2.7 m, $t_s = 2.7 \text{ m}$;
- Permeability of the low-permeability soil (m/s) is $1.3 \times 10^{-7} \text{ m/s}$, $k_s = 1.3 \times 10^{-7} \text{ m/s}$.

Properties of circular defect

- Contact good, number of defects (n) is 1~4;
- Contact poor, number of defects (n) is 10~20;
- Diameter of defect (d) is 0.00028 m.

4.3.2 Case 2: Geometry of rectangular defect

- Considered geomembrane area (A) is 4000 m^2 , $A = 4000 \text{ m}^2$;
- Hydraulic head of the geomembrane (m) is 0.29 m, $h = 0.29 \text{ m}$;
- Thickness of the low-permeability soil (m) is 2.7 m, $t_s = 2.7 \text{ m}$;
- Permeability of the low-permeability soil (m/s) is $1.3 \times 10^{-7} \text{ m/s}$, $k_s = 1.3 \times 10^{-7} \text{ m/s}$.

Properties of circular defect

- Contact good, number of defects (n) is 1~4;
- Contact poor, number of defects (n) is 10~20;
- Diameter of defect (d) is 0.00028 m.
- Width of defect (b) is 0.0028 m, $b = 0.0028$;
- Length of defect (B) is 0.018 m, $B = 0.018$.

- Good contact conditions:

a. Circular

From Table 4, $n = 1, 2, 3, 4$

$$Q = n \cdot 0.976 \cdot C_{qo} \cdot [1 + 0.1 \cdot (h/t_s)^{0.95}] \cdot D^{0.2} \cdot h^{0.9} \cdot k_s^{0.74} \cdot A$$

$$n = 1$$

$$Q = 1 * 0.976 * 0.21 * (1 + 0.1 * (0.29/2.7) ^ 0.95) * (0.00028 ^ 0.2) * (0.29 ^ 0.9) * (1.3 * 0.0000001 ^ 0.74) * 4000 = 0.0000455, \text{ m}^3/(\text{m}^2.\text{d})$$

$$n = 2$$

$$Q = 2 * 0.976 * 0.21 * (1 + 0.1 * (0.29/2.7) ^ 0.95) * (0.00028 ^ 0.2) * (0.29 ^ 0.9) * (1.3 * 0.0000001 ^ 0.74) * 4000 = 0.0000911, \text{ m}^3/(\text{m}^2.\text{d})$$

$$n = 3$$

$$Q = 3 * 0.976 * 0.21 * (1 + 0.1 * (0.29/2.7)^{0.95}) * (0.00028 \wedge 0.2) * (0.29 \wedge 0.9) * (1.3 * 0.0000001 \wedge 0.74) * 4000 = 0.00140, \text{ m}^3/(\text{m}^2 \cdot \text{d})$$

$$n = 4$$

$$Q = 4 * 0.976 * 0.21 * (1 + 0.1 * (0.29/2.7)^{0.95}) * (0.00028 \wedge 0.2) * (0.29 \wedge 0.9) * (1.3 * 0.0000001 \wedge 0.74) * 4000 = 0.00180, \text{ m}^3/(\text{m}^2 \cdot \text{d})$$

b. Square

From Table 4, $n = 1, 2, 3, 4$

$$Q = n \cdot C_{qo} \cdot [1 + 0.1 \cdot (h/t_s)^{0.95}] \cdot b^{0.2} \cdot h^{0.9} \cdot k_s^{0.74} \cdot A$$

$$n = 1$$

$$Q = 1 * 0.21 * (1 + 0.1 * (0.29/2.7)^{0.95}) * (0.0028 \wedge 0.2) * (0.29 \wedge 0.9) * (1.3 * 0.0000001 \wedge 0.74) * 4000 = 0.0000739, \text{ m}^3/(\text{m}^2 \cdot \text{d})$$

$$n = 2$$

$$Q = 2 * 0.21 * (1 + 0.1 * (0.29/2.7)^{0.95}) * (0.0028 \wedge 0.2) * (0.29 \wedge 0.9) * (1.3 * 0.0000001 \wedge 0.74) * 4000 = 0.00150, \text{ m}^3/(\text{m}^2 \cdot \text{d})$$

$$n = 3$$

$$Q = 3 * 0.21 * (1 + 0.1 * (0.29/2.7)^{0.95}) * (0.0028 \wedge 0.2) * (0.29 \wedge 0.9) * (1.3 * 0.0000001 \wedge 0.74) * 4000 = 0.0022, \text{ m}^3/(\text{m}^2 \cdot \text{d})$$

$$n = 4$$

$$Q = 4 * 0.21 * (1 + 0.1 * (0.29/2.7)^{0.95}) * (0.0028 \wedge 0.2) * (0.29 \wedge 0.9) * (1.3 * 0.0000001 \wedge 0.74) * 4000 = 0.0030, \text{ m}^3/(\text{m}^2 \cdot \text{d})$$

c. Rectangular

From Table 4, $n = 1, 2, 3, 4$

$$Q = n \cdot C_{qo} \cdot [1 + 0.1 \cdot (h/t_s)^{0.95}] \cdot b^{0.2} \cdot h^{0.9} \cdot k_s^{0.74} \cdot A + n \cdot C_{qoo} \cdot [1 + 0.2 \cdot (h/t_s)^{0.95}] \cdot (B - b)^{0.1} \cdot h^{0.45} \cdot k_s^{0.87} \cdot A$$

$$n = 1$$

$$Q = 1 * 0.21 * (1 + 0.1 * (0.29/2.7)^{0.95}) * (0.0028 \wedge 0.2) * (0.29 \wedge 0.9) * (1.3 * 0.0000001 \wedge 0.74) * 4000 + 1 * 0.52 * (1 + 0.2 * (0.29/2.7)^{0.95}) * (0.018 - 0.0028) \wedge 0.1 * (0.29 \wedge 0.45) * (1.3 * 0.0000001 \wedge 0.74) * 4000 = 0.00760, \text{ m}^3/(\text{m}^2 \cdot \text{d})$$

$$n = 2$$

$$Q = 2 * 0.21 * (1 + 0.1 * (0.29/2.7)^{0.95}) * (0.0028 \wedge 0.2) * (0.29 \wedge 0.9) * (1.3 * 0.0000001 \wedge 0.74) * 4000 + 2 * 0.52 * (1 + 0.2 * (0.29/2.7)^{0.95}) * (0.018 - 0.0028) \wedge 0.1 * (0.29 \wedge 0.45) * (1.3 * 0.0000001 \wedge 0.74) * 4000 = 0.0153, \text{ m}^3/(\text{m}^2 \cdot \text{d})$$

$$n = 3$$

$$Q = 3 * 0.21 * (1 + 0.1 * (0.29/2.7)^{0.95}) * (0.0028 \wedge 0.2) * (0.29 \wedge 0.9) * (1.3 * 0.0000001 \wedge 0.74) * 4000 + 3 * 0.52 * (1 + 0.2 * (0.29/2.7)^{0.95}) * (0.018 - 0.0028) \wedge 0.1 * (0.29 \wedge 0.45) * (1.3 * 0.0000001 \wedge 0.74) * 4000 = 0.0229, \text{ m}^3/(\text{m}^2 \cdot \text{d})$$

$$^{\wedge} 0.95) * (0.018 - 0.0028) \wedge 0.1 * (0.29 \wedge 0.45) * (1.3 * 0.0000001 \wedge 0.74) * 4000 = 0.0229, \text{ m}^3/(\text{m}^2 \cdot \text{d})$$

$$n = 4$$

$$Q = 4 * 0.21 * (1 + 0.1 * (0.29/2.7)^{0.95}) * (0.0028 \wedge 0.2) * (0.29 \wedge 0.9) * (1.3 * 0.0000001 \wedge 0.74) * 4000 + 4 * 0.52 * (1 + 0.2 * (0.29/2.7)^{0.95}) * (0.018 - 0.0028) \wedge 0.1 * (0.29 \wedge 0.45) * (1.3 * 0.0000001 \wedge 0.74) * 4000 = 0.0305, \text{ m}^3/(\text{m}^2 \cdot \text{d})$$

2. Poor contact conditions:

a. Circular

From Table 4, $n = 10, 11, \dots, 20$

$$Q = n \cdot 0.976 \cdot C_{qo} \cdot [1 + 0.1 \cdot (h/t_s)^{0.95}] \cdot D^{0.2} \cdot h^{0.9} \cdot k_s^{0.74} \cdot A$$

$$n = 10$$

$$Q = 10 * 0.976 * 1.15 * (1 + 0.1 * (0.29/2.7)^{0.95}) * (0.00028 \wedge 0.2) * (0.29 \wedge 0.9) * (1.3 * 0.0000001 \wedge 0.74) * 4000 = 0.0249, \text{ m}^3/(\text{m}^2 \cdot \text{d})$$

$$n = 11$$

$$Q = 11 * 0.976 * 1.15 * (1 + 0.1 * (0.29/2.7)^{0.95}) * (0.00028 \wedge 0.2) * (0.29 \wedge 0.9) * (1.3 * 0.0000001 \wedge 0.74) * 4000 = 0.0274, \text{ m}^3/(\text{m}^2 \cdot \text{d})$$

$$n = 12$$

$$Q = 12 * 0.976 * 1.15 * (1 + 0.1 * (0.29/2.7)^{0.95}) * (0.00028 \wedge 0.2) * (0.29 \wedge 0.9) * (1.3 * 0.0000001 \wedge 0.74) * 4000 = 0.0299, \text{ m}^3/(\text{m}^2 \cdot \text{d})$$

$$n = 13$$

$$Q = 13 * 0.976 * 1.15 * (1 + 0.1 * (0.29/2.7)^{0.95}) * (0.00028 \wedge 0.2) * (0.29 \wedge 0.9) * (1.3 * 0.0000001 \wedge 0.74) * 4000 = 0.0324, \text{ m}^3/(\text{m}^2 \cdot \text{d})$$

$$n = 14$$

$$Q = 14 * 0.976 * 1.15 * (1 + 0.1 * (0.29/2.7)^{0.95}) * (0.00028 \wedge 0.2) * (0.29 \wedge 0.9) * (1.3 * 0.0000001 \wedge 0.74) * 4000 = 0.0349, \text{ m}^3/(\text{m}^2 \cdot \text{d})$$

$$n = 15$$

$$Q = 15 * 0.976 * 1.15 * (1 + 0.1 * (0.29/2.7)^{0.95}) * (0.00028 \wedge 0.2) * (0.29 \wedge 0.9) * (1.3 * 0.0000001 \wedge 0.74) * 4000 = 0.0374, \text{ m}^3/(\text{m}^2 \cdot \text{d})$$

$$n = 16$$

$$Q = 16 * 0.976 * 1.15 * (1 + 0.1 * (0.29/2.7)^{0.95}) * (0.00028 \wedge 0.2) * (0.29 \wedge 0.9) * (1.3 * 0.0000001 \wedge 0.74) * 4000 = 0.0399, \text{ m}^3/(\text{m}^2 \cdot \text{d})$$

$$n = 17$$

$$Q = 17 * 0.976 * 1.15 * (1 + 0.1 * (0.29/2.7)^{0.95}) * (0.00028 \wedge 0.2) * (0.29 \wedge 0.9) * (1.3 * 0.0000001 \wedge 0.74) * 4000 = 0.0424, \text{ m}^3/(\text{m}^2 \cdot \text{d})$$

$$n = 18$$

$$Q = 18 * 0.976 * 1.15 * (1 + 0.1 * (0.29/2.7)^{0.95}) * (0.00028 \wedge 0.2) * (0.29 \wedge 0.9) * (1.3 * 0.0000001 \wedge 0.74) * 4000 = 0.0449, \text{ m}^3/(\text{m}^2 \cdot \text{d})$$

$$* 0.0000001 \wedge 0.74) * 4000 = 0.0449, \text{ m}^3/(\text{m}^2 \cdot \text{d})$$

$$n = 19$$

$$Q = 19 * 0.976 * 1.15 * (1 + 0.1 * (0.29/2.7) \wedge 0.95) * (0.0028 \wedge 0.2) * (0.29 \wedge 0.9) * (1.3 * 0.0000001 \wedge 0.74) * 4000 = 0.0474 \text{ m}^3/(\text{m}^2 \cdot \text{d})$$

$$n = 20$$

$$Q = 20 * 0.976 * 1.15 * (1 + 0.1 * (0.29/2.7) \wedge 0.95) * (0.0028 \wedge 0.2) * (0.29 \wedge 0.9) * (1.3 * 0.0000001 \wedge 0.74) * 4000 = 0.0499, \text{ m}^3/(\text{m}^2 \cdot \text{d})$$

b. Square

From Table 4, $n = 10, 11, \dots, 20$

$$Q = n \cdot C_{qo} \cdot [1 + 0.1 \cdot (ht_s)^{0.95}] \cdot b^{0.2} \cdot h^{0.9} \cdot k_s^{0.74} \cdot A$$

$$n = 10$$

$$Q = 10 * 1.15 * (1 + 0.1 * (0.29/2.7) \wedge 0.95) * (0.0028 \wedge 0.2) * (0.29 \wedge 0.9) * (1.3 * 0.0000001 \wedge 0.74) * 4000 = 0.0405, \text{ m}^3/(\text{m}^2 \cdot \text{d})$$

$$n = 11$$

$$Q = 11 * 1.15 * (1 + 0.1 * (0.29/2.7) \wedge 0.95) * (0.0028 \wedge 0.2) * (0.29 \wedge 0.9) * (1.3 * 0.0000001 \wedge 0.74) * 4000 = 0.0446, \text{ m}^3/(\text{m}^2 \cdot \text{d})$$

$$n = 12$$

$$Q = 12 * 1.15 * (1 + 0.1 * (0.29/2.7) \wedge 0.95) * (0.0028 \wedge 0.2) * (0.29 \wedge 0.9) * (1.3 * 0.0000001 \wedge 0.74) * 4000 = 0.0486, \text{ m}^3/(\text{m}^2 \cdot \text{d})$$

$$n = 13$$

$$Q = 13 * 1.15 * (1 + 0.1 * (0.29/2.7) \wedge 0.95) * (0.0028 \wedge 0.2) * (0.29 \wedge 0.9) * (1.3 * 0.0000001 \wedge 0.74) * 4000 = 0.0527, \text{ m}^3/(\text{m}^2 \cdot \text{d})$$

$$n = 14$$

$$Q = 14 * 1.15 * (1 + 0.1 * (0.29/2.7) \wedge 0.95) * (0.0028 \wedge 0.2) * (0.29 \wedge 0.9) * (1.3 * 0.0000001 \wedge 0.74) * 4000 = 0.0567, \text{ m}^3/(\text{m}^2 \cdot \text{d})$$

$$n = 15$$

$$Q = 15 * 1.15 * (1 + 0.1 * (0.29/2.7) \wedge 0.95) * (0.0028 \wedge 0.2) * (0.29 \wedge 0.9) * (1.3 * 0.0000001 \wedge 0.74) * 4000 = 0.0608, \text{ m}^3/(\text{m}^2 \cdot \text{d})$$

$$n = 16$$

$$Q = 16 * 1.15 * (1 + 0.1 * (0.29/2.7) \wedge 0.95) * (0.0028 \wedge 0.2) * (0.29 \wedge 0.9) * (1.3 * 0.0000001 \wedge 0.74) * 4000 = 0.0648, \text{ m}^3/(\text{m}^2 \cdot \text{d})$$

$$n = 17$$

$$Q = 17 * 1.15 * (1 + 0.1 * (0.29/2.7) \wedge 0.95) * (0.0028 \wedge 0.2) * (0.29 \wedge 0.9) * (1.3 * 0.0000001 \wedge 0.74) * 4000 = 0.0689, \text{ m}^3/(\text{m}^2 \cdot \text{d})$$

$$n = 18$$

$$Q = 18 * 1.15 * (1 + 0.1 * (0.29/2.7) \wedge 0.95) * (0.0028 \wedge 0.2) * (0.29 \wedge 0.9) * (1.3 * 0.0000001 \wedge 0.74) * 4000 = 0.0729, \text{ m}^3/(\text{m}^2 \cdot \text{d})$$

$$n = 19$$

$$Q = 19 * 1.15 * (1 + 0.1 * (0.29/2.7) \wedge 0.95) * (0.0028 \wedge 0.2) * (0.29 \wedge 0.9) * (1.3 * 0.0000001 \wedge 0.74) * 4000 = 0.0770, \text{ m}^3/(\text{m}^2 \cdot \text{d})$$

$$n = 20$$

$$Q = 20 * 1.15 * (1 + 0.1 * (0.29/2.7) \wedge 0.95) * (0.0028 \wedge 0.2) * (0.29 \wedge 0.9) * (1.3 * 0.0000001 \wedge 0.74) * 4000 = 0.0810, \text{ m}^3/(\text{m}^2 \cdot \text{d})$$

c. Rectangular

From Table 4, $n = 10, 11, \dots, 20$

$$Q = n \cdot C_{qo} \cdot [1 + 0.1 \cdot (ht_s)^{0.95}] \cdot b^{0.2} \cdot h^{0.9} \cdot k_s^{0.74} \cdot A + n \cdot C_{q\infty} \cdot [1 + 0.2 \cdot (ht_s)^{0.95}] \cdot (B - b)^{0.1} \cdot h^{0.45} \cdot k_s^{0.87} \cdot A$$

$$n = 10$$

$$Q = 10 * 1.15 * (1 + 0.1 * (0.29/2.7) \wedge 0.95) * (0.0028 \wedge 0.2) * (0.29 \wedge 0.9) * (1.3 * 0.0000001 \wedge 0.74) * 4000 + 10 * 1.22 * (1 + 0.2 * (0.29/2.7) \wedge 0.95) * (0.018 - 0.0028) \wedge 0.1 * (0.29 \wedge 0.45) * (1.3 * 0.0000001 \wedge 0.74) * 4000 = 0.2023, \text{ m}^3/(\text{m}^2 \cdot \text{d})$$

$$n = 11$$

$$Q = 11 * 1.15 * (1 + 0.1 * (0.29/2.7) \wedge 0.95) * (0.0028 \wedge 0.2) * (0.29 \wedge 0.9) * (1.3 * 0.0000001 \wedge 0.74) * 4000 + 11 * 1.22 * (1 + 0.2 * (0.29/2.7) \wedge 0.95) * (0.018 - 0.0028) \wedge 0.1 * (0.29 \wedge 0.45) * (1.3 * 0.0000001 \wedge 0.74) * 4000 = 0.2225, \text{ m}^3/(\text{m}^2 \cdot \text{d})$$

$$n = 12$$

$$Q = 12 * 1.15 * (1 + 0.1 * (0.29/2.7) \wedge 0.95) * (0.0028 \wedge 0.2) * (0.29 \wedge 0.9) * (1.3 * 0.0000001 \wedge 0.74) * 4000 + 12 * 1.22 * (1 + 0.2 * (0.29/2.7) \wedge 0.95) * (0.018 - 0.0028) \wedge 0.1 * (0.29 \wedge 0.45) * (1.3 * 0.0000001 \wedge 0.74) * 4000 = 0.2427, \text{ m}^3/(\text{m}^2 \cdot \text{d})$$

$$n = 13$$

$$Q = 13 * 1.15 * (1 + 0.1 * (0.29/2.7) \wedge 0.95) * (0.0028 \wedge 0.2) * (0.29 \wedge 0.9) * (1.3 * 0.0000001 \wedge 0.74) * 4000 + 13 * 1.22 * (1 + 0.2 * (0.29/2.7) \wedge 0.95) * (0.018 - 0.0028) \wedge 0.1 * (0.29 \wedge 0.45) * (1.3 * 0.0000001 \wedge 0.74) * 4000 = 0.2630, \text{ m}^3/(\text{m}^2 \cdot \text{d})$$

$$n = 14$$

$$Q = 14 * 1.15 * (1 + 0.1 * (0.29/2.7) \wedge 0.95) * (0.0028 \wedge 0.2) * (0.29 \wedge 0.9) * (1.3 * 0.0000001 \wedge 0.74) * 4000 + 14 * 1.22 * (1 + 0.2 * (0.29/2.7) \wedge 0.95) * (0.018 - 0.0028) \wedge 0.1 * (0.29 \wedge 0.45) * (1.3 * 0.0000001 \wedge 0.74) * 4000 = 0.2832, \text{ m}^3/(\text{m}^2 \cdot \text{d})$$

$$n = 15$$

$$Q = 15 * 1.15 * (1 + 0.1 * (0.29/2.7) \wedge 0.95) * (0.0028 \wedge 0.2) * (0.29 \wedge 0.9) * (1.3 * 0.0000001 \wedge 0.74) * 4000 + 15 * 1.22 * (1 + 0.2 * (0.29/2.7) \wedge 0.95) * (0.018 - 0.0028) \wedge 0.1 * (0.29 \wedge 0.45) * (1.3 * 0.0000001 \wedge 0.74) * 4000 = 0.3034, \text{ m}^3/(\text{m}^2 \cdot \text{d})$$

$$\wedge 0.74) * 4000 + 15 * 1.22 * (1 + 0.2 * (0.29/2.7) \wedge 0.95) * (0.018 - 0.0028) \wedge 0.1 * (0.29 \wedge 0.45) * (1.3 * 0.0000001 \wedge 0.74) * 4000 = 0.3034, \text{ m}^3/(\text{m}^2.\text{d})$$

$$n = 16$$

$$Q = 16 * 1.15 * (1 + 0.1 * (0.29/2.7) \wedge 0.95) * (0.0028 \wedge 0.2) * (0.29 \wedge 0.9) * (1.3 * 0.0000001 \wedge 0.74) * 4000 + 16 * 1.22 * (1 + 0.2 * (0.29/2.7) \wedge 0.95) * (0.018 - 0.0028) \wedge 0.1 * (0.29 \wedge 0.45) * (1.3 * 0.0000001 \wedge 0.74) * 4000 = 0.3237, \text{ m}^3/(\text{m}^2.\text{d})$$

$$n = 17$$

$$Q = 17 * 1.15 * (1 + 0.1 * (0.29/2.7) \wedge 0.95) * (0.0028 \wedge 0.2) * (0.29 \wedge 0.9) * (1.3 * 0.0000001 \wedge 0.74) * 4000 + 17 * 1.22 * (1 + 0.2 * (0.29/2.7) \wedge 0.95) * (0.018 - 0.0028) \wedge 0.1 * (0.29 \wedge 0.45) * (1.3 * 0.0000001 \wedge 0.74) * 4000 = 0.3439, \text{ m}^3/(\text{m}^2.\text{d})$$

$$n = 18$$

$$Q = 18 * 1.15 * (1 + 0.1 * (0.29/2.7) \wedge 0.95) * (0.0028 \wedge 0.2) * (0.29 \wedge 0.9) * (1.3 * 0.0000001 \wedge 0.74) * 4000 + 18 * 1.22 * (1 + 0.2 * (0.29/2.7) \wedge 0.95) * (0.018 - 0.0028) \wedge 0.1 * (0.29 \wedge 0.45) * (1.3 * 0.0000001 \wedge 0.74) * 4000 = 0.3641, \text{ m}^3/(\text{m}^2.\text{d})$$

$$n = 19$$

$$Q = 19 * 1.15 * (1 + 0.1 * (0.29/2.7) \wedge 0.95) * (0.0028 \wedge 0.2) * (0.29 \wedge 0.9) * (1.3 * 0.0000001 \wedge 0.74) * 4000 + 19 * 1.22 * (1 + 0.2 * (0.29/2.7) \wedge 0.95) * (0.018 - 0.0028) \wedge 0.1 * (0.29 \wedge 0.45) * (1.3 * 0.0000001 \wedge 0.74) * 4000 = 0.3843, \text{ m}^3/(\text{m}^2.\text{d})$$

$$n = 20$$

$$Q = 20 * 1.15 * (1 + 0.1 * (0.29/2.7) \wedge 0.95) * (0.0028 \wedge 0.2) * (0.29 \wedge 0.9) * (1.3 * 0.0000001 \wedge 0.74) * 4000 + 20 * 1.22 * (1 + 0.2 * (0.29/2.7) \wedge 0.95) * (0.018 - 0.0028) \wedge 0.1 * (0.29 \wedge 0.45) * (1.3 * 0.0000001 \wedge 0.74) * 4000 = 0.4046, \text{ m}^3/(\text{m}^2.\text{d})$$

To state three shapes of GM defect, such as: circular, square, rectangular. And put out three calculate equations, to take two cases (circular defect, rectangular defect (also including square defect, which is a special condition)). The calculated results are shown as:

when in good contact conditions, the defect shape is circular, $n = 1\sim 4$, $Q \in [0.0000455, 0.00180](\text{m}^3/(\text{m}^2.\text{d}))$; the defect shape is square, $n = 1\sim 4$, $Q \in [0.0000739, 0.0030](\text{m}^3/(\text{m}^2.\text{d}))$; the defect shape is rectangular, $n = 1\sim 4$, $Q \in [0.00760, 0.0305](\text{m}^3/(\text{m}^2.\text{d}))$;

when in poor contact conditions, the defect shape is circular, $n = 10\sim 20$, $Q \in [0.0249, 0.0499](\text{m}^3/(\text{m}^2.\text{d}))$; the defect shape is square, $n = 10\sim 20$,

$Q \in [0.0405, 0.0810](\text{m}^3/(\text{m}^2.\text{d}))$; the defect shape is rectangular, $n = 10\sim 20$, $Q \in [0.2023, 0.4046](\text{m}^3/(\text{m}^2.\text{d}))$.

5 CONCLUSIONS

In this paper, Hydraulic conductivity tests were performed to obtain seepage coefficient of GCLs, and the conclusions are as follows:

1. An apparatus is applied to measure the hydraulic conductivity coefficient of GT, and seepage properties of GCLs in normal stress conditions which is measured with different equipment and penetration of liquid water. To take free swelling or hydration swelling test to do research on the influence factors of GCLs, which including load sequences, normal stress, and hydration fluid and bentonite of GCLs test. The results showed that the factors affect the swelling properties of the GCLs.
2. In order to get hydraulic conductivity of GCLs, several test must be taken, several liquids, such as leachate (with a single species of cation hydration, and osmotic liquid solution), deionized water, and distilled water. The results showed that the concentration of cation and valence of cation penetration of liquids in hydration and ionic radius of hydration effect on hydraulic conductivity of GCLs. The results show that the conditions such as horizontal strain, the normal stress and hydration loading sequence, have some effects to hydraulic conductivity.
3. Absorption ability of GCLs during liquid permeation is studied, and its influencing factors are also discussed, including hydration liquid and permeation time. The results show that GCLs has large absorption ability on the permeation of liquids. But when increase of permeation volume, the ability is decreasing, and the types of hydration liquids take much effect on the variation of GCLs absorption.
4. In this study, Analysis was made to combine the conclusion to obtain with practical engineering projects, and proposals of building method of GCLs are advanced.

ACKNOWLEDGMENT

This work was supported Project (KLE-TJGE-0802) (Tongji University); Project (GZ2007-09) (Chengdu University of Science and technology). *Xiaobo Xiong, corresponding author, E-mail: thongtao2006@163.com.

REFERENCES

- Chen Sheng-shui, Zheng Cheng-feng, Yang Mingchang. 2006. Experimental study of A new type of GCL anti-seepage material [J]. *Hydro-Science and Engineering*, (3): 34–38. (in Chinese).
- Chen Yun-min, Xie Hai-jian, Ke Han, et al. 2006. Analytical solution of contaminant diffusion through multi-layered soils [J]. *Chinese Journal of Geotechnical Engineering*, 28(4): 521–524. (in Chinese).
- Foose G.J., Benson C.H., Edil T.B., et al. 2001. Predicting leakage through composite landfill liners[J]. *Journal of Geotechnical and Geoenvironmental Engineering*, 127: 510–520.
- He Jun, Fan Ying. 2008. Effect of groundwater table on performance of liners in waste landfill [J]. *Advances in Science and Technology of Water Resources*, 28(1): 32–34. (in Chinese).
- He Jun, Xiao Heng-lin, Kong Xiang-yi. 2011. Hydraulic conductivity tests on damaged geosynthetic clay liners [J]. *Advances in Science and Technology of Water Resources*, 31(6): 16–18+26. (in Chinese).
- J.P. Giroud and R. Bonaparte. 1989. Leakage Through Liners Constructed with Geomembranes, Part I, Geomembrane Liners, Geotextiles and Geomembranes, 8, 1: 27–67.
- Li Zhibin. 2007. Research on Anti-Seepage Availability of Geosynthetic Clay Liners and Related Mechanism Analysis, Shanghai: Tongji University. (in Chinese).
- Qian Xuede, Shi Jianyong, Guo Zhiping et al. 2004. contaminant migration of clay liner system [J]. *Journal of Hohai University (Natural Science)*, 32 (4):415–420. (in Chinese).
- Rowe R.K. 2005. Long-term performance of contaminant barrier systems (45th Rankin Lecture) [J]. *Géotechnique*. 55(9): 631–677.
- Shen Junfeng, Sheng-Rong Li, He Shaohui, et al. 2006. Research on Hydration expansion stress characteristics of GCL bentonite waterproof blanket [J]. *Journal of Geological*: 1632. (in Chinese).
- USEPA, 1991. Design and Construction of RCRA/CERCLA Final Covers, EPA/625/4-91/025, Office of Research and Development, U.S. Environmental Protection Agency, Washington, D.C., May.
- Wang Baohui, Dong Huisi, Xu Zhaoming, et al. 2010. Research development in migration model of pollutant solute in porous media [J]. *Chemical Industry And Engineering Progress*, 29(7): 1338–1342+1368. (in Chinese).
- Xie HJ, Ke H, Chen YM. 2006. Analysis of one-dimensional organic contaminants diffusion through composite liner under time-dependent concentration conditions [J]. *Acta Scientie Circum stantiae*, 26(6):930–935. (in Chinese).
- Xing Yuhang, Wang Hongyu, Peng Fei. 2012. Research review on hydraulic characteristic of impermeable liner in solid waste landfill [J]. *Ningxia Engineering Technology*, 11(2): 186–189. (in Chinese).
- Xu Chao, Qi Chang-wei, Li Zhi-bin. 2011. Adsorption ability of geosynthetic clay liner to cations and organics in landfill leachate [J]. *Hydrogeology & Engineering Geology*. 38(3):77–81. (in Chinese).
- Yang Hui, Guo Xujing, Chen Gang. 2009. Mechanism and mathematical model of the solute transport in landfill leachate [J] *Industrial Safety and Environmental Protection*, 35 (1): 33–35. (in Chinese).
- Yang Yu-chun. 2013. Material Characteristics and Anti-Water Mechanism of Anti-Water Geosynthetics Clay Liner [J]. *Power System and Clean Energy*. 29(10): 109–113. (in Chinese).
- Young H.M., Johnson B, Carson D, et al. 2004. Characterization of infiltration rates from landfills: supporting groundwater modeling efforts [J]. *Environmental Monitoring and Assessment*. 96: 283–311.
- Zhan LT, Guan C, Xie HJ, Chen YM. 2014. Vertical migration of leachate pollutants in clayey soils beneath an uncontrolled landfill at Huainan, China: a field and theoretical investigation. *Science of the Total Environment*, 470–471: 290–298. (in Chinese).

The analysis of the contrasted love in *Women in Love*

Hong Yun Du, Xiao Nan Peng & Lei Zhang

English Office 2, Beijing University of Chinese Medicine Dongfang College, Oriental University City, Langfang, Hebei Province, China

ABSTRACT: D.H Lawrence is a great writer in the 20th century. *Women in Love* is one of his greatest novels. In the novel, D.H Lawrence shows the ideal love between man and woman through two contrasted love, the love between Birkin and Ursula and the love between Gerald and Gudrun. He thinks the star-equilibrium relationship between man and woman is the ideal love. Besides, the blood-brotherhood relationship between man and man is the complementary love of human beings. This paper will discuss the two contrasted love affairs from three parts: contrasted attitudes towards love and marriage; contrasted love process towards love and marriage; contrasted fates towards love and marriage.

Keywords: star-equilibrium; blood-brotherhood; contrast

1 INTRODUCTION

As a great writer in the 20th century, D.H Lawrence has great influence in the literary history. E.M. Foster considered: “he was the greatest imaginative novelist of his generation.” [1] and Aldous Huxley thought: “Vitality has the attractiveness of beauty, and in Lawrence there was a continuously springing fountain of vitality.” [2] D.H Lawrence expresses his attitude towards love in *Women in Love*. He believes the love between man and woman is the basic love of human beings. He expresses his ideal relationship between man and woman is the star-equilibrium relationship through Birkin in *Women in Love*, “what I want is a strange conjunction with you-” he said quietly; ‘not meeting and mingling-you are quite right-but an equilibrium, a pure balance of two single beings-as the stars balance each other.’ [3] That means man and woman should be harmonious in mind and in body; On the other side, they should keep a certain distance and have their own freedom, balancing each other like two stars. Besides, there is the love between man and man, which is the blood-brotherhood, it is complementary to the love between man and women. D.H Lawrence shows the ideal love through the two contrasted love affairs in *Women in Love*, the love between Birkin and Ursula and the love between Gerald and Gudrun. This paper will illustrate D.H Lawrence’s ideas towards love from three parts: the two pairs of lovers have contrasted attitudes, contrasted love processes and contrasted fates towards love and marriage.

2 SECTION ONE: CONTRASTED ATTITUDES TOWARDS LOVE AND MARRIAGE

The different endings of the two contrasted love affairs base on the main characters’ contrasted attitudes towards love and marriage.

2.1 *Ursula’s and Gudrun’s contrasted attitudes towards love and marriage*

In the first chapter, when the two sisters talk about love and marriage

“Don’t you think one need the experience of having been married?” She asked.

“Do you think it need be an experience?” replied Ursula.

“Bound to be, in some way or other” said Gudrun, coolly. [4] (D.H Lawrence, 1994: 1).

These words imply the two sister’s different attitudes towards love and marriage. In Gudrun’s opinion, love and marriage is just an experience and marriage is an opportunity to compete with man, this shows Gudrun’s will of dominance. In contrast, in Ursula’s opinion, love and marriage is not the simple experience, she will not marry if she could not find the real love. The two sister’s contrasted attitudes towards love and marriage imply that Ursula has the real love attitude while Gudrun has the attitude towards love that is just an experience and dominance. Their different attitudes towards love and marriage will affect their love and marriage in the feature. Ursula gets her happy and harmonious love in the end while Gudrun’s love goes to death.

2.2 *Birkin's and Gerald's contrasted attitudes towards love and marriage*

In chapter five in the train, Birkin and Gerald show their contrasted attitudes towards love and marriage.

"I find," he said, "that one needs some one really pure single activity-I should call love a single pure activity. But I don't really love any body-not know." ...

"Yes. I want the finality of love." ...

"I don't believe a woman, and nothing but a woman, will ever make my life," said Gerald. (D.H Lawrence, 1994: 63).

These words show the two man's different attitudes towards love and marriage. In Birkin's opinion, love is a single pure activity and the only woman is his love. In contrast, in Gerald's mind, woman is only an experience to him and a woman is not enough. Birkin wants to find his true love while Gerald treats marriage as an experience and the will of dominance. The two men's contrasted attitudes towards love and marriage also affect their love in the future. In the end, Birkin finds his true love while Gerald's love goes to death.

Besides, Birkin and Gerald have different views towards the love between man and man that is the blood-brotherhood. In Birkin's mind, the love between man and woman is the basic love of human beings. The love between man and man is complementary to the basic human love. Only the love between man and woman is not sufficient to human beings. In the whole novel, Birkin offers several times the blood-brotherhood love to Gerald, but Gerald refuses at last.

Through Birkin's mouth, D.H Lawrence expresses his own ideas about love and marriage. The ideal love between man and woman is through mutual understanding, not through the dominance of the others. And love is a process of transfiguration from the old self into the new state of being, the harmonious mutual unison between man and woman to get the balance of the equilibrium, but not through fighting to dominate the others. Besides, there is the love between man and man, which is complementary to the basic love between man and woman.

3 SECTION TWO: CONTRASTED LOVE PROCESS TOWARDS LOVE AND MARRIAGE

The two love affairs have different love processes: Birkin and Ursula's love process is through mutual understanding while Gerald and Gudrun's love Process is through the will of dominating the others.

3.1 *Love between Birkin and Ursula*

Birkin and Ursula's love is based on mutual understanding and gradually fighting to get a better understanding. But at the beginning of the novel, Birkin is loved by Hermione, who is the representative of the modern industrial society and has the strong traditional will of dominance. He rejects her at last and turns to Ursula who has the spiritual freedom. With the time going on, Birkin and Ursula fall in love with each other, but at first, they disagree with each other in terms of love. Ursula wants her lover to love her absolutely, with complete self-abandon and she would in turn be his humble slave, while Birkin values individuality more than love, he does not want to merge but want them to be balanced like two stars in conjunction. According to Birkin, love is a single pure activity and he does not like the traditional domestic love, he longs for the spiritual love. Ursula could not at first accept Birkin's unconventional ideas and behaviors. Because of the different views about love and marriages, they quarrel a lot. Their love experiences ups and downs. In the episode of the ring, Ursula throws away the ring which is the symbol of the traditional love. In the episode of the chair, they give away the chair which is the symbol of the conventional domestic life, and hunt for the spiritual love and the new life. The two lovers have the same attitude towards the love and marriage at last.

Ursula finally finds truth in Birkin's ideas, in the climax chapter Continental, Ursula said to Gudrun,

"Love is too human and little. I believe in something inhuman, of which love is only a little part. I believe what we must fulfill comes out of the unknown to us, and it is something infinitely more than love. It isn't some merely human." (D.H Lawrence, 1994: 493).

This is Birkin's idea about love. It reflects that Ursula totally accepts Birkin's idea about love. At the same time, she is changing Birkin's idea about love and marriage day by day, and Birkin sees the true part in Ursula's idea about love and marriage. From Ursula, Birkin finds a salvation for the dying civilization. So Birkin and Ursula's love process is a kind of mutual fighting, they get the balanced relationship between man and woman, that is a kind of equilibrium, their love process is exploratory and creative, which is the ideal relationship between man and women according to D.H Laurence.

3.2 *Love between Gerald and Gudrun*

Gerald and Gudrun's love has the tendency of dominating the others. Gudrun was attracted by Gerald's appearance when she first saw him far away and wanted to know him. There was

something strange and northern about him that attracted her. With the time going on, she envied Gerald when she saw him swimming in the isolation of water. Gudrun was attracted so much that she envied him strongly for his freedom as a man. This implies that Gudrun has the will of dominance in her mind and does things according to the mental consciousness. Gudrun also has the strong will to dominate the others, just like Gerald. In the scene of Gerald and the mare, the attitude that Gerald treats the mare is cruel, cold and indifferent. It not only shows Gerald's strong dominate will, but at the same time, it also illustrates Gudrun's mind is always obsessed with dominance and violence. At that very moment, Gudrun feels, "the world reeled and passed into nothingness for Gudrun, she could not know any more." (D.H Lawrence, 1994: 124) This shows that she is cold, hard and indifferent to others just as Gerald. They both want to dominate the others. Therefore, in their love process, they are fighting for the dominate will over the other. So their love is unharmonious, which will go to destruction.

The two contrasted love affairs have different endings: Birkin and Ursula's love got a kind of equilibrium while Gerald and Gudrun's love went to destruction. Through the two contrasted love processes, D.H Lawrence shows his attitudes towards the ideal love which is through mutual understanding and at last form the balance of the star-equilibrium.

4 SECTION THREE: CONTRASTED FATES TOWARDS LOVE AND MARRIAGE

In *Women in Love*, D.H Lawrence uses many scenes to illustrate his view about the contrasted fates of the two love affairs. Birkin and Ursula are always connected with the rebirth scenes which predict their love will end in rebirth while Gerald and Gudrun are always connected with death scenes which predict their love will end in death.

4.1 *Rebirth scenes about Birkin and Ursula*

In many scenes, Birkin has the deep thought of death and destruction. To him, corruption and reform, destruction and creation, death and rebirth could not be separated absolutely. Death is the beginning of the rebirth. In the chapter water-party, Birkin and Ursula talk about the death of Diana. He thinks the destruction of the old world brings a new circle of creation. He thinks death and rebirth, destruction and creation goes together. New creation will be born in the process of destruction, rebirth comes after death. Human beings could revive only through the process of casting off the

old self and going to the new self. In the chapter a chair, in the market, Ursula and Birkin pick up an old beautiful chair for their home, but at last, they give it away. The chair is the symbol of the old traditional marriage life. Birkin and Ursula have the same recognition that they do not want a conventional domestic life. They want to cast off the old dead marriage life, which only leads to destruction and death. They do not belong to the old conventional world, but wants to go to a new world which will lead to happiness and rebirth.

4.2 *Death scenes about Gerald and Gudrun*

When Birkin and Ursula are connected with rebirth, Gerald and Gudrun are connected with death. Gerald's association with death is shown in the episode water-party. This accident shows that Gerald and Gudrun are closely connected with death. As a local magnate and master, Gerald organized the annual public festival for the people in the district. When Gerald and Gudrun were boating on the lake, there was the news that Gerald's sister and her fiancé were drowned in the water. Because Gerald had hurt his hand, he could not save his sister from the water; at last, this accident leads to the death of his sister Dania and her fiancé. This foresees that the fate of Gerald and Gudrun's love is connected with death. After Gerald's father's death, he is very empty in the heart. With the gloomy state of mind, he goes to Gudrun's room. When he enters Gudrun's room, he has the mud on his shoes from his newly death father's tomb. It also shows that Gerald and Gudrun are connected with death. The final fate of their love would go to destruction.

Birkin and Ursula's love is always connected with the scenes that have the meaning of rebirth while Gerald and Gudrun's love is always connected with scenes have the meaning of destruction. This is the fate of the two love affairs: Birkin and Ursula's love will go to rebirth while Gerald and Gudrun's love will go to destruction.

5 CONCLUSION

In *Women in Love*, the two pairs of love affairs have different fates: Birkin and Ursula's love goes to rebirth and construction while Gerald and Gudrun's love goes to death and destruction. They have the contrasted fates in the end because of their different attitudes towards love and marriage and their different love processes. Through the two contrasted love, D.H Lawrence expresses his ideas towards love: the love between man and woman is the basic love of the human beings. The star-equilibrium relationship is the ideal relationship between man and woman.

Besides, the love between man and man that is the blood-brotherhood is complementary to the basic love. In this way, people can get the perfect state in their lives in the respect of love.

REFERENCES

- [1] Frank N. Magil, *Critical Survey of Long Fiction*, New York: Salem Press, (1983), p.1580.
- [2] Aldous Huxley, "Introduction" to *The Letters of D.H. Lawrence*, New York: Salem Press, (1932), pp.1263–67.
- [3] D.H. Lawrence, *Women in Love* [M]. Dover Publications Inc, (2003), p.126.
- [4] D.H. Lawrence, *Women in Love*. Beijing: Foreign language press, (1994), p.1.

Design of a pallet pool in Inner Mongolia

Jian Wei Ren

Transportation Institute, Inner Mongolia University, Hohhot, China

ABSTRACT: Pallets move the world. It is necessary to establish a pallet pool in Inner Mongolia, but how to establish it has not been studied. Firstly, the feature, examples, and operation process of Third-Party Owned Pool, Cooperative Pool, Third-Party Managed Pool, and Private Pool are analyzed in detail. Then, a third-party owned pool is proposed to be established in Inner Mongolia based on our analysis. Finally, we suggest that the third-party owned pallet pool in Inner Mongolia should be with seven branch companies at Hohhot, Baotou, Wuhai, Chifeng, Tongliao, Erods and Hulun Buir and its headquarter should be located in Hohhot.

Keywords: pallet pool; Inner Mongolia

1 INTRODUCTION OF PALLETS AND PALLET POOLS

Pallets move the world. In the United States, an estimated 4 billion pallets are in daily service. Nationwide, on an annual basis, an estimated 441 million new pallets are manufactured and 357 million pallets are repaired or rebuilt from discarded pallets (Buehlmann, Philip, Bush, 2010). In China, about 910 million pallets are in daily service and 50 million new pallets are manufactured (Jin, 2014). In Inner Mongolia, there is not a pallets manufacture, while pallets have been used in warehouse and transportation.

As pallets are viewed as assets, their management becomes essential to fully reap their benefits and to receive a measurable return on investment (Harris and Worrell, 2008). Although there are three kinds of pallets management methods (transfer of ownership, pallet exchange and pallet pooling), pallet pooling has increasingly become more popular.

Naval Inventory Control Point (2006) pointed out there are three kinds of Pallet Pool (Third-party Owned Pool, Third-party Managed Pool and Private Pool), but we believe there is another kind of pallet pool which is named Pallet Alliance Pool. So we think there are four kinds of pallet pools as follows,

- Third-party Owned Pool
- Pallet Alliance Pool
- Third-party Managed Pool
- Private Pool.

It is necessary to establish a pallet pool in Inner Mongolia, but how to establish it has not been studied. We are fuscous on this problem.

2 WHICH KIND OF PALLET POOLS SHOULD BE ESTABLISHED IN INNER MONGOLIA

2.1 *Third-party owned pool*

Pallets of a third-party owned pool are owned by a third-party that manages all aspects of the pallet pool (Naval Inventory Control Point, 2006; Harris and Worrell, 2008). A third-party owned pool always is operated by a pallet rental company.

There are about 22 pallet rental companies in the whole world. And they are mainly locates in Eastern America, Southeastern Canada, Western and Central Europe, Australia, Southern Africa and Eastern Asia.

In China, there are about 5 third-party owned pools. None third-party owned pool in Inner Mongolia.

The basic operation processes of a third-party owned pool are as:

1. Headquarters manage the whole pallet pool. Especially, it coordinates its service depots.
2. The nearest service depot issue pallets to a customer when the customer demands pallets.
3. The customer loads their goods on pallets and does business. When off-loads their goods, the customer or its partner calls the service depots to take empty pallets back.
4. The nearest service depot inspects, picks-up, sorts, and repairs or recycles these pallets.

**A service depot can transfer pallets to another depot that lacks of pallets.*

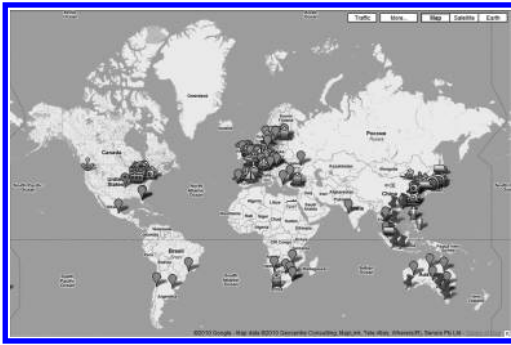


Figure 1. Distribution of pallet rental companies.

2.2 Cooperative pool

A Cooperative Pool consists of many pallet rental companies, pallet manufacture companies, pallet recovery companies and so on. A Cooperative Pool committee should maintain a pool-wide quality assurance and inspection standard for the pool's pallet and provide an efficient interchange system for their members. And a cooperative pool committee also may offer a variety of services to their members including education, training, and management tools.

There are about five cooperative pools, such as CPC, EPAL and APP.

None cooperative pool is exist in Inner Mongolia.

The basic operation processes of a cooperative pool are as:

1. Pallet alliance committee maintain a pool-wide quality assurance and inspection standard for the pool's pallets, provides an efficient interchange system for their members, offer a variety of services to their members.
2. The nearest member of a cooperative pool issues pallets to a customer when the customer demands pallets.
3. The customer loads their goods on pallets and does business. When off-loads the goods, the customer or its partner calls nearest member of the cooperative pool to take empty pallets back.
4. The nearest member of the cooperative pool inspects, picks-up, sorts, and repairs or recycles these pallets.

**The members of a Cooperative Pool can exchange their pallets.*

2.3 Third-party managed pool

The pallets of a third-party managed pool are owned by the user, but all aspects of the pallet pool are managed by a third party. The third party is

responsible for the retrieval and recovery of the pallets, tracking of the inventory, and maintaining the pallet's condition. This type of pool is highly customized to meet a specific company's objectives (Naval Inventory Control Point, 2006; Harris and Worrell, 2008).

For instance, IFCO as a third-party management server focus on pallet procurement, repair, shipping, tracking, sorting, and retrieval solutions, to provide total, 360-degree Pallet-Management-Services for their clients. The company operates principally in Europe, the United States, and Canada. Nine of the top 25 World Retailers are IFCO's Pallet Management Partners and twenty of the top 100 largest publicly held U.S. manufacturing companies are IFCO's Pallet Management customers.

As far as we known, there is not a pallet pool is managed by a third party in Inner Mongolia.

The basic operation processes of a third-party managed pool are as:

1. The third-party management server provides many kinds of services, including shipping, tracking, test, sorting, repair, etc, to manage the whole pallet pool for its customer.
2. The third-party management server moves pallets from the nearest pallets supplier to a pallet demander when the demander demands pallets.
3. The demander loads their goods on pallets and does business. When off-loads the goods, the demander or its partner calls the third party management server to take empty pallets back.
4. The third-party management server inspects, picks-up, sorts, and repairs or recycles these pallets. And then, it moves these pallets to another pallets demander. The ex-pallets-demander becomes the pallets supplier.

**A pallets supplier is a depot who has adequate pallets and a pallets demander is a depot who needs pallets.*

2.4 Private pool

As to a private pool, a manufacturer owns the pallets and manages all aspects of the pallet pool. It creates the specifications and arranges for pallet delivery and return (Naval Inventory Control Point, 2006; Harris and Worrell, 2008).

There are many private pools. For example, US Postal service manages its pallets, including wood pallets, INCA presswood pallets and plastic pallets, by itself. The USPS operated a "pallet round-up" program which helped recover 57,000 pallets, for a savings of \$1.1 million. And the USPS has been developing a "closed-loop" pallet inventory system.

There are private pools in Inner Mongolia, but there is not a professional private pool. For example, Mengniu Group owns lots of pallets and its logistics management center manages all of these pallets, however, as far as we known, they didn't operate any pallet program to make their pallets are used more efficiently.

The basic operation processes of a private pool are as:

1. A pallet management department manages a whole pallet pool.
2. The pallet management department moves pallets from the nearest pallets supplier to a pallet demander when the demander demands pallets.
3. The demander loads their goods on pallets and does business. When off-loads the goods, the demander or its partner calls the pallet management department to take empty pallets back.
4. Then pallet management department inspects, picks-up, sorts, and repairs or recycles these pallets. And then, the pallet management department moves these pallets to another pallets demander. The ex-pallets-demander becomes the pallets supplier.

**A pallets supplier is a depot who has adequate pallets and a pallets demander is a depot who needs pallets.*

**In some companies, there may be not a pallet management department and its pallet pool may be managed by another department like transport department.*

2.5 Choose

According to the analysis above, third-party owned pools are the most popular pallet pools and managers could reap more social benefits from a third-party owned pool than the other kinds of pallet pools. So, we propose to establish a third-party owned pool in Inner Mongolia.

3 A THIRD-PARTY OWNED POOL IN INNER MONGOLIA

It is hard to establish a third-party owned pool in Inner Mongolia because its whole territory is about 1,180,000 square kilometers while it is sparsely populated. But almost the most important enterprises are located in Hohhot, Baotou, Wuhai, Chifeng, Tongliao, Erosds and Hulun Buir, so if a third-party could success operate a pallet pool in these seven cities, they could make good business in Inner Mongolia.

Therefore, a third-party pallet pool in Inner Mongolia should establish at least seven branch

Table 1. Registered enterprises of prefecture—level cities (leagues) of inner Mongolia.

City/league	Registered enterprises
Hohhot	7362
Baotou	6865
Wuhai	1515
Chifeng	10988
Tongliao	7771
Erdos	4162
Hulun Buir	6906
Bayan Nur	246
Ulanqab	199
Hinggan league	377
Xilingol league	667
Alxa league	702

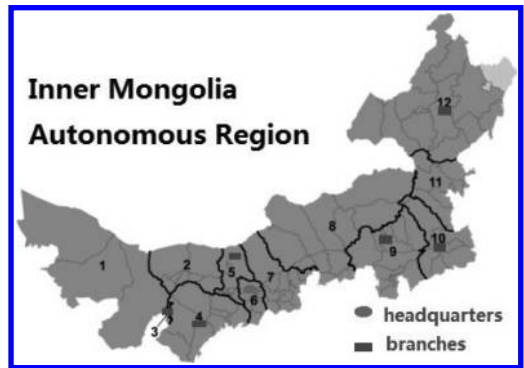


Figure 2. Service centers of a third-party pallet pool in Inner Mongolia. 1 Alxa, 2 Bayannur, 3 Wuhai, 4 Ordos, 5 Baotou, 6 Hohhot, 7 Ulanqab, 8 Xilingol, 9 Chifeng, 10 Tongliao, 11 Hinggan, 12 Hulunbuir.

companies, and these seven branch companies should locate at Hohhot, Baotou, Wuhai, Chifeng, Tongliao, Erosds and Hulun Buir. As Hohhot is the capital of the Inner Mongolian Autonomous Region, serving as the region's administrative, economic, and cultural centre, it is necessary to locate its headquarter in Hohhot.

4 CONCLUSION

First of all, we analyzed the feature, examples, and operation process of the four kinds of pallet pools which are Third-Party Owned Pool, Cooperative Pool, Third-Party Managed Pool, and Private Pool. Then, a third-party owned pool is proposed to established in Inner Mongolia. Finally, we suggest that the third-party pallet pool in Inner Mongolia should be with seven branch companies

at Hohhot, Baotou, Wuhai, Chifeng, Tongliao, Eros and Hulun Buir and its headquarter should be located in Hohhot.

REFERENCES

- Buehlmann, Urs, Philip A.A.R. Bush.2010. Pallet reuse and recycling saves high value material from landfills. *Engagement Matters*. 2(1):8, 10.
- Harris, J.S. and J.S. Worrell. 2008. Pallet management system: a study of the implementation of UID/RFID technology for tracking shipping materials within the department of defense distribution network. *NAVAL Postgraduate School*. Monterey, CA, 12–13.
- Naval Inventory Control Point. 2006. Investigation of non-wood pallets for use in Navy supply: Phase 1 report (Code M0772 Publication). Mechanicsburg, PA: Author.
- Jin, W. Chinese pallet industry development in 2013 and 2014, *Logistics & Material Handling*, 2014(3):61–62.

Design of a harbor station in Nansha Islands

Jian Wei Ren, Jia Wei Cao & Xue Wei

Transportation Institute, Inner Mongolia University, Hohhot, China

ABSTRACT: South China Sea is the immanent territory of China. It is urgent to build South China Sea islands. The paper is focus on the design of a harbor station in the Nansha Islands in the South China Sea. Firstly, Meiji reef is chosen to build harbor station based on the analysis of four typical islands or reefs of Nansha Islands by AVEE method. Then the layout design of the harbor station on Meiji reef is proposed.

Keywords: harbor station; layout design; location; Nansha Islands

1 INTRODUCTION

South China Sea is the immanent territory of China. Based on the concision of rights protection and exploitation of the South China Sea, it is urgent to build South China Sea islands.

The Nansha Islands are a disputed group of more than 750 reefs, islets, atolls, cays and islands in the South China Sea. The islands contain approximately 4 km² of actual land area spread over a vast area of more than 425,000 km². The Nansha Islands are one of three archipelagos in the South China Sea which comprise more than 30,000 islands and reefs. In view of the serious

situation of the Nansha Islands, it is necessary to strengthen the construction of Nansha Islands to ensure the safety of the South China Sea.

The paper is focus on the design of a harbor station in the Nansha Islands, because only if there is a harbor station, Nansha Islands is probably safe in a long time.

2 LOCATION OF THE HARBOR STATION

The location of a harbor station is vital to make it successful. In order to choose a good location for the harbor station in Nansha Islands, SAVEE

Table 1. The value evaluation factors.

Value evaluation factors	Value and weight coefficient
Location (the distance to a main channel and Yongxing islands)	$V = K \left[e^{-\frac{-(x+1)}{ A }} \right]^5, K = 1$
The area of dry rock	$V = K \left\{ 1 - \left[e^{-\frac{-(x+1)}{ A }} \right]^5 \right\}, K = 0.8$
The area of reef	$V = K \left\{ 1 - \left[e^{-\frac{-(x+1)}{ A }} \right]^5 \right\}, K = 0.7$
The elevation of a island or reef	>2 m, the value is 0; 0~2 m, -0.2; -2~0 m, -0.5; -2~-5 m, -0.6; <-5 m, -0.8
Growth index β'	0.916 < $\beta' < 0.993$ semi-closed atoll, the value is 0.75; $\beta' > 0.993$ closed atoll, the value is 0.3; 0.702 < $\beta' < 0.916$ semi-open atoll, the value is 0; $\beta' < 0.702$ open atoll, the value is -0.3
The condition of anchorage	Excellent, 0.6; good, 0.2; normal, -0.2; bad, -0.6
Water depth of anchorage	10~25 m, 0.5; <2 m or >40 m, -0.5; others, 0
Tidal rage	<1.0 m, 0.5; 1.0~2.0 m, 0.3; 2.0~3.0 m, 0; >3.0 m, -0.5
Safe condition	Excellent, 0.5; good, 0.25; normal, -0.25; bad, -0.5
Fishery resources	Excellent, 0.5; good, 0.2; normal, 0; bad, -0.5
The number of unmanned islands or reefs within 12 nautical mile	$V = KX/X_{max}, K = 0.7$

Table 2. The raw value of evaluation factors.

Evaluation factors	Zhubi reef (Subi reef)	Nanxun reef (Gaven reef)	Yongshu reef (Fiery cross reef)	Meiji reef (Mischief reef)
The distance to a main channel (km)	51.2	119.0	84.8	212
The distance to the Yongxing island (km)	684	765	806	846
The area of reef (km ²)	15.76	2.76	108	45.31
The area of dry rock (km ²)	0.01	0.01	0.01	0.07
Growth index	Closed atoll	0.611	0.350	0.930
The elevation of a island or reef (m)	1	2	0.5	1
The condition of anchorage	Excellent	Normal	Good	Excellent
Water depth of anchorage	20	20	28	25
Tidal rage	2	1.5	1.5	2
Safe condition	Excellent	Bad	Normal	Excellent
Fishery resources	Good	Good	Normal	Good
The number of unmanned islands or reefs within 12 nautical mile	0	0	0	3

Table 3. Result.

Evaluation factor	Zhubi reef	Nanxun reef	Yongshu reef	Meiji reef
The distance to a main channel	0.292	0.059	0.132	0.007
The distance to the Yongxing island	0.017	0.011	0.008	0.007
The area of reef	0.432	0.128	0.795	0.706
The area of dry rock	0.7	0.7	0.7	0.7
Growth index	0.3	-0.3	-0.3	0.75
The elevation of a island or reef	-0.2	0	-0.2	0
The condition of anchorage	0.6	-0.2	0.2	0.6
Water depth of anchorage	0.5	0.5	0	0.5
Tidal rage	0	0.3	0.3	0
Safe condition	0.4	-0.4	-0.25	0.4
Fishery resources	0.2	0.2	0	0.2
The number of unmanned islands or reefs within 12 nautical mile	0	0	0	0.7
Grade	0.9899	0.797	0.9294	0.9994

method is used (Loh, Hsieh, 1994, 1995, 1996, 1998).

Four typical islands or reefs of Nansha Islands are chosen as the research objects based on qualitative analysis. The four islands or reefs are Subi reef, Gaven reef, Yongshu reef, and Meiji reef. The value evaluation factors are chosen based on the research of Chen (Chen, 2011) as shown in Table 1. The raw value of these factors of the four islands or reefs is also partly from the research of Chen (Chen, 2011) as shown in Table 2. The result is shown in Table 3.

As shown in Table 3, the grade of Meiji reef is the highest, so the Meiji reef is the best position to build harbor station in the Nansha Islands.

Meiji reef is a large reef, located at 9° 55' N, 115° 32'E, in the Nansha Islands in the South China Sea and is controlled by China. Meiji reef is an atoll

reef which consists of an annular reef rim surrounding a central lagoon. The area surrounding is rich in yet unexplored oil and gas fields. Meiji reef is a natural sheltered harbor. So it is really a good place to build a harbor station.

3 LAYOUT DESIGN OF THE HARBOR STATION

Based on the analysis of Meiji reef, the layout design of the harbor station in Nansha Islands is as shown in Figure 1.

Remarks:

1. The airport runway is outside. The tarmac is inside. The taxiway is middle. On the ends of runway is the clearway. And the hangar is bottom.

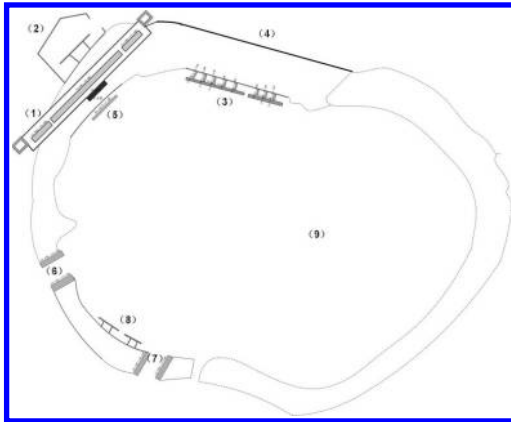


Figure 1. Layout design of the harbor station.

2. Outer pier. It is mainly used for the maintenance of facilities.
3. The main pier. It is used as ship berth.
4. Breakwater
5. Auxiliary pier
6. The main entrance
7. Auxiliary entrance
8. Simple berth
9. Anchorage.

The dotted portion is the originally contour of Meiji reef and the solid part is contour of artificial buildings.

4 CONCLUSION

The paper is focus on the design of a harbor station in Nansha Islands. Firstly, Meiji reef is chosen to build harbor station based on the analysis of four typical islands or reefs of Nansha Islands by AVEE method. Then the layout design of the harbor station in Meiji reef is proposed.

REFERENCES

- Chen S.Y. Interests and strategy value evaluation of Nansha Islands based on SAVEE. *Chinese Fishers Economics*, 2011, 29(3):63–67.
- Loh D.K., Hsieh Y.T.C., Choo Y.K., et al. Integration of a rule-based expert system with GIS through a relational database management system for forest resource management. *Computers and Electronics in Agriculture*, 1994(11):215–228.
- Loh D.K., Hsieh Y.T.C. Incorporating rule-based reasoning in the spatial modeling of succession in a savanna landscape. *AI Applications: Natural Resources, Agriculture & Environmental Science*, 1995, 9(1):29.
- Loh D.K. Spatially constrained reasoning for the determination of wildlife foraging areas. *Computers and Electronics in Agriculture*, 1996(15):323–334.
- Loh D.K. Automated construction of rule bases for forest resource planning. *Computers and Electronics in Agriculture*, 1998(21):117–133.

Re-discussion on the measurement of tourist environment capacity in large-scale scenic areas

Kun Qiang Wang

Sanya Vocational Polytechnic College, Sanya, Hainan, China

Qiang Bai

Sanya College, Sanya, Hainan, China

ABSTRACT: This paper summarized the academic fruits of tourist environment capacity and their distinguish features both at home and abroad. The traditional measurement formula widely applied in our country was evaluated and the defects existed in this formula were pointed out. We proposed an amended formula for tourist environment capacity measurement and its application range. Finally, several problems were fully discussed in the practical application on tourist environment capacity measurement.

Keywords: tourist environment capacity; measurement formula; large-scale scenic area

1 INTRODUCTION

Tourist environment capacity is also named as tourist capacity or tourism carrying capacity [1]. The concept of carrying capacity first appears in the ecological study, which is “the upper limit of individuals’ existence number at a certain environment condition (which is mainly referring to the combination of ecological factors such as the living space, nutrient substance, sunlight, etc.)” [2]. Afterwards this word is applied in the environmental science and then the concept “environment carrying capacity” is formed. It is defined as the human activity threshold that the environment of a certain district can bear at a certain time period, a certain state or condition [3].

The systematic foreign research concerning the tourist environment capacity is started in the 60th of 20th century. In the year of 1964, the American researcher J. Alan and Wagar published his academic monograph named as “The Carrying Capacity of Wild Lands for Recreation”. Wagar believed the recreational environment capacity was defined as a recreational use quantity that the tourist quality could be long-term maintained for a recreation area. In 1971, Lim and George H. Stankey made further discussion on the problem of recreational environment capacity. They proposed that, recreational environment capacity was the utilize strength with maintaining a certain use standard for tourist, but without destroy of environment and influence of tourist experience. Afterwards, numbers of researchers concerning the tourist environment capacity problem gradually increased. The peak

for researching recreational environment capacity problems appeared from the 60th to 80th of 20 century. There were many researchers in most of the American colleges studying the environment capacity problem at the end of 70th of 20th century [4].

In the comprehensive view of foreign researches on the tourist environment capacity, the main characteristic is that they do not pay much attention to the concept of “quantity”, but concern much more about “how to change the environment in an acceptable way”. In general, the researchers in our country have gained a lot of valuable research achievements on the tourist environment capacity study, and they were widely applied in the specific practice during the plan and management of tourist. In the Appendix A of “General specification for tourism planning” established by national tourism administration in 2003, the tourist capacity is divided into space capacity, apparatus capacity, ecological capacity, and social psychological capacity based on the existing research results. It is proposed that for a scenic area, measurement of day space capacity and day apparatus capacity is the most basic rule. In the appendix, the formulas for measuring day space capacity and day apparatus capacity have been listed: [5]

Formula for measuring day space capacity:

$$C = \sum C_i = \sum X_i \times Z_i / Y_i \quad (1)$$

C is the total day space capacity of scenic areas. Its value is equal to the sum of that of the each scenic area.

C_i is the day space capacity of the scenic area numbered as i .

X_i is the area that can be visited of the scenic area numbered as i .

Y_i is the basic space standard of the scenic area numbered as i , that is the average reasonable visit space of each tourist takes.

Z_i is the day turnover of the scenic area numbered as i .

Formula for measuring day apparatus capacity:

$$C = \sum C_i = \sum X_i \times Y_i \quad (2)$$

The calculation method of day apparatus capacity is almost similar with that of day space capacity.

The former formulas provide a specific and operability method for qualified the tourist capacity of a scenic area. However, as a static state model formula, it still has some limitation. We name formula (1) as the traditional measurement formula of tourist capacity for convenient discussion [7].

After comparison of the tourist environment capacity research between our country and the abroad, it is discovered that two different routes are chosen by the homeland and foreign researchers of tourist environment capacity. In the abroad, the starting point of research tourist environment capacity is the concept of recreational experience management, which respect is controlling the environment influence. Only if the indirect method (visitor management) is not work, they start to control the number of tourist. With regard of the tourist environment capacity research of our country, especially in the plan and management practice of tourist, they mostly put their views on controlling the number of tourists. The number of tourists is also the final indicator when the tourist environment capacity quantitative model is applied. It should be mentioned that the two different technological routes on one hand indicate the gap exists for the tourist environment capacity research and management level in our homeland and the abroad. On the other hand, our national characteristic is also revealed. Under the limit of national conditions such as large population, fast development of tourist industry, low overall quality of the population, and the low management level of scenic areas, at this stage it has a much stronger practical significance to take the number of tourist as the final indicator of research tourist environment capacity.

2 THE MAJOR DEFECTS EXISTING IN THE TRADITIONAL MEASUREMENT FORMULAS OF TOURIST CAPACITY

In the tourist plan and management practice in our country, the traditional measurement formulas of

tourist capacity are more and more widely used in the estimating tourist capacity and managing scenic spot of scenic areas. Peicong Luo (1997) made quantitative analysis on the tourist environment capacity of Wuyi Mountain national scenic spot [8]. Qingyou Liu et al. (2003) estimated the tourist environment capacity of Lu Mountain scenic spot [9]. Jing Guo et al. (2003) quantitatively researched the tourist environment capacity of the scenic spot in the eastern suburbs of Nanjing City [10]. All of the as-mentioned tourist environment capacity of large scenic spots are quantitatively measured according to the principle of traditional measurement formulas.

It should be mentioned that the traditional measurement formula as a technological method enhances the operability of tourist environment capacity research and scenic spot capacity control. However, we discover that, there is a large limitation existing during the tourist plan and practice of this traditional measurement formula. More and more drawbacks expose in the large number of tourist plans and researches in our country. If the traditional measurement formula cannot be utilized correctly, the scenic spot management might be misguided and further influence the sustainable development of tourist area. Based on our working experience about tourist plan and practice, the main defects of traditional measurement formulas of tourist capacity are as follows:

1. The tourism demand of different kinds of tourists are not be considered. That means the differentiation of tourist capacity limitation factors between different types of tourism areas is not reflected. The different kinds of tourists have different kinds of demands. But the traditional measurement formula is a kind of static model, which is basically only suitable for the sightseeing type of tourist area. As mentioned in the Appendix A of "General specification for tourism planning", the day apparatus capacity is relative with the former day space capacity. The two kinds of capacities are combined together. It is also proposed that the environment capacity of a tourism area depends on the minimum value among the ecological environment capacity, social psychological capacity, and the sum of space capacity and apparatus capacity. However, this static combination just ignores the characterized differentiation between different tourism areas. In fact, for a sightseeing type of tourism area, the apparatus capacity has large elasticity but small rigidity, and has no dominated effect on the tourist capacity of tourism area. While for a pure vocation tourism area, the apparatus capacity has large rigidity and small elasticity, which is a decisive factor for

tourist capacity of tourism area. Therefore, the single, static measurement formula has large limitation in the tourist plan and management practice.

2. The structure of traditional measurement formula has a big defect, so the application range is narrow in the tourist plan and management practice. The technological route of traditional measurement formula is dividing a big tourism area into several scenic spots, and to calculate the day space capacity (day turnover included) of each scenic spot, then summarize the day space capacity of all scenic spots to get the total day space capacity of this big tourism area. This technological route has fully considered the non-uniformity of basic space standard between every functional partition of tourism area and every scenic spot, showing a scientific and reasonable feature. However, the disperse measurement of day turnover of each scenic spot will make the scenic spots become independent, and the interrelation of visitors flow between every scenic spot will be cut off, causing the double counting of visitors and the exaggerating the tourism capacity of the entire tourism area objectively.

3 AMENDMENT OF TOURIST CAPACITY MEASUREMENT FORMULA

1. Definition of the suitable scope

Because the tourist environment carrying is a very complicated concept system, and its influence factors are very wide, it is difficult to make a generally suitable tourist capacity static model. But in some tourism areas with the similar feature, establishing a tourist capacity static model is benefit for making sure of the tourist capacity of tourism area scientifically, and making a better balance between source protection and tourism explore and utilization. In this work, the traditional measurement formula of tourist capacity is amended and its suitable scope is assumed as follows:

- a. The function of scenic tourism area is mainly sightseeing, relaxation, and entertainment, and the vocational function could be included as well. These areas are dominantly referred to the comprehensive large scenic tourism area.
- b. The functional regions or the scenic spots inside of scenic tourism area are different with each other with a non-uniform basic space standard.
- c. The scenic spots exhibit good combination with nearby position and strong accessibility.
- d. The scenic tourism area is a relatively closed system to the outside, while the scenic spots

(subsystems) inside of the tourism area is open to each other. This means the management of visitors is mainly located at the grade of scenic tourism area, and the management of visitors in the scenic spots inside of tourism area is an assistance.

2. Amendment of measurement formula

The amendment of tourist capacity measurement formula is mainly revising the structural defects of the traditional measurement formula, solving the exaggerating problem of tourist capacity of scenic area. The definite solution is retain the reasonable content that different basic space standard should be adopted by different scenic spots. At the same time, considering the flowing of visitors between the scenic spots, the day turnover of each scenic spot is no longer calculated separately. As a substitution, the day turnover is calculated by using the average visit time of the whole scenic tourism area. The specified amended formula is as follows:

$$C = \sum \frac{X_i}{Y_i} \cdot \frac{T}{t} = \sum D_i \cdot Z$$

C is the total day space capacity of tourism area;

X_i is the area that can be visited in the scenic spot numbered as i ;

Y_i is the area that is suitable to be visited for tourist in the scenic spot numbered as i , that is the average basic space standard taken by one tourist;

T is the effect opening time in one day of scenic tourism area;

t is the average visiting time for one visitor in the scenic tourism area;

D_i is the transient capacity of the scenic spot numbered as i ;

Z is the day turnover of the whole scenic tourism area.

Based on the former research results and according to the tourist capacity amendment formula, this work chooses four scenic areas including Wuyi Mountain [10], Lu Mountain [11], Qixing Park in Guilin [10], and Sun Yat-sen Mausoleum in Nanjing [13]. The tourist capacity of these scenic areas is measured again and the comparative results are listed in Table 1.

Because the data is lacked in the original article, the average visiting time of visitors in Wuyi Mountain scenic area is equal to the sum of average visiting time of 8 scenic spots inside of the scenic area, which is 29 hours (settled according to the original article). The average visiting time of visitors in Qixing Park in Guilin is referred to the relative large value among the same type of scenic spots in our country, which is 5 hours.

Table 1. Comparative results of traditional formula and amendment formula*.

Tourist capacity	Wuyi mountain		Lu mountain		Qixing park in Guilin		Sun Yat-sen Mausoleum in Nanjing	
	C (person)	Cy (ten thousand person)	C (person)	Cy (ten thousand person)	C (person)	Cy (ten thousand person)	C (person)	Cy (ten thousand person)
Traditional formula	37377	1364	22234	134	36112	1318	16223	592
Amendment formula	6993	255	5920	104	24735	903	3152	115

*: C is the day space capacity of tourism area, Cy is the year space capacity of tourism area.

4 DISCUSSION ON THE PRACTICAL APPLICATION OF TOURIST ENVIRONMENT CAPACITY

The as-mentioned amendment formula proposes a static model for measuring the tourist capacity in an assumption condition. However, in the practical application, the characterization of different scenic tourism areas differs in thousands of ways. It should be adjusted according to the practical situation of tourism areas.

1. The demand category should be defined firstly before the confirming of tourist capacity.

The type of visitors must be firstly defined when the tourist capacity is scientifically measured. The tourist demand of different types of visitors is different and they are suitable to different basic space standard. Meanwhile, from the point of view of sustainable development of the tourist area, the tourist activity which is suitable for different quality of tourist source is also different. For a typical tourist source, a suitable tourist activity form should be defined.

2. The structural feature should be considered fully, especially whether there is bottleneck restriction factor in the tourist capacity of scenic area.

Generally speaking, some of the restriction factors are rigid and some of them are elastic, which should be separately treated according to the practical situation. For a scenic tourism area, the scenic original structure has a crucial effect on the touring lines organization and visitors' tourist activity. For example, Dai Peak of Tai Mountain is a scenic area which will must be visited by every visitor, and all of the mountaineering lines are directly to the Dai Peak. Therefore the tourist capacity of Dai Peak constitute a bottleneck of the whole scenic area. The visiting ways towards Dai Peak (apparatus) capacity is also related with the bottleneck. Fengjun Cui (1997) discussed this characterization in his research on the Tai Mountain tourism environment carrying ability. Another similar case is the research of Chenglin Huang (1997) to the tourism environment capacity of Huang Mountain scenic area [10].

3. The space distribution structure and managing mode of scenic spots inside of the scenic area also have important effect on the measurement of tourist capacity.

In the as-mentioned assumption about the tourist capacity amendment formula, the third and fourth clues are all involved in this point. If the scenic spots in a scenic area are relatively dispersive, the combination of scenic spots is poor, the inter-attraction is not strong, at the same time the management of scenic spot is

relative independent, the tourist capacity measurement of scenic area should not be calculated in an entirety, and it should be calculated separately to every scenic spot. In this case, the traditional tourist capacity measurement formula can be just suitable.

4. The basic space standard of tourist place is of great significance on the tourist capacity measurement, which should be formulated and improved as soon as possible.

At present, our country has not a basic space standard for the improvement of scenic tourism area. There is only the government standard "Scenic area planning and specification" (GB 50298-1999) to be used for reference [11]. However, the basic space standard in this specification considers in a narrow scope, which cannot be fit for the increasingly diverse demand of the visitors and the constant rich and developed function of tourism area. In addition, the Appendix A of "General specification for tourism planning" established by national tourism administration has also proposed a basic space standard about the tourism serve apparatus. Therefore, the basic space standard of tourism place should be set by organizing experts as soon as possible in order to avoid the randomness during tourist capacity measurement.

REFERENCES

- [1] Lisle S. Mitchell. Geography and tourism [J]. *Annals of Tourism Research*. 1991, 18 (1) 57–70.
- [2] Harry Coccossis, Apostolos Parpairis. Tourism and the environment-some observations on the concept of carrying capacity [J]. *Tourism and the Environment*. 1992, 2 (2), 23–33.
- [3] Fengjun Cui. Study on the tourist environment bearing capacity [J]. *Economic Geography*. 1995, 15 (1), 105–109.
- [4] George H. Stankey, Stephen F. McCool and Gerald L. Stokes. Limits of acceptable change: a new framework for managing the bob Marshall Wilderness complex [J]. *Western Wild lands*, Fall. 1984, 10 (3), 33–37.
- [5] Donald Getz. Models in tourism planning: towards integration of theory and practice [J]. *Tourism Management*. 1986, 7 (1), 21–32.
- [6] Yang Rui. Preliminary study on environmental capacity of scenic spots. *Urban Planning Forum*. 1996, 6 (4), 12–32.
- [7] Xu Xiaoyin. Discussion on the measuring methods of tourism environmental capacity in scenic spots. *Journal of Central China Normal University (Natural Science)*. 1999, 33 (3), 455–459.
- [8] Lu Lin. A study on the tourist flows in mountain resorts a case study in Huangshan Mountain [J]. *Acta Geographica Sinica*. 1994, 49 (3), 236–246.
- [9] Huang Zhenfeng, Chen Zhigang, Yuan Linwang. A summary of study on regional tourism environment in China. *Geography and Geo-information Science*. 2004, 20 (3), 99–104.
- [10] Zhang Xiaoping, Zhu Zhongfu. An analysis of tourism environment capacity in Jiuzhaigou Scenic area. *Tourism Tribune*. 2007, 22 (9), 50–57.
- [11] GB50298-1999, Scenic area planning and specification.

The design of dual purpose crib based on man-machine research

Li-Li Liu & Jing Bian

*Jiangsu Key Laboratory of Large Engineering Equipment Detection and Control,
Xuzhou Institute of Technology, Xuzhou, Jiangsu Province, China*

ABSTRACT: Based on the current status of the development of the crib on the market, we focus on the man-machine relations as the entry point, study and analyze the existing disadvantages and problems of the crib. The design of the dual purpose crib can not only be used as the normal crib, but also can be used when the babies grow up.

With the improvement of people's living standards and economic level, people think more about the pursuit of the material quality now, at the same time, they also slowly begin to pay more attention to the ecological environment protection and the importance of reducing energy consumption. Children's bed is an infant from birth possessions, and people become more and more highly for the requirement of its safety and comfort. However, most of the Children's beds currently on the market are still focused on the design of the appearance design, without considering the problem whether it can be used after the babies grow up. And how to make the invisible waste to become resources is more and more important. Moreover, in the current promotion of "green design" situation, we should understand the importance of conserving resources. So for the sharp increase in children's bed needs, we will design a children's bed that has the basic functions, but also design features into the sofa, to meet the needs of different periods, and reduce the unnecessary waste of resources.

Keywords: children's beds; dual purpose; man-machine analysis; cozy

1 THE ANALYSIS OF ENTRY POINT FOR PRODUCT DESIGN

Product design is a process of creating new and improved products for people to use. Its first consideration is safety, functionality, usability, price and appearance. Children's beds are one of the essential items after the baby was born. As baby's first hotbed, comfort and safety of it will determine the initial development of the fine baby. Generally long after the baby was born is left in the crib, so parents must ensure the safety of the Children's beds to avoid the accident. Choose a Children's bed is particularly important conform to safety standards, through the survey found that the average Children's beds bed bar because there is gap between cracks, so that the baby is likely the danger caused by the head trapped, even cause suffocation and crisis to the baby's life. In addition, when the baby began to crawl slowly began to practice, because the clothes could also entangled in bed around prominent obstacles, which can potentially cause baby in danger of falling from the Children's beds. Finally, because as children grow up slowly, after Children's beds can't satisfy their needs, so we can consider from the Angle of utility, when you can't use, can satisfy other functions, and not wasteful.

2 THE MAIN PROBLEM OF THE 2 MAN-MACHINE RELATIONSHIP EXISTING PRODUCTS

Ergonomics, which is the application of anthropometry, are human body mechanics, physiology, labor physiology research methods such as subject. The study of human body structure characteristic and the function characteristic provide the human body each part of the size, weight, surface area, specific gravity, center of gravity, and the relationship of the human body each part in the activity and reach range human body structure characteristic parameters. In addition, we discuss the factors that affect mental state at work and the influence of psychological factors on the efficiency and so on. In this article, through the analysis and research about the existing range of Children's beds, we sum up the following several problems, and the solutions to these problems as an important target of Children's beds design.

First of all, from the psychological point of view, the current market of Children's beds is single form, lack of fashion sense, and there is no sense of novelty.

Secondly, from the consideration on the existing Children's beds function, single structure, the lack

of humanization design, even if it appeared on the market at present multi-function Children's beds design. But the function transformation is not convenient. Therefore, we can consider in the design on the basis of adding features, convenient conversion, to make it more humane, and more comfortable.

Finally, from a security point of view, most of the Children's beds design on the market at present is mainly focused on brand and quality, while also protean appearance but from the main body, make body single shape. And according to the survey, a researcher said that most of the babies are not suitable for shaking, because of the newborn infant brain organizations are very fragile, shaking for a long time can make the baby's brain and skull constantly scratches can sometimes lead to trace damage can affect the health of baby's body. In addition, when it converted to sofa chair, let the user feel more comfortable, more human.

3 DUAL PURPOSE DESIGN POINTS OF THE CRIB FUNCTION DESIGN

Please conform to the law of scientific design program. Adopt different ways of regulating changes, in the guarantee of safety and comfort at the same time. Fully consider the crib after use can't continue to use lead to occupy a space problem. The baby's bed and sofa in the form of contact with restructuring, mainly from the Children's beds to the secondary sofa, again from the sofa as the main auxiliary crib two directions to consider, in the security and the uniqueness and everything else is a breakthrough for products on the market. As shown in [Figure 1](#) & [Figure 2](#).



Figure 1. The baby bed used as sofa.

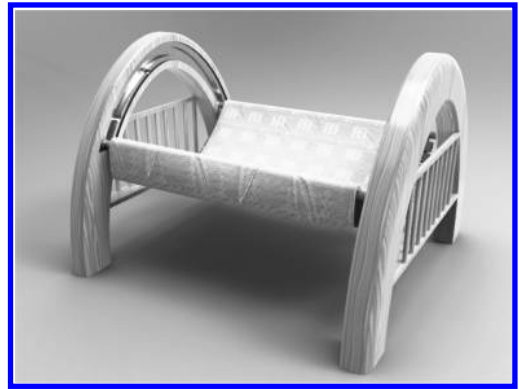


Figure 2. The baby bed.

4 SHAPE DESIGN

As is known to all, the baby in her mother's belly, is amniotic fluid around, such as one day suddenly left the mother's belly to the outside world, the baby will be insecure. So we can from the baby's physiological and psychological aspects of in-depth thinking. It can copy the shape of the cradle designed, let the baby lying on it, like a lie in her mother's arms. It was wrapped around, let the baby sleep more comfortable, more sweetly. In addition, from the transformation into the sofa of form after consideration, the morphology change is more easy and convenient, and at the same time, people also can sit experience a space of love and the warmth of love.

5 RECEIVE A CONCEPTION

Many of the products on the market at present on the product function and appearance also began to pay attention to the product to receive way. The aim is to make the product when removing and installing more convenient, and this also is helpful for the transportation of products, reducing the transportation cost, not only make it more humane, but also conforms to the "green design". As shown in [Figure 3](#).

6 THE MAN-MACHINE ANALYSIS

The so-called human nature products, is containing the man-machine engineering products, as long as it is "people" the use of the product, should be on the man-machine engineering into consideration, the modeling of products is combined with man-machine engineering. The design of the product cannot be without the man-machine engineering.

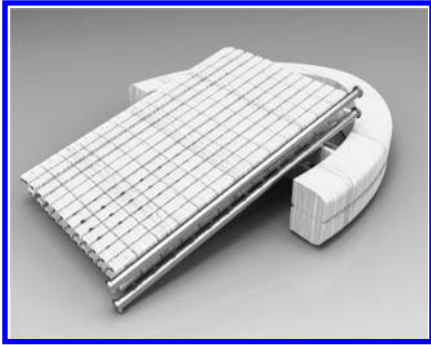


Figure 3. Analysis diagram.

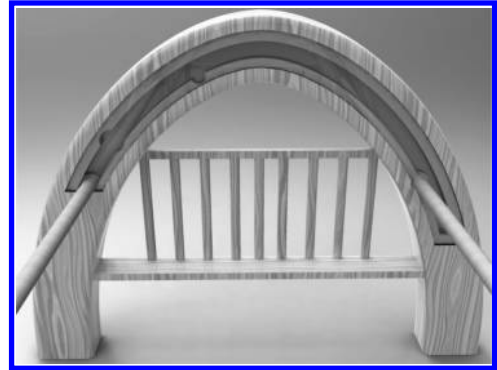


Figure 4. Details of the figure.

A product is, however, how to evaluate it in terms of ergonomics is in accordance with the specification?

1. For Children's beds should be paid attention to when choose cylindrical bars. The distance between the two fences is no more than 6 cm (this is the new standard of Numbers), to prevent the baby's head from the middle. Some moms like pattern are more complex, the vulture act the role of more Children's beds, in fact, this bed is safe enough for children. Because bed or bed raised vulture act the role to hook for children's clothing, children try to break free, it may impact injury. In addition, when the mattress to its highest position, it has to do with the distance of the side of bed must be at least 40 centimeters of above. Mattress with bedstead tight closely together on both sides of the distance on both sides of guardrail for less than 2 cm (mattress), in order to prevent the baby into it. On the choice of the mattress, the traditional cotton quilts is a good choice. Finally, on the use of Children's beds on both sides of the fence, the height of the fence is 50 centimeters above the mattress. If it is too low, by the time the children can catch fence stand, is in danger of falling climb over the fence at any time.
2. As a double sofa the size of each part should be consistent with the requirements of human body engineering, in order to suit the curved surface of structure of human body physiology had better. The sofa seat surface height should be equal to the people of the lower leg and the height of the heel or slightly low altitude, for about 35 to 42 cm; Single person sofa seat in the front of the width should not be less than 48 cm; Double sofa should be above 95 cm, on the surface of the seat depth should be between the 48–55 cm. When the body sits on the sofa, the maximum with knee still outside the sofa face advisable; After the height of the back of a chair to sit down



Figure 5. Details of the figure.

when it is advisable to achieve between shoulder and ear, a back of a chair from the ground at the top of the roughly 68–68 cm; After the inclination of the back of a chair, it is advisable to between 100–108 degrees. The both sides of the height of the armrest in 62–65 cm.

3. As it is shown in Figure 4, the details of the slide bar graph, which has three slots, from left to right is the first imported groove, and the second is as a rod notches on the sofa, and the third is as a crib in the slot. Rod can be used to track the sliding into the primary slot, simple and safe operation. In addition, as shown in Figure 5 is a fixed pole figure, the details of the above on a cotton padded covering, so people won't feel stiff, sit on it to increase its comfort. Adjust the surface using bamboo, natural pollution-free, freedom and activities.

7 CONCLUSION

Children's beds have had the very big development in our country, but the design of new products

research and development is always a topic. For Children's beds combination design, to find and solve the problems of the family is the need of young parents, so is the need of times development. The design solves the baby crib bed taking up space and transforming complicated problem.

The design of dual purpose crib based on Man-machine is an Innovation. It's Simple style. The dual purpose crib is in the form of combination on the basis of ensure safety and comfort in the baby and make it when not in use take up the question of family space and into the sofa, pay more attention to its effectiveness. The amphibious Children's beds modeling concise, simple structure, and transform is very convenient, and every part of considering the baby's comfort and safety, considering the effect of the adult is comfortable. Every size and parameters according to the theory of ergonomics are reference for scientific data.

This subject adopts a novel way to solved the problem of the recycle of the new design of dual crib to meet the psychological needs of the consumers.

If we can combine intelligent adjustment function with it, I believe that this solution can rush out a new land in the future market.

REFERENCES

- [1] Zhang Xianrong. The design theory and method of industry [M]. Beijing: Beijing Institute of Technology press, 1996.
- [2] Wang Ming purpose. Product design [M]. Beijing: Chinese Youth Press, 2002.
- [3] Tong Huiming for life and design [M]. Beijing: China Fine Arts Publishing House, 1998.
- [4] (Germany) Bernhard.E. Boolean Dirk. Industrial Design: product shapehistory. The theory and practice of Hu Feize [J]. Beijing: Chinese Architecture Industry Press, 2007.
- [5] Tang Yong medium. Modular fixture assembly technology [M]. Beijing: National Defence Industry Press, 1979.
- [6] Ding YuLan. The man-machine engineering [M]. Beijing:Beijing Institute of Technology Press, 2005.

A design study on optoelectronic textiles in cases of LED lighting and solar powered handbags

Ju-Yi Shih & Shu-Ling Lai

Department of Digital Media Design, Asia University, Taichung, Taiwan

Huai-Tzu Cheng

Industrial Economics and Knowledge Research Center, ITRI, Hsinchu, Taiwan

ABSTRACT: At the present stage, the major optoelectronic technologies used in textile design are LED lighting and solar cells. Due to the progress of these technologies is very rapid, the feasibility of practical application and commercial promotion is gradually apparent. This paper focuses on a design study of optoelectronic textiles in cases of LED lighting and solar powered handbags. The composition of components and the assembly of handbags have been described and discussed. These products are the strengths of Taiwan industries, thus it will be worth to develop and promote for the clothing industry in Taiwan.

Keywords: green textile; LED; solar cell; textile design; handbag

1 INTRODUCTION

Optoelectronic components, including LED lighting and solar cells, are appeared in the market for more than 20 years [1–5]. There are many related textile products has been introduced in the market, but these products are still not accepted by most of people. Aside from the continuous technology improvement should be executed to invent better components, the related design study would also require to be enhanced. There are many applied research works about the optoelectronic textile, but just a little concern the case of handbag [6–10].

This publication contains a design study of optoelectronic textiles in cases of LED lighting and solar powered handbags. The purpose of this study is to introduce the utilization of optoelectronic products in textile industry and potential market, as well as provide design reference for the designers who are interested in the textile design of this field.

In the application of optoelectronic components in handbag design, a concept can be illustrated by Figure 1. LED components can be used in handbags as a light source for the purposes of decoration or warning signal, and solar cells may be applied as a power source, which can supply electricity to a mobile phone, a digital camera or any other consumer electric product. Besides these components, the electric components, such as battery, charger, controller, switch, and connection lead are also needed to assemble a final complete product with correct functions.

2 DESIGN AND FABRICATION OF LED LIGHTING HANDBAG

Currently LED components used in the textile include soft packaging, optical fiber and LED yarn [11]. Among these components, LED yarns have the advantages of easy use, superior performance and reasonable cost. The LED yarn was developed by Taiwan Textile Research Institute in cooperation with some manufacturers of electronic products in 2011 [11]. This product shows the characteristics of flexibility, abrasion resistance and strength with the potential of market application.

As shown in Figure 2, LED chips are encapsulated on a conductive fiber, and then coated with an optically transparent resin to form a LED yarn. LED yarns can be sewn on appropriate locations of clothes, and connected to battery boxes,

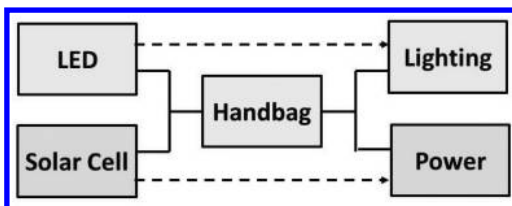


Figure 1. Concept and function of optoelectronic handbags.

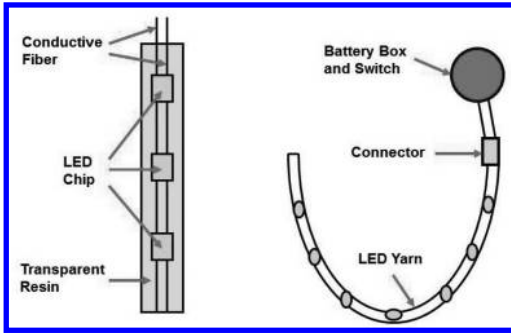


Figure 2. The structure and the product of LED yarn [6].

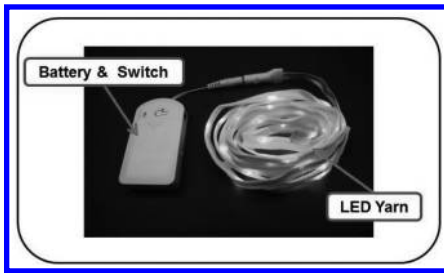


Figure 3. LED lighting system [12].



Figure 4. A LED handbag.

switches, and circuit boards. Therefore, one can turn on a start switch when LED light is required. LED yarns can be provided by a roll base with an outer diameter of 2.5 mm. The maximum current consumption is 240 mA/m when the input voltage is DC 4.5 V, and the service time is about 20,000 hours.

The LED lighting system using by this study is described as Figure 3. This LED yarn and a power box with switch was provided by the Fabric King Group in Taiwan [12]. The LED yarn has composed by two colors of LED chips. With one color

is red and the other color is blue, the variation of color change is more chromatic, and the warming and shining effect can be enhanced.

A handbag with LED lighting is shown in Figure 4. A kind of thick cotton canvas fabric with waterproof treatment was used for the exterior layer, and nylon fabric was selected to be the internal layer. Gray and brown colors of canvas fabrics were cut to the shape of long bar separately, and sawed together in a staggered form to obtain a handbag. In addition, a brown bag strap made by canvas fabric was used for easy to carry. The LED yarn was sewed along the bottom side of this handbag, and the power box was installed in a pocket inside this handbag. Due to a lithium battery with the capacity 1,000 mAh was used, the shining time of LED yarn could be 12 hours for continuous lighting, and 24 hours for flashing lighting.

3 DESIGN AND FABRICATION OF SOLAR POWERED HANDBAG

Traditional solar cells used in the textile are very monotonous with blue color and rectangular shape. Recently, colored solar cells are appeared in the market, and there are different kinds of products for selection, such as multilayer antireflection, color modulation layer, colorized encapsulation layer, and colorized frame [9].

Tropical Solar photovoltaic Company locates in central Taiwan and has developed a colorized encapsulation layer type of solar cell with various shapes. As shown in Figure 5, there are two solar cells with different shapes of leaf and circle [13]. In addition, the color of solar cell is blue, and the color of frame is green. The strong point of these solar cells is very interesting and can attract admiring eyesight and aesthetic judgment.

The material of this handbag was leather with brown color as shown in Figure 6(a). A piece of leather was used for both the front part and the back part of this bag, and a strap of leather was used for the side part. The connection of leathers utilized hand-sewn process with a big needle. The solar cell and electric components used in this study

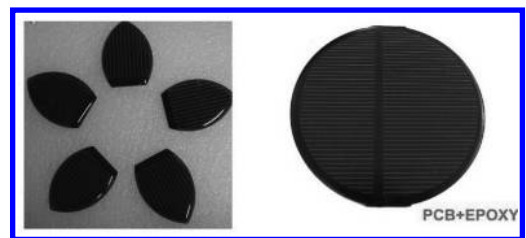


Figure 5. Colored and shaped solar cell [13].

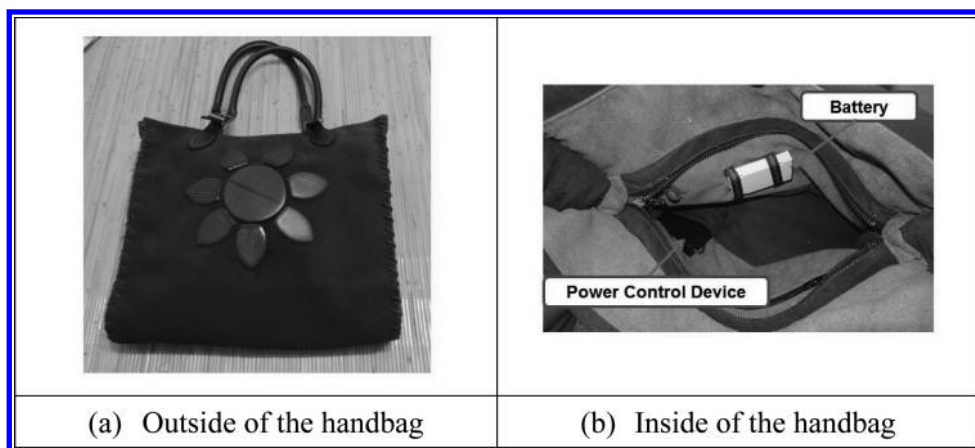


Figure 6. A solar powered handbag.

is directly supplied by Tropical Solar photovoltaic Company. The solar cell with a shape of sunflower was attached in the front part of this bag as shown in Figure 6(a), and the electric components are fixed in the inner part as shown in Figure 6(b).

A power control device in Figure 6(b) is used to control the charging process if necessary, and can provide electricity for charging a mobile phone through a USB connector. Besides, electricity obtained from solar cell can be controlled by the power control device for storing in the lithium battery. The solar cell is a kind of single crystal type, and cannot generate power in a cloudy day or inside a house. It can only produce electricity under the sunshine of a clear day. Although this solar cell cannot provide enough electricity for a mobile phone, it still can replenish electrical energy and extend the operation time of a mobile phone.

4 CONCLUDING REMARKS

A design of optoelectronic textiles in cases of LED lighting and solar powered handbags had been illustrated and completed, which can provide design reference for the designers who are interested in the optoelectronic textile design.

In order to promote LED components to be used in the textile industry and market, it needs the creativity of more fashion designers and the participation of more apparel manufacturers. Thus, a training effort for fashion designers to be familiar with the application of optoelectronic components in textile design is very important. In the future, the LED textile will combine with a trend of intelligent electronic evolution to access a wider range of applications.

ACKNOWLEDGEMENTS

This work was supported in part by the Ministry of Economic Affairs of Taiwan, under Contract 101-EC-17-A-02-S1-201. The authors like to appreciate all of helps from Tropical Solar photovoltaic Company in Nantou, Taiwan, Fabric King Textile Co. in Taipei, Taiwan and Strong & Young Technology Development Co. in Taipei, Taiwan.

REFERENCES

- [1] Kuo, H.C., Lai, F.Y. and Kuo, S.Y. Principle and application of LED, Wu-Nan Culture Enterprise, Taipei, Taiwan, 2009.
- [2] Wang, C.L.: An application study of LED in textile, MS Thesis, Wuhan Textile University, China 2011.
- [3] Bedeloglu, A., Demir, A., Bozkurt, Y. and Sariciftci, N.S. Text. Res. J. 80(11) (2010) 1065–1074.
- [4] Werner, J.H., Wagner, T.A., Berge, C.E.M., Brendle, W. and Schubert, M.B. Proceedings of 3rd World Conference on Photovoltaic Energy Conversion 2 (2003) 1272–1275.
- [5] Schubert, M.B., Ishikawa, Y.A., Kramer, J.W. Gemmer C.E.M. and Werner, J.H. Proceedings of 31st IEEE Photovoltaic Specialists Conference and Exhibition (2005) 1488–1494.
- [6] Shih, J.Y., Lai, S.L. and Cheng, H.T. Int. J. Adv. Mat. Res., 821–822 (2013) 453–458.
- [7] Shih, J.Y., Lai, S.L. and Cheng, H.T. Int. J. App. Mech. & Mat. Res., 368–370 (2013) 702–707.
- [8] Shih, J.Y., Lai, S.L. and Cheng, H.T. Int. J. Adv. Mat. Res. 706–708 (2013) 420–425.
- [9] Shih, J.Y., Lai, S.L. and Cheng, H.T. Int. J. Adv. Mat. Res. 655–657 (2012) 2017–2024.
- [10] Shih, J.Y., Lai, S.L. and Cheng, H.T. Int. J. Adv. Mat. Res. 655–657 (2012) 2042–2047.
- [11] Lee, C.L. Ind. Mat. Mag. 292 (2011) 117–127.
- [12] Information on <http://www.fabric-k.com>.
- [13] Information on <http://www.chip-city.com.tw>.

Author index

- Abdeljaber, O. 627
Abu-Bakar, A. 45
Afshari, A. 849, 855
Ahmad, Z. 45
Al Rjoub, Y.S. 627
Amiri, M. 849
Azhar, A.T.S. 37
Aziman, M. 37
- Bačová, K. 17
Bai, L.M. 773, 777, 781
Bai, Q. 917
Bao, S.R.N. 327
Baratzadeh, V. 855
Bi, X.F. 715
Bian, J. 923
Bocci, E. 55
Brozovský, J. 817
Burkovic, K. 861
- Cai, J.L. 553
Cajka, M. 861
Cajka, R. 861
Cao, J.W. 913
Čápayová, S. 17
Ceselsky, J. 807
Chae, S.-U. 639
Chai, S.B. 419
Chatakorn, S. 643
Chen, C.-H. 25
Chen, C.T. 623
Chen, D.Q. 307
Chen, F.-Y. 7
Chen, H.K. 789
Chen, H.-Y. 481
Chen, J. 173
Chen, J.L. 499
Chen, L.-Q. 121
Chen, M.C. 413
Chen, Q.W. 239
Chen, S.G. 391
Chen, S.Y. 577
Chen, W. 219
Chen, X. 569
Chen, X.J. 233
Chen, X.M. 131
- Chen, X.X. 169
Chen, Y. 695
Chen, Y. 877, 883
Chen, Y.R. 485
Chen, Z.G. 757
Chen, Z.J. 525
Cheng, H.-T. 927
Cheng, W. 201
Cheng, X.W. 323
Chitral, W.D. 37
Chung, H. 1
Cui, D. 887
- Dai, F. 769
Dai, G.L. 763, 795
Deng, D.H. 333
Deng, R.G. 689
Deng, X.B. 789
Deng, Y. 173
Deng, Z.S. 51
Di Carlo, A. 55
Ding, R.S. 333
Ding, X.X. 189
Djakfar, L. 753
Dong, K. 801
Dong, Z.Q. 211
Du, B. 543, 547
Du, H.Y. 905
Du, J.G. 343
Du, Y.L. 107
Du, Y.-R. 13
Duan, J. 131
- Edrisian, Y. 855
- Fan, J. 769
Fan, W.J. 573
Fan, Y. 561
Fang, B. 711
Fang, F. 451
Fang, Q.W. 801
Fauziah, A. 37
Feng, X.P. 529
Ferko, M. 807
Fu, D. 363
Fu, D.B. 495
- Fu, L. 319
Fu, X.D. 419
Fu, X.J. 225
Fu, Y.R. 503
- Gao, G.Y. 407
Gao, L.-L. 785
Gao, M. 435
Gao, M.X. 327
Gao, Z. 499
Gong, W.M. 763, 795
Gu, J.M. 211
Guo, G.L. 347
Guo, H. 795
Guo, H.H. 521
Guo, X.Y. 373
- Han, F. 577
Han, J.M. 695
Han, Q.L. 445
Han, W. 69
Han, Y.G. 455
Hassanzadeh, M. 849
Hazreek, Z.A.M. 37
He, J.B. 463
He, J.H. 185
He, M.L. 477
He, X.-J. 869
He, Y.W. 499
Hearunyakij, M. 643
Hong, Y. 611
Hou, Q.H. 671
Hou, T.B. 313
Hsieh, T.-K. 13
Hu, B.N. 517
Hu, G.W. 429
Hu, H.J. 711
Hu, L. 297
Hu, M. 689
Hu, S.P. 581
Hu, Z.Q. 61
Huang, H. 413
Huang, H. 873
Huang, H.F. 359
Huang, J.C. 829
Huang, M.F. 319

Huang, Q. 707
 Huang, T. 377
 Huang, Y. 211
 Huang, Y.M. 347
 Huang, Y.W. 841
 Huang, Z.F. 679
 Huang, Z.Y. 313
 Hwang, C.L. 623

 Imran, I. 507

 Jia, L.M. 683
 Jia, X.Y. 69
 Jia, Z. 137
 Jiang, Q.C. 883
 Jiang, X. 201
 Jiao, Y.Y. 605
 Jin, S. 873
 Jin, W.G. 169
 Jin, X. 173
 Jun, S.J. 407

 Kang, W. 1
 Kaveh, S. 849, 855
 Kim, H.-Y. 639
 Kong, X.L. 445
 Kucera, J. 807
 Kweon, O.-S. 639
 Kwon, I.-K. 639

 Labudek, P. 861
 Lai, J.Y. 801
 Lai, S.-L. 927
 Lei, S.Y. 229
 Li, A.H. 257
 Li, C. 125
 Li, C. 367
 Li, C.B. 117
 Li, C.-G. 179
 Li, C.H. 829
 Li, C.R. 521
 Li, G. 553
 Li, H. 323
 Li, H.T. 327
 Li, J.F. 455
 Li, J.J. 107
 Li, J.X. 539
 Li, K.P. 359
 Li, L.F. 419
 Li, L.L. 703
 Li, P. 73, 77
 Li, Q.L. 455
 Li, S. 195
 Li, S.M. 333
 Li, S.Q. 581

 Li, X.K. 195
 Li, Y. 87, 91
 Li, Y. 605
 Li, Y. 703
 Li, Y.G. 131
 Li, Z.Z. 455
 Liang, A.H. 525
 Liang, C.Y. 367
 Liang, J.-H. 7
 Liang, L.J. 211
 Liang, X. 711
 Liang, Y.-Y. 7
 Liao, M.J. 69
 Limongan, A.H. 623
 Lin, B.H. 499
 Lin, F. 391
 Lin, H.B. 319
 Lin, R.L. 731, 735, 739, 743
 Lin, X.C. 343
 Lin, X.-M. 121
 Lin, Y.-B. 25
 Ling, G.X. 543, 547
 Ling, Y.H. 347
 Liou, Y.-C. 25
 Liu, C.-C. 25
 Liu, H.B. 205
 Liu, H.B. 467
 Liu, H.F. 377
 Liu, H.M. 275, 293
 Liu, J. 307, 313
 Liu, J. 333
 Liu, J.J. 367, 413
 Liu, L.J. 485
 Liu, L.-L. 923
 Liu, M. 695
 Liu, N. 499
 Liu, Q.J. 577
 Liu, R.Q. 307, 313
 Liu, S.J. 585
 Liu, S.K. 495
 Liu, W. 51
 Liu, X. 529
 Liu, X.H. 117
 Liu, Y. 205
 Liu, Y. 877, 883
 Liu, Y.F. 727
 Liu, Z.H. 275
 Liu, Z.L. 107
 Long, J.W. 373
 Long, W.X. 543, 547
 Lu, H.M. 537
 Lu, R.J. 667
 Lu, S. 683
 Lu, X. 243
 Lu, Y. 585

 Luo, J.N. 251
 Luo, S. 51
 Luo, Y.R. 319
 Luo, Z.G. 789
 Lv, P. 513
 Lv, Y.M. 459

 Ma, C.L. 21
 Ma, H. 653
 Ma, H.W. 347
 Ma, L. 395
 Ma, R.Y. 499
 Ma, X. 359
 Ma, X.J. 577
 Mahemuti, M. 157
 Mamuti, M. 157
 Meng, Q.L. 151
 Meng, Y.D. 503
 Mikolasek, D. 811, 817
 Mo, S.X. 195
 Mohsan, N.M. 31
 Moneti, M. 55

 Nasution, H. 635
 Ni, T. 111
 Norshariza, M.B. 45

 Pan, Q.X. 219, 377
 Pang, X.Q. 61
 Pang, Y.C. 521
 Pang, Y.G. 257
 Peng, I.-W. 7
 Peng, X.N. 905
 Phuoc, H.T. 623
 Pi, F.M. 615
 Proske, Z. 807

 Qi, C.H. 327
 Qi, H. 131
 Qi, H.W. 723
 Qi, X.L. 435
 Qi, X.X. 263
 Qian, G.P. 377
 Qian, X.Q. 801
 Qie, E.T. 605
 Qie, R.Q. 649
 Qiu, J. 595
 Qu, Y.X. 403, 407

 Ren, J.W. 909, 913
 Ren, X.M. 205
 Ren, Y.Y. 663
 Risdianto, Y. 623
 Rosli, S. 37
 Rouzi, K. 157

Sabbagh, F. 849, 855
 Sang, H.T. 789
 Setiawan, J. 507
 Shang, J.L. 229
 Shao, L.-L. 513
 Shen, L. 485
 Sheng, Q. 419
 Shih, J.-Y. 927
 Shu, X.P. 477
 Song, L. 373
 Song, Y.P. 267
 Su, H. 287
 Su, M.Y. 189
 Su, Y. 293
 Su, Y. 561
 Sucharda, O. 811, 817
 Sudarsana, D.K. 753
 Sulaiman, A. 31
 Sulistio, H. 753
 Sun, M. 747
 Sun, W.G. 485
 Sun, X. 581
 Sun, Y.X. 267
 Sun, Z.J. 383

 Tahir, M.Md. 31
 Tahir, P. 45
 Tang, B. 215, 363
 Tang, L. 111
 Tang, L.S. 789
 Tang, Z. 297
 Tao, Z. 233
 Teng, K. 225
 Tesfamariam, M.G. 623
 Tsai, H.-Y. 13
 Tuan, B.L.A. 623

 Vasek, J. 811
 Vecchione, L. 55
 Vojvodikova, B. 807

 Wan, T.-L. 825
 Wang, C.L. 103
 Wang, C.T. 605
 Wang, D. 95, 99
 Wang, J.-J. 423
 Wang, K. 429
 Wang, K.Q. 917
 Wang, K.S. 521
 Wang, L. 715
 Wang, L. 795
 Wang, M.M. 619
 Wang, P. 151
 Wang, P. 689
 Wang, Q. 125

 Wang, S. 891
 Wang, S.Y. 747
 Wang, W. 169
 Wang, W. 303, 557
 Wang, W.H. 671
 Wang, W.M. 367
 Wang, X. 455
 Wang, X.Y. 573
 Wang, Y. 569
 Wang, Y.P. 569, 723
 Wang, Y.Y. 163
 Wang, Z. 463
 Wang, Z.H. 657
 Wei, S.J. 239, 243, 247
 Wei, X. 913
 Wei, Y. 459
 Wen, H. 111
 Wen, Q.M. 247
 Wen, Z. 439
 Weng, Z.C. 333
 Wicaksono, A. 753
 Wu, D.Z. 591
 Wu, H. 343
 Wu, J.H. 591
 Wu, J.Y. 353
 Wu, J.Y. 841
 Wu, W. 163
 Wu, X.F. 841
 Wu, X.Y. 581
 Wu, Y.Z. 347
 Wu, Z. 499

 Xi, X. 513
 Xia, C. 495
 Xia, L.B. 595
 Xiang, Y.M. 543, 547
 Xiao, Y. 663
 Xie, L. 215, 363
 Xie, Z.P. 619
 Xin, H.W. 359
 Xiong, X.B. 895
 Xu, D. 73, 77
 Xu, D.J. 715
 Xu, H.D. 225
 Xu, J. 145, 257
 Xu, J.C. 343
 Xu, L. 403
 Xu, M.Y. 263
 Xu, Q. 467
 Xu, X. 297
 Xu, X.W. 619
 Xu, Y. 169
 Xu, Y.L. 769
 Xue, K. 439
 Xue, S.F. 117

 Xue, W.B. 565
 Xue, X.H. 257

 Yan, H. 615
 Yang, B. 219
 Yang, C. 179
 Yang, C. 763
 Yang, C.-D. 833
 Yang, C.L. 303
 Yang, D. 239, 243, 247,
 399, 403, 407
 Yang, D.J. 333
 Yang, H.L. 195
 Yang, J.H. 619
 Yang, K. 83
 Yang, M.S. 565
 Yang, Q.L. 297
 Yang, W.-R. 869
 Yang, X.F. 619
 Yang, X.M. 455
 Yang, Y. 707
 Yang, Y.L. 679
 Yang, Z. 873
 Ye, D.P. 711
 Ye, Z.C. 553
 Yin, J. 689
 Ying, W.Z. 599
 Yu, C.H. 435
 Yu, J. 525
 Yu, P.Q. 485
 Yu, Q. 103
 Yu, R.G. 117
 Yu, T.-C. 25
 Yu, X.F. 451
 Yu, Y.J. 141, 145
 Yuan, K. 225
 Yuan, K.F. 383, 387
 Yuan, Z.H. 263
 Yungmin, Y. 1

 Zeng, D.G. 233
 Zeng, T. 319
 Zeng, X.-S. 65
 Zeng, Z. 333
 Zeng, Z.Y. 353
 Zha, X.D. 219
 Zhan, R.Q. 577
 Zhang, B. 517
 Zhang, H. 229
 Zhang, H. 251
 Zhang, H. 391
 Zhang, K. 869
 Zhang, L. 533
 Zhang, L. 905
 Zhang, L.H. 403, 407

Zhang, L.H. 467, 553	Zhang, Z.Q. 499	Zhu, H.Y. 251
Zhang, L.Y. 459	Zhang, Z.-X. 513	Zhu, J. 163, 719
Zhang, M. 117	Zhao, T. 327	Zhu, M.-X. 121
Zhang, M. 239, 243, 399	Zhao, W.-J. 179	Zhu, Q.S. 675
Zhang, M.L. 439	Zhao, Z.J. 117	Zhu, S.H. 719
Zhang, M.X. 707	Zheng, D.S. 719	Zhu, S.L. 327
Zhang, P. 869	Zheng, H.K. 367	Zhu, S.Y. 21
Zhang, R.N. 141	Zheng, L.-X. 179	Zhu, X.G. 303, 557
Zhang, T.G. 229	Zheng, Q.L. 473	Zhu, Z.R. 763
Zhang, X.J. 239, 399	Zheng, X.G. 333	Zidek, L. 817
Zhang, Y. 757	Zheng, Y. 195	Zong, X.M. 723
Zhang, Y.-C. 785	Zhong, Z.B. 689	Zou, Y. 125
Zhang, Y.M. 117	Zhou, G.Y. 279	Zuo, X. 279
Zhang, Y.M. 429	Zhou, P. 841	Zuzulová, A. 17
Zhang, Z.H. 477	Zhou, Y.Q. 419	